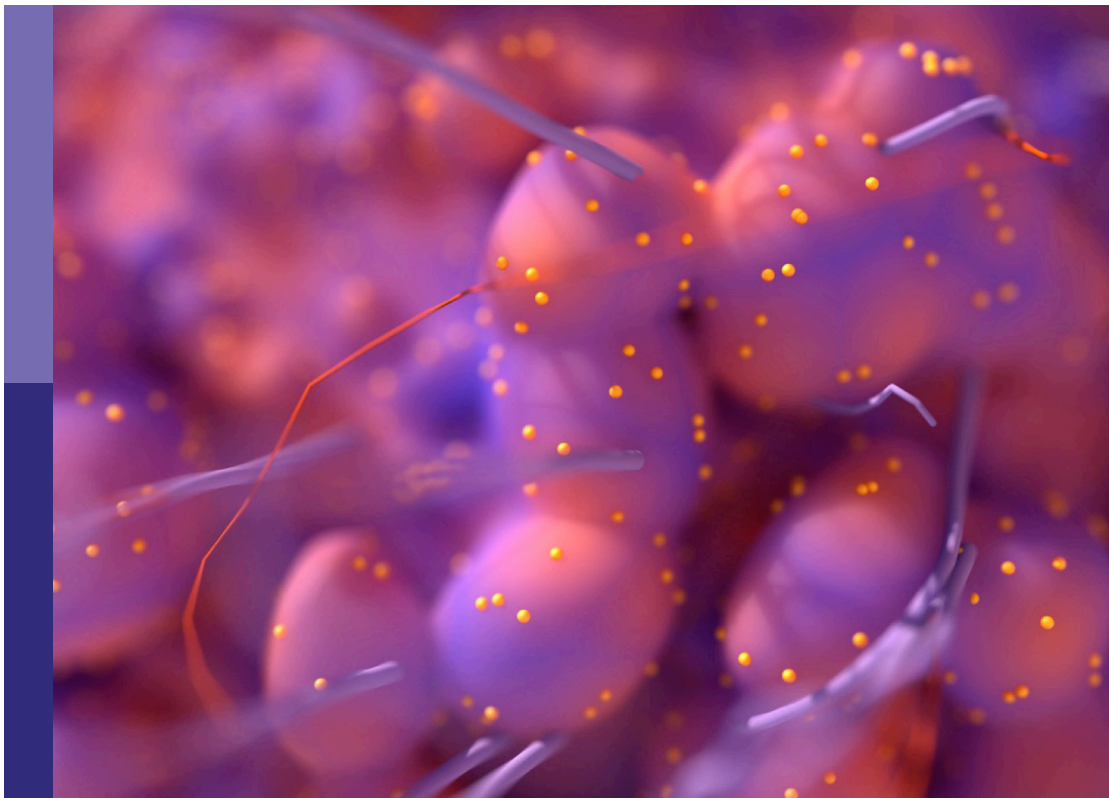
frontiers | Research Topics

Nanomaterials and multimodal tumor therapy

Edited by
Zeming Liu, Kelong Ai and Jiangbo Yu

Published in
Frontiers in Oncology
Frontiers in Pharmacology
Frontiers in Bioengineering and Biotechnology



FRONTIERS EBOOK COPYRIGHT STATEMENT

The copyright in the text of individual articles in this ebook is the property of their respective authors or their respective institutions or funders. The copyright in graphics and images within each article may be subject to copyright of other parties. In both cases this is subject to a license granted to Frontiers.

The compilation of articles constituting this ebook is the property of Frontiers.

Each article within this ebook, and the ebook itself, are published under the most recent version of the Creative Commons CC-BY licence. The version current at the date of publication of this ebook is CC-BY 4.0. If the CC-BY licence is updated, the licence granted by Frontiers is automatically updated to the new version.

When exercising any right under the CC-BY licence, Frontiers must be attributed as the original publisher of the article or ebook, as applicable.

Authors have the responsibility of ensuring that any graphics or other materials which are the property of others may be included in the CC-BY licence, but this should be checked before relying on the CC-BY licence to reproduce those materials. Any copyright notices relating to those materials must be complied with.

Copyright and source acknowledgement notices may not be removed and must be displayed in any copy, derivative work or partial copy which includes the elements in question.

All copyright, and all rights therein, are protected by national and international copyright laws. The above represents a summary only. For further information please read Frontiers' Conditions for Website Use and Copyright Statement, and the applicable CC-BY licence.

ISSN 1664-8714
ISBN 978-2-83251-117-6
DOI 10.3389/978-2-83251-117-6

About Frontiers

Frontiers is more than just an open access publisher of scholarly articles: it is a pioneering approach to the world of academia, radically improving the way scholarly research is managed. The grand vision of Frontiers is a world where all people have an equal opportunity to seek, share and generate knowledge. Frontiers provides immediate and permanent online open access to all its publications, but this alone is not enough to realize our grand goals.

Frontiers journal series

The Frontiers journal series is a multi-tier and interdisciplinary set of open-access, online journals, promising a paradigm shift from the current review, selection and dissemination processes in academic publishing. All Frontiers journals are driven by researchers for researchers; therefore, they constitute a service to the scholarly community. At the same time, the *Frontiers journal series* operates on a revolutionary invention, the tiered publishing system, initially addressing specific communities of scholars, and gradually climbing up to broader public understanding, thus serving the interests of the lay society, too.

Dedication to quality

Each Frontiers article is a landmark of the highest quality, thanks to genuinely collaborative interactions between authors and review editors, who include some of the world's best academicians. Research must be certified by peers before entering a stream of knowledge that may eventually reach the public - and shape society; therefore, Frontiers only applies the most rigorous and unbiased reviews. Frontiers revolutionizes research publishing by freely delivering the most outstanding research, evaluated with no bias from both the academic and social point of view. By applying the most advanced information technologies, Frontiers is catapulting scholarly publishing into a new generation.

What are Frontiers Research Topics?

Frontiers Research Topics are very popular trademarks of the *Frontiers journals series*: they are collections of at least ten articles, all centered on a particular subject. With their unique mix of varied contributions from Original Research to Review Articles, Frontiers Research Topics unify the most influential researchers, the latest key findings and historical advances in a hot research area.

Find out more on how to host your own Frontiers Research Topic or contribute to one as an author by contacting the Frontiers editorial office: frontiersin.org/about/contact

Nanomaterials and multimodal tumor therapy

Topic editors

Zeming Liu — Huazhong University of Science and Technology, China

Kelong Ai — Central South University, China

Jiangbo Yu — University of Washington, United States

Citation

Liu, Z., Ai, K., Yu, J., eds. (2023). *Nanomaterials and multimodal tumor therapy*. Lausanne: Frontiers Media SA. doi: 10.3389/978-2-83251-117-6

Table of contents

07 Editorial: Nanomaterials and multimodal tumor therapy
Yongqi Yang, Qiaohui Chen, Yige Qiu, Yiying Wang, Qiong Huang and Kelong Ai

11 Exosomes as Smart Nanoplatforms for Diagnosis and Therapy of Cancer
Yuying Zhao, Piaoxue Liu, Hanxu Tan, Xiaojia Chen, Qi Wang and Tongkai Chen

35 Facile Synthesis of Holmium-Based Nanoparticles as a CT and MRI Dual-Modal Imaging for Cancer Diagnosis
Tianqi Zhang, Mo Deng, Lei Zhang, Zerun Liu, Yang Liu, Shuyan Song, Tingting Gong and Qinghai Yuan

45 Advanced Nano-Carriers for Anti-Tumor Drug Loading
Jia Xiang, Rui Zhao, Bo Wang, Xinran Sun, Xu Guo, Songwen Tan and Wenjie Liu

52 A Novel H_2O_2 Generator for Tumor Chemotherapy-Enhanced CO Gas Therapy
Yang Li, Zeming Liu, Weng Zeng, Ziqi Wang, Chunping Liu, Ning Zeng, Keli Zhong, Dazhen Jiang and Yiping Wu

59 An Injectable Hydrogel for Enhanced FeGA-Based Chemodynamic Therapy by Increasing Intracellular Acidity
Wen Zeng, Dazhen Jiang, Zeming Liu, Weilong Suo, Ziqi Wang, Daoming Zhu and Qinqin Huang

68 Doxorubicin-Loaded Tumor-Targeting Peptide-Decorated Polypeptide Nanoparticles for Treating Primary Orthotopic Colon Cancer
Guoliang Liu, Min Wang, Hongyu He and Jiannan Li

80 $SnFe_2O_4$ Nanozyme Based TME Improvement System for Anti-Cancer Combination Thermoradiotherapy
Wen Zeng, Chunping Liu, Shuntao Wang, Ziqi Wang and Qinqin Huang

88 Achieving NIR Light-Mediated Tumor-Specific Fenton Reaction-Assisted Oncotherapy by Using Magnetic Nanoclusters
Shaoyou Qin, Jinru Xue, Erna Jia, Na Ren, Yongqiang Dong and Changyu Zhou

101 Platelet Membranes Coated Gold Nanocages for Tumor Targeted Drug Delivery and Amplificated Low-Dose Radiotherapy
Mingzhu Chen, Ping Wang, Dazhen Jiang, Zhirong Bao and Hong Quan

110 Ultrasmall PEI-Decorated Bi_2Se_3 Nanodots as a Multifunctional Theranostic Nanoplatform for *in vivo* CT Imaging-Guided Cancer Photothermal Therapy
Peng Zhang, Lei Wang, Xiuying Chen, Xiang Li and Qinghai Yuan

119 Delivery of siRNA Using Functionalized Gold Nanorods Enhances Anti-Osteosarcoma Efficacy
Man Zhang, Jinti Lin, Jiakang Jin, Wei Yu, Yiying Qi and Huimin Tao

133 Mitochondria-Targeting Chemodynamic Therapy Nanodrugs for Cancer Treatment
Qiaohui Chen, Niansheng Li, Xiaoyuan Wang, Yuqi Yang, Yuting Xiang, Xingyu Long, Jinping Zhang, Jia Huang, Li Chen and Qiong Huang

140 Nanomaterial Technology and Triple Negative Breast Cancer
Kai Hou, Zeng Ning, Hongbo Chen and Yiping Wu

146 Applications and Biocompatibility of Mesoporous Silica Nanocarriers in the Field of Medicine
Chengcheng Zhang, Hongyi Xie, Zhengyan Zhang, Bingjian Wen, Hua Cao, Yan Bai, Qishi Che, Jiao Guo and Zhengquan Su

164 Recent Advance of Nanomaterial-Mediated Tumor Therapies in the Past Five Years
Xinyan Hao, Junyong Wu, DaXiong Xiang and Yongyu Yang

177 Emerging Bismuth Chalcogenides Based Nanodrugs for Cancer Radiotherapy
Jia Huang, Qiong Huang, Min Liu, Qiaohui Chen and Kelong Ai

185 Effective Delivery of siRNA-Loaded Nanoparticles for Overcoming Oxaliplatin Resistance in Colorectal Cancer
Yue Zhou, Qing Zhang, Minjia Wang, Chengzhi Huang and Xueqing Yao

198 Corrigendum: Effective Delivery of siRNA-Loaded Nanoparticles for Overcoming Oxaliplatin Resistance in Colorectal Cancer
Yue Zhou, Qing Zhang, Minjia Wang, Chengzhi Huang and Xueqing Yao

200 Fabrication of *In Situ* Grown Hydroxyapatite Nanoparticles Modified Porous Polyetheretherketone Matrix Composites to Promote Osteointegration and Enhance Bone Repair
Ningning Wang, Desheng Qi, Lu Liu, Yanlin Zhu, Hong Liu and Song Zhu

213 Docetaxel-Loaded Novel Nano-Platform for Synergistic Therapy of Non-Small Cell Lung Cancer
Xing Feng, Xiaoling Xiong and Shenglin Ma

223 Corrigendum: Docetaxel-loaded novel nano-platform for synergistic therapy of non-small cell lung cancer
Xing Feng, Xiaoling Xiong and Shenglin Ma

224 Study on the Mechanism of Astragalus Polysaccharide in Treating Pulmonary Fibrosis Based on "Drug-Target-Pathway" Network
Pingping Bing, Wenhu Zhou and Songwen Tan

234 Melanoma and Nanotechnology-Based Treatment
Hong Zeng, Jia Li, Kai Hou, Yiping Wu, Hongbo Chen and Zeng Ning

240 pH-Responsive Polymer Nanomaterials for Tumor Therapy
Shunli Chu, Xiaolu Shi, Ye Tian and Fengxiang Gao

262 Biomimetic ZIF8 Nanosystem With Tumor Hypoxia Relief Ability to Enhance Chemo-Photothermal Synergistic Therapy
Ziming Zhao, Zhaorong Liu, Yabing Hua, Yuanjie Pan, Ge Yi, Shengyue Wu, Cong He, Yanzhuo Zhang and Yihua Yang

276 Exosome-Based Nanoplatforms: The Emerging Tools for Breast Cancer Therapy
Quan Liu, Xian Zhang and Jun Zhang

284 Principles and Protocols For Post-Cryopreservation Quality Evaluation of Stem Cells in Novel Biomedicine
Jingxian Xie, Marlene Davis Ekpo, Jian Xiao, Hongbin Zhao, Xiaoyong Bai, Yijie Liang, Guang Zhao, Dong Liu and Songwen Tan

293 Synergistic Radiosensitization Mediated by Chemodynamic Therapy *via* a Novel Biodegradable Peroxidases Mimicking Nanohybrid
Jun Zhang, Dazhen Jiang, Meng Lyu, Shiqi Ren, Yunfeng Zhou and Zhen Cao

302 Nucleus-Targeting Phototherapy Nanodrugs for High-Effective Anti-Cancer Treatment
Xingyu Long, Xiaojie Zhang, Qiaohui Chen, Min Liu, Yuting Xiang, Yuqi Yang, Zuoxiu Xiao, Jia Huang, Xiaoyuan Wang, Chong Liu, Yayun Nan and Qiong Huang

310 Nanodrugs Detonate Lysosome Bombs
Yuting Xiang, Niansheng Li, Min Liu, Qiaohui Chen, Xingyu Long, Yuqi Yang, Zuoxiu Xiao, Jia Huang, Xiaoyuan Wang, Yunrong Yang, Jinping Zhang, Chong Liu and Qiong Huang

317 Smart Nanoparticles for Breast Cancer Treatment Based on the Tumor Microenvironment
Xiao Luo, Qi Zhang, Hongbo Chen, Kai Hou, Ning Zeng and Yiping Wu

325 Research Progress in Exosome-Based Nanoscale Drug Carriers in Tumor Therapies
Wei Fu, Tingting Li, Hongbo Chen, Shu Zhu and Changkai Zhou

334 Nanomaterial Technology and Soft Tissue Sarcomas
Changkai Zhou, Xue Chen, Ying Huang, Qi Zhang, Shu Zhu and Wei Fu

342 Recent Advances in Nanotheranostic Agents for Tumor Microenvironment–Responsive Magnetic Resonance Imaging
Longhai Jin, Chenyi Yang, Jianqiu Wang, Jiannan Li and Nannan Xu

349 Nanoparticle-Based Combination Therapy for Melanoma
Hongbo Chen, Kai Hou, Jing Yu, Le Wang and Xue Chen

358 Cu-Hemin Nanosheets and Indocyanine Green Co-Loaded Hydrogel for Photothermal Therapy and Amplified Photodynamic Therapy
Shu Zhu, Shuntao Wang, Chunping Liu, Meng Lyu and Qinqin Huang

367 Injectable Hydrogel System for Camptothecin Initiated Nanocatalytic Tumor Therapy With High Performance
Shuntao Wang, Qi Zhang, Ning Zeng, Pengyuan Qi, Chunyu Huang and Qinqin Huang

375 Nanozyme Hydrogels for Self-Augmented Sonodynamic/Photothermal Combination Therapy
Shuntao Wang, Ning Zeng, Qi Zhang, Mingzhu Chen and Qinqin Huang

383 Research Progress of Photothermal Nanomaterials in Multimodal Tumor Therapy
Xiaolu Shi, Ye Tian, Yang Liu, Zhengrong Xiong, Shaobo Zhai, Shunli Chu and Fengxiang Gao

410 Nanotech Probes: A Revolution in Cancer Diagnosis
Qi Zhang, Kai Hou, Hongbo Chen, Ning Zeng and Yiping Wu

416 Genetic Variants in Double-Strand Break Repair Pathway Genes to Predict Platinum-Based Chemotherapy Prognosis in Patients With Lung Cancer
Jun-Yan Liu, Ting Zou, Ji-Ye Yin, Zhan Wang, Chong Liu, Han-Xue Huang, Fei-Xiang Ding, Meng-Rong Lei, Ying Wang, Min Liu, Zhao-Qian Liu, Li-Ming Tan and Juan Chen

426 Nanodrugs Manipulating Endoplasmic Reticulum Stress for Highly Effective Antitumor Therapy
Yuting Xiang, Min Liu, Yunrong Yang, Yubo Wang, Yige Qiu, Shiqi Tu, Yitian Jiang, Yayun Nan, Xiaojie Zhang and Qiong Huang

433 Current Progress in Cancer Treatment Using Nanomaterials
Ruirui Zhu, Fangyuan Zhang, Yudong Peng, Tian Xie, Yi Wang and Yin Lan

442 Recent Advance in Tumor Microenvironment-Based Stimuli-Responsive Nanoscale Drug Delivery and Imaging Platform
Fengzhi Cui, Jianhua Liu, Siwen Pang and Bo Li

frontiers | Frontiers in Oncology

TYPE Editorial
PUBLISHED 08 December 2022
DOI 10.3389/fonc.2022.1081687

Check for updates

OPEN ACCESS

EDITED AND REVIEWED BY
Olivier Feron,
Université catholique de Louvain

*CORRESPONDENCE
Kelong Ai
aikelong@csu.edu.cn

†The authors have contributed equally to this work

SPECIALTY SECTION
This article was submitted to Pharmacology of Anti-Cancer Drugs, a section of the journal Frontiers in Oncology

RECEIVED 27 October 2022
ACCEPTED 21 November 2022
PUBLISHED 08 December 2022

CITATION
Yang Y, Chen Q, Qiu Y, Wang Y, Huang Q and Ai K (2022) Editorial: Nanomaterials and multimodal tumor therapy.
Front. Oncol. 12:1081687.
doi: 10.3389/fonc.2022.1081687

COPYRIGHT
© 2022 Yang, Chen, Qiu, Wang, Huang and Ai. This is an open-access article distributed under the terms of the Creative Commons Attribution License (CC BY). The use, distribution or reproduction in other forums is permitted, provided the original author(s) and the copyright owner(s) are credited and that the original publication in this journal is cited, in accordance with accepted academic practice. No use, distribution or reproduction is permitted which does not comply with these terms.

Editorial: Nanomaterials and multimodal tumor therapy

Yongqi Yang[1,2†], Qiaohui Chen[1,2†], Yige Qiu[1,2], Yiying Wang[1,2], Qiong Huang[3,4] and Kelong Ai[1,2*]

[1]Xiangya School of Pharmaceutical Sciences, Central South University, Changsha, Hunan, China, [2]Hunan Provincial Key Laboratory of Cardiovascular Research, Xiangya School of Pharmaceutical Sciences, Central South University, Changsha, China, [3]Department of Pharmacy, Xiangya Hospital, Central South University, Changsha, Hunan, China, [4]National Clinical Research Center for Geriatric Disorders, Xiangya Hospital, Central South University, Changsha, Hunan, China

KEYWORDS

nanomaterials, multimodal therapy, drug delivery, cancer treatment, tumor microenvironment

Editorial on the Research Topic
Nanomaterials and multimodal tumor therapy

Although cancer treatment has improved dramatically over recent decades, it continues to remain among the most challenging public health issues. Comprehensive cancer management continues to evolve from use of earlier modalities such as surgery, radiotherapy (RT) and chemotherapy (CHT), to increasingly sophisticated approaches incorporating thermal therapy (e.g., photothermal therapy (PTT), magnetic-thermal therapy), dynamic therapy (e.g., photodynamic therapy (PDT), chemodynamic therapy (CDT), sonodynamic therapy (SDT) (1)) and more recently, immunotherapy (2). Such emerging therapies minimize tissue trauma, enhance targeting of malignant cells, reduce systemic side effects and improve patient prognosis.

However, monomodal therapeutic strategies that depend on a single mechanism of action are often inherently flawed. For instance, efficacy of thermal ablation by PTT is often lessened by expression of heat shock proteins produced under stress; treatment of deep-tissue tumors is thus often limited by the depth of light penetration. Oxygen-dependent dynamic therapy, which utilizes oxygen to produce reactive oxygen species (ROS) particularly toxic to cancer cells, is known to exacerbate hypoxia in the tumor microenvironment (TME) and thus exhibit poor efficacy. Similarly, tumor-driven immunosuppression is known to frequently render immunotherapy (IT) ineffective. Development of multimodal tumor therapies is thus urgently warranted.

Major advances in nanotechnology have paved the way for the exploitation of multi-functional therapeutic platforms. Elaborate nanoplatforms constructed *via* drug loading, structure optimization and surface modification, can thus be expected to exhibit efficacious anti-tumor activity.

In comparison with monomodal tumor therapy, nanomaterial-based multimodal therapy (Figure 1) possesses major advantages. First, use of multimodal therapy can exert multi-faceted anti-neoplastic effects while minimizing risks of multidrug resistance and

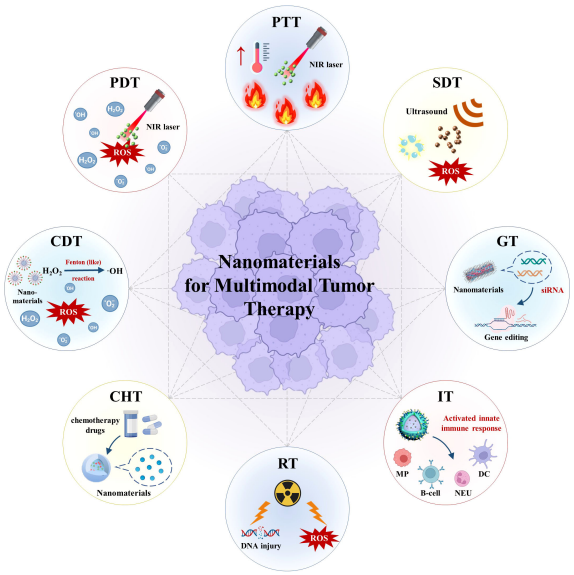


FIGURE 1
Schematic illustration of nanomaterials for multimodal tumor therapy. (PTT, photothermal therapy; PDT, photodynamic therapy; NIR, near-infrared; ROS, reactive oxygen species; CDT, chemodynamic therapy; SDT, sonodynamic therapy; CHT, chemotherapy; RT, radiotherapy; GT, gene therapy; IT, immunotherapy; MP, macrophage; NEU, neutrophil; DC , dendritic cell).

untargeted toxicity. Second, multimodal therapeutic strategies can apply precision medicine approaches to treat a variety of malignancies. Third, nanomaterial optimization can effectively achieve controlled drug delivery to tumor tissues and thus significantly improve pharmacotherapeutic outcomes.

As mentioned by Shi et al., combination strategies based on synergistically enhanced interactions among two or more treatments tend to produce super-additive "1+1>2" effects. They introduced common inorganic, organic and composite photothermal nanomaterials in the context of multimodal cancer treatment, highlighting the great potential of photothermal nanomaterial use.

In PTT/PDT dual-modal therapy, PTT achieves thermal ablation *via* near-infrared (NIR) light irradiation utilizing a specific wavelength, while PDT kills cells *via* photosensitization and induction of cytotoxic ROS generation. Zhu et al. prepared NIR-responsive injectable agarose hydrogels containing Cu-Hemin and indocyanine green (ICG). As a photothermal agent, ICG was found to effectually absorb and convert NIR light energy emitted by an 808 nm laser into thermal energy. Resultant heating and softening of the hydrogel matrix released Cu-Hemin to mediate antioxidant glutathione (GSH) consumption. Furthermore, ICG was reported to act as a photosensitizer that facilitated production of significant quantities of cytotoxic ROS in tumor cells. As such, PTT/PDT therapy utilizing Cu-Hemin and ICG effectively modulates GSH content within the TME and amplifies the anti-neoplastic effects of PDT.

Utilizing low-intensity ultrasound to generate ROS within tumor cells, SDT has been shown to effectively induce apoptosis. However, marked oxygen consumption in the setting of SDT was reported to aggravate TME hypoxia and thus limit its therapeutic use. Wang et al. designed a multifunctional hydrogel capable of co-delivering nanozyme prussian blue (PB) and sonosensitizer chlorin e6 (Ce6). After photoirradiation using an 808 nm laser, PB was found to convert light energy into heat. After heat-induced hydrogel softening, release of PB and Ce6 was achieved. Resultant catalysis of endogenous H_2O_2 to O_2 by PB alleviated hypoxia within the TME and enhanced Ce6-mediated SDT. Both *in vivo* and *in vitro* results have underscored promise in utilizing PTT/SDT synergy in cancer treatment.

Autophagy was reported to render pharmacotherapy ineffective by facilitating drug resistance among cancer cells, which assists to clear damaged and aging organelles timely and maintains their persistent abnormal proliferation. As such, clinical use of PTT-induced thermal ablation remains challenging. Zhang et al. designed a PTT/gene therapy (GT) platform to load transcription factor EB (TFEB)-siRNA by cell penetrating membrane peptides (CPP)-functionalized gold nanorods (GNRs) with good stable photothermal conversion rate. Importantly, use of CPP was found to enhance the cell permeability of GNRs. Under NIR irradiation, this platform accurately delivered siRNA targeting the autolysosomes, which could weaken the drug resistance of osteosarcoma cells and enhance PTT efficacy. In addition, TFEB silencing by this platform was reported to efficiently inhibit pulmonary metastasis by osteosarcoma cells because TFEB associated autophagy with lysosomal biogenesis and promoted cancer metastasis.

Although generation of hydroxyl radicals (·OH) *via* Fenton or Fenton-like reactions triggers oxidative damage, CDT efficiency remains limited by the delivery rate of Fenton reagents and complex TME conditions. Qin et al. attempted to synergistically enhance the Fenton reaction utilizing PTT/CDT by developing a novel NIR-mediated, tumor-specific nanoplatform based on magnetic iron oxide nanoclusters (MNCs). MNCs were found to possess excellent magnetic response characteristics and facilitate delivery of Fenton reagents to tumor sites *via* magnetophoresis. Furthermore, MNCs exhibited excellent photothermal characteristics and Fenton-like nano-catalysts activity, which accelerated Fenton reactivity and enhanced therapeutic effects *via* an increase in temperature. As such, incorporation of PTT and the Fenton reaction was found to produce superior anti-tumor effects as compared to monotherapy both *in vitro* and *in vivo*, with MNCs + NIR group almost completely inhibiting *in vivo* tumor growth. Similarly, Zeng et al. developed a chemodynamic hydrogel system based on iron-gallic acid nanoparticles (FeGA) and α-cyano-4-hydroxycinnamic acid (α-CHCA) that

also utilized PTT/CDT co-therapy. Irradiation of FeGA by an 808 nm NIR laser resulted in conversion of light energy into thermal energy, with Fe^{2+} simultaneously enhancing Fenton reactivity to damage tumor cells. Furthermore, diffusion of α-CHCA into the TME was found to increase intracellular acidity and contribute to ·OH production by CDT.

Profound nonspecific side effects of CHT significantly affect patient quality of life and limit patient compliance to treatment. As such, nanomaterials-based combination therapy utilizing PTT and CHT has recently emerged as a focus of study. Zhao et al. designed a biomimetic nanosystem based on a zeolitic imidazolate framework 8 (ZIF8) that employed particles loaded with doxorubicin hydrochloride (DOX·HCl) and photothermal agent copper sulfide (CuS), and that were coated with red cell membrane and catalase (CAT) components. With its biodegradation dependent on pH, ZIF8 rapidly degraded in the acidic TME and facilitated targeted co-delivery of both CHT and PTT agents. Furthermore, catalysis of H_2O_2 decomposition functioned to provide sufficient O_2 for PTT activity, thus enhancing DOX delivery and cytotoxicity. Combined utilization of PTT and RT was similarly reported to optimize treatment while lowering required radiation doses and minimizing side effects. Hydrogel-encapsulated $SnFe_2O_4$ (SFO) nanozyme was reported by Zeng et al. to exploit GSH oxidase (GSH-OXD) and CAT activity in addition to PTT effects, thus reducing GSH levels in tumor tissues and effectively catalyzing formation of large quantities of O_2. Thus, the anti-cancer properties of RT were enhanced *via* alleviation of hypoxia within the TME and minimization of resistance. *In vivo* anti-tumor findings revealed almost complete inhibition of tumor growth in the PTT/RT group. Moreover, Huang et al. highlighted the advantages of Bi_2X_3-based nanomaterials as photothermal agents in the context of PTT enhancement that improves ROS production in RT and thus broadens the clinical application of Bi_2X_3-based nanomaterials in RT use.

In addition to PTT-based strategies, other bimodal approaches also optimize multi-faceted therapeutic outcomes. Incorporation of CDT and RT by Zhang et al. entailed fixation of glucose oxidase (GOD) and Hemin on the surface of biodegradable mesoporous silica nanospheres (MSN). Oxidation of glucose by GOD generated significant quantities of H_2O_2; subsequent conversion of H_2O_2 into ROS by Hemin markedly enhanced RT efficacy and produced an *in-vivo* tumor suppression rate as high as 91.5%. Chen et al. designed a CHT/RT platform employing platelet membrane-coated gold nanocages (AuNs) loaded with cisplatin capable of directly destroying tumor cell DNA and enhancing RT efficacy. This platform almost completely inhibited increases in tumor volume *in vivo*. Yang et al. encapsulated camptothecin (CPT) and the CO prodrug MnCO in ZIF8 nanocarriers that decomposed in the acidic TME, releasing CPT to destroy tumor mass and produce significant quantities of H_2O_2. Subsequently, MnCO triggered a Fenton-like reaction with H_2O_2 to generate CO; this localized increase in CO levels inhibited mitochondrial respiration and induced tumor cell apoptosis. Such enhancement of CHT in the setting of CDT was reported to suppress approximately 90% of tumor cells *in vitro* and almost entirely inhibit tumor volume growth in mice with CT26 tumors.

Importantly, multimodality was reported to exhibit even greater superiority over monomodal and bimodal approaches. Feng et al. constructed an intelligent PTT/CHT/IT nanoplatform using Mn^{III}PC@DTX@poly-acylcosugar acid (PLGA)@Mn^{2+}@hyaluronic acid (HA) (MDPMH) for treatment of non-small cell lung cancer. Mn-modified phthalocyanine derivative (Mn^{III}PC) was employed as a photothermal agent to facilitate PTT while docetaxel (DTX) was delivered in a targeted fashion to the tumor site to minimize non-targeted toxicity to normal tissues. Endocytosis of Mn^{2+} by macrophages, dendritic cells and lymphocytes resulted in activation of the innate immune response. *In vitro* findings confirmed this platform to be significantly more effective in inducing tumor cell apoptosis as compared to monomodal or bimodal strategies.

Use of multimodal strategies in concert with PTT/CHT/CDT overcomes a number of practical limitations such as penetration depth in PTT and decreases drug resistance. Wang et al. studied use of encapsulated CPT and pyrite (FeS_2) with injectable hydrogels. A photothermal agent, FeS_2 simultaneously functioned as a peroxidase (POD), mediated PTT and catalyzed production of ·OH within the TME *via* Fenton reactivity. The GSH-OXD activity of FeS_2 resulted in consumption of excess intracellular GSH and further amplified oxidative stress. Moreover, this hydrogel system allowed for controlled release of nanomaterials, enhancing the selective chemotherapeutic effect of CPT, maintaining within the therapeutic window, and ultimately showing favorable tumor-specific cytotoxicity. Of note, PTT/CHT/CDT treatment group was reported to be most efficacious in mice.

In summary, incorporation of existing nanomaterial-based drug delivery platforms to rationally design multimodal cancer treatment strategies holds great promise for future clinical applications. Their cooperations are typically complementary between two or more therapies, including, but not limited to, examples within this research topic. But it is regrettable that research progress in this area has remained slow and most of the aforementioned therapies remain at the laboratory level. As such, further systematic study of potential contradictions and side effects in the context of multimodal treatment strategies is urgently warranted.

The emerging field of nanomedicine offers increased clinical precision in the management of malignancies. In order to successfully translate laboratory findings into clinical practice, thorough study of nanomaterial properties is necessary to characterize compound stability, excretion rates, safety profiles and metabolism, as well as identify possible physiological effects

of short and long-term exposure. Adoption of diagnostic and treatment gold standards, preclinical and clinical evaluation protocols, as well as large-scale manufacturing specifications for nanomaterial drugs or vectors, is similarly mandated. Finally, although many nanomaterials offer remarkable efficacy with relatively few side effects, much interdisciplinary research remains to be performed for the purposes of optimizing their clinical value and minimizing costs of clinical applications. Fortunately, including the authors of this topic, a multitude of other talented scientists are working as hard as ever to accomplish the aforementioned objectives and improve patient outcomes.

Author contributions

All authors listed have made a substantial, direct, and intellectual contribution to the work.

Funding

This work was supported by the National Natural Science Foundation of China (No. 81974508, 21974134), the Hunan Science Fund for Distinguished Young Scholar of China (No. 2021JJ10067), Innovation-Driven Project of Central South University (No. 202045005), Hunan Provincial Natural Science Foundation of China (No. 2021JJ31066), Central South University Research Programme of Advanced Interdisciplinary Studies (2023QYJC017).

Conflict of interest

The authors declare that the research was conducted in the absence of any commercial or financial relationships that could be construed as a potential conflict of interest.

Publisher's note

All claims expressed in this article are solely those of the authors and do not necessarily represent those of their affiliated organizations, or those of the publisher, the editors and the reviewers. Any product that may be evaluated in this article, or claim that may be made by its manufacturer, is not guaranteed or endorsed by the publisher.

References

1. Xiao Z, Chen Q, Yang Y, Tu S, Wang B, Qiu Y, et al. State of the Art Advancements in Sonodynamic Therapy (Sdt): Metal-Organic Frameworks for Sdt. *Chemical Engineering Journal* (2022) 449:137889. doi: 10.1016/j.cej.2022.137889.

2. Yang Y, Zhao T, Chen Q, Li Y, Xiao Z, Xiang Y, et al. Nanomedicine Strategies for Heating "Cold" Ovarian Cancer (Oc): Next Evolution in Immunotherapy of Oc. *Advanced science (Weinheim, Baden-Wurttemberg, Germany)* (2022) 9(28):e2202797. doi: 10.1002/advs.202202797.

frontiers in Oncology

REVIEW
published: 26 August 2021
doi: 10.3389/fonc.2021.743189

Exosomes as Smart Nanoplatforms for Diagnosis and Therapy of Cancer

*Yuying Zhao[1,2], Piaoxue Liu[1], Hanxu Tan[3], Xiaojia Chen[4], Qi Wang[1] and Tongkai Chen[1]**

[1] Science and Technology Innovation Center, Guangzhou University of Chinese Medicine, Guangzhou, China, [2] Department of Mammary Disease, Guangdong Provincial Hospital of Chinese Medicine, The Second Clinical Collage of Guangzhou University of Chinese Medicine, Guangzhou, China, [3] School of Fundamental Medical Science, Guangzhou University of Chinese Medicine, Guangzhou, China, [4] State Key Laboratory of Quality Research in Chinese Medicine, Institute of Chinese Medical Sciences, University of Macau, Macau, China

Exosomes are composed of a lipid bilayer membrane, containing proteins, nucleic acids, DNA, RNA, etc., derived from donor cells. They have a size range of approximately 30-150 nm. The intrinsic characteristics of exosomes, including efficient cellular uptake, low immunogenicity, low toxicity, intrinsic ability to traverse biological barriers, and inherent targeting ability, facilitate their application to the drug delivery system. Here, we review the generation, uptake, separation, and purification methods of exosomes, focusing on their application as carriers in tumor diagnosis and treatment, especially in brain tumors, as well as the patent applications of exosomes in recent years.

Keywords: exosomes, biomarker, cancer diagnosis, cancer therapy, brain cancer

OPEN ACCESS

Edited by:
Kelong Ai,
Central South University, China

Reviewed by:
Qiong Huang,
Central South University, China
Welch Jack,
Nanjing University of Chinese Medicine, China

***Correspondence:**
Tongkai Chen
chentongkai@gzucm.edu.cn

Specialty section:
This article was submitted to Pharmacology of Anti-Cancer Drugs, a section of the journal Frontiers in Oncology

Received: *17 July 2021*
Accepted: *09 August 2021*
Published: *26 August 2021*

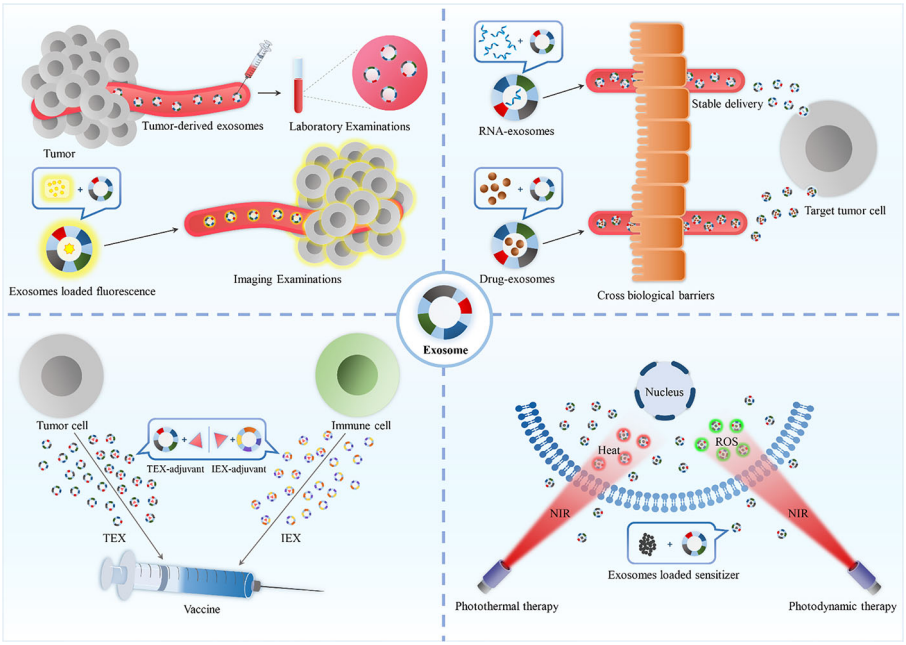
Citation:
Zhao Y, Liu P, Tan H, Chen X, Wang Q and Chen T (2021) Exosomes as Smart Nanoplatforms for Diagnosis and Therapy of Cancer. Front. Oncol. 11:743189. doi: 10.3389/fonc.2021.743189

INTRODUCTION

Most cells secrete various types of membrane vesicles, called extracellular vehicles (EVs) (1). EVs are classified into (1) ectosomes and (2) exosomes based on their size, biogenesis, and biophysical properties (2). Ectosomes are ubiquitous vesicles, approximately 100 to 500 mm in diameter, that are directly released from the plasma membrane (PM).

In the early 1980s, Pan and Johnstone first identified exosomes while studying the process of maturation of reticulocytes into erythrocytes (3). Exosomes are formed by the exocytosis of intraluminal vesicles (ILVs)-containing multivesicular bodies (MVBs) that are formed by the sequential invagination of the PM. The released exosomes have an approximate diameter of 40 to 160 nm (average ~ 100 nm) (4).

Exosomes possess a unique ability to facilitate complex biological responses, which promotes their use as diagnostic and therapeutic tools to treat various diseases, including neurodegenerative, cardiovascular, and cancer (5). The heterogeneity of exosomes is based on the different combinations of various characteristics, including size, original cells (source), content (cargo molecules), and effect on the functioning of the recipient cells (6). Recent studies are actively exploring exosomes as therapeutic agents to deliver drug payloads based on their ability to deliver various cargo molecules, including specific proteins, metabolites, lipids, and nucleic acids (7). Unlike liposomes, injected exosomes can effectively enter other cells and provide functional cargo molecules without getting attacked by the immune system and inducing toxicity due to its biogenetic derivation (8, 9).



GRAPHICAL ABSTRACT |

Compared with other nanomaterials such as polymer-based nanomaterials and inorganic nanomaterials, they both have excellent pharmacokinetic properties, bioavailability (10), biodistribution, and can decrease the side effects of free drugs (11, 12). As a novel drug carrier, exosomes possess several unique structural and physicochemical properties, including low toxicity and immunogenicity, efficient cellular entry, intrinsic ability to cross biological barriers, increased circulatory stability, and active targeting potential (9). Interestingly, cancer cells are known to secrete excessive amounts of exosomes compared to normal cells and support tumor progression by promoting angiogenesis, modulating the immune system, and remodeling the surrounding parenchymal tissue (13, 14). Currently, there are several clinical trials with varying objectives, investigating the role of exosomes as tumor markers. This review summarizes the recent research on exosome as a carrier in tumor diagnosis and treatment, especially brain tumors, to facilitate the application of exosomes in the development of tumor therapy.

BACKGROUND OF EXOSOMES

Different Periods of Exosomes

The Biogenesis of Exosomes

Exosomes are derived from the early-sorting endosomes (ESEs), late-classified endosomes (LSEs), and ultimately ILVs-containing intracellular MVBs *via* the endosomal pathway (**Figure 1**). ESEs are cup-shaped structures formed by the initial invagination of the PM, which includes cell-surface proteins and extracellular soluble proteins. In some cases, the newly formed ESE might merge with the preexisting ESE. Consequently, ESEs mature into LSEs, leading to the formation of ILVs-filled MVBs *via* the second invagination of the PM. Ultimately, the fusion of MVBs with the PM results in the secretion of ILVs *via* exocytosis (15).

There are two major pathways involved in the generations of exosomes: Endosomal Sorting Complex Required for Transport (ESCRT)-dependent pathway and ESCRT-independent pathway (16). The ESCRT mechanism involves four major complexes, ESCRT-0, ESCRT-I, ESCRT-II, and ESCRT-III, comprising several subunits which play distinct roles. The ESCRT-0 complex identifies and separates ubiquitinated transmembrane proteins in the endosomal membrane; ESCRT- I, along with ESCRT-II, initiate the local budding of the endosomal membrane, followed by ESCRT-III-mediated vesicle segregation (17). The ESCRT-independent mechanism of exosome biogenesis requires the generation of ceramide by type 2-neutral sphingomyelinase (18). Additionally, ESCRT-independent endosomal sorting is regulated by proteins from the tetraspanin family and exosome-rich CD63 (19). Thus, it seems that both mechanisms might operate synergistically for the biogenesis of exosomes. Moreover, the cell type, cellular homeostasis, and cargo molecules could be vital for regulating the secretion of exosomes (20).

The Release (Secretion) of Exosomes

Exosomes are secreted as ILVs post the fusion of MVBs with the PM. Alternatively, MVBs are directed to lysosomes for degradation (18). The mechanism of regulation of the balance between intracellular degradation or the release of exosomes is

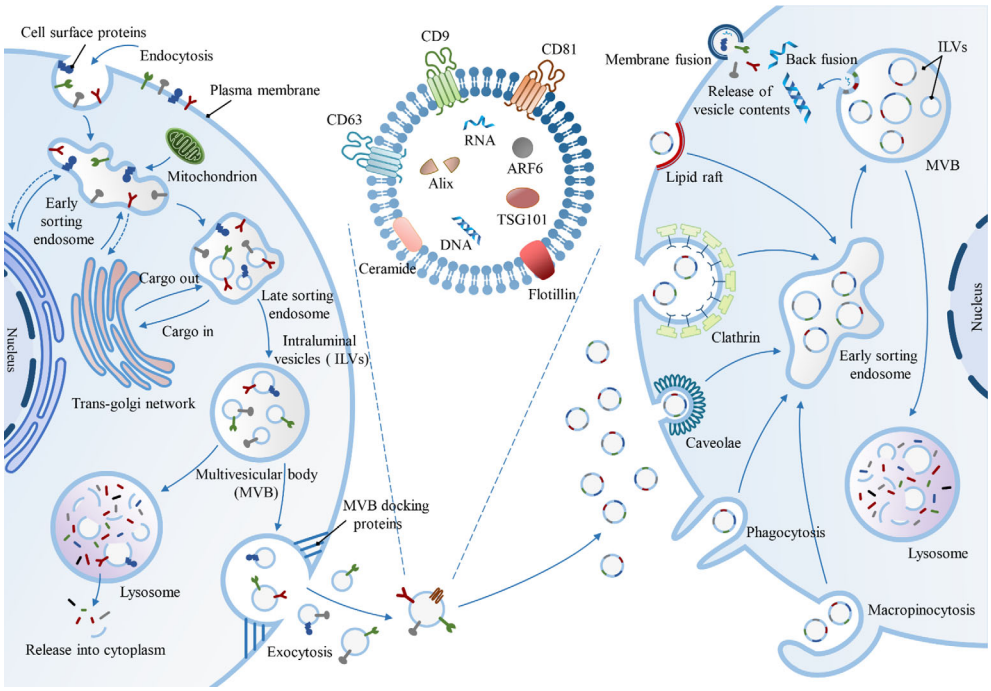


FIGURE 1 | Biogenesis, biomarkers and uptake of exosomes.

unclear. Recent studies have provided insights into a possible mechanism, where the ISGylation of MVB proteins facilitates their fusion with lysosomes, directing MVBs toward the degradation pathway and away from the secretory pathway (21); intracellular transport of MVB *via* microtubules to the PM (22), the formation of docking sites in the PM (23), or recruitment of Soluble NSF Attachment Protein Receptor (SNARE) proteins and synaptotagmin family members that facilitate their fusion with either lysosomes or the PM (24). Molecular regulators associated with the release of exosomes include several molecules involved in MVB docking, such as RAB27A and RAB27B32 and their respective effectors, synaptotagmin-like protein 4 and exophilin 5 (20). Furthermore, studies have shown that autophagosomes fuse with MVBs and direct them to lysosomes to prevent exosome secretion (20). Similarly, previous studies have been shown that the prion protein (PrP) inhibits the formation of autophagosomes by interacting with caveolin to promote exosome secretion (25).

The Uptake of Exosomes

There are several pathways involved in the uptake of exosomes, including receptor-mediated endocytosis, clathrin-mediated endocytosis, lipid raft-mediated endocytosis, phagocytosis, caveolin-mediated endocytosis, micropinocytosis (26), and membrane fusion (27), which increase the complexity of exosomes in intercellular communication (**Figure 1**). For instance, mutated KRAS expression generates oncogenic signals that promote the uptake of exosomes in human pancreatic cancer cells through macrocytosis (28), clathrin-dependent endocytosis mediates exosome uptake in neurosecretory PC12 cells (derived from rat adrenal medullary tumor) (29).

A recent study identified a different exosome internalization pathway involving filopodia-mediated recruitment, followed by endocytosis by a process resembling virus entry (30). However, variable conditions impact exosome uptake and subsequent biological activity, such as the preferential uptake of small exosomes by cells of different sizes, exosome uptake is inhibited at low temperatures (31). Some proteins are known to facilitate exosome uptake, such as the tetraspanin membrane proteins CD9 and CD81 and intercellular adhesion molecule (ICAM)-1 (32). Additionally, proton pump inhibition or cellular pH changes in melanoma cells are known to limit exosome uptake (33).

Content and Function of Exosomes

Previous studies on the composition of exosomes have revealed the presence of various cargo molecules, including membrane proteins, cytosolic and nuclear proteins, extracellular matrix proteins, metabolites, and nucleic acids, such as mRNA, noncoding RNA species, and DNA (34, 35). The composition can vary widely based on cellular origin, heterogeneity in size, cellular microenvironment, and inherent biology of cells (4).

The diverse composition of exosomes results in the complexity of their functions. Additionally, the effects of exosomes on receptor cells vary based on the expression of receptors on the cell surface. Generally, exosomes are involved in eliminating excess metabolites to maintain cellular homeostasis (36) and intercellular

communication, which has been associated with numerous physiological and pathological functions (37). In cancer cells, exosomes are known to support tumor progression by promoting angiogenesis, regulating the immune system, and remodeling the surrounding parenchymal tissue (38). In breast milk, breast milk-derived exosomes contain miRNAs with immunomodulatory functions to regulate immune tolerance and promote postnatal health and growth (39).

Recent studies on the central nervous system have indicated that exosomes secreted by oligodendrocytes enhance neuronal viability as well as an increase in the neuron firing rate (40). In a syngeneic mouse model of melanoma, melanoma-derived exosomes induced lung vascular leakiness and recruited bone marrow-derived macrophages to metastatic sites. Moreover, chemotherapy and radiation therapy also impact the composition and functioning of exosomes with potential implications on therapy outcomes (41).

Separation and Purification of Exosomes

Current studies are involved in the exploration of exosomes as a new method for the cellular delivery of drug payload. There are several techniques being used to separate exosomes from EVs (**Table 1**); however, there are still many challenges regarding the efficient and economic production, separation, and purification of exosomes in adequate quantities, which prevent their clinical use (9).

Therefore, it is imperative to promote a standardized method that is practical, efficient, and feasible to isolate and purify exosomes from the cell culture medium.

APPLYING OF EXOSOME TO IMPROVE CANCER DIAGNOSIS

Timely detection is vital for the effective treatment of cancer. Currently, clinical diagnosis of cancer includes laboratory examinations, imaging studies, and tissue biopsy which is regarded as the gold standard. However, since biopsies are invasive, the first two methodologies are more widely used. Unfortunately, laboratory examination and imaging analysis have low sensitivity and have an insignificant role in the diagnosis of early-stage cancer. For several years now, scientists have discussed the application of exosomes in clinical diagnosis, especially in improving the sensitivity of laboratory and imaging studies. Moreover, an early cancer diagnosis is directly related to improved survival rates.

Application in Laboratory Examinations

Exosomes can transport DNA, RNA, and proteins into biological fluids to mediate intercellular communication (4). Tumor cell-derived exosomes contain oncogenic information that facilitates cancer growth and metastasis (51). Thus, it was recently predicted that exosomes could act as tumor biomarkers (52, 53). A study showed that TAG72-rich and CA125-rich exosomes could act as biomarkers of colorectal cancer (54). A significant increase in the serum/plasma levels of miR-547-3p was observed in patients with osteosarcoma (55) or hepatocellular carcinoma (56) and considered as a diagnostic biomarker, and miR-547-3p levels were significantly reduced post-radiotherapy in patients with glioma (57). Exosomes can be detected in the early stages of cancer, suggesting that they might be vital candidates for laboratory examinations.

Tumor-derived exosomes possess tumor markers, and tumors can be identified based on the levels of tumor-derived exosomes in bodily fluids (**Figure 2A**) (60). However, during the early stages of development, tumors secrete few exosomes, which are difficult to detect, and thus, detachable microfluidic devices were invented to detect early-stage tumors using electrochemical aptamer sensors (DeMEA). This equipment can improve the sensitivity of the detection of tumor-secreted exosomes (61). It provides the possibility of early detection of cancer. When a tumor progresses to a terminal stage, it is critical to determine its level of metastasis to develop the treatment strategy. Thus, an ingenious microfluidic device was designed to detect exosomes based on the specific binding of lectins to unique glycans on the surface of cancer cell-derived exosomes, which could distinguish between metastatic and non-metastatic pancreatic cancer while

TABLE 1 | Isolation technique of exosomes.

Isolation technique	Isolation methods	Advantages	Limitations	Ref.
Ultracentrifugation	Differential centrifugal forces	Low equipment cost, fast procedure and high yield	Time-consuming, costly instrumentation; exosomes may be damaged by repeated centrifugation	(42, 43)
Sucrose-gradient centrifugation	Ultracentrifugation combined with sucrose density gradients	Yields highly pure exosomes.	It is difficult to achieve pure vesicle purification through density-based procedures, which might provide enrichment at best.	(44)
Size-exclusion chromatography	Separation based on gel filtration	The biological activity and integrity of the isolated exosomes are retained.	Since it is a time-intensive process, the processing of several samples is difficult.	(45)
Immunoaffinity capture	Positive selection: magnetic bead-bound antibodies bind to targeted exosomes. Negative selection: magnetic bead-bound antibodies bind and isolate irrelevant exosomes.	Highly efficient, can be used for quantification and qualitative analysis of the isolated exosomes.	Expensive; the strong antibody-antigen binding makes the dissociation of bound exosomes difficult for further analyses.	(46)
Polymer-based precipitation	Polymers, such as PEG, considerably reduce the solubility of exosomes, which can then be isolated *via* low-speed centrifugation.	Easy operation, rapid processing, does not require specialized equipment.	Expensive; exosome isolation may contain contaminating proteins.	(47, 48)
Microfluidics-based isolation	This microscale technique uses differences in size, density, and immunoaffinity to isolate exosomes.	Rapid, great precision, and sensitive detection	Low yield	(49, 50)

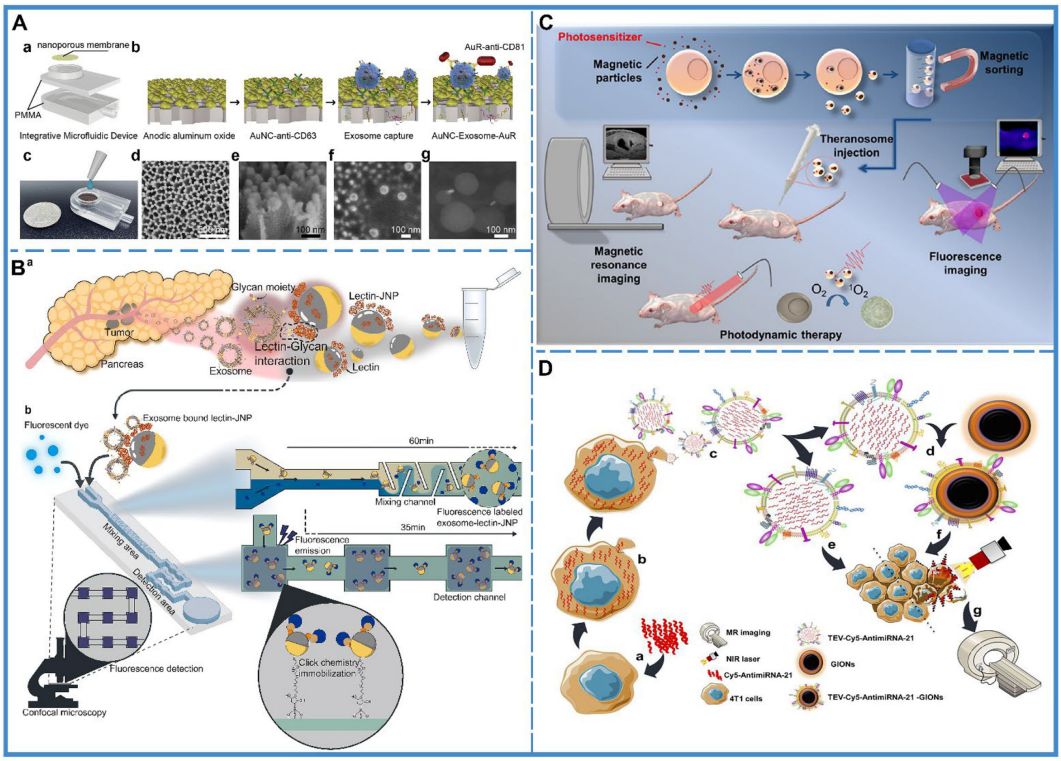


FIGURE 2 | Cancer diagnosis. **(A)** An integrative microfluidic device (IMD) for the isolation and detection of exosomes. (a) The model design of the IMD. (b) The *in-situ* detection of exosomes. (c) An image of the IMD. (d) A scanning electron micrograph of the Au nanoparticles deposited on a 50-mm-thick AAO membrane; side view presented in (e). (f) A scanning electron micrograph of the captured exosomes on the AAO membrane, and (g) A scanning electron micrograph of the AuNC-Exosome-AuR complex. Reproduced with permission from Ref (60). Copyright 2020 Elsevier. **(B)** Schematic illustration of the capturing of pancreatic cancer exosomes *via* Exo-chip system. (a) Isolation of the exosomes from the patient blood specimens/pancreatic cancer cell line culture medium. (b) After addition to the Exo-chip with Janus nanoparticles (JNPs), the sample was visualized *via* fluorescence imaging and analysis. Lectin-conjugated JNPs mediate the interaction between exosomes and the chip substrate *via* click reactions (maleimide-functionalized JNPs and thiol-functionalized substrate) that bind the substrate in a laminar flow system. Reproduced with permission from ref (58). Copyright 2020 Elsevier. **(C)** Schematic illustration of the synthesis of tumor derived extracellular vehicles loaded Cy5 and antimiRNA-21 (TEVs-Cy5-antimiRNA-21) and TEVs-Cy5-antimiRNA-21-coated gold iron oxide nanotheranostics (GIONs). (a) Cy5-antimiRNA-21 was transfected into the donor 4T1 cells, (b) Cy5-antimiRNA-21-packed donor 4T1 cells, (c) *In situ* generation of 4T1 tumor cell-derived Cy5-antimiRNA-21-loaded extracellular vesicles, (d) Top-down fabrication synthesis of TEVs-Cy5-antimiRNA-21-coated GIONs, (e) TEVs-Cy5-antimiRNA-21-mediated cancer therapy, (f) TEVs-Cy5-antimiRNA-21-GIONs-mediated multimodal imaging and photothermal cancer therapy, (g) MRI of 4T1 cancer cells delivered by TEVs-Cy5-antimiRNA-21-GIONs. Reproduced with permission from ref (59). Copyright 2013 American Chemical Society. **(D)** Schematic representation of theranosome generation from drug-loaded magnetic precursor cells along with their application in photodynamic therapy and dual-mode MRI and fluorescence imaging. Reproduced with permission from ref (66). Copyright 2018 American Chemical Society.

improving the accuracy of pancreatic cancer diagnosis (**Figure 2B**) (58).

Application in Imaging Examinations

Compared with laboratory examinations, imaging examinations are more intuitive and visual (62). Exosomes are considered to be natural delivery vesicles that can slow down the endocytosis of macrophages and extend blood circulation time to avoid clearance *via* the kidney, liver, and the immune system (28), implying that their biocompatibility and transcellular permeability present them as probable vehicles for theranostic applications. Currently, for imaging analysis, the cargo molecules that can be loaded by the exosomes include inorganic molecules (63), magnetic materials (**Figure 2C**) (59), and fluorescent molecules (64). Besides, there is two main preparation method of exosome theranostics: *in-vitro* biosynthesis and in-situ biosynthesis.

In-vitro biosynthesis is a more controllable technique. In a study, chlorin e6 (Ce6) molecules were loaded on the surface of inorganic Au nanoparticles (Au@Ce6), followed by embedding the Au@Ce6 into exosomes, which were collected and purified from the urine of gastric cancer patients. The results showed that the nanovehicles could successfully improve the cellular uptake of cancer cells and reduce the endocytosis of macrophages, which further enhanced the accumulation of targeted tumor sites for superior real-time fluorescence imaging (63). Another study used superparamagnetic iron oxide (SPIO)-loaded exosomes for magnetic particle imaging (MPI), which enabled the acquisition of *in vivo* images with greater contrast, sensitivity,

and quantitation than magnetic resonance imaging (MRI) (65). Apart from this, gold-iron oxide nanoparticles-loaded exosomes also demonstrated excellent T2 contrast in MRI (**Figure 2D**) (66).

In-situ biosynthesis is a more sensitive technique where the raw materials of the bioprobe are injected into the organism, followed by their self-assembly in the tumor microenvironment (TME). After the bioprobe assembly is complete, it gets embedded into the exosome as metabolic trash and excreted outside the cell. Thus, it can be found in the early stages of cancer. A study utilized TME for bioimaging with in-situ biosynthesized nanoscale gold and iron probes and subsequently disseminated Au-Fe nanoclusters from cargo exosomes within the circulation, which could be subsequently used as fluorescence, Computed Tomography (CT), and MRI imaging tools for cancer diagnosis (67).

Application in Brain Cancer Diagnosis

In clinical studies, the application of biopsy to brain cancers is limited due to the location of the nidus. Usually, the diagnosis is confirmed by imaging analysis and laboratory examination, and biopsy is performed only when there are clinical symptoms; however, by then, the cancer has developed to middle or advanced stages. Therefore, it is necessary to improve the sensitivity of imaging techniques and laboratory examination and strive for early diagnosis. The use of exosomes in the diagnosis may solve this problem. In the laboratory diagnosis, once the TME is established, exosomes containing oncogenic information are released into the peripheral blood, which can be detected by laboratory tests (57). As for the image-based diagnosis, encapsulating particles with imaging capabilities in exosomes can be absorbed by the brain cancer cells due to their capability to cross the blood-brain barrier (BBB) (65, 68) or be transported from the nidus to the peripheral blood (67), which can effectively improve the imaging signals of CT or MRI and enhance the sensitivity of imaging diagnosis. Based on these conclusions, the combination of improved laboratory tests and imaging techniques by exosome can facilitate early diagnosis of brain cancers, reduce the rate of missed diagnosis, and achieve early treatment of brain cancers.

In summary, exosomes could improve the sensitivity of laboratory tests and imaging to detect tumors. In laboratory examinations, the presence of exosomes with tumor markers in bodily fluids could be used to detect tumors. Further research invented numerous devices to improve the sensitivity of detecting early tumors as well as for distinguishing whether tumors were metastatic by analyzing exosomes, with improved clinical efficacy. In imaging examinations, exosomes derived from tumor cells were found to enhance the signal at the tumor site by loading inorganic molecules, magnetic materials or fluorescent molecules. These involved two methods: (1) *in vitro* biosynthesis where fluorescent molecules were loaded into the exosomes *in vitro* and then transported to tumors through the homing ability of exosomes; (2) in-situ biosynthesis where the raw materials of the bioprobe were injected into the organisms and then self-assembled in the tumor microenvironment (TME).

USE OF EXOSOMES TO IMPROVE RNAI-BASED CANCER THERAPY

Until now, RNAs interference (RNAi)-based therapy, such as small interfering RNAs (siRNAs) and micro RNAs (miRNAs) (**Table 2**), have been demonstrated to be effective for cancer treatment (85, 86). However, rapid hydrolysis, poor bioavailability (87), and the inability to cross the biological barriers have restricted the development of RNAi-based therapies (88). Thus, an effective delivery system is needed that protects RNAs from nuclease degradation and releases them into the cytoplasm of targeted cells without adverse effects (89). Currently, there exist three classes of delivery vehicles: viruses, polycationic polyethyleneimine (PEI)-based nanoparticles, and liposomes. With the delivery of viruses, RNAs can enter host cells and survive in host cells for a long time *via* genome integration. But there are some serious drawbacks to using viruses. They get cleared by preexisting antibodies in the bloodstream and active complement or coagulation factors in the circulating blood; furthermore, gamma retroviral vectors were used for clinical gene therapy in ten patients with X-linked SCID (SCID-X1), and four of them developed T-cell leukemia after treatment. Viruses may also cause malignancies (90). PEI nanoparticles or liposomes, which are more safe compared with viruses, can protect RNAs from degradation in the bloodstream and facilitate cellular uptake, but they may induce cellular stress, inflammatory response, and apoptosis (91). On the contrary, exosomes have high target specificity, high permeability, and low toxicity. Meanwhile, they also provide serum stability (**Figure 3A**) (69). and facilitate cellular uptake by cancer cells, without immune response or inflammatory reaction (4). Given the limitations of these three vehicles, exosomes, a natural intercellular communication system, are more suitable vehicles over existing RNAs delivery vehicles (93, 94).

Application in Stable Delivery

As mentioned above, the use of RNAs in oncology has been limited by their easy degradation by nucleases, which reduces their stability in the blood (95). Furthermore, the pore size of the glomerular basement membrane (GBM) is approximately 6-10 nm (96), while the length of naked RNA is only 7 nm; thus, it can be filtered through GBM and pass into the urine quickly (97). Currently, scientists assume that this defect in RNAs could be remedied by using the exosome. Several experiments have been designed to verify this hypothesis. For example, one study found a significant increase in the storage stability of RNAs after loading with exosomes compared with only PEIs-modified siRNAs (92). Plasma-derived exosomes also protected miRNAs from nuclease degradation and successfully promoted apoptosis of the HepG2 hepatocellular carcinoma cells (77). Again, siRNAs loaded with milk-derived exosomes are stable and resist degradation; the combination of exosomes and siRNAs eventually silence the expression of target genes by approximately 2-10 folds (**Figure 3A**) (69). Thus, exosomes, with no inherent toxicity and intrinsic biocompatibility, can

TABLE 2 | Exosome-mediated siRNA delivery.

Tumor	Source of exosomes	Cargos	Loading methods	Drug loading (%)	Encapsulation efficiency (%)	Zeta potential (mV)	Particle size (nm)	Improvements	Ref
Lung cancer	Bovine milk	siRNA	Electroporation and chemical transfection (Exo-Fect) methods.	30	/	/	/	More stale, higher drug delivery efficiency, higher cellular uptake.	(69)
Lung cancer	tLyp-1-lamp2b transfected HEK293T cell	siRNA	Electroporation	/	61.53 ± 0.32	/	~100	Desirable targeting efficacy.	(70)
Bladder cancer	Bone marrow derived mesenchymal stem cells	microRNA-9-3p	/	/	/	/	~120 nm	Desirable inhibition of tumor growth and metastasis.	(71)
Human Prostate Cancer	Human bone marrow-derived MSC (BMSC)	microRNA-143	/	/	/	/	132.5 ± 37.4	Desirable targeting efficacy.	(72)
Pancreatic ductal adenocarcinoma	Human umbilical cord mesenchymal stromal cells	miR-145-5p	Chemical transfection (Exo-Fect)	/	/	/	119	Higher delivery efficiency.	(73)
Gastric cancer	HEK293T cells	miR-374a-5p inhibitor	Chemical transfection (Exo-Fect)	/	/	/	/	More stale, higher drug delivery efficiency, lower toxicity and immunogenicity.	(74)
Oral squamous cell carcinoma	T cells	miR-138	Chemical transfection (Exo-Fect)	/	/	/	50 - 200	Desirable targeting efficacy, lower toxicity.	(75)
Malignant mesothelioma	HUVECs	MiR-126	Chemical transfection (Exo-Fect)	/	/	/	/	Desirable therapeutic efficacy to cancer stroma.	(76)
Hepatocellular carcinoma	Plasma	miR-31 and miR-451a	Middle electroporation	/	31.63 ± 5.94	/	/	Less enzymatic degradation of miRNA, desirable targeting efficacy.	(77)
Pancreatic Cancer	Bone Marrow Mesenchymal Stem Cell	MicroRNA-126-3p	/	/	/	/	100	Desirable targeting efficacy.	(78)
Glioblastoma	293T cell	microRNA-21	Electroporation	1.68 ± 0.23	/	-10 and -3	15 - 50	Higher BBB transportation and delivery efficiency of AMO	(79)
Colorectal cancer	THLG-293T or LG-293T cells	miR-21 inhibitor	Electroporation	5-FU: 3.1 miR-21i: 0.5	/	– 11 ± 2.7	110 ± 11.3	Higher cellular uptake, desirable targeting efficacy.	(80)
Breast Cancer	Mesenchymal Stem Cells	LNA-antimiR-142-3p	Electroporation	/	57	/	103	Desirable ability to penetrate the cancer stem cells	(81)
Myeloid leukemia	Human bone marrow mesenchymal stem cells	miR-222-3p	chemical transfection (Exo-Fect)	/	/	/	~200	Desirable targeting efficacy.	(82)
Breast cancer	Breast cancer cells	siRNA (siS100A4)	incubation and extrusion method	/	86.70 ± 1.22	-33.61 ± 0.81	173.63 ± 0.77	Less degradation in blood circulation, desirable inhibition of tumor growth and metastasis.	(83)
Digestive system tumors	Milk	bcl-2 siRNA	Ultrasound method	66.9 ± 4.5	/	/	60 - 90	Higher cell membrane crossing efficacy and less degradation in serum.	(84)

"/" represents that information was not mentioned in the original article.

protect RNAs from nuclease degradation and renal filtration and help maintain the stability of RNAs in blood.

Application in Crossing Biological Barriers

However, only maintaining stability is not enough. Since naked RNAs have a poor ability of cell penetration, it is hard for RNAs to enter into the cell (98). Even after entering the cell, they run the risk of being hydrolyzed by lysosomes (89). Consequently, the success of therapeutic RNAs depends on efficient cell internalization and timely endosomal escape. It is well known that exosomes have the innate ability to cross biological barriers; thus, engineered exosomes could efficiently facilitate cellular uptake of miRNAs and significantly reduce cancer proliferation (80). Professor Lin has proved that milk-derived exosomes can transport across the gastrointestinal barrier (99), and small interfering RAN (bcl-2 siRNA) encapsulated by milk-derived exosomes can effectively pass through cell membranes and inhibit the growth of cancer cells (84). Additionally, a study demonstrated

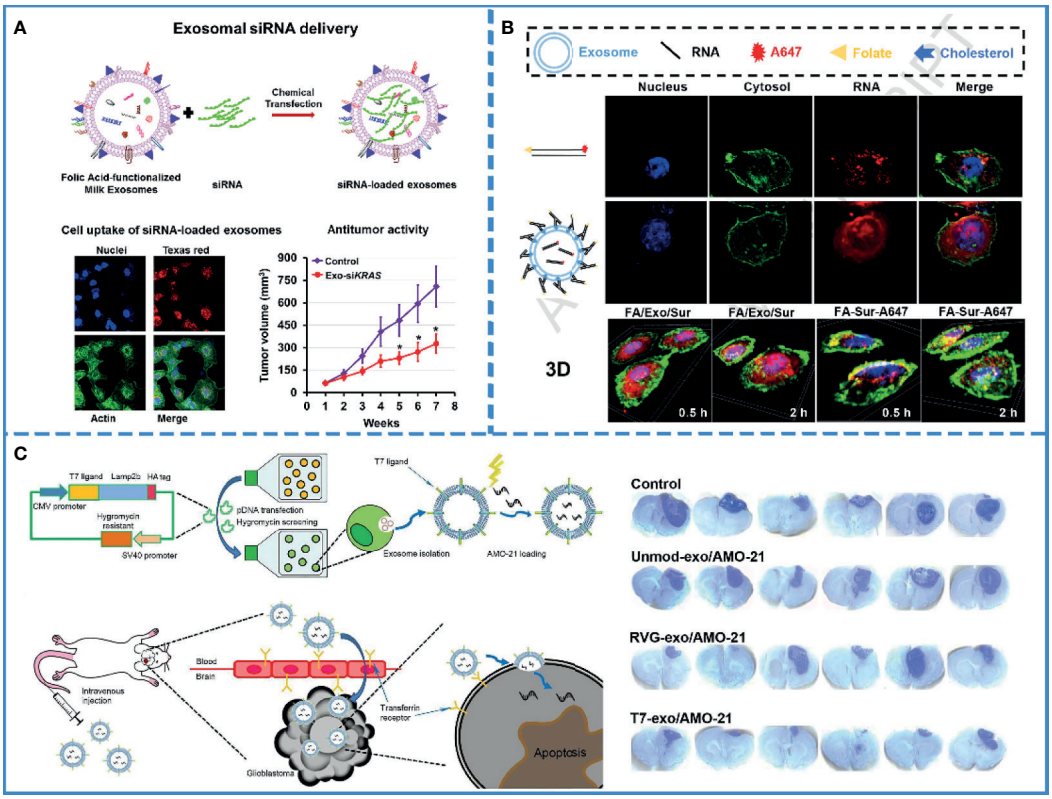


FIGURE 3 | RNAi-based cancer therapy. **(A)** Schematic illustration of folic acid-functionalized milk exosomes loaded with siRNA *via* chemical transfection. Reproduced with permission from ref (69). Copyright 2019 Elsevier. **(B)** FA-decorated exosomes loaded with siRNA were uniformly distributed in the cytoplasm, and there was little overlap with the endosomes/lysosomes in the cells, indicating that exosomes with folate targeting had effective cytosol delivery property. Reproduced with permission from ref (100). Copyright 2019 Elsevier. **(C)** Schematic illustration of the synthesis of a T7 peptide-decorated exosome (T7-exo). After systemic administration, the T7-exo could cross the BBB, bind to glioblastoma, and enhance the efficiency of AMO delivery. Reproduced with permission from ref (79). Copyright 2019 Elsevier.

that sometimes, exosomes fused with the target cell membranes, releasing their cargos directly into the cytoplasm. Thus, exosomes could help avoid the endosome trapping, enabling the full functionality of the RNAs and effectively inhibiting tumor growth (**Figure 3B**) (100). If the exosome was internalized *via* the clathrin-mediated or clathrin-independent endocytosis, it could also help RNAs escape digestion by reverse fusion with the limiting membrane of the MVE or by being re-secretion *via* the early endocytic recycling pathway (30).

Application in Overcoming Off-Target Effect

RNA therapy runs the risk of off-target effects, which can result in unanticipated phenotypes (89). Currently, active targeting might constitute the best way to solve this problem. Compared with other vehicles, exosomes have better targeting ability. First, exosomes have been proved to have a weak homing effect, i.e., cancer-derived exosomes are preferentially absorbed by the cancer cells (65, 101). Second, the exosomes originate from the cell membrane (4); thus, they can be modified *via* different targeted peptides or proteins and then can actively target cancer cells. Recently, exosomes were modified by a variety of target ligands, such as tLyp-1 (70), folic acid (69), iRGD peptide (102), and T7-peptide (79) in RNAs-based cancer therapy. Thus, this approach can limit the off-target effects and promote cellular uptake of RNAs by cancer cells, either passive targeting or active targeting.

Application in Brain Cancer RNAs Interference Based Therapy

The poor diagnostics, therapeutics, and prognosis of brain cancer are well known. It mainly includes glioblastoma, medulloblastoma, and oligodendroglioma. Currently, a standard treatment for brain cancer is surgical resection, followed by radiotherapy and chemotherapy. However, surgical resection is limited because of the diffusive nature of brain cancer and the intolerance in some patients. Also, chemotherapy and radiotherapy can have serious adverse effects; thus, brain cancer has a low cure rate and a high recurrence rate clinically. Therefore, a drug with low-toxicity, low-immunogenicity, high bioavailability, ability to cross the blood-brain barrier (BBB), and active targeting is needed. Most naked molecules do not meet

these requirements. Fortunately, exosomes possess an invisibility cloak, increasing their functionality by wrapping them in a vesicle. In other words, they can carry the cargos and pass through biological barriers smoothly, including BBB; thus, improving the biological availability of cargos (103). Additionally, exosomes are non-toxic, which will not lead to acute immune rejection, thus giving the cargos high biocompatibility (7). Also, exosomes present a customizable surface and can be modified for different applications (104). These characteristics of exosomes are exclusive to them (105), making them the preferred carriers in brain treatment.

For the treatment of brain tumors, RNA therapy is not only hindered by the BBB but also by the off-target effects. The complex and mysterious structure of the brain makes the adverse effects of off-target unpredictable. One study analyzed the delivery of miRNA-21 using T7-peptide-decorated exosomes *via* intravenous injection. After systemic administration, this compound showed a brilliant brain-targeting ability and reduced tumor size in orthotopic glioblastoma models without adverse effects. Similarly, Lamp2b and rabies virus glycoprotein (RVG) are also known to target glioblastoma (**Figure 3C**) (79). If unmodified exosomes are used to deliver RNAs, then intra-tumor injection may be the most efficient and safe method (106).

In summary, exosome-loaded RNA for tumor treatment could improve the disadvantages of RNA, such as rapid hydrolysis, poor bioavailability, and inability to cross the biological barriers. Experiments have shown that exosomes can store RNA, avoiding RNA degradation by enzymes and maintaining its stability in the blood. In addition, exosomes can carry RNA across biological barriers, such as the blood-brain barrier and the gastrointestinal barrier. Finally, RNA therapy has the risk of off-target effects. Thus, exosomes can help RNA overcome off-target effects and improve targeting ability, in turn improving anti-tumor efficacy.

USE OF EXOSOME TO IMPROVE CANCER CHEMOTHERAPY

Several chemotherapeutic drugs, which exhibit potent anti-cancer effects *in vitro*, do not show similar efficacy *in vivo* due to low bioavailability and low biocompatibility. Also, long-term chemotherapy induces drug resistance in cancer cells (107), which causes further complications. A drug needs a drug delivery system to exert its therapeutic effect *in vivo* to improve its bioavailability, as well as its solubility in water, stability in blood, permeability to biological barriers, and accumulation in cancer tissues. Additionally, it is also necessary to improve their active targeting ability, hide their immunogenicity, and make them self-degradable. Exosomes as "natural nanoparticles," can not only meet the above requirements but also help to overcome cancer drug resistance; thus, they can work as valuable carriers for drug delivery (**Table 3**) (118).

Use in Enhancing Bioavailability

Several natural products and extracts, such as paclitaxel, curcumin, celastrol, anthocyanin, etc. suffer from low bioavailability *in vivo* despite having excellent anti-cancer properties. Numerous experiments have shown that exosomes can improve the bioavailability of these drugs and improve their efficacy in cancer treatment. For example, aminoethylanisamide-polyethylene glycol-vectorized exosomes loaded with paclitaxel (AA-PEG-exoPTX) exhibit a high loading capacity, excellent accumulation in cancer cells upon systemic administration, and improved therapeutic efficiency (111). In this previous study, AA-PEG-vectorized exosomes increased the aqueous solubility of PTX and promoted the accumulation of PTX in tumor tissues. In another experiment, the poor aqueous solubility and instability in the blood of celastrol were improved *via* exosome wrapping. Thus, exosomes improved the bioavailability of celastrol and enhanced its anti-cancer efficacy (119).

Compared with systemic administration, oral administration is non-invasive and easy for the patient; thus, it constitutes an excellent treatment method for chemotherapy. However, the gastrointestinal barrier hinders the absorption of drugs, especially gastric acid, which reduces the stability of drugs. Fortunately, milk-derived exosomes can stably exist in gastric acid; thus, avoiding the degradation of the cargo molecules (99). Curcumin is well known for its excellent anti-cancer properties but poor aqueous solubility. Its hydrophobic nature results in not only poor aqueous solubility but also rapid intestinal hepatic metabolism. A study showed that exosome-encapsulated curcumin could stably exist in gastric acid and smoothly cross the gastrointestinal barrier to improve the bioavailability of curcumin. Additionally, compared with the pure curcumin group, exo-curcumin showed significantly improved accumulation in tumor cells as well as enhanced anti-tumor efficacy (108).

Application in Enhancing Biocompatibility

Most chemical drugs, such as adriamycin, cisplatin, oxaliplatin, etc. suffer from low biocompatibility. The adverse effects of these drugs limit their clinical application. Theoretically, carriers with active targeting ability, low immunogenicity, and self-degradability should solve this problem. Autologous-derived exosomes elicit a negligible immune response or an inflammatory reaction, as well as possess the ability of self-degradation and active/passive targeting *via* surface or gene modification. These characteristics make exosomes more suitable than other carriers to improve the biocompatibility of chemical drugs (120). A study developed A33 antibody, which is uniformly expressed in colorectal cancer, positive exosomes loading doxorubicin (Dox) to improve the targeting ability, and this system showed high efficacy for the treatment of colorectal cancer without causing cardiotoxicity. Additionally, it demonstrated that exosomes fused with target cells more efficiently under acidic conditions, implying that exosomes facilitated drug release in acidic cancer cells (**Figure 4A**) (112). Furthermore, autologous exosomes can also reduce the hepatotoxicity and nephrotoxicity of gemcitabine by mediating the delivery of drugs to the cancer site due to its special homing effect (117). Additionally, the use of exosomes increased cancer cell uptake, minimized immunogenicity, and enhanced the biocompatibility of aspirin (**Figure 4B**) (115).

TABLE 3 | Exosome-mediated anti-tumor drug delivery.

Source of exosomes	Drugs	Tumor	Drug loading (%)	Encapsulation efficiency (%)	Zeta potential (mV)	Particle size (nm)	Improvements	Ref
Bovine milk	Paclitaxel	Lung cancer	8	/	-7	75 ± 0.6	Improve oral bioavailability	(99)
Bovine milk	Curcumin	Cervical cancer	18–24	53.9 ± 6.7	/	93 ± 6	Improve low water solubility, rapid intestinal/hepatic metabolism, oral bioavailability	(108)
Bovine milk	Bilberry-derived anthos	Lung cancer	20	/	/	83 ± 1.7	Improve low solubility, low permeability, and poor oral bioavailability	(109)
FBS	Curcumin	Breast cancer	/	/	-24.1 ± 2.2	122.7 ± 6.5	Cross the BBB and facilitate accurate glioma recognition and improvement of the curative effect	(110)
Macrophage	Paclitaxel	Lung cancer	33	/	-4.4 ± 0.1	280.8 ± 3.1	High loading capacity, profound ability to accumulate in cancer cells, and improved therapeutic outcomes.	(111)
LIM1215 cells	Doxorubicin	Colorectal Cancer	2.60	9.06	-9.57 ± 0.38	187.83 ± 6.76	Improve the therapeutic effect of Dox and reduce its systemic toxicity.	(112)
MCF7, Caco2, PC3 and HepG2 cell lines	Bioactive compounds from black bean extract	Gastric cancer	Soyasaponin α: 17.31 soyasaponin β: 16.08	/	-19.23 ± 2.42	142.80 ± 23.67	Improve low solubility, poor penetration into cells, hepatic disposition, narrow therapeutic index, and rapid uptake by normal tissues	(113)
J774A.1 cells	Doxorubicin	Breast cancer	99	/	-26 ± 3	177 ± 21	Higher drug accumulation in target cells and improve small molecule stability and blood circulation time	(114)
Breast and colorectal cancer cells	Aspirin	Breast and colorectal cancer	/	/	/	50-150	Improve the poor water-solubility of aspirin	(115)
Bone marrow mesenchymal stem cells	Pancreatic ductal adenocarcinoma, paclitaxel (PTX) and gemcitabine monophosphate (GEMP)	Pancreatic cancer	GEMP: 8.78 PTX: 1.25	GEMP: 5.92 PTX: 2.62	-10.46 ± 0.55	75.5 ± 1.4	Surpass the restrictions of pathological ECM and increase the accumulation of therapeutics in the tumor site.	(116)
Autologous pancreatic cancer	Gemcitabine	Pancreatic cancer	11.68 ± 3.68	/	/	70 - 150	Facilitate cellular uptake of GEM and contributed to significantly increased cytotoxic effect of GEM	(117)

"/" represents that information was not mentioned in the original article.

Application in Overcoming Multidrug Resistance

Clinically, multidrug resistance is a fatal blow to cancer chemotherapy. Additionally, the TME is well known for its potential for drug resistance. In fact, exosomes play a crucial role in this process since they transmit the information related to drug resistance between cancer cells. On the contrary, for cancer treatment, exosomes can also be used to transmit information about reversing drug resistance between cancer cells. Thus, caudally injected exo-anti-miR-214 was shown to reverse the resistance to cisplatin in gastric cancer and repress cancer growth *in vivo* by downregulating the expression of miR-214, which promoted gastric cancer chemoresistance (121). Additionally, in pancreatic ductal adenocarcinoma, chemoresistance to gemcitabine (GEM) significantly reduced the sensitivity of chemotherapeutic agents. The downregulation of key proteins, such as human equilibrium nucleotide transporter 1 (hENT1) and deoxynivalenol kinase (dCK), reduced the transport of GEM to the cytoplasm and insufficient conversion of GEM phosphorylation products, resulting in GEM-related chemoresistance. The internalization of exosomes into the cell was shown to be energy-dependent and was mediated by clathrin-independent endocytosis and macropinocytosis. Thus, GEM could enter the cytoplasm through a different internalization *via* exosomes, avoiding the primitive transport involved in human equilibrium nucleotide transporter protein 1 (hENT1) and thus, resist resistance (116). Drug resistance has been associated with an efflux transporter known as P-glycoprotein (P-gp) that is located in the cellular membrane (122). A study showed that the PTX-loaded exosome could bypass P-gp-mediated drug efflux in the resistant cancer cells to overcome the chemoresistance (**Figure 4C**) (123).

Application in Brain Cancer Chemotherapy

Due to chemoresistance and the limitations related to BBB, most chemotherapy drugs show poor therapeutic efficacy in brain tumors. The exosome is an extraordinary carrier with improved drug bioavailability, biocompatibility, and the ability to cross the BBB, which is helpful in improving the efficacy of drugs. For example, doxorubicin- and paclitaxel-loaded exosomes can cross BBB smoothly, with good bioavailability and anticancer efficacy (**Figure 4D**) (124). In another study, neuropilin-1-targeted peptide (RGE) was conjugated with the exosome membrane to improve its biocompatibility (110). As previously mentioned, brain cancer is also affected by multidrug resistance. It has been

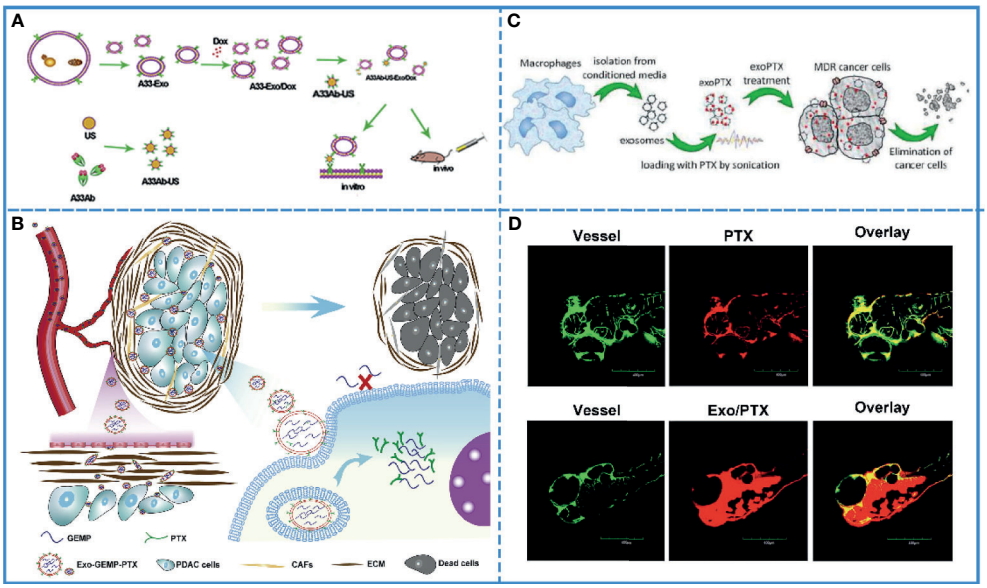


FIGURE 4 | Cancer chemotherapy. **(A)** Schematic illustration of A33Ab-US-Exo/Dox complex formation between A33 antibody-coated surface-carboxyl Fe_3O_4 superparamagnetic nanoparticles (US) (A33Ab-US) and exosomes (A33-Exo) released from doxorubicin-loaded LIM1215 cells (A33-Exo/Dox). Reproduced with permission from ref (112). Copyright 2018 Elsevier. **(B)** Exosomes loaded with GEMP and PTX were used for targeted chemotherapy of pancreatic cancer *via* dual functions, i.e., stromal penetrability and anti-matrix and overcame chemoresistance. Reproduced with permission from ref (115). Copyright 2019 Elsevier. **(C)** Paclitaxel (PTX)-loaded exosomes (exoPTX), derived from autologous macrophages, exhibited high loading capacity, sustained drug release, profound ability to accumulate in resistant cancer cells, and elevated cytotoxicity compared to PTX. Reproduced with permission from ref (123). Copyright 2016 Elsevier. **(D)** Injection of fluorescence-labeled PTX alone and those complexed with bEND3 exosomes in zebrafish embryos showed that Exo/PTX effectively crossed the BBB into the brain. Reproduced with permission from ref (124). Copyright 2015 Springer Science.

proved that miR-9 plays an important role in the development of drug resistance in glioblastoma cells against temozolomide by inducing an increase in P-gp. After entering the cells by exosomes, anti-miR-9 could reverse the expression of the multidrug transporter and sensitize glioblastoma cells to temozolomide (125). Thus, exosomes can be used to increase the therapeutic efficacy in brain cancer, especially in crossing BBB and overcoming chemoresistance.

In summary, the anti-tumor effect of chemotherapy was mainly inhibited by the low bioavailability and poor biocompatibility of the drug and the drug resistance in cancer cells. Exosomes could improve their bioavailability, stability, trans-biological barrier capacity, and overcome tumor drug resistance, improving the antitumor effect of chemotherapy.

USE OF EXOSOME IN COMBINATION WITH CANCER IMMUNOTHERAPY

The immunosuppressive TME is known to help the cancer cells evade the immune system (126). For example, apoptotic tumor cells are rarely recognized as antigens, and TME has the ability to upregulate the expression of regulatory T (Treg) cells or myeloid-derived suppressor cells and downregulate that of the cytotoxic T cells (127). Therefore, the inhibition of immune escape is the focus of tumor immunotherapy (128). Recent studies have shown that tumor-derived exosomes (TEXs) and immune cell-derived exosomes (IEXs) exhibit outstanding immunomodulatory effects and can overcome tumor immunosuppression (**Table 4**) (143, 144). Among them, dendritic cell-derived exosomes (DEXs) and tumor cell-derived exosomes are widely used because of their high specificity (145).

Application in Immunotherapy of TEXs and IEXs

Tumor-derived exosomes are known to carry immunosuppressive signals from tumor cells and transmit them between cells (146, 147). However, they are rich in tumor antigens as they carry tumor cell-related information (134). Therefore, isolating TEXs and injecting them into the organism could help with antigen presentation, which could generate an immune response, and produce enough cytotoxic T cells to kill tumor cells.

Several experiments have shown that the immunostimulatory ability of dendritic cell-derived exosomes (DEXs) is the same as that of the donor cells (148), and they directly or indirectly stimulate cytotoxic T cells *via* the major histocompatibility complex class I (MHC I) and major histocompatibility complex class II (MHC II) (149). Additionally, DCs are highly immunogenic, and different mature DC-derived exosomes have different functions. Mature, activated DC-derived exosomes often express MHC-I and MHC-II molecules as well as co-

TABLE 4 | Exosome-assisted immunotherapy.

Source of exosomes	Tumor	Size	Characteristics	Ref
Ovalbumin (OVA)-pulsed dendritic cells	/	153 nm	1. Exosomes carry high levels of OVA and induce a more potent antigen-specific response. 2. Induce antigen-specific CD8+ T cells. 3. Induce antigen-specific IgG production. 4. Facilitate interferon gamma production in mouse splenocytes.	(129)
Natural killer (NK) cells exposed to the NB cell	Neuroblastoma	less than 100 nm	1. The exosomes secreted by NK cells exposed to NB cells showed efficient cytotoxicity against NB tumors. 2. The exosomes, capable of transferring their content into naive NKs, exerts a powerful cytotoxic effect on target cells. 3. Overcome the immune resistance of malignant cells.	(130)
HEK293T cells transfected with plasmid DNA encoding SIRPa variant	Colon adenocarcinoma	100 nm	1. Tumor-derived exosomes enhance the effectiveness of CD47-targeted therapy. 2. Tumor-derived exosomes induce innate and adaptive anti-tumor responses.	(131)
Glioblastoma cells	Glioblastoma	30 - 50 nm	1. Exosomes derived from tumor cells are effective antigens, which are convenient to store and extract, and can be used to load DCs. 2. DC loaded with exosomes presents highly efficient uptake, prolonged storage presentation and long-lasting processing. 3. Exosomes efficiently transfer antigens from professional antigen-presenting cells (APCs) to other APCs, facilitating antigen-specific immune responses.	(132)
Dendritic cell	Hepatocellular carcinoma	50-150 nm	1. DEXAFP elicited a strong antigen-specific immune response. 2. The tumor microenvironment was significantly improved following DEXAFP treatment, resulting an increase in CD8+ T lymphocytes and a decrease in regulatory T (Treg) cells.	(133)
Pancreatic cancer cells	Pancreatic cancer	/	1. TEX carries tumor-associated antigens. 2. Because TEX are preferentially recruited to the MHCII loading compartment it is rarely degraded by lysosomes 3. TEX is enriched in newly delivered MHCII molecules and preferentially activates CD4 helper T cells.	(134)
Dendritic cells	Cervical cancer	/	1. Dendritic cell (DC)-derived exosomes (Dexo) are capable of inducing anti-tumor immune responses. 2. Dexo effectively induced cytotoxic activity of CD8+ T cells against TC-1 tumor cells. 3. Dexo promoted the immune response to *in vitro* restimulation induced by antigen E7 in inoculated mouse splenocytes.	(135)
Hepatocellular carcinoma tumor cells	Hepatocellular carcinoma	30-100 nm	1. After DC-TEX treatment, the number of T regulatory cells decreased and the number of CD8+ T cells increased. 2. After DC-TEX treatment, the number of PD-1+ increased significantly.	(136)
Cell- and serum-derived exosomes	/	~140 nm	Fetal bovine serum-derived exosomes (bo-EXO), which have the ability to reach the surface zone (macrophage zone) and the paracortical zone (T-cell zone) of lymph nodes, are effective in delivering immunostimulatory molecules to antigen-presenting cells and T cells.	(137)
Natural Killer cells	Glioblastoma	~100 nm	1. Natural killer (NK)-exosomes have antitumor activity against glioblast cells. 2. Natural killer (NK)-exosomes have the ability of tumor targeting. 3. Natural killer (NK)-exosomes can be loaded with other anticancer drugs, enhancing their antitumor effects and tumor specificity and facilitating their passage through the BBB.	(138)
RenCa cells	Renal cell carcinoma	30-100 nm	1. Exosomes carry high levels of OVA and induce a more potent antigen-specific response. 2. Induces antigen-specific CD8+ T cells. 3. Induces antigen-specific IgG production. 4. Facilitate interferon gamma production in mouse splenocytes.	(139)
Fetal bovine serum	Breast cancer	109 nm	1. The exosomes secreted by NK cells exposed to NB cells showed efficient cytotoxicity against NB tumors. 2. The exosomes, capable of transferring their content into naive NKs, exerts a powerful cytotoxic effect on target cells. 3. Overcome the immune resistance of malignant cells.	(140)
Tumor cell	/	/	1. Tumor-derived exosomes enhance the effectiveness of CD47-targeted therapy. 2. Tumor-derived exosomes induce innate and adaptive anti-tumor responses.	(141)
Bone marrow mesenchymal stem cell	Pancreatic ductal adenocarcinoma	140 ± 37.6 nm	1. BM-MSC-derived exosomes significantly improve tumor targeting and increase drug accumulation at the tumor site. 2. Protect the cargo gene.	(142)

"/" represents that information was not mentioned in the original article.

stimulatory molecules (CD40, CD80, CD86, etc.) and are therefore able to induce effective antigen-specific T and B cell responses and activate cytotoxic T cells and natural killer (NK) cells. Studies have shown that DC-derived exosomes induce antigen-specific responses against tumor cells by activating innate and adaptive immune cells and overcoming tumor-induced immunosuppression (**Figure 5A**) (150). Based on these characteristics, DEXs have been extensively used in free-cell tumor vaccines (133). Along with dendritic cells, the exosomes derived from macrophages, natural killer cells, B cells, and T cells also possess the immunoregulatory ability and can be used in tumor immunotherapy (151, 152).

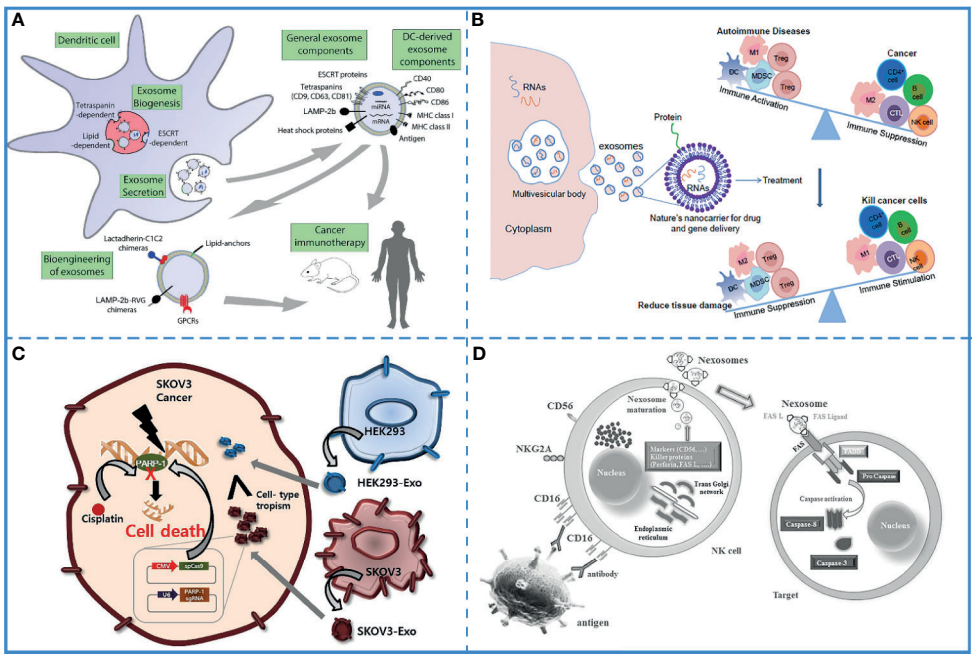


FIGURE 5 | Immunotherapy. **(A)** DEXs can overcome tumor immunosuppression. Reproduced with permission from ref (150). Copyright 2015 Elsevier. **(B)** DC-derived exosomes have been used for immunotherapy in animal studies and human clinical trials. It can also be bioengineered to contain specific cargoes. Reproduced with permission from ref (155). Copyright 2014 Elsevier. **(C)** Compared with epithelial cell-derived exosomes (HEK293-exo), tumor -derived exosomes (SKOV3-Exo) accelerates their accumulation in SKOV3 tumor cells due to their cell tropism. Reproduced with permission from ref (156). Copyright 2017 Elsevier. **(D)** Nexosomes (NK-derived exosomes) entrap CD markers, perforin, and FAS-L, which mediates cytotoxicity by interacting with FAS on exposed cell membranes. Reproduced with permission from ref (130). Copyright 2017 Wolters Kluwer Health, Inc.

Application in Tumor Antigens or Adjuvants Delivering by TEXs and IEXs

The successful delivery of tumor antigens or adjuvants to antigen-presenting cells (APCs) is the most effective method to induce an anti-tumor immune response. Therefore, a novel carrier that can deliver tumor antigens and adjuvants to APCs is required for the development of cancer immunotherapy. Exosomes are natural vesicles produced by cells, which carry cargo molecules stably and safely, can smoothly cross biological barriers, and can target cells accurately. Furthermore, exosomes are also suitable as carriers in immunotherapy because (i) they can simulate the transmission of pathogens to antigen-presenting cells (153), (ii) they can carry a wide range of cargo molecules, such as tumor-specific antigens, peptides, and toll-like receptor (TLR) ligands (154), (iii) the loading method is optional and convenient, the cargos can be loaded directly into the exosomes isolated from the donor cells or indirectly by co-incubation with donor cells (**Figure 5B**) (155).

Application in Tumor Antigens or Adjuvants Delivering by TEXs

Compared with other exosomes, TEXs carry a higher number of tumor-associated antigens and can effectively target tumor cells (156) (**Figure 5C**). Additionally, the surface of TEXs is rich in proteins that promote cell-to-cell interaction; thus, they can be easily absorbed by the target cells (157). A study demonstrated that TEXs painted with the functional domain of high-mobility group nucleosome-binding protein 1 (TEX-N1ND), a potent adjuvant, enhanced DC immunogenicity; thus, eliciting long-lasting anti-tumor immunity and tumor suppression. Also, N1ND-decorated TEXs are known to promote N1ND uptake because of the surface proteins of TEXs (141). Another experiment used the early secretory antigenic target-6 (ESAT-6) from *Mycobacterium tuberculosis* as an immune response-inducing antigen and found that TEXs expressing ESAT-6 or its epitopes on the surface could be captured by APCs to induce immune responses against the tumor cells. The pathogenic antigen presented on the TEXs surfaces acted as an "artificial neoepitope" and was recognized by DCs as a "danger signal", leading to the activation of an antitumor immune response (158). Furthermore, the TEXs-based tumor antigens-adjuvant co-delivery system was more efficient, which effectively activated DC2.4 cells and enhanced tumor antigen presentation capacity (159).

Application in Tumor Antigens or Adjuvants Delivering by DEXs

Compared with tumor cell lysates, DEXs are more easily absorbed by DCs and have excellent antigen storage, presentation, and processing ability (149). Meanwhile, compared with other microvesicles, DEXs can induce a more effective immune response. For instance, among the microvesicles and exosomes

from antigen Ovalbumin (OVA)-pulsed DCs, only DEXs elicit antigen-specific CD8+ T-cells and antigen-specific IgG production (129). Another experiment demonstrated that DEXs loaded OVA with poly(I:C), a ligand of TLR-3, induced a strong protective immune response and markedly inhibited the tumor growth and improved the survival rate of the tumor-bearing mice (135). Similarly, thymic stromal lymphopoietin (TSLP) induced DEXs, which were enriched with OX40 ligand (OX40L), promoted proliferation of $CD4^+$ T cells, upregulated the level of IL-4, and promoted Th2 differentiation (160).

Application in Tumor Antigens or Adjuvants Delivering by Other IEXs

The mutual communication between innate immune cells and acquired immune cells results in a perfect immune system, and the exosomes secreted by them are the bridge of their communication (152). For example, the exosomes secreted by innate immune cells can not only be received by other types of innate immune cells but also recognized by acquired immune cells, affecting the differentiation, activation, tissue recruitment, and production of cytokines by the acquired immune cells (**Figure 5D**) (124, 130). Therefore, exosomes derived from immune cells loaded with tumor antigens or adjuvants are easier to be recognized by the immune system; thus, activating the immune response and effectively killing the tumor cells (143). By carrying the adjuvant heat shock protein 70, these exosomes can effectively induce an immune response and cause tumor regression in the animal model (161). Additionally, T cell-derived exosomes loaded with CD40L can promote B cell proliferation and differentiation (162).

Different Application Between TEXs and IEXs Delivering Tumor Antigens or Adjuvants

Exosomes derived from immune cells and tumor cells loaded with tumor antigens or adjuvants are easily recognized by the immune system; thus, these are used as antigen carriers for cancer immunotherapy. Compared with IEXs, TEXs have a stronger ability to target tumor cells and efficiently deliver multiple tumor antigens to DCs (163). TEXs, which are recovered and enriched from patient serum might provide an optimized, individual-specific source of antigen for DCs vaccination (164). Nevertheless, numerous studies have shown that TEXs have immunosuppressive effects on the immune system since they can interfere with the maturation of DCs, weaken the activation of NK cells, induce suppressor cells of myeloid origin, and transform macrophages into tumor-promoting phenotype (165–167). Compared with TEXs, IEXs are more easily absorbed by DCs and have better antigen storage, presentation, and processing capabilities; hence, the exosome fraction is known to be more immunogenic *in vivo* and produces fewer side effects (168). However, treatment with single IEXs might be more resistant to immunomodulatory events occurring in tumors than other immunotherapies (149). IEXs can be modified by multiple methods to increase their targeting ability and become a promising delivery system (169, 170). Further research is required to fully utilize the advantages of TEXs and IEXs, and bypass their disadvantages to regulate tumor immunity, which has great application potential in cancer treatment (171).

Application in Brain Cancer Immunotherapy of TEXs and IEXs

Based on their carrier and immunomodulatory ability, exosomes play a vital role in immunotherapy against the brain tumor. For example, co-delivery of tumor-derived exosomes with α-galactosylceramide (α-GalCer) on a DC-based vaccine induced strong activation and proliferation of tumor-specific cytotoxic T lymphocytes and destroyed tumor immunosuppressive environment, showing a powerful effect in glioblastoma (132). Additionally, DEXs loaded with chaperone-rich cell lysates (CRCLs) derived from GL261 glioma cells promoted proliferation and activity of $CD4^+$ and $CD8^+$ T cells, enhanced T cell infiltration in intracranial glioma tissues, and induced the generation of anti-tumor cytokines, including IL-2 and IFN-γ. Therefore, they significantly prolonged the survival of mice with tumors and inhibited tumor growth *in vivo* (172). A study used natural killer cell-derived exosomes (NK-Exos) to treat glioblastoma and found that NK-Exos exerted an innate therapeutic effect in glioblastoma. It demonstrated that NK-Exos possessed strong antitumor activity toward glioblastoma cells and could facilitate the transfer of other anti-cancer agents through the BBB by wrapping them (138).

In summary, collecting tumor-derived exosomes and reinjecting them into the organism could aid antigen presentation and elicit an immune response. While the dendritic cell-derived exosomes have the same immunostimulatory capacity as donor cells, the tumor-derived exosomes are able to activate innate and adaptive immune cells and overcome tumor-induced immunosuppression, triggering an antigen-presentation response against the tumor cells. Furthermore, in addition to their own biological activity, exosomes can transport tumor antigens or adjuvants to antigen-presenting cells and induce antitumor immune responses.

APPLICATION OF EXOSOME TO IMPROVE CANCER PHOTODYNAMIC THERAPY OR PHOTOTHERMAL THERAPY

Recently, substantial breakthroughs have been made in the use of near-infrared light (NIR) in anti-cancer treatment. However, both photodynamic therapy (PDT) and photothermal therapy (PTT) need an effective carrier delivery system to deliver photosensitizers (173) or photothermal transducers (174). PDT kills the cancer cells by irradiating the photosensitizer to produce the toxic singlet oxygen. On the contrary, PTT induces the thermal killing effect by using photothermal transducers to convert light energy into thermal energy. Currently, exosomes are being used as carriers in PDT and PTT to improve their effectiveness.

Application in Photodynamic Therapy

Currently, the transport efficiency of photosensitizers in PDT is low. Recent studies on the excellent carrier performance of

exosomes have attracted the attention of researchers. Studies have shown that exosomes can smoothly carry the photosensitizer to the tumor site. The engineered exosome can be endowed with the ability to target tumor cells; thus, enhancing the therapeutic efficiency of PDT. For example, exosomes collected and purified from the urine of gastric cancer patients have the ability to passively target tumor sites due to natural cell membranes and antigens. Meanwhile, the exosomes are known to promote the internalization of Exo-PMA/Au-BSA@Ce6. Au NPs are transferred into aqueous solution by amphiphilic polymer (PMA) coating, and after surface coupling of the BSA layer, Ce6 is trapped into the BSA network and finally embedded in the exosome nanocarriers toward the cancer cells, avoiding endocytosis by macrophages and prolonging their blood circulation time. The results have shown that the nanoparticles could be released inside cancer cells under 633 nm laser irradiation, producing a large number of singlet oxygen species, killing the tumor cells (**Figure 6A**) (63). However, the short lifespan and limited diffusion length of cytotoxic reactive oxygen species (ROS) generated by the photosensitizer reduces the anti-tumor effects. Therefore, a nucleus targeted exosome was designed to enhance the PDT effect, engineered using a chimeric peptide (ChiP-Exo). In this study, a dual-stage light strategy was used for precise PDT by sequentially destroying the PM and nucleus of the cancer cells. Based on these exosomes, it could activate ROS *in situ* to disrupt the nuclei, which greatly inhibited tumor growth with minimized systemic toxicity (**Figures 6B, C**) (175). As mention above, tumor-derived exosomes can be used as immunostimulants. Based on this feature, the combination of photodynamic therapy and immunotherapy can be used to treat tumors through exosomes. For instance, recombinant exosomes derived from tumors (R-Exo) are used as drug delivery vehicles and immunostimulants at the same time. During exosomal re-assemble, a chlorin e6 photosensitizer was loaded into tumor-derived exosomes. After this modification, R-Exo retains its original average size and has the same membrane protein, so that it can target tumor cells. The R-Exo loaded with chlorine e6 (Ce6-R-Exo) can be observed by photoacoustic imaging, and it can effectively produce reactive oxygen species inside tumor cells under laser irradiation. In addition, Ce6-R-Exo enhances the ability of immune cells to release cytokines, which indicates that these modified exosomes can also be used as immunotherapeutic (**Figure 6D**) (176).

Application in Photothermal Therapy

Compared with traditional therapy, PTT is controllable, noninvasive, and has minimal adverse effects. With the help of exosome delivery, photothermal transducers are carried to tumor cells and produce a thermal effect after NIR irradiation. For instance, an exosome with gold nanoparticles has been designed that assembles into a popcorn-like nanostructure. The formulated nanopopcorn, consisting of self-grown gold nanoparticles and exosomes loaded with DOX, was shown to retain the photothermal conversion of gold nanoparticles and cytotoxicity of DOX. The use of exosomes improved cellular internalization, controlled drug release, enhanced anti-tumor efficacy, and minimized adverse effects (**Figure 7A**) (177). However, it was found that PTT was blocked by heat shock proteins and other stress proteins, resulting in thermal tolerance. Thus, a higher temperature was required to achieve anti-tumor effects. However, the high temperature could damage the surrounding tissue. Therefore, the low-temperature nucleus-targeted PTT in the NIR-II region is conceptualized. For example, vanadium carbide quantum dots (V2C QDs) with good photothermal effect in the NIR-II region were modified with TAT peptides and packaged into exosomes with RGD modification. This carrier exhibited good biocompatibility, long circulation time, and endosomal escape ability. More importantly, it could target the cell and enter into the nucleus to achieve low-temperature PTT with advanced tumor destruction efficiency (**Figure 7B**) (178).

In summary, both PDT and PTT require delivery of the photosensitizer to the treatment site. Exosomes, as carriers of the photosensitizer, can increase the circulation time of the photosensitizer in the blood, and help the photosensitizer cross the blood-brain barrier. Additionally, the modified exosomes could carry photosensitizers to target the nucleus and improve the effectiveness of PDT or PTT.

PATENTS OF EXOSOMES IN CANCER THERAPY

In the past ten years, research on exosomes has grown exponentially. The functions of exosomes have expanded from transporting intracellular garbage to participating in cell-to-cell communication as well as tumor growth and metastasis. Despite this growing trend, the lack of reference standards for exosomes, the inability to replicate experimental results, and the lack of clinical transformation have resulted in an incomplete acceptance of exosomes in some scientific fields. Fortunately, many patents are trying to address these problems, and many more are expected to support the multiple roles of exosomes.

Currently, there are several techniques to separate exosomes with their individual advantages and disadvantages; however, there is no uniform standard of characterization for isolated exosomes, which adds uncertainty to further experiments. In response, EP3690434 provided a method to analyze EVs using the size-specific fractionation ability of size-exclusion chromatography and specific binding of probes to EVs. This method could speed up and facilitate the quantitative analysis of EVs (types and quantities) present in the samples, the physicochemical analysis of EVs, and an analysis of the specificity or affinity of binding of the probes to the components of EVs. This kit could detect whether the isolated exosomes contained other vesicles, which can be used as a standard for testing the purity of exosomes. In view of the low output of exosomes, researchers have proposed to artificially synthesize exosome analogs with identical physiological functions and can be mass produced.

Tumor-derived exosomes contain tumor markers and can be used in tumor diagnosis. If the clinical transformation of tumor diagnosis by exosomes can be achieved, the early detection of

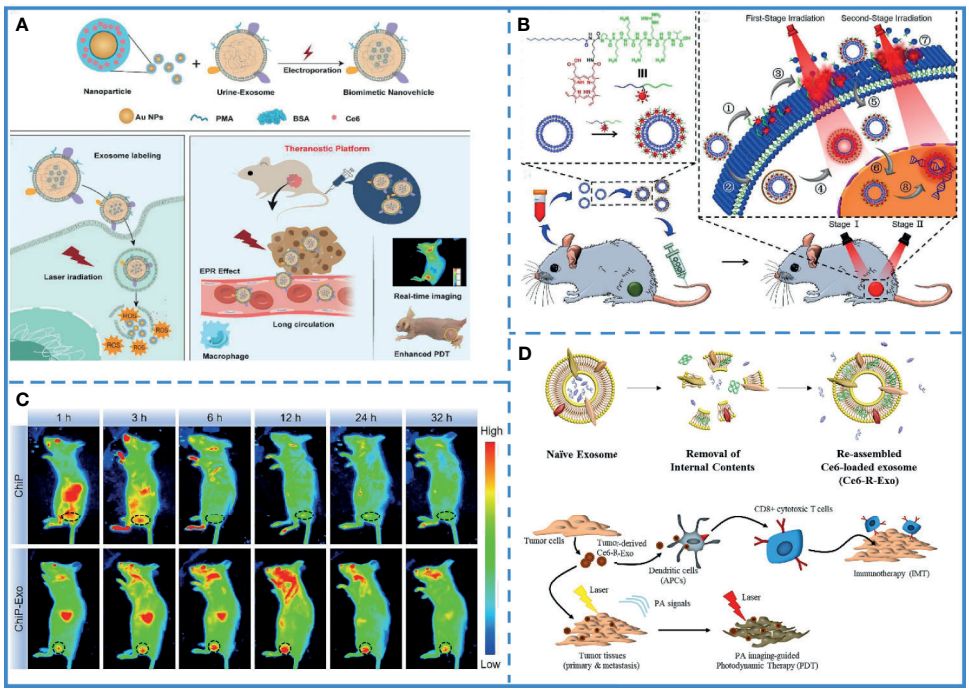


FIGURE 6 | Photodynamic therapy. **(A)** Synthesis of Exo-PMA/Au-BSA@Ce6 nanovehicles. Laser irradiation at 633 nm under acidic conditions resulted in the collapse of the structure of nanovehicles, leading to the release of PMA/Au-BSA@Ce6 nanoparticles into the cancer cells, producing singlet oxygen species, inhibiting tumor cell growth. Reproduced with permission from ref (63). Copyright 2019 Elsevier. **(B)** Intravenous injection of ChiP-Exo and dual-stage light-guided PDT against the tumor. ChiP-Exo underwent the following steps: (1) PM-targeted delivery; (2) Endocytic delivery; (3) PM fluctuation; (4) Lysosomal escape after the first-stage light irradiation; (5) Photochemical internalization (PCI); (6) Nucleus-targeted translocation; this was followed by (7) PM rupture, and (8) Nucleus destruction under the second-stage light irradiation. Reproduced with permission from ref (175). Copyright 2019 Elsevier. **(C)** ChiP has several limitations, including a relatively shorter half-life *in vivo* and poor retention in tumor tissues. On the contrary, ChiP-Exo continuously accumulates in the tumor and exhibits superior tumor treatment ability. Reproduced with permission from ref (175). Copyright 2019 Elsevier. **(D)** Combined photodynamic therapy and immunotherapy *via* exosomes to treat tumors. Reproduced with permission from ref (176). Copyright 2020 Elsevier.

tumors and timely treatment will be possible and would significantly benefit the patients. Currently, several kits have been developed for the detection of different tumors and applied for patents. WO2020159181 developed a kit to predict the recurrence probability of acute myeloid leukemia by detecting CD53 and CD47 expression of exosomes in the blood collected from the patients; WO2020147252 developed a kit to detect breast cancer, mainly to detect the TII protein of exosomes derived from the body fluids of the patients; WO2019093717 developed a kit to diagnose lung cancer and predict prognosis. The use of exosomes in tumor diagnosis has substantial future prospects. The nearly noninvasive, simple, and rapid diagnosis technique can eliminate the concerns of patients and improve the rate of early diagnosis of tumors.

Many experiments have confirmed that exosomes can significantly improve the efficacy of tumor treatment, but most of them are in the experimental stage and need to gradually transition to clinical applications. Thus, it is necessary to apply for patents to promote the transformation of exosomes into clinical practice. Exosomes as carriers can increase the efficacy of drug therapy, but most of the synthesis techniques are difficult to reproduce, which is not conducive to further research. WO2020132946 and WO2020141369 have provided a detailed process of preparing exosomes to carry cargo molecules for tumor treatment and have recorded the conditions, reagents, and instruments used in the preparation process, with high reproducibility, which will be implemented in clinical trials in the future. Additionally, the addition of the function of exosomes as a carrier to the original research would help with the further advancement of technology and would help maintain the patent protection period. Apart from being a carrier, exosomes themselves have an anti-tumor effect; WO2020032379 confirmed that exosomes derived from macrophages exposed to death cells could reach cancer cells and inhibit the epithelial-mesenchymal cell conversion in cancer cells as well as infiltration of cancer cells; thereby preventing or treating cancer. The successful application for the patent of exosomes for tumor therapy indicates that exosomes have great potential in assisting chemotherapy, RNA interference therapy, immunotherapy, and phototherapy (**Table 5**), which can significantly improve the efficacy of tumor treatment and optimize the current tumor treatment strategy.

Until January 2021, there were 205 clinical trials related to exosome research. Of the 205 trials, around 87 trials involved

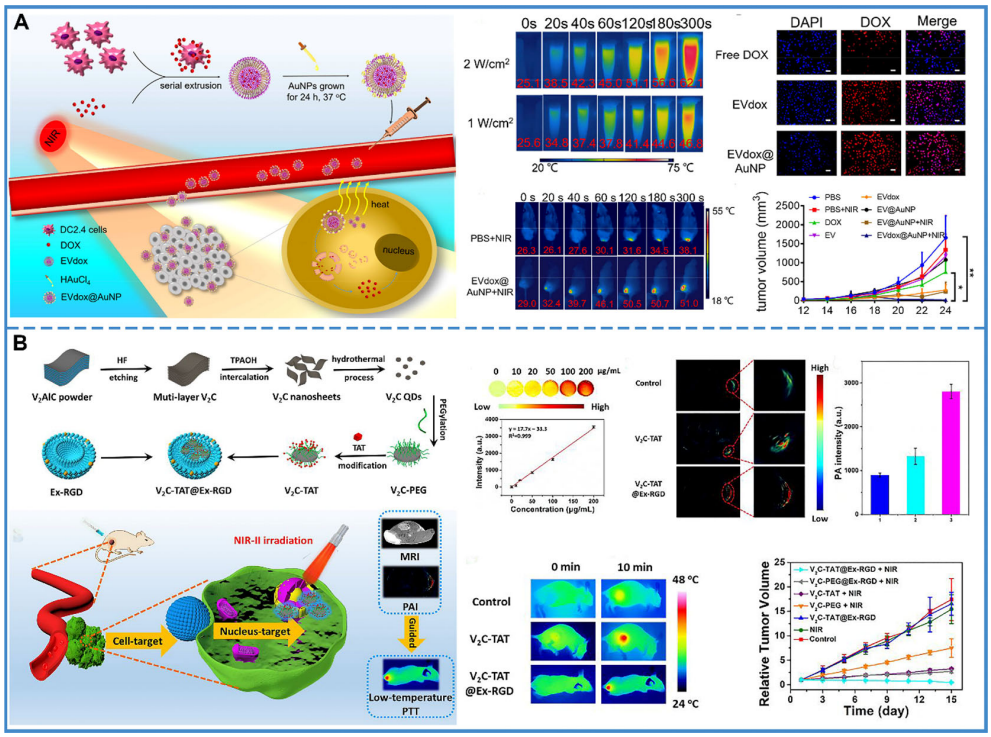


FIGURE 7 | Photothermal therapy. **(A)** The prepared EVdox@AuNP (EVs encapsulating DOX were first obtained (EVdox), and self-growth of gold nanoparticles around EVdox) plays a synergistic role of photothermal and chemotherapy for tumor treatment. In this system, AuNPs have a good thermal effect and exosomes can assist DOX aggregation within tumor cells, thus inducing effective tumor elimination. Reproduced with permission from ref (177). Copyright 2019 Elsevier. **(B)** V2C-TAT@Ex-RGD (The small fluorescent V2C QDs were modified with TAT peptides and packaged into Ex with RGD modification) targeted the cancer cell membrane & nucleus organelle for low-temperature imaging-guided PTT in NIR-II. The PA intensity at the tumor site was 2.11-fold higher in V2C-TAT@Ex-RGD-treated mice than in V2C-PEG-TAT-treated mice. It was shown that the efficient tumor accumulation of V2C-TAT@Ex-RGD was due to the Ex-RGD coating. After 10 min of 1064 nm laser irradiation at a power density of 0.96 W/cm^2, the tumor site warming was higher in the V2C-TAT@Ex-RGD-treated mice compared with the control group and the V2C-TAT-treated mice. And, the V2C-TAT@Ex-RGD +1064 nm laser irradiation group could effectively inhibit tumor growth without recurrence. Reproduced with permission from ref (178). Copyright 2019 American Chemical Society.

cancer-related studies (179). Among these clinical trials, exosome-based phase I and II clinical trials have been completed in advanced lung cancer patients showing promising data (148). Notably, DEX-based phase I and II clinical trials have been performed in non-small cell lung cancer (NSCLC), indicating the safety and feasibility of the approach, as well as the preference of these nanovesicles to stimulate T cell- and NK cell-based immune responses in patients (149). A vaccination trial with tumor antigen-loaded dendritic cell-derived exosomes showed the safety and feasibility of DEXs vaccines (NCT01159288). Based on these promising results of exosomes for clinical treatment, significant progress in this field could be expected in the future.

CONCLUSIONS AND FUTURE PERSPECTIVE

In 1983, exosomes were first discovered in sheep reticulocytes, were named "exosomes" by Johnstone in 1987. Since its discovery, exosomes have always been regarded as a way for cells to excrete waste. Now, with many studies on its biological origin, material composition and transport, intercellular signal transduction, and distribution in body fluids, it has been found that exosomes have several functions. All body fluids contain exosomes, such as blood, saliva, urine, cerebrospinal fluid, and milk. Although exosomes come from a wide range of sources, their yield is very small. There are many kinds of purification methods, the most common one being ultracentrifugation, which results in large amounts of exosomes, but with low purity, and some researchers have proposed that the exosomes may contain other EVs rather than being pure exosomes. Another method is sucrose-gradient centrifugation, which generates highly pure exosomes, but the process is complicated and has a low yield. Additionally, there are filtration centrifugation, immunomagnetic beads method, PS affinity method, chromatography, etc. It is important to note that since there are multiple methods of separation and purification, there is a wide gap in the characteristics of the isolated exosomes. Therefore, a reliable and unified standard is needed to purify, separate, and characterize the exosomes.

TABLE 5 | Patents of exosomes.

Patent/Application Number	Title	Description	Tumor	Source	Therapeutic strategy	Country	Filling Year
EP3548005	Exosomes for delivery of therapeutic agents	This invention provides a method of preparing an exosome as drug delivery vehicles, and a method of making a composition which a therapeutic agent encapsulated within such an exosome, as well as methods of delivering such exosome and composition to specific tissues and organs.	/	Milk	Chemotherapy	European	2017
CN106943432	Umbilical cord mesenchymal stem cells-derived exosome and application of exosome in preparation of medicine for treating liver cancer	This invention focuses on the preparation of umbilical cord mesenchymal stem cell-derived exosome-loaded compound CP1-6, which has a significant inhibitory doing effect on hepatocellular carcinoma.	Liver cancer	Umbilical cord mesenchymal stem cells	Chemotherapy	China	2017
WO2017223186	Exosome-guided treatment of cancer	This invention is a novel assay for detecting the efficacy of cancer treatment by analyzing proteins in exosomes associated with mutations known to drive growth, metastasis, and/or proliferation.	Extensive treatment	Whole blood, serum, plasma, and urine	Immunotherapy/ chemotherapy/ RNA interference therapy	USA	2017
CN107119015	Exosome as well as preparation method and application thereof in preparing medicine for treating lung cancer	This invention provides a new preparation method that enables efficient *in vitro* exosome preparation by stimulating the cellular secretion of exosomes using KRN7000 and ATP, and the prepared exosomes have relatively good cytotoxic effects and lung antitumor activity.	Lung cancer	Umbilical cord blood cell	Immunotherapy	China	2017
CN109432427	Preparation method of tumor targeting heat therapy material taking exosome as carrier and product of preparation method	This invention provides a method of preparing a thermal therapy material with tumor-targeting ability using exosomes as carriers, the composition having photothermal efficacy and targeting lung cancer.	Lung cancer	Lung cancer cell A549	Phototherapy	China	2018
US20180193266	Exosomal compositions and methods for the treatment of disease	This invention provides an exosome composition that treats cancer by intranasal, intraoral or intratumoral administration	Extensive treatment	Bodily fluid	Chemotherapy	USA	2018
WO2019128952	Method for preparing immune cell exosome carrying chimeric antigen receptor and application thereof	The invention focuses on exosomes from chimeric antigen receptor (CAR) T cells in cancer therapy	Extensive treatment	T cell of patients	Immunotherapy	China	2019
CN110075122	Therapeutic exosome medicine for liver cancer	This invention provides an exosome with down-regulated VPS35 gene expression secreted by hepatocellular carcinoma cells, and mRNA molecule for the treatment of hepatocellular carcinoma.	Liver cancer	Liver cancer	RNA interference therapy	China	2019
WO2018151445	Exosome-based nanoparticle composite and method for preparing same	This invention provides a new exosome-based nanoparticle composite, and a method for its preparation. The nanocomposite improves *in vivo* stability and redispersibility through biocompatible polymers.	Breast cancer	RAW264.7 macrophage cell/breast cell line MDA-MB231	Chemotherapy	Korean	2019
CN110051833	Method for preparing cancer vaccine by using leukemia cell exosome	This invention is a cancer vaccine prepared using an exosome secreted by leukemia cells	Leukemia	Leukemia cell	Immunotherapy	China	2019
CN109675032	Medicament prepared from photothermal material and exosome-mediated chemotherapeutic drug and application thereof	This invention discloses a medicinal composition comprising a photothermal material and an exosome-mediated chemotherapeutic drug.	Breast cancer/ liver cancer/ cervical cancer	Breast cancer cell/liver cancer cell/ cervical cancer cell	Phototherapy and chemotherapy	China	2019

Exosomes have several advantages as drug delivery systems, such as good biocompatibility, low immunogenicity, targeting specificity, and the ability to overcome membrane barriers. Based on these characteristics, exosomes are widely used in tumor diagnosis, prognosis, treatment, and are gradually applied to clinical trials. For tumor diagnosis, TEXs carry tumor specificity markers, which can be detected by laboratory tests or imaging analysis, to achieve early detection and early treatment.

Furthermore, by analyzing the composition of TEXs, we can evaluate the short-term therapeutic effect, which would act as a reference for clinical treatment. Apart from providing an efficient and safe drug delivery system, exosomes display different synergistic effects in different tumor treatment strategies to reduce the adverse effects and improve the therapeutic effect. For example, in RNAs interference-based therapy, exosomes can not only ensure the stability of RNA but also reduce the risk of off-target effects; for chemotherapy, exosomes can not only efficiently transport drugs but also minimize drug resistance; for immunotherapy, the role of exosomes is more diverse, TEXs can be used as tumor antigens without any modification, thus activating the immune system. Moreover, exosomes derived from different sources of immune cells can not only have the same immune function as donor cells but also modulate the TME and inhibit tumor immune escape. In PDT/PTT, the exosomes can transport more photosensitizers and photothermal transducers into tumor cells. Also, as the exosome inherits the heat sensitivity of the lipid membrane, it is easy for materials to achieve endosomal escape after light. Interestingly, exosomes purified from patients themselves can be used in personalized therapy.

Brain tumors are different from other types of tumors due to the special position of the brain and the tight barrier system. Brain tumors are not easy to diagnose and even more difficult to treat. Many general tumor treatment strategies are not effective for brain tumors, and thus, the fatality rate of brain tumors remains high. The high permeability, biosafety, and exosome targeting are indispensable factors in the brain tumor treatment strategy. Many experiments have shown that the addition of exosomes to the original tumor treatment strategy can greatly improve the therapeutic efficacy of brain tumor treatment. Exosomes are like a natural ferry, which can carry the necessary substances for treatment across the BBB without destroying its integrity. Thus, the addition of exosomes might promote the treatment of brain tumors and reduce their mortality.

AUTHOR CONTRIBUTIONS

YZ and TC contributed to the conception and design of the study. YZ and PL wrote the first draft of the manuscript. HT drew the drawings and collected the data. XC, QW, and TC revised the manuscript. All authors contributed to the article and approved the submitted version.

FUNDING

Financial supports from the Guangdong Basic and Applied Basic Research Foundation (2019B1515120043), the Research Fund of University of Macau (File no. MYRG2019-00121-ICMS and MYRG2018-00207-ICMS), the Science and Technology Development Fund, Macau SAR (File no. 0098/2020/A), and the Key Project of Basic Research of Shenzhen (JCYJ20200109113603854) are gratefully acknowledged.

REFERENCES

1. Schorey JS, Cheng Y, Singh PP, Smith VL. Exosomes and Other Extracellular Vesicles in Host-Pathogen Interactions. *EMBO Rep* (2015) 16(1):24–43. doi: 10.15252/embr.201439363
2. Cocucci E, Meldolesi J. Ectosomes and Exosomes: Shedding the Confusion Between Extracellular Vesicles. *Trends Cell Biol* (2015) 25(6):364–72. doi: 10.1016/j.tcb.2015.01.004
3. Colombo M, Raposo G, Théry C. Biogenesis, Secretion, and Intercellular Interactions of Exosomes and Other Extracellular Vesicles. *Annu Rev Cell Dev Biol* (2014) 30(1):255–89. doi: 10.1146/annurev-cellbio-101512-122326
4. Kalluri R, LeBleu VS. The Biology, Function, and Biomedical Applications of Exosomes. *Science* (2020) 367(1):6478–977. doi: 10.1126/science.aau6977
5. Tang Y, Zhang P, Wang Y, Wang J, Su M, Wang Y, et al. The Biogenesis, Biology, and Clinical Significance of Exosomal PD-L1 in Cancer. *Front Immunol* (2020) 11:604. doi: 10.3389/fimmu.2020.00604
6. Kowal J, Arras G, Colombo M, Jouve M, Morath JP, Primdal-Bengtson B, et al. Proteomic Comparison Defines Novel Markers to Characterize Heterogeneous Populations of Extracellular Vesicle Subtypes. *Proc Natl Acad Sci U S A* (2016) 113(8):E968–77. doi: 10.1073/pnas.1521230113
7. Batrakova EV, Kim MS. Using Exosomes, Naturally-Equipped Nanocarriers, for Drug Delivery. *J Control Release* (2015) 219:396–405. doi: 10.1016/j.jconrel.2015.07.030
8. Kalluri R. The Biology and Function of Exosomes in Cancer. *J Clin Invest* (2016) 126(4):1208–15. doi: 10.1172/JCI81135
9. Yang XX, Sun C, Wang L, Guo XL. New Insight Into Isolation, Identification Techniques and Medical Applications of Exosomes. *J Control Release* (2019) 308:119–29. doi: 10.1016/j.jconrel.2019.07.021
10. Wang Y, Pei H, Jia Y, Liu J, Li Z, Ai K, et al. Synergistic Tailoring of Electrostatic and Hydrophobic Interactions for Rapid and Specific Recognition of Lysophosphatidic Acid, an Early-Stage Ovarian Cancer Biomarker. *J Am Chem Soc* (2017) 139(33):11616–21. doi: 10.1021/jacs.7b06885
11. Huang Q, Wu W, Ai K, Liu J. Highly Sensitive Polydiacetylene Ensembles for Biosensing and Bioimaging. *Front Chem* (2020) 8:565782. doi: 10.3389/fchem.2020.565782
12. Wang J, Sui L, Huang J, Miao L, Nie Y, Wang K, et al. MoS2-Based Nanocomposites for Cancer Diagnosis and Therapy. *Bioact Mater* (2021) 6 (11):4209–42. doi: 10.1016/j.bioactmat.2021.04.021
13. Kharaziha P, Ceder S, Li Q, Panaretakis T. Tumor Cell-Derived Exosomes: A Message in a Bottle. *Biochim Biophys Acta* (2012) 1826(1):103–11. doi: 10.1016/j.bbcan.2012.03.006
14. Hessvik NP, Llorente A. Current Knowledge on Exosome Biogenesis and Release. *Cell Mol Life Sci* (2018) 75(2):193–208. doi: 10.1007/s00018-017-2595-9
15. McAndrews KM, Kalluri R. Mechanisms Associated With Biogenesis of Exosomes in Cancer. *Mol Cancer* (2019) 18(1):52–62. doi: 10.1186/s12943-019-0963-9
16. Grad LI, Yerbury JJ, Turner BJ, Guest WC, Pokrishevsky E, O'Neill MA, et al. Intercellular Propagated Misfolding of Wild-Type Cu/Zn Superoxide Dismutase Occurs *via* Exosome-Dependent and -Independent Mechanisms. *Proc Natl Acad Sci U S A* (2014) 111(9):3620–5. doi: 10.1073/pnas.1312245111
17. Colombo M, Moita C, van Niel G, Kowal J, Vigneron J, Benaroch P, et al. Analysis of ESCRT Functions in Exosome Biogenesis, Composition and Secretion Highlights the Heterogeneity of Extracellular Vesicles. *J Cell Sci* (2013) 126(Pt 24):5553–65. doi: 10.1242/jcs.128868
18. van Niel G, D'Angelo G, Raposo G. Shedding Light on the Cell Biology of Extracellular Vesicles. *Nat Rev Mol Cell Biol* (2018) 19(4):213–28. doi: 10.1038/nrm.2017.125
19. van Niel G, Charrin S, Simoes S, Romao M, Rochin L, Saftig P, et al. The Tetraspanin CD63 Regulates ESCRT-Independent and -Dependent

Endosomal Sorting During Melanogenesis. *Dev Cell* (2011) 21(4):708–21. doi: 10.1016/j.devcel.2011.08.019
20. Maas SLN, Breakefield XO, Weaver AM. Extracellular Vesicles: Unique Intercellular Delivery Vehicles. *Trends Cell Biol* (2017) 27(3):172–88. doi: 10.1016/j.tcb.2016.11.003
21. Villarroya-Beltri C, Baixauli F, Mittelbrunn M, Fernandez-Delgado I, Torralba D, Moreno-Gonzalo O, et al. ISGylation Controls Exosome Secretion by Promoting Lysosomal Degradation of MVB Proteins. *Nat Commun* (2016) 7:13588–98. doi: 10.1038/ncomms13588
22. Mittelbrunn M, Vicente Manzanares M, Sanchez-Madrid F. Organizing Polarized Delivery of Exosomes at Synapses. *Traffic* (2015) 16(4):327–37. doi: 10.1111/tra.12258
23. Sinha S, Hoshino D, Hong NH, Kirkbride KC, Grega-Larson NE, Seiki M, et al. Cortactin Promotes Exosome Secretion by Controlling Branched Actin Dynamics. *J Cell Biol* (2016) 214(2):197–213. doi: 10.1083/jcb.201601025
24. Jahn R, Scheller RH. SNAREs–engines for Membrane Fusion. *Nat Rev Mol Cell Biol* (2006) 7(9):631–43. doi: 10.1038/nrm2002
25. Dias MV, Teixeira BL, Rodrigues BR, Sinigaglia-Coimbra R, Porto-Carreiro I, Roffe M, et al. PRNP/prion Protein Regulates the Secretion of Exosomes Modulating CAV1/caveolin-1-Suppressed Autophagy. *Autophagy* (2016) 12 (11):2113–28. doi: 10.1080/15548627.2016.1226735
26. Mulcahy LA, Pink RC, Carter DR. Routes and Mechanisms of Extracellular Vesicle Uptake. *J Extracell Vesicles* (2014) 3:24641–55. doi: 10.3402/jev.v3.24641
27. Pironti G, Strachan RT, Abraham D, Mon-Wei Yu S, Chen M, Chen W, et al. Circulating Exosomes Induced by Cardiac Pressure Overload Contain Functional Angiotensin II Type 1 Receptors. *Circulation* (2015) 131 (24):2120–30. doi: 10.1161/CIRCULATIONAHA.115.015687
28. Kamerkar S, LeBleu VS, Sugimoto H, Yang S, Ruivo CF, Melo SA, et al. Exosomes Facilitate Therapeutic Targeting of Oncogenic KRAS in Pancreatic Cancer. *Nature* (2017) 546(7659):498–503. doi: 10.1038/nature22341
29. Tian T, Zhu YL, Zhou YY, Liang GF, Wang YY, Hu FH, et al. Exosome Uptake Through Clathrin-Mediated Endocytosis and Macropinocytosis and Mediating miR-21 Delivery. *J Biol Chem* (2014) 289(32):22258–67. doi: 10.1074/jbc.M114.588046
30. Heusermann W, Hean J, Trojer D, Steib E, von Bueren S, Graff-Meyer A, et al. Exosomes Surf on Filopodia to Enter Cells at Endocytic Hot Spots, Traffic Within Endosomes, and Are Targeted to the ER. *J Cell Biol* (2016) 213: (2):173–84. doi: 10.1083/jcb.201506084
31. He C, Zheng S, Luo Y, Wang B. Exosome Theranostics: Biology and Translational Medicine. *Theranostics* (2018) 8(1):237–55. doi: 10.7150/thno.21945
32. Yu B, Kim HW, Gong M, Wang J, Millard RW, Wang Y, et al. Exosomes Secreted From GATA-4 Overexpressing Mesenchymal Stem Cells Serve as a Reservoir of Anti-Apoptotic microRNAs for Cardioprotection. *Int J Cardiol* (2015) 182:349–60. doi: 10.1016/j.ijcard.2014.12.043
33. Parolini I, Federici C, Raggi C, Lugini L, Palleschi S, De Milito A, et al. Microenvironmental pH is a Key Factor for Exosome Traffic in Tumor Cells. *J Biol Chem* (2009) 284(49):34211–22. doi: 10.1074/jbc.M109.041152
34. Keerthikumar S, Chisanga D, Ariyaratne D, Al Saffar H, Anand S, Zhao K, et al. ExoCarta: A Web-Based Compendium of Exosomal Cargo. *J Mol Biol* (2016) 428(4):688–92. doi: 10.1016/j.jmb.2015.09.019
35. Lasda E, Parker R. Circular RNAs Co-Precipitate With Extracellular Vesicles: A Possible Mechanism for circRNA Clearance. *PloS One* (2016) 11(2):e0148407–17. doi: 10.1371/journal.pone.0148407
36. Baixauli F, Lopez-Otin C, Mittelbrunn M. Exosomes and Autophagy: Coordinated Mechanisms for the Maintenance of Cellular Fitness. *Front Immunol* (2014) 5:403. doi: 10.3389/fimmu.2014.00403
37. Record M, Carayon K, Poirot M, Silvente-Poirot S. Exosomes as New Vesicular Lipid Transporters Involved in Cell-Cell Communication and Various Pathophysiologies. *Biochim Biophys Acta* (2014) 1841(1):108–20. doi: 10.1016/j.bbalip.2013.10.004
38. Becker A, Thakur BK, Weiss JM, Kim HS, Peinado H, Lyden D. Extracellular Vesicles in Cancer: Cell-To-Cell Mediators of Metastasis. *Cancer Cell* (2016) 30(6):836–48. doi: 10.1016/j.ccell.2016.10.009
39. Foster BP, Balassa T, Benen TD, Dominovic M, Elmadjian GK, Florova V, et al. Extracellular Vesicles in Blood, Milk and Body Fluids of the Female and Male Urogenital Tract and With Special Regard to Reproduction. *Crit Rev Clin Lab Sci* (2016) 53(6):379–95. doi: 10.1080/10408363.2016.1190682
40. Fruhbeis C, Frohlich D, Kuo WP, Amphornrat J, Thilemann S, Saab AS, et al. Neurotransmitter-Triggered Transfer of Exosomes Mediates Oligodendrocyte-Neuron Communication. *PloS Biol* (2013) 11(7): e1001604–22. doi: 10.1371/journal.pbio.1001604
41. Cesselli D, Parisse P, Aleksova A, Veneziano C, Cervellin C, Zanello A, et al. Extracellular Vesicles: How Drug and Pathology Interfere With Their Biogenesis and Function. *Front Physiol* (2018) 9:1394. doi: 10.3389/fphys.2018.01394
42. Greening DW, Xu R, Ji H, Tauro BJ, Simpson RJ. A Protocol for Exosome Isolation and Characterization: Evaluation of Ultracentrifugation, Density-Gradient Separation, and Immunoaffinity Capture Methods. *Proteomic Profiling. Methods Mol Biol* (2015) p:179–209. doi: 10.1007/978-1-4939-2550-6_15
43. Helwa I, Cai J, Drewry MD, Zimmerman A, Dinkins MB, Khaled ML, et al. A Comparative Study of Serum Exosome Isolation Using Differential Ultracentrifugation and Three Commercial Reagents. *PloS One* (2017) 12 (1):e0170628–49. doi: 10.1371/journal.pone.0170628
44. Taylor DD, Shah S. Methods of Isolating Extracellular Vesicles Impact Down-Stream Analyses of Their Cargoes. *Methods* (2015) 87:3–10. doi: 10.1016/j.ymeth.2015.02.019
45. Boing AN, van der Pol E, Grootemaat AE, Coumans FA, Sturk A, Nieuwland R. Single-Step Isolation of Extracellular Vesicles by Size-Exclusion Chromatography. *J Extracell Vesicles* (2014) 3:23430–40. doi: 10.3402/jev.v3.23430
46. Fitzgerald J, Leonard P, Darcy E, Sharma S, O'Kennedy R. Immunoaffinity Chromatography: Concepts and Applications. *Methods Mol Biol* (2017) 1485:27–51. doi: 10.1007/978-1-4939-6412-3_3
47. Taylor DD, Zacharias W, Gercel-Taylor C. Exosome Isolation for Proteomic Analyses and RNA Profiling. *Methods Mol Biol* (2011) 728:235–46. doi: 10.1007/978-1-61779-068-3_15
48. Zeringer E, Barta T, Li M, Vlassov AV. Strategies for Isolation of Exosomes. *Cold Spring Harb Protoc* (2015) 2015(4):319–23. doi: 10.1101/pdb.top074476
49. Liga A, Vliegenthart AD, Oosthuyzen W, Dear JW, Kersaudy-Kerhoas M. Exosome Isolation: A Microfluidic Road-Map. *Lab Chip* (2015) 15 (11):2388–94. doi: 10.1039/c5lc00240k
50. Dorayappan KDP, Gardner ML, Hisey CL, Zingarelli RA, Smith BQ, Lightfoot MDS, et al. A Microfluidic Chip Enables Isolation of Exosomes and Establishment of Their Protein Profiles and Associated Signaling Pathways in Ovarian Cancer. *Cancer Res* (2019) 79(13):3503–13. doi: 10.1158/0008-5472.CAN-18-3538
51. Hoshino A, Costa-Silva B, Shen TL, Rodrigues G, Hashimoto A, Tesic Mark M, et al. Tumour Exosome Integrins Determine Organotropic Metastasis. *Nature* (2015) 527(7578):329–35. doi: 10.1038/nature15756
52. Jalalian SH, Ramezani M, Jalalian SA, Abnous K, Taghdisi SM. Exosomes, New Biomarkers in Early Cancer Detection. *Anal Biochem* (2019) 571:1–13. doi: 10.1016/j.ab.2019.02.013
53. Cheng N, Du D, Wang X, Liu D, Xu W, Luo Y, et al. Recent Advances in Biosensors for Detecting Cancer-Derived Exosomes. *Trends Biotechnol* (2019) 37(11):1236–54. doi: 10.1016/j.tibtech.2019.04.008
54. Xiao Y, Li Y, Yuan Y, Liu B, Pan S, Liu Q, et al. The Potential of Exosomes Derived From Colorectal Cancer as a Biomarker. *Clin Chim Acta* (2019) 490:186–93. doi: 10.1016/j.cca.2018.09.007
55. Allen-Rhoades W, Kurenbekova L, Satterfield L, Parikh N, Fuja D, Shuck RL, et al. Cross-Species Identification of a Plasma microRNA Signature for Detection, Therapeutic Monitoring, and Prognosis in Osteosarcoma. *Cancer Med* (2015) 4(7):977–88. doi: 10.1002/cam4.438
56. Shen X, Xue Y, Cong H, Wang X, Ju S. Dysregulation of Serum microRNA-574-3p and Its Clinical Significance in Hepatocellular Carcinoma. *Ann Clin Biochem* (2018) 55(4):478–84. doi: 10.1177/0004563217741908
57. Li Z, Ye L, Wang L, Quan R, Zhou Y, Li X. Identification of miRNA Signatures in Serum Exosomes as a Potential Biomarker After Radiotherapy

Treatment in Glioma Patients. *Ann Diagn Pathol* (2020) 44:151436–41. doi: 10.1016/j.anndiagpath.2019.151436
58. Choi Y, Park U, Koo HJ, Park JS, Lee DH, Kim K, et al. Exosome-Mediated Diagnosis of Pancreatic Cancer Using Lectin-Conjugated Nanoparticles Bound to Selective Glycans. *Biosens Bioelectron* (2021) 177:112980–9. doi: 10.1016/j.bios.2021.112980
59. Silva AKA, Kolosnjaj-Tabi J, Bonneau S, Marangon I, Boggetto N, Kelly A, et al. Magnetic and Photoresponsive Theranosomes Translating Cell-Released Vesicles Into Smart Nanovectors for Cancer Therapy. *ACS Nano* (2013) 7(6):4954–66. doi: 10.1021/nn400269x
60. Yang Q, Cheng L, Hu L, Lou D, Zhang T, Li J, et al. An Integrative Microfluidic Device for Isolation and Ultrasensitive Detection of Lung Cancer-Specific Exosomes From Patient Urine. *Biosens Bioelectron* (2020) 163:112290–8. doi: 10.1016/j.bios.2020.112290
61. Kashefi-Kheyrabadi L, Kim J, Chakravarty S, Park S, Gwak H, Kim SI, et al. Detachable Microfluidic Device Implemented With Electrochemical Aptasensor (DeMEA) for Sequential Analysis of Cancerous Exosomes. *Biosens Bioelectron* (2020) 169:112622–30. doi: 10.1016/j.bios.2020.112622
62. Kooijmans SAA, Schiffelers RM, Zarovni N, Vago R. Modulation of Tissue Tropism and Biological Activity of Exosomes and Other Extracellular Vesicles: New Nanotools for Cancer Treatment. *Pharmacol Res* (2016) 111:487–500. doi: 10.1016/j.phrs.2016.07.006
63. Pan S, Pei L, Zhang A, Zhang Y, Zhang C, Huang M, et al. Passion Fruit-Like Exosome-PMA/Au-BSA@Ce6 Nanovehicles for Real-Time Fluorescence Imaging and Enhanced Targeted Photodynamic Therapy With Deep Penetration and Superior Retention Behavior in Tumor. *Biomaterials* (2020) 230:119606–35. doi: 10.1016/j.biomaterials.2019.119606
64. Dai W, Su L, Lu H, Dong H, Zhang X. Exosomes-Mediated Synthetic Dicer Substrates Delivery for Intracellular Dicer Imaging Detection. *Biosens Bioelectron* (2020) 151-176:111907. doi: 10.1016/j.bios.2019.111907
65. Jung KO, Jo H, Yu JH, Gambhir SS, Pratx G. Development and MPI Tracking of Novel Hypoxia-Targeted Theranostic Exosomes. *Biomaterials* (2018) 177:139–48. doi: 10.1016/j.biomaterials.2018.05.048
66. Bose RJC, Uday Kumar S, Zeng Y, Afjei R, Robinson E, Lau K, et al. Tumor Cell-Derived Extracellular Vesicle-Coated Nanocarriers: An Efficient Theranostic Platform for the Cancer-Specific Delivery of Anti-miR-21 and Imaging Agents. *ACS Nano* (2018) 12(11):10817–32. doi: 10.1021/acsnano.8b02587
67. Rehman FU, Du T, Shaikh S, Jiang X, Chen Y, Li X, et al. Nano in Nano: Biosynthesized Gold and Iron Nanoclusters Cargo Neoplastic Exosomes for Cancer Status Biomarking. *Nanomedicine* (2018) 14(8):2619–31. doi: 10.1016/j.nano.2018.07.014
68. Chen CC, Liu L, Ma F, Wong CW, Guo XE, Chacko JV, et al. Elucidation of Exosome Migration Across the Blood-Brain Barrier Model *In Vitro*. *Cell Mol Bioeng* (2016) 9(4):509–29. doi: 10.1007/s12195-016-0458-3
69. Aqil F, Munagala R, Jeyabalan J, Agrawal AK, Kyakulaga AH, Wilcher SA, et al. Milk Exosomes - Natural Nanoparticles for siRNA Delivery. *Cancer Lett* (2019) 449:186–95. doi: 10.1016/j.canlet.2019.02.011
70. Bai J, Duan J, Liu R, Du Y, Luo Q, Cui Y, et al. Engineered Targeting Tlyp-1 Exosomes as Gene Therapy Vectors for Efficient Delivery of siRNA Into Lung Cancer Cells. *Asian J Pharm Sci* (2019) 15(4):461–71. doi: 10.1016/j.ajps.2019.04.002
71. Cai H, Yang X, Gao Y, Xu Z, Yu B, Xu T, et al. Exosomal MicroRNA-9-3p Secreted From BMSCs Downregulates ESM1 to Suppress the Development of Bladder Cancer. *Mol Ther Nucleic Acids* (2019) 18:787–800. doi: 10.1016/j.omtn.2019.09.023
72. Che Y, Shi X, Shi Y, Jiang X, Ai Q, Shi Y, et al. Exosomes Derived From miR-143-Overexpressing MSCs Inhibit Cell Migration and Invasion in Human Prostate Cancer by Downregulating Tff3. *Mol Ther Nucleic Acids* (2019) 18:232–44. doi: 10.1016/j.omtn.2019.08.010
73. Ding Y, Cao F, Sun H, Wang Y, Liu S, Wu Y, et al. Exosomes Derived From Human Umbilical Cord Mesenchymal Stromal Cells Deliver Exogenous miR-145-5p to Inhibit Pancreatic Ductal Adenocarcinoma Progression. *Cancer Lett* (2019) 442:351–61. doi: 10.1016/j.canlet.2018.10.039
74. Ji R, Zhang X, Gu H, Ma J, Wen X, Zhou J, et al. miR-374a-5p: A New Target for Diagnosis and Drug Resistance Therapy in Gastric Cancer. *Mol Ther Nucleic Acids* (2019) 18:320–31. doi: 10.1016/j.omtn.2019.07.025
75. Li L, Lu S, Liang X, Cao B, Wang S, Jiang J, et al. gammadeltaTDEs: An Efficient Delivery System for miR-138 With Anti-Tumoral and Immunostimulatory Roles on Oral Squamous Cell Carcinoma. *Mol Ther Nucleic Acids* (2019) 14:101–13. doi: 10.1016/j.omtn.2018.11.009
76. Monaco F, Gaetani S, Alessandrini F, Tagliabracci A, Bracci M, Valentino M, et al. Exosomal Transfer of miR-126 Promotes the Anti-Tumour Response in Malignant Mesothelioma: Role of miR-126 in Cancer-Stroma Communication. *Cancer Lett* (2019) 463:27–36. doi: 10.1016/j.canlet.2019.08.001
77. Pomatto MAC, Bussolati B, D'Antico S, Ghiotto S, Tetta C, Brizzi MF, et al. Improved Loading of Plasma-Derived Extracellular Vesicles to Encapsulate Antitumor miRNAs. *Mol Ther Methods Clin Dev* (2019) 13:133–44. doi: 10.1016/j.omtm.2019.01.001
78. Wu DM, Wen X, Han XR, Wang S, Wang YJ, Shen M, et al. Bone Marrow Mesenchymal Stem Cell-Derived Exosomal MicroRNA-126-3p Inhibits Pancreatic Cancer Development by Targeting Adam9. *Mol Ther Nucleic Acids* (2019) 16:229–45. doi: 10.1016/j.omtn.2019.02.022
79. Kim G, Kim M, Lee Y, Byun JW, Hwang DW, Lee M. Systemic Delivery of microRNA-21 Antisense Oligonucleotides to the Brain Using T7-Peptide Decorated Exosomes. *J Control Release* (2020) 317:273–81. doi: 10.1016/j.jconrel.2019.11.009
80. Liang G, Zhu Y, Ali DJ, Tian T, Xu H, Si K, et al. Engineered Exosomes for Targeted Co-Delivery of miR-21 Inhibitor and Chemotherapeutics to Reverse Drug Resistance in Colon Cancer. *J Nanobiotechnol* (2020) 18 (1):10–24. doi: 10.1186/s12951-019-0563-2
81. Naseri Z, Oskuee RK, Forouzandeh-Moghadam M, Jaafari MR. Delivery of LNA-antimiR-142-3p by Mesenchymal Stem Cells-Derived Exosomes to Breast Cancer Stem Cells Reduces Tumorigenicity. *Stem Cell Rev Rep* (2020) 16(3):541–56. doi: 10.1007/s12015-019-09944-w
82. Zhang F, Lu Y, Wang M, Zhu J, Li J, Zhang P, et al. Exosomes Derived From Human Bone Marrow Mesenchymal Stem Cells Transfer miR-222-3p to Suppress Acute Myeloid Leukemia Cell Proliferation by Targeting IRF2/INPP4B. *Mol Cell Probes* (2020) 51:101513–20. doi: 10.1016/j.mcp.2020.101513
83. Zhao L, Gu C, Gan Y, Shao L, Chen H, Zhu H. Exosome-Mediated siRNA Delivery to Suppress Postoperative Breast Cancer Metastasis. *J Control Release* (2020) 318:1–15. doi: 10.1016/j.jconrel.2019.12.005
84. Tao H, Xu H, Zuo L, Li C, Qiao G, Guo M, et al. Exosomes-Coated Bcl-2 siRNA Inhibits the Growth of Digestive System Tumors Both *In Vitro* and *In Vivo*. *Int J Biol Macromol* (2020) 161:470–80. doi: 10.1016/j.ijbiomac.2020.06.052
85. Liang X, Li D, Leng S, Zhu X. RNA-Based Pharmacotherapy for Tumors: From Bench to Clinic and Back. *Biomed Pharmacother* (2020) 125:109997. doi: 10.1016/j.biopha.2020.109997
86. Buzdin A, Sorokin M, Garazha A, Glusker A, Aleshin A, Poddubskaya E, et al. RNA Sequencing for Research and Diagnostics in Clinical Oncology. *Semin Cancer Biol* (2020) 60:311–23. doi: 10.1016/j.semcancer.2019.07.010
87. Arnold A, Czupiel P, Shoichet M. Engineered Polymeric Nanoparticles to Guide the Cellular Internalization and Trafficking of Small Interfering Ribonucleic Acids. *J Control Release* (2017) 259:3–15. doi: 10.1016/j.jconrel.2017.02.019
88. Wittrup A, Ai A, Liu X, Hamar P, Trifonova R, Charisse K, et al. Visualizing Lipid-Formulated siRNA Release From Endosomes and Target Gene Knockdown. *Nat Biotechnol* (2015) 33(8):870–6. doi: 10.1038/nbt.3298
89. Subhan MA, Torchilin VP. Efficient Nanocarriers of siRNA Therapeutics for Cancer Treatment. *Transl Res* (2019) 214:62–91. doi: 10.1016/j.trsl.2019.07.006
90. Hacein-Bey-Abina S, Garrigue A, Wang G, Soulier J, Lim A, Morillon E, et al. Insertional Oncogenesis in 4 Patients After Retrovirus-Mediated Gene Therapy of SCID-X1. *J Clin Invest* (2008) 118(9):3132–42. doi: 10.1172/jci35700
91. Hornung V, Bauernfeind F, Halle A, Samstad E, Kono H, Rock K, et al. Silica Crystals and Aluminum Salts Activate the NALP3 Inflammasome Through Phagosomal Destabilization. *Nat Immunol* (2008) 9(8):847–56. doi: 10.1038/ni.1631
92. Zhupanyn P, Ewe A, Buch T, Malek A, Rademacher P, Muller C, et al. Extracellular Vesicle (ECV)-Modified Polyethylenimine (PEI) Complexes

for Enhanced siRNA Delivery *In Vitro* and *In Vivo*. *J Control Release* (2019) 319:63–76. doi: 10.1016/j.jconrel.2019.12.032
93. Shahabipour F, Barati N, Johnston TP, Derosa G, Maffioli P, Sahebkar A. Exosomes: Nanoparticulate Tools for RNA Interference and Drug Delivery. *J Cell Physiol* (2017) 232(7):1660–8. doi: 10.1002/jcp.25766
94. Darband SG, Mirza-Aghazadeh-Attari M, Kaviani M, Mihanfar A, Sadighparvar S, Yousefi B, et al. Exosomes: Natural Nanoparticles as Bio Shuttles for RNAi Delivery. *J Control Release* (2018) 289:158–70. doi: 10.1016/j.jconrel.2018.10.001
95. Galvanin A, Dostert G, Ayadi L, Marchand V, Velot É, Motorin Y. Diversity and Heterogeneity of Extracellular RNA in Human Plasma. *Biochimie* (2019) 164:22–36. doi: 10.1016/j.biochi.2019.05.011
96. Du B, Jiang X, Das A, Zhou Q, Yu M, Jin R, et al. Glomerular Barrier Behaves as an Atomically Precise Bandpass Filter in a Sub-Nanometre Regime. (2017) *Nat Nanotechnol* 12(11):1096–102. doi: 10.1038/nnano.2017.170
97. Choi HS, Liu W, Misra P, Tanaka E, Zimmer JP, Itty Ipe B, et al. Renal Clearance of Quantum Dots. *Nat Biotechnol* (2007) 25(10):1165–70. doi: 10.1038/nbt1340
98. Kim T, Viard M, Afonin KA, Gupta K, Popov M, Salotti J, et al. Characterization of Cationic Bolaamphiphile Vesicles for siRNA Delivery Into Tumors and Brain. *Mol Ther Nucleic Acids* (2020) 20:359–72. doi: 10.1016/j.omtn.2020.02.011
99. Agrawal AK, Aqil F, Jeyabalan J, Spencer WA, Beck J, Gachuki BW, et al. Milk-Derived Exosomes for Oral Delivery of Paclitaxel. *Nanomedicine* (2017) 13(5):1627–36. doi: 10.1016/j.nano.2017.03.001
100. Zheng Z, Li Z, Xu C, Guo B, Guo P. Folate-Displaying Exosome Mediated Cytosolic Delivery of siRNA Avoiding Endosome Trapping. *J Control Release* (2019) 311-312:43–9. doi: 10.1016/j.jconrel.2019.08.021
101. Emam SE, Abu Lila AS, Elsadek NE, Ando H, Shimizu T, Okuhira K, et al. Cancer Cell-Type Tropism is One of Crucial Determinants for the Efficient Systemic Delivery of Cancer Cell-Derived Exosomes to Tumor Tissues. *Eur J Pharm Biopharm* (2019) 145:27–34. doi: 10.1016/j.ejpb.2019.10.005
102. Yang R, Yan X, Zhang S, Guo H. Mp88-16 Targeted Exosome-Mediated Delivery of Survivin siRNA for the Treatment of Bladder Cancer. *J Urol* (2017) 197(4):e1180. doi: 10.1016/j.juro.2017.02.2741
103. Yuan D, Zhao Y, Banks WA, Bullock KM, Haney M, Batrakova E, et al. Macrophage Exosomes as Natural Nanocarriers for Protein Delivery to Inflamed Brain. *Biomaterials* (2017) 142:1–12. doi: 10.1016/j.biomaterials.2017.07.011
104. Gilligan KE, Dwyer RM. Engineering Exosomes for Cancer Therapy. *Int J Mol Sci* (2017) 18(6):1122–33. doi: 10.3390/ijms18061122
105. Kim HJ, Kim A, Miyata K, Kataoka K. Recent Progress in Development of siRNA Delivery Vehicles for Cancer Therapy. *Adv Drug Delivery Rev* (2016) 104:61–77. doi: 10.1016/j.addr.2016.06.011
106. Katakowski M, Buller B, Zheng X, Lu Y, Rogers T, Osobamiro O, et al. Exosomes From Marrow Stromal Cells Expressing miR-146b Inhibit Glioma Growth. *Cancer Lett* (2013) 335(1):201–4. doi: 10.1016/j.canlet.2013.02.019
107. Narayanan S, Cai C, Assaraf Y, Guo H, Cui Q, Wei L, et al. Targeting the Ubiquitin-Proteasome Pathway to Overcome Anti-Cancer Drug Resistance. *Drug Resist Updat* (2020) 48:100663. doi: 10.1016/j.drup.2019.100663
108. Aqil F, Munagala R, Jeyabalan J, Agrawal AK, Gupta R. Exosomes for the Enhanced Tissue Bioavailability and Efficacy of Curcumin. *AAPS J* (2017) 19 (6):1691–702. doi: 10.1208/s12248-017-0154-9
109. Munagala R, Aqil F, Jeyabalan J, Agrawal AK, Mudd AM, Kyakulaga AH, et al. Exosomal Formulation of Anthocyanidins Against Multiple Cancer Types. *Cancer Lett* (2017) 393:94–102. doi: 10.1016/j.canlet.2017.02.004
110. Jia G, Han Y, An Y, Ding Y, He C, Wang X, et al. NRP-1 Targeted and Cargo-Loaded Exosomes Facilitate Simultaneous Imaging and Therapy of Glioma *In Vitro* and *In Vivo*. *Biomaterials* (2018) 178:302–16. doi: 10.1016/j.biomaterials.2018.06.029
111. Kim MS, Haney MJ, Zhao Y, Yuan D, Deygen I, Klyachko NL, et al. Engineering Macrophage-Derived Exosomes for Targeted Paclitaxel Delivery to Pulmonary Metastases: *In Vitro* and *In Vivo* Evaluations. *Nanomedicine* (2018) 14(1):195–204. doi: 10.1016/j.nano.2017.09.011
112. Li Y, Gao Y, Gong C, Wang Z, Xia Q, Gu F, et al. A33 Antibody-Functionalized Exosomes for Targeted Delivery of Doxorubicin Against Colorectal Cancer. *Nanomedicine* (2018) 14(7):1973–85. doi: 10.1016/j.nano.2018.05.020
113. Donoso-Quezada J, Guajardo-Flores D, González-Valdéz J. Exosomes as Nanocarriers for the Delivery of Bioactive Compounds From Black Bean Extract With Antiproliferative Activity in Cancer Cell Lines. *Materials Today: Proc* (2019) 13:362–9. doi: 10.1016/j.matpr.2019.03.166
114. Rayamajhi S, Nguyen TDT, Marasini R, Aryal S. Macrophage-Derived Exosome-Mimetic Hybrid Vesicles for Tumor Targeted Drug Delivery. *Acta Biomater* (2019) 94:482–94. doi: 10.1016/j.actbio.2019.05.054
115. Tran PHL, Wang T, Yin W, Tran TTD, Nguyen TNG, Lee BJ, et al. Aspirin-Loaded Nanoexosomes as Cancer Therapeutics. *Int J Pharm* (2019) 572:118786–97. doi: 10.1016/j.ijpharm.2019.118786
116. Zhou Y, Zhou W, Chen X, Wang Q, Li C, Chen Q, et al. Bone Marrow Mesenchymal Stem Cells-Derived Exosomes for Penetrating and Targeted Chemotherapy of Pancreatic Cancer. *Acta Pharm Sin B* (2019) 10(8):1563–75. doi: 10.1016/j.apsb.2019.11.013
117. Li YJ, Wu JY, Wang JM, Hu XB, Cai JX, Xiang DX. Gemcitabine Loaded Autologous Exosomes for Effective and Safe Chemotherapy of Pancreatic Cancer. *Acta Biomater* (2020) 101:519–30. doi: 10.1016/j.actbio.2019.10.022
118. Pullan JE, Confeld MI, Osborn JK, Kim J, Sarkar K, Mallik S. Exosomes as Drug Carriers for Cancer Therapy. *Mol Pharm* (2019) 16(5):1789–98. doi: 10.1021/acs.molpharmaceut.9b00104
119. Aqil F, Kausar H, Agrawal AK, Jeyabalan J, Kyakulaga AH, Munagala R, et al. Exosomal Formulation Enhances Therapeutic Response of Celastrol Against Lung Cancer. *Exp Mol Pathol* (2016) 101(1):12–21. doi: 10.1016/j.yexmp.2016.05.013
120. Di C, Zhang Q, Wang Y, Wang F, Chen Y, Gan L, et al. Exosomes as Drug Carriers for Clinical Application. *Artif Cells Nanomed Biotechnol* (2018) 46 (sup3):S564–S70. doi: 10.1080/21691401.2018.1501381
121. Wang X, Zhang H, Bai M, Ning T, Ge S, Deng T, et al. Exosomes Serve as Nanoparticles to Deliver Anti-miR-214 to Reverse Chemoresistance to Cisplatin in Gastric Cancer. *Mol Ther* (2018) 26(3):774–83. doi: 10.1016/j.ymthe.2018.01.001
122. Wang C, Guan W, Peng J, Chen Y, Xu G, Dou H. Gene/paclitaxel Co-Delivering Nanocarriers Prepared by Framework-Induced Self-Assembly for the Inhibition of Highly Drug-Resistant Tumors. *Acta Biomater* (2020) 103:247–58. doi: 10.1016/j.actbio.2019.12.015
123. Kim MS, Haney MJ, Zhao Y, Mahajan V, Deygen I, Klyachko NL, et al. Development of Exosome-Encapsulated Paclitaxel to Overcome MDR in Cancer Cells. *Nanomedicine* (2016) 12(3):655–64. doi: 10.1016/j.nano.2015.10.012
124. Yang T, Martin P, Fogarty B, Brown A, Schurman K, Phipps R, et al. Exosome Delivered Anticancer Drugs Across the Blood-Brain Barrier for Brain Cancer Therapy in Danio Rerio. *Pharm Res* (2015) 32(6):2003–14. doi: 10.1007/s11095-014-1593-y
125. Munoz J, Bliss S, Greco S, Ramkissoon S, Ligon K, Rameshwar P. Delivery of Functional Anti-miR-9 by Mesenchymal Stem Cell-Derived Exosomes to Glioblastoma Multiforme Cells Conferred Chemosensitivity. *Mol Ther Nucleic Acids* (2013) 2:e126. doi: 10.1038/mtna.2013.60
126. Kalantari Khandani N, Ghahremanloo A, Hashemy SI. Role of Tumor Microenvironment in the Regulation of PD-L1: A Novel Role in Resistance to Cancer Immunotherapy. *J Cell Physiol* (2020) 235(10):6496–506. doi: 10.1002/jcp.29671
127. Syn N, Wang L, Sethi G, Thiery JP, Goh BC. Exosome-Mediated Metastasis: From Epithelial-Mesenchymal Transition to Escape From Immunosurveillance. *Trends Pharmacol Sci* (2016) 37(7):606–17. doi: 10.1016/j.tips.2016.04.006
128. Kothandan VK, Kothandan S, Kim DH, Byun Y, Lee YK, Park IK, et al. Crosstalk Between Stress Granules, Exosomes, Tumour Antigens, and Immune Cells: Significance for Cancer Immunity. *Vaccines (Basel)* (2020) 8(2):172–89. doi: 10.3390/vaccines8020172
129. Wahlund CJE, Güclüler G, Hiltbrunner S, Veerman RE, Näslund TI, Gabrielsson S. Exosomes From Antigen-Pulsed Dendritic Cells Induce Stronger Antigen-Specific Immune Responses Than Microvesicles. *In Vivo. Sci Rep* (2017) 7(1):17095–103. doi: 10.1038/s41598-017-16609-6
130. Shoae-Hassani A, Hamidieh AA, Behfar M, Mohseni R, Mortazavi-Tabatabaei SA, Asgharzadeh S. NK Cell-Derived Exosomes From NK Cells Previously Exposed to Neuroblastoma Cells Augment the Antitumor Activity of Cytokine-Activated NK Cells. *J Immunother* (2017) 40(7):265–76. doi: 10.1097/cji.0000000000000179

131. Koh E, Lee EJ, Nam GH, Hong Y, Cho E, Yang Y, et al. Exosome-SIRPalpha, a CD47 Blockade Increases Cancer Cell Phagocytosis. *Biomaterials* (2017) 121:121–9. doi: 10.1016/j.biomaterials.2017.01.004
132. Liu H, Chen L, Liu J, Meng H, Zhang R, Ma L, et al. Co-Delivery of Tumor-Derived Exosomes With Alpha-Galactosylceramide on Dendritic Cell-Based Immunotherapy for Glioblastoma. *Cancer Lett* (2017) 411:182–90. doi: 10.1016/j.canlet.2017.09.022
133. Lu Z, Zuo B, Jing R, Gao X, Rao Q, Liu Z, et al. Dendritic Cell-Derived Exosomes Elicit Tumor Regression in Autochthonous Hepatocellular Carcinoma Mouse Models. *J Hepatol* (2017) 67(4):739–48. doi: 10.1016/j.jhep.2017.05.019
134. Xiao L, Erb U, Zhao K, Hackert T, Zoller M. Efficacy of Vaccination With Tumor-Exosome Loaded Dendritic Cells Combined With Cytotoxic Drug Treatment in Pancreatic Cancer. *Oncoimmunology* (2017) 6(6):e1319044–88. doi: 10.1080/2162402X.2017.1319044
135. Chen S, Lv M, Fang S, Ye W, Gao Y, Xu Y. Poly(I:C) Enhanced Anti-Cervical Cancer Immunities Induced by Dendritic Cells-Derived Exosomes. *Int J Biol Macromol* (2018) 113:1182–7. doi: 10.1016/j.ijbiomac.2018.02.034
136. Shengbin S, Quan R, Chuangnian Z, Xiuyuan Z, Qin Y, Niu Z. Dendritic Cells Pulsed With Exosomes in Combination With PD-1 Antibody Increase the Efficacy of Sorafenib in Hepatocellular Carcinoma Model. *Trans Oncol* (2018) 11(2):250–8. doi: 10.1016/j.tranon.2018.01.001
137. Yu G, Jung H, Kang YY, Mok H. Comparative Evaluation of Cell- and Serum-Derived Exosomes to Deliver Immune Stimulators to Lymph Nodes. *Biomaterials* (2018) 162:71–81. doi: 10.1016/j.biomaterials.2018.02.003
138. Zhu L, Oh JM, Gangadaran P, Kalimuthu S, Baek SH, Jeong SY, et al. Targeting and Therapy of Glioblastoma in a Mouse Model Using Exosomes Derived From Natural Killer Cells. *Front Immunol* (2018) 9:824. doi: 10.3389/fimmu.2018.00824
139. Xu HY, Li N, Yao N, Xu XF, Wang HX, Liu XY, et al. CD8+ T Cells Stimulated by Exosomes Derived From RenCa Cells Mediate Specific Immune Responses Through the FasL/Fas Signaling Pathway and, Combined With GMCSF and IL12, Enhance the Antirenal Cortical Adenocarcinoma Effect. *Oncol Rep* (2019) 42(2):866–79. doi: 10.3892/or.2019.7208
140. Shi X, Cheng Q, Hou T, Han M, Smbatyan G, Lang JE, et al. Genetically Engineered Cell-Derived Nanoparticles for Targeted Breast Cancer Immunotherapy. *Mol Ther* (2020) 28(2):536–47. doi: 10.1016/j.ymthe.2019.11.020
141. Zuo B, Qi H, Lu Z, Chen L, Sun B, Yang R, et al. Alarmin-Painted Exosomes Elicit Persistent Antitumor Immunity in Large Established Tumors in Mice. *Nat Commun* (2020) 11(1):1790–805. doi: 10.1038/s41467-020-15569-2
142. Zhou W, Zhou Y, Chen X, Ning T, Chen H, Guo Q, et al. Pancreatic Cancer-Targeting Exosomes for Enhancing Immunotherapy and Reprogramming Tumor Microenvironment. *Biomaterials* (2021) 268:120546. doi: 10.1016/j.biomaterials.2020.120546
143. Veerman RE, Güçlüler Akpinar G, Eldh M, Gabrielsson S. Immune Cell-Derived Extracellular Vesicles – Functions and Therapeutic Applications. *Trends Mol Med* (2019) 25(5):382–94. doi: 10.1016/j.molmed.2019.02.003
144. Dutta A. Exosomes-Based Cell-Free Cancer Therapy: A Novel Strategy for Targeted Therapy. *Immunol Med* (2021) 44(2):116–23. doi: 10.1080/25785826.2020.1818482
145. Nam GH, Choi Y, Kim GB, Kim S, Kim SA, Kim IS. Emerging Prospects of Exosomes for Cancer Treatment: From Conventional Therapy to Immunotherapy. *Adv Mater* (2020) 32(51):e2002440. doi: 10.1002/adma.202002440
146. Hong CS, Sharma P, Yerneni SS, Simms P, Jackson EK, Whiteside TL, et al. Circulating Exosomes Carrying an Immunosuppressive Cargo Interfere With Cellular Immunotherapy in Acute Myeloid Leukemia. *Sci Rep* (2017) 7(1):14684–93. doi: 10.1038/s41598-017-14661-w
147. Whiteside TL. Exosomes Carrying Immunoinhibitory Proteins and Their Role in Cancer. *Clin Exp Immunol* (2017) 189(3):259–67. doi: 10.1111/cei.12974
148. Besse B, Charrier M, Lapierre V, Dansin E, Lantz O, Planchard D, et al. Dendritic Cell-Derived Exosomes as Maintenance Immunotherapy After First Line Chemotherapy in NSCLC. *Oncoimmunology* (2016) 5(4):e1071008–51. doi: 10.1080/2162402X.2015.1071008
149. Pitt JM, Andre F, Amigorena S, Soria JC, Eggermont A, Kroemer G, et al. Dendritic Cell-Derived Exosomes for Cancer Therapy. *J Clin Invest* (2016) 126(4):1224–32. doi: 10.1172/JCI81137
150. Bell BM, Kirk ID, Hiltbrunner S, Gabrielsson S, Bultema JJ. Designer Exosomes as Next-Generation Cancer Immunotherapy. *Nanomedicine* (2016) 12(1):163–9. doi: 10.1016/j.nano.2015.09.011
151. Gehrmann U, Naslund TI, Hiltbrunner S, Larssen P, Gabrielsson S. Harnessing the Exosome-Induced Immune Response for Cancer Immunotherapy. *Semin Cancer Biol* (2014) 28:58–67. doi: 10.1016/j.semcancer.2014.05.003
152. Yan W, Jiang S. Immune Cell-Derived Exosomes in the Cancer-Immunity Cycle. *Trends Cancer* (2020) 6(6):506–17. doi: 10.1016/j.trecan.2020.02.013
153. Kurywchak P, Tavormina J, Kalluri R. The Emerging Roles of Exosomes in the Modulation of Immune Responses in Cancer. *Genome Med* (2018) 10(1):23–6. doi: 10.1186/s13073-018-0535-4
154. Syn NL, Wang L, Chow EK, Lim CT, Goh BC. Exosomes in Cancer Nanomedicine and Immunotherapy: Prospects and Challenges. *Trends Biotechnol* (2017) 35(7):665–76. doi: 10.1016/j.tibtech.2017.03.004
155. Tran TH, Mattheolabakis G, Aldawsari H, Amiji M. Exosomes as Nanocarriers for Immunotherapy of Cancer and Inflammatory Diseases. *Clin Immunol* (2015) 160(1):46–58. doi: 10.1016/j.clim.2015.03.021
156. Kim SM, Yang Y, Oh SJ, Hong Y, Seo M, Jang M. Cancer-Derived Exosomes as a Delivery Platform of CRISPR/Cas9 Confer Cancer Cell Tropism-Dependent Targeting. *J Control Release* (2017) 266:8–16. doi: 10.1016/j.jconrel.2017.09.013
157. Kibria G, Ramos EK, Wan Y, Gius DR, Liu H. Exosomes as a Drug Delivery System in Cancer Therapy: Potential and Challenges. *Mol Pharm* (2018) 15(9):3625–33. doi: 10.1021/acs.molpharmaceut.8b00277
158. Koyama Y, Ito T, Hasegawa A, Eriguchi M, Inaba T, Ushigusa T, et al. Exosomes Derived From Tumor Cells Genetically Modified to Express Mycobacterium Tuberculosis Antigen: A Novel Vaccine for Cancer Therapy. *Biotechnol Lett* (2016) 38(11):1857–66. doi: 10.1007/s10529-016-2185-1
159. Morishita M, Takahashi Y, Matsumoto A, Nishikawa M, Takakura Y. Exosome-Based Tumor Antigens-Adjuvant Co-Delivery Utilizing Genetically Engineered Tumor Cell-Derived Exosomes With Immunostimulatory CpG DNA. *Biomaterials* (2016) 111:55–65. doi: 10.1016/j.biomaterials.2016.09.031
160. Huang L, Zhang X, Wang M, Chen Z, Yan Y, Gu W, et al. Exosomes From Thymic Stromal Lymphopoietin-Activated Dendritic Cells Promote Th2 Differentiation Through the OX40 Ligand. *Pathobiol* (2019) 86:111–7. doi: 10.1159/000493013
161. Behzadi E, Hosseini HM, Halabian R, Fooladi AAI. Macrophage Cell-Derived Exosomes/Staphylococcal Enterotoxin B Against Fibrosarcoma Tumor. *Microb Pathog* (2017) 111:132–8. doi: 10.1016/j.micpath.2017.08.027
162. Tay N, Lee D, Chua Y, Prabhu N, Gascoigne N, Kemeny D. CD40L Expression Allows CD8 T Cells to Promote Their Own Expansion and Differentiation Through Dendritic Cells. *Front Immunol* (2017) 8:1484. doi: 10.3389/fimmu.2017.01484
163. Rao Q, Zuo B, Lu Z, Gao X, You A, Wu C, et al. Tumor-Derived Exosomes Elicit Tumor Suppression in Murine Hepatocellular Carcinoma Models and Humans *In Vitro*. *Hepatology* (2016) 64(2):456–72. doi: 10.1002/hep.28549
164. Gu X, Erb U, Buchler MW, Zoller M. Improved Vaccine Efficacy of Tumor Exosome Compared to Tumor Lysate Loaded Dendritic Cells in Mice. *Int J Cancer* (2015) 136(4):E74–84. doi: 10.1002/ijc.29100
165. Chen W, Jiang J, Xia W, Huang J. Tumor-Related Exosomes Contribute to Tumor-Promoting Microenvironment: An Immunological Perspective. *J Immunol Res* (2017) 2017:1073947. doi: 10.1155/2017/1073947
166. Whiteside TL. Exosomes and Tumor-Mediated Immune Suppression. *J Clin Invest* (2016) 126(4):1216–23. doi: 10.1172/JCI81136
167. Olejarz W, Dominiak A, Zolnierzak A, Kubiak-Tomaszewska G, Lorenc T. Tumor-Derived Exosomes in Immunosuppression and Immunotherapy. *J Immunol Res* (2020) 2020:6272498. doi: 10.1155/2020/6272498
168. Wen C, Seeger RC, Fabbri M, Wang L, Wayne AS, Jong AY. Biological Roles and Potential Applications of Immune Cell-Derived Extracellular Vesicles. *J Extracell Vesicles* (2017) 6(1):1400370. doi: 10.1080/20013078.2017.1400370
169. Veerman RE, Gucluler Akpinar G, Eldh M, Gabrielsson S. Immune Cell-Derived Extracellular Vesicles - Functions and Therapeutic Applications. *Trends Mol Med* (2019) 25(5):382–94. doi: 10.1016/j.molmed.2019.02.003

170. Wu M, Wang G, Hu W, Yao Y, Yu XF. Emerging Roles and Therapeutic Value of Exosomes in Cancer Metastasis. *Mol Cancer* (2019) 18(1):53. doi: 10.1186/s12943-019-0964-8
171. Liu Y, Gu Y, Cao X. The Exosomes in Tumor Immunity. *Oncoimmunology* (2015) 4(9):e1027472. doi: 10.1080/2162402X.2015.1027472
172. Bu N, Wu H, Zhang G, Zhan S, Zhang R, Sun H, et al. Exosomes From Dendritic Cells Loaded With Chaperone-Rich Cell Lysates Elicit a Potent T Cell Immune Response Against Intracranial Glioma in Mice. *J Mol Neurosci* (2015) 56(3):631–43. doi: 10.1007/s12031-015-0506-9
173. Chen J, Fan T, Xie Z, Zeng Q, Xue P, Zheng T, et al. Advances in Nanomaterials for Photodynamic Therapy Applications: Status and Challenges. *Biomaterials* (2020) 237:119827. doi: 10.1016/j.biomaterials.2020.119827
174. Yang W, Liang H, Ma S, Wang D, Huang J. Gold Nanoparticle Based Photothermal Therapy: Development and Application for Effective Cancer Treatment. *Sustain Materials Technol* (2019) 19(7):1979–94. doi: 10.1016/j.susmat.2019.e00109
175. Cheng H, Fan JH, Zhao LP, Fan GL, Zheng RR, Qiu XZ, et al. Chimeric Peptide Engineered Exosomes for Dual-Stage Light Guided Plasma Membrane and Nucleus Targeted Photodynamic Therapy. *Biomaterials* (2019) 211:14–24. doi: 10.1016/j.biomaterials.2019.05.004
176. Jang Y, Kim H, Yoon S, Lee H, Hwang J, Jung J, et al. Exosome-Based Photoacoustic Imaging Guided Photodynamic and Immunotherapy for the Treatment of Pancreatic Cancer. *J Control Release* (2021) 330:293–304. doi: 10.1016/j.jconrel.2020.12.039
177. Zhang D, Qin X, Wu T, Qiao Q, Song Q, Zhang Z. Extracellular Vesicles Based Self-Grown Gold Nanopopcorn for Combinatorial Chemo-Photothermal Therapy. *Biomaterials* (2019) 197:220–8. doi: 10.1016/j.biomaterials.2019.01.024
178. Cao Y, Wu T, Zhang K, Meng X, Dai W, Wang D, et al. Engineered Exosome-Mediated Near-Infrared-II Region V2C Quantum Dot Delivery for Nucleus-Target Low-Temperature Photothermal Therapy. *ACS Nano* (2019) 13(2):1499–510. doi: 10.1021/acsnano.8b07224
179. Huda MN, Nafiujjaman M, Deaguero IG, Okonkwo J, Hill ML, Kim T, et al. Potential Use of Exosomes as Diagnostic Biomarkers and in Targeted Drug Delivery: Progress in Clinical and Preclinical Applications. *ACS Biomater Sci Eng* (2021) 7(6):2106–49. doi: 10.1021/acsbiomaterials.1c00217

Conflict of Interest: The authors declare that the research was conducted in the absence of any commercial or financial relationships that could be construed as a potential conflict of interest.

Publisher's Note: All claims expressed in this article are solely those of the authors and do not necessarily represent those of their affiliated organizations, or those of the publisher, the editors and the reviewers. Any product that may be evaluated in this article, or claim that may be made by its manufacturer, is not guaranteed or endorsed by the publisher.

Copyright © 2021 Zhao, Liu, Tan, Chen, Wang and Chen. This is an open-access article distributed under the terms of the Creative Commons Attribution License (CC BY). The use, distribution or reproduction in other forums is permitted, provided the original author(s) and the copyright owner(s) are credited and that the original publication in this journal is cited, in accordance with accepted academic practice. No use, distribution or reproduction is permitted which does not comply with these terms.

frontiers in Oncology

ORIGINAL RESEARCH
published: 26 August 2021
doi: 10.3389/fonc.2021.741383

Facile Synthesis of Holmium-Based Nanoparticles as a CT and MRI Dual-Modal Imaging for Cancer Diagnosis

Tianqi Zhang[1], Mo Deng[2], Lei Zhang[3], Zerun Liu[4], Yang Liu[5], Shuyan Song[5], Tingting Gong[1] and Qinghai Yuan[1]**

[1] Department of Radiology, The Second Hospital of Jilin University, Changchun, China, [2] Department of Clinical Laboratory, The Second Hospital of Jilin University, Changchun, China, [3] Department of Neurology, The Second Hospital of Jilin University, Changchun, China, [4] Department of Clinical Pharmacy, Jilin University School of Pharmaceutical Science, Changchun, China, [5] State Key Laboratory of Rare Earth Resource Utilization, Changchun Institute of Applied Chemistry, Chinese Academy of Sciences, Changchun, China

OPEN ACCESS

Edited by:
Kelong Ai,
Central South University, China

Reviewed by:
Zhen Liu,
Beijing University of Chemical Technology, China
Yunlu Dai,
University of Macau, China

***Correspondence:**
Tingting Gong
gongtt01@jlu.edu.cn
Qinghai Yuan
yqh@jlu.edu.cn

Specialty section:
This article was submitted to Pharmacology of Anti-Cancer Drugs, a section of the journal Frontiers in Oncology

Received: *14 July 2021*
Accepted: *03 August 2021*
Published: *26 August 2021*

Citation:
Zhang T, Deng M, Zhang L, Liu Z, Liu Y, Song S, Gong T and Yuan Q (2021) Facile Synthesis of Holmium-Based Nanoparticles as a CT and MRI Dual-Modal Imaging for Cancer Diagnosis. Front. Oncol. 11:741383. doi: 10.3389/fonc.2021.741383

The rapid development of medical imaging has boosted the abilities of modern medicine. As single modality imaging limits complex cancer diagnostics, dual-modal imaging has come into the spotlight in clinical settings. The rare earth element Holmium (Ho) has intrinsic paramagnetism and great X-ray attenuation due to its high atomic number. These features endow Ho with good potential to be a nanoprobe in combined x-ray computed tomography (CT) and T_2-weighted magnetic resonance imaging (MRI). Herein, we present a facile strategy for preparing HoF_3 nanoparticles (HoF_3 NPs) with modification by PEG 4000. The functional PEG-HoF_3 NPs have good water solubility, low cytotoxicity, and biocompatibility as a dual-modal contrast agent. Currently, there is limited systematic and intensive investigation of Ho-based nanomaterials for dual-modal imaging. Our PEG-HoF_3 NPs provide a new direction to realize *in vitro* and *vivo* CT/MRI imaging, as well as validation of Ho-based nanomaterials will verify their potential for biomedical applications.

Keywords: nanomaterial, cancer, diagnosis, dual-model imaging, contrast agent

INTRODUCTION

Imaging technology plays an important role in modern medicine due to its ability to provide noninvasive but detailed information of anatomical structure and functional activities during the progress of a disease. However, single-model imaging methods cannot always meet the criteria for diagnosing co2mplex diseases (1, 2); thus, multi-modal imaging has become the new direction for imaging technology development (3–6). There are two main means to achieve multi-modal imaging (1): endow one device with multiple imaging capabilities; or (2) construct multi-modal contrast agents (CAs) for diagnosis. Conflicts between various methods and high costs have limited the feasibility of the first method. Hence, researchers are focusing their efforts on developing multi-modal CAs that can be widely used in magnetic resonance imaging (MRI), X-ray computed tomography (CT), as well as fluorescence imaging (FI) (7–13). Due to the penetrative limitation of FI *in vivo*, CT and MRI are more commonly applied for clinical diagnosis (14–17). CT is the most cost-effective examination and offers strong X-ray penetration, which has very high resolution for bone and calcification but poor resolution for soft tissue. Notably, MRI can remedy this

shortcoming. Therefore, the combination of CT and MRI can significantly improve diagnostic ability (2, 18–24).

At present, CT and MRI examinations are used independently in clinical settings. Small iodinated molecule nanomaterials are routinely applied as CT CAs to assist in disease diagnosis. Due to the lack of X-ray absorption, a very large amount of such CAs for intravenous injection is needed to meet the contrast requirement, usually 80-150 ml per adult for angiography (25, 26). Such a high dose is not only likely to cause allergy, but it can also lead to irreversible renal damage (27–29). Furthermore, as small molecular iodide is quickly excreted by the kidney, its short circulation lifetime can affect imaging quality for certain diseases. Similarly, MRI has its own limitations. Gd-chelates are the most commonly used commercial MRI CAs in clinical settings. However, Gd-based CAs can accumulate in the central nervous system and lead to renal fibrosis (30). Another notable disadvantage of MRI is that the optimum magnetic field strength for current Gd-based CAs is less than 1.0 T (31), whereas the trend in clinical MRI is to use ultra-high magnetic fields of 7.0 T or even higher because of the better imaging quality (32). 7.0 T MRI has been available in the market since 2017, and ultra-high field strength MRI equipment will become mainstream in the future. As a result, several researchers have been focusing on developing new CAs to suit this powerful visualization tool. Tb, Ho, and Dy are the elements with the largest magnetic moments in the periodic table and can cause considerable transverse relaxation of hydrogen protons in free water. Thus, Tb, Ho, and Dy-based materials are the best choices for ultra-high field T_2 CAs (33–36). Against the background of continuous pursuit of ultra-high field intensity MRI, research on MRI CAs based on large magnetic moment elements is likely to experience rapid growth in the near future. Thus, we developed a facile strategy to construct control-sized PEGylated HoF_3 nanoparticles (PEG-HoF_3 NPs) as a dual-modal imaging CA. **Scheme 1**. illustrates the design of our study. We used a facile one-pot solvothermal approach to obtain Ho-based nanomaterial, which has a high X-ray attenuation and large magnetic moment. PEG-HoF_3 NPs offer great biocompatibility and low cytotoxicity due to the existence of poly(ethylene glycol) (PEG). As a result, these NPs could be used as CT/MRI dual-modal imaging CAs both *in vitro* and *in vivo*, confirming the potential of Ho-based nanomaterials for bioapplication research.

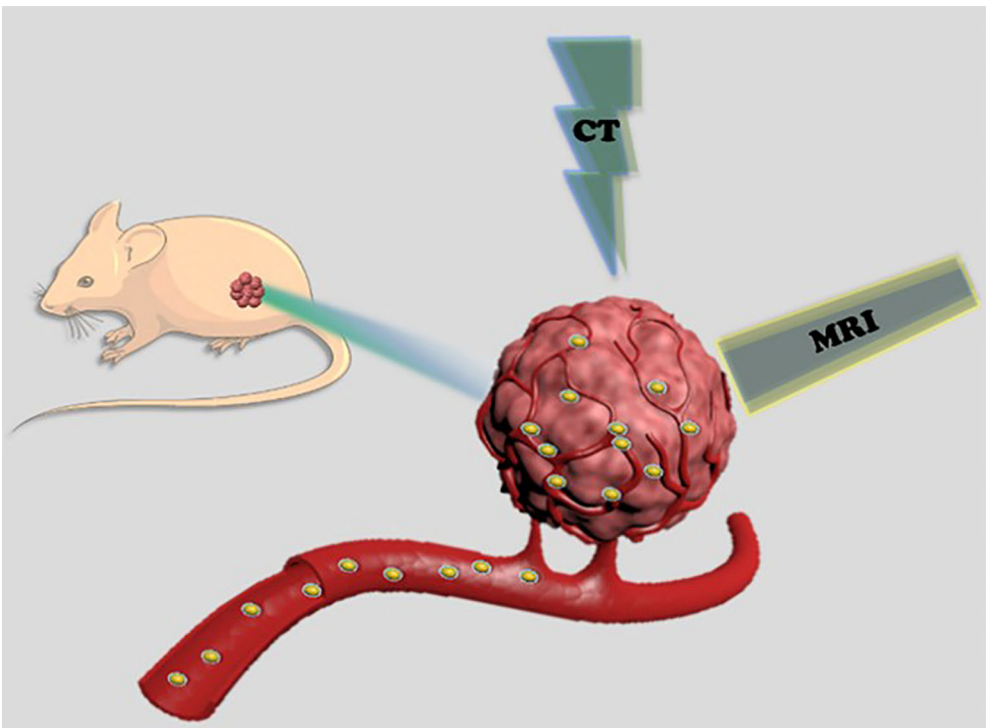
MATERIALS AND METHODS

Chemicals

$HoCl_3{\bullet}6H_2O$, poly(ethylene glycol) (PEG, MW = 4000 Da) was obtained from Sigma-Aldrich. NH_4F and ethylene glycol (EG) were obtained from Beijing Chemicals. Dimethyl sulfoxide (DMSO) were obtained from Sigma-Aldrich. DMEM and FBS were purchased from Gibco.

Preparation of PEG-HoF_3 NPs

PEG-HoF_3 NPs were fabricated *via* a one-pot solvothermal method. Firstly, 0.8 mmol $HoCl_3{\bullet}6H_2O$ was dissolved in 5 mL



SCHEME 1 | Schematic illustration of PEG-HoF_3 NPs for enhanced CT and T_2-weighted duel-model imaging.

of EG to form a clear solution. Then, 0.6 g of PEG 4000 was added to 15 mL of EG to form a clear solution. Next, prepared EG with 2.4 mmol NH_4F added to the mixture of above two solutions. This mixed solutions were vigorously stirred for about 40 min and then transferred to a 50 mL Teflon-lined autoclave and kept at 200°C for 10 h. When the system was cooled down, all collected NPs were washed several times.

In Vitro Cytotoxicity Assessment

Human cervix cancer cells (HeLa) and mouse fibroblast cells (L929) were cultured in DMEM with 10% FBS, 1% penicillin, and 1% streptomycin at a 37°C in a 5% CO_2 incubator. After incubation in 96-well cell culture plates for 24 h, different concentrations of PEG-HoF_3 NPs (0, 25, 50, 100, 200, 300 μg/mL) were added to the HeLa cells and L929 cells and incubated for another 24 h. Next, 10 μL (5 mg/mL) MTT was added to 96-well cell culture plates and kept for an additional 4 h at 37°C. Finally, the medium was removed and DMSO was added for 15 min to dissolve the formazan. The absorbance peak at 570 nm was measured by a microplate reader.

Histological and Hematology Assessment

Kunming mice (18-25 g) were obtained from the Center for Experimental Animals, Jilin University (Changchun, China). All operations are carried out in accordance with relevant national regulations. For histological assessment, 100 μL PEG-HoF_3 NPs (300 μg/mL) and 100 μL 0.9% NaCl solution were administered to Kunming mice *via* tail vein. After 30 days, Major organs and tissues (heart, liver, spleen, lung, kidney, and muscle) were collected. All tissues samples were formalin-fixed, paraffin-embedded, and stained with H&E. Tissue sections were observed under an optical microscope (×10). Blood samples were also obtained from the PEG-HoF_3 NPs and NaCl injected mouse groups for routine blood testing and biochemical indices testing.

CT Imaging

Different concentration of PEG-HoF_3 NPs and Iohexol aqueous solutions (I or Ho 0, 0.25, 0.5, 1, 2, 4 mmol/mL) were prepared for *in vitro* CT imaging. When the suitable con-centration was determined, *in vivo* CT images were obtained on Kunming mice. After intraperitoneal anesthesia with chloral hydrate, 100 μL PEG-HoF_3 NPs (2 mg/mL) were injected into these mice *via* tail vein and images were obtained at different times (0, 1, 2, 6, 12, 24 h). CT was performed using a clinical CT scanner, and the parameters were tube voltage of 120 kVp, tube current of 300 mAs, 0.9 mm thickness, 0.99 pitch, window width of 200 HU, and window level of 45 HU.

T_2-Weighted MRI

Different concentrations of PEG-HoF_3 NPs aqueous solutions (Ho 0, 0.0625, 0.125, 0.25, 0.5, 1 mmol/mL) were prepared for *in vitro* T_2-weighted MRI. Preliminary preparation was similar to the above steps. MRI was performed on a clinical MR scanner. 100 uL PEG-HoF_3 NPs (0.8 mg/mL) were injected into mice as above. These mice were scanned pre-injection and 1, 2, 4, 12, and 24 h post-injection. The MR scanner parameters were TR=7279.7 ms, TE=113 ms and FOV=240x240 mm.

RESULTS AND DISCUSSION

Preparation and Characterization of PEG-HoF_3 NPs

Uniform HoF_3 NPs were prepared through a one-pot solvothermal method using PEG 4000 as a surfactant, as illustrated in **Figure 1A**. The TEM images demonstrate the good dispersivity of PEG-HoF_3 NPs, and the existence of Ho and F element is proved by HADDF-STEM image and EDS mapping (**Figures 1B–F**), and the high-resolution TEM image shows that the width of lattice fringes about PEG-HoF_3 NPs was 0.3401 nm. The SEM image shows the spherical nanoparticles with an average diameter of 38 nm; the diameter of PEG-HoF_3 NPs was normally distributed in the range of 30–55 nm (**Figure S1**). In order to ascertain the hydrodynamic diameters of PEG-HoF_3 NPs, the dynamic light scattering (DLS) was performed, and the results show the average hydrodynamic diameter are suitable for using in organism in different solvents (**Figure 2A**). Meanwhile, the Zeta potential of PEG-HoF_3 NPs was 5.83 mV with the decoration of PEG. These value are suitable for nanomaterial which will be applied *in vivo*. XRD analysis exhibited several strong peaks, which indicated the highly crystalline nanostructure of this material. The diffraction peaks of the nanoparticles can be indexed to orthorhombic HoF_3, which matches the card (PDF 00-023-0284) in **Figure 2B** (34). XPS spectra verified that the NPs contained Ho 4d, F 1s (**Figures 2C, D**), further confirming the existence of HoF_3 NPs. The peaks of C and O confirmed the presence of PEG (**Figure S2**). The peak in 3391 cm^{-1} of FTIR spectrum further confirm the existence of PEG (**Figure S3**). Due to the low toxicity and bio-tolerability of PEG, it was approved for use in biopharmaceuticals by the US FDA several years ago (37, 38). Using PEG 4000 to modify the surface of HoF_3 NPs not only reduced cytotoxicity, but also enhanced dispersibility in water and phosphate-buffered saline (PBS) solution. The picture shows good stability of PEG-HoF_3 NPs in normal saline and PBS solution (**Figure S4**). There was no obvious Ho^{3+} ion dissociation after long-term dialysis in PBS solution (pH=7.4) with PEG-HoF_3 NPs.

Biocompatibility Assessment of PEG-HoF_3 NPs

Biocompatibility assessment should be carried out before nanomaterial imaging probes are applied *in vivo*. Due to the lack of data about the application of Ho-based nanomaterial *in vivo*, we carried out a variety of tests to assess the safety of PEG-HoF_3 NPs. The cytotoxicity of PEG-HoF_3 NPs was evaluated by the MTT cell proliferation assay. We chose HeLa and L929 cells to evaluate the toxicity of the new Ho-based nanomaterial by observing damage in cancer cells and normal cells, respectively. The cell viability results are depicted in **Figures 3A, B**. The two cell types were exposed to PEG-HoF_3 NPs at different extracellular

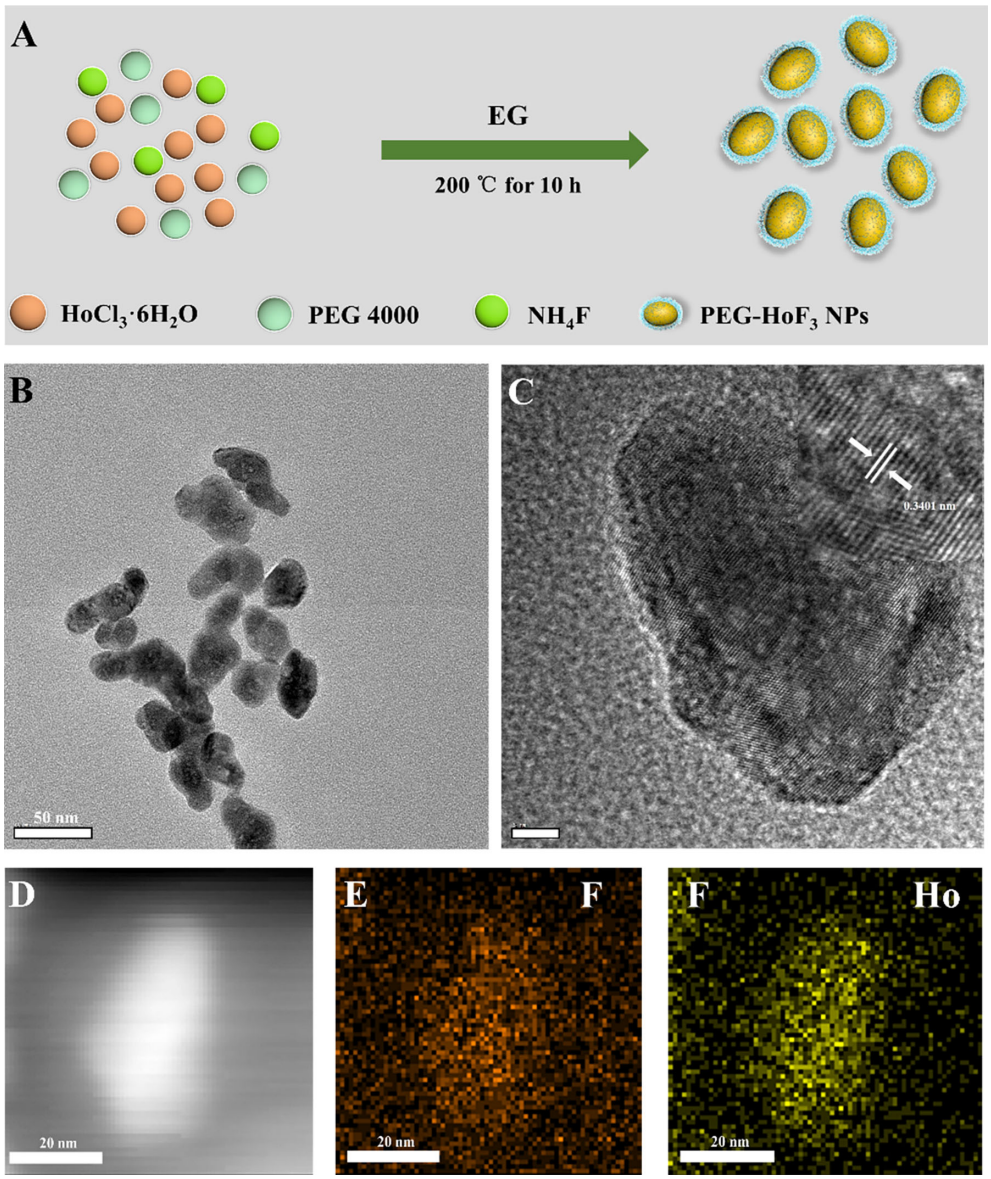


FIGURE 1 | **(A)** The synthetic process of PEG-HoF_3 NPs; **(B, C)** TEM image of PEG-HoF_3 NPs, the particles size is about 30-40nm and its lattice fringes; **(D–F)**. HADDF-STEM image of PEG-HoF_3 and EDS mapping of F, Ho element.

concentrations (0-300 μg/mL). As expected, the new PEGylated Ho-based nanoparticles had great biocompatibility. Cell viability was still about 85% of the highest concentration (300 μg/mL) in both cell strains. We further investigated histological damage caused by PEG-HoF_3 NPs through long-term toxicity assessment. Thirty days after injection, the two groups' mice were sacrificed. The main organs and tissues (heart, liver, spleen, lung, kidney, and muscle) underwent H&E staining for histopathological assessment.

Paraffin sections conformed that there was no significant damage or severe inflammation in organs or tissues in either the control group or PEG-HoF_3 NPs injection group (**Figure 3C**). Encouraged by these results, quantitative analysis of PEG-HoF_3 NPs potential toxicity was carried out *via* blood testing and biochemical examination. Routine blood tests can be used to observe changes in the distribution of blood cells to judge the condition of mice, and biochemical examination can be used to detect various products of metabolism in blood to show the condition of organs such as liver or kidney. Thirty days after injection, there were no significant abnormalities in the morphology or indices of blood cells **Figure 4**. Metabolism of the main organs also remained stable, which was consistent with the physiological status of the mice. Taken together, the results confirmed that Ho-based nanomaterials offer great potential for bio-application researches due to their high biocompatibility.

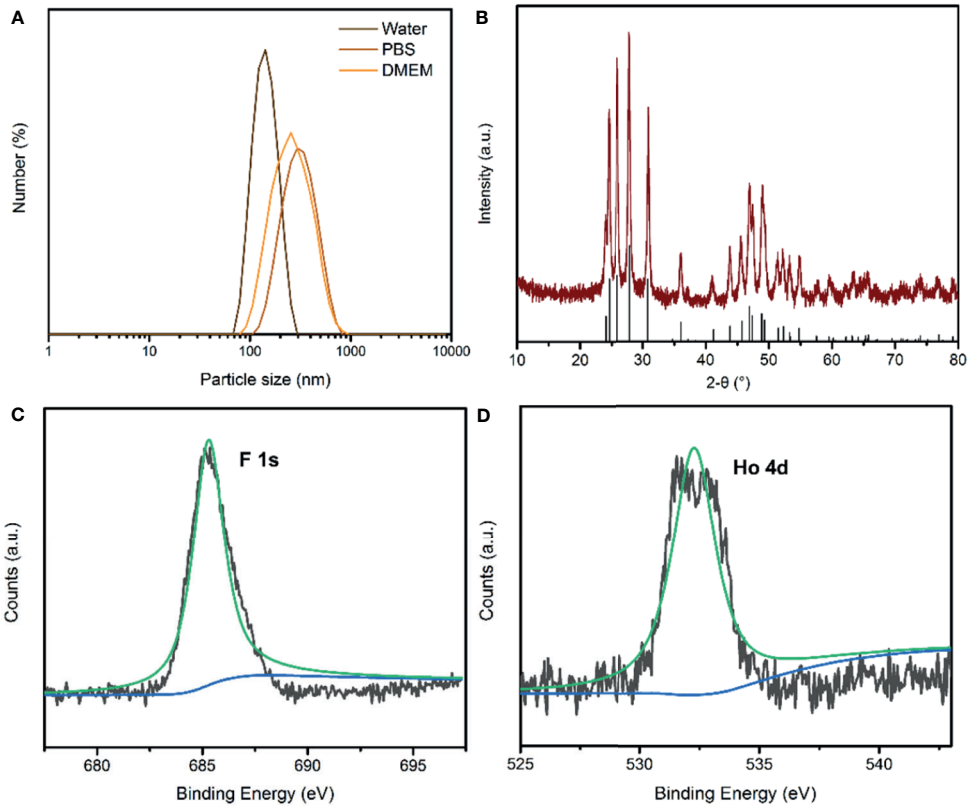


FIGURE 2 | **(A)** The dynamic light scattering (DLS) of PEG-HoF_3 NPs; **(B)** XRD pattern of PEG-HoF_3 NPs; **(C, D)** Higher-resolution XPS spectra of Ho 4d and F1s, respectively.

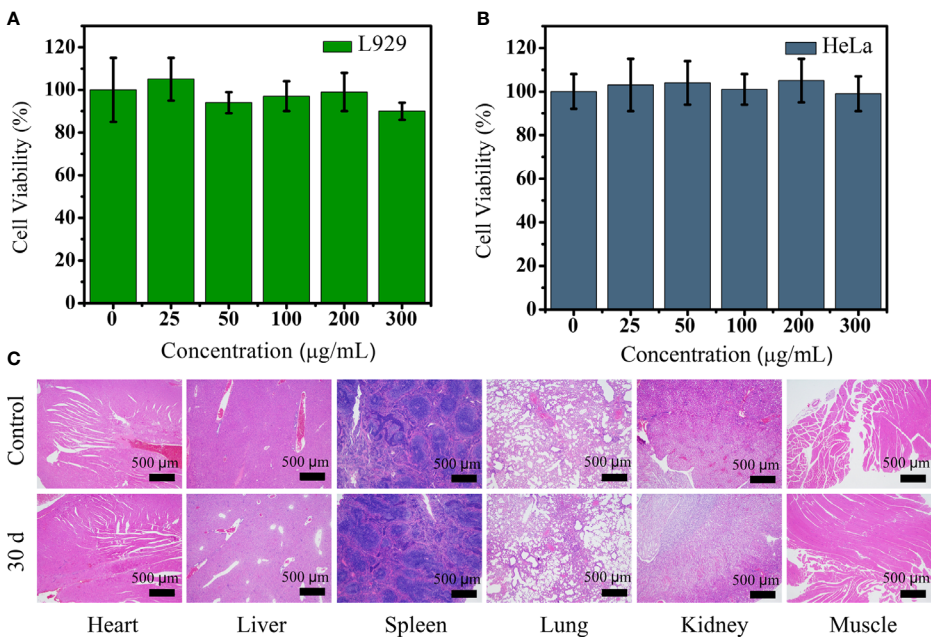


FIGURE 3 | **(A, B)** Viability of L929 and HeLa cells after incubation with different concentrations of PEG-HoF_3 NPs; **(C)** Tissue sections of 6 major organs from mouse which injected with PEG-HoF_3 NPs *via* tail vein.

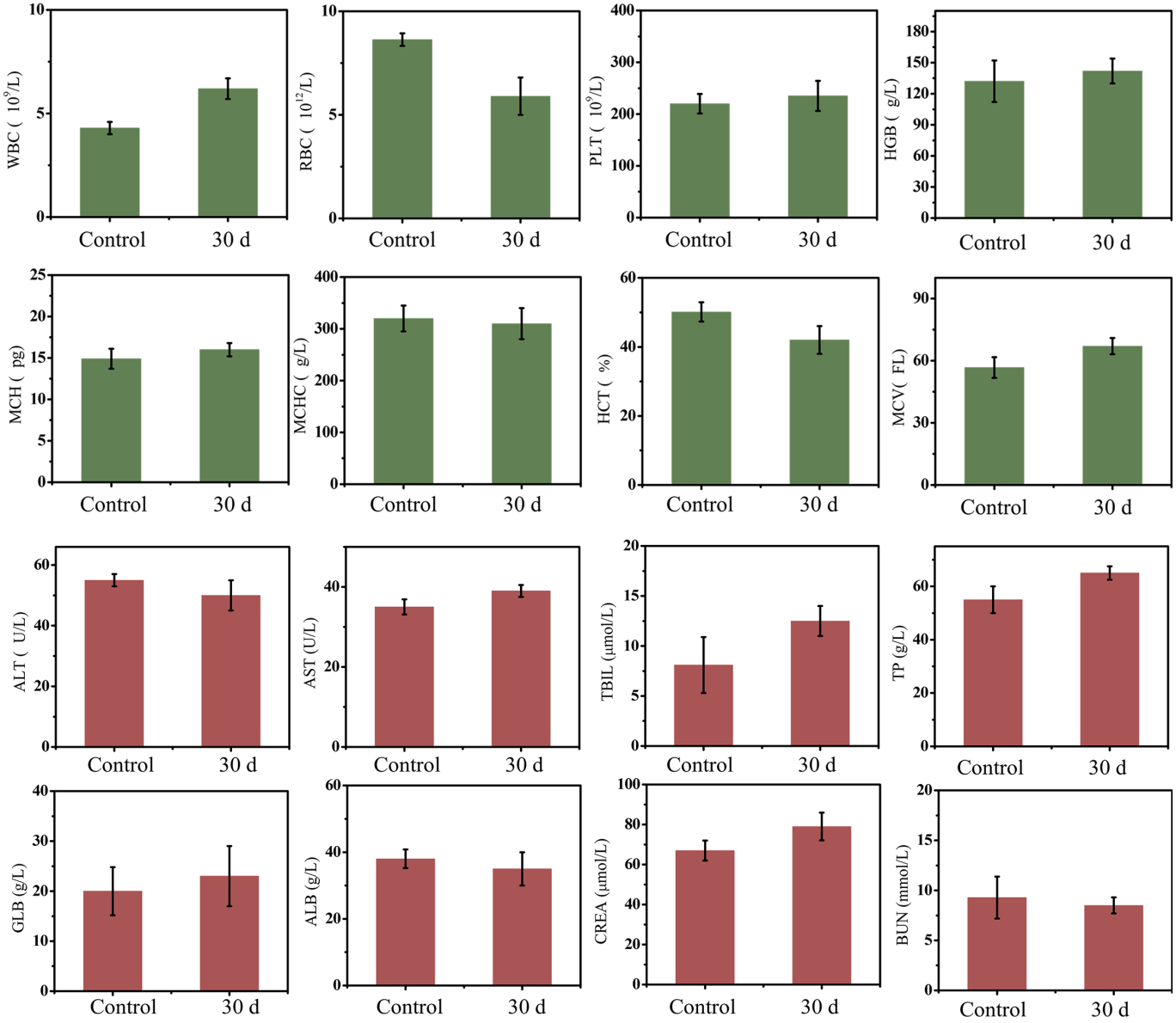


FIGURE 4 | Mice blood testing and biochemical examination, there is no evitable changes in two groups.

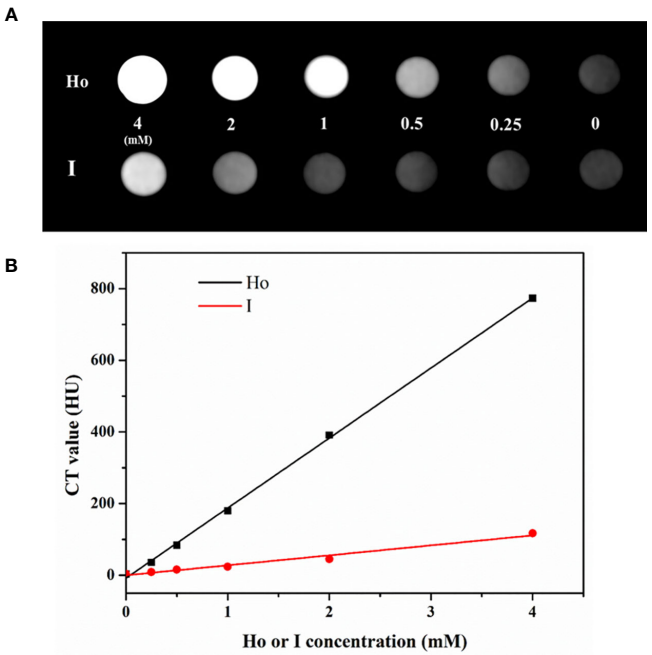


FIGURE 5 | **(A)** *In vitro* CT images of PEG-HoF_3 NPs and Iohexol aqueous solution with different concentration; **(B)** CT value of corresponding tube of A.

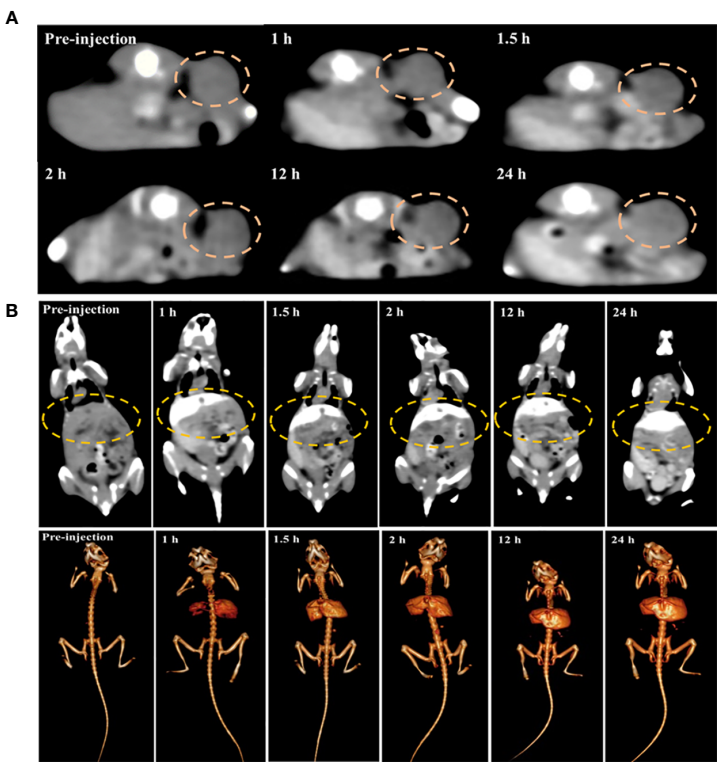


FIGURE 6 | **(A, B)** Changes of tumor site and mouse liver in different time point before versus post-injection of PEG-HoF_3 NPs.

CT Imaging

As a rare earth element, Ho has an atomic number of 67, which is much higher than iodine's atomic number of 53. The inherent characteristics of Ho, specifically its high x-ray attenuation, result in the significantly improved imaging ability of Ho-based CAs in CT. The *in vitro* CT imaging results are shown in **Figure 5A**. Different concentrations of PEG-HoF_3 NPs and Iohexol aqueous solution (0-4 mM) were prepared in Eppendorf tubes and the solutions became brighter as the concentration increased. As shown in **Figure 5B**, the Hounsfield Units (HU) value of PEG-HoF_3 NPs was significantly higher than that of iodine-based CAs, as we expected, and the HU values for both increased linearly. Therefore, the necessary dose of PEG-HoF_3 NPs is much lower than that of iodine-based CAs to achieve the same contrast effect *in vivo*, which may reduce the risks of large doses of CAs (39).

After cytotoxicity assessment of PEG-HoF_3 NPs, tumor-bearing Kunming mice were selected to test the CT contrast effect *in vivo*. The distribution of PEG-HoF_3 NPs was monitored by a CT scanner at different time points. We then compared the images at these time points with the images pre-injection: the brightness of the tumor site was obviously higher after 24 h (**Figure 6A**).

We also tracked the brightness of the liver and kidney after administering PEG-HoF_3 NPs *via* the tail vein (**Figures 6B** and **S5**). Usually, small molecule iodine CAs are not long-lasting in the liver, which decreases the diagnostic ability of liver disease to some extent. However, as shown in **Figure S5**, the liver of the

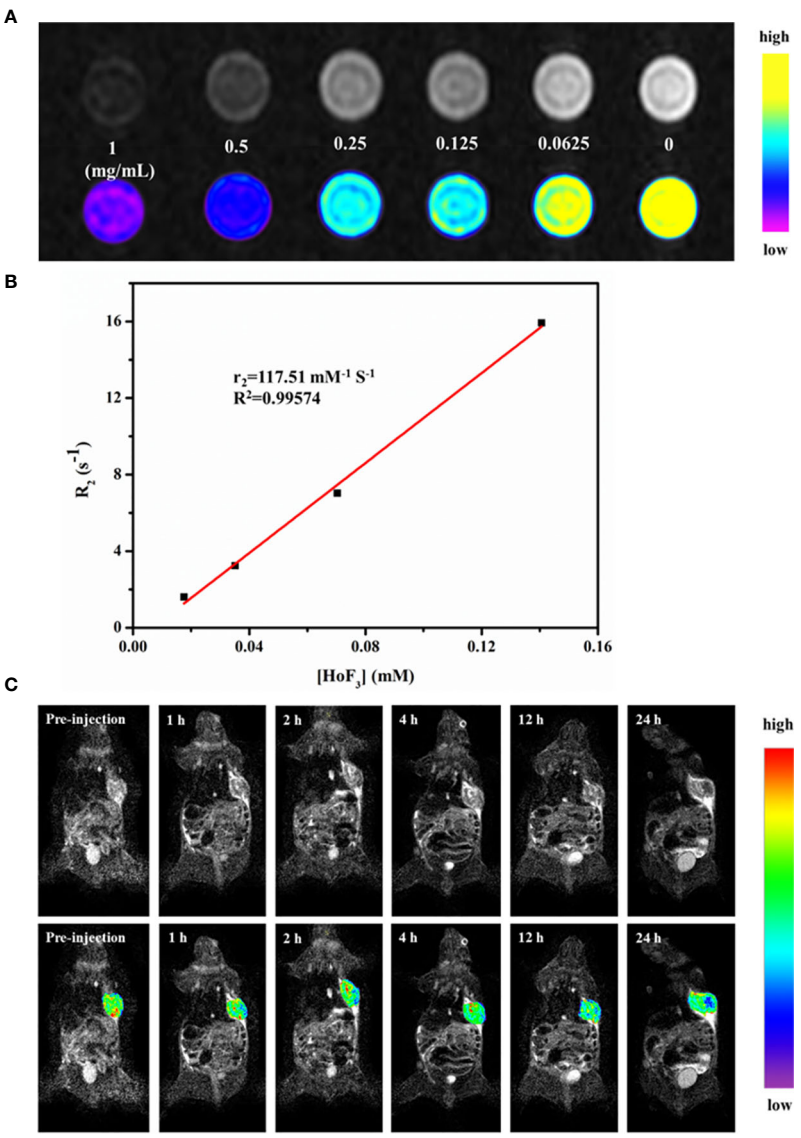


FIGURE 7 | **(A)** *In vitro* T_2-weighted MRI images of PEG-HoF_3 NPs with different concentration; **(B)** The r_2 relaxivity plot of PEG-HoF_3 NPs; **(C)** Signal changes of tumor site in different time point before and post-injection of PEG-HoF_3 NPs.

mice maintained a high contrast effect after 24 h, which likely indicates the uptake of PEG-HoF_3 NPs by hepatocytes. However, there was no obvious enhancement in the kidney at the time points we used. This may indicate that the uptake of PEG-HoF_3 NPs by renal cells is limited and that the size and shape of PEG-HoF_3 NPs prevented its filtration through the kidney. It is possible that the above mechanism can decrease the side effects of CAs on the kidney, and warrants further study.

T_2-Weighted MRI

To date, there have been few studies on Ho-based MRI imaging. It has been confirmed that Ho-based nanomaterial has T_2-weighted MRI contrast ability owing to its intrinsic paramagnetism. However, the magnetic resonance relaxivity of NPs can differ due to their size, form, and even synthesis methods. For this reason, we firstly validated the feasibility of PEG-HoF_3 NPs as a T_2-weighted MRI CAs *in vitro*. Different concentrations of PEG-HoF_3 NPs aqueous solution were tested on a clinical MR scanner. T_2-weighted images of PEG-HoF_3 NPs aqueous solution (0-1 mg/mL) gradually darkened with an increasing Ho concentration (**Figure 7A**). According to the concentration of PEG-HoF_3 NPs, the r_2 relaxivity value of this new contrast agent is 117.51 mM^{-1} S^{-1} (**Figure 7B**). Next, we further explored the potential of PEG-HoF_3 NPs as negative MRI CAs in tumor-bearing mice. T_2-weighted MRI was performed on the same scanner at different times (1, 2, 4, 12, 24 h) after intravenous injection of PEG-HoF_3 NPs (**Figure 7C**). The results showed no significant changes in the signal of the tumor site within 0 to 2 h. However, after 12 h, the signal of the tumor site decreased significantly and a large dark area gradually presented. At 24 h, the negative contrast agent filled the center of tumor site. These results also confirm long term circulation of PEG-HoF_3 NPs, which will be helpful for improving the detection of tumors at specific places.

CONCLUSIONS

We firstly synthesized a new Ho-based NP *via* a one-pot solvothermal method. The new PEG-HoF_3 NPs had a uniform size and showed good dispersibility in aqueous solution. Cytotoxicity assessment and histological analysis indicated that the new Ho-based NPs had good biocompatibility and low toxicity for applications *in vivo*. We then further verified the imaging ability of the PEG-HoF_3 NPs *in vitro* and *vivo*. The results showed that PEG-HoF_3 NPs had an excellent contrast effect in both CT and T_2-weighted MRI. Based on this desirable performance, we expect that PEG-HoF_3 NPs hold great promise for dual-modal imaging and that Ho-based nanomaterials warrant further research.

DATA AVAILABILITY STATEMENT

The original contributions presented in the study are included in the article/**Supplementary Material**. Further inquiries can be directed to the corresponding authors.

ETHICS STATEMENT

The animal study was reviewed and approved by Laboratory Animal Center of Jilin University.

AUTHOR CONTRIBUTIONS

TZ contributed to conception and design of the study. MD and LZ provided the database of mice. ZL contributed to the data of revised manuscript. YL and SS provided the testing instrument and site. TZ wrote the first draft of the manuscript. TG and QY revised and edited the manuscript. All authors contributed to the article and approved the submitted version.

FUNDING

This work was supported by the Program of Science and Technology Development Plan of Jilin Province of China (Nos. 20190201218JC), the Health Special Project of Jilin Province Department of Finance (Nos. 2019SCE7025, 2020SCZT088).

SUPPLEMENTARY MATERIAL

The Supplementary Material for this article can be found online at: https://www.frontiersin.org/articles/10.3389/fonc.2021.741383/full#supplementary-material.

REFERENCES

1. Shi J, Sun X, Zheng S, Li J, Fu X, Zhang H. A New Near-Infrared Persistent Luminescence Nanoparticle as a Multifunctional Nanoplatform for Multimodal Imaging and Cancer Therapy. *Biomaterials* (2018) 152:15–23. doi: 10.1016/j.biomaterials.2017.10.032
2. Padmanabhan P, Kumar A, Kumar S, Chaudhary RK, Gulyas B. Nanoparticles in Practice for Molecular-Imaging Applications: An Overview. *Acta Biomater* (2016) 41:1–16. doi: 10.1016/j.actbio.2016.06.003
3. Chen C, Liu J, Chen Y, Li C, Liu X, Huang H, et al. Sub-10 Nm Sr2LuF7:Yb/Er@Sr2GdF7@SrF2 Up-Conversion Nanocrystals for Up-Conversion Luminescence-Magnetic Resonance-Computed Tomography Trimodal Bioimaging. *ACS Appl Mater Interfaces* (2017) 9(7):5748–56. doi: 10.1021/acsami.6b14007
4. Jin L, Liu J, Tang Y, Cao L, Zhang T, Yuan Q, et al. MnO2-Functionalized Co-P Nanocomposite: A New Theranostic Agent for pH-Triggered T1/T2 Dual-Modality Magnetic Resonance Imaging-Guided Chemo-Photothermal Synergistic Therapy. *ACS Appl Mater Interfaces* (2017) 9(48):41648–58. doi: 10.1021/acsami.7b10608
5. Li Q, Li X, Zhang L, Zuo J, Zhang Y, Liu X, et al. An 800 Nm Driven NaErF4@NaLuF4 Upconversion Platform for Multimodality Imaging and Photodynamic Therapy. *Nanoscale* (2018) 10(26):12356–63. doi: 10.1039/c8nr00446c
6. Ma S, Zhang J, Xia S, Yin W, Qin Y, Lei R, et al. Three-Dimensional Angiography Fused With CT/MRI for Multimodal Imaging of Nanoparticles Based on Ba4Yb3F17:Lu(3+),Gd(3+). *Nanoscale* (2018) 10(28):13402–9. doi: 10.1039/c8nr03054e
7. van Schooneveld MM, Cormode DP, Koole R, van Wijngaarden JT, Calcagno C, Skajaa T, et al. A Fluorescent, Paramagnetic and PEGylated Gold/Silica

Nanoparticle for MRI, CT and Fluorescence Imaging. *Contrast Media Mol Imaging* (2010) 5(4):231–6. doi: 10.1002/cmmi.376
8. Curcio A, Silva AKA, Cabana S, Espinosa A, Baptiste B, Menguy N, et al. Iron Oxide Nanoflowers @ CuS Hybrids for Cancer Tri-Therapy: Interplay of Photothermal Therapy, Magnetic Hyperthermia and Photodynamic Therapy. *Theranostics* (2019) 9(5):1288–302. doi: 10.7150/thno.30238
9. Zhang X, Xi ZQ, Machuki JO, Luo JJ, Yang DZ, Li JJ, et al. Gold Cube-In-Cube Based Oxygen Nanogenerator: A Theranostic Nanoplatform for Modulating Tumor Microenvironment for Precise Chemo-Phototherapy and Multimodal Imaging. *ACS Nano* (2019) 13(5):5306–25. doi: 10.1021/acsnano.8b09786
10. Wang ZX, Wu LM, Chen M, Zhou SX. Facile Synthesis of Superparamagnetic Fluorescent Fe3O4/ZnS Hollow Nanospheres. *J Am Chem Soc* (2009) 131 (32):11276–+. doi: 10.1021/ja903246e
11. Jeffrey RB. Imaging Pancreatic Cysts With CT and MRI. *Digest Dis Sci* (2017) 62(7):1787–95. doi: 10.1007/s10620-017-4501-6
12. Schieda N, Lim RS, McInnes MDF, Thomassin I, Renard-Penna R, Tavolaro S, et al. Characterization of Small (<4cm) Solid Renal Masses by Computed Tomography and Magnetic Resonance Imaging: Current Evidence and Further Development. *Diagn Intervent Imaging* (2018) 99(7-8):443–55. doi: 10.1016/j.diii.2018.03.004
13. Ahlawat S, Baig A, Blakeley JO, Jacobs MA, Fayad LM. Multiparametric Whole-Body Anatomic, Functional, and Metabolic Imaging Characteristics of Peripheral Lesions in Patients With Schwannomatosis. *J Magnet Resonance Imaging: JMRI* (2016) 44(4):794–803. doi: 10.1002/jmri.25236
14. Shan X, Chen Q, Yin X, Jiang C, Li T, Wei S, et al. Polypyrrole-Based Double Rare Earth Hybrid Nanoparticles for Multimodal Imaging and Photothermal Therapy. *J Mater Chem B* (2020) 8(3):426–37. doi: 10.1039/c9tb02254f
15. Lyu M, Zhu DM, Duo YH, Li Y, Quan H. Bimetallic Nanodots for Tri-Modal CT/MRI/PA Imaging and Hypoxia-Resistant Thermoradiotherapy in the NIR-II Biological Windows. *Biomaterials* (2020) 233:119656. doi: 10.1016/j.biomaterials.2019.119656
16. Li Z, Guan M, Sun D, Xu Y, Li F, Xiong W. A Novel MRI- and CT-Based Scoring System to Differentiate Malignant From Osteoporotic Vertebral Fractures in Chinese Patients. *BMC Musculoskelet Disord* (2018) 19(1):406. doi: 10.1186/s12891-018-2331-0
17. Jin X, Fang F, Liu J, Jiang C, Han X, Song Z, et al. An Ultrasmall and Metabolizable PEGylated NaGdF4:Dy Nanoprobe for High-Performance T (1)/T(2)-Weighted MR and CT Multimodal Imaging. *Nanoscale* (2015) 7 (38):15680–8. doi: 10.1039/c5nr04065e
18. Park EA, Lee W, Kang DK, Kim SJ, Kim YJ, Kim Y, et al. Comparison of Iohexol-380 and Iohexol-350 for Coronary CT Angiography: A Multicenter, Randomized, Double-Blind Phase 3 Trial. *Korean J Radiol* (2016) 17(3):330–8. doi: 10.3348/kjr.2016.17.3.330
19. Bolen MA, Brinza E, Renapurkar RD, Kim ESH, Gornik HL. Screening CT Angiography of the Aorta, Visceral Branch Vessels, and Pelvic Arteries in Fibromuscular Dysplasia. *JACC Cardiovasc Imaging* (2017) 10(5):554–61. doi: 10.1016/j.jcmg.2016.04.010
20. Nijssen EC, Rennenberg RJ, Nelemans PJ, Essers BA, Janssen MM, Vermeeren MA, et al. Prophylactic Hydration to Protect Renal Function From Intravascular Iodinated Contrast Material in Patients at High Risk of Contrast-Induced Nephropathy (AMACING): A Prospective, Randomised, Phase 3, Controlled, Open-Label, Non-Inferiority Trial. *Lancet* (2017) 389 (10076):1312–22. doi: 10.1016/S0140-6736(17)30057-0
21. Wang Z, Jia T, Sun QQ, Kuang Y, Liu B, Xu MS, et al. Construction of Bi/phthalocyanine Manganese Nanocomposite for Trimodal Imaging Directed Photodynamic and Photothermal Therapy Mediated by 808 Nm Light. *Biomaterials* (2020) 228:119569. doi: 10.1016/j.biomaterials.2019.119569
22. Ai K, Huang J, Xiao Z, Yang Y, Bai Y, Peng J. Localized Surface Plasmon Resonance Properties and Biomedical Applications of Copper Selenide Nanomaterials. *Mater Today Chem* (2021) 20:100402. doi: 10.1016/j.mtchem.2020.100402
23. Wang J, Sui L, Huang J, Miao L, Nie Y, Wang K, et al. MoS2-Based Nanocomposites for Cancer Diagnosis and Therapy. *Bioactive Mater* (2021) 6(11):4209–42. doi: 10.1016/j.bioactmat.2021.04.021
24. Huang Q, Wu W, Ai K, Liu J. Highly Sensitive Polydiacetylene Ensembles for Biosensing and Bioimaging. *Front Chem* (2020) 8:565782. doi: 10.3389/fchem.2020.565782
25. Estelrich J, Sanchez-Martin MJ, Busquets MA. Nanoparticles in Magnetic Resonance Imaging: From Simple to Dual Contrast Agents. *Int J Nanomed* (2015) 10:1727–41. doi: 10.2147/IJN.S76501
26. Rohrer M, Bauer H, Mintorovitch J, Requardt M, Weinmann HJ. Comparison of Magnetic Properties of MRI Contrast Media Solutions at Different Magnetic Field Strengths. *Invest Radiol* (2005) 40(11):715–24. doi: 10.1097/01.rli.0000184756.66360.d3
27. Kraff O, Quick HH. 7t: Physics, Safety, and Potential Clinical Applications. *J Magnet Resonance Imaging: JMRI* (2017) 46(6):1573–89. doi: 10.1002/jmri.25723
28. Chen L, Huang Q, Zhao T, Sui L, Wang S, Xiao Z, et al. Nanotherapies for Sepsis by Regulating Inflammatory Signals and Reactive Oxygen and Nitrogen Species: New Insight for Treating COVID-19. *Redox Biol* (2021) 45:102046. doi: 10.1016/j.redox.2021.102046
29. Sui L, Wang J, Xiao Z, Yang Y, Yang Z, Ai K. ROS-Scavenging Nanomaterials to Treat Periodontitis. *Front Chem* (2020) 8:595530. doi: 10.3389/fchem.2020.595530
30. Ni D, Zhang J, Bu W, Zhang C, Yao Z, Xing H, et al. PEGylated NaHoF4 Nanoparticles as Contrast Agents for Both X-Ray Computed Tomography and Ultra-High Field Magnetic Resonance Imaging. *Biomaterials* (2016) 76:218–25. doi: 10.1016/j.biomaterials.2015.10.063
31. Gonzalez-Mancebo D, Becerro AI, Rojas TC, Garcia-Martin ML, de la Fuente JM, Ocana M. HoF3 and DyF3 Nanoparticles as Contrast Agents for High-Field Magnetic Resonance Imaging. *Part Part Syst Char* (2017) 34(10): 1700116. doi: 10.1002/Ppsc.201700116
32. Das GK, Johnson NJ, Cramen J, Blasiak B, Latta P, Tomanek B, et al. NaDyF4 Nanoparticles as T2 Contrast Agents for Ultrahigh Field Magnetic Resonance Imaging. *J Phys Chem Lett* (2012) 3(4):524–9. doi: 10.1021/jz201664h
33. Marasini S, Yue H, Ho SL, Jung KH, Park JA, Cha H, et al. D-Glucuronic Acid-Coated Ultrasmall Paramagnetic Ln(2)O(3) (Ln = Tb, Dy, and Ho) Nanoparticles: Magnetic Properties, Water Proton Relaxivities, and Fluorescence Properties. *Eur J Inorg Chem* (2019) 2019(34):3832–9. doi: 10.1002/ejic.201900378
34. D'Souza AA, Shegokar R. Polyethylene Glycol (PEG): A Versatile Polymer for Pharmaceutical Applications. *Expert Opin Drug Deliv* (2016) 13(9):1257–75. doi: 10.1080/17425247.2016.1182485
35. Ai K, Liu Y, Liu J, Yuan Q, He Y, Lu L. Large-Scale Synthesis of Bi(2)S(3) Nanodots as a Contrast Agent for *In Vivo* X-Ray Computed Tomography Imaging. *Adv Mater* (2011) 23(42):4886–91. doi: 10.1002/adma.201103289
36. Liu JH, Wang L, Zhang TQ, Wang JQ, Gong X, Cui FZ, et al. Facile Synthesis of Biocompatible Fe3O4-Based Nanoparticles for pH-Responsive Dual-Model Magnetic Resonance Imaging- Guided Tumour Eradication by Photothermal Therapy. *Chin J Anal Chem* (2019) 47(5):678–85. doi: 10.1016/S1872-2040(19)61158-8
37. Zhang TQ, Han XL, He YY, He XJ, Wang JQ, Yuan QH, et al. Facile Synthesis of PEGylated Tungsten-Based Nanoprobes for Gastric Computed Tomography Imaging. *Chin J Anal Chem* (2018) 46(10):1539–43. doi: 10.1016/S1872-2040(18)61116-8
38. Li NS, Chen L, Xiao ZX, Yang YQ, Ai KL. Progress in Detection of Biomarker of Ovarian Cancer: Lysophosphatidic Acid. *Chin J Anal Chem* (2020) 48 (12):1597–606. doi: 10.19756/j.issn.0253.3820.201339
39. Zhu S, Tian R, Antaris AL, Chen X, Dai H. Near-Infrared-II Molecular Dyes for Cancer Imaging and Surgery. *Adv Mater* (2019) 31(24):e1900321. doi: 10.1002/adma.201900321

Conflict of Interest: The authors declare that the research was conducted in the absence of any commercial or financial relationships that could be construed as a potential conflict of interest.

Publisher's Note: All claims expressed in this article are solely those of the authors and do not necessarily represent those of their affiliated organizations, or those of the publisher, the editors and the reviewers. Any product that may be evaluated in this article, or claim that may be made by its manufacturer, is not guaranteed or endorsed by the publisher.

Copyright © 2021 Zhang, Deng, Zhang, Liu, Liu, Song, Gong and Yuan. This is an open-access article distributed under the terms of the Creative Commons Attribution License (CC BY). The use, distribution or reproduction in other forums is permitted, provided the original author(s) and the copyright owner(s) are credited and that the original publication in this journal is cited, in accordance with accepted academic practice. No use, distribution or reproduction is permitted which does not comply with these terms.

frontiers in Oncology

MINI REVIEW
published: 16 September 2021
doi: 10.3389/fonc.2021.758143

Advanced Nano-Carriers for Anti-Tumor Drug Loading

Jia Xiang[†], *Rui Zhao*[†], *Bo Wang*, *Xinran Sun*, *Xu Guo*, *Songwen Tan*[*] *and Wenjie Liu*

Xiangya School of Pharmaceutical Sciences, Central South University, Changsha, China

Chemotherapy is one of the important means of tumor therapy. However, most of the anti-tumor drugs that currently used in clinic are hydrophobic non-specific drugs, which seriously affect the efficacy of drugs. With the development of nanotechnology, drug efficacy can be improved by selecting appropriate biodegradable nanocarriers for achieving the controlled release, targeting and higher bioavailability of drugs. This paper reviewed the research progress of anti-tumor drug nanoparticle carriers, which mainly summarized the materials used for anti-tumor drug nanoparticle carriers and their effects in anti-tumor drugs, as well as the targeted drug delivery methods of anti-tumor drugs based on nanocarriers.

Keywords: cancer, chemotherapy, antitumor drug, nano drug carrier, targeted transportation

OPEN ACCESS

Edited by:
Kelong Ai,
Central South University, China

Reviewed by:
Hongwen Wu,
Liuzhou Workers Hospital, China
Xinchun He,
Hunan Normal University, China

****Correspondence:***
Songwen Tan
songwen.tan@csu.edu.cn

[†]These authors have contributed equally to this work and share first authorship

Specialty section:
This article was submitted to Pharmacology of Anti-Cancer Drugs, a section of the journal Frontiers in Oncology

Received: *13 August 2021*
Accepted: *30 August 2021*
Published: *16 September 2021*

Citation:
Xiang J, Zhao R, Wang B, Sun X, Guo X, Tan S and Liu W (2021) Advanced Nano-Carriers for Anti-Tumor Drug Loading. Front. Oncol. 11:758143. doi: 10.3389/fonc.2021.758143

INTRODUCTION

Tumor is still one of the main fatal diseases of human beings, and chemotherapy is one of the main methods to treat tumor in clinic (1). However, most anti-tumor drugs have poor water solubility and low bioavailability (2), which leads to the limited therapeutic effect of drugs on tumor tissues (3). In addition, chemotherapy will have serious toxic and side effects on other normal tissues and cells (4), which not only damages patients' body function, but also causes patients to develop drug resistance (4), which seriously affects the curative effect. In 1978, Marty first used nanoparticles as drug carriers (5). Nanocarriers are nano-sized carriers based on the concept of targeted drug delivery system (TDDS) (4). At present, it has become a research hotspot due to its advantages of controlled release, targeting, high efficiency, low toxicity and high stability (6). With the development of nanotechnology, the anti-tumor drug with nanoparticles as carriers can achieve controlled release and targeted drug delivery through using special materials and surface modification (4). It can also improve the stability and bioavailability of anti-tumor drugs, overcome the limitations of traditional anti-tumor drugs, which has been widely used. In this review, we introduced main types of nano-drug carrier materials and their effects and discussed the targeted transport modes of nano-drug carriers.

NANO CARRIERS FOR ANTI-TUMOR DRUG

The nanoparticles used as anti-tumor drug loading system have a size of 1–100 nm (4) and mainly include nano-liposomes, nano-polymers, nano-gene carriers, nano-inorganic materials and other drug carriers. **Figure 1** showed the development of nano-sized anti-tumor drug carriers. **Table 1** presented the materials used as anti-tumor drugs delivery carriers.

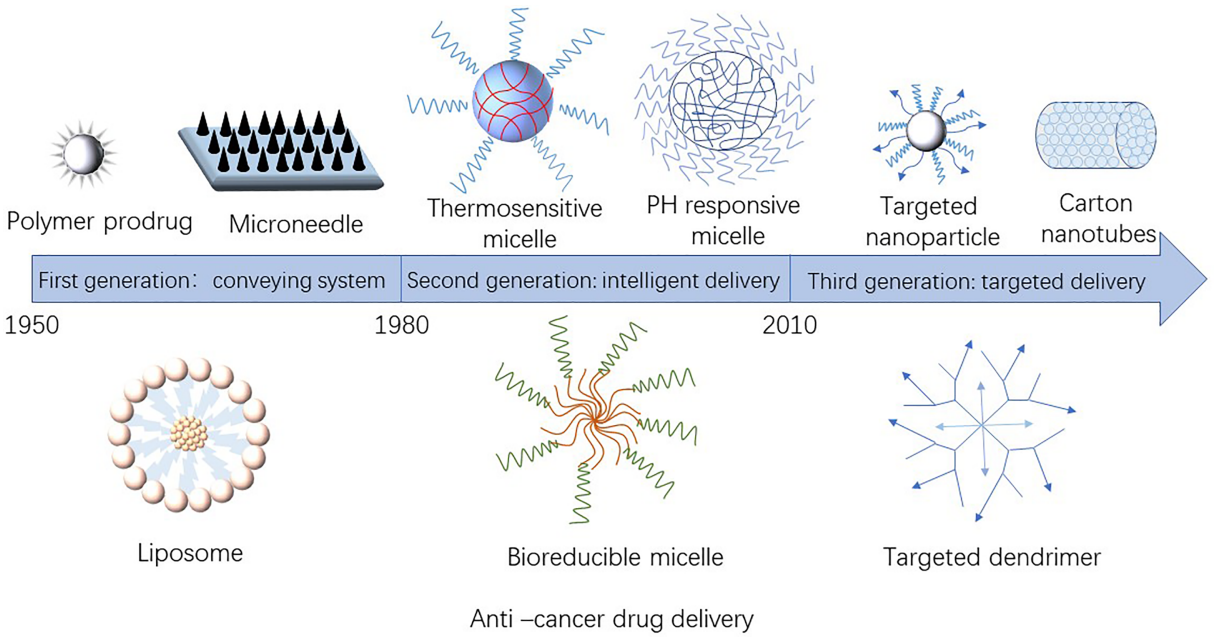


FIGURE 1 | Development of nano-carriers for anti-tumor drug.

TABLE 1 | Different materials as anti-tumor drugs delivery carrier.

Nanomaterial	Modification	Anti-cancer drug	Results	Reference
Liposomes	No	Luteolin	Improve solubility and bioavailability of Luteolin and obtain better anticancer effect	(7)
	Anti-GD2 antibodies	Doxorubicin	Improve the targeting of drugs to Human Neuroblastoma	(8)
	NGR peptides	Bortezomib	Reduce side effects and improve anti-tumor effect	(9)
hyaluronic	Chitosan	Paclitaxel	Improve the targeting and stability of drug	(10)
PLA	No	Tamoxifen	Reduce side effects and improve anti-tumor effect	(11)
	methoxy poly (ethylene glycol)	verapamil and doxorubicin	Reduce drug resistance and improve anti-cancer effect	(12)
	PEG	Anastrozole	Effectively deliver Anastrozole to target cells	(13)
PLGA	Chitosan and PEG	curcumin	Improve the targeting of drug	(14)
PEG	Fe_3O_4	doxorubicin	Improve the therapeutic effect	(15)
Poly(anhydride)	Cyclodextrins	Camptothecin	Improve bioavailability of Camptothecin	(16)
Chitosan	No	Chlorambucil	Reduce the abnormal toxicity and enhance the uptake of tumor cells	(17)
carbon nanotubes	Folate (covalent)	Doxorubicin and cell impermeant propidium iodide	Improve the drug loading and stability	(18)
	Fluorescent probe labeled single strand DNA (non-covalent)	No	Improve the targeting response ability	(19)
Silica Nanoparticles	Econazole	Fluconazole	Enhance targeting and permeability and reduce side effects	(20)
Au nanorods	5' thiol end	Doxorubicin and platinum	Improve the targeting and response activity	(21)
ZnO nanoparticle	PEG	Doxorubicin	Increase blood concentration and anti-tumor efficiency	(22)
	No	Ibuprofen	Reduce dissolution rate and improve anti-tumor ability	(23)
Quantum dots	Boron nitride	Doxorubicin	Improve drug activity and anti-tumor ability	(24)

Nano-Liposomes

Liposomes are structures, similar to biofilms, composed of hydrophilic head and lipophilic tail, which can encapsulate drugs in aqueous solution to form monolayer or multilayer vesicles (25). Liposomes are considered as promising drug carriers due to their low toxicity, high safety, high biocompatibility, strong drug loading capacity and more flexible regulation of drug release (25–27). Luteolin (LUT) is a kind of natural flavonoids widely distributed in a variety of plants and has anti-tumor activity. Due to the poor water solubility and low bioavailability of luteolin, so Wu et al. (7) prepared liposome LUT with encapsulation efficiency of up to 90%. *In vitro* studies show that LUT encapsulated by liposome can inhibit tumor growth by inducing apoptosis of tumor cells and has superior anti-tumor effect on mouse colon cancer cell CT26 compared with LUT without liposome.

Nano-Polymers

Nano-polymer carriers have good biocompatibility and biodegradability (28), and have been widely studied in the medical field. Currently, nano-polymer carriers used for anti-tumor drugs mainly divided into natural and synthetic nano-polymer carriers. Natural nano-polymer carriers mainly include hyaluronic acid-based polymers, agarose, collagen and chitosan while synthetic nano-polymer carriers include poly anhydrides, poly (ϵ-caprolactone) (PCL), polylactic acid (PLA), polyethylene glycol (PEG), polyglutamic acid(PGA),and poly D,L-lactide-co-glocolide(PLGA),etc. Among them, PEG with low toxicity have been the focus of research in recent years. PEG is a polymer material obtained by ring-opening polymerization of ethylene oxide. Its main characteristics are controllable polymerization degree, stable structure (29), and can avoid the recognition of human immune system, which has the property of "stealth" *in vivo*. Genexol-PM® in Korea and Paclical® in Russia are polymer nanodrugs that have been approved clinically, and both of them are polymer nanomedicine formulations of paclitaxel. Furthermore, there are many polymer nano-drugs that have entered preclinical research (30), such as Opaxio and Xyotax.

Nano-Gene Carriers

Gene therapy played an important role in cancer treatment (31). The carrier of gene therapy was the key to the success of gene therapy (32). At present, the commonly used gene vectors mainly include viral vectors and non-viral vectors. The difficulty and high cost in preparing viral vectors and the potential carcinogenicity limit their application in gene therapy (33). As a potential substitute for viral vectors, non-viral vectors are simple to prepare, high in portability and low in toxicity, and most of them are nano-vectors including peptides, liposome, polymers and so on (34–36). Wang et al. (37) prepared a multifunctional tumor therapeutic carrier transport plasmid Cas9-sgPlk-1 by electrostatic interaction with lipid encapsulated gold nanoparticles, which provides a multifunctional method for efficient targeted gene editing and makes nano-gene carriers more widely used *in vivo* and *in vitro* experiments.

Inorganic Nanoparticles

In recent years, inorganic nanoparticles have been widely used in tumor imaging and treatment (38) mainly including metals (e.g., gold, zinc, silver and iron nanoparticles), metal oxides (iron and titanium oxide nanoparticles), carbon dots, carbon nanotubes and semiconductors etc. (39, 40). Due to the unique physical and chemical properties and good stability of inorganic nanoparticles, especially optical, magnetic and other physical properties, inorganic nanoparticles may be more suitable for cancer treatment than traditional organic nanocarriers (38). Chen et al. (41) modify Fe_3O_4 nanoparticles onto carbon nanotubes to provide a double-targeted drug delivery system with about 110% excellent drug-loading capacity for tumor-targeted optical imaging and magnetic-targeted drug delivery. However, the toxicity of inorganic nanoparticles greatly limits its clinical application (42).

TARGETED DELIVERY OF NANO-DRUG CARRIERS

Although traditional chemotherapy drugs can kill tumor cells with high efficiency, they also have toxic and side effects on normal tissues due to their lack of specificity while nanotechnology provides a new opportunity for tumor targeted therapy (43). At present, anti-tumor drugs based on nanoparticles can be targeted to transport drugs through three ways: passive transport, active transport and physical and chemical transport, which can identify cancerous tissues more accurately in complex organisms and release them at cancerous tissues to reduce toxic and side effects on normal cells.

Passive Targeted Transport

Passive targeting, mainly through permeation and retention effect(EPR), enables the drug to be swallowed by macrophages as a foreign body immediately after entering the human body, so as to reduce non-specific binding with non-target sites and reach the targeted sites for selective binding (44). Drug carriers, such as liposomes, mainly transported drugs through passive targeting (45). Mitra et al. (46) embedded adriamycin glucan complex in long-circulating nanoparticles, and enriched the drug targeting to the tumor site of mice by EPR effect, so as to achieve the purpose of slow targeting, high efficiency and low toxicity of drugs. At present, many passive targeting nanoparticles have shown promising therapeutic effects in clinical trials, such as Marqibo, Myocet and lysosomes (47).

Active Targeted Transport

The limitation of passive targeting is that it has lower specificity to tumor site, while active targeting has higher targeting. It is found that some antigens or receptors are over-expressed on the surface of tumor cells, while normal cells express them normally (48), such as folate receptor (49), prostate-specific membrane antigen (50), biotin receptors (51), transferrin receptor (52), peptide (53) and the carbonic anhydrase IX (54). Active targeting is based on the specific recognition between receptor and ligand or the covalent modification of targeting groups on the surface. Mackiewicz et al. (55) designed multifunctional poly (ethylene glycol)-block-poly(lactic acid)) nanoparticles modified by folic acid and fluorescent probes, which can achieve the purposes of cell imaging and targeted delivery of anti-tumor drugs at the same time.

Physical and Chemical Targeted Transport

The microenvironment of tumor cells is different from that of normal cells. Based on the unique physical and chemical environment of tumor site, researchers have developed a series of nano-drug carriers with stimulus response, which can achieve targeted release by controlling exogenous stimulus (change of temperature, magnetic field, light or electric pulse) or endogenous stimulus (change of PH value or redox), thereby improving drug efficacy and reducing side effects (56–59).

Magnetic-Responsive Nanocarriers

Since Widder et al. (60) proposed the targeted therapy of magnetic drugs in the 1970s, the research on magnetic targeted drug delivery system (MTDS) has become an important part of the current research on tumor diagnosis and treatment. Magnetic nanoparticles were fixed by external magnetic field, and then heated by alternating magnetic field to kill tumor cells (61). MTDS usually used core-shell nanoparticles (62), magnetic liposomes (63) and nanoporous metal capsules (64) as magnetic responsive nanocarriers. Among them, superparamagnetic iron oxide nano drug-loaded particles have become the current research focus due to their low cytotoxicity, chemical and magnetic stability. Shalaby et al. (65) combined magnetic nanoparticles with adenovirus to transfect them into human fibroma cells under the action of external magnetic field. The results showed that magnetic transfection could significantly inhibit cell proliferation and induce apoptosis.

PH-Responsive Nanocarriers

pH value in tumor cells is generally lower than that in normal tissues. The pH value of normal tissue is about 7.4, while the pH value of tumor extracellular microenvironment is about 6.5~7.2 (66). Researchers have developed pH-responsive drug carrier systems by introducing alkaline polymers containing multiple amino groups into polymers, or acetals, orthoesters, hydrazine bonds that can be broken in acidic environments (67–69). This carrier systems were often used to control drug release in specific organs (such as the gastrointestinal tract or vagina) or organelles (such as nucleosomes or lysosomes) and trigger drug release when microenvironment changes are associated with pathological conditions (70). Deng et al. (71) found that the amino protonation caused by chitosan swelling would lead to the release of tumor necrosis factor-α (TNF-α) encapsulated in chitosan in tumor tissues in local acidic environment.

Temperature-Responsive Nanocarriers

Temperature-responsive nanocarriers maintain structural integrity in normal tissues (37°C), and the drug is well encapsulated in nanomaterials, but the tumor tissue temperature of the patients treated by hyperthermia therapy is as high as 39.5°C, therefore, when the nano-carrier reaches the tumor site, at least one component of the nano-material responds to the nonlinear rapid change of temperature, the structure of the system is destroyed and the drug is released, thus realizing targeted drug delivery at the tumor site (72). Temperature-responsive nanocarriers usually included liposomes and polymer micelles (n-isopropylacrylamide). Shah et al. (73) wrapped photosensitizer tetrakis(hydroxymethyl)phosphonium chloride and anticancer drug doxorubicin in hydrophobic lipid bilayer membrane, and wrapped magnetic nanoparticles in hydrophilic inner capsule, realizing simultaneous magnetocaloric therapy, photodynamic therapy and chemotherapy. Experimental results show that combined therapy can almost eliminate completely cancer cells, and the therapeutic effect is remarkable.

Photo-Responsive Nano-Carrier

The photo-responsive nano-carrier can respond to specific wavelength light to achieve targeted drug delivery (74). The photosensitive azobenzene group and its derivatives can be optically isomerized from trans to cis under the irradiation of 300-380 nm, and can also be optically isomerized from cis to trans in the visible region, which makes it possible to optically control drug release (75). Because soft tissue has strong scattering in the ultraviolet visible region less than 700 nm, the penetration depth of light-responsive nanocarriers is low (~ 10 mm), which is only suitable for body parts that can be directly irradiated (such as eyes and skin, etc.) (74). Today, near infrared lasers (NIR) with wavelengths ranging from 700 to 1000 nm have wide clinical applications due to their low scattering, deep tissue penetration, and micro-tissue damage (76). YOU et al. (77) designed and synthesized multifunctional doxorubicin hollow gold nanoparticles, which accelerated the release of drugs under the irradiation of near infrared light. Compared with traditional chemotherapy methods, the anti-cancer activity was increased, and the systemic toxicity was reduced, proving that the NIR technology has a broad prospect.

Redox-Responsive Nanocarriers

Concentration of Glutathione (GSH) in tumor cells was about several hundred times higher than that in extracellular cells. In general, redox-responsive nanocarriers can intelligently target drug release in tumor cells by introducing disulfide or diselenide bonds (78), which is of great significance to many drug molecules (e. g. camptothecin, doxorubicin, etc.) that exert their effects in the organelles of tumor cells. Disulfide bonds are very stable under normal physiological condition but will be reduced and broken in the presence of high concentration GSH in tumor cells (79). Based on this principle, Wang et al. (80) developed Camptothecin (CPT) conjugated core cross-linked micelles that can break down disulfide bonds by oxidation-reduction, thus, destroying the micelle structure and releasing CPT rapidly. In vitro cytotoxicity study showed that the anti-cancer activity of redox-responsive core cross-linked micelles was significantly higher than that of nonresponsive micelles.

CONCLUSION AND PROSPECT

Great progress has been made in the research of nano anti-tumor drug carrier, which effectively overcomes the limitations of poor solubility, low bioavailability and non-specificity of traditional chemotherapy drugs, and obviously improves the curative effect of drugs. At present, nano-carriers for anti-tumor drugs mainly include nano-liposomes, nano-polymers and nano-gene carriers, which belong to nano-organic materials and nano-inorganic materials. The application of anti-tumor drug nanocarriers can truly achieve targeted drug delivery at the focus, and its targeted transportation modes mainly include passive transportation, active

transportation and physical and chemical transportation (according to the changes of temperature, magnetic field, light or electric pulse, PH and redox). However, most of the research on nano anti-tumor drug carrier focuses on the basic theory, and few drugs can be used clinically, which limits the wide application of nano anti-tumor drug carriers (81–83). In the future, researchers need to continuously explore and design nanoporous carriers of anti-tumor drugs with high drug loading, high efficiency, low toxicity, low cost and clinical application value. The modification of nanoparticles is combined with single surface group modification and combined physicochemical modification so as to establish a new route of administration, which is conducive to the interdisciplinary comprehensive research and maximize its scientific value and market value.

AUTHOR CONTRIBUTIONS

JX wrote the paper. ZR participated in the design and drafting of this manuscript. BW, XS and XG performed the literature search and revised the paper. WL and ST guided the writing of the paper and reviewed the manuscript. All authors contributed to the article and approved the submitted version.

ACKNOWLEDGMENTS

JX and RZ contributed to this work and should be considered co-first authors.

REFERENCES

1. Nygren P. What Is Cancer Chemotherapy? *Acta Oncol* (2001) 40(2–3):166–74. doi: 10.1080/02841860151116204
2. Chen H, Zheng Y, Tian G, Tian Y, Zeng X, Liu G, et al. Oral Delivery of DMAB-Modified Docetaxel-Loaded PLGA-TPGS Nanoparticles for Cancer Chemotherapy. *Nanoscale Res Lett* (2011) 6(1):4. doi: 10.1007/s11671-010-9741-8
3. Jain KK. An Overview of Drug Delivery Systems. *Methods Mol Biol* (2020) 1–54. doi: 10.1007/978-1-4939-9798-5_1
4. Van Vlerken LE, Amiji MM. Multi-Functional Polymeric Nanoparticles for Tumour-Targeted Drug Delivery. *Expert Opin Drug Deliv* (2006) 3(2):205–16. doi: 10.1517/17425247.3.2.205
5. Kreuter J. Nanoparticles—A Historical Perspective. *Int J Pharmaceut* (2007) 331(1):1–10. doi: 10.doi:10.1016/j.ijpharm.2006.10.021
6. Saltzman WM, Fung LK. Polymeric Implants for Cancer Chemotherapy. *Adv Drug Deliv Rev* (1997) 26(2-3):209–30. doi: 10.1016/s0169-409x(97)00036-7
7. Wu G, Li J, Yue J, Zhang S, Yunusi K. Liposome Encapsulated Luteolin Showed Enhanced Antitumor Efficacy to Colorectal Carcinoma. *Mol Med Rep* (2018) 17(2):2456–64. doi: 10.3892/mmr.2017.8185
8. Pastorino F, Brignole C, Marimpietri D, Sapra P, Moase EH, Allen TM, et al. Doxorubicin-Loaded Fab' Fragments of Anti-Disialoganglioside Immunoliposomes Selectively Inhibit the Growth and Dissemination of Human Neuroblastoma in Nude Mice. *Cancer Res* (2003) 63(1):86–92. doi: 10.1186/s13054-015-0752-9
9. Zuccari G, Milelli A, Pastorino F, Loi M, Petretto A, Parise A, et al. Tumor Vascular Targeted Liposomal-Bortezomib Minimizes Side Effects and Increases Therapeutic Activity in Human Neuroblastoma. *J Control Release* (2015) 211:44–52. doi: 10.1016/j.jconrel.2015.05.286
10. Li J, Huang P, Chang L, Long X, Dong A, Liu J, et al. Tumor Targeting and pH-Responsive Polyelectrolyte Complex Nanoparticles Based on Hyaluronic Acid-Paclitaxel Conjugates and Chitosan for Oral Delivery of Paclitaxel. *Macromol Res* (2013) 21(12):1331–7. doi: 10.1007/s13233-013-1171-x
11. Pandey SK, Ghosh S, Maiti P, Haldar C. Therapeutic Efficacy and Toxicity of Tamoxifen Loaded PLA Nanoparticles for Breast Cancer. *Int J Biol Macromol* (2015) 72:309–19. doi: 10.1016/j.ijbiomac.2014.08.012
12. Zheng W, Li M, Lin Y, Zhan X. Encapsulation of Verapamil and Doxorubicin by MPEG-PLA to Reverse Drug Resistance in Ovarian Cancer. *Biomed Pharmacother* (2018) 108:565–73. doi: 10.1016/j.biopha.2018.09.039
13. Goudarzi F, Asadi A, Afsharpour M, Jamadi RH. *In Vitro* Characterization and Evaluation of the Cytotoxicity Effects of Nisin and Nisin-Loaded PLA-PEG-PLA Nanoparticles on Gastrointestinal (AGS and KYSE-30), Hepatic (HepG2) and Blood (K562) Cancer Cell Lines. *AAPS PharmSciTech* (2018) 19 (4):1554–66. doi: 10.1208/s12249-018-0969-4
14. Arya G, Das M, Sahoo SK. Evaluation of Curcumin Loaded Chitosan/PEG Blended PLGA Nanoparticles for Effective Treatment of Pancreatic Cancer. *Biomed Pharmacother* (2018) 102:555–66. doi: 10.1016/j.biopha.2018.03.101
15. Dutta B, Shetake NG, Gawali SL, Barick BK, Barick KC, Babu PD, et al. PEG Mediated Shape-Selective Synthesis of Cubic Fe 3 O 4 Nanoparticles for Cancer Therapeutics. *J Alloy Compd* (2018) 737:347–55. doi: 10.1016/j.jallcom.2017.12.028
16. Huarte J, Espuelas S, Lai Y, He B, Tang J, Irache JM. Oral Delivery of Camptothecin Using Cyclodextrin/Poly(Anhydride) Nanoparticles. *Int J Pharm* (2016) 506(1-2):116–28. doi: 10.1016/j.ijpharm.2016.04.045
17. Shayegh A, Khalatbari F, Zonoubi N, Zarazvand F, Monavvari F, Hejazinia H, et al. Chlorambucil-Chitosan Nano-Conjugate: An Efficient Agent Against Breast Cancer Targeted Therapy. *Curr Drug Deliv* (2021). doi: 10.2174/1567201817666201027122620
18. Kapri S, Maiti S, Bhattacharyya S. Lemon Grass Derived Porous Carbon Nanospheres Functionalized for Controlled and Targeted Drug Delivery. *Carbon* (2016) 100:223–35. doi: 10.1016/j.carbon.2016.01.017
19. Li C, Meng Y, Wang S, Qian M, Wang J, Lu W, et al. Mesoporous Carbon Nanospheres Featured Fluorescent Aptasensor for Multiple Diagnosis of Cancer *In Vitro* and *In Vivo*. *ACS Nano* (2015) 9(12):12096–103. doi: 10.1021/acsnano.5b05137
20. Firooz A, Nafisi S, Maibach HI. Novel Drug Delivery Strategies for Improving Econazole Antifungal Action. *Int J Pharm* (2015) 495(1):599–607. doi: 10.1016/j.ijpharm.2015.09.015
21. Shanmugam V, Chien YH, Cheng YS, Liu TY, Huang CC, Su CH, et al. Oligonucleotides–assembled Au Nanorod-Assisted Cancer Photothermal Ablation and Combination Chemotherapy With Targeted Dual-Drug Delivery of Doxorubicin and Cisplatin Prodrug. *ACS Appl Mater Interfaces* (2014) 6(6):4382–93. doi: 10.1021/am5000905
22. Alarifi S, Ali D, Alkahtani S, Verma A, Ahamed M, Ahmed M, et al. Induction of Oxidative Stress, DNA Damage, and Apoptosis in a Malignant Human Skin Melanoma Cell Line After Exposure to Zinc Oxide Nanoparticles. *Int J Nanomedicine* (2013) 8:983–93. doi: 10.2147/ijn.S42028
23. Condello M, De Berardis B, Ammendolia MG, Barone F, Condello G, Degan P, et al. ZnO Nanoparticle Tracking From Uptake to Genotoxic Damage in Human Colon Carcinoma Cells. *Toxicol In Vitro* (2016) 35:169–79. doi: 10.1016/j.tiv.2016.06.005
24. Umrao S, Maurya AK, Shukla V, Grigoriev A, Ahuja R, Vinayak M, et al. Anticarcinogenic Activity of Blue Fluorescent Hexagonal Boron Nitride Quantum Dots: As an Effective Enhancer for DNA Cleavage Activity of Anticancer Drug Doxorubicin. *Mater Today Bio* (2019) 1:100001. doi: 10.1016/j.mtbio.2019.01.001
25. Tapeinos C, Battaglini M, Ciofani ,G. Advances in the Design of Solid Lipid Nanoparticles and Nanostructured Lipid Carriers for Targeting Brain Diseases. *J Control Release* (2017) 264:306–32. doi: 10.1016/j.jconrel.2017.08.033
26. Zhao S, Minh LV, Li N, Garamus VM, Handge UA, Liu J, et al. Doxorubicin Hydrochloride-Oleic Acid Conjugate Loaded Nanostructured Lipid Carriers for Tumor Specific Drug Release. *Colloids Surf B Biointerfaces* (2016) 145:95–103. doi: 10.1016/j.colsurfb.2016.04.027
27. Patil A, Lakhani P, Taskar P, Wu KW, Sweeney C, Avula B, et al. Formulation Development, Optimization, and *In Vitro-In Vivo* Characterization of Natamycin-Loaded PEGylated Nano-Lipid Carriers for Ocular Applications. *J Pharm Sci* (2018) 107(8):2160–71. doi: 10.1016/j.xphs.2018.04.014

28. Astete CE, Sabliov CM. Synthesis and Characterization of PLGA Nanoparticles. *Biomat Sci-Polym E* (2006) 17(3):247–89. doi: 10.1163/156856206775997322
29. Barratt G. Colloidal Drug Carriers: Achievements and Perspectives. *Cell Mol Life Sci* (2003) 60(1):21–37. doi: 10.1007/s000180300002
30. Palazzolo S, Bayda S, Hadla M, Caligiuri I, Corona G, Toffoli G, et al. The Clinical Translation of Organic Nanomaterials for Cancer Therapy: A Focus on Polymeric Nanoparticles, Micelles, Liposomes and Exosomes. *Curr Med Chem* (2018) 25(34):4224–68. doi: 10.2174/0929867324666170830113755
31. Krishnagopal A, Reddy A, Sen D. Stent-Mediated Gene and Drug Delivery for Cardiovascular Disease and Cancer: A Brief Insight. *J Gene Med* (2017) 19(5): e2954. doi: 10.1002/jgm.2954
32. Kohn DB, Sadelain M, Glorioso JC. Occurrence of Leukaemia Following Gene Therapy of X-Linked SCID. *Nat Rev Cancer* (2003) 3(7):477–88. doi: 10.1038/nrc1122
33. Robbins PD, Ghivizzani SC. Viral Vectors for Gene Therapy. *Pharmacol Therapeut* (1998) 80(1):35–47. doi: 10.1016/S0163-7258(98)00020-5
34. Yin H, Kanasty RL, Eltoukhy AA, Vegas AJ, Dorkin JR, Anderson DG. Non-viral vectors for gene-based therapy. *Nat Rev Genet* (2014) 15(8):541–55. doi: 10.1038/nrg3763
35. Zhang Y, Satterlee A, Huang L. *In Vivo* Gene Delivery by Nonviral Vectors: Overcoming Hurdles? *Mol Ther* (2012) 20(7):1298–304. doi: 10.1038/mt.2012.79
36. Fang H, Feng Y, Chen J, Tian H, Chen X. Constructing Efficient Polycationic Gene Carriers Through Regulating the Physicochemical Properties. *Mater Today Chem* (2019) 11:269–82. doi: 10.1016/j.mtchem.2018.11.007
37. Wang P, Zhang L, Zheng W, Cong L, Guo Z, Xie Y, et al. Thermo-Triggered Release of CRISPR-Cas9 System by Lipid-Encapsulated Gold Nanoparticles for Tumor Therapy. *Angew Chem Int Ed Engl* (2018) 57(6):1491–6. doi: 10.1002/anie.201708689
38. Huang HC, Barua S, Sharma G, Dey SK, Rege K. Inorganic Nanoparticles for Cancer Imaging and Therapy. *J Control Release* (2011) 155(3):344–57. doi: 10.1016/j.jconrel.2011.06.004
39. Bayda S, Hadla M, Palazzolo S, Riello P, Corona G, Toffoli G, et al. Inorganic Nanoparticles for Cancer Therapy: A Transition From Lab to Clinic. *Curr Med Chem* (2018) 25(34):4269–303. doi: 10.2174/0929867325666171229141156
40. Pugazhendhi A, Edison T, Karuppusamy I, Kathirvel B. Inorganic Nanoparticles: A Potential Cancer Therapy for Human Welfare. *Int J Pharm* (2018) 539(1-2):104–11. doi: 10.1016/j.ijpharm.2018.01.034
41. Chen ML, He YJ, Chen XW, Wang JH. Quantum Dots Conjugated With Fe3O4-Filled Carbon Nanotubes for Cancer-Targeted Imaging and Magnetically Guided Drug Delivery. *Langmuir* (2012) 28(47):16469–76. doi: 10.1021/la303957y
42. Winnik FM, Maysinger D. Quantum Dot Cytotoxicity and Ways to Reduce it. *Acc Chem Res* (2013) 46(3):672–80. doi: 10.1021/ar3000585
43. You C, Wu H, Wang M, Wang S, Shi T, Luo Y, et al. A Strategy for Photothermal Conversion of Polymeric Nanoparticles by Polyaniline for Smart Control of Targeted Drug Delivery. *Nanotechnology* (2017) 28 (16):165102. doi: 10.1088/1361-6528/aa645f
44. Maeda H, Wu J, Sawa T, Matsumura Y, Hori K. Tumor Vascular Permeability and the EPR Effect in Macromolecular Therapeutics: A Review. *J Control Release* (2000) 65(1-2):271–84. doi: 10.1016/S0168-3659(99)00248-5
45. Nichols JW, Bae YH. EPR: Evidence and Fallacy. *J Control Release* (2014) 190:451–64. doi: 10.1016/j.jconrel.2014.03.057
46. Mitra S, Gaur U, Ghosh PC, Maitra AN. Tumour Targeted Delivery of Encapsulated Dextran-Doxorubicin Conjugate Using Chitosan Nanoparticles as Carrier. *J Control Release* (2001) 74(1-3):317–23. doi: 10.1016/s0168-3659(01)00342-x
47. Subhan MA, Yalamarty SSK, Filipczak N, Parveen F, Torchilin VP. Recent Advances in Tumor Targeting via EPR Effect for Cancer Treatment. *J Pers Med* (2021) 11(6):571. doi: 10.3390/jpm11060571
48. Lu Y, Low PS. Folate-Mediated Delivery of Macromolecular Anticancer Therapeutic Agents. *Adv Drug Deliv Rev* (2002) 54(5):675–93. doi: 10.1016/s0169-409x(02)00042-x
49. Elnakat H, Ratnam M. Role of Folate Receptor Genes in Reproduction and Related Cancers. *Front Biosci* (2006) 11:506–19. doi: 10.2741/1815
50. Kularatne SA, Zhou Z, Yang J, Post CB, Low PS. Design, Synthesis, and Preclinical Evaluation of Prostate-Specific Membrane Antigen Targeted (99m)Tc-Radioimaging Agents. *Mol Pharm* (2009) 6(3):790–800. doi: 10.1021/mp9000712
51. Bhuniya S, Maiti S, Kim EJ, Lee H, Sessler JL, Hong KS, et al. An Activatable Theranostic for Targeted Cancer Therapy and Imaging. *Angew Chem Int Ed Engl* (2014) 53(17):4469–74. doi: 10.1002/anie.201311133
52. Högemann-Savellano D, Bos E, Blondet C, Sato F, Abe T, Josephson L, et al. The Transferrin Receptor: A Potential Molecular Imaging Marker for Human Cancer. *Neoplasia* (2003) 5(6):495–506. doi: 10.1016/s1476-5586(03)80034-9
53. Reubi JC. Peptide Receptors as Molecular Targets for Cancer Diagnosis and Therapy. *Endocr Rev* (2003) 24(4):389–427. doi: 10.1210/er.2002-0007
54. Krall N, Pretto F, Decurtins W, Bernardes GJ, Supuran CT, Neri D. A Small-Molecule Drug Conjugate for the Treatment of Carbonic Anhydrase IX Expressing Tumors. *Angew Chem Int Ed Engl* (2014) 53(16):4231–5. doi: 10.1002/anie.201310709
55. Mackiewicz N, Nicolas J, Handke N, Noiray M, Mougin J, Daveu C, et al. Precise Engineering of Multifunctional PEGylated Polyester Nanoparticles for Cancer Cell Targeting and Imaging. *Chem Mater* (2014) 26(5):1834–47. doi: 10.1021/cm403822w
56. Thambi T, Son S, Lee DS, Park JH. Poly(ethylene Glycol)-B-Poly(Lysine) Copolymer Bearing Nitroaromatics for Hypoxia-Sensitive Drug Delivery. *Acta Biomater* (2016) 29:261–70. doi: 10.1016/j.actbio.2015.10.011
57. Thambi T, Deepagan VG, Yoon HY, Han HS, Kim SH, Son S, et al. Hypoxia-Responsive Polymeric Nanoparticles for Tumor-Targeted Drug Delivery. *Biomaterials* (2014) 35(5):1735–43. doi: 10.1016/j.biomaterials.2013.11.022
58. Zhang YJ, Gallis B, Taya M, Wang S, Ho RJ, Sasaki T. pH-Responsive Artemisinin Derivatives and Lipid Nanoparticle Formulations Inhibit Growth of Breast Cancer Cells *In Vitro* and Induce Down-Regulation of HER Family Members. *PLoS One* (2013) 8(3):e59086. doi: 10.1371/journal.pone.0059086
59. Zelzer M, Todd SJ, Hirst AR, Mcdonald TO, Ulijn RV. Enzyme Responsive Materials: Design Strategies and Future Developments. *Biomater Sci* (2013) 1 (1):11–39. doi: 10.1039/c2bm00041e
60. Widder KJ, Senyel AE, Scarpelli GD. Magnetic Microspheres: A Model System of Site Specific Drug Delivery *In Vivo*. *Proc Soc Exp Biol Med* (1978) 158 (2):141–6. doi: 10.3181/00379727-158-40158
61. Yang HW, Hua MY, Liu HL, Huang CY, Tsai RY, Lu YJ, et al. Self-Protecting Core-Shell Magnetic Nanoparticles for Targeted, Traceable, Long Half-Life Delivery of BCNU to Gliomas. *Biomaterials* (2011) 32(27):6523–32. doi: 10.1016/j.biomaterials.2011.05.047
62. Zhang L, Wang T, Yang L, Liu C, Wang C, Liu H, et al. General Route to Multifunctional Uniform Yolk/Mesoporous Silica Shell Nanocapsules: A Platform for Simultaneous Cancer-Targeted Imaging and Magnetically Guided Drug Delivery. *Chemistry* (2012) 18(39):12512–21. doi: 10.1002/chem.201200030
63. Yang C, Rait A, Pirollo KF, Dagata JA, Farkas N, Chang EH. Nanoimmunoliposome Delivery of Superparamagnetic Iron Oxide Markedly Enhances Targeting and Uptake in Human Cancer Cells *In Vitro* and *In Vivo*. *Nanomedicine* (2008) 4(4):318–29. doi: 10.1016/j.nano.2008.05.004
64. Zhang F, Braun GB, Pallaoro A, Zhang Y, Shi Y, Cui D, et al. Mesoporous Multifunctional Upconversion Luminescent and Magnetic "Nanorattle" Materials for Targeted Chemotherapy. *Nano Lett* (2012) 12(1):61–7. doi: 10.1021/nl202949y
65. Shalaby SM, Khater MK, Perucho AM, Mohamed SA, Helwa I, Laknaur A, et al. Magnetic Nanoparticles as a New Approach to Improve the Efficacy of Gene Therapy Against Differentiated Human Uterine Fibroid Cells and Tumor-Initiating Stem Cells. *Fertil Steril* (2016) 105(6):1638–1648.e1638. doi: 10.1016/j.fertnstert.2016.03.001
66. Stubbs M, Mcsheehy PM, Griffiths JR, Bashford CL. Causes and Consequences of Tumour Acidity and Implications for Treatment. *Mol Med Today* (2000) 6 (1):15–9. doi: 10.1016/s1357-4310(99)01615-9
67. Du JZ, Du XJ, Mao CQ, Wang J. Tailor-Made Dual pH-Sensitive Polymer-Doxorubicin Nanoparticles for Efficient Anticancer Drug Delivery. *J Am Chem Soc* (2011) 133(44):17560–3. doi: 10.1021/ja207150n
68. Qiu L, Zhu M, Gong K, Peng H, Ge L, Zhao L, et al. pH-Triggered Degradable Polymeric Micelles for Targeted Anti-Tumor Drug Delivery. *Mater Sci Eng C Mater Biol Appl* (2017) 78:912–22. doi: 10.1016/j.msec.2017.04.137
69. Zheng L, Zhang X, Wang Y, Liu F, Peng J, Zhao X, et al. Fabrication of Acidic pH-Cleavable Polymer for Anticancer Drug Delivery Using a Dual Functional

Monomer. *Biomacromolecules* (2018) 19(9):3874–82. doi: 10.1021/acs.biomac.8b01001
70. Sawant RM, Hurley JP, Salmaso S, Kale A, Tolcheva E, Levchenko TS, et al. "SMART" Drug Delivery Systems: Double-Targeted pH-Responsive Pharmaceutical Nanocarriers. *Bioconjug Chem* (2006) 17(4):943–9. doi: 10.1021/bc060080h
71. Deng Z, Zhen Z, Hu X, Wu S, Xu Z, Chu PK. Hollow Chitosan-Silica Nanospheres as pH-Sensitive Targeted Delivery Carriers in Breast Cancer Therapy. *Biomaterials* (2011) 32(21):4976–86. doi: 10.1016/j.biomaterials.2011.03.050
72. Fan T, Li M, Wu X, Li M, Wu Y. Preparation of Thermoresponsive and pH-Sensitivity Polymer Magnetic Hydrogel Nanospheres as Anticancer Drug Carriers. *Colloids Surf B Biointerfaces* (2011) 88(2):593–600. doi: 10.1016/j.colsurfb.2011.07.048
73. Shah SA, Aslam Khan MU, Arshad M, Awan SU, Hashmi MU, Ahmad N. Doxorubicin-Loaded Photosensitive Magnetic Liposomes for Multi-Modal Cancer Therapy. *Colloids Surf B Biointerfaces* (2016) 148:157–64. doi: 10.1016/j.colsurfb.2016.08.055
74. Fomina N, Sankaranarayanan J, Almutairi A. Photochemical Mechanisms of Light-Triggered Release From Nanocarriers. *Adv Drug Deliv Rev* (2012) 64(11):1005–20. doi: 10.1016/j.addr.2012.02.006
75. Schulze-Lefert P, Becker-André M, Schulz W, Hahlbrock K, Dangl JL. Functional Architecture of the Light-Responsive Chalcone Synthase Promoter From Parsley. *Plant Cell* (1989) 1(7):707–14. doi: 10.1105/tpc.1.7.707
76. Yang J, Lee J, Kang J, Oh SJ, Ko HJ, Son JH, et al. Smart Drug-Loaded Polymer Gold Nanoshells for Systemic and Localized Therapy of Human Epithelial Cancer. *Adv Mater* (2009) 21(43):4339–42. doi: 10.1002/adma.200900334
77. You J, Zhang R, Xiong C, Zhong M, Melancon M, Gupta S, et al. Effective Photothermal Chemotherapy Using Doxorubicin-Loaded Gold Nanospheres That Target EphB4 Receptors in Tumors. *Cancer Res* (2012) 72(18):4777–86. doi: 10.1158/0008-5472.Can-12-1003
78. Xia J, Du Y, Huang L, Chaurasiya B, Tu J, Webster TJ, et al. Redox-Responsive Micelles From Disulfide Bond-Bridged Hyaluronic Acid-Tocopherol Succinate for the Treatment of Melanoma. *Nanomedicine* (2018) 14(3):713–23. doi: 10.1016/j.nano.2017.12.017
79. Li Y, Liu T, Zhang G, Ge Z, Liu S. Tumor-Targeted Redox-Responsive Nonviral Gene Delivery Nanocarriers Based on Neutral-Cationic Brush Block Copolymers. *Macromol Rapid Commun* (2014) 35(4):466–73. doi: 10.1002/marc.201300719
80. Wang H, Tang L, Tu C, Song Z, Yin Q, Yin L, et al. Redox-Responsive, Core-Cross-Linked Micelles Capable of on-Demand, Concurrent Drug Release and Structure Disassembly. *Biomacromolecules* (2013) 14(10):3706–12. doi: 10.1021/bm401086d
81. Lammers T, Kiessling F, Hennink WE, Storm G. Drug Targeting to Tumors: Principles, Pitfalls and (Pre-) Clinical Progress. *J Control Release* (2012) 161(2):175–87. doi: 10.1016/j.jconrel.2011.09.063
82. Bae Y, Kataoka K. Intelligent Polymeric Micelles From Functional Poly(Ethylene Glycol)-Poly(Amino Acid) Block Copolymers. *Adv Drug Deliv* (2009) 61(10):768–84. doi: 10.1016/j.addr.2009.04.016
83. Holback H, Yeo Y. Intratumoral Drug Delivery With Nanoparticulate Carriers. *Pharm Res* (2011) 28(8):1819–30. doi: 10.1007/s11095-010-0360-y

Conflict of Interest: The authors declare that the research was conducted in the absence of any commercial or financial relationships that could be construed as a potential conflict of interest.

The handling editor declared a shared affiliation, though no other collaboration with the authors at the time of the review.

Publisher's Note: All claims expressed in this article are solely those of the authors and do not necessarily represent those of their affiliated organizations, or those of the publisher, the editors and the reviewers. Any product that may be evaluated in this article, or claim that may be made by its manufacturer, is not guaranteed or endorsed by the publisher.

Copyright © 2021 Xiang, Zhao, Wang, Sun, Guo, Tan and Liu. This is an open-access article distributed under the terms of the Creative Commons Attribution License (CC BY). The use, distribution or reproduction in other forums is permitted, provided the original author(s) and the copyright owner(s) are credited and that the original publication in this journal is cited, in accordance with accepted academic practice. No use, distribution or reproduction is permitted which does not comply with these terms.

frontiers in Oncology

ORIGINAL RESEARCH
published: 21 September 2021
doi: 10.3389/fonc.2021.738567

A Novel H_2O_2 Generator for Tumor Chemotherapy-Enhanced CO Gas Therapy

Yang Li[2†], Zeming Liu[1†], Weng Zeng[3†], Ziqi Wang[4], Chunping Liu[1], Ning Zeng[1], Keli Zhong[2], Dazhen Jiang[5*] and Yiping Wu[1*]*

[1] Department of Plastic Surgery, Tongji Hospital, Tongji Medical College, Huazhong University of Science and Technology, Wuhan, China, [2] Department of Gastrointestinal Surgery, Shenzhen People's Hospital (The Second Clinical Medical College, Jinan University, The First Affiliated Hospital, Southern University of Science and Technology), Shenzhen, China, [3] Department of Ophthalmology, Zhongnan Hospital of Wuhan University, Wuhan, China, [4] Key Laboratory of Artificial Micro- and Nano-Structures of Ministry of Education, School of Physics and Technology, Wuhan University, Wuhan, China, [5] Department of Radiation and Medical Oncology, Hubei Key Laboratory of Tumor Biological Behaviors, Hubei Cancer Clinical Study Center, Zhongnan Hospital of Wuhan University, Wuhan, China

OPEN ACCESS

Edited by:
Husain Yar Khan,
Wayne State University, United States

Reviewed by:
Wei Wei,
Memorial Sloan Kettering Cancer Center, United States
Ting Zhuang,
Xinxiang Medical University, China
Jia Huang,
Central South University, China

***Correspondence:**
Keli Zhong
zhongkeli@126.com
Dazhen Jiang
jiangdazhen@whu.edu.cn
Yiping Wu
wuyipingtj@163.com

[†]These authors have contributed equally to this work

Specialty section:
This article was submitted to Pharmacology of Anti-Cancer Drugs, a section of the journal Frontiers in Oncology

Received: *09 July 2021*
Accepted: *25 August 2021*
Published: *21 September 2021*

Citation:
Li Y, Liu Z, Zeng W, Wang Z, Liu C, Zeng N, Zhong K, Jiang D and Wu Y (2021) A Novel H_2O_2 Generator for Tumor Chemotherapy-Enhanced CO Gas Therapy. Front. Oncol. 11:738567. doi: 10.3389/fonc.2021.738567

Carbon monoxide (CO) gas therapy is a promising cancer treatment. However, gas delivery to the tumor site remains problematic. Proper tunable control of CO release in tumors is crucial to increasing the efficiency of CO treatment and reducing the risk of CO poisoning. To overcome such challenges, we designed ZCM, a novel stable nanotechnology delivery system comprising manganese carbonyl (MnCO) combined with anticancer drug camptothecin (CPT) loaded onto a zeolitic imidazole framework-8 (ZIF-8). After intravenous injection, ZCM gradually accumulates in cancerous tissues, decomposing in the acidic tumor microenvironment, releasing CPT and MnCO. CPT acts as a chemotherapy agent destroying tumors and producing copious H_2O_2. MnCO can react with the H_2O_2 to generate CO, powerfully damaging the tumor. Both *in vitro* and *in vivo* experiments indicate that the ZCM system is both safe and has excellent tumor inhibition properties. ZCM is a novel system for CO controlled release, with significant potential to improve future cancer therapy.

Keywords: H_2O_2 generator, CO gas therapy, camptothecin, ZIF-8 nanoparticles, TME (tumor microenvironment)

INTRODUCTION

The targeted development of cancer treatment technology—including chemotherapy, radiotherapy, and immunotherapy—has enormous potential in tumor treatment, although most such technologies are yet to be used routinely in the clinic (1–5). Among therapeutic approaches being developed, treating cancer with CO gas is both novel and practical, yet remains underexplored. High-dose CO can reduce cell protein synthesis by inhibiting cellular mitochondrial respiration and induce cancer cell apoptosis (6–8). The safety and potency of CO therapy relies on the precise release of large amounts of CO directly into the tumor (8). However, most CO-related anticancer treatments are still in their initial stages, as the gaseous nature of CO makes controlled release highly problematic.

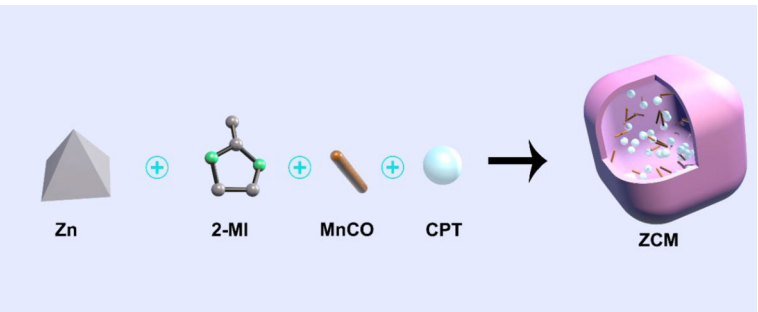
As a CO prodrug, manganese carbonyl (MnCO) has a Fenton-like reaction with H_2O_2 to generate CO gas *in situ* (9). CO can then bind hemoglobin in tumor tissue, reducing its capacity for oxygen transport, causing mitochondrial damage, and thus achieving an anticancer effect without causing side effects systemically (9). Zhu and coworkers designed a novel type of CO delivery system using the immune evasion ability and tumor targeting of tumor-derived exosomes (EXO), encapsulating MnCO into exosomes by electroporation method to form the MMV system (6); this system could achieve a powerful antitumor effect in combination with low-dose radiotherapy. Both *in vivo* and *in vitro* experiments have verified the rationality of the MMV combined with RT designed by their team, and there is no inflammatory reaction and other side effects during the treatment period, which has good biological safety. Jin and his team used hollow mesoporous silica nanoparticle (hMSN) nanocarriers to effectively encapsulate MnCO and constructed a nano-drug (MnCO@hMSN) for antitumor research (10). After being internalized into the tumor tissue, the nanomedicine (MnCO@hMSN) will react with H_2O_2 in the tumor (a new Fenton-like reaction that releases CO gas *in situ*) to achieve antitumor effects. *In vivo* experiments have shown that within the treatment cycle. The weight of the mice did not have any abnormalities, and the tumor proliferation was significantly inhibited (10). However, in cancer cells, although intracellular H_2O_2 concentration can reach 50 μM, endogenous H_2O_2 is unable to achieve satisfactory efficiency (11–13). Insufficient H_2O_2 in the tumor microenvironment (TME) is a profound problem for MnCO-based cancer therapy. CPT is a natural product topoisomerase inhibitor operating *via* several mechanisms including induction of cellular DNA damage (14–16). It is also an H_2O_2 enhancer, inducing high levels of H_2O_2 in the tumor (14). This property has interested several researchers. Tang et al. overcame the lack of target-specific, high-intensity luminescence by creating a target-specific chemiluminescence strategy, where CPT was loaded into the CLDRS system, enhancing H_2O_2 concentration and chemiluminescence (14). However, CPT has poor delivery to tumors and low water solubility, limiting its systemic use in cancer therapy.

Use of new nanocarriers allows for the design of secure and efficient multifunctional nanoplatforms for accurate drug delivery and effective cancer treatment. As a new metal-organic framework (MOF), ZIF-8 has good drug delivery properties and biocompatibility (17–21). Compared to other metal-organic framework (MOF) materials (22–26), ZIF-8 has several unique characteristics. ZIF-8 comprises 2-methylimidazole and Zn^{2+}. Zinc is the second most abundant transition metal in biology, while biogenic amino acid histidine contains an imidazole group (27). ZIF-8 has exceptional chemical and thermal stability, particularly in aqueous conditions; high specific surface area; and negligible physiological toxicity (28). Moreover, decomposition occurs easily under acidic conditions (pH 5.0–6.0), making ZIF-8 suitable for stimulus-responsive controlled drug release of payloads in the acidic tumor microenvironments (18). ZIF-8 is thus an ideal template for preparing hollow nanomaterials with adjustable sizes for small-molecule drug delivery. The ZIF-8-loaded drugs are less likely to leak during transit to their site of action, retaining pharmaceutical activity until they reach their target tumors (29, 30). Efficient delivery of CPT/MnCO using ZIF-8 nano-frameworks is expected to overcome many limitations of current CO gas therapy.

We designed a therapeutic strategy that combines chemotherapy drug CPT and CO gas prodrug MnCO in a ZIF-8 nanocarrier with good drug delivery properties forming a composite system we named ZCM (**Scheme 1**). After intravenous injection, ZCM circulates systemically, reaching the tumor target, where it is endocytosed. Subsequently, CPT and MnCO are released in response to the acidic tumor microenvironment, where CPT also acts as a H_2O_2 generator increasing the concentration of H_2O_2 in the tumor, synergistically improving the anticancer activity of MnCO. MnCO reacts with H_2O_2 to generate CO *in situ*, directly damaging mitochondria. *In vitro* and *in vivo* experiments indicate that the ZCM system has a high antitumor effect and does not induce significant off-target toxicity, since ZCM does not leak MnCO. The development of ZCM highlights a powerful new approach to MOF-based nanomedicines.

RESULTS AND DISCUSSION

ZIF-8 nanomaterials of approximately 100 nm were prepared using a simple stirring method (30). Then ZCMs were



SCHEME 1 | Illustration of a novel H_2O_2 generator for enhanced CO gas therapy.

synthesized by simultaneous embedment of CPT and MnCO into ZIF-8 to form a ZCM system, as shown in **Figures 1A, B** for transmission electron microscope (TEM) images of pure ZIF-8 and ZCM. A TEM image of ZCM, as measured in an acidic environment (**Figure 1C**), suggests that ZCM can decompose in an acidic environment. The diameter of ZCM (**Figure 1D**) showed almost no changes, again indicating that ZCM was stable and did not alter due to inclusion of drugs. The absorption of CPT, ZIF-8, MnCO, and ZCM was measured using UV–vis absorption spectroscopy, with results indicating the successful preparation of ZCM (**Figure 1E**). The drug loading efficiency of CPT and MnCO in ZCM was found to be 14.6% and 17.8%. ZCM's drug release ability was also studied (**Figure 1F**). Under neutral conditions, ZCM did not decompose and CPT was not released. At pH = 6.5, after 48 h of coculture, CPT release was approximately 30%. At pH = 5.5, CPT release was approximately 38% at 24 h; after 48 h, this had reached almost 90%, with the CPT almost completely released. As shown in **Figure S1**, the release rate of CO rapidly enhances with increasing H_2O_2 concentrations. This indicated that ZCM can release CO in response to the tumor microenvironment. This indicates that ZCM can help control payload release in the tumor environment, which is expected to alter the tumor microenvironment and realize CO gas therapy.

Our ZCM system performs well, and we are actively conducting *in vitro* antitumor trials. Although MnCO greatly inhibits tumors, the CO yield generated by the H_2O_2-MnCO reaction is affected by the H_2O_2 concentration in the tumor: at 50–100 μM, this is higher than in ordinary cells, but is still limited. Therefore, it is necessary to increase the tumor H_2O_2 concentration. Our system contains the chemotherapeutic drug CPT, which produces H_2O_2. We verified the ability of ZCM to produce CO; see **Figures 2A, D**. The control group and single ZIF-8 or ZC showed no fluorescence, suggesting a low intracellular CO concentration. ZM containing MnCO shows weak fluorescence. The green fluorescence of the ZCM treatment group was the strongest, since CPT can generate H_2O_2 in TME, promoting the reaction between MnCO and H_2O_2. Changes in mitochondrial membrane potential (MMP) in tumor cells were monitored using the JC-1(5,5′,6,6′-tetrachloro-1,1′,3,3′-tetraethyl-imidacarbocyanine) probe method. Typically, JC-1 dye accumulates in the mitochondria, where it aggregates, producing a red fluorescence. However, in damaged mitochondria where MMP is reduced, monomeric dye is released into the cytoplasm, producing green fluorescence. **Figures 2B, E** shows the high green/red fluorescence ratio of cells treated with ZCM. This is consistent with reduced mitochondrial damage due to ZCM. Once ZCM is decomposed by the acidic environment of tumor cells, MnCO will react with H_2O_2 in TME to produce CO gas *in situ*. This causes serious mitochondrial damage. In addition, we measured the ROS content of different formulations: the ZCM group had high fluorescence, while that of the ZC and ZM groups was much lower (**Figure 2C**). This may be because CPT alters the tumor microenvironment and MnCO produces elevated ROS. ROS can degrade cellular protein and DNA, thus killing tumor cells (27, 31–33). An MTT assay test indicated that the cell viability of the control and ZIF-8 groups was minimally affected, while ZC alone or ZM induced moderate tumor growth inhibition (**Figure 2F**). Our ZCM system showed the greatest tumor inhibition, reaching 90%. There are significant differences when compared to other experimental groups, suggesting that ZCM-

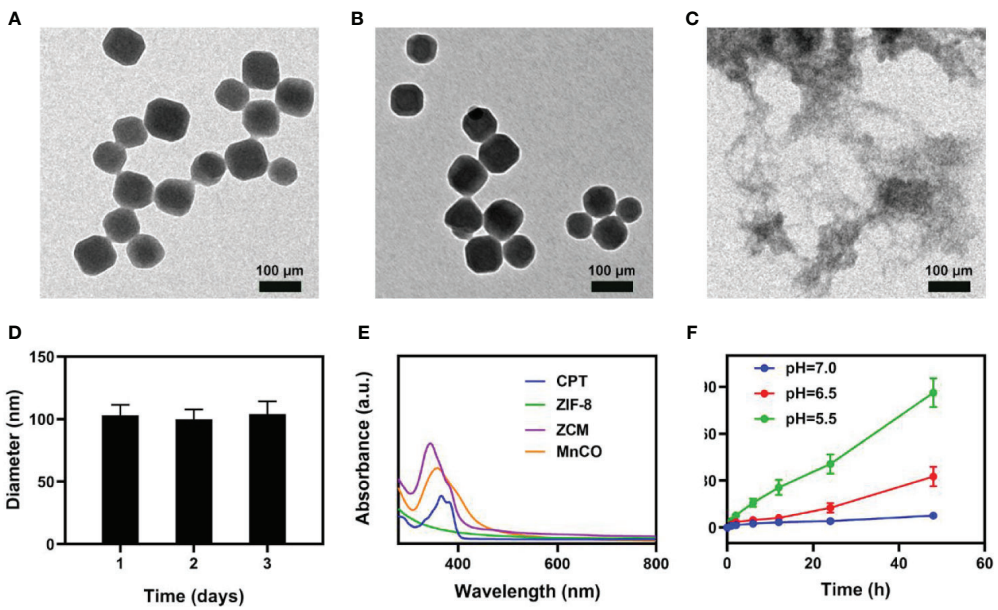


FIGURE 1 | Characterization of ZCM. **(A)** TEM image of ZIF-8 and **(B)** ZCM. **(C)** TEM image of decomposed ZCM. **(D)** DLS was used to measure the hydrodynamic diameter of ZCM. **(E)** UV–vis spectra for CPT, ZIF-8, MnCO, and ZCM in PBS. **(F)** *In vitro* CPT release profile at different pH from ZCM.

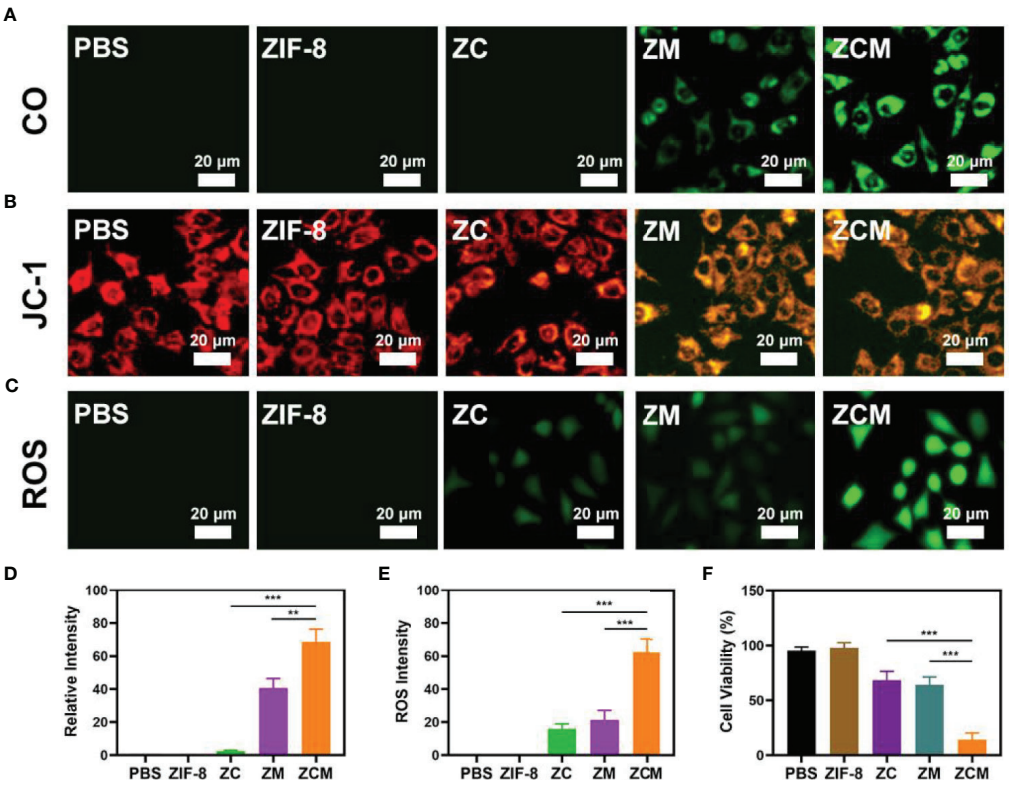


FIGURE 2 | *In vitro* synergetic therapeutic effects of the ZCM. **(A–C)** CO (FL-CO-1), JC-1 (green for JC-1 monomer and red for JC-1 aggregate), and ROS (DCFH-DA) fluorescence images under different treatments. **(D)** Quantification analysis of CO **(A)** based on the relative intensity of counts of at least 100 cells per treatment group (n = 3). **(E)** Fluorescence intensity of ROS in **(C)** based on the relative intensity of counts of at least 100 cells per treatment group (n = 3). **(F)** The survival of CT26 cells with different treatments. **p < 0.01, ***p < 0.005; Student's t-test.

mediated increased H_2O_2 concentrations of TME can enhance the effect of MnCO, inhibiting tumor growth.

We next evaluated the ZCM-mediated antitumor efficacy in mice with CT26 tumors. To investigate the principal effect of ZCM, BALB/c mice were injected subcutaneously into the right flank with 1×10^6 CT26 cells. The mice were treated when the primary tumor volume reached 200 mm^3. Tumor-bearing mice were randomly divided into five groups (five mice per group): (1) PBS; (2) ZIF-8; (3) ZC; (4) ZM; and (5) ZCM. The equivalent CPT dose was 10 mg/kg in groups 3 and 5. Treatment was conducted every 3 days for 16 days. During treatment, the tumor volumes of the control and ZIF-8 groups rose rapidly, which is shown in **Figures 3A, B**. The ZC or ZM group showed a moderate tumor suppression effect. When ZIF-8 reaches the tumor and is endocytosed, the acidic tumor microenvironment causes the ZIF-8 framework to decompose, releasing its drug payload and inducing a therapeutic effect. The ZCM system had the most marked therapeutic effect, with tumor volume growth almost entirely suppressed during treatment. During this study, no weight changes were detected in the treatment group, indicating no significant systemic toxicity (**Figure 3C**). This is crucial since many treatments have clear systemic toxicity, which significantly decreases their potential utility (34–37). We used the FL-Co-1 + $PdCl_2$ fluorescence probe to detect the CO content of tumors, confirming that combining CPT and MnCO in ZCM greatly enhanced CO generation in the tumor. We took tumor tissue sections for staining. H&E, TUNEL, and Ki-67 staining (**Figures 3D, E** and **S2, S3**) confirmed there was significant cell necrosis in the ZCM group. As shown in **Figure 4**, there was likewise no inflammatory damage, and liver and kidney indexes were normal. The *in vivo* results indicate that our novel treatment achieved both good biological safety therapy and increased tumor H_2O_2 concentration, reinforcing the effect of ZCM with profound CO-based therapy.

CONCLUSION

We designed a novel H_2O_2 generator ZCM to realize enhanced CO gas therapy. Encapsulated chemotherapeutic agents CPT and MnCO can increase the concentration of H_2O_2 in the tumor microenvironment driving CO gas therapy, with an enhanced ability to induce tumor cell apoptosis. The *in vitro* and *in vivo* results indicate our system has an excellent tumor inhibition effect. Our ZCM system exhibited no clear toxicity during

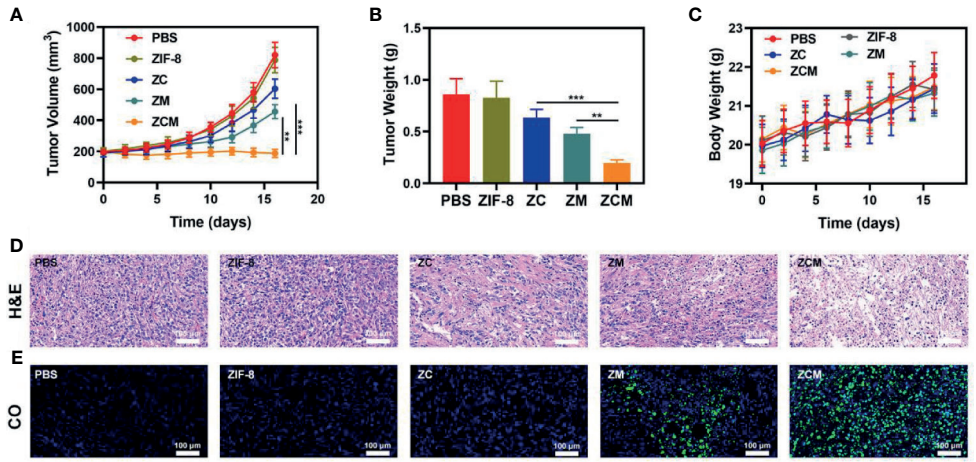


FIGURE 3 | *In vivo* therapy. **(A)** Tumor volume, **(B)** weight, and **(C)** murine body weight were monitored in the five treatment groups (n = 5). **(D)** Tumor sections were stained for H&E. **(E)** Fluorescence imaging for co-localization of the tumor region to test CO production. (Blue: DAPI, green: FL-CO-1). **p < 0.01, ***p < 0.005; Student's t-test.

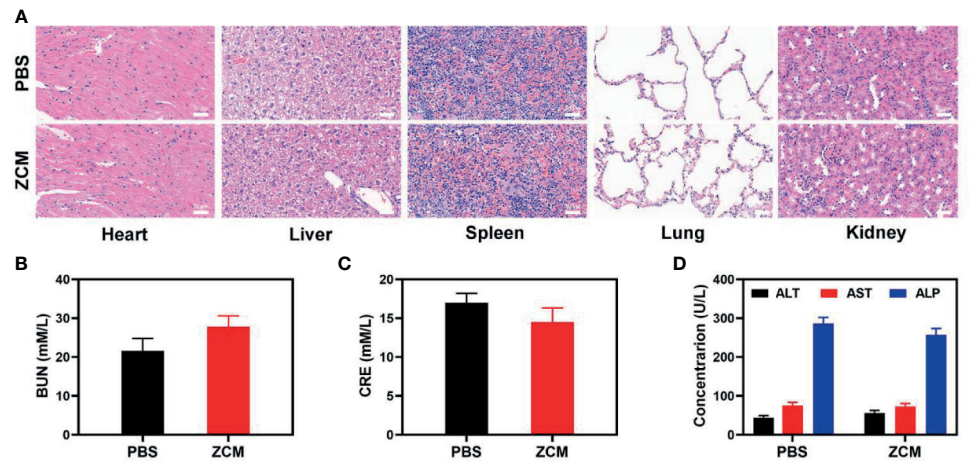


FIGURE 4 | **(A)** Histopathologic examination of the tissues including the heart, liver, spleen, lung, and kidney from tumor-bearing mice after PBS or ZCM treatment. **(B)** Blood biochemistry data for kidney function marker BUN. **(C)** Blood biochemistry data including kidney function marker CRE. **(D)** Liver function markers: ALT, AST, and ALP.

treatment. As non-toxic materials have better application potential and will also reduce the pain of patients during treatment. Although many materials have good antitumor effects, their systemic toxicity significantly affects the application value. We will explore the biological application of our combination of MnCO and other novel nanotechnology vehicles, optimizing our treatment plan.

DATA AVAILABILITY STATEMENT

The raw data supporting the conclusions of this article will be made available by the authors, without undue reservation.

ETHICS STATEMENT

The animal study was reviewed and approved by the Institutional Animal Care and Use Committee of Wuhan University.

AUTHOR CONTRIBUTIONS

Conceived and designed the experiments: YL, ZL, and WZ. Performed the experiments: YL, ZL, DJ, YW, KZ, and CL. Contributed reagents/materials/analysis tools: NZ, DJ, YW, KZ, and CL. Revised and polished the article: NZ, YL, ZL, DJ, YW, KZ, and CL. All authors contributed to the article and approved the submitted version.

FUNDING

This work was supported by the National Natural Science Foundation of China (81901771) and Zhongnan Hospital of Wuhan University Science, Technology and Innovation Seed Fund, Project znpy2019022.

SUPPLEMENTARY MATERIAL

The Supplementary Material for this article can be found online at: https://www.frontiersin.org/articles/10.3389/fonc.2021.738567/full#supplementary-material

REFERENCES

1. Chen Q, Xu L, Liang C, Wang C, Peng R, Liu Z. Photothermal Therapy With Immune-Adjuvant Nanoparticles Together With Checkpoint Blockade for Effective Cancer Immunotherapy. *Nat Commun* (2016) 7:13193. doi: 10.1038/ncomms13193
2. Zhang F, Lei Z. Molecular Engineering of NIR-II Fluorophores for Improved Biomedical Detection. *Angewandte Chemie* (2020) 60:16294–308.
3. Liang C, Zhang X, Yang M, Wang W, Chen P, Dong X. Remodeling Tumor Microenvironment by Multifunctional Nanoassemblies for Enhanced Photodynamic Cancer Therapy. *ACS Materials Lett* (2020) 2(10):1268–86. doi: 10.1021/acsmaterialslett.0c00259
4. Wang J, Sui L, Huang J, Miao L, Nie Y, Wang K, et al. MoS2-Based Nanocomposites for Cancer Diagnosis and Therapy. *Bioact Mater* (2021) 6 (11):4209–42. doi: 10.1016/j.bioactmat.2021.04.021
5. Ai K, Huang J, Xiao Z, Yang Y, Bai Y, Peng J. Localized Surface Plasmon Resonance Properties and Biomedical Applications of Copper Selenide Nanomaterials. *Mater Today Chem* (2021) 20:100402. doi: 10.1016/j.mtchem.2020.100402
6. Zhu D, Liu Z, Li Y, Huang Q, Xia L, Li K. Delivery of Manganese Carbonyl to the Tumor Microenvironment Using Tumor-Derived Exosomes for Cancer Gas Therapy and Low Dose Radiotherapy. *Biomaterials* (2021) 274:120894. doi: 10.1016/j.biomaterials.2021.120894
7. Wu L, Cai X, Zhu H, Li J, Shi D, Su D, et al. PDT-Driven Highly Efficient Intracellular Delivery and Controlled Release of CO in Combination With Sufficient Singlet Oxygen Production for Synergistic Anticancer Therapy. *Adv Funct Mater* (2018) 28(41):1804324. doi: 10.1002/adfm.201804324
8. Wang S, Shang L, Li L, Yu Y, Chi C, Wang K, et al. Metal-Organic-Framework-Derived Mesoporous Carbon Nanospheres Containing Porphyrin-Like Metal Centers for Conformal Phototherapy. *Adv Mater* (2016) 28(38):8379–87. doi: 10.1002/adma.201602197
9. Wu D, Duan X, Guan Q, Liu J, Yang X, Zhang F, et al. Mesoporous Polydopamine Carrying Manganese Carbonyl Responds to Tumor Microenvironment for Multimodal Imaging-Guided Cancer Therapy. *Adv Funct Mater* (2019) 29(16):1900095. doi: 10.1002/adfm.201900095
10. Jin Z, Wen Y, Xiong L, Yang T, Zhao P, Tan L, et al. Intratumoral H2O2-Triggered Release of CO From a Metal Carbonyl-Based Nanomedicine for Efficient CO Therapy. *Chem Commun* (2017) 53(40):5557–60. doi: 10.1039/C7CC01576C
11. Li WP, Su CH, Chang YC, Lin YJ, Yeh CS. Ultrasound-Induced Reactive Oxygen Species Mediated Therapy and Imaging Using a Fenton Reaction Activable Polymersome. *ACS Nano* (2016) 10(2):2017–27. doi: 10.1021/acsnano.5b06175
12. Tang Z, Zhang H, Liu Y, Ni D, Zhang H, Zhang J, et al. Antiferromagnetic Pyrite as the Tumor Microenvironment-Mediated Nanoplatform for Self-Enhanced Tumor Imaging and Therapy. *Adv Mater* (2017) 29(47):1701683. doi: 10.1002/adma.201701683
13. Huo M, Wang L, Chen Y, Shi J. Tumor-Selective Catalytic Nanomedicine by Nanocatalyst Delivery. *Nat Commun* (2017) 8(1):357. doi: 10.1038/s41467-017-00424-8
14. Tang Y, Lu X, Yin C, Zhao H, Hu W, Hu X, et al. Chemiluminescence-Initiated and in Situ-Enhanced Photoisomerization for Tissue-Depth-Independent Photo-Controlled Drug Release. *Chem Sci* (2019) 10(5):1401–9. doi: 10.1039/C8SC04012E
15. Gong L, Zhang Y, Liu C, Zhang M, Han S. Application of Radiosensitizers in Cancer Radiotherapy. *Int J Nanomed* (2021) 16:1083–102. doi: 10.2147/IJN.S290438
16. Liang Q, Bie N, Yong T, Tang K, Shi X, Wei Z, et al. The Softness of Tumour-Cell-Derived Microparticles Regulates Their Drug-Delivery Efficiency. *Nat Biomed Eng* (2019) 3(9):729–40. doi: 10.1038/s41551-019-0405-4
17. Su L, Wu Q, Tan L, Huang Z, Fu C, Ren X, et al. High Biocompatible ZIF-8 Coated by ZrO2 for Chemo-Microwave Thermal Tumor Synergistic Therapy. *ACS Appl Mater Interf* (2019) 11(11):10520–31. doi: 10.1021/acsami.8b22177
18. Shao F, Wu Y, Tian Z, Liu S. Biomimetic Nanoreactor for Targeted Cancer Starvation Therapy and Cascade Amplificated Chemotherapy. *Biomaterials* (2021) 274:120869. doi: 10.1016/j.biomaterials.2021.120869
19. Maleki A, Shahbazi MA, Alinezhad V, Santos HA. The Progress and Prospect of Zeolitic Imidazolate Frameworks in Cancer Therapy, Antibacterial Activity, and Biomineralization. *Advanced Healthcare Mater* (2020) 9(12):e2000248. doi: 10.1002/adhm.202000248
20. Meng X, Jia K, Sun K, Zhang L, Wang Z. Smart Responsive Nanoplatform *via in Situ* Forming Disulfiram-Copper Ion Chelation Complex for Cancer Combination Chemotherapy. *Chem Eng J* (2021) 415. doi: 10.1016/j.cej.2021.128947
21. Geng S, Lou R, Yin Q, Li S, Yang R, Zhou J. Reshaping the Tumor Microenvironment for Increasing the Distribution of Glucose Oxidase in Tumor and Inhibiting Metastasis. *J Mater Chem B* (2021) 9(5):1424–31. doi: 10.1039/D0TB02468F
22. Huang C, Ding S, Jiang W, Wang FB. Glutathione-Depleting Nanoplatelets for Enhanced Sonodynamic Cancer Therapy. *Nanoscale* (2021) 13:4512–8. doi: 10.1039/D0NR08440A
23. Yang G, Xu L, Chao Y, Xu J, Sun X, Wu Y, et al. Hollow MnO2 as a Tumor-Microenvironment-Responsive Biodegradable Nano-Platform for Combination Therapy Favoring Antitumor Immune Responses. *Nat Commun* (2017) 8(1):902. doi: 10.1038/s41467-017-01050-0
24. Fan W, Bu W, Shen B, He Q, Cui Z, Liu Y, et al. Intelligent MnO2 Nanosheets Anchored With Upconversion Nanoprobes for Concurrent pH-/H2O2-Responsive UCL Imaging and Oxygen-Elevated Synergetic Therapy. *Adv Mater* (2015) 27(28):4155–61. doi: 10.1002/adma.201405141
25. Zhu Y, Shi H, Li T, Yu J, Guo Z, Cheng J, et al. A Dual Functional Nanoreactor for Synergistic Starvation and Photodynamic Therapy. *ACS Appl Mater Interf* (2020) 12(16):18309–18. doi: 10.1021/acsami.0c01039
26. Song C, Xu W, Wei Z, Ou C, Wu J, Tong J, et al. Anti-LDLR Modified TPZ@Ce6-PEG Complexes for Tumor Hypoxia-Targeting Chemo-/Radio-/Photodynamic/Photothermal Therapy. *J Mater Chem B* (2020) 8(4):648–54. doi: 10.1039/C9TB02248A
27. Liu X, Liu Z, Dong K, Wu S, Sang Y, Cui T, et al. Tumor-Activatable Ultrasmall Nanozyme Generator for Enhanced Penetration and Deep Catalytic Therapy. *Biomaterials* (2020) 258:120263. doi: 10.1016/j.biomaterials.2020.120263
28. Li Y, Xu N, Zhu W, Wang L, Liu B, Zhang J, et al. Nanoscale Melittin@Zeolitic Imidazolate Frameworks for Enhanced Anticancer Activity and Mechanism Analysis. *ACS Appl Mater Interf* (2018) 10(27):22974–84. doi: 10.1021/acsami.8b06125
29. Zhao Q, Gong Z, Li Z, Wang J, Zhang J, Zhao Z, et al. Target Reprogramming Lysosomes of CD8+ T Cells by a Mineralized Metal-Organic Framework for Cancer Immunotherapy. *Adv Mater* (2021) 30:2100616. doi: 10.1002/adma.202100616
30. Li S, Tan L, Meng X. Nanoscale Metal-Organic Frameworks: Synthesis, Biocompatibility, Imaging Applications, and Thermal and Dynamic Therapy of Tumors. *Adv Funct Mater* (2020) 30(13):1908924. doi: 10.1002/adfm.201908924
31. Ding S, Liu Z, Huang C, Zeng N, Jiang W, Li Q. Novel Engineered Bacterium/Black Phosphorus Quantum Dot Hybrid System for Hypoxic Tumor Targeting and Efficient Photodynamic Therapy. *ACS Appl Mater Interf* (2021). doi: 10.1021/acsami.0c20254
32. Zhang C, Yan L, Gu Z, Zhao Y. Strategies Based on Metal-Based Nanoparticles for Hypoxic-Tumor Radiotherapy. *Chem Sci* (2019) 10(29):6932–43. doi: 10.1039/C9SC02107H

33. Chang M, Hou Z, Wang M, Yang C, Wang R, Li F, et al. Single-Atom Pd Nanozyme for Ferroptosis-Boosted Mild-Temperature Photothermal Therapy. *Angewandte Chemie* (2021) 60(23):12971–9. doi: 10.1002/anie.202101924
34. Guo B, Wu M, Shi Q, Dai T, Xu S, Jiang J, et al. All-In-One Molecular Aggregation-Induced Emission Theranostics: Fluorescence Image Guided and Mitochondria Targeted Chemo- and Photodynamic Cancer Cell Ablation. *Chem Mater* (2020) 32(11):4681–91. doi: 10.1021/acs.chemmater.0c01187
35. Yu W, Liu T, Zhang M, Wang Z, Ye J, Li CX, et al. O2 Economizer for Inhibiting Cell Respiration To Combat the Hypoxia Obstacle in Tumor Treatments. *ACS Nano* (2019) 13(2):1784–94. doi: 10.1021/acsnano.8b07852
36. Zhu D, Zhang J, Luo G, Duo Y, Tang BZ. Bright Bacterium for Hypoxia-Tolerant Photodynamic Therapy Against Orthotopic Colon Tumors by an Interventional Method. *Adv Sci* (2021) (8):2004769. doi: 10.1002/advs.202004769
37. Huang C, Chen B, Chen M, Jiang W, Liu W. Injectable Hydrogel for Cu(2+) Controlled Release and Potent Tumor Therapy. *Life (Basel)* (2021) 11(5):391. doi: 10.3390/life11050391

Conflict of Interest: The authors declare that the research was conducted in the absence of any commercial or financial relationships that could be construed as a potential conflict of interest.

Publisher's Note: All claims expressed in this article are solely those of the authors and do not necessarily represent those of their affiliated organizations, or those of the publisher, the editors and the reviewers. Any product that may be evaluated in this article, or claim that may be made by its manufacturer, is not guaranteed or endorsed by the publisher.

Copyright © 2021 Li, Liu, Zeng, Wang, Liu, Zeng, Zhong, Jiang and Wu. This is an open-access article distributed under the terms of the Creative Commons Attribution License (CC BY). The use, distribution or reproduction in other forums is permitted, provided the original author(s) and the copyright owner(s) are credited and that the original publication in this journal is cited, in accordance with accepted academic practice. No use, distribution or reproduction is permitted which does not comply with these terms.

frontiers in Oncology

ORIGINAL RESEARCH
published: 22 September 2021
doi: 10.3389/fonc.2021.750855

An Injectable Hydrogel for Enhanced FeGA-Based Chemodynamic Therapy by Increasing Intracellular Acidity

Wen Zeng[1,2†], Dazhen Jiang[3†], Zeming Liu[4†], Weilong Suo[1], Ziqi Wang[5], Daoming Zhu[1] and Qinqin Huang[1]*

[1] Department of Molecular Pathology, The Second Affiliated Hospital of Zhengzhou University, Zhengzhou, China, [2] Department of Ophthalmology, Zhongnan Hospital of Wuhan University, Wuhan, China, [3] Department of Radiation and Medical Oncology, Hubei Key Laboratory of Tumor Biological Behaviors, Hubei Cancer Clinical Study Center, Zhongnan Hospital of Wuhan University, Wuhan, China, [4] Department of Plastic and Cosmetic Surgery, Tongji Hospital, Tongji Medical College, Huazhong University of Science and Technology, Wuhan, China, [5] Key Laboratory of Artificial Micro- and Nano-Structures of Ministry of Education, School of Physics and Technology, Wuhan University, Wuhan, China

OPEN ACCESS

Edited by:
Cyril Corbet, Fonds National de la Recherche Scientifique (FNRS), Belgium

Reviewed by:
Qiong Huang, Central South University, China
Honghe Liu, Johns Hopkins University, United States
Ke Jiang, Sun Yat-sen University Cancer Center (SYSUCC), China

***Correspondence:**
Qinqin Huang
qqhuang@zzu.edu.cn

[†]These authors have contributed equally to this work

Specialty section:
This article was submitted to Pharmacology of Anti-Cancer Drugs, a section of the journal Frontiers in Oncology

Received: *31 July 2021*
Accepted: *02 September 2021*
Published: *22 September 2021*

Citation:
Zeng W, Jiang D, Liu Z, Suo W, Wang Z, Zhu D and Huang Q (2021) An Injectable Hydrogel for Enhanced FeGA-Based Chemodynamic Therapy by Increasing Intracellular Acidity. Front. Oncol. 11:750855. doi: 10.3389/fonc.2021.750855

Hydroxyl radical (•OH)-mediated chemodynamic therapy (CDT) is an emerging antitumor strategy, however, acid deficiency in the tumor microenvironment (TME) hampers its efficacy. In this study, a new injectable hydrogel was developed as an acid-enhanced CDT system (AES) for improving tumor therapy. The AES contains iron–gallic acid nanoparticles (FeGA) and α-cyano-4-hydroxycinnamic acid (α-CHCA). FeGA converts near-infrared laser into heat, which results in agarose degradation and consequent α-CHCA release. Then, as a monocarboxylic acid transporter inhibitor, α-CHCA can raise the acidity in TME, thus contributing to an increase in ·OH-production in FeGA-based CDT. This approach was found effective for killing tumor cells both *in vitro* and *in vivo*, demonstrating good therapeutic efficacy. *In vivo* investigations also revealed that AES had outstanding biocompatibility and stability. This is the first study to improve FeGA-based CDT by increasing intracellular acidity. The AES system developed here opens new opportunities for effective tumor treatment.

Keywords: FeGA, hydrogel, α-CHCA, chemodynamic therapy and tumor therapy, intracellular acidity

INTRODUCTION

Cancer, as one of the primary diseases affecting human health, has a profound impact on human life, and the patient's condition becomes due to the rapid propagation and diffusion of cancer cells, and the lower efficacy of the currently used chemotherapeutic agents (1–5). However, cancer cells are very sensitive to reactive oxygen species (ROS), increased ROS levels can cause cell redox imbalance, thus resulting in permanent damage to the orgate and, eventually, apoptosis (6, 7). Based on this fact, researchers have developed a range of new treatment approaches to enhance tumor ROS levels, such as radiotherapy (RT), photodynamic therapy (PDT), CDT, and so on (8–10). However, the light-treated PDT is limited in the body, and long-term RT results in diverse side effects (11–13). Furthermore, increasing evidence suggests that the CDT for foreign iron treatment offers a significant advantage (14, 15). In TME, Fe^{2+} can react with enough hydrogen peroxide (H_2O_2), thus producing toxic •OH. Several other kinds of iron-containing formulations such as

tetraned iron nanoparticles, iron oxide nanoparticles, and FeGA particles have been utilized as a catalyst for Fenton-reacted cell death, either alone or in combination with other catalysts (16, 17). Liu et al. used food acid and Fe^{2+} mixed ultra-small FeGA complex for achieving improved CDT (18). The catalytic stability of free Fe^{2+} was greatly improved due to GA-mediated Fe^{3+}, and the combined glutathione (GSH) consumpant BSO was significantly improved as FeGA could consume GSH. This in turn improved oxidative stress in tumors, resulting in a considerable improvement in the treatment effect of simultaneous chemotherapy or radiotherapy. Although a significant anti-tumor efficacy is attained, the Fenton reaction's effect is highly associated with the acidity of the tumor (19). With the decrease of pH, the reaction rate of Fe2+ with H_2O_2 increases. TME frequently exhibits a weak acid environment due to aberrant cancer cell metabolism and is unable to attain the optimal pH range of Fanton, which has a significant effect on CDT.

Cancer cells, unlike normal cells, are more likely to "ferment" glucose into lactic acid to produce adenosine triphosphate for energy rather than oxidative phosphorylation of mitochondria, even in normoxic conditions. This is the Warburg effect (20, 21). Furthermore, some tumor tissues continue to deteriorate lactic acid *via* the tricarboxylic acid (TCA) cycle to prevent long-term accumulation of lactic acid in the cells, thus inducing cell disorders. This is the metabolic process that tumor cells go through (22). As a result, disrupting the tumor's metabolic equilibrium by affecting the cyclic impact of TCG or the lactic acid transfer chain will eventually result in a substantial lactic acid accumulation in the cell and leads to cell acidosis (23). This in turn results in improved anti-tumor effects. Wan et al. used α-CHCA, a monocarboxylic acid transport inhibitor, to destroy the delivery process of lactic acid, alter the metabolic homeostasis, and used it in combination with H_2S to achieve a powerful tumor-killing effect (23). This approach only targets cancer tissues during therapy and does not produce inflammatory reactions or other organ side effects, thus demonstrating a high level of biological safety. However, most small-molecule drugs are administered *via* intravenous injection. The drugs are incapable of evading the immune system and cannot actively target tumor cells (24). A considerable number of drugs are removed through the bloodstream, and the drugs reaching the tumor are uncontrolled. These factors greatly limit the treatment efficacy.

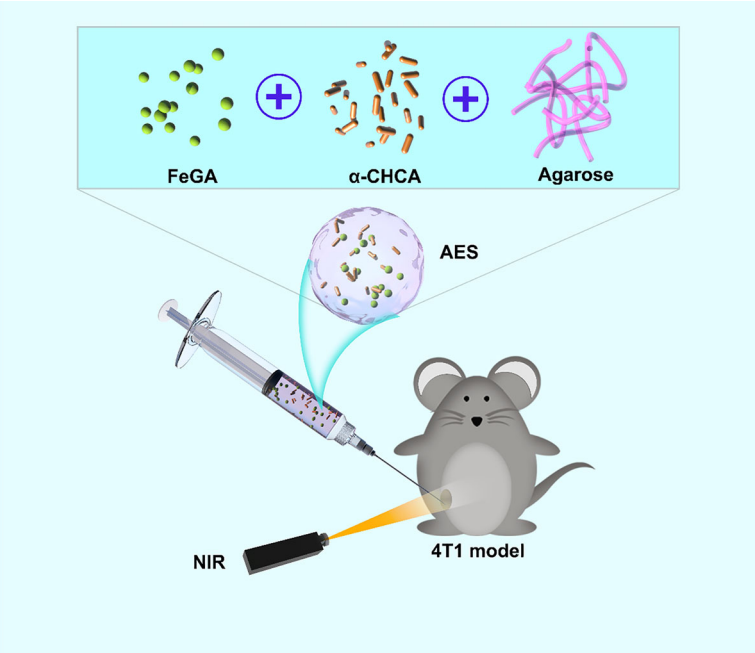
Traditional drug delivery systems usually have issues such as poor drug loading, difficult manufacturing processes, and early drug leakage or slow release (25–27). Although many inorganic and organic materials are also widely used in biological applications, most of them are injected intravenously, with high material loss rate and difficulty in reaching tumor tissues (28). Moreover, it is difficult to achieve controlled release of these materials or require complex modifications to improve their biological applicability, which is not conducive to clinical applications (29, 30). The long-term toxicity induced by the carrier persisting in the body for an extended period is also an important aspect. Light-responsive hydrogels with minimal invasiveness have recently gained popularity as a controlled drug release platform (31–33). The hydrogel gradually solidifies after being injected into tumor tissue and can be utilized as a military rationing depot for a longer period, this characteristic is attributed to the rapid decrease of the temperature of the hydrogel and the increase of the storage modulus, which leads to the solidification of the hydrogel and its long-term residence in the body (34, 35). After one injection, this form of local administration can be used again and again. Furthermore, the drug release rate can be changed by optimizing parameters such as laser strength and laser irradiation period and extending the treatment method's application. For the first time, Zhu et al. used an agarose hydrogel to deliver the AIEgen material for anti-tumor treatment. As a photothermal agent (PTA), prussian blue (PB) nanozyme stimulated the disintegration of the hydrogel while also acting as a CAT enzyme to catalyze H_2O_2 for improving the TME (31). Following that, a low-power white light was used. AIEgens produced ROSs under sufficient oxygen levels for promoting tumor ablation upon irradiation. As a result of these findings, we are encouraged to use hydrogels to deliver α-CHCA for disrupting the tumor's ecological balance and boosting the efficacy of FeGA-based CDT.

We designed an injectable hydrogel with FeGA nanoparticles and α-CHCA for intratumoral injection of chemodynamic and photothermal therapy (**Scheme 1**). The US Food and Drug Administration (FDA) has declared agarose hydrogels to be safe. FeGA nanoparticles and α-CHCA were placed into an agarose hydrogel for producing the FeGA reservoir and acid enhance system (AES). In this system, the FeGA nanoparticles serve as a PTA due to their outstanding photothermal performance. FeGA turns light energy into heat energy upon irradiating the AES system with an 808 nm near-infrared (NIR) laser, thus causing the temperature rise of the agarose hydrogel, as a result, reversible hydrolysis and softening occur. α-CHCA diffuses into the TME, inhibiting lactic acid efflux and intracellular accumulation in tumor cells, resulting in tumor acidosis. The Fenton reaction, which is driven by Fe^{2+}, can then produce a high amount of •OH, which can damage tumor cells. The AES can be employed as a FeGA storage controller for achieving the controlled release of the drug and for intratumor injection of local tumors. This is the first study to show that increasing intracellular acidity *in situ* improves FeGA-based CDT. In conclusion, the FH nanosystem has a wide range of clinical applications in synergetic therapy.

RESULTS AND DISCUSSION

Characterization of FeGA Nanoparticles and AES

Figure 1A shows a transmission electron microscope image of FeGA. The results show better dispersibility and smaller size of FeGA, with an average of 2.36 ± 1.2 nm. The nanoparticles of smaller than 10 nm in size are easily cleared by the kidney, which limits its therapeutic efficacy. Therefore, the applicability of FeGA can be greatly improved through the hydrogel delivery system. The particle size of FeGA was measured for three consecutive days (**Figure 1C**), and the size fluctuation range was found small, reflecting the good stability of FeGA. Thus, in turn



SCHEME 1 | Schematic illustration of an injectable hydrogel for enhanced FeGA-based chemodynamic therapy by increasing intracellular acidity.

makes it a good system in clinical application prospects. Even though many materials have a beneficial biological impact, their high instability restricts their future value (36). The agarose hydrogel has been authorized by the FDA as a safe material that does not cause any toxicity in the body and is metabolized by the body's natural processes following dissolution. The scanning electron microscope (SEM) image of the agarose hydrogel is shown in **Figure 1B**. The pore size of the hydrogel is larger and the AES system was then developed by encapsulating FeGA and α-CHCA in a hydrogel. **Figure 1D** demonstrates the good photothermal heating potential of AES while the developed hydrogel remains solid. The hydrogel gradually dissolves after 10 minutes of 808 nm laser irradiation. The drug and nanoparticles in the gel are almost totally dissolved and are released. Infrared thermal imaging further indicated that following irradiation, the temperature of AES increased dramatically. **Figure 1E** shows the ultraviolet-visible absorption of FeGA. FeGA has a quite high absorption bandwidth in the 600-800 nm range, with a distinctive peak near 600 nm. X-ray photoelectron spectroscopy (XPS) was used to measure the Fe 2p spectrum in FeGA (**Figure 1F**). Zeta potential of FeGA was detected to be -18.1 ± 6.57mV. The rheological value of AES was evaluated at various temperatures (**Figure 1G**), and the results revealed that as the temperature increases, AES rapidly dissolves, accompanied by a gradual decrease in storage modulus. This is in line with the hydrogel's rheological properties. We then put AES to the test to see if it could regulate the release of materials and the results are described in **Figure 1H**. Laser irradiation can partially disintegrate AES and liberate the α-CHCA within it. The hydrogel becomes cool and hardens after the laser irradiation is stopped, and the drug will remain protected. The drug is usually released completely after four laser switching cycles. This also demonstrates that our AES system has a strong ability to control drug release, which inhibits lactic acid efflux, strengthens the tumor's acidic environment, and keeps the cells in an acidic environment, which is likely to promote FeGA-mediated CDT.

Photo-Thermal of the FeGA for PTT

One of the most essential factors for evaluating PTA is photothermal stability. A powerful photothermal treatment can be assisted by a good photothermal agent. To test the photothermal performance of FeGA nanoparticles, FeGA solutions were prepared with different concentrations (0, 25, 50, 100, 200 μg/mL). **Figure 2A** shows that assuming all other parameters remain constant, the heating impact of the solution increases as the FeGA concentration rises. The temperature of 100 μg/mL FeGa increased by roughly 16.6°C after 5 min of laser irradiation. For 5 minutes, the 200 μg/mL FeGA solution was repeatedly heated with the 808 nm NIR laser (**Figures 2B, D, E**), then the solution was allowed to cool to ambient temperature. The heating curves of each cycle were identical, and the variations in peak temperature changes were minor, demonstrating that the FeGA nanoparticles' photothermal conversion capability was found to be stable and reproducible over repeated 4 heating and cooling cycles. These findings suggest that the FeGA nanoparticles have good photothermal stability. Furthermore, the photo-thermal conversion efficiency (η) of the FeGA was calculated from the data of **Figures 2C, F**, and was found as 42.6%, which was higher than various materials such as Au nanorods (21%) and Ti_3C_2 nanosheets (30.6%) (37, 38). Above all, FeGA nanoparticles are an excellent PTA for photothermal conversion to anti-tumor.

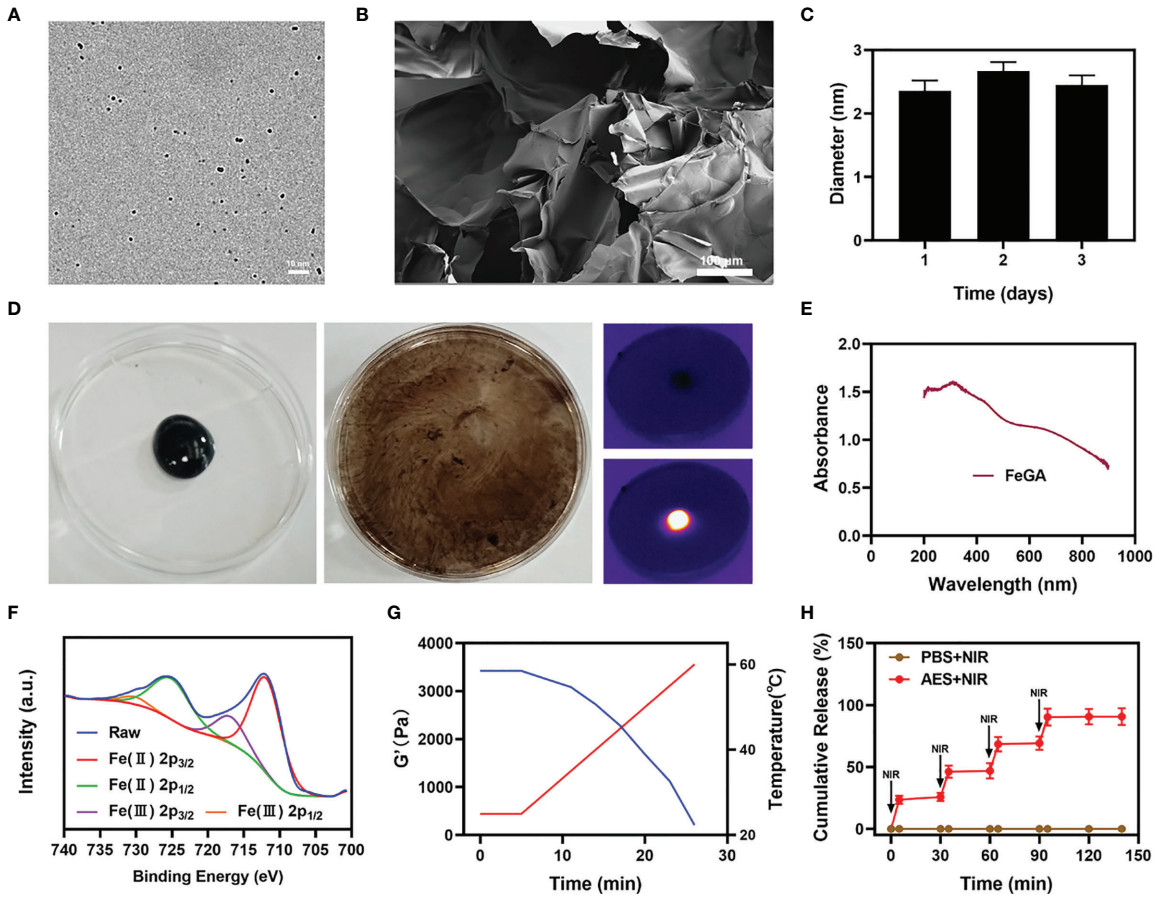


FIGURE 1 | Characterization of AES. **(A)** TEM image of FeGA. **(B)** SEM image of the hydrogel. **(C)** Statistical graph of the measured diameter of FeGA. (n = 3). **(D)** The morphology of the prepared AES before and after 0.5 W/cm^2 808 nm laser irradiation for 10 min and infrared thermal images of the prepared AES after being irradiated. **(E)** FeGA absorbance spectra. **(F)** Fe 2p spectrum of XPS spectra of fresh GA–Fe. **(G)** Rheological and temperature curves (blue and red, respectively) for the prepared AES in response to 0.5 W/cm^2 808 nm laser irradiation. **(H)** *In vitro* AES release profile in the presence and absence of 808 nm laser irradiation, with red arrows being used to indicate irradiation time points (n = 3). The results were expressed as mean ± SD.

In Vitro Combination Therapy

Furthermore, we assessed the ROS content of several formulations. There is no green fluorescence in the control group, the NIR group, or the AES group when treated alone. The AES + NIR group had high fluorescence, whereas the FeGA + NIR group had much lower fluorescence. This could be because α-CHCA alters the tumor acid microenvironment, and FeGA reacts with enough H_2O_2 to produce increased ROS. ROS can cause cellular protein and DNA damage, resulting in the death of tumor cells (39). In several experimental groups, we continued to evaluate the lactic acid concentration of the TME. The results revealed that, despite the presence of α-CHCA in the AES group, α-CHCA was unable to affect the cells due to the hydrogel's encapsulation, but the AES + NIR group had increased lactic acid concentration. α-CHCA can be released after laser irradiation, changing the lactic acid ecological microenvironment of tumor cells. Hence, the AES + NIR group was able to produce good lactate accumulating effect. The acidic environment is conducive to the subsequent FeGA-mediated Fenton reaction. FeGA was incubated with 4T1 cells at various concentrations (0, 10, 20, 30, 40 μg/mL) for 24 hours. Even at high concentrations, cell viability did not decrease significantly. The findings suggested that FeGA NPs are highly biocompatible. The cell viability of the control group was largely unaffected by the MTT experiment, whereas the NIR with FeGA group demonstrated a little inhibition in tumor growth (**Figure 2G**). AES + NIR system exhibited the best tumor growth inhibition rate (about 88.5%), with significant differences compared to other experiment groups indicating that AES mediated controlled release of α-CHCA can effectively increase the acidity of TME, thereby enhancing the CDT effect and inhibiting tumor growth. These findings motivate our ongoing research to proceed with the developed formulation for anti-tumor efficacy *in vivo*.

In Vivo Anti-tumor Study

As stated earlier, the good performance of AES *in vitro* as a PTA and acid boosting system has prompted us to investigate the

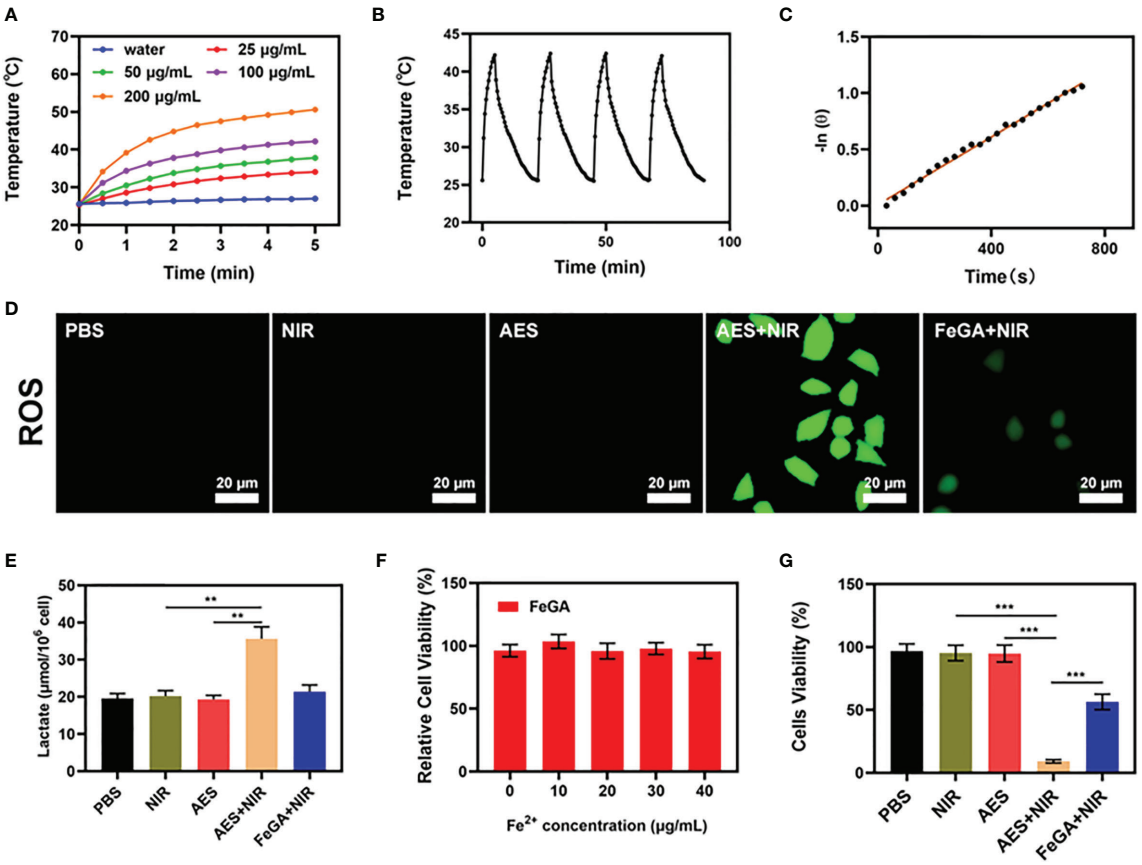


FIGURE 2 | *In vitro* synergetic therapeutic effects of the AES. **(A)** Temperature increase for the different FeGA concentrations upon laser irradiation at 808 nm and 0.5 W/cm^2 for 5min. **(B)** Temperature variation of a FeGA solution at 100 μg/mL under cyclic laser irradiation. **(C)** Calculation of the time constant for the heat transfer using linear regression of the cooling profile. **(D)** Measurement of tumor cell ROS fluorescence after the indicated treatments (n = 5). **(E)** *In vitro* lactate accumulation effect of different formulations (n = 5). **(F)** Dark cytotoxicity of FeGA on 4T1 cells (n = 5). **(G)** *In vitro* cytotoxicity of different formulations against 4T1 cells (n = 5). **P < 0.01, ***P < 0.005; Student's t-test. The results were expressed as mean ± SD.

photothermal conversion effect of FeGA *in vivo*. BALB/c mice were used to establish 4T1 subcutaneous tumor models. After invading the tumor tissue, we measured the temperature rise of AES under laser irradiation. The PBS group rarely heated up after laser irradiation, as seen in **Figures 3A, B**, whereas the temperature of the tumor in the AES group increased dramatically, showing that AES has strong photothermal performance. This finding is similar to the *in vitro* photothermal findings, demonstrating that AES can provide *in vivo* photothermal therapy and drug release. Tumor tissues' heat resistance was lowered when compared to normal cells, resulting in tumor cell-selective apoptosis at high temperatures (42 – 47°C) (17). Following that, we measured the amount of lactic acid in the tumor after various treatments. The lactic acid level of the tumor increased considerably after 4 hours of AES plus NIR treatment, as seen in **Figure 3C**. However, no obvious signals of increase were observed in the other groups, demonstrating that the released -CHCA can effectively prevent tumor cell lactic acid efflux and intracellular accumulation, leading to tumor acidosis (**Figure 3C**). The anti-tumor efficacy of AES-mediated anti-tumor therapy was next evaluated in mice with 4T1 tumors. BALB/c mice were injected subcutaneously with 1×10^6 4T1 cells in the right flank to assess the main effect of AES. The mice were treated after reaching the primary tumor volume to 200 mm^3. Tumor-bearing mice were randomly divided into 4 groups (5 mice per group): (1) PBS; (2) NIR; (3) AES and (4) AES + NIR. The equivalent FeGA dose was 5 mg/kg in groups 3 and 4. For 16 days, treatment was given every 4 days. The body mass of treated and control mice remained normal after treatment, showing the safety of our technique (**Figure 3F**). This is quite interesting because many treatments are associated with severe systemic toxicity, which is detrimental to the material's future clinical application (40). The tumor volumes of the PBS and NIR treated groups increased substantially during the 2 weeks of treatment, as illustrated in **Figure 3D**. In addition, the AES group had essentially no tumor-suppressive effect. The hydrogel entrapped FeGA and CHCA are unable to kill tumors. The AES + NIR system, which included both FeGA, had the most potent therapeutic response as the tumor volume growth curves being nearly reduced during therapy (**Figures 3D, E**). When the AES hydrogel is exposed to laser radiation after intratumoral injection, it

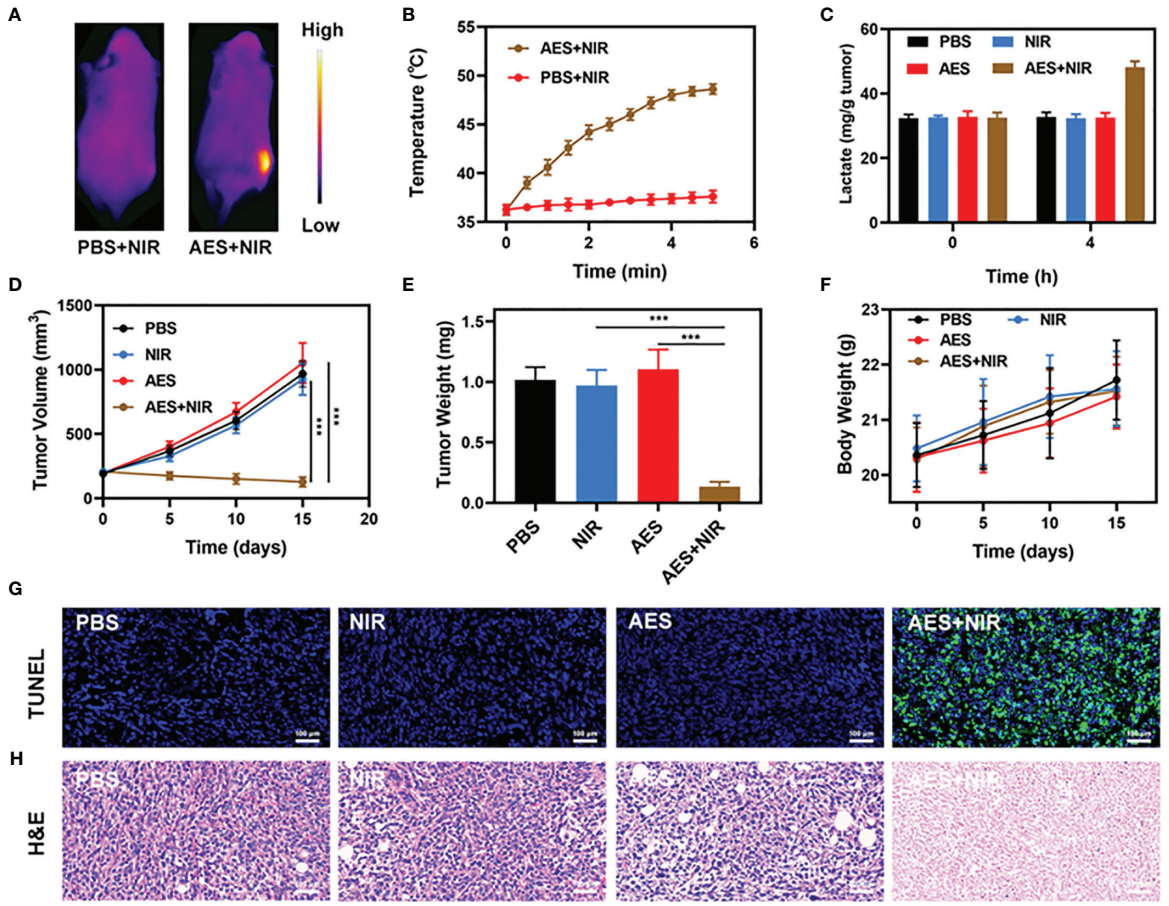


FIGURE 3 | *In vivo* therapy. **(A)** IR thermal images of tumors following an 808 nm laser irradiation (0.5 W/cm^2) for 5 min in the indicated treatment groups (n = 3). **(B)** Temperature increase in mice implanted with 4T1 tumors following 808 nm laser irradiation (0.5 W/cm^2) for 5 min in the indicated treatment groups. **(C)** Lactate accumulation effect of different *in vivo* treatments (n = 5). **(D)** Tumor volume changes over time in groups treated as indicated (n = 5). **(E)** Average tumor weight values associated with the indicated treatments (n = 5). **(F)** Changes in body weight in response to the indicated treatments (n = 5). **(G)** TUNEL and **(H)** H&E stained tumor sections from the indicated treatment groups (n = 5). ***P < 0.005; Student's t-test. The results were expressed as mean ± SD.

dissolves and releases FeGA and α-CHCA in FH. α-CHCA would raise the tumor's lactic acid concentration. FeGA then combines with intratumoral H_2O_2 to produce •OH in situ, which kills the tumor. We tested the fluorescence intensity of ROS in different groups *in vivo*, and the results also showed that AES + NIR group showed the strongest green fluorescence, and produced a large amount of ROS to promote tumor apoptosis. The tumor mass of mice was also in agreement with the volume curve (**Figure 3E**). We obtained slices of tumor tissue for staining. TUNEL and H&E staining (**Figures 3G, H**) also confirmed the large amount of cell necrosis in the AES combined NIR treatment group.

Histological Analysis

Furthermore, FeGA activation did not cause any loss to systems, as shown in **Figure 4**. After the treatment of mice's vital organs (heart, liver, spleen, lungs, and kidney), there was no inflammation, and damage in the body, and the liver, and kidney indexes were also normal. As many nanomaterials possess great therapeutic efficacy, they are also associated with systemic toxicity, which limits their future clinical applications (41). *In vivo* data show that our novel combination therapy not only achieves a high level of biological safety but also increases tumor •OH content, thus enhancing the effect of FH-enhanced therapy.

CONCLUSION

Finally, we developed an injectable light-controlled hydrogel system, called an acid to enhance system AES, by encapsulating FeGA nanoparticles and α CHCA in agarose hydrogel. The nano-system can be combined with 808 nm laser irradiation for achieving outstanding tumor treatment effects. FeGA nanoparticles can be employed as an ideal PTA due to their superior photothermal effect in the NIR-I region. The agarose hydrogel underwent controlled and reversible hydrolysis and softening states under the NIR laser power, resulting in light-triggered FeGA nanoparticles release and

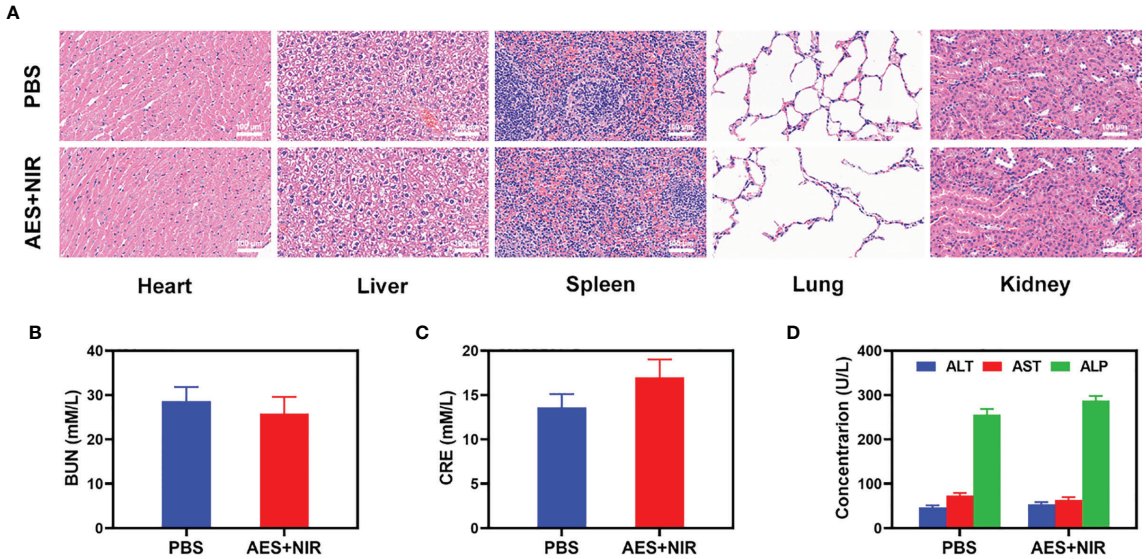


FIGURE 4 | Result of *in vivo* safety experiments. **(A)** Histopathological analysis results (H&E-stained images) of the major organs, heart, lung, liver, kidneys, and spleen, of mice that were exposed to different treatments of 16 days post-injection. Blood biochemistry data including kidney function markers: **(B)** liver function markers: BUN, **(C)** CRE, and **(D)** ALT, ALP, and AST after various treatments (n = 5). The results were expressed as mean ± SD.

degradation of hydrogel. Then, α-CHCA would then cause tumor acidosis in the region, causing an increase in the Fenton reaction. The AES exhibits outstanding cancer cell killing and tumor ablation properties in both *in vitro* and *in vivo* tests, with good stability, low toxicity, and biocompatibility. This is the first study to show that increasing intracellular acidity in FeGA-based CDT improves its performance. Thus, we may conclude that the AES has great anti-cancer potential in combination therapy.

DATA AVAILABILITY STATEMENT

The raw data supporting the conclusions of this article will be made available by the authors, without undue reservation.

ETHICS STATEMENT

The animal experiments were carried out according to the protocol approved by the Ministry of Health in People's Republic of PR China and were approved by the Administrative Committee on Animal Research of the Zhengzhou University.

AUTHOR CONTRIBUTIONS

Conceived and designed the experiments: ZW, WZ, ZL, WS, DJ, and QH. Performed the experiments: WZ, DZ, ZL, ZW, and WS. Contributed reagents/materials/analysis tools: ZW, WS, WZ, DJ and QH. All authors contributed to the article and approved the submitted version.

FUNDING

This work was supported by the National Natural Science Foundation of China (31800085) and Zhongnan Hospital of Wuhan University Science, Technology and Innovation Seed Fund, Project znpy2019022.

SUPPLEMENTARY MATERIAL

The Supplementary Material for this article can be found online at: https://www.frontiersin.org/articles/10.3389/fonc.2021.750855/full#supplementary-material

REFERENCES

1. Zhu D, Lyu M, Jiang W, Suo M, Huang Q, Li K. A Biomimetic Nanozyme/Camptothecin Hybrid System for Synergistically Enhanced Radiotherapy. *J Materr Chem B* (2020) 8:5312–9. doi: 10.1039/D0TB00676A
2. Zhu D, Lyu M, Huang Q, Suo M, Liu Y, Jiang W, et al. Stellate Plasmonic Exosomes for Penetrative Targeting Tumor NIR-II Thermo-Radiotherapy. *ACS Appl Materr Interfaces* (2020) 12(33):36928–37. doi: 10.1021/acsami.0c09969
3. Huang C, Wang FB, Liu L, Jiang W, Liu W, Ma W, et al. Hypoxic Tumor Radiosensitization Using Engineered Probiotics. *Adv Healthcare Materr* (2021) 10:2002207. doi: 10.1002/adhm.202002207
4. Ding S, Liu Z, Huang C, Zeng N, Jiang W, Li Q. Novel Engineered Bacterium/Black Phosphorus Quantum Dot Hybrid System for Hypoxic Tumor Targeting and Efficient Photodynamic Therapy. *ACS Appl Materr Interfaces* (2021) 13(8):10564–73. doi: 10.1021/acsami.0c20254
5. Yu W, Liu T, Zhang M, Wang Z, Ye J, Li CX, et al. O2 Economizer for Inhibiting Cell Respiration To Combat the Hypoxia Obstacle in

Tumor Treatments. *ACS Nano* (2019) 13(2):1784–94. doi: 10.1021/acsnano.8b07852
6. Cheng Y-J, Qin S-Y, Ma Y-H, Chen X-S, Zhang A-Q, Zhang X-Z. Super-pH-Sensitive Mesoporous Silica Nanoparticle-Based Drug Delivery System for Effective Combination Cancer Therapy. *ACS Biomater Sci Eng* (2019) 5 (4):1878–86. doi: 10.1021/acsbiomaterials.9b00099
7. Liu LH, Zhang YH, Qiu WX, Zhang L, Gao F, Li B, et al. Dual-Stage Light Amplified Photodynamic Therapy Against Hypoxic Tumor Based on an O2 Self-Sufficient Nanoplatform. *Small* (2017) 13(37):1701621. doi: 10.1002/smll.201701621
8. Guo J, Huang L. Membrane-Core Nanoparticles for Cancer Nanomedicine. *Adv Drug Delivery Rev* (2020) 156:23–39. doi: 10.1016/j.addr.2020.05.005
9. Wang X-Q, Wang W, Peng M, Zhang X-Z. Free Radicals for Cancer Theranostics. *Biomaterials* (2021) 266:120474. doi: 10.1016/j.biomaterials.2020.120474
10. Li S, Tan L, Meng X. Nanoscale Metal-Organic Frameworks: Synthesis, Biocompatibility, Imaging Applications, and Thermal and Dynamic Therapy of Tumors. *Adv Funct Mater* (2020) 30(13):1908924. doi: 10.1002/adfm.201908924
11. Zhao LP, Zheng RR, Chen HQ, Liu LS, Zhao XY, Liu HH, et al. Self-Delivery Nanomedicine for O2-Economized Photodynamic Tumor Therapy. *Nano Lett* (2020) 20(3):2062–71. doi: 10.1021/acs.nanolett.0c00047
12. Ren SZ, Wang B, Zhu XH, Zhu D, Liu M, Li SK, et al. Oxygen Self-Sufficient Core-Shell Metal-Organic Framework-Based Smart Nanoplatform for Enhanced Synergistic Chemotherapy and Photodynamic Therapy. *ACS Appl Materr Interfaces* (2020) 12(22):24662–74. doi: 10.1021/acsami.0c08534
13. Jin C, Bai L, Wu H, Tian F, Guo G. Radiosensitization of Paclitaxel, Etanidazole and Paclitaxel+Etanidazole Nanoparticles on Hypoxic Human Tumor Cells In Vitro. *Biomaterials* (2007) 28(25):3724–30. doi: 10.1016/j.biomaterials.2007.04.032
14. Fu S, Yang R, Zhang L, Liu W, Du G, Cao Y, et al. Biomimetic CoO@AuPt Nanozyme Responsive to Multiple Tumor Microenvironmental Clues for Augmenting Chemodynamic Therapy. *Biomaterials* (2020) 257:120279. doi: 10.1016/j.biomaterials.2020.120279
15. Meng X, Jia K, Sun K, Zhang L, Wang Z. Smart Responsive Nanoplatform via in Situ Forming Disulfiram-Copper Ion Chelation Complex for Cancer Combination Chemotherapy. *Chem Eng J* (2021) 415:128947. doi: 10.1016/j.cej.2021.128947
16. Zhang X, He C, Chen Y, Chen C, Yan R, Fan T, et al. Cyclic Reactions-Mediated Self-Supply of H2O2 and O2 for Cooperative Chemodynamic/Starvation Cancer Therapy. *Biomaterials* (2021) 275:120987. doi: 10.1016/j.biomaterials.2021.120987
17. He Y, Guo S, Zhang Y, Liu Y, Ju H. NIR-II Reinforced Intracellular Cyclic Reaction to Enhance Chemodynamic Therapy With Abundant H2O2 Supply. *Biomaterials* (2021) 275:120962. doi: 10.1016/j.biomaterials.2021.120962
18. Dong Z, Feng L, Chao Y, Hao Y, Chen M, Gong F, et al. Amplification of Tumor Oxidative Stresses With Liposomal Fenton Catalyst and Glutathione Inhibitor for Enhanced Cancer Chemotherapy and Radiotherapy. *Nano Lett* (2019) 19(2):805–15. doi: 10.1021/acs.nanolett.8b03905
19. Li M, Lan X, Han X, Shi S, Sun H, Kang Y, et al. Acid-Induced Self-Catalyzing Platform Based on Dextran-Coated Copper Peroxide Nanoaggregates for Biofilm Treatment. *ACS Appl Materr Interfaces* (2021) 13(25):29269–80. doi: 10.1021/acsami.1c03409
20. Liberti MV, Locasale JW. The Warburg Effect: How Does it Benefit Cancer Cells? *Trends Biochem Sci* (2016) 41(3):211–8. doi: 10.1016/j.tibs.2015.12.001
21. Icard P, Shulman S, Farhat D, Steyaert JM, Alifano M, Lincet H. How the Warburg Effect Supports Aggressiveness and Drug Resistance of Cancer Cells? *Drug Resist Updates Rev Commentaries Antimicrob Anticancer Chemother* (2018) 38:1–11. doi: 10.1016/j.drup.2018.03.001
22. Gao F, Tang Y, Liu WL, Zou MZ, Huang C, Liu CJ, et al. Intra/Extracellular Lactic Acid Exhaustion for Synergistic Metabolic Therapy and Immunotherapy of Tumors. *Adv Materr* (2019) e1904639. doi: 10.1002/adma.201904639
23. Chen Q-W, Wang J-W, Wang X-N, Fan J-X, Liu X-H, Li B, et al. Inhibition of Tumor Progression Through the Coupling of Bacterial Respiration With Tumor Metabolism. *Angewandte Chemie (International Ed English)* (2020) 59 (48):21562–70. doi: 10.1002/anie.202002649
24. Huang C, Ding S, Jiang W, Wang FB. Glutathione-Depleting Nanoplatelets for Enhanced Sonodynamic Cancer Therapy. *Nanoscale* (2021) 13:4512–8. doi: 10.1039/D0NR08440A
25. Ren C, Cheng Y, Li W, Liu P, Yang L, Lu Q, et al. Ultra-Small Bi2S3 Nanodot-Doped Reversible Fe(ii/iii)-Based Hollow Mesoporous Prussian Blue Nanocubes for Amplified Tumor Oxidative Stress-Augmented Photo-/Radiotherapy. *Biomater Sci* (2020) 8(7):1981–95. doi: 10.1039/C9BM02014D
26. Jin L, Hu P, Wang Y, Wu L, Qin K, Cheng H, et al. Fast-Acting Black-Phosphorus-Assisted Depression Therapy With Low Toxicity. *Adv Materr* (2020) 32(2):e1906050. doi: 10.1002/adma.201906050
27. Zhu Y, Shi H, Li T, Yu J, Guo Z, Cheng J, et al. Functional Nanoreactor for Synergistic Starvation and Photodynamic Therapy. *ACS Appl Materr Interfaces* (2020) 12(16):18309–18. doi: 10.1021/acsami.0c01039
28. Wang J, Sui L, Huang J, Miao L, Nie Y, Wang K, et al. MoS2-Based Nanocomposites for Cancer Diagnosis and Therapy. *Bioact Mater* (2021) 6 (11):4209–42. doi: 10.1016/j.bioactmat.2021.04.021
29. Huang Q, Wu W, Ai K, Liu J. Highly Sensitive Polydiacetylene Ensembles for Biosensing and Bioimaging. *Front Chem* (2020) 8:565782. doi: 10.3389/fchem.2020.565782
30. Wang Y, Pei H, Jia Y, Liu J, Li Z, Ai K, et al. Synergistic Tailoring of Electrostatic and Hydrophobic Interactions for Rapid and Specific Recognition of Lysophosphatidic Acid, an Early-Stage Ovarian Cancer Biomarker. *J Am Chem Soc* (2017) 139(33):11616–21. doi: 10.1021/jacs.7b06885
31. Zhu D, Zheng Z, Luo G, Suo M, Li X, Duo Y, et al. Single Injection and Multiple Treatments: An Injectable Nanozyme Hydrogel as AIEgen Reservoir and Release Controller for Efficient Tumor Therapy. *Nano Today* (2021) 37:101091. doi: 10.1016/j.nantod.2021.101091
32. Huang C, Chen B, Chen M, Jiang W, Liu W. Injectable Hydrogel for Cu(2+) Controlled Release and Potent Tumor Therapy. *Life (Basel)* (2021) 11(5):391. doi: 10.3390/life11050391
33. Chen D, Chen C, Huang C, Chen T, Liu Z. Injectable Hydrogel for NIR-II Photo-Thermal Tumor Therapy and Dihydroartemisinin-Mediated Chemodynamic Therapy. *Front Chem* (2020) 8:251. doi: 10.3389/fchem.2020.00251
34. Meng Z, Zhou X, Xu J, Han X, Dong Z, Wang H, et al. Light-Triggered In Situ Gelation to Enable Robust Photodynamic-Immunotherapy by Repeated Stimulations. *Adv Materr* (2019) 31(24):e1900927. doi: 10.1002/adma.201900927
35. Qiu M, Wang D, Liang W, Liu L, Zhang Y, Chen X, et al. Novel Concept of the Smart NIR-Light-Controlled Drug Release of Black Phosphorus Nanostructure for Cancer Therapy. *Proc Natl Acad Sci USA* (2018) 115 (3):501–6. doi: 10.1073/pnas.1714421115
36. Chang M, Hou Z, Jin D, Zhou J, Wang M, Wang M, et al. Colorectal Tumor Microenvironment-Activated Bio-Decomposable and Metabolizable Cu2 O@CaCO3 Nanocomposites for Synergistic Oncotherapy. *Adv Materr* (2020) 32 (43):2004647. doi: 10.1002/adma.202004647
37. Song G, Liang C, Gong H, Li M, Zheng X, Cheng L, et al. Core-Shell MnSe@Bi2 Se3 Fabricated via a Cation Exchange Method as Novel Nanotheranostics for Multimodal Imaging and Synergistic Thermoradiotherapy. *Adv Materr* (2015) 27(40):6110–7. doi: 10.1002/adma.201503006
38. Chen G, Yang Y, Xu Q, Ling M, Lin H, Ma W, et al. Self-Amplification of Tumor Oxidative Stress With Degradable Metallic Complexes for Synergistic Cascade Tumor Therapy. *Nano Lett* (2020) 20(11):8141–50. doi: 10.1021/acs.nanolett.0c03127
39. Zhang X, Li G, Wu D, Li X, Hu N, Chen J, et al. Recent Progress in the Design Fabrication of Metal-Organic Frameworks-Based Nanozymes and Their Applications to Sensing and Cancer Therapy. *Biosensors Bioelectron* (2019) 137:178–98. doi: 10.1016/j.bios.2019.04.061
40. Zhou J, Wang M, Han Y, Lai J, Chen J. Multistage-Targeted Gold/Mesoporous Silica Nanocomposite Hydrogel as In Situ Injectable Drug Release System for Chemophotothermal Synergistic Cancer Therapy. *ACS Appl Bio Mater* (2019) 3(1):421–31. doi: 10.1021/acsabm.9b00895
41. Chen Q, Xu L, Liang C, Wang C, Peng R, Liu Z. Photothermal Therapy With Immune-Adjuvant Nanoparticles Together With Checkpoint Blockade for Effective Cancer Immunotherapy. *Nat Commun* (2016) 7:13193. doi: 10.1038/ncomms13193

Conflict of Interest: The authors declare that the research was conducted in the absence of any commercial or financial relationships that could be construed as a potential conflict of interest.

Publisher's Note: All claims expressed in this article are solely those of the authors and do not necessarily represent those of their affiliated organizations, or those of the publisher, the editors and the reviewers. Any product that may be evaluated in

this article, or claim that may be made by its manufacturer, is not guaranteed or endorsed by the publisher.

Copyright © 2021 Zeng, Jiang, Liu, Suo, Wang, Zhu and Huang. This is an open-access article distributed under the terms of the Creative Commons Attribution License (CC BY). The use, distribution or reproduction in other forums is permitted, provided the original author(s) and the copyright owner(s) are credited and that the original publication in this journal is cited, in accordance with accepted academic practice. No use, distribution or reproduction is permitted which does not comply with these terms.

frontiers in Pharmacology

ORIGINAL RESEARCH
published: 15 October 2021
doi: 10.3389/fphar.2021.744811

Doxorubicin-Loaded Tumor-Targeting Peptide-Decorated Polypeptide Nanoparticles for Treating Primary Orthotopic Colon Cancer

Guoliang Liu[1†], *Min Wang*[2†], *Hongyu He*[1] *and Jiannan Li*[2*]

[1]Operating Theater and Department of Anesthesiology, The Second Hospital of Jilin University, Changchun, China, [2]Department of General Surgery, The Second Hospital of Jilin University, Changchun, China

Colorectal cancer is the third most common malignant disease worldwide, and chemotherapy has been the standard treatment for colorectal cancer. However, the therapeutic effects of chemotherapy are unsatisfactory for advanced and recurrent colorectal cancers. Thus, increasing the treatment efficacy of chemotherapy in colorectal cancer is a must. In this study, doxorubicin (DOX)-loaded tumor-targeting peptide-decorated mPEG-P(Phe-co-Cys) nanoparticles were developed to treat orthotopic colon cancer in mice. The peptide VATANST (STP) can specifically bind with vimentin highly expressed on the surface of colon cancer cells, thus achieving the tumor-targeting effects. The nanoparticles are core-shell structured, which can protect the loaded DOX while passing through the blood flow and increase the circulation time. The disulfide bonds within the nanoparticles are sensitive to the glutathione-rich microenvironment of tumor tissues. Rupture of disulfide bonds of the nanoparticles leads to the continuous release of DOX, thus resulting in the apoptosis of the tumor cells. The *in vivo* experiments in mice with orthotopic colon cancer demonstrated that the synthesized DOX-loaded tumor-targeting peptide-decorated polypeptide nanoparticles showed properties of drug delivery systems and exhibited good antitumor properties. The synthesized nanoparticles show appropriate properties as one of the drug delivery systems and exhibit good antitumor properties after encapsulating DOX.

Keywords: colorectal cancer, chemotherapy, nanoparticles, tumor targeting, drug delivery system

OPEN ACCESS

Edited by:
Kelong Ai,
Central South University, China

Reviewed by:
Jia Huang,
Central South University, China
Zhi Li,
Fuzhou University, China
Shuyi Li,
Johns Hopkins Medicine, United States

***Correspondence:**
Jiannan Li
jnli@ciac.ac.cn

†These authors have contributed equally to this work

Specialty section:
This article was submitted to Pharmacology of Anti-Cancer Drugs, a section of the journal Frontiers in Pharmacology

Received: *21 July 2021*
Accepted: *15 September 2021*
Published: *15 October 2021*

Citation:
Liu G, Wang M, He H and Li J (2021) Doxorubicin-Loaded Tumor-Targeting Peptide-Decorated Polypeptide Nanoparticles for Treating Primary Orthotopic Colon Cancer. Front. Pharmacol. 12:744811. doi: 10.3389/fphar.2021.744811

INTRODUCTION

Colorectal cancer was the third most common malignant disease worldwide, and the number of patients was rising, with approximately 500,000 deaths each year (Jemal et al., 2011; Laroui et al., 2011). With the innovation of treatment theories, chemotherapy was highlighted. Recent advances in chemotherapy, including the use of irinotecan, oxaliplatin, fluoropyrimidines, cetuximab, bevacizumab, and radiation therapy, have increased the median survival of patients (Ortiz et al., 2012). However, advanced and recurrent colorectal cancers were still hard to be cured (Chaudhary et al., 2011). Therefore, patients with colorectal cancer needed more efficient chemotherapy (Soster et al., 2012; Prados et al., 2013).

With the development of nanotechnology, plenty of nanoscale drug delivery systems (DDSs) have been applied to the chemotherapy drug delivery, such as micelles, vesicles, nanogels, and dendrimer

(Gu et al., 2015; Li et al., 2018; Chen et al., 2020; Su et al., 2020). Among them, the polymer nanoparticles were possibly the most promising (Choi et al., 2012; Wang et al., 2012; Ai et al., 2021). Through special design, nanoparticles could achieve specific functions, such as increasing the solubility of chemotherapy drugs and improving the stability in circulation (Cherukuri and Curley, 2010; Laroui et al., 2011). Nanoparticles have attracted worldwide interest and made great progress in design and fabrication.

In general, most nanoparticles possessed good biocompatibility and biosecurity (Zhu et al., 2010; Cho et al., 2012). Therefore, the loading of antitumor drugs into nanoparticles is needed to treat cancer. For the package of antitumor drugs, small-molecule drugs were promising, such as doxorubicin (DOX) and curcumin (Kaminskas et al., 2012). DOX is a kind of antitumor antibiotic with a wide antitumor spectrum (Cui et al., 2012; Maeda, 2012). Clinically, DOX could inhibit some common tumors and had been used to treat breast cancer, bladder cancer, lung cancer, ovarian cancer, colorectal cancer, and so on (Ta et al., 2009). However, the broad distribution of DOX limited the treatment efficiency and caused a variety of side effects, such as inhibition of medullary hematopoiesis function, nephrotoxicity, and cardiotoxicity (Lee et al., 2006).

In this study, a kind of mPEG-P(Phe-co-Cys) copolymers was developed, which could self-assemble into nanoparticles in aqueous solutions. The mPEG-P(Phe-co-Cys) nanoparticles (mNPs) were decorated with peptide VATANST (STP), and DOX was encapsulated within the nanoparticles to obtain STP-mNPs/DOX. STP-mNPs/DOX are core-shell structured with DOX as the core and the PEG as the shell. The appropriate particle size can prolong the circulation time while passing through the blood flow. STP could specifically bind with vimentin highly expressed on the surface of colon cancer cells (Kim et al., 2020; Vermani et al., 2020), thus increasing the tumor-targeting effects of STP-mNPs/DOX. The disulfide bonds within the nanoparticles were sensitive to the glutathione-rich microenvironment of colon cancer (GSH) (Zinczuk et al., 2020). The disulfide bonds of STP-mNPs/DOX are ruptured in the tumor tissues and led to the continuous release of loaded DOX, thus increasing the necrosis of tumor cells. The treatment efficacy of STP-mNPs/DOX in primary orthotopic colon cancer was evaluated using mice in this study.

MATERIALS AND METHODS

The preparation of mPEG-P(Phe-*co*-Cys) nanoparticles (mNPs) and STP-mNPs and characterizations of mNPs and STP-mNPs are in the Supplementary Material.

Materials

Polyethylene glycol monomethyl ether (mPEG), L-phenylalanine (L-Phe), L-cysteine (L-Cys), and deuterated trifluoroacetic acid (TFA-*d*) were purchased from Sigma-Aldrich (Shanghai, PR China). The STP, DOX hydrochloride (DOX HCl), and GSH were obtained from Gill Biochemical Co., Ltd. (Shanghai, PR China). Cell culture products, including Dulbecco's modified Eagle's medium (DMEM) and fetal bovine serum (FBS), were provided by Gibco (USA). Penicillin and streptomycin were obtained from Huabei Pharmaceutical Co., Ltd. (Hebei, PR China). Sodium cyanoborohydride (NaBH3CN), 3-(4,5-dimethyl-thiazol-2-yl)-2,5-diphenyl tetrazolium bromide (MTT), and 4′,6-diamidino-2-phenylindole dihydrochloride (DAPI) were purchased from Sigma-Aldrich (Shanghai, P. China). Terminal deoxynucleotidyl transferase-mediated deoxyuridine triphosphate nick-end labeling (TUNEL) kit was purchased from Roche Company (Mannheim, Germany). The purified deionized water was prepared by the Milli-Q plus system (Millipore Co., Billerica, MA, USA).

Preparations of mNPs/DOX and STP-mNPs/DOX

DOX was loaded into mNPs and STP-mNPs through a nanoprecipitation technique. In brief, DOX HCl was dissolved in 2.0 ml of phosphate-buffered saline (PBS) solution, and then the solution was slowly added to 18.0 ml *N*,*N*-dimethylformamide (DMF) (10.0 mg ml^{-1}) containing mNPs or STP-mNPs. After that, 18.0 ml distilled water and 2.0 ml PBS were added to the mixed solution. The solution was continuously stirred at room temperature for 12 h and then dialyzed in deionized water for 12 h (molecular weight cut-off (MWCO) = 3,500 Da). At last, the mNPs/DOX and STP-mNPs/DOX were obtained by lyophilization.

Characterizations of mNPs/DOX and STP-mNPs/DOX

The drug loading content (DLC) of mNPs/DOX and STP-mNPs/DOX was calculated using DLC (%) = (the amount of drug in the nanoparticles/total mass of the nanoparticles × 100%). The drug loading efficiency (DLE) of mNPs/DOX and STP-mNPs/DOX was calculated using DLE (%) = (the amount of drug in the nanoparticles/total amount of the drug × 100%).

The morphologies of mNPs/DOX and STP-mNPs/DOX were revealed by transmission electron microscopy (TEM) on a JEM-1011 (JEOL, Tokyo, Japan). The hydrodynamic diameters (D_h) were detected by dynamic laser scattering (DLS) measurements with a scattering angle at 90° on a WyattQELS instrument (DAWN EOS, Wyatt Technology Corporation, Santa Barbara, CA, USA).

DOX Release *In Vitro*

The DOX release profiles of mNPs/DOX and STP-mNPs/DOX *in vitro* were determined at pH 5.5, 6.8, and 7.4 with or without 10.0 mM glutathione (GSH) in PBS solution. The DOX-loaded freeze-dried micelles were dissolved into PBS at pH 5.5, 6.8, and 7.4 with or without 10.0 mM GSH, and the concentration of the solution was 100.0 μg ml^{-1}, respectively. Then 10.0 ml of each solution was transferred into a dialysis bag (MWCO = 3,500 Da). Extremity-sealed dialysis bags were then placed into the homologous 100.0 ml of PBS for the release assay with 75 rpm electric shock at 37°C, which simulated the circulation *in vivo*. At

pre-set times, 2.0 ml of external soaking solution was taken out and the equivalent fresh PBS of different pH with or without GSH was replenished into the homologous sample. Afterward, the accumulative DOX release was tested by fluorescence spectroscopy using the standard curve method (λ_{ex} = 480 nm).

Cellular Uptake and Intracellular DOX Release

Murine colon cancer cell line CT26 was cultured in complete DMEM with 10% (v/v) FBS, penicillin (50.0 IU ml^{-1}), and streptomycin (50.0 IU ml^{-1}) at 37°C in a 5% (v/v) carbon dioxide atmosphere. The cellular uptake and intracellular release DOX profiles of DOX-loaded nanoparticles were detected by both flow cytometry (FCM) and confocal laser scanning microscopy (CLSM) using CT26 cells. Germfree coverslips were put onto 6-well plates, one for each well. The CT26 cells were seeded into the well with a density of 2.0×10^5 cells per well in 2.0 ml of DMEM and cultured for 12 h. Then, three wells were chosen, and 200 μl of buthionine-sulfoximine (BSO) PBS solution was added to the selected wells with a concentration of 0.01 mmol ml^{-1}. After 12 h of culture at 37°C in a 5% (v/v) carbon dioxide atmosphere, another three wells were selected, and 200 μl of GSH solution in PBS with the same concentration of BSO solution was added to the wells. After 2 h of culture, the medium was replaced with free DOX, mNPs/DOX, or STP-mNPs/DOX solution in DMEM at a final DOX concentration of 10.0 μg ml^{-1}. Then, after 2 h of culture, the coverslips that were adhered with CT26 cells were washed with PBS and then fixed with 4% PBS-buffered formaldehyde for 30 min at room temperature. Subsequently, the coverslips were counterstained with DAPI (blue color) for cellular nuclei. The cellular microimages were determined on the CLSM (LSM 780, Carl Zeiss, Jena, Germany). For the FCM assay, the CT26 cells were cultured similarly to CLSM tests without any coverslips. After culture with free DOX, mNPs/DOX, or STP-mNPs/DOX for 2 h, the culture media were removed. The obtained cells were washed three times with PBS. The cells in each well were then suspended in 1.0 ml of PBS and centrifuged for 4 min at 3,000 rpm. The cells were then resuspended in 0.3 ml of PBS, and the data for 10,000 gated events were collected. The data were analyzed on a flow cytometer (Beckman, California, USA).

Cytotoxicity Assays *In Vitro*

The cytotoxicity of free DOX, mNPs/DOX, and STP-mNPs/DOX *in vitro* in the different external environments was demonstrated using the MTT assay. The CT26 cells were seeded in 96-well plates, 7,000 cells per well, in 200.0 μl of complete DMEM and cultured for 12 h. Then, BSO solution with a concentration of 0.01 mmol ml^{-1} was added to three lists of wells. After 12 h of culture, another three lists were selected for adding GSH solution with the same concentration of BSO solution and then cultured at constant temperature for 2 h. Subsequently, the culture medium was replaced with 200.0 μl of fresh medium containing free DOX, mNPs/DOX, or STP-mNPs/DOX at a final DOX concentration of 10.0 μg ml^{-1}. The cells were subjected to MTT assay after 48 h culture. The stock solution containing 0.05 mg of MTT in PBS was added to each well and then cultured for another 4 h. Subsequently, the medium was replaced with 150 μl of DMSO. Furthermore, mNPs and STP-mNPs (0–40.0 mg L^{-1}) were also cultured with CT26 cells as above, but BSO or GSH solutions were not used. The absorbency of the above solution was measured on a Bio-Rad 680 microplate reader at 490 nm. The cell viability was calculated using the following: cell viability (%)= (absorbance of sample/absorbance of control × 100%).

Pharmacokinetics of DOX *In Vivo*

For the *in vivo* research of pharmacokinetics of free DOX, mNPs/DOX, and STP-mNPs/DOX, male Kunming mice weighing about 200 g were fasted for 12 h before the test. Free DOX, mNPs/DOX, and STP-mNPs/DOX were dissolved with PBS. After intravenous administration of 5.0 mg kg^{-1} of free DOX and an equivalent dose of mNPs/DOX and STP-mNPs/DOX, blood was collected from the retrobulbar vein into heparinized 1.5 ml centrifuge tubes at 0, 5, 15, and 30 min and 1, 2, 3, 4, 6, 8, 10, 12, and 24 h. To separate the plasma and blood cells, blood samples were centrifuged at 10,000 rpm and 4°C for 10 min. The supernatant (200.0 μl) was transferred into a new centrifuge tube with 1.0 ml of methyl alcohol. After vibration by the vortex mixer for 10 min, the samples were centrifuged again. Then, the supernatants were removed into glass tubes, respectively; moreover, the samples were blow-dried using a nitrogen concentrator at 35°C. Subsequently, the samples were redissolved with 200.0 μl of methyl alcohol, and the amounts of DOX of samples were detected with the High-Performance Liquid Chromatography (HPLC) method. Waters liquid chromatographic system (Waters e2695 Separations Module, USA) was equipped with a fluorescence detector (Waters 2475 Multi-λ Fluorescence Detector, USA) with the excitation and emission wavelengths at 472 and 592 nm, respectively. A Waters Symmetry C18 analytical column (5 μm, 4.6 × 250 mm) was used at 35°C.

In Vivo Antitumor Assay

The *in vivo* antitumor efficacy of free DOX, mNPs/DOX, and STP-mNPs/DOX was demonstrated using a drug-induced *in situ* tumor model in 6–8 -eek-old male Balb/C mice. Dimethyl hydrazine (DMH) was the inducer and was dissolved in ethylene diamine tetraacetic acid (EDTA) solution. EDTA was dissolved in PBS solution, and the concentration was 1 mmol L^{-1}. The concentration of DMH solution was 3 mg ml^{-1}. DMH solution was injected into the mice's abdominal cavity, and the drug was absorbed through the peritoneal. The given dose was 30 mg per kilogram of body weight. The injection was performed on Tuesday and Friday every week, and the whole process lasted 16 weeks. After the last injection, one mouse was sacrificed, and the colon was dissected to confirm the formation of the tumor. After 3 days, mice were randomly divided into four groups. The tumor-bearing mice were treated with free DOX, mNPs/DOX, STP-mNPs/DOX, and PBS. The tail vein injections of 0.2 ml of PBS alone or DOX-loaded micelles of free DOX with an equivalent DOX dosage (5.0 mg DOX per kilogram body

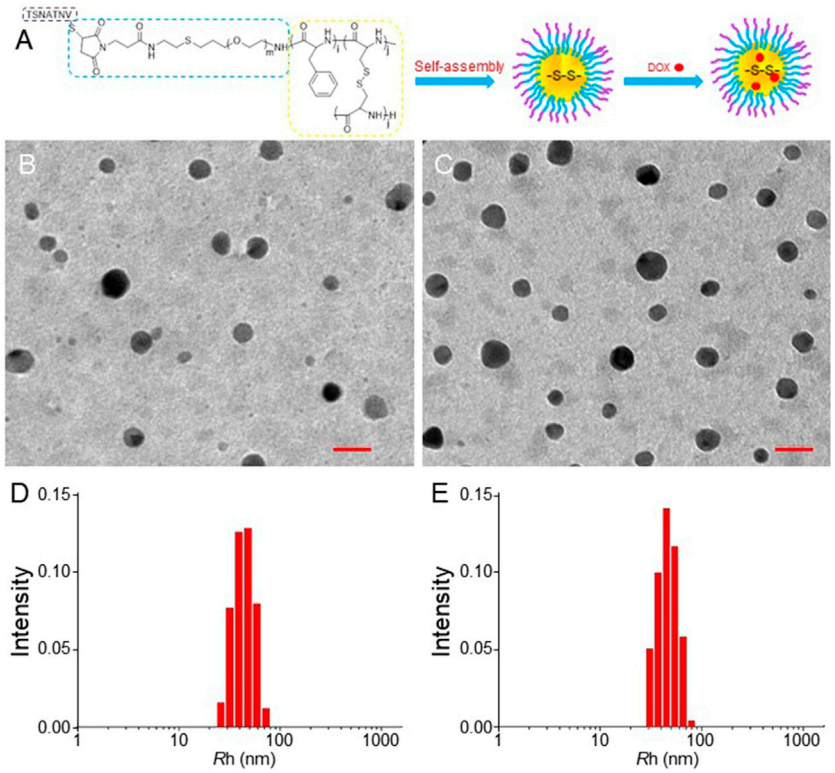


FIGURE 1 | Preparation of STP-mNPs/DOX and characterizations of mNPs-DOX and STP-mNPs/DOX. **(A)** Schematic illustration of preparation of STP-mNPs/DOX. TEM analysis of **(B)** mNPs/DOX and **(C)** STP-mNPs/DOX and R_hs of **(D)** mNPs/DOX and (E) STP-mNPs/DOX. Scale bars = 100 nm.

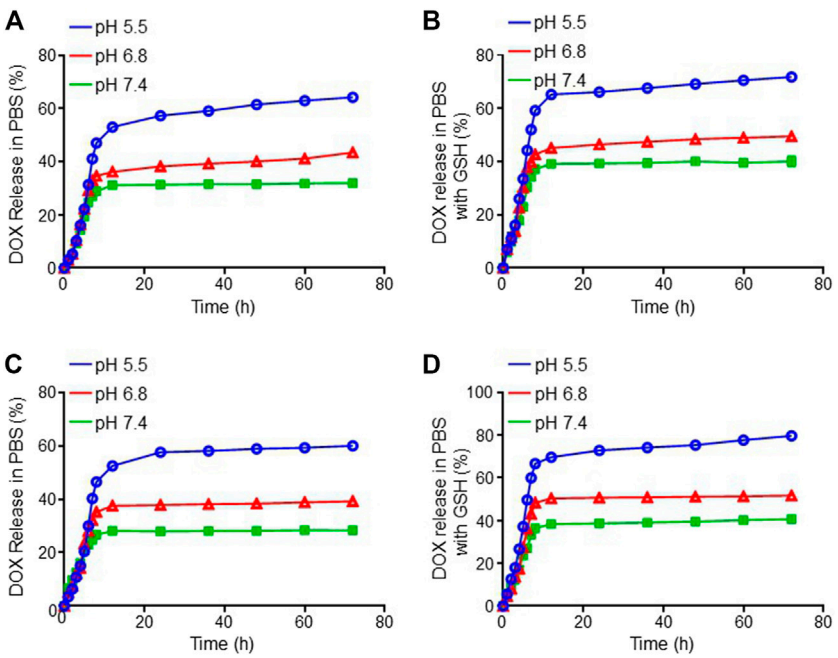


FIGURE 2 | DOX release profiles of mNPs/DOX in **(A)** PBS and **(B)** PBS with GSH and STP-mNPs/DOX in **(C)** PBS and **(D)** PBS with GSH *in vitro* at 37°C, pH 5.5, 6.8, and 7.4, respectively. Data were presented as mean ± SD (n = 3).

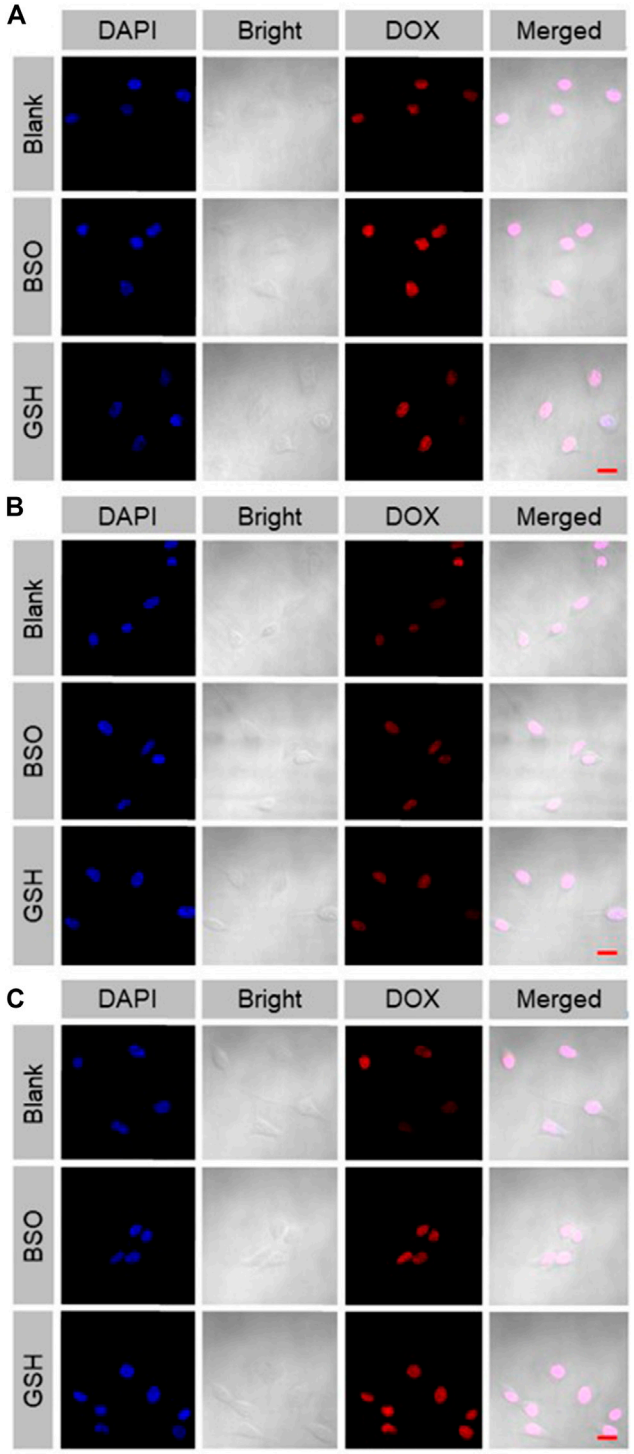


FIGURE 3 | Cellular uptake and intracellular DOX release of **(A)** free DOX, **(B)** mNPs/DOX, and **(C)** STP-mNPs/DOX after incubation with CT26 cells for 2 h detected by CLSM. Scale bars = 20 μm.

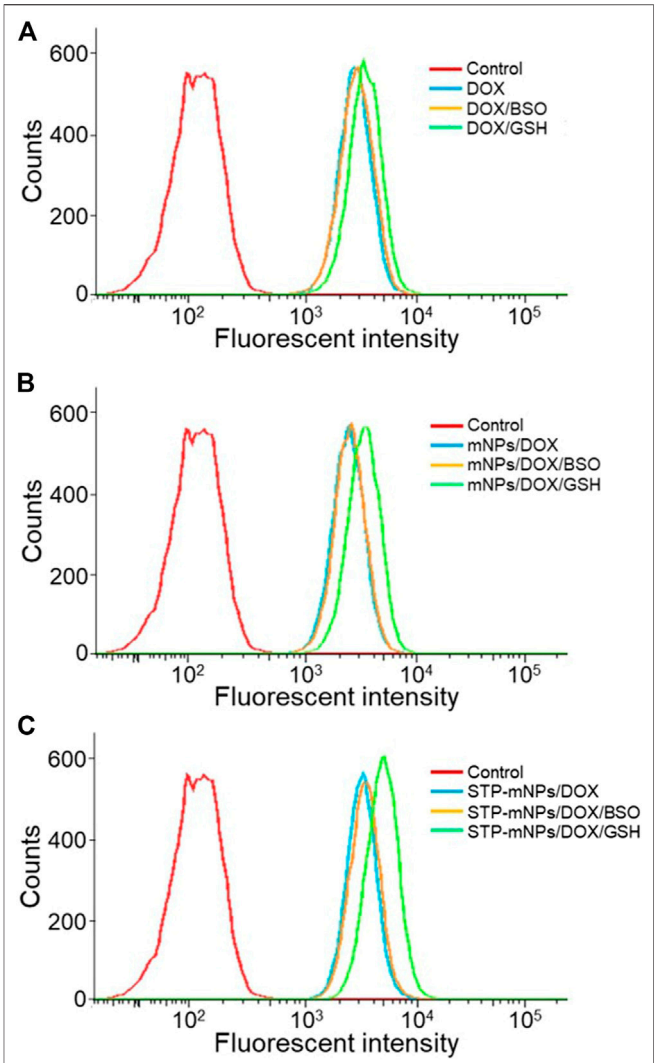


FIGURE 4 | Cellular uptake and intracellular DOX release of DOX, mNPs/DOX, and STP-mNPs/DOX after incubation with CT26 cells for 2 h detected by FCM.

weight) in PBS were performed on days 1, 5, 9, 13, 17, and 21. Free DOX and PBS were administred as positive and negative controls, respectively.

Histological and Immunohistochemical Analyses

Five days after the last injection, all the mice were sacrificed, and the colons were dissected along the longitudinal axis. The lining of the colons was rinsed in deionized water, flattened, and photographed. Then, the colon segments were rinsed in deionized water again, flattened, and photographed. The number of the tumor sites larger than 2 mm in each mouse was recorded. The colons and major organs (i.e., heart, liver, spleen, lung, and kidney) of other mice were collected and fixed in 4% (w/v) PBS-buffered paraformaldehyde overnight and then embedded in paraffin. The paraffin-embedded organs were cut into 5.0 μm slices. The slices were stained with hematoxylin and eosin (H&E) and cut into 0.3 μm sheets for immunohistochemical analyses (i.e., Ki-67, PARP, TUNEL). The histological and immunohistochemical alterations were

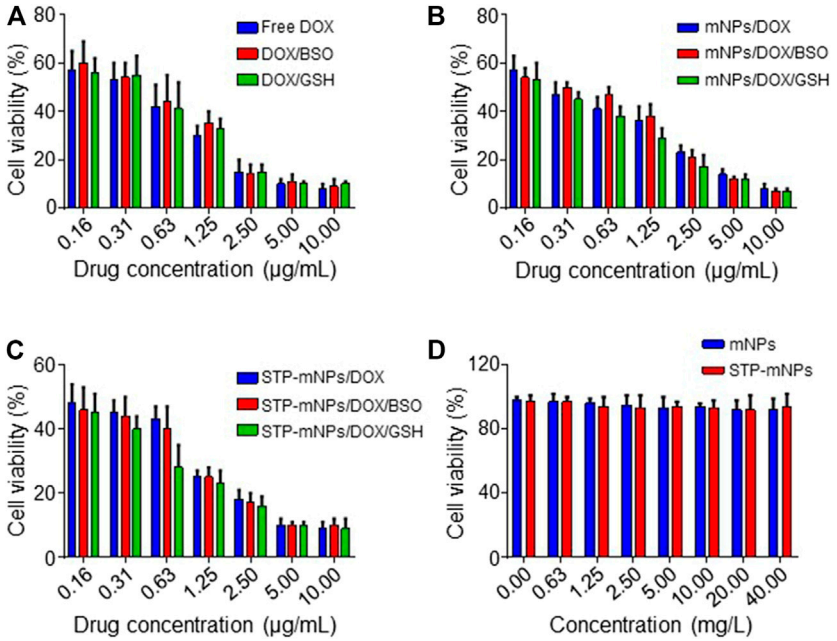


FIGURE 5 | Cytotoxicities *in vitro* of free DOX, mNPs, STP-mNPs, mNPs/DOX, and STP-mNPs/DOX after incubation with CT26 cells for 48 h. Data were presented as mean ± SD (n = 3).

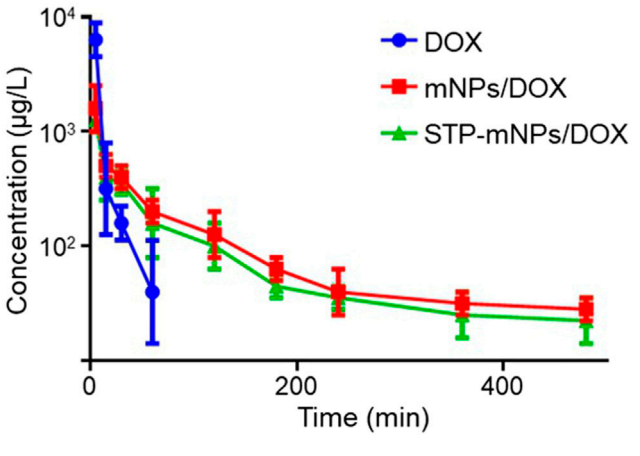


FIGURE 6 | Pharmacokinetics of free DOX, mNPs/DOX, and STP-mNPs/DOX *in vivo*. Data were presented as mean ± SD (n = 3).

detected by microscope (Nikon Eclipse *Ti*, Optical Apparatus Co., Ardmore, PA) and subsequently analyzed with CLSM and ImageJ software (National Institutes of Health, Bethesda, Maryland).

Statistical Analyses

All experiments were performed at least three times, and the results were represented as means ± standard deviation (SD). Data were analyzed using SPSS 14.0 (SPSS Inc., Chicago, IL, USA). $^{*}p < 0.05$ was considered statistically significant, and $^{**}p < 0.01$ and $^{***}p < 0.001$ were considered highly significant.

RESULTS AND DISCUSSION

In this study, DOX-loaded tumor-targeting peptide-decorated polypeptide nanoparticles were developed for treating primary orthotopic colon cancer in mice. Vimentin was a kind of epithelial-to-mesenchymal (EMT) marker highly expressed in many cancers, including colorectal cancer (Kim et al., 2020; Vermani et al., 2020). STP could specifically bind with vimentin, which can increase the tumor-targeting effects of mNPs (Qiu et al., 2020). The STP-mNPs/DOX are core-shell structured with DOX loaded in the core, and the PEG shell can protect the inside DOX while allowing the blood flow through. The STP-mNPs/DOX is based on mPEG-P(Phe-co-Cys) copolymers, and the disulfide bonds within the nanoparticles were sensitive to the GSH-rich microenvironment of colon cancer (Wen et al., 2019; Zinczuk et al., 2019). The concentrations of GSH were 1.0–2.0 μmol/L, 2.0–20.0 μmol/L, and 2.0–10.0 mmol/L in plasma, normal tissues, and tumor cells, respectively (Schafer and Buettner, 2001). The GSH concentration in tumor cells was about 500 times higher than that in normal tissues. The rupture of disulfide bonds of STP-mNPs/DOX led to the continuous release of loaded DOX, thus increasing the necrosis of tumor cells (Wang et al., 2020; Wang et al., 2021). As a result, under the enhanced permeability and retention (EPR) and tumor-targeting effects, STP-mNPs/DOX can accumulate in tumor tissues. Large amounts of DOX can be released under high levels of GSH within the tumor cells. Furthermore, the efficacy of STP-mNPs/DOX in the treatment of primary orthotopic colon cancer was evaluated in this study.

Based on our previous study (Qiu et al., 2020), the mNPs/DOX and STP-mNPs/DOX were successfully synthesized.

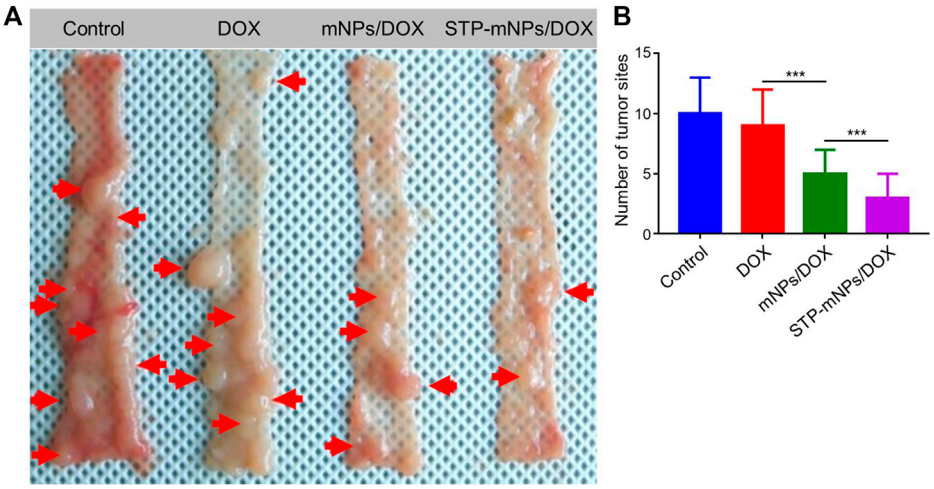


FIGURE 7 | The treatment efficacy of STP-mNPs/DOX toward primary orthotopic colon cancer in mice. **(A)** The tumor and colon were dissected from mice treated with free DOX, mNPs, or STP-mNPs/DOX, with PBS as control. The red arrows pointed to tumors that are larger than 2 mm in diameter. **(B)** The number of tumor sites which are larger than 2 mm in diameter. Data were presented as mean ± SD (n = 6, ***p < 0.001).

Supplementary Figure S1 shows the proton nuclear magnetic resonance (1H NMR) and Fourier-transform infrared (FTIR) spectroscopy of mNPs and STP-mNPs. Detailed descriptions are provided in the Supplementary Material. The DLC and DLE of mNPs/DOX are 6.42 ± 1.05 wt% and 36.12 ± 1.85 wt%, respectively. The DLC and DLE of STP-mNPs/DOX are 7.12 ± 1.85 wt% and 37.20 ± 2.55 wt%, respectively. The decoration of STP did not change the DLC or DLE of mNPs/DOX significantly.

Figure 1A shows the schematic illustration of the preparation of STP-mNPs/DOX. The morphology and size of mNPs/DOX and STP-mNPs/DOX were determined by TEM and DLS. As shown in **Figures 1B,C**, both mNPs/DOX and STP-mNPs/DOX are spherical particles in an aqueous environment with similar sizes. DLS shows the diameters of mNPs/DOX and STP-mNPs/DOX are 88.34 ± 4.26 nm and 90.74 ± 4.65 nm, respectively (**Figures 1D,E**). For nanoparticles, size was a crucial property for distribution. Some studies have suggested that the particles with a radius larger than 100 nm would be captured by the reticuloendothelial system, and the particles with a radius smaller than 30 nm would be eliminated from plasma rapidly (Peer et al., 2007; Wang et al., 2012). This result indicated that the sizes of mNPs/DOX and STP-mNPs/DOX were appropriate for DDSs. Moreover, the morphology of the drug delivery systems plays an important role in the distribution within the body tissues. Spherical nanoparticles are more likely to be endocytosed within tumor cells (Qiu et al., 2020). Benefiting from the appropriate size and spherical morphology of nanoparticles, mNPs/DOX and STP-mNPs/DOX prolonged circulation and increased DOX accumulation in tumor sites through the EPR effect (Kobayashi et al., 2013).

The DOX release behaviors from both mNPs/DOX and STP-mNPs/DOX with or without GSH in different pH values *in vitro* were detected, respectively. As shown in **Figure 2**, a similar rapid release of DOX from mNPs/DOX and STP-mNPs/DOX is observed at 6 h, and DOX is released in a more steady pattern till 72 h subsequently. The data of DOX release behavior showed that both mNPs/DOX and STP-mNPs/DOX had a better release effect in the pH value 5.5 environments compared with pH values 6.8 and 7.4. The different pH values 5.5, 6.8, and 7.4 were similar to the pH values of the internal environment of tumor cells, the interstitial fluid, and the plasma, respectively. Therefore, the release of DOX from both mNPs/DOX and STP-mNPs/DOX is less in plasma than in the internal environment of tumor cells, showing that the nanoparticles prolonged the circulation time. More DOX was released from mNPs/DOX and STP-mNPs/DOX in the GSH environment than that in non-GSH environment, indicating that high levels of GSH in the tumor microenvironment could lead to more DOX release. The core-shell structure of STP-mNPs/DOX increases the stability of the nanoparticles in blood circulation and protects the loaded DOX. The disulfide bonds of STP-mNPs/DOX are ruptured within tumor tissues because of the rich GSH environment, and large amounts of DOX can be released. Due to the specific structure and the disulfide bonds, the developed STP-mNPs/DOX can deliver DOX to tumor cells in a targeted manner.

The cellular internalization and intracellular release of DOX were performed on the murine colon cancer cell line CT26. The CT26 cells were observed by CLSM after being treated with free DOX, mNPs/DOX, and STP-mNPs/DOX. DOX was directly used to measure the cellular internalization without any other additional markers due to its self-fluorescent characteristic, and the fluorescence intensity was directly proportional to the amount of internalized DOX (Hossain et al., 2013). As shown in **Figure 3**, the red fluorescence of DOX can be observed in the cell nuclei treated with free DOX, mNPs/DOX, and STP-mNPs/DOX, demonstrating the cellular internalization of mNPs/DOX and STP-mNPs/DOX and the intracellular DOX release of mNPs/DOX and STP-mNPs/DOX. For further evaluation, the cellular uptake of free DOX, mNPs/DOX, and STP-mNPs/DOX of the

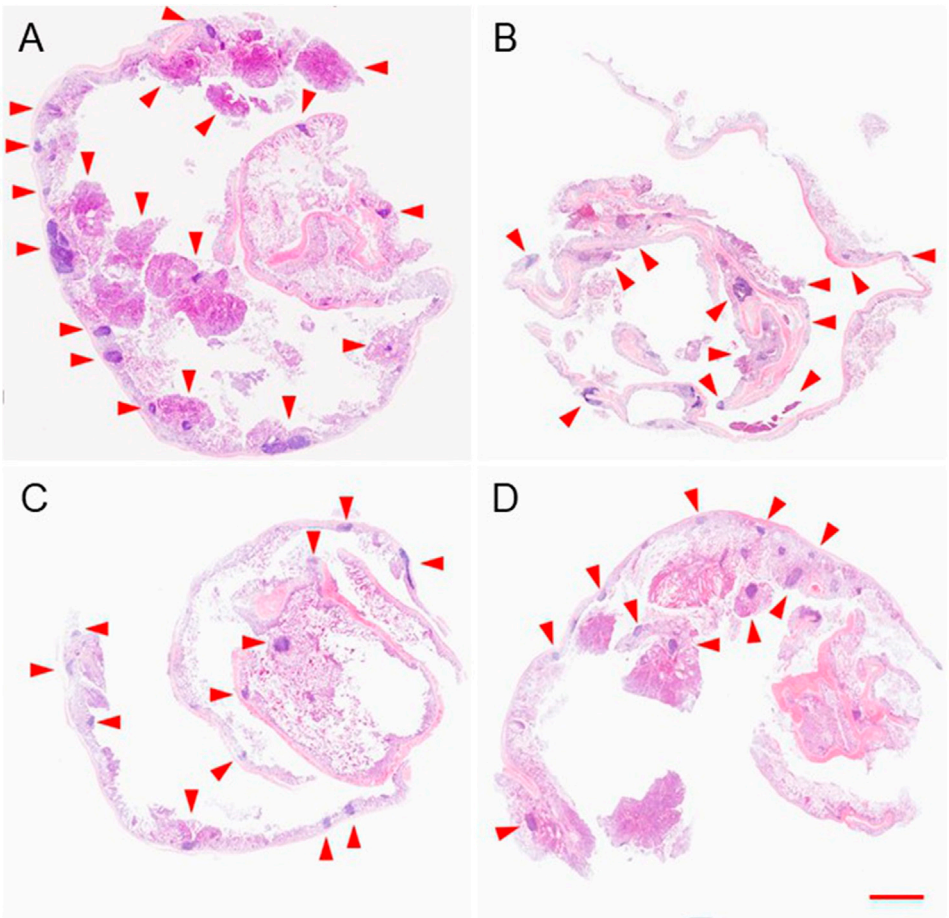


FIGURE 8 | Colon and tumor sections of mice after treatment of **(A)** PBS, **(B)** free DOX, **(C)** mNPs/DOX, or **(D)** STP-mNPs/DOX were stained by H&E. The red arrows pointed to tumors. Scale bar = 5 mm.

CT26 cells is analyzed with fluorescence-activated FCM (**Figure 4**). There is no significant difference in cellular internalization in the free DOX group after being treated for 2 h in PBS, PBS with BSO, or PBS with GSH. However, the cellular internalization or intracellular DOX release of mNPs/DOX and STP-mNPs/DOX in the PBS with GSH was more than PBS or PBS with BSO due to disulfide bonds in the mNPs/DOX and STP-mNPs/DOX possibly. BSO could inhibit the effects of GSH and mNPs/DOX and STP-mNPs/DOX are more stable after BSO treatment. However, GSH could increase the rupture of disulfide bonds, thus leading to more DOX being released. Therefore, fractures are more likely to occur in the GSH-induced reductive environment, thus accelerating DOX release from dissociated nanoparticles. These results further indicate that the rich GSH environment of tumor tissues can lead to large amounts of DOX release for tumor killing.

MTT assay was used to determine the cytotoxicity of free DOX, mNPs, STP-mNPs, mNPs/DOX, and STP-mNPs/DOX. CT26 cells were cultured in 96-well plates with PBS, BSO PBS solution, or GSH PBS solution, as previously described and treated with free DOX, mNPs/DOX, or STP-mNPs/DOX at an equal dosage of DOX, proceeding with MTT assay after 48 h. **Figures 5A–C** show that the viability of the CT26 cell decreases with the increase of DOX concentration and there is no significant difference between cell viability in the cells cultured with PBS, BSO PBS solution, or GSH PBS solution in the free DOX treated group. However, in mNPs/DOX and STP-mNPs/DOX treated group, the cell viability of cells cultured with GSH PBS solution was significantly lower than that of the cells cultured with PBS or BSO PBS solution, indicating that the cytotoxicity of mNPs/DOX and STP-mNPs/DOX was enhanced in reductive conditions, consistent with the previous result of DOX intracellular release. **Figure 5D** shows that mNPs and STP-mNPs have no toxic effect toward CT26 cells. The cell viability is still at a relatively high level with the increasing of mNPs and STP-mNPs concentrations. The synthesized mNPs and STP-mNPs indicated no cytotoxicity toward CT26 cells and can be safely applied for DOX delivery. STP-mNPs/DOX shows the best cytotoxicity toward CT26 cells under a rich GSH environment.

HPLC was used to evaluate the plasma pharmacokinetics of the free DOX, mNPs/DOX, and STP-mNPs/DOX (Zhu et al.,

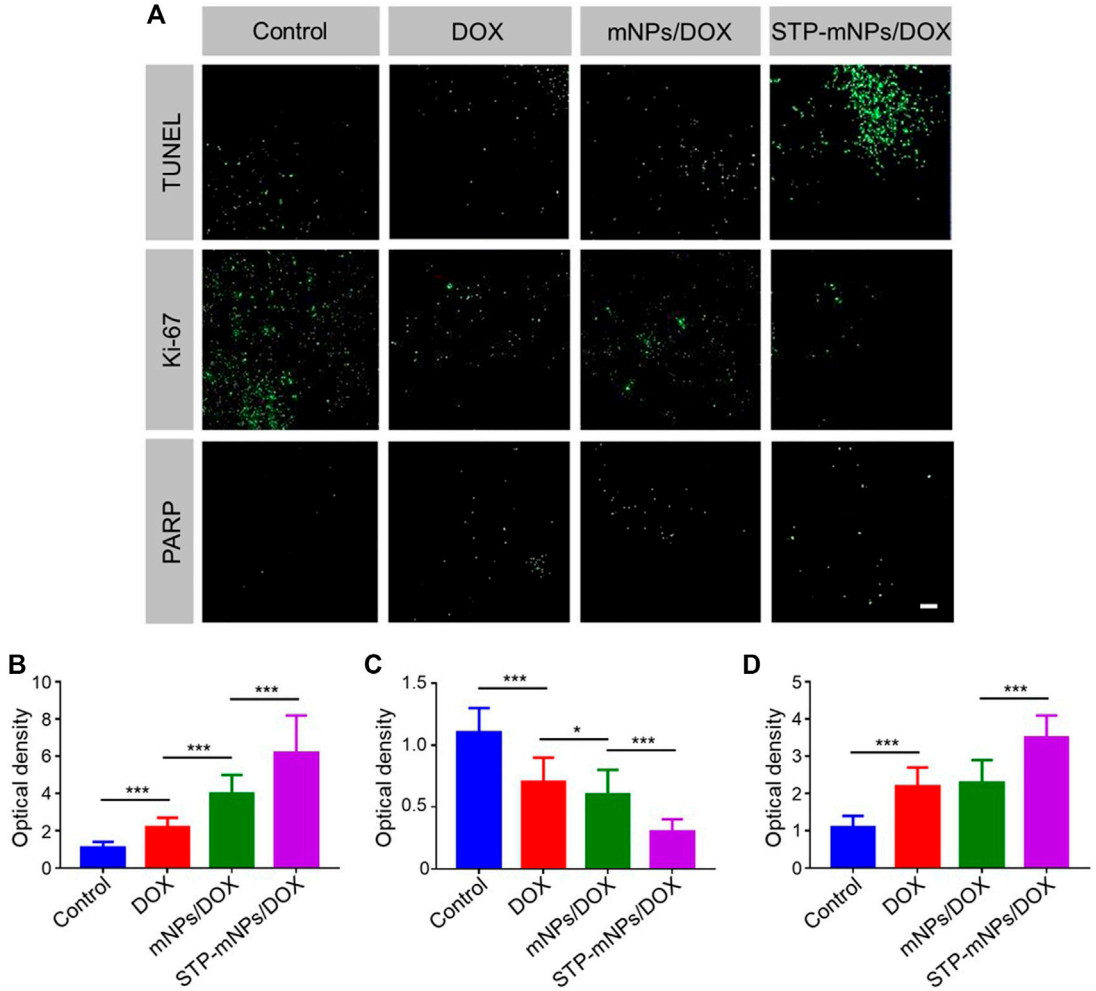


FIGURE 9 | Immunofluorescence analysis of TUNEL, Ki-67, and PARP in Control, DOX, mNPs/DOX, and STP-mNPs/DOX groups. **(A)** CLSM of the immunofluorescence images in different groups. Semiquantitative analysis of **(B)** TUNEL, **(C)** Ki-67, and **(D)** PARP in different groups. Data were presented as mean ± SD (n = 3, $^{*}p < 0.05$ and $^{***}p < 0.001$). Scale bar = 50 μm.

2010; Cho et al., 2012). **Figure 6** shows that the DOX in plasma is cleared from blood circulation rapidly and can hardly be detected after being injected into the plasma for 60 min. In contrast, the DOX concentration of mNPs/DOX and STP-mNPs/DOX decreases relatively slower, showing that both mNPs/DOX and STP-mNPs/DOX increased the DOX stability in plasma in a slow-release mode. The results were consistent with previous DOX release profiles *in vitro*. The longer circulation time of mNPs/DOX and STP-mNPs/DOX could reduce the side effects of DOX to other major organs and increase the DOX accumulation in the tumor tissues (Qiu et al., 2020). The PEG shell of mNPs/DOX and STP-mNPs/DOX could seal DOX within the nanoparticles and protect the agent while passaging the blood flow. The disulfide bonds within the nanoparticles were stable in normal tissues but were sensitive to the microenvironment of tumor tissues with high levels of GSH. The suitable particle size of mNPs/DOX and STP-mNPs/DOX could also help maintain longer blood circulation time (Kolate et al., 2014). As mentioned above, the diameter of STP-mNPs/DOX (90.74 ± 4.65 nm) enables the effective delivery of DOX to tumor cells without being captured by the reticuloendothelial system or eliminated from plasma rapidly (Peer et al., 2007; Wang et al., 2012).

DMH was used as the inducer to establish the colon cancer *in situ* tumor animal models (Samanta et al., 2008; Baskar et al., 2012). Hematochezia occurred in many Balb/C mice, and ascites occurred in only two mice during the drug-induced process caused by colon cancer formed in the intestines possibly. The growth or burst of colon cancer could cause bleeding within the colonic cavity. The DMH-induced process lasted for 4 months. After the last intraperitoneal injection, mice were randomly divided into PBS, free DOX, mNPs/DOX, and STP-mNPs/DOX groups, respectively, and administred with a DOX dose of 5 mg kg^{-1} through intravenous injection every 4 days for a total of six injections. Free DOX and PBS were administred as positive and negative controls, respectively. The mice were sacrificed, and

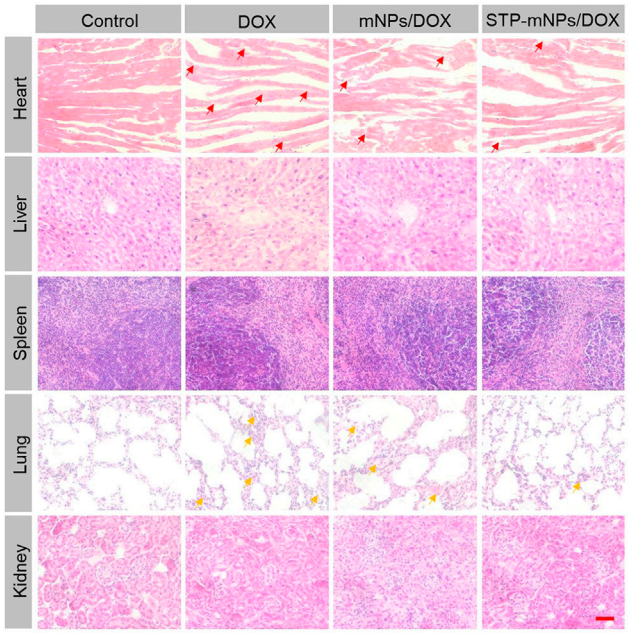


FIGURE 10 | *In vivo* histological (H&E) analyses of major organs (heart, liver, spleen, lung, and kidney) sections form *in situ* tumor model mice after treatment with free DOX, mNPs/DOX, STP-mNPs/DOX, or PBS (as control). Red arrows indicate myocardial injuries and yellow arrows indicate lung injuries. Scale bar = 100 μm.

the colon tissues were dissected and washed out in deionized water after the treatment process. **Figure 7A** shows the photographed results of the flattened colons. Tumor sites with diameters larger than 2 mm were counted. The amount of the tumor of the STP-mNPs/DOX treated mouse is significantly less than the others (**Figure 7B**), indicating that the STP-mNPs/DOX has the best treatment effect. Subsequently, the flattened colons were curled up along the long axis and fixed with 4% paraformaldehyde. The winding colon was sliced along the winding direction and the tissues were H&E stained and photographed under the microscope. **Figure 8** shows that the nucleus gathered zones are tumor sections. The amount of the tumor of STP-mNPs/DOX treated mice was significantly less than the other mice on the micro-level. The accumulation of nanoparticles at the tumor site was enhanced due to the EPR effect (Kobayashi et al., 2013) and tumor-targeting effect (Qiu et al., 2020), leading to the enhanced antitumor efficacy of STP-mNPs/DOX. The disulfide bonds made STP-mNPs/DOX release DOX more efficiently in the intercellular environment.

To further evaluate the antitumor efficacy of DOX, mNPs/DOX, and STP-mNPs/DOX, the colons were collected after the mice dead and sectioned for TUNEL assay. The DNA of tumor cells was fractured caused by chemotherapy drugs, and the fragmentation of DNA could be dyed with green fluorescence by a fluorescein isothiocyanate marked TUNEL kit. **Figure 9A** shows that the flake and punctiform green fluorescent signals are observed in DOX-loaded nanoparticles or free DOX treated tumor, and the green fluorescence signal is relative to the tumor cell apoptosis. The images are taken from the junction of the tumor and normal tissue, showing that there was no visible fluorescence signal in the location of normal tissue. However, in the tumor location, more fluorescence signal was observed in the tumor of the STP-mNPs/DOX treated group than the other groups, indicating that more apoptosis took place in the STP-mNPs/DOX treated tumor. Therefore, the antitumor efficacy of STP-mNPs/DOX was better than that of the others. The results were also confirmed by semiquantitative analysis. The fluorescence intensity of the control group was defined as "1," and the optical densities of the other groups were defined as the ratio of the sample group and the control group. **Figure 9B** shows that the STP-mNPs/DOX treated group has the most TUNEL expression compared to the other groups. The Ki-67 and PARP assays were processed in the tumor area to confirm the tumor apoptosis further. **Figure 9A** shows different results because the Ki-67 and PARP assays are a pair of opposite markers. The tumor treated with STP-mNPs/DOX shows the lowest fluorescent signal in the Ki-67 assay, reflecting the lowest tumor proliferation ability in STP-mNPs/DOX group. The STP-mNPs/DOX group also showed the highest fluorescent signal in PARP assay, reflecting tumor apoptosis. The results indicate that STP-mNPs/DOX can effectively promote tumor apoptosis and inhibit tumor proliferation, consistent with **Figure 9A**. **Figures 9C,D** also show the least and most fluorescent intensities of TUNEL and PARP in the STP-mNPs/DOX group, respectively. The histopathological studies show that STP-mNPs/DOX can significantly prevent the progression of colon cancer by inhibiting tumor proliferation and increasing tumor apoptosis.

For antitumor drugs, security assessments were crucial in the clinical application (Ding et al., 2011). The major organs (heart, liver, spleen, lung, and kidney) were dissected from mice after death to evaluate the safety of STP-mNPs/DOX. The organs were sliced and stained by H&E. The stained sections were photographed for histopathological analyses. As shown in **Figure 10**, the images of major organs of each group are exhibited. The images of organs of the control group show that no significant tissue damage occurs, and every organ has a relatively normal histological structure. However, other groups treated with DOX formulation showed different degrees of myocardial injuries, such as myocardial cell edema, irregular arrangement of the myocardial cell, and inflammatory cell infiltration. In the meantime, pathological lung changes could be observed in the DOX formulation treated group, such as thickening and blocking alveolar walls. Moreover, the organ damage level of the STP-mNPs/DOX treated group was lower than that of mNPs/DOX or free DOX treated group. Nevertheless, all the visible changes were slight, and no significant morphological changes could be detected, showing the high biosecurity of STP-mNPs/DOX.

CONCLUSION

DOX-loaded tumor-targeting peptide-decorated polypeptide nanoparticles were synthesized to treat DMH-induced *in situ* colon cancer in mice. *In vitro* experiments of STP-mNPs/DOX showed appropriate size for tumor tissue accumulation, improved DOX release and internalization, and enhanced

antitumor efficacy against CT26 cells. *In vivo* experiments in mice with the orthotopic colon cancer model demonstrated that STP-mNPs/DOX possess better antitumor efficacy than mNPs/DOX and free DOX. The synthesized STP-mNPs/DOX shows appropriate properties as one of the DDSs and exhibits good antitumor properties after encapsulating DOX. Therefore, STP-mNPs can be applied in delivering a series of small-molecule chemotherapeutic drugs for cancer therapy.

DATA AVAILABILITY STATEMENT

The raw data supporting the conclusion of this article will be made available by the authors, without undue reservation.

ETHICS STATEMENT

The animal study was reviewed and approved by Animal Experimental Center of Jilin University.

AUTHOR CONTRIBUTIONS

GL and MW wrote the manuscript. GL, MW, and HH performed the study. HH analyzed the data. JL revised the manuscript. GL and MW contributed equally to this work.

FUNDING

This work was supported by Science and Technology Development Project of Jilin Province (#3D5197434429), the Youth Program of the National Natural Science Foundation of China (#3A4205367429), and the Education Project of Jilin University (#419070600046).

SUPPLEMENTARY MATERIAL

The Supplementary Material for this article can be found online at: https://www.frontiersin.org/articles/10.3389/fphar.2021.744811/full#supplementary-material

REFERENCES

Ai, K., Huang, J., Xiao, Z., Yang, Y., Bai, Y., and Peng, J. (2021). Localized Surface Plasmon Resonance Properties and Biomedical Applications of Copper Selenide Nanomaterials. *Mater. Today Chem.* 20, 100402. doi:10.1016/j.mtchem.2020.100402

Baskar, A. A., Al Numair, K. S., Gabriel Paulraj, M., Alsaif, M. A., Muamar, M. A., and Ignacimuthu, S. (2012). β-Sitosterol Prevents Lipid Peroxidation and Improves Antioxidant Status and Histoarchitecture in Rats with 1,2-Dimethylhydrazine-Induced Colon Cancer. *J. Med. Food* 15, 335–343. doi:10.1089/jmf.2011.1780

Chaudhary, A., Sutaria, D., Huang, Y., Wang, J., and Prabhu, S. (2011). Chemoprevention of colon Cancer in a Rat Carcinogenesis Model Using a Novel Nanotechnology-Based Combined Treatment System. *Cancer Prev. Res. (Phila)* 4, 1655–1664. doi:10.1158/1940-6207.CAPR-11-0129

Chen, L., Zhao, L., Hu, G., Jin, R., Cai, B., Bai, Y., et al. (2020). Tumor-Specific Nanomedicine via Sequential Catalytic Reactions for Accurate Tumor Therapy. *J. Mater. Chem. B* 8, 6857–6865. doi:10.1039/c9tb02812a

Cherukuri, P., and Curley, S. A. (2010). "Use of Nanoparticles for Targeted, Noninvasive Thermal Destruction of Malignant Cells," in *Cancer Nanotechnology: Methods and Protocols*. Editors S.R. Grobmyer and B.M. Moudgil (Clifton, NJ: Methods in Molecular Biology), 359–373. doi:10.1007/978-1-60761-609-2_24

Cho, H. J., Yoon, I. S., Yoon, H. Y., Koo, H., Jin, Y. J., Ko, S. H., et al. (2012). Polyethylene Glycol-Conjugated Hyaluronic Acid-Ceramide Self-Assembled Nanoparticles for Targeted Delivery of Doxorubicin. *Biomaterials* 33, 1190–1200. doi:10.1016/j.biomaterials.2011.10.064

Choi, K. Y., Jeon, E. J., Yoon, H. Y., Lee, B. S., Na, J. H., Min, K. H., et al. (2012). Theranostic Nanoparticles Based on PEGylated Hyaluronic Acid for the Diagnosis, Therapy and Monitoring of colon Cancer. *Biomaterials* 33, 6186–6193. doi:10.1016/j.biomaterials.2012.05.029

Cui, J., Yan, Y., Wang, Y., and Caruso, F. (2012). Templated Assembly of pH-Labile Polymer-Drug Particles for Intracellular Drug Delivery. *Adv. Funct. Mater.* 22, 4718–4723. doi:10.1002/adfm.201201191

Ding, J., Shi, F., Xiao, C., Lin, L., Chen, L., He, C., et al. (2011). One-Step Preparation of Reduction-Responsive Poly(ethylene Glycol)-Poly(amino Acid)s Nanogels as Efficient Intracellular Drug Delivery Platforms. *Polym. Chem.* 2, 2857–2864. doi:10.1039/c1py00360g

Gu, X., Ding, J., Zhang, Z., Li, Q., Zhuang, X., and Chen, X. (2015). Polymeric Nanocarriers for Drug Delivery in Osteosarcoma Treatment. *Curr. Pharm. Des.* 21, 5187–5197. doi:10.2174/1381612821666150923095618

Hossain, S., Yamamoto, H., Chowdhury, E. H., Wu, X., Hirose, H., Haque, A., et al. (2013). Fabrication and Intracellular Delivery of Doxorubicin/Carbonate Apatite Nanocomposites: Effect on Growth Retardation of Established Colon Tumor. *Plos One* 8, e60428. doi:10.1371/journal.pone.0060428

Jemal, A., Bray, F., Center, M. M., Ferlay, J., Ward, E., and Forman, D. (2011). Global Cancer Statistics. *CA Cancer J. Clin.* 61, 69–90. doi:10.3322/caac.20107

Kaminskas, L. M., Mcleod, V. M., Kelly, B. D., Sberna, G., Boyd, B. J., Williamson, M., et al. (2012). A Comparison of Changes to Doxorubicin Pharmacokinetics, Antitumor Activity, and Toxicity Mediated by PEGylated Dendrimer and PEGylated Liposome Drug Delivery Systems. *Nanomedicine* 8, 103–111. doi:10.1016/j.nano.2011.05.013

Kim, T. W., Lee, Y. S., Yun, N. H., Shin, C. H., Hong, H. K., Kim, H. H., et al. (2020). MicroRNA-17-5p Regulates EMT by Targeting Vimentin in Colorectal Cancer. *Br. J. Cancer* 123, 1123–1130. doi:10.1038/s41416-020-0940-5

Kobayashi, H., Watanabe, R., and Choyke, P. L. (2013). Improving Conventional Enhanced Permeability and Retention (EPR) Effects; what Is the Appropriate Target. *Theranostics* 4, 81–89. doi:10.7150/thno.7193

Kolate, A., Baradia, D., Patil, S., Vhora, I., Kore, G., and Misra, A. (2014). PEG - A Versatile Conjugating Ligand for Drugs and Drug Delivery Systems. *J. Control. Release* 192, 67–81. doi:10.1016/j.jconrel.2014.06.046

Laroui, H., Wilson, D. S., Dalmasso, G., Salaita, K., Murthy, N., Sitaraman, S. V., et al. (2011). Nanomedicine in GI. *Am. J. Physiol. Gastrointest. Liver Physiol.* 300, G371–G383. doi:10.1152/ajpgi.00466.2010

Lee, C. C., Gillies, E. R., Fox, M. E., Guillaudeu, S. J., Fréchet, J. M., Dy, E. E., et al. (2006). A Single Dose of Doxorubicin-Functionalized Bow-Tie Dendrimer Cures Mice Bearing C-26 Colon Carcinomas. *Proc. Natl. Acad. Sci. U S A.* 103, 16649–16654. doi:10.1073/pnas.0607705103

Li, J., Xu, W., Li, D., Liu, T., Zhang, Y. S., Ding, J., et al. (2018). Locally Deployable Nanofiber Patch for Sequential Drug Delivery in Treatment of Primary and Advanced Orthotopic Hepatomas. *Acs Nano* 12, 6685–6699. doi:10.1021/acsnano.8b01729

Maeda, H. (2012). Macromolecular Therapeutics in Cancer Treatment: The EPR Effect and Beyond. *J. Control. Release* 164, 138–144. doi:10.1016/j.jconrel.2012.04.038

Ortiz, R., Prados, J., Melguizo, C., Arias, J. L., Ruiz, M. A., Alvarez, P. J., et al. (2012). 5-Fluorouracil-Loaded Poly(ε-Caprolactone) Nanoparticles Combined with Phage E Gene Therapy as a New Strategy against colon Cancer. *Int. J. Nanomedicine* 7, 95–107. doi:10.2147/IJN.S26401

Peer, D., Karp, J. M., Hong, S., Farokhzad, O. C., Margalit, R., and Langer, R. (2007). Nanocarriers as an Emerging Platform for Cancer Therapy. *Nat. Nanotechnol* 2, 751–760. doi:10.1038/nnano.2007.387

Prados, J., Melguizo, C., Ortiz, R., Perazzoli, G., Cabeza, L., Alvarez, P. J., et al. (2013). Colon Cancer Therapy: Recent Developments in Nanomedicine to Improve the Efficacy of Conventional Chemotherapeutic Drugs. *Anticancer Agents Med. Chem.* 13, 1204–1216. doi:10.2174/18715206113139990325

Qiu, R., Sun, D., Bai, Y., Li, J., and Wang, L. (2020). Application of Tumor-Targeting Peptide-Decorated Polypeptide Nanoparticles with Doxorubicin to Treat Osteosarcoma. *Drug Deliv.* 27, 1704–1717. doi:10.1080/10717544.2020.1856221

Samanta, S., Swamy, V., Suresh, D., Rajkumar, M., Rana, B., Rana, A., et al. (2008). Protective Effects of Vanadium against DMH-Induced Genotoxicity and Carcinogenesis in Rat colon: Removal of O(6)-Methylguanine DNA Adducts, P53 Expression, Inducible Nitric Oxide Synthase Downregulation and Apoptotic Induction. *Mutat. Res.* 650, 123–131. doi:10.1016/j.mrgentox.2007.11.001

Schafer, F. Q., and Buettner, G. R. (2001). Redox Environment of the Cell as Viewed through the Redox State of the Glutathione Disulfide/glutathione Couple. *Free Radic. Biol. Med.* 30, 1191–1212. doi:10.1016/s0891-5849(01)00480-4

Soster, M., Juris, R., Bonacchi, S., Genovese, D., Montalti, M., Rampazzo, E., et al. (2012). Targeted Dual-Color Silica Nanoparticles Provide Univocal Identification of Micrometastases in Preclinical Models of Colorectal Cancer. *Int. J. Nanomedicine* 7, 4797–4807. doi:10.2147/IJN.S33825

Su, T., Yang, B., Gao, T., Liu, T., and Li, J. (2020). Polymer Nanoparticle-Assisted Chemotherapy of Pancreatic Cancer. *Ther. Adv. Med. Oncol.* 12, 1758835920915978. doi:10.1177/1758835920915978

Ta, H. T., Dass, C. R., Larson, I., Choong, P. F., and Dunstan, D. E. (2009). A Chitosan-Dipotassium Orthophosphate Hydrogel for the Delivery of Doxorubicin in the Treatment of Osteosarcoma. *Biomaterials* 30, 3605–3613. doi:10.1016/j.biomaterials.2009.03.022

Vermani, L., Kumar, R., Kannan, R. R., Deka, M. K., Talukdar, A., and Kumar, N. S. (2020). Expression Pattern of ALDH1, E-Cadherin, Vimentin and Twist in Early and Late Onset Sporadic Colorectal Cancer. *Biomark Med.* 14, 1371–1382. doi:10.2217/bmm-2020-0206

Wang, A. Z., Langer, R., and Farokhzad, O. C. (2012). Nanoparticle Delivery of Cancer Drugs. *Annu. Rev. Med.* 63, 185–198. doi:10.1146/annurev-med-040210-162544

Wang, J., Sui, L., Huang, J., Miao, L., Nie, Y., Wang, K., et al. (2021). MoS2-Based Nanocomposites for Cancer Diagnosis and Therapy. *Bioact Mater.* 6, 4209–4242. doi:10.1016/j.bioactmat.2021.04.021

Wang, X., Yang, L., Fang, Q., Xu, J., Cheng, X., Xue, Y., et al. (2020). GLUT1-Targeting and GSH-Responsive DOX/L61 Nanodrug Particles for Enhancing MDR Breast Cancer Therapy. *Part. Part. Syst. Charact.* 37, 2000165. doi:10.1002/ppsc.202000165

Wen, Y., Zhang, Z. J., Huang, Y. P., Wang, K. P., Liu, K., Zou, H., et al. (2019). Application of the Ethyl Acetate Extract of Cichorium as a Potential Photosensitizer in Photodynamic Therapy Induces Apoptosis and Autophagy in Colorectal Cancer Cell Lines via the Protein Kinase R-Like Endoplasmic Reticulum Kinase Pathway. *J. Biomed. Nanotechnol* 15, 1867–1880. doi:10.1166/jbn.2019.2825

Zhu, S., Hong, M., Tang, G., Qian, L., Lin, J., Jiang, Y., et al. (2010). Partly PEGylated Polyamidoamine Dendrimer for Tumor-Selective Targeting of Doxorubicin: The Effects of PEGylation Degree and Drug Conjugation Style. *Biomaterials* 31, 1360–1371. doi:10.1016/j.biomaterials.2009.10.044

Zinczuk, J., Maciejczyk, M., Zareba, K., Pryczynicz, A., Dymicka-Piekarska, V., Kaminska, J., et al. (2020). Pro-Oxidant Enzymes, Redox Balance and Oxidative Damage to Proteins, Lipids and DNA in Colorectal Cancer Tissue. Is Oxidative Stress Dependent on Tumour Budding and Inflammatory Infiltration. *Cancers* 12, 1636. doi:10.3390/cancers12061636

Zinczuk, J., Maciejczyk, M., Zareba, K., Romaniuk, W., Markowski, A., Kedra, B., et al. (2019). Antioxidant Barrier, Redox Status, and Oxidative Damage to Biomolecules in Patients with Colorectal Cancer. Can Malondialdehyde and Catalase Be Markers of Colorectal Cancer Advancement. *Biomolecules* 9, 637. doi:10.3390/biom9100637

Conflict of Interest: The authors declare that the research was conducted in the absence of any commercial or financial relationships that could be construed as a potential conflict of interest.

Publisher's Note: All claims expressed in this article are solely those of the authors and do not necessarily represent those of their affiliated organizations, or those of the publisher, the editors and the reviewers. Any product that may be evaluated in this article, or claim that may be made by its manufacturer, is not guaranteed or endorsed by the publisher.

Copyright © 2021 Liu, Wang, He and Li. This is an open-access article distributed under the terms of the Creative Commons Attribution License (CC BY). The use, distribution or reproduction in other forums is permitted, provided the original author(s) and the copyright owner(s) are credited and that the original publication in this journal is cited, in accordance with accepted academic practice. No use, distribution or reproduction is permitted which does not comply with these terms.

frontiers in Oncology

ORIGINAL RESEARCH
published: 20 October 2021
doi: 10.3389/fonc.2021.768829

$SnFe_2O_4$ Nanozyme Based TME Improvement System for Anti-Cancer Combination Thermoradiotherapy

Wen Zeng[1,2†], *Chunping Liu*[3†], *Shuntao Wang*[3†], *Ziqi Wang*[4] *and Qinqin Huang*[1*]

[1] Department of Molecular Pathology, The Second Affiliated Hospital of Zhengzhou University, Zhengzhou, China, [2] Department of Ophthalmology, Zhongnan Hospital of Wuhan University, Wuhan, China, [3] Department of Breast and Thyroid Surgery, Union Hospital, Tongji Medical College, Huazhong University of Science and Technology, Wuhan, China, [4] Key Laboratory of Artificial Micro- and Nano-Structures of Ministry of Education, School of Physics and Technology, Wuhan University, Wuhan, China

OPEN ACCESS

Edited by:
Kelong Ai,
Central South University, China

Reviewed by:
Yaswanth Kuthati,
Cathay General Hospital, Taiwan
Ke Jiang,
Sun Yat-sen University Cancer Center (SYSUCC), China
Jialiu Wei,
Chinese Academy of Medical Sciences and Peking Union Medical College, China

***Correspondence:**
Qinqin Huang
qqhuang@zzu.edu.cn

[†]These authors have contributed equally to this work

Specialty section:
This article was submitted to Pharmacology of Anti-Cancer Drugs, a section of the journal Frontiers in Oncology

Received: 01 September 2021
Accepted: 27 September 2021
Published: 20 October 2021

Citation:
Zeng W, Liu C, Wang S, Wang Z and Huang Q (2021) $SnFe_2O_4$ Nanozyme Based TME Improvement System for Anti-Cancer Combination Thermoradiotherapy. Front. Oncol. 11:768829. doi: 10.3389/fonc.2021.768829

High doses of radiotherapy (RT) are associated with resistance induction. Therefore, highly selective and controllable radiosensitizers are urgently needed. To address this issue, we developed a tin ferrite (SFO)-based tumor microenvironment (TME)-improved system (SIS) that can be used in combination with low-dose radiation. The SIS was delivered *via* intratumoral injection directly to the tumor site, where it was stored as a ration depot. Due to the photothermal properties of SFO, SIS steadily dissolved under near-infrared (NIR) laser irradiation. Simultaneously, the dual glutathione oxidase (GSH-OXD) and catalase (CAT) activities of the SFO nanozyme significantly lowered the content of GSH in tumor tissues and efficiently catalyzed the conversion of intracellular hydrogen peroxide to produce a large amount of oxygen (O_2) for intracellular redox homeostasis disruption, thus reducing radiotherapy resistance. Our *in vivo* and *in vitro* studies suggested that combining the SIS and NIR irradiation with RT (2Gy) significantly reduced tumor proliferation without side effects such as inflammation. To conclude, this study revealed that SFO-based nanozymes show great promise as a catalytic, radiosensitizing anti-tumor therapy.

Keywords: radiotherapy, photothermal therapy, hydrogel, nanozymes, tumor therapy

INTRODUCTION

Cancer, which can strike at any age and affect anybody, remains a serious threat to human life and health in today's society, despite current scientific advancements (1–3). Radiotherapy (RT), either alone or in combination with other cutting-edge treatments, is widely utilized to treat cancer patients (4). RT is based on the use of high-energy X-rays or gamma rays to generate radiation-induced DNA damage and triggers the development of large amounts of harmful reactive oxygen species (ROS) (4). Both radiation-induced DNA damage and ROS production that exceeds the potential of the cell to neutralize these free radicals result in cell death by apoptosis reducing the size of the tumor (5, 6). However, while RT kills tumor cells, it does so at the expense of nearby cells and tissues in the human body. Radiation produces ROS in a dose-dependent manner, resulting in better treatment outcomes at higher doses (7, 8). However, high-dose radiotherapy might cause systemic

effects, including fatigue, loss of appetite, bone marrow suppression, radiotherapy-induced secondary and primary malignancies, and infertility, as well as local radiation damage. Local liver injury can lead to altered activity or even liver failure in more serious cases (9, 10). Furthermore, while RT has some efficacy, the tumor microenvironment (TME) in solid tumors frequently exhibits high levels of glutathione oxidase (GSH-OXD) expression, since GSH plays an essential role in anti-tumor radiation *via* GSH spontaneous reaction or GSH S-transferase catalyzed reaction with xenoorganisms (11–13). Moreover, since GSH is a reducing agent it can directly eliminate ROS which reduces the effectiveness of ROS-based therapies (14). Therefore, a decrease in cellular GSH content can effectively promote radiation sensitization and, thus, improve RT efficacy (15, 16). The employment of alternative catalysts to decrease the levels of GSH is expected to have a good synergistic impact when paired with irradiation, allowing a reduction of the dose of radiation without compromising the therapeutic effect.

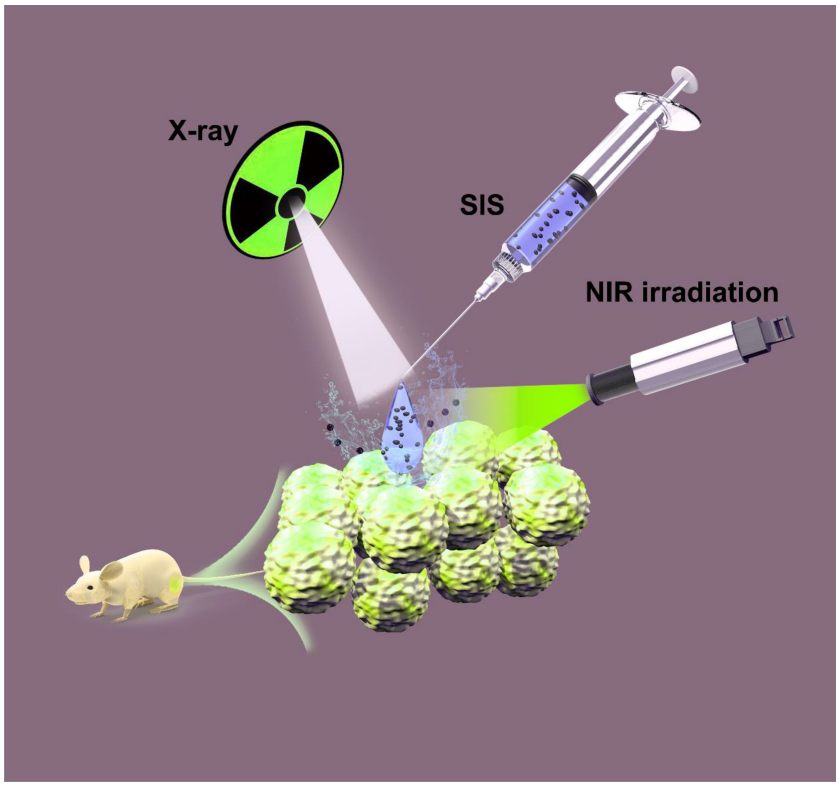
Since there are various pathways of GSH metabolism and various types of chemical reactions involving GSH, its elimination can be accomplished in a variety of ways (17, 18). Converting GSH to its oxidized state through direct interactions has become one of the most commonly used methods for lowering GSH levels (11, 13, 19). For example, Bao et al. achieved radiation sensitization by creating a composite nanomaterial containing MnO_2 to improve tumor hypoxia and lower intracellular GSH levels (20). Qu et al. developed MoS_2@AIBI-PCM, a composite nanomaterial in which GSH oxidation is effectively achieved through reaction with MoS_2 without releasing hazardous metal ions, resulting in significant tumor death and good biocompatibility during therapy (21). Tin ferrite ($SnFe_2O_4$, abbreviated as SFO) is a novel nanomaterial that stimulates both GSH-OXD and high-activity CAT (22). SFO can reduce GSH and act as a catalyst for the conversion of H_2O_2 to O_2 to produce sufficient O_2 to sensitize the TME, and is expected to act synergistically with RT. These nanomaterials can reach tumor tissues *via* blood circulation upon intravenous injection. Despite the fact that these nanomaterials have proven effective against the GSH system they are vulnerable to the activity of the immune system and are easily cleared from the bloodstream by the liver and kidneys, which considerably reduces their anti-tumor efficiency. Various drug delivery systems such as liposomes have been designed and developed in recent years that represent safer and more effective cancer treatments (17, 23). However, the interference of a series of *in vivo* biological barriers, including the blood circulation, vascular extravasation, accumulation at the tumor location, tumor depth of stromal infiltration, and tumor cell internalization, have limited intracellular drug release.

Traditional drug delivery systems are susceptible to issues such as poor drug loading, complicated synthesis methods, early drug leakage or slow-release, and the long-term toxicity brought on by the carrier's presence in the body over an extended period (24, 25). Recently, light-responsive hydrogels with minimum invasiveness have received a lot of attention as a controlled drug release platform (26–28). The hydrogel progressively solidifies after being injected into tumor tissue and can serve as a rationing depot over a long period (29). After one injection, this form of local administration can be used repeatedly. Furthermore, parameters such as laser power and irradiation period can be modified to alter the medication release rate, extending the applicability of this treatment method. Recently, Zhu et al. were the first to employ an agarose hydrogel to deliver anti-tumor aggregation-induced emission-based luminogens (AIEgen) material. As a photothermal agent, Prussian blue (PB) nanozyme stimulates the disintegration of the hydrogel while also stimulating CAT to scavenge H_2O_2 to sensitize the tumor microenvironment (30). Following that, under the irradiation of low-power white light, AIEgens can produce ROS under sufficient oxygen levels to promote tumor ablation. Zhang et al. developed a black phosphorus-based injectable hydrogel for photothermal therapy, which employs external photoexcitation to release cancer drugs, resulting in accurate and safe cancer treatment (31). In addition, thermal-radiotherapy is a combined treatment mode. Photothermal therapy can not only kill tumors alone, but also inactivate cells, thus sensitizing radiotherapy (32). In view of these findings, we hypothesized that delivering SFO to the TME using hydrogels would enhance the efficacy of low-dose radiation.

In this study, we developed a method using intratumoral delivery of an injectable hydrogel containing SFO nanoparticles for combined photothermal and radiotherapy (**Scheme 1**). Agarose hydrogels have been approved by the US Food and Drug Administration (FDA) owing to their reliable biosafety. Therefore, we prepared an SFO-based TME-improved system (SIS) by loading SFO nanoparticles into an agarose hydrogel. SFO nanoparticles serve as a photothermal agent (PTA) in this system due to their outstanding photothermal performance. SFO turns light energy into heat energy when an 808 nm near-infrared (NIR) laser irradiates the SIS system, causing the temperature of the agarose hydrogel to rise and reversible hydrolysis and softening to occur. When SIS diffuses into the local TME, the SFO nanozyme lowers intracellular GSH levels and simultaneously catalyzes the conversion of H_2O_2 to O_2, due to its stimulation of GSH-OXD and CAT activities, respectively, increasing the sensitivity of the TME to radiation. The SIS functions as an SFO storage control, to achieve regulated drug release following its intratumoral injection of local malignancies. Our *in vivo* and *in vitro* experiments showed that SIS is effective in treating tumors without any off-target toxicity. In conclusion, the SIS nanosystem has a wide range of clinical potential in synergetic anti-tumor therapy.

RESULTS AND DISCUSSION

We first obtained a transmission electron microscope (TEM) image of SFO, as shown in **Figure 1A**. SFO has outstanding dispersibility and small size with an average of 16.4 ± 1.4 nm. Since nanomaterials are easily cleared by the kidney it is difficult to achieve the desired therapeutic effect by methods that require circulation in the bloodstream (33). Therefore, we used a hydrogel delivery technique that considerably improved the applicability of SFO. The hydrogel was prepared using a basic hydrothermal technique and analyzed by scanning electron microscopy (SEM). As shown in **Figure 1B**, the SEM images reveal the complex pore structure of the hydrogel. The results of X-ray diffraction (XRD) and X-ray



SCHEME 1 | SIS system was used for anti-cancer combination thermoradiotherapy.

photoelectron spectroscopy (XPS) are shown in **Figures 1C, E**, respectively. The ability of SFO nanozymes to produce O_2 from hydrogen peroxide is essential for the treatment of hypoxic tumors. **Figure 1D** shows that SFO nanozyme interacts with H_2O_2 and effectively produces O_2. The rheological values of SIS were measured at various temperatures (**Figure 1F**). The results revealed that as the temperature rises SIS gradually dissolves, accompanied by a gradual decrease in storage modulus. This is in line with the hydrogel's rheological properties. One of the most essential factors for evaluating PTA is photothermal stability (34, 35). A powerful photothermal treatment can be assisted by a good photothermal agent. **Figure 1G** shows that SFO has a wide absorption region (650-900 nm). To test the photothermal performance of SFO nanoparticles, solutions were prepared with different concentrations of SFO (0, 50, 100, 200 μg/mL). **Figure 1H** shows that, assuming all other parameters remain constant, the heating impact of the solution increases as the SFO concentration rises. At 100 μg/mL SFO, the temperature increased by roughly 19.5°C after 5 min of laser irradiation. Next, a 200 μg/mL SFO solution was repeatedly heated for 5 min using an 808 nm NIR laser and allowed to cool to ambient temperature (**Figure 1I**). The heating curves of each cycle were identical and the variations in peak temperatures were minor, demonstrating that the photothermal conversion capability of the SFO nanoparticles was stable and reproducible over 4 repeated heating and cooling cycles. These findings suggested that the SFO nanoparticles had good photothermal stability. Furthermore, the photothermal conversion efficiency (η) of the SFO was calculated from the data of **Figure 1I** and was found to be 38.5%, which was greater than various other materials such as Au nanostars (36.4%) and Ti3C2 nanosheets (30.6%) (36, 37).

The SIS system is well-structured and performance oriented. Anti-tumor experiments *in vitro* are presently underway. While SFO has the potential to disrupt the ecological balance of cancer cells and hence increase the efficacy of radiation, it can do so only when it is present in tumor tissue. The immune system may recognize stimuli from a variety of foreign invaders and part of that stimulation may trigger the immune response, resulting in immunity, while other stimuli may result in tolerance. When tumor cells are exposed to radiation, double-stranded DNA breaks (DSB) occur at certain sites, providing insight into radiation sensitization (38). Measuring the fluorescence intensity of the histone variant H_2AX phosphorylated is a specific and sensitive technique to detect DSB formation following DNA damage (39). Therefore, we analyzed the density of H2AX foci in the nuclei of 4T1 cells after various treatments, including 1) PBS + NIR; 2) RT (2Gy); 3) SIS + NIR; 4) High dose RT (6Gy); and 5) SIS + NIR + RT, both under normoxic and hypoxic conditions. Under normoxic conditions, 2 Gy of radiation caused substantial DNA damage and when the dose was raised to 6Gy, the DSB effect increased. However, in hypoxic cells, the effect was not satisfactory. The DSB effect in the 6 Gy RT group under hypoxia conditions was only about 40.6%. It is important to mention that 808 nm laser irradiation combined

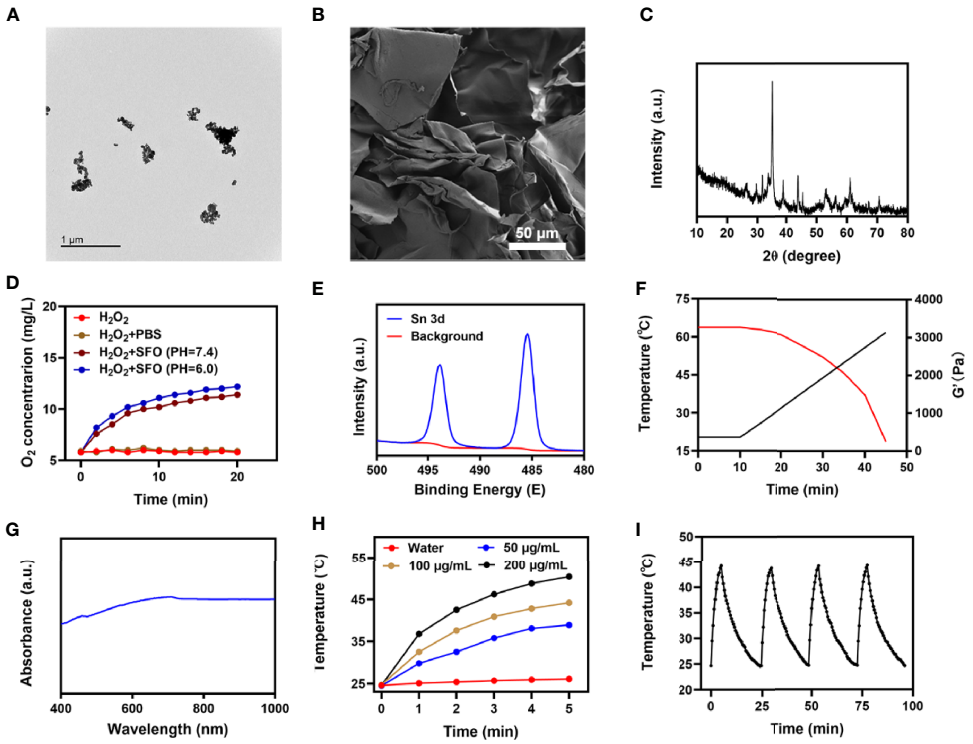


FIGURE 1 | **(A)** TEM image of SFO. **(B)** SEM image of hydrogel. **(C)** XRD pattern of SFO. **(D)** O_2 generation in H_2O_2 solution added with PBS or SFO under different pH values (7.4 and 6.0). **(E)** Sn 3d spectrum of XPS spectra of fresh SFO. **(F)** Rheological and temperature curves (red and black, respectively) for the prepared SIS in response to 0.5 W/cm^2 808 nm laser irradiation. **(G)** SFO absorbance spectra. **(H)** Heating curves for the different concentrations of SFO nanoparticles solutions upon laser irradiation at 808 nm (0.5 W/cm^2) for 5 min. **(I)** Temperature variation of an SFO solution at 200 μg/mL under cyclic laser irradiation.

with SIS achieved about 40% γ-H2AX formation whether in hypoxia or normoxia conditions. Notably, SIS + NIR + RT displayed the strongest effect, up to 76.4% and 72.6% γ-H2AX foci development in normoxic and hypoxic conditions, respectively, which was greater than the 6 Gy RT groups (**Figures 2A–D**). The uniform and significant differences between each experimental group were linked to the synergistic effect of SIS as a photothermal agent in PTT, SFO as CAT and GSH-OXD, and sensitization to low-dose radiation. Colony formation assays also showed that the SIS + NIR + RT group demonstrated considerable tumor growth inhibition compared with controls under both normoxic and hypoxic conditions (**Figures 2E, F**, respectively). SFO was added to 4T1 cells at various doses (0, 5, 10, 20, 40 μg/mL) and after 24 hours of incubation cell viability was assessed (**Figure 2G**). Even at high concentrations, cell viability did not decline significantly. Therefore, our results show that SFO NPs exhibit high biocompatibility. GSH is a rich endogenous antioxidant that can maintain cellular redox balance and inhibit cell damage caused by ROS (40). Therefore, we studied the ability of SFO nanozymes to deplete GSH. With increasing SFO concentrations, GSH depletion increased significantly (**Figure 2H**). Taken together, these findings motivated us to fully investigate the anti-tumor efficacy of SFO *in vivo*.

The proliferation of malignant tumors is associated with local intratumoral hypoxia and, as a result, cancerous tissues are less susceptible to the lethal DNA damaging effects of ionizing radiation than aerobic cells, reducing the sensitivity and increasing the resistance towards radiotherapy (41). We explored the effect of SIS on the oxygen content of the tumor. The results showed that SIS + NIR reduced the hypoxic staining (PIMO-positive cells) in the tumor (**Figure 3A**), while the control group (PBS + NIR) showed obvious hypoxic areas, confirming that the SFO actively catalyzes the conversion of local H_2O_2, producing a large amount of oxygen to relieve the tumor hypoxia. In view of its good *in vitro* performance as a PTA and radiosensitizer, we next investigated the photothermal conversion impact of SFO *in vivo*. BALB/c mice were injected subcutaneously with 4T1 cells to develop tumors. **Figure 3B** shows the temperature change curves for the PBS and SIS groups after 10 minutes of 808 nm NIR laser irradiation at 0.5 W/cm^2. Within 10 minutes of receiving SIS, the temperature increased about 20.4°C, whereas the PBS group experienced only little increase in temperature. Tumor tissues have lower heat resistance than normal cells, resulting in tumor cells being selectively destroyed at high temperatures (42–47°C). The efficacy of SIS-mediated anti-tumor activity was then tested in mice bearing 4T1 tumors. To investigate the primary effect of the SIS, BALB/c mice were subcutaneous injected into the right flank with 1×10^6 4T1 cells. When the primary tumor volumes reached 200 mm^3, the mice were randomly divided into 5 groups (each group included 5 mice): 1) PBS + NIR; 2) RT (2Gy); 3) SIS + NIR; 4) High dose RT

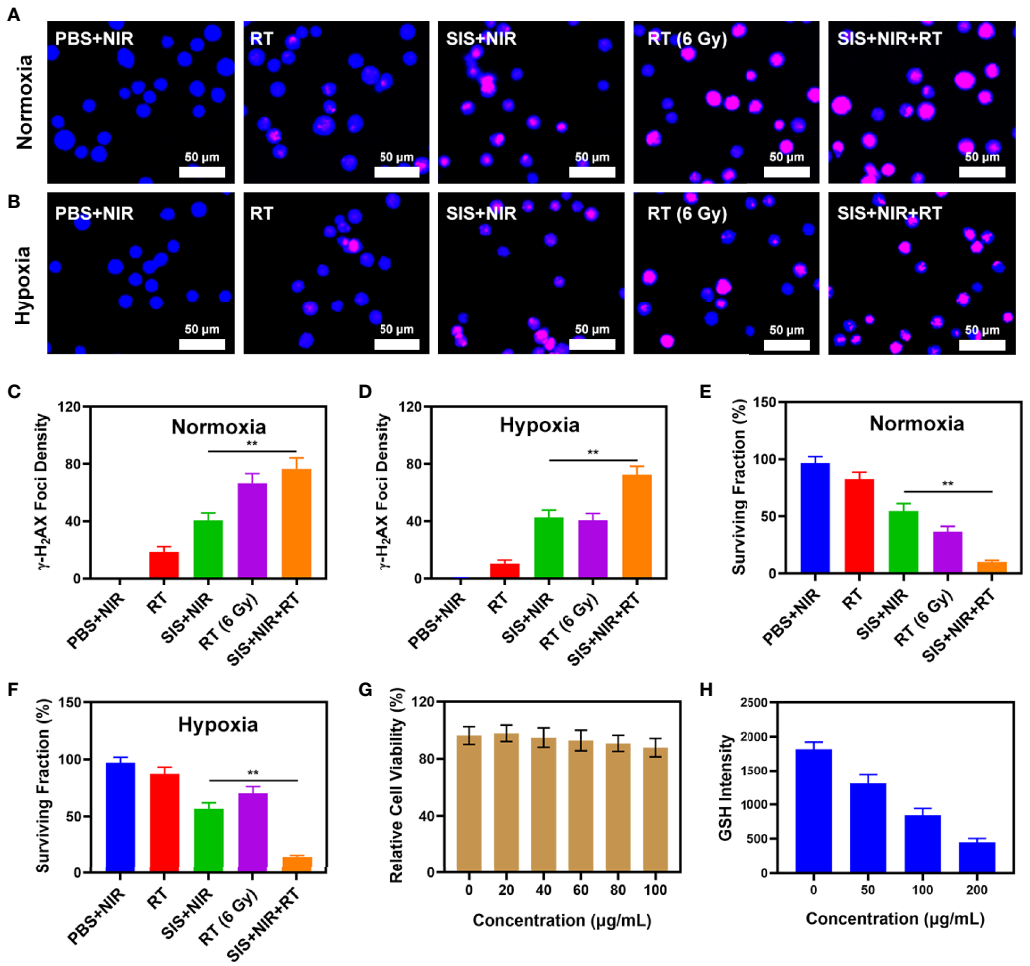


FIGURE 2 | **(A)** The CLSM images of 4T1 cells under different treatment in normoxia condition. The nuclei were stained with DAPI (blue) and DSBs were stained with γ-H_2AX (red). **(B)** The CLSM images of 4T1 cells under different treatment in hypoxia condition. The nuclei were stained with DAPI (blue) and DSBs were stained with γ-H_2AX (red). **(C)** The density of γ-H_2AX foci in **(A)** was determined based on analyses of 100 cells per treatment group (γ-H_2AX foci/100 μm^2, n = 3). **(D)** The density of γ-H_2AX foci in **(B)** was determined based on analyses of 100 cells per treatment group (γ-H_2AX foci/100 μm^2, n = 3). **(E)** Colony formation assays were conducted using 4T1 cells treated with radiation under normoxia condition (n = 3). **(F)** Colony formation assays were conducted using 4T1 cells treated with radiation under hypoxia condition (n = 3). **(G)** Dark cytotoxicity of SFO on 4T1 cells. **(H)** Quantitative analysis of GSH levels for different SFO concentration. **P < 0.01; Student's t-test.

(6Gy); 5) SIS + NIR + RT. The SFO concentration was 1 mg/kg in groups 3, and 5. The mice received therapy every five days for 16 days. The tumor volumes of the PBS + NIR group and the low dosage RT treated group increased rapidly over the 2 weeks of treatment, as illustrated in **Figure 3C**. The SIS + NIR treatment had a tumor-suppressing impact that was moderate. Following intratumoral injection of SIS, the hydrogel will disintegrate once subjected to laser radiation and release SFO. SFO then catalyzes the intratumoral conversion of H_2O_2 to produce O_2 in situ, which increases radiation sensitization. Furthermore, SFO decreases GSH levels in the tumors, further amplifying the radiation effect. The SIS + NIR + RT treatment, which included SFO, had the most potent therapeutic impact, with growth curves of tumor volume nearly completely suppressed during therapy. As the combination of 808 nm laser irradiation and RT could play the role of mutual promotion, SFO could simultaneously enhance RT and PTT. The tumor mass of the mice was also in agreement with the volume curve (**Figure 3D**). No weight changes were observed in the treatment group throughout the study, indicating that the treatment did not cause any significant systemic toxicity in the mice (**Figure 3E**), which is noteworthy because many treatments are associated with severe systemic toxicity, which severely hampers future medical applications of the material (30). We obtained slices of tumor tissue for staining. Hematyloxin and eosin (H&E) and TUNEL staining (**Figure 3F**) revealed that tumors from the SIS combined thermal radiation group had a significant percentage of cell necrosis. Furthermore, SFO activation did not result in systemic loss, as shown in **Figure 4**. Following the treatment, the vital organs (heart, liver, spleen, lungs, and kidney) were without any inflammation or damage. Moreover, the liver and kidney indexes were also normal. While many nanomaterials have high therapeutic efficacy, they also have a high risk of systemic

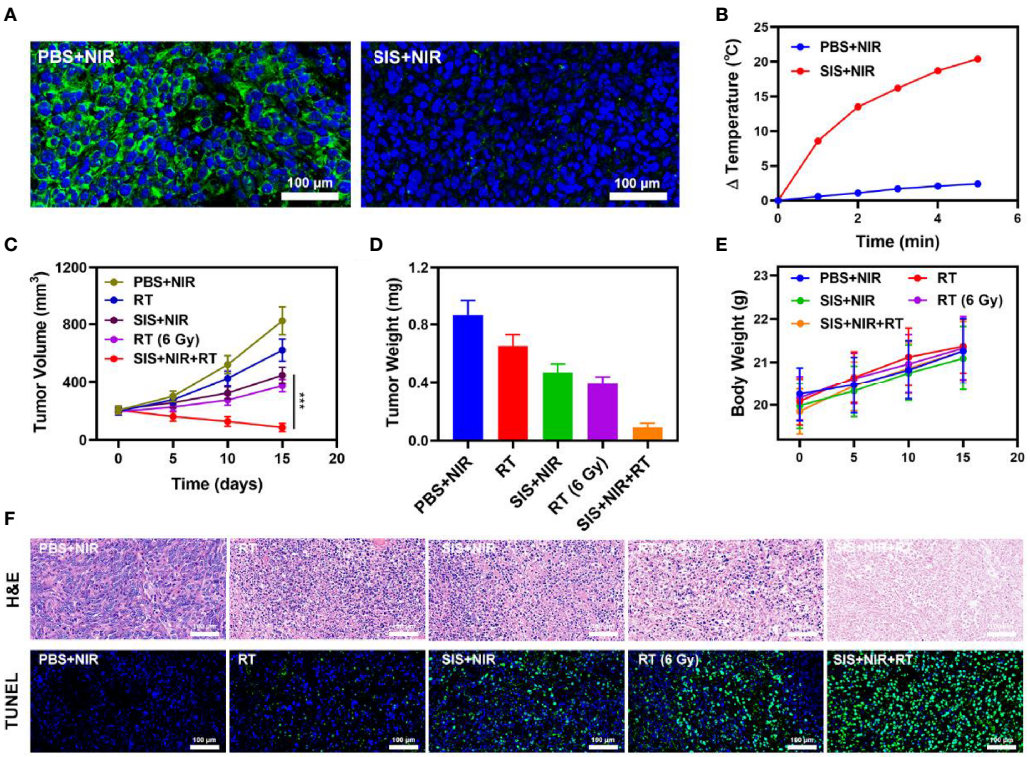


FIGURE 3 | **(A)** Representative images of tumor tissue sections stained with anti-PIMO (green) and DAPI (blue) following the indicated treatments. **(B)** Temperature increases in mice implanted with 4T1 tumors following 808 nm laser irradiation (0.5 W/cm2) for 5 min in the indicated treatment groups. **(C)** Tumor volume change over time in groups treated as indicated. **(D)** Average tumor weight values associated with the indicated treatments. **(E)** Changes in body weight in response to the indicated treatments. **(F)** H&E and TUNEL stained tumor sections from the indicated treatment groups. ***P < 0.005; Student's t-test.

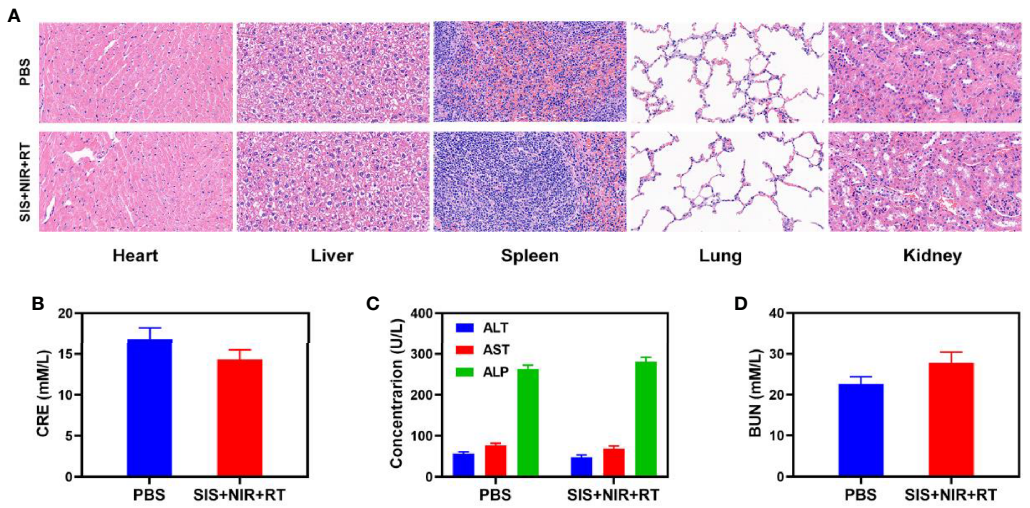


FIGURE 4 | Result of *in vivo* safety experiments. **(A)** Histopathological analysis results (H&E stained images) of the major organs, heart, lung, liver, kidneys, and spleen, of mice that were exposed to different treatments 16 days post-injection. Blood biochemistry data including kidney function markers: **(B)** liver function markers: CRE, **(C)** ALT, ALP, and AST and **(D)** BUN after various treatments.

toxicity, which limits their future clinical applications. Our *in vivo* results showed that our unique and powerful SIS-enhanced combination treatment not only achieved a high level of biological safety but also sensitized the TME, enhancing the efficacy of RT.

CONCLUSION

In conclusion, by encapsulating SFO nanozymes in an agarose hydrogel, we developed an injectable light-controlled SFO-based hydrogel as a TME-sensitizing system named SIS. The nano-system allowed the combination of low-dose radiation with other therapies greatly improving tumor treatment outcomes. SFO nanoparticles are outstanding radiosensitizers and PTAs due to the nanozyme catalysis and superior photothermal effect in the NIR-I region. The agarose hydrogel underwent regulated and reversible hydrolysis and a softening under the NIR laser power, resulting in the light-triggered release of SFO nanoparticles and hydrogel deterioration. The release rate of SFO nanoparticles is adjustable by changing the parameters. More importantly, by injecting the hydrogel intratumorally, the concentration of SFO nanoparticles in tumor tissues will be significantly raised, a single injection allowing for multiple treatments *in vivo*. It is worth emphasizing that after photothermal treatment, we observed an increase in of O_2 content of the tumor cells, which considerably boosted radiotherapy efficacy. The SIS exhibits outstanding cancer cell killing efficacy and tumor ablation properties in both *in vitro* and *in vivo* tests, with good stability and biocompatibility, and low toxicity. In conclusion, SIS has great potential in anti-cancer combination therapy.

DATA AVAILABILITY STATEMENT

The original contributions presented in the study are included in the article/**Supplementary Material**. Further inquiries can be directed to the corresponding author.

ETHICS STATEMENT

The animal study was reviewed and approved by Administrative Committee on Animal Research of the Zhengzhou University.

AUTHOR CONTRIBUTIONS

Conceived and designed the experiments: ZW, WZ, QH, and SW. Performed the experiments: ZW and CL. Contributed reagents/materials/analysis tools: ZW and WZ. Revised the polished the article: QH. All authors contributed to the article and approved the submitted version.

FUNDING

This work was supported by the National Natural Science Foundation of China (31800085).

SUPPLEMENTARY MATERIAL

The Supplementary Material for this article can be found online at: https://www.frontiersin.org/articles/10.3389/fonc.2021.768829/full#supplementary-material

REFERENCES

1. Jin L, Hu P, Wang Y, Wu L, Qin K, Cheng H, et al. Fast-Acting Black-Phosphorus-Assisted Depression Therapy With Low Toxicity. *Adv Mater* (2020) 32(2):e1906050. doi: 10.1002/adma.201906050
2. Chen C, Ni X, Jia S, Liang Y, Wu X, Kong D, et al. Massively Evoking Immunogenic Cell Death by Focused Mitochondrial Oxidative Stress Using an AIE Luminogen With a Twisted Molecular Structure. *Adv Mater* (2019) 31 (52):e1904914. doi: 10.1002/adma.201904914
3. Chang M, Hou Z, Jin D, Zhou J, Wang M, Wang M, et al. Colorectal Tumor Microenvironment-Activated Bio-Decomposable and Metabolizable Cu2 O@ Caco3 Nanocomposites for Synergistic Oncotherapy. *Adv Mater* (2020) 32 (43):e2004647. doi: 10.1002/adma.202004647
4. Gong L, Zhang Y, Liu C, Zhang M, Han S. Application of Radiosensitizers in Cancer Radiotherapy. *Int J Nanomed* (2021) 16:1083–102. doi: 10.2147/IJN.S290438
5. Xie J, Gong L, Zhu S, Yong Y, Gu Z, Zhao Y. Emerging Strategies of Nanomaterial-Mediated Tumor Radiosensitization. *Advanced Mterials* (2019) 31(3):e1802244. doi: 10.1002/adma.201802244
6. Liu T, Yang K, Liu Z. Recent Advances in Functional Nanomaterials for X-Ray Triggered Cancer Therapy. *Prog Natural Science: Materials Int* (2020) 30 (5):567–76. doi: 10.1016/j.pnsc.2020.09.009
7. Pallares RM, Abergel RJ. Nanoparticles for Targeted Cancer Radiotherapy. *Nano Res* (2020) 13(11):2887–97. doi: 10.1007/s12274-020-2957-8
8. Wang SB, Zhang C, Chen ZX, Ye JJ, Peng SY, Rong L, et al. A Versatile Carbon Monoxide Nanogenerator for Enhanced Tumor Therapy and Anti-Inflammation. *ACS Nano* (2019) 13(5):5523–32. doi: 10.1021/acsnano.9b00345
9. Fan W, Bu W, Zhang Z, Shen B, Zhang H, He Q, et al. X-Ray Radiation-Controlled NO-Release for on-Demand Depth-Independent Hypoxic Radiosensitization. *Angewandte Chemie* (2015) 54(47):14026–30. doi: 10.1002/anie.201504536
10. Rocca JD, Werner ME, Kramer SA, Huxford-Phillips RC, Sukumar R, Cummings ND, et al. Polysilsesquioxane Nanoparticles for Triggered Release of Cisplatin and Effective Cancer Chemoradiotherapy. *Nanomedicine* (2015) 11(1):31–8. doi: 10.1016/j.nano.2014.07.004
11. Wu Y, Guo T, Qiu Y, Lin Y, Yao Y, Lian W, et al. An Inorganic Prodrug, Tellurium Nanowires With Enhanced ROS Generation and GSH Depletion for Selective Cancer Therapy. *Chem Sci* (2019) 10(29):7068–75. doi: 10.1039/C9SC01070J
12. Liu Y, Zhai S, Jiang X, Liu Y, Wang K, Wang C, et al. Intracellular Mutual Promotion of Redox Homeostasis Regulation and Iron Metabolism Disruption for Enduring Chemodynamic Therapy. *Advanced Funct Materials* (2021). doi: 10.1002/adfm.202010390
13. Yin W, Li J, Ke W, Zha Z, Ge Z. Integrated Nanoparticles to Synergistically Elevate Tumor Oxidative Stress and Suppress Antioxidative Capability for Amplified Oxidation Therapy. *ACS Appl Mater Interfaces* (2017) 9 (35):29538–46. doi: 10.1021/acsami.7b08347
14. Cheng X, Xu HD, Ran HH, Liang G, Wu FG. Glutathione-Depleting Nanomedicines for Synergistic Cancer Therapy. *ACS Nano* (2021) 15 (5):18039–68. doi: 10.1021/acsnano.1c00498
15. Lan J-S, Liu L, Zeng R-F, Qin Y-H, Hou J-W, Xie S-S, et al. Tumor-Specific Carrier-Free Nanodrugs With GSH Depletion and Enhanced ROS Generation for Endogenous Synergistic Anti-Tumor by a Chemotherapy-Photodynamic Therapy. *Chem Eng J* (2021) 407. doi: 10.1016/j.cej.2020.127212

16. Dong Z, Feng L, Hao Y, Li Q, Chen M, Yang Z, et al. Synthesis of Caco3-Based Nanomedicine for Enhanced Sonodynamic Therapy *via* Amplification of Tumor Oxidative Stress. *Chem* (2020) 6(6):1391–407. doi: 10.1016/j.chempr.2020.02.020
17. Huang C, Ding S, Jiang W, Wang FB. Glutathione-Depleting Nanoplatelets for Enhanced Sonodynamic Cancer Therapy. *Nanoscale* (2021) 13:4512–8. doi: 10.1039/D0NR08440A
18. Wu H, Liu L, Song L, Ma M, Gu N, Zhang Y. Enhanced Tumor Synergistic Therapy by Injectable Magnetic Hydrogel Mediated Generation of Hyperthermia and Highly Toxic Reactive Oxygen Species. *ACS Nano* (2019) 13(12):14013–23. doi: 10.1021/acsnano.9b06134
19. Gao S, Zhang W, Wang R, Hopkins SP, Spagnoli JC, Racin M, et al. Nanoparticles Encapsulating Nitrosylated Maytansine to Enhance Radiation Therapy. *ACS Nano* (2020) 14(2):1468–81. doi: 10.1021/acsnano.9b05976
20. Lyu M, Zhu D, Kong X, Yang Y, Ding S, Zhou Y, et al. Glutathione-Depleting Nanoenzyme and Glucose Oxidase Combination for Hypoxia Modulation and Radiotherapy Enhancement. *Adv Healthcare Mater* (2020) 9(11): e1901819. doi: 10.1002/adhm.201901819
21. Wu S, Liu X, Ren J, Qu X. Glutathione Depletion in a Benign Manner by Mos2 -Based Nanoflowers for Enhanced Hypoxia-Irrelevant Free-Radical-Based Cancer Therapy. *Small* (2019) 15(51):e1904870.
22. Feng L, Liu B, Xie R, Wang D, Qian C, Zhou W, et al. An Ultrasmall $SnFe_2O_4$ Nanozyme With Endogenous Oxygen Generation and Glutathione Depletion for Synergistic Cancer Therapy. *Adv Funct Mater* (2020) 31(5):2006216. doi: 10.1002/adfm.202006216
23. Huang C, Wang FB, Liu L, Jiang W, Liu W, Ma W, et al. Hypoxic Tumor Radiosensitization Using Engineered Probiotics. *Adv Healthcare Mater* (2021) 10:e2002207. doi: 10.1002/adhm.202002207
24. Zhu D, Lyu M, Jiang W, Suo M, Huang Q, Li K. A Biomimetic Nanozyme/ Camptothecin Hybrid System for Synergistically Enhanced Radiotherapy, Journal of Materials Chemistry. *J Materials Chem B* (2020) 8:5312–9. doi: 10.1039/D0TB00676A
25. Zhu D, Zhang J, Luo G, Duo Y, Tang BZ. Bright Bacterium for Hypoxia-Tolerant Photodynamic Therapy Against Orthotopic Colon Tumors by an Interventional Method. *Adv Sci* (2021) 8(15):e2004769. doi: 10.1002/advs.202004769
26. Chen M, Tan Y, Dong Z, Lu J, Han X, Jin Q, et al. Injectable Anti-Inflammatory Nanofiber Hydrogel to Achieve Systemic Immunotherapy Post Local Administration. *Nano Lett* (2020) 20(9):6763–73. doi: 10.1021/acs.nanolett.0c02684
27. Chen D, Chen C, Huang C, Chen T, Liu Z. Injectable Hydrogel for NIR-II Photo-Thermal Tumor Therapy and Dihydroartemisinin-Mediated Chemodynamic Therapy. *Front Chem* (2020) 8:251. doi: 10.3389/fchem.2020.00251
28. Luo S, Wu J, Jia Z, Tang P, Sheng J, Xie C, et al. Bifunctional Hydrogel With Photothermal Effects for Tumor Therapy and Bone Regeneration. *Macromol Biosci* (2019) 19(9):e1900047. doi: 10.1002/mabi.201900047
29. Huang C, Chen B, Chen M, Jiang W, Liu W. Injectable Hydrogel for Cu(2+) Controlled Release and Potent Tumor Therapy. *Life (Basel)* (2021) 11(5):391. doi: 10.3390/life11050391
30. Zhu D, Zheng Z, Luo G, Suo M, Li X, Duo Y, et al. Single Injection and Multiple Treatments: An Injectable Nanozyme Hydrogel as Aiegen Reservoir and Release Controller for Efficient Tumor Therapy. *Nano Today* (2021) 37:101091. doi: 10.1016/j.nantod.2021.101091
31. Qiu M, Wang D, Liang W, Liu L, Zhang Y, Chen X, et al. Novel Concept of the Smart NIR-Light-Controlled Drug Release of Black Phosphorus Nanostructure for Cancer Therapy. *Proc Natl Acad Sci USA* (2018) 115 (3):501–6. doi: 10.1073/pnas.1714421115
32. Lyu M, Zhu D, Li Y, Quan H. Bimetallic Nanodots for Tri-Modal CT/MRI/PA Imaging and Hypoxia-Resistant Thermoradiotherapy in the NIR-II Biological Windows. *Biomaterials* (2019) 233:119656. doi: 10.1016/j.biomaterials. 2019.119656
33. Zhao LP, Zheng RR, Chen HQ, Liu LS, Zhao XY, Liu HH, et al. Self-Delivery Nanomedicine for O2-Economized Photodynamic Tumor Therapy. *Nano Lett* (2020) 20(3):2062–71. doi: 10.1021/acs.nanolett.0c00047
34. Yu X, Li A, Zhao C, Yang K, Chen X, Li W. Ultrasmall Semimetal Nanoparticles of Bismuth for Dual-Modal Computed Tomography/ Photoacoustic Imaging and Synergistic Thermoradiotherapy. *ACS Nano* (2017) 11(4):3990–4001. doi: 10.1021/acsnano.7b00476
35. Yuan Z, Qu S, He Y, Xu Y, Liang L, Zhou X, et al. Thermosensitive Drug-Loading System Based on Copper Sulfide Nanoparticles for Combined Photothermal Therapy and Chemotherapy *In Vivo*. *Biomaterials Sci* (2018) 6(12):3219–30. doi: 10.1039/C8BM00799C
36. Zhu D, Lyu M, Huang Q, Suo M, Liu Y, Jiang W, et al. Stellate Plasmonic Exosomes for Penetrative Targeting Tumor NIR-II Thermo-Radiotherapy. *ACS Appl Mat Interfaces* (2020) 12(33):36928–37. doi: 10.1021/acsami.0c09969
37. Yang J, Xie R, Feng L, Liu B, Lv R, Li C, et al. Hyperthermia and Controllable Free Radical Coenhanced Synergistic Therapy in Hypoxia Enabled by Near-Infrared-II Light Irradiation. *ACS Nano* (2019) 13(11):13144–60. doi: 10.1021/acsnano.9b05985
38. Chen Q, Chen J, Yang Z, Xu J, Xu L, Liang C, et al. Nanoparticle-Enhanced Radiotherapy to Trigger Robust Cancer Immunotherapy. *Advanced Materials* (2019) 31(10):e1802228. doi: 10.1002/adma.201802228
39. Gao S, Li T, Guo Y, Sun C, Xianyu B, Xu H. Selenium-Containing Nanoparticles Combine the NK Cells Mediated Immunotherapy With Radiotherapy and Chemotherapy. *Advanced Materials* (2020) 32(12): e1907568. doi: 10.1002/adma.201907568
40. Zhang C, Yan L, Wang X, Dong X, Zhou R, Gu Z, et al. Tumor Microenvironment-Responsive Cu2(OH)PO4 Nanocrystals for Selective and Controllable Radiosentization *via* the X-Ray-Triggered Fenton-Like Reaction. *Nano Lett* (2019) 19(3):1749–57. doi: 10.1021/acs.nanolett.8b04763
41. Huang C, Chen T, Zhu D, Huang Q. Enhanced Tumor Targeting and Radiotherapy by Quercetin Loaded Biomimetic Nanoparticles. *Front Chem* (2020) 8:225. doi: 10.3389/fchem.2020.00225

Conflict of Interest: The authors declare that the research was conducted in the absence of any commercial or financial relationships that could be construed as a potential conflict of interest.

Publisher's Note: All claims expressed in this article are solely those of the authors and do not necessarily represent those of their affiliated organizations, or those of the publisher, the editors and the reviewers. Any product that may be evaluated in this article, or claim that may be made by its manufacturer, is not guaranteed or endorsed by the publisher.

Copyright © 2021 Zeng, Liu, Wang, Wang and Huang. This is an open-access article distributed under the terms of the Creative Commons Attribution License (CC BY). The use, distribution or reproduction in other forums is permitted, provided the original author(s) and the copyright owner(s) are credited and that the original publication in this journal is cited, in accordance with accepted academic practice. No use, distribution or reproduction is permitted which does not comply with these terms.

frontiers in Oncology

ORIGINAL RESEARCH
published: 25 October 2021
doi: 10.3389/fonc.2021.777295

Achieving NIR Light-Mediated Tumor-Specific Fenton Reaction-Assisted Oncotherapy by Using Magnetic Nanoclusters

Shaoyou Qin[1], *Jinru Xue*[2], *Erna Jia*[1], *Na Ren*[2], *Yongqiang Dong*[3] *and Changyu Zhou*[1]*

[1] Department of Gastroenterology and Hepatology, China-Japan Union Hospital of Jilin University, Jilin University, Changchun, China, [2] Department of Thoracic Surgery, China-Japan Union Hospital of Jilin University, Jilin University, Changchun, China, [3] Department of Thyroid Surgery, First Affiliated Hospital of Zhengzhou University, Zhengzhou, China

As an emerging strategy for oncotherapy, Fenton chemistry can efficiently improve the conversion from endogenous H_2O_2 into highly toxic ·OH in the whole high-performance therapeutic process. Although promising, the efficiency of Fenton reaction in tumor regions is highly limited by the inefficient delivery of Fenton reagents and the restrictive conditions of tumor microenvironment. One promising strategy against the above limitations is to specifically increase the temperature around the tumor regions. In this study, a novel NIR light-mediated tumor-specific nanoplatform based on magnetic iron oxide nanoclusters (MNCs) was rationally designed and well developed for photothermally enhanced Fenton reaction-assisted oncotherapy. MNCs could accumulate into the tumor regions with the help of an external magnet field to enable T_2-weighted magnetic resonance (MR) imaging of tumors and MR imaging-guided combined antitumor therapy. Our well-prepared MNCs also revealed excellent photothermal effect upon a NIR light irradiation, promising their further important role as a photothermal therapy (PTT) agent. More importantly, heat induced by the PTT of MNCs could accelerate the release of Fe from MNCs and enhance the efficiency of Fenton reaction under H_2O_2-enriched acidic tumor microenvironment. Results based on long-term toxicity investigations demonstrated the overall safety of MNCs after intravenous injection. This work therefore introduced a novel nanoplatform based on MNCs that exerted a great antitumor effect *via* photothermally enhanced tumor-specific Fenton chemistry.

Keywords: magnetic nanomaterials, photothermal effect, Fenton chemistry, oncotherapy, long-term toxicity

OPEN ACCESS

Edited by:
Kelong Ai,
Central South University, China

Reviewed by:
Meng Li,
Hebei Medical University, China
Yan Yan Huang,
Nanjing Forestry University, China

****Correspondence:***
Changyu Zhou
cyzhou@jlu.edu.cn

Specialty section:
This article was submitted to Pharmacology of Anti-Cancer Drugs, a section of the journal Frontiers in Oncology

Received: *15 September 2021*
Accepted: *06 October 2021*
Published: *25 October 2021*

Citation:
Qin S, Xue J, Jia E, Ren N, Dong Y and Zhou C (2021) Achieving NIR Light-Mediated Tumor-Specific Fenton Reaction-Assisted Oncotherapy by Using Magnetic Nanoclusters. Front. Oncol. 11:777295. doi: 10.3389/fonc.2021.777295

INTRODUCTION

Reactive oxygen species (ROS) are a series of chemicals originated from complete or partial reduction of oxygen in living organisms. As the main by-products of oxygen metabolism, ROS including H_2O_2, $^1O_2$, ·OH, and $O_2^{\cdot-}$ play essential roles during the regulation process of various physiological functions, while overproduction of ROS can introduce serious cellular oxidative stress *via* DNA damage, protein denaturation, as well as lipid peroxidation (1–6). Accordingly, numerous

efforts have been devoted to using excessive harmful ROS to regulate the intracellular redox status for oncotherapy. Compared with classical approaches of surgery and chemotherapy, current novel ROS-mediated therapeutic strategies with the assistance of exogenous/endogenous light, ultrasound, radiation, and chemical species hold more advantages including non-invasiveness, high selectivity, and negligible side effects (7–13). Although promising, the clinical efficiency of the above strategies in solid tumors is severely restricted by the hypoxic tumor microenvironment and the intratumoral ROS generation efficiency. Thus, it is urgently needed to develop novel therapeutic strategies towards further oxygen-independent ROS-mediated oncotherapy.

Exploitation of the typical Fenton reaction and Fenton-like chemical reaction for oncotherapy has attracted increasing attention in recent years (14–16). Briefly, Fenton reaction containing ferrous ions/ferric ions (Fe^{2+}/Fe^{3+}) is able to efficiently catalyze the transformation of endogenous H_2O_2 into highly toxic ·OH in tumors. Compared with other ROS-mediated antitumor strategies, mild acidity and elevated levels of H_2O_2 of tumor microenvironment can significantly endow intratumoral Fenton chemistry with more advantages in therapeutic selectivity and specificity as compared to normal tissues (17–20). However, Fenton reaction alone cannot achieve a satisfactory clinical antitumor efficiency due to the endogenous lake of Fenton catalysts and relatively limited reaction conditions including excess reducing glutathione in tumors. As well known, the amount of Fenton catalysts in tumors is directly related to the generation efficacy of ·OH, and effective delivery of Fenton catalysts to the tumor regions accordingly has been considered as an important feature in a Fenton reaction-mediated oncotherapy (21–23). In addition, recent studies indicate that raising temperature of reaction system can highly increase efficiency of Fenton reaction in some research fields including the treatment of hazardous organic pollutants in water based on the classical thermodynamic molecular collision theory (24–26). Therefore, a strategy to deliver Fenton catalysts and simultaneously increase the temperature of tumor regions can achieve a localized and adaptive Fenton reaction with an enhanced antitumor therapeutic effect.

Thanks to the remarkable breakthroughs in the field of nanotechnology and materials science, a great deal of novel nanomaterials with unique physicochemical properties have been rationally designed and well prepared as next-generation therapeutic reagents for biomedical usages (27–31). As a series of important nanomaterials, magnetic iron oxide nanoparticles have been widely explored in versatile biomedical fields including magnetic resonance (MR) imaging, magnetic hyperthermia, photothermal therapy, chemodynamic therapy, nanozyme-based bioanalysis, magnetic field-assisted targeted drug delivery, and magnetic separation of biomolecules (32–42). Recent studies indicate that magnetic nanoparticles exhibit distinct toxicity under different physiological conditions (43–45). In detail, magnetic nanoparticles can decompose H_2O_2 into non-toxic O_2 and H_2O under neutral condition with catalase-like activity while they convert H_2O_2 into highly toxic ·OH under acidic condition and behave like Fenton nanocatalysts. Significantly, U. S. Food and Drug Administration-approved magnetic nanoparticles named ferumoxytol can inhibit the growth of early mammary cancers and prevent the hepatic metastasis *via* the increase of pro-inflammatory M1 macrophages in tumor regions, which is closely related to the generation of ROS *via* Fenton reaction. In that case, we envision that magnetic nanoparticles can achieve enhanced ROS-mediated oncotherapy with their intrinsic photothermal effect. More importantly, magnetic nanoparticles can efficiently target tumor regions with the assistance of external magnetic field. All these exciting lines of evidence encourage us to using magnetic nanoparticles as new-generation biocompatible antitumor reagents with new therapeutic mechanism and high therapeutic efficiency.

In this study, a novel NIR light-mediated tumor-specific nanoplatform based on magnetic iron oxide nanoclusters (MNCs) was rationally designed and well developed for photothermally enhanced Fenton reaction-assisted oncotherapy. MNCs with excellent magnetic response character could efficiently accumulate into the tumor regions under an external magnet field, favoring further T_2-weighted MR imaging of tumors and MR imaging-guided combined antitumor therapy. Upon a NIR light irradiation, these MNCs exhibited great photothermal effect, promising their important role as a photothermal therapy (PTT) agent. It is worth noting that heat induced by the PTT of MNCs could accelerate the release of Fe from MNCs and enhance the efficiency of Fenton reaction under H_2O_2-enriched acidic tumor microenvironment. Toxicity investigations after intravenous injection of MNCs indicated their overall safety. Taken together, a new magnetic nanoparticle-based therapeutic strategy against solid tumors was developed *via* photothermally enhanced tumor-specific Fenton chemistry, promising for further preclinical or clinical applications.

MATERIALS AND METHODS

Chemicals

$FeCl_3{\cdot}6H_2O$, urea, polyethylene glycol (PEG, M_w = 2000) and sodium citrate were purchased from Aladdin Reagent. Calcein AM and propidium iodide (PI) were achieved from Sigma-Aldrich. Dulbecco's modified Eagle's medium (DMEM) and fetal bovine serum (FBS) were obtained from Beyotime Biotechnology. All chemicals were of analytical grade and used directly without any purification. Water used in all experiments was obtained *via* a Milli-Q water system.

Synthesis of Magnetic Iron Oxide Nanoclusters

Magnetic iron oxide nanoclusters (MCNs) were synthesized *via* a facile one-pot hydrothermal method. Typically, $FeCl_3{\cdot}6H_2O$ (2 mmol), sodium citrate (4 mmol), urea (6 mmol), and PEG (2.0 g) were dissolved in distilled water (40 ml). After the above mixture was dissolved totally, the solution was transferred to a Teflon-

lined autoclave (50 ml) and maintained at 200°C for 12 h. After cooling down to room temperature, MCNs were collected by magnetic separation, washed with distilled water and absolute ethanol, and dried under vacuum overnight for further use.

Photothermal Effect of MNCs

MNCs dispersed in 0.9% NaCl solution with different concentrations were irradiated under an 808-nm laser with a power intensity of 2 W/cm^2. Solution temperatures were recoded every 30 s by using an infrared thermal camera (FLIR I3). Relative photothermal photos of MNCs after near-infrared irradiation with a period of 5 min were collected at the same time.

Time-Dependent Fe Release

MNCs were added into various PBS (10 mM, 10 ml) with different pH values under 37°C. Final concentration of MNCs was defined as 1 mg/ml. At each given time interval, solution was collected after magnetic separation of residual MNCs, and the release amount of Fe in each group was quantitatively analyzed *via* ICP-MS. Three independent repeated experiments were done in the abovementioned groups.

Catalytic Effect of MNCs

A colorimetric method based on the oxidation of TMB was used to explore the Fenton reaction performance of MNCs. Briefly, absorbance changes at 652 nm of TMB at pH 7.4 or 6.5 with or without H_2O_2 were measured in the presence or absence of MNCs at 37°C. In order to simulate the heat from the photothermal effect of MNCs, reaction temperature was maintained at 50°C and the temperature effect on the Fenton reaction of MNCs was investigated. Concentrations of MNCs, TMB, and H_2O_2 in the above experiments were 50 μg/ml, 1 mM, and 20 mM, respectively. Co-incubation period of above reaction system was defined as 5 min.

Cell Culture

4T1 mouse breast tumor cell line (4T1 cells) was obtained from the Type Culture Collection Committee of the Chinese Academy of Sciences (Shanghai, China) and was cultured in DMEM containing 10% FBS in an incubator (37°C, 5% CO_2).

Cytotoxicity of MNCs

4T1 cells were seeded into a 96-well plate to allow the cellular attachment at first (n = 4). Twelve hours later, medium was replaced by medium containing MNCs. After further co-incubation for 24 h, cell viabilities were evaluated by using MTT assay. Moreover, similar experiments were carried out and above cellular suspension was collected for LDH leakage analysis (n = 4). For cellular live-dead staining analysis of MNCs, 4T1 cells were seeded into a six-well plate to allow the cellular attachment. Twelve hours later, medium was replaced by medium containing MNCs. After co-incubation for 12 h, medium containing MNCs was removed, live-dead staining was performed, and stained cells were observed under an Olympus BX-51 imaging system.

Animals

Balb/c mice weighing about 25 g were purchased from Charles River (Beijing, China). The protocol of all the animal studies was approved by the Institutional Animal Care and Use Committee at Jilin University.

Assays of Hemolysis and Coagulation

Fresh mouse blood samples stabilized by EDTA were obtained from Balb/c mice. After centrifugation at 1,000 rpm, red blood cells were diluted to a quarter of their volumes with 0.9% NaCl solution. Diluted red blood cells (0.2 ml) were mixed with 0.9% NaCl solution (0.8 ml) as negative group, distilled water (0.8 ml) as positive group, and 0.9% NaCl solution containing a series of concentrations of MNCs (0.8 ml) as experimental groups. The above samples were further vortexed and maintained for another 2 h. Then, the absorbance of supernatants at 541 nm was determined *via* a UV-vis spectroscopy (n = 4). For coagulation assays, plasma from volunteers was mixed with 0.9% NaCl solution containing MNCs at first. Then, a fully automatic blood coagulation analyzer was used to read out the values of activated partial thromboplastin time (APTT) and prothrombin time (PT) in the presence of MNCs with different co-incubation concentrations (n = 4).

Light-Induced Cytotoxicity of MNCs

4T1 cells were seeded into a 96-well plate and cultured overnight (n = 4). Then, medium was replaced by medium containing MNCs. Six hours later, cells were irradiated with an 808-nm laser with different power intensities for 5 min. After another 6 h incubation, cell viabilities were evaluated by using the MTT assay.

Fenton Reaction-Mediated Cytotoxicity of MNCs

4T1 cells were seeded into a 96-well plate and cultured overnight (n = 4). Then, medium was replaced by medium containing a series of concentrations of MNCs and H_2O_2 (100 μM) at pH 7.4 or 6.5. After 12 h co-incubation, cell viabilities were evaluated by using MTT assay.

Combined Antitumor Effect of MNCs *In Vitro*

4T1 cells were seeded into a 96-well plate and cultured overnight (n = 4). Cells were divided into eight groups, namely, control, NIR, H_2O_2, H_2O_2+NIR, MNCs, MNCs+H_2O_2, MNCs+NIR, and MNCs+H_2O_2+NIR. MNCs with a concentration of 100 μg/ml, H_2O_2 with a concentration of 100 μM, pH value of 6.5, an 808-nm laser with a power intensity of 2 W/cm^2, and an irradiation period of 5 min were used throughout our current experimental design. Twelve hours after the above various treatments, cell viabilities of various groups were evaluated by using the MTT assay.

Live/Dead Staining

4T1 cells were seeded into a six-well plate and cultured overnight. Then, medium was replaced by fresh medium with

different components. Detailed treatments were similar to those of combined antitumor effect of MNCs *in vitro*. Acidified medium was used throughout all groups except the control group. After the above treatments, cells were stained with calcein AM and PI, and fluorescence microscopy images were collected on an Olympus BX-51 imaging system. In addition, trypan blue solution (0.4%) was used to distinguish live/dead cells under an optical microscope.

Cellular ROS Detection

4T1 cells were seeded into a six-well plate and cultured overnight. Then, medium was replaced by fresh medium with different components. Detailed treatments were similar to those of combined antitumor effect of MNCs *in vitro*. Acidified medium was used throughout all groups except the control group. After the above treatments, cells were washed with cool 0.9% NaCl solution. After the co-incubation with DCFH-DA for another 20 min, cells were observed under an Olympus BX-51 imaging system.

Preparation of 4T1 Tumor-Bearing Mice

4T1 tumor xenografts were implanted into the axillaries of Balb/c mice by subcutaneous injection of 10^6 4T1 cells. When tumor volumes reached about 100 mm^3, MR imaging, thermal imaging, and antitumor effect of MNCs were explored in detail.

MR Imaging

MR imaging was carried out on a 1.5-T clinical MR imaging instrument (Siemens Medical System). A series of concentrations of MNCs fixed in low concentration of agarose gel were mixed with water at first and prepared for the following *in vitro* T_2-weighted MR imaging. For *in vivo* T_2-weighted MR imaging, 0.9% NaCl solution containing MNCs (1 mg/ml, 1 ml) was intravenously injected into tumor-bearing mice under the assistance of magnet. Mice were imaged before intravenous administration and 5 min after injection of MNCs under the above MR imaging system.

Thermal Imaging

Firstly, 0.9% NaCl solution containing MNCs (1 mg/ml, 1 ml) was intravenously injected into tumor-bearing mice under the assistance of magnet. Secondly, tumors were irradiated by an 808-nm laser with a power density of 2 W/cm^2 for 5 min to obtain thermal imaging. During the irradiation, the spot size of laser beam was well adjusted to cover the whole region of tumors. Tumor-bearing mice without intravenous administration of MNCs was selected as the control group to highlight the photothermal effect of MNCs *in vivo*. Both groups were imaged by using an infrared thermal camera. Meanwhile, temperature changes around tumors were recorded.

Antitumor Effect *In Vivo*

When tumor volumes reached about 100 mm^3, mice were randomly divided into four groups including control, MNCs, NIR, and MNCs+NIR (n = 4). 0.9% NaCl solution containing MNCs (1 mg/ml, 1 ml) was intravenously injected under the assistance of magnet in the groups of MNCs and MNCs+NIR. 1 h after the injection of MNCs, tumors were irradiated with an 808-nm laser (2 W/cm^2, 5 min) in the group of MNCs+NIR. To achieve a great antitumor effect, the above irradiation was conducted every other day for three treatments. Similar irradiation treatment was also carried out in the group of NIR. Tumor sizes of the above four groups were measured every day during the whole experimental period. Tumor volumes were calculated *via* the following formula: volume = (tumor length) × (tumor width)^2/2. Two weeks after the first irradiation treatment, mice were sacrificed, tumors were excised and weighed, and tumor sections were examined after hematoxylin and eosin (H&E) staining.

Biosafety of MNCs

For biosafety evaluation of MNCs, mice with similar body weight were randomly divided into two groups, which were defined as control and test (n = 4). Mice in the test group were intravenously injected of high dosages of MNCs (5 mg pre mouse weighted about 25 g). Mice in the control group were administered of 0.9% NaCl solution with the same volume. Body weight measurements of the above mice were recorded for a month. Then, blood of mice in the above groups was collected for further assays of blood biochemical and inflammatory cytokines. Last but not least, mice in the above two groups were sacrificed, and main organs including heart, liver, spleen, lung, and kidney were harvested for further H&E staining.

Statistical Analysis

All data were expressed as mean ± standard deviation and carried out at least three times. A p-value < 0.05 was considered as statistical significances. Statistical analysis was performed *via* one-way analysis of variance together with a *post hoc* LSD test.

RESULTS AND DISCUSSION

Figure 1A schematically illustrated our rational strategy of NIR light-mediated tumor-specific Fenton reaction-assisted oncotherapy and relative proposed antitumor mechanism of magnetic iron oxide nanoclusters (MNCs). With the help of external magnetic field, MNCs could efficiently target and accumulate into 4T1 tumor sites after intravenous injection. Upon multiple NIR irradiation, MNCs could elevate the temperature of tumor sites, resulting in an effective PTT against solid tumors. During the whole process of PTT, the heat could accelerate the release of Fe from MNCs with the assistance of acid tumor microenvironment, improved the conversion of endogenous H_2O_2 into ·OH, and achieved a PTT-enhanced catalytic cancer therapy. Typically, MNCs were well synthesized *via* a facile one-pot hydrothermal method according to previous studies with some modification (40). Images achieved by scanning electron microscopy (SEM) and transmission electron microscopy (TEM) demonstrated the uniform and non-aggregated characteristic of MNCs, which held an average diameter of 140 nm (**Figures 1B, C**). Wide-angle x-ray diffraction (XRD) pattern of MNCs showed a pure-phase cubic structure, promising their well-defined magnetite phase (**Figure 1D**). High-resolution TEM image revealed that

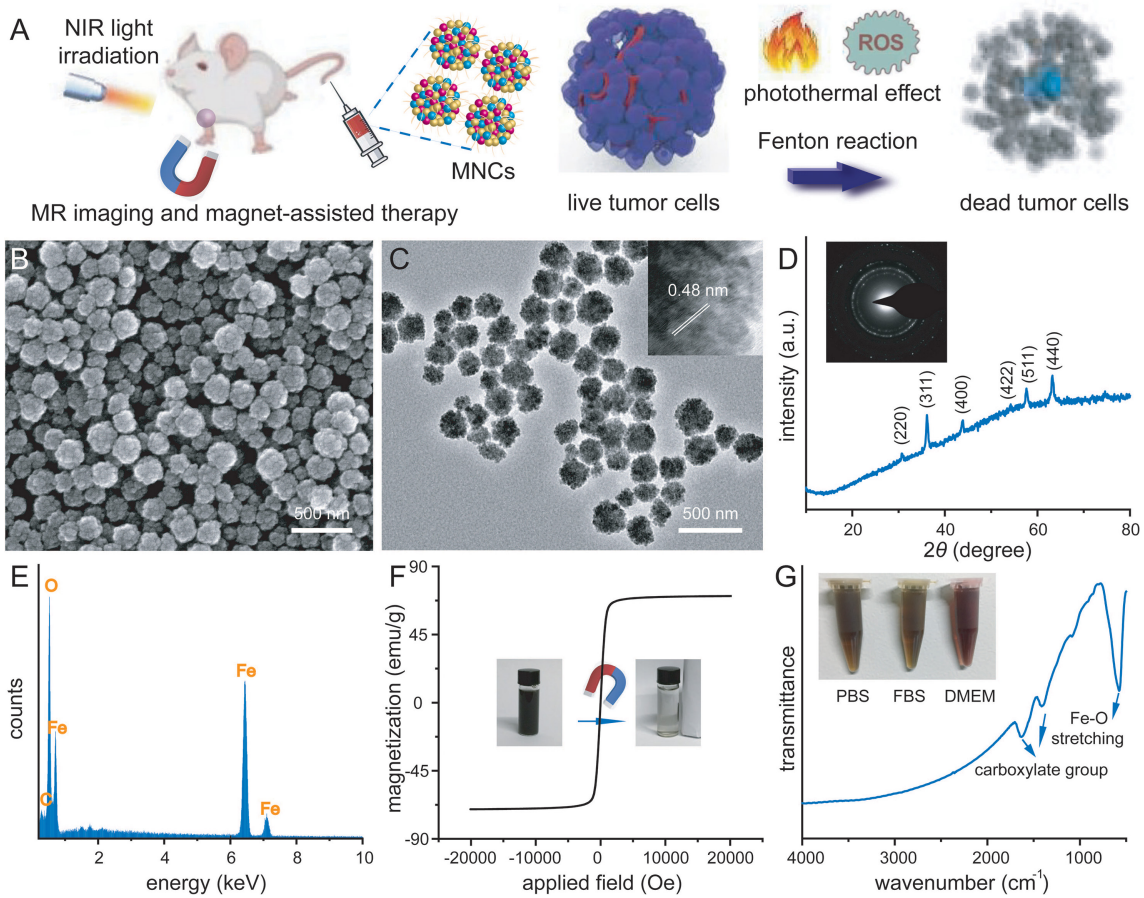


FIGURE 1 | Schematic illustration of tumor-targeting therapy *via* a PTT-enhanced Fenton reaction and relative antitumor mechanism **(A)**. SEM image **(B)**, TEM image **(C)**, wide-angle XRD pattern **(D)**, EDS analysis **(E)**, room temperature magnetic hysteresis loop **(F)**, and FT-IR spectrum **(G)** of well-prepared magnetic nanoclusters (MNCs). Inset of **(C)**: HR-TEM image of MNCs. Inset of D: SEAD image of MNCs. Inset of **(F)**: photo of magnetic separation process. Inset of **(G)**: photos of MNCs dispersed in different physiological solutions.

MNCs were composed of many smaller particles (inset of **Figure 1C**). Interlayer distance could be calculated as 0.48 nm, which matched well with the separation between (111) lattice planes. A selective area electronic diffraction (SAED) pattern exhibited polycrystalline-like diffraction rings and further supported the polycrystalline nature of MNCs (inset of **Figure 1D**). Energy-dispersive spectroscopy (EDS) analysis confirmed that MNCs were composed of Fe, O, and C elements (**Figure 1E**). The absence of a hysteresis loop based on field-dependent magnetization measurement demonstrated the superparamagnetic nature of MNCs with a relatively high saturation magnetization value of 70.43 emu/g at room temperature (**Figure 1F**). In addition, the photo inset of **Figure 1F** revealed a direct magnetic response of MNCs in water towards magnet. C-H vibrating and carboxylate vibrating in FT-IR spectra indicated the presence of PEG molecule and citrate capped on MNCs, which endowed their great dispersion in various physiological solution including PBS, FBS, and DMEM (**Figure 1G**). Moreover, the addition of PEG molecules and citrate in the typical synthesis implied the presence of negative charge density on the surface of MNCs according to their negative *Z*-potential value. The above results thus promised that our MNCs prepared in aqueous solution instead of organic solvents exhibited more advantages in further biomedical applications.

UV-vis-NIR spectra demonstrated that MNCs in water exhibited a broad absorption in the NIR region, which inspired us to explore their photothermal performance (**Figure 2A**). To assess the photothermal properties of MNCs, temperature changes of dispersion containing MNCs with different concentrations were recorded under continuous NIR irradiation (35, 36). As shown in **Figure 2B**, obvious concentration- and irradiation period-dependent temperature increases could be clearly detected, which were then visually confirmed *via* relative NIR thermal imaging photos (**Figure 2C**). In detail, the temperature of a dispersion containing MNCs with a concentration of 100 μg/ml increased by 34.1°C within 5 min of NIR irradiation while the temperature of water increased only 2.5°C. All these results suggested that MNCs could efficiently convert NIR irradiation energy into heat energy. As another vital feature of NIR light-mediated Fenton antitumor therapy, we further explored the

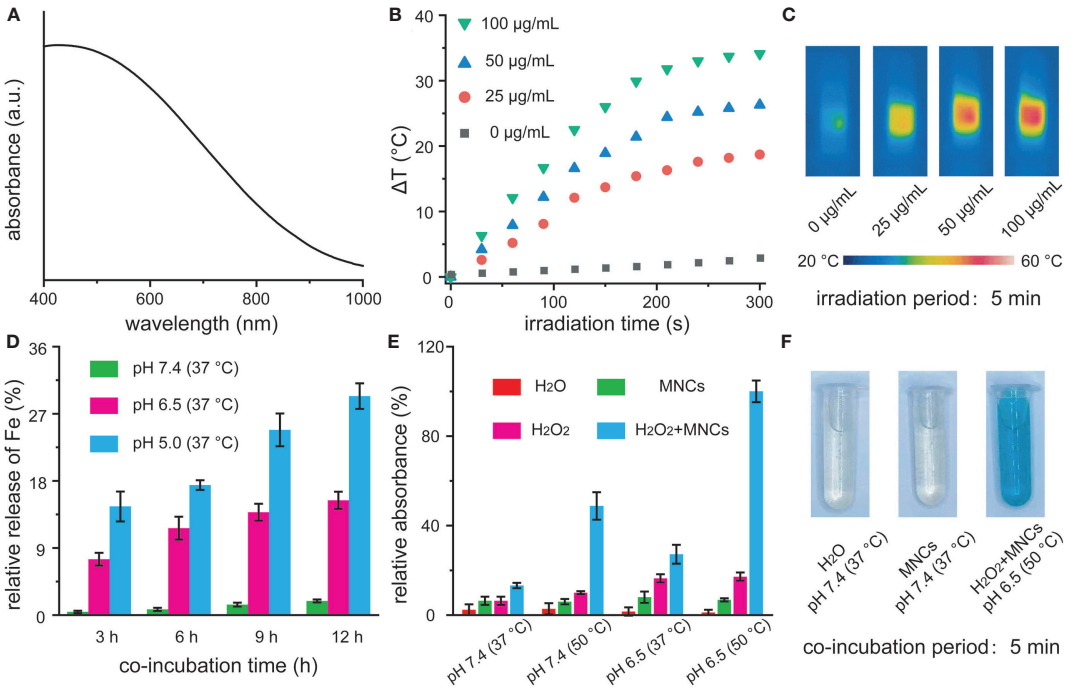


FIGURE 2 | UV-vis-NIR absorption spectra of MNCs in water **(A)**. Temperature change **(B)** and relative near-infrared photos **(C)** of MNCs under an 808-nm laser irradiation with a power intensity of 2 W/cm^2. Time-dependent Fe release percentages from MNCs with a concentration of 1 mg/ml at different pH values **(D)**. Relative absorbance of TMB at 652 nm **(E)** and corresponding photos **(F)** after various treatments. The concentrations of MNCs, TMB, and H_2O_2 used in **(E, F)** were 50 μg/ml, 1 mM, and 20 mM, respectively.

release performance of Fe from MNCs under different stimulation conditions. In general, tumor microenvironment was featured with regional hypoxia, low pH, and nutritional deprivation. Moreover, lysosome produced by the rupture of Golgi apparatus usually contained many acid enzymes, and the pH value of lysosome was about 5.0. Therefore, pH 6.5 and pH 5.0 were used to simulate the acid conditions of tumor microenvironment and lysosome, respectively. As shown in **Figure 2D**, a clear time- and pH-dependent Fe release behavior could be found in MNCs with different conditions. After 12 h of co-incubation, 28% Fe release could be detected at pH 5.0 and 17% Fe release occurred at pH 6.5 while less than 3% Fe release was found at pH 7.4. These results thus promised that MNC-based Fenton antitumor therapy could efficiently work in tumor sites instead of other normal tissues or organs. In order to simulate the heat from photothermal effect of MNCs, we further explored reaction temperature effect on the Fenton reaction of MNCs. Based on our experimental design, TMB was used to study the catalytic performance of MNCs by monitoring the generation of ·OH. As shown in **Figure 2E**, upon the addition of MNCs, solution containing TMB and H_2O_2 held a temperature- or pH value-dependent manner. Significantly, high temperature or low pH value could lead to obvious absorbance increase at 652 nm. More importantly, maximum absorbance reached only when the experimental condition was defined as low pH value of 6.5 and high temperature of 50°C. Generally, only when the localized photothermal temperature was over 43°C could cellular apoptosis and necrosis be well achieved. Meanwhile, low temperature-induced photothermal effect could be easily resisted by the intracellular regulation, such as heat shock protein-assisted physiological process. Similar to a very recent study, 50°C was therefore selected and used as the typical experimental temperature in our study (24). According to the above findings, heat and low pH value could extremely improve the efficiency of Fenton reaction catalyzed by MNCs, which were also confirmed by the photos of oxTMB colorimetry experiments (**Figure 2F**).

Prior to the use of MNCs for further biomedical usages, their cytotoxicity and blood compatibility were well explored at first. According to the results of MTT assay and live/dead staining shown in **Figures 3A, B**, all the viabilities of 4T1 cells were not hindered after the co-incubation with different concentrations of MNCs, and cellular morphology was not affected by MNCs with the same experimental concentrations, which indicated that MNCs possessed negligible cytotoxicity. Moreover, the results based on lactose dehydrogenase (LDH) leakage revealed that nearly no LDH could be detected even under the maximum co-incubation concentration, promising the integrity of cell membrane in the presence of MNCs (**Figure 3C**). As an essential method towards the exploration of interaction between any newly developed nanomaterial and blood components, hemolytic assay in the presence of MNCs was further investigated. Based on both qualitative and quantitative results shown in **Figures 3D, E** and **Table S1**, MNCs were not even able to cause slight injury of red blood cells, and all the hemolysis percentages were lower than 2%. In addition, activated partial

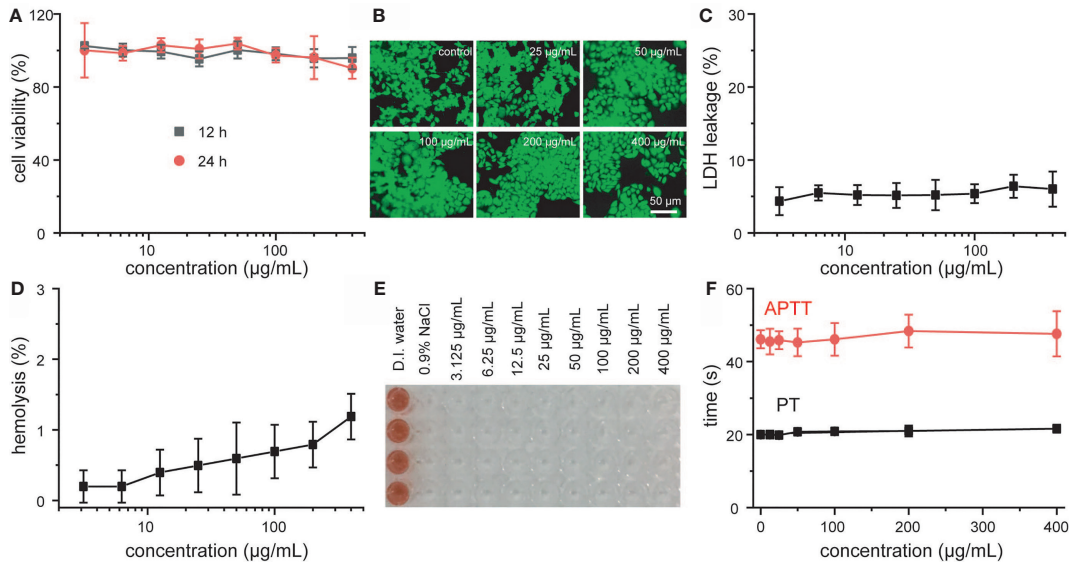


FIGURE 3 | Viability **(A)**, live-dead staining images **(B)**, and LDH leakage **(C)** of 4T1 cells treated with MNCs. Hemolysis assay **(D)**, photo of hemolysis **(E)**, and blood coagulation assay **(F)** after co-incubation with MNCs.

thromboplastin time (APTT) and prothrombin time (PT) were used to explore the blood coagulation of MNCs. As expected, no obvious differences in APTT and PT could be found between the samples treated with a series of concentrations of MNCs and the reference one, thus demonstrating the negligible effect of MNCs on blood coagulation time (**Figure 3F**). All of these exciting results indicated the negligible cytotoxicity and high blood compatibility of MNCs.

Encouraged by the excellent properties of MNCs so far, we further investigated their antitumor effect *in vitro*. Cytotoxicity of 4T1 cells against H_2O_2 under different pH values was explored at first in order to confirm the experimental concentration of H_2O_2 in cell culture. As shown in **Figure 4A**, 100 μM was considered as a reasonable concentration of H_2O_2 for further cell culture because 200 μM or 400 μM of H_2O_2 could induce more or less death of 4T1 cells upon different co-incubation pH values including pH 7.4 and pH 6.5 (23–25). Moreover, no apparent cytotoxicity could be detected even at a high concentration of MNCs up to 100 μg/ml, both at pH 7.4 and pH 6.5, further demonstrating their high biocompatibility (**Figure 4B**). With the assistance of an 808-nm laser irradiation, viabilities of 4T1 cells significantly decreased along with the increasing of the concentrations of MNCs or laser intensities (**Figure 4C**). For instance, fewer than 40% of 4T1 cells survived when treated with MNCs at 100 μg/ml and a 2 W/cm^2 laser irradiation, indicating the excellent PTT effect of MNCs *in vitro*. We then evaluated the Fenton reaction-mediated antitumor effects of MNCs. As shown in **Figure 4D**, MNCs exhibited a slight cytotoxicity when incubated at pH 7.4 with H_2O_2, while an obvious concentration-dependent antitumor effect was found at pH 6.5 with H_2O_2. In detail, viability of 4T1 cells decreased to their 40% in the presence of 100 μg/ml of MNCs at pH 6.5 with 100 μM of H_2O_2. In the following experiments, we further explored the NIR laser-assisted combined antitumor effect of MNCs in the presence of H_2O_2 at relatively low pH value, which was used to simulate tumor microenvironment. Detailed experimental information was illustrated in **Figure 4E**. No more than 60% of 4T1 cells were killed in the groups of MNCs+H_2O_2 and MNCs +NIR; however, more than three-quarters of 4T1 cells were killed in the group of MNCs+H_2O_2+NIR, which exhibited a clearly enhanced antitumor effect than PTT alone or Fenton reaction alone. Live-dead staining images and trypan blue staining images further demonstrated the combined antitumor effects of MNCs *via* both PTT and Fenton reaction (**Figures 4F, G**). No dead cells could be detected in the groups of control, NIR, H_2O_2, NIR +H_2O_2, and MNCs. However, nearly all the 4T1 cells were damaged or killed in the group of MNCs+H_2O_2+NIR. The generation of ROS in 4T1 cells by Fenton reaction was then detected with the help of DCFH-DA. As shown in **Figure 4H**, green fluorescence could be easily found in the groups with the addition of H_2O_2. Compared with that of the group of H_2O_2 or the group of NIR+H_2O_2, much stronger fluorescence could be detected in the group of MNCs+H_2O_2+NIR, which could be ascribed to the effect of photothermally enhanced Fenton reaction. All these exciting results thus demonstrated the excellent combined antitumor effects of MNCs under simulated tumor microenvironment.

Figure 5A schematically illustrated the detailed timeline for NIR light-mediated tumor-specific Fenton reaction-assisted oncotherapy. When tumor volumes grew to 100 mm^3, 0.9% NaCl solution containing MNCs was intravenously injected with the assistance of an external magnetic field around the tumors.

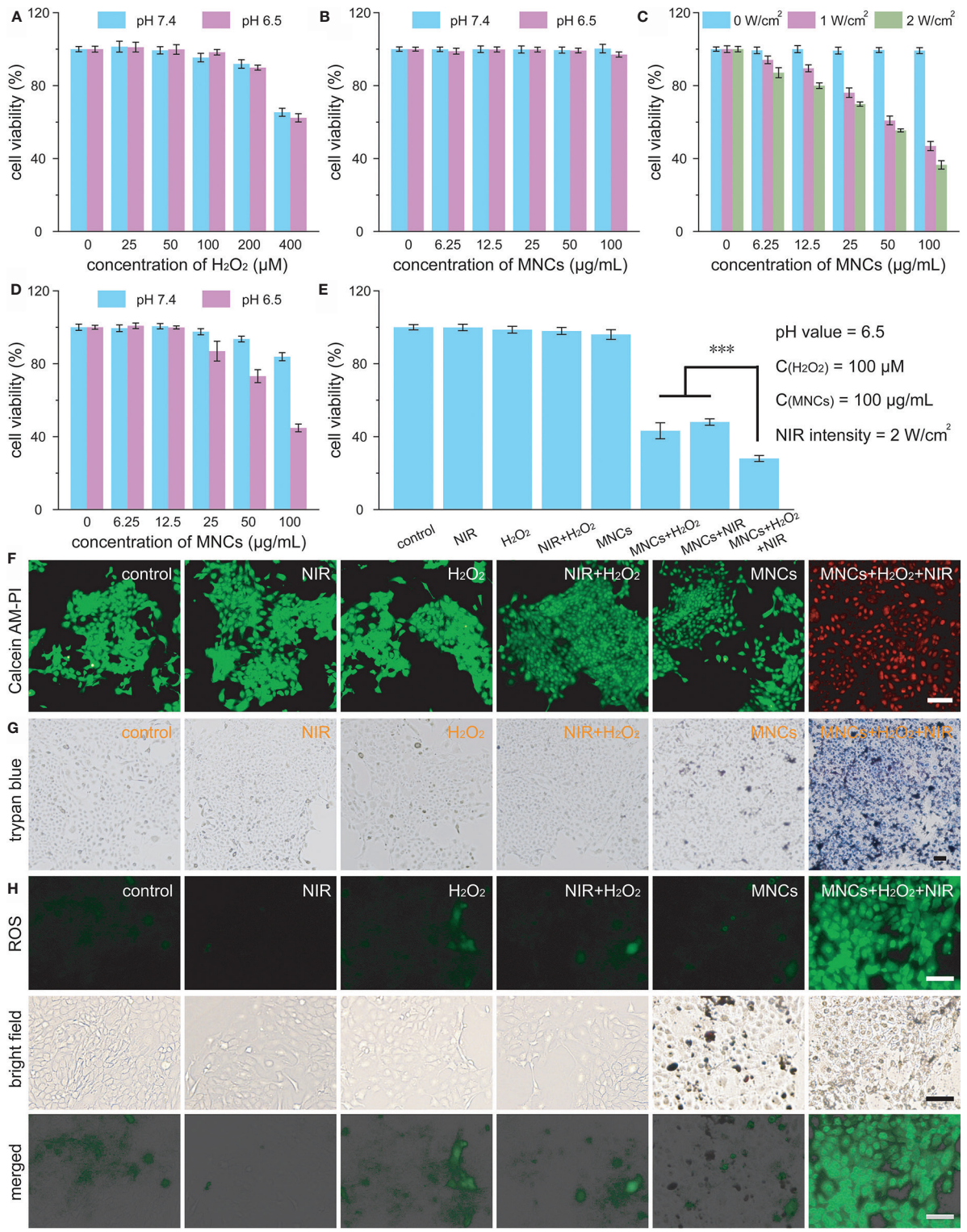


FIGURE 4 | Viabilities of 4T1 cells treated with H_2O_2 **(A)** and MNCs **(B)** under different pH values. Cellular viabilities under laser irradiation in the presence of MNCs **(C)**. Cellular viabilities under different pH values in the presence H_2O_2 and MNCs **(D)**. The concentration of H_2O_2 in D was 100 μM. Combined *in vitro* antitumor effect of MNCs with laser irradiation and H_2O_2 under acidic pH value **(E)**. Inset of E: detailed experimental conditions. Live-dead staining images **(F)**, trypan blue staining images **(G)**, and ROS staining images **(H)** of 4T1 cells after various treatments. Scale bars are equal to 100 μm. Asterisks indicated statistical significances (*$p < 0.05$, **$p < 0.01$, ***$p < 0.001$).

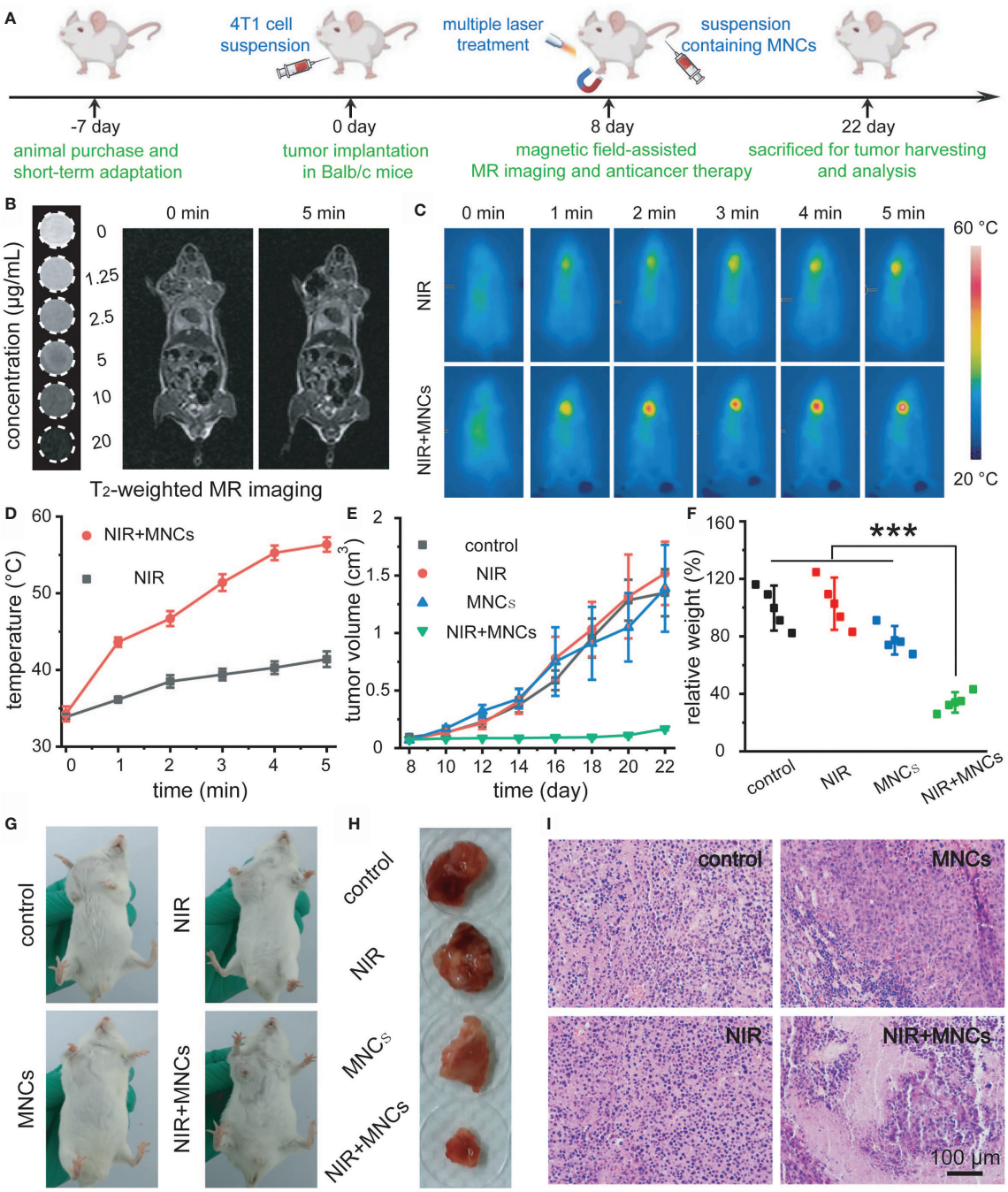


FIGURE 5 | Schematic illustration of the timeline for NIR light-mediated tumor-specific Fenton reaction-assisted oncotherapy **(A)**. T_2-weighted MR image of MNCs in aqueous solution and *in vivo* magnet-assisted MR imaging before and 5 min after intravenous administration of MNCs **(B)**. Thermal images of tumor-bearing mice **(C)** and relative temperature profiles of tumor sites in mice **(D)** under different treatments. Tumor growth curves **(E)** and relative tumor weights at the end of the whole therapy period **(F)** for the indicated treatments. Photos of tumors in mice **(G)** and relative tumor tissues collected from mice **(H)** at the end of the whole therapy period upon different treatments. H&E staining of tumor tissues after various treatments **(I)**. Asterisks indicated statistical significances (*$p < 0.05$, **$p < 0.01$, ***$p < 0.001$).

Then, an 808-nm laser with a power density of 2 W/cm^2 was used to perform irradiation for the following tumor thermal imaging and tumor ablation experiment. Moreover, magnetic field-assisted MR imaging was carried out at the same time owing to the excellent magnetic property of MNCs. As shown in **Figure 5B**, all the tubes containing MNCs appeared darker and darker according to T_2-weighted MR images along with the increasing of concentrations of MNCs while the tube without the

addition of MNCs remained bright. *In vivo* T_2-weighted images before and after administration of MNCs demonstrated that our well-designed MNCs could efficiently accumulate into tumor upon the help of magnetic field even within a very short response period of 5 min. In detail, a significant darkening effect in the tumor region of 4T1 tumor-bearing mouse could be easily detected as compared with the image recorded before administration of MNCs. These results thus indicated the feasibility of MNCs as MR imaging-guided antitumor theranostic reagents. NIR light-induced temperature changes *in vivo* by MNCs were then explored with the assistance of a thermal imaging camera. As shown in **Figures 5C, D**, the temperature of tumor region administered with MNCs could easily increase from mouse body temperature to about 55°C during the whole NIR light irradiation, while other regions, which were not exposed to the NIR light, exhibited no temperature changes. Additionally, a no more than 5°C increase occurred around the tumor region without the injection of MNCs. Before the evaluation of antitumor effects of MNCs *in vivo*, 4T1 tumor-bearing mice were randomly divided into four groups at first, which were then defined as control, MNCs, NIR, and MNCs+NIR. During the whole treatment period of 2 weeks, tumor volumes were monitored to assess the therapeutic effects of above groups. As shown in **Figure 5E**, groups of control, NIR, and MNCs exhibited relatively rapid tumor growth while nearly total tumor suppression could be easily found in the group of MNCs+NIR. At the end of the whole antitumor treatment period, mice were sacrificed, and tumors were excised and weighted. As shown in **Figures 5F–H**, average tumor weights in the above four groups were consistent with our tumor volume measurements. However, tumor weights in the group of MNCs revealed somewhat lighter than those in the groups of control and NIR because of the appearance of partial tumor cavity after tumor ablation, indicating the effects of Fenton reaction-mediated antitumor therapy. Significantly, photothermal effect of MNCs could extremely enhance the effect of Fenton reaction based on our current study. **Figure 5I** provided the H&E staining of tumor sections collected from the mice at the end of antitumor treatment. As expected, no obvious tumor cell damage was found in the groups of control and NIR. However, most tumor cells in the group of MNCs+NIR were killed while some cell damage was detected in tumors from mice treated with MNCs, which re-confirmed the superior antitumor

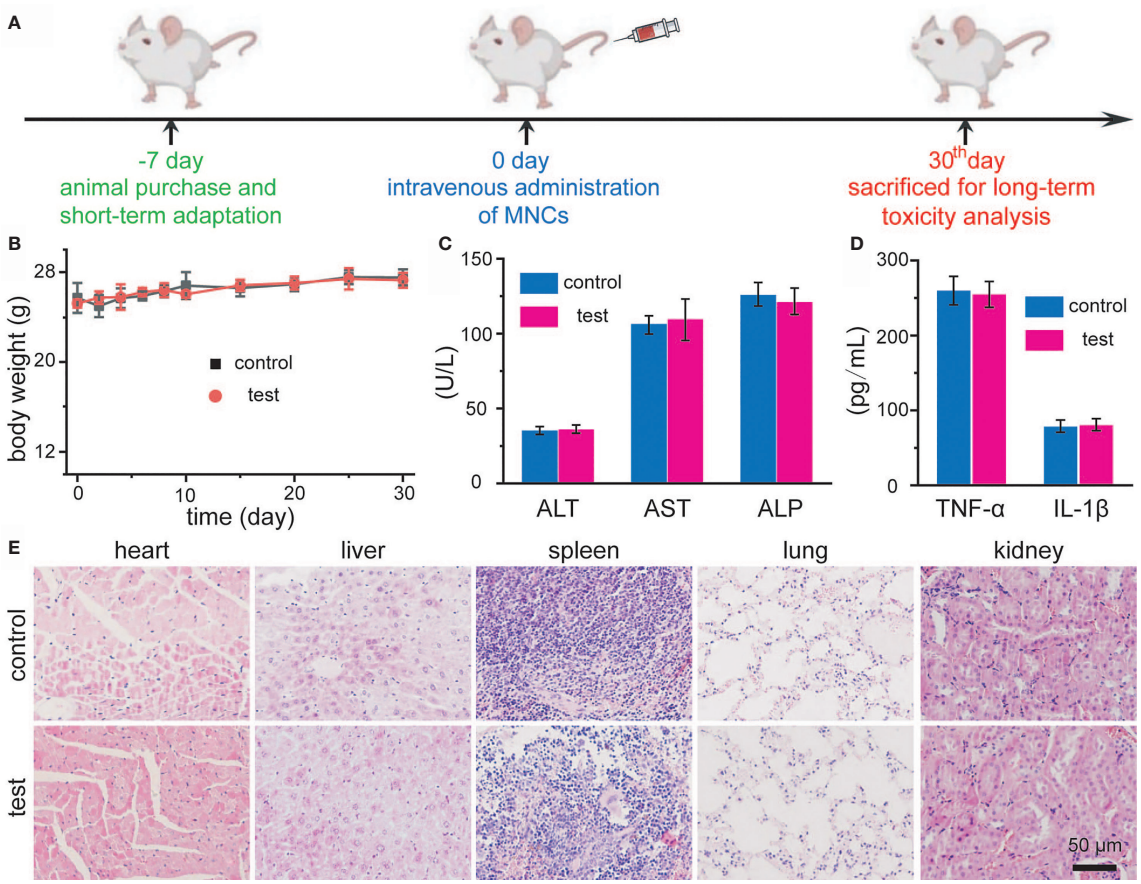


FIGURE 6 | Schematic illustration of *in vivo* toxicity evaluation of MNCs **(A)**. Body-weight changes of Balb/c mice after intravenous injection of MNCs **(B)**. Serum levels of ALT, AST, and ALP in mice **(C)**. Serum levels of TNF-α and IL-β in mice **(D)**. H&E staining images of mouse main exposed organs after different treatments **(E)**.

effect of MNCs based on the rationally combined PTT and Fenton reaction.

To determine whether MNCs could induce any harmful effect after systemic administration, we then explored the long-term toxicity of MNCs. The timeline of our experimental design is illustrated in **Figure 6A**. Firstly, mice adapt to diet about 1 week before the initiation of experimentation. Secondly, MNCs with a relative high dosage dispersed in 0.9% NaCl solution were intravenously injected. As shown in **Figure 6B**, no differences in body weight could be detected between the control group and the test group during the whole experimental period of a month. In addition, mice in both groups did not exhibit any behavior abnormality. A month after the intravenous injection of MNCs, assays of blood biochemicals and inflammatory cytokines were used to provide more quantitative toxicity evaluation of these MNCs. Results shown in **Figure 6C** demonstrated that MNCs did not alter the hepatic function indexes, such as alanine aminotransferase (ALT), alkaline phosphatasein (ALP), and aspartate aminotransferase (AST). Serum levels of inflammatory cytokines including TNF-α and IL-β in mice exhibited negligible differences at the same time (**Figure 6D**). H&E histology analysis of main exposed organs a month after the injection of MNCs was used to indicate the potential signs of inflammation and injuries. Compared with those of the control group, no obvious inflammation and injuries were observed in the test group (**Figure 6E**). All these results thus supported the extremely low systemic toxicity of MNCs and the high feasibility of our current therapeutic strategy.

CONCLUSION

In summary, a novel NIR light-mediated tumor-specific nanoplatform based on efficient MNCs has been well developed for photothermally enhanced Fenton reaction-assisted oncotherapy. These MNCs were synthesized *via* a green hydrothermal method without any organic solvent. By virtue of their superparamagnetic nature, these MNCs can act as a T_2-weighted MR imaging-guided antitumor theranostic reagent. Meanwhile, relatively high saturation magnetization value endows these MNCs with the capacity for tumor targeting with the help of an external magnet field. Because of their high photothermal effect, MNCs can serve as an efficient PTT agent for antitumor therapy. Significantly, heat produced by the PTT effect can extremely accelerate the release of Fe from MNCs and achieve an enhanced Fenton reaction under H_2O_2-enriched acidic tumor microenvironment for oncotherapy. Both *in vitro* and *in vivo* results confirm the superior antitumor effect of MNCs based on combined PTT and Fenton reaction, promising the high feasibility of our current therapeutic strategy. Last but not least, long-term toxicity exploration of MNCs after intravenous administration suggests their low systemic toxicity and high biocompatibility. Accordingly, our present approach not only develops a new concept of photothermally enhanced Fenton chemistry based on magnetic nanomaterials, but also provides a meaningful insight for further nanoplatform-assisted combined tumor therapy.

DATA AVAILABILITY STATEMENT

The original contributions presented in the study are included in the article/**Supplementary Material**. Further inquiries can be directed to the corresponding author.

ETHICS STATEMENT

The animal study was reviewed and approved by the Institutional Animal Care and Use Committee at Jilin University.

AUTHOR CONTRIBUTIONS

SQ and JX contributed equally to this work. SQ, JX, and CZ conceived and designed the experiments and wrote the manuscript. SQ, JX, EJ, NR, and YD performed the experiments. All authors contributed to the article and approved the submitted version.

FUNDING

Financial support was provided by the Jilin Provincial Health Special Project (2018SCZ015) and the National Natural Science Foundation of China (81900521).

SUPPLEMENTARY MATERIAL

The Supplementary Material for this article can be found online at: https://www.frontiersin.org/articles/10.3389/fonc.2021.777295/full#supplementary-material

REFERENCES

1. Yang B, Chen Y, Shi J, Bowen R. Reactive Oxygen Species (Ros)-Based Nanomedicine. *Chem Rev* (2019) 119:4881–985. doi: 10.1021/acs.chemrev.8b00626
2. Chen L, Huang Q, Zhao T, Sui L, Wang S, Xiao Z, et al. Nanotherapies for Sepsis by Regulating Inflammatory Signals and Reactive Oxygen and Nitrogen Species: New Insight for Treating COVID-19. *Redox Biol* (2021) 45:102046. doi: 10.1016/j.redox.2021.102046
3. Huang Y, Liu Z, Liu C, Ju E, Zhang Y, Ren J, et al. Self-Assembly of Multi-Nanozymes to Mimic an Intracellular Antioxidant Defense System. *Angew Chem Int Ed* (2016) 55:6646–50. doi: 10.1002/anie.201600868
4. Sui L, Wang J, Xiao Z, Yang Y, Yang Z, Ai K. ROS-Scavenging Nanomaterials to Treat Periodontitis. *Front Chem* (2020) 8:595530. doi: 10.3389/fchem.2020.595530
5. Bao X, Zhao J, Sun J, Hu M, Yang X. Polydopamine Nanoparticles as Efficient Scavengers for Reactive Oxygen Species in Periodontal Disease. *ACS Nano* (2018) 12:8882–92. doi: 10.1021/acsnano.8b04022

6. Zhao T, Wu W, Sui L, Huang Q, Nan Y, Liu J, et al. Reactive Oxygen Species-Based Nanomaterials for the Treatment of Myocardial Ischemia Reperfusion Injuries. *Bioact Mater* (2022) 7:47–72. doi: 10.1016/j.bioactmat.2021.06.006
7. Li S, Shang L, Xu B, Wang S, Gu K, Wu Q, et al. A Nanozyme With Photo-Enhanced Dual Enzyme-Like Activities for Deep Pancreatic Cancer Therapy. *Angew Chem Int Ed* (2019) 58:12624–31. doi: 10.1002/anie.201904751
8. Ma P, Xiao H, Yu C, Liu J, Cheng Z, Song H, et al. Enhanced Cisplatin Chemotherapy by Iron Oxide Nanocarrier-Mediated Generation of Highly Toxic Reactive Oxygen Species. *Nano Lett* (2017) 17:928–37. doi: 10.1021/acs.nanolett.6b04269
9. Wang J, Sui L, Huang J, Miao L, Nie Y, Wang K, et al. Mos_2-Based Nanocomposites for Cancer Diagnosis and Therapy. *Bioact Mater* (2021) 6:4209–42. doi: 10.1016/j.bioactmat.2021.04.021
10. Du J, Gu Z, Yan L, Yong Y, Yi X, Zhang X, et al. Poly(Vinylpyrollidone)-and Selenocysteine-Modified Bi_2Se_3 Nanoparticles Enhance Radiotherapy Efficacy in Tumors and Promote Radioprotection in Normal Tissues. *Adv Mater* (2017) 29:1701268. doi: 10.1002/adma.201701268
11. Liang S, Xiao X, Bai L, Liu B, Yuan M, Ma P, et al. Conferring Ti-Based Mofs With Defects for Enhanced Sonodynamic Cancer Therapy. *Adv Mater* (2021) 33:2100333. doi: 10.1002/adma.202100333
12. Ai K, Huang J, Xiao Z, Yang Y, Bai Y, Peng J. Localized Surface Plasmon Resonance Properties and Biomedical Applications of Copper Selenide Nanomaterials. *Mater Today Chem* (2021) 20:100402. doi: 10.1016/j.mtchem.2020.100402
13. Wang H, Yu D, Fang J, Cao C, Liu Z, Ren J, et al. Renal-Clearable Porphyrinic Metal-Organic Framework Nanodots for Enhanced Photodynamic Therapy. *ACS Nano* (2019) 13:9206–17. doi: 10.1021/acsnano.9b03531
14. Tang Z, Zhao P, Wang H, Liu Y, Bu W. Biomedicine Meets Fenton Chemistry. *Chem Rev* (2021) 121:1981–2019. doi: 10.1021/acs.chemrev.0c00977
15. Ji S, Jiang B, Hao H, Chen Y, Dong J, Mao Y, et al. Matching the Kinetics of Natural Enzymes With a Single-Atom Iron Nanozyme. *Nat Catal* (2021) 4:407–17. doi: 10.1038/s41929-021-00609-x
16. Huo M, Wang L, Chen Y, Shi J. Tumor-Selective Catalytic Nanomedicine by Nanocatalyst Delivery. *Nat Commun* (2017) 8:357. doi: 10.1038/s41467-017-00424-8
17. Kim J, Cho H, Jeon H, Kim D, Song C, Lee N, et al. Continuous O_2–Evolving $Mnfe_2o_4$ Nanoparticle-Anchored Mesoporous Silica Nanoparticles for Efficient Photodynamic Therapy in Hypoxic Cancer. *J Am Chem Soc* (2017) 139:10992–5. doi: 10.1021/jacs.7b05559
18. Junttila M, Sauvage F. Influence of Tumour Micro-Environment Heterogeneity on Therapeutic Response. *Nature* (2013) 501:346–54. doi: 10.1038/nature12626
19. Li N, Chen L, Xiao Z, Yang Y, Ai K. Progress in Detection of Biomarker of Ovarian Cancer: Lysophosphatidic Acid. *Chin J Anal Chem* (2020) 48:1597–606. doi: 10.1016/S1872-2040(20)60062-7
20. Li W, Su C, Chang Y, Lin Y, Yeh C. Ultrasound-Induced Reactive Oxygen Species Mediated Therapy and Imaging Using a Fenton Reaction Activable Polymersome. *ACS Nano* (2016) 10:2017–27. doi: 10.1021/acsnano.5b06175
21. Tang Z, Liu Y, He M, Bu W. Chemodynamic Therapy: Tumour Microenvironment-Mediated Fenton and Fenton-Like Reactions. *Angew Chem Int Ed* (2019) 58:946–56. doi: 10.1002/anie.201805664
22. Liu Y, Jiang Y, Zhang M, Tang Z, He M, Bu W. Modulating Hypoxia *via* Nanomaterials Chemistry for Efficient Treatment of Solid Tumors. *Acc Chem Res* (2018) 51:2502–11. doi: 10.1021/acs.accounts.8b00214
23. Tang Z, Zhang H, Liu Y, Ni D, Zhang H, Zhang J, et al. Antiferromagnetic Pyrite as the Tumor Microenvironment-Mediated Nanoplatform for Self-Enhanced Tumor Imaging and Therapy. *Adv Mater* (2017) 29:1701683. doi: 10.1002/adma.201701683
24. Min H, Qi Y, Zhang Y, Han X, Cheng K, Liu Y, et al. A Graphdiyne Oxide-Based Iron Sponge With Photothermally Enhanced Tumor-Specific Fenton Chemistry. *Adv Mater* (2020) 32:2000038. doi: 10.1002/adma.202000038
25. Bai J, Jia X, Zhen W, Cheng W, Jiang X. A Facile Ion-Doping Strategy to Regulate Tumor Microenvironments for Enhanced Multimodal Tumor Theranostics. *J Am Chem Soc* (2018) 140:106–9. doi: 10.1021/jacs.7b11114
26. Neyens E, Baaeyens J. A Review of Classic Fenton's Peroxidation as an Advanced Oxidation Technique. *J Hazard Mater* (2003) B98:33–50. doi: 10.1016/S0304-3894(02)00282-0
27. Lee H, Shin T, Cheon J, Weissleder R. Recent Developments in Magnetic Diagnostic Systems. *Chem Rev* (2015) 115:10690–724. doi: 10.1021/cr500698d
28. Liu Y, Shi J. Antioxidative Nanomaterials and Biomedical Applications. *Nano Today* (2019) 27:146–77. doi: 10.1016/j.nantod.2019.05.008
29. Izci M, Maksoudian C, Manshian B, Soenen S. The Use of Alternative Strategies for Enhanced Nanoparticle Delivery to Solid Tumors. *Chem Rev* (2021) 121:1746–803. doi: 10.1021/acs.chemrev.0c00779
30. Zhou J, Rao L, Yu G, Cook T, Chen X, Huang F. Supramolecular Cancer Nanotheranostics. *Chem Soc Rev* (2021) 50:2839–91. doi: 10.1039/d0cs00011f
31. Liang M, Yan X. Nanozymes: From New Concepts, Mechanisms, and Standards to Applications. *Acc Chem Res* (2019) 52:2190–200. doi: 10.1021/acs.accounts.9b00140
32. Jeon M, Halbert M, Stephen Z, Zhang M. Iron Oxide Nanoparticles as T_1 Contrast Agents for Magnetic Resonance Imaging: Fundamentals, Challenges, Applications, and Prospectives. *Adv Mater* (2021) 33:1906539. doi: 10.1002/adma.201906539
33. Lu Y, Xu Y, Zhang G, Ling D, Wang M, Zhou Y, et al. Iron Oxide Nanoclusters for T_1 Magnetic Resonance Imaging of non-Human Primates. *Nat BioMed Eng* (2017) 1:637–43. doi: 10.1038/s41551-017-0116-7
34. Gao L, Zhuang J, Nie L, Zhang J, Zhang Y, Gu N, et al. Intrinsic Peroxidase-Like Activity of Ferromagnetic Nanoparticles. *Nat Nanotechnol* (2007) 2:577–83. doi: 10.1038/nnano.2007.260
35. Shen S, Wang S, Zheng R, Zhu X, Jiang X, Fu D, et al. Magnetic Nanoparticle Clusters for Photothermal Therapy With Near-Infrared Irradiation. *Biomaterials* (2015) 39:67–74. doi: 10.1016/j.biomaterials.2014.10.064
36. Chu M, Shao Y, Peng J, Dai X, Li H, Wu Q, et al. Near-Infrared Laser Light Mediated Cancer Therapy by Photothermal Effect of Fe_3O_4 Magnetic Nanoparticles. *Biomaterials* (2013) 34:4078–88. doi: 10.1016/j.biomaterials.2013.01.086
37. Yoo D, Jeong H, Preihs C, Choi J, Shin T, Sessler J, et al. Double-Effector Nanoparticles: A Synergistic Approach to Apoptotic Hyperthermia. *Angew Chem Int Ed* (2012) 51:12482–5. doi: 10.1002/anie.201206400
38. Ding W, Chen Z, Gu Y, Chen Z, Zheng Y, Sun F. Magnetic Testis Targeting and Magnetic Hyperthermia for Noninvasive, Controllable Male Contraception *via* Intravenous Administration. *Nano Lett* (2021) 21:6289–97. doi: 10.1021/acs.nanolett.1c02181
39. Zwi-Dantsis L, Wang B, Marijon C, Zonetti S, Ferrini A, Massi L, et al. Remote Magnetic Nanoparticle Manipulation Enables the Dynamic Patterning of Cardiac Tissues. *Adv Mater* (2020) 32:1904598. doi: 10.1002/adma.201904598
40. Liu Z, Li M, Li Z, Pu F, Ren J, Qu X. Easy Access to Selective Binding and Recyclable Separation of Histidine-Tagged Proteins Using Ni^{2+}-Decorated Superparamagnetic Nanoparticles. *Nano Res* (2012) 5:450–9. doi: 10.1007/s12274-012-0230-5
41. Shao M, Ning F, Zhao J, Wei M, Evans D, Duan X. Preparation of Fe_3O_4@Sio_2@Layered Double Hydroxide Core-Shell Microspheres for Magnetic Separation of Proteins. *J Am Chem Soc* (2012) 134:1071–7. doi: 10.1021/ja2086323
42. Ling D, Lee N, Hyeon T. Chemical Synthesis and Assembly of Uniformly Sized Iron Oxide Nanoparticles for Medical Applications. *Acc Chem Res* (2015) 48:1276–85. doi: 10.1021/acs.accounts.5b00038
43. Zanganeh S, Hutter G, Spitler R, Lenkov O, Mahmoudi M, Shaw A, et al. Iron Oxide Nanoparticles Inhibit Tumour Growth by Inducing Pro-Inflammatory Macrophage Polarization in Tumour Tissues. *Nat Nanotechnol* (2016) 11:986–94. doi: 10.1038/nnano.2016.168
44. Chen Z, Yin J, Zhou Y, Zhang Y, Song L, Song M, et al. Dual Enzyme-Like Activities of Iron Oxide Nanoparticles and Their Implication for Diminishing Cytotoxicity. *ACS Nano* (2012) 6:4001–12. doi: 10.1021/nn300291r
45. Qian X, Zhang J, Gu Z, Chen Y. Nanocatalysts-Augmented Fenton Chemical Reaction for Nanocatalytic Tumor Therapy. *Biomaterials* (2019) 211:1–13. doi: 10.1016/j.biomaterials.2019.04.023

Conflict of Interest: The authors declare that the research was conducted in the absence of any commercial or financial relationships that could be construed as a potential conflict of interest.

Publisher's Note: All claims expressed in this article are solely those of the authors and do not necessarily represent those of their affiliated organizations, or those of the publisher, the editors and the reviewers. Any product that may be evaluated in

this article, or claim that may be made by its manufacturer, is not guaranteed or endorsed by the publisher.

Copyright © 2021 Qin, Xue, Jia, Ren, Dong and Zhou. This is an open-access article distributed under the terms of the Creative Commons Attribution License (CC BY). The use, distribution or reproduction in other forums is permitted, provided the original author(s) and the copyright owner(s) are credited and that the original publication in this journal is cited, in accordance with accepted academic practice. No use, distribution or reproduction is permitted which does not comply with these terms.

frontiers in Oncology

ORIGINAL RESEARCH
published: 24 November 2021
doi: 10.3389/fonc.2021.793006

Platelet Membranes Coated Gold Nanocages for Tumor Targeted Drug Delivery and Amplificated Low-Dose Radiotherapy

Mingzhu Chen[1†], Ping Wang[2†], Dazhen Jiang[3], Zhirong Bao[3] and Hong Quan[1*]*

[1] Key Laboratory of Artificial Micro- and Nano-Structures of Ministry of Education, School of Physics and Technology, Wuhan University, Wuhan, China, [2] Department of Molecular Pathology, Henan Cancer Hospital, Affiliated Tumor Hospital of Zhengzhou University, Zhengzhou, China, [3] Department of Radiation and Medical Oncology, Hubei Key Laboratory of Tumor Biological Behaviors, Hubei Cancer Clinical Study Center, Zhongnan Hospital of Wuhan University, Wuhan, China

OPEN ACCESS

Edited by:
Kelong Ai,
Central South University, China

Reviewed by:
Jia Huang,
Central South University, China
Wang Ying,
Beijing University of Chinese Medicine, China

***Correspondence:**
Zhirong Bao
bao_zhirong@163.com
Hong Quan
00007962@whu.edu.cn

[†]These authors have contributed equally to this work

Specialty section:
This article was submitted to Pharmacology of Anti-Cancer Drugs, a section of the journal Frontiers in Oncology

Received: *11 October 2021*
Accepted: *01 November 2021*
Published: *24 November 2021*

Citation:
Chen M, Wang P, Jiang D, Bao Z and Quan H (2021) Platelet Membranes Coated Gold Nanocages for Tumor Targeted Drug Delivery and Amplificated Low-Dose Radiotherapy. Front. Oncol. 11:793006. doi: 10.3389/fonc.2021.793006

Continuous high doses of radiation can cause irreversible side effects and radiation resistance; thus, advanced radiosensitizers are urgently needed. To overcome this problem, we developed a nano platelet radiosensitization system (PCA) by coating the chemotherapeutic drug cisplatin (CDDP) loaded gold nanocages (AuNs) within the platelet membrane. The developed PCA system may enable AuNs to have immune escape and targeting capabilities. After administration, PCA will actively target tumor cells and avoid being cleared by the immune system. Subsequently, CDDP, which destroys tumor cell DNA, can not only kill tumor cells directly but also combine with AuNs, which deposit radiation energy into tumor tissues, reducing RT resistance. *In vivo* and *in vitro* studies revealed that the combination of PCA with RT (2Gy) efficiently inhibits tumor proliferation without causing side effects such as inflammation. To conclude, this is the first attempt to use platelet membranes to correctly transport AuNs while also accomplishing low-dose RT, which could help AuNs-based tumor RT become more effective.

Keywords: platelet membranes, gold nanocages, drug delivery, low-dose radiotherapy, cisplatin

INTRODUCTION

Despite current scientific advancements, cancer, which can strike at any age and affect anybody, remains a severe threat to human life and health (1–3). Radiotherapy (RT) is widely used to treat cancer patients, either alone or in combination with other cutting-edge treatments (4). RT is based on the use of high-energy X-rays or gamma rays to cause radiation-induced DNA damage and triggers the generation of reactive oxygen species (ROS) in increased concentrations (5). Both radiation-induced DNA damage and ROS generation that exceeds the cell's ability to neutralize these free radicals result in apoptosis, which reduces tumor size (6). However, while RT kills tumor cells, it also kills adjacent cells and tissues in the human body (7). RT produces ROS in a dose-dependent manner, with higher doses resulting in better therapeutic outcomes (8). However, high-dose RT might cause systemic effects such as fatigue, loss of appetite, bone marrow suppression, RT-induced secondary and primary malignancies, and infertility, as well as local RT damage (9–11). Local liver damage can lead to changes in activity or, in the worst-case scenario, liver failure (12).

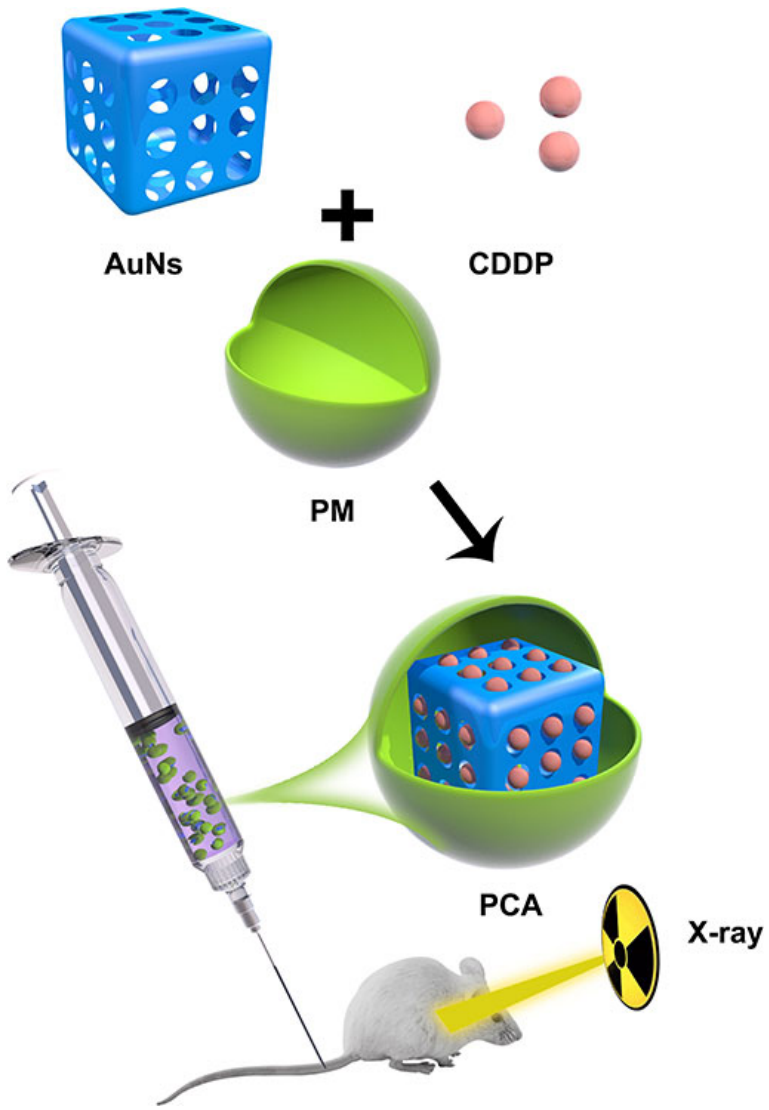
Therefore, there is a definite need to find novel methods to improve RT effectiveness in cancer patients.

The emergence of nanoplatforms has enabled more and more novel nanomaterials to be delivered to tumor tissues to accomplish radiosensitization while reducing systemic toxicity, as a result of the integration of nanotechnology in the area of cancer treatment (13). MoS_2-based nanomaterials and copper selenide nanomaterials have been explored to realize radiosensitization (14, 15). These studies provide new insights for the selection of radiotherapy sensitizers. Gold nanomaterials, such as gold nanorods, gold nanostars, gold nanocages, and other High-Z nanomaterials, are the most common of these (16–18). Gold, a High-Z nanomaterial, can enhance the deposition of radiation energy in the tumor and improve the effectiveness of RT (19). For example, Liu et al. developed a new type of gold nanostar probe that can simultaneously realize tumor imaging and photothermal therapy *in vivo* (20). Unlike other gold nanomaterials, gold nanocages have the excellent drug-carrying ability. Zhu et al. (21) designed paclitaxel-loaded gold nanocages and wrapped them with red blood cell membranes to achieve combined anti-tumor effects *in vitro*. However, no article has yet been published that describes the usage of gold nanocages to produce radiosensitization.

For a long time, people have known that platelets play an important role in hemostasis through clotting and blood vessel damage (22–24). Platelets can also interact with tumor cells by directly binding or secreting cytokines. Taking advantage of the natural pathophysiological affinity and targeting ability of platelets to tumors, a biomimetic drug delivery system based on platelet membranes has also been developed for tumor treatment (25, 26). Compared with artificial drug delivery platforms, they are less likely to cause clearance reactions, so vesicles administered with the platelet membrane itself provide a better prospect for drug delivery (27, 28). Platelet membranes are easier to penetrate from blood vessels to tumor tissues for precision medication administration or nanomaterial delivery due to the properties of membrane proteins. The oxidative stress amplifying drug cinnamaldehyde (CA) coated platelet membrane hybrid nanosystem (PSCI) was developed by Huang et al. using the peculiarities of platelet membranes (PM) to transport CA to tumor tissues and achieve up to 90% tumor growth suppression (22). Therefore, it stimulates us to add gold nanocages to PM to overcome radiation resistance and immune clearance.

For the first time, a study on the combined application of AuNs and PM to improve low-dose RT was published in this study. A composite nanosystem PCA was constructed by coating AuNs containing the anticancer drug cisplatin (CDDP) with PM (**Scheme 1**). The platelet membrane can protect CDDP and AuNs, prevent these medicines from leaking in advance, and successfully improve the blood circulation time of AuNs in the body because PCA has targeting and radiosensitization capabilities. At the same time, it helps the drug overcome the renal effect and immune clearance, and actively targets tumor cells. Subsequently, CDDP, which destroys tumor cell DNA, can not only directly kill tumor cells, but also can combine with AuNs that deposit RT energy to tumor tissues to achieve high-efficiency sensitization RT. It needs to be pointed out that in the treatment window, we only need 2 Gy of RT and PCA synergistic treatment to obtain a strong radiation sensitization effect. PCA system provides a higher biological potential for long-term use. Finally, these findings broaden the use of gold nanocages and provide new insights for the development of platelet membrane-based tumor treatment systems.As shown in **Scheme 1**, we firstly extracted platelet vesicles (PV) from platelets. The AuNs and CDDP were co-coated with PV to obtain a PV-coated composite nano-system (PCA). **Figure 1A** shows a transmission electron microscopy (TEM) image of the prepared AuNs and PCA. PCA exhibited a gray-scale platelet membrane (PM) of about 8.5 nm. PCA and platelet membrane showed the same P-selectin protein profile, as shown in **Figure 1B**, indicating that platelet membrane proteins are completely retained in PCA. These results showed that we have successfully prepared AuNs and composite material PCA. Platelet membranes have a lot of potential in the field of substance delivery because of this characteristic, which makes them far superior to standard drug delivery methods like liposomes or red blood cell membranes that don't target anything (29, 30). P-selectin in platelet membranes can specifically recognize corresponding ligands on the surface of tumor cells, and these interactions give PCA the ability to actively target tumor cells. None of these materials increase the penetration of the substance into the tumor tissue. The successful coating of PV allows the poorly targeted CDDP and AuNs to stay in the bloodstream for longer, evade immune system attacks, and actively target tumor cells. And we continued to measure the zeta potential of different materials, as shown in **Figure 1C**. During the three days, the particle sizes of AuNs were 95.4 ± 4.8 nm, 93.8 ± 4.2 nm, and 94.5 ± 5.1 nm, respectively, while the particle sizes of PCA were 103.4 ± 6.2 nm, 101.7 ± 5.2 nm, and 102.5 ± 5.7 nm (**Figure 1D**), which also indicates that both AuNs and hybrid PCA have good stability and can be used in subsequent biological experiments. The drug releasing ability of PCA have been investigated, as shown in **Figure 1E**, PCA hardly releases CDDP without X-ray exposure (**Figure 1E**). Once irradiated by X-rays, the platelet membrane will be damaged, and gradually release the drugs. The drug loading efficiency (DLE) was determined using high-performance liquid chromatography (HPLC). DLE was 94.6 ± 5.2%. These results suggest that PCA has a PM structure and that would be released from 4T1 tumor cells *via* extracellular action to change the tumor micro-environment.

The PCA system is well-structured and characterized in terms of performance. We are actively conducting *in vitro* anti-tumor trials. Although AuNs and CDDP can change the ecological balance of the tumor microenvironment and therefore enhance the efficacy of radiation, they can only do so when they are located at the tumor tissue. The immune system can recognize the stimulation of various foreign invaders, and some of the stimulation can trigger the immune response, resulting in immunity, and inhibit the immune system from responding to other stimuli, resulting in tolerance (31, 32). However, the platelets are not attacked by the immune system, which is related to PM proteins. Unlike other drug delivery systems that



SCHEME 1 | Schematic illustration of platelet membranes coated gold nanocages for tumor targeted drug delivery and amplificated low-dose radiotherapy.

do not have targeting capabilities rearranged nanomaterial-coated PCA may be directed to tumor cells, identified by cancer cells, and engorged to release nanomaterial. This internalization effect was tracked by staining RCA (red blood cell membrane comprising AuNs which have been loaded with CDDP) and PCA nanovesicles with Dil dye and co-incubation with 4T1 cells and staining with commercial lysosome Lyso-Tracker Green probe to verify the ability of PCA to be internalized by tumor cells *in vitro* (co-localization assay). After 2 h of incubation, it was clear that a significant quantity of PCA had been endocytosed, whereas RCA only had a partial measured fluorescence impact of Dil (**Figure 2C**), demonstrating that PM may be used as an excellent carrier of AuNs to target tumor tissues. When tumor cells are exposed to radiation, double-stranded DNA breaks (DSB) occur, providing insight into radiation sensitization. Measuring the fluorescence intensity of γ-H2AX is a good and intelligent technique to verify the formation of DSB after cell damage (33). Therefore, we detected H_2AX foci in the nucleus after treatment in different groups. There was moderate DNA damage after low dose (2 Gy) RT. Notably, it is worth noting that 2Gy RT combined with PA only achieved about 53.6% γ-H2AX formation, while 2Gy combined with PCA achieved the best γ-H_2AX foci formation, as high as 70.2% (**Figures 2A, B**). Compared with each experimental group, there was a uniform and significant difference, which was attributed to the targeting ability of platelet membrane and RT sensitization effect of CDDP and AuNs. Furthermore, the Colony formation assays test showed that the cell viability of the control group was almost unaffected, while RT combined with the PA group had moderate tumor growth inhibition (**Figure 2D**).

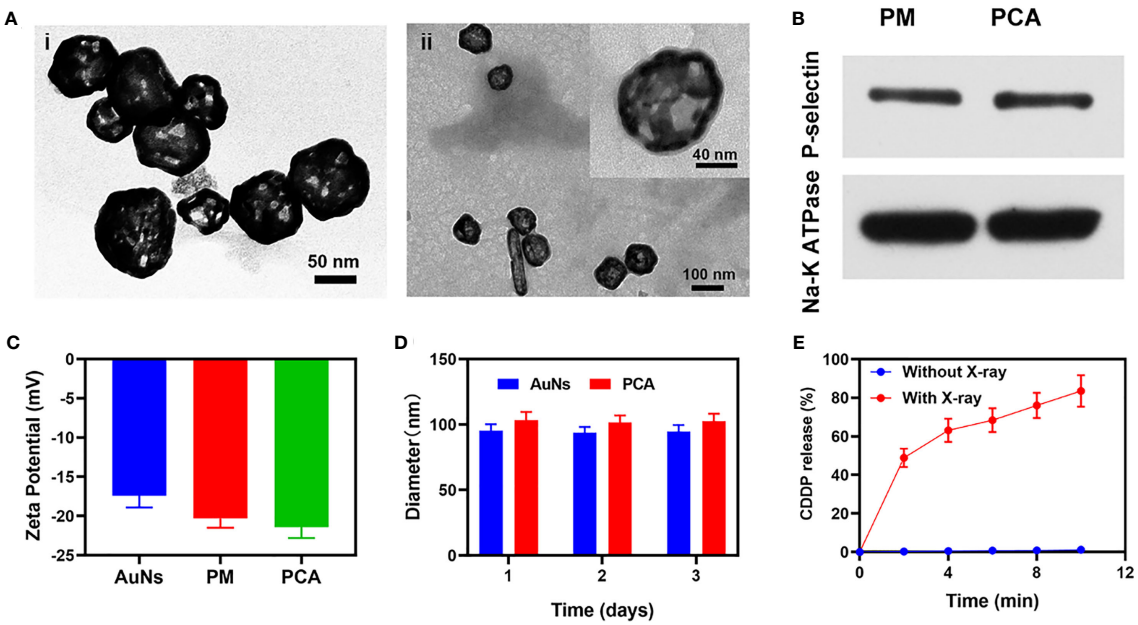


FIGURE 1 | **(A)** TEM image of (i) AuNs and (ii) PCA. Insert: single PCA with high magnification. **(B)** The expressions of the key protein P-selectin on PCA with PM as a control. **(C)** Zeta potential of AuNs, PM, and PCA. **(D)** Statistical graph of the measured diameter of AuNs and PCA. **(E)** CDDP release profiles under different conditions.

Although Au can deposit RT rays to enhance its therapeutic efficacy, the single sensitization effect is limited. There were significant differences in tumor growth inhibition rates (the tumor inhibition rate reached 92.5%) between the PCA + RT system and the other experiment groups, indicating that CDDP in PCA mediated destroying DNA of tumor cells can effectively exert influence on cellular viability balance and thus enhance the effect of RT to achieve tumor growth inhibition. Together, these results drive continued exploration of anti-tumor efficacy *in vivo*.

Because an *in vitro* investigation of the tumor-killing effect revealed significant potential. We further explore *in vivo* intensification of PCA effects. Therefore, we conducted *in vivo* pharmacokinetic experiments to investigate the effect of platelet membranes on blood retention. Mice were intravenously injected with RCA or PCA at a dose of 1 mg CDDP/kg (**Figure 3A**). Next, we studied the biological distribution (**Figure 3B**). After 12 h of administration, the CDDP mainly accumulated in the liver and spleen of the RCA group of mice, while the PCA group showed good tumor targeting and low organ accumulation, further proving the targeting ability of the platelet membrane. Both PCA and RCA showed a stronger blood retention effect. Although the coating of erythrocyte membrane made AuNs and CDDP impervious to immune system attack, it lacked tumor targeting, and CDDP accumulation in tumor tissues was only marginally increased, with the PCA group having the most visible tumor accumulation. We next evaluated PCA-mediated anti-tumor efficiency in mice bearing 4T1 tumors. To investigate the primary effect of the PCA, BALB/c mice were subcutaneous injected with 1×10^6 4T1 cells into the right flank. The mice were grouped and treated when the primary tumor volume reached 200 mm^3. Tumor-bearing mice were divided randomly into 5 groups (each group included 5 mice): 1) Control (PBS); 2) Radiotherapy (RT, 2Gy); 3) PCA; 4) PA + RT; 5) PCA + RT. The CDDP concentration was 1 mg/kg in groups 3 and 5. The AuNs concentration was 5 mg/kg in groups 3, 4, and 5. The treatment was conducted every 5 days for 15 days. During the 2 weeks treatment, the tumor volumes of the control group and RT treated group rose rapidly, as shown in **Figure 3C**. The PCA group also hardly inhibited tumor growth. The group of PA + RT also showed an almost moderate tumor suppressant effect. Although Au element can deposit RT rays to expand the RT therapeutic effect, the single sensitization effect is limited. When these nanomaterials are injected into the caudal vein, the PCA circulates to the tumor tissue and is endocytosed by tumor cells. As a result of the tumor cells' endocytosis, AuNs are released into the tumor microenvironment (TME), having a therapeutic effect. Specifically, the PCA + RT system, which carried both CDDP and AuNs, achieved the most powerful therapeutic effect, with tumor volume growth curves almost completely suppressed during treatment. The tumor mass of mice was also consistent with the corresponding volume curve (**Figure 3D**). The treatment group did not gain or lose weight during the study, indicating that the treatment did not cause any significant systemic toxicity (**Figure 3E**). This is significant because many treatments are associated with extremely systemic toxicity, which is extremely detrimental to the future clinical application of the material. We took tumor tissue sections for H&E staining (**Figure 3F**) also confirmed that there was a large amount of cell necrosis in the

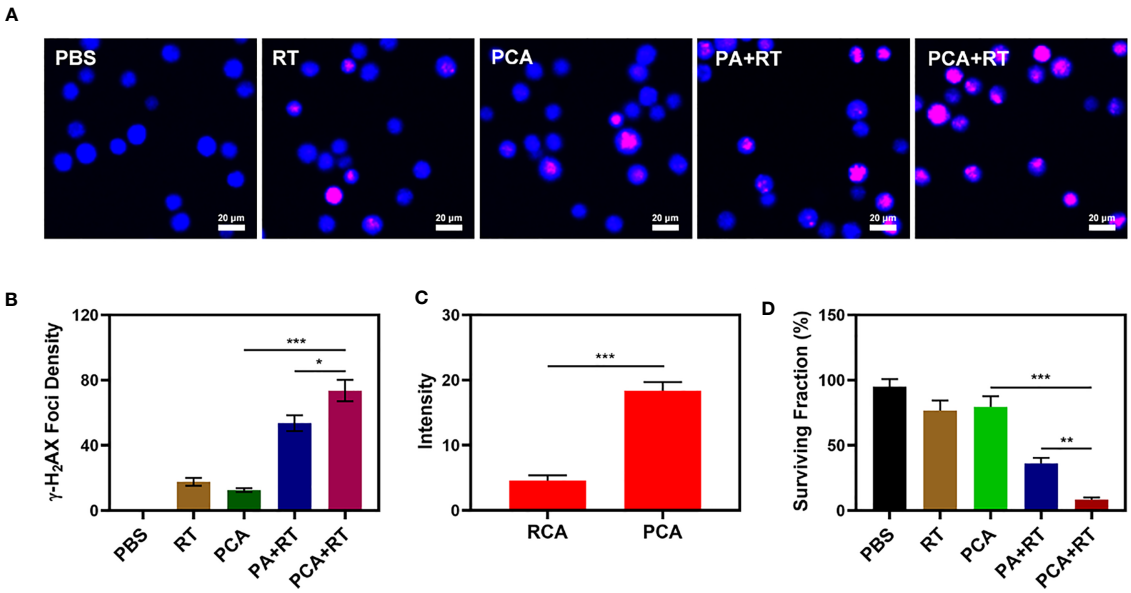


FIGURE 2 | The CLSM images of 4T1 cells with different treatments. The nuclei were stained with DAPI (blue) and DSBs were stained with γ-H_2AX (red). **(B)** Average fluorescence intensity of γ-H_2AX from figure **(A)**. **(C)** Co-localization of Lyso-Tracker Green FM (blue) and Dil (red) for RCA and PCA over time in 4T1 tumor cells. **(D)** Colony formation assays were conducted using 4T1 cells treated with 2 Gy of radiation (n = 3). Significant differences among groups as calculated using the Student's t-test. *P < 0.05, **P < 0.01, ***P < 0.005.

PCA combined RT treatment group. As shown in **Figure 4**, during PCA activation treatment of mice, their vital organs (heart, liver, spleen, lungs, and kidney) were found to be healthy and free of inflammation and damage throughout the body. Furthermore, the liver and kidney indices were found to be normal as well. as many nanomaterials possess great therapeutic efficacy, they are also associated with systemic toxicity, which limits their future clinical applications (34, 35). The *in vivo* results demonstrate that this novel combined treatment not only achieves a good biological safety therapy but gives damage to tumor cell DNA, reinforces the effect of RT with profound PCA-enhanced therapy.

CONCLUSION

In a nutshell, we developed a platelet membrane-based RT sensitizer to achieve enhanced RT results. The nano-agent AuNs and chemotherapeutic drugs encapsulated in PCA can deposit RT rays or damage tumor DNA to reduce RT resistance. Platelet membranes endow PCA with excellent targeting ability. These elements have a greater ability to induce tumor cell apoptosis. Both *in vitro* and *in vivo* results indicate that PCA system shows good tumor suppression. What matters is that the method we developed has no visible adverse effects during therapy. We will continue to investigate the biological applications of PM in combination with other new nanomaterials in the future, as well as combine additional nanotechnology to improve treatment approach.

MATERIALS AND METHODS

Materials and Reagents

Deionized (DI) water was obtained by an 18 MΩ cm (SHRO-plus DI) system. Phosphate buffer solution (PBS) and bovine serum albumin (BSA) were purchased from Thermo-Fisher (USA). AuNs were obtained from XFNano (Nanjing, China)., 1'-dioctadecyl-3, 3, 3', 3'-tetramethylindocarbocyanine perchlorates (Dil) was obtained from Sigma-Aldrich (USA). The γ-H2AX antibody was purchased from Abcam Company. The other reagents used in this work were purchased from Sinopharm Chemical Reagent (China) and Aladdin-Reagent (China).

Preparation and Characterization of PLT-Vesicles (PM)

Platelets (PLTs) from whole blood were isolated through gradient centrifugation. 10 mL mice whole blood was centrifuged at 100 × g for 20 min with no brake. Afterward, the supernatant was centrifuged at 800 × g for 20 min. The PLTs were washed by PBS and centrifuged repeatedly. The preparation processes were monitored using a conventional microscope (IX71, Olympus, Japan). PLT membranes were derived by a repeated freeze–thaw process. Aliquots of PLT suspensions were first frozen at −80°C, thawed at room temperature, and pelleted by centrifugation at 4000 × g for 3 min. After three repeated washes with PBS mixed with protease inhibitor tablets, the pelleted PLT membranes were suspended in water, sonicated in a capped glass vial for 5 min using a bath sonicator at a frequency of 53 kHz and a power of 100 W, and then extruded

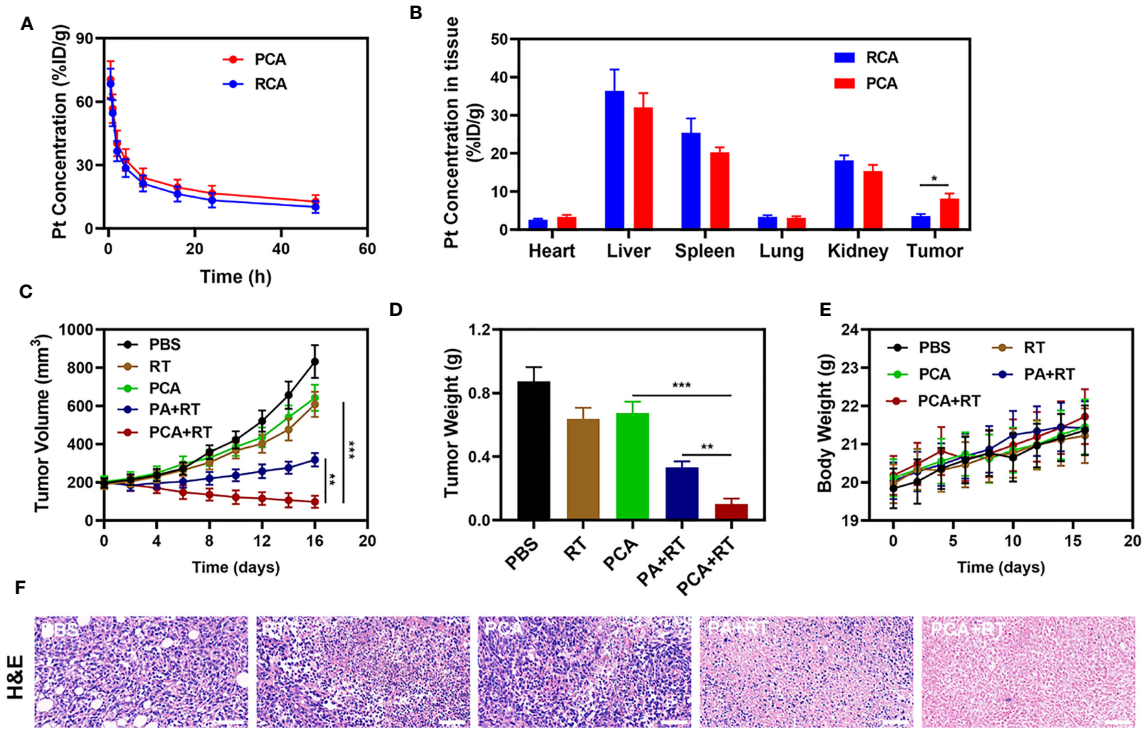


FIGURE 3 | **(A)** Pharmacokinetic behavior of RCA and PCA in mice following i.v. administration. Data are presented as mean ± SD (n = 3). **(B)** Quantitative analysis of Pt biodistribution in tissues and tumors of tumor-bearing mice injected with RCA or PCA at CDDP dose of 5 mg/kg, respectively (n = 3). **(C)** Change in tumor-volume curves of 4T1 tumor-bearing mice after treatments (n = 5). **(D)** Changes in tumor weight following treatment (n = 5). **(E)** Body weight of 4T1 tumor-bearing mice as recorded every 2 days following treatment (n = 5). **(F)** Representative hematoxylin-eosin staining (H&E) stained tumor slice images of mice following treatment (n = 5), scale bars = 100 μm. Significant differences among groups as calculated using the student's t-test. *P < 0.05, **P < 0.01, ***P < 0.005.

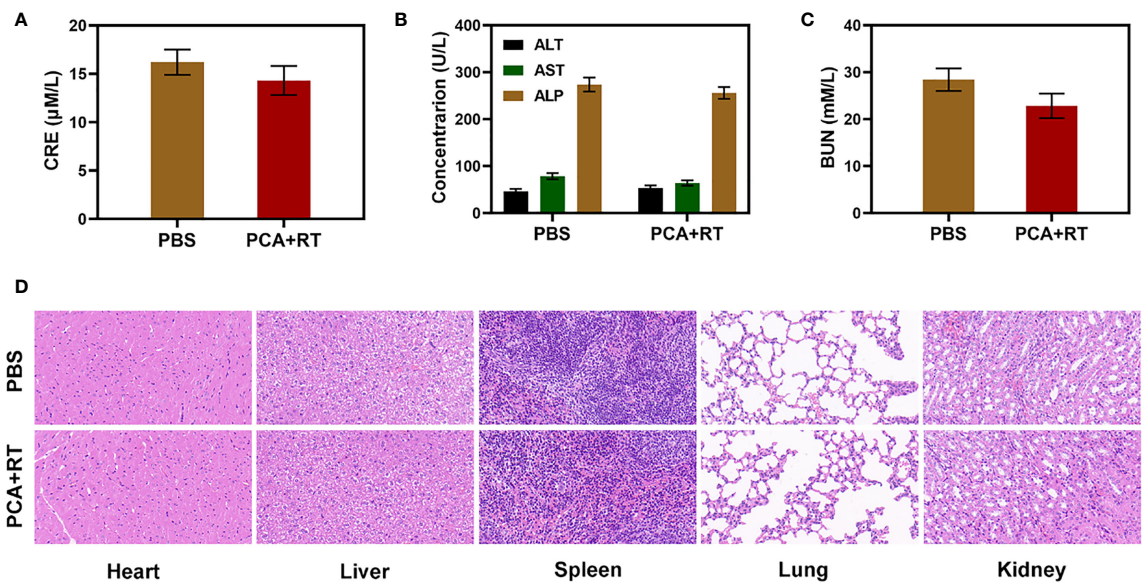


FIGURE 4 | Result of *in vivo* safety experiments. Blood biochemistry data including kidney/liver function markers: **(A)** CRE, **(B)** ALT, ALP, and AST, and **(C)** BUN after various treatments. **(D)** Histopathological analysis results (H&E) stained images of the major organs, heart, lung, liver, kidneys, and spleen, of mice that were exposed to different treatments 16 days' post-injection under laser irradiation.

sequentially through 400 and 200 nm polycarbonate porous membranes on a mini extruder (Avanti Polar Lipids, USA).

Preparation of PCA

To prepare the PCA, the mixture of 100 μg AuNs, CDDP (20 μg dispersed in PBS) and PM was sonicated for 0.5 h. Thereafter, a polycarbonate membrane containing 200 nm pore size was used for extruding the mixture 10 times using an extruder. The final mixture was centrifuged and washed with PBS to remove the residual free materials.

Characterization of the PCA Nanoparticles

The morphology structures of AuNs and PCA nanoparticles were observed by the TEM (JEOL-2100). Hydrodynamic diameter and zeta potential were detected by the dynamic light scattering (Nano-ZS ZEN3600). Drug loading efficiency (DLE) = (weight of loaded drug/weight of feeding drug) × 100%.

Drug Release Studies

1mg of PCA were dispersed in 1ml PBS solution. The solution was exposed to X-ray irradiation (2 Gy) for 5min. At the given time points, the released CDDP was measured by High Performance Liquid Chromatography (HLPC). No X-ray irradiation was used as a control group.

Cell Lines and Animal Model

4T1 mouse breast cancer cell lines were provided by the College of Life Science of Wuhan University. All the cells were cultured in the standard cell medium recommended by American Type Culture Collection. Female Balb/c mice aged 4-5 weeks were purchased from Vital River Company (Beijing, China). 5×10^6 4T1 cells suspended in 100 μL PBS were subcutaneously injected into each mouse to establish the tumor models. After the tumor volume reached around 200 mm^3, the tumor bearing mice were used for further experiments. The animal experiments were carried out according to the protocol approved by the Ministry of Health in the People's Republic of PR China and were approved by the Administrative Committee on Animal Research of the Wuhan University.

Western Blotting for the Key Proteins in PM and PCA

The total cellular protein in PM and PCA were extracted using a protein extraction kit (Dingguo, China). The extracted proteins were separated using SDS-PAGE electrophoresis. After electrophoresis, the gel was treated with Coomassie blue staining. Extraction of protein for western blot was performed as described above. The proteins were then transferred onto polyvinylidene fluoride (PVDF) membranes (BioRad). This was followed by a blocking step for 1 h with 5% skim milk, and then the membrane was incubated with the primary antibody against P-selectin (Proteintech) overnight at 4°C using Na,K-ATPase as the control. Finally, the membrane was incubated with the secondary antibody for 1 h at room temperature.

In Vitro Tumor-Specific Uptake

At first, Dil labeled RCA and PCA (Containing 100 μg/mL AuNs) were incubated with 4T1 cells for 2 h at 37°C. The cells were then washed with PBS several times, fixed with PFA for 30 min at room temperature, stained with Lyso-Tracker Green and then imaged by using a fluorescence microscope (IX81, Olympus, Japan). The fluorescence intensity was measured by IamgeJ software.

γ-H_2AX Immunofluorescence Analysis

4T1 cells were seeded in 24-well plates and then cultured for 24 h at 37°C under hypoxia condition. Then the cells were treated with 1) Control (PBS); 2) Radiotherapy (RT, 2Gy); 3) PCA; 4) PA + RT; 5) PCA + RT. The AuNs concentration was 200 μg/mL in groups 3, 4, and 5. After RT treatment for 2 h, the cells were fixed with 4% paraformaldehyde for 10 min, rinsed with PBS, permeabilized with methanol for 15 min at -20°C and then rinsed with PBS again. Then the cells were exposed to a blocking buffer (1% bovine serum albumin (BSA) in PBS solution) for 1 h at room temperature and further incubated with anti- phospho-histone γ-H2AX mouse monoclonal antibody (dilution 1:500) overnight at 4°C. After washing with PBS, the cells were incubated with Cy5-conjugated sheep anti-mouse secondary antibody (dilution 1:500) for 1 h at room temperature. Excess antibody was removed by rinsing the coverslips in PBS. Cell nuclei were stained by DAPI for 5 min at room temperature. The cells were imaged *via* confocal fluorescence microscopy (IX81). Quantitative analysis of γ-H2AX foci density (foci/100 μm2) was performed by automatic counting using the ImageJ software for n = 100 cells in each treatment group.

Clonogenic Assay

4T1 cells were seeded in 6-well plates with a different amount (125, 250, 500, 1000 and 2000) per well and incubated at 37°C for 24 h Then the cells were treated with five groups: 1) Control (PBS); 2) Radiotherapy (RT, 2Gy); 3) PCA; 4) PA + RT; 5) PCA + RT. The AuNs concentration was 200 μg/mL in groups 3, 4, and 5. After that, cells were washed with PBS and fresh medium was replaced every three days for 10 days. The colonies were fixed by 4% paraformaldehyde and then stained with Giemsa dye. Only colonies containing at least 50 cells were counted. At last, an evaluation of the effects of different treatments was conducted by counting the survival fraction of the colonies. Each treatment was performed in triplicate.

In Vivo Pharmacokinetics and Distribution Study

4T1 tumor bearing BALB/c mice (n = 3) received an intravenous (i.v.) injection of 100 μL PBS containing RCA, or PCA at the concentration of 1 mg/kg CDDP. At various time points after the injection (i.e.,0.5, 1, 2, 4, 8, 16, 24, and 48 h), 20 μL blood was collected from the tail veins, treated with aqua regia, and then on heated at 70°C until to obtain clear solutions. And the resultant mixture was left standing still at room temperature for 12 h and then kept in oil bath at 70°C for 6 h to remove acids, yielding samples for Pt content quantification by using an ICP-AES (iris Intrepid II XSP, Thermo Elemental, USA). To study the

biodistribution of particles in various organs, at 24 h after the injection, all mice were euthanized and their hearts, livers, spleens, kidneys, lungs, and tumors were carefully collected, weighted, and finally quantitatively analyzed with ICP-AES as described above.

In Vivo Antitumor Study

1×10^6 4T1 cells suspended in 100 μL PBS were subcutaneously injected into each mouse to establish the tumor models. When tumor size reached approximately 200 mm3, the mice were divided randomly into 5 groups (each group included 5 mice): 1) Control (PBS); 2) Radiotherapy (RT, 2Gy); 3) PCA; 4) PA + RT; 5) PCA + RT. The CDDP dose was 1mg/kg in groups 3 and 5. The treatment was conducted every 5 days for 15 days. Mice body weight and tumor volume in all groups were monitored every 2 days. A caliper was employed to measure the tumor length and tumor width and the tumor volume was calculated according to the following formula. Tumor volume = tumor length × tumor width^2/2. After 16 days of treatment, all the mice were sacrificed. Their blood samples and major organs (i.e., hearts, livers, spleens, lungs, and kidneys) were collected. Three important hepatic indicators (i.e., ALT: alanine aminotransferase, AST: aspartate aminotransferase, and ALP: alkaline phosphatase) and two indicators for kidney functions (i.e., BUN: blood urea nitrogen and CRE: creatinine) were measured by using a blood biochemical autoanalyzer (7080, HITACHI, Japan). And the tumor tissues were weighed, and fixed in 4% neutral buffered formalin, processed routinely into paraffin, and sectioned at 4 μm. Then the sections were stained with hematoxylin and eosin (H&E) staining and finally examined by using an optical microscope (BX51, Olympus, Japan). Part of their organs were stained with H&E and examined as described above.

Statistical Analysis

Data analyses were conducted using the GraphPad Prism 5.0 software. Significance between every two groups was calculated by the Student's t-test. *P < 0.05, **P < 0.01, ***P < 0.005.

DATA AVAILABILITY STATEMENT

The original contributions presented in the study are included in the article/**Supplementary Material**. Further inquiries can be directed to the corresponding authors.

ETHICS STATEMENT

The animal experiments were carried out according to the protocol approved by the Ministry of Health in the People's Republic of PR China and were approved by the Administrative Committee on Animal Research of the Wuhan University.

AUTHOR CONTRIBUTIONS

MC and ZB: analysis. MC: drafting. DJ and HQ: interpretation of data. PW: revising. All authors contributed to the article and approved the submitted version.

FUNDING

We greatly acknowledged the financial support from the National Natural Science Foundation of China (Grant No. 12005158). This work was supported by the Elekta-Wuhan University Medical Physics Teaching and Research Fund (250000200).

SUPPLEMENTARY MATERIAL

The Supplementary Material for this article can be found online at: https://www.frontiersin.org/articles/10.3389/fonc.2021.793006/full#supplementary-material

REFERENCES

1. Gao F, Tang Y, Liu WL, Zou MZ, Huang C, Liu CJ, et al. Intra/Extracellular Lactic Acid Exhaustion for Synergistic Metabolic Therapy and Immunotherapy of Tumors. *Advanced Mater* (2019) 31;51:e1904639. doi: 10.1002/adma.201904639
2. Yang K, Yu G, Yang Z, Yue L, Zhang X, Sun C, et al. Supramolecular Polymerization-Induced Nanoassemblies for Self-Augmented Cascade Chemotherapy and Chemodynamic Therapy of Tumor. *Angewandte Chem* (2021) 60(32):17570–8. doi: 10.1002/ange.202103721
3. Tang ZM, Liu YY, He MY, Bu WB. Chemodynamic Therapy: Tumour Microenvironment-Mediated Fenton and Fenton-Like Reactions, Angew. *Chem-Int Edit* (2019) 58(4):946–56. doi: 10.1002/anie.201805664
4. Zhu D, Lyu M, Jiang W, Suo M, Huang Q, Li K. A Biomimetic Nanozyme/Camptothecin Hybrid System for Synergistically Enhanced Radiotherapy. *J Mater Chem B* (2020) 8:5312–9. doi: 10.1039/D0TB00676A
5. Pallares RM, Abergel RJ. Nanoparticles for Targeted Cancer Radiotherapy. *Nano Res* (2020) 13(11):2887–97. doi: 10.1007/s12274-020-2957-8
6. Jin C, Bai L, Wu H, Tian F, Guo G. Radiosensitization of Paclitaxel, Etanidazole and Paclitaxel+Etanidazole Nanoparticles on Hypoxic Human Tumor Cells *In Vitro*. *Biomaterials* (2007) 28(25):3724–30. doi: 10.1016/j.biomaterials.2007.04.032
7. Yu X, Li A, Zhao C, Yang K, Chen X, Li W. Ultrasmall Semimetal Nanoparticles of Bismuth for Dual-Modal Computed Tomography/Photoacoustic Imaging and Synergistic Thermoradiotherapy. *ACS Nano* (2017) 11(4):3990–4001. doi: 10.1021/acsnano.7b00476
8. Liu Y, Liu Y, Bu W, Xiao Q, Sun Y, Zhao K, et al. Radiation-/Hypoxia-Induced Solid Tumor Metastasis and Regrowth Inhibited by Hypoxia-Specific Upconversion Nanoradiosensitizer. *Biomaterials* (2015) 49:1–8. doi: 10.1016/j.biomaterials.2015.01.028
9. Wang Z, Shao D, Chang Z, Lu M, Wang Y, Yue J, et al. Janus Gold Nanoplatform for Synergetic Chemoradiotherapy and Computed Tomography Imaging of Hepatocellular Carcinoma. *ACS Nano* (2017) 11(12):12732–41. doi: 10.1021/acsnano.7b07486
10. Huang H, He L, Zhou W, Qu G, Wang J, Yang N, et al. Stable Black Phosphorus/Bi2O3 Heterostructures for Synergistic Cancer Radiotherapy. *Biomaterials* (2018) 171:12–22. doi: 10.1016/j.biomaterials.2018.04.022
11. Lyu M, Zhu D, Li Y, Quan H. Bimetallic Nanodots for Tri-Modal CT/MRI/PA Imaging and Hypoxia-Resistant Thermoradiotherapy in the NIR-II Biological Windows. *Biomaterials* (2019) 223:119656. doi: 10.1016 j.biomaterials.2019.119656

12. Yu X, Tang X, He J, Yi X, Xu G, Tian L, et al. Polydopamine Nanoparticle as a Multifunctional Nanocarrier for Combined Radiophotodynamic Therapy of Cancer. *Particle Particle Syst Characterization* (2017) 34(2):1600296. doi: 10.1002/ppsc.201600296
13. Zhang C, Yan L, Wang X, Dong X, Zhou R, Gu Z, et al. Tumor Microenvironment-Responsive Cu2(OH)PO4 Nanocrystals for Selective and Controllable Radiosentization *via* the X-Ray-Triggered Fenton-Like Reaction. *Nano Lett* (2019) 19(3):1749–57. doi: 10.1021/acs.nanolett.8b04763
14. Ai K, Huang J, Xiao Z, Yang Y, Bai Y, Peng J. Localized Surface Plasmon Resonance Properties and Biomedical Applications of Copper Selenide Nanomaterials. *Mater Today Chem* (2021) 20:100402. doi: 10.1016/j.mtchem.2020.100402
15. Wang J, Sui L, Huang J, Miao L, Nie Y, Wang K, et al. MoS2-Based Nanocomposites for Cancer Diagnosis and Therapy. *Bioact Mater* (2021) 6 (11):4209–42. doi: 10.1016/j.bioactmat.2021.04.021
16. Zhu D, Lyu M, Huang Q, Suo M, Liu Y, Jiang W, et al. Stellate Plasmonic Exosomes for Penetrative Targeting Tumor NIR-II Thermo-Radiotherapy. *ACS Appl Mater Interfaces* (2020) 12(33):36928–37. doi: 10.1021/acsami.0c09969
17. Deng X, Liang S, Cai X, Huang S, Cheng Z, Shi Y, et al. Yolk-Shell Structured Au Nanostar@Metal-Organic Framework for Synergistic Chemo-Photothermal Therapy in the Second Near-Infrared Window. *Nano Lett* (2019) 19(10):6772–80. doi: 10.1021/acs.nanolett.9b01716
18. Sun H, Su J, Meng Q, Yin Q, Chen L, Gu W, et al. Cancer Cell Membrane-Coated Gold Nanocages With Hyperthermia-Triggered Drug Release and Homotypic Target Inhibit Growth and Metastasis of Breast Cancer. *Advanced Funct Mater* (2017) 27(3):1604300. doi: 10.1002/adfm.201604300
19. Li S, Tan L, Meng X. Nanoscale Metal-Organic Frameworks: Synthesis, Biocompatibility, Imaging Applications, and Thermal and Dynamic Therapy of Tumors. *Advanced Funct Mater* (2020) 30(13):1908924. doi: 10.1002/adfm.201908924
20. Liu Y, Ashton JR, Moding EJ, Yuan H, Register JK, Fales AM, et al. A Plasmonic Gold Nanostar Theranostic Probe for *In Vivo* Tumor Imaging and Photothermal Therapy. *Theranostics* (2015) 5(9):946–60. doi: 10.7150/thno.11974
21. Zhu DM, Xie W, Xiao YS, Suo M, Zan MH, Liao QQ, et al. Erythrocyte Membrane-Coated Gold Nanocages for Targeted Photothermal and Chemical Cancer Therapy. *Nanotechnology* (2018) 29(8):084002. doi: 10.1088/1361-6528/aa9ca1
22. Huang C, Ding S, Jiang W, Wang FB. Glutathione-Depleting Nanoplatelets for Enhanced Sonodynamic Cancer Therapy. *Nanoscale* (2021) 13:4512–8. doi: 10.1039/D0NR08440A
23. Liu WL, Zou MZ, Qin SY, Cheng YJ, Ma YH, Sun YX, et al. Recent Advances of Cell Membrane-Coated Nanomaterials for Biomedical Applications. *Advanced Funct Mater* (2020) 30(39):2003559. doi: 10.1002/adfm.202003559
24. Rao L, Meng Q-F, Huang Q, Wang Z, Yu G-T, Li A, et al. Platelet-Leukocyte Hybrid Membrane-Coated Immunomagnetic Beads for Highly Efficient and Highly Specific Isolation of Circulating Tumor Cells. *Advanced Funct Mater* (2018) 28(34):1803531. doi: 10.1002/adfm.201803531
25. Dehaini D, Wei X, Fang RH, Masson S, Angsantikul P, Luk BT, et al. Erythrocyte-Platelet Hybrid Membrane Coating for Enhanced Nanoparticle Functionalization. *Advanced Mater* (2017) 29(16):1606209. doi: 10.1002/adma.201606209
26. Wang Z, Zeng W, Chen Z, Suo W, Quan H, Tan ZJ. An Intratumoral Injectable Nanozyme Hydrogel for Hypoxia-Resistant Thermoradiotherapy. *Colloids Surfaces B Biointerfaces* (2021) 207:112026. doi: 10.1016/j.colsurfb.2021.112026
27. Zhu D, Zhang J, Luo G, Duo Y, Tang BZ. Bright Bacterium for Hypoxia-Tolerant Photodynamic Therapy Against Orthotopic Colon Tumors by an Interventional Method. *Advanced Sci* (2021) e2004769. doi: 10.1002/advs.202004769
28. Zhu DM, Duo YH, Suo M, Zhao YH, Xia LG, Zheng Z, et al. Tumor-Exocytosed Exosome/Aggregation-Induced Emission Luminogen Hybrid Nanovesicles Facilitate Efficient Tumor Penetration and Photodynamic Therapy, Angew. *Chem-Int Edit* (2020) 59(33):13836–43. doi: 10.1002/anie.202003672
29. Zhao Q, Gong Z, Li Z, Wang J, Zhang J, Zhao Z, et al. Target Reprogramming Lysosomes of CD8+ T Cells by a Mineralized Metal-Organic Framework for Cancer Immunotherapy. *Advanced Mater* (2021) 33(17):e2100616. doi: 10.1002/adma.202100616
30. Duan F, Feng X, Yang X, Sun W, Jin Y, Liu H, et al. A Simple and Powerful Co-Delivery System Based on pH-Responsive Metal-Organic Frameworks for Enhanced Cancer Immunotherapy. *Biomaterials* (2017) 122:23–33. doi: 10.1016/j.biomaterials.2017.01.017
31. Chen Q, Xu L, Liang C, Wang C, Peng R, Liu Z. Photothermal Therapy With Immune-Adjuvant Nanoparticles Together With Checkpoint Blockade for Effective Cancer Immunotherapy. *Nat Commun* (2016) 7:13193. doi: 10.1038/ncomms13193
32. Liu X, Liu Z, Dong K, Wu S, Sang Y, Cui T, et al. Tumor-Activatable Ultrasmall Nanozyme Generator for Enhanced Penetration and Deep Catalytic Therapy. *Biomaterials* (2020) 258:120263. doi: 10.1016/j.biomaterials.2020.120263
33. Huang C, Wang FB, Liu L, Jiang W, Liu W, Ma W, et al. Hypoxic Tumor Radiosensitization Using Engineered Probiotics. *Advanced Healthcare Mater* (2021) 10(10):e2002207. doi: 10.1002/adhm.202002207
34. Zhu Y, Shi H, Li T, Yu J, Guo Z, Cheng J, et al. A Dual Functional Nanoreactor for Synergistic Starvation and Photodynamic Therapy. *ACS Appl Mater Interfaces* (2020) 12(16):18309–18. doi: 10.1021/acsami.0c01039
35. Jin L, Hu P, Wang Y, Wu L, Qin K, Cheng H, et al. Fast-Acting Black-Phosphorus-Assisted Depression Therapy With Low Toxicity. *Advanced Mater* (2020) 32(2):e1906050. doi: 10.1002/adma.201906050

Conflict of Interest: The authors declare that the research was conducted in the absence of any commercial or financial relationships that could be construed as a potential conflict of interest.

Publisher's Note: All claims expressed in this article are solely those of the authors and do not necessarily represent those of their affiliated organizations, or those of the publisher, the editors and the reviewers. Any product that may be evaluated in this article, or claim that may be made by its manufacturer, is not guaranteed or endorsed by the publisher.

Copyright © 2021 Chen, Wang, Jiang, Bao and Quan. This is an open-access article distributed under the terms of the Creative Commons Attribution License (CC BY). The use, distribution or reproduction in other forums is permitted, provided the original author(s) and the copyright owner(s) are credited and that the original publication in this journal is cited, in accordance with accepted academic practice. No use, distribution or reproduction is permitted which does not comply with these terms.

frontiers in Pharmacology

ORIGINAL RESEARCH
published: 02 December 2021
doi: 10.3389/fphar.2021.795012

Ultrasmall PEI-Decorated Bi_2Se_3 Nanodots as a Multifunctional Theranostic Nanoplatform for *in vivo* CT Imaging-Guided Cancer Photothermal Therapy

Peng Zhang[1], *Lei Wang*[1], *Xiuying Chen*[1], *Xiang Li*[2] *and Qinghai Yuan*[1]*

[1]Department of Radiology, The Second Hospital of Jilin University, Changchun, China, [2]Department of Radiology, Jilin Province FAW General Hospital, Changchun, China

Bi-based nanomaterials, such as Bi_2Se_3, play an important part in biomedicine, such as photothermal therapy (PTT) and computed tomography (CT) imaging. Polyethylenimine (PEI)-modified ultrasmall Bi_2Se_3 nanodots were prepared using an ultrafast synthetic method at room temperature (25°C). Bi_2Se_3 nanodots exhibited superior CT imaging performance, and could be used as effective photothermal reagents owing to their broad absorption in the ultraviolet–visible–near infrared region. Under irradiation at 808 nm, PEI-Bi_2Se_3 nanodots exhibited excellent photothermal-conversion efficiency of up to 41.3%. Good biocompatibility and significant tumor-ablation capabilities were demonstrated *in vitro* and *in vivo*. These results revealed that PEI-Bi_2Se_3 nanodots are safe and a good nanotheranostic platform for CT imaging-guided PTT of cancer.

Keywords: photothermal therapy, Bi2Se3 nanodots, ultrafast synthesis, CT imaging, cancer therapy

OPEN ACCESS

Edited by:
Kelong Ai,
Central South University, China

Reviewed by:
Dan Li,
The Fifth Affiliated Hospital of Sun Yat-sen University, China
Jing Wang,
Huazhong University of Science and Technology, China

***Correspondence:**
Qinghai Yuan
yuanqinghai123@sina.com

Specialty section:
This article was submitted to Pharmacology of Anti-Cancer Drugs, a section of the journal Frontiers in Pharmacology

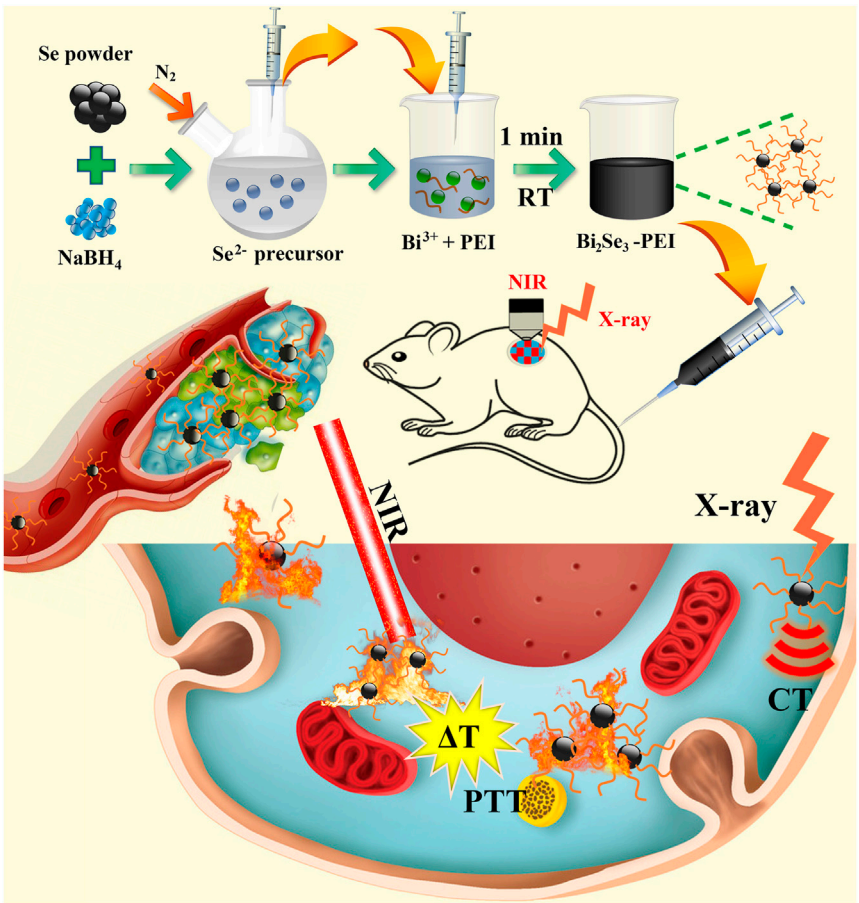
Received: *14 October 2021*
Accepted: *16 November 2021*
Published: *02 December 2021*

Citation:
Zhang P, Wang L, Chen X, Li X and Yuan Q (2021) Ultrasmall PEI-Decorated Bi_2Se_3 Nanodots as a Multifunctional Theranostic Nanoplatform for in vivo CT Imaging-Guided Cancer Photothermal Therapy. Front. Pharmacol. 12:795012. doi: 10.3389/fphar.2021.795012

INTRODUCTION

The early diagnosis of cancer and "precision" medicine are major challenges for oncologists. Scientists need to develop multifunctional biocompatible nanotheranostic platforms that integrate diagnostic and therapeutic functions (Barreto et al., 2011; Ho et al., 2015; Chen et al., 2016). As a non-invasive method, phototherapy can alleviate the side-effects and suffering of treatment as compared with that using resection, chemotherapy, or radiotherapy (Cheng et al., 2014; Fan et al., 2017; Lei et al., 2018; Basak et al., 2019).

Photothermal therapy (PTT) has attracted significant research attention because it is highly efficient, minimally invasive, and controllable (Liu et al., 2019; Meng et al., 2020; Zhao et al., 2020). Recently, PTT agents, such as precious metals (e.g., Au, Pt, or Pd nanoparticles) (Yin et al., 2014; Tang et al., 2015; Zhu et al., 2017; Zhang et al., 2019), metal chalcogenides (e.g., CuS nanoparticles, Bi_2S_3 nanoparticles, Bi_2Se_3 nanosheets, MoS_2 nanosheets, or $MoSe_2$ nanosheets) (Liu et al., 2014; Yang et al., 2016; You et al., 2017; Huang et al., 2019; Wang et al., 2019), carbon derivatives (Bao et al., 2018; Ortega-Liebana et al., 2019), and polymeric nanoparticles (Han et al., 2018; Zhang et al., 2018), have aroused widespread research interest. In particular, Bi_2Se_3, with its broad near absorption in the infrared (NIR) region, excellent efficiency for photothermal conversion, good biocompatibility, and metabolizability, has been used as a PTT agent (Song et al., 2015; Cheng et al., 2016; Xie et al., 2017; Huang et al., 2019). Moreover, due to the high X-ray attenuation coefficient (5.74 cm^2 g^{-1}, 100 keV) and atomic number (Z = 83) of Bi than those of the extensively



SCHEME 1 | Fabrication of PEI-Bi_2Se_3 nanodots for CT imaging-guided PTT of cancer.

applied contrast agent iobitridol (X-ray attenuation coefficient of 1.94 $cm^2\ g^{-1}$, 100 keV; Z = 53), Bi-based nanomaterials can be used as potential contrast agents for computed tomography (CT) (Lei et al., 2017). Thus, Bi_2Se_3 has been used widely as a powerful nanotheranostic agent in CT imaging-guided PTT of cancer. However, most reports have focused on the synthesis of Bi_2Se_3 nanosheets at high temperatures (Xiao et al., 2017; Xie et al., 2017). Nevertheless, the synthesis is more complicated, and a larger particle size is not conducive to biological metabolism. Only a few reports have focused on the ultrarapid synthesis of water-soluble ultrasmall Bi_2Se_3 nanodots at room temperature (25°C).

We report a facile room-temperature method for synthesizing ultrasmall polyethylenimine-decorated Bi_2Se_3 (PEI-Bi_2Se_3) nanodots for CT imaging-guided PTT of cancer *in vitro* and *in vivo*. Compared with strategies reported previously, the rapid synthesis of PEI-Bi_2Se_3 nanodots may improve the efficiency of the synthesis and prevent further surface modification. Furthermore, the raw materials are inexpensive, and the organic solvents are nontoxic and environmentally friendly, thereby making the process suitable for future production at a large scale.

The synthesized nanodots exhibited excellent absorption properties and the efficiency of photothermal conversion was high under laser irradiation at 808 nm. Moreover, the outstanding CT imaging and photothermal-ablation capacity observed *in vitro* and *in vivo*, and non-significant long-term toxicity observed *in vivo*, revealed that PEI-Bi_2Se_3 nanodots could achieve CT imaging-guided PTT of cancer. Hence, PEI-Bi2Se3 nanodots could be powerful and safe nanotheranostic agents in cancer therapy.

RESULTS AND DISCUSSION

The Synthesis and Characterization of PEI-Bi_2Se_3 Nanodots

A novel NIR light-responsive nanotheranostic platform based on PEI-Bi_2Se_3 nanodots for CT imaging-guided PTT of cancer was fabricated (**Scheme 1**). Under the protection of an inert-gas atmosphere and ice-water bath, Se powder was reduced by $NaBH_4$ under magnetic stirring at room temperature (25°C) to obtain NaHSe solution (Se^{2-} precursor solution). An appropriate amount of the Se^{2-} precursor solution was

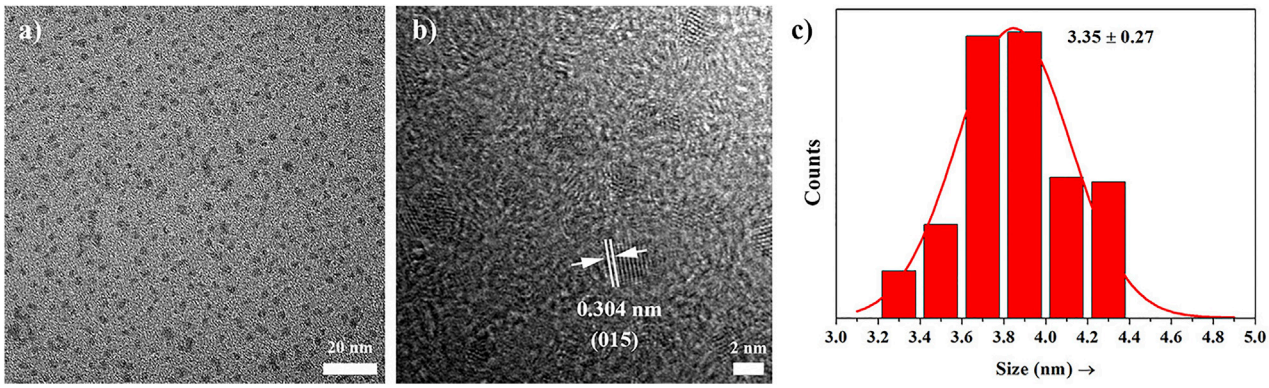


FIGURE 1 | (A) TEM image, **(B)** HRTEM image, and **(C)** size histogram of PEI-Bi_2Se_3 nanodots.

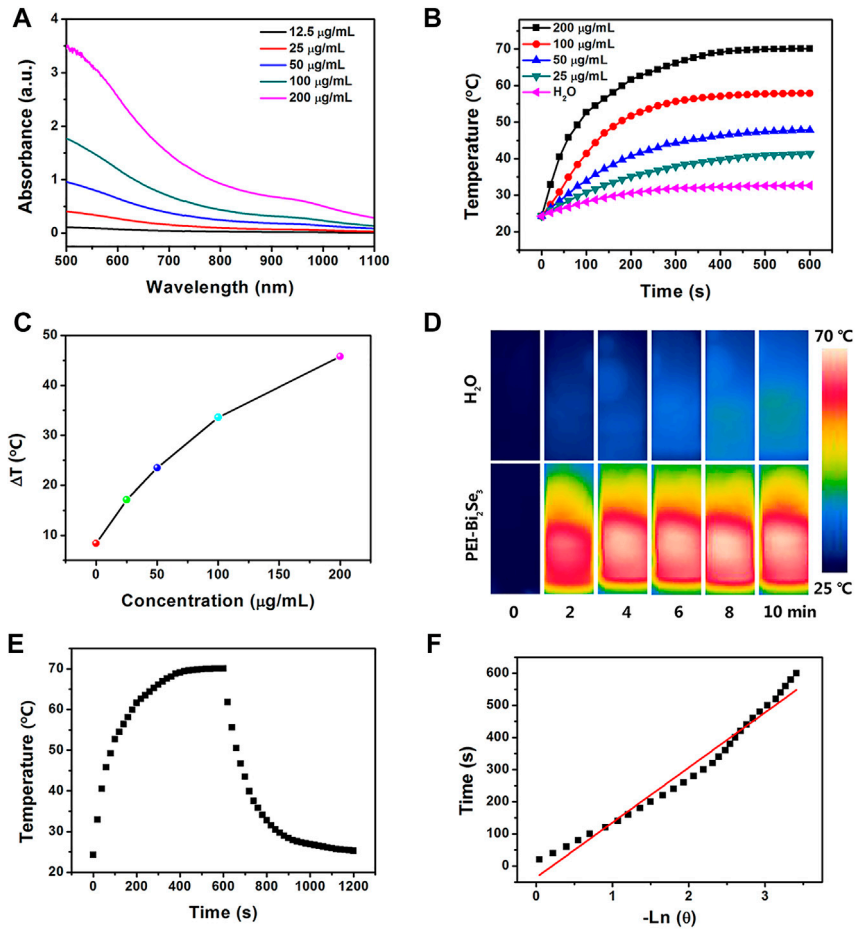


FIGURE 2 | (A) UV–Vis–NIR absorption spectra of PEI-Bi_2Se_3 nanodots in water with different concentrations of Bi^{+3}. **(B)** Plot of temperature increase of pure water and aqueous solutions of PEI-Bi_2Se_3 nanodots of different concentrations upon exposure to a NIR laser at 808 nm (1.0 Wcm^{-2}) as a function of irradiation duration. The temperature was measured every 10 s using a thermocouple microprobe. **(C)** Plot of temperature change (Δ*T*) over a period of 600 s vs. the concentration of PEI-Bi_2Se_3 nanodots. **(D)** IR thermal images of an aqueous solution of PEI-Bi_2Se_3 nanodots (200 μg ml^{-1}) and pure water after irradiation for 10 min (808 nm, 1.0 W cm^{-2}). **(E)** Photothermal response of an aqueous solution of PEI-Bi_2Se_3 nanodots (200 μg ml^{-1}) after irradiation for 600 s with an NIR laser (808 nm, 1.0 W cm^{-2}). Subsequently, the laser was turned off. **(F)** Linear time data vs. −ln*θ* obtained after a cooling period of **(E)**.

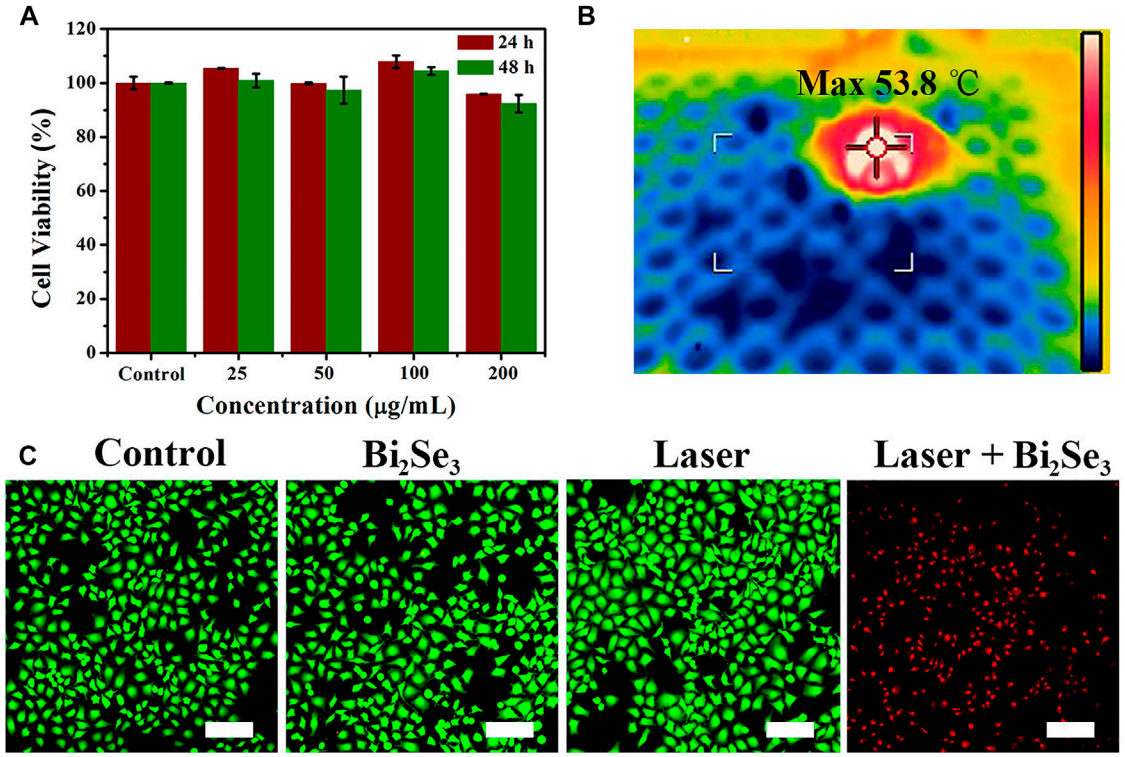


FIGURE 3 | (A) Viability of A549 cells incubated with PEI-Bi_2Se_3 nanodots (0–200 μg ml^{-1}) for 24 and 48 h **(B)** IR thermal images of A549 cells in a 96-well plate incubated with PEI-Bi_2Se_3 nanodots after irradiation for 10 min (808 nm, 1.0 W cm^{-2}). **(C)** Fluorescence images of A549 cells stained with calcein-AM (live cells, green) and PI (dead cells, red) after various treatments. Scale bar = 200 μm.

transferred rapidly to a mixed solution of ethylene glycol and water containing $Bi(NO_3)_3{\cdot}5H_2O$ and PEI. The reaction solution turned black rapidly, indicating that the reaction was ultra-facile and efficient (within 1 min). In the Experimental section in Supplementary Material, the experimental details are presented. Moreover, Bi_2Se_3 nanodots had promising potential for CT imaging-guided PTT of cancer owing to an efficient photothermal performance, strong absorption in the NIR region, and the high X-ray attenuation coefficient of Bi^{3+}.

A transmission electron microscopy (TEM) image of the obtained PEI-Bi_2Se_3 nanodots is shown in **Figure 1A**. A clear lattice fringe with a distance of 0.304 nm can be seen on the high-resolution TEM image (**Figure 1B**), which can be attributed to the (015) planes of Bi_2Se_3. Furthermore, the prepared PEI-Bi_2Se_3 nanodots, as uniform spheres with relatively narrow size distribution, had a mean diameter of 3.56 nm (**Figure 1C**). The X-ray diffraction (XRD) patterns of the prepared PEI-Bi_2Se_3 nanodots are shown in **Supplementary Figure S1**. All the characteristic XRD peaks matched well with the standard hexagonal phase of Bi_2Se_3 (Joint Committee on Powder Diffraction Standards = 33-0214). Moreover, PEI-Bi_2Se_3 nanodots could maintain good dispersity in various solutions, such as Dulbecco's modified Eagle's medium, phosphate-buffered saline (PBS), NaCl, and water, for several months (**Supplementary Figure S2**), indicating that the PEI modification was beneficial for improving the stability of PEI-Bi_2Se_3 nanodots.

Photothermal Performance of PEI-Bi_2Se_3 Nanodots *in vitro*

PEI-Bi_2Se_3 nanodots showed a broad ultraviolet–visible–NIR (UV–Vis–NIR) absorption spectrum ranging from 500 to 1,100 nm (**Figure 2A**). As the concentration of Bi^{3+} increased, the absorption intensity of PEI-Bi_2Se_3 nanodots was enhanced, and the colorless solution turned dark black (**Supplementary Figure S3**). Absorbance at 808 nm increased linearly (**Supplementary Figure S4**), which suggested that PEI-Bi_2Se_3 nanodots exhibited good dispersibility in water, and could be excellent photothermal agents for PTT. To investigate the photothermal performance, pure water (control) and aqueous solutions of PEI-Bi_2Se_3 nanodots (25, 50, 100, 200 μg/ml) were exposed to a NIR laser (808 nm, 1.0 W cm^{-2}) for 10 min. The temperatures of the different PEI-Bi_2Se_3 nanodot solutions increased rapidly, exhibiting noticeable concentration- and irradiation time-dependent behavior (**Figure 2B**). This finding indicated that the temperature of the PEI-Bi_2Se_3 solution could reach up to 70.1°C at a concentration of 200 μg ml^{-1} (1.0 W cm^{-2}, 10 min), which is highly effective for killing tumor cells *via* hyperthermia. In contrast, under identical experimental conditions, the temperature of pure water increased by up to 8.4°C (**Figure 2C**). The IR thermal images of pure water and

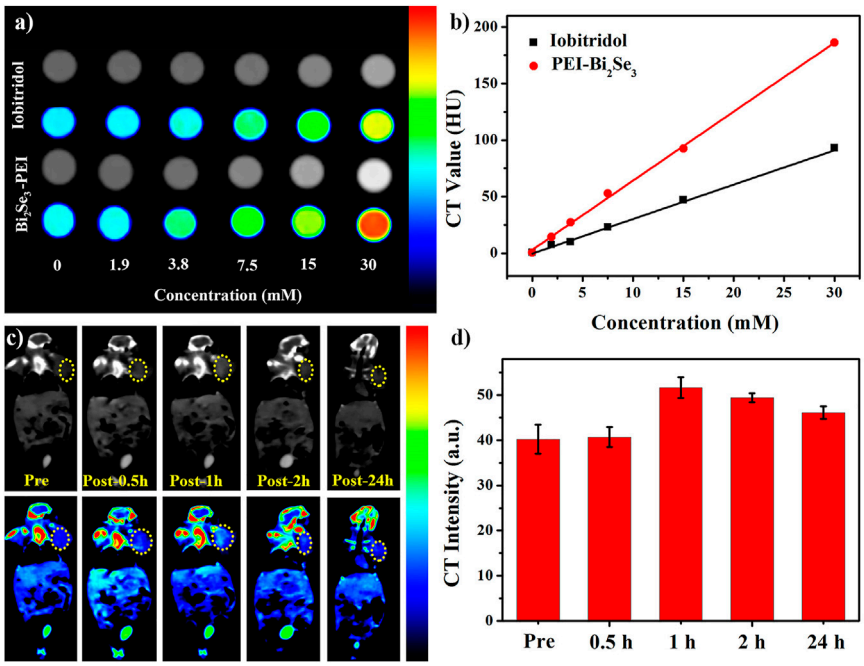


FIGURE 4 | (A) *In vitro* CT images of iobitridol and PEI-Bi_2Se_3 nanodots at different concentrations. **(B)** Concentration-dependent CT signals of iobitridol (black line) and PEI-Bi_2Se_3 nanodots (red line) *in vitro*. **(C)** Time-dependent CT imaging of tumor-bearing mice before and after intravenous injection of PEI-Bi_2Se_3 nanodots. **(D)** CT signal intensities of the tumor area at different times.

aqueous solution of PEI-Bi_2Se_3 nanodots (200 μg ml^{-1}) after a certain duration of irradiation are shown in **Figure 2D**. The temperature of the PEI-Bi_2Se_3 aqueous solution (200 μg ml^{-1}) increased rapidly with an increase in the irradiation duration using a laser at 808 nm whereas, under identical conditions, the temperature of pure water increased slowly.

PEI-Bi_2Se_3 nanodots could therefore convert NIR energy into thermal energy rapidly and efficiently, and act as potential photothermal agents during PTT. In particular, the efficiency of photothermal conversion of PEI-Bi_2Se_3 nanodots was up to 41.3% (**Figures 2E,F**), which is much higher than that of currently reported photothermal agents, such as PVP-Bi nanodots (~30%) (Lei et al., 2017), Bi_2Se_3 nanosheets (~33%) (Xie et al., 2017), and $Cu_{2-x}Se$ nanocrystals (~22%) (Hessel et al., 2011). Photostability is another prerequisite for evaluating the performance of photothermal agents during PTT. After irradiation of the aqueous solution of PEI-Bi_2Se_3 nanodots (200 μg ml^{-1}) using a continuous-wave NIR laser at 808 nm for 1 h (1.0 W cm^{-2}), the color of the solution, UV–Vis–NIR spectrum, and morphology exhibited no distinct changes (**Supplementary Figures S5, S6**). Hence, PEI-Bi_2Se_3 nanodots possessed satisfactory photothermal stability. All the results shown above (excellent photothermal effect and good photostability) highlighted the potential of PEI-Bi_2Se_3 nanodots as suitable agents for PTT of cancer.

Studies on Cytotoxicity and Photothermal Ablation of Tumor Cells

Evaluation of the cytotoxicity of PEI-Bi_2Se_3 nanodots is important. The cytotoxicity of PEI-Bi_2Se_3 nanodots was tested by the Cell Counting Kit-8 assay. Even at a high concentration of PEI-Bi_2Se_3 nanodots (200 μg ml^{-1}), the viability of A549 cells was 96 and 92% after incubation for 24 h (red bars) and 48 h (green bars), respectively (**Figure 3A**). These results indicated that PEI-Bi_2Se_3 nanodots exhibited no distinct toxicity towards A549 cells.

Because of the outstanding photothermal performance of PEI-Bi_2Se_3 nanodots, we investigated their photothermal effects against tumor cells. The IR thermal images of A549 cells incubated with PEI-Bi_2Se_3 nanodots in a 96-well plate are shown in **Figure 3B**. Notably, the temperature could increase up to 53.8°C under irradiation at 808 nm (1.0 W cm^{-2}) after addition of PEI-Bi_2Se_3 nanodots to the culture. Cancer cells are sensitive to heat, and can be killed effectively at >42°C. To identify further the anti-cancer effect of PEI-Bi_2Se_3 nanodots on A549 cells, live and dead cells were imaged using a fluorescence microscope after staining with calcein acetoxymethyl ester (green fluorescence) and propidium iodide (red fluorescence), respectively. In the control groups, notable cytotoxicity was not observed (PBS, PEI-Bi_2Se_3 nanodots only, laser only), whereas almost no living cells were observed in the PEI-Bi_2Se_3 + laser group (**Figure 3C**). These results suggested that the as-synthesized PEI-Bi_2Se_3 nanodots with low cytotoxicity would produce satisfactory results upon *in vivo* cancer treatment. In addition, endocytosis pathways were determined in order to identify the uptake mechanism of extracellular PEI-Bi_2Se_3 nanodots. The cellular uptake of PEI-Bi_2Se_3 was evaluated by monitoring the fluorescence of FITC in the A549 cells at various incubation times (1, 3, and 6 h). As shown in **Supplementary Figure S7**, green fluorescence of FITC was observed after 1 h incubation with FITC-labeled PEI-Bi_2Se_3. The

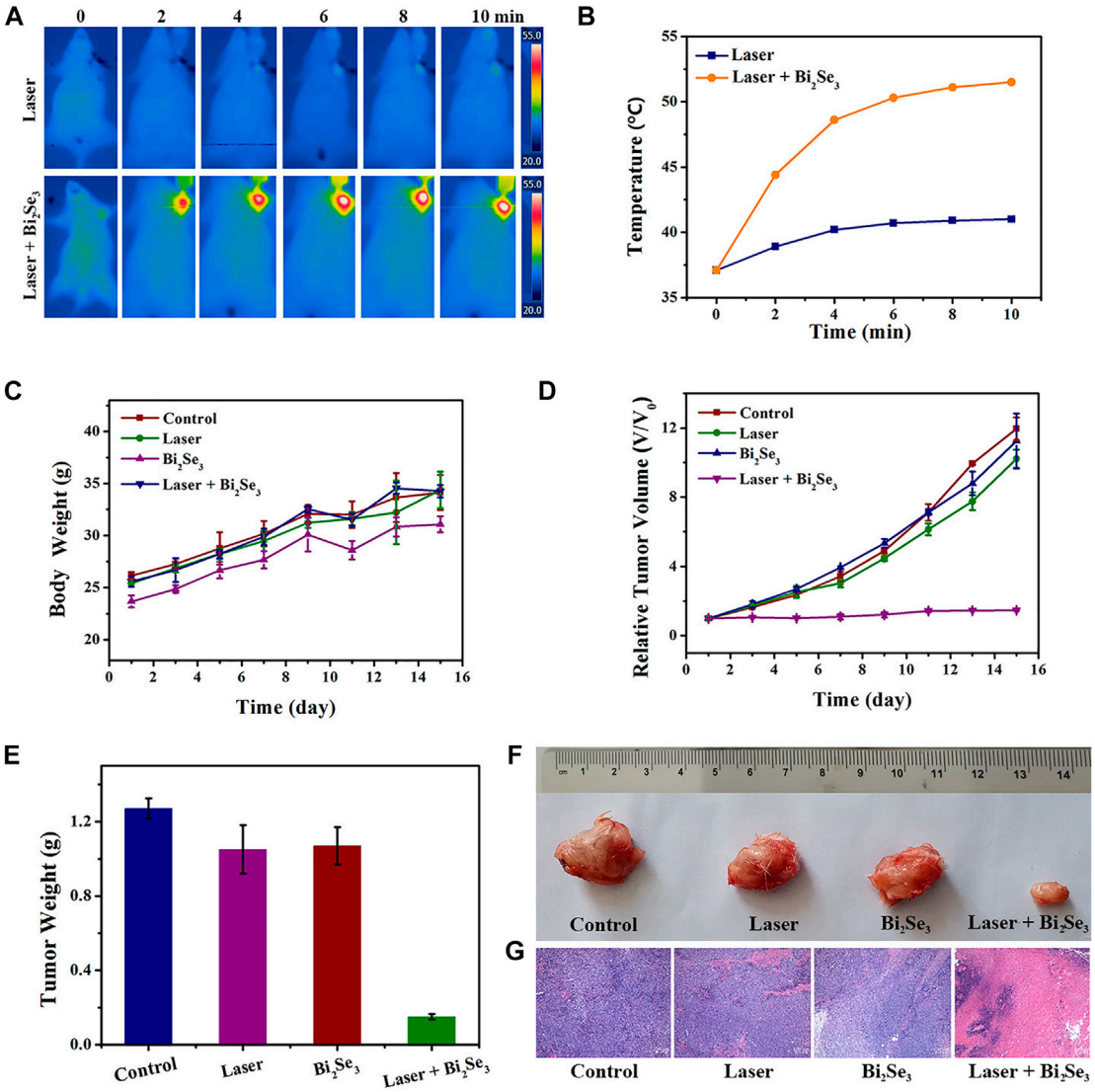


FIGURE 5 | (A) IR thermal images and **(B)** corresponding curve showing the temperature variation of tumor-bearing mice injected (i.v.) with PBS (control) or PEI-Bi_2Se_3 nanodots, followed by irradiation with a laser at 808 nm for 10 min **(C)** Bodyweight of mice and **(D)** curves showing relative tumor growth in different groups after various treatments. **(E)** Mean tumor weight of each group after various treatments. **(F)** Photographs of tumors of each group and **(G)** H&E staining of tumor slides collected from different groups. All scale bars = 100 μm.

signals increase obviously with incubation time, demonstrating efficient internalization of PEI-Bi_2Se_3 by cancer cells.

CT Imaging *in vitro* and *in vivo*

High resolution, easy manipulation, and high penetrability make CT imaging an important part of medical diagnoses (Lee et al., 2013; Du et al., 2020). Bi element with its large atomic number and high electron density has promising capacity for X-ray attenuation (Kinsella et al., 2011; Li et al., 2016). The X-ray absorption coefficient and iobitridol were compared to evaluate the *in vitro* CT imaging capability of PEI-Bi_2Se_3 nanodots. The latter exhibited a much higher CT density than that of iobitridol at equivalent concentrations (**Figure 4A**), whereas the Hounsfield unit (HU) values of both contrast agents exhibited a typical linear dependence on the concentration (**Figure 4B**). Compared with the curve for iobitridol, the curve for PEI-Bi_2Se_3 nanodots had a steeper slope. Hence, the as-synthesized PEI-Bi_2Se_3 nanodots had superior ability in CT imaging and were effective contrast agents.

Inspired by the satisfactory CT effect *in vitro*, we assessed the feasibility of using PEI-Bi_2Se_3 nanodots as CT contrast agents *in vivo*. Time-dependent CT imaging was undertaken after tumor-bearing mice were injected (i.v.) with PEI-Bi_2Se_3 nanodots (Bi concentration = 30 mM, 150 μL). At 0 h–1 h after injection, the CT density at the tumor site brightened gradually (**Figure 4C**), which was caused by passive accumulation of PEI-Bi_2Se_3 nanodots at the tumor site through the enhanced permeability and retention effect. Thereafter, the density decreased because some PEI-Bi_2Se_3 nanodots had metabolized. The mean HU value

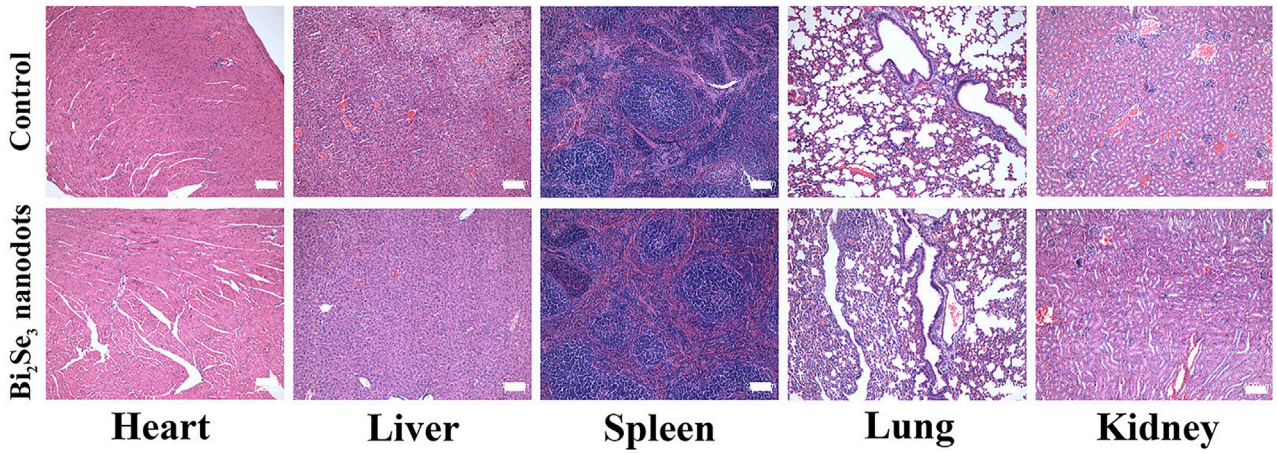


FIGURE 6 | H&E staining of major organs (heart, liver, spleen, lungs, and kidneys) of mice 30 days after injection of PEI-Bi_2Se_3 nanodots. All scale bars = 100 μm.

increased from 40.2 HU (pre-injection) to 40.7 HU (0.5 h) and 51.6 HU (1 h) and decreased gradually from 49.4 HU (2 h) to 46.1 HU (24 h) at the tumor site (**Figure 4D**). These results demonstrated that PEI-Bi_2Se_3 nanodots could serve as promising *in vivo* CT contrast agents for the accurate diagnosis of cancer.

Photothermal Effect, Photothermal Therapy, and Long-Term Toxicity of PEI-Bi_2Se_3 Nanodots *in vivo*

Based on the good properties of PEI-Bi_2Se_3 nanodots at tumor sites (i.e., excellent *in vitro* photothermal effect, satisfactory CT imaging effect, and outstanding passive targeted accumulation), we studied the feasibility of CT imaging-guided PTT of cancer *in vivo*. PEI-Bi_2Se_3 nanodots (Bi concentration = 20 mg kg^{-1}) were injected (i.v.) into tumor-bearing mice. Obvious enhancement was observed 1 h after injection, so the tumor was irradiated using a laser at 808 nm (1.0 W cm^{-2}) 1-h later, and the photothermal effect *in vivo* was monitored by an IR thermal camera. The temperature at the tumor site in the treatment group increased rapidly as the duration of irradiation increased (**Figure 5A**) but the temperature at the tumor site did not show a significant change compared with that in the control group. The corresponding curve detailing temperature variation is shown as **Figure 5B**. After 10 min of NIR irradiation (808 nm, 1.0 W cm^{-2}), in the presence of PEI-Bi_2Se_3 nanodots, the temperature at the tumor sites was as high as 51.1°C whereas, in the control group, a minor increase in temperature was observed. Hence, PEI-Bi_2Se_3 nanodots could serve as excellent photothermal agents for *in vivo* tumor ablation: they could kill cancer cells and inhibit their continued diffusion.

A tumor model was established by injecting (s.c.) U14 cells into the left axilla of female Kunming mice. Once the tumors had grown to ~100 mm^3, mice were used for experimentation. The mice bearing the U14 cells were divided randomly into four groups of six: 1) control; 2) laser only; 3) PEI-Bi_2Se_3 nanodots; 4) PEI-Bi_2Se_3 nanodots + laser. The tumors in mice were irradiated (808 nm) 1 h after injection of PEI-Bi_2Se_3 nanodots. The bodyweight and tumor volume of mice were measured every 2 days to evaluate therapeutic efficacy. After various treatments, the bodyweight of mice showed a steady increase (**Figure 5C**), thereby indicating that PEI-Bi_2Se_3 nanodots did not produce toxic side-effects during PTT. The tumor volume of each mouse was measured using a Vernier caliper, and plotted as a function of the relative tumor volume and treatment duration (**Figure 5D**). The average weights of excised tumors are shown in **Figure 5E**, and representative tumor photographs of each group are shown in **Figure 5F**. Compared with groups 1–3, the growth of tumors in group 4 was inhibited significantly after 14 days of PTT. In addition, hematoxylin and eosin (H&E) staining revealed no appreciable damage in groups 1–3; simultaneously, severe shrinkage and discrete cancer cells were observed clearly in group 4 (**Figure 5G**). Taken together, these results demonstrated that PEI-Bi_2Se_3 nanodots possessed potential as ideal and safe photothermal agents for cancer treatment.

The potential long-term toxicity of PEI-Bi_2Se_3 nanodots *in vivo* was also investigated. Thirty days after injection, pathological samples of major organs (heart, lungs, liver, spleen, kidneys) from control mice and treated mice were obtained. H&E staining (**Figure 6**) revealed no distinct tissue damage or inflammatory lesions in any major organ. Moreover, there were no abnormal signs in treated mice during the entire observation period. These results confirmed that PEI-Bi_2Se_3 nanodots were not significantly toxic *in vivo*.

CONCLUSION

Ultrasmall PEI-Bi_2Se_3 nanodots were fabricated *via* an ultrafast, facile, and environmentally friendly method. The obtained PEI-Bi_2Se_3 nanodots could ensure good contrast enhancement owing to their high X-ray attenuation coefficient, and showed good photothermal killing effects *in vitro* and *in vivo* owing to considerable photothermal-conversion effects. Moreover, PEI-Bi_2Se_3 nanodots possessed negligible long-term toxicity *in vivo*.

Therefore, we believe that the as-synthesized PEI-Bi_2Se_3 nanodots are useful theranostic agents for CT-imaging-guided PTT of cancer.

DATA AVAILABILITY STATEMENT

The original contributions presented in the study are included in the article/**Supplementary Material**, further inquiries can be directed to the corresponding author.

ETHICS STATEMENT

The animal study was reviewed and approved by the Laboratory Animal Center of Jilin University.

AUTHOR CONTRIBUTIONS

PZ contributed to the conception and design of the study. XL provided the database for mice experiments. LW contributed to the data analysis of the revised manuscript. XL and XC provided the testing instruments and site. PZ wrote the first draft of the manuscript. XC and QY revised and edited the manuscript. All authors contributed to the manuscript and approved the submitted version.

FUNDING

This work was supported by the Bethune Science Support Program of Jilin University (No. 2018B33), Program of Science and Technology Development Plan of Jilin Province of China (No. 20190201218JC), the Health Special Project of Jilin Province Department of Finance (Nos. 2019SCE7025, 2020SCZT088).

SUPPLEMENTARY MATERIAL

The Supplementary Material for this article can be found online at: https://www.frontiersin.org/articles/10.3389/fphar.2021.795012/full#supplementary-material

REFERENCES

Bao, X., Yuan, Y., Chen, J. Q., Zhang, B. H., Li, D., Zhou, D., et al. (2018). *In Vivo* Theranostics with Near-Infrared-Emitting Carbon Dots – Highly Efficient Photothermal Therapy Based on Passive Targeting after Intravenous Administration. *Light-sci. Appl.* 7, 11. doi:10.1038/s41377-018-0090-1

Barreto, J. A., O'Malley, W., Kubeil, M., Graham, B., Stephan, H., and Spiccia, L. (2011). Nanomaterials: Applications in Cancer Imaging and Therapy. *Adv. Mater.* 23 (12), H18–H40. doi:10.1002/adma.201100140

Basak, K., Luís Deán-Ben, X., Gottschalk, S., Reiss, M., and Razansky, D. (2019). Non-invasive Determination of Murine Placental and Foetal Functional Parameters with Multispectral Optoacoustic Tomography. *Light Sci. Appl.* 8, 71. doi:10.1038/s41377-019-0181-7

Chen, G., Roy, I., Yang, C., and Prasad, P. N. (2016). Nanochemistry and Nanomedicine for Nanoparticle-Based Diagnostics and Therapy. *Chem. Rev.* 116 (5), 2826–2885. doi:10.1021/acs.chemrev.5b00148

Cheng, L., Shen, S., Shi, S., Yi, Y., Wang, X., Song, G., et al. (2016). FeSe2-Decorated Bi2Se3 Nanosheets Fabricated via Cation Exchange for Chelator-free 64Cu-Labeling and Multimodal Image-Guided Photothermal-Radiation Therapy. *Adv. Funct. Mater.* 26 (13), 2185–2197. doi:10.1002/adfm.201504810

Cheng, L., Wang, C., Feng, L., Yang, K., and Liu, Z. (2014). Functional Nanomaterials for Phototherapies of Cancer. *Chem. Rev.* 114 (21), 10869–10939. doi:10.1021/cr400532z

Du, K., Lei, P., Dong, L., Zhang, M., Gao, X., Yao, S., et al. (2020). *In Situ* decorating of Ultrasmall Ag2Se on Upconversion Nanoparticles as Novel Nanotheranostic Agent for Multimodal Imaging-Guided Cancer Photothermal Therapy. *Appl. Mater. Today* 18, 100497. doi:10.1016/j.apmt.2019.100497

Fan, W., Yung, B., Huang, P., and Chen, X. (2017). Nanotechnology for Multimodal Synergistic Cancer Therapy. *Chem. Rev.* 117 (22), 13566–13638. doi:10.1021/acs.chemrev.7b00258

Han, Y., Chen, Z., Zhao, H., Zha, Z., Ke, W., Wang, Y., et al. (2018). Oxygen-independent Combined Photothermal/Photodynamic Therapy Delivered by Tumor Acidity-Responsive Polymeric Micelles. *J. Control Release* 284, 15–25. doi:10.1016/j.jconrel.2018.06.012

Hessel, C. M., Pattani, V. P., Rasch, M., Panthani, M. G., Koo, B., Tunnell, J. W., et al. (2011). Copper Selenide Nanocrystals for Photothermal Therapy. *Nano Lett.* 11 (6), 2560–2566. doi:10.1021/nl201400z

Ho, D. A., Wang, C. H. K., and Chow, E. K. H. (2015). Nanodiamonds: the Intersection of Nanotechnology, Drug Development, and Personalized Medicine. *Sci. Adv.* 1 (7), 14. doi:10.1126/sciadv.1500439

Huang, Y., Huang, J., Jiang, M., and Zeng, S. (2019). NIR-triggered Theranostic Bi2S3 Light Transducer for On-Demand NO Release and Synergistic Gas/Photothermal Combination Therapy of Tumors. *ACS Appl. Bio Mater.* 2 (11), 4769–4776. doi:10.1021/acsabm.9b00522

Kinsella, J. M., Jimenez, R. E., Karmali, P. P., Rush, A. M., Kotamraju, V. R., Gianneschi, N. C., et al. (2011). X-Ray Computed Tomography Imaging of Breast Cancer by Using Targeted Peptide-Labeled Bismuth Sulfide Nanoparticles. *Angew. Chem. Int. Ed. Engl.* 50 (51), 12308–12311. doi:10.1002/anie.201104507

Lee, N., Choi, S. H., and Hyeon, T. (2013). Nano-sized CT Contrast Agents. *Adv. Mater.* 25 (19), 2641–2660. doi:10.1002/adma.201300081

Lei, P., An, R., Zhang, P., Yao, S., Song, S., Dong, L., et al. (2017). Ultrafast Synthesis of Ultrasmall Poly(Vinylpyrrolidone)-Protected Bismuth Nanodots as a Multifunctional Theranostic Agent for *In Vivo* Dual-Modal CT/Photothermal-imaging-guided Photothermal Therapy. *Adv. Funct. Mater.* 27 (35), 1702018. doi:10.1002/adfm.201702018

Lei, P., An, R., Zheng, X., Zhang, P., Du, K., Zhang, M., et al. (2018). Ultrafast Synthesis of Ultrasmall Polyethylenimine-Protected AgBiS2 Nanodots by "rookie Method" for *In Vivo* Dual-Modal CT/PA Imaging and Simultaneous Photothermal Therapy. *Nanoscale* 10 (35), 16765–16774. doi:10.1039/c8nr04870c

Li, Z., Liu, J., Hu, Y., Howard, K. A., Li, Z., Fan, X., et al. (2016). Multimodal Imaging-Guided Antitumor Photothermal Therapy and Drug Delivery Using Bismuth Selenide Spherical Sponge. *ACS Nano* 10 (10), 9646–9658. doi:10.1021/acsnano.6b05427

Liu, T., Wang, C., Gu, X., Gong, H., Cheng, L., Shi, X., et al. (2014). Drug Delivery with PEGylated MoS2 Nano-Sheets for Combined Photothermal and Chemotherapy of Cancer. *Adv. Mater.* 26 (21), 3433–3440. doi:10.1002/adma.201305256

Liu, Y., Bhattarai, P., Dai, Z., and Chen, X. (2019). Photothermal Therapy and Photoacoustic Imaging via Nanotheranostics in Fighting Cancer. *Chem. Soc. Rev.* 48 (7), 2053–2108. doi:10.1039/c8cs00618k

Meng, X., Zhang, B., Yi, Y., Cheng, H., Wang, B., Liu, Y., et al. (2020). Accurate and Real-Time Temperature Monitoring during MR Imaging Guided PTT. *Nano Lett.* 20 (4), 2522–2529. doi:10.1021/acs.nanolett.9b05267

Ortega-Liebana, M. C., Encabo-Berzosa, M. M., Casanova, A., Pereboom, M. D., Alda, J. O., Hueso, J. L., et al. (2019). Upconverting Carbon Nanodots from Ethylenediaminetetraacetic Acid (EDTA) as Near-Infrared Activated Phototheranostic Agents. *Chemistry* 25 (21), 5539–5546. doi:10.1002/chem.201806307

Song, G., Liang, C., Gong, H., Li, M., Zheng, X., Cheng, L., et al. (2015). Core-Shell MnSe@Bi2Se3Fabricated via a Cation Exchange Method as Novel Nanotheranostics for Multimodal Imaging and Synergistic Thermoradiotherapy. *Adv. Mater.* 27 (40), 6110–6117. doi:10.1002/adma.201503006

Tang, S., Chen, M., and Zheng, N. (2015). Multifunctional Ultrasmall Pd Nanosheets for Enhanced Near-Infrared Photothermal Therapy and Chemotherapy of Cancer. *Nano Res.* 8 (1), 165–174. doi:10.1007/s12274-014-0605-x

Wang, Y., Zhao, J. X., Chen, Z., Zhang, F., Wang, Q., Guo, W., et al. (2019). Construct of $MoSe_2/Bi_2Se_3$ Nanoheterostructure: Multimodal CT/PT Imaging-Guided PTT/PDT/Chemotherapy for Cancer Treating. *Biomaterials* 217, 13. doi:10.1016/j.biomaterials.2019.119282

Xiao, L., Zhu, A., Xu, Q., Chen, Y., Xu, J., and Weng, J. (2017). Colorimetric Biosensor for Detection of Cancer Biomarker by Au Nanoparticle-Decorated Bi2Se3 Nanosheets. *ACS Appl. Mater. Inter.* 9 (8), 6931–6940. doi:10.1021/acsami.6b15750

Xie, H., Shao, J., Wang, J., Sun, Z., Yu, X.-F., and Wang, Q.-Q. (2017). Near-infrared Optical Performances of Two Bi2Se3nanosheets. *RSC Adv.* 7 (79), 50234–50238. doi:10.1039/c7ra09872c

Yang, W., Guo, W., Le, W., Lv, G., Zhang, F., Shi, L., et al. (2016). Albumin-bioinspired Gd:CuS Nanotheranostic Agent for *In Vivo* Photoacoustic/Magnetic Resonance Imaging-Guided Tumor-Targeted Photothermal Therapy. *ACS Nano* 10 (11), 10245–10257. doi:10.1021/acsnano.6b05760

Yin, Z., Zhang, W., Fu, Q., Yue, H., Wei, W., Tang, P., et al. (2014). Construction of Stable Chainlike Au Nanostructures via Silica Coating and Exploration for Potential Photothermal Therapy. *Small* 10 (18), 3619–3624. doi:10.1002/smll.201400474

You, Q., Sun, Q., Wang, J., Tan, X., Pang, X., Liu, L., et al. (2017). A Single-Light Triggered and Dual-Imaging Guided Multifunctional Platform for Combined Photothermal and Photodynamic Therapy Based on TD-Controlled and ICG-Loaded CuS@mSiO2. *Nanoscale* 9 (11), 3784–3796. doi:10.1039/c6nr09042g

Zhang, H., Wang, Y., Zhong, H., Li, J., and Ding, C. (2019). Near-infrared Light-Activated Pt@Au Nanorings-Based Probe for Fluorescence Imaging and Targeted Photothermal Therapy of Cancer Cells. *ACS Appl. Bio Mater.* 2 (11), 5012–5020. doi:10.1021/acsabm.9b00712

Zhang, L., Qin, Y., Zhang, Z., Fan, F., Huang, C., Lu, L., et al. (2018). Dual pH/Reduction-Responsive Hybrid Polymeric Micelles for Targeted Chemo-Photothermal Combination Therapy. *Acta Biomater.* 75, 371–385. doi:10.1016/j.actbio.2018.05.026

Zhao, S., Tian, R., Shao, B., Feng, Y., Yuan, S., Dong, L., et al. (2020). UCNP-bi 2 Se 3 Upconverting Nanohybrid for Upconversion Luminescence and CT Imaging and Photothermal Therapy. *Chem. Eur. J.* 26, 1127–1135. doi:10.1002/chem.201904586

Zhu, H., Wang, Y., Chen, C., Ma, M., Zeng, J., Li, S., et al. (2017). Monodisperse Dual Plasmonic Au@Cu2-xE (E= S, Se) Core@Shell Supraparticles: Aqueous Fabrication, Multimodal Imaging, and Tumor Therapy at *In Vivo* Level. *ACS Nano* 11 (8), 8273–8281. doi:10.1021/acsnano.7b03369

Conflict of Interest: The authors declare that the research was conducted in the absence of any commercial or financial relationships that could be construed as a potential conflict of interest.

Publisher's Note: All claims expressed in this article are solely those of the authors and do not necessarily represent those of their affiliated organizations, or those of the publisher, the editors and the reviewers. Any product that may be evaluated in this article, or claim that may be made by its manufacturer, is not guaranteed or endorsed by the publisher.

Copyright © 2021 Zhang, Wang, Chen, Li and Yuan. This is an open-access article distributed under the terms of the Creative Commons Attribution License (CC BY). The use, distribution or reproduction in other forums is permitted, provided the original author(s) and the copyright owner(s) are credited and that the original publication in this journal is cited, in accordance with accepted academic practice. No use, distribution or reproduction is permitted which does not comply with these terms.

frontiers in Pharmacology

ORIGINAL RESEARCH
published: 20 December 2021
doi: 10.3389/fphar.2021.799588

Delivery of siRNA Using Functionalized Gold Nanorods Enhances Anti-Osteosarcoma Efficacy

Man Zhang [1,2,3†], Jinti Lin [1,2,3†], Jiakang Jin [1,2,3], Wei Yu [1,2,3], Yiying Qi [1,2,3]* and Huimin Tao [1,2,3]**

[1]Department of Orthopedic Surgery, the Second Affiliated Hospital, Zhejiang University School of Medicine, Hangzhou, China, [2]Orthopedics Research Institute of Zhejiang University, Hangzhou, China, [3]Key Laboratory of Motor System Disease Research and Precision Therapy of Zhejiang Province, Hangzhou, China

Gold nanorods (GNRs) are intensively explored for the application in cancer therapy, which has motivated the development of photothermal therapy (PTT) multifunctional nanoplatforms based on GNRs to cure osteosarcoma (OS). However, the major limitations include the toxicity of surface protectants of GNRs, unsatisfactory targeting therapy, and the resistant effects of photothermal-induced autophagy, so the risk of relapse and metastasis of OS increase. In the present study, the GNR multifunctional nanoplatforms were designed and synthesized to deliver transcription factor EB (TFEB)-siRNA–targeting autophagy; then, the resistance of autophagy to PTT and the pH-sensitive cell-penetrating membrane peptide (CPP) was weakened, which could improve the tumor-targeting ability of the GNR nanoplatforms and realize an efficient synergistic effect for tumor treatment. Meanwhile, it is worth noting that the GNR nanoplatform groups have anti-lung metastasis of OS. This study provides a new reference to improve the efficacy of OS clinically.

Keywords: gold nanorods, photothermal therapy, RNA interference, osteosarcoma, autophagy

OPEN ACCESS

Edited by:
Kelong Ai,
Central South University, China

Reviewed by:
Chao Fang,
Shanghai Jiao Tong University, China
Jia Huang,
Central South University, China

***Correspondence:**
Wei Yu
11818244@zju.edu.cn
Yiying Qi
qiyiying@zju.edu.cn
Huimin Tao
2187040@zju.edu.cn

†These authors have contributed equally to this work

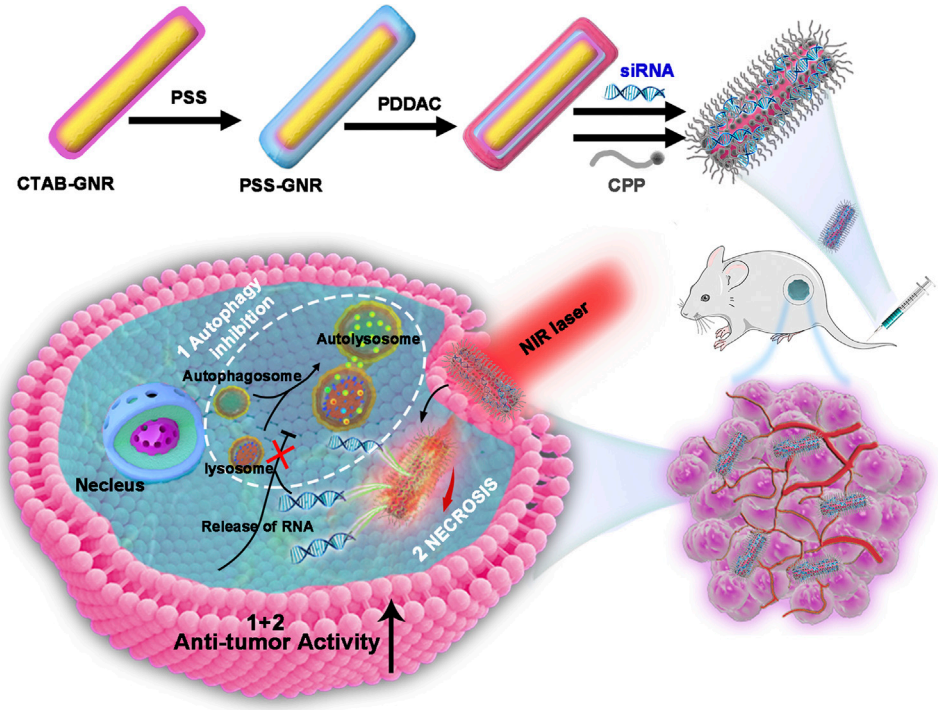
Specialty section:
This article was submitted to Pharmacology of Anti-Cancer Drugs, a section of the journal Frontiers in Pharmacology

Received: *21 October 2021*
Accepted: *22 November 2021*
Published: *20 December 2021*

Citation:
Zhang M, Lin J, Jin J, Yu W, Qi Y and Tao H (2021) Delivery of siRNA Using Functionalized Gold Nanorods Enhances Anti-Osteosarcoma Efficacy. Front. Pharmacol. 12:799588. doi: 10.3389/fphar.2021.799588

INTRODUCTION

Surgical resection of solid tumors and postoperative chemotherapy and radiotherapy are currently adopted for the treatment of malignant tumor, but the side effects of chemotherapeutic drugs and the development of resistant tumor cells lead to patient intolerance, tumor recurrence, and distant metastases (Holohan et al., 2013; Wyld et al., 2015; Zugazagoitia et al., 2016). Photothermal therapy (PTT) is a promising and effective approach in cancer therapy, and it applies light-absorbing nanomaterials to convert light radiation into heat so as to kill tumor cells (Riley and Day 2017). The approach displays many advantages, including high penetration depth in the biological tissues, minimal invasiveness to normal tissues, high spatial precision, and so on (Xu et al., 2020). It has been studied that NIR triggers nanomaterial-induced PTT that could be used as an effective way to treat deep tissue pancreatic cancer and gallbladder disease (Ma et al., 2018; Cai et al., 2020; Jia et al., 2020). PTT also could enhance the antitumor immune response after the highly immunogenic thermal death of tumor cells (Liu et al., 2018) and promote tumor infiltration of CAR T cells (Chen et al., 2019), which makes. These characteristics of PTT enable it suitable for the treatment of some highly malignant and aggressive metastatic tumors that are difficult to be completely removed with surgery,



Graphical Abstract | Schematic representation of the photothermal therapy approach using GNR@siRNA/CPP multifunctional nanoplatforms in osteosarcoma.

such as osteosarcoma (OS). For the malignant tumor with the highest incidence in the skeletal system (Luetke et al., 2014), a major problem, as yet unsolved, is that patients with relapsed or unresectable OS have dismal prognosis (Ritter and Bielack 2010; Harrison et al., 2018). A recent study has revealed that PTT inhibited the tumor growth in an OS mouse model (Xiong et al., 2021). However, the nanomaterial-triggered PTT could not exhaustively eradicate the tumor for the nonuniform distribution of hyperthermia (Zhang et al., 2013; Li et al., 2015) and the production of resistant tumor cells. Therefore, the development of an advanced PTT-based strategy with a stable photothermal conversion rate could improve cancer cell killing *via* countering resistance, with great potential for clinical transformation.

In the process of photothermal treatment of the tumor, the photothermal absorption capacity is highly dependent on the photothermal conversion rate of the photothermal material and the laser wavelength (Liu et al., 2017). With prominent optical absorption and excellent photothermal conversion efficiency in the near-infrared (NIR) window, MoS_2-based nanocomposites can be used for cancer therapy. However, it is still difficult to synthesize stable MoS_2 nanocomposites that may also interfere with the reproductive system (Ai et al., 2021). Another nanomaterial, namely, copper selenide, has broad application prospects in the field of near-infrared thermal ablation for its localized surface plasmon resonance (LSPR) in the near-infrared region. But copper selenide is easy to be oxidized to release copper ions, thus causing LSPR changes, and trigger adverse effects *in vivo*, and these characteristics limit its clinical application (Wang et al., 2021). Gold nanorods (GNRs) have a mature synthetic method without genotoxicity (Zarska et al., 2018). Meanwhile, GNRs have been explored as light-absorbing nanomaterials for cancer therapy for their unique biological characteristics, strong absorption of light in the near-infrared region, and excellent photothermal conversion (Huang et al., 2009). The size of the gap between tumor vascular endothelial cells and normal vascular endothelial cells is different, and thus, the number of nanocarriers was designed to enhance passive accumulation and extend blood circulation at tumor sites by increasing permeability and retention (EPR) (Golombek et al., 2018) effects, which could weaken cellular uptake, in turn.

A cell-penetrating membrane peptide (CPP) is a small molecule polypeptide which can carry various cargoes across the cellular membranes in an intact, such as liposomes, full-length proteins, nucleic acids, and nanoparticles (Taylor and Zahid 2020). Studies have confirmed that CPP-functionalized gold nanorods could improve the cell penetration, exert excellent efficacy (Riveros et al., 2020), and improve the targeting of tumor cells (Tan et al., 2017). The characteristic features of acidosis in tumor microenvironments are taken as advantages to synthesize pH-responsive CPP and realize the targeting of therapeutic drugs to tumor tissue, and it is undoubtedly a strategy for the treatment of tumors. One study pointed out that pH-controllable CPP provided an active cell-penetrating characteristic in tumors (Lee et al., 2017), while the role of CPP-functionalized gold nanorods in the treatment of OS was rarely been reported.

As a physiological activity of cells to maintain substance metabolism, internal environment stability, and genome integrity, autophagy also plays an important role in the abnormal proliferation of tumor cells (Levy et al., 2017). The activation of autophagy helps to remove damaged and aging organelles timely and maintain the continuous abnormal proliferation of tumor cells (Ravanan et al., 2017). In addition, the development of drug resistance in cancer cells has become a major barrier for the effective treatment of cancer with chemotherapy, and autophagy has been proved to be involved in the production of resistant cancer cells (Li et al., 2017; Taylor et al., 2018). In addition, the activation of autophagy provides necessary energy and nutritional supply for DNA repair and delays cell apoptosis following photothermal therapy (Wu et al., 2018; Zhang et al., 2019). On the other hand, the surface chemistry of GNRs mediates their biological toxicity, and CTAB-GNRs induce cell apoptosis and autophagy by damaging the mitochondria and activating intracellular reactive oxygen species (ROS) (Wan et al., 2015). Research studies have confirmed that near-infrared photothermal therapy using gold nanoparticles could increase autophagic cell death in breast cancer (Zhang et al., 2017), and the autophagy suppressor enhances the efficacy of PTT in tumor cells (Ma et al., 2018). In the process of clinical application, near-infrared photothermal therapy could overcome autophagy-induced resistance to PTT and chemotherapy in the treatment of tumors, increase the dose of chemotherapeutic drugs, the treatment temperature, or extend the irradiation time, which may result in unpredictable damage to normal tissues. Gene silencing is a promising technique for cancer treatment with precision and few side effects. The silencing of the transcription factor EB (TFEB) gene has positive effects on autophagy inhibition and antitumor activities (Golombek et al., 2018; Li et al., 2019; Astanina et al., 2021). However, the renal clearance, nuclease degradation, and the positive charge of siRNA prevent its diffusion across cellular membranes during siRNA delivery (Kulkarni et al., 2019), which still needs to be addressed.

In this report, the aim was to construct a multifunctional GNR-based therapeutic system combined with pH-sensitive CPP to improve the uptake efficiency of cells and tumor targeting. Importantly, efficient delivery of siRNA (target lysosomes) significantly restrained the PTT-induced autophagy and then weakened the resistance of autophagy to PTT. Therefore, this study provides a potential platform for PTT to treat cancer with superior efficacy.

MATERIALS AND METHODS

Chemical and Reagents

TFEB siRNA was designed by TSINGKE (Beijing, China). The sequences are as follows: 5'-: GAUGUCAUUGACAACAUUATT and R: UAAUGUUGUCAAUGACAUCTT-3'. Chloroauric acid (HAuCl4.4H2O), sodium chloride, hexadecyltrimethylammonium bromide (CTAB), L-Ascorbic acid, sodium borohydride (NaBH4), silver nitrate (AgNO3), L-ascorbic acid, poly (diallyldimethylammonium chloride) (PDDAC, MW 100,000–200,000 g/mol), and poly (sodium 4-styrenesulfonate) (PSS) were purchased from Aldrich (Shanghai, China). Hydrochloric acid (HCl) was obtained from Sinopharm Chemical Reagent Co., Ltd. (Shanghai, China). Cell-penetrating peptides [CPP, Pep-TH, AGYLLGHINLHHLAHL (Aib) HHIL-Cys] (**Supplementary Figure S1A**) were supplied by Shanghai Apeptide Co., Ltd. (Shanghai, China). More than 95% of the pure peptide was analyzed by LC-MS and 2467.90 of the molecule was analyzed by high-performance liquid chromatography (HPLC) (**Supplementary Figures S1B,C**).

Synthesis of GNRs, GNR@siRNA, and GNR@siRNA/CPP

To synthesize the GNRs, a seed-mediated growth method (El-Sayed, 2003) was adopted. Briefly, under vigorous stirring, 0.6 ml of 10 mM fresh $NaBH_4$ was immediately injected into 5 ml of 0.5 mM HAuCl4, and they were mixed with 5 ml of 0.2 M CTAB solution. The color changed from yellow to bright brown, and the stirring was stopped. This seed solution was aged at least 1 h before being used. A total of 15 ml (0.1 M) $AgNO_3$ and 1.2 ml (5 mM) HAuCl4 were added to 6 ml (0.2 M) CTAB together. Afterward, 720 ml (10 M) Mascorbic acid and 15 ml (1.2 M) HCl were added to the solution and swirled until the color changed from dark orange to colorless. Then, 12 ml of the seed solution was added. Finally, the GNRs were harvested by centrifugation at 10,000 rpm for 10 min. In the synthesis of GNR@siRNA/CPP, the GNRs are scattered to 2 ml of 10 mg/mLPSS (dispersed in 1 mM NaCl) and stirred for 2 h at room temperature to get PSS-coated GNRs (GNR/PSS) by adopting a similar method to the PDDAC further coated. Subsequently, the GNRs/PSS/PDDAC were mixed with different amounts of siRNAs and incubated for 1 h to obtain GNR/PSS/PDDAC@siRNA (GNR@siRNA). In the synthesis of GNR@siRNA/CPP, the GNR@siRNA nanoplex was mixed with different amounts of CPP by pipetting and incubated for 24 h at room temperature.

Cell Culture

Human OS cell lines (HOSs), U2-OS (U2), 143B, and MG-63 were purchased from the Cell Bank of the Chinese Academy of Sciences (Shanghai, China, cultured in Dulbecco's modified Eagle's medium) (DMEM), supplemented with 10% fetal bovine serum (FBS) and 1% antibiotics (penicillin–streptomycin). All cells were maintained at an appropriate atmosphere.

Characterizations

The molecular weight and the purity of the sample were confirmed by Shimadzu LCMS-2020 and high-performance liquid chromatography (HPLC), respectively. Transmission electron microscopy (TEM, Hitachi H-7650) was used to observe the morphology of GNR nanoplatforms. The zeta potentials of the samples were investigated on a zetasizer (Malvern Instruments, UK), and the absorption spectra were performed on a TU-1810 UV-V spectrophotometer.

Agarose Gel Electrophoresis

The GNR nanoplexes with different siRNA ratios were loaded onto 1% agarose gels with 0.5 mg/ml ethidium bromide. The gels

were electrophoresed at 100 V (15 min) and acquired by using UV light on a Gel Doc 2000 imager system (Bio-Rad, Munich, Germany).

In Vitro Photothermal Measurement

Cells were plated on 12-well tissue culture plates and incubated for 24 h, and the culture medium was then removed and replaced with a culture medium containing the conjugated nanoparticles. Afterward, each sample was exposed or unexposed to a near-infrared (NIR) laser (808 nm, Tengxing Electronic Technology Co., Ltd. Guangdong, China) at 1 W/cm^2 for 5 min. Finally, a high-precision infrared thermal imager (ST9450, Xima, Guangzhou, China) was applied to monitor the temperature change.

Cell Invasion and Migration Assays

Cells were seeded into the well plate with different treatment. After 24 h, the Cell Counting Kit-8 (Dojindo, Japan) dye was added to investigate cellular survival. For the wound-healing assay, a wound was made using a pipette tip, and when the cell proliferation reached approximately 80% confluence in the 6-well plate, it was used to detect cell migration. Transwell chambers (Corning Life Science, United States) were chosen to determine cell invasion and migration abilities.

Measurement of Endocytosis

Cells were grown to about 80% confluence in 12-well plates and then incubated with siRNA (labeled with the green fluorescent FAM), GNR@siRNA, and GNR@siRNA/CPP for 24 h, respectively. After the culture medium was removed, a confocal laser microscope (Nikon, A1PLUS, Tokyo, Japan) was used to capture fluorescence images immediately, and the densities of the fluorescence intensity were analyzed using ImageJ software (NIH, Bethesda, MD, United States).

Live/Dead Staining

Cells were seeded in well plates and grown to about 80%, treated with different nanoparticles for 24 h, and then irradiated under 808 nm NIR laser (1 W/cm2) for 5 min. Next, 2 μM calcein (Beyotime, China) and 50 μg/ml PI (Beyotime, China) were used to stain the cells for 10 min before observation by confocal laser microscopy (Nikon, A1PLUS, Tokyo, Japan).

In Vivo Experiments

All animal experiments complied with the guidelines and followed a protocol that was approved by the Research Ethics Committee of Zhejiang University, China (Permit No. 2019/053). Nude mice (4-week-old, male) were obtained from the Shanghai Laboratory Animal Center (Chinese Academy of Science, Shanghai, China). The mice were raised under specific pathogen-free conditions and inoculated with 2 × 106 HOS cells *via* the marrow cavity of the right tibia and armpit subcutaneously. After 7 days, these mice were randomized into four groups. The mice received the GNR complex (10 mg/kg) and an equivalent volume of PBS (CON group) with a time interval of 4 days, respectively. Tibial axillary and armpit tumors were harvested 3 weeks after treatment, with each tumor being weighed. The tumor sizes were calculated as volume (cm^3) = [π × width^2 (cm^2) × length (cm)]/6.

Western Blotting

Cellular proteins (60 μg) were transferred onto a polyvinylidene fluoride membrane (Bio-Rad Laboratories), and after being blocked by 5% fat-free milk for 1.5 h, the membranes were incubated with the following primary antibodies: active caspase-3 (1:1,000, CST), LC3I/II (1:1,000, Proteintech Group, Inc.), and GAPDH (Cat: RT1210-1, Huabio) overnight at 4°C. Then, the membranes were incubated with a secondary antibody for 1 h. The signals were visualized with the ChemiDoc^{TM} XRS + Imaging System (Bio-Rad Laboratories, Hercules, CA, United States).

Immunofluorescence

After the samples were fixed with 4% paraformaldehyde and blocked by 5% bovine serum albumin (BSA), the samples were incubated with the following primary antibodies: active caspase-3 (1:100, CST) and LC3B (1:200, Proteintech Group, Inc.) at 4°C overnight. Afterward, the samples were incubated with the secondary antibody (1:1,000, Huabio), and the sections were then restained with an anti-fluorescent quench sealant (Yeasen). The fluorescence images were captured by confocal laser microscopy (Nikon, A1PLUS, Tokyo, Japan), and the densities of the fluorescence intensity were analyzed using ImageJ software (NIH, Bethesda, MD, United States).

Hematoxylin and Eosin

Tissues were harvested and fixed in 4% (w/v) paraformaldehyde for 24 h, after gradient alcohol dehydration and being embedded in paraffin wax. The sections were then prepared and mounted on slides for H&E and cresyl violet staining. Images were obtained by light microscopy.

Statistical Analysis

All data were presented as means ± SEM. Differences between two groups were determined using Student's t-test, whereas one-way ANOVA followed by Dunnett's *post hoc* test was used to determine differences among multiple groups. p value < 0.05 was considered to be significant.

RESULTS AND DISCUSSION

Synthesis and Characterization of the GNR@siRNA/CPP System

In this study, the GNR@siRNA/CPP delivery vehicle was acquired *via* a well-developed layer-by-layer assembly approach. Before PDDA (positively charged) coating, the original CTAB on the surface of GNRs was replaced by the sodium polystyrene sulfonate (query) (PSS, negatively charged) layer. Meanwhile, the PDDA made the siRNA electrostatic bond with GNRs. Next, CPP was immobilized on the GNR surface by sulfur–gold bonds (**Figure 1A**). As revealed by TEM (**Figure 1B**), the GNR@siRNA/CPP indicated a regular rod-shaped and well-

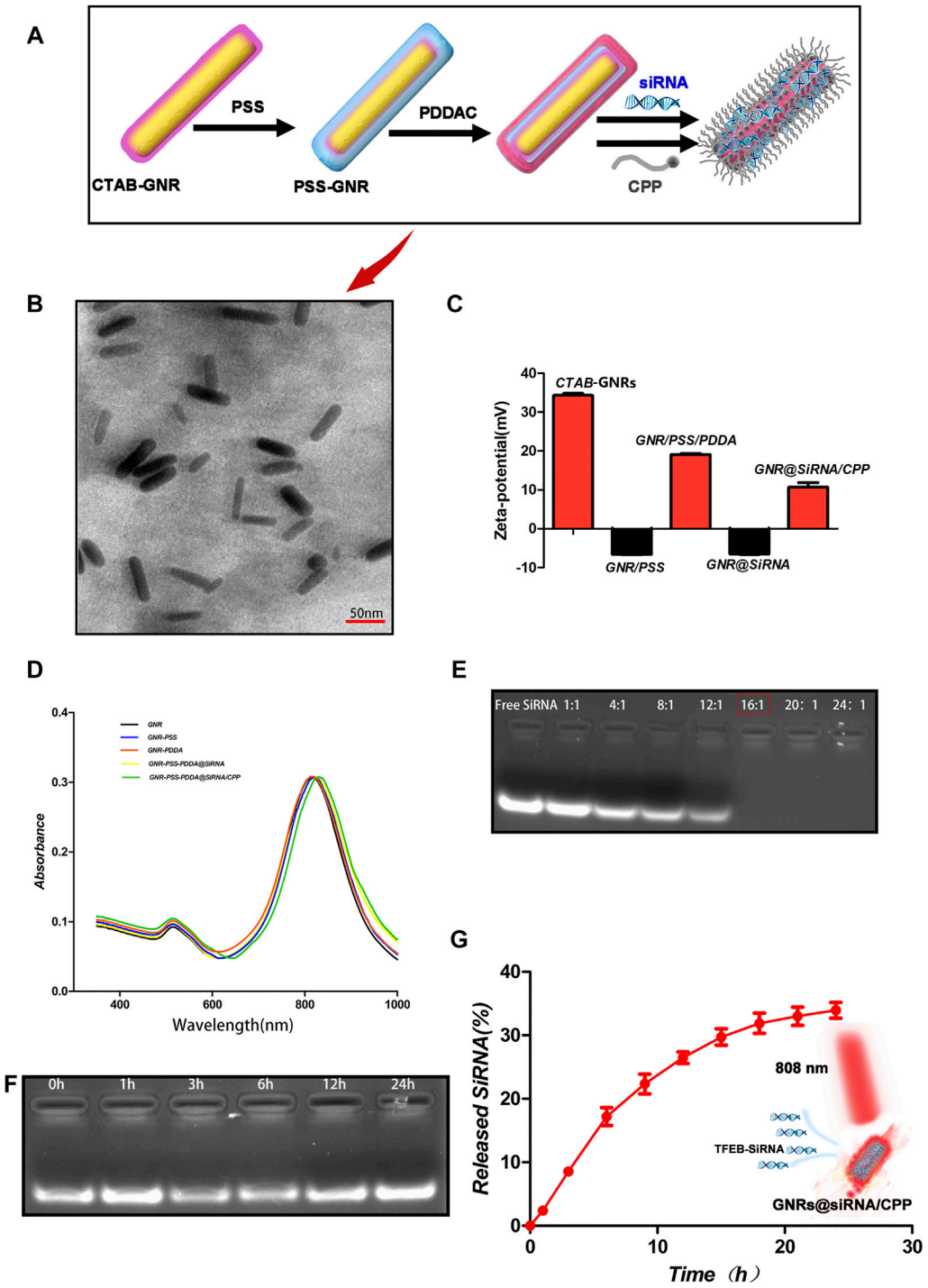


FIGURE 1 | Characterization of the nanoplatforms. **(A)** Schematic illustration of the synthesis of GNR@siRNA/CPP nanorods. **(B)** TEM images of GNR@siRNA/CPP nanorods. **(C, D)** Zeta potential and UV-vis spectrum of GNRs, GNR-PSS, GNR-PSS-PDDAC, GNRs-PSS-PDDAC-siRNA (GNRs@siRNA), and GNR/PSS/PDDAC-siRNA-CPP (GNR@siRNA/CPP). **(E, F)** Agarose gel retardation assay of GNR/siRNA complexes under various weight ratios and protection of siRNA against fetal bovine serum digestion. **(G)** siRNA cumulative release from GNR@siRNA/CPP complexes at different points in time.

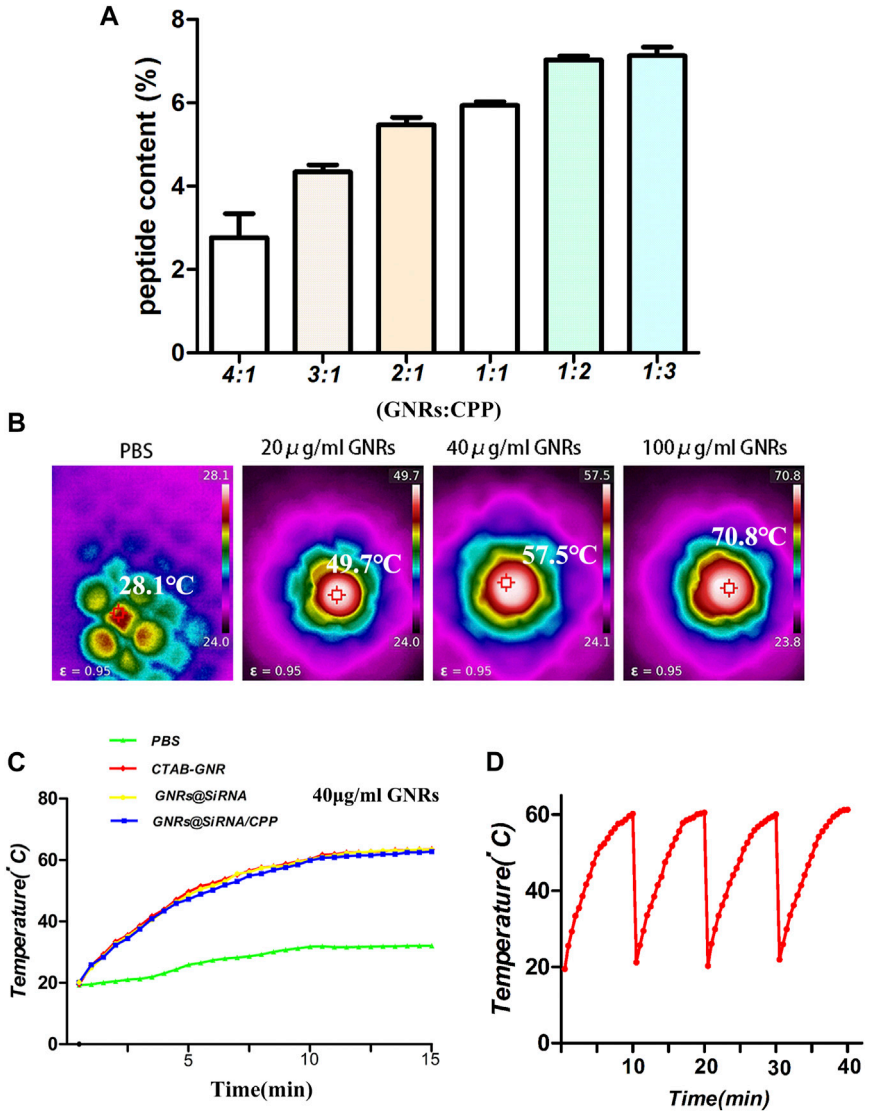


FIGURE 2 | Characterization of the GNR/CPP complexes. **(A)** Peptide content on GNR/CPP complexes surface under various weight ratios. **(B)** Temperature plot of different concentrations of GNRs irradiated by 808 nm laser irradiation (1 W/cm^2). **(C)** Temperature changes of GNRs and GNR complexes irradiated by 808 nm NIR laser. **(D)** Temperature change curves of the GNR@siRNA and GNR@siRNA/CPP irradiated by 808 nm laser.

dispersed character, and being proved after modification and conjugation, GNRs were still in a well-dispersed status. The zeta potential values of the CTAB–GNRs, PSS-GNRs, PSS-PDDA–GNRs, PSS-PDDA–GNR@siRNA, and PSS-PDDA–GNR@siRNA/CPP were + 34.3, −6.5, + 19.1, −6.4, and + 10.7 mV, respectively (**Figure 1C**). After the incubation of the cationic GNR/PSS/PDDAC substrate with anionic siRNA, the zeta potentials reverse from positive to negative, while that after the anionic GNR/PSS/PDDAC/siRNA substrate with cationic CPP, the zeta potentials reverse from negative to positive, which suggests the binding of CPP with GNRs-siRNA in the final GNRs-siRNA/CPP. Being attributed to the siRNAl and CPP doping, the GNR complex exhibited a continuous red shift that was observed from the longitudinal SPR (LSPR) in the absorption spectra (**Figure 1D**). Based on the above experimental results, we concluded that the siRNA and CPP were successfully bound to the surface of GNRs.

Two important factors, the binding stability and release of siRNA, needed to be considered before the siRNA delivery platform was performed. The agarose gel electrophoresis assay was used to investigate the optimal binding ratio of GNRs to TFEB siRNA. As shown in **Figure 1E**, when the mass ratio of GNRs to siRNA is 16:1, siRNA almost completely binds to GNRs. And then, the GNR@siRNA was incubated in 50% fetal bovine serum (FBS) at 37°C for different time periods, and after 24 h of incubation, the particle-bound siRNA still remained intact, which confirms the stability of the delivery system siRNA that binds to GNRs. The released siRNA was also tested from the GNR@

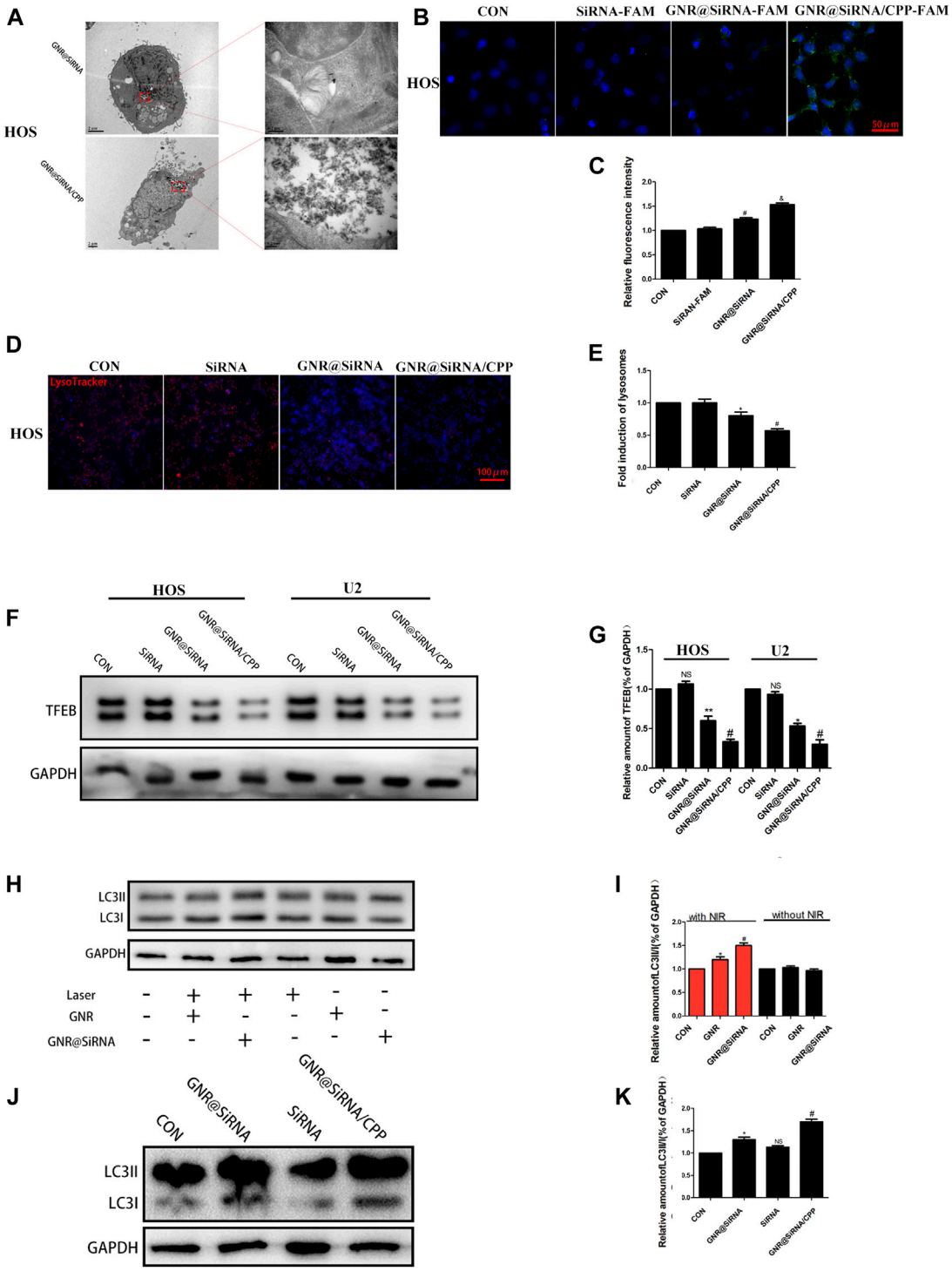


FIGURE 3 | Nanoplatforms inhibits lysosome formation. **(A)** TEM images of GNR@siRNA and GNR@siRNA/CPP in OS cells. **(B, C)** Fluorescent images of OS cells incubated with siRNA (labeled with the green fluorescent FAM), GNR@siRNA, and GNR@siRNA/CPP, respectively. **(D, E)** Confocal microscopic images of Lyso Tracker for lysosomes (red) in OS cells. **(F, G)** Protein expression and densitometric quantification of TFEB in different groups. **(H–K)** Protein expression and densitometric quantification of LC3B in different groups. ($n = 5$ per group; $^{*}p < 0.05$ vs. CON group, $^{**}p < 0.01$ vs. siRNA group, $^{\#}p < 0.05$ vs. siRNA group or GNR@siRNA group; $^{\&}p < 0.05$ vs. GNR@siRNA group).

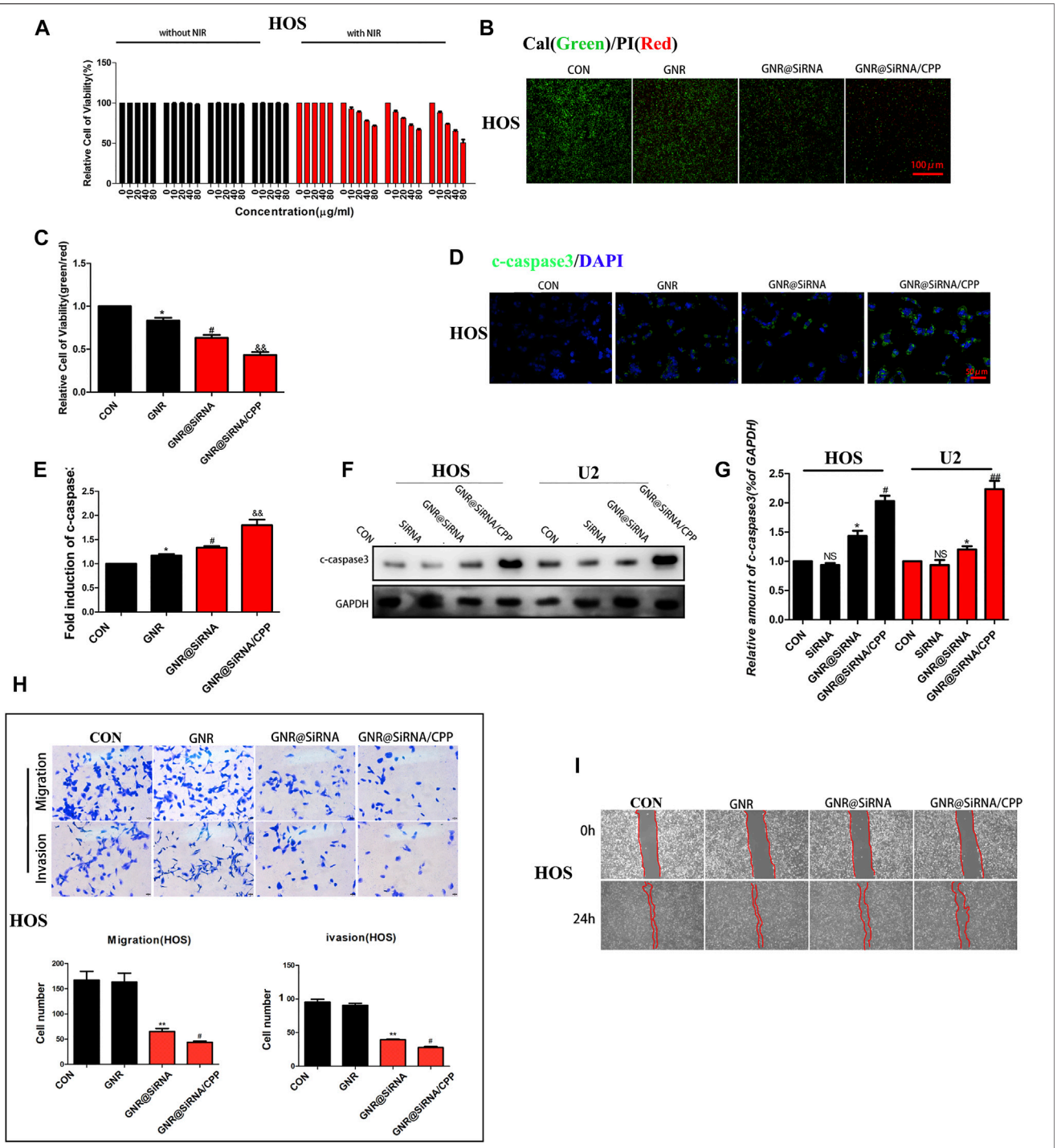


FIGURE 4 | Nanoplatforms inhibit OS cell activity *in vitro*. **(A)** Cell-survival rate in OS cells. **(B, C)** Living/dead staining of OS cells incubated with 100 μg/ml GNRs and GNR complexes for 24 h and then irradiated under 808 nm NIR laser (1 W/cm^2). **(D, E)** Immunofluorescence staining of c-caspase-3 in different groups. **(F, G)** Western blotting and densitometric quantification. **(H)** Migration and invasion assay in different groups. **(I)** Wound-healing assay in different groups. (n = 5 per group; $^{**}p < 0.01$ or $^{***}p < 0.001$ vs. CON group; $^{\#\#}p < 0.01$ vs. GNR@siRNA group; $^{\#}p < 0.05$ vs. GNR@siRNA group).

siRNA/CPP *via* the absorbance of the supernatant at 260 nm. After 24 h, the accumulated siRNA release reached about 35% (**Figure 1G**) that was enough to make the biological availability. The Micro BCA assay was used to measure the peptide contents on the GNRs (**Figure 2A**). When the ratio between the peptide and GNRs was greater than 1:1, about 6% of the total weight of GNR@siRNA/CPP can provide excellent biological functions. In addition, the photothermal conversion ability of the GNR

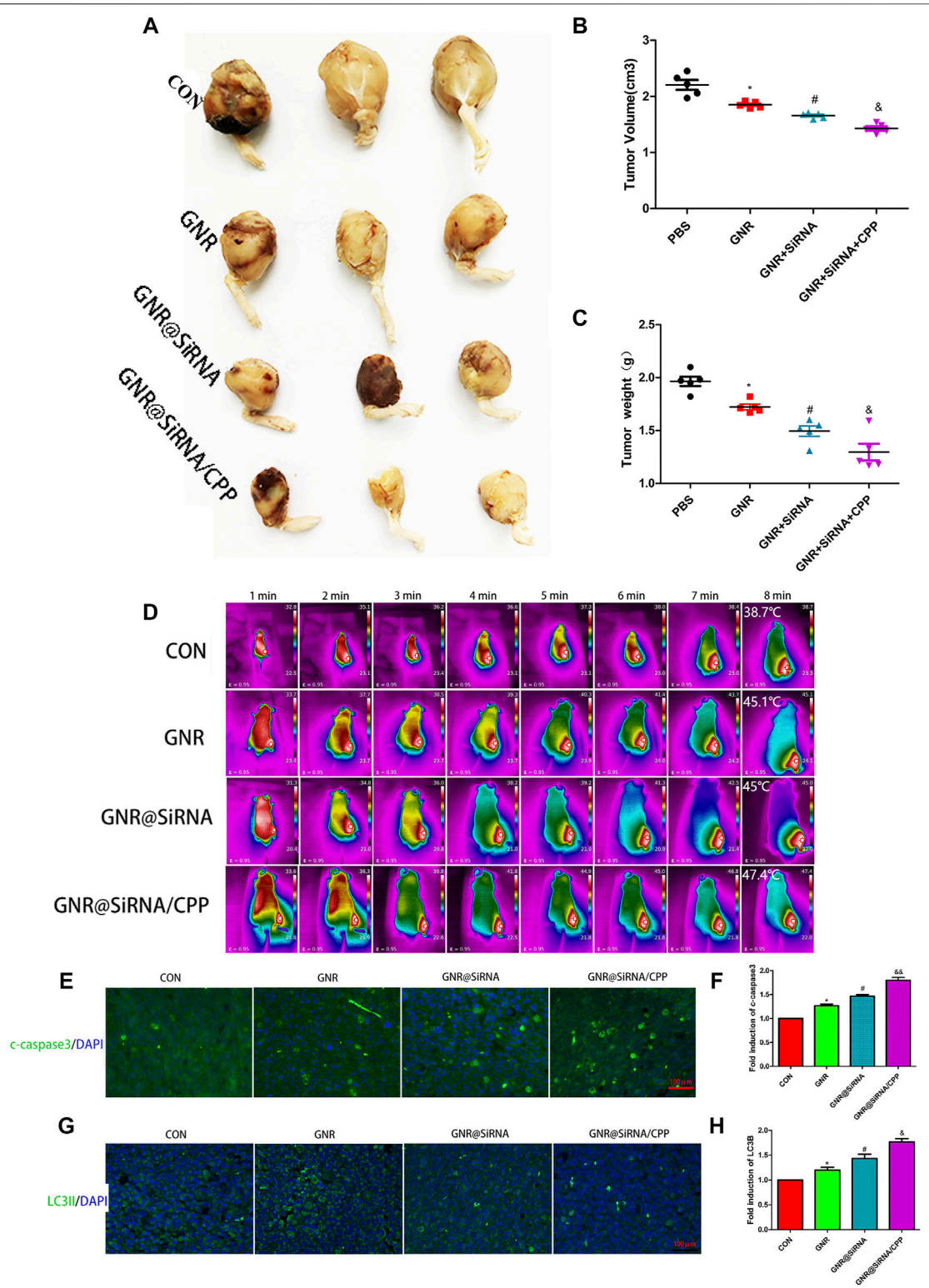


FIGURE 5 | Nanoplatforms inhibit the growth of the marrow cavity of OS *in vivo*. **(A–C)** Photographs of harvested xenograft tumors in different groups. **(D)** Thermographs of mice recorded in different groups by NIR irradiation for various times. **(E–H)** Immunofluorescence staining of c-caspase3 and LC3B in different groups. (n = 5 per group; $^{*}p < 0.05$ vs. CON group; $^{\#}p < 0.05$ vs. GNR group; $^{\&}p < 0.05$ or $^{\&\&}p < 0.01$ vs. GNR@siRNA group).

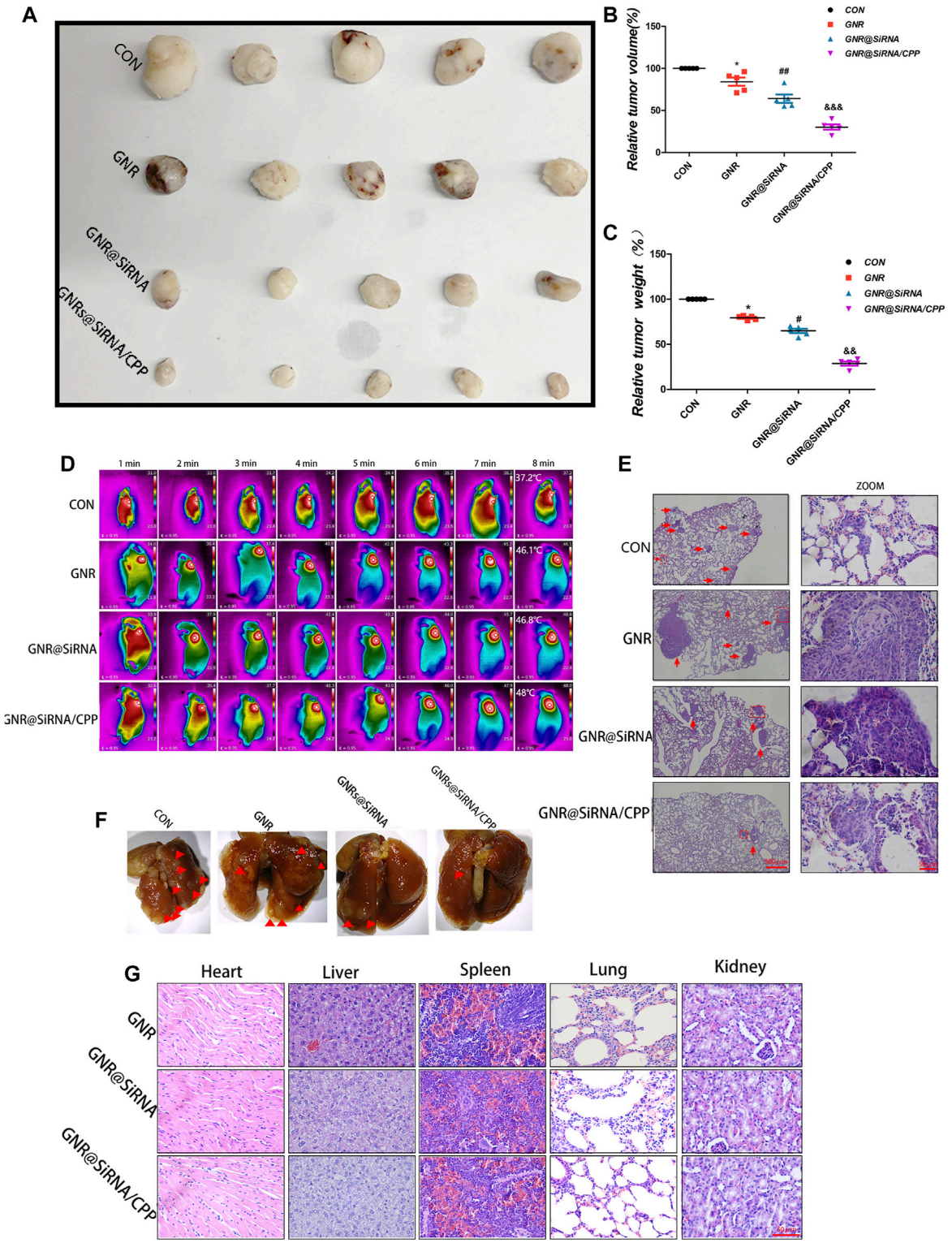


FIGURE 6 | Nanoplatforms inhibit the growth of OS subcutaneously and pulmonary metastasis *in vivo*. **(A–C)** Tumor formation in different groups. **(D)** Thermographs of mice recorded in different groups by NIR irradiation for various times. **(E, F)** Photographs and H&E staining of lung tissues in different groups. **(G)** H&E staining of organ tissues of mice in different groups. ($n = 5$ per group; $^{*}p < 0.05$ vs. CON group; $^{\#}p < 0.05$ or $^{\#\#}p < 0.01$ vs. GNR group; $^{\&\&}p < 0.01$ or $^{\&\&\&}p < 0.001$ vs. GNR@siRNA group).

complex was also tested. Various concentrations of GNR complexes can be heated from room temperature to about 49.7–70.8°C after 5 min irradiation under an 808 nm laser (**Figures 2B,C**), and all GNR complexes can realize ternary heating–cooling cycle for the excellent photothermal stability (**Figure 2F**).

Cellular Uptake of the GNR@siRNA/CPP System.

The pharmacokinetic and biodistribution of nanoplatforms need to be considered before treatment. It has been reported that coated gold nanorods were injected intravenously in mice, and their concentration peaked in the blood about 1 h later. After 24 h, they were basically cleared and gradually increased in tissues and organs. Meanwhile, they could still be detected after 24 h, mainly in the spleen, liver, and tumor tissues (Arunkumar et al., 2015; Puleio et al., 2020). The cellular uptake of GNR@siRNA/CPP was detected in HOS and U2 osteosarcoma cell lines. As illustrated in **Figures 3B,C** and **Supplementary Figures S2A,B**, FAM siRNA was observed in GNR complex groups by laser confocal, and the fluorescence intensity follows the hierarchy: GNR@siRNA/CPP > GNR@siRNA > GNRs > CON group. TEM images were used to visualize the nanorods in the cells, and the results (**Figure 3A**; **Supplementary Figure S2C**) showed the same results as laser confocal. These results suggested that CPP increased the amount of GNR complex cellular uptake by OS cells. To further explore the effectiveness of siRNA vectors, the expression of the target protein TFEB and the lysosomes was detected in OS cells. As anticipated, free siRNA did not have effects on the expression of TFEB protein levels; the GNR complexes inhibited the expression of TFEB protein, and the GNR complex with CPP showed stronger inhibition in OS cells (**Figures 3F,G**). The LysoTracker red staining assay was conducted to investigate the number of lysosomes in OS cells. As demonstrated in **Figures 3D,E** and **Supplementary Figures S2D,E**, the number of lysosomes in OS was unaffected by free siRNA, and the GNR complexes inhibited the lysosomal formation in OS cells. The autophagy-related protein LC3B was also investigated in OS cells. As displayed in **Figure 3K**, the expression of LC3B was significantly increased in the GNR group, which was reversed by the GNR@siRNA group under NIR irradiation. However, it did not have that trend without NIR irradiation in OS cells. Additionally, the free siRNA did not inhibit the LC3B protein expression, and compared with the GNR@siRNA group, the GNR@siRNA/CPP group exerted much effective ability for the promotion of the expression of LC3B protein in OS cells (**Figures 3H–K**; **Supplementary Figures S2F–I**). Therefore, it was concluded that an siRNA delivery vector that can efficiently transport siRNA and realize the efficient gene silencing of the target gene was constructed successfully.

In Vitro Photothermal Effects

The cytotoxicities of GNR complexes on OS cells were first investigated by the cell survival rate *via* the CCK8 assay. As shown in **Figure 4A**; **Supplementary Figures S3A–C**, GNR complexes have no effects on the survival rate of OS cells without laser irradiation, suggesting that the GNR complexes are non-toxic themselves. When OS cells were exposed to GNR complexes, the survival decreased was dose-dependent under laser irradiation conditions. Furthermore, due to higher cellular uptake of GNR@siRNA/CPP, the GNR@siRNA/CPP group had better ability to kill tumor cells, which was further confirmed by Cal/PI double staining and Western blot for the apoptotic protein (**Figures 4B,C**; **Supplementary Figures S3D,G**). Hence, it can be concluded that gene silencing by GNR complexes and photothermal effects can synergically kill OS cells, and CPP increases GNR complex entry into tumor cells and promotes apoptosis. Most cancer-related deaths are attributable to metastases, but the current clinical treatments are unsatisfactory (Liao et al., 2021). Transcription factor EB (TFEB) links autophagy to lysosomal biogenesis (Settembre et al., 2011) and promotes metastasis in cancer (Liang et al., 2018; He et al., 2019). Moreover, autophagy has been confirmed to be involved in modulating tumor cell motility and invasion (Sharifi et al., 2016). Hence, the experiment was performed to determine whether GNR complexes have effects on the migration of OS cells, and the GNR complexes were exposed to the OS cells under 808-nm near-infrared (NIR) light, where the temperature was regulated without affecting the cell viability/proliferation. Our results demonstrated that the invasion and migration of the GNR complex groups were significantly abrogated in OS cells, compared with those in CON and GNR groups (**Figure 4H**; **Supplementary Figures S3H–J**), which was similar to the results observed in the wound-healing assay (**Figure 4I**; **Supplementary Figure S3K**), suggesting that the nanocarrier successfully transported the interfering gene with inhibitory effects on OS cells *in vitro*.

In Vivo Experiment

To further verify the efficacy of the GNR complex for OS, we tested *in situ* and subcutaneous mouse models of OS. In *in situ* mouse models, the GNR complex decreases the growth of the tumors compared with that of the control group and decreases the growth of the tumors with the following hierarchy: GNR@siRNA/CPP > GNR@siRNA GNRs > CONgroup (**Figures 5A–C**). Being encouraged by the antitumor efficacy of the GNR complex *in vivo*, it was necessary to evaluate the conversion property of nanocomposites under NIR light *in vivo*. We investigated the photothermal therapy of GNR complexes by performing with an 808 nm laser. After irradiation for 8 min, the tumor area in CON, GNR, GNR@siRNA, and GNR@siRNA/CPP showed temperatures of 38.7°C, 45.1°C, 45°C, and 47.4°C, respectively (**Figure 5D**), which were enough to achieve the effects of tumor ablation in the GNR and GNR complex groups. pH-sensitive CPP increased the GNR complex into the tumor cells, thus leading to sufficient tumor ablation. In subcutaneous mouse models, the GNR complex presented the same inhibiting tumor growth tendency and photothermal conversion ability with that *in*

situ mouse models (**Figures 6A–D**). Next, the cleaved caspase-3 and LC3B-positive cells in the tumor tissue were detected. The GNR@siRNA/CPP group resulted in a more remarkable increased apoptosis of tumor cells than other groups (**Figures 5E,F**). The hierarchy of the amount of LC3B-positive cells is as follows: GNR@siRNA/CPP > GNR @siRNA > GNRs > CON group (**Figures 5G,H**). This indicated that the silencing of the TFEB gene by the GNR complex reduced the generation of lysosomes and the binding between lysosomes and autophagosomes, thereby leading to the blocked autophagy. LC3B accumulation increases the photothermal effects and tumor cell apoptosis.

In vitro, we have demonstrated that GNR complexes abrogated the invasion and migration of OS cells, and some studies have revealed that patients with osteosarcoma had evidence of metastases at diagnosis, mostly in the lungs (Meazza and Scanagatta, 2016). Therefore, we examined the influences of the GNR complex on lung metastasis of OS *in vivo*. As presented in **Figures 6E,F**, the lungs of the CON group exhibited multiple small metastatic tumor nodules which increased compared with the GNR complex group, and the hierarchy of the GNR complex inhibited lung metastasis of OS as follows: GNR@ siRNA/CPP > GNR @siRNA > GNRs > CON, indicating that the nanocarrier is successful in transporting cargoes and facilitating biological functions of the cargo *in vivo*. The biosecurity of the GNR complex was also detected by the H&E-stained vital organs, and no obvious damage was observed in H&E-stained histopathological slices of the heart, liver, spleen, lungs, and kidneys (**Figure 6G**). In summary, the GNR complex was designed and synthesized by exerting an admirable ability to carry siRNA, and pH-sensitive CPP increased the tumor-targeting ability of the GNR complex, which plays a synergistic role in gene silencing and photothermal ablation of tumor *in vivo* experiments.

CONCLUSION

In this study, the GNR@siRNA/CPP nanoplatforms were designed to efficiently deliver siRNA oligos targeting TFEB so as to promote photothermal therapy. The multifunctional nanoplatforms exhibited excellent biocompatibility, photothermal conversion property, and stability. The GNR conjugation with pH-sensitive CPP resulted in the uptake efficiency of the nanoplatforms by OS cells, and tumor targeting was improved. In addition, the multifunctional nanoplatforms provide an effective protection of siRNA from unexpected degradation and a stable release rate. It was demonstrated that TFEB-siRNA delivered efficient intracellularly by GNR significantly, weakened the formation of autolysosomes, induced the inhibition of autophagy in OS cells, and then weakened the resistance of autophagy to PTT. Most importantly, the GNR@siRNA/CPP nanoplatforms exerted efficacy to suppress metastasis of OS. Both *in vitro* and *in vivo* anti-osteosarcoma effects were remarkably enhanced, which attributes to the synergistic effects by GNR@siRNA/CPP nanoplatforms under NIR irradiation conditions. Therefore, this study indicated a potential multifunctional nanocarrier system for tumor therapy and metastasis.

DATA AVAILABILITY STATEMENT

The original contributions presented in the study are included in the article/**Supplementary Material**; further inquiries can be directed to the corresponding authors.

ETHICS STATEMENT

The animal study was reviewed and approved by the Research Ethics Committee of Zhejiang University.

AUTHOR CONTRIBUTIONS

HT, YQ, and WY conceived and designed the research. MZ performed the experiments. JL analyzed the data and interpreted results of experiments. JJ drafted and reviewed the manuscript. All authors read and approved the manuscript.

FUNDING

This study was supported by the grants from the National Science Foundation of China (81772325, 82072413) and the National Scientific and Technological Achievements Promotion Project for college students (2021R401233, 2020R401216). Thanks for the technical support by the Core Facilities, Zhejiang University School of Medicine.

SUPPLEMENTARY MATERIAL

The Supplementary Material for this article can be found online at: https://www.frontiersin.org/articles/10.3389/fphar.2021.799588/full#supplementary-material

Supplementary Figure S1 | Characterization of the GNR/CPP complexes. **(A)** Structural diagram of the cell-penetrating membrane peptide (CPP). **(B, C)** Molecular weight of CPP detected by MS and the purity of CPP detected by HPLC.

Supplementary Figure S2 | Nanoplatforms inhibit lysosome formation. **(A, B)** Fluorescent images of OS cells incubated with siRNA (labeled with the green fluorescent FAM), GNR@siRNA, and GNR@siRNA/CPP, respectively. **(C)** TEM images of GNR@siRNA and GNR@siRNA/CPP in OS cells. **(D, E)** Confocal microscope images of Lyso Tracker for lysosomes (red) in OS cells. **(F–I)** Protein expression and densitometric quantification of LC3 in different groups. (n = 5 per group; $^{*}p < 0.05$ vs. CON group, $^{**}p < 0.01$ vs. siRNA group, $^{\#}p < 0.05$ vs. siRNA group or GNR@siRNA group; $^{\&}p < 0.05$ vs. GNR@siRNA group).

Supplementary Figure S3 | Nanoplatforms inhibit OS cell activity *in vitro*. **(A–C)** Cell survival rate in OS cells. **(D, G)** Living/dead staining of OS cells incubated with 100 μg/ml GNRs and GNR complexes for 24 h and then irradiated under 808 nm NIR laser (1 W/cm^2). **(E, F)** Immunofluorescence staining of c-caspase3 in different groups. **(H–J)** Migration and invasion assay in different groups. **(K)** Wound-healing assay in different groups. (n = 5 per group; $^{**}p < 0.01$ or $^{***}p < 0.001$ vs. CON group; $^{\#\#}p < 0.01$ vs. GNR@siRNA group; $^{\#}p < 0.05$ vs. GNR@siRNA group).

REFERENCES

Ai, K., Huang, J., Xiao, Z., Yang, Y., Bai, Y., and Peng, J. (2021). Localized Surface Plasmon Resonance Properties and Biomedical Applications of Copper Selenide Nanomaterials. *Mater. Today Chem.* 20, 100402. doi:10.1016/j.mtchem.2020.100402

Arunkumar, P., Raju, B., Vasantharaja, R., Vijayaraghavan, S., Preetham Kumar, B., Jeganathan, K., et al. (2015). Near Infra-red Laser Mediated Photothermal and Antitumor Efficacy of Doxorubicin Conjugated Gold Nanorods with Reduced Cardiotoxicity in Swiss Albino Mice. *Nanomedicine* 11 (6), 1435–1444. doi:10.1016/j.nano.2015.03.012

Astanina, E., Bussolino, F., and Doronzo, G. (2021). Multifaceted Activities of Transcription Factor EB in Cancer Onset and Progression. *Mol. Oncol.* 15 (2), 327–346. doi:10.1002/1878-0261.12867

Cai, Q., Wang, X., Wang, S., Jin, L., Ding, J., Zhou, D., et al. (2020). Gallbladder Cancer Progression Is Reversed by Nanomaterial-Induced Photothermal Therapy in Combination with Chemotherapy and Autophagy Inhibition. *Int. J. Nanomedicine* 15, 253–262. doi:10.2147/ijn.s231289

Chen, Q., Hu, Q., Dukhovlinova, E., Chen, G., Ahn, S., Wang, C., et al. (2019). Photothermal Therapy Promotes Tumor Infiltration and Antitumor Activity of CAR T Cells. *Adv. Mater.* 31 (23), e1900192. doi:10.1002/adma.201900192

El-Sayed, B. N. a. M. A. (2003). Preparation and Growth Mechanism of Gold Nanorods (NRs) Using Seed-Mediated Growth Method. *Chem. Mater.* 15, 1957–1962.

Golombek, S. K., May, J. N., Theek, B., Appold, L., Drude, N., Kiessling, F., et al. (2018). Tumor Targeting via EPR: Strategies to Enhance Patient Responses. *Adv. Drug Deliv. Rev.* 130, 17–38. doi:10.1016/j.addr.2018.07.007

Harrison, D. J., Geller, D. S., Gill, J. D., Lewis, V. O., and Gorlick, R. (2018). Current and Future Therapeutic Approaches for Osteosarcoma. *Expert Rev. Anticancer Ther.* 18 (1), 39–50. doi:10.1080/14737140.2018.1413939

He, R., Wang, M., Zhao, C., Shen, M., Yu, Y., He, L., et al. (2019). TFEB-driven Autophagy Potentiates TGF-β Induced Migration in Pancreatic Cancer Cells. *J. Exp. Clin. Cancer Res.* 38 (1), 340. doi:10.1186/s13046-019-1343-4

Holohan, C., Van Schaeybroeck, S., Longley, D. B., and Johnston, P. G. (2013). Cancer Drug Resistance: an Evolving Paradigm. *Nat. Rev. Cancer* 13 (10), 714–726. doi:10.1038/nrc3599

Huang, X., Neretina, S., and El-Sayed, M. A. (2009). Gold Nanorods: from Synthesis and Properties to Biological and Biomedical Applications. *Adv. Mater.* 21 (48), 4880–4910. doi:10.1002/adma.200802789

Jia, X., Xu, W., Ye, Z., Wang, Y., Dong, Q., Wang, E., et al. (2020). Functionalized Graphene@Gold Nanostar/Lipid for Pancreatic Cancer Gene and Photothermal Synergistic Therapy under Photoacoustic/Photothermal Imaging Dual-Modal Guidance. *Small* 16 (39), e2003707. doi:10.1002/smll.202003707

Kulkarni, J. A., Witzigmann, D., Chen, S., Cullis, P. R., and van der Meel, R. (2019). Lipid Nanoparticle Technology for Clinical Translation of siRNA Therapeutics. *Acc. Chem. Res.* 52 (9), 2435–2444. doi:10.1021/acs.accounts.9b00368

Lee, D., Noh, I., Yoo, J., Rejinold, N. S., and Kim, Y. C. (2017). pH-Controllable Cell-Penetrating Polypeptide that Exhibits Cancer Targeting. *Acta Biomater.* 57, 187–196. doi:10.1016/j.actbio.2017.05.040

Levy, J. M. M., Towers, C. G., and Thorburn, A. (2017). Targeting Autophagy in Cancer. *Nat. Rev. Cancer* 17 (9), 528–542. doi:10.1038/nrc.2017.53

Li, P., Shi, Y. W., Li, B. X., Xu, W. C., Shi, Z. L., Zhou, C., et al. (2015). Photothermal Effect Enhances the Efficiency of Radiotherapy Using Arg-Gly-Asp Peptides-Conjugated Gold Nanorods that Target αvβ3 in Melanoma Cancer Cells. *J. Nanobiotechnology* 13, 52. doi:10.1186/s12951-015-0113-5

Li, S., Song, Y., Quach, C., Guo, H., Jang, G. B., Maazi, H., et al. (2019). Transcriptional Regulation of Autophagy-Lysosomal Function in BRAF-Driven Melanoma Progression and Chemoresistance. *Nat. Commun.* 10 (1), 1693. doi:10.1038/s41467-019-09634-8

Li, Y. J., Lei, Y. H., Yao, N., Wang, C. R., Hu, N., Ye, W. C., et al. (2017). Autophagy and Multidrug Resistance in Cancer. *Chin. J. Cancer* 36 (1), 52. doi:10.1186/s40880-017-0219-2

Liang, J., Jia, X., Wang, K., and Zhao, N. (2018). High Expression of TFEB Is Associated with Aggressive Clinical Features in Colorectal Cancer. *Onco Targets Ther.* 11, 8089–8098. doi:10.2147/ott.s180112

Liao, J., Shi, K., Jia, Y., Wu, Y., and Qian, Z. (2021). Gold Nanorods and Nanohydroxyapatite Hybrid Hydrogel for Preventing Bone Tumor Recurrence via Postoperative Photothermal Therapy and Bone Regeneration Promotion. *Bioact Mater.* 6 (8), 2221–2230. doi:10.1016/j.bioactmat.2021.01.006

Liu, Y., Crawford, B. M., and Vo-Dinh, T. (2018). Gold Nanoparticles-Mediated Photothermal Therapy and Immunotherapy. *Immunotherapy* 10 (13), 1175–1188. doi:10.2217/imt-2018-0029

Liu, Y., Zhang, X., Liu, Z., Wang, L., Luo, L., Wang, M., et al. (2017). Gold Nanoshell-Based Betulinic Acid Liposomes for Synergistic Chemo-Photothermal Therapy. *Nanomedicine* 13 (6), 1891–1900. doi:10.1016/j.nano.2017.03.012

Luetke, A., Meyers, P. A., Lewis, I., and Juergens, H. (2014). Osteosarcoma Treatment - where Do We Stand? A State of the Art Review. *Cancer Treat. Rev.* 40 (4), 523–532. doi:10.1016/j.ctrv.2013.11.006

Ma, Y., Chen, H., Hao, B., Zhou, J., He, G., Miao, Z., et al. (2018). A Chloroquine-Loaded Prussian Blue Platform with Controllable Autophagy Inhibition for Enhanced Photothermal Therapy. *J. Mater. Chem. B* 6 (37), 5854–5859. doi:10.1039/c8tb01987h

Meazza, C., and Scanagatta, P. (2016). Metastatic Osteosarcoma: a Challenging Multidisciplinary Treatment. *Expert Rev. Anticancer Ther.* 16 (5), 543–556. doi:10.1586/14737140.2016.1168697

Puleio, R., Licciardi, M., Varvarà, P., Scialabba, C., Cassata, G., Cicero, L., et al. (2020). Effect of Actively Targeted Copolymer Coating on Solid Tumors Eradication by Gold Nanorods-Induced Hyperthermia. *Int. J. Pharm.* 587, 119641. doi:10.1016/j.ijpharm.2020.119641

Ravanan, P., Srikumar, I. F., and Talwar, P. (2017). Autophagy: The Spotlight for Cellular Stress Responses. *Life Sci.* 188, 53–67. doi:10.1016/j.lfs.2017.08.029

Riley, R. S., and Day, E. S. (2017). Gold Nanoparticle-Mediated Photothermal Therapy: Applications and Opportunities for Multimodal Cancer Treatment. *Wiley Interdiscip. Rev. Nanomed Nanobiotechnol* 9 (4). doi:10.1002/wnan.1449

Ritter, J., and Bielack, S. S. (2010). Osteosarcoma. *Ann. Oncol.* 21 (Suppl. 7), vii320–5. doi:10.1093/annonc/mdq276

Riveros, A. L., Eggeling, C., Riquelme, S., Adura, C., López-Iglesias, C., Guzmán, F., et al. (2020). Improving Cell Penetration of Gold Nanorods by Using an Amphipathic Arginine Rich Peptide. *Int. J. Nanomedicine* 15, 1837–1851. doi:10.2147/ijn.s237820

Settembre, C., Di Malta, C., Polito, V. A., Garcia Arencibia, M., Vetrini, F., Erdin, S., et al. (2011). TFEB Links Autophagy to Lysosomal Biogenesis. *Science* 332 (6036), 1429–1433. doi:10.1126/science.1204592

Sharifi, M. N., Mowers, E. E., Drake, L. E., Collier, C., Chen, H., Zamora, M., et al. (2016). Autophagy Promotes Focal Adhesion Disassembly and Cell Motility of Metastatic Tumor Cells through the Direct Interaction of Paxillin with LC3. *Cell Rep* 15 (8), 1660–1672. doi:10.1016/j.celrep.2016.04.065

Tan, H., Huang, Y., Xu, J., Chen, B., Zhang, P., Ye, Z., et al. (2017). Spider Toxin Peptide Lycosin-I Functionalized Gold Nanoparticles for *In Vivo* Tumor Targeting and Therapy. *Theranostics* 7 (12), 3168–3178. doi:10.7150/thno.19780

Taylor, M. A., Das, B. C., and Ray, S. K. (2018). Targeting Autophagy for Combating Chemoresistance and Radioresistance in Glioblastoma. *Apoptosis* 23 (11-12), 563–575. doi:10.1007/s10495-018-1480-9

Taylor, R. E., and Zahid, M. (2020). Cell Penetrating Peptides, Novel Vectors for Gene Therapy. *Pharmaceutics* 12 (3). doi:10.3390/pharmaceutics12030225

Wan, J., Wang, J. H., Liu, T., Xie, Z., Yu, X. F., and Li, W. (2015). Surface Chemistry but Not Aspect Ratio Mediates the Biological Toxicity of Gold Nanorods *In Vitro* and *In Vivo*. *Sci. Rep.* 5, 11398. doi:10.1038/srep11398

Wang, J., Sui, L., Huang, J., Miao, L., Nie, Y., Wang, K., et al. (2021). MoS2-based Nanocomposites for Cancer Diagnosis and Therapy. *Bioact Mater.* 6 (11), 4209–4242. doi:10.1016/j.bioactmat.2021.04.021

Wu, X., Wu, Y., Wang, Z., Liu, L., Sun, C., Chen, Y., et al. (2018). A Cascade-Targeting Nanocapsule for Enhanced Photothermal Tumor Therapy with Aid of Autophagy Inhibition. *Adv. Healthc. Mater.* 7 (11), e1800121. doi:10.1002/adhm.201800121

Wyld, L., Audisio, R. A., and Poston, G. J. (2015). The Evolution of Cancer Surgery and Future Perspectives. *Nat. Rev. Clin. Oncol.* 12 (2), 115–124. doi:10.1038/nrclinonc.2014.191

Xiong, S., Xiong, G., Li, Z., Jiang, Q., Yin, J., Yin, T., et al. (2021). Gold Nanoparticle-Based Nanoprobes with Enhanced Tumor Targeting and

Photothermal/photodynamic Response for Therapy of Osteosarcoma. *Nanotechnology* 32 (15), 155102. doi:10.1088/1361-6528/abd816

Xu, X., Lu, H., and Lee, R. (2020). Near Infrared Light Triggered Photo/Immuno-Therapy toward Cancers. *Front. Bioeng. Biotechnol.* 8, 488. doi:10.3389/fbioe.2020.00488

Zarska, M., Sramek, M., Novotny, F., Havel, F., Babelova, A., Mrazkova, B., et al. (2018). Biological Safety and Tissue Distribution of (16-mercaptohexadecyl) trimethylammonium Bromide-Modified Cationic Gold Nanorods. *Biomaterials* 154, 275–290. doi:10.1016/j.biomaterials.2017.10.044

Zhang, M., Kim, H. S., Jin, T., and Moon, W. K. (2017). Near-infrared Photothermal Therapy Using EGFR-Targeted Gold Nanoparticles Increases Autophagic Cell Death in Breast Cancer. *J. Photochem. Photobiol. B* 170, 58–64. doi:10.1016/j.jphotobiol.2017.03.025

Zhang, Y., Zhang, L., Gao, J., and Wen, L. (2019). Pro-Death or Pro-survival: Contrasting Paradigms on Nanomaterial-Induced Autophagy and Exploitations for Cancer Therapy. *Acc. Chem. Res.* 52 (11), 3164–3176. doi:10.1021/acs.accounts.9b00397

Zhang, Z., Wang, J., and Chen, C. (2013). Near-infrared Light-Mediated Nanoplatforms for Cancer Thermo-Chemotherapy and Optical Imaging. *Adv. Mater.* 25 (28), 3869–3880. doi:10.1002/adma.201301890

Zugazagoitia, J., Guedes, C., Ponce, S., Ferrer, I., Molina-Pinelo, S., and Paz-Ares, L. (2016). Current Challenges in Cancer Treatment. *Clin. Ther.* 38 (7), 1551–1566. doi:10.1016/j.clinthera.2016.03.026

Conflict of Interest: The authors declare that the research was conducted in the absence of any commercial or financial relationships that could be construed as a potential conflict of interest.

Publisher's Note: All claims expressed in this article are solely those of the authors and do not necessarily represent those of their affiliated organizations, or those of the publisher, the editors, and the reviewers. Any product that may be evaluated in this article, or claim that may be made by its manufacturer, is not guaranteed or endorsed by the publisher.

Copyright © 2021 Zhang, Lin, Jin, Yu, Qi and Tao. This is an open-access article distributed under the terms of the Creative Commons Attribution License (CC BY). The use, distribution or reproduction in other forums is permitted, provided the original author(s) and the copyright owner(s) are credited and that the original publication in this journal is cited, in accordance with accepted academic practice. No use, distribution or reproduction is permitted which does not comply with these terms.

frontiers in Pharmacology

MINI REVIEW
published: 10 January 2022
doi: 10.3389/fphar.2022.847048

Mitochondria-Targeting Chemodynamic Therapy Nanodrugs for Cancer Treatment

*Qiaohui Chen[1,2†], Niansheng Li[1,2†], Xiaoyuan Wang[1,2], Yuqi Yang[3,4], Yuting Xiang[1,2], Xingyu Long[1,2], Jinping Zhang[3,4], Jia Huang[1,2], Li Chen[1,2] and Qiong Huang[3,4]**

[1]Xiangya School of Pharmaceutical Sciences, Central South University, Changsha, China, [2]Hunan Provincial Key Laboratory of Cardiovascular Research, Xiangya School of Pharmaceutical Sciences, Central South University, Changsha, China, [3]Department of Pharmacy, Xiangya Hospital, Central South University, Changsha, China, [4]National Clinical Research Center for Geriatric Disorders, Xiangya Hospital, Central South University, Changsha, China

Mitochondria, as one of the most critical subcellular organelles of cancer cells, are very vulnerable and often on the verge of oxidative stress. The classic chemodynamic therapy (CDT) directly employs endogenous chemical energy to trigger reactive oxygen species (ROS) burst and destroy tumor cells. However, the effectiveness of CDT is restricted by the limited diffusion distance and short half-life of ROS. From this perspective, the treatment method (mitochondria-targeting chemodynamic therapy nanodrugs, M-CDT nanodrugs) that can generate high levels of ROS at the mitochondrial site is extremely efficient and promising for cancer treatment. Currently, many emerging M-CDT nanodrugs have been demonstrated excellent spatial specificity and anti-cancer efficacy. In this minireview, we review various proof-of-concept researches based on different M-CDT nanodrugs designs to overcome the limits of the efficacy of CDT, mainly divided into four strategies: supplying H_2O_2, non-H_2O_2 dependent CDT, eliminating GSH and enhancing by hyperthermia therapy (HT). These well-designed M-CDT nanodrugs greatly increase the efficacy of CDT. Finally, the progress and potential of M-CDT nanodrugs are discussed, as well as their limitations and opportunities.

Keywords: chemodynamic therapy, mitochondria-targeting, nanomaterials, cancer therapy, reactive oxygen species

OPEN ACCESS

Edited by:
Zeming Liu,
Huazhong University of Science and Technology, China

Reviewed by:
Wu-Yi Sun,
Anhui Medical University, China
Wensheng Chen,
Texas A&M University, United States

****Correspondence:***
Qiong Huang
qionghuang@csu.edu.cn

[†]These authors have contributed equally to this work

Specialty section:
This article was submitted to Pharmacology of Anti-Cancer Drugs, a section of the journal Frontiers in Pharmacology

Received: *01 January 2022*
Accepted: *17 January 2022*
Published: *10 January 2022*

Citation:
Chen Q, Li N, Wang X, Yang Y, Xiang Y, Long X, Zhang J, Huang J, Chen L and Huang Q (2022) Mitochondria-Targeting Chemodynamic Therapy Nanodrugs for Cancer Treatment. Front. Pharmacol. 13:847048. doi: 10.3389/fphar.2022.847048

INTRODUCTION

Many new therapeutic targets and emerging therapies have been developed to find the Achilles heel of cancer cells (de Lázaro and Mooney, 2021). However, most therapy methods cannot completely kill malignant tumors or prevent the formation and recurrence of metastatic tumors (Chen et al., 2020). Mitochondria, as one of the most critical organelles in cancer cells, play a vital role in the energy supply, calcium homeostasis regulation, and signal transduction of cancer cells (Jiang et al., 2021). Mitochondria are also the key regulators of the apoptosis pathway. Damaged mitochondria release pro-apoptotic proteins (like cytochrome c) from the mitochondrial membrane space to the cytoplasm to trigger apoptosis in a typical apoptotic pathway (Bock and Tait, 2020). Moreover, the mitochondria of cancer cells usually undergo metabolic reprogramming for rapid proliferation and invasion, that is, they are more inclined to glycolysis than oxidative phosphorylation to produce ATP (Martínez-Reyes and Chandel, 2021). This process also produces a higher level of reactive oxygen species (ROS), which makes the mitochondria themselves on the verge of oxidative stress (Hayes

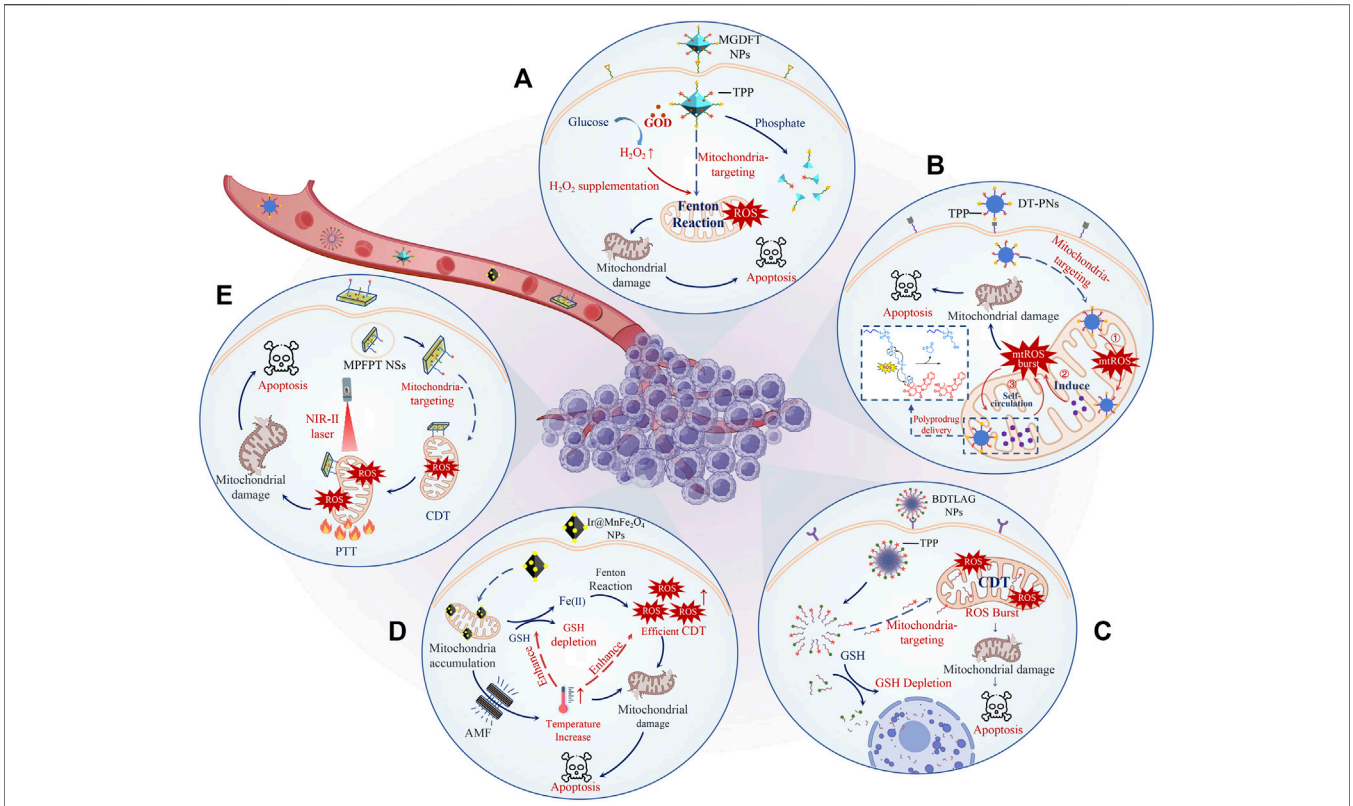


FIGURE 1 | Schematic illustration of representative M-CDT nanodrugs. The therapeutic efficacy of M-CDT nanodrugs is further increased by H_2O_2 supplementation **(A)**, non-H_2O_2 dependent CDT **(B)**, GSH depletion **(C)**, and combination with MHT **(D)** or PTT **(E)**. To be specific, MGDFT NPs catalyzed the decomposition of glucose into H_2O_2 and gluconic acid through loaded GOD, significantly increasing the level of H_2O_2 **(A)**. DT-PNs delivered non-H_2O_2 CDT agents to mitochondria through a poly-prodrug delivery strategy, triggering a ROS burst *in situ* and efficiently killing tumor cells **(B)**. BDTLAG NPs rapidly consumed GSH and released CDT agents through the reaction of disulfide bonds with GSH, which significantly improved the tumor killing effect of ROS **(C)**. Ir@$MnFe_2O_4$ NPs generated high temperatures locally in the mitochondria under the AMF, greatly promoting the rate of Fenton reaction and thus producing a high level of ROS to induce mitochondria damage **(D)**. MPFPT NSs with high photothermal conversion efficiency efficiently accelerated the rate of the Fenton reaction by heating mitochondria, indicating the superiority of PTT-CDT with mitochondria targeting **(E)**.

et al., 2020). ROS has strong oxidative activity and can cause severe oxidative damage (Qin et al., 2021). Therefore, it is an extremely efficient strategy to promote mitochondrial damage to kill cancer cells by increasing the level of ROS in the mitochondrial region (Guo et al., 2021).

ROS-based cancer therapy such as chemodynamic therapies (CDT), photodynamic therapy (PDT), and sonodynamic therapy (SDT) have attracted substantial attention in recent years with the advantages of noninvasiveness, high tumor specificity, minimal toxicity, and low drug resistance (Wang et al., 2021a; Gao et al., 2020a). Among them, CDT has more unique advantages than other methods because it directly employs endogenous H_2O_2 in tumor site to generate toxic ROS through Fenton/Fenton-like reactions (**Eq. 1**) or other ways to kill cancer cells with no need for external energy input or O_2 (Tian et al., 2021). However, ROS is a short-lived and efficient "killer" with a lifetime of less than 0.1 ms and a diffusion range of only 10–20 nm (Zhang et al., 2019). The initial location of ROS production has a significant impact on the therapeutic effect of CDT. CDT agents with targeting mitochondria can produce a high level of ROS *in situ* on mitochondria to cause severely mitochondrial damage and further trigger cell death (Zeng et al., 2021). However, the transport of CDT agents to the mitochondria of cancer cells is a huge bottleneck. In addition, the effect of CDT is greatly limited by the high concentration of glutathione (GSH), the unsustainable supply of H_2O_2, and the low Fenton reaction rate at the tumor site (Wang et al., 2020). Fortunately, the mitochondrial membrane potential of cancer cells is much higher than that in normal cells (~−220 mV vs. ~ −140 mV) (Fantin et al., 2006; Bagkos et al., 2014), which means mitochondria targeting groups with positive electricity and lipophilicity can be preferentially enriched into mitochondria of cancer cells (Shen et al., 2020; Xie et al., 2021). Moreover, the rapid development of nanodrugs has brought new hope for an ideal CDT agent delivery system. Well-designed nanodrugs can greatly increase the penetration of CDT agents at tumor sites by the enhanced permeation and retention (EPR) effect or active targeting (Li et al., 2021a; Nadar et al., 2021). Currently, many emerging CDT nanodrugs with mitochondria-targeting (M-CDT nanodrugs) have recently been demonstrated excellent spatial specificity and anti-cancer efficacy. More importantly, the therapeutic efficacy of M-CDT nanodrugs is further increased by GSH depletion (Wang et al., 2021b), H_2O_2 supplementation (Sun et al., 2021), non-H_2O_2 dependent CDT (Zhang et al., 2019), and combination hyperthermia

TABLE 1 | Nanodrugs for mitochondria-targeting chemodynamic therapy.

Category	Strategy	Nanomaterials	Tumor cell-targeting ligands	Mitochondria-targeting molecules	Size	Fenton agent	Adjuvant therapy
Self-enhanced M-CDT nanodrugs	H_2O_2 supplement	FG/T-Nanoprodrug (Sun et al., 2021)	—	TPP	142 nm	Ferrocene, LND	—
		MGDFT NPs (Peng et al., 2021)	FA	TPP	~400 nm	Fe (II)	Chemotherapy (CT)
		FC-BBR/IND@GOD@HA NPs (Cheng et al., 2022)	HA	Berberine	156 nm	Ferrocene	CT
	non-H_2O_2 dependent CDT	DT-PNs(Zhang et al., 2019)	cRGD	TPP	~55 nm	CPT	—
	GSH depletion	BDTLAG NPs (Wang et al., 2021b)	Biotin	TPP	~140 nm	α-TOS, LND	CT
		CDTLG NPs (Wang et al., 2021c)	Glycyrrhetinic acid	TPP	~147 nm	α-TOS, LND	CT
		TLDCAG NPs (Wang et al., 2021d)	—	TPP	~185 nm	α-TOS, LND	CT
HT enhanced M-CDT nanodrugs	CDT + MHT	Ir@$MnFe_2O_4$ NPs (Shen et al., 2020)	—	Iridium (III) complexes	11.24 ± 1.11 nm	Fe (II)	MHT
	CDT + PTT	CuO@AuCu-TPP nanocarriers (Li et al., 2020)	—	TPP	255 nm	Cu (I)	PTT
		MPFPT NSs(Li et al., 2021c)	—	TPP	~7.2 nm (thickness)	Fe (II)	PTT
		PTFHD nanoplatforms (Jin et al., 2020)	HA	TPP	120 nm	Fe (II)	PTT, CT
	CDT + PDT	TPP-PEG-Au–Ag cages (Wen et al., 2021)	—	TPP	~50 nm	Ag (I)	PDT, PTT
		Fe_3O_4@Dex-TPP/PpIX/ss-mPEG NPs (Hou et al., 2019)	—	TPP	64.34 ± 2.63 nm	Fe (II)	PDT
		UCSRF(Hu et al., 2017)	—	Ru (II) complex	60–80 nm	Fe (II)	PDT

therapy. This minireview focuses on the latest progress of M-CDT nanodrugs because of the significance of M-CDT nanodrugs and many advances in this research field. We divide these M-CDT nanodrugs into two parts to comprehensively summarize: Firstly, self-enhanced M-CDT nanodrugs with H_2O_2 supplementation, non-H_2O_2 dependent CDT, and GSH depletion; Secondly, HT enhanced M-CDT nanodrugs (**Figure 1**; **Table 1**). Finally, we propose the future development direction and challenges of M-CDT nanodrugs. This review provides the most advanced treatment methods and valuable information for cancer treatment.

$$H_2O_2+Fe^{2+} \rightarrow \cdot OH + OH^- + Fe^{3+} \quad (1)$$

SELF-ENHANCED M-CDT NANODRUGS

Cancer cells have a much higher level of H_2O_2 (up to 100 mM) than normal cells (20 nM), which is also the first prerequisite for CDT treatment (Tang et al., 2020). However, H_2O_2 cannot be continuously supplied, which greatly limits the effect of CDT (Xuan et al., 2020). In addition, cancer cells have high concentrations of GSH to balance the oxidative stress caused by ROS (Langford et al., 2018). The ROS can easily be eliminated by the GSH-Glutathione peroxidase system during CDT treatment. Currently, three strategies are developed to greatly improve the efficacy of M-CDT nanodrugs: supplying H_2O_2, non-H_2O_2 dependent CDT, and eliminating GSH in cancer cells.

H_2O_2 is still insufficient for continuous ·OH generation during Fenton reaction-based CDT. Therefore, M-CDT nanodrugs with H_2O_2-supplement are advantageous for maintaining continuous oxidative damage (Cheng et al., 2022). For example, Peng et al. (2021) designed phosphate-degradable nanoparticles based on metal-organic frameworks nanocarriers (MGDFT NPs) with glucose oxidase (GOD) and doxorubicin (DOX) for CDT of cancer. Mil-101 (Fe) was selected as the nanocarrier for DOX and GOD, as well as the iron source for the Fenton reaction. Then Mil-101 (Fe) was modified by folic acid (FA) and triphenylphosphonium (TPP) to get a sequential targeting efficiency to cancer cells and mitochondria in cancer cells, respectively. Furthermore, MIL-101(Fe) was phosphate-sensitive and easy to degrade in cancer cells with the high concentration of phosphate, and MGDFT NPs disintegrated quickly to release iron ions and GOD. GOD catalyzed efficiently the reaction of glucose and O_2 to produce gluconic acid and H_2O_2, which supplied the Fenton reaction substrate and prolonged CDT treatment duration. The level of ROS produced by MGDFT NPs was 4.4 times that of the NPs without GOD in 4T1 cells. The growth of cancer cells was successfully inhibited by MGDFT NPs without obvious side effects. Similarly, Sun et al. (2021) developed M-CDT nanodrugs loaded with GOD and lonidamine (FG/T-Nanoprodrug) for the chemotherapy and CDT combination therapy. The FG/T-Nanoprodrug was prepared in two steps: First, a T-Prodrug containing polylysine, TPP, and lonidamine self-assembled to form nanoparticles; Secondly, GOD and ferrocene (a Fenton reaction catalyst) were linked to the surface of nanoparticles to prepare the FG/T-Nanoprodrug. The FG/T-Nanoprodrug

entered the mitochondria of cancer cells mediated by TPP and then released lonidamine and GOD. Lonidamine, as a hexokinase inhibitor (the rate-limiting enzyme of glycolysis), reduced glucose utilization by inhibiting mitochondrial energy metabolism, which allowed more glucose to be converted by GOD into H_2O_2 in cancer cells. The FG/T-Nanoprodrug continuously produced abundant ROS to destroy mitochondria and release cytochrome c. Tumor tissues treated with the FG/T-Nanoprodrug had a 7-fold increase of ROS levels compared to the saline group after 7 days. The FG/T-Nanoprodrug demonstrated extremely strong tumor suppression and ablation in a tumor xenograft model.

Non-H_2O_2 dependent CDT completely avoids the bottleneck problem that H_2O_2 cannot be continuously supplied in cancer cells (Gao et al., 2020b). Some chemotherapy drugs can directly stimulate the generation of endogenous ROS by interacting with the mitochondrial respiratory chain complex, which is considered to have CDT effect as well (Wang et al., 2021c; Wang et al., 2021d). For example, camptothecin (CPT), as an atypical CDT agent, can not only inhibit DNA topoisomerase I but stimulate the production of endogenous mitochondrial ROS to hyperpolarize mitochondria (Sánchez-Alcázar et al., 2000; Sen et al., 2004). Recently, Zhang et al. (2019) developed ROS-responsive polyprodrug nanoreactors with dual-targeting properties (DT-PNs) for cancer therapy. DT-PNS was self-assembled with two polyprodrug amphiphiles connected with multi-CPTs through the ROS-responsive thioketal linkage: cRGD-PDMA-bPCPTSM and TPP-PDMA-bPCPTSM. The decorated cyclic Arg-Gly-Asp (cRGD) peptide and TPP targeted the overexpressed integrins on the surface of cancer cells and mitochondria, respectively. As a result, DT-PNs internalized by cancer cells precisely anchored the mitochondria and released the initial CPT in response to endogenous upregulated mitochondrial ROS, while the CPT released *in situ* further triggered mitochondrial ROS, and finally formed a CPT-ROS circulation to generate a ROS burst in mitochondria. The self-circulation of CPT release and ROS burst led to mitochondrial-dependent apoptosis and efficiently killed cancer cells.

Very recently, Wang et al. (2021b) constructed a sequential multi-stage targeting nanoparticles (BDTLAG NPs) to increase the effect of non-H_2O_2 dependent CDT by GSH depletion. The BDTLAG NPs consisted of three parts: two mitochondria targeting CDT agents (TPP-PEG_{2K}-LND and TPP-PEG_{2K}-TOS) and a GSH scavenging group (Bio-PEG_{2K}-S-S-CPT). The TPP group mediated the mitochondria targeting of lonidamine (LND) and α-tocopheryl succinate (α-TOS), both of which interfered with the mitochondrial energy metabolism to stimulate endogenous ROS production. Importantly, the Bio-PEG_{2K}-S-S-CPT part of BDTLAG NPs actively targeted cancer cells because the surface of the cancer cells expresses biotin (Bio) receptors. The disulfide bond in the BDTLAG NPs broke to release CPT, LND, and TOS by reacting with GSH in cancer cells. The effect of depletion GSH was measured by the released CPT. Bio-PEG_{2K}-S-S-CPT effectively removed GSH in cancer cells, and the CPT released by Bio-PEG_{2K}-S-S-CPT was 6.8 times higher than that by the group without GSH response in cancer cells. At the same time, LND and TOS entered the mitochondria and caused high concentrations of ROS *in situ* on mitochondria, which led to mitochondria damage to induce the death of cancer cells. Compared with the CPT group and the BDG NPs group (without mitochondria targeting), BDTLAG NPs had the best tumor suppression effect because of their mitochondria targeting and efficient GSH depletion.

HT ENHANCED M-CDT NANODRUGS

The slower reaction rate of CDT based on Fenton reaction is also a major factor limitation of the effectiveness of CDT (Cao et al., 2021). The high temperature from hyperthermia therapy (HT) can improve the rate of the Fenton/Fenton-like reaction to greatly increase the efficacy of CDT (Liu et al., 2019; Danewalia and Singh, 2021). Recently, Shen et al. (2020) reported $MnFe_2O_4$ NPs functionalized with Ir (III) complexes (Ir@$MnFe_2O_4$ NPs) for magnetic hyperthermia therapy (MHT) enhanced CDT. Cyclometalated iridium (III) complexes effectively targeted tumor cells inner mitochondrial membrane with high membrane potential. $MnFe_2O_4$ with superparamagnetism responded quickly to external magnetic fields and had excellent magnetothermal-properties including high magnetothermal conversion efficiency and magnetothermal stability. Therefore, Ir@$MnFe_2O_4$ NPs were internalized into cancer cells via the EPR effect and localized in mitochondria with help of cyclometalated iridium (III) complexes. GSH in cancer cells reduced the Fe (III) to Fe (II) on Ir@$MnFe_2O_4$ NPs surfaces to catalyze the Fenton reaction. More importantly, Ir@$MnFe_2O_4$ NPs generated high temperatures locally in the mitochondria under the alternating magnetic field (AMF), which produced a high level of ROS to induce mitochondria damage by greatly promoting the rate of the Fenton reaction. Ir@$MnFe_2O_4$NPs + AMF demonstrated a much stronger effect of inhibiting tumor growth than Ir@$MnFe_2O_4$NPs and AMF due to the synergistic effect of MHT and CDT.

Local high temperature through near-infrared light is also an effective strategy to enhance the efficacy of CDT (Zhou et al., 2019; Li et al., 2021b). For example, Jin et al. (2020) recently reported dual-targeted core-shell nanoplatforms (PTFHD nanoplatforms) for photothermal therapy (PTT) enhanced CDT. The PTFHD nanoplatforms were composed of hyaluronic acid (HA) and TPP co-modified polydopamine (PDA) nanoparticles loaded with DOX and Fe ions. HA and TPP mediated the sequential multistage-targeting of PTFHD nanoplatforms from cancer cells to their mitochondria. The PTFHD nanoplatforms catalyzed Fenton reaction by Fe ions in mitochondria after enzymolysis of HA shell and exposure of PDA-TPP-Fe core. PDA was a high-efficiency photothermal agent with high photothermal conversion efficiency. The PTFHD nanoplatforms lead to the local high temperature of mitochondria site under the irradiation of near-infrared laser (808 nm), which greatly promoted the rate of the Fenton reaction and damages the mitochondria. The second near-infrared (1,000–1,350 nm, NIR-II) has deeper tissue penetration and higher maximum allowable exposure than the first near-infrared (750–1,000 nm, NIR-I) light

(Wang et al., 2021e; Liu et al., 2021; Zhang et al., 2021). Very recently, Li et al. (2021c) developed mitochondria-targeted MoS_2@PDA-Fe@PEG/TPP nanosheets (MPFPT NSs) for the combination therapy of NIR-II-activated PTT and CDT. MPFPT NSs had a high photothermal conversion efficiency at NIR-II (34.9%). In addition, the Fe doped in MPFPT NSs was adopted as a Fenton reaction catalyst. MPFPT NSs significantly led to mitochondrial dysfunction and cancer cell apoptosis through TPP-mediated mitochondria targeting under NIR-II light (1,064 nm). The MPFPTNSs had a better tumor suppressive effect than similar nanoagents without mitochondria targeting ability or relying on single-mode therapy thanks to the superiority of PTT-CDT with mitochondria targeting.

Iron-based Fenton reaction has a low reaction rate. In addition, the optimal pH value for iron-based Fenton reaction is usually pH 2-5, and the reaction rate is low in the neutral intracellular environment of tumor cells (pH7.4) (Bao et al., 2021). The Fenton reaction rate of Cu(I) ($1 \times 10^4\ M^{-1}s^{-1}$) is much higher than that of Fe (II) ($76\ M^{-1}s^{-1}$) (Hu et al., 2019; Li et al., 2019; Lin et al., 2019). Meanwhile, the pH range required for the reaction of Cu(I) is wider than that of Fe(II), which can be carried out in weakly acidic and neutral media (Ma et al., 2019). Recently, Li et al. (2020) proposed an exo/endogenous dual-augmented mitochondria targeting nanoplatform (CuO@AuCu-TPP) for PTT-enhanced CDT by Cu(I) mediated Fenton reaction. The CuO@AuCu was prepared by *in-situ* reduction of chloroauric acid on Cu_2O truncated octahedron. In this process, the Cu(I) in truncated octahedron was converted to Cu (II), and chloroauric acid was reduced to small gold nanoparticles on the surface of Cu_2O truncated octahedrons. The CuO@AuCu were further modified with TPP (CuO@AuCu-TPP) to target the mitochondria of cancer cells. The aggregates of small gold nanoparticles on the surface of CuO@AuCu-TPP were adopted as a powerful photothermal agent because of their strong near-infrared absorption. Cu (II) was reduced into Cu (I) by GSH after CuO@AuCu-TPP were enriched in mitochondria, which deleted GSH and initiated a rapid Fenton reaction. Moreover, ROS generation efficiency of the CuO@AuCu-TPP further increased by 4.6 times under the irradiation of near-infrared light (808 nm). The CuO@AuCu-TPP possessed an excellent antitumor effect due to the PTT enhanced CDT and GSH depletion in Balb/c mice tumor models.

CONCLUSION AND PROSPECT

Traditional anticancer drugs including CDT agents are limited by their poor pharmacokinetic properties, such as low bioavailability, short half-life and low stability. Fortunately, nanotechnology can effectively improve the pharmacokinetic characteristics of traditional drugs by changing the size, shape and material characteristics of nanomaterials (Liu et al., 2012; Chen et al., 2021; Zhao et al., 2022; Zhu et al., 2022). Especially, well-designed nanodrugs can greatly increase the penetration of drugs at tumor sites and improve their pharmacokinetic and pharmacodynamic properties by the EPR effect. After decades of development, some nanodrugs have been approved for clinical cancer treatment, such as liposomes, polymer micelles, and inorganic nanomaterials (Cheng et al., 2021). However, most of these nanodrugs are carried with traditional chemotherapeutic drugs. Fundamentally, these nanodrugs are difficult to solve the resistance of cancer cells to traditional chemotherapeutic drugs, and have limited efficacy for cancer. Mitochondria are probably the most vulnerable part of cancer cells, because mitochondria not only play an irreplaceable core role in cancer cells but are also a key link in the apoptosis pathway of cancer cells. Therefore, mitochondria are likely to be the Achilles heel of cancer cells. Compared with non-mitochondria-targeting treatments, M-CDT nanodrugs exhibit higher therapeutic effect with lower dosage of drugs via precise and severe damage to mitochondria. More importantly, M-CDT nanodrugs are expected to solve the resistance of traditional drugs, because the resistance of cancer cells is generally ATP-dependent. For example, P-glycoproteins use ATP produced by mitochondria to pump a variety of anti-cancer drugs with different structures and different molecular weights out of the cancer cell, which is why cancer cells acquire multiple drug resistance. These emerging M-CDT nanodrugs destroy mitochondria very efficiently and fundamentally eliminate the multi-drug resistance of cancer cells. In short, M-CDT nanodrugs have great advantages over traditional drugs and conventional CDT nanodrugs, and have demonstrated amazing effects of cancer treatment. However, M-CDT nanodrugs still have some challenges to overcome.

First, M-CDT nanodrugs with the classic iron-based Fenton reaction face the bottleneck of insufficient reaction rate. Iron is a ubiquitous element in the human body and has excellent biocompatibility. However, the biggest problem lies in its low efficiency under the conditions of the cancer microenvironment. Hyperthermia can increase the reaction rate, but it brings complexity to the treatment and does not fundamentally solve the problem. In addition, other transition metals such as Cu, Pt, etc. are adopted to increase the reaction rate. However, the biocompatibility of transition metals is far less than that of iron (Ai et al., 2021). Reducing the pH of cancer cells is a very promising solution. The deduction of pH in tumor cells reinforces the response rate of the classic Fenton reaction-based CDT and simultaneously induces mitochondrial calcium overload, and these two resulting effects synergistically cause mitochondrial dysfunction and therefore tumor cell death (Bao et al., 2021). Secondly, for non-H_2O_2-dependent M-CDT nanodrugs, precise control of CDT drugs release on the mitochondria is a great challenge. Most of these CDT drugs can produce ROS only when they interfere with the mitochondrial respiratory chain in the inner mitochondrial membrane. In addition, these CDT drugs generally belong to traditional high toxic chemotherapy drugs, and their uncontrollable release can cause great side effects. Third, cancer cells themselves have sophisticated antioxidant defense systems, such as abundant GSH and antioxidant enzyme systems, etc (Su et al., 2021). Therefore, M-CDT nanodrugs often need to intervene in the various factor of antioxidant defense systems. Integrating multiple functions on M-CDT nanodrugs is still a great challenge.

Nevertheless, M-CDT nanodrugs are very promising in cancer treatment. M-CDT nanodrugs will be undergoing rapid

development with a deeper understanding of tumor pathology and treatment methods. We hope that a new way for the clinical transformation of the M-CDT nanodrugs will be opened through the optimized design of M-CDT nanodrugs.

AUTHOR CONTRIBUTIONS

All authors listed have made a substantial, direct, and intellectual contribution to the work and approved it for publication.

FUNDING

This work was supported by the National Natural Science Foundation of China (No. 81974508, 21974134), the Hunan Science Fund for Distinguished Young Scholar of China (No. 2021JJ10067), Innovation-Driven Project of Central South University (No. 202045005), Hunan Provincial Natural Science Foundation of China (No. 2021JJ31066), Changsha Science and Technology Project (No. kq2001048), Key Research Project of Ningxia Hui Autonomous Region in 2021 of China (Major Project) (No. 2021BEG01001).

REFERENCES

Ai, K., Huang, J., Xiao, Z., Yang, Y., Bai, Y., and Peng, J. (2021). Localized Surface Plasmon Resonance Properties and Biomedical Applications of Copper Selenide Nanomaterials. *Mater. Today Chem.* 20, 100402. doi:10.1016/j.mtchem.2020.100402

Bagkos, G., Koufopoulos, K., and Piperi, C. (2014). A New Model for Mitochondrial Membrane Potential Production and Storage. *Med. Hypotheses* 83, 175–181. doi:10.1016/j.mehy.2014.05.001

Bao, W., Liu, M., Meng, J., Liu, S., Wang, S., Jia, R., et al. (2021). MOFs-based Nanoagent Enables Dual Mitochondrial Damage in Synergistic Antitumor Therapy via Oxidative Stress and Calcium Overload. *Nat. Commun.* 12, 6399. doi:10.1038/s41467-021-26655-4

Bock, F. J., and Tait, S. W. G. (2020). Mitochondria as Multifaceted Regulators of Cell Death. *Nat. Rev. Mol. Cel Biol* 21, 85–100. doi:10.1038/s41580-019-0173-8

Cao, W., Jin, M., Yang, K., Chen, B., Xiong, M., Li, X., et al. (2021). Fenton/Fenton-like Metal-Based Nanomaterials Combine with Oxidase for Synergistic Tumor Therapy. *J. Nanobiotechnol* 19, 325. doi:10.1186/s12951-021-01074-1

Chen, J., Zhu, Y., Wu, C., and Shi, J. (2020). Nanoplatform-based cascade Engineering for Cancer Therapy. *Chem. Soc. Rev.* 49, 9057–9094. doi:10.1039/d0cs00607f

Chen, L., Huang, Q., Zhao, T., Sui, L., Wang, S., Xiao, Z., et al. (2021). Nanotherapies for Sepsis by Regulating Inflammatory Signals and Reactive Oxygen and Nitrogen Species: New Insight for Treating COVID-19. *Redox Biol.* 45, 102046. doi:10.1016/j.redox.2021.102046

Cheng, Y., Ji, Y., and Ouyang, D. (2022). FC-BBR/IND-induced Glucose Oxidase Nanodrugs for Targeted Combination Therapy. *Int. J. Pharm.* 611, 121349. doi:10.1016/j.ijpharm.2021.121349

Cheng, Z., Li, M., Dey, R., and Chen, Y. (2021). Nanomaterials for Cancer Therapy: Current Progress and Perspectives. *J. Hematol. Oncol.* 14, 85. doi:10.1186/s13045-021-01096-0

Danewalia, S. S., and Singh, K. (2021). Bioactive Glasses and Glass-Ceramics for Hyperthermia Treatment of Cancer: State-Of-Art, Challenges, and Future Perspectives. *Mater. Today Bio* 10, 100100. doi:10.1016/j.mtbio.2021.100100

de Lázaro, I., and Mooney, D. J. (2021). Obstacles and Opportunities in a Forward Vision for Cancer Nanomedicine. *Nat. Mater.* 20, 1469–1479. doi:10.1038/s41563-021-01047-7

Fantin, V. R., St-Pierre, J., and Leder, P. (2006). Attenuation of LDH-A Expression Uncovers a Link between Glycolysis, Mitochondrial Physiology, and Tumor Maintenance. *Cancer cell* 9, 425–434. doi:10.1016/j.ccr.2006.04.023

Gao, D., Guo, X., Zhang, X., Chen, S., Wang, Y., Chen, T., et al. (2020). Multifunctional Phototheranostic Nanomedicine for Cancer Imaging and Treatment. *Mater. Today Bio* 5, 100035. doi:10.1016/j.mtbio.2019.100035

Gao, F., Wang, F., Nie, X., Zhang, Z., Chen, G., Xia, L., et al. (2020). Mitochondria-targeted Delivery and Light Controlled Release of Iron Prodrug and CO to Enhance Cancer Therapy by Ferroptosis. *New J. Chem.* 44, 3478–3486. doi:10.1039/c9nj05860e

Guo, X., Yang, N., Ji, W., Zhang, H., Dong, X., Zhou, Z., et al. (2021). Mito-Bomb: Targeting Mitochondria for Cancer Therapy. *Adv. Mater.* 33, 2007778. doi:10.1002/adma.202007778

Hayes, J. D., Dinkova-Kostova, A. T., and Tew, K. D. (2020). Oxidative Stress in Cancer. *Cancer cell* 38, 167–197. doi:10.1016/j.ccell.2020.06.001

Hou, H., Huang, X., Wei, G., Xu, F., Wang, Y., and Zhou, S. (2019). Fenton Reaction-Assisted Photodynamic Therapy for Cancer with Multifunctional Magnetic Nanoparticles. *ACS Appl. Mater. Inter.* 11, 29579–29592. doi:10.1021/acsami.9b09671

Hu, P., Wu, T., Fan, W., Chen, L., Liu, Y., Ni, D., et al. (2017). Near Infrared-Assisted Fenton Reaction for Tumor-specific and Mitochondrial DNA-Targeted Photochemotherapy. *Biomaterials* 141, 86–95. doi:10.1016/j.biomaterials.2017.06.035

Hu, R., Fang, Y., Huo, M., Yao, H., Wang, C., Chen, Y., et al. (2019). Ultrasmall Cu2-xS Nanodots as Photothermal-Enhanced Fenton Nanocatalysts for Synergistic Tumor Therapy at NIR-II Biowindow. *Biomaterials* 206, 101–114. doi:10.1016/j.biomaterials.2019.03.014

Jiang, L., Zhou, S., Zhang, X., Li, C., Ji, S., Mao, H., et al. (2021). Mitochondrion-specific Dendritic Lipopeptide Liposomes for Targeted Sub-cellular Delivery. *Nat. Commun.* 12, 2390. doi:10.1038/s41467-021-22594-2

Jin, R., Wang, Q., Dou, G., Bai, Y., Liu, S., Cai, B., et al. (2020). Stimuli Responsive Nanoplatform with Mitochondria-specific Multiple Model Therapeutics for Effective Tumor Treatment. *Applied Materials Today* 21, 100883. doi:10.1016/j.apmt.2020.100883

Langford, T. F., Huang, B. K., Lim, J. B., Moon, S. J., and Sikes, H. D. (2018). Monitoring the Action of Redox-Directed Cancer Therapeutics Using a Human Peroxiredoxin-2-Based Probe. *Nat. Commun.* 9, 3145. doi:10.1038/s41467-018-05557-y

Li, X., Hao, S., Han, A., Yang, Y., Fang, G., Liu, J., et al. (2019). Intracellular Fenton Reaction Based on Mitochondria-Targeted Copper(II)-peptide Complex for Induced Apoptosis. *J. Mater. Chem. B* 7, 4008–4016. doi:10.1039/c9tb00569b

Li, W., Wang, S., Ren, C., Liu, P., Lu, Q., Yang, L., et al. (2020). Exo/endogenous Dual-Augmented Chemodynamic Therapy Based on Bio-Reducible and Bio-Breakable Copper (Ⅱ)-based Truncated Octahedron. *Chem. Eng. J.* 396, 125280. doi:10.1016/j.cej.2020.125280

Li, S. L., Jiang, P., Jiang, F. L., and Liu, Y. (2021). Recent Advances in Nanomaterial-Based Nanoplatforms for Chemodynamic Cancer Therapy. *Adv. Funct. Mater.* 31, 2100243. doi:10.1002/adfm.202100243

Li, X., Yuan, H. J., Tian, X. M., Tang, J., Liu, L. F., and Liu, F. Y. (2021). Biocompatible Copper Sulfide-Based Nanocomposites for Artery Interventional Chemo-Photothermal Therapy of Orthotropic Hepatocellular Carcinoma. *Mater. Today Bio* 12, 100128. doi:10.1016/j.mtbio.2021.100128

Li, X., Xiao, H., Xiu, W., Yang, K., Zhang, Y., Yuwen, L., et al. (2021). Mitochondria-Targeting MoS2-Based Nanoagents for Enhanced NIR-II Photothermal-Chemodynamic Synergistic Oncotherapy. *ACS Appl. Mater. Inter.* 13, 55928–55938. doi:10.1021/acsami.1c18311

Lin, K., Lin, Z., Li, Y., Zheng, Y., and Zhang, D. (2019). Ultrasound-induced Reactive Oxygen Species Generation and Mitochondria-specific Damage by Sonodynamic Agent/metal Ion-Doped Mesoporous Silica. *RSC Adv.* 9, 39924–39931. doi:10.1039/c9ra08142a

Liu, Y., Ai, K., and Lu, L. (2012). Nanoparticulate X-ray Computed Tomography Contrast Agents: From Design Validation to *In Vivo* Applications. *Acc. Chem. Res.* 45, 1817–1827. doi:10.1021/ar300150c

Liu, X., Liu, Y., Wang, J., Wei, T., and Dai, Z. (2019). Mild Hyperthermia-Enhanced Enzyme-Mediated Tumor Cell Chemodynamic Therapy. *ACS Appl. Mater. Inter.* 11, 23065–23071. doi:10.1021/acsami.9b08257

Liu, S., Li, Y., Zhang, J., Zhang, H., Wang, Y., Chuah, C., et al. (2021). A Two-In-One Janus NIR-II AIEgen with Balanced Absorption and Emission for Image-

Guided Precision Surgery. *Mater. Today Bio* 10, 100087. doi:10.1016/j.mtbio.2020.100087

Ma, B., Wang, S., Liu, F., Zhang, S., Duan, J., Li, Z., et al. (2019). Self-Assembled Copper-Amino Acid Nanoparticles for *In Situ* Glutathione "AND" H2O2 Sequentially Triggered Chemodynamic Therapy. *J. Am. Chem. Soc.* 141, 849–857. doi:10.1021/jacs.8b08714

Martínez-Reyes, I., and Chandel, N. S. (2021). Cancer Metabolism: Looking Forward. *Nat. Rev. Cancer* 21, 669–680. doi:10.1038/s41568-021-00378-6

Nadar, R. A., Franssen, G. M., Van Dijk, N. W. M., Codee-van der Schilden, K., de Weijert, M., Oosterwijk, E., et al. (2021). Bone Tumor-Targeted Delivery of Theranostic 195mPt-Bisphosphonate Complexes Promotes Killing of Metastatic Tumor Cells. *Mater. Today Bio* 9, 100088. doi:10.1016/j.mtbio.2020.100088

Peng, H., Qin, Y. T., Feng, Y. S., He, X. W., Li, W. Y., and Zhang, Y. K. (2021). Phosphate-Degradable Nanoparticles Based on Metal-Organic Frameworks for Chemo-Starvation-Chemodynamic Synergistic Antitumor Therapy. *ACS Appl. Mater. Inter.* 13, 37713–37723. doi:10.1021/acsami.1c10816

Qin, X., Wu, C., Niu, D., Qin, L., Wang, X., Wang, Q., et al. (2021). Peroxisome Inspired Hybrid Enzyme Nanogels for Chemodynamic and Photodynamic Therapy. *Nat. Commun.* 12, 5243. doi:10.1038/s41467-021-25561-z

Sánchez-Alcázar, J. A., Ault, J. G., Khodjakov, A., and Schneider, E. (2000). Increased Mitochondrial Cytochrome C Levels and Mitochondrial Hyperpolarization Precede Camptothecin-Induced Apoptosis in Jurkat Cells. *Cell Death Differ* 7, 1090–1100. doi:10.1038/sj.cdd.4400740

Sen, N., Das, B. B., Ganguly, A., Mukherjee, T., Tripathi, G., Bandyopadhyay, S., et al. (2004). Camptothecin Induced Mitochondrial Dysfunction Leading to Programmed Cell Death in Unicellular Hemoflagellate Leishmania Donovani. *Cel Death Differ* 11, 924–936. doi:10.1038/sj.cdd.4401435

Shen, J., Rees, T. W., Zhou, Z., Yang, S., Ji, L., and Chao, H. (2020). A Mitochondria-Targeting Magnetothermogenic Nanozyme for Magnet-Induced Synergistic Cancer Therapy. *Biomaterials* 251, 120079. doi:10.1016/j.biomaterials.2020.120079

Su, X., Cao, Y., Liu, Y., Ouyang, B., Ning, B., Wang, Y., et al. (2021). Localized Disruption of Redox Homeostasis Boosting Ferroptosis of Tumor by Hydrogel Delivery System. *Mater. Today Bio* 12, 100154. doi:10.1016/j.mtbio.2021.100154

Sun, M., Wang, C., Lv, M., Fan, Z., and Du, J. (2021). Mitochondrial-targeting Nanoprodrugs to Mutually Reinforce Metabolic Inhibition and Autophagy for Combating Resistant Cancer. *Biomaterials* 278, 121168. doi:10.1016/j.biomaterials.2021.121168

Tang, Y., Ji, Y., Yi, C., Cheng, D., Wang, B., Fu, Y., et al. (2020). Self-accelerating H2O2-Responsive Plasmonic Nanovesicles for Synergistic Chemo/starving Therapy of Tumors. *Theranostics* 10, 8691–8704. doi:10.7150/thno.45392

Tian, Q., Xue, F., Wang, Y., Cheng, Y., An, L., Yang, S., et al. (2021). Recent Advances in Enhanced Chemodynamic Therapy Strategies. *Nano Today* 39, 101162. doi:10.1016/j.nantod.2021.101162

Wang, X., Zhong, X., Liu, Z., and Cheng, L. (2020). Recent Progress of Chemodynamic Therapy-Induced Combination Cancer Therapy. *Nano Today* 35, 100946. doi:10.1016/j.nantod.2020.100946

Wang, X. Q., Wang, W., Peng, M., and Zhang, X. Z. (2021). Free Radicals for Cancer Theranostics. *Biomaterials* 266, 120474. doi:10.1016/j.biomaterials.2020.120474

Wang, N., Liu, C., Yao, W., Zhou, H., Yu, S., Chen, H., et al. (2021). A Traceable, Sequential Multistage-Targeting Nanoparticles Combining Chemo/Chemodynamic Therapy for Enhancing Antitumor Efficacy. *Adv. Funct. Mater.* 31, 2101432. doi:10.1002/adfm.202101432

Wang, N., Liu, C., Yao, W., Wang, X., Zhou, H., Chen, H., et al. (2021). A Sequential Multistage-Targeted Nanoparticles for MR Imaging and Efficient Chemo/chemodynamic Synergistic Therapy of Liver Cancer. *Applied Materials Today* 24, 101147. doi:10.1016/j.apmt.2021.101147

Wang, N., Liu, C., Yao, W., Zhou, H., Yu, S., Chen, H., et al. (2021). Endogenous Reactive Oxygen Species Burst Induced and Spatiotemporally Controlled Multiple Drug Release by Traceable Nanoparticles for Enhancing Antitumor Efficacy. *Biomater. Sci.* 9, 4968–4983. doi:10.1039/d1bm00668a

Wang, J., Sui, L., Huang, J., Miao, L., Nie, Y., Wang, K., et al. (2021). MoS2-based Nanocomposites for Cancer Diagnosis and Therapy. *Bioact Mater.* 6, 4209–4242. doi:10.1016/j.bioactmat.2021.04.021

Wen, Y. L., Chen, L., Leng, F., Yang, Z. Y., and Yu, C. (2021). Bimetallic Au-Ag Nanocages Extended TPP Conjugate Structure for Self-Enhancing Therapy of Tumors. *J. Nanostructure Chem.* doi:10.1007/s40097-021-00457-y

Xie, L., Wang, L., Guan, R., Ji, L., and Chao, H. (2021). Anti-metastasis and Anti-proliferation Effect of Mitochondria-Accumulating Ruthenium(II) Complexes via Redox Homeostasis Disturbance and Energy Depletion. *J. Inorg. Biochem.* 217, 111380. doi:10.1016/j.jinorgbio.2021.111380

Xuan, W., Xia, Y., Li, T., Wang, L., Liu, Y., and Tan, W. (2020). Molecular Self-Assembly of Bioorthogonal Aptamer-Prodrug Conjugate Micelles for Hydrogen Peroxide and pH-independent Cancer Chemodynamic Therapy. *J. Am. Chem. Soc.* 142, 937–944. doi:10.1021/jacs.9b10755

Zeng, Z., Fang, C., Zhang, Y., Chen, C.-X., Zhang, Y.-F., and Zhang, K. (2021). Mitochondria-Targeted Nanocarriers Promote Highly Efficient Cancer Therapy: A Review. *Front. Bioeng. Biotechnol.* 9, 1060. doi:10.3389/fbioe.2021.784602

Zhang, W., Hu, X., Shen, Q., and Xing, D. (2019). Mitochondria-specific Drug Release and Reactive Oxygen Species Burst Induced by Polyprodrug Nanoreactors Can Enhance Chemotherapy. *Nat. Commun.* 10, 1704. doi:10.1038/s41467-019-09566-3

Zhang, Y., Zhang, S., Zhang, Z., Ji, L., Zhang, J., Wang, Q., et al. (2021). Recent Progress on NIR-II Photothermal Therapy. *Front. Chem.* 9, 728066. doi:10.3389/fchem.2021.728066

Zhao, T., Wu, W., Sui, L., Huang, Q., Nan, Y., Liu, J., et al. (2022). Reactive Oxygen Species-Based Nanomaterials for the Treatment of Myocardial Ischemia Reperfusion Injuries. *Bioactive Mater.* 7, 47–72. doi:10.1016/j.bioactmat.2021.06.006

Zhou, W., Guan, H., Sun, K., Xing, Y., and Zhang, J. (2019). FeOOH/Polypyrrole Nanocomposites with an Islands-In-Sea Structure toward Combined Photothermal/Chemodynamic Therapy. *ACS Appl. Bio Mater.* 2, 2708–2714. doi:10.1021/acsabm.9b00435

Zhu, Y., Zhao, T., Liu, M., Wang, S., Liu, S., Yang, Y., et al. (2022). Rheumatoid Arthritis Microenvironment Insights into Treatment Effect of Nanomaterials. *Nano Today* 42, 101358. doi:10.1016/j.nantod.2021.101358

Conflict of Interest: The authors declare that the research was conducted in the absence of any commercial or financial relationships that could be construed as a potential conflict of interest.

Publisher's Note: All claims expressed in this article are solely those of the authors and do not necessarily represent those of their affiliated organizations, or those of the publisher, the editors and the reviewers. Any product that may be evaluated in this article, or claim that may be made by its manufacturer, is not guaranteed or endorsed by the publisher.

Copyright © 2022 Chen, Li, Wang, Yang, Xiang, Long, Zhang, Huang, Chen and Huang. This is an open-access article distributed under the terms of the Creative Commons Attribution License (CC BY). The use, distribution or reproduction in other forums is permitted, provided the original author(s) and the copyright owner(s) are credited and that the original publication in this journal is cited, in accordance with accepted academic practice. No use, distribution or reproduction is permitted which does not comply with these terms.

frontiers in Oncology

REVIEW
published: 12 January 2022
doi: 10.3389/fonc.2021.828810

Nanomaterial Technology and Triple Negative Breast Cancer

Kai Hou[†], *Zeng Ning*[†], *Hongbo Chen and Yiping Wu*[*]

Department of Plastic and Cosmetic Surgery, Tongji Hospital, Tongji Medical College, Huazhong University of Science and Technology, Wuhan, China

Triple negative breast cancer (TNBC) is a malignant breast cancer subtype that is prone to progression, with high associated metastasis and five-year mortality rates and an overall poor prognosis. Chemotherapy is usually administered to treat TNBC without additional targeted therapies. Novel nanomaterials have a variety of excellent physical and chemical properties and biological functions (including targeting specificity), and contrast agents and drug delivery vectors based on nanotechnology are progressing towards a more accurate and targeted direction. This review discusses the mechanisms of action and prospects for the use of nanotechnology in the treatment of TNBC, thus providing potential new strategies for the diagnosis and treatment of TNBC.

Keywords: nanomaterial, nanotechnology, nanobiosensors, triple negative breast cancer, drug delivery, vaccines

OPEN ACCESS

Edited by:
Kelong Ai,
Central South University, China

Reviewed by:
Ping Wang,
Zhengzhou University, China
Liang Zhang,
Wuhan University, China
Yuqi Yang,
Central South University, China

***Correspondence:**
Yiping Wu
wuyipingtj@163.com

[†]*These authors have contributed equally to this work*

Specialty section:
This article was submitted to Pharmacology of Anti-Cancer Drugs, a section of the journal Frontiers in Oncology

Received: *04 December 2021*
Accepted: *23 December 2021*
Published: *12 January 2022*

Citation:
Hou K, Ning Z, Chen H and Wu Y (2022) Nanomaterial Technology and Triple Negative Breast Cancer. Front. Oncol. 11:828810. doi: 10.3389/fonc.2021.828810

INTRODUCTION

Cancer is a major public health problem worldwide and the second leading cause of death in the United States. Cancer mortality rates have been rising throughout most of the 20th and 21st centuries, with 1,898,160 new cancer cases and 608,570 cancer deaths expected in the United States as of 2021 (1). From 2010 to 2016, the five-year overall survival rate for all diagnosed cancers in the United States was 67% (68% for Caucasians and 63% for African Americans) (1, 2). Prostate cancer (98%), melanoma (93%) and female breast cancer (90%) had the highest associated survival rates, while pancreatic cancer (10%), liver cancer (20%), esophageal cancer (20%) and lung cancer (21%) had the lowest survival rates (3, 4).

Improved cancer survival rates seen in recent decades are mainly due to advances in diagnosis and treatment, specifically reflecting advances in screening, diagnosis, and surgery (e.g., pathological staging, thoracoscopic surgery). Therapies for metastatic disease include targeted therapy (e.g., precision medicine), chemotherapy, radiotherapy, immunotherapy (e.g., programmed cell death protein-1 and programmed death ligand-1 inhibitors), and novel material-based therapies (1, 5–9).

Abbreviations: COVID-19, coronavirus disease 2019; HER2, human epidermal growth factor receptor 2; ER, estrogen receptors; PR, progesterone receptors; TNBC, triple negative breast cancer; BL1, basal like 1; BL2, basal like 2; ML, mesenchymal like; MSL, mesenchymal stemlike; LAR, intracavitary androgen receptor; IM, immune regulation; ROS, reactive oxygen species; TME, tumor microenvironment; DOX, doxorubicin.

The disruptive effects of the coronavirus disease 2019 (COVID-19) pandemic on healthcare delivery include disruptive effects with respect to the diagnosis and treatment of cancer patients due to delays in diagnosis and treatment, reduced access to care, and delays or closures of healthcare facilities and systems. These factors are likely to result in short-term, spurious declines in cancer rates followed by an increase in advanced disease and associated cancer mortality rates (1, 10, 11).

BREAST CANCER

Women comprise 49.5 percent of the global population, and are disproportionately represented among elderly people over age 60. In fact, due to population growth and aging, the global cancer burden for women has been increasing in all countries regardless of income level. Breast cancer is the most common malignancy among women worldwide, with one study estimating that approximately 160,000 patients with advanced breast cancer were diagnosed in the United States as of 2017 (12).

Due to the influence of multi-modal factors, such as genetic susceptibility, lifestyle, and other environmental factors, breast cancer incidence and mortality show extreme variance across countries and demographics (13). For example, breast cancer incidence is higher in high-income regions (e.g., 92 per 100,000 in North America) as compared with low-income regions (e.g., 27 per 100,000 in Central Africa and East Asia) (14). However, many low-income and middle-income countries, including countries in sub-Saharan Africa and developing countries in Asia, have low breast cancer incidence rates due to delays in healthcare delivery, late diagnoses, and limited access to treatment due to low mammography coverage and limited overall treatment options (15).

At the molecular level, breast cancer molecular signatures include the activation of human epidermal growth factor receptor 2 (HER2, encoded by *ERBB2*), the activation of hormone receptors (estrogen receptors and progesterone receptors), and *BRCA* mutations (16, 17). Intrinsic classifications delineated in 2000 distinguish four breast cancer subtypes: Luminal A and Luminal B, HER2-enriched, and triple negative breast cancer (TNBC). This classification system shifts the clinical management of breast cancer from a cancer burden-based approach to a biologically-centered approach. Currently, clinical practice classifies five breast cancer subtypes (luminal A, luminal B, HER2-enriched (HER2+), basal-like and normal-like) based on histological and molecular characteristics, including TNBC. TNBC is defined according to the following criteria: estrogen receptor-negative (ER–), progesterone receptor-negative (PR–), HER2–, high grade, and high Ki67 index tumors, either NST (no special type) histology or special type histology (metaplastic, adenoid cystic, medullary-like, secretory), and a generally poor prognosis (18).

There are differences in prognosis among breast cancer subtypes. Approximately 10-15% of TNBC cases present with poor prognoses due to the lack of targeted therapy for TNBC, aside from chemotherapy (19, 20). Morphologically, approximately 90% of TNBC cases present as infiltrating ductal carcinoma, while the remaining cases are classified as apocrine carcinoma, lobular carcinoma, adenoid cystic carcinoma, and metaplastic carcinoma (21–23). There are six different TNBC subtypes, including basal like 1, basal like 2, mesenchymal like, mesenchymal stemlike, intracavitary androgen receptor, and immune regulation subtypes. TNBC heterogeneity clinically refers to different breast cancer subtypes presenting with a triple negative phenotype. Gene expression profiles and genetic outcomes for each class show differences, thus illustrating the inherent complexity of TNBC (21).

Triple-negative breast cancer is more likely to recur as compared with other breast cancer subtypes, with five-year specific survival rates of 85% for stage 3 triple-negative cancer, as compared with survival rates ranging from 94-99% for hormone receptor-positive and ERBB2-positive cancers (24). The distribution of breast cancer molecular subtypes varies by race, with African and African American women having the highest rates of TNBC. TNBC presents with a higher rate of metastasis and the highest proportion of poorly differentiated or undifferentiated grades among all subtypes. These factors result in reduced survival rates (25).

BREAST CANCER DIAGNOSIS AND TREATMENT

Therapeutic strategies for treating breast cancer include local therapies (e.g., surgery, radiotherapy) as well as systemic therapies. Molecular subtypes have a profound influence on the therapeutic strategies selected for breast cancer. Specifically, systemic therapies have been developed primarily on the basis of molecular characteristics, including targeted chemotherapy, endocrine therapy for hormone receptor-positive diseases, anti-HER2 therapy for HER2-positive diseases, polymerase inhibitors for *BRCA* mutation carriers, and novel immunotherapy modalities (18).

In addition to surgical topical treatment, patients with hormone-receptor-positive cancer need endocrine therapy. A few of these patients also receive chemotherapy. Patients with ERBB2-positive cancer are treated with ERBB2-targeted antibodies or small molecule inhibitors combined with chemotherapy. Patients with triple-negative cancer typically receive only chemotherapy or radiation. Whether breast cancer patients receive radiotherapy is determined according to their specific indications. More and more patients are choosing to undergo systemic treatments, including targeted preoperative chemotherapy (i.e., neoadjuvant chemotherapy) following preoperative puncture examination (24). Breast cancer treatments based on nanotechnology are the focus of the current review.

NANOTECHNOLOGY AND CANCER

Advances in nanotechnology over the past two decades offer potential new strategies for treating various diseases (26–32).

Nanotechnology-based contrast agents and drug delivery vectors for disease diagnosis and treatment are progressing towards a more accurate and targeted direction. Currently, nanocarriers are mainly comprised of polymers, metals, lipids, nucleic acids, and proteins, including nanoparticles/tubes, micelles, dendrimers and liposomes (33). These smart nanoparticles can encapsulate drugs or probes and are coated with specially modified ligands that bind to receptors expressed at cell sites and ultimately affect cell function for the accurate and effective diagnosis and treatment of disease (34, 35).

Nanooncology is a branch of nanomedicine. Cancer diagnosis and treatment based on nanotechnology has received wide attention on a worldwide scale in the past decades (36–40). For example, in diagnostics, some nanoparticles have been developed into biomolecular vectors that can detect cancer biomarkers and play an important role in assisting cancer detection and monitoring cancer biomarkers, including proteins, antibody fragments, DNA fragments, and RNA fragments (37). For example, nanobiosensors are very sensitive and can detect multiple protein biomarkers within seconds (41, 42). Additionally, nanotechnology assisted molecular diagnostic technology has been increasingly implemented in imaging applications, which is conducive to the identification of cancer at an earlier and more accurate stage (43, 44).

In terms of treatment, nanotechnology has unique physicochemical properties, including a high surface volume ratio. In recent years, drug delivery systems based on nanomaterials, including micelles, nanoemulsions and liposomes, have been widely used. Nanomaterials can bind and load bioactive molecules, including DNA, RNA, drugs, and proteins. These bioactive molecules can easily cross many biological barriers and can easily be transported to the target. Therefore, nanomaterials are widely used in the loading and delivery of drugs for treating various cancers so as to improve the efficacy of chemotherapy combined with radiotherapy and photodynamic cancer therapy (7, 25, 45–47). To achieve complete tumor eradication, therapeutic agents need to be infused at extremely high levels. Moreover, within cancer immunotherapy using nanotechnology, nanoparticles carry T cells or natural killer cells and higher concentrations of anti-cancer drugs, achieving a strong and lasting anticancer immune response due to low concentrations of immune regulators (48, 49). Advances in nanotechnology, including virus-like sizes and high surface-volume ratios and surfaces that can be modified to precisely target specific cell types can be widely used in designing cancer vaccines (50).

Additionally, the cancer microenvironment plays a critical role in determining cancer survival and reducing mortality. Microenvironmental factors, such as cancer hypoxia or hyperglycemia and inflammation, are also directly associated with the survival and expansion of cancer cells. Interventions aimed at changing the microenvironment of cancer cells can induce cancer cell death and form the basis for new anticancer therapies (51).

NANOTECHNOLOGY AND TNBC

TNBC is an important and recalcitrant breast cancer subtype. The treatment of patients with TNBC remains an immense clinical challenge, characterized by aggressive progression, high metastasis rates, and poor overall prognoses (52). Because standard endocrine therapy (i.e., HER2 targeting therapy) does not affect TNBC, anthracycline-based drugs and taxane chemotherapy are major means to achieving TNBC systemic treatment. These treatment modalities are highly effective. However, many cycles of chemotherapy and high doses of cytotoxic drugs employed to destroy cancer cells are likewise toxic to nearby healthy cells, causing adverse systemic effects such as hair loss, gastrointestinal symptoms, and thrombocytopenia (53, 54).

Moreover, chemotherapy resistance caused by P-glycoprotein overexpression, DNA damage repair, topoisomerase II mutations, low solubility and bioavailability of chemotherapy drugs, and the immune escape of cancer cells limits the therapeutic effects of drugs on TNBC. Chemotherapy resistance results in a recurrence rate of 50% and a mortality rate of 37% for TNBC (55, 56). Invasive proliferation, heterogeneity, and cancer resistance to therapeutic drugs are extreme challenges in the treatment metastatic breast cancer, which mainly metastasizes to local lymph nodes, bones, and the lungs (57).

Therefore, in order to avoid non-specific targeting and chemotherapy side effects among TNBC patients, the need to open up new molecular targets and treatments is much more urgent than for other types of breast cancer. Nanotechnology-based drug delivery systems are auspicious tools that can selectively target tumors and eliminate the cytotoxicity of drugs to other organs (58).

Drug Delivery Systems for Nanotechnology

Nanodrug delivery systems mostly rely on enhanced permeation and retention effects for targeting drug delivery (59). In general, nanoparticles that can be applied to cancer treatment within nanoscience have the following physiochemical properties: tailored size and conformation, appropriate encapsulation capacity, high adhesion to the cancer environment, selective localization, enhanced cancer internalization through endocytosis, sustained and controllable drug release, a long cyclic half-life, minimal systemic toxicity, and safe biological elimination (60, 61). Research on the high expression of cancer targets and ligands *via* nanomaterials combined with other therapies (such as photodynamic therapy, chemotherapy, and radiotherapy) to produce therapeutic synergistic effects will be the key to the application of nanomaterials within TNBC.

Photothermal therapy (PTT) is ineffective in the treatment of TNBC due to the lack of effective therapeutic targets. In order to solve this problem, Cheng et al., used gold nanocage (AuNC) as a photothermal conversion agent combined with anti-heat shock protein monoclonal antibody (cmHSP) as a target ligand in order to prepare a microwave triggered heat shock protein (HSP)-tar gold nanosystem (CMHSP-AUNC). Microwave irradiation can effectively activate HSP70 overexpression in TNBC, thus meaningfully improving the targeting ability, accumulation in cancer area, and anti-cancer efficacy of CMHSP-AUNC (62). Xu et al. developed a nanoemulsion formulation with high stability for the systematic delivery of puerarin nanoPue. This modality reshapes the stromal microenvironment through nanoparticle

treatment, down-regulates intracanceral reactive oxygen species (ROS) and oxidative stress, meaningfully reduces the connective tissue formation response within different types of solid tumors and enables nanoparticles to infiltrate more effectively into cancer parenchyma. Simultaneously, nanoPue, a powerful tumor microenvironment (TME) modulator, meaningfully improves the cancer immune microenvironment as well as the therapeutic efficiency of α-PD-L1 in TNBC models (63). Bhattacharya et al. have also developed thyquinone (TQ)-loaded hyaluronic acid (HA) coupled with Pluronic ® P123 and F127 copolymer nanoparticles (HA-TQ-NPS) as selective drug carriers to deliver anticancer phytochemical TQ to TNBC cells. HA-TQ-NPS meaningfully promotes apoptosis, anti-metastasis, and anti-angiogenesis in TNBC cells *via* upregulation of microRNA-361 with no associated toxicity to normal cells (64).

Nanomaterials as Adjuvant Immunotherapy for TNBC

The immune microenvironment affects the occurrence and development of breast cancer according to the principles of immune monitoring and immune editing. In the early stages of tumorigenesis, the immune microenvironment plays an anti-cancer role mainly through the cytokine environment (i.e., activated CD8+ and CD4+ T cells). In contrast, once the cancer becomes aggressive, the cellular composition of the microenvironment, including fibroblasts and the cytokine content associated with cancer, facilitates cancer promotion and is invaded by breast cancer cells (63).

Using immune cells within targeted cancer therapy is in line with the concept of using internal mechanisms within the host immune system to fight cancer. In this study, Prof. James Allison and Prof. Tasuku Honjo, the winners of the 2018 Nobel Prize in Medicine, investigated the use of immune checkpoint blockades in cancer treatment *via* inhibiting negative immune regulation. Immunotherapy has achieved some success thus far, thereby providing a new therapeutic strategy for TNBC treatment. Current immunotherapies include immune checkpoint blockers, cytotoxic T lymphocyte (CTL) exchange activation, adaptive cell transfer therapy (ACT), and TME regulation. Nanotechnology presents a novel immunomodulatory strategy that can be implemented as a personalized immunotherapy modality for TNBC (65).

Nanotechnology provides efficient and intelligent nanodelivery systems that facilitate the delivery of immune-stimulating adjuvants and cancer antigens to enhance antigen presentation and immunity and aid in the treatment of metastases. Nanoparticle carriers improve the solubility and bioavailability of immunotherapy modalities, including protection from degradation, thereby increasing therapeutic efficacy. Currently, nanoparticles (NPs) are already implemented to help improve antigen expression pathways by delivering epigenetic regulators and immune-stimulating cytokines (66). For example, Tran et al. evaluated different polyethylene-oxidation-polylactic acid (PEO-PLA) copolymer micelles, with vorinostat (HDACi) demonstrating better biosolubility, an increased half-life, and improved pharmacokinetics as compared with other modalities (67). NP-carrying bevacizumab and CRLX101 likewise showed good efficacy in TNBC treatment (68). Sulforaphane (SFN) downregulates histone deacetylase (HDAC6) mediated phosphatase and inhibits MDA-MB-231 and MDA-MB-468 cells. The expression of tensin homolog (PTEN) induces autophagy, meaningfully increasing the sensitivity of TNBC to doxorubicin (DOX). Thus, inhibition of cancer growth *via* autophagy induction due to SFN combined with therapeutic DOX may provide an effective approach for TNBC treatment (69). Although targeted nanodrugs have good potential, due to the biological distributions, pharmacokinetics, targeted population biodegradability, immunogenicity, and the complexity of dosing system design for nanodrugs, only a portion of nanodrug systems (e.g., polymer micelles, liposomes, nanoparticle couplings) progress to the clinical administration stage. More research is needed with respect to TNBC nanodrugs.

Vaccines Based on Nanotechnology

Cancer vaccines are comprised of cancer cells and/or cancer antigens and lead to an effective anti-cancer host immune response. Cancer vaccines include DNA vaccines, Ab vaccines against idiotypic types and cancer-associated pathogens, and dendritic cell vaccines (70, 71). In Liu's study, the researchers (including the authors of the current review) constructed nanoparticles to deliver an mRNA vaccine encoding the cancer-associated antigen MUC1 to dendritic cells (DCs) in lymph nodes, thus activating cancer-specific T cells. In this study, combining a simple mRNA vaccine with an anti-CTLA-4 monoclonal antibody meaningfully enhanced the anti-cancer host immune response and anti-cancer effects. These data support the use NP as messenger RNA vaccine vectors as well as the combined implementation of TNBC immunotherapies, NP-based messenger RNA vaccines, and CTLA-4 inhibitors (52).

CONCLUSIONS

Triple negative breast cancer is a difficult and often intractable disease because of its high heterogeneity and low associated survival rates. Currently, the available treatment methods for patients diagnosed with TNBC are limited, especially with respect to refractory TNBC. Novel nanotechnology modalities represent auspicious strategies for efficient and accurate diagnoses and targeted therapies for TNBC due to their tailored physical and chemical properties and biological functions. Our work guides and informs future research directions and will ultimately contribute to informing medical guidelines.

AUTHOR CONTRIBUTIONS

All authors contributed to the design of the study and writing of the manuscript. KH and HC undertook the research, YW and ZN wrote the main manuscript text and prepared figures. YW revised the article critically for important intellectual content and final approval of the version to be submitted. All authors contributed to the article and approved the submitted version.

REFERENCES

1. Siegel RL, Miller KD, Fuchs HE, Jemal A. Cancer Statistics, 2021. *CA Cancer J Clin* (2021) 71(1):7–33. doi: 10.3322/caac.21654
2. Sung H, Ferlay J, Siegel RL, Laversanne M, Soerjomataram I, Jemal A, et al. Global Cancer Statistics 2020: GLOBOCAN Estimates of Incidence and Mortality Worldwide for 36 Cancers in 185 Countries. *CA Cancer J Clin* (2021) 71(3):209–49. doi: 10.3322/caac.21660
3. American Cancer Society Cancer Statistics 2021 Report. *J Nucl Med* (2021) 62 (3):12N.
4. Ferlay J, Colombet M, Soerjomataram I, Parkin DM, Pineros M, Znaor A, et al. Cancer Statistics for the Year 2020: An Overview. *Int J Cancer* (2021). doi: 10.1002/ijc.33588
5. Malhotra J, Jabbour SK, Aisner J. Current State of Immunotherapy for Non-Small Cell Lung Cancer. *Transl Lung Cancer Res* (2017) 6(2):196–211. doi: 10.21037/tlcr.2017.03.01
6. Zeng W, Jiang D, Liu Z, Suo W, Wang Z, Zhu D, et al. An Injectable Hydrogel for Enhanced FeGA-Based Chemodynamic Therapy by Increasing Intracellular Acidity. *Front Oncol* (2021) 11:750855. doi: 10.3389/fonc.2021.750855
7. Suo M, Liu Z, Tang W, Guo J, Jiang W, Liu Y, et al. Development of a Novel Oxidative Stress-Amplifying Nanocomposite Capable of Supplying Intratumoral H2O2 and O2 for Enhanced Chemodynamic Therapy and Radiotherapy in Patient-Derived Xenograft (PDX) Models. *Nanoscale* (2020) 12(45):23259–65. doi: 10.1039/d0nr06594c
8. Li Y, Appius A, Pattipaka T, Feyereislova A, Cassidy A, Ganti AK. Real-World Management of Patients With Epidermal Growth Factor Receptor (EGFR) Mutation-Positive Non-Small-Cell Lung Cancer in the USA. *PloS One* (2019) 14(1):e0209709. doi: 10.1371/journal.pone.0209709
9. Horn L, Spigel DR, Vokes EE, Holgado E, Ready N, Steins M, et al. Nivolumab Versus Docetaxel in Previously Treated Patients With Advanced Non-Small-Cell Lung Cancer: Two-Year Outcomes From Two Randomized, Open-Label, Phase III Trials (CheckMate 017 and CheckMate 057). *J Clin Oncol* (2017) 35 (35):3924–33. doi: 10.1200/JCO.2017.74.3062
10. Li J, Gao R, Wu G, Wu X, Liu Z, Wang H, et al. Clinical Characteristics of Emergency Surgery Patients Infected With Coronavirus Disease 2019 (COVID-19) Pneumonia in Wuhan, China. *Surgery* (2020) 168(3):398–403. doi: 10.1016/j.surg.2020.05.007
11. Li M, Cheng B, Zeng W, Chen S, Tu M, Wu M, et al. Analysis of the Risk Factors for Mortality in Adult COVID-19 Patients in Wuhan: A Multicenter Study. *Front Med (Lausanne)* (2020) 7:545. doi: 10.3389/fmed.2020.00545
12. Mariotto AB, Etzioni R, Hurlbert M, Penberthy L, Mayer M. Estimation of the Number of Women Living With Metastatic Breast Cancer in the United States. *Cancer Epidemiol Biomarkers Prev* (2017) 26(6):809–15. doi: 10.1158/1055-9965.EPI-16-0889
13. Ginsburg O, Bray F, Coleman MP, Vanderpuye V, Eniu A, Kotha SR, et al. The Global Burden of Women's Cancers: A Grand Challenge in Global Health. *Lancet* (2017) 389(10071):847–60. doi: 10.1016/S0140-6736(16)31392-7
14. Torre LA, Siegel RL, Ward EM, Jemal A. Global Cancer Incidence and Mortality Rates and Trends–An Update. *Cancer Epidemiol Biomarkers Prev* (2016) 25(1):16–27. doi: 10.1158/1055-9965.EPI-15-0578
15. Allemani C, Weir HK, Carreira H, Harewood R, Spika D, Wang XS, et al. Global Surveillance of Cancer Survival 1995-2009: Analysis of Individual Data for 25,676,887 Patients From 279 Population-Based Registries in 67 Countries (CONCORD-2). *Lancet* (2015) 385(9972):977–1010. doi: 10.1016/S0140-6736(14)62038-9
16. Perou CM, Sorlie T, Eisen MB, van de Rijn M, Jeffrey SS, Rees CA, et al. Molecular Portraits of Human Breast Tumours. *Nature* (2000) 406 (6797):747–52. doi: 10.1038/35021093
17. N. Cancer Genome Atlas. Comprehensive Molecular Portraits of Human Breast Tumours. *Nature* (2012) 490(7418):61–70. doi: 10.1038/nature11412
18. Harbeck N, Penault-Llorca F, Cortes J, Gnant M, Houssami N, Poortmans P, et al. Breast Cancer. *Nat Rev Dis Primers* (2019) 5(1):66. doi: 10.1038/s41572-019-0111-2
19. Salgado R, Denkert C, Demaria S, Sirtaine N, Klauschen F, Pruneri G, et al. The Evaluation of Tumor-Infiltrating Lymphocytes (TILs) in Breast Cancer: Recommendations by an International TILs Working Group 2014. *Ann Oncol* (2015) 26(2):259–71. doi: 10.1093/annonc/mdu450
20. Kojima YA, Wang X, Sun H, Compton F, Covinsky M, Zhang S. Reproducible Evaluation of Tumor-Infiltrating Lymphocytes (TILs) Using the Recommendations of International TILs Working Group 2014. *Ann Diagn Pathol* (2018) 35:77–9. doi: 10.1016/j.anndiagpath.2018.05.007
21. Mendes TF, Kluskens LD, Rodrigues LR. Triple Negative Breast Cancer: Nanosolutions for a Big Challenge. *Adv Sci (Weinh)* (2015) 2(11):1500053. doi: 10.1002/advs.201500053
22. Boyle P. Triple-Negative Breast Cancer: Epidemiological Considerations and Recommendations. *Ann Oncol* (2012) 23(Suppl 6):vi7–12. doi: 10.1093/annonc/mds187
23. Gonzalez-Angulo AM, Timms KM, Liu S, Chen H, Litton JK, Potter J, et al. Incidence and Outcome of BRCA Mutations in Unselected Patients With Triple Receptor-Negative Breast Cancer. *Clin Cancer Res* (2011) 17(5):1082–9. doi: 10.1158/1078-0432.CCR-10-2560
24. Waks AG, Winer EP. Breast Cancer Treatment: A Review. *JAMA* (2019) 321 (3):288–300. doi: 10.1001/jama.2018.19323
25. Zhu D, Liu Z, Li Y, Huang Q, Xia L, Li K. Delivery of Manganese Carbonyl to the Tumor Microenvironment Using Tumor-Derived Exosomes for Cancer Gas Therapy and Low Dose Radiotherapy. *Biomaterials* (2021) 274:120894. doi: 10.1016/j.biomaterials.2021.120894
26. Oliveira MB, do Prado AH, Bernegossi J, Sato CS, Lourenco Brunetti I, Scarpa MV, et al. Topical Application of Retinyl Palmitate-Loaded Nanotechnology-Based Drug Delivery Systems for the Treatment of Skin Aging. *BioMed Res Int* (2014) 2014:632570. doi: 10.1155/2014/632570
27. Saraiva C, Praca C, Ferreira R, Santos T, Ferreira L, Bernardino L. Nanoparticle-Mediated Brain Drug Delivery: Overcoming Blood-Brain Barrier to Treat Neurodegenerative Diseases. *J Control Release* (2016) 235:34–47. doi: 10.1016/j.jconrel.2016.05.044
28. Zhu XJ, Feng JQ, Zheng MZ, Yang ZR, Zhao L, Zhang W, et al. Metal-Protein Nanoparticles Facilitate Anti-VSV and H1N1 Viruses Through the Coordinative Actions on Innate Immune Responses and METTL14. *Macromol Biosci* (2021) 21(4):e2000382. doi: 10.1002/mabi.202000382
29. Zhang Y, Yang Z, Xiang Y, Xu R, Zheng Y, Lu Y, et al. Evolutions of Antibiotic Resistance Genes (ARGs), Class 1 Integron-Integrase (Inti1) and Potential Hosts of ARGs During Sludge Anaerobic Digestion With the Iron Nanoparticles Addition. *Sci Total Environ* (2020) 724:138248. doi: 10.1016/j.scitotenv.2020.138248
30. Lalotra AS, Singh V, Khurana B, Agrawal S, Shrestha S, Arora D. A Comprehensive Review on Nanotechnology-Based Innovations in Topical Drug Delivery for the Treatment of Skin Cancer. *Curr Pharm Des* (2020) 26 (44):5720–31. doi: 10.2174/1381612826666200819202821
31. Greco SJ, Rameshwar P. Mesenchymal Stem Cells in Drug/Gene Delivery: Implications for Cell Therapy. *Ther Delivery* (2012) 3(8):997–1004. doi: 10.4155/tde.12.69
32. Liu Y, Hong H, Xue J, Luo J, Liu Q, Chen X, et al. Near-Infrared Radiation-Assisted Drug Delivery Nanoplatform to Realize Blood-Brain Barrier Crossing and Protection for Parkinsonian Therapy. *ACS Appl Mater Interfaces* (2021) 13(31):37746–60. doi: 10.1021/acsami.1c12675
33. Kumari P, Ghosh B, Biswas S. Nanocarriers for Cancer-Targeted Drug Delivery. *J Drug Target* (2016) 24(3):179–91. doi: 10.3109/1061186X.2015.1051049
34. Setyawati MI, Kutty RV, Leong DT. DNA Nanostructures Carrying Stoichiometrically Definable Antibodies. *Small* (2016) 12(40):5601–11. doi: 10.1002/smll.201601669
35. Del Pilar Chantada-Vazquez M, Lopez AC, Vence MG, Vazquez-Estevez S, Acea-Nebril B, Calatayud DG, et al. Proteomic Investigation on Bio-Corona of Au, Ag and Fe Nanoparticles for the Discovery of Triple Negative Breast Cancer Serum Protein Biomarkers. *J Proteomics* (2020) 212:103581. doi: 10.1016/j.jprot.2019.103581
36. Gao A, Hu XL, Saeed M, Chen BF, Li YP, Yu HJ. Overview of Recent Advances in Liposomal Nanoparticle-Based Cancer Immunotherapy. *Acta Pharmacol Sin* (2019) 40(9):1129–37. doi: 10.1038/s41401-019-0281-1
37. Thambiraj S, Hema S, Shankaran DR. An Overview on Applications of Gold Nanoparticle for Early Diagnosis and Targeted Drug Delivery to Prostate Cancer. *Recent Pat Nanotechnol* (2018) 12(2):110–31. doi: 10.2174/1872210511666171101120157
38. Song X, Ruan L, Zheng T, Wei J, Zhang J, Lu H, et al. A Reduction Active Theranostic Nanoparticle for Enhanced Near-Infrared Imaging and

Phototherapy by Reducing Glutathione Level in Cancer Cells. *J Nanosci Nanotechnol* (2021) 21(12):5965–71. doi: 10.1166/jnn.2021.19514
39. Zhang J, Wang L, You X, Xian T, Wu J, Pang J. Nanoparticle Therapy for Prostate Cancer: Overview and Perspectives. *Curr Top Med Chem* (2019) 19 (1):57–73. doi: 10.2174/1568026619666190125145836
40. Pekkanen AM, DeWitt MR, Rylander MN. Nanoparticle Enhanced Optical Imaging and Phototherapy of Cancer. *J BioMed Nanotechnol* (2014) 10 (9):1677–712. doi: 10.1166/jbn.2014.1988
41. Chaturvedi VK, Singh A, Singh VK, Singh MP. Cancer Nanotechnology: A New Revolution for Cancer Diagnosis and Therapy. *Curr Drug Metab* (2019) 20(6):416–29. doi: 10.2174/1389200219666180918111528
42. Tran S, DeGiovanni PJ, Piel B, Rai P. Cancer Nanomedicine: A Review of Recent Success in Drug Delivery. *Clin Transl Med* (2017) 6(1):44. doi: 10.1186/s40169-017-0175-0
43. Mansur AA, Mansur HS, Soriano-Araujo A, Lobato ZI. Fluorescent Nanohybrids Based on Quantum Dot-Chitosan-Antibody as Potential Cancer Biomarkers. *ACS Appl Mater Interfaces* (2014) 6(14):11403–12. doi: 10.1021/am5019989
44. Jayanthi V, Das AB, Saxena U. Recent Advances in Biosensor Development for the Detection of Cancer Biomarkers. *Biosens Bioelectron* (2017) 91:15–23. doi: 10.1016/j.bios.2016.12.014
45. Karlsson J, Vaughan HJ, Green JJ. Biodegradable Polymeric Nanoparticles for Therapeutic Cancer Treatments. *Annu Rev Chem Biomol Eng* (2018) 9:105–27. doi: 10.1146/annurev-chembioeng-060817-084055
46. Kemp JA, Shim MS, Heo CY, Kwon YJ. "Combo" Nanomedicine: Co-Delivery of Multi-Modal Therapeutics for Efficient, Targeted, and Safe Cancer Therapy. *Adv Drug Delivery Rev* (2016) 98:3–18. doi: 10.1016/j.addr.2015.10.019
47. Chen D, Chen C, Huang C, Chen T, Liu Z. Injectable Hydrogel for NIR-II Photo-Thermal Tumor Therapy and Dihydroartemisinin-Mediated Chemodynamic Therapy. *Front Chem* (2020) 8:251. doi: 10.3389/fchem.2020.00251
48. Siegler EL, Kim YJ, Chen X, Siriwon N, Mac J, Rohrs JA, et al. Combination Cancer Therapy Using Chimeric Antigen Receptor-Engineered Natural Killer Cells as Drug Carriers. *Mol Ther* (2017) 25(12):2607–19. doi: 10.1016/j.ymthe.2017.08.010
49. Meir R, Shamalov K, Betzer O, Motiei M, Horovitz-Fried M, Yehuda R, et al. Nanomedicine for Cancer Immunotherapy: Tracking Cancer-Specific T-Cells in Vivo With Gold Nanoparticles and CT Imaging. *ACS Nano* (2015) 9 (6):6363–72. doi: 10.1021/acsnano.5b01939
50. Mi Y, t. Hagan CT, Vincent BG, Wang AZ. Emerging Nano-/Microapproaches for Cancer Immunotherapy. *Adv Sci (Weinh)* (2019) 6 (6):1801847. doi: 10.1002/advs.201801847
51. Vishwakarma M, Piddini E. Outcompeting Cancer. *Nat Rev Cancer* (2020) 20 (3):187–98. doi: 10.1038/s41568-019-0231-8
52. Liu L, Wang Y, Miao L, Liu Q, Musetti S, Li J, et al. Combination Immunotherapy of MUC1 mRNA Nano-Vaccine and CTLA-4 Blockade Effectively Inhibits Growth of Triple Negative Breast Cancer. *Mol Ther* (2018) 26(1):45–55. doi: 10.1016/j.ymthe.2017.10.020
53. Shi Y, Jin J, Ji W, Guan X. Therapeutic Landscape in Mutational Triple Negative Breast Cancer. *Mol Cancer* (2018) 17(1):99. doi: 10.1186/s12943-018-0850-9
54. Bayraktar S, Gluck S. Molecularly Targeted Therapies for Metastatic Triple-Negative Breast Cancer. *Breast Cancer Res Treat* (2013) 138(1):21–35. doi: 10.1007/s10549-013-2421-5
55. Sharma A, Goyal AK, Rath G. Recent Advances in Metal Nanoparticles in Cancer Therapy. *J Drug Target* (2018) 26(8):617–32. doi: 10.1080/1061186X.2017.1400553
56. Denkert C, Liedtke C, Tutt A, von Minckwitz G. Molecular Alterations in Triple-Negative Breast Cancer-the Road to New Treatment Strategies. *Lancet* (2017) 389(10087):2430–42. doi: 10.1016/S0140-6736(16)32454-0
57. Gradishar WJ, Moran MS, Abraham J, Aft R, Agnese D, Allison KH, et al. NCCN Guidelines(R) Insights: Breast Cancer, Version 4.2021. *J Natl Compr Canc Netw* (2021) 19(5):484–93. doi: 10.6004/jnccn.2021.0023
58. Thakur V, Kutty RV. Recent Advances in Nanotheranostics for Triple Negative Breast Cancer Treatment. *J Exp Clin Cancer Res* (2019) 38(1):430. doi: 10.1186/s13046-019-1443-1
59. Wang Y, Pei H, Jia Y, Liu J, Li Z, Ai K, et al. Synergistic Tailoring of Electrostatic and Hydrophobic Interactions for Rapid and Specific Recognition of Lysophosphatidic Acid, an Early-Stage Ovarian Cancer Biomarker. *J Am Chem Soc* (2017) 139(33):11616–21. doi: 10.1021/jacs.7b06885
60. Setyawati MI, Kutty RV, Tay CY, Yuan X, Xie J, Leong DT. Novel Theranostic DNA Nanoscaffolds for the Simultaneous Detection and Killing of Escherichia Coli and Staphylococcus Aureus. *ACS Appl Mater Interfaces* (2014) 6 (24):21822–31. doi: 10.1021/am502591c
61. Wang J, Sui L, Huang J, Miao L, Nie Y, Wang K, et al. MoS2-Based Nanocomposites for Cancer Diagnosis and Therapy. *Bioact Mater* (2021) 6 (11):4209–42. doi: 10.1016/j.bioactmat.2021.04.021
62. Cheng Y, Bao D, Chen X, Wu Y, Wei Y, Wu Z, et al. Microwave-Triggered/HSP-Targeted Gold Nano-System for Triple-Negative Breast Cancer Photothermal Therapy. *Int J Pharm* (2021) 593:120162. doi: 10.1016/j.ijpharm.2020.120162
63. Xu H, Hu M, Liu M, An S, Guan K, Wang M, et al. Nano-Puerarin Regulates Tumor Microenvironment and Facilitates Chemo- and Immunotherapy in Murine Triple Negative Breast Cancer Model. *Biomaterials* (2020) 235:119769. doi: 10.1016/j.biomaterials.2020.119769
64. Bhattacharya S, Ghosh A, Maiti S, Ahir M, Debnath GH, Gupta P, et al. Delivery of Thymoquinone Through Hyaluronic Acid-Decorated Mixed Pluronic(R) Nanoparticles to Attenuate Angiogenesis and Metastasis of Triple-Negative Breast Cancer. *J Control Release* (2020) 322:357–74. doi: 10.1016/j.jconrel.2020.03.033
65. Jia H, Truica CI, Wang B, Wang Y, Ren X, Harvey HA, et al. Immunotherapy for Triple-Negative Breast Cancer: Existing Challenges and Exciting Prospects. *Drug Resist Update* (2017) 32:1–15. doi: 10.1016/j.drup.2017.07.002
66. Hu X, Zhang J, Xu B, Jiang Z, Ragaz J, Tong Z, et al. Multicenter Phase II Study of Apatinib, a Novel VEGFR Inhibitor in Heavily Pretreated Patients With Metastatic Triple-Negative Breast Cancer. *Int J Cancer* (2014) 135 (8):1961–9. doi: 10.1002/ijc.28829
67. Tran TH, Ramasamy T, Truong DH, Shin BS, Choi HG, Yong CS, et al. Development of Vorinostat-Loaded Solid Lipid Nanoparticles to Enhance Pharmacokinetics and Efficacy Against Multidrug-Resistant Cancer Cells. *Pharm Res* (2014) 31(8):1978–88. doi: 10.1007/s11095-014-1300-z
68. Pham E, Yin M, Peters CG, Lee CR, Brown D, Xu P, et al. Preclinical Efficacy of Bevacizumab With CRLX101, an Investigational Nanoparticle-Drug Conjugate, in Treatment of Metastatic Triple-Negative Breast Cancer. *Cancer Res* (2016) 76(15):4493–503. doi: 10.1158/0008-5472.CAN-15-3435
69. Yang F, Wang F, Liu Y, Wang S, Li X, Huang Y, et al. Sulforaphane Induces Autophagy by Inhibition of HDAC6-Mediated PTEN Activation in Triple Negative Breast Cancer Cells. *Life Sci* (2018) 213:149–57. doi: 10.1016/j.lfs.2018.10.034
70. Postmus PE, Kerr KM, Oudkerk M, Senan S, Waller DA, Vansteenkiste J, et al. Early and Locally Advanced Non-Small-Cell Lung Cancer (NSCLC): ESMO Clinical Practice Guidelines for Diagnosis, Treatment and Follow-Up. *Ann Oncol* (2017) 28(suppl_4):iv1–iv21. doi: 10.1093/annonc/mdx222
71. Vansteenkiste J, De Ruysscher D, Eberhardt WE, Lim E, Senan S, Felip E, et al. Early and Locally Advanced Non-Small-Cell Lung Cancer (NSCLC): ESMO Clinical Practice Guidelines for Diagnosis, Treatment and Follow-Up. *Ann Oncol* (2013) 24(Suppl 6):vi89–98. doi: 10.1093/annonc/mdt241

Conflict of Interest: The authors declare that the research was conducted in the absence of any commercial or financial relationships that could be construed as a potential conflict of interest.

Publisher's Note: All claims expressed in this article are solely those of the authors and do not necessarily represent those of their affiliated organizations, or those of the publisher, the editors and the reviewers. Any product that may be evaluated in this article, or claim that may be made by its manufacturer, is not guaranteed or endorsed by the publisher.

Copyright © 2022 Hou, Ning, Chen and Wu. This is an open-access article distributed under the terms of the Creative Commons Attribution License (CC BY). The use, distribution or reproduction in other forums is permitted, provided the original author(s) and the copyright owner(s) are credited and that the original publication in this journal is cited, in accordance with accepted academic practice. No use, distribution or reproduction is permitted which does not comply with these terms.

frontiers in Pharmacology

REVIEW
published: 28 January 2022
doi: 10.3389/fphar.2022.829796

Applications and Biocompatibility of Mesoporous Silica Nanocarriers in the Field of Medicine

Chengcheng Zhang[1,2], Hongyi Xie[1,2], Zhengyan Zhang[1,2], Bingjian Wen[1,2], Hua Cao[3], Yan Bai[4], Qishi Che[5], Jiao Guo[1] and Zhengquan Su[1,2]**

[1]Guangdong Engineering Research Center of Natural Products and New Drugs, Guangdong Provincial University Engineering Technology Research Center of Natural Products and Drugs, Guangdong Pharmaceutical University, Guangzhou, China, [2]Guangdong Metabolic Diseases Research Centre of Integrated Chinese and Western Medicine, Guangdong Pharmaceutical University, Guangzhou, China, [3]School of Chemistry and Chemical Engineering, Guangdong Pharmaceutical University, Zhongshan, China, [4]School of Public Health, Guangdong Pharmaceutical University, Guangzhou, China, [5]Guangzhou Rainhome Pharm & Tech Co., Ltd., Guangzhou, China

Mesoporous silica nanocarrier (MSN) preparations have a wide range of medical applications. Studying the biocompatibility of MSN is an important part of clinical transformation. Scientists have developed different types of mesoporous silica nanocarriers (MSNs) for different applications to realize the great potential of MSNs in the field of biomedicine, especially in tumor treatment. MSNs have achieved good results in diagnostic bioimaging, tissue engineering, cancer treatment, vaccine development, biomaterial application and diagnostics. MSNs can improve the therapeutic efficiency of drugs, introduce new drug delivery strategies, and provide advantages that traditional drugs lack. It is necessary not only to innovate MSNs but also to comprehensively understand their biological distribution. In this review, we summarize the various medical uses of MSN preparations and explore the factors that affect their distribution and biocompatibility in the body based on metabolism. Designing more reasonable therapeutic nanomedicine is an important task for the further development of the potential clinical applications of MSNs.

Keywords: mesoporous silica, MSN, cancer, targeted drug delivery, gene delivery, biodistribution

OPEN ACCESS

Edited by:
Zeming Liu,
Huazhong University of Science and Technology, China

Reviewed by:
Kapil Dev Patel,
Korea University, South Korea
Tiancong Zhao,
Fudan University, China

****Correspondence:***
Jiao Guo
gyguoyz@163.com
Zhengquan Su
suzhq@scnu.edu.cn

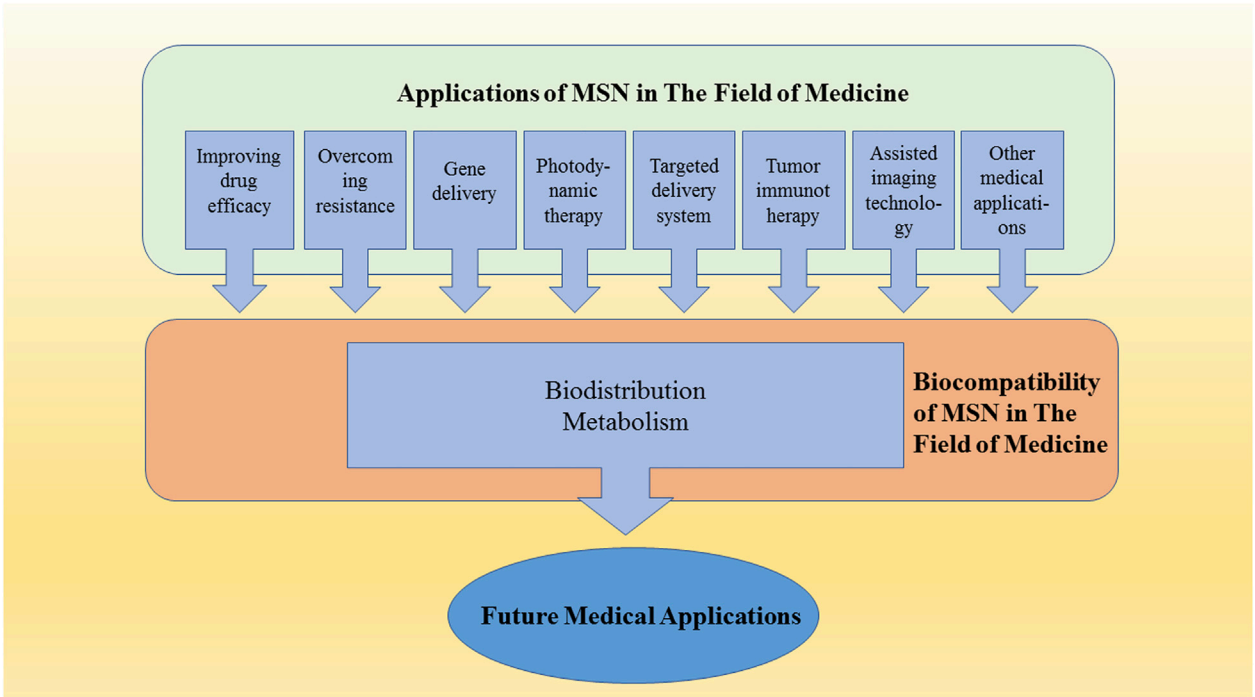
Specialty section:
This article was submitted to Pharmacology of Anti-Cancer Drugs, a section of the journal Frontiers in Pharmacology

Received: *06 December 2021*
Accepted: *10 January 2022*
Published: *28 January 2022*

Citation:
Zhang C, Xie H, Zhang Z, Wen B, Cao H, Bai Y, Che Q, Guo J and Su Z (2022) Applications and Biocompatibility of Mesoporous Silica Nanocarriers in the Field of Medicine. Front. Pharmacol. 13:829796. doi: 10.3389/fphar.2022.829796

INTRODUCTION

The completion of the Human Genome Project (HGP) marks the entry of human beings into the postgenome era.(Ginsburg and Phillips, 2018). The "precision medicine initiative" was proposed in the State of the Union address in 2015, and $215 million was allocated in 2016 to fund related scientific research and innovation development (The White House, 2015). In 2012, the British government announced the launch of the Genome Project, investing $523 million in cancer and rare disease research. Chinese nanomedicine is also actively being explored and has achieved good results (Zhao, 2018). Precision medicine (Adams and Petersen, 2016; Konig et al., 2017) is playing an increasingly prominent role in disease prevention, diagnosis and treatment and improving the health of the population, especially through the use of gene sequencing technology, (Ji et al., 2018; Nagahashi et al., 2019; Wakai et al., 2019), targeted drug delivery, accurate diagnostic and treatment methods, and the establishment of large-scale data for predicting health risks (Vogt et al., 2018). In practical applications, such as precision prevention, precision medicine (Bertier et al., 2016) has become the future direction of biomedicine development; compared with traditional



GRAPHICAL ABSTRACT | Mesoporous silica nanocarrier (MSN) preparations have a wide range of medical applications. Studying the biocompatibility of MSN is an important part of clinical transformation.

empirical medicine, nanomedicine (Bjornmalm et al., 2017; Shi et al., 2017) can overcome medical problems based on nanotechnology. Nanomedicine integrates information about the human body and disease obtained through modern technologies, such as precision instruments and life sciences, with information obtained from traditional experience and can thus greatly reduce the uncertainty of clinical practice, improving diagnosis and treatment, especially surgical treatment. Nanomedicine (Shi et al., 2017; Bayda et al., 2019) has become a research hotspot in the international medical sciences. A variety of nanocarriers and nanomedicines have been developed, including those based on inorganic materials (such as gold (Zhang et al., 2019), iron oxide, silver (Rai et al., 2009), silica (Rotow and Bivona, 2017; Ni et al., 2018; Assaraf et al., 2019; Hu et al., 2019), and graphene) and organic nanoparticles (such as liposomes, micelles, polymers, and vesicles). Among them, mesoporous silica nanocarriers (MSNs) have many advantages, which will be discussed in detail, as follows: 1) the high specific surface area yields a high drug loading capacity for both hydrophilic and hydrophobic drugs; 2) the particle size and shape are easy to adjust to meet different drug delivery needs; 3) the easily modified active surface groups allow different coatings and targeting strategies to be applied to improve uptake, targeting and bioavailability and reduce toxic effects, thereby achieving the purpose of precision treatment and improved efficacy; 4) the mesoporous structure is ordered; MSNs with pore channels which build up an effective nano-network path enable the diffusion and extended release of drugs (Letchmanan et al., 2017). And 5) the biocompatibility is hilicic acid, are absorbed by the body or are excreted through the urinary system. It is precisely because of the above advantages that mesoporous silica has shown great prospects for applications in biomedicine and other fields. The M41S family of ordered mesoporous silica (Kresge et al., 1992) was first reported in the early 1990s. Silica-based diagnostic nanoparticles in the form of Cornell dots (C dots) have been approved by the FDA for phase I human clinical trials, (Benezra et al., 2011), which is a landmark achievement. However, for MSNs to be transformed into clinical medicines, it is necessary to understand the biological behavior and related clinical data of mesoporous silica.

The mechanism of interaction between nanoparticles and various cells and tissues in the human body is the key to determining the medical applicability of nanotechnology. Compared with soluble molecules and drugs, the delivery of drugs using nanocarriers is more complicated because the behavior of nanocarriers is related not only to the molecular weight, solubility, and physical and chemical properties of the loaded drugs but also to the pore size distribution, and particle size of the nanocarrier. Coatings, targeting groups and other factors are also closely related. Therefore, for drug delivery using nanocarriers, it is necessary to detect, understand and optimize the release parameters, distribution, metabolism, excretion and biocompatibility of the drugs in the body for optimal clinical results. These are the current challenges in nanomedicine.

In this review, we summarize the current reliable research data and describe the application of mesoporous silica as a nanocarrier in gene therapy, photodynamic therapy, molecular targeted drug

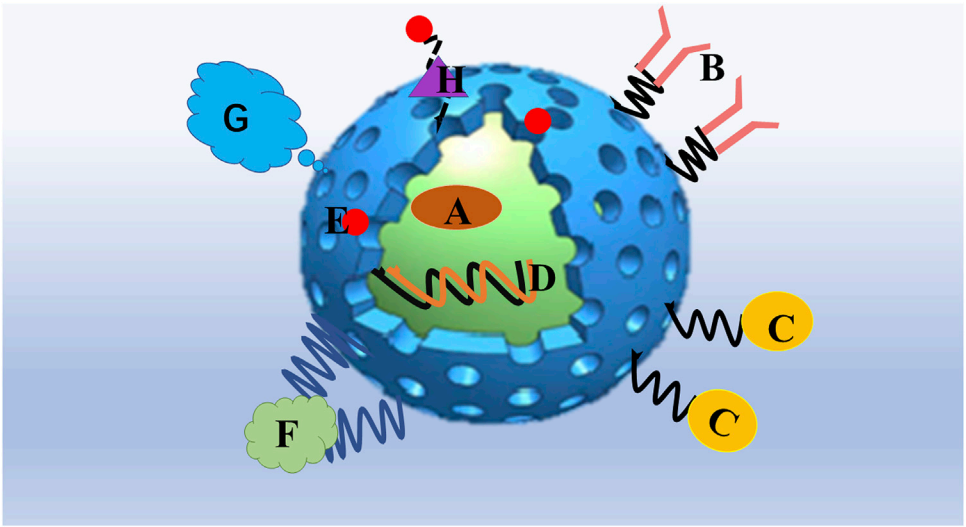


FIGURE 1 | Mesoporous silica nanoparticles are particularly promising as a platform for drug delivery. **(A)** Hydrophobic/hydrophilic drug and combining drugs could be entrapped in the interior of the MSN. **(B)** Targeting ligands such as antibodies. **(C)** Bioimaging agents such as magnetic nanoparticles, quantum dots. or fluorophores. **(D)** gene therapy agents such as plasmids, DNA, small interfering RNA (siRNA), micro RNA (miRNA), and short-hairpin RNA (shRNA). **(E)** nanoparticles attached to MSNs as functional gatekeepers. **(F)** Stimuli-responsive polymers. **(G)** Grafting with a protecting polymer, such as PEG, shields the MSN surface from interacting with opsonizing proteins. **(H)** Stimuli-responsive linkers, which chemically attach MSNs and gatekeepers.

delivery, vaccine delivery, and imaging, among others. MSN distribution and metabolism are discussed in detail. The importance of biodistribution and biocompatibility is explained, and key points of future research are discussed.

APPLICATIONS IN MEDICINE

MSNs have the advantages of an ordered mesoporous structure, an adjustable pore size, a high specific surface area, and easily modified active surface groups (Baek et al., 2015). MSNs are particularly promising as nanodrug carriers; biomedical applications require MSNs to maintain a high degree of dispersion and colloidal stability. Aggregation affects MSN internalization by cells, which increases the difficulty of controlling the biodistribution; furthermore, larger particle sizes caused by agglomeration may lead to increased biological toxicity. Based on the easy-to-modify hydroxyl groups on the MSN surface, chemical modifications, such as with a protein, polymer coating, or phospholipid bilayer, can be used to maintain its colloidal stability and reduce the occurrence of agglomeration. (**Figure 1**). Various MSNs have been developed for targeted drug, gene, and protein delivery, along with composite nanomedicines for diagnostic bioimaging, tissue engineering, cancer treatment, vaccine development, biomaterial applications, and theranostics (Singh et al., 2017); (**Table 1**)

Improving the Efficacy and Reducing the Side Effects of Anticancer Drugs

At present, chemotherapy is one of the most effective methods for the treatment of cancer, and chemotherapy, surgery and radiotherapy together form the three pillars of cancer treatment. In chemotherapy, drugs are used to kill cancer cells to achieve the goal of treatment. However, whether is the drugs are taken by mouth, injection, intraperitoneal injection, or other routes, they will enter the systemic circulation and cause uncontrollable side effects. MSNs have a high drug loading capacity and can be loaded with small-molecule drugs, especially hydrophobic drugs; at the same time, this approach can prevent drug degradation and physiological toxicity to healthy tissues caused by premature drug exposure. Thus, MSNs are of great significance for the delivery of hydrophobic anticancer drugs, drugs with narrow therapeutic windows, and chemotherapeutics with significant side effects. Drugs with narrow therapeutic windows is also called narrow therapeutic index (NTI). NTI drugs can be defined based on the steepness of the dose–response relationship and the degree of overlap between the effective and the toxic concentrations. MSNs are good tool about solving the problem of NTI, because they could improve the efficacy and reduce the side effects of drugs (Zenych et al., 2020; Habet, 2021). Duo et al (Duo et al., 2017) designed the doxorubicin (DOX)-loaded mesoporous silica nanomedicine MSN-DOX@PDA-PEG for the treatment of breast cancer; compared with free DOX, the nanomedicine showed a higher cell uptake efficiency in MCF-7 and MDA cells. The cytotoxicity test in MB-231 cells proved that the nanomedicine had almost no cytotoxicity. *In vivo* experiments showed that the smallest tumor volume and greater anticancer efficacy in the mesoporous silica nanomedicine group; additionally, body weight monitoring and hematoxylin and eosin (H&E) staining of organ (including heart, liver, spleen, lung and kidney) tissue sections showed no histopathological abnormalities, indicating MSN-

TABLE 1 | Applications and biocompatibility of MSNs.

Nanomedicine	Purpose of treatment	Nanodrug size	Cargo	Modification	Modification function	Citation
MSNs-DOX@PDA-PEG	Improving the efficacy and reducing the side effects of anticancer drugs	198 nm	DOX	PEG-PDA	PEG increases the stability and biocompatibility; PDA functions as a pH-sensitive gatekeeper	Duo et al. (2017)
LM@MSNs/DOX@HA	Inhibiting solid tumor growth under near-infrared (NIR) irradiation by synergistic photothermal therapy/chemotherapy	160 nm	DOX	Liquid metal HA	Synergistic photothermal therapy/chemotherapy	Hu et al. (2019)
M-MSNs-DOX	Improving the efficacy and reducing the side effects of anticancer drugs	200 nm	DOX	PEG	PEG increases the stability and biocompatibility	Shao et al. (2016)
H-MSNs-DOX/siRNA	Inhibiting MDR tumor growth	70 nm	DOX/siRNA	—	—	Sun et al. (2017)
PTX/GEM LB-MSNPs	Synergistically suppressing pancreatic cancer stromal volume and tumor size	112 nm	GEM/PTX	Lipid-coated	Facilitate coentrapment of hydrophobic drugs	Meng et al. (2015)
PTX/TET-CTAB@MSNs	Combining drugs for antitumor activity and the reversal of MDR activities	125 nm	PTX/TET	CTAB	pH-responsive release property	Jia et al. (2015)
PMSN-PEI-CQ	Highly efficient transfection of plasmid DNA and reducing cytotoxicity	174.5–215 nm	CQ; pDNA	PEI	Protect the pDNA from nuclease degradation	Zarei et al. (2018)
MSN-2NH_2/CpG	CpG oligodeoxynucleotide delivery	178 nm	CpG ODN	NH_2-TES, 2NH_2-TES, 3NH_2-TES	Larger loading capacity, significantly enhance the serum stability of CpG ODN	Xu et al. (2015)
MSNs-NH_2/dsDNA	Enhancing the delivery efficiency of immunostimulatory DNA drugs	190 nm	dsDNA	-NH2	Higher efficiency of cell uptake	Tao et al. (2014)
MSNPs-PEI-DOX/MDR1-siRNA	MDR cancer	150 nm	DOX MDR1-siRNA	PEI	Efficient transfection into KBV cells	Wang et al. (2018)
PEG-PEI@MSNs@siRNA	siRNA delivery	113 nm	siRNA	PEI-PEG	Good synthesis reproducibility and scalability	Ngamcherdtrakul et al. (2018)
KIT-6-MSNs@siRNA	High nucleic acid loading capacity	200–400 nm	siRNA	—	—	Meka et al. (2016)
LPMSNs@TRAF3-shRNA	Inhibiting the mRNA and protein expression of TRAF3	170 nm	shRNA-TRAF3	—	—	Zhang J. et al. (2016)
MONs–PTAT@pDNA	Highly efficient intranuclear gene delivery	160 nm	pDNA	PTAT	High loading capacity, improved protection for the loaded gene, enhanced transfection efficiencies of EGFP plasmid	Wu et al. (2015)
CP-MSNPs@siRNA	Delivering siRNA for cancer therapeutics	105 nm	siRNA	CP	Positive charge for the loading of siRNA	Shen J. et al. (2014)
CM/SLN/Ce6	Tumor-targeted PDT of gastric cancer	115 nm	Ce6	Cellular membrane (CM)	High biocompatibility and inheritance of the merits of the source cells	Yang et al. (2019)
AuNRs@MSNs-RLA/CS(DMA)-PEG	Enhancing photodynamic and photothermal tumor therapy	200 nm	ICG AuNR	RLA/CS(DMA)-PEG	Tumor targeting and pH response	Liu et al. (2018)
^{64}Cu-HMSN-ZW800-TRC105	Tumor-targeted positron emission tomography (PET)/near-infrared fluorescence (NIRF) dual-modality imaging	150 nm	^{64}Cu	TRC105	Target tumor vasculature	Chen et al. (2014)
YSPMOs(DOX)@CuS	Multifunctional triple-responsive platform for chemo-photothermal therapy	222.6 nm	DOX	CuS	Avoid premature leakage in the delivery process, provide the photothermal therapy (PTT) ability	Cheng et al. (2018)
$HmSiO_2$-FA-CuS-PEG/DOX	Nanoplatform for targeted chemo-photothermal therapy	155 nm	DOX	FA CuS	Target cancer cells Chemo-photothermal therapy	Liu et al. (2014)
PSiNPs@PELA-PEG	Synergistic effects and MDR inhibition	286 nm	Afatinib, rapamycin, docetaxel	PELA-PEG	Achieve high biocompatibility and low permeability	Zhang et al. (2019)
CuS@MSNs-TRC105	Photothermal ablation properties and tumor vasculature targeting	65 nm	CuS	TRC105	Target tumor vasculature	Chen et al. (2015)

(Continued on following page)

TABLE 1 | (*Continued*) Applications and biocompatibility of MSNs.

Nanomedicine	Purpose of treatment	Nanodrug size	Cargo	Modification	Modification function	Citation
MSNP-CYS-5FU-FA-BA@DOX-CD	Augmented the innate and adaptive immune defense mechanisms, Significantly reduced the tumor load and enhanced the survival of the animals	110 nm	Dox; 5-FU	FA	Active targeting by folic acid directs drugs in the close proximities of the tumor cells, causing efficient killing and significant growth inhibition	Srivastava et al. (2020)
Ru@MSNs	Exhibited high *in vivo* antitumor activity, the nanosystems at 20 nm exhibited low toxicity, the larger (80 nm) showed superior potential for overcoming MDR.	20 nm, 40nm, 80 nm	Ru	FA	Facilitate selectivity toward hepatocellular carcinoma cells	(Tang et al., 2013; Ma et al., 2018)
DTX-Lac-MSN	A hepatoma-targeting drug delivery system	100 nm	DTX	Lactose	Specifically target ASGPR	Quan et al. (2015)
MSNs-FA-Q	Targeted delivery with enhanced bioavailability	200 nm	Quercetin	FA	Target breast cancer cells	Sarkar et al. (2016)
MSNs-FA-TAN-MB	Ultrasound response property, tumor targeting and imaging in tumor therapy	2,608 nm	Tanshinone IIA (TAN)	FA MB	Tumor targeting, high biocompatibility	Lv et al. (2017)
MSR-MSNs	Dual-scale vaccine transport into host dendritic cells (DCs) to enhance cancer immunotherapy	150 nm	OVA, CpG-ODNs	—	—	Nguyen et al. (2020)
Trp2@HMSNs	Improved the antigen-loading efficacy, sustained drug release profiles, enhanced the phagocytosis efficiency, enabled DCs maturation and Th1 immunity, sustained immunological memory, and enhanced the adjuvant effect	200 nm	Trp2	PEI	Acted as an etching agent, protecting agent, soft template, and promoter	Liu et al. (2019)
LB-MSNs-OVA	Intradermal antigen delivery system	213 nm	OVA	Lipid bilayer	Significantly improve the colloidal stability and reduce the premature release of OVA	Tu et al. (2017)
Gd@SiO_2-DOX/ICG-PDC	Cancer treatment and magnetic resonance imaging	214 nm	DOX, ICG Gd(III)	PDC	Protect from quick release of drugs and increase cellular uptake	Cao et al. (2015)
MSNs-DOX-Ag_2Se	Chemo-photothermal therapy	130 nm	DOX	Ag_2Se QD	Enhance photothermal properties and act as “gatekeepers"	Li et al. (2019)
Apt-PTPA-MSHNs	Highly efficient MRI contrast agents	200 nm	PTPA	EpCAM	Anti-EpCAM aptamer was conjugated with epoxy-functionalized PTPA MSHNs to improve selectivity toward the cancerous cells	Dineshkumar et al. (2019)
Mn-DTPA-MSNSs	Liver-specific positive MRI contrast agent	116 nm	—	Mn^{2+}	MRI contrast agent	Pálmai et al. (2017)
Fe_3O_4@$mSiO_2$/PDDA/BSA-Gd_2O_3	T_1-T_2 molecular magnetic resonance imaging of renal carcinoma cells	345 nm	BSA-Gd_2O_3, Fe_3O_4	AS1411	Specifically combine with nucleolin on the surface of the tumor cell	Li et al. (2018)
MSNs-GTMC-PMMA	Functionalization for orthopedic surgery to prevent post-surgery infection	100–400 nm	GTMC	PMMA	Critical weight-bearing mechanical properties	Letchmanan et al. (2017)
GTMC/TBMC/MSN/Simplex-P	The combination of excellent mechanical properties and sustainable drug delivery efficiency demonstrates the potential applicability for orthopedic surgery to prevent post-surgery infection	400 nm	GTMC TBMC	PMMA	Critical weight-bearing mechanical properties, bending modulus and compression strength of bone cement	Letchmanan et al. (2017)
SiO_2-PMMA	Mimicking the mechanical properties of human enamel and hardness compatibility with human enamel	7 nm	—	PMMA	Achieve hardness compatible with that of human enamel and an elastic modulus similar to that of human dentin	Ikeda et al. (2019)
PDG-MSNPs	Improved the engraftment of islets (i.e., enhanced revascularization and reduced inflammation), re-establishment of glycemic control	120 nm	Glutamine	Polydopa-mine	Resulted in a delay in the release of glutamine	Razavi et al. (2020)

(Continued on following page)

TABLE 1 | (*Continued*) Applications and biocompatibility of MSNs.

Nanomedicine	Purpose of treatment	Nanodrug size	Cargo	Modification	Modification function	Citation
OST-MSNs-PA@ PEI-siRNA	Increase expression of osteogenic related genes improving the bone microarchitecture	100 nm	Osteostatin SOST siRNA	alendronate (ALN) modified PEG	Confer the nanoparticles good colloidal stability and bone targeting capacity	Mora-Raimundo et al. (2021)
Ag@Vm-ge	Combined with the gentamicin delivery, the pathogenic bacteria in diabetic wound can be completely eradicated	145 nm	Gentamicin	—	—	Wang et al. (2021)
colchicine MSNs/ chitosan-pullulan hydrogel	Enhanced the drug skin permeation and therapeutic activity in comparison to conventional free colchicine	167.1 ± 51.36 nm	Colchicine	Carboxyethyl chitosan/ oxidized pullulan	Efficient transdermal delivery	Mohamed et al. (2020)
Ce@MSNs	Stimulated osteoblast cells to produce bone matrix and demonstrated antioxidant properties in a co-culture cells without osteogenic supplements	80 nm	Ce	—	—	Pinna et al. (2021)

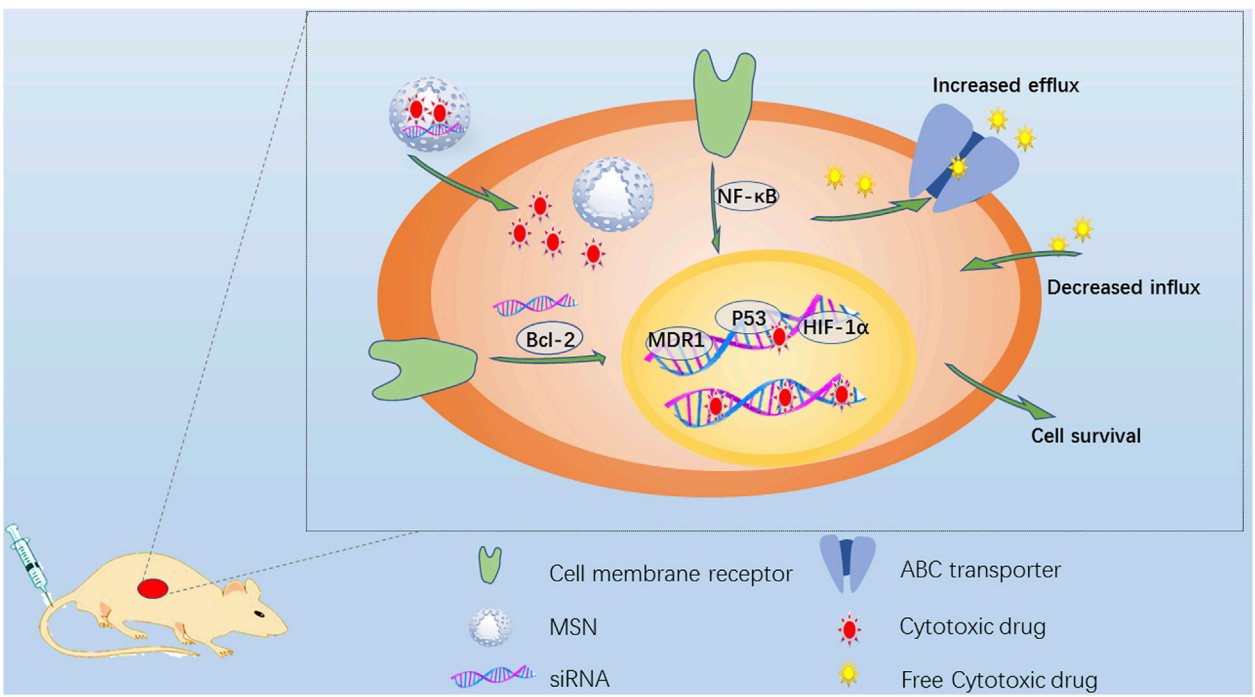


FIGURE 2 | Schematic diagram of strategies to overcome MDR. Drug-resistant cancer cells have many ways to escape cytotoxic drugs, including the overexpression of ABC transporter to increase drug efflux, repair DNA and inhibit drug-induced apoptosis. The anti-apoptotic signal transduction pathway always involves the activation of Bcl-2, MDR1, NF-κB and HIF-1 overexpression and the mutation of tumor suppressor gene p53. MSN is endocytosed into drug-resistant cancer cells, and the loaded cytotoxic drugs and/or siRNA targeting related genes can be continuously released to reduce drug resistance.

DOX@PDA-PEG has good biocompatibility and low *in vivo* toxicity.

Mesoporous silica nanomedicine can not only improve the therapeutic effect of the anticancer drug DOX but also reduce its side effects. Hu et al. (Hu et al., 2019) designed a DOX-loaded MSN (LM@MSN) via surface modification and liquid metal immobilization for cancer treatment; the near-infrared (NIR) dye indocyanine green (ICG) was encapsulated in the nanosystem. *In vivo* fluorescence imaging was performed to evaluate its targeting performance. The results of *in vitro* fluorescence imaging showed aggregation of the targeted drug in the tumor. After 36 h, the content of heparin in the tumor was

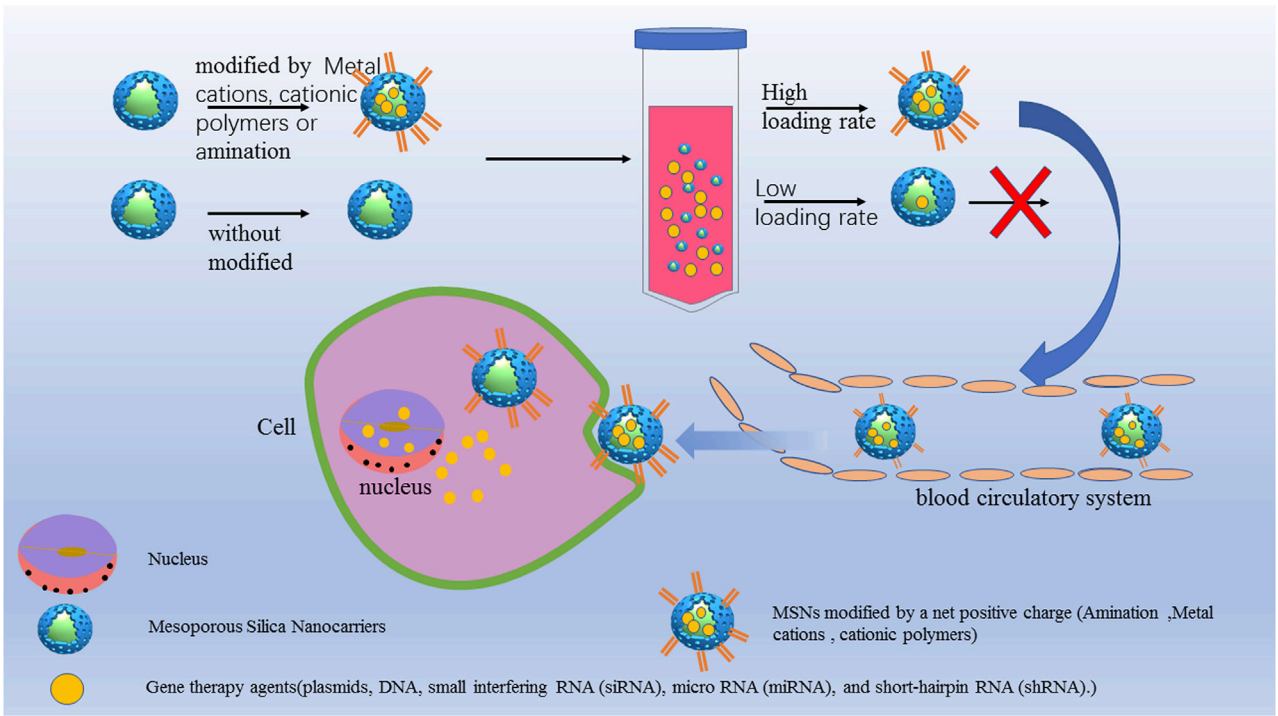


FIGURE 3 | MSNs for gene therapy to increase the cell uptake and transfection efficiency. MSNs modified by a net positive charge such as amination modification, metal cations and cationic polymers. The aminated MSN delivery systems had a higher loading capacity and showed greater delivery efficiency and protection, resulting in significantly improved serum stability without cytotoxicity.

higher than that in the heart, spleen, kidney and other organs. When tested in tumor cells (4T1, HeLa, MCF-7) and normal cells (3T3), the normal cells showed a viability of greater than 80%, demonstrating low toxicity and good activity even at relatively high concentrations, in turn indicating that this MSN has good biocompatibility. Shao et al (Shao et al., 2016) designed a "nanobullet" consisting of magnetic Fe_3O_4 as the head and DOX-loaded MSN as the body (M-MSN-DOX); this multifunctional nanocomposite material showed excellent targeting, with greater uptake by HepG2 tumor cells. The administration of DOX and M-MSN-DOX via a tail vein injection for 16 days effectively inhibited the growth of orthotopic liver tumors and the deterioration of other analyzed liver tumor mouse model parameters, including body weight, blood chemistry and major organ and tissue toxicological indicators. No pathological damage was observed in mouse brain, heart, liver, spleen, lung or kidney tissue sections, indicating that this mesoporous silica nanomedicine not only has good biocompatibility but is also effective for improving the efficacy and reducing the side effects of the drug.

Combining Drugs and Overcoming Resistance

The current important standard for cancer treatment (Yardley, 2013) is based on increasing the dosage and scheduling intensity of therapeutic drugs to avoid chemotherapy resistance. Multidrug resistance (MDR) (Rotow and Bivona, 2017; Fang et al., 2018; Assaraf et al., 2019) is the main obstacle to cancer chemotherapy; MDR can severely hinder the efficacy of anticancer drugs and even lead to treatment failure. The drug resistance mechanism of tumor tissue is very complex and involves multiple dynamic mechanisms. MDR can usually be divided into two categories. Drug efflux pump (P-glycoprotein (Thorat et al., 2020) and multidrug resistance protein MRP1) overexpression is an effective method (**Figure 2**).

Drug transport pumps can actively prevent the treatment of tumors. The drug is pumped out of the cell, increasing the efflux of the drug and reducing the accumulation of the drug in the cell. The second category mainly refers to the activation of cell antiapoptotic defense pathways, such as by drug-induced B-cell lymphoma 2 (BCL-2), inhibitor of apoptosis protein (IAP) and FLIP protein expression, leading to reduced drug sensitivity. These two mechanisms are sometimes active at the same time. In view of the unique properties of mesoporous silica, different drug delivery strategies have been designed to overcome drug resistance. The energy-dependent endocytosis of MSNs promotes cell absorption, improves drug efficacy and bypasses drug efflux pumps to overcome drug resistance. Sun et al. (Sun et al., 2017) designed a unique core-shell-level mesoporous silica/silicone nanosystem. The small mesopores in the core were loaded with small-molecule drugs, and the large mesopores in the shell were integrated with siRNA by disulfide bonds. During treatment, the reactivity of the disulfide bonds in the shell to the

tumor microenvironment (TME) caused them to break down, first releasing the siRNA to inhibit the expression of P-gp to inhibit MDR and then releasing the small-molecule drug DOX from the core to exert a therapeutic effect. *In vivo* experiments showed that the tumor inhibition rate in the free DOX group was 50.7%, while that in the H-MSN-DOX/siRNA group reached 87%, demonstrating a significant inhibitory effect on drug resistance. At the same time, mice in the free DOX group lost weight, but those in the other groups, including the H-MSN-DOX/siRNA group, showed normal weight changes. Compared with the injection of free drug, administration of the H-MSN-DOX/siRNA delivery system greatly enhanced the therapeutic efficacy while significantly reducing the side effects of the delivered anticancer drug. MSNs loaded with different drugs may overcome the problem of drug resistance by strategically improving the therapeutic efficacy of the drugs. Meng et al (Meng et al., 2015) designed a mesoporous silica nanoparticle (MSNP) carrier to jointly deliver paclitaxel (PTX) and gemcitabine (GEM) for the synergistic treatment of pancreatic cancer. The codelivery of PTX/GEM by the LB-MSNP yielded better results than the delivery of free GEM and Abraxane in xenotransplantation and orthotopic tumor animal models, with a therapeutic effect equivalent to that of 12 times the dose of Abraxane. Similarly, Jia et al (Jia et al., 2015) designed multifunctional MSNPs loaded with the antitumor drug PTX and the multidrug resistance reversal agent tetrandrine (TET). The results of experiments in MCF-7 human breast cancer cells and MCF-7/ADR multidrug-resistant cells showed that the PTX/TET-CTAB@MSNs significantly inhibited the proliferation of the drug-resistant cells and completely reversed the resistance to PTX.

The combination of medications can improve the therapeutic effect of the drugs; additionally, different drugs can be selected for loading according to different treatment strategies and individual differences. This approach can reduce the side effects of anticancer drugs and avoid the development of drug resistance.

MSNs for Gene Delivery

Gene therapy has broad prospects, but naked nucleic acids are not easily internalized by cells; they have poor biological stability and a short half-life and are subject to intracellular degradation prior to entering the nucleus. The systemic delivery of carrier particles can overcome these problems. At present, gene delivery systems can be divided into two categories: viral vectors and nonviral vectors. Although viral vectors have advantages in delivering genes, they have potential safety hazards. Nonviral vectors have been a research hotspot in recent years, including polymers, recombinant proteins, cationic compounds and inorganic nanoparticles. However, cationic materials are usually associated with high toxicity, recombinant proteins show low cost performance, and liposomes can enable effective gene transfection but are unstable. Compared with other nanoparticles, inorganic nanoparticles are simple to prepare and easy to functionalize and have good biocompatibility and excellent physical and chemical stability. MSNs have favorable characteristics for gene delivery, including a narrow pore size distribution and the ability to can effectively protect the cargo up to the release point, and the surface chemical structure facilitates the optimization of adsorption and release characteristics. Thus, MSNs are considered promising carriers for gene therapy.

The current methods to improve the performance of mesoporous silica-loaded genes are as follows: 1) positive charge functionalization, such as by amination (Cheang et al., 2012; Tao et al., 2014; Xu et al., 2015; Zhang M. et al., 2016) and cationic polymer (Ngamcherdtrakul et al., 2018; Wang et al., 2018) functionalization, yielding modified MSNs with a net positive charge that promotes gene loading by enhancing electrostatic interactions with nucleic acids; (**Figure 3**); 2) synthesizing large pore size MSNs to realize improved gene protection and transportation. (Wu et al., 2015; Zhang J. et al., 2016; Meka et al., 2016).

To study the effect of amination on the delivery efficiency of nucleic acids, Xu et al.(Xu et al., 2015) modified MSNs with NH2-TES, 2NH2-TES and 3NH2-TES and loaded them with CpG oligodeoxynucleotide (CpG ODN) to form MSN-NH2/CpG, MSN-2NH2/CpG, MSN-3NH2/CpG complexes. The aminated MSN delivery systems had a higher loading capacity and showed greater delivery efficiency and protection, resulting in significantly improved serum stability without cytotoxicity. Similarly, the modification of mesoporous silica with cationic polymers can also improve the gene loading performance. Shen et al (Shen J. et al., 2014) designed a universal siRNA carrier composed of MSNPs functionalized with polyethyleneimine (PEI) grafted with cyclodextrin (CP), allowing the positive charge loading and release of siRNA *in vivo* through electrostatic interaction. Compared with free siRNA, the CP-MSNPs reduced the intracellular degradation rate of siRNA by 47.4%, and the cell internalization rate reached 99.2% within 24 h. *In vivo* microscopy monitoring in a tumor mouse model showed that the maximum concentration at the tumor site could be reached in 20 min, targeting and effectively inhibiting the gene expression of glycolytic pyruvate kinase isoenzyme (PKM2). Wang et al (Wang et al., 2018) designed MSNs carrying MDR1-siRNA to block the expression of MDR1 and loaded them with the anticancer drug DOX. The cationic polymer PEI was used to modify the MSNs to obtain a positive charge for better MDR1-siRNA loading. Meka et al. (Meka et al., 2016) prepared MSNs with 9 nm mesopores. The hydrophobic octadecyl-conjugated MSNs showed a high loading capacity and effectively delivered siRNA to cancer cells, inhibiting cancer cell proliferation. Wu et al (Wu et al., 2015) successfully developed mesoporous organosilica nanoparticles (MONs) with cell-penetrating peptides (TAT) for efficient nuclear gene delivery with a high drug loading capacity, which resulted in better loaded gene protection and improved EGFP plasmid transfection efficiency.

At present, surface amino and cationic modification as well as large-pore-size mesoporous silica can effectively improve gene delivery and have broad prospects for application in cancer therapy drug/gene delivery.

Application of Mesoporous Silica in Photo-Triggered Therapy

Both photothermal therapy (PTT) and photodynamic therapy (PDT) are important class of therapy approach by MSNs, have

been demonstrated the priorities to elevate cancer therapeutic efficacies and diminish undesired side effects through different mechanisms in cancer treatment. Photothermal therapy (PTT) (Shen et al., 2016) is a minimally invasive method selectively ablate cancer cells by converting light energy into heat. It has become a promising alternative to radiotherapy and chemotherapy. The basic principle of PDT is that the irradiation of photosensitizers at specific wavelengths causes cells to produce create cytotoxic singlet oxygen or ROS, leading to cell death (Singh et al., 2017; Liang et al., 2020; Wang et al., 2020).

To improve the therapeutic effect, synergistic effects between photothermal agents and antitumor drugs (Youssef et al., 2018; Hu et al., 2019; Yang et al., 2019; Zhang et al., 2019) have become a new hot topic of research. Many dosage forms of DOX-loaded mesoporous silica for cancer treatment have been developed and achieved good results. Hu et al (Hu et al., 2019) designed immobilized liquid metal nanoparticles based on a surface mesoporous silica coating strategy (LM@MSNs) and loaded them with the anticancer drug DOX and decorated them with hyaluronic acid (HA), resulting in the construction of the tumor-targeted nanomedicine LM@MSN/DOX@HA. Under NIR irradiation, the immobilized LM nanoparticles exerted a photothermal effect and a synergist effect with the anticancer drug to kill cancer cells. HA helped the nanocarrier achieve targeted recognition and reduced its toxic side effects on normal tissues. Similarly, Liu et al (Liu et al., 2018) designed a multifunctional nanoplatform based on mesoporous silica-coated gold nanorods (AuNRs@MSNs) that were loaded with ICG and RLA peptide with plasma membrane permeability and a mitochondrial targeting ability ([RLARLAR]2) and capped with β-cyclodextrin (β-CD). The weakly acidic microenvironment of tumor tissue induced polymer dissociation and re-exposure of the RLA peptide, promoting targeted accumulation of the nanocarrier in mitochondria. When irradiated with an 800 nm laser, the local electric field enhancement of the AuNRs significantly increased the ROS production of ICG, yielding a photothermal effect. The production of ROS and local hyperthermia led to mitochondrial dysfunction, leading to obvious tumor cell apoptosis and necrosis. Zhang et al (Zhang et al., 2019) used microfluidic technology to encapsulate mesoporous silica and AuNRs in a hybrid polymer body to construct a composite material. The hybrid polymer was composed of a combination of poly (ethylene glycol)-b-poly (lactic acid) diblock copolymer and phospholipids, resulting in high biocompatibility and low permeability. This material could be used to realize combined antitumor, photothermal, and targeted therapy.

Copper sulfide (CuS) nanoparticles have the characteristics of a low synthesis cost, a wide NIR absorption range, good biocompatibility and a good NIR photothermal conversion efficiency. An increasing number of nanodrugs based on the photothermal effect of CuS are being developed (Chen et al., 2014; Cheng et al., 2018). Liu et al. (Liu et al., 2014) developed hollow MSNPs loaded with CuS as a photosensitizer, DOX as an anticancer drug, and folic acid (FA) as a targeting agent. The system showed a good photothermal effect and an excellent DOX loading capacity. It enters cancer cells through a targeted receptor-mediated endocytic pathway; the change in pH and exposure to NIR irradiation trigger the release of DOX, driving the synergy of chemotherapy and PTT.

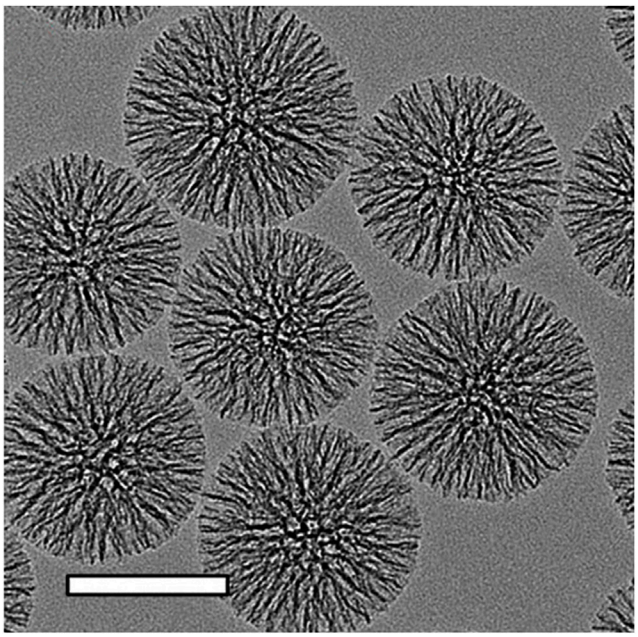


FIGURE 4 | Transmission electron microscopic images of MSNs. The scalebars in TEM images is 100 nm. Reproduced with permission from ref (Shen et al., 2014); copyright 2014 American Chemical Society.

Wang et al. (Wang et al., 2020)reported a redox nanocarrier (called RN) is prepared by hollow mesoporous silica sphere (HMSNs) and a redox-responsive polymer ligand. The nanocarrier is loaded with catalase, metformin, and photosensitizer chlorin e6 (Ce6). With optimal size, redox-responsive drug release behavior and excellent singlet oxygen production, the RN have potential to enhance anti-tumor efficiency. The *in vitro* chemo-photodynamic synergetic experiments indicated that the NPs had excellent reactive oxygen species generation and remarkable cancer cell killing efficiency under laser irradiation.

The critical challenges in photodynamic and photothermal chemotherapies of cancer are the limited penetration depth of light, instability of photosensitizers, and non-degradable character of inorganic nanomaterials (Cheng et al., 2020; Wang et al., 2020). Improving the photothermal conversion efficiency and reducing the laser power density have become the directions of PTT development. Combination photo-chemotherapy, including photothermal-chemotherapy, photodynamic-chemotherapy, and photodynamic-photothermal-chemotherapy, has demonstrated the priorities to elevate cancer therapeutic efficacies and diminish undesired side effects through different mechanisms in cancer treatment.

Targeted Delivery System Based on Mesoporous Silica

Targeted drug delivery systems (TDDSs) (Chen et al., 2015; Foster et al., 2017) consist of drug delivery systems conjugated

with carriers, ligands or antibodies to selectively concentrate drugs in target organs, tissues, cells, or intracellular structures through local, oral or systemic administration. At present, the targeted delivery of nanoparticles can be achieved by active and passive targeting. Passive targeting (Meng et al., 2011; Tang et al., 2013; Tang et al., 2014) is mainly based on the enhanced permeability and retention (EPR) effect. Compared with the microvascular endothelial space in tumor tissue, the microvascular endothelial space in normal tissue is dense, and the structure is complete. Solid tumor tissue is rich in blood vessels and has a large vascular wall surface area, poor structural integrity, and a lack of lymphatic drainage. Such tissue demonstrates selectivity, high permeability and retention of nanoparticles. The EPR effect promotes the selective distribution of macromolecular substances in tumor tissues, which can increase the efficacy and reduce the systemic side effects of drugs. To explore the role of particle size in determining biological characteristics and antitumor activity, Li et al. (Tang et al., 2014) compared nanoparticles 20, 50, and 200 nm in size according to radiolabeling, lung pathology, mathematical modeling and other research results and showed that the 50 nm MSNs performed best in terms of the size-dependent biodistribution, penetration and clearance of tumor tissue, and anticancer efficacy in various tumor models.

Active targeting is achieved through the use of specific targeting ligands, which can enhance specific uptake by cells and increase the intracellular drug concentration. Quan et al. (Quan et al., 2015) designed a drug delivery system called Lac-MSN, in which a 3-aminopropyltriethoxysilane-modified MSN was conjugated with the liver-targeting agent lactose and loaded with the water-insoluble anticancer drug docetaxel (DTX). The system mediated the targeted delivery of asialoglycoprotein receptor (ASGPR) and increased the concentration of the drug in the target organs, resulting in improved bioavailability. Sarkar et al (Sarkar et al., 2016) designed FA-modified quercetin-loaded mesoporous silica nanoparticles (MSNs-FA-Q) targeting breast cancer cells overexpressing folate receptors to enhance cell uptake and improve bioavailability. Lv et al (Lv et al., 2017) modified the folate MSN drug delivery system to achieve active targeting, thus increasing both the drug concentration in the target organ and the therapeutic efficacy.

MSNs allow high loading of drugs, and protects them inside the channeled pores until they reach target and release. The MSNs with optimal drug allow potential possess high loading of drugs, sustained and controlled release, and targeted delivery actions. An increasing number of targeted nanodrugs have been modified through diverse preparations to achieve targeted delivery for different needs.

Tumor Immunotherapy Based on Mesoporous Silica

Cancer immunotherapy can be achieved with cancer vaccines, (Nguyen et al., 2020), which are considered to be a promising tool to fight cancer (**Figure 4**) (Shen D. et al., 2014). Mesoporous silica materials are promising candidates to improve cancer immunotherapy based on their attractive properties that include high specific surface area, high biocompatibility, the easily modified surface groups, and self-adjuvanticity (Lee et al., 2020). Compared with nonporous silica nanoparticles, MSNs not only include self-adjuvanticity, but also could load Toll-like receptor (TLR) agonists, cytosine-phosphonothioate-guanine (CpG), ovalbumin, and immunomodulatory drug (gardiquimod) for mounting a highly potent and long-lasting antitumor immune response. (Nguyen et al., 2019; Nguyen et al., 2020; Seth et al., 2020). Adjuvants (Wang et al., 2012; Liu et al., 2013; Mody et al., 2013) can improve the efficacy of a vaccine by increasing the immunogenicity of the antigen, thus inducing a stronger immune response and promoting the immune memory of the antigen. Liu et al (Liu et al., 2013) designed different structures of silica nanoparticles (SNs) loaded with ovalbumin (OVA) to study the potential for application in protein vaccines. The results showed an effect of the SN structure and size and the medium on protein loading. When mice were vaccinated with SN-OVA preparations, the SNs could upregulate the humoral immune response. Tu et al (Tu et al., 2017) successfully developed lipid-encapsulated MSNPs (LB-MSN-OVA) loaded with OVA as an antigen, which were found to be suitable for the intradermal delivery of encapsulated protein antigens. Modifying nano-microneedles can improve compliance with vaccination, and loading nanoparticles with an antigen can increase and alter the immune response to the antigen. Composite nanomaterials based on mesoporous silica are equally effective in immune delivery systems. Nguyen TL et al (Nguyen et al., 2020) designed an injectable dual-scale mesoporous silica vaccine consisting of coupled mesoporous silica microrods (MSRs) and MSNPs. Compared with the same dose of the MSN vaccine, the MSR-MSN vaccine promoted the production of a large number of cytotoxic antigen-specific T cells against cancer. Compared with the MSR vaccine, the MSR-MSN vaccine showed enhanced antitumor efficacy. The enhanced efficacy of the dual-scale nanoparticle cancer vaccine is due to the improvement in the uptake of MSNs by dendritic cells (DCs) and the migration of the MSNs to lymph nodes over time.

Assisted Imaging Technology Based on Mesoporous Silica

The use of mesoporous silica in auxiliary imaging technology has made good progress (Caltagirone et al., 2015) and can be divided into three categories: 1) fluorescent agents for fluorescence imaging; (Rashidi et al., 2017); 2. loaded contrast agents for magnetic resonance imaging (MRI); (Cao et al., 2015); and 3) radiolabeled MSNs for positron emission tomography (PET) imaging (Ni et al., 2018).

The MSN that is used in fluorescence imaging is optically transparent due to its nanoscale particle size (Koenderink et al., 2001) and will not interfere with the emission of fluorescent agents. At present, imaging agents based on mesoporous silica mainly include quantum dots (QDs), (Li et al., 2019), organic dyes (Rashidi et al., 2016; Rashidi et al., 2017; Fulaz et al., 2019) or rare-earth elements (Chu et al., 2019). Li et al (Li et al., 2019) designed Ag2Se QD-modified MSNPs. Ag2Se QDs have near-infrared fluorescence, excellent

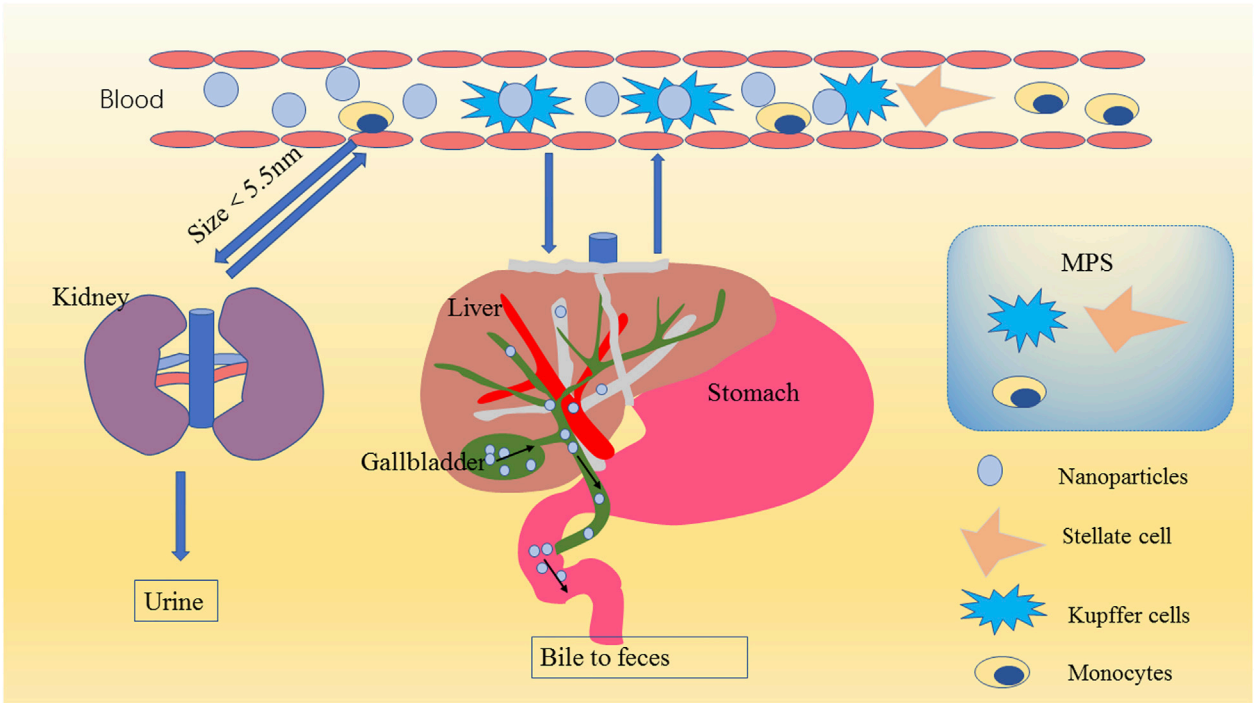


FIGURE 5 | Schematic diagram of nanoparticle metabolism. MSNs in the blood are eliminated mainly through the kidneys (urine) or liver (bile to feces) after encountering the mononuclear phagocyte system (MPS). Because of the filtration effect of the glomerulus and because the physiological pore size of the glomerulus is approximately 5.5 nm, MSNs smaller than 5.5 nm are excreted mainly in the urine through the kidney; MSNs larger than 5.5 nm transition from the peripheral circulation to the liver, and the nanomaterials that escape through the liver return to the systemic circulation through the central vein and are finally returned to the liver (or another MPS organ). This process is repeated until the nanomaterial is removed from the blood. The liver degrades the MSNs into various types of silicic acid, which are excreted in the urine through the hepatic vein to the kidney, usually within 4 weeks. The undegraded MSNs enter the common bile duct, are excreted to the duodenum through the sphincter of Oddi, and finally pass through the entire gastrointestinal tract to be cleared in the feces.

biocompatibility and good dispersibility. Relying on the remarkable photothermal conversion rate (approximately 27.8%) of Ag2Se QDs and the anticancer drug DOX to achieve the effect of combined treatment, responsive multifunctional composite nanomaterials that release drugs at specific sites can achieve effective and accurate cancer treatment. Duan et al (Duan et al., 2017) designed a multifunctional imaging-guided MSN-based therapeutic platform for combined fluorescence/photoacoustic (PA)/computed tomography (CT) imaging and gene/chemical/photothermal therapy. The X-ray opacity and PA properties of AuNRs were used for CT and PA imaging; the fluorescent QDs further improved the imaging sensitivity; and DOX and therapeutic pDNA were used to achieve collaborative imaging-guided cancer treatment.

MRI (Taylor et al., 2008; Cao et al., 2015) is an effective biomedical tool that has the ability to acquire anatomical and metabolic/functional information with high spatiotemporal resolution nondestructively, and MSN-based MRI contrast agents exhibit strong relaxation, high sensitivity and a highly active core payload (Pálmai et al., 2017) due to their flexibility and large surface area. MSNs modified by targeting ligands can effectively identify abnormal tissues for diagnostic purposes. The accumulation of MSN-based MR contrast agent at the target site helps to improve imaging sensitivity. Marcell et al. (Pálmai et al., 2017) designed a silica-based MRI contrast agent with a shortened longitudinal (T1) relaxation time due to the presence of Mn^{2+}. The functionalized MSNs showed significant contrast enhancement on MRI both *in vivo* and *in vitro*. Similarly, Li et al. (Li et al., 2018) designed a mesoporous silica-based T1-T2 dual-core contrast agent loaded with Fe_3O_4 and BSA-Gd2O3 nanoparticles. It has been verified that T1-T2 dual-mode MRI avoids the false-positive signals observed in single-mode imaging and provides more accurate and complementary information.

PET imaging (Ni et al., 2018) of radiolabeled SiNPs is used for analysis of the distribution of drugs in organs/tissues, pharmacokinetic determination and tumor targeting monitoring and has the advantages of high sensitivity, noninvasiveness and quantitation. The U.S. FDA approved the use of 124 I-labeled ultrasmall SiNPs (C dots) for PET imaging in patients with metastatic melanoma as an investigational new drug (IND), which is a significant milestone for the development of useful mesoporous silica products. At present, MSNPs labeled with different radioactive elements (64Cu, 89Zr, 18F, 68Ga, 124I, etc.) have been developed for cancer treatment.

Clinically, the new technology of combined PET/MRI imaging (Forte et al., 2019) has demonstrated high sensitivity and good accuracy and has value in the early detection and diagnosis of

many diseases (especially tumors and the most common heart and brain diseases). In the future, imaging technology will continue to move toward integration and development, which will increase the requirements for imaging agents based on mesoporous silica.

Other Medical Applications

MSNs have great potential for applications in other biomedical fields due to their excellent properties. MSNs loaded with antibiotics and bone cement for functional application in orthopedic surgery have excellent mechanical properties and sustainable drug delivery efficiency (Shen et al., 2011; Letchmanan et al., 2017). A large number of studies have shown that such materials can efficiently and continuously release antibiotics, thereby reducing the risk of postoperative joint infections. Recently, Hiroshi Ikeda et al (Ikeda et al., 2019) designed a mesoporous silica-based organic-inorganic composite material with a nanoscale double-mesh structure to achieve the mechanical properties of human enamel, and the material demonstrated hardness compatible with that of human enamel. Furthermore, Li et al (Li et al., 2015) developed a removable denture base or orthodontic appliance loaded antibiotics to achieve a continuous sterilization effect.

BIOCOMPATIBILITY AND BIODISTRIBUTION

The safety of MSNs is very important. We summarized the metabolic process of mesoporous silica in the body, which is of great significance for its biosafety and biocompatibility, according to a large amount of literature (**Figure 5**); (Fischer et al., 2006; He et al., 2011; Fu et al., 2013)

Drugs based on liposome nanocarriers have been used in clinical treatment; (Bozzuto and Molinari, 2015; Rudokas et al., 2016); current clinical data show that these carriers are sufficiently safe, possibly due to the biocompatibility of phospholipids (Allen and Cullis, 2013; Palazzolo et al., 2018). Similarly, polylactic acid-glycolic acid copolymer is a biodegradable functional organic polymer that can be used as a polymeric nanocarrier (Kamaly et al., 2012; Palazzolo et al., 2018) with good biocompatibility, no toxicity, good encapsulation and easy formation. Due to its performance, this material has been approved by the FDA and officially included in the United States Pharmacopeia as a pharmaceutical excipient. Although these nanocarriers have demonstrated satisfactory biocompatibility, they still have some shortcomings, such as problems related to stability, controlled drug release, and biological barriers. However, MSNs show good performance in these aspects. In this section, we focus on the progress in research on MSN biodistribution and biocompatibility.

Influence of MSN Shape, Size and Surface Modification

The biosafety of MSNs is related to their surface modification. Studies have shown that the cytotoxicity of MSNs is mainly related to their surface silanol groups, which may nonspecifically bind to certain proteins on the cell membrane and cause cell lysis and necrosis (Slowing et al., 2009; Lin and Haynes, 2010; Shinto et al., 2019; Tsamesidis et al., 2020). The surface properties of MSNs have an impact on their biodistribution and biocompatibility. Researchers have found that using polyethylene glycol (PEG) for functional modification to change the surface characteristics of MSNs can reduce the capture of MSNs by the liver, spleen, and lungs, thereby prolonging their circulation time (He et al., 2011). Breznan et al (Breznan et al., 2018) designed a series of MSNs of different sizes (25, 70, 100, 170 and 600 nm) and with different surface features (pristine, C_3-COOH moieties and C_{11}-COOH moieties) to study their cytotoxicity and inflammatory potential. *In vitro* and *in vivo* experiments showed that the toxicity of mesoporous silica was lower than that of nonporous nanoparticles and that changing the surface charge of MSNs can further reduce their cytotoxicity. Further analysis showed that particle size, zeta potential and surface modification were important factors affecting MSN cytotoxicity. Yu et al.'s (Yu et al., 2011) cytotoxicity and hemolysis test results for MSNs also support this conclusion. Roggers et al.(Roggers et al., 2014) found that lipid bilayer-coated MSNs showed significantly better blood compatibility than phosphatidylcholine-coated and uncoated MSNs. Through electron microscopy, ultraviolet-visible spectroscopy and flow cytometry analysis, it was observed that these inorganic/organic composite nanomaterials could contact red blood cells without damaging the cells even at relatively high concentrations. This finding also reflects that changing the surface properties of MSNs through different surface modification strategies can improve their biocompatibility. Liu et al. (Liu et al., 2011) showed that in a mouse model, the lethal dose of 110 nm MSNs was higher than 1,000 mg/kg. Repeated dose toxicity studies showed that no deaths occurred within 14 days of the intravenous administration of repeated MSN doses of 20, 40 and 80 mg/kg. These results also indicated that the toxicity of MSNs is lower when administered via a single-dose intravenous injection than when administered repeatedly. These data show good biocompatibility.

To explore the effects of particle size, dose and cell type on MSN biodistribution and toxicity, Kim et al.(Kim et al., 2015) synthesized MSNs with particle sizes of 20, 60, 100, and 200 nm and cultured them with A549 human alveolar cancer cells and HepG2 lung cancer cells. In addition, in NIH/3T3 mouse embryonic fibroblasts, MSNs of a uniform particle size, to eliminate the experimental uncertainty caused by mixed particle size, were used to explore the effect of particle size on cytotoxicity. By analyzing cell viability, membrane destruction, oxidative stress, and cell uptake, this research showed that MSN cytotoxicity was closely related to particle size, cell type and MSN dose.

The biodistribution and biological toxicity of MSNPs are closely related to their physical and chemical properties. While surface modifications have the greatest influence, different surface modifications have different degrees of influence. The size of the nanoparticle, the surface charge, surface modification, geometric shape and biodistribution are closely related to the

biodistribution and biological toxicity. This suggests that when designing nanoparticles, the size and surface modifications should be selected according to the drug delivery strategy and treatment requirements.

Biodistribution of MSNs

To obtain the best therapeutic effect, nanoparticles should accumulate in diseased tissue as much as possible while having no adverse effects on normal tissue. Upon completing the task of drug delivery, nanoparticles should be cleared from the body and nontarget sites and not persist in the organism.(Pérez-Herrero and Fernández-Medarde, 2015). Although smaller nanoparticles exhibit stronger tissue penetration, they cannot distinguish between healthy and diseased tissues.(Heldin et al., 2004).

At present, there are six main methods for administering nanoparticles: intravenous injection; subcutaneous injection; intratumoral injection; pulmonary inhalation; oral administration; and transdermal administration. Intravenous injection can achieve the rapid delivery and distribution of nanoparticles in the circulatory system, but it can also cause them to be cleared by the kidneys, liver or reticuloendothelial system (RES). The advantage of intravenous injection, subcutaneous injection and intratumoral administration is that these methods can overcome the "first-pass effect" of the liver; after subcutaneous injection, according to the size of the nanoparticles, large nanoparticles (tens of nanometers) enter the lymphatic circulation, and small nanoparticles (a few nanometers) enter the blood circulation through the capillaries. It has been shown that larger materials can last longer at the injection site, and intertumoral injection has been the most common method used in animal experiments; (Brigger et al., 2002; Heldin et al., 2004); this method can achieve more precise targeting and overcome the limitations of systemic administration. Pulmonary inhalation (Gehr et al., 1978; Patton and Byron, 2007) is a feasible method for treating lung diseases or for systemic delivery to treat other diseases because the lungs (alveoli and airways) have a large internal surface area and high endothelial permeability. Nanomaterials that reach the alveolar exchange area are cleared by alveolar macrophages (phagocytes that may leave or remain in the lungs) or DCs and then transported to the draining lymph nodes of the lungs. The oral administration of nanomedicine (Desai et al., 2012) is relatively convenient and has high patient compliance. However, in enzymatic degradation in acidic environments, the intestinal tissue barrier and the "first-pass effect" of the liver (Zhang YN. et al., 2016) all lead to poor oral bioavailability.(Yun et al., 2013). Additionally, healthy human skin is an effective barrier to nanoparticles.(Lodén et al., 2011). Systemic treatment though transdermal delivery is therefore unlikely, but the use of this route for the treatment of local diseases (such as psoriasis) is still promising.(Boakye et al., 2017).

The physical and chemical properties of nanomaterials affect not only the biological distribution but also the biodegradation rate of the nanomaterials in the body. The biodistribution of nanomaterials is related to many factors, including the size, surface properties and dissolution rate of the nanomaterials, as well as tissue- or organ-dependent factors, such as tissue permeability and barrier properties. After intravenous, oral and subcutaneous delivery, nanomaterials can be found in the liver, spleen, kidneys, bone marrow, central nervous system, and local and systemic lymph nodes, (Alexis et al., 2008; Huang et al., 2011; Khlebtsov and Dykman, 2011; Meng et al., 2011), but the liver is the target organ because the liver contains many vascular endothelial cells and Kupffer cells (KCs) and is the main organ for removing macromolecules and microorganisms in the circulation. More than 99% of the particles will be removed by cells in the liver and other organs of the RES. Unexpectedly, when nanomaterials enter and pass through the liver, their speed is reduced by 1,000 times, which increases the possibility of nanomaterials interacting with and subsequently being absorbed and eliminated by a variety of liver cells. These cells are mainly KCs, liver B cells and sinusoidal endothelial cells.(Ray, 2016). He et al. studied the effects of PEGylation and particle size on the biodistribution of MSNs *in vivo*. Nanoparticles 80–390 nm in size were injected into the tail vein of mice and rats. The biodistribution of the nanoparticles was tracked using fluorescein isothiocyanate (FITC), and the results showed higher concentrations of particles in the spleen, liver, and lungs and lower concentrations of particles in the kidneys and heart. The size of nanoparticles also showed a negative correlation with the circulation time. MSNs 80 nm in size showed the longest cycle time, and PEGylation could significantly extend the cycle time. Larger nanoparticles showed faster degradation, which may have been caused by the RES.(He et al., 2011). Xie et al.'s study on the size of MSNs also supports the above conclusion.(Xie et al., 2010). By changing the pore size, geometry and surface characteristics to study the biological distribution, Yu et al. found that the tissue distribution depends on the pore size and surface charge of the particles and that the surface charge and pore size are more important than geometric properties.(Yu et al., 2012).

The biodistribution of MSNPs is closely related to their physical and chemical properties. The size of the nanoparticle greatly affects its biodistribution, and the surface charge, surface modification, geometric shape and biodistribution are closely related to the biodistribution. While surface modifications have the greatest influence, different surface modifications have different degrees of influence. This suggests that when designing nanoparticles, the size and surface modifications should be selected according to the drug delivery strategy and treatment requirements.

Biological Toxicity of MSNs

Now, we understand the metabolism of MSNs, the factors that affect their metabolism, and their distribution in the body. However, understanding these facets is not sufficient. To realize the clinical transformation of MSNs, only investigating the acute toxicity and subacute toxicity of nanoparticles cannot fully reflect their biological toxicity (Hosseinpour et al., 2020; Mohammapdour and Ghandehari, 2022). It is necessary to understand the toxicity of nanoparticles to various types of cells *in vivo*. At present, scientists have paid attention to the immunotoxicity and cytotoxicity of nanoparticles. However, research on MSN that can cross the blood-brain barrier is still insufficient, because it may damage nerve cells. And the research

on the influence of MSNs on DNA is far from enough. In future experiments, more evidence is needed to clarify the biological toxicity of MSN, particularly the following four aspects: immunotoxicity, cytotoxicity, (Manke et al., 2013), neurotoxicity, (Xue et al., 2012), and genetic toxicity.(Donaldson et al., 2010).

Immunotoxicity: The body's first line of defense includes monocytes and macrophages. Nanoparticles entering the human body interact with immune cells and can cause the production of proinflammatory factors, in turn leading to cell apoptosis, which is considered to be the mechanism of nanoparticle-induced immunotoxicity.(Lee et al., 2011). When the therapeutic doses of nanoparticles are given to patients, what will happen to their immune system? How long does it take for the MSNs to degrade and be cleared from MPS? Weather MPS is saturated or not? And what may happen when MPS is saturated? How does this influence the function of the immune system and the normal functions of saturated macrophages? We can't ignore these problems.(Shahbazi et al., 2013).

Cytotoxicity: MSNs can induce oxidative stress and mediate apoptosis in a size- and dose-dependent manner through the mitochondrial pathway. ROS-mediated toxicity is considered to be an important mechanism of nanoparticle toxicity.(Fu et al., 2014).

Neurotoxicity: Very small nanoparticles can be transported across the blood-brain barrier and damage nerve cells. Studies have shown that direct contact with neuroblastoma cells induces adverse reactions, including markers of Alzheimer's disease.(Yang et al., 2014).

Genotoxicity: MSNs can directly interact with DNA, consuming antioxidants, oxidizing DNA, disrupting the cell cycle and causing abnormal gene expression. These are considered to be the potential mechanisms of nanoparticle-induced genotoxicity.(Donaldson et al., 2010; Tarantini et al., 2015).

Currently, it is believed that the main mechanism of biological MSN toxicity is the induction of oxidative stress, which causes toxicity to cells, including immune and nerve cells, as well as DNA. Of course, the toxicity of MSNs is strongly related to the dose, particle size, shape, and surface properties of the MSNs. This is also a research direction that will continue to be explored in the future. For the development of effective mesoporous silica-based clinical drugs, it is necessary to study the potential mechanisms of toxicity.

CONCLUSION AND OUTLOOK

This review provides a detailed introduction to the applications of MSNs in the field of medicine and how they can improve the bioavailability of drugs, reduce antitumor drug resistance, and facilitate targeted therapy and bioimaging, among others. MSNs have achieved remarkable results in animal experiments. The US FDA has also approved the first silica material, C dots, for clinical research. Porous silica holds great promise. Scientists have conducted much research to develop MSNs and apply them as drug delivery systems or in therapeutic strategies. The biodistribution and long-term fate of these MSNs are critical to the applicability and efficacy of drugs, and gaining an understanding of these outcomes is essential to promote the clinical application of mesoporous silica.

In the development of drug delivery strategies, scientists continue to make advances in synthesis methods, surface modifications, and targeting strategies. Composite materials and multifunctional materials that can achieve active targeting and bioimaging while delivering drugs are constantly emerging. In oncology, better therapeutic effects can be achieved through the combination loading of pharmaceuticals and genetic vectors, with the potential to result in a full response. Now, not only reactive oxygen and acid-base responses but also precision delivery under external conditions can be achieved via controlled release in response to photonic, ultrasonic, or magnetic stimuli. In future research, the development of multifunctional responsive materials through different targeting and response strategies and in combination with various imaging technologies will lead to the efficient treatment of target tissues with reduced side effects.

Currently, research on the biodistribution and biosafety of mesoporous silica is very important for its application as a nanocarrier. Studying the biological toxicity of MSNs, particularly their immunotoxicity, cytotoxicity, neurotoxicity and genotoxicity, is important for achieving the clinical application of MSNs.

AUTHOR CONTRIBUTIONS

CZ is the main writer of the review, completes the collection and analysis of relevant literature and the writing of the first draft of the paper; HX, ZZ and BW participates in the analysis and sorting of the literature and data; HC, YB and QC helped with the analysis through constructive discussions. JG and ZS are the creator and person in charge of the project, and guide essay writing. All authors have read and agreed to the final text.

FUNDING

This work was financially supported by the Science and Technology Program of Guangzhou, China (No.202103000089), the Guangdong Demonstration base for Joint Cultivation of Postgraduates, the Science Foundation for Distinguished Young Scholars of Guangdong (No. 2020B1515020026).

REFERENCES

Adams, S. A., and Petersen, C. (2016). Precision Medicine: Opportunities, Possibilities, and Challenges for Patients and Providers. *J. Am. Med. Inform. Assoc.* 23 (4), 787–790. doi:10.1093/jamia/ocv215

Alexis, F., Pridgen, E., Molnar, L. K., and Farokhzad, O. C. (2008). Factors Affecting the Clearance and Biodistribution of Polymeric Nanoparticles. *Mol. Pharm.* 5 (4), 505–515. doi:10.1021/mp800051m

Allen, T. M., and Cullis, P. R. (2013). Liposomal Drug Delivery Systems: from Concept to Clinical Applications. *Adv. Drug Deliv. Rev.* 65 (1), 36–48. doi:10.1016/j.addr.2012.09.037

Assaraf, Y. G., Brozovic, A., Gonçalves, A. C., Jurkovicova, D., Linē, A., Machuqueiro, M., et al. (2019). The Multi-Factorial Nature of Clinical Multidrug Resistance in Cancer. *Drug Resist. Updat* 46, 100645. doi:10.1016/j.drup.2019.100645

Baek, S., Singh, R. K., Khanal, D., Patel, K. D., Lee, E. J., Leong, K. W., et al. (2015). Smart Multifunctional Drug Delivery towards Anticancer Therapy Harmonized in Mesoporous Nanoparticles. *Nanoscale* 7 (34), 14191–14216. doi:10.1039/C5NR02730F

Bayda, S., Adeel, M., Tuccinardi, T., Cordani, M., and Rizzolio, F. (2019). The History of Nanoscience and Nanotechnology: From Chemical-Physical Applications to Nanomedicine. *Molecules* 25 (1), 112. doi:10.3390/molecules25010112

Benezra, M., Penate-Medina, O., Zanzonico, P. B., Schaer, D., Ow, H., Burns, A., et al. (2011). Multimodal Silica Nanoparticles Are Effective Cancer-Targeted Probes in a Model of Human Melanoma. *J. Clin. Invest.* 121 (7), 2768–2780. doi:10.1172/JCI45600

Bertier, G., Carrot-Zhang, J., Ragoussis, V., and Joly, Y. (2016). Integrating Precision Cancer Medicine into Healthcare-Policy, Practice, and Research Challenges. *Genome Med.* 8 (1), 108. doi:10.1186/s13073-016-0362-4

Björnmalm, M., Thurecht, K. J., Michael, M., Scott, A. M., and Caruso, F. (2017). Bridging Bio-Nano Science and Cancer Nanomedicine. *ACS Nano* 11 (10), 9594–9613. doi:10.1021/acsnano.7b04855

Boakye, C. H. A., Patel, K., Doddapaneni, R., Bagde, A., Marepally, S., and Singh, M. (2017). Novel Amphiphilic Lipid Augments the Co-delivery of Erlotinib and IL36 siRNA into the Skin for Psoriasis Treatment. *J. Control. Release* 246, 120–132. doi:10.1016/j.jconrel.2016.05.017

Bozzuto, G., and Molinari, A. (2015). Liposomes as Nanomedical Devices. *Int. J. Nanomedicine* 10, 975–999. doi:10.2147/ijn.S68861

Breznan, D., Das, D. D., MacKinnon-Roy, C., Bernatchez, S., Sayari, A., Hill, M., et al. (2018). Physicochemical Properties Can Be Key Determinants of Mesoporous Silica Nanoparticle Potency *In Vitro*. *ACS Nano* 12 (12), 12062–12079. doi:10.1021/acsnano.8b04910

Brigger, I., Dubernet, C., and Couvreur, P. (2002). Nanoparticles in Cancer Therapy and Diagnosis. *Adv. Drug Deliv. Rev.* 54 (5), 631–651. doi:10.1016/s0169-409x(02)00044-3

Caltagirone, C., Bettoschi, A., Garau, A., and Montis, R. (2015). Silica-based Nanoparticles: a Versatile Tool for the Development of Efficient Imaging Agents. *Chem. Soc. Rev.* 44 (14), 4645–4671. doi:10.1039/c4cs00270a

Cao, M., Wang, P., Kou, Y., Wang, J., Liu, J., Li, Y., et al. (2015). Gadolinium(III)-Chelated Silica Nanospheres Integrating Chemotherapy and Photothermal Therapy for Cancer Treatment and Magnetic Resonance Imaging. *ACS Appl. Mater. Inter.* 7 (45), 25014–25023. doi:10.1021/acsami.5b06938

Cheang, T. Y., Tang, B., Xu, A. W., Chang, G. Q., Hu, Z. J., He, W. L., et al. (2012). Promising Plasmid DNA Vector Based on APTES-Modified Silica Nanoparticles. *Int. J. Nanomedicine* 7, 1061–1067. doi:10.2147/IJN.S28267

Chen, F., Hong, H., Goel, S., Graves, S. A., Orbay, H., Ehlerding, E. B., et al. (2015). *In Vivo* Tumor Vasculature Targeting of CuS@MSN Based Theranostic Nanomedicine. *ACS nano* 9 (4), 3926–3934. doi:10.1021/nn507241v

Chen, F., Hong, H., Shi, S., Goel, S., Valdovinos, H. F., Hernandez, R., et al. (2014). Engineering of Hollow Mesoporous Silica Nanoparticles for Remarkably Enhanced Tumor Active Targeting Efficacy. *Sci. Rep.* 4, 5080. doi:10.1038/srep05080

Cheng, X., Li, D., Lin, A., Xu, J., Wu, L., Gu, H., et al. (2018). Fabrication of Multifunctional Triple-Responsive Platform Based on CuS-Capped Periodic Mesoporous Organosilica Nanoparticles for Chemo-Photothermal Therapy. *Int. J. Nanomedicine* 13, 3661–3677. doi:10.2147/ijn.S167407

Cheng, Y.-J., Hu, J.-J., Qin, S.-Y., Zhang, A.-Q., and Zhang, X.-Z. (2020). Recent Advances in Functional Mesoporous Silica-Based Nanoplatforms for Combinational Photo-Chemotherapy of Cancer. *Biomaterials* 232, 119738. doi:10.1016/j.biomaterials.2019.119738

Chu, C. H., Cheng, S. H., Chen, N. T., Liao, W. N., and Lo, L. W. (2019). Microwave-Synthesized Platinum-Embedded Mesoporous Silica Nanoparticles as Dual-Modality Contrast Agents: Computed Tomography and Optical Imaging. *Int. J. Mol. Sci.* 20 (7). doi:10.3390/ijms20071560

Desai, P. P., Date, A. A., and Patravale, V. B. J. D. D. T. T. (2012). Overcoming Poor Oral Bioavailability Using Nanoparticle Formulations - Opportunities and Limitations. *Drug Discov. Today Technol.* 9 (2), e71–e95. doi:10.1016/j.ddtec.2011.12.001

Dineshkumar, S., Raj, A., Srivastava, A., Mukherjee, S., Pasha, S. S., Kachwal, V., et al. (2019). Facile Incorporation of "Aggregation-Induced Emission"-Active Conjugated Polymer into Mesoporous Silica Hollow Nanospheres: Synthesis, Characterization, Photophysical Studies, and Application in Bioimaging. *ACS Appl. Mater. Inter.* 11 (34), 31270–31282. doi:10.1021/acsami.9b07664

Donaldson, K., Poland, C. A., and Schins, R. P. (2010). Possible Genotoxic Mechanisms of Nanoparticles: Criteria for Improved Test Strategies. *Nanotoxicology* 4, 414–420. doi:10.3109/17435390.2010.482751

Duan, S., Yang, Y., Zhang, C., Zhao, N., and Xu, F. J. (2017). NIR-responsive Polycationic Gatekeeper-Cloaked Hetero-Nanoparticles for Multimodal Imaging-Guided Triple-Combination Therapy of Cancer. *Small* 13 (9), 1603133. doi:10.1002/smll.201603133

Duo, Y., Li, Y., Chen, C., Liu, B., Wang, X., Zeng, X., et al. (2017). DOX-loaded pH-Sensitive Mesoporous Silica Nanoparticles Coated with PDA and PEG Induce Pro-death Autophagy in Breast Cancer. *RSC Adv.* 7 (63), 39641–39650. doi:10.1039/c7ra05135b

Fang, J., Zhang, S., Xue, X., Zhu, X., Song, S., Wang, B., et al. (2018). Quercetin and Doxorubicin Co-delivery Using Mesoporous Silica Nanoparticles Enhance the Efficacy of Gastric Carcinoma Chemotherapy. *Int. J. Nanomedicine* 13, 5113–5126. doi:10.2147/IJN.S170862

Fischer, H. C., Liu, L., Pang, K. S., and Chan, W. C. W. (2006). Pharmacokinetics of Nanoscale Quantum Dots: *In Vivo* Distribution, Sequestration, and Clearance in the Rat. *Adv. Funct. Mater.* 16, 1299–1305. doi:10.1002/adfm.200500529

Forte, E., Fiorenza, D., Torino, E., Costagliola di Polidoro, A., Cavaliere, C., Netti, P. A., et al. (2019). Radiolabeled PET/MRI Nanoparticles for Tumor Imaging. *J. Clin. Med.* 9 (1), 89. doi:10.3390/jcm9010089

Foster, C., Watson, A., Kaplinsky, J., and Kamaly, N. (2017). Improved Targeting of Cancers with Nanotherapeutics. *Methods Mol. Biol.* 1530, 13–37. doi:10.1007/978-1-4939-6646-2_2

Fu, C., Liu, T., Li, L., Liu, H., Chen, D., and Tang, F. (2013). The Absorption, Distribution, Excretion and Toxicity of Mesoporous Silica Nanoparticles in Mice Following Different Exposure Routes. *Biomaterials* 34 (10), 2565–2575. doi:10.1016/j.biomaterials.2012.12.043

Fu, P. P., Xia, Q., Hwang, H. M., Ray, P. C., and Yu, H. (2014). Mechanisms of Nanotoxicity: Generation of Reactive Oxygen Species. *J. Food Drug Anal.* 22 (1), 64–75. doi:10.1016/j.jfda.2014.01.005

Fulaz, S., Hiebner, D., Barros, C. H. N., Devlin, H., Vitale, S., Quinn, L., et al. (2019). Ratiometric Imaging of the *In Situ* pH Distribution of Biofilms by Use of Fluorescent Mesoporous Silica Nanosensors. *ACS Appl. Mater. Inter.* 11 (36), 32679–32688. doi:10.1021/acsami.9b09978

Gehr, P., Bachofen, M., and Weibel, E. R. (1978). The normal Human Lung: Ultrastructure and Morphometric Estimation of Diffusion Capacity. *Respir. Physiol.* 32 (2), 121–140. doi:10.1016/0034-5687(78)90104-4

Ginsburg, G. S., and Phillips, K. A. (2018). Precision Medicine: From Science to Value. *Health Aff. (Millwood)* 37 (5), 694–701. doi:10.1377/hlthaff.2017.1624

Habet, S. (2021). Narrow Therapeutic Index Drugs: Clinical Pharmacology Perspective. *J. Pharm. Pharmacol.* 73 (10), 1285–1291. doi:10.1093/jpp/rgab102

He, Q., Zhang, Z., Gao, F., Li, Y., and Shi, J. (2011). *In Vivo* biodistribution and Urinary Excretion of Mesoporous Silica Nanoparticles: Effects of Particle Size and PEGylation. *Small* 7 (2), 271–280. doi:10.1002/smll.201001459

Heldin, C. H., Rubin, K., Pietras, K., and Ostman, A. (2004). High Interstitial Fluid Pressure - an Obstacle in Cancer Therapy. *Nat. Rev. Cancer* 4 (10), 806–813. doi:10.1038/nrc1456

Hosseinpour, S., Walsh, L. J., and Xu, C. (2020). Biomedical Application of Mesoporous Silica Nanoparticles as Delivery Systems: a Biological Safety Perspective. *J. Mater. Chem. B* 8 (43), 9863–9876. doi:10.1039/d0tb01868f

Hu, J. J., Liu, M. D., Chen, Y., Gao, F., Peng, S. Y., Xie, B. R., et al. (2019). Immobilized Liquid Metal Nanoparticles with Improved Stability and Photothermal Performance for Combinational Therapy of Tumor. *Biomaterials* 207, 76–88. doi:10.1016/j.biomaterials.2019.03.043

Huang, X., Li, L., Liu, T., Hao, N., Liu, H., Chen, D., et al. (2011). The Shape Effect of Mesoporous Silica Nanoparticles on Biodistribution, Clearance, and Biocompatibility *In Vivo*. *ACS Nano* 5 (7), 5390–5399. doi:10.1021/nn200365a

Ikeda, H., Nagamatsu, Y., and Shimizu, H. (2019). Preparation of Silica-Poly(methyl Methacrylate) Composite with a Nanoscale Dual-Network Structure and Hardness Comparable to Human Enamel. *Dent Mater.* 35 (6), 893–899. doi:10.1016/j.dental.2019.03.006

Ji, Y., Si, Y., McMillin, G. A., and Lyon, E. (2018). Clinical Pharmacogenomics Testing in the Era of Next Generation Sequencing: Challenges and Opportunities for Precision Medicine. *Expert Rev. Mol. Diagn.* 18 (5), 411–421. doi:10.1080/14737159.2018.1461561

Jia, L., Li, Z., Shen, J., Zheng, D., Tian, X., Guo, H., et al. (2015). Multifunctional Mesoporous Silica Nanoparticles Mediated Co-delivery of Paclitaxel and Tetrandrine for Overcoming Multidrug Resistance. *Int. J. Pharm.* 489 (1-2), 318–330. doi:10.1016/j.ijpharm.2015.05.010

Kamaly, N., Xiao, Z., Valencia, P. M., Radovic-Moreno, A. F., and Farokhzad, O. C. (2012). Targeted Polymeric Therapeutic Nanoparticles: Design, Development and Clinical Translation. *Chem. Soc. Rev.* 41 (7), 2971–3010. doi:10.1039/c2cs15344k

Khlebtsov, N., and Dykman, L. (2011). Biodistribution and Toxicity of Engineered Gold Nanoparticles: a Review of *In Vitro* and *In Vivo* Studies. *Chem. Soc. Rev.* 40 (3), 1647–1671. doi:10.1039/c0cs00018c

Kim, I. Y., Joachim, E., Choi, H., and Kim, K. (2015). Toxicity of Silica Nanoparticles Depends on Size, Dose, and Cell Type. *Nanomedicine* 11 (6), 1407–1416. doi:10.1016/j.nano.2015.03.004

Koenderink, G. H., Sacanna, S., Pathmamanoharan, C., Raşa, M., and Philipse, A. P. (2001). Preparation and Properties of Optically Transparent Aqueous Dispersions of Monodisperse Fluorinated Colloids. *Langmuir* 17 (20), 6086–6093. doi:10.1021/la010181y

König, I. R., Fuchs, O., Hansen, G., von Mutius, E., and Kopp, M. V. (2017). What Is Precision Medicine. *Eur. Respir. J.* 50 (4), 1700391. doi:10.1183/13993003.00391-2017

Kresge, C. T., Leonowicz, M. E., Roth, W. J., Vartuli, J. C., and Beck, J. S. (1992). Ordered Mesoporous Molecular Sieves Synthesized by a Liquid-crystal Template Mechanism. *Nature* 359 (6397), 710–712. doi:10.1038/359710a0

Lee, J. Y., Kim, M. K., Nguyen, T. L., and Kim, J. (2020). Hollow Mesoporous Silica Nanoparticles with Extra-large Mesopores for Enhanced Cancer Vaccine. *ACS Appl. Mater. Inter.* 12 (31), 34658–34666. doi:10.1021/acsami.0c09484

Lee, S., Yun, H. S., and Kim, S. H. (2011). The Comparative Effects of Mesoporous Silica Nanoparticles and Colloidal Silica on Inflammation and Apoptosis. *Biomaterials* 32 (35), 9434–9443. doi:10.1016/j.biomaterials.2011.08.042

Letchmanan, K., Shen, S. C., Ng, W. K., Kingshuk, P., Shi, Z., Wang, W., et al. (2017). Mechanical Properties and Antibiotic Release Characteristics of Poly(methyl Methacrylate)-Based Bone Cement Formulated with Mesoporous Silica Nanoparticles. *J. Mech. Behav. Biomed. Mater.* 72, 163–170. doi:10.1016/j.jmbbm.2017.05.003

Li, H., Gu, J., Shah, L. A., Siddiq, M., Hu, J., Cai, X., et al. (2015). Bone Cement Based on Vancomycin Loaded Mesoporous Silica Nanoparticle and Calcium Sulfate Composites. *Mater. Sci. Eng. C Mater. Biol. Appl.* 49, 210–216. doi:10.1016/j.msec.2014.12.082

Li, J., You, J., Wu, C., Dai, Y., Shi, M., Dong, L., et al. (2018). T1-T2 Molecular Magnetic Resonance Imaging of Renal Carcinoma Cells Based on Nano-Contrast Agents. *Int. J. Nanomedicine* 13, 4607–4625. doi:10.2147/IJN.S168660

Li, X., Liu, Z., Luo, K., Yin, X., Lin, X., and Zhu, C. (2019). Biomimetic Synthesis of Ag2 Se Quantum Dots with Enhanced Photothermal Properties and as "Gatekeepers" to Cap Mesoporous Silica Nanoparticles for Chemo-Photothermal Therapy. *Chem. Asian J.* 14 (1), 155–161. doi:10.1002/asia.201801388

Liang, J., Jin, X., Chen, B., Hu, J., Huang, Q., Wan, J., et al. (2020). Doxorubicin-loaded pH-responsive nanoparticles coated with chlorin e6 for drug delivery and synergetic chemo-photodynamic therapy. *Nanotechnology* 31 (19), 195103. doi:10.1088/1361-6528/ab6fd5

Lin, Y. S., and Haynes, C. L. (2010). Impacts of Mesoporous Silica Nanoparticle Size, Pore Ordering, and Pore Integrity on Hemolytic Activity. *J. Am. Chem. Soc.* 132 (13), 4834–4842. doi:10.1021/ja910846q

Liu, J., Liang, H., Li, M., Luo, Z., Zhang, J., Guo, X., et al. (2018). Tumor Acidity Activating Multifunctional Nanoplatform for NIR-Mediated Multiple Enhanced Photodynamic and Photothermal Tumor Therapy. *Biomaterials* 157, 107–124. doi:10.1016/j.biomaterials.2017.12.003

Liu, Q., Zhou, Y., Li, M., Zhao, L., Ren, J., Li, D., et al. (2019). Polyethylenimine Hybrid Thin-Shell Hollow Mesoporous Silica Nanoparticles as Vaccine Self-Adjuvants for Cancer Immunotherapy. *ACS Appl. Mater. Inter.* 11 (51), 47798–47809. doi:10.1021/acsami.9b19446

Liu, T., Li, L., Teng, X., Huang, X., Liu, H., Chen, D., et al. (2011). Single and Repeated Dose Toxicity of Mesoporous Hollow Silica Nanoparticles in Intravenously Exposed Mice. *Biomaterials* 32 (6), 1657–1668. doi:10.1016/j.biomaterials.2010.10.035

Liu, T., Liu, H., Fu, C., Li, L., Chen, D., Zhang, Y., et al. (2013). Silica Nanorattle with Enhanced Protein Loading: a Potential Vaccine Adjuvant. *J. Colloid Interf. Sci* 400, 168–174. doi:10.1016/j.jcis.2013.03.005

Liu, X., Fu, F., Xu, K., Zou, R., Yang, J., Wang, Q., et al. (2014). Folic Acid-Conjugated Hollow Mesoporous silica/CuS Nanocomposites as a Difunctional Nanoplatform for Targeted Chemo-Photothermal Therapy of Cancer Cells. *J. Mater. Chem. B* 2 (33), 5358–5367. doi:10.1039/c4tb00919c

Lodén, M., Beitner, H., Gonzalez, H., Edström, D. W., Akerström, U., Austad, J., et al. (2011). Sunscreen Use: Controversies, Challenges and Regulatory Aspects. *Br. J. Dermatol.* 165 (2), 255–262. doi:10.1111/j.1365-2133.2011.10298.x

Lv, Y., Cao, Y., Li, P., Liu, J., Chen, H., Hu, W., et al. (2017). Ultrasound-Triggered Destruction of Folate-Functionalized Mesoporous Silica Nanoparticle-Loaded Microbubble for Targeted Tumor Therapy. *Adv. Healthc. Mater.* 6 (18), 1700354. doi:10.1002/adhm.201700354

Ma, B., He, L., You, Y., Mo, J., and Chen, T. (2018). Controlled Synthesis and Size Effects of Multifunctional Mesoporous Silica Nanosystem for Precise Cancer Therapy. *Drug Deliv.* 25 (1), 293–306. doi:10.1080/10717544.2018.1425779

Manke, A., Wang, L., and Rojanasakul, Y. (2013). Mechanisms of Nanoparticle-Induced Oxidative Stress and Toxicity. *Biomed. Res. Int.* 2013, 942916. doi:10.1155/2013/942916

Meka, A. K., Niu, Y., Karmakar, S., Hartono, S. B., Zhang, J., Lin, C. X. C., et al. (2016). Facile Synthesis of Large-Pore Bicontinuous Cubic Mesoporous Silica Nanoparticles for Intracellular Gene Delivery. *ChemNanoMat* 2 (3), 220–225. doi:10.1002/cnma.201600021

Meng, H., Wang, M., Liu, H., Liu, X., Situ, A., Wu, B., et al. (2015). Use of a Lipid-Coated Mesoporous Silica Nanoparticle Platform for Synergistic Gemcitabine and Paclitaxel Delivery to Human Pancreatic Cancer in Mice. *ACS nano* 9 (4), 3540–3557. doi:10.1021/acsnano.5b00510

Meng, H., Xue, M., Xia, T., Ji, Z., Tarn, D. Y., Zink, J. I., et al. (2011). Use of Size and a Copolymer Design Feature to Improve the Biodistribution and the Enhanced Permeability and Retention Effect of Doxorubicin-Loaded Mesoporous Silica Nanoparticles in a Murine Xenograft Tumor Model. *ACS Nano* 5 (5), 4131–4144. doi:10.1021/nn200809t

Mody, K. T., Popat, A., Mahony, D., Cavallaro, A. S., Yu, C., and Mitter, N. (2013). Mesoporous Silica Nanoparticles as Antigen Carriers and Adjuvants for Vaccine Delivery. *Nanoscale* 5 (12), 5167–5179. doi:10.1039/c3nr00357d

Mohamed, A. L., Elmotasem, H., and Salama, A. A. A. (2020). Colchicine Mesoporous Silica Nanoparticles/hydrogel Composite Loaded Cotton Patches as a New Encapsulator System for Transdermal Osteoarthritis Management. *Int. J. Biol. Macromol* 164, 1149–1163. doi:10.1016/j.ijbiomac.2020.07.133

Mohammapdour, R., and Ghandehari, H. (2022). Mechanisms of Immune Response to Inorganic Nanoparticles and Their Degradation Products. *Adv. Drug Deliv. Rev.* 180, 114022. doi:10.1016/j.addr.2021.114022

Mora-Raimundo, P., Lozano, D., Benito, M., Mulero, F., Manzano, M., and Vallet-Regí, M. (2021). Osteoporosis Remission and New Bone Formation with Mesoporous Silica Nanoparticles. *Adv. Sci. (Weinh)* 8 (16), e2101107. doi:10.1002/advs.202101107

Nagahashi, M., Shimada, Y., Ichikawa, H., Kameyama, H., Takabe, K., Okuda, S., et al. (2019). Next Generation Sequencing-Based Gene Panel Tests for the Management of Solid Tumors. *Cancer Sci.* 110 (1), 6–15. doi:10.1111/cas.13837

Ngamcherdtrakul, W., Sangvanich, T., Reda, M., Gu, S., Bejan, D., and Yantasee, W. (2018). Lyophilization and Stability of Antibody-Conjugated Mesoporous

Silica Nanoparticle with Cationic Polymer and PEG for siRNA Delivery. *Int. J. Nanomedicine* 13, 4015–4027. doi:10.2147/IJN.S164393

Nguyen, T. L., Cha, B. G., Choi, Y., Im, J., and Kim, J. (2020). Injectable Dual-Scale Mesoporous Silica Cancer Vaccine Enabling Efficient Delivery of Antigen/adjuvant-Loaded Nanoparticles to Dendritic Cells Recruited in Local Macroporous Scaffold. *Biomaterials* 239, 119859. doi:10.1016/j.biomaterials.2020.119859

Nguyen, T. L., Choi, Y., and Kim, J. (2019). Mesoporous Silica as a Versatile Platform for Cancer Immunotherapy. *Adv. Mater.* 31 (34), e1803953. doi:10.1002/adma.201803953

Ni, D., Jiang, D., Ehlerding, E. B., Huang, P., and Cai, W. (2018). Radiolabeling Silica-Based Nanoparticles via Coordination Chemistry: Basic Principles, Strategies, and Applications. *Acc. Chem. Res.* 51 (3), 778–788. doi:10.1021/acs.accounts.7b00635

Palazzolo, S., Bayda, S., Hadla, M., Caligiuri, I., Corona, G., Toffoli, G., et al. (2018). The Clinical Translation of Organic Nanomaterials for Cancer Therapy: A Focus on Polymeric Nanoparticles, Micelles, Liposomes and Exosomes. *Curr. Med. Chem.* 25 (34), 4224–4268. doi:10.2174/0929867324666170830113755

Pálmai, M., Pethő, A., Nagy, L. N., Klébert, S., May, Z., Mihály, J., et al. (2017). Direct Immobilization of Manganese Chelates on Silica Nanospheres for MRI Applications. *J. Colloid Interf. Sci* 498, 298–305. doi:10.1016/j.jcis.2017.03.053

Patton, J. S., and Byron, P. R. (2007). Inhaling Medicines: Delivering Drugs to the Body through the Lungs. *Nat. Rev. Drug Discov.* 6 (1), 67–74. doi:10.1038/nrd2153

Pérez-Herrero, E., and Fernández-Medarde, A. (2015). Advanced Targeted Therapies in Cancer: Drug Nanocarriers, the Future of Chemotherapy. *Eur. J. Pharm. Biopharm.* 93, 52–79. doi:10.1016/j.ejpb.2015.03.018

Pinna, A., Torki Baghbaderani, M., Vigil Hernández, V., Naruphontjirakul, P., Li, S., McFarlane, T., et al. (2021). Nanoceria Provides Antioxidant and Osteogenic Properties to Mesoporous Silica Nanoparticles for Osteoporosis Treatment. *Acta Biomater.* 122, 365–376. doi:10.1016/j.actbio.2020.12.029

Quan, G., Pan, X., Wang, Z., Wu, Q., Li, G., Dian, L., et al. (2015). Lactosaminated Mesoporous Silica Nanoparticles for Asialoglycoprotein Receptor Targeted Anticancer Drug Delivery. *J. Nanobiotechnology* 13, 7. doi:10.1186/s12951-015-0068-6

Rai, M., Yadav, A., and Gade, A. (2009). Silver Nanoparticles as a New Generation of Antimicrobials. *Biotechnol. Adv.* 27 (1), 76–83. doi:10.1016/j.biotechadv.2008.09.002

Rashidi, L., Ganji, F., and Vasheghani-Farahani, E. (2017). Fluorescein Isothiocyanate-Dyed Mesoporous Silica Nanoparticles for Tracking Antioxidant Delivery. *IET Nanobiotechnol* 11 (4), 454–462. doi:10.1049/iet-nbt.2016.0120

Rashidi, L., Vasheghani-Farahani, E., and Ganji, F. J. I. N. (2016). FITC-dyed Mesoporous Silica Nanoparticles for Tracking Antioxidant Delivery. *Nanobiotechnology* 11 (4), 454–462. doi:10.1049/iet-nbt.2016.0120

Ray, K. (2016). Liver: Clearance of Nanomaterials in the Liver. *Nat. Rev. Gastroenterol. Hepatol.* 13 (10), 560. doi:10.1038/nrgastro.2016.136

Razavi, M., Primavera, R., Kevadiya, B. D., Wang, J., Ullah, M., Buchwald, P., et al. (2020). Controlled Nutrient Delivery to Pancreatic Islets Using Polydopamine-Coated Mesoporous Silica Nanoparticles. *Nano Lett.* 20 (10), 7220–7229. doi:10.1021/acs.nanolett.0c02576

Roggers, R. A., Joglekar, M., Valenstein, J. S., and Trewyn, B. G. (2014). Mimicking Red Blood Cell Lipid Membrane to Enhance the Hemocompatibility of Large-Pore Mesoporous Silica. *ACS Appl. Mater. Inter.* 6 (3), 1675–1681. doi:10.1021/am4045713

Rotow, J., and Bivona, T. G. (2017). Understanding and Targeting Resistance Mechanisms in NSCLC. *Nat. Rev. Cancer* 17 (11), 637–658. doi:10.1038/nrc.2017.84

Rudokas, M., Najlah, M., Alhnan, M. A., and Elhissi, A. (2016). Liposome Delivery Systems for Inhalation: A Critical Review Highlighting Formulation Issues and Anticancer Applications. *Med. Princ Pract.* 25 (Suppl. 2), 60–72. doi:10.1159/000445116

Sarkar, A., Ghosh, S., Chowdhury, S., Pandey, B., and Sil, P. C. (2016). Targeted Delivery of Quercetin Loaded Mesoporous Silica Nanoparticles to the Breast Cancer Cells. *Biochim. Biophys. Acta* 1860 (10), 2065–2075. doi:10.1016/j.bbagen.2016.07.001

Seth, A., Gholami Derami, H., Gupta, P., Wang, Z., Rathi, P., Gupta, R., et al. (2020). Polydopamine-Mesoporous Silica Core-Shell Nanoparticles for Combined Photothermal Immunotherapy. *ACS Appl. Mater. Inter.* 12 (38), 42499–42510. doi:10.1021/acsami.0c10781

Shahbazi, M. A., Hamidi, M., Mäkilä, E. M., Zhang, H., Almeida, P. V., Kaasalainen, M., et al. (2013). The Mechanisms of Surface Chemistry Effects of Mesoporous Silicon Nanoparticles on Immunotoxicity and Biocompatibility. *Biomaterials* 34 (31), 7776–7789. doi:10.1016/j.biomaterials.2013.06.052

Shao, D., Li, J., Zheng, X., Pan, Y., Wang, Z., Zhang, M., et al. (2016). Janus "Nano-Bullets" for Magnetic Targeting Liver Cancer Chemotherapy. *Biomaterials* 100, 118–133. doi:10.1016/j.biomaterials.2016.05.030

Shen, D., Yang, J., Li, X., Zhou, L., Zhang, R., Li, W., et al. (2014). Biphase Stratification Approach to Three-Dimensional Dendritic Biodegradable Mesoporous Silica Nanospheres. *Nano Lett.* 14 (2), 923–932. doi:10.1021/nl404316v

Shen, J., Kim, H. C., Su, H., Wang, F., Wolfram, J., Kirui, D., et al. (2014). Cyclodextrin and Polyethylenimine Functionalized Mesoporous Silica Nanoparticles for Delivery of siRNA Cancer Therapeutics. *Theranostics* 4 (5), 487–497. doi:10.7150/thno.8263

Shen, S. C., Ng, W. K., Shi, Z., Chia, L., Neoh, K. G., and Tan, R. B. (2011). Mesoporous Silica Nanoparticle-Functionalized Poly(methyl Methacrylate)-Based Bone Cement for Effective Antibiotics Delivery. *J. Mater. Sci. Mater. Med.* 22 (10), 2283–2292. doi:10.1007/s10856-011-4397-1

Shen, Y., Shuhendler, A. J., Ye, D., Xu, J. J., and Chen, H. Y. (2016). Two-photon Excitation Nanoparticles for Photodynamic Therapy. *Chem. Soc. Rev.* 45 (24), 6725–6741. doi:10.1039/c6cs00442c

Shi, J., Kantoff, P. W., Wooster, R., and Farokhzad, O. C. (2017). Cancer Nanomedicine: Progress, Challenges and Opportunities. *Nat. Rev. Cancer* 17 (1), 20–37. doi:10.1038/nrc.2016.108

Shinto, H., Fukasawa, T., Yoshisue, K., Tsukamoto, N., Aso, S., Hirohashi, Y., et al. (2019). Effect of Interfacial Serum Proteins on the Cell Membrane Disruption Induced by Amorphous Silica Nanoparticles in Erythrocytes, Lymphocytes, Malignant Melanocytes, and Macrophages. *Colloids Surf. B Biointerfaces* 181, 270–277. doi:10.1016/j.colsurfb.2019.05.067

Singh, R. K., Patel, K. D., Leong, K. W., and Kim, H. W. (2017). Progress in Nanotheranostics Based on Mesoporous Silica Nanomaterial Platforms. *ACS Appl. Mater. Inter.* 9 (12), 10309–10337. doi:10.1021/acsami.6b16505

Slowing, I. I., Wu, C. W., Vivero-Escoto, J. L., and Lin, V. S. (2009). Mesoporous Silica Nanoparticles for Reducing Hemolytic Activity towards Mammalian Red Blood Cells. *Small* 5 (1), 57–62. doi:10.1002/smll.200800926

Srivastava, P., Hira, S. K., Paladhi, A., Singh, R., Gupta, U., Srivastava, D. N., et al. (2020). Studies on Interaction Potency Model Based on Drug Synergy and Therapeutic Potential of Triple Stimuli-Responsive Delivery of Doxorubicin and 5-Fluoro-2-Deoxyuridine against Lymphoma Using Disulfide-Bridged Cysteine over Mesoporous Silica Nanoparticles. *J. Mater. Chem. B* 8 (7), 1411–1421. doi:10.1039/c9tb02628b

Sun, L., Wang, D., Chen, Y., Wang, L., Huang, P., Li, Y., et al. (2017). Core-shell Hierarchical Mesostructured Silica Nanoparticles for Gene/chemo-Synergetic Stepwise Therapy of Multidrug-Resistant Cancer. *Biomaterials* 133, 219–228. doi:10.1016/j.biomaterials.2017.04.028

Tang, L., Gabrielson, N. P., Uckun, F. M., Fan, T. M., and Cheng, J. (2013). Size-dependent Tumor Penetration and *In Vivo* Efficacy of Monodisperse Drug-Silica Nanoconjugates. *Mol. Pharm.* 10 (3), 883–892. doi:10.1021/mp300684a

Tang, L., Yang, X., Yin, Q., Cai, K., Wang, H., Chaudhury, I., et al. (2014). Investigating the Optimal Size of Anticancer Nanomedicine. *Proc. Natl. Acad. Sci. U S A.* 111 (43), 15344–15349. doi:10.1073/pnas.1411499111

Tao, C., Zhu, Y., Xu, Y., Zhu, M., Morita, H., and Hanagata, N. (2014). Mesoporous Silica Nanoparticles for Enhancing the Delivery Efficiency of Immunostimulatory DNA Drugs. *Dalton Trans.* 43 (13), 5142–5150. doi:10.1039/c3dt53433b

Tarantini, A., Huet, S., Jarry, G., Lanceleur, R., Poul, M., Tavares, A., et al. (2015). Genotoxicity of Synthetic Amorphous Silica Nanoparticles in Rats Following Short-Term Exposure. Part 1: Oral Route. *Environ. Mol. Mutagen* 56 (2), 218–227. doi:10.1002/em.21935

Taylor, K. M., Kim, J. S., Rieter, W. J., An, H., Lin, W., and Lin, W. (2008). Mesoporous Silica Nanospheres as Highly Efficient MRI Contrast Agents. *J. Am. Chem. Soc.* 130 (7), 2154–2155. doi:10.1021/ja710193c

The White House (2015). FACT SHEET: President Obama's Precision Medicine Initiative. [Online]. Available: https://obamawhitehouse.archives.gov/the-

press-office/2015/01/30/fact-sheet-president-obama-s-precision-medicine-initiative (Accessed 01 15, 2015).

Thorat, N. D., Bauer, J., Tofail, S. A. M., Gascón Pérez, V., Bohara, R. A., and Yadav, H. M. (2020). Silica Nano Supra-assembly for the Targeted Delivery of Therapeutic Cargo to Overcome Chemoresistance in Cancer. *Colloids Surf. B Biointerfaces* 185, 110571. doi:10.1016/j.colsurfb.2019.110571

Tsamesidis, I., Pouroutzidou, G. K., Lymperaki, E., Kazeli, K., Lioutas, C. B., Christodoulou, E., et al. (2020). Effect of Ion Doping in Silica-Based Nanoparticles on the Hemolytic and Oxidative Activity in Contact with Human Erythrocytes. *Chem. Biol. Interact* 318, 108974. doi:10.1016/j.cbi.2020.108974

Tu, J., Du, G., Reza Nejadnik, M., Mönkäre, J., van der Maaden, K., Bomans, P. H. H., et al. (2017). Mesoporous Silica Nanoparticle-Coated Microneedle Arrays for Intradermal Antigen Delivery. *Pharm. Res.* 34 (8), 1693–1706. doi:10.1007/s11095-017-2177-4

Vogt, H., Green, S., and Broderson, J. (2018). Precision Medicine in the Clouds. *Nat. Biotechnol.* 36 (8), 678–680. doi:10.1038/nbt.4210

Wakai, T., Prasoon, P., Hirose, Y., Shimada, Y., Ichikawa, H., and Nagahashi, M. (2019). Next-generation Sequencing-Based Clinical Sequencing: toward Precision Medicine in Solid Tumors. *Int. J. Clin. Oncol.* 24 (2), 115–122. doi:10.1007/s10147-018-1375-3

Wang, D., Xu, X., Zhang, K., Sun, B., Wang, L., Meng, L., et al. (2018). Codelivery of Doxorubicin and MDR1-siRNA by Mesoporous Silica Nanoparticles-Polymerpolyethylenimine to Improve Oral Squamous Carcinoma Treatment. *Int. J. Nanomedicine* 13, 187–198. doi:10.2147/IJN.S150610

Wang, P., Jiang, S., Li, Y., Luo, Q., Lin, J., Hu, L., et al. (2021). Virus-like Mesoporous Silica-Coated Plasmonic Ag Nanocube with strong Bacteria Adhesion for Diabetic Wound Ulcer Healing. *Nanomedicine: Nanotechnology, Biol. Med.* 34, 102381. doi:10.1016/j.nano.2021.102381

Wang, T., Jiang, H., Zhao, Q., Wang, S., Zou, M., and Cheng, G. (2012). Enhanced Mucosal and Systemic Immune Responses Obtained by Porous Silica Nanoparticles Used as an Oral Vaccine Adjuvant: Effect of Silica Architecture on Immunological Properties. *Int. J. Pharm.* 436 (1-2), 351–358. doi:10.1016/j.ijpharm.2012.06.028

Wang, X., Ding, X., Yu, B., Zhang, X., Shen, Y., and Cong, H. (2020). Tumor microenvironment-responsive polymer with chlorin e6 to interface hollow mesoporous silica nanoparticles-loaded oxygen supply factor for boosted photodynamic therapy. *Nanotechnology* 31 (30), 305709. doi:10.1088/1361-6528/ab89d1

Wu, M., Meng, Q., Chen, Y., Du, Y., Zhang, L., Li, Y., et al. (2015). Large-pore Ultrasmall Mesoporous Organosilica Nanoparticles: Micelle/precursor Co-templating Assembly and Nuclear-Targeted Gene Delivery. *Adv. Mater.* 27 (2), 215–222. doi:10.1002/adma.201404256

Xie, G., Sun, J., Zhong, G., Shi, L., and Zhang, D. (2010). Biodistribution and Toxicity of Intravenously Administered Silica Nanoparticles in Mice. *Arch. Toxicol.* 84 (3), 183–190. doi:10.1007/s00204-009-0488-x

Xu, Y., Claiden, P., Zhu, Y., Morita, H., and Hanagata, N. (2015). Effect of Amino Groups of Mesoporous Silica Nanoparticles on CpG Oligodexynucleotide Delivery. *Sci. Technol. Adv. Mater.* 16 (4), 045006. doi:10.1088/1468-6996/16/4/045006

Xue, Y., Wu, J., and Sun, J. (2012). Four Types of Inorganic Nanoparticles Stimulate the Inflammatory Reaction in Brain Microglia and Damage Neurons *In Vitro*. *Toxicol. Lett.* 214 (2), 91–98. doi:10.1016/j.toxlet.2012.08.009

Yang, J., Teng, Y., Fu, Y., and Zhang, C. (2019). Chlorins e6 loaded silica nanoparticles coated with gastric cancer cell membrane for tumor specific photodynamic therapy of gastric cancer. *Int. J. Nanomedicine* 14, 5061–5071. doi:10.2147/IJN.S202910

Yang, X., He, C., Li, J., Chen, H., Ma, Q., Sui, X., et al. (2014). Uptake of Silica Nanoparticles: Neurotoxicity and Alzheimer-like Pathology in Human SK-N-SH and Mouse Neuro2a Neuroblastoma Cells. *Toxicol. Lett.* 229 (1), 240–249. doi:10.1016/j.toxlet.2014.05.009

Yardley, D. A. (2013). Drug Resistance and the Role of Combination Chemotherapy in Improving Patient Outcomes. *Int. J. Breast Cancer* 2013, 137414. doi:10.1155/2013/137414

Youssef, Z., Jouan-Hureaux, V., Colombeau, L., Arnoux, P., Moussaron, A., Baros, F., et al. (2018). Titania and silica nanoparticles coupled to Chlorin e6 for anti-cancer photodynamic therapy. *Photodiagnosis Photodyn Ther.* 22, 115–126. doi:10.1016/j.pdpdt.2018.03.005

Yu, T., Hubbard, D., Ray, A., and Ghandehari, H. (2012). *In Vivo* biodistribution and Pharmacokinetics of Silica Nanoparticles as a Function of Geometry, Porosity and Surface Characteristics. *J. Control. Release* 163 (1), 46–54. doi:10.1016/j.jconrel.2012.05.046

Yu, T., Malugin, A., and Ghandehari, H. (2011). Impact of Silica Nanoparticle Design on Cellular Toxicity and Hemolytic Activity. *ACS Nano* 5 (7), 5717–5728. doi:10.1021/nn2013904

Yun, Y., Cho, Y. W., and Park, K. (2013). Nanoparticles for Oral Delivery: Targeted Nanoparticles with Peptidic Ligands for Oral Protein Delivery. *Adv. Drug Deliv. Rev.* 65 (6), 822–832. doi:10.1016/j.addr.2012.10.007

Zarei, H., Kazemi Oskuee, R., Hanafi-Bojd, M. Y., Gholami, L., Ansari, L., and Malaekeh-Nikouei, B. (2018). Enhanced Gene Delivery by Polyethyleneimine Coated Mesoporous Silica Nanoparticles. *Pharm. Dev. Technol.* 24 (1), 127–132. doi:10.1080/10837450.2018.1431930

Zenych, A., Fournier, L., and Chauvierre, C. (2020). Nanomedicine Progress in Thrombolytic Therapy. *Biomaterials* 258, 120297. doi:10.1016/j.biomaterials.2020.120297

Zhang, H., Cui, W., Qu, X., Wu, H., Qu, L., Zhang, X., et al. (2019). Photothermal-responsive Nanosized Hybrid Polymersome as Versatile Therapeutics Codelivery Nanovehicle for Effective Tumor Suppression. *Proc. Natl. Acad. Sci. U S A.* 116 (16), 7744–7749. doi:10.1073/pnas.1817251116

Zhang, J., Guo, S., Zhang, W., Niu, D., and Gong, J. (2016). Large-pore Mesoporous Silica Nanospheres as Vehicles for Delivering TRAF3-shRNA Plasmids to Kupffer Cells. *Biochem. Biophys. Res. Commun.* 469 (2), 196–202. doi:10.1016/j.bbrc.2015.11.101

Zhang, M., Kim, Y. K., Cui, P., Zhang, J., Qiao, J., He, Y., et al. (2016). Folate-conjugated Polyspermine for Lung Cancer-Targeted Gene Therapy. *Acta Pharm. Sin B* 6 (4), 336–343. doi:10.1016/j.apsb.2016.03.010

Zhang, Y. N., Poon, W., Tavares, A. J., McGilvray, I. D., and Chan, W. C. W. (2016). Nanoparticle-liver Interactions: Cellular Uptake and Hepatobiliary Elimination. *J. Control. Release* 240, 332–348. doi:10.1016/j.jconrel.2016.01.020

Zhao, Y. (2018). Nanomedicine in China. *Adv. Healthc. Mater.* 7 (20), e1801051. doi:10.1002/adhm.201801051

Conflict of Interest: Author QC is employed by Guangzhou Rainhome Pharm & Tech Co., Ltd.

The remaining authors declare that the research was conducted in the absence of any commercial or financial relationships that could be construed as a potential conflict of interest.

Publisher's Note: All claims expressed in this article are solely those of the authors and do not necessarily represent those of their affiliated organizations, or those of the publisher, the editors and the reviewers. Any product that may be evaluated in this article, or claim that may be made by its manufacturer, is not guaranteed or endorsed by the publisher.

Copyright © 2022 Zhang, Xie, Zhang, Wen, Cao, Bai, Che, Guo and Su. This is an open-access article distributed under the terms of the Creative Commons Attribution License (CC BY). The use, distribution or reproduction in other forums is permitted, provided the original author(s) and the copyright owner(s) are credited and that the original publication in this journal is cited, in accordance with accepted academic practice. No use, distribution or reproduction is permitted which does not comply with these terms.

frontiers in Pharmacology

REVIEW
published: 18 February 2022
doi: 10.3389/fphar.2022.846715

Recent Advance of Nanomaterial-Mediated Tumor Therapies in the Past Five Years

Xinyan Hao[1,2,3], *Junyong Wu*[1,2,3], *DaXiong Xiang*[1,2,3] *and Yongyu Yang*[1,2,3]*

[1]*Department of Pharmacy, The Second Xiangya Hospital, Central South University, Changsha, China,* [2]*Hunan Provincial Engineering Research Centre of Translational Medicine and Innovative Drug, Changsha, China,* [3]*Institute of Clinical Pharmacy, Central South University, Changsha, China*

Cancer has posed a major threat to human life and health with a rapidly increasing number of patients. The complexity and refractory of tumors have brought great challenges to tumor treatment. In recent years, nanomaterials and nanotechnology have attracted more attention and greatly improved the efficiency of tumor therapies and significantly prolonged the survival period, whether for traditional tumor treatment methods such as radiotherapy, or emerging methods, such as phototherapy and immunotherapy, sonodynamic therapy, chemodynamic therapy and RNA interference therapeutics. Various monotherapies have obtained positive results, while combination therapies are further proposed to prevent incomplete eradication and recurrence of tumors, strengthen tumor killing efficacy with minimal side effects. In view of the complementary promotion effects between different therapies, it is vital to utilize nanomaterials as the link between monotherapies to achieve synergistic performance. Further development of nanomaterials with efficient tumor-killing effect and better biosafety is more in line with the needs of clinical treatment. In a word, the development of nanomaterials provides a promising way for tumor treatment, and here we will review the emerging nanomaterials towards radiotherapy, phototherapy and immunotherapy, and summarized the developed nanocarriers applied for the tumor combination therapies in the past 5 years, besides, the advances of some other novel therapies such as sonodynamic therapy, chemodynamic therapy, and RNA interference therapeutics have also been mentioned.

Keywords: nanomaterial, radiotherapy, phototherapy, immunotherapy, combination therapies

OPEN ACCESS

Edited by:
Zeming Liu,
Huazhong University of Science and Technology, China

Reviewed by:
Peng Li,
Xinxiang Medical University, China
Hua De Liao,
Central South University, China

***Correspondence:**
Yongyu Yang
yongyuyang@csu.edu.cn

Specialty section:
This article was submitted to Pharmacology of Anti-Cancer Drugs, a section of the journal Frontiers in Pharmacology

Received: *31 December 2021*
Accepted: *31 January 2022*
Published: *18 February 2022*

Citation:
Hao X, Wu J, Xiang D and Yang Y (2022) Recent Advance of Nanomaterial-Mediated Tumor Therapies in the Past Five Years. Front. Pharmacol. 13:846715. doi: 10.3389/fphar.2022.846715

INTRODUCTION

Cancer has severely threatened human life worldwide, and malignant tumors are still a serious problem that needs to be solved urgently (Siegel et al., 2020). Traditional tumor treatment methods mainly include surgery, chemotherapy and radiotherapy, while some limitations are also manifested, such as the damage to surrounding tissues, poor effect on hypoxic tumors, possible wound complications, and inconvenience of treatment (Kaur and Asea, 2012; Sundaram et al., 2020). Research on development of tumor therapies is aimed to better eradicate tumors while minimizing side effects.

The application of nanomaterials has further optimized traditional tumor therapies and provided more options for emerging tumor therapies such as phototherapy, immunotherapy, sonodynamic therapy, chemodynamic therapy and RNA interference (RNAi) therapeutics (Song et al., 2017; Hou

et al., 2018). The unique properties of nanomaterials made them applicative for tumor diagnose and treatment (He et al., 2015). The nano-scale size facilitates the penetration cross biological barriers, increases the drug delivery efficiency and controls the release behavior, thus achieving better therapeutic effects (Sun et al., 2014). In addition, appropriate nanomaterials can be effectively targeted to the tumor site and reduce systemic toxicity; Modified nanomaterials have been widely applied for both traditional and novel tumor therapies due to the specific physicochemical properties and targeting ability (Sun et al., 2014; Aikins et al., 2020). Nanocarriers have also been constructed to overcome hypoxia of the tumor microenvironment to obtain more efficient tumor killing effects (Abbasi et al., 2016; Meng et al., 2018). Nevertheless, although monotherapy strategies such as radiotherapy and phototherapy are proven effective methods for tumor treatment, there may be a potential risk of tumor recurrence or the refractory of deep-seated tumors. Based on this, tumor combination therapy has been proposed to eradicate tumors synergistically and effectively in a complementary manner, minimizing systemic toxicity and side effects as much as possible. Studies have demonstrated that radiotherapy can break through the limitation of insufficient tissue penetration of phototherapy. In turn, photothermal therapy can promote oxygen perfusion to relieve the hypoxic environment of tumors, which is beneficial to the efficiency of oxygen-dependent therapies such as radiotherapy, photodynamic therapy and sonodynamic therapy. In addition, a large amount of evidence has shown that the therapies can induce the release of tumor-associated antigens locally to activate the immune response, therefore, combination therapies with immunotherapy are a smart approach to achieve synergistic tumor treatment effects (Hou et al., 2018; Chen et al., 2019; Galon and Bruni, 2019). On this basis, recent research has also focused on the development of nanomaterials for the construction of carriers for combination therapy.

The review is aim to outline the recent advances in nanomaterial-mediated radiotherapy, phototherapy, and immunotherapy, and some other therapies (sonodynamic therapy, chemodynamic therapy, and RNAi therapeutics). Besides, we will present innovate strategies for combined tumor treatment based on nanomaterials in the past 5 years.

APPLICATION OF NANOMATERIALS IN RADIOTHERAPY

Radiotherapy utilizes high-dose radiation to induce DNA destruction and generate free radicals to kill tumor cells, including internal and external radiotherapy, usually in conjunction with chemotherapy or surgery (Sundaram et al., 2020; Zeng et al., 2021). However, traditional radiotherapy causes irreversible damage to surrounding normal tissues due to the large amount of radiation. Besides, the hypoxic environment limits oxygen-dependent DNA damage, which in turn leads to tumor resistance to radiation (Jarosz-Biej et al., 2019). Hypoxia also protects dormant cancer stem cells, allowing them to retain the potential for proliferation and differentiation, thus leading to a potential risk of recurrence (Wang et al., 2019a). Therefore, it is necessary to improve the sensitivity of tumor cells to irradiation, overcome the hypoxic environment at the tumor site and increase oxidative stress, strengthen the killing effect on tumor cells and alleviate its side effects on normal tissues (**Figure 1**).

High-Z materials such as gold (Dong et al., 2020), silver (Liu Z. et al., 2018), platinum (Li et al., 2019) and gadolinium (Du and Sun, 2020) have been widely reported to be used as radiosensitizers and accelerate the generation of reactive oxygen species (ROS) through photoelectric effect, Auger electronics and Compton effect (Sundaram et al., 2020). Lan et al. developed a metal-organic frameworks (MOF) hierarchically composed of Hf-based secondary building units and Ir-based bridging ligands, encapsulated $(P_2W_{18}O_{62})^{6-}$ (W_{18}) polyoxometalates through electrostatic adsorption to further enhance the sensitivity of radiotherapy (Lan et al., 2019). The hierarchical structure facilitated the generation of hydroxyl radical ($^{\bullet}OH$), singlet oxygen ($^1O_2$) and superoxide (O_2^-), which is an excellent radio-enhancer for the treatment of MC38 and CT26 tumor bearing mice (Lan et al., 2019).

Among high-Z materials, gold-based nanoparticles (AuNPs) have received extensive attention due to the good biocompatibility and surface modifiability. Studies have further enhanced its superiority in radiotherapy sensitization by changing the size, structure or surface properties (Yang et al., 2014; Dong et al., 2020). Dong et al. prepared gold sub-nanoparticles encapsulating cell cycle regulator α-difluoromethylornithine, and modified them with arginine-glycine-aspartic acid (RGD) penetrating peptide to promote its penetration of the blood-brain barrier. The results showed enhanced sensitivity to radiation and significant therapeutic effects in low-dose radiation (Dong et al., 2021). AuNPs can also be modified to improve targeting ability. A conjugated complex composed of AuNPs and a plectin-1 targeting peptide showed more aggregation at the tumor site, and induced tumor cell apoptosis with better biosafety (Dong et al., 2020).

Hypoxia of the tumor microenvironment hinders radiation therapy sensitivity and the formation of ROS. Hypoxia-inducible factor 1 (HIF-1) is stably expressed under hypoxic conditions, which has been shown to participate in the proliferation and metastasis of tumor cells by regulating its downstream signaling molecules (Meng et al., 2018; Sundaram et al., 2020). Based on this, studies utilized nanocarriers combined with tumor oxygenation agents such as catalase and MnO_2 to decompose the over-expressed H_2O_2 into oxygen, thereby alleviating the tumor hypoxia and enhancing the sensitivity of radiotherapy (Abbasi et al., 2016; Song et al., 2016). Meng et al. encapsulated the HIF-1 inhibitor acriflavine into MnO_2 nanoparticles to generate oxygen in tumor tissues and improve the effect of radiotherapy. On the other hand, acriflavine inhibited the expression of HIF-1 and down-regulated its downstream signaling molecules such as vascular endothelial growth factor and glucose transporter, showing an 84.70% tumor inhibition rate in abscopal tumors (Meng et al., 2018).

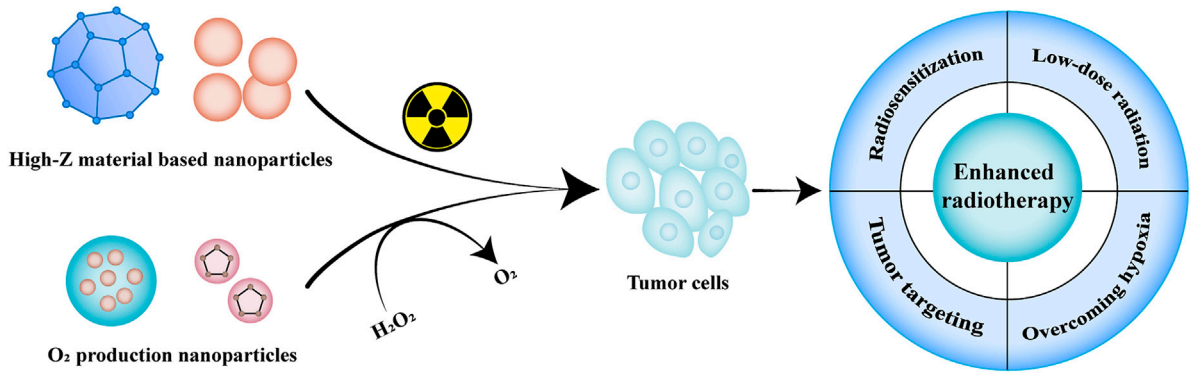


FIGURE 1 | Illustration of nanomaterials used in radiotherapy. The commonly used nanomaterials in radiotherapy mainly include high-Z materials-based nanoparticles and oxygen-producing nanoparticles, which can effectively enhance the accumulation at the tumor site, improve the sensitivity of radiotherapy, overcome the hypoxic environment of tumors and enhance the radiotherapy efficiency.

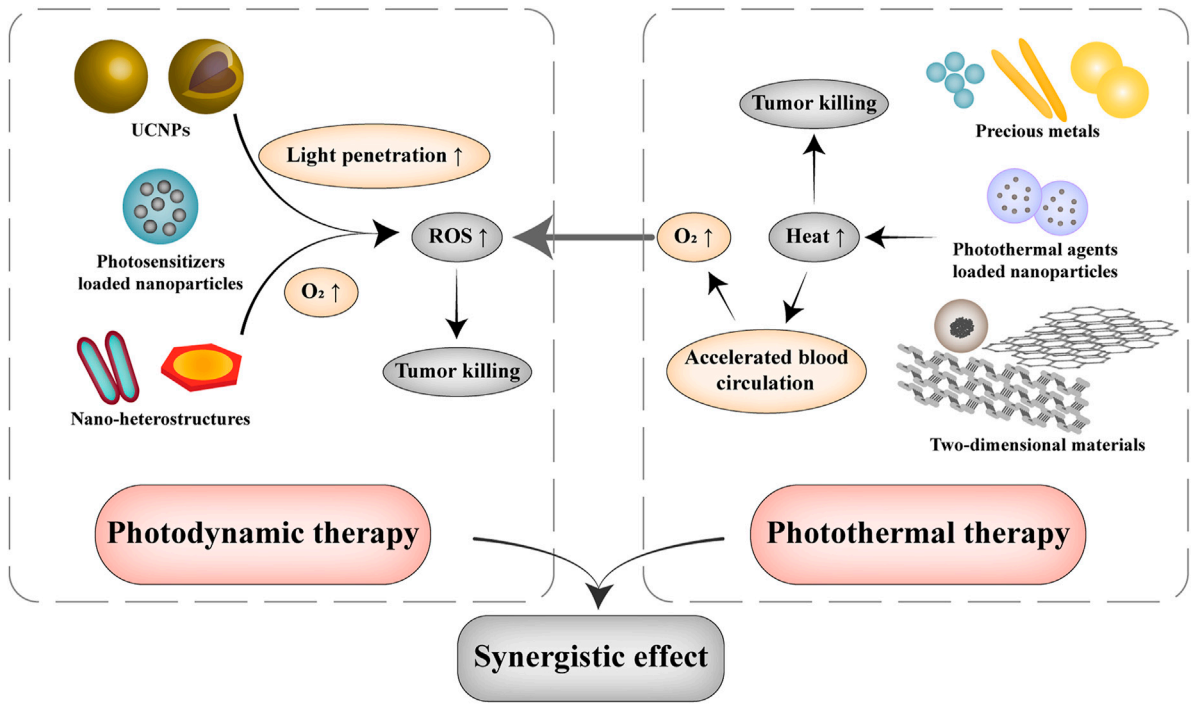


FIGURE 2 | Illustration of nanomaterials used in photothermal therapy and photodynamic therapy. Photodynamic therapy stimulates photosensitizers to produce ROS in an oxygen-dependent manner. UCNPs are applied to enhance the tissue permeability of light by converting NIR into UV or visible light, and nano heterostructures have been proposed for the simultaneous generation of ROS and O_2 through electron-hole separation under normoxia or hypoxia condition. Photothermal therapy uses NIR to excite nanomaterials with good light-to-heat conversion capabilities for tumor ablation, which can effectively accelerate the blood circulation and increase the oxygen concentration of tumor tissue, which in turn facilitates the performance of photodynamic therapy.

NANOMATERIALS USED IN PHOTOTHERMAL THERAPY AND PHOTODYNAMIC THERAPY

Photothermal therapy and photodynamic therapy are currently the most common phototherapy for tumor treatment. Photothermal therapy is to gather materials with high light-to-heat conversion efficiency in the tumor tissue and heat it to ablate cancer cells under the irradiation of external light source (Hou et al., 2018). And photodynamic therapy utilizes a specific wavelength of light to irradiate a photosensitizer at the tumor site and generate ROS to kill tumor cells. Compared with traditional tumor therapy, both photothermal and photodynamic therapy can be applied accurately and

effectively with less side effects and greatly reduce the patient's pain in a noninvasive way (**Figure 2**) (Li et al., 2020).

Photothermal agents are materials with good light-to-heat conversion capabilities, mainly including noble metals (gold (Wang et al., 2013), silver (Park et al., 2020), platinum (Ma et al., 2020), etc.), two-dimensional materials (graphene (Chen et al., 2016), black phosphorus (BP) (Geng et al., 2019), transition metal-based materials (Xie et al., 2019), etc.), and some organic small molecule photothermal agents (porphyrin, phthalocyanine, cyanine, etc.) (Lv et al., 2020). The current research aims to develop materials with excellent biocompatibility in addition to photothermal performance. Most metal-free 2D materials such as graphene oxide and BP have great biocompatibility and biodegradability, and have attracted more attention as candidate materials for photothermal therapy in recent years (Liu S. et al, 2020). Graphene has been a hotspot of scientific research since its discovery. Recently, graphene derivatives have been favored due to its better drug loading efficiency and photothermal conversion capacity (Chen et al., 2016). It is proved that folic acid coupled chitosan functionalized graphene oxide (FA-CS-GO) can completely destroy cancer cells under near-infrared (NIR) light irradiation *in vitro*, and showed excellent anti-tumor effect *in vivo* with no recurrence in 20 days (Jun et al., 2020). Besides, BP has been considered as a promising photothermal material, but its rapid degradation in the physiological environment limits its application. Based on this, Geng et al. assembled NIR-II responsive carbon dots on BP nanosheets to construct a hybrid photothermal agent, which improved the stability of BP and showed synergistic photothermal effect, attained higher light-to-heat conversion efficiency in the NIR-I and NIR-II window (77.3 and 61.4%, respectively), and the deep tumors were eradicated under the 1,064 nm laser (Geng et al., 2019). Shao et al. prepared a core-shell structured nanospheres with black phosphorous quantum dots (BPQDs) encapsulated in poly (lactic-co-glycolic acid) (PLGA), and the nanospheres achieved a better passive targeting effect, retained good photothermal performance with excellent stability (Shao et al., 2016).

As for photodynamic therapy, there have been many studies on nanocarriers loaded photosensitizers such as photofrin (Kano et al., 2013), 5-aminolevulinic acid (Zhang et al., 2015) and chlorine e6 (Ce6) (Yang et al., 2019) to improve delivery efficiency and enhance tumor killing effects, but the hypoxia microenvironment greatly limits the therapeutic efficiency. In addition to the strategies of delivering MnO_2 and catalase to increase the production of oxygen, studies have indicated that nano-heterostructure can promote electron-hole separation and the accumulation of ROS, which is considered an effective material for photodynamic therapy (Cheng et al., 2020). Zhang et al. designed a bismuth sulfide (Bi_2S_3)-bismuth (Bi) Z-type heterostructure with a good electron-hole separation ability, simultaneously generated ROS and O_2 under NIR irradiation, improved photodynamic therapy efficiency with excellent biocompatibility and biodegradability (Cheng et al., 2020). Qiu et al. also prepared bismuth/bismuth oxide (Bi/BiOx) lateral nano-heterostructures based on the regioselective oxidation strategy. Under 660 nm laser irradiation, $^1O_2$ can be effectively generated under normal oxygen conditions, and cytotoxic •OH and H_2 can be generated under hypoxic conditions, showing synergetic photodynamic performance on tumor elimination (Qiu et al., 2021).

Furthermore, studies used up-conversion nanomaterials (UCNPs) to emit visible light under NIR excitation and stimulate photosensitizers to effectively produce ROS, overcome the limitation of weak tissue penetration of visible light, and improve the efficacy of photodynamic therapy (Liang et al., 2020a; Liu et al., 2020b). Liu et al. constructed a Nd^{3+} ion-doped UCNPs surface-modified porphyrin-like metal-organic framework and functionalized it to target the mitochondria to achieve enhanced photodynamic therapy under the trigger of NIR irradiation (Liu et al., 2020c). Liang et al. developed UCNPs modified with oleic acid-polyamide dendrimers to form hydrophobic and hydrophilic pockets on the surface of nanoparticles through click reaction, loaded with photosensitizer Ce6 and catalase, which can effectively overcome tumor hypoxia and improve photodynamic therapy efficiency, indicating significant anti-tumor effect through synergistic mitochondrial targeting modification (Liang et al., 2020b).

In addition, photodynamic and photothermal therapy are usually applied in combination due to their synergistic tumor killing effect (**Figure 2**). Photothermal therapy generates heat locally can not only ablate tumor cells, but also accelerate blood circulation and accumulate oxygen in the tumor's hypoxic microenvironment to provide suitable conditions for photodynamic therapy (Yang et al., 2021). Guan et al. prepared covalent organic framework nanoparticles with a particle size of ~140 nm that co-loaded the photosensitizer porphyrin and the photothermal agent naphthalocyanine. The temperature increase led by the photothermal effect significantly enhanced the sensitivity of photodynamic therapy by destroying lysosomes and mitochondria (Guan et al., 2019). Yang et al. synthesized TiO_2@RP nanorods with red phosphorus (RP) as the shell and TiO_2 as the core. After being irradiated with 808 nm NIR light for 5 min, the nanorods can reach 39.3–44.1°C and induce the production of $^1O_2$, effectively killing cancer cells in deep tissues of renal cell carcinoma (Yang et al., 2021).

NANOMATERIAL-MEDIATED IMMUNOTHERAPY

Immunotherapy is based on the regulation of the immune system, activating a long-term immune response against malignant tumor cells, thereby eradicating tumors and inhibiting tumor metastasis (Riley et al., 2019). Tumor associate antigens derived from necrotic or apoptotic tumor cells can be taken up and processed by antigen-presenting cells, presented to T cells in lymph nodes, inducing the activation of immature T cells to effector T cells. T cell-mediated cellular immune response is the key to tumor immunity (Song et al., 2017).

Tumor vaccines can effectively trigger potent immune responses for tumor prevention and treatment specifically. Nanomaterials are applied to co-deliver antigens and adjuvants

(Zhu et al., 2018), increase the uptake of antigen-presenting cells, improve the ability of cross presentation, or directly target lymph nodes to induce strong effective immune response (Li H. et al, 2017; Zhong et al., 2019a). Zhu et al. co-encapsulated B16 melanoma-derived tyrosinase-related protein 2 (Trp2) peptides and toll-like receptor agonists (CpG oligonucleotides and monophosphoryl lipid A) in a mesoporous silica vector, which improved the efficiency of antigen delivery to dendritic cells, effectively activated T cell-specific immune responses and prolonged the survival period of tumor-bearing mice significantly (Zhu et al., 2018). Li et al. prepared micelles composed of polycaprolactone-polyethyleneimine and polycaprolactone-polyethylene glycol, and co-loaded Trp2 and the adjuvant CpG oligodeoxynucleotide, which showed higher activity of cytotoxic T lymphocytes (CTLs) and stronger anti-tumor ability in B16F10 melanoma mice compared with the mixture of free Trp2 and CpG (Li M. et al, 2017).

The antigen captured by dendritic cells are presented to the major histocompatibility complex class I (MHCI) or major histocompatibility complex class II (MHCII) molecules extracellularly (Song et al., 2017). For tumor immunotherapy, it is vital that exogenous antigens escape from lysosomes and activate $CD8^+$T cells through the MHCI pathway through cross presentation (Du et al., 2020). Suitable nanomaterials are applied according to the unique acidic environment of the lysosome to promote the escape of antigen from the lysosome and enhance cross presentation (Li H. et al, 2017; Du et al., 2020). The most commonly used methods are cationic polymer modifications such as polyethylenimine (Li M. et al, 2017), 1,2-dioleoyl-3-trimethylammonium-propane (Zhang et al., 2019) and dimethyl dioctadecylammonium bromide (Xia et al., 2018), inducing the proton sponge effect to cause the destruction of the endosomal membrane, thereby increasing the endosomal escape of the antigen (Du et al., 2020). Recent studies have shown that pH-sensitive materials can also promote cross presentation by inducing endosomal membrane fusion and transferring antigens through the cytosol (Zhong et al., 2019b; Du et al., 2020). MOFs have attracted attention due to their excellent drug-carrying capacity and pH-sensitive properties. Zhong et al. used zeolite imidazole skeleton (ZIF-8), a pH-sensitive degradable MOF, co-loaded antigen and CpG for subcutaneous injection, which decomposed in the lysosome to release the antigen into the cytoplasm and enhanced cross presentation, remarkably inhibiting EG7-OVA tumor growth (Zhong et al., 2019a). In another study, the MOF composed of guanine monophosphate and lanthanide ions can be actively internalized by antigen presenting cells, release the antigen and promote its escape from the lysosome, significantly improving the CTL response (Duan et al., 2017).

Although tumor vaccines have shown excellent anti-tumor effects, the immunosuppressive microenvironment presents a major challenge for tumor immunotherapy, and immune checkpoint inhibitors have been considered as a promising strategy in recent years (Song et al., 2017). Blocking the immune checkpoints facilitates the recognition of T cells and initiates an effective anti-tumor immune response, thus preventing tumor immune escape and improving the efficiency of anti-tumor immunotherapy (Song et al., 2017; Chen et al., 2018). The most studied inhibitory receptors are cytotoxic T lymphocyte-associated protein 4 (CTLA-4) and programmed death 1 (PD-1). CTLA-4 is expressed on activated T cells and interacts with costimulatory molecules on antigen presenting cells to impede T cell activation (Ruan et al., 2019). And PD-1 is up-regulated on activated T cells, interacts with the corresponding ligand PD-L1 on tumor cells to inhibit the function of T cells. Anti-CTLA-4 monoclonal antibody ipilimumab and anti-PD-1/PD-L1 antibodies such as pembrolizumab and avelumab have been approved by the United States Food and Drug Administration (FDA) for clinical cancer treatment (Chen et al., 2018; Ruan et al., 2019). Studies have shown that combining tumor vaccines with immune checkpoint inhibitors can effectively combat tumors and prevent the recurrence (Kuai et al., 2017; Kim et al., 2020). Kim et al. used biocompatible phospholipid nanoparticles to co-encapsulate tumor antigens and CpG adjuvants, which showed strong anti-tumor effects in the prevention and treatment of EG7 tumor models, but the vaccine induced T-cell exhaustion by increasing PD-L1 expression, leading to tumor recurrence. Combining anti-PD-1 therapy with nano-vaccine suppressed tumor recurrence and showed a synergistic anti-tumor effect (Kim et al., 2020).

DEVELOPED NANOMATERIALS TOWARDS THE TUMOR COMBINATION THERAPIES

Nanomaterials have exhibited great potential in tumor treatment and obtained remarkable results in both traditional and emerging therapies. However, there are still some limitations in monotherapy such as the inability to completely eliminate the tumor or the potential risk of tumor recurrence. The application of nanomaterials in combination therapy is emphasized to achieve synergistic effects for tumor treatment (**Figure 3**).

Radiotherapy Combined With Phototherapy

NIR light used in photothermal therapy has a limited penetration depth and fails to eradicate tumor cells in the deep tissue. Relatively, radiotherapy has a stronger penetrating ability, which can effectively break through the restriction while also improving the photothermal conversion capability (Zheng et al., 2021). At the same time, photothermal therapy can improve oxygen perfusion and relieve hypoxic environment, thus amplifying the effect of radiotherapy (Luo et al., 2020). Research has shown that nanomaterials based on high-Z element can simultaneously promote photothermal therapy and radiotherapy. Zheng designed a $W_{18}O_{49}$ nanosphere which showed excellent radiation sensitization and photothermal performance, promoted the production of $^1O_2$ and •OH, increased radiation-induced DNA damage and significantly inhibited tumor cell proliferation and metastasis (Zheng et al., 2021). In addition, the combined application with nano-heterostructure is conducive to the production of ROS. Cai et al. prepared a copper sulfide nano-heterostructure modified by platinum gold nanoparticles with enhanced

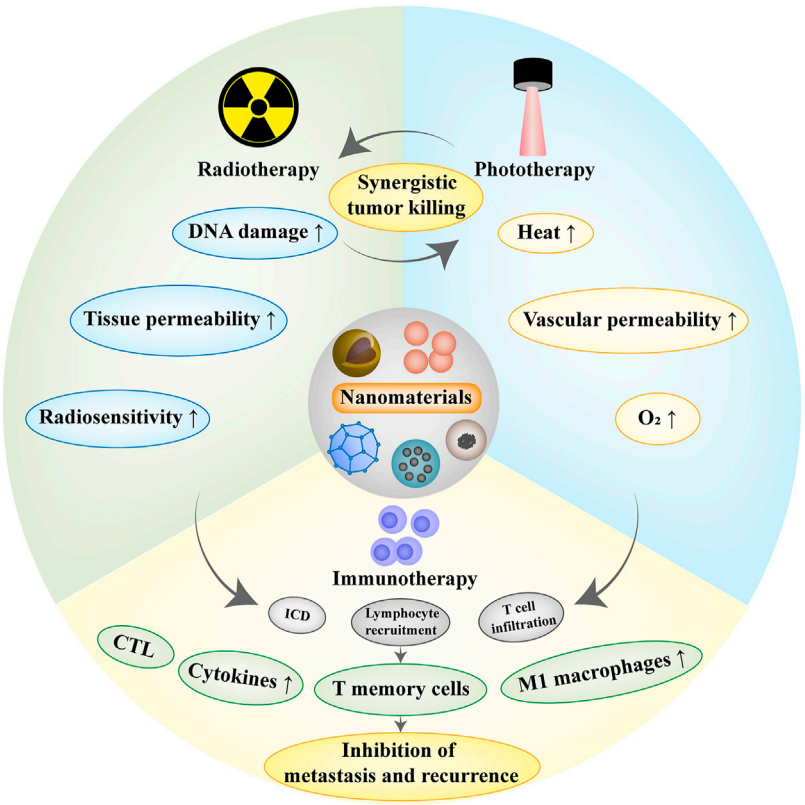


FIGURE 3 | Schematic diagram of tumor combination therapies. Radiotherapy can break through the limitation of insufficient tissue penetration of phototherapy. In turn, photothermal therapy can improve vascular permeability and increase O_2 concentration, which facilitates the performance of radiotherapy. Radiotherapy/phototherapy can induce immunogenic cell death (ICD), release tumor-associated antigens locally and increase T cell infiltration, and the combination with immunotherapy can effectively inhibit tumor metastasis and recurrence.

light-to-heat conversion capacity, leading to efficient glutathione clearance and formation of ROS with the co-excitation of NIR and X-ray. The nano-heterostructure can effectively remove tumors and inhibit tumor recurrence, exerting the synergistic anti-tumor effect of radiotherapy and photothermal therapy (Cai et al., 2021). Similarly, Huang et al. developed a dumbbell-shaped heterostructure based on copper selenide-gold nanoparticles for enhanced radiophotothermal therapy. The heterostructure possesses excellent photothermal conversion efficiency due to enhanced localized surface plasmon resonance and also has better X-ray attenuation based on the synergy of multiple elements, indicating a remarkable tumor cell elimination effect (Huang et al., 2019).

The combination of radiotherapy and photodynamic therapy can also solve the limitation of tissue penetration to eliminate deep-seated tumors. Studies have demonstrated that the strategy of combining high-Z materials and photosensitizers has achieved remarkable results. Sun et al. successfully synthesized polymer nanodots based on gadolinium ions and the clinically used photosensitizer Rose Bengal through solvothermal reaction. The nanodots induced the generation efficiency of $^1O_2$ increased by 1.9 times compared with Rose Bengal, significantly inhibiting tumor growth with a tumor suppression rate of 98.8% without systemic toxicity or long-term side effects (Sun et al., 2020). Another promising approach is to combine scintillator materials and photosensitizers to activate radiotherapy and photodynamic therapy under the same ionizing radiation. Scintillators are developed to absorb X-rays and convert them into photons to activate photosensitizers to generate ROS, providing a new strategy for treatment of deep tumors (Zhong et al., 2019b). Ahmad et al. prepared a scintillating nanoparticle CeF_3:Gd^{3+}, Tb^{3+}coated with mesoporous silica and loaded Bengal Rose for X-ray-induced photodynamic therapy. Low-dose X-ray irradiation confirmed a better tumor regression effect of synergistic therapies relative to radiotherapy alone by down-regulating the amino acids involved in protein and DNA synthesis (Ahmad et al., 2019). Shi et al. prepared mesoporous zinc gallium germanate long afterglow nanoparticles ($Zn_3Ga_2GeO_8$:Cr^{3+}, Yb^{3+}, Er^{3+}), which can penetrate muscle tissue to achieve effective afterglow imaging in mice. Under X-ray irradiation, the nanoparticles emitted NIR long afterglow thus activating the photosensitizer to kill cancer cells and effectively inhibiting the growth of liver tumors *in situ* (Shi et al., 2020). Zhong et al. prepared a rod-like structure of $NaCeF_4$: Gd, Tb nano scintillation crystals to enhance the local radiation intensity, which was also activated as an X-ray responsive

TABLE 1 | List of nanomaterials in tumor combination therapy based on immunotherapy.

No	Design	Activity	Ref
—	Radiotherapy combined with immunotherapy	—	—
1	PLGA nanoparticle co-loaded with catalase and Toll-like receptor-7 agonist R837 combined with anti-CTLA-4 therapy	Decomposed H_2O_2 and increased the oxygen in the tumor to enhance efficacy of radiotherapy, triggered a stronger tumor immune response effectively and inhibited the growth of distant tumors	Chen et al. (2019)
2	RGD modified triangular star tellurium nanomaterials combined with anti-PD-1 therapy	Increased the accumulation of ROS and improved radiotherapy effect, promoted the polarization of M2 to M1 phenotype macrophages	Huang et al. (2020)
3	Metal-organic layers composed of Hf-oxo clusters and porphyrin-based bridging ligands, combined with anti-PD-1 polypeptides	Enhanced the radiotherapeutic effects and the generation of ROS, efficiently triggered strong immune response and antimetastatic effects	Patel et al. (2019)
4	Nanoparticles comprised of CpG and pH-responsive polymer PC7A coated with bacterial membrane and modified with maleimide	The nanoparticle can capture cancer neoantigens following radiotherapy, enhance the cross presentation and effectively activate T cell response and anti-tumor immune memory	Ni et al. (2019)
—	Photodynamic/photothermal therapy combined with immunotherapy	—	—
1	Pd nanosheets loaded with CpG ODNs	Increased the levels of TNF-α and IL-6 and induced a strong CTL response, significantly improved the survival rate of tumor-bearing mice	Ming et al. (2020)
2	FePSe3 wrapped in CT26 membrane, loaded with anti-PD-1 polypeptides	Improved the accumulation at the tumor site, induced the activation of T cells, and significantly prolonged the survival time of tumor-bearing mice	Fang et al. (2021)
3	Catalase-Ce6 mixed with polymeric matrix polyethylene glycol diacrylate to form an *in-situ* hydrogel, loaded with R837 and combined with anti-CTLA-4 therapy	Inhibited the growth of distant tumors, and provided effective immune memory protection	Meng et al. (2019)
4	pH-sensitive dextran-hyaluronidase nanoparticles followed by application of Ce6@liposome, combined with anti-PD-L1 therapy	Degraded hyaluronic acid in the extracellular matrix to alleviate the hypoxic environment and effectively inhibited the growth of distant tumors	Wang et al. (2019a)
5	$NaGdF_4$: Yb/Er upconversion layer-coated PDA nanoparticles loaded with Ce6, combined with anti-PD-1 therapy	Increased the levels of IL-6 and TNF-α and decreased the level of IL-10, activated CTLs and T memory cells and inhibited tumor metastasis and recurrence effectively	Yan et al. (2019)
6	Au/Ag nanorod combined with anti-CTLA-4 therapy	Induced a strong immune memory effect and prevented tumor recurrence	Jin et al. (2021)

photosensitizer to generate a large amount of O_2^- and •OH (Zhong et al., 2019b).

In addition, it is demonstrated that the combination of photothermal and X-ray-induced photodynamic therapy has a better therapeutic effect, as photothermal therapy is believed to enhance the permeability of nanoparticles in tumors and increase oxygen accumulation, which is conducive to improving the efficacy of oxygen-dependent treatments such as photodynamic therapy and radiotherapy (Guo et al., 2017; Luo et al., 2020). Based on this, Luo et al. conjugated europium complex scintillators and mesoporous silica coated gold nanorods, loaded with photosensitizer hematoporphyrin to applied for the synergistic treatment of radiotherapy/photodynamic/photothermal therapy. The nanoparticle has strong NIR absorption and X-ray conversion efficiency, showed excellent photothermal effect and radiosensitization ability, and realized the effective treatment for deep tumor with minimal side effects upon low-dose laser and X-rays (Luo et al., 2020). Guo et al. constructed bovine serum albumin (BSA)-encapsulated $BiOI@Bi_2S_3$ semiconductor heterojunction nanoparticles, in which bismuth and iodine were used as radiotherapy sensitizers due to the strong X-ray attenuation ability, and the electron-hole pairs and heterojunction structure in semiconductors can promote the generation of ROS through the photodynamic therapy process. Besides, bismuth sulfide was used as a photothermal agent to kill hypoxic cells insensitive to radiotherapy, improved the hypoxic environment of tumors and achieved a synergistic tumor-inhibiting effect superior to monotherapy (Guo et al., 2017).

Radiotherapy/Phototherapy Combined With Immunotherapy

Currently, immunotherapy has received a lot of attention and showed a gratifying rapid development. However, the therapeutic effect is unsatisfactory in the treatment of "cold tumors" (Bonaventura et al., 2019). "Hot tumors" and "cold tumors" refer to tumors with or without lymphocytes infiltration and inflammation respectively. Cold tumors greatly limit the effectiveness of tumor immunotherapy, especially the application of immune checkpoint inhibitors (Galon and Bruni, 2019). In recent years, it has been discovered that tumor therapies such as radiotherapy, chemotherapy or phototherapy can stimulate the immune system by inducing immunogenic cell death to release tumor-related antigens and damage-related molecular patterns, recruit lymphocytes and enhance T cell infiltration by destroying tumor microenvironment and turn cold tumors into hot tumors, which facilitates the induction of stronger T cell immune responses to attack tumors cells and inhibit tumor metastasis and recurrence (Bonaventura et al., 2019; Galon and Bruni, 2019). Therefore, the combination of multiple tumor therapies is considered a promising strategy to achieve synergistic anti-tumor effects and nanomaterial-based strategies have been proven to achieve remarkable therapeutic outcomes (**Table 1**).

Studies have shown that combining radiotherapy enhancement methods with immune adjuvants or immune checkpoint inhibitors can obtain ideal anti-tumor effects (Ni et al., 2019; Patel et al., 2019). Chen et al. prepared a PLGA nanoparticle (PLGA-R837@Cat) that co-loaded catalase and

Toll-like receptor-7 agonist (R837), which can effectively decompose H_2O_2 and increase the oxygen in the tumor to enhance efficacy of radiotherapy. Radiotherapy based on PLGA-R837@Cat induced the immunogenic death of tumor cells and triggered a stronger tumor immune response with the assistance of R837. Furthermore, the results proved that the combination therapy with anti-CTLA-4 antibody can effectively inhibit the growth of distant tumors (Chen et al., 2019). Huang et al. synthesized the triangular star tellurium nanomaterials and modified RGD polypeptide to target the tumor, which increased the accumulation of ROS and the efficacy of radiotherapy. Combined treatment with anti-PD-1 enhanced the infiltration of cytotoxic T lymphocytes in tumor tissues, promoted the polarization of protumorigenic M2 phenotype macrophages to tumoricidal M1 phenotype macrophages, and the proportion of M2 phenotype macrophages decreased from 24.46 to 4.66%, effectively inhibiting the growth of distal tumors (Huang et al., 2020).

Phototherapy combined with immunotherapy is also considered to be a promising strategy (Chen et al., 2021; Feng et al., 2021). The application of nanomaterials with high light-to-heat conversion efficiency in combination with immune adjuvants or immune checkpoint inhibitors has shown excellent tumor treatment effects (Ming et al., 2020; Fang et al., 2021). Ming et al. utilized the photothermal material Pd nanosheets to deliver CpG ODNs, which effectively inhibited tumors under NIR irradiation. The levels of TNF-α and IL-6 were significantly increased, and a strong CTL response was induced, which greatly improved the survival rate of tumor-bearing mice (Ming et al., 2020). Fang et al. designed a two-dimensional material $FePSe_3$ wrapped in colon CT26 membrane, loaded with anti-PD-1 polypeptides, which showed significant accumulation at the tumor site, promoted the maturation of dendritic cells and the activation of T cells, remarkably prolonged the survival period of mice under the irradiation of infrared laser (Fang et al., 2021).

As for photodynamic therapy combined immunotherapy, Meng et al. prepared a light-triggered *in situ* gelation system for tumor treatment: modified catalase with photosensitizer Ce6 and mixed with polymeric matrix polyethylene glycol diacrylate, and R837 was added as an immune adjuvant. After injection into the tumor, it was irradiated with 660 nm light to form an *in-situ* hydrogel for multiple rounds of photodynamic therapy. In combination with CTLA-4 inhibitors, it further inhibited the growth of distant tumors, and also provided effective long-term immune memory protection to avoid tumor recurrence (Meng et al., 2019). Wang et al. designed pH-sensitive nanoparticles through the reaction of dextran and hyaluronidase, which can rapidly degrade hyaluronic acid in the extracellular matrix by releasing hyaluronidase in the acidic microenvironment of the tumor, thereby alleviating the hypoxic environment. It was proved that the nanoparticles can improve the efficacy of subsequent photodynamic therapy of Ce6@liposome and further enhance the infiltration of CTLs in tumor tissues after combining with anti-PD-L1, showing a significantly stronger anti-tumor effect and effectively inhibiting the growth of distant tumors. (Wang et al., 2019b). Shao et al. prepared a core-shell nanostructure formed by porphyrinic MOFs and UCNPs. Besides, a hypoxia-activated prodrug tilapazamin was loaded to achieve an excellent synergistic therapeutic effect on CT26 tumor-bearing mice (Shao et al., 2020).

Given that photothermal and photodynamic therapy have a great synergistic effect, its further combination with immunotherapy has also obtained ideal results. Yan et al. prepared NaGdF4: Yb/Er upconversion layer-coated polydopamine (PDA) nanoparticles, and modified the photosensitizer Ce6 to maximize the synergistic effect of phototherapy under 980 nm laser irradiation. Higher concentrations of cytokines such as IL-6 and TNF-α and lower level of IL-10 were induced, which proved the activation of a stronger immune response and the reduction of M2 suppressive macrophages, respectively. When combined with anti-PD-1 treatment, the survival rate of mice reached up to 77.8%, significantly higher than the group without PD-1 blockade antibody. Besides, the activation of CTLs and T memory cells can inhibit tumor metastasis and recurrence effectively (Yan et al., 2019). Jin et al. constructed a corn-like Au/Ag nanorod irradiated with a 1,064 nm laser to induce ICD of tumor cells. Combined with anti-CTLA-4 treatment can induce a strong immune memory effect, which was an effective method to reverse the immunosuppressive cold tumor microenvironment and prevent the tumor from recurring (Jin et al., 2021).

OTHER TUMOR THERAPIES BASED ON NANOMATERIALS

Sonodynamic Therapy

Sonodynamic therapy uses ultrasound to focus acoustic energy on tumor tissue, activating sonosensitizers to generate ROS and trigger anti-tumor effects. Various nanocarriers have been constructed to deliver small molecule sonosensitizers such as porphyrin, hematoporphyrin monomethyl ether, and rose bengal to enhance the accumulation at tumor sites (Liang et al., 2020a). Besides, inorganic sonosensitizers are favored due to the better physicochemical properties. TiO_2 is a traditional sonosensitizer and its modification has always been the focus of research (Çeşmeli and Biray Avci, 2019). The combination of modified TiO_2 and noble metals can effectively prevent the recombination of electrons and holes generated by ultrasound excitation. ROS generation efficiency of Au-TiO_2 nanosheets is significantly higher than that of TiO_2 itself (Cao et al., 2019). In addition, the combination of BP and Au was also found to improve the efficiency of sonodynamic therapy, inhibiting tumor growth with less side effects (Ouyang et al., 2018).

Ultrasound poses stronger penetration ability through biological tissues to achieve better therapeutic effect on deep tumors, which can effectively overcome the limitation of insufficient tissue penetration of phototherapy. Besides, some sonosensitizers or nanomaterials can be activated by ultrasound and laser at the same time, so as to achieve synergistic therapeutic effect, which is a novel therapeutic strategy to provide a promising solution for the treatment of deep-seated tumors (Liang et al., 2020b). Liang et al. synthesized a complex

composed of CuS and Pt, and the hollow cavity of CuS could be loaded with the sonosensitizer tetra (4-aminophenyl) porphyrin. Furthermore, the deposition of Pt enhanced the photothermal performance and catalyzed the generation of O_2 from H_2O_2 to accumulate sufficient ROS and induce tumor cell apoptosis. Besides, the heat generated by the laser can accelerate the catalytic activity of Pt and increase the oxygen level, which can further promote sonodynamic therapy efficacy and achieve synergistic tumor killing effect (Liang et al., 2019). In addition, sonodynamic therapy can also induce the release of damage-related molecular pattern molecules and trigger anti-tumor immune responses. Yue et al. prepared a liposome containing sonosensitizer hematoporphyrin monomethyl ether and immune adjuvant R837, which elicited strong anti-tumor immune responses, and the combination with anti-PD-L1 checkpoint blocker induced a potent memory immune response (Yue et al., 2019).

Chemodynamic Therapy

Chemodynamic therapy is to activate the Fenton/Fenton-like reaction in the tumor microenvironment to generate ROS and kill tumor cells. Chemodynamic therapy can also generate O_2 at tumor sites without tissue depth limitations (Xin et al., 2021). Nanomaterials with high catalytic efficiency and excellent biocompatibility have been applied in chemodynamic therapy, including iron-based nanomaterials, other metal-based nanomaterials such as manganese (Ding et al., 2020) and molybdenum (Dhas et al., 2021), and some organic nanomaterials such as MOF (Zhang S. et al, 2020). Copper-based nanomaterials have received extensive attention in recent years due to the low cost and easy availability (Ai et al., 2021). Cu-MOF nanoparticles can be rapidly degraded after exposure to the tumor microenvironment, release Cu^{2+} to deplete glutathione and generate highly cytotoxic •OH to enhance the chemodynamic therapy effect (Zhang K. et al, 2020). Similarly, Ma et al. designed a Zn^{2+}/Cu^{2+} co-doped MOF loaded with cisplatin and achieved excellent tumor inhibitory effect (Ma et al., 2021). The combination of chemodynamic therapy and other therapies has been found to obtain a synergistic effect, and the generated ROS and O_2 can effectively overcome tumor hypoxia and enhance the efficacy of radiotherapy and photodynamic therapy (Liu S. et al, 2020). In addition, chemodynamic therapy combined with photothermal therapy has great potential to improve the therapeutic performance: the temperature increase induced by photothermal therapy promotes the production of ROS, which in turn enhances tumor cell sensitization, thus achieving a stronger anti-tumor effect (Zhang S. et al, 2020). Studies have also shown that further combination of checkpoint blockade therapy can successfully inhibit distant tumor growth and cancer metastasis (Hu et al., 2020).

Nano-Based Delivery of RNA Interference Therapeutics

RNA interference (RNAi) is an important gene expression regulation method, which is a gene silencing process induced by endogenous or artificially transfected small interfering double-stranded RNA (Xin et al., 2017). A major challenge for RNAi therapeutics is the construction of efficient vectors, and various cationic polymer nanoparticles and lipid-based carriers have been applied for RNAi delivery (Xin et al., 2017). More effective delivery systems are needed to specifically target tumors according to the tumor microenvironment. Gold nanoclusters are favored due to the unique ultra-small size, which can increase the aggregation of nerve growth factor small interfering RNA (NGF siRNA) at tumor sites, and effectively interfere with the NGF gene to inhibit tumor development (Lei et al., 2017). Xu et al. synthesized a pH-responsive siRNA nanoparticle, which was modified with polyethylene glycol to attain long-circulating effect, and could rapidly release siRNA in the tumor microenvironment, thereby leading to effective gene silencing and significantly inhibiting the growth of prostate cancer (Xu et al., 2017). In addition, the development of multifunctional nanocarriers and combination therapies can achieve better therapeutic effects. Liu et al. synthesized a siRNA-loaded amorphous iron oxide nanoparticle, which can inhibit the up-regulation of monocarboxylic acid transporter in tumor cells to induce cellular acidosis, and catalyze H_2O_2 to generate ROS through Fenton-like reaction, thereby killing tumor cells and inhibiting tumor growth (Liu Y. et al, 2018).

CONCLUSION AND PROSPECT

Here we reviewed the progress of nanomaterials used in radiotherapy, phototherapy, immunotherapy and some other therapies such as sonodynamic therapy, chemodynamic therapy and RNAi therapeutics in the past 5 years, listed some creative designs of nanocarriers and summarized the major development direction of tumor combination therapies. The application of nanomaterials has been a promising strategy in both traditional and emerging therapies, and a variety of suitable nanomaterial-based carriers with specific properties have been gradually developed to effectively accumulate at the tumor site and overcome the adverse tumor microenvironment, which have shown great potential for improving the efficiency of tumor treatment. Recent studies have been focused on the development of the combination of multiple therapies in order to maximize the therapeutic effect. The combination of radiotherapy and phototherapy can effectively combat deep-seated tumors with minimal side effects, and the oxygen perfusion lead by photothermal therapy is conducive to oxygen-dependent therapies such as radiotherapy and photodynamic therapy. In addition, various therapies have been proved to activate the immune response to a certain extent in the process of tumor treatment. Therefore, combining immunotherapy can synergistically strengthen the therapeutic outcome and dramatically prevent tumor metastasis and recurrence.

Despite satisfactory progress in the development and application of nanomaterials, some challenges remain to be addressed. The clinical translation of nanomaterials is the most critical issue for tumor treatment, so the materials

should possess excellent biocompatibility and biodegradability, and FDA-approved materials ought to be prioritized for consideration. Similarly, the scale-up process from the laboratory to the clinic usually requires optimization or changes of the preparation method, so the efforts should be made to establish nanocarriers that facilitate the scale-up production while ensuring the effectiveness of tumor treatment. Besides, the toxicity and safety of nanomaterials are still pressing issues, and research should give more consideration to the long-term and potential toxicity of nanomaterials. In addition, it is of great importance to develop nanomaterials with specific physicochemical properties to meet the needs of different tumor therapies. Currently combination therapy is favored due to its synergistic anti-tumor efficacy, accordingly, nanomaterials with multiple functional properties are gradually developed to simplify the design of the carriers and achieve better therapeutic effect. It is vital to explore multifunctional nanomaterials to trigger multiple therapeutic effects in further research. The complexity of the tumor microenvironment presents a great challenge for the design of nanocarriers. With the continuous deepening of current research, the relationship between tumor therapies and its further mechanism has gradually become clear. According to the actual tumor conditions, suitable carriers can be designed to reverse unfavorable microenvironment to enhance the therapeutic outcome through monotherapies or combination therapies. The development of nanomaterials with suitable properties and biosafety to achieve remarkable therapeutic effect is the vital topic for tumor treatment in the future.

AUTHOR CONTRIBUTIONS

XH: wrote the manuscript and drew the drawings. JW and DX: read and improved the scientific quality. YY: read and improved the scientific quality; supervision and correction of the manuscript. All authors contributed to the article and approved the submitted version.

REFERENCES

Abbasi, A. Z., Gordijo, C. R., Amini, M. A., Maeda, A., Rauth, A. M., DaCosta, R. S., et al. (2016). Hybrid Manganese Dioxide Nanoparticles Potentiate Radiation Therapy by Modulating Tumor Hypoxia. *Cancer Res.* 76, 6643–6656. doi:10.1158/0008-5472.CAN-15-3475

Ahmad, F., Wang, X., Jiang, Z., Yu, X., Liu, X., Mao, R., et al. (2019). Codoping Enhanced Radioluminescence of Nanoscintillators for X-ray-Activated Synergistic Cancer Therapy and Prognosis Using Metabolomics. *ACS Nano* 13, 10419–10433. doi:10.1021/acsnano.9b04213

Ai, K., Huang, J., Xiao, Z., Yang, Y., Bai, Y., and Peng, J. (2021). Localized Surface Plasmon Resonance Properties and Biomedical Applications of Copper Selenide Nanomaterials. *Mater. Today Chem.* 20, 100402. doi:10.1016/j.mtchem.2020.100402

Aikins, M. E., Xu, C., and Moon, J. J. (2020). Engineered Nanoparticles for Cancer Vaccination and Immunotherapy. *Acc. Chem. Res.* 53, 2094–2105. doi:10.1021/acs.accounts.0c00456

Bonaventura, P., Shekarian, T., Alcazer, V., Valladeau-Guilemond, J., Valsesia-Wittmann, S., Amigorena, S., et al. (2019). Cold Tumors: A Therapeutic Challenge for Immunotherapy. *Front. Immunol.* 10, 168. doi:10.3389/fimmu.2019.00168

Cai, R., Xiang, H., Yang, D., Lin, K. T., Wu, Y., Zhou, R., et al. (2021). Plasmonic AuPt@CuS Heterostructure with Enhanced Synergistic Efficacy for Radiophotothermal Therapy. *J. Am. Chem. Soc.* 143, 16113–16127. doi:10.1021/jacs.1c06652

Cao, Y., Wu, T., Dai, W., Dong, H., and Zhang, X. (2019). TiO2 Nanosheets with the Au Nanocrystal-Decorated Edge for Mitochondria-Targeting Enhanced Sonodynamic Therapy. *Chem. Mater.* 31, 9105–9114. doi:10.1021/acs.chemmater.9b03430

Çeşmeli, S., and Biray Avci, C. (2019). Application of Titanium Dioxide (TiO2) Nanoparticles in Cancer Therapies. *J. Drug Target.* 27, 762–766. doi:10.1080/1061186X.2018.1527338

Chen, C., Song, M., Du, Y., Yu, Y., Li, C., Han, Y., et al. (2021). Tumor-Associated-Macrophage-Membrane-Coated Nanoparticles for Improved Photodynamic Immunotherapy. *Nano Lett.* 21, 5522–5531. doi:10.1021/acs.nanolett.1c00818

Chen, Q., Chen, J., Yang, Z., Xu, J., Xu, L., Liang, C., et al. (2019). Nanoparticle-Enhanced Radiotherapy to Trigger Robust Cancer Immunotherapy. *Adv. Mater.* 31, e1802228. doi:10.1002/adma.201802228

Chen, Q., Wang, C., Chen, G., Hu, Q., and Gu, Z. (2018). Delivery Strategies for Immune Checkpoint Blockade. *Adv. Healthc. Mater.* 7, e1800424. doi:10.1002/adhm.201800424

Chen, Y. W., Su, Y. L., Hu, S. H., and Chen, S. Y. (2016). Functionalized Graphene Nanocomposites for Enhancing Photothermal Therapy in Tumor Treatment. *Adv. Drug Deliv. Rev.* 105, 190–204. doi:10.1016/j.addr.2016.05.022

Cheng, Y., Kong, X., Chang, Y., Feng, Y., Zheng, R., Wu, X., et al. (2020). Spatiotemporally Synchronous Oxygen Self-Supply and Reactive Oxygen Species Production on Z-Scheme Heterostructures for Hypoxic Tumor Therapy. *Adv. Mater.* 32, e1908109. doi:10.1002/adma.201908109

Dhas, N., Kudarha, R., Garkal, A., Ghate, V., Sharma, S., Panzade, P., et al. (2021). Molybdenum-based Hetero-Nanocomposites for Cancer Therapy, Diagnosis and Biosensing Application: Current Advancement and Future Breakthroughs. *J. Control. Release* 330, 257–283. doi:10.1016/j.jconrel.2020.12.015

Ding, B., Zheng, P., Ma, P., and Lin, J. (2020). Manganese Oxide Nanomaterials: Synthesis, Properties, and Theranostic Applications. *Adv. Mater.* 32, e1905823. doi:10.1002/adma.201905823

Dong, C. Y., Hong, S., Zheng, D. W., Huang, Q. X., Liu, F. S., Zhong, Z. L., et al. (2021). Multifunctionalized Gold Sub-nanometer Particles for Sensitizing Radiotherapy against Glioblastoma. *Small* 17, e2006582. doi:10.1002/smll.202006582

Dong, W., Cai, Z., Pang, J., Wang, J., Tang, N., Zhang, W., et al. (2020). Radiotherapy Enhancement for Human Pancreatic Carcinoma Using a Peptide-Gold Nanoparticle Hybrid. *J. Biomed. Nanotechnol* 16, 352–363. doi:10.1166/jbn.2020.2898

Du, G., and Sun, X. (2020). Engineering Nanoparticulate Vaccines for Enhancing Antigen Cross-Presentation. *Curr. Opin. Biotechnol.* 66, 113–122. doi:10.1016/j.copbio.2020.06.015

Du, Y., Sun, H., Lux, F., Xie, Y., Du, L., Xu, C., et al. (2020). Radiosensitization Effect of AGuIX, a Gadolinium-Based Nanoparticle, in Nonsmall Cell Lung Cancer. *ACS Appl. Mater. Inter.* 12, 56874–56885. doi:10.1021/acsami.0c16548

Duan, F., Feng, X., Yang, X., Sun, W., Jin, Y., Liu, H., et al. (2017). A Simple and Powerful Co-delivery System Based on pH-Responsive Metal-Organic Frameworks for Enhanced Cancer Immunotherapy. *Biomaterials* 122, 23–33. doi:10.1016/j.biomaterials.2017.01.017

Fang, X., Wu, X., Li, Z., Jiang, L., Lo, W. S., Chen, G., et al. (2021). Biomimetic Anti-PD-1 Peptide-Loaded 2D FePSe3 Nanosheets for Efficient Photothermal and Enhanced Immune Therapy with Multimodal MR/PA/Thermal Imaging. *Adv. Sci. (Weinh)* 8, 2003041. doi:10.1002/advs.202003041

Feng, Y., Xie, X., Zhang, H., Su, Q., Yang, G., Wei, X., et al. (2021). Multistage-responsive Nanovehicle to Improve Tumor Penetration for Dual-Modality

Imaging-Guided Photodynamic-Immunotherapy. *Biomaterials* 275, 120990. doi:10.1016/j.biomaterials.2021.120990

Galon, J., and Bruni, D. (2019). Approaches to Treat Immune Hot, Altered and Cold Tumours with Combination Immunotherapies. *Nat. Rev. Drug Discov.* 18, 197–218. doi:10.1038/s41573-018-0007-y

Geng, B., Shen, W., Li, P., Fang, F., Qin, H., Li, X. K., et al. (2019). Carbon Dot-Passivated Black Phosphorus Nanosheet Hybrids for Synergistic Cancer Therapy in the NIR-II Window. *ACS Appl. Mater. Inter.* 11, 44949–44960. doi:10.1021/acsami.9b15569

Guan, Q., Zhou, L. L., Li, Y. A., Li, W. Y., Wang, S., Song, C., et al. (2019). Nanoscale Covalent Organic Framework for Combinatorial Antitumor Photodynamic and Photothermal Therapy. *ACS Nano* 13, 13304–13316. doi:10.1021/acsnano.9b06467

Guo, Z., Zhu, S., Yong, Y., Zhang, X., Dong, X., Du, J., et al. (2017). Synthesis of BSA-Coated BiOI@Bi2 S3 Semiconductor Heterojunction Nanoparticles and Their Applications for Radio/Photodynamic/Photothermal Synergistic Therapy of Tumor. *Adv. Mater.* 29. doi:10.1002/adma.201704136

He, W., Ai, K., and Lu, L. (2015). Nanoparticulate X-ray CT Contrast Agents. *Sci. China Chem.* 58, 753–760. doi:10.1007/s11426-015-5351-8

Hou, X., Tao, Y., Pang, Y., Li, X., Jiang, G., and Liu, Y. (2018). Nanoparticle-based Photothermal and Photodynamic Immunotherapy for Tumor Treatment. *Int. J. Cancer* 143, 3050–3060. doi:10.1002/ijc.31717

Hu, C., Cai, L., Liu, S., Liu, Y., Zhou, Y., and Pang, M. (2020). Copper-Doped Nanoscale Covalent Organic Polymer for Augmented Photo/Chemodynamic Synergistic Therapy and Immunotherapy. *Bioconjug. Chem.* 31, 1661–1670. doi:10.1021/acs.bioconjchem.0c00209

Huang, Q., Zhang, S., Zhang, H., Han, Y., Liu, H., Ren, F., et al. (2019). Boosting the Radiosensitizing and Photothermal Performance of Cu2- xSe Nanocrystals for Synergetic Radiophotothermal Therapy of Orthotopic Breast Cancer. *ACS Nano* 13, 1342–1353. doi:10.1021/acsnano.8b06795

Huang, W., He, L., Ouyang, J., Chen, Q., Liu, C., Tao, W., et al. (2020). Triangle-shaped Tellurium Nanostars Potentiate Radiotherapy by Boosting Checkpoint Blockade Immunotherapy. *Matter* 3, 1725–1753. doi:10.1016/j.matt.2020.08.027

Jarosz-Biej, M., Smolarczyk, R., Cichoń, T., and Kułach, N. (2019). Tumor Microenvironment as A "Game Changer" in Cancer Radiotherapy. *Int. J. Mol. Sci.* 20. doi:10.3390/ijms20133212

Jin, L., Shen, S., Huang, Y., Li, D., and Yang, X. (2021). Corn-like Au/Ag Nanorod-Mediated NIR-II Photothermal/photodynamic Therapy Potentiates Immune Checkpoint Antibody Efficacy by Reprogramming the Cold Tumor Microenvironment. *Biomaterials* 268, 120582. doi:10.1016/j.biomaterials.2020.120582

Jun, S. W., Manivasagan, P., Kwon, J., Nguyen, V. T., Mondal, S., Ly, C. D., et al. (2020). Folic Acid-Conjugated Chitosan-Functionalized Graphene Oxide for Highly Efficient Photoacoustic Imaging-Guided Tumor-Targeted Photothermal Therapy. *Int. J. Biol. Macromol* 155, 961–971. doi:10.1016/j.ijbiomac.2019.11.055

Kano, A., Taniwaki, Y., Nakamura, I., Shimada, N., Moriyama, K., and Maruyama, A. (2013). Tumor Delivery of Photofrin® by PLL-G-PEG for Photodynamic Therapy. *J. Control. Release* 167, 315–321. doi:10.1016/j.jconrel.2013.02.016

Kaur, P., and Asea, A. (2012). Radiation-induced Effects and the Immune System in Cancer. *Front. Oncol.* 2, 191. doi:10.3389/fonc.2012.00191

Kim, Y., Kang, S., Shin, H., Kim, T., Yu, B., Kim, J., et al. (2020). Sequential and Timely Combination of a Cancer Nanovaccine with Immune Checkpoint Blockade Effectively Inhibits Tumor Growth and Relapse. *Angew. Chem. Int. Ed. Engl.* 59, 14628–14638. doi:10.1002/anie.202006117

Kuai, R., Ochyl, L. J., Bahjat, K. S., Schwendeman, A., and Moon, J. J. (2017). Designer Vaccine Nanodiscs for Personalized Cancer Immunotherapy. *Nat. Mater.* 16, 489–496. doi:10.1038/nmat4822

Lan, G., Ni, K., Veroneau, S. S., Luo, T., You, E., and Lin, W. (2019). Nanoscale Metal-Organic Framework Hierarchically Combines High-Z Components for Multifarious Radio-Enhancement. *J. Am. Chem. Soc.* 141, 6859–6863. doi:10.1021/jacs.9b03029

Lei, Y., Tang, L., Xie, Y., Xianyu, Y., Zhang, L., Wang, P., et al. (2017). Gold Nanoclusters-Assisted Delivery of NGF siRNA for Effective Treatment of Pancreatic Cancer. *Nat. Commun.* 8, 15130. doi:10.1038/ncomms15130

Li, H., Li, Y., Wang, X., Hou, Y., Hong, X., Gong, T., et al. (2017a). Rational Design of Polymeric Hybrid Micelles to Overcome Lymphatic and Intracellular Delivery Barriers in Cancer Immunotherapy. *Theranostics* 7, 4383–4398. doi:10.7150/thno.20745

Li, M., Li, Y., Peng, K., Wang, Y., Gong, T., Zhang, Z., et al. (2017b). Engineering Intranasal mRNA Vaccines to Enhance Lymph Node Trafficking and Immune Responses. *Acta Biomater.* 64, 237–248. doi:10.1016/j.actbio.2017.10.019

Li, X., Lovell, J. F., Yoon, J., and Chen, X. (2020). Clinical Development and Potential of Photothermal and Photodynamic Therapies for Cancer. *Nat. Rev. Clin. Oncol.* 17, 657–674. doi:10.1038/s41571-020-0410-2

Li, Y., Yun, K. H., Lee, H., Goh, S. H., Suh, Y. G., and Choi, Y. (2019). Porous Platinum Nanoparticles as a High-Z and Oxygen Generating Nanozyme for Enhanced Radiotherapy *In Vivo*. *Biomaterials* 197, 12–19. doi:10.1016/j.biomaterials.2019.01.004

Liang, S., Deng, X., Chang, Y., Sun, C., Shao, S., Xie, Z., et al. (2019). Intelligent Hollow Pt-CuS Janus Architecture for Synergistic Catalysis-Enhanced Sonodynamic and Photothermal Cancer Therapy. *Nano Lett.* 19, 4134–4145. doi:10.1021/acs.nanolett.9b01595

Liang, S., Deng, X., Ma, P., Cheng, Z., and Lin, J. (2020b). Recent Advances in Nanomaterial-Assisted Combinational Sonodynamic Cancer Therapy. *Adv. Mater.* 32, e2003214. doi:10.1002/adma.202003214

Liang, S., Sun, C., Yang, P., Ma, P., Huang, S., Cheng, Z., et al. (2020a). Core-shell Structured Upconversion Nanocrystal-Dendrimer Composite as a Carrier for Mitochondria Targeting and Catalase Enhanced Anti-cancer Photodynamic Therapy. *Biomaterials* 240, 119850. doi:10.1016/j.biomaterials.2020.119850

Liu, C., Cao, Y., Cheng, Y., Wang, D., Xu, T., Su, L., et al. (2020c). An Open Source and Reduce Expenditure ROS Generation Strategy for Chemodynamic/photodynamic Synergistic Therapy. *Nat. Commun.* 11, 1735. doi:10.1038/s41467-020-15591-4

Liu, C., Liu, B., Zhao, J., Di, Z., Chen, D., Gu, Z., et al. (2020b). Nd3+ -Sensitized Upconversion Metal-Organic Frameworks for Mitochondria-Targeted Amplified Photodynamic Therapy. *Angew. Chem. Int. Ed. Engl.* 59, 2634–2638. doi:10.1002/anie.201911508

Liu, S., Pan, X., and Liu, H. (2020a). Two-Dimensional Nanomaterials for Photothermal Therapy. *Angew. Chem. Int. Ed. Engl.* 59, 5890–5900. doi:10.1002/anie.201911477

Liu, Y., Ji, X., Tong, W. W. L., Askhatova, D., Yang, T., Cheng, H., et al. (2018b). Engineering Multifunctional RNAi Nanomedicine to Concurrently Target Cancer Hallmarks for Combinatorial Therapy. *Angew. Chem. Int. Ed. Engl.* 57, 1510–1513. doi:10.1002/anie.201710144

Liu, Z., Tan, H., Zhang, X., Chen, F., Zhou, Z., Hu, X., et al. (2018a). Enhancement of Radiotherapy Efficacy by Silver Nanoparticles in Hypoxic Glioma Cells. *Artif. Cell Nanomed Biotechnol* 46, S922–S30. doi:10.1080/21691401.2018.1518912

Luo, L., Sun, W., Feng, Y., Qin, R., Zhang, J., Ding, D., et al. (2020). Conjugation of a Scintillator Complex and Gold Nanorods for Dual-Modal Image-Guided Photothermal and X-ray-Induced Photodynamic Therapy of Tumors. *ACS Appl. Mater. Inter.* 12, 12591–12599. doi:10.1021/acsami.0c01189

Lv, S., Miao, Y., Liu, D., and Song, F. (2020). Recent Development of Photothermal Agents (PTAs) Based on Small Organic Molecular Dyes. *Chembiochem* 21, 2098–2110. doi:10.1002/cbic.202000089

Ma, Y., Su, Z., Zhou, L., He, L., Hou, Z., Zou, J., et al. (2021). Biodegradable Metal-Organic Framework-Gated Organosilica for Tumor Microenvironment-Unlocked Glutathione Depletion-Enhanced Synergistic Therapy. *Adv. Mater.*, 2107560. doi:10.1002/adma.202107560

Ma, Z., Zhang, Y., Zhang, J., Zhang, W., Foda, M. F., Dai, X., et al. (2020). Ultrasmall Peptide-Coated Platinum Nanoparticles for Precise NIR-II Photothermal Therapy by Mitochondrial Targeting. *ACS Appl. Mater. Inter.* 12, 39434–39443. doi:10.1021/acsami.0c11469

Meng, L., Cheng, Y., Tong, X., Gan, S., Ding, Y., Zhang, Y., et al. (2018). Tumor Oxygenation and Hypoxia Inducible Factor-1 Functional Inhibition via a Reactive Oxygen Species Responsive Nanoplatform for Enhancing Radiation Therapy and Abscopal Effects. *ACS Nano* 12, 8308–8322. doi:10.1021/acsnano.8b03590

Meng, Z., Zhou, X., Xu, J., Han, X., Dong, Z., Wang, H., et al. (2019). Light-Triggered *In Situ* Gelation to Enable Robust Photodynamic-Immunotherapy by

Repeated Stimulations. *Adv. Mater.* 31, e1900927. doi:10.1002/adma.201900927

Ming, J., Zhang, J., Shi, Y., Yang, W., Li, J., Sun, D., et al. (2020). A Trustworthy CpG Nanoplatform for Highly Safe and Efficient Cancer Photothermal Combined Immunotherapy. *Nanoscale* 12, 3916–3930. doi:10.1039/c9nr09402d

Ni, K., Lan, G., Chan, C., Duan, X., Guo, N., Veroneau, S. S., et al. (2019). Ultrathin Metal-Organic Layer-Mediated Radiotherapy-Radiodynamic Therapy Enhances Immunotherapy of Metastatic Cancers. *Matter* 1, 1331–1353. doi:10.1016/j.matt.2019.06.007

Ouyang, J., Deng, L., Chen, W., Sheng, J., Liu, Z., Wang, L., et al. (2018). Two Dimensional Semiconductors for Ultrasound-Mediated Cancer Therapy: the Case of Black Phosphorus Nanosheets. *Chem. Commun. (Camb)* 54, 2874–2877. doi:10.1039/c8cc00392k

Park, T., Lee, S., Amatya, R., Cheong, H., Moon, C., Kwak, H. D., et al. (2020). ICG-loaded PEGylated BSA-Silver Nanoparticles for Effective Photothermal Cancer Therapy. *Int. J. Nanomedicine* 15, 5459–5471. doi:10.2147/IJN.S255874

Patel, R. B., Ye, M., Carlson, P. M., Jaquish, A., Zangl, L., Ma, B., et al. (2019). Development of an *In Situ* Cancer Vaccine via Combinational Radiation and Bacterial-Membrane-Coated Nanoparticles. *Adv. Mater.* 31, e1902626. doi:10.1002/adma.201902626

Qiu, M., Wang, D., Huang, H., Yin, T., Bao, W., Zhang, B., et al. (2021). A Regioselectively Oxidized 2D Bi/BiOx Lateral Nano-Heterostructure for Hypoxic Photodynamic Therapy. *Adv. Mater.* 33, 2102562. doi:10.1002/adma.202102562

Riley, R. S., June, C. H., Langer, R., and Mitchell, M. J. (2019). Delivery Technologies for Cancer Immunotherapy. *Nat. Rev. Drug Discov.* 18, 175–196. doi:10.1038/s41573-018-0006-z

Ruan, H., Bu, L., Hu, Q., Cheng, H., Lu, W., and Gu, Z. (2019). Strategies of Combination Drug Delivery for Immune Checkpoint Blockades. *Adv. Healthc. Mater.* 8, e1801099. doi:10.1002/adhm.201801099

Shao, J., Xie, H., Huang, H., Li, Z., Sun, Z., Xu, Y., et al. (2016). Biodegradable Black Phosphorus-Based Nanospheres for *In Vivo* Photothermal Cancer Therapy. *Nat. Commun.* 7, 12967. doi:10.1038/ncomms12967

Shao, Y., Liu, B., Di, Z., Zhang, G., Sun, L. D., Li, L., et al. (2020). Engineering of Upconverted Metal-Organic Frameworks for Near-Infrared Light-Triggered Combinational Photodynamic/Chemo-/Immunotherapy against Hypoxic Tumors. *J. Am. Chem. Soc.* 142, 3939–3946. doi:10.1021/jacs.9b12788

Shi, T., Sun, W., Qin, R., Li, D., Feng, Y., Chen, L., et al. (2020). X-Ray-Induced Persistent Luminescence Promotes Ultrasensitive Imaging and Effective Inhibition of Orthotopic Hepatic Tumors. *Adv. Funct. Mater.* 30, 2001166. doi:10.1002/adfm.202001166

Siegel, R. L., Miller, K. D., Fidler-Benaoudia, M., Keegan, T. H., Hipp, H. S., and Jemal, A. (2020). Cancer Statistics for Adolescents and Young Adults, 2020. *CA Cancer J. Clin.* 70, 443–459. doi:10.3322/caac.21637

Song, G., Chen, Y., Liang, C., Yi, X., Liu, J., Sun, X., et al. (2016). Catalase-Loaded TaOx Nanoshells as Bio-Nanoreactors Combining High-Z Element and Enzyme Delivery for Enhancing Radiotherapy. *Adv. Mater.* 28, 7143–7148. doi:10.1002/adma.201602111

Song, W., Musetti, S. N., and Huang, L. (2017). Nanomaterials for Cancer Immunotherapy. *Biomaterials* 148, 16–30. doi:10.1016/j.biomaterials.2017.09.017

Sun, T., Zhang, Y. S., Pang, B., Hyun, D. C., Yang, M., and Xia, Y. (2014). Engineered Nanoparticles for Drug Delivery in Cancer Therapy. *Angew. Chem. Int. Ed. Engl.* 53, 12320–12364. doi:10.1002/anie.201403036

Sun, W., Luo, L., Feng, Y., Qiu, Y., Shi, C., Meng, S., et al. (2020). Gadolinium-Rose Bengal Coordination Polymer Nanodots for MR-/Fluorescence-Image-Guided Radiation and Photodynamic Therapy. *Adv. Mater.* 32, e2000377. doi:10.1002/adma.202000377

Sundaram, A., Peng, L., Chai, L., Xie, Z., Ponraj, J. S., Wang, X., et al. (2020). Advanced Nanomaterials for Hypoxia Tumor Therapy: Challenges and Solutions. *Nanoscale* 12, 21497–21518. doi:10.1039/d0nr06271e

Wang, H., Jiang, H., Van De Gucht, M., and De Ridder, M. (2019b). Hypoxic Radioresistance: Can ROS Be the Key to Overcome it? *Cancers (Basel)* 11. doi:10.3390/cancers11010112

Wang, H., Han, X., Dong, Z., Xu, J., Wang, J., and Liu, Z. (2019a). Hyaluronidase with pH-responsive Dextran Modification as an Adjuvant Nanomedicine for Enhanced Photodynamic-Immunotherapy of Cancer. *Adv. Funct. Mater.* 29, 1902440. doi:10.1002/adfm.201902440

Wang, X., Liu, H., Chen, D., Meng, X., Liu, T., Fu, C., et al. (2013). Multifunctional Fe3O4@P(St/MAA)@chitosan@Au Core/shell Nanoparticles for Dual Imaging and Photothermal Therapy. *ACS Appl. Mater. Inter.* 5, 4966–4971. doi:10.1021/am400721s

Xia, Y., Wu, J., Du, Y., Miao, C., Su, Z., and Ma, G. (2018). Bridging Systemic Immunity with Gastrointestinal Immune Responses via Oil-In-Polymer Capsules. *Adv. Mater.* 30, e1801067. doi:10.1002/adma.201801067

Xie, Z., Chen, S., Duo, Y., Zhu, Y., Fan, T., Zou, Q., et al. (2019). Biocompatible Two-Dimensional Titanium Nanosheets for Multimodal Imaging-Guided Cancer Theranostics. *ACS Appl. Mater. Inter.* 11, 22129–22140. doi:10.1021/acsami.9b04628

Xin, J., Deng, C., Aras, O., Zhou, M., Wu, C., and An, F. (2021). Chemodynamic Nanomaterials for Cancer Theranostics. *J. Nanobiotechnol* 19, 192. doi:10.1186/s12951-021-00936-y

Xin, Y., Huang, M., Guo, W. W., Huang, Q., Zhang, L. Z., and Jiang, G. (2017). Nano-based Delivery of RNAi in Cancer Therapy. *Mol. Cancer* 16, 134. doi:10.1186/s12943-017-0683-y

Xu, X., Saw, P. E., Tao, W., Li, Y., Ji, X., Yu, M., et al. (2017). Tumor Microenvironment-Responsive Multistaged Nanoplatform for Systemic RNAi and Cancer Therapy. *Nano Lett.* 17, 4427–4435. doi:10.1021/acs.nanolett.7b01571

Yan, S., Zeng, X., Tang, Y., Liu, B. F., Wang, Y., and Liu, X. (2019). Activating Antitumor Immunity and Antimetastatic Effect through Polydopamine-Encapsulated Core-Shell Upconversion Nanoparticles. *Adv. Mater.* 31, e1905825. doi:10.1002/adma.201905825

Yang, C., Zhu, Y., Li, D., Liu, Y., Guan, C., Man, X., et al. (2021). Red Phosphorus Decorated TiO 2 Nanorod Mediated Photodynamic and Photothermal Therapy for Renal Cell Carcinoma. *Small* 17, 2101837. doi:10.1002/smll.202101837

Yang, J., Teng, Y., Fu, Y., and Zhang, C. (2019). Chlorins e6 loaded silica nanoparticles coated with gastric cancer cell membrane for tumor specific photodynamic therapy of gastric cancer. *Int. J. Nanomedicine* 14, 5061–5071. doi:10.2147/IJN.S202910

Yang, Y. S., Carney, R. P., Stellacci, F., and Irvine, D. J. (2014). Enhancing Radiotherapy by Lipid Nanocapsule-Mediated Delivery of Amphiphilic Gold Nanoparticles to Intracellular Membranes. *ACS Nano* 8, 8992–9002. doi:10.1021/nn502146r

Yue, W., Chen, L., Yu, L., Zhou, B., Yin, H., Ren, W., et al. (2019). Checkpoint Blockade and Nanosonosensitizer-Augmented Noninvasive Sonodynamic Therapy Combination Reduces Tumour Growth and Metastases in Mice. *Nat. Commun.* 10, 2025. doi:10.1038/s41467-019-09760-3

Zeng, L., Cao, Y., He, L., Ding, S., Bian, X. W., and Tian, G. (2021). Metal-ligand Coordination Nanomaterials for Radiotherapy: Emerging Synergistic Cancer Therapy. *J. Mater. Chem. B* 9, 208–227. doi:10.1039/d0tb02294b

Zhang, K., Meng, X., Yang, Z., Dong, H., and Zhang, X. (2020b). Enhanced Cancer Therapy by Hypoxia-Responsive Copper Metal-Organic Frameworks Nanosystem. *Biomaterials* 258, 120278. doi:10.1016/j.biomaterials.2020.120278

Zhang, L., Wu, S., Qin, Y., Fan, F., Zhang, Z., Huang, C., et al. (2019). Targeted Codelivery of an Antigen and Dual Agonists by Hybrid Nanoparticles for Enhanced Cancer Immunotherapy. *Nano Lett.* 19, 4237–4249. doi:10.1021/acs.nanolett.9b00030

Zhang, S., Cao, C., Lv, X., Dai, H., Zhong, Z., Liang, C., et al. (2020a). A H2O2 Self-Sufficient Nanoplatform with Domino Effects for thermal-responsive Enhanced Chemodynamic Therapy. *Chem. Sci.* 11, 1926–1934. doi:10.1039/c9sc05506a

Zhang, Z., Wang, S., Xu, H., Wang, B., and Yao, C. (2015). Role of 5-aminolevulinic Acid-Conjugated Gold Nanoparticles for Photodynamic Therapy of Cancer. *J. Biomed. Opt.* 20, 51043. doi:10.1117/1.JBO.20.5.051043

Zheng, N., Zhang, S., Wang, L., Qi, Z., Peng, Q., Jian, L., et al. (2021). Boosting Image-Guiding Radiation Therapy through W18O49 Nanospheres and the Second Near-Infrared Light Irradiation. *Nano Res.* doi:10.1007/s12274-021-3814-0

Zhong, X., Wang, X., Zhan, G., Tang, Y., Yao, Y., Dong, Z., et al. (2019a). NaCeF4: Gd,Tb Scintillator as an X-ray Responsive Photosensitizer for Multimodal Imaging-Guided Synchronous Radio/Radiodynamic Therapy. *Nano Lett.* 19, 8234–8244. doi:10.1021/acs.nanolett.9b03682

Zhong, X., Zhang, Y., Tan, L., Zheng, T., Hou, Y., Hong, X., et al. (2019b). An Aluminum Adjuvant-Integrated Nano-MOF as Antigen Delivery System to Induce strong Humoral and Cellular Immune Responses. *J. Control. Release* 300, 81–92. doi:10.1016/j.jconrel.2019.02.035

Zhu, M., Ding, X., Zhao, R., Liu, X., Shen, H., Cai, C., et al. (2018). Co-delivery of Tumor Antigen and Dual Toll-like Receptor Ligands into Dendritic Cell by Silicon Microparticle Enables Efficient Immunotherapy against Melanoma. *J. Control. Release* 272, 72–82. doi:10.1016/j.jconrel.2018.01.004

Conflict of Interest: The authors declare that the research was conducted in the absence of any commercial or financial relationships that could be construed as a potential conflict of interest.

The reviewer (HDL) declared a past co-authorship with the author(s) (DX) to the handling editor.

Publisher's Note: All claims expressed in this article are solely those of the authors and do not necessarily represent those of their affiliated organizations, or those of the publisher, the editors, and the reviewers. Any product that may be evaluated in this article, or claim that may be made by its manufacturer, is not guaranteed or endorsed by the publisher.

Copyright © 2022 Hao, Wu, Xiang and Yang. This is an open-access article distributed under the terms of the Creative Commons Attribution License (CC BY). The use, distribution or reproduction in other forums is permitted, provided the original author(s) and the copyright owner(s) are credited and that the original publication in this journal is cited, in accordance with accepted academic practice. No use, distribution or reproduction is permitted which does not comply with these terms.

frontiers in Pharmacology

MINI REVIEW
published: 18 February 2022
doi: 10.3389/fphar.2022.844037

Emerging Bismuth Chalcogenides Based Nanodrugs for Cancer Radiotherapy

Jia Huang[1,2†], *Qiong Huang*[3,4†], *Min Liu*[3,4], *Qiaohui Chen*[1,2] *and Kelong Ai*[1,2*]

[1]Xiangya School of Pharmaceutical Sciences, Central South University, Changsha, China, [2]Hunan Provincial Key Laboratory of Cardiovascular Research, Xiangya School of Pharmaceutical Sciences, Central South University, Changsha, China, [3]Department of Pharmacy, Xiangya Hospital, Central South University, Changsha, China, [4]National Clinical Research Center for Geriatric Disorders, Xiangya Hospital, Central South University, Changsha, China

Radiotherapy (RT), as one of the main methods of clinical tumor treatment, has been applied to the treatment of most solid tumors. However, the effect of RT is compromised by the radiation resistance of tumor hypoxic environment and non-specific damage caused by high-dose radiation. Bismuth chalcogenides (Bi_2X_3, X = S, Se) based nanodrugs have attracted widespread attention as highly efficient radiosensitizers due to their high photoelectric effect and excellent biocompatibility. More importantly, specially designed nanocomposites can effectively alleviate the radiation resistance of tumor tissues. Here, for the first time, we systematically summarize the latest progresses of Bi_2X_3 nanodrugs to enhance RT by alleviating the hypoxic tumor microenvironment. These emerging Bi_2X_3 nanodrugs mainly include three aspects, which are Bi_2X_3 nanocomposites with high-efficient O_2 supply, non-O_2-dependent Bi_2X_3 nanocomposites RT enhancers, and Bi_2X_3 nanocomposites-based photothermal-enhanced radiosensitizers. These Bi_2X_3 nanodrugs can effectively overcome the RT resistance of tumor hypoxic microenvironment, and have extremely high therapeutic effects and clinical application prospects. Finally, we put forward the challenges and prospects of Bi_2X_3 nanomaterials in the field of RT.

Keywords: bismuth chalcogenides, nanomaterials, cancer radiotherapy, radiosensitizers, tumor hypoxia microenvironment

OPEN ACCESS

Edited by:
Christian Celia,
University of Studies G. d'Annunzio Chieti and Pescara, Italy

Reviewed by:
Xianwen Wang,
Anhui Medical University, China
Kai Yang,
Soochow University, China

***Correspondence:**
Kelong Ai
aikelong@csu.edu.cn

†These authors have contributed equally to this work

Specialty section:
This article was submitted to Pharmacology of Anti-Cancer Drugs, a section of the journal Frontiers in Pharmacology

Received: *27 December 2021*
Accepted: *28 January 2022*
Published: *18 February 2022*

Citation:
Huang J, Huang Q, Liu M, Chen Q and Ai K (2022) Emerging Bismuth Chalcogenides Based Nanodrugs for Cancer Radiotherapy. Front. Pharmacol. 13:844037. doi: 10.3389/fphar.2022.844037

INTRODUCTION

Radiotherapy (RT) has many advantages for cancer treatment compared with surgery or chemotherapy, like non-invasive, excellent targeting, and low cost (Begg et al., 2011). Currently, half of new cancers are treated with RT (Bentzen, 2006). RT adopts ionizing radiation (usually X-ray) to irradiate the tumor site through direct and indirect action to induce cancer cell death. Ionizing radiation can directly destroy DNA or protein by breaking the bonds in these molecules. More importantly, high-energy ionizing radiation can easily ionize and split H_2O to produce many reactive oxygen species (ROS) in tumor tissues (**Eq. 1**) (Le Caër, 2011). These ROS further cause the death of cancer cells by damaging DNA and proteins (Wu et al., 2019; Yao et al., 2021a). This indirect effect is the main tumor-killing effect of RT because the water content is the highest (generally 65%) in tumor tissues. However, there are two bottlenecks which greatly limit the effectiveness of RT. Firstly, a larger dose of X-rays is usually required to kill tumor cells because cancer tissues absorb X-rays very weakly, which also cause damage to normal tissues, especially the immune system (De Martino et al., 2021). Secondly, the hypoxic tumor microenvironment (TME) greatly

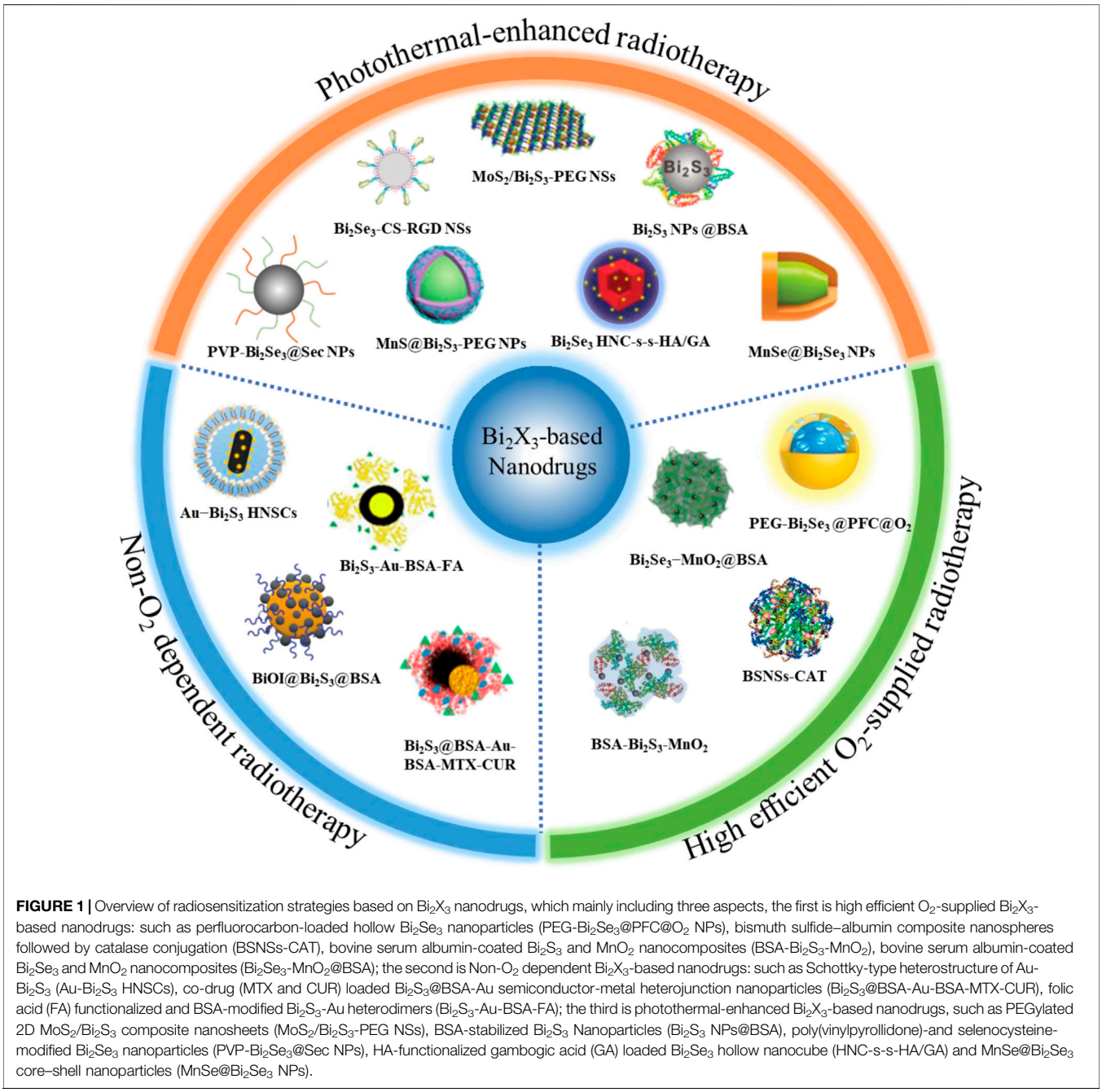


FIGURE 1 | Overview of radiosensitization strategies based on Bi_2X_3 nanodrugs, which mainly including three aspects, the first is high efficient O_2-supplied Bi_2X_3-based nanodrugs: such as perfluorocarbon-loaded hollow Bi_2Se_3 nanoparticles (PEG-Bi_2Se_3@PFC@O_2 NPs), bismuth sulfide–albumin composite nanospheres followed by catalase conjugation (BSNSs-CAT), bovine serum albumin-coated Bi_2S_3 and MnO_2 nanocomposites (BSA-Bi_2S_3-MnO_2), bovine serum albumin-coated Bi_2Se_3 and MnO_2 nanocomposites (Bi_2Se_3-MnO_2@BSA); the second is Non-O_2 dependent Bi_2X_3-based nanodrugs: such as Schottky-type heterostructure of Au-Bi_2S_3 (Au-Bi_2S_3 HNSCs), co-drug (MTX and CUR) loaded Bi_2S_3@BSA-Au semiconductor-metal heterojunction nanoparticles (Bi_2S_3@BSA-Au-BSA-MTX-CUR), folic acid (FA) functionalized and BSA-modified Bi_2S_3-Au heterodimers (Bi_2S_3-Au-BSA-FA); the third is photothermal-enhanced Bi_2X_3-based nanodrugs, such as PEGylated 2D MoS_2/Bi_2S_3 composite nanosheets (MoS_2/Bi_2S_3-PEG NSs), BSA-stabilized Bi_2S_3 Nanoparticles (Bi_2S_3 NPs@BSA), poly(vinylpyrollidone)-and selenocysteine-modified Bi_2Se_3 nanoparticles (PVP-Bi_2Se_3@Sec NPs), HA-functionalized gambogic acid (GA) loaded Bi_2Se_3 hollow nanocube (HNC-s-s-HA/GA) and MnSe@Bi_2Se_3 core–shell nanoparticles (MnSe@Bi_2Se_3 NPs).

reduces the effect of RT. O_2 is a very important RT sensitizer and is easy to accept a free electron to form superoxide radicals ($O_2^-\cdot$), which is then further converted into other highly oxidative active ROS (e.g. hydrogen peroxide and hydroxyl radicals) (Zhao et al., 2022; Zhu et al., 2022). Compared with normal cells, cancer cells are 3-times more resistant to RT-induced killing in a tumor hypoxia environment (Evans et al., 1997).

$$H_2O \xrightarrow{Ionizing\ Radiation} e^- + \cdot OH + H\cdot + HO_2\cdot + H_2O_2 + H_3O^+ + HO^- \quad (1)$$

Drugs containing high atomic number elements can be very effective in enhancing RT because they have a much higher X-ray absorption capacity than human tissues. Currently, many kinds of elements with high atomic number have been researched for radiosensitization, such as Au, Ta, W, Yb, Hf, and Bi (Tang et al., 2019; Xie et al., 2019; Zang et al., 2019; Peng et al., 2020; Liu et al., 2021; Xue et al., 2021). For example, NBTXR3 based on HfO_2 has been approved by the FDA to enter Phase III clinical studies, and demonstrated excellent RT effect for advanced soft-tissue sarcoma (Bonvalot et al., 2019). However, most of the high-Z elements are heavy metal elements with high toxicity, and their

TABLE 1 | The overview of emerging Bi_2X_3-based nanodrugs for RT.

Category	Nanomaterials	Advantages of nanomaterials	Ref
High efficient O_2-supplied radiotherapy	PEG-Bi_2Se_3@PFC@O_2 NPs	Efficient oxygen carrying capacity; powerful radiosensitization performance	Song et al. (2016)
	BSA-Bi_2S_3-CAT NSs	Effective tumor homing and tumor hypoxia relief	Zhang et al. (2018)
	Bi_2Se_3-MnO_2-BSA	Excellent CAT-like catalytic activity; high colloidal stability and biocompatibility	Yao et al. (2021b)
	BSA-Bi_2S_3-MnO_2	Remarkable radiotherapeutic enhancement effect; without obvious toxic and side effects	Zhang et al. (2019)
Non-O_2 dependent radiotherapy	Schottky-type heterostructure of Au-Bi_2S_3	Significant electron-hole separation efficiency, high-efficiency radiosensitization properties	Wang et al. (2019)
	Bi_2S_3@BSA-Au-BSA-MTX-CUR hybrid system	Efficient electron-hole separation efficiency and synergistic anti-tumor effects of radio-chemotherapy	Nosrati et al. (2022)
	Bi_2S_3-Au-BSA-FA hybrids	Effective radiosensitization and tumor targeting	Abhari et al. (2020)
Photothermal-enhanced radiotherapy	Bi_2S_3 nanorods	Remarkable radio-photothermal synergistic therapeutic effect	Cheng et al. (2017)
	BSA-capped Bi_2S_3 NPs	Ultra-small size; remarkable X-ray and photothermal response properties (η= 51%)	Wang et al. (2016)
	BSA-Bi_2Se_3 nanodots	High photothermal conversion efficiency (η= 50.7%); effective radiosensitization ratio (6%)	Mao et al. (2016)
	PVP-Bi_2Se_3@Sec NPs	Effective biodegradability; promoting the body's immune function	Du et al. (2017)
	HA-functionalized gambogic acid (GA) loaded Bi_2Se_3 hollow nanocubes (HNC-s-s-HA/GA)	Effective accumulation and uptake by CD44 overexpressing cancer cells; specifical drug releasing; avoiding heat damage	Song et al. (2019)
	Heterogeneous	—	
	Bi_2S_3-MoS_2 NPs	satisfactory photothermal performance; enhanced radiosensitization effectively inhibit the TNBC metastasis	Fei Gao et al. (2020)
	MoS_2/Bi_2S_3-PEG composite nanosheets	—	
	Core–Shell MnSe@Bi_2Se_3-PEG	Desirable photothermal performance, colloidal stability and biocompatibility	Wang et al. (2015)
	$FeSe_2$/Bi_2Se_3-PEG composite nanostructures	Additional MRI performance; photothermal-enhanced RT efficiency	Song et al. (2015)
		Excellent compatibility, remarkable synergistic tumor destruction effect; no appreciable toxic side effect	Cheng et al. (2016)

application in the field of biomedicine has been greatly restricted.

Bismuth, as an element with high atomic number (Z = 83), has surprising biocompatibility and been active in the biomedical field for hundreds of years. A variety of bismuth-based compounds have been widely used to treat diseases such as gastrohelcoma and bacterial infections (Peterson et al., 1996; Nomiya et al., 2004). Bismuth chalcogenides (Bi_2X_3, X = S, Se) based nanodrugs have been favored in tumor RT due to their many unique characteristics: 1) low toxicity and high biological safety *in vivo*; 2) low cost and easy synthesis; 3) strong X-ray absorption (The X-ray attenuation coefficient of Bi element is 5.74 > Au = 5.16 > Pt = 4.99 > Ta = 4.3 $cm^2\ g^{-1}$ at 100 keV). After Bi_2X_3-based nanodrugs specifically enrich in the tumor area by passively or actively targeting effect, the tumor can be effectively killed at a lower X-ray dose, and the damage to other normal tissues can also be greatly reduced (Zhang et al., 2014; Song et al., 2017; Alejo-Martinez et al., 2019). Nevertheless, the RT effect of these nanodrugs is still greatly reduced by the hypoxic tumor microenvironment. Currently, many emerging Bi_2X_3 nanodrugs are developed to further improve the efficiency of RT, and have demonstrated very impressive tumor-killing effects. Here, a systematic review is provided to summarize the breakthrough progresses of Bi_2X_3 nanodrugs for overcoming the limitations of the tumor hypoxia microenvironment in the field of RT. Currently, three strategies have been developed to improve the RT efficiency of Bi_2X_3 nanodrugs (**Figure 1**; **Table 1**). Firstly, elaborately designed Bi_2X_3-based nanocomposites increase the supply of O_2 to relieve the hypoxic state of the TME; the second strategy is non-O_2 dependent RT: Bi_2X_3-based nanocomposites with distinctive heterojunction structure to promote the production of non-O_2 dependent radicals; the third is photothermal-enhanced RT: local high temperature of the tumor site can not only relieve the hypoxic tumor microenvironment, but also increase the yield and speed of ROS production in RT. Finally, we discussed the challenges and prospects of bismuth chalcogenides nanocomposites in the field of cancer RT.

High-Efficient O_2-Supplied Radiotherapy

Many well-designed Bi_2X_3-based nanocomposites have shown great potential in improving tumor hypoxia and RT efficiency. Bi_2X_3-based nanocomposites with ideal structure and morphology can be prepared through specific synthesis strategies due to their unique and flexible physical and chemical properties, such as hollow structure (Song et al., 2016; Zhang et al., 2020), mesoporous structure (Sun et al.,

2019; Yang et al., 2021), core-shell structure (Li et al., 2017; Li et al., 2018). For example, Song et al. (2016) prepared PEGylated hollow Bi_2Se_3 nanoparticles (PEG-Bi_2Se_3 NPs) through cation exchange reaction based on the Kirkendall effect. Perfluorocarbon, a highly efficient oxygen loading solvent, was then filled into the hollow structure of PEG-Bi_2Se_3 NPs (PEG-Bi_2Se_3@PFC@O_2). The oxygen carrying capacity of PEG-Bi_2Se_3@PFC@O_2 was significantly higher than that of the hollow PEG-Bi_2Se_3 NPs, up to 96.9 ± 9.4 μmol/g of PEG-Bi_2Se_3. Moreover, the O_2 retention time exceeded 1 h, and the gradual release of O_2 effectively improved the hypoxic microenvironment in the tumor site. At the same X-ray dose, the anti-tumor effect of PEG-Bi_2Se_3@PFC@O_2 was significantly better than that of PEG-Bi_2Se_3 and RT group. Another effective strategy to improve tumor hypoxia is to convert the high concentration H_2O_2 into O_2 in the tumor microenvironment (Zhang et al., 2018; Zhang et al., 2019; Yuzhu Yao et al., 2021). For example, Zhang et al. (2018) developed a Bi_2S_3-albumin composite nanospheres combined with catalase (abbreviated as BSNSs-CAT) for cancer treatment. CAT at BSNSs-CAT efficiently catalyzed the conversion of H_2O_2 into O_2 after BSNSs-CAT accumulated in tumor tissues through enhanced penetration and retention effect (EPR effect). The percentage of O_2 saturation concentration treated with BSNSs-CAT increased significantly from 52.5% to about 59.2% in the tumor site. BSNSs-CAT + RT had the best tumor growth inhibition effect thanks to the strong reflective absorption of Bi and the improvement of the hypoxic microenvironment, followed by BSNSs + RT, then RT group. However, CAT, as a natural enzyme, is easily degraded and inactivated by proteases *in vivo*. Some catalase-mimick nanozymes can catalyze H_2O_2 to produce H_2O and O_2 (Dai et al., 2021). Very recently, Yuzhu Yao et al. (2021) developed a nanocomposite of Bi_2Se_3, MnO_2 and bovine serum albumin (Bi_2Se_3-MnO_2@BSA) for RT. MnO_2 showed high-efficiency catalase-like properties and excellent stability *in vivo*. Moreover, the CAT activity of Bi_2Se_3-MnO_2@BSA was 2.46 times higher than that of MnO_2@BSA, because the Mn atoms of Bi_2Se_3-MnO_2@BSA was in an electron-rich state and easier to provide electrons for H_2O_2. The Bi_2Se_3-MnO_2@BSA + RT group showed a stronger tumor-killing effect compared to the MnO_2@BSA + RT group and the RT group in the *in vivo* treatments.

Non-O_2 Dependent Radiotherapy

Non-O_2 dependent RT has great advantages in RT, because it can directly avoid the RT resistance from the hypoxic microenvironment. As we all know, Bi chalcogenide compounds, as a narrow band gap semiconductor, can theoretically be excited by X-rays to generate free electrons and holes in the conduction band (CB) and valence band (VB), respectively (Meng et al., 2016; Waiskopf et al., 2016). These electron-hole pairs further react with H_2O or H_2O_2 to generate highly cytotoxic hydroxyl radicals (·OH) to induce cancer cells apoptosis by intense oxidative damages. However, the generation of ·OH is significantly suppressed in Bi chalcogenide nanomaterials due to the rapid recombination of electron-hole pairs (Zhang et al., 2012). The heterojunction structure of Bi_2X_3 nanocomposites can separate electrons and holes to greatly reduce the recombination of electron and hole pairs (Wang et al., 2019; Abhari et al., 2020; Nosrati et al., 2022). For example, Wang et al. (2019) designed Au-Bi_2S_3 nanocomposites with Schottky-type heterostructures (Au-Bi_2S_3 HNSCs) for non-O_2 dependent RT. Au-Bi_2S_3 HNSCs were prepared by *in-situ* growth of gold nanocrystals on Bi_2S_3 nanorods. The Schottky barrier was a low interface voltage region on the metal-semiconductor boundary. Semiconductor Bi_2S_3 generated low-energy electron-hole pairs under X-ray irradiation in Au-Bi_2S_3 HNSCs, and then electrons and holes were effectively separated because the electrons were easily transferred to gold *via* Schottky barrier. The current response of Au-Bi_2S_3 HNSCs was 1.5-times higher than pure Bi_2S_3 and the ·OH production was 1.6-times than that of Au and Bi_2S_3 mixture under X-ray irradiation. More importantly, the RT effect of Au-Bi_2S_3 HNSCs was significantly better than that of the pure Bi_2S_3 group or the Au and Bi_2S_3 mixture group both in the *in vitro* and *in vivo* experiments. In addition, Bi_2S_3-Au Schottky-type heterostructures can be adopted as a multifunctional drug delivery platform to combine chemotherapy and RT. This combination therapy has shown great potential in improving the efficiency of RT and minimizing the systemic toxicity of chemotherapeutic drugs (Nadar et al., 2021). Very recently, Nosrati et al. (2022) developed a methotrexate and curcumin co-loaded BSA-encapsulated Bi_2S_3-Au nanocomposite (Bi_2S_3@BSA-Au-BSA-MTX-CUR) for the combined treatment of chemotherapy and RT. In Bi_2S_3@BSA-Au-BSA-MTX-CUR, Bi_2S_3@BSA-Au heterojunctions enhance the generation of ·OH to increase the RT efficiency, while MTX efficiently promoted cellular uptake and interfere the biosynthesis of DNA of cancer cells. Interestingly, the combined treatment of chemotherapy and RT achieved a significant anti-cancer effect *in vivo* only under a single dose Bi_2S_3@BSA-Au-BSA-MTX-CUR injection and one-time X-ray irradiation, and the tumors was completely eradicated after 20 days of treatment.

Photothermal-Enhanced Radiotherapy

In recent years, photothermal therapy (PTT), as a specific emerging cancer therapy, has been extensively researched in the field of tumor treatment (Liu et al., 2019; Danewalia and Singh, 2021). Many transition metal nanomaterials have been researched for PTT, such as MoS_2-based nanomaterials (Jianling Wang et al., 2021), CoS_2 nanomaterials (Wang et al., 2020a), copper-based nanomaterials (Ai et al., 2021; Wang et al., 2021b; Li et al., 2021), titanium-based nanomaterials (Wang et al., 2020b; Wang et al., 2021c), covalent organic frameworks (COFs) (Yao et al., 2021b), etc. Compared with above PTT agents, Bi_2X_3-based nanomaterials have been proven to be a kind of more excellent photosensitizers due to the strong near-infrared absorption performance and high photothermal conversion efficiency of Bi_2X_3 (Xie et al., 2016; Cheng et al., 2018). Local high temperature can directly increase the oxygen content of the tumor microenvironment by increasing blood flow in the tumor. Moreover, high temperature induced by PTT can facilitate the generation of O_2-dependent ROS for RT by inhibiting the expression of hypoxia-inducible factor (HIF-1α) to increase oxygen concentration in tumor site. In addition, photothermal effects also interfere with DNA repair by

reducing the expression of DNA repair related proteins (DNA repair enzymes, PARP, Rad 51), and downregulating angiogenic factors to inhibit tumor metastasis (Oei et al., 2015; Cheng et al., 2017). Therefore, the combination of photothermal therapy and RT is an effective radiosensitization strategy. For example, Wang et al. (2016) prepared ultra-small BSA-coated Bi_2S_3 nanodots (BSA-Bi_2S_3 NPs) for photothermal-enhanced RT. BSA-Bi_2S_3 NPs had the excellent X-ray and photothermal response properties (the photothermal conversion efficiency was as high as 51%). Moreover, The BSA-Bi_2S_3 NPs with ultra-small size (about only 6 nm) were more conducive to being taken up by tumor cells. Compared with the RT sensitization group (Bi_2S_3+X-ray) or the PTT group (Bi_2S_3+NIR), the 4T1-tumor bearing mice treated with radio-photothermal combination therapy group (Bi_2S_3+X-ray + NIR) achieved complete tumor eradication, and the survival rate of mice reached 100% over 40 days after treatment. In addition, it is also extremely important to protect adjacent normal tissues from radiation damage during RT. Recently, Du et al. (2017) reported a Bi_2Se_3 nanoparticles modified with polyvinylpyrrolidone and selenocysteine (PVP-Bi_2Se_3@Sec NPs) for photothermal-enhanced RT. The photothermal effect of Bi_2Se_3 NPs effectively improved tumor hypoxia microenvironment to enhance the radiosensitivity of cancer cells. Moreover, the PVP-Bi_2Se_3@Sec NPs were degraded *in vivo*, and part of the Se released from the NPs to enhance the body's immune function. Compared with RT, the PVP-Bi_2Se_3@Sec NPs group effectively protected the immune system, and the key cytokines level (like interleukin 6 and 2) were restored in the blood.

The efficiency of RT can be further increased by improving the photothermal conversion efficiency of the Bi_2X_3-based nanocomposites. Fox example, Fei Gao et al. (2020) developed heterogeneous Bi_2S_3-MoS_2 nanoparticles (BMNPs) for photothermal enhanced RT. BMNPs had a higher photothermal conversion efficiency than Bi_2S_3 nanoparticles (BNPs) (35.8 vs 28.1%). The BMNPs reduced the quasi-threshold X-ray dose from 1.39 to 0.92 Gy, and the sensitivity enhancement ratio increased by 17.9%. The effect of NIR + RT + BMNP group was much better than that of RT group and RT + BMNPs group in the treatment of triple-negative breast cancer. The survival rate of mice in the NIR + RT + BMNP group was as high as 100% at 28 days after treatment, while the RT group and RT + BMNPs group had only 0 and 20%, respectively. When the temperature of the tumor area rises, the tumor cells resisting heating-caused damage by up-regulating the expression of heat shock proteins (HSPs) (Ge Gao et al., 2020). Therefore, the photothermal enhanced RT can be further increased by inhibiting the activity of HSPs. Moreover, avoiding thermal damage and inflammation of adjacent normal tissues caused by hyperthermia also needs to be considered. Recently, Song et al. reported a hyaluronic acid (HA) modification and gambogic acid (GA) loaded hollow Bi_2Se_3 nanotube (HNC-ss-HA/GA) for low-temperature radio-photothermal combination therapy. HA ligands promoted the accumulation of HNC-ss-HA/GA in tumors due to its specifical affinity with CD44 receptor in cancer cells. Glutathione, one of the most important antioxidants in cells, is known to be overexpressed in cancer cells (Ding et al., 2021). Interestingly, the disulfide bond between HNC and HA can be rapidly cleaved by glutathione to release GA. GA, as an effective inhibitor of HSPs, which could enhance the heat sensitivity of cancer cells (Su et al., 2021), thereby improve the efficacy of photothermal-enhanced RT. The combined therapy group (HNC-s-s-HA/GA + NIR + X-ray) demonstrated the strongest suppress tumor growth effect *in vivo* compared to other monotherapy groups (HNC-s-s-HA/GA + NIR and HNC-s-s-HA/GA + X-ray).

SUMMARY AND OUTLOOK

In summary, this review summarizes the latest research progress of Bi_2X_3-based nanodrugs for RT. Bi_2X_3-based nanodrugs have great clinical application prospects in the field of RT because of their super-high RT effect and biocompatibility. Nevertheless, there are still many challenges to overcome in achieving clinical translation of these treatment strategies. Firstly, the excellent RT effects of these Bi_2X_3-based nanodrugs are all achieved in mice models. However, the huge species difference between human and mice makes these nanodrugs face a big bottleneck for clinical translation. For example, mice tumor models generally take about 15 days, while human cancers often take months or even years. Therefore, the tumor microenvironment of human may be very different from that of mice models, which may lead to unsatisfactory clinical effects of Bi_2X_3-based nanodrugs. Therefore, from the perspective of clinical application, it is necessary to verify the radiosensitizing effect of Bi_2X_3-based nanodrugs in humanized animal models, such as the monkey models. Secondly, metabolic pathway of Bi_2X_3-based nanodrugs needs further study *in vivo*. As we all know, as a heavy metal element, excessive Bi may cause some side effects such as renal toxicity, brain toxicity and neurological decline, which can be attributed to the tendency of Bi to bind to sulfhydryl groups in many important enzymes in the human body, resulting in the denaturation of enzymes and destroys its functionality. At present, most of the metabolism and toxicity of Bi_2X_3-based nanodrugs have only been done for about a month, and the longer-term toxicity and metabolic mechanisms still need to be further explored. Therefore, exploring biodegradable and clearable Bi_2X_3-based nanodrugs is of great significance for thier clinical translation (Wang et al., 2021a). Fortunately, there is rare Bi element in the human body itself. Therefore, the distribution, metabolism, and excretion process of Bi_2X_3-based nanodrugs can be easily tracked by the content and valence of Bi *in vivo*. Thirdly, the large-scale and controllable preparation of Bi_2X_3-based nanodrugs need to be further optimized. In commercial preparation, it is necessary to maintain precise control of the size, morphology, charge, and composition of nanomaterials to ensure uniformity and strict quality control. Therefore, exploring a simpler, faster, more precise and controllable synthesis process is vital for the clinical translation and commercial production of Bi_2X_3-based nanodrugs in the field of RT. Nevertheless, Bi_2X_3-based nanodrugs still have great clinical application prospects of RT. As mentioned earlier, NBTXR3 based on HfO_2 have shown excellent effects in clinical phase III. In theory, Bi_2X_3-based

nanodrugs have stronger biocompatibility and radiosensitization effect than HfO_2 nanoparticles. We believe that Bi_2X_3-based nanodrugs will achieve true clinical RT treatment with the joint efforts of scientists from multiple disciplines such as chemistry, medicine, and biology in the near future.

AUTHOR CONTRIBUTIONS

All authors listed have made a substantial, direct, and intellectual contribution to the work and approved it for publication.

FUNDING

This work was supported by the National Natural Science Foundation of China (Nos. 21974134 and 81974508), the Hunan Science Fund for Distinguished Young Scholar of China (No. 2021JJ10067), Innovation-Driven Project of Central South University (No. 202045005), Hunan Provincial Natural Science Foundation of China (No. 2021JJ31066), Changsha Science and Technology Project (No. kq2001048), Key Research Project of Ningxia Hui Autonomous Region in 2021 of China (Major Project) (No. 2021BEG01001).

REFERENCES

Abhari, F., Charmi, J., Rezaeejam, H., Karimimoghaddam, Z., Nosrati, H., Danafar, H., et al. (2020). Folic Acid Modified Bismuth Sulfide and Gold Heterodimers for Enhancing Radiosensitization of Mice Tumors to X-ray Radiation. *ACS Sustain. Chem. Eng.* 8 (13), 5260–5269. doi:10.1021/acssuschemeng.0c00182

Ai, K., Huang, J., Xiao, Z., Yang, Y., Bai, Y., and Peng, J. (2021). Localized Surface Plasmon Resonance Properties and Biomedical Applications of Copper Selenide Nanomaterials. *Mater. Today Chem.* 20, 100402. doi:10.1016/j.mtchem.2020.100402

Alejo-Martinez, H., Sevilla-Moreno, A. C., Ondo-Mendéz, A., Quintero, J. H., and Páez, C. J. (2019). Comparison of Bi 2 S 3 and Ta 2 O 5 as Alternative Materials to Gold in Nanoparticles Used as Agents to Increase the Dose in Radiotherapy. *J. Phys. Conf. Ser.* 1247 (1), 012050. doi:10.1088/1742-6596/1247/1/012050

Begg, A. C., Stewart, F. A., and Vens, C. (2011). Strategies to Improve Radiotherapy with Targeted Drugs. *Nat. Rev. Cancer* 11 (4), 239–253. doi:10.1038/nrc3007

Bentzen, S. M. (2006). Preventing or Reducing Late Side Effects of Radiation Therapy: Radiobiology Meets Molecular Pathology. *Nat. Rev. Cancer* 6 (9), 702–713. doi:10.1038/nrc1950

Bonvalot, S., Rutkowski, P. L., Thariat, J., Carrère, S., Ducassou, A., Sunyach, M. P., et al. (2019). NBTXR3, a First-In-Class Radioenhancer Hafnium Oxide Nanoparticle, Plus Radiotherapy versus Radiotherapy Alone in Patients with Locally Advanced Soft-Tissue Sarcoma (Act.In.Sarc): a Multicentre, Phase 2-3, Randomised, Controlled Trial. *Lancet Oncol.* 20 (8), 1148–1159. doi:10.1016/S1470-2045(19)30326-2

Cheng, L., Shen, S., Shi, S., Yi, Y., Wang, X., Song, G., et al. (2016). FeSe2-Decorated Bi2Se3 Nanosheets Fabricated *via* Cation Exchange for Chelator-free 64Cu-Labeling and Multimodal Image-Guided Photothermal-Radiation Therapy. *Adv. Funct. Mater.* 26 (13), 2185–2197. doi:10.1002/adfm.201504810

Cheng, X., Yong, Y., Dai, Y., Song, X., Yang, G., Pan, Y., et al. (2017). Enhanced Radiotherapy Using Bismuth Sulfide Nanoagents Combined with Photothermal Treatment. *Theranostics* 7 (17), 4087–4098. doi:10.7150/thno.20548

Cheng, Y., Chang, Y., Feng, Y., Jian, H., Tang, Z., and Zhang, H. (2018). Deep-Level Defect Enhanced Photothermal Performance of Bismuth Sulfide-Gold Heterojunction Nanorods for Photothermal Therapy of Cancer Guided by Computed Tomography Imaging. *Angew. Chem. Int. Ed. Engl.* 57 (1), 246–251. doi:10.1002/anie.201710399

Dai, Y., Ding, Y., and Li, L. (2021). Nanozymes for Regulation of Reactive Oxygen Species and Disease Therapy. *Chin. Chem. Lett.* 32 (9), 2715–2728. doi:10.1016/j.cclet.2021.03.036

Danewalia, S. S., and Singh, K. (2021). Bioactive Glasses and Glass-Ceramics for Hyperthermia Treatment of Cancer: State-Of-Art, Challenges, and Future Perspectives. *Mater. Today Bio* 10, 100100. doi:10.1016/j.mtbio.2021.100100

De Martino, M., Daviaud, C., and Vanpouille-Box, C. (2021). Radiotherapy: An Immune Response Modifier for Immuno-Oncology. *Semin. Immunol.* 52, 101474. doi:10.1016/j.smim.2021.101474

Ding, Y., Dai, Y., Wu, M., and Li, L. (2021). Glutathione-mediated Nanomedicines for Cancer Diagnosis and Therapy. *Chem. Eng. J.* 426, 128880. doi:10.1016/j.cej.2021.128880

Du, J., Gu, Z., Yan, L., Yong, Y., Yi, X., Zhang, X., et al. (2017). Poly(Vinylpyrollidone)- and Selenocysteine-Modified Bi2 Se3 Nanoparticles Enhance Radiotherapy Efficacy in Tumors and Promote Radioprotection in Normal Tissues. *Adv. Mater.* 29 (34), 1701268. doi:10.1002/adma.201701268

Evans, S. M., Jenkins, W. T., Shapiro, M., and Koch, C. J. (1997). "Evaluation of the Concept of "Hypoxic Fraction" as a Descriptor of Tumor Oxygenation Status," in *Oxygen Transport to Tissue XVIII*. Editors E. M. Nemoto, J. C. LaManna, C. Cooper, D. Delpy, K. Groebe, T. K. Hunt, et al. (Boston, MA: Springer US), 215–225. doi:10.1007/978-1-4615-5865-1_26

Gao, F., Wang, D., Zhang, T., Ghosal, A., Guo, Z., Miao, Y., et al. (2020). Facile Synthesis of Bi2S3-MoS2 Heterogeneous Nanoagent as Dual Functional Radiosensitizer for Triple Negative Breast Cancer Theranostics. *Chem. Eng. J.* 395, 125032. doi:10.1016/j.cej.2020.125032

Gao, G., Jiang, Y. W., Guo, Y., Jia, H. R., Cheng, X., Deng, Y., et al. (2020). Enzyme-Mediated Tumor Starvation and Phototherapy Enhance Mild-Temperature Photothermal Therapy. *Adv. Funct. Mater.* 30 (16), 1909391. doi:10.1002/adfm.201909391

Le Caër, S. (2011). Water Radiolysis: Influence of Oxide Surfaces on H2 Production under Ionizing Radiation. *Water* 3 (1), 235–253. doi:10.3390/w3010235

Li, Y., Sun, Y., Cao, T., Su, Q., Li, Z., Huang, M., et al. (2017). A Cation-Exchange Controlled Core-Shell MnS@Bi2S3 Theranostic Platform for Multimodal Imaging Guided Radiation Therapy with Hyperthermia Boost. *Nanoscale* 9 (38), 14364–14375. doi:10.1039/c7nr02384g

Li, L., Lu, Y., Jiang, C., Zhu, Y., Yang, X., Hu, X., et al. (2018). Actively Targeted Deep Tissue Imaging and Photothermal-Chemo Therapy of Breast Cancer by Antibody-Functionalized Drug-Loaded X-Ray-Responsive Bismuth Sulfide@Mesoporous Silica Core-Shell Nanoparticles. *Adv. Funct. Mater.* 28 (5), 1704623. doi:10.1002/adfm.201704623

Li, X., Yuan, H. J., Tian, X. M., Tang, J., Liu, L. F., and Liu, F. Y. (2021). Biocompatible Copper Sulfide-Based Nanocomposites for Artery Interventional Chemo-Photothermal Therapy of Orthotropic Hepatocellular Carcinoma. *Mater. Today Bio* 12, 100128. doi:10.1016/j.mtbio.2021.100128

Liu, Y., Bhattarai, P., Dai, Z., and Chen, X. (2019). Photothermal Therapy and Photoacoustic Imaging via Nanotheranostics in Fighting Cancer. *Chem. Soc. Rev.* 48 (7), 2053–2108. doi:10.1039/c8cs00618k

Liu, J., Zhang, J., Song, K., Du, J., Wang, X., Liu, J., et al. (2021). Tumor Microenvironment Modulation Platform Based on Composite Biodegradable Bismuth-Manganese Radiosensitizer for Inhibiting Radioresistant Hypoxic Tumors. *Small* 17 (34), 2101015. doi:10.1002/smll.202101015

Mao, F., Wen, L., Sun, C., Zhang, S., Wang, G., Zeng, J., et al. (2016). Ultrasmall Biocompatible Bi2Se3 Nanodots for Multimodal Imaging-Guided Synergistic Radiophototherapy against Cancer. *ACS Nano* 10 (12), 11145–11155. doi:10.1021/acsnano.6b06067

Meng, X., Liu, L., Ouyang, S., Xu, H., Wang, D., Zhao, N., et al. (2016). Nanometals for Solar-To-Chemical Energy Conversion: From Semiconductor-Based Photocatalysis to Plasmon-Mediated Photocatalysis and Photo-Thermocatalysis. *Adv. Mater.* 28 (32), 6781–6803. doi:10.1002/adma.201600305

Nadar, R. A., Franssen, G. M., Van Dijk, N. W. M., Codee-van der Schilden, K., de Weijert, M., Oosterwijk, E., et al. (2021). Bone Tumor-Targeted Delivery of Theranostic 195mPt-Bisphosphonate Complexes Promotes Killing of Metastatic Tumor Cells. *Mater. Today Bio* 9, 100088. doi:10.1016/j.mtbio.2020.100088

Nomiya, K., Sekino, K., Ishikawa, M., Honda, A., Yokoyama, M., Chikaraishi Kasuga, N., et al. (2004). Syntheses, crystal Structures and Antimicrobial

Activities of Monomeric 8-coordinate, and Dimeric and Monomeric 7-coordinate Bismuth(III) Complexes with Tridentate and Pentadentate Thiosemicarbazones and Pentadentate Semicarbazone Ligands. *J. Inorg. Biochem.* 98 (4), 601–615. doi:10.1016/j.jinorgbio.2004.01.011

Nosrati, H., Attari, E., Abhari, F., Barsbay, M., Ghaffarlou, M., Mousazadeh, N., et al. (2022). Complete Ablation of Tumors Using Synchronous Chemoradiation with Bimetallic Theranostic Nanoparticles. *Bioactive Mater.* 7, 74–84. doi:10.1016/j.bioactmat.2021.05.015

Oei, A. L., Vriend, L. E., Crezee, J., Franken, N. A., and Krawczyk, P. M. (2015). Effects of Hyperthermia on DNA Repair Pathways: One Treatment to Inhibit Them All. *Radiat. Oncol.* 10 (1), 165. doi:10.1186/s13014-015-0462-0

Peng, C., Liang, Y., Chen, Y., Qian, X., Luo, W., Chen, S., et al. (2020). Hollow Mesoporous Tantalum Oxide Based Nanospheres for Triple Sensitization of Radiotherapy. *ACS Appl. Mater. Inter.* 12 (5), 5520–5530. doi:10.1021/acsami.9b20053

Peterson, W. L., Ciociola, A. A., Sykes, D. L., McSorley, D. J., and Webb, D. D. (1996). Ranitidine Bismuth Citrate Plus Clarithromycin Is Effective for Healing Duodenal Ulcers, Eradicating *H. pylori* and Reducing Ulcer Recurrence. RBC *H. pylori* Study Group. *Aliment. Pharmacol. Ther.* 10 (3), 251–261. doi:10.1111/j.0953-0673.1996.00251.x

Song, G., Liang, C., Gong, H., Li, M., Zheng, X., Cheng, L., et al. (2015). Core-Shell MnSe@Bi2 Se3 Fabricated via a Cation Exchange Method as Novel Nanotheranostics for Multimodal Imaging and Synergistic Thermoradiotherapy. *Adv. Mater.* 27 (40), 6110–6117. doi:10.1002/adma.201503006

Song, G., Liang, C., Yi, X., Zhao, Q., Cheng, L., Yang, K., et al. (2016). Perfluorocarbon-Loaded Hollow Bi2Se3 Nanoparticles for Timely Supply of Oxygen under Near-Infrared Light to Enhance the Radiotherapy of Cancer. *Adv. Mater.* 28 (14), 2716–2723. doi:10.1002/adma.201504617

Song, Z., Chang, Y., Xie, H., Yu, X.-F., Chu, P. K., and Chen, T. (2017). Decorated Ultrathin Bismuth Selenide Nanosheets as Targeted Theranostic Agents for *In Vivo* Imaging Guided Cancer Radiation Therapy. *NPG Asia Mater.* 9 (10), e439. doi:10.1038/am.2017.167

Song, Y., Wang, Y., Zhu, Y., Cheng, Y., Wang, Y., Wang, S., et al. (2019). Biomodal Tumor-Targeted and Redox-Responsive Bi2 Se3 Hollow Nanocubes for MSOT/CT Imaging Guided Synergistic Low-Temperature Photothermal Radiotherapy. *Adv. Healthc. Mater.* 8 (16), e1900250. doi:10.1002/adhm.201900250

Su, X., Cao, Y., Liu, Y., Ouyang, B., Ning, B., Wang, Y., et al. (2021). Localized Disruption of Redox Homeostasis Boosting Ferroptosis of Tumor by Hydrogel Delivery System. *Mater. Today Bio* 12, 100154. doi:10.1016/j.mtbio.2021.100154

Sun, L., Hou, M., Zhang, L., Qian, D., Yang, Q., Xu, Z., et al. (2019). PEGylated mesoporous Bi2S3 nanostars loaded with chlorin e6 and doxorubicin for fluorescence/CT imaging-guided multimodal therapy of cancer. *Nanomedicine* 17, 1–12. doi:10.1016/j.nano.2018.12.013

Tang, W., Dong, Z., Zhang, R., Yi, X., Yang, K., Jin, M., et al. (2019). Multifunctional Two-Dimensional Core-Shell MXene@Gold Nanocomposites for Enhanced Photo-Radio Combined Therapy in the Second Biological Window. *ACS Nano* 13 (1), 284–294. doi:10.1021/acsnano.8b05982

Wang, J., Sui, L., Huang, J., Miao, L., Nie, Y., Wang, K., et al. (2021). MoS2-based Nanocomposites for Cancer Diagnosis and Therapy. *Bioact Mater.* 6 (11), 4209–4242. doi:10.1016/j.bioactmat.2021.04.021

Waiskopf, N., Ben-Shahar, Y., Galchenko, M., Carmel, I., Moshitzky, G., Soreq, H., et al. (2016). Photocatalytic Reactive Oxygen Species Formation by Semiconductor-Metal Hybrid Nanoparticles. Toward Light-Induced Modulation of Biological Processes. *Nano Lett.* 16 (7), 4266–4273. doi:10.1021/acs.nanolett.6b01298

Wang, S., Li, X., Chen, Y., Cai, X., Yao, H., Gao, W., et al. (2015). A Facile One-Pot Synthesis of a Two-Dimensional MoS2/Bi2S3 Composite Theranostic Nanosystem for Multi-Modality Tumor Imaging and Therapy. *Adv. Mater.* 27 (17), 2775–2782. doi:10.1002/adma.201500870

Wang, Y., Wu, Y., Liu, Y., Shen, J., Lv, L., Li, L., et al. (2016). BSA-mediated Synthesis of Bismuth Sulfide Nanotheranostic Agents for Tumor Multimodal Imaging and Thermoradiotherapy. *Adv. Funct. Mater.* 26 (29), 5335–5344. doi:10.1002/adfm.201601341

Wang, X., Zhang, C., Du, J., Dong, X., Jian, S., Yan, L., et al. (2019). Enhanced Generation of Non-oxygen Dependent Free Radicals by Schottky-type Heterostructures of Au-Bi2S3 Nanoparticles via X-ray-Induced Catalytic Reaction for Radiosensitization. *ACS Nano* 13 (5), 5947–5958. doi:10.1021/acsnano.9b01818

Wang, X., Zhong, X., Zha, Z., He, G., Miao, Z., Lei, H., et al. (2020). Biodegradable CoS2 Nanoclusters for Photothermal-Enhanced Chemodynamic Therapy. *Appl. Mater. Today* 18, 100464. doi:10.1016/j.apmt.2019.100464

Wang, X., Wang, X., Zhong, X., Li, G., Yang, Z., Gong, Y., et al. (2020). V-TiO2 Nanospindles with Regulating Tumor Microenvironment Performance for Enhanced Sonodynamic Cancer Therapy. *Appl. Phys. Rev.* 7 (4), 041411. doi:10.1063/5.0027606

Wang, X., Zhong, X., Li, J., Liu, Z., and Cheng, L. (2021). Inorganic Nanomaterials with Rapid Clearance for Biomedical Applications. *Chem. Soc. Rev.* 50 (15), 8669–8742. doi:10.1039/d0cs00461h

Wang, X., Shi, Q., Zha, Z., Zhu, D., Zheng, L., Shi, L., et al. (2021). Copper Single-Atom Catalysts with Photothermal Performance and Enhanced Nanozyme Activity for Bacteria-Infected Wound Therapy. *Bioact Mater.* 6 (12), 4389–4401. doi:10.1016/j.bioactmat.2021.04.024

Wang, X., Zhong, X., and Cheng, L. (2021). Titanium-based Nanomaterials for Cancer Theranostics. *Coord. Chem. Rev.* 430, 213662. doi:10.1016/j.ccr.2020.213662

Wu, M., Ding, Y., and Li, L. (2019). Recent Progress in the Augmentation of Reactive Species with Nanoplatforms for Cancer Therapy. *Nanoscale* 11 (42), 19658–19683. doi:10.1039/c9nr06651a

Xie, H., Li, Z., Sun, Z., Shao, J., Yu, X. F., Guo, Z., et al. (2016). Metabolizable Ultrathin Bi2 Se3 Nanosheets in Imaging-Guided Photothermal Therapy. *Small* 12 (30), 4136–4145. doi:10.1002/smll.201601050

Xie, J., Gong, L., Zhu, S., Yong, Y., Gu, Z., and Zhao, Y. (2019). Emerging Strategies of Nanomaterial-Mediated Tumor Radiosensitization. *Adv. Mater.* 31 (3), e1802244. doi:10.1002/adma.201802244

Xue, J., Duosiken, D., Zhong, S., Cao, J. J., Hu, L. Y., Sun, K., et al. (2021). The Dependence of Radio-Sensitization Efficiency on Mitochondrial Targeting with NaGdF4:Yb,Er Nanoparticles. *Acta Biomater.* 131, 508–518. doi:10.1016/j.actbio.2021.06.041

Yang, C., Chang, M., Yuan, M., Jiang, F., Ding, B., Zhao, Y., et al. (2021). NIR-Triggered Multi-Mode Antitumor Therapy Based on Bi 2 Se 3/Au Heterostructure with Enhanced Efficacy. *Small* 17 (28), 2100961. doi:10.1002/smll.202100961

Yao, S., Zhao, X., Wan, X., Wang, X., Huang, T., Zhang, J., et al. (2021). π-π Conjugation Promoted Nanocatalysis for Cancer Therapy Based on a Covalent Organic Framework. *Mater. Horiz* 8 (12), 3457–3467. doi:10.1039/d1mh01273h

Yao, S., Liu, Z., and Li, L. (2021). Recent Progress in Nanoscale Covalent Organic Frameworks for Cancer Diagnosis and Therapy. *Nanomicro Lett.* 13 (1), 176. doi:10.1007/s40820-021-00696-2

Yao, Y., Li, P., He, J., Wang, D., Hu, J., and Yang, X. (2021). Albumin-Templated Bi2Se3-MnO2 Nanocomposites with Promoted Catalase-like Activity for Enhanced Radiotherapy of Cancer. *ACS Appl. Mater. Inter.* 13 (24), 28650–28661. doi:10.1021/acsami.1c05669

Zang, Y., Gong, L., Mei, L., Gu, Z., and Wang, Q. (2019). Bi2WO6 Semiconductor Nanoplates for Tumor Radiosensitization through High- Z Effects and Radiocatalysis. *ACS Appl. Mater. Inter.* 11 (21), 18942–18952. doi:10.1021/acsami.9b03636

Zhang, Z., Wang, W., Wang, L., and Sun, S. (2012). Enhancement of Visible-Light Photocatalysis by Coupling with Narrow-Band-Gap Semiconductor: A Case Study on Bi2S3/Bi2WO6. *ACS Appl. Mater. Inter.* 4 (2), 593–597. doi:10.1021/am2017199

Zhang, X.-D., Chen, J., Min, Y., Park, G. B., Shen, X., Song, S.-S., et al. (2014). Metabolizable Bi2Se3Nanoplates: Biodistribution, Toxicity, and Uses for Cancer Radiation Therapy and Imaging. *Adv. Funct. Mater.* 24 (12), 1718–1729. doi:10.1002/adfm.201302312

Zhang, Q., Chen, J., Ma, M., Wang, H., and Chen, H. (2018). A Bioenvironment-Responsive Versatile Nanoplatform Enabling Rapid Clearance and Effective Tumor Homing for Oxygen-Enhanced Radiotherapy. *Chem. Mater.* 30 (15), 5412–5421. doi:10.1021/acs.chemmater.8b02251

Zhang, L., Chen, Q., Zou, X., Chen, J., Hu, L., Dong, Z., et al. (2019). Intelligent Protein-Coated Bismuth Sulfide and Manganese Oxide Nanocomposites Obtained by Biomineralization for Multimodal Imaging-Guided Enhanced Tumor Therapy. *J. Mater. Chem. B* 7 (34), 5170–5181. doi:10.1039/c9tb00991d

Zhang, C., Li, D., Pei, P., Wang, W., Chen, B., Chu, Z., et al. (2020). Rod-based Urchin-like Hollow Microspheres of Bi2S3: Facile Synthesis, Photo-Controlled Drug Release for Photoacoustic Imaging and Chemo-Photothermal Therapy of Tumor Ablation. *Biomaterials* 237, 119835. doi:10.1016/j.biomaterials.2020.119835

Zhao, T., Wu, W., Sui, L., Huang, Q., Nan, Y., Liu, J., et al. (2022). Reactive Oxygen Species-Based Nanomaterials for the Treatment of Myocardial Ischemia Reperfusion Injuries. *Bioactive Mater.* 7, 47–72. doi:10.1016/j.bioactmat.2021.06.006

Zhu, Y., Zhao, T., Liu, M., Wang, S., Liu, S., Yang, Y., et al. (2022). Rheumatoid Arthritis Microenvironment Insights into Treatment Effect of Nanomaterials. *Nano Today* 42, 101358. doi:10.1016/j.nantod.2021.101358

Conflict of Interest: The authors declare that the research was conducted in the absence of any commercial or financial relationships that could be construed as a potential conflict of interest.

Publisher's Note: All claims expressed in this article are solely those of the authors and do not necessarily represent those of their affiliated organizations, or those of the publisher, the editors and the reviewers. Any product that may be evaluated in this article, or claim that may be made by its manufacturer, is not guaranteed or endorsed by the publisher.

Copyright © 2022 Huang, Huang, Liu, Chen and Ai. This is an open-access article distributed under the terms of the Creative Commons Attribution License (CC BY). The use, distribution or reproduction in other forums is permitted, provided the original author(s) and the copyright owner(s) are credited and that the original publication in this journal is cited, in accordance with accepted academic practice. No use, distribution or reproduction is permitted which does not comply with these terms.

frontiers in Oncology

ORIGINAL RESEARCH
published: 21 February 2022
doi: 10.3389/fonc.2022.827891

Effective Delivery of siRNA-Loaded Nanoparticles for Overcoming Oxaliplatin Resistance in Colorectal Cancer

Yue Zhou[1,2,3†], *Qing Zhang*[1,2,3,4†], *Minjia Wang*[1,2,3,5†], *Chengzhi Huang*[2,3,5*†] *and Xueqing Yao*[1,2,3,5*]

[1] The Second School of Clinical Medicine, Southern Medical University, Guangzhou, China, [2] Department of Gastrointestinal Surgery, Ganzhou Municipal Hospital, Ganzhou, China, [3] Department of Gastrointestinal Surgery, Department of General Surgery, Guangdong Provincial People's Hospital, Guangdong Academy of Medical Sciences, Guangzhou, China, [4] Department of Gastrointestinal and Anorectal Surgery, The First People's Hospital of Zhaoqing, Zhaoqing, China, [5] School of Medicine, South China University of Technology, Guangzhou, China

OPEN ACCESS

Edited by:
Zeming Liu,
Huazhong University of Science and Technology, China

Reviewed by:
Ming Xu,
Chongqing Medical University, China
Chaohui Zheng,
Fujian Medical University, China

***Correspondence:**
Xueqing Yao
syyaoxueqing@scut.edu.cn
Chengzhi Huang
huangchengzhi93@hotmail.com

[†]*These authors have contributed equally to this work*

Specialty section:
This article was submitted to Pharmacology of Anti-Cancer Drugs, a section of the journal Frontiers in Oncology

Received: *02 December 2021*
Accepted: *20 January 2022*
Published: *21 February 2022*

Citation:
Zhou Y, Zhang Q, Wang M, Huang C and Yao X (2022) Effective Delivery of siRNA-Loaded Nanoparticles for Overcoming Oxaliplatin Resistance in Colorectal Cancer. Front. Oncol. 12:827891. doi: 10.3389/fonc.2022.827891

Chemotherapy resistance represents a formidable obstacle in advanced or metastatic colorectal cancer (CRC) patients. It is reported that ATPase copper transporting alpha (ATP7A) plays an important role in chemotherapy resistance in CRC. Here, we identified ATP7A as a potentially key gene of OXA resistance in CRC. The patients with higher expression of ATP7A tended to have platinum drug resistance. While the lower expression of ATP7A by siRNA knockdown resulted in enhancement of OXA sensitivity and increased OXA-induced apoptosis. Further, we demonstrated a novel and safe strategy to increase CRC chemosensitivity by delivering siRNA into tumor cells *via* a novel nanoparticle, DAN. In summary, our study provided a novel nanocarrier-based delivery of ATP7A to interfere in a key gene of chemo-resistance in CRC, which may be a novel therapeutic strategy to overcome chemotherapy resistance in CRC.

Keywords: oxaliplatin, chemoresistance, siRNA delivery, colorectal cancer, ATP7A

INTRODUCTION

Although the rapid development of cancer therapeutic methods, colorectal cancer (CRC) is still the third most common cancer in the world (1). The early-stage CRC patients may benefit from radical surgical resection with a higher disease-free survival (DFS) rate of nearly 90% (2, 3). However, the advanced or metastatic CRC patients might not have the chance to accept the radical surgical resection (3, 4). As a result, chemotherapy, targeted therapy, or immunotherapy might be a better preferable therapeutic method for those patients.

Oxaliplatin (OXA), a Pt-based chemotherapy drug, combined with 5-fluorouracil (5-Fu) or capecitabine was introduced for first-line chemotherapy methods for advanced CRC patients (5, 6). The FOLFOX protocol (OXA combined with 5-Fu) or CapeOx protocol (OXA combined with capecitabine) were significantly improved the clinical prognosis (7–9). However, the overall survival (OS) or DFS for advanced CRC patients remained low. One of the most important reasons for poor prognosis might be the resistance against Pt-based chemotherapy (10). New studies

are raising more and more questions nowadays about the mechanism based on chemotherapy resistance. Researches found that the primary mechanisms of platinum resistance included drug accumulation, the ability of DNA or RNA repair efficiency, and self-detoxification of cells (11). Of those, reduction in drug accumulation is one of the most generally acknowledged mechanisms of acquired OXA resistance (12).

ATPase copper efflux transporter A (ATP7A) is a member of intracellular copper transporters, ubiquitously expressed and transports copper out of the cell to maintain cellular copper homeostasis (13, 14). Additionally, ATP7A is also found to be one of the key regulators of intracellular platinum levels by delivering platinum to the extracellular space, reducing intracellular drug accumulation, thus compromising therapeutic efficacy (15–17). Furthermore, it has been reported that ATP7A is related to the resistance of platinum-based chemotherapy in various kinds of cancers, such as CRC and breast cancer (14, 18). Therefore, the development of the strategy to specifically knockdown ATP7A is considered to be a feasible treatment for colorectal cancer.

Gene interference, a relatively novel technique for switching off individual genes by delivering small interfering RNA (siRNA), has become an anti-tumor therapy with broad application prospects (19). The siRNA aimed to knockdown a targeted gene by delivering a specific sequence into a cell (20). Owing to the instability, poor blood circulation, and low uptake efficiency of free siRNA, the key to gene interference is how to transport therapeutic genes and drugs safely and efficiently to the tumor site (21, 22). Therefore, it is significant to find an effective delivery to transfer siRNA into cancer cells for anti-tumor treatment (23). (1,2-Dioleoyl-3-trimethylammonium-propane) DOTAP-assisted nanoparticles (DANs) could overcome the challenge of siRNA delivery, which helps effectively deliver siRNA, mRNA, or plasmid into cancer cells (24–26).

In the current research, we encapsulated siRNA using DANs and confirmed that DAN-siATP7A could be effectively downregulated the target gene *in vitro* and *in vivo*. As expected, after systemic injection of DAN-siATP7A into the model mice of CRC, the antitumor efficacy of OXA has been significantly enhanced with the size and weight of the tumor decreasing dramatically. Meanwhile, in terms of the weight curve, blood index, and organ index of the mice, combination therapy is relatively safe with few or minimal undesired systematic toxic effects. These results verified our hypothesis that nanocarrier-mediated interference of ATP7A could overcome oxaliplatin resistance in CRC. The combination use of nanoparticles and OXA represents a potential alternative therapy method against advanced cancer.

MATERIALS AND METHODS

Patients and Tissues Specimens

The tumor tissue specimens of CRC patients obtained from palliative or radical surgical resection were randomly chosen between 2015 to 2016 from Guangdong Provincial People's Hospital (Guangdong Academy of Medical Sciences). The inclusion criteria were: 1) All the patients were underwent palliative or radical surgical resection, and was pathologically diagnosed as adenocarcinoma. 2) All the included patients were received standardized OXA-based chemotherapy protocol. The exclusion criteria were: 1) pathologically diagnosed as gastrointestinal stromal tumors or squamous carcinoma.

Tumor stages were defined according to the 8th edition of the TNM staging system. To evaluate the therapeutic effect of OXA-based chemotherapy, we analyzed the results of radiology or pathology examination and referred to the following criteria: partial response (PR), complete response (CR), stable disease (SD), and progressive disease (PD). In our study, the OXA-response was defined as PR or CR, and the SD, PD were considered as OXA-resistance. All specimens were obtained with written informed consent and the study was approved by the Institutional Review Board of Guangdong Provincial People's Hospital under the grant number: GDREC2019504H(R2).

Immunohistochemistry and Hematoxylin-Eosin Staining

To further evaluate the potential association of ATP7A with OXA-resistance in CRC, immunohistochemistry (IHC) analysis was performed in our research as previously described (27). In brief, the primary antibody against ATP7A was purchased from BBI LIFE Science Corporation, (D161470, BBI, China). Two qualified pathologists independently analyzed the IHC results of the ATP7A protein expression based on the percentage of positive cells and staining intensity of the cytoplasm and nucleus. The score of percentage in positive cells was defined as 0 (<10%), 1 (10–25%), 2 (25-50%), and 3 (>50%), and the score of staining intensity were defined as 0 (negative staining), 1 (weakly staining), 2 (moderately staining), and 3 (strongly staining). The sum of the two scores was regarded as the final IHC score. High expression of ATP7A was defined as an IHC score from 4 to 6, while 0 to 3was regarded as low expression. We also performed Hematoxylin-Eosin (HE) staining in tumor tissues and viscus tissues from nude mice following the instruction of the manufactory (Biosharp, China).

Cell Culture and Transfection

We obtained human CRC cell lines, HCT116 and LOVO, from the iCell Bioscience (iCell, Shanghai, China). These cells were cultured in RPMI-1640 medium (BL303A, Biosharp, China) containing 10% fetal bovine serum (FBS, BL201A, Biosharp, China) supplemented with 1X penicillin-streptomycin solution (BL505A, Biosharp, China) at 37°C in a humidified incubator containing 5% CO2.

The siATP7A and cy5-labeled siNC were synthesized in Suzhou Gene Pharma and transfected into HCT116 and LOVO cells at a final concentration of 50 nM to knockdown ATP7A messenger RNA. The Lipofectamine 3000 (Invitrogen, USA) was utilized in the transfection procedure. Meanwhile, western- blotting and qPCR were utilized to evaluate the transfection efficacy following the manufacturer's protocol. The target of siATP7A sequence is as follows: 5'- UAUCCUAUGGUUAAACCUCUG-3', The scrambled (NC) siRNA sequence is 5'-UUCUCCGAACGUGUCACGU-3'.

Bioinformatic Analysis

The expression and Kaplan-Meier survival analysis of ATP7A in CRC patient cohorts were performed in Gene Expression Profiling Interactive Analysis (GEPIA, http://gepia.cancer-pku.cn/index.html) database (28).

Western-Blot

The Western Blot was performed as previously described (27). In brief, total protein of cells was extracted with RIPA buffer (Beyotime, China) supplemented with protease inhibitor, phenylmethylsulfonyl fluoride (PMSF, Beyotime, China) at 4°C, 14000 rpm for 20 min. BCA assay (Fudebio, China) was used for protein quantification. The protein was isolated by electrophoresis using 10% SDS-polyacrylamide gel (PAGE) and then transferred to the PVDF membrane (Immobilon P, Millipore, USA). 5% fat-free milk (Beyotime, China) in Tris-buffered saline with Tween-20 (TBST) was used to block nonspecific binding sites at room temperature for 1h. Then, the membranes were immunoblotted with primary antibody overnight at 4°C: anti-ATP7A (1:1000, D161470, Sangon Biotech, China) and anti-GAPDH antibody (1:1000, AP0066, Bioworld Technology, USA). After being washed with TBST 3 times, blots were incubated with secondary peroxidase-conjugated antibodies, the goat anti-rabbit secondary antibody (1:5000, BS13278, Bioworld Technology, USA) for 1 h at room temperature. The membranes were performed with an enhanced chemiluminescence system and scanned by the Syngene Imaging System (Frederick, USA).s

Quantitative Real-Time Polymerase Chain Reaction

Total RNA of CRC cells was extracted with TRIzol RNA Isolation Reagents (ThermoFisher Scientific, USA) as previously described. The 500ng of extracted RNA was reverse-transcribed into complementary DNA (cDNA) using the First-strand cDNA Synthesis Kit (K1072, Apexbio, USA) following the manufacturer's protocol. qPCR was performed on the LightCycler 480 (Roche, Swiss) instrument by using 2X SYBR Green PCR Mix (K1070, Apexbio, USA). ΔΔCT was calculated to analyze the results of qPCR and data from each experiment were normalized to the expression of a control gene (GAPDH). The following primers were used:

ATP7A, forward 5′-TGACCCTAAACTACAGACTCCAA-3′ and reverse: 5′-CGCCGTAACAGTCAGAAACAA-3′; GAPDH, forward 5′-TCAACGGATTTGGTCGTATTGGGCG-3′ and reverse 5′-CTCGCTCCTGGAAGATGGTGATGGG-3′.

Cell Viability Assay

For detection of OXA cytotoxicity (A8648, Apexbio), the CRC cells were seeded at a density of 3,000 per well into 96-well plates and cultured in a complete medium containing different concentrations of OXA for 48 h. Then, the Cell Counting Kit-8 (CCK-8) detection Kit (K1018, Apexbio, USA) was used to assess the inhibitory concentration of OXA. After continuing incubation for 4 h, the absorbance in 450 nm was detected *via* a microplate reader (BIO-Tek SYNERGY H1, USA). For detection of cell viability, 1,000 cells were seeded into each well of the 96-well plate with OXA of the 50% inhibitory concentration (IC50). CCK-8 solution was added to the wells at the time point of 0, 24, 48, and 72 h. The absorbance of stained cells was measured at 450 nm after continuing incubation for 4 h.

Apoptosis Detection

Cell Apoptosis Detection Kit (E-CK-A217, Elabscience, China) was utilized in apoptosis detection assays. The cultured cells were digested by trypsin, resuspended in 500 μL of binding buffer, and stained with Annexin V-FITC and propidium iodide (PI) for 15 min in dark. All samples were detected by a flow cytometer (BD FACS Verse, BD bioscience, USA) and the results were analyzed using the FlowJo 10.6 software (BD bioscience, USA).

Wound-Healing Assay

Cells in each group were seeded into a 6-well plate at a density of 2×10^6 per well to confluence After being cultured in pure RPMI-1640 medium without FBS, two straight wounds were made by a 200ul pipette tip (ThermoFisher Scientific, USA) in each well. At the time point of 0h, 24h, and 48 h, the migration status was photographed at the same location of wells using a light microscope (Olympus BX63, Japan) The result was analyzed by the ImageJ software.

Colony Formation Assay

Cells in each group were seeded into 6-well plates at a density of 1000 per well and continuously cultured for 2 weeks. The RPMI-1640 complete culture medium was replaced every 3 days. At the end of the experiment, 0.1% crystal violet (PH1322, Phygene Scientific, China) was used to stain the colonies. The number of colonies was counted by ImageJ software (29, 30).

Migration Assay

For migration assay, 8 μm-pore transwell chambers (Corning Costar, USA) were used without Matrigel. Each well of 24-well plates was filled with the RPMI-1640 complete culture medium containing 10% FBS. Then, approximately 1×10^5 cells in 500ul FBS-free medium were pipette into the upper chamber slowly. The incubation time is 48 h for HCT116 and LOVO. After being washed by PBS 3 times, cells on the upper surface of the chamber were removed lightly using a cotton swab. Then, the cells migrated to the lower surface of the chamber were fixed using 4% paraformaldehyde (PFA). At the end of the experiment, cells were stained with 0.1% crystal violet solution and counted and analyzed by ImageJ software.

Construction of Nanoparticles

Nanoparticles (DANs) encapsulating siRNA were prepared through a double emulsion solvent evaporation technique as previously described (24, 31). The PEG5k-b-PLGA11k (molar ratio: LA/GA=75/25) was purchased from Kelanbio (Guangzhou, China) and 1,2-Dioleoyl-3-trimethylammonium-propane (DOTAP) was purchased from Topscience (Shanghai, China) (24). Firstly, 25 μL DNase/RNase-free water containing 5 OD siRNA and 500 μL chloroform containing DOTAP (1 mg) and PEG5K-b-PLGA11K (25 mg) were emulsified for 1 min at 80W in an ice bath by sonication using Sonics Materials™

ultrasonic Processor VCX130-220V (Sonics & Materials, Inc, Newtown, USA). Then, 5 mL DNase/RNase-free water was added to the primary emulsion and further emulsified for 1 min. Finally, the organic solvent was removed with a rotary evaporator RV10 auto control (IKA, Germany). The diameter of DANsiATP7A was monitored at 25°C with Malvern Zetasizer Nano ZSE (Worcestershire, UK).

Cellular Uptake of DANsiRNA *In Vitro*

Cy5-siNC was encapsulated into DAN (DANCy5-siNC) to investigate cellular uptake of DAN by confocal laser scanning microscopy (CLSM). Cells were seeded into an observation dish for 24h and then incubated with DANCy5-siNC or free Cy5-siNC for 8 h. After the cell nucleus stained with DAPI (Beyotime, China), samples were photographed by Carl Zeiss LSM880 confocal microscope.

Establishment Mice CRC Model

The nude mice (6-8 weeks old) were randomly allocated to control and experimental groups, and the mice were all bred in specific pathogen-free (SPF) conditions. Mice were injected subcutaneously with 5×10^6 HCT116 cells. The tumor volume was calculated using the formula: Tumor Volume (mm^3) = (longest diameter) * (shortest diameter)^2 * 0.5. When the size of the tumor reaches 150mm^3, and the mice were randomly divided into 4 groups (PBS, free OXA, DAN-siATP7A, and combination use of DAN-siATP7A and OXA). After treatments, the tumors, organs, and blood from mice were dissected for further analysis. The animal experiment was proved by the Institutional Review Board of Guangdong Provincial People's Hospital under the grant number: GDREC2019506A.

TUNEL Staining for Apoptosis

Terminal deoxynucleotidyl transferase-mediated nick end labeling (TUNEL) assay is applied to determine the apoptotic cells. The CRC samples of mice were fixed in 4% PFA for 24 h, subsequently embedded in paraffin, and sliced (4–5 μm). The TUNEL staining was performed using the DAB (SA-HRP) TUNEL Cell Apoptosis Detection Kit (Servicebio, Wuhan, China) following the manufacturer's protocol. Streptavidin labeled with horse-Radish peroxidase (HRP) (SA-HRP) was then detected the biotin-labeled DNA terminal. Finally, HRP substrate mixture (DAB) was added for color reaction, so that the apoptotic cell nucleus was dyed brown and yellow, which can be detected by the ordinary light microscope. The rate of apoptosis was displayed as the ratio of TUNEL positive nuclei to hematoxylin-stained nuclei.

In-Vivo Toxicity Analysis

To further evaluate the *in vivo* toxicity of DAN nanoparticles, the crucial organs of the mice, such as the heart, liver, spleen, lung, kidney, and brain, were dissected for HE staining. Two experienced pathologists were invited to analyze the potential toxicity of the nanoparticles through the slides. Blood samples of mice have been collected to analyze the concentration of alanine aminotransferase (ALT), aspartate aminotransferase (AST), glutamyl transferase (GGT), blood urea nitrogen (BUN), Creatinine (Cr), and uric acid (UC) according to the manufacture's instructions (Nanjing Jiancheng, China).

Statistical Analysis

Statistical analysis was performed using Prism 9.0 (GraphPad, La Jolla, CA, USA) and Stata 15.0 (Stata Corp, USA). Data are presented as mean ± standard deviation (SD). The difference between the two groups was analyzed by the Student's *t*-test or unpaired *t*-test. Comparison of three or more groups were using the one-way ANOVA analysis. The experiments had been performed in triplicate. A $p<0.05$ was considered as statistical significance.

RESULTS

Implications of ATP7A Expression and Clinical Characteristic

In our cohort, a total of 41 advanced CRC cases were included and received standard eight-cycle OXA-based chemotherapy (FOLFOX or CapeOx protocol). 20 CRC patients benefit from the chemotherapy, while 21 patients suffered from chemotherapy resistance. The analysis of IHC staining implied that the chemotherapy resistance CRC patients had a higher expression of ATP7A protein than the chemotherapy response patients (**Figures 1A, B**, P<0.001). Our analysis also implied that the metastatic CRC patients (TNM Stage IV) had a higher expression of ATP7A in tumor tissue than locally advanced CRC patients (TNM Stage III, P<0.01). However, there was no statistical significance in survival (OS and DFS) between the higher and lower expression of ATP7A CRC patients (**Supplementary Figure 1**). The correlation between ATP7A expression and clinicopathologic features of CRC patients could be found in **Supplemental Table 1**.

Based on the GEPIA database, the bioinformatic analysis of ATP7A implied that there was no statistical significance between ATP7A high-expressed and low-expressed CRC patients in OS (**Supplemental Figure 2A**). However, the higher expression of ATP7A CRC may have a worse prognosis in DFS (**Supplemental Figure 2B**, HR=1.5, P=0.048). There was no ATP7A expression difference between the adjacent normal tissue and tumor tissue (**Supplemental Figure 2C**), and the bioinformatic analysis displayed that the ATP7A expression was not related to the TNM stage (**Supplemental Figure 2D**).

ATP7A Inhibition Reverse OXA Resistance *In Vitro*

To investigate the biological role of ATP7A in CRC, we knocked down ATP7A using siRNA. HCT116 and LOVO cell lines were transfected with siATP7A. The western blot and qPCR results revealed that in siATP7A-transfected HCT116 and LOVO cells, ATP7A was downregulated obviously (**Figure 2A**, P<0.001). To further research the effects of ATP7A in CRC cell chemosensitivity, ATP7A-knockdown CRC cells were treated with various concentrations of OXA for 48h, and the cytotoxic effects of OXA were measured using the CCK-8 assay

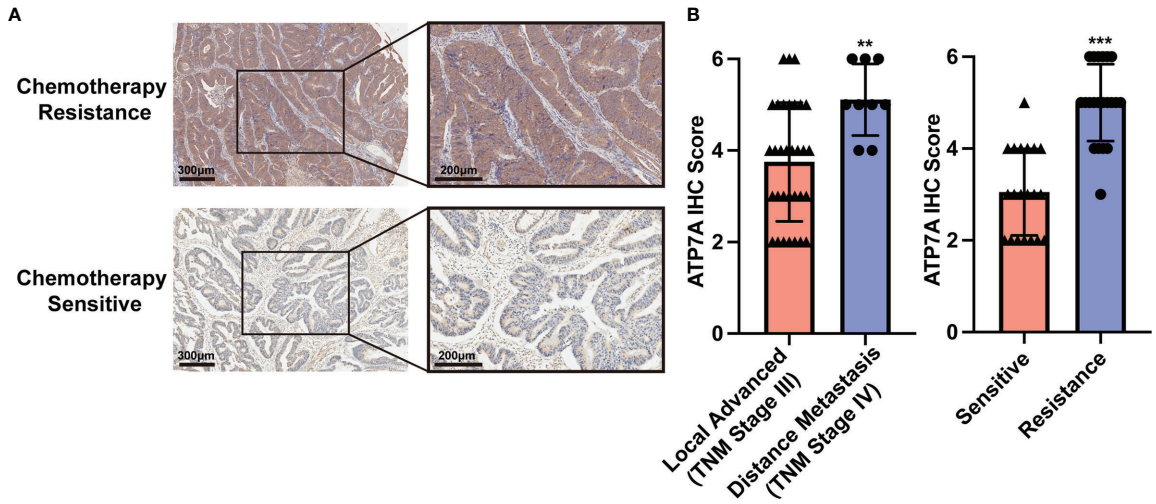


FIGURE 1 | Implications of ATP7A expression and clinical characteristics. **(A)** Expression of ATP7A in OXA resistance and OXA responder of CRC patients. **(B)** IHC staining scores of chemotherapy resistance patients and chemotherapy responders. **P < 0.01 and ***P < 0.001 when compared to the control group.

(**Figure 2B**). When ATP7A was knocked down, the IC50 value of OXA in siATP7A-transfected HCT116 (IC50 = 1.604 μg/ml, 95% CI = 1.419 to 1.807 μg/ml) was substantially lower than that in siNC-transfected HCT116 (IC50 = 8.407 μg/ml, 95% CI = 6.883 to 10.24 μg/ml). Similarly, the IC50 value of OXA for siATP7A-transfected LOVO (IC50 = 1.713μg/ml, 95% CI = 1.389 to 2.071 μg/ml) was significantly lower than that of siNC-transfected LOVO (IC50 = 5.439μg/ml, 95% CI =4.653 to 6.340μg/ml, **Figure 2C**, P<0.001). Furthermore, the CCK-8 assay proved that the cell viability of ATP7A downregulation cells was reduced compared to the negative control (**Figure 2D**, P<0.001). The results indicated that ATP7A downregulation noticeably increased and resensitized the chemosensitivity of CRC cells to OXA.

Knockdown of ATP7A Expression May Inhibit Cancer Tumorigenesis *In Vitro*

The results of colony-forming assay showed that ATP7A knockdown significantly decreased the colony formation ability with OXA treatment (**Figure 3A**, P<0.001). As for the apoptosis detection by FACS, the results suggested that the combination of ATP7A knockdown and OXA treatment largely inhibited the cell growth and improved the ratio of late apoptosis (**Figure 3B** P<0.001). To assess the effect of ATP7A on CRC cell motility, we performed wound-healing assays and transwell assays. Both HCT116 and LOVO treated with siATP7A knockdown plus OXA show the decreased ability of migration compared with the control (**Figures 3C, D**, P<0.001).

Construction of DAN Nanoparticle

To deliver siATP7A effectively *in vitro* and *in vivo*, the copolymer PEG5K-b-PLGA11K and a cationic lipid (DOTAP) were chosen to encapsulate siATP7A *via* a double-emulsion method. The components used for DAN-siATP7A preparation are shown in **Figure 4A**. In addition, the diameter of DAN-siATP7A was 101.4 ± 13.84 nm (**Figure 4B**) and the zeta potential was 21.77 ± 3.26mV (**Figure 4C**). To evaluate the stability of DAN-siATP7A, we incubated it in PRIM-1640 with 10% FBS for 48 h and the size of DAN-siATP7A changed very slightly (**Figure 4D**), which implied that DAN-siATP7A was relatively stable in blood circulation. Meanwhile, we further investigate the DAN-siATP7A in the following *in vitro* and *in vivo* studies. After being transferred by DAN-siATP7A, the ATP7A protein expression and mRNA expression in CRC cells showed the same significant inhibition (**Figures 4E, F**, P<0.001). Further, we investigate the cellular uptake of DAN-siRNA. As shown in **Figure 4G**, confocal images indicated that Cy-5 labeled siRNA can be delivered into the CRC cells successfully by DAN over time. *In vivo* study, we evaluated the transfection efficiency in the colorectal cancer model of nude mice (**Figure 4H**). Then, the result of IHC showed that the DAN-siATP7A group displayed a significant reduction of ATP7A protein expression compared to the free siATP7A group (**Figure 4I**, P<0.001), indicating that DAN-siATP7A could be delivered into the CRC tissue and played a significant role in knocking down.

siRNA-Loaded Nanoparticle Reverses Chemoresistance *In Vivo*

A xenografted HCT116 model of human CRC in nude mice was established to investigate the therapeutic effect of different groups *in vivo* (**Figure 5A**). **Figures 5B, C** showed tumor images and weight curves. The tumor size treated in the combination group (OXA+DAN-siATP7A) was smaller compared with others: free OXA, free DAN-siATP7A, and control group. We also recorded the tumor volume changes at different time points to evaluate the therapeutic efficacy. As **Figure 5D** shown, the tumor volumes of mice after treatment in combination therapy were also much smaller (P < 0.001),

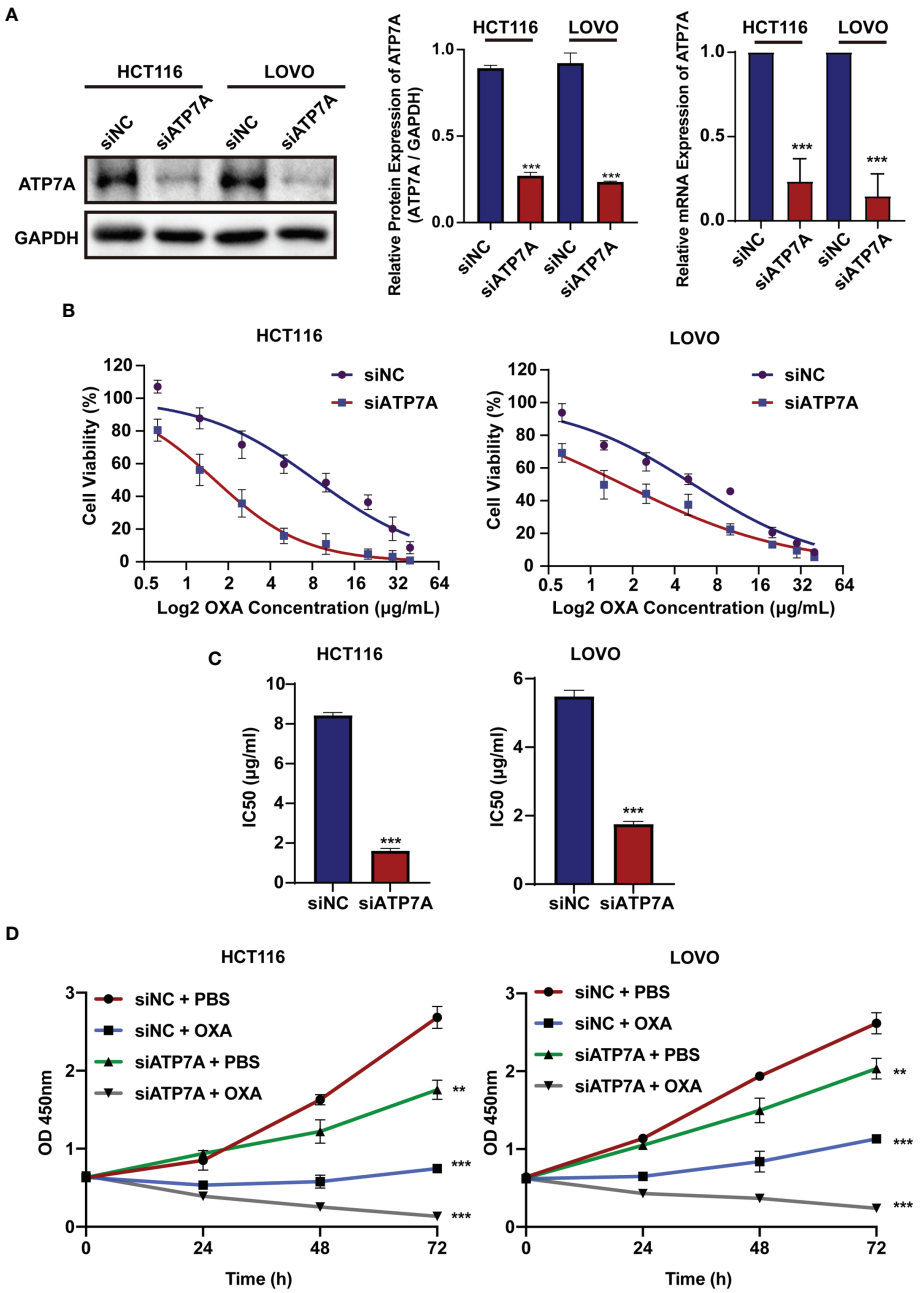


FIGURE 2 | ATP7A inhibition reverse OXA resistance *in vitro*. **(A)** ATP7A protein and ATP7A mRNA expression were inhibited by the siATP7A in HCT116 and LOVO cell lines. **(B)** OXA sensitivity in HCT116 and LOVO cell lines treated with siATP7A was determined using the CCK-8 test after treatment with various concentrations of OXA for 48 h. **(C)** The IC50 of OXA for siNC and siRNA transfected HCT116 or LOVO cells. **(D)** Together with OXA, decreased expression of ATP7A significantly suppressed cancer cell lines proliferation. **P < 0.01 and ***P < 0.001 when compared to the control group.

indicating the increased combinational therapeutic efficacy and the reversal effect of DAN-siATP7A on OXA resistance *in vivo*. Furthermore, the quantitative analysis of TUNEL staining was applied to analyze the tumor apoptosis *in vivo* (**Figure 5F** and **Supplemental Figure 3**). The highest apoptosis rate was observed in the combination of DAN-siATP7A and OXA treatment groups. Similarly, H&E staining (**Figure 5F**) shows the same trend, indicating the reversal role of DAN-siATP7A on OXA resistance *in vivo* during the antitumor process.

In Vivo Toxicity Analysis

We also evaluated the systematic toxicity of OXA and DAN-siATP7A by monitoring the body weights of nude mice for 42

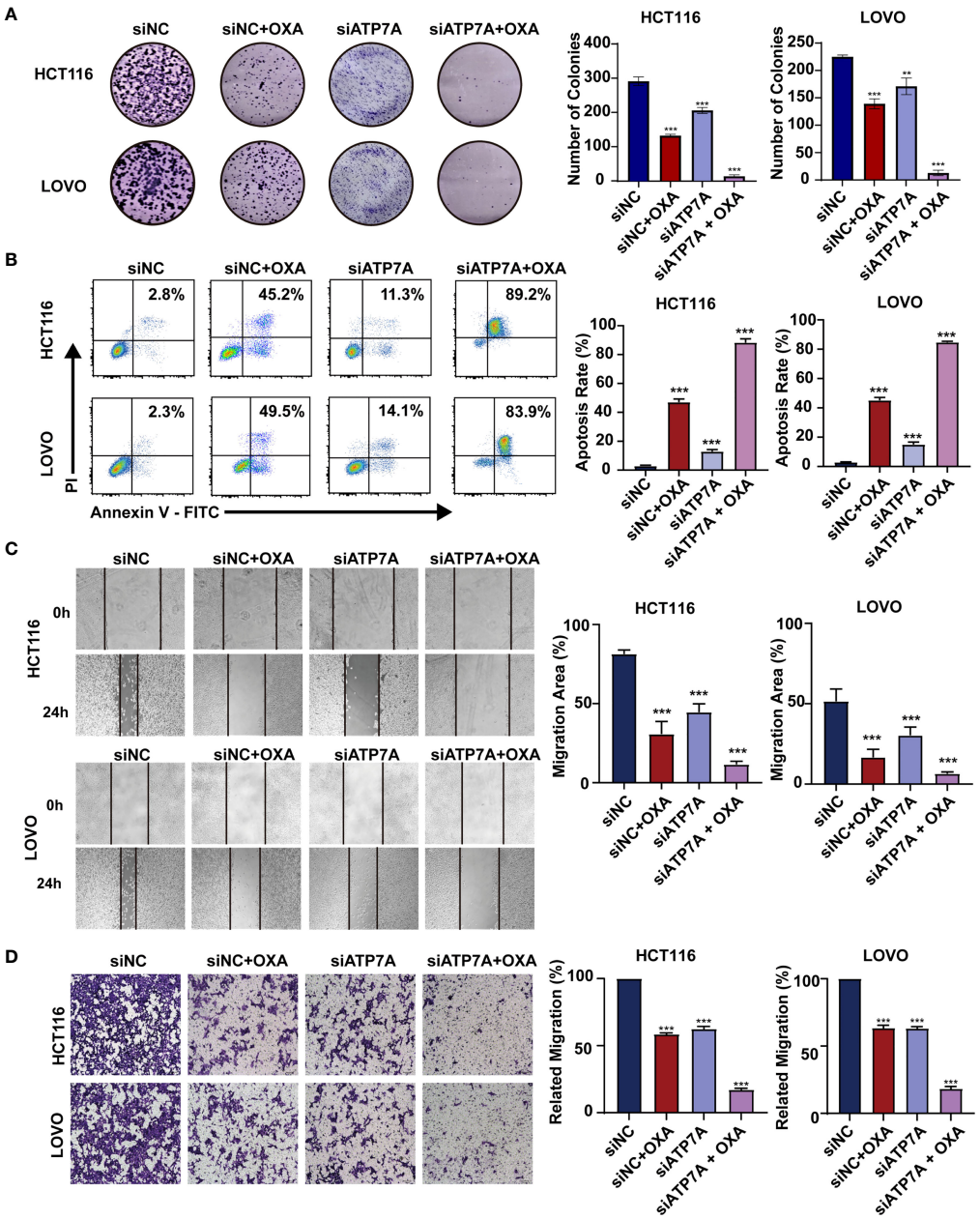


FIGURE 3 | Knockdown of ATP7A expression may inhibit cancer tumorigenesis *in vitro*. **(A)** Colony formation assays in HCT116 and LOVO cells. **(B)** A flow cytometer was performed to assess the apoptosis rate of HCT116 and LOVO cells. **(C)** Wound healing assay of HCT116 and LOVO cells. **(D)** Transwell assay was performed to evaluate the invasion of HCT116 and LOVO cells. *P < 0.05; **P < 0.01 and ***P < 0.001 when compared to the control group.

days. The body weight of the control, free OXA, and free DAN-siATP7A groups displayed increasing over time due to the increased tumor growth of the three groups. However, the body weights of the OXA and DAN-siATP7A groups did not seem to significantly change (**Figure 5E**), suggesting that the combination treatment do not have obvious toxicity to the mice. In addition, the main organs of mice were dissected, H&E stained, and observed by optical microscopy (**Figures 6A, B**). The organ index was calculated by the following formula: Organ Index(%) = [(the weight of the organ)/(the weight of the mice)] *100. As displayed in **Figure 6A**, there was no difference was found in each group of organ index. We also evaluate the potential hepatic and renal impairment from the blood sample of the nude mice, including the index of ALT, AST, GGT, BUN, Cr, and UC (**Figure 6C**). Our results indicated that no obvious adverse effects to the major organs of mice were observed after the mice were treated with the combination treatment of OXA and DAN-siATP7A.

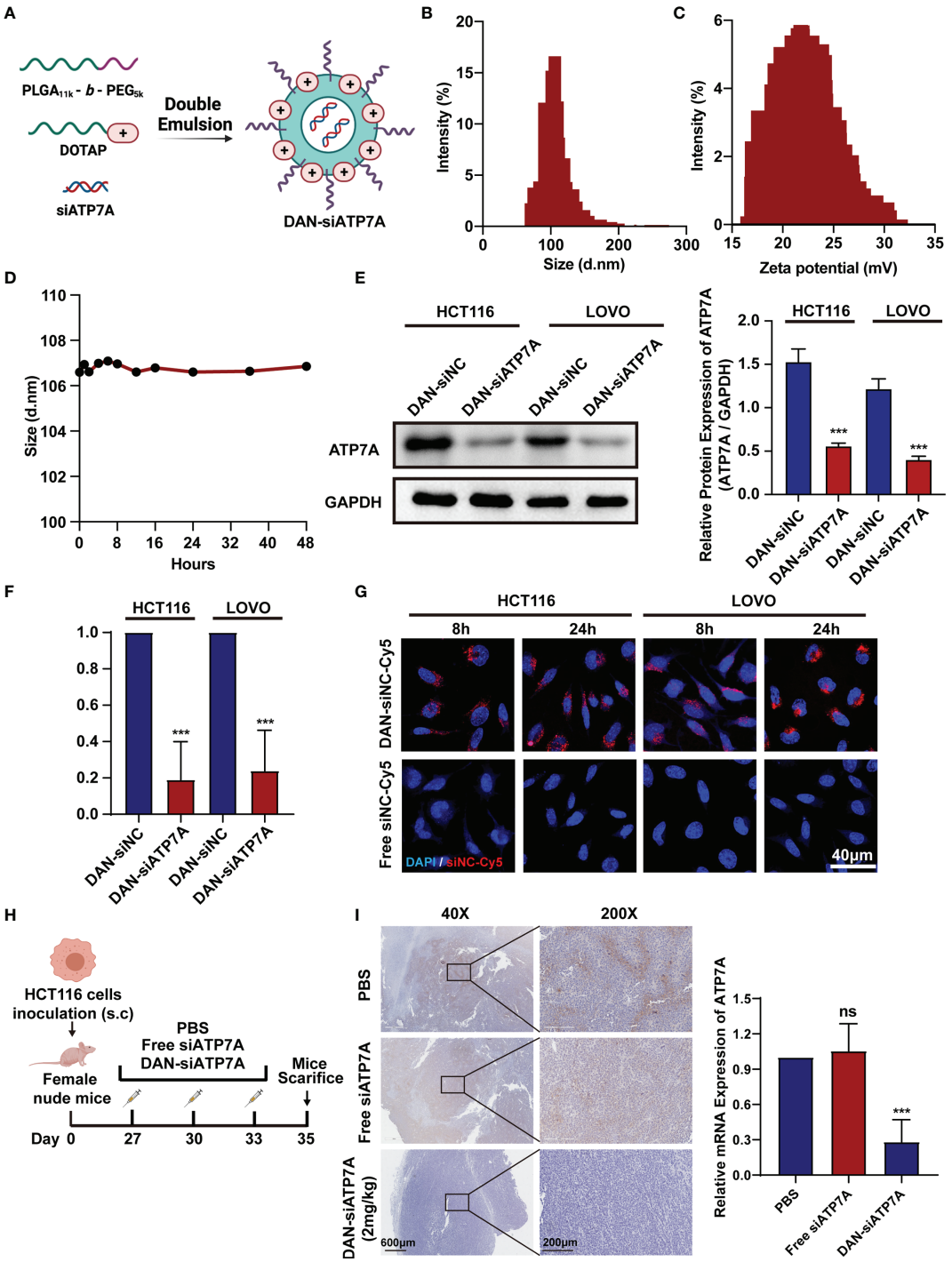


FIGURE 4 | Construction of DAN nanoparticle. **(A)** The schematic illustration of the nanoparticle DAN-siATP7A construction. The size **(B)** and zeta potential **(C)** distribution of DAN-siATP7A. **(D)** The size measurement of DANsiATP7A in the RPMI-1640 supplemented with 10% FBS. The protein expression **(E)** and mRNA expression **(F)** of ATP7A after being transfected with DAN-siATP7A in HCT116 and LOVO cell lines. **(G)** The in Virto cellular uptake of Cy5-labeled DAN-siNC and free Cy5-labeled siNC *in vitro*. The confocal image was captured 8 hours and 24hours after the transfection of HCT116 and LOVO cell lines. **(H)** The scheme of medication on tumor-bearing mice. **(I)** The IHC analysis of ATP7A and the PCR analysis of ATP7A mRNA in tumor tissue implied effective knockdown of ATP7A *via* DAN-siATP7A nanoparticles. ***P < 0.001 and ns, not significance, when compared to the control group.

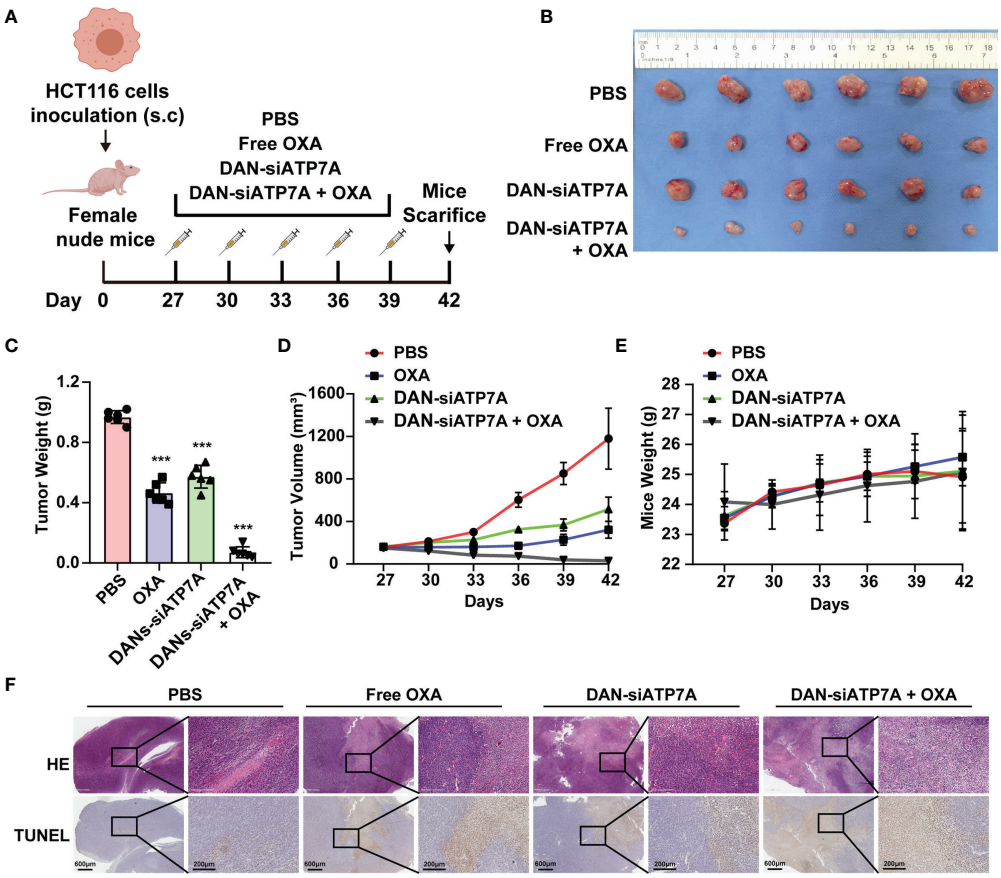


FIGURE 5 | siRNA-loaded nanoparticle reverses chemoresistance in HCT116-bearing mice. **(A)** The scheme of medication on tumor-bearing mice. **(B)** The image of the tumor was dissected from the nude mice at the end of the *in vivo* study. Tumor weight **(C)**, tumor volume **(D)** and mice weight **(E)** after the treatment. **(F)** The HE staining and TUNEL analysis of the tumor tissue of the nude mice. ***P < 0.001 when compared to the control group.

DISCUSSION

Oxaliplatin-based chemotherapy is currently the first-line clinical treatment for advanced CRC patients. However, chemotherapy failure or resistance was the major cause of recurrence and poor prognosis in CRC patients. It is of great importance to identify the therapy targets and develop novel therapeutic strategies to overcome chemotherapy resistance to improve the survival of the patients.

Previous reports demonstrated that the mechanisms of OXA resistance include uptake and metabolic abnormalities, changes in the tumor microenvironment. Herein, enhanced drug efflux and decreased drug concentration both contributed to chemotherapy resistance, in which ATP-binding cassette (ABC) transporters were the most prominent (32–34). Previous researches found out that the up-regulated ATP7A was correlated to the platinum drug resistance in colon cancer, esophageal squamous cell cancer, gastric carcinoma, and ovarian cancer (14). In the research of esophageal squamous cell cancer, researchers found out that the ATP7A knockdown by siRNA partially reversed resistance, and may provide novel strategies to overcome platinum drug resistance (35).

Hence, in our study, we identified ATP7A as a potentially key gene of OXA resistance in CRC. In our cohorts, the patients with higher expression ATP7A tended to have platinum drug resistance. The lower expression of ATP7A by siRNA knockdown resulted in enhancement of OXA sensitivity and increased OXA-induced apoptosis. We also demonstrated a novel strategy to increase CRC chemosensitivity by delivering siRNAs into tumor cells by developing a novel nano-particles, DAN. The nanoparticles exhibit an ideal anti-tumor effect combined with the OXA *in vivo*. DAN nanoparticles were based on the FDA-approved material, PEG-PLGA (24). As a result, it displayed less *in vivo* toxicity in the mouse xenograft. In brief, we identified a key gene in CRC chemoresistance *via* clinical samples and *in vitro* experiments, and develop novel and effective nanoparticles to overcome the platinum drug resistance in colon cancer.

In the survival analysis, there was not enough evidence revealing that the lower-expression of ATP7A CRC patients benefit from a better clinical prognosis in our cohort (**Supplementary Figure 1**). To find out its cause, the results may be concluded from the limited samples from our cohorts (41 patients) and advanced CRC patients enrolled in our study may

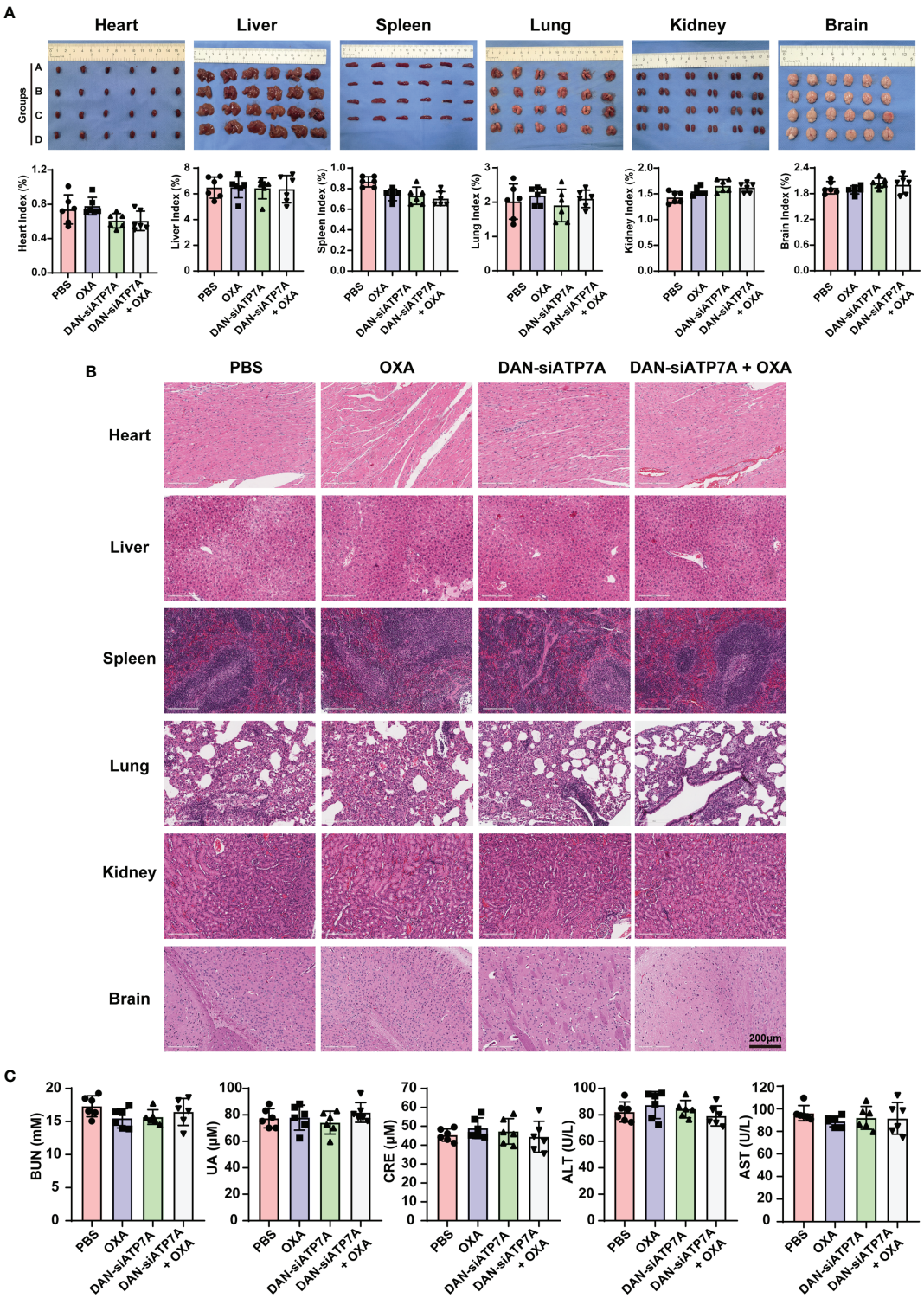


FIGURE 6 | *In vivo* toxicity analysis. **(A)** The image of organs including heart, liver, spleen, lung, kidney, and brain from the nude mice at the end of the *in vivo* study and the organ index (organ index = the weight of the organ/the weight of the mice) of the nude mice. Data were expressed as means ± SD. Group A stands for PBS; Group B stands for OXA; Group C stands for DAN-siATP7A and Group D stands for DAN-ATP7A + OXA. **(B)** The HE staining of organs. **(C)** The blood test of ALT, AST, BUN, Cr, UC of the nude mice, and no toxicity were found in our *in vivo* experiment.

have poor prognosis than the early-stage CRC patients. Despite no prognosis difference in OS analysis, the bioinformatic analysis revealed that the lower ATP7A expressed CRC patients may have a better clinical prognosis in DFS (**Supplementary Figure 2B**, $P<0.05$). Due to the conflicted conclusion of survival analysis, we implied that the ATP7A may not act as a prognostic indicator for CRC patients.

We provided the pieces of clinical evidence that the ATP7A was upregulated in OXA-resistant CRC patients compared to those patients who respond to chemotherapy (**Figure 1**). The previous researches found out the higher expression of ATP7A was correlated with the chemotherapy resistance. Samimi G et al. demonstrated that after being transfected with an ATP7A-expression construct, the human ovarian carcinoma cells also conferred resistance to DDP, CBDCA, and OXA (36). As a result, we hypothesis that higher ATP7A expression may be correlated to the OXA-based chemoresistance in CRC patients. The lower ATP7A expression CRC patients may benefit from the chemotherapy. However, due to the limited sample size of our study, it could not be concluded that the ATP7A may be a key regulator of CRC chemoresistance, and all the results of clinical analysis has no clinical implications currently. A multi-center with larger cohorts study should be conducted further to support the conclusion.

In our study, the present results indicated that knockdown of ATP7A by siRNA enhanced OXA sensitivity and reversed chemoresistance both *in vitro* and *in vivo*. *In vitro*, increased chemosensitivity and apoptosis, and decreased cell proliferation were evident in CRC cells following siRNA-mediated knockdown of ATP7A, suggesting that ATP7A is one of the important biomarkers for OXA resistance in CRC. Further, we found that the combination of OXA and siATP7A could inhibit the migration of CRC cells (**Figures 3C, D**).

Moreover, the analysis of IHC staining implied that the chemotherapy resistance CRC patients had a higher expression of ATP7A protein than the chemotherapy response patients and the metastatic CRC patients (TNM Stage IV) had a higher expression of ATP7A in tumor tissue than locally advanced CRC patients (**Figure 1B**). Our findings provide evidence that decreased drug efflux by knockdown ATP7A in CRC cells could lead up to higher tissue distribution and intracellular drug accumulation to form destructive DNA-platinum adducts which ultimately destroy cancer cells. These results all suggested that ATP7A played a vital role in the modulation of Pt-resistance.

Since when genetic interference was discovered in 1998, siRNA has been recognized as a powerful genetic interference tool to specifically silence the target genes to tackle cancer angiogenesis, invasion, and metastasis (23). Oxaliplatin therapy might have unrealized clinical benefits due to a lack of an appropriate carrier delivering siATP7A. Unfortunately, it is a great challenge for delivery of siRNA to tumors *in vivo* in consideration of the barrier of the blood circulation and poor cellular uptake (20, 21). In the present study, our strategy may provide a solution to this challenge. We explore a novel nanocarrier-based delivery of ATP7A as a therapeutic strategy for nanoparticles-mediated chemotherapy sensitization, which was based on the PEG-PLGA and DOTAP (24). Specifically, we encapsulated siRNA targeting ATP7A using DANs and confirmed that DAN-siATP7A could be effectively enriched in tumor tissue and downregulate the target gene (**Figure 4**). The therapeutic efficacy of different forms *in vivo* was verified by the enhanced cell apoptosis rate and the enhanced tumor inhibition efficacy (**Figure 5**). In addition, the combination therapy is relatively safe as confirmed by the detection of various organs and blood indexes (**Figure 6**). Let it be added here that the composition of DANs, PEG-PLGA, is a pharmaceutically approved drug for clinical by Food and Drug Administration (FDA). Yet the biosecurity and anti-tumor effect of DAN-siATP7A in OXA-resistance patients is by far less well understood. Most of these data are derived from *in vitro* drug-exposed tumor cells and in nude mice, which have not yet entered the clinical stage and need further verifications.

In conclusion, our findings demonstrate that ATP7A may act as a therapeutic target for CRC patients. The delivery of siATP7A *via* nanoparticles increases the sensitivity of CRC cells to oxaliplatin, thereby providing a new treatment strategy for CRC. However, due to the limitations in our study, such as limited cohorts from single-center retrospective study, the conclusions of clinical analysis may only implied the higher expression of ATP7A may correlated with chemo-resistance in CRC patients. All the results from clinical analysis currently have no clinical implications and needed to be further validated.

DATA AVAILABILITY STATEMENT

The original contributions presented in the study are included in the article/**Supplementary Material**. Further inquiries can be directed to the corresponding authors.

ETHICS STATEMENT

The studies involving human participants were reviewed and approved by Guangdong Provincial People's Hospital. The patients/participants provided their written informed consent to participate in this study. The animal study was reviewed and approved by Guangdong Provincial People's Hospital.

AUTHOR CONTRIBUTIONS

The study concept and design were carried out by all the authors who participate in the study. The experiments were performed by YZ, QZ, MW, and CH, YZ, QZ, and MW wrote the draft of the manuscript. All the authors conducted the critical revision of the manuscript and finally approved the version.

FUNDING

This work was supported by grants from the Science and Technology Planning Project of Guangdong Provincial People's

Hospital (Guangdong Academy of Medical Sciences, No. DFJH201913), CSCO-Roche Cancer Research Foundation (No. Y-2019Roche-190), CSCO-Haosen Research Foundation (No. Y-HS2019/2-050), the Science and Technology Planning Project of Ganzhou (No. 202101074816).

REFERENCES

1. Siegel RL, Miller KD, Fuchs HE, Jemal A. Cancer Statistics, 2021. *CA Cancer J Clin* (2021) 71(1):7–33. doi: 10.3322/caac.21654
2. Burnett-Hartman AN, Lee JK, Demb J, Gupta S. An Update on the Epidemiology, Molecular Characterization, Diagnosis, and Screening Strategies for Early-Onset Colorectal Cancer. *Gastroenterology* (2021) 160 (4):1041–9. doi: 10.1053/j.gastro.2020.12.068
3. Yelorda KL, Fu SJ, Owens DK. Analysis of Survival Among Adults With Early-Onset Colorectal Cancer. *JAMA Netw Open* (2021) 4(6):e2112878. doi: 10.1001/jamanetworkopen.2021.12878
4. Garcia-Alfonso P, Munoz Martin AJ, Ortega Moran L, Soto Alsar J, Torres Perez-Solero G, Blanco Codesido M, et al. Oral Drugs in the Treatment of Metastatic Colorectal Cancer. *Ther Adv Med Oncol* (2021) 13:17588359211009001. doi: 10.1177/17588359211009001
5. McQuade RM, Stojanovska V, Bornstein JC, Nurgali K. Colorectal Cancer Chemotherapy: The Evolution of Treatment and New Approaches. *Curr Med Chem* (2017) 24(15):1537–57. doi: 10.2174/0929867324666170111152436
6. Rad AH, Aghebati-Maleki L, Kafil HS, Abbasi A. Molecular Mechanisms of Postbiotics in Colorectal Cancer Prevention and Treatment. *Crit Rev Food Sci Nutr* (2021) 61(11):1787–803. doi: 10.1080/10408398.2020.1765310
7. Glimelius B, Stintzing S, Marshall J, Yoshino T, de Gramont A. Metastatic Colorectal Cancer: Advances in the Folate-Fluoropyrimidine Chemotherapy Backbone. *Cancer Treat Rev* (2021) 98:102218. doi: 10.1016/j.ctrv.2021.102218
8. Guo Y, Xiong BH, Zhang T, Cheng Y, Ma L. XELOX vs. FOLFOX in Metastatic Colorectal Cancer: An Updated Meta-Analysis. *Cancer Invest* (2016) 34(2):94–104. doi: 10.3109/07357907.2015.1104689
9. Jung F, Guidolin K, Lee MH, Lam-Tin-Cheung K, Zhao G, Doshi S, et al. Interventions and Outcomes for Neoadjuvant Treatment of T4 Colon Cancer: A Scoping Review. *Curr Oncol* (2021) 28(3):2065–78. doi: 10.3390/curroncol28030191
10. Rottenberg S, Disler C, Perego P. The Rediscovery of Platinum-Based Cancer Therapy. *Nat Rev Cancer* (2021) 21(1):37–50. doi: 10.1038/s41568-020-00308-y
11. Huang D, Savage SR, Calinawan AP, Lin C, Zhang B, Wang P, et al. A Highly Annotated Database of Genes Associated With Platinum Resistance in Cancer. *Oncogene* (2021) 40(46):6395–405. doi: 10.1038/s41388-021-02055-2
12. Zhou J, Kang Y, Chen L, Wang H, Liu J, Zeng S, et al. The Drug-Resistance Mechanisms of Five Platinum-Based Antitumor Agents. *Front Pharmacol* (2020) 11:343. doi: 10.3389/fphar.2020.00343
13. Lukanovic D, Herzog M, Kobal B, Cerne K. The Contribution of Copper Efflux Transporters ATP7A and ATP7B to Chemoresistance and Personalized Medicine in Ovarian Cancer. *BioMed Pharmacother* (2020) 129:110401. doi: 10.1016/j.biopha.2020.110401
14. Li YQ, Yin JY, Liu ZQ, Li XP. Copper Efflux Transporters ATP7A and ATP7B: Novel Biomarkers for Platinum Drug Resistance and Targets for Therapy. *IUBMB Life* (2018) 70(3):183–91. doi: 10.1002/iub.1722
15. Petruzzelli R, Polishchuk RS. Activity and Trafficking of Copper-Transporting ATPases in Tumor Development and Defense Against Platinum-Based Drugs. *Cells* (2019) 8(9):1–18. doi: 10.3390/cells8091080
16. Kuo MT, Chen HH, Song IS, Savaraj N, Ishikawa T. The Roles of Copper Transporters in Cisplatin Resistance. *Cancer Metastasis Rev* (2007) 26(1):71–83. doi: 10.1007/s10555-007-9045-3
17. Lai YH, Kuo C, Kuo MT, Chen HHW. Modulating Chemosensitivity of Tumors to Platinum-Based Antitumor Drugs by Transcriptional Regulation of Copper Homeostasis. *Int J Mol Sci* (2018) 19(5):1–18. doi: 10.3390/ijms19051486
18. Shanbhag V, Jasmer-McDonald K, Zhu S, Martin AL, Gudekar N, Khan A, et al. ATP7A Delivers Copper to the Lysyl Oxidase Family of Enzymes and Promotes Tumorigenesis and Metastasis. *Proc Natl Acad Sci USA* (2019) 116 (14):6836–41. doi: 10.1073/pnas.1817473116
19. Alvarez-Erviti L, Seow Y, Yin H, Betts C, Lakhal S, Wood MJ. Delivery of siRNA to the Mouse Brain by Systemic Injection of Targeted Exosomes. *Nat Biotechnol* (2011) 29(4):341–5. doi: 10.1038/nbt.1807

SUPPLEMENTARY MATERIAL

The Supplementary Material for this article can be found online at: https://www.frontiersin.org/articles/10.3389/fonc.2022.827891/full#supplementary-material

20. Liu Y, Wang J, Xiong Q, Hornburg D, Tao W, Farokhzad OC. Nano-Bio Interactions in Cancer: From Therapeutics Delivery to Early Detection. *Acc Chem Res* (2021) 54(2):291–301. doi: 10.1021/acs.accounts.0c00413
21. Kanasty R, Dorkin JR, Vegas A, Anderson D. Delivery Materials for siRNA Therapeutics. *Nat Mater* (2013) 12(11):967–77. doi: 10.1038/nmat3765
22. Nikam RR, Gore KR. Journey of siRNA: Clinical Developments and Targeted Delivery. *Nucleic Acid Ther* (2018) 28(4):209–24. doi: 10.1089/nat.2017.0715
23. Singh A, Trivedi P, Jain NK. Advances in siRNA Delivery in Cancer Therapy. *Artif Cells Nanomed Biotechnol* (2018) 46(2):274–83. doi: 10.1080/21691401.2017.1307210
24. Xu CF, Iqbal S, Shen S, Luo YL, Yang X, Wang J. Development of "CLAN" Nanomedicine for Nucleic Acid Therapeutics. *Small* (2019) 15(16):e1900055. doi: 10.1002/smll.201900055
25. Charbe NB, Amnerkar ND, Ramesh B, Tambuwala MM, Bakshi HA, Aljabali AAA, et al. Small Interfering RNA for Cancer Treatment: Overcoming Hurdles in Delivery. *Acta Pharm Sin B* (2020) 10(11):2075–109. doi: 10.1016/j.apsb.2020.10.005
26. Kang L, Gao Z, Huang W, Jin M, Wang Q. Nanocarrier-Mediated Co-Delivery of Chemotherapeutic Drugs and Gene Agents for Cancer Treatment. *Acta Pharm Sin B* (2015) 5(3):169–75. doi: 10.1016/j.apsb.2015.03.001
27. Huang C, Wang M, Wang J, Wu D, Gao Y, Huang K, et al. Suppression MGP Inhibits Tumor Proliferation and Reverses Oxaliplatin Resistance in Colorectal Cancer. *Biochem Pharmacol* (2021) 189:114390. doi: 10.1016/j.bcp.2020.114390
28. Tang Z, Li C, Kang B, Gao G, Li C, Zhang Z. GEPIA: A Web Server for Cancer and Normal Gene Expression Profiling and Interactive Analyses. *Nucleic Acids Res* (2017) 45(W1):W98–W102. doi: 10.1093/nar/gkx247
29. Schneider CA, Rasband WS, Eliceiri KW. NIH Image to ImageJ: 25 Years of Image Analysis. *Nat Methods* (2012) 9(7):671–5. doi: 10.1038/nmeth.2089
30. Schindelin J, Arganda-Carreras I, Frise E, Kaynig V, Longair M, Pietzsch T, et al. Fiji: An Open-Source Platform for Biological-Image Analysis. *Nat Methods* (2012) 9(7):676–82. doi: 10.1038/nmeth.2019
31. Huang H, Jiang CT, Shen S, Liu A, Gan YJ, Tong QS, et al. Nanoenabled Reversal of IDO1-Mediated Immunosuppression Synergizes With Immunogenic Chemotherapy for Improved Cancer Therapy. *Nano Lett* (2019) 19(8):5356–65. doi: 10.1021/acs.nanolett.9b01807
32. Wang Y, Wang Y, Qin Z, Cai S, Yu L, Hu H, et al. The Role of Non-Coding RNAs in ABC Transporters Regulation and Their Clinical Implications of Multidrug Resistance in Cancer. *Expert Opin Drug Metab Toxicol* (2021) 17 (3):291–306. doi: 10.1080/17425255.2021.1887139
33. Chen Z, Shi T, Zhang L, Zhu P, Deng M, Huang C, et al. Mammalian Drug Efflux Transporters of the ATP Binding Cassette (ABC) Family in Multidrug Resistance: A Review of the Past Decade. *Cancer Lett* (2016) 370(1):153–64. doi: 10.1016/j.canlet.2015.10.010
34. Robey RW, Pluchino KM, Hall MD, Fojo AT, Bates SE, Gottesman MM. Revisiting the Role of ABC Transporters in Multidrug-Resistant Cancer. *Nat Rev Cancer* (2018) 18(7):452–64. doi: 10.1038/s41568-018-0005-8
35. Li ZH, Zheng R, Chen JT, Jia J, Qiu M. The Role of Copper Transporter ATP7A in Platinum-Resistance of Esophageal Squamous Cell Cancer (ESCC). *J Cancer* (2016) 7(14):2085–92. doi: 10.7150/jca.16117
36. Samimi G, Varki NM, Wilczynski S, Safaei R, Alberts DS, Howell SB. Increase in Expression of the Copper Transporter ATP7A During Platinum Drug-Based Treatment Is Associated With Poor Survival in Ovarian Cancer Patients. *Clin Cancer Res* (2003) 9(16 Pt 1):5853–9.

Conflict of Interest: The authors declare that the research was conducted in the absence of any commercial or financial relationships that could be construed as a potential conflict of interest.

Publisher's Note: All claims expressed in this article are solely those of the authors and do not necessarily represent those of their affiliated organizations, or those of the publisher, the editors and the reviewers. Any product that may be evaluated in

this article, or claim that may be made by its manufacturer, is not guaranteed or endorsed by the publisher.

Copyright © 2022 Zhou, Zhang, Wang, Huang and Yao. This is an open-access article distributed under the terms of the Creative Commons Attribution License (CC BY). The use, distribution or reproduction in other forums is permitted, provided the original author(s) and the copyright owner(s) are credited and that the original publication in this journal is cited, in accordance with accepted academic practice. No use, distribution or reproduction is permitted which does not comply with these terms.

frontiers | Frontiers in Oncology

CORRECTION
published: 27 June 2022
doi: 10.3389/fonc.2022.916983

Corrigendum: Effective Delivery of siRNA-Loaded Nanoparticles for Overcoming Oxaliplatin Resistance in Colorectal Cancer

Yue Zhou[1,2,3†], *Qing Zhang*[1,2,3,4†], *Minjia Wang*[1,2,3,5†], *Chengzhi Huang*[2,3,5*†] *and Xueqing Yao*[1,2,3,5*]

[1] The Second School of Clinical Medicine, Southern Medical University, Guangzhou, China, [2] Department of Gastrointestinal Surgery, Ganzhou Municipal Hospital, Ganzhou, China, [3] Department of Gastrointestinal Surgery, Department of General Surgery, Guangdong Provincial People's Hospital, Guangdong Academy of Medical Sciences, Guangzhou, China, [4] Department of Gastrointestinal and Anorectal Surgery, The First People's Hospital of Zhaoqing, Zhaoqing, China, [5] School of Medicine, South China University of Technology, Guangzhou, China

Keywords: oxaliplatin, chemoresistance, siRNA delivery, colorectal cancer, ATP7A

OPEN ACCESS

Edited and reviewed by:
Zeming Liu,
Huazhong University of Science and Technology, China

***Correspondence:**
Xueqing Yao
syyaoxueqing@scut.edu.cn
Chengzhi Huang
huangchengzhi93@hotmail.com

†*These authors have contributed equally to this work*

Specialty section:
This article was submitted to Pharmacology of Anti-Cancer Drugs, a section of the journal Frontiers in Oncology

Received: *10 April 2022*
Accepted: *09 May 2022*
Published: *27 June 2022*

Citation:
Zhou Y, Zhang Q, Wang M, Huang C and Yao X (2022) Corrigendum: Effective Delivery of siRNA-Loaded Nanoparticles for Overcoming Oxaliplatin Resistance in Colorectal Cancer. Front. Oncol. 12:916983. doi: 10.3389/fonc.2022.916983

A Corrigendum on:

Effective Delivery of siRNA-Loaded Nanoparticles for Overcoming Oxaliplatin Resistance in Colorectal Cancer

By Zhou Y, Zhang Q, Wang M, Huang C and Yao X (2022). Front. Oncol. 12:827891. doi: 10.3389/fonc.2022.827891

In the original article, there was a mistake in **Figure 3** as published. While preparing the figures, the labels of the bar charts in **Figure 3** were misspelled. The corrected **Figure 3** appears below.

In the published article, there was also an error in affiliation 3. Instead of "Department of Gastrointestinal Surgery, Department of General Surgery, Guangdong Provincial People's Hospital, Guangdong Academy of Medical Sciences, School of Medicine, South China University of Technology, Guangzhou, China", it should be "Department of Gastrointestinal Surgery, Department of General Surgery, Guangdong Provincial People's Hospital, Guangdong Academy of Medical Sciences, Guangzhou, China".

There was a further error as an affiliation was omitted for authors Minjia Wang, Chengzhi Huang and Xueqing Yao. These authors should also have affiliation 5 – "School of Medicine, South China University of Technology, Guangzhou, China".

The authors apologize for these errors and state that this does not change the scientific conclusions of the article in any way. The original article has been updated.

Publisher's Note: All claims expressed in this article are solely those of the authors and do not necessarily represent those of their affiliated organizations, or those of the publisher, the editors and the reviewers. Any product that may be evaluated in this article, or claim that may be made by its manufacturer, is not guaranteed or endorsed by the publisher.

Copyright © 2022 Zhou, Zhang, Wang, Huang and Yao. This is an open-access article distributed under the terms of the Creative Commons Attribution License (CC BY). The use, distribution or reproduction in other forums is permitted, provided the original author(s) and the copyright owner(s) are credited and that the original publication in this journal is cited, in accordance with accepted academic practice. No use, distribution or reproduction is permitted which does not comply with these terms.

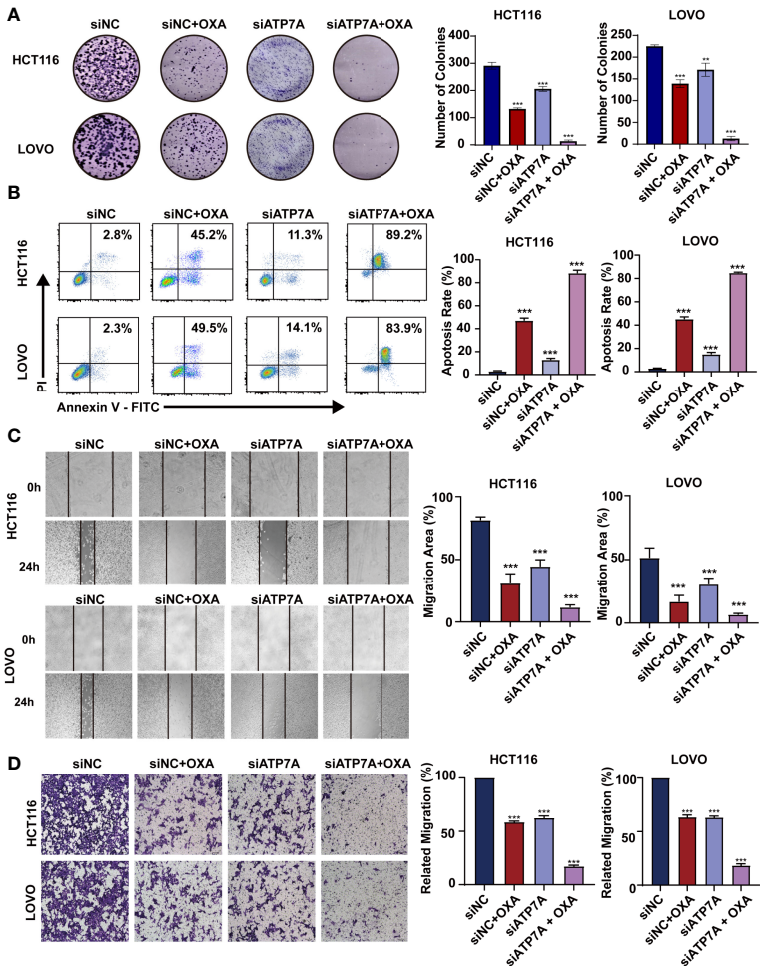


FIGURE 3 | Knockdown of ATP7A expression may inhibit cancer tumorigenesis *in vitro* **(A)** Colony formation assays in HCT116 and LOVO cells. **(B)** A flow cytometer was performed to assess the apoptosis rate of HCT116 and LOVO cells. **(C)** Wound healing assay of HCT116 and LOVO cells. **(D)** Transwell assay was performed to evaluate the invasion of HCT116 and LOVO cells. $^{**}P < 0.01$ and $^{***}P < 0.001$ when compared to the control group.

frontiers in Bioengineering and Biotechnology

ORIGINAL RESEARCH
published: 28 February 2022
doi: 10.3389/fbioe.2022.831288

Fabrication of *In Situ* Grown Hydroxyapatite Nanoparticles Modified Porous Polyetheretherketone Matrix Composites to Promote Osteointegration and Enhance Bone Repair

Ningning Wang[1], *Desheng Qi*[2], *Lu Liu*[3], *Yanlin Zhu*[4], *Hong Liu*[5] *and Song Zhu*[1]*

[1]Department of Prosthetic Dentistry, School and Hospital of Stomatology, Jilin University, Changchun, China, [2]College of Chemistry, Engineering Research Center of Special Engineering Plastics, Ministry of Education, Jilin University, Changchun, China, [3]Department of Stomatology, China-Japan Friendship Hospital, Jilin University, Changchun, China, [4]Department of Oral Implantology, School and Hospital of Stomatology, Jilin University, Changchun, China, [5]Department of General Dentistry, School and Hospital of Stomatology, Jilin University, Changchun, China

OPEN ACCESS

Edited by:
Zeming Liu,
Huazhong University of Science and Technology, China

Reviewed by:
Kelong Ai,
Central South University, China
Xiaoyuan Wang,
Central South University Changsha, China in collaboration with KA Yunlu Dai,
University of Macau, China

***Correspondence:**
Song Zhu
zhusong1965@163.com

Specialty section:
This article was submitted to Biomaterials, a section of the journal Frontiers in Bioengineering and Biotechnology

Received: 08 December 2021
Accepted: 17 January 2022
Published: 28 February 2022

Citation:
Wang N, Qi D, Liu L, Zhu Y, Liu H and Zhu S (2022) Fabrication of In Situ Grown Hydroxyapatite Nanoparticles Modified Porous Polyetheretherketone Matrix Composites to Promote Osteointegration and Enhance Bone Repair. Front. Bioeng. Biotechnol. 10:831288. doi: 10.3389/fbioe.2022.831288

The repairment of critical-sized bone defects is a serious problem that stimulates the development of new biomaterials. In this study, nanohydroxyapatite (nHA)-doped porous polyetheretherketone (pPEEK) were successfully fabricated by the thermally induced phase separation method and hydrothermal treatment. Structural analysis was performed by X-ray diffraction. The water contact angles and scanning electron microscopy were measured to assess physical properties of surfaces. The mechanical strength of the composites is also determined. Microcomputed tomography is used to characterize the nHA content of the composites. The *in vitro* bioactivity of the composites with or without nHA was investigated by using murine pre-osteoblasts MC3T3-E1, and the results of cytotoxicity and cell proliferation assays revealed that the cytocompatibility of all specimens was good. Adherence assays were employed to examine the adhesion and morphology of cells on different materials. However, nHA-doped composites induced cell attachment and cell spreading more significantly. Osteogenic differentiation was investigated using alkaline phosphatase activity and alizarin red staining, and these *in vitro* results demonstrated that composites containing nHA particles enhanced osteoblast differentiation. Its effectiveness for promoting osteogenesis was also confirmed in an *in vivo* animal experiment using a tibial defective rat model. After 8 weeks of implantation, compared to the pure PEEK and pPEEK without nHA groups, the nHA-pPEEK group showed better osteogenic activity. The results indicate that the nHA-pPEEK composites are possibly a well-designed bone substitute for critical-sized bone defects by promoting bone regeneration and osteointegration successfully.

Keywords: nanohydroxyapatite, polyetheretherketone, differentiation, animal model, osteointegration

1 INTRODUCTION

Bone defects, which are caused by trauma, tumor surgery, and inflammation, affect the quality of life of patients seriously and remain a major clinical challenge (Huang et al., 2019; Xie et al., 2020). Autologous bone grafts are considered the gold standard as bone implants due to their ideal osteo-inductive properties, preventing the histocompatibility problem. However, the associated risk of donor site disease and limited supplementation are disadvantages of the treatment (Beigi et al., 2019; Kohli et al., 2021). Metals (e.g., titanium alloys) are widely used as prostheses because of the high mechanical strength and excellent frictional resistance (Yan et al., 2018). Some disadvantages, however, have been pointed out for metal implants: image distortion in postoperative observations, stress shielding effect on the bone around the implant, and the need of additional surgery for removal (Hughes et al., 2018; Ko et al., 2021).

In recent years, there has been rising interest to develop the new medical devices based on polyetheretherketone (PEEK) because of its good biocompatibility and mechanical properties that can match the cortical bone tissue (Vaezi et al., 2016; Feng et al., 2019). Unlike metal implants, which create artifacts in radiography, computed tomography (CT), and magnetic resonance imaging (MRI), PEEK does not generate such artifacts (Fukuda et al., 2018; Sunarso et al., 2020). However, PEEK is not a material with bioactivity, which possesses poor osseointegration, owing to its bioinert nature (Dai et al., 2019). Therefore, the development of new modification techniques to enhance the bioactivity of PEEK is an important requirement.

Several strategies have been studied to improve the bioinert nature of PEEK with bioactive materials (Wan et al., 2020), and synthetic hydroxyapatite (HA), which is most similar to mature bone, has been widely applied as a bone substitute for the requirement of bone defects in orthopedic surgery (Pujari-Palmer et al., 2017; Zakrzewski et al., 2020). To enhance the osteointegration of PEEK-based implants, several techniques have already been developed for various orthopedic uses: 1) the incorporation of HA into the PEEK matrix, 2) coating PEEK implants with HA, and 3) adding porosity into PEEK implants (Zhong et al., 2019). Due to the natural structure of native bone tissues, pores in implants play a key role in bone regeneration (Lin et al., 2019) because biocompatible porous implants that mimic the natural bone structure have given the most hopeful results due to their promoting effect on cell proliferation and neovascularization (Paraš et al., 2020). Among these methods, the use of HA combined with the porosity has been considered a desirable technology for improving the osteointegration of PEEK-based devices (Torstrick et al., 2018). Some investigators have reported that the incorporation of bioactive molecules and porosity to PEEK are effective approaches to improve the osteointegration of PEEK-based implants (Chubrik et al., 2020; Conrad and Roeder, 2020; Swaminathan et al., 2020; Huang et al., 2021; Venkatraman et al., 2021).

In summary, two major methods have been performed to improve the biological activity of porous PEEK (po-PEEK) materials with the synthetic HA. One approach is to fabricate PEEK-based composites by incorporating bioactive molecules into PEEK substrates, but this may influence the mechanical strength. Another strategy is to activate the surface of PEEK with HA coating. However, PEEK surface coatings may lead to insufficient cohesion and delamination, resulting in tissue inflammation (Han et al., 2019).

The objective in this study is to prepare a new kind of porous composite based on porogens in a PEEK matrix by using a novel experimental technique. Subsequently, HA is generated *in situ* inside the porosity of Po-PEEK biomaterial *via* hydrothermal synthesis, aiming to develop a bioactive composite with good biological performances for bone regeneration and reconstruction. A schematic diagram of the experimental protocol is illustrated in **Scheme 1**.

2 MATERIALS AND METHODS

2.1 Preparation of Porous PEEK

2.1.1 Fabrication

Briefly, diphenyl sulfone was added into a 1 L round-bottom flask and heated to 140°C until completely dissolved. PEEK powder (melt flow rate = 13, offered by Jilin University Special Plastic Engineering Research Center) was added and slowly warmed to 350°C. Then, the solution was stirred until the powder was dissolved completely. Finally, sodium chloride was added, and the solution continued to be stirred until it was homogeneous. The product was poured into the mold and cooled to room temperature. Subsequently, the resulted polymer was further purified by Soxhlet extractions for 3 days with acetone and distilled water to remove diphenyl sulfone and excess inorganic salts. Throughout the manuscript, two types of Po-PEEK with different solid contents were synthesized, and different degrees of compression were processed to improve the mechanical properties. Materials were divided into four groups: PK50-20% (50% solid content and 20% compression), PK50-10% (50% solid content and 10% compression), PK50 (50% solid content), and PK40 (40% solid content). The solid content was calculated as shown below:

$$Solid\ content = \frac{M_{PEEK}}{M_{PEEK} + M_{diphenyl\ sulfone}}$$

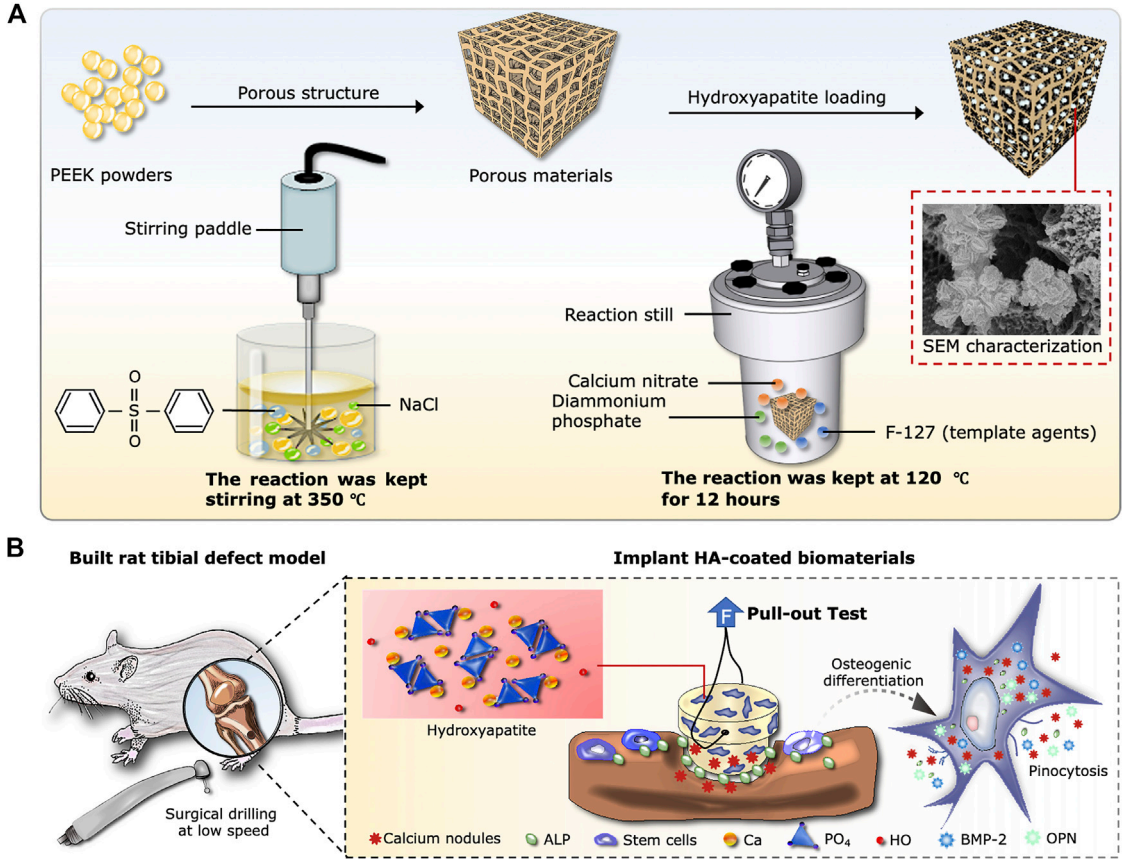
Where M_{PEEK} and $M_{diphenyl\ sulfone}$ represented the mass of PEEK powder and diphenyl sulfone in the reaction system, respectively.

2.1.2 SEM Observation

The material was broken up with liquid nitrogen, and the cross-sections were sputtered with gold for 60 s. The samples were then observed and photographed with a scanning electron microscope (SEM, Hitachi S4800; Japan).

2.1.3 Density and Porosity

The density of materials was tested by a density/specific gravity meter DA-510 (Kyoto Electronics Manufacturing, Kyoto, Japan) at room temperature and the porosity was calculated based on the formula as follows:



SCHEME 1 | Design of the experiment. **(A)** Schematic diagram of synthesis process, including the Po-PEEK with thermally induced phase separation and nHA with hydrothermal methods. **(B)** Implantation procedure of rat tibial defect model and cellular responses around the host bones after the operation.

$$P = 1 - \frac{\rho}{\rho_0}$$

where P denoted the porosity of fabricated material, and ρ indicated the density of the material in its natural state, and ρ_0 represented the absolute solid density of this material.

2.1.4 Mechanical Strength

The materials were cut into 1 cm cubes for tests of mechanical properties, with an Instron universal tester 5,966 (Instron, Norwood, MA, United States).

2.2 Fabrication of Nanohydroxyapatite-Doped Porous PEEK

2.2.1 Synthesis Process

The nanohydroxyapatite (nHA) was synthesized in the laboratory *via* a hydrothermal treatment method. Specifically, di-ammonium hydrogen phosphate (AR grade) was dissolved in 10 ml of Millipore water, and Po-PEEK with 50% solid content was immersed in it under vacuum to make the solution infiltrate the pores of the samples. Afterwards, the materials were frozen at −20°C and lyophilized. Calcium nitrate and pluronic F127 were dissolved in 10 ml of Millipore water and stirred until complete homogenization. Pluronic F127 was selected as a soft template to obtain the porous structure (Gong J. et al., 2020). The lyophilized samples were immersed in the solution of calcium nitrate under vacuum to make theoluteion infiltrate the pores again, and the precipitation was carried out by adding di-ammonium hydrogen phosphate dropwise to the calcium nitrate solution under constant stirring, followed by being transferred into reaction kettles at 120°C for about 12 h. Following the termination of the experiment, all samples were washed with distilled water to remove remaining salts and Pluronic F127, keeping the samples dried at 60°C in the vacuum oven.

2.2.2 SEM Observation

The operation was performed essentially as described previously.

2.2.3 Water Contact Angle Test

The water contact angle of the sample surface was analyzed by the contact angle-measuring instrument (DSA25, Kruss, Germany). The test materials were then cut into samples of 20 mm length, 10 mm width, and an average thickness of 2 mm. The droplets were laid onto the sample surfaces, and the images were captured using the camera. The contact angle was measured by recording the contact angle values.

2.2.4 X-Ray Diffraction Analysis (XRD)

The synthesized nHA powders on an XRD grid were exposed to the measurements, and the structures of which were characterized by using an X-ray diffract meter (XRD-6000; Shimadzu, Tokyo, Japan) in the 2θ range from 10° to 80° at a scanning rate of 10°/min.

2.2.5 Experiment Sizes of Samples

The experiments were conducted using two different sizes of materials. For *in vivo* experiments, the samples were 1 mm thick and 10 mm in diameter. *In vivo* samples were T-shaped columns, with 3 mm diameter at the bottom and 4 mm diameter at the top. Both sections measured 2 mm in length for a total length of 4 mm. The top section had a 0.75 mm diameter transverse hole for pull-out testing. **Figure 1A** shows a schematic of this appearance.

2.3 *In Vitro* Assays

2.3.1 Cytotoxicity Assay

In vitro cytotoxicity was measured by MTT assays with MC3T3-E1 osteoblasts, which were purchased from the American Type Culture Collection (Manassas, VA, United States). The cells were grown in DMEM with 10% fetal bovine serum (FBS) and 1% penicillin–streptomycin (all Sigma-Aldrich, MO, United States). The cells were incubated at 37°C and 5% CO_2. The experiment was conducted with extracts of all groups. Cells were seeded into 96-well cell culture plates at a density of 10^4 cells/well and routinely incubated. After 24 h, the medium was removed and replaced with the prepared extracts, and culture was continued for another 24 h. Cell viability was tested using the MTT assay kit (Solarbio, Beijing, China) according to the manufacturer's instructions. To display the cell viability more intuitively, the live/dead staining was carried out with Calcein-AM/PI Double Stain Kit (Solarbio, Beijing, China). Live cells were stained in green by Calcein-AM, whereas dead cells were stained red by PI. The staining results were captured under an inversion fluorescence microscope (BX51WI; Olympus, Tokyo, Japan).

2.3.2 Cell Proliferation Activity

Cells were seeded into different materials with a density of 2×10^3 /well. Cell proliferation was performed according to the CCK8 kit (CCK8, Dojindo, Japan) manufacturer's protocol on 1, 3, and 5 days.

2.3.3 Cell Adhesion Evaluation

For each group, 4×10^4 cells were seeded onto the different samples, cultured for 24 h. The cell morphology was observed with SEM. In detail, the cells were rinsed with phosphate-buffered saline (PBS) and then fixed with 2.5% glutaraldehyde for 2 h. After the removal of the fixative, samples were rinsed with PBS again. Subsequently, dehydration was carried out with the gradient-ethanol method, with critical point drying in CO_2 and gold coating. The cell morphology was visualized *via* SEM and photographed. To further validate the impact of the materials on cell morphology and cytoskeleton organization, the fluorescence staining of actin cytoskeleton was performed. In brief, cells were fixed with 4% paraformaldehyde (PFA) for 15–20 min, and then fixed cells were stained with FITC-phalloidin and DAPI (all Sigma-Aldrich, MO, United States) for cytoskeleton and cellular nuclei staining, respectively. Images were captured and recorded with the confocal laser scanning microscope (Fluo View FV-1000; Olympus, Tokyo, Japan).

2.3.4 Cell Seeding Efficiency

To investigate the adhesive ability of cells on the materials over short time periods, the percent attachment was calculated after 4 h co-culturing time. MC3T3-E1 cells were seeded onto the materials at a density of 10^5 cells/sample and incubated for 4 h. The medium was removed, and the cells were rinsed with PBS collected into the centrifuge tubes. Then, the residual cells on the materials were digested with trypsin (Solarbio, Beijing, China) and suspended in a suitable volume of culture medium, followed by counting with a cell-counting plate. The cell seeding efficiency was calculated as follows:

$$\eta = \frac{X}{X_0}$$

where η indicates the seeding efficiency, X the number of the residual cells, and X_0 the initial number of cells seeded onto the samples.

2.4 Osteogenic Differentiation *in vitro*

MC3T3-E1 cells, which are pre-osteoblast derived from mouse calvaria, are used as model cells, being capable of differentiating to mature mineralizing osteoblasts. In this study, once the cells reached confluence, the culture medium was switched to osteogenesis inductive medium, composed of culture medium supplemented with 10 mM β-glycerophosphate, 10 nM dexamethasone, 50 μg/ml ascorbic acid (all Sigma-Aldrich, MO, United States).

2.4.1 Alkaline Phosphatase Activity

MC3T3-E1 cells were seeded onto the different sample surfaces at a density of 2×10^4 cells/well. The analysis of ALP activity and ALP staining was performed after osteogenically induction for 7 and 14 days. ALP was stained using an ALP staining kit (Beyotime, Shanghai, China) according to the manufacturers' instructions. The intracellular ALP activity was also evaluated quantitatively. According to the manufacturers' protocols, the BCA kit (Beyotime, Shanghai, China) was used to determine the total protein content and ALP activity was investigated by an ALP activity kit (Jiancheng, Nanjing, China).

2.4.2 Alizarin Red s Staining

Detection of mineral deposition was performed using alizarin red staining and semi-quantification method. Cells were seeded onto the sample surfaces at a density of 2×10^4 cells/well and cultured for 21 days with osteogenic medium. For ARS staining, cells were fixed in 4% paraformaldehyde and stained with 1% ARS (Solarbio, Beijing, China) for about 30 min. Images of the stained materials were taken by using a scanner (Perfection V600I; Epson, United States). To quantify calcium deposition,

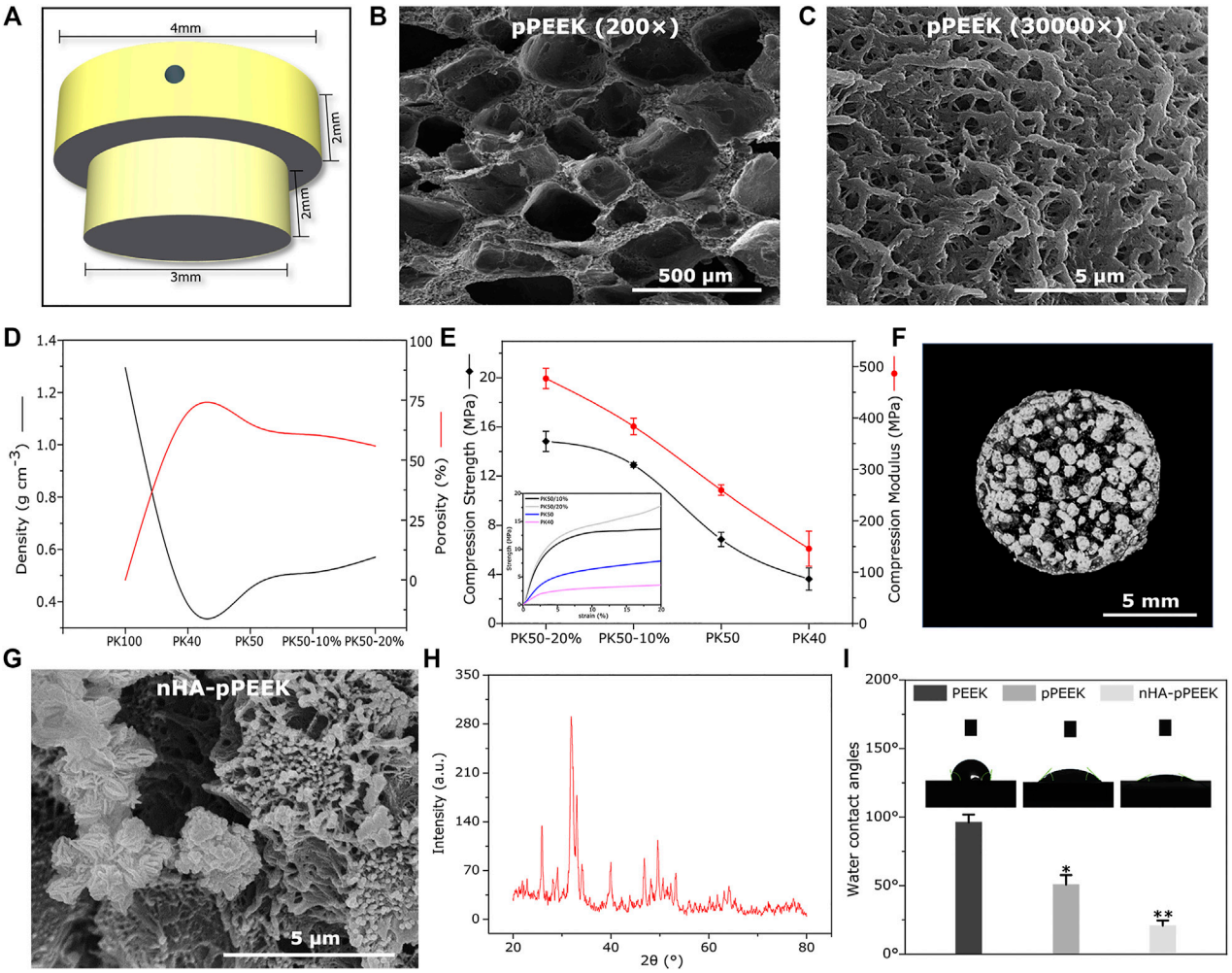


FIGURE 1 | Characterization. **(A)** 3D schematic of the implant material **(B,C)** SEM images of porous materials with different magnification. **(D)** Density and porosity of all groups with different solid content and compressive degrees. **(E)** Mechanical strength of all groups with different solid content and compressive degrees. **(F)** Micro-CT image of the material in the PK50-20% group. **(G)** SEM picture of synthetic nHA. **(H)** XRD diffractogram for samples of synthetic nHA. **(I)** The water contact angle analysis of the different samples.

materials with cells were in treatment with 10% (v/v) cetylpyridinium chloride monohydrate (Aladdin, Shanghai, China) aqueous solution to extract the ARS dye, quantified at an OD of 562 nm (Gong L. et al., 2020).

2.5 Osteogenic Assay *in vivo*

2.5.1 Rat Tibial Defect Model

Osteointegration of surfaces was evaluated by using the implant-plug model, creating the defective area in the proximal tibia of the rat. All surgical processes were approved by the Institutional Animal Care and Use Committee of Jilin University (IACUC No. 20210507-02). A total of 15 male Sprague–Dawley rats (n = 5) were in use (Weitong Lihua, Beijing, China). Animals were 12 weeks old and their mean body weight was 397 g. Animals were pre-anesthetized with isoflurane, and subsequently, an intraperitoneal injection of a urethane/acepromazine maleate mix was carried out to anesthetize the animal. Both hind limbs were prepared, and a 1 cm incision was made, with muscle released and the medial collateral ligament transected. The bone surfaces were exposed, and a 2.5 mm puncher (Integra Miltex, Plainsboro, NJ, United States) was used to generate holes in the bone tissues. Each implant was pressed into the hole, and it was made sure that the lip of the implant was flushed on the cortex. The incisions were sutured in a routine manner. Each animal was implanted one material in each leg, and experimental groups were randomized between animals and legs. All animals were euthanized after 8 weeks by carbon dioxide asphyxiation. Animal samples were fixed in PFA until further testing.

2.5.2 Small Animal Microcomputed Tomography (μCT)

All samples were scanned with μCT prior to biomechanical testing and histologic examination. All the samples were examined using a μCT system (Bruker, Kontich, Belgium) to evaluate the amount of new-formed bones. Three-dimensional

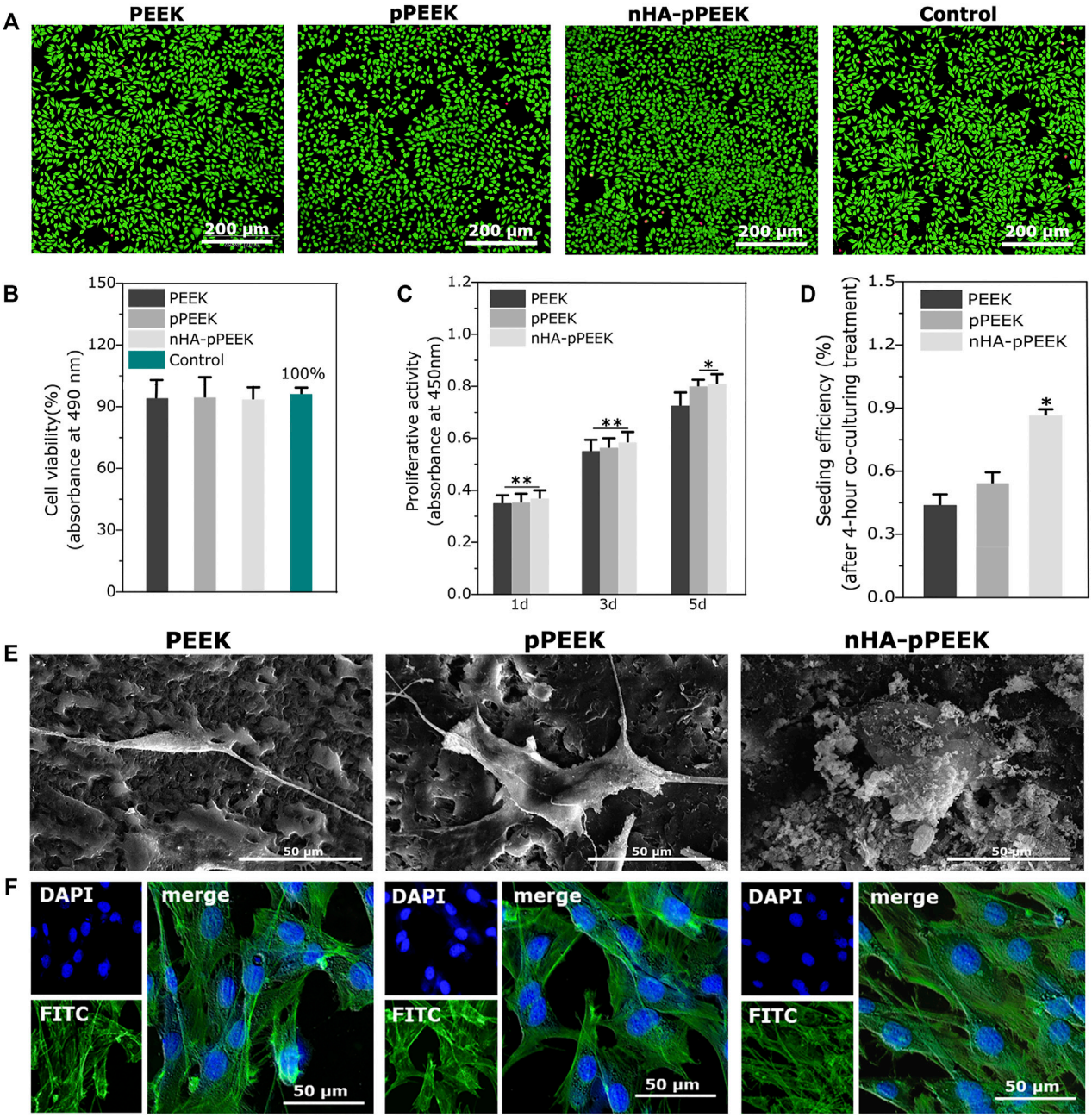


FIGURE 2 | Biocompatibility of prepared materials. **(A)** Live/dead cell staining for evaluation of different extracts from all groups. **(B)** Cell cytotoxicity quantitative measurement by the MTT assay. **(C)** Analysis of cell proliferation on different surfaces of all groups. **(D)** Seeding efficiency for MC3T3-E1 cells on the different materials. **(E)** Cell morphology in SEM of MC3T3-E1 osteoblast cells after co-culture with different samples. **(F)** Fluorescent staining of cells with FITC-phalloidin (actin cytoskeleton, green) and DAPI (nucleus, blue).

(3D) images of μCT were performed using the CTVox software, and bone regeneration was expressed as the bone volume/tissue volume (BV/TV) ratio and trabecular number (Tb. N) using Dataviewer and CTAn (all Brucker, Kontich, Belgium).

2.5.3 Pull-Out Test

A biomechanical pull-out test was carried out to assess the osteointegration for each implant surface. All pullout tests were conducted using a universal testing machine (Instron 5500R, MA, United States). Each tibia was secured with a custom fixture, and the implant was linked to a 100 N load cell by passing a piano wire through the prepared hole. Pre-loaded samples (1.0 N) were placed to a constant tensile displacement rate of 0.1 mm/s. The tensile force is the maximum load reached before implant dislodgement or failure.

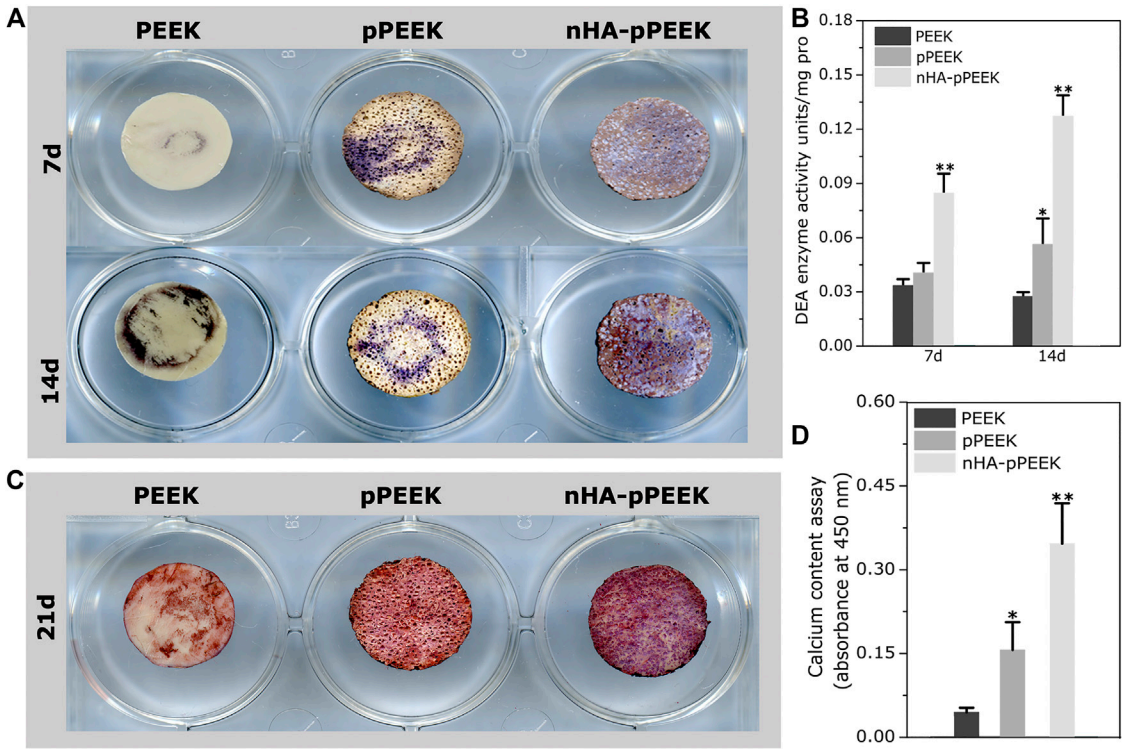


FIGURE 3 | Osteogenic differentiation of MC3T3-E1 cells. **(A)** ALP staining assays of cells on the different materials after 7 and 14 days co-culture time. **(B)** ALP activity in cell lysates collected from cells co-cultured with different materials. **(C)** ARS staining of cells on the different materials. **(D)** Quantification of ARS staining in **(C)**.

2.5.4 Surface Patterns of Implants

Surface changes of implants were analyzed using SEM-EDX (energy-dispersive X-ray) system. SEM was used to observe and compare the implant surface morphology before and after implantation. Elemental analysis was performed using an EDX spectrometer for carbon, oxygen, calcium, and phosphorus, which represented osteogenesis-related elemental types.

2.5.5 Histological and Immunohistochemical Analysis

After pull-out testing, the samples collected for histological analysis were fixed in 4% formalin and decalcified with 10% EDTA for 16 weeks until fully decalcified. After decalcification, all the specimens were paraffin-embedded and sectioned at 4 μm thickness and subjected to staining for histological evaluation. Histological analyses were conducted using hematoxylin and eosin (HE) staining and Masson's trichrome (MTC) staining. Immunohistochemical staining for the bone morphogenetic protein-2 (BMP-2) and osteocalcin (OCN) of tissue sections was performed using a standard, indirect three-step immunoperoxidase technique.

2.6 Data Analysis

Statistical significance was determined by the independent-sample *t*-test for the comparison of two groups and one-way ANOVA for comparison of three or more groups. $p < 0.05$ was taken to indicate statistical significance, $^{*}p < 0.05$ and $^{**}p < 0.01$.

3 RESULTS

3.1 Material Characterization

Po-PEEK materials obtained from the thermally induced phase separation technology are characterized by SEM, and the findings are reported in **Figures 1B,C** with two different magnifications, showing a network of well-connected pores with different dimensions. **Figure 1D** shows the differences and trends in the densities and porosity of different groups, indicating that the decline of densities is greater in the PK40 group (40% solid content), and that of PK50 (50% solid content) is rebounded somewhat. However, the densities of PK50 are increased with increasing degrees of compression, where PK50-10% or PK50-20% means that Po-PEEK with 50% solid content is compressed by 10% or 20%. The porosities as expected, show an opposite trend with the densities in the same groups. The mechanical strength tests of different groups are displayed in **Figure 1E**, and these results are consistent with the density results in the trend of change. Taken together, the PK50-20% group is the best outcome for density, porosity, and strength as the bone substitute materials. Therefore, PK50-20% was chosen for the subsequent experiments (pPEEK). For samples doped with nHA particles, a CT analysis of the composites (nHA-pPEEK) is presented in **Figure 1F**. As can be seen, HA nanoparticles embedded in pPEEK were clearly visible, showing the high-density shadows. The SEM image of nHA crystals is presented in **Figure 1G**, indicating that the synthetic

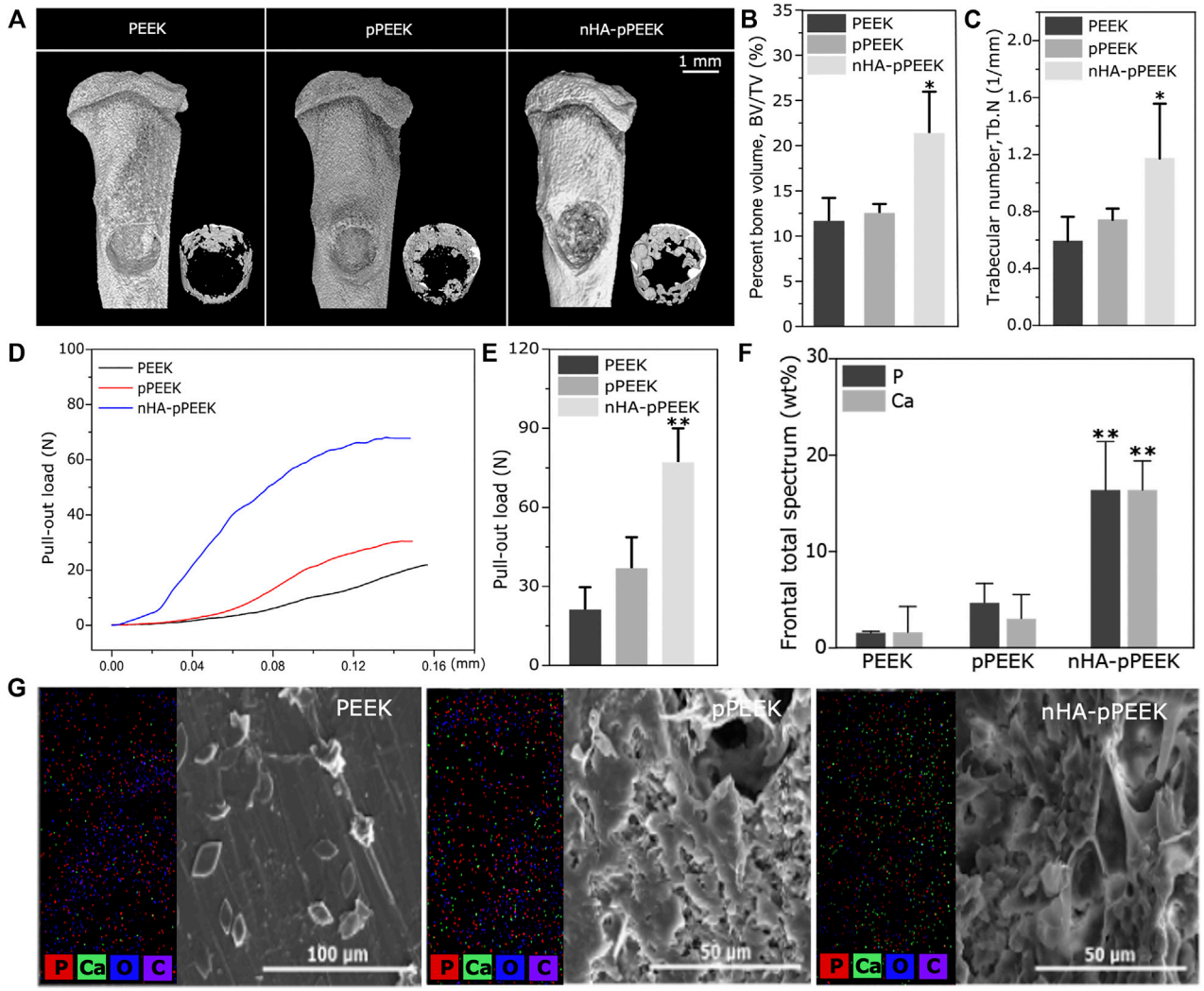


FIGURE 4 | *In vivo* analysis on osseointegration. **(A)** Three-dimensional images obtained from μCT reconstruction. Overall pattern of tibia (upper); new bone in the defect part (lower). **(B)** BV/TV, and **(C)** Tb. N of the defective aera calculated using accessory software. (D) Pull-out strength of the implanted materials in all groups, having different effects on osseointegration. **(E)** The maximum values of pull-out load taken for quantitative analysis. **(F)** Quantitative analyses of phosphorus and calcium. **(G)** The surface composition of each sample analysis by SEM-EDX system, including SEM images and distribution maps of the elements of carbon, oxygen, phosphorus, and calcium.

nHA particles occur in the form of crystal clusters and the mean length of a single crystal is about 300 nm with a needle shape. The XRD result shows HA typical diffraction peaks and confirms the nucleation of HA in all samples (**Figure 1H**). Appropriate hydrophilic surfaces will be more conducive to initial cell attachment (Chen Y. et al., 2017). The hydrophilic–hydrophobic property of the different materials was characterized by water static contact angles (**Figure 1I**). The contact angle analysis shows 99° on the material surface of the control group while showing 50° and 21° on the material surfaces of the pPEEK and nHA-pPEEK groups. It is generally believed that contact angles greater than 90° indicate hydrophobic properties, while smaller than 45° denotes clearly hydrophilic ones (Peters, 2017). Thus, as far as hydrophilic properties, statistically significant difference is observed among the control groups (PEEK and pPEEK) and experimental groups (nHA-pPEEK) ($p < 0.01$). Interestingly, the hydrophilic ability of pPEEK is better than PEEK ($p < 0.05$), which means that the porous structure may also improve the hydrophobicity of the original biomaterial.

3.2 Cellular Compatibility

The conditions of the cultures contacted with extracts from the materials (indirect methods) are assessed using image analysis and quantitative analysis. Results are presented in **Figures 2A,B**), and all groups do not show any toxicity, thus showing that the synthetic materials are cell compatible completely. To investigate possible influences of the material surface on the proliferation of the cells, CCK8 assessment is taken, and the results are shown in **Figure 2C**. The cell proliferation in each group increases based on the culturing time, and all groups show higher values than the

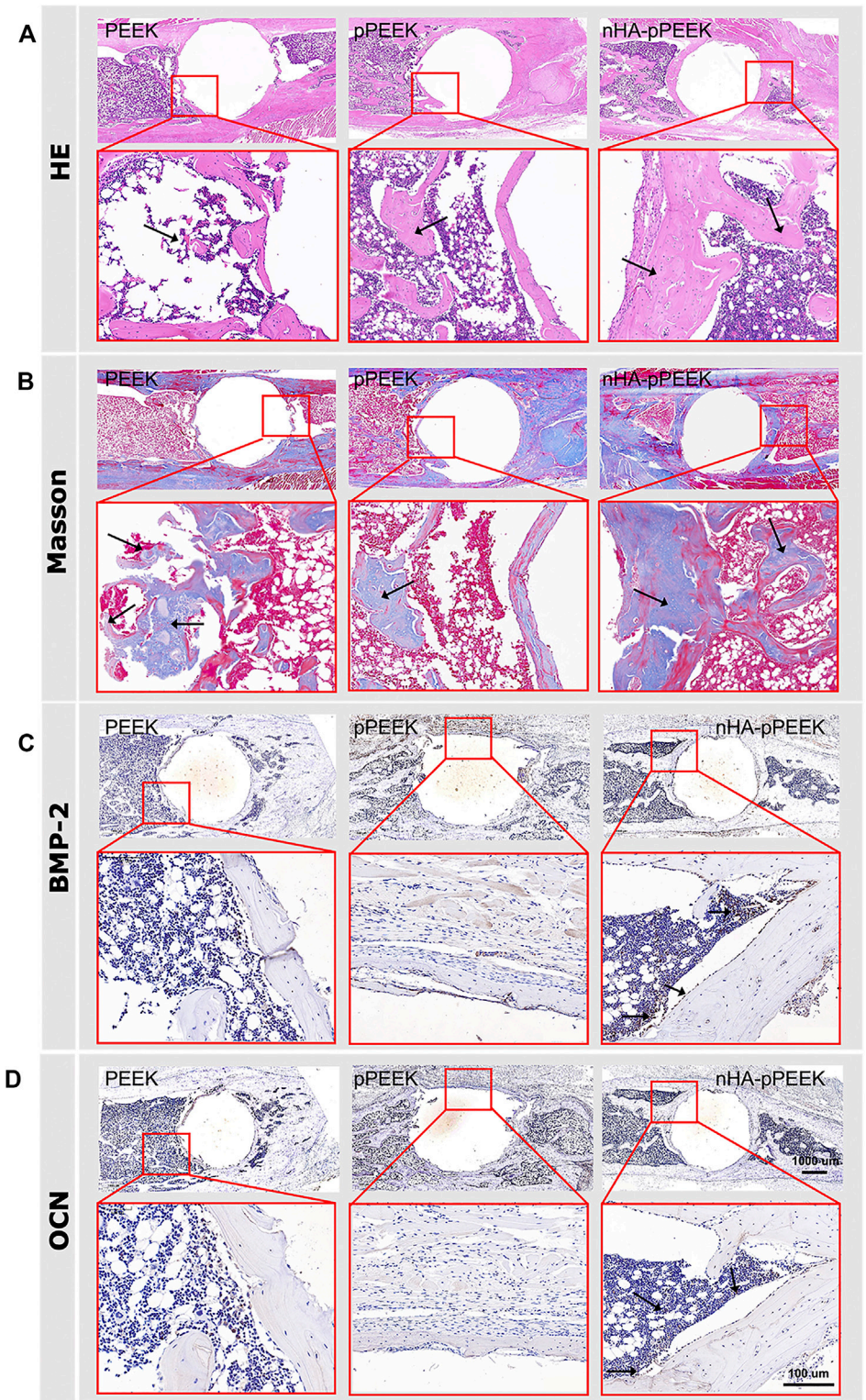


FIGURE 5 | Histological analysis. **(A)** Representative displays of hematoxylin–eosin (HE) staining of tibia tissue sections, revealing that nHA-pPEEK composites markedly promoted new bone formation (black arrows). **(B)** Results of MTC staining for the collagenous fiber distinguished as blue (black arrows), showing that the experimental group had a large number of blue collagen fibrils and fibrous tissue. **(C)** Results of BMP-2 protein immunolocalization *via* immunohistochemistry staining to make a successful differential diagnosis (black arrows). **(D)** OCN immunolocalization *via* immunohistochemistry staining to make a successful differential diagnosis (black arrows).

frontier group ($p < 0.01$). On day 5, pPEEK and nHA-pPEEK groups show higher values than the PEEK control group ($p < 0.05$), which means that a porous structure may promote the ability of cell proliferation, but nHA does not show apparent superior performance. Cell seeding efficiency is a cell adherence assay to evaluate the effect of materials on cell adhesion. From the results (**Figure 2D**), nHA-pPEEK can stimulate the adhesion of MC3T3-E1 cells compared with other groups ($p < 0.05$). The morphology of MC3T3-E1 cells adhered on the surfaces of materials is observed under SEM (**Figure 2E**), revealing that nHA-pPEEK can promote the expansion of cells apparently from the difference in cellular area. Cell morphology and spreading are closely related to cytoskeletal structure, so cell fluorescent staining is performed. Results are displayed in **Figure 2F**, where nuclear staining is blue and cytoskeletal staining is green. Compared to PEEK and pPEEK groups, there are a greater number of cells and larger amounts of cytoskeleton fibers of each cell in the nHA-pPEEK group. The cytoskeleton is the key component that regulates cell migration and differentiation, and some studies believe that osteogenic gene activation is mediated by cytoskeletal change (Wei et al., 2020).

3.3 *In Vitro* Osteogenic Differentiation Assays

We have analyzed the osteogenic potential of the synthetic materials *in vitro*. ALP activity is a marker of early-stage osteogenesis (Chen E. E. M. et al., 2017). The samples show different degrees of ALP staining (**Figure 3A**), where the results in day 14 are greater than day 7 overall. At each specific time point, the nHA-pPEEK group shows deepest staining, indicating that ALP activity is highest, followed in decreasing order by the pPEEK and PEEK groups. To investigate whether the differences among the groups are highly significant, ALP activity quantitative assessment is performed (**Figure 3B**). In agreement with staining results, there are statistically important differences in ALP activity between the nHA-PEEK and other groups ($p < 0.01$). Notably, the ALP activity in the pPEEK group on day 14 is higher than PEEK groups ($p < 0.05$), which means that pPEEK has a certain degree of osteoinductive abilities. Mineralization is considered an *in vitro* endpoint of osteogenic differentiation (Lin et al., 2017). Thus, ARS staining is performed on day 21 and results are presented in **Figure 3C**. The red color is deeper and deeper in order of PEEK, pPEEK, and nHA-pPEEK, indicating that the content of calcium is more and more. The result of quantification of ARS is consistent with the result of ARS staining (**Figure 3D**), where the nHA-pPEEK group has a higher content of calcium than other groups ($p < 0.01$), and pPEEK is also slightly elevated compared to PEEK ($p < 0.05$).

3.4 *In Vivo* Bone Integration

To demonstrate implant functionality, the osseointegration of implants placed around rat tibias is analyzed. Eight weeks after the implantation, materials with surrounding tissues are harvested for analysis. The μCT scanning-reconstructed images for different groups are shown in **Figure 4A**. From the results, bone density and the amount of new bone volume in nHA-pPEEK are apparently higher than the PEEK and pPEEK groups, which indicates that the osteoinductivity and osteoconductivity of nHA-pPEEK composites are greater than others. Results of bone parameters, including BV/TV (**Figure 4B**) and Tb. N (**Figure 4C**), are consistent with reconstructed images, showing that nHA-pPEEK has the best performance in osteogenesis ($p < 0.05$). The biomechanical pull-out test is utilized to evaluate the quality of osseointegration of the implants, and the results (**Figures 4D,E**) show that there are significant differences observed among materials ($p < 0.01$), which illustrates that nHA-pPEEK has the ability to enhance the osteogenic capacity of biomaterials. After pull-out, SEM is employed to characterize the morphology of the surfaces on the implants. Results show that new bone tissues deposit on the surface of the materials in each group and intensity differs among the groups (**Figure 4G**). Quantification indicates statistical significance (**Figure 4F**, $p < 0.01$), further confirming the osteogenic capacity of the nHA-pPEEK implants. According to the results of HE and Masson staining (**Figures 5A,B**) 8 weeks after bone graft in the tibiae of rats, the osteogenic area can be clearly seen in the nHA-pPEEK group, which shows cell aggregation at the osteogenic front of the newly formed bone and where the area presents collagen fiber bundles of high content. **Figures 5C,D** shows that the osteogenic differentiation of cells was observed by positive immunohistochemical staining for BMP-2 and OCN and the results confirm that the nHA-pPEEK materials can effectively promote stem cells to differentiate to the bone cells compared to other groups.

4 DISCUSSION

HA-based biomaterials are widely used as bone substitute material because its osteoinductive activity is generally recognized, because biosafety is a prerequisite for bone-substitute *in vivo* applications (Tang et al., 2017). To date, there are many ways in which HA participates in the PEEK materials, as described before, but with a variety of weaknesses consistently present. In this paper, a new technique based on thermally induced phase separation method and hydrothermal synthesis technology is used for producing bioactive nHA-pPEEK composites. The technique is also an efficient method for fabricating Po-PEEK with changeable porosity. The nHA-pPEEK biocomposites produced exhibit good biocompatibility and cell attachment, while the incorporation of nHA into PEEK does not result in the reduction of mechanical strength because the HA particles are attached on the surface rather than embedded in PEEK substrate. SEM and XRD results confirm the formation of crystalline nHA on the porous pPEEK materials after the hydrothermal method. Upon the addition of nHA biomolecules, nHA-pPEEK composites' hydrophilic properties are improved compared with other groups. The surface hydrophilicity will promote the attachment of many different cells, and cell spreading, proliferation, and differentiation have also been related to it in addition to initial cellular attachment (Pan et al., 2015; Pajoumshariati et al., 2018).

In the biomedical field, cell viability is often used to determine the biocompatibility of biomaterials. According to ISO 10993-5, cell viability results can be interpreted as following: >80% no cytotoxicity, 80%–60% weak cytotoxicity, 60%–40% moderate cytotoxicity, and <40% strong cytotoxicity (Ciorita et al., 2020).

The results show that all fabricated materials are compatible with MC3T3-E1 cells with no cytotoxicity. Cell proliferation is another of the cell activities required for tissue regeneration (Del Castillo-Santaella et al., 2019). The cell proliferation rate of cells cultured on the material surfaces changes at different time points, and the results in the pPEEK and nHA-pPEEK groups are superior to that in the control group on day 5, which means that porous structure can promote cell proliferation and nHA particles have no proliferation-promoting effect significantly despite the higher levels of cell viability ($p > 0.05$). This is probably because the porous structures allow for the optimal interaction of the materials with the cells, oxygen and other nutrients are delivered to nourish the attached and embedded cells (Tong et al., 2016). The material properties can influence cellular reaction when cells attach the surfaces, and material–cell interactions are further evaluated by cell adhesion tests (Cui et al., 2017). Cell seeding efficiency on the surfaces of synthetic materials in a short period of time correlates with almost surface property changes, and nHA particles occupy a preponderant place in the cell attachment. Next, the morphologies of cell spreading within 3D matrix are obtained using SEM after co-culturing with different groups for 24 h. The results show that cells have a more homogenous spreading distribution in the nHA-pPEEK group, which is possibly associated with cell differentiations. Hence, the better performance of nHA-modified samples in improving cell differentiation is probably associated to the functions and bioactivity of nHA (Jiang et al., 2020). Cell spreading is often accompanied by changes in the structure and composition of the cytoskeleton (Ma et al., 2016), and the beneficial outcome of cytoskeleton staining further confirms the effect of nHA and porous structure on MC3T3-E1 cells. The cell-spreading area and the cell numbers can be helpful data for cell evaluation on materials.

During early stages of cell differentiation, osteoblasts synthesize ALP and other related markers, which ultimately leads to the extracellular matrix calcification, where the degree of osteoblastic differentiation is evaluated by the expression of the aforementioned osteoblast markers (Zhang et al., 2017). The expression of ALP is monitored using ALP staining and ALP activity assay. Results show that a significantly greater ALP activity is observed in the nHA-pPEEK group compared with other groups at any point in time. Interestingly, cells in the pPEEK group have a higher level than the PEEK groups in the ALP activity quantification experiment, which is possibly related to the morphology of porous structure (Feng et al., 2020). The degree of the extracellular matrix mineralization is determined using ARS staining and the semi-quantification of cultured osteoblasts to detect bone nodules. Results indicate that the number of calcium nodules is increased obviously in the nHA-pPEEK group, and a mild increase is observed in the pPEEK group, which is consistent with the ALP quantification results above. In the osteogenic experiments, nHA-pPEEK composites show better osteogenic ability with enhanced ALP activity and more calcium deposition. Lastly, the current results are obtained from *in vitro* experiments and need to be validated *in vivo*.

In this study, the effect of synthesized composite materials on osteointegration is investigated in a well-established rat tibial bone defect model. At the end of the eighth week, rats are sacrificed, and tibias are detected by μCT, and the data reveal that the amount of new bone formation on the surfaces of the nHA-pPEEK group is significantly higher than other groups, showing a high amount of newly formed bone in the defect areas. A quantitative analysis involving BV/TV and Tb. N further tests this idea. The osteointegration of the newly formed bone is examined by the pull-out test, and the results are expressed as the maximum pull-out force, which is consistently higher for the nHA-pPEEK than for the pPEEK, and pure PEEK groups. This could be partially explained by biomimetic mineralization (Zhao et al., 2020). Porous nHA-pPEEK composites mimic the structure of natural bones in the sense that nHA acts as the bone salt and pPEEK the porous structure to cancellous bone. The biomechanical strength of bone–implant integration is measured by the pull-out test, and the surfaces of the extracted materials are examined by SEM-EDX for the analysis of new bone formation. The present experimental results show that the pull-out force is the maximum in the nHA-pPEEK group, hindered by the newly formed coupled bone. SEM images show that the nHA-pPEEK composites appear to have a rough surface morphology. The measurements of calcium and phosphorus on the surfaces performed with EDX identify these elements in all treatment groups, but the nHA-pPEEK group has the greatest amount compared to others and based on the results of the quantitative analysis. The HE histological staining is used to demonstrate different tissue structures, and the newly formed bulk bone tissues are displayed, where the collagenous regions contain a lacuna structure that is surrounded with osteoid. The results of Masson staining are expected, which show that the nHA-pPEEK group has the most blue staining area of collagen fibrils. BMP-2 and OCN are the respective mid-later stage markers in the osteogenic differentiation process of stem cells (Shuang et al., 2016; Shalumon et al., 2018; Dashtimoghadam et al., 2020), and so the evaluation is necessary to assess. There is significantly greater positive OCN or BMP-2 staining in the nHA-pPEEK group compared with other two groups, which illustrates the successful osteogenic differentiation of MC3T3 cells, further proving the excellent osteoinductive performance of the nHA-pPEEK composites. The *in vivo* experiment further indicates that nHA-pPEEK induces more new bone formation and tighter bone bonding.

5 CONCLUSION

In this study, an nHA-pPEEK was developed and its potential to successfully promote bone integration *in vivo* was demonstrated. The nHA-pPEEK composites were fabricated by thermally induced phase separation method and hydrothermal reaction technology. In the *in vitro* experiments, the composites displayed good osteogenesis and biocompatibility. After 8 weeks of implantation, significantly higher new bone formation within the defective area as well as at the implant–bone interface was achieved in the nHA-pPEEK group compared to that of the PEEK and pPEEK groups. The results showed that the nHA-pPEEK biomaterials can be a promising bone substitute for the treatment of bone defects.

DATA AVAILABILITY STATEMENT

The original contributions presented in the study are included in the article/Supplementary Materials, further inquiries can be directed to the corresponding author.

ETHICS STATEMENT

The animal study was reviewed and approved by the Institutional Animal Care and Use Committee of Jilin University.

AUTHOR CONTRIBUTIONS

NW, DQ, LL, YZ, HL, and SZ designed and performed the whole experiment. NW and DQ analyzed all data and wrote the paper. All authors contributed to the article and approved the submitted version.

FUNDING

This work was supported by the following funds: The Natural Science Foundation of China (Grant no. 81771123 and 82071163).

REFERENCES

Beigi, M.-H., Safaie, N., Nasr-Esfahani, M.-H., and Kiani, A. (2019). 3D Titania Nanofiber-like Webs Induced by Plasma Ionization: A New Direction for Bioreactivity and Osteoinductivity Enhancement of Biomaterials. *Sci. Rep.* 9, 17999. doi:10.1038/s41598-019-54533-z

Chen, E. E. M., Zhang, W., Ye, C. C. Y., Gao, X., Jiang, L. L. J., Zhao, T. T. F., et al. (2017a). Knockdown of SIRT7 Enhances the Osteogenic Differentiation of Human Bone Marrow Mesenchymal Stem Cells Partly via Activation of the Wnt/β-Catenin Signaling Pathway. *Cell Death Dis* 8, e3042. doi:10.1038/cddis.2017.429

Chen, Y., Liu, X., Liu, R., Gong, Y., Wang, M., Huang, Q., et al. (2017b). Zero-order Controlled Release of BMP2-Derived Peptide P24 from the Chitosan Scaffold by Chemical Grafting Modification Technique for Promotion of Osteogenesis *In Vitro* and Enhancement of Bone Repair *In Vivo*. *Theranostics* 7, 1072–1087. doi:10.7150/thno.18193

Chubrik, A., Senatov, F., Kolesnikov, E., Orlova, P., Poponova, M., Grunina, T., et al. (2020). Highly Porous PEEK and PEEK/HA Scaffolds with Escherichia Coli-Derived Recombinant BMP-2 and Erythropoietin for Enhanced Osteogenesis and Angiogenesis. *Polym. Test.* 87, 106518. doi:10.1016/j.polymertesting.2020.106518

Ciorita, A., Suciu, M., Macavei, S., Kacso, I., Lung, I., Soran, M.-L., et al. (2020). Green Synthesis of Ag-MnO2 Nanoparticles Using Chelidonium Majus and Vinca Minor Extracts and Their *In Vitro* Cytotoxicity. *Molecules* 25, 21. doi:10.3390/molecules25040819

Conrad, T. L., and Roeder, R. K. (2020). Effects of Porogen Morphology on the Architecture, Permeability, and Mechanical Properties of Hydroxyapatite Whisker Reinforced Polyetheretherketone Scaffolds. *J. Mech. Behav. Biomed. Mater.* 106, 103730. doi:10.1016/j.jmbbm.2020.103730

Cui, X., Huang, C., Zhang, M., Ruan, C., Peng, S., Li, L., et al. (2017). Enhanced Osteointegration of Poly(methylmethacrylate) Bone Cements by Incorporating Strontium-Containing Borate Bioactive Glass. *J. R. Soc. Interf.* 14, 20161057. doi:10.1098/rsif.2016.1057

Dai, Y., Guo, H., Chu, L., He, Z., Wang, M., Zhang, S., et al. (2019). Promoting Osteoblasts Responses *In Vitro* and Improving Osteointegration *In Vivo* through Bioactive Coating of Nanosilicon Nitride on Polyetheretherketone. *J. Orthop. Transl* 24, 198–208. doi:10.1016/j.jot.2019.10.011

Dashtimoghadam, E., Fahimipour, F., Tongas, N., and Tayebi, L. (2020). Microfluidic Fabrication of Microcarriers with Sequential Delivery of VEGF and BMP-2 for Bone Regeneration. *Sci. Rep.* 10, 11764. doi:10.1038/s41598-020-68221-w

Del Castillo-Santaella, T., Ortega-Oller, I., Padial-Molina, M., O'Valle, F., Galindo-Moreno, P., Jódar-Reyes, A. B., et al. (2019). Formulation, Colloidal Characterization, and *In Vitro* Biological Effect of BMP-2 Loaded PLGA Nanoparticles for Bone Regeneration. *Pharmaceutics* 11, 388. doi:10.3390/pharmaceutics11080388

Feng, X., Ma, L., Liang, H., Liu, X., Lei, J., Li, W., et al. (2020). Osteointegration of 3D-Printed Fully Porous Polyetheretherketone Scaffolds with Different Pore Sizes. *ACS Omega* 5, 26655–26666. doi:10.1021/acsomega.0c03489

Feng, X., Yu, H., Liu, H., Yu, X., Feng, Z., Bai, S., et al. (2019). Three-Dimensionally-Printed Polyether-Ether-Ketone Implant with a Cross-Linked Structure and Acid-Etched Microporous Surface Promotes Integration with Soft Tissue. *Int. J. Mol. Med.* 20, 3811. doi:10.3390/ijms20153811

Fukuda, N., Kanazawa, M., Tsuru, K., Tsuchiya, A., Sunarso, S., Toita, R., et al. (2018). Synergistic Effect of Surface Phosphorylation and Micro-roughness on Enhanced Osseointegration Ability of Poly(ether Ether Ketone) in the Rabbit Tibia. *Sci. Rep.* 8, 10. doi:10.1038/s41598-018-35313-7

Gong, J., Schuurmans, C. C. L., Genderen, A. M., Cao, X., Li, W., Cheng, F., et al. (2020a). Complexation-induced Resolution Enhancement of 3D-Printed Hydrogel Constructs. *Nat. Commun.* 11, 1267. doi:10.1038/s41467-020-14997-4

Gong, L., Chen, B., Zhang, J., Sun, Y., Yuan, J., Niu, X., et al. (2020b). Human ESC-sEVs Alleviate Age-Related Bone Loss by Rejuvenating Senescent Bone Marrow-Derived Mesenchymal Stem Cells. *J. Extracell Vesicles* 9, 1800971. doi:10.1080/20013078.2020.1800971

Han, X., Sharma, N., Xu, Z., Scheideler, L., Geis-Gerstorfer, J., Rupp, F., et al. (2019). An *In Vitro* Study of Osteoblast Response on Fused-Filament Fabrication 3D Printed PEEK for Dental and Cranio-Maxillofacial Implants. *J. Clin. Med.* 8, 16. doi:10.3390/jcm8060771

Huang, X., Cen, X., Sun, W., Xia, K., Yu, L., Liu, J., et al. (2019). CircPOMT1 and circMCM3AP Inhibit Osteogenic Differentiation of Human Adipose-Derived Stem Cells by Targeting miR-6881-3p. *Am. J. Transl Res.* 11, 4776–4788.

Huang, Z., Wan, Y., Zhu, X., Zhang, P., Yang, Z., Yao, F., et al. (2021). Simultaneous Engineering of Nanofillers and Patterned Surface Macropores of Graphene/hydroxyapatite/polyetheretherketone Ternary Composites for Potential Bone Implants. *Mater. Sci. Eng. C-mater Biol. Appl.* 123, 111967. doi:10.1016/j.msec.2021.111967

Hughes, E. A. B., Parkes, A., Williams, R. L., Jenkins, M. J., and Grover, L. M. (2018). Formulation of a Covalently Bonded Hydroxyapatite and Poly(ether Ether Ketone) Composite. *J. Tissue Eng.* 9, 13. doi:10.1177/2041731418815570

Jiang, P., Zhang, Y., Hu, R., Wang, X., Lai, Y., Rui, G., et al. (2020). Hydroxyapatite-modified Micro/nanostructured Titania Surfaces with Different Crystalline Phases for Osteoblast Regulation. *Bioact Mater.* 6, 1118–1129. doi:10.1016/j.bioactmat.2020.10.006

Ko, H., Lee, S., and Jho, J. (2021). Synthesis and Modification of Hydroxyapatite Nanofiber for Poly(Lactic Acid) Composites with Enhanced Mechanical Strength and Bioactivity. *Nanomaterials* 11, 213. doi:10.3390/nano11010213

Kohli, N., Sharma, V., Orera, A., Sawadkar, P., Owji, N., Frost, O. G., et al. (2021). Pro-angiogenic and Osteogenic Composite Scaffolds of Fibrin, Alginate and Calcium Phosphate for Bone Tissue Engineering. *J. Tissue Eng.* 12, 20417314211005610. doi:10.1177/20417314211005610

Lin, T., Wang, H., Cheng, W., Hsu, H., and Yeh, M. (2019). Osteochondral Tissue Regeneration Using a Tyramine-Modified Bilayered PLGA Scaffold Combined with Articular Chondrocytes in a Porcine Model. *Int. J. Mol. Med.* 20, 326. doi:10.3390/ijms20020326

Lin, Y., Chen, C., Chou, L., Chen, C., Kang, L., and Wang, C. (2017). Enhancement of Bone Marrow-Derived Mesenchymal Stem Cell Osteogenesis and New Bone Formation in Rats by Obtusilactone A. *Int. J. Mol. Med.* 18, 2422. doi:10.3390/ijms18112422

Ma, J., Zhao, N., and Zhu, D. (2016). Bioabsorbable Zinc Ion Induced Biphasic Cellular Responses in Vascular Smooth Muscle Cells. *Sci. Rep.* 6, 26661. doi:10.1038/srep26661

Pajoumshariati, S., Shirali, H., Yavari, S. K., Sheikholeslami, S. N., Lotfi, G., Mashhadi Abbas, F., et al. (2018). GBR Membrane of Novel Poly (Butylene Succinate-Co-Glycolate) Co-polyester Co-polymer for Periodontal Application. *Sci. Rep.* 8, 7513. doi:10.1038/s41598-018-25952-1

Pan, J. L., Shu, N., Sun, L., and Sun, H. (2015). Application of Avidin-Biotin Technology to Improve Cell Adhesion on Nanofibrous Matrices. *J. Nanobiotechnol* 13, 37. doi:10.1186/s12951-015-0096-2

Paraš, S., Trišić, D., Mitrović Ajtić, O., Prokić, B., Drobne, D., Živković, S., et al. (2020). Toxicological Profile of Nanostructured Bone Substitute Based on Hydroxyapatite and Poly(lactide-Co-Glycolide) after Subchronic Oral Exposure of Rats. *Nanomaterials* 10, 918. doi:10.3390/nano10050918

Peters, E. N. (2017). Poly(phenylene Ether) Based Amphiphilic Block Copolymers. *Polymers* 9, 433. doi:10.3390/polym9090433

Pujari-Palmer, S., Lu, X., and Karlsson Ott, M. (2017). The Influence of Hydroxyapatite Nanoparticle Morphology on Embryonic Development in a Zebrafish Exposure Model. *Nanomaterials* 7, 89. doi:10.3390/nano7040089

Shalumon, K. T., Kuo, C.-Y., Wong, C.-B., Chien, Y.-M., Chen, H.-A., and Chen, J.-P. (2018). Gelatin/Nanohyroxyapatite Cryogel Embedded Poly(lactic-Co-Glycolic Acid)/Nanohydroxyapatite Microsphere Hybrid Scaffolds for Simultaneous Bone Regeneration and Load-Bearing. *Polymers* 10, 620. doi:10.3390/polym10060620

Shuang, Y., Yizhen, L., Zhang, Y., Fujioka-Kobayashi, M., Sculean, A., and Miron, R. J. (2016). *In Vitro* characterization of an Osteoinductive Biphasic Calcium Phosphate in Combination with Recombinant BMP2. *BMC Oral Health* 17, 35. doi:10.1186/s12903-016-0263-3

Sunarso, Tsuchiya, A., Toita, R., Tsuru, K., and Ishikawa, K. (2020). Enhanced Osseointegration Capability of Poly(ether Ether Ketone) via Combined Phosphate and Calcium Surface-Functionalization. *Int. J. Mol. Med.* 21, 13. doi:10.3390/ijms21010198

Swaminathan, P. D., Uddin, M. N., Wooley, P., and Asmatulu, R. (2020). Fabrication and Biological Analysis of Highly Porous PEEK Bionanocomposites Incorporated with Carbon and Hydroxyapatite Nanoparticles for Biological Applications. *Molecules* 25, 3572. doi:10.3390/molecules25163572

Tang, Y., Wu, C., Wu, Z., Hu, L., Zhang, W., and Zhao, K. (2017). Fabrication and *In Vitro* Biological Properties of Piezoelectric Bioceramics for Bone Regeneration. *Sci. Rep.* 7, 43360. doi:10.1038/srep43360

Tong, S. X., Xu, D. P., Liu, Z. M., Du, Y., and Wang, X. K. (2016). Synthesis of and *In Vitro* and *In Vivo* Evaluation of a Novel TGF-β1-SF-CS Three-Dimensional Scaffold for Bone Tissue Engineering. *Int. J. Mol. Med.* 38, 367–380. doi:10.3892/ijmm.2016.2651

Torstrick, F. B., Lin, A. S. P., Potter, D., Safranski, D. L., Sulchek, T. A., Gall, K., et al. (2018). Porous PEEK Improves the Bone-Implant Interface Compared to Plasma-Sprayed Titanium Coating on PEEK. *Biomaterials* 185, 106–116. doi:10.1016/j.biomaterials.2018.09.009

Vaezi, M., Black, C., Gibbs, D. M. R., Oreffo, R. O. C., Brady, M., Moshrefi-Torbati, M., et al. (2016). Characterization of New PEEK/HA Composites with 3D HA Network Fabricated by Extrusion Freeforming. *Molecules* 21, 687. doi:10.3390/molecules21060687

Venkatraman, P., Bohmann, N., Gadalla, D., Rader, C., and Foster, E. J. (2021). Microstructured Poly(ether-Ether-Ketone)-Hydroxyapatite Composites for Bone Replacements. *J. Compos. Mater.* 55, 2263–2271. doi:10.1177/0021998320983870

Wan, T., Jiao, Z., Guo, M., Wang, Z., Wan, Y., Lin, K., et al. (2020). Gaseous Sulfur Trioxide Induced Controllable Sulfonation Promoting Biomineralization and Osseointegration of Polyetheretherketone Implants. *Bioact Mater.* 5, 1004–1017. doi:10.1016/j.bioactmat.2020.06.011

Wei, Q., Holle, A., Li, J., Posa, F., Biagioni, F., Croci, O., et al. (2020). BMP-2 Signaling and Mechanotransduction Synergize to Drive Osteogenic Differentiation via YAP/TAZ. *Adv. Sci.* 7, 1902931. doi:10.1002/advs.201902931

Xie, L., Liu, N., Xiao, Y., Liu, Y., Yan, C., Wang, G., et al. (2020). *In Vitro* and *In Vivo* Osteogenesis Induced by Icariin and Bone Morphogenetic Protein-2: A Dynamic Observation. *Front. Pharmacol.* 11, 10. doi:10.3389/fphar.2020.01058

Yan, J., Wang, C., Li, K., Zhang, Q., Yang, M., Di-Wu, W., et al. (2018). Enhancement of Surface Bioactivity on Carbon Fiber-Reinforced Polyether Ether Ketone via Graphene Modification. *Int. J. Nanomed* 13, 3425–3440. doi:10.2147/IJN.S160030

Zakrzewski, W., Dobrzynski, M., Nowicka, J., Pajaczkowska, M., Szymonowicz, M., Targonska, S., et al. (2020). The Influence of Ozonated Olive Oil-Loaded and Copper-Doped Nanohydroxyapatites on Planktonic Forms of Microorganisms. *Nanomaterials* 10, 21. doi:10.3390/nano10101997

Zhang, Y., Shen, L., Mao, Z., Wang, N., Wang, X., Huang, X., et al. (2017). Icariin Enhances Bone Repair in Rabbits with Bone Infection during Post-infection Treatment and Prevents Inhibition of Osteoblasts by Vancomycin. *Front. Pharmacol.* 8, 784. doi:10.3389/fphar.2017.00784

Zhao, W., Li, Y., Zhou, A., Chen, X., Li, K., Chen, S., et al. (2020). Controlled Release of Basic Fibroblast Growth Factor from a Peptide Biomaterial for Bone Regeneration. *R. Soc. Open Sci.* 7, 191830. doi:10.1098/rsos.191830

Zhong, G., Vaezi, M., Mei, X., Liu, P., and Yang, S. (2019). Strategy for Controlling the Properties of Bioactive Poly-Ether-Ether-Ketone/Hydroxyapatite Composites for Bone Tissue Engineering Scaffolds. *ACS Omega* 4, 19238–19245. doi:10.1021/acsomega.9b02572

Conflict of Interest: The authors declare that the research was conducted in the absence of any commercial or financial relationships that could be construed as a potential conflict of interest.

Publisher's Note: All claims expressed in this article are solely those of the authors and do not necessarily represent those of their affiliated organizations, or those of the publisher, the editors and the reviewers. Any product that may be evaluated in this article, or claim that may be made by its manufacturer, is not guaranteed or endorsed by the publisher.

Copyright © 2022 Wang, Qi, Liu, Zhu, Liu and Zhu. This is an open-access article distributed under the terms of the Creative Commons Attribution License (CC BY). The use, distribution or reproduction in other forums is permitted, provided the original author(s) and the copyright owner(s) are credited and that the original publication in this journal is cited, in accordance with accepted academic practice. No use, distribution or reproduction is permitted which does not comply with these terms.

frontiers in Pharmacology

ORIGINAL RESEARCH
published: 02 March 2022
doi: 10.3389/fphar.2022.832725

Docetaxel-Loaded Novel Nano-Platform for Synergistic Therapy of Non-Small Cell Lung Cancer

Xing Feng[1,2], *Xiaoling Xiong*[3] *and Shenglin Ma*[4]*

[1]Department of Thoracic Surgery, The Affiliated Hangzhou Hospital of Nanjing Medical University, Hangzhou, China, [2]Department of Thoracic Surgery, Affiliated Hangzhou First People's Hospital, Zhejiang University School of Medicine, Hangzhou, China, [3]Department of Nephrology, Sir Run Run Shaw Hospital, Zhejiang University School of Medicine, Hangzhou, China, [4]Department of Oncology, The Affiliated Hangzhou Hospital of Nanjing Medical University, Hangzhou, China

Nowadays, non-small cell lung cancer (NSCLC) is threatening the health of all mankind. Although many progresses on treatment of lung cancer have been achieved in the past few decades, the current treatment methods are still traditional surgery, radiotherapy, and chemotherapy, which had poor selectivity and side effects. Lower-toxicity and more efficient treatments are in sore need. In this paper, a smart nanodelivery platform based on photothermal therapy, chemotherapy, and immunotherapy was constructed. The nanoparticles are composed of novel photothermal agents, Mn-modified phthalocyanine derivative ($Mn^{III}PC$), docetaxel (DTX), and an effective targeting molecule, hyaluronic acid. The nanoplatform could release Mn^{2+} from $Mn^{III}PC$@DTX@PLGA@Mn^{2+}@HA(MDPMH) and probably activate tumor immunity through cGAS-STING and chemotherapy, respectively. Furthermore, DTX could be released in the process for removal of tumor cells. The "one-for-all" nanomaterial may shed some light on treating NSCLC in multiple methods.

Keywords: non-small cell lung cancer, targeted therapy, immunotherapy, hotothermal therapy, cGAS-STING

OPEN ACCESS

Edited by:
Kelong Ai,
Central South University, China

Reviewed by:
Wang Ying,
Beijing University of Chinese Medicine, China
Jia Huang,
Central South University, China

***Correspondence:**
Shenglin Ma
mashenglin0607@163.com

Specialty section:
This article was submitted to Pharmacology of Anti-Cancer Drugs, a section of the journal Frontiers in Pharmacology

Received: *10 December 2021*
Accepted: *18 January 2022*
Published: *02 March 2022*

Citation:
Feng X, Xiong X and Ma S (2022) Docetaxel-Loaded Novel Nano-Platform for Synergistic Therapy of Non-Small Cell Lung Cancer. Front. Pharmacol. 13:832725. doi: 10.3389/fphar.2022.832725

INTRODUCTION

Nowadays, lung cancer is still one of the most fatal tumors worldwide and the main cause of cancer-related mortality (Lim, 2016). Lung cancer is classified into small cell lung cancer (SCLC) and non-small cell lung cancer (NSCLC) according to the different histological performance, in which NSCLC comprises about 85% of total cases (Jonna and Subramaniam, 2019; Lee and Cheah, 2019). The mainstay of treatments for NSCLC is still the conventional therapies, including chemotherapy, surgery, radiotherapy, and synergistic therapy. The physical damage caused by surgical treatment, dose dependence, low selectivity, and side effects of chemotherapy and radiotherapy often bring great suffering to the patient (Camidge et al., 2019; Duma et al., 2019). Therefore, it is urgent to develop a new strategy which is effective against NSCLC but low side effects to normal tissues.

Photothermal therapy (PTT), utilizing photothermal agents [e.g., noble metal nanoparticles (Liu et al., 2020; Zheng et al., 2020), transition metal sulfides (Ai et al., 2021; Dhas et al., 2021), black phosphorus (Jana et al., 2020), phthalocyanines (PCs) (Taratula et al., 2015; Jin et al., 2019; Li et al., 2019)], could efficiently absorb light and convert photon energy into heat and cause the thermal ablation of adjacent tumor cells (Camidge et al., 2019). However, some drawbacks, particularly poor thermal stability and low biocompatibility, had severely limited its wide application in biomedicine. Recently, metal phthalocyanines (MPCs) have caught the attention of researchers with strong NIR

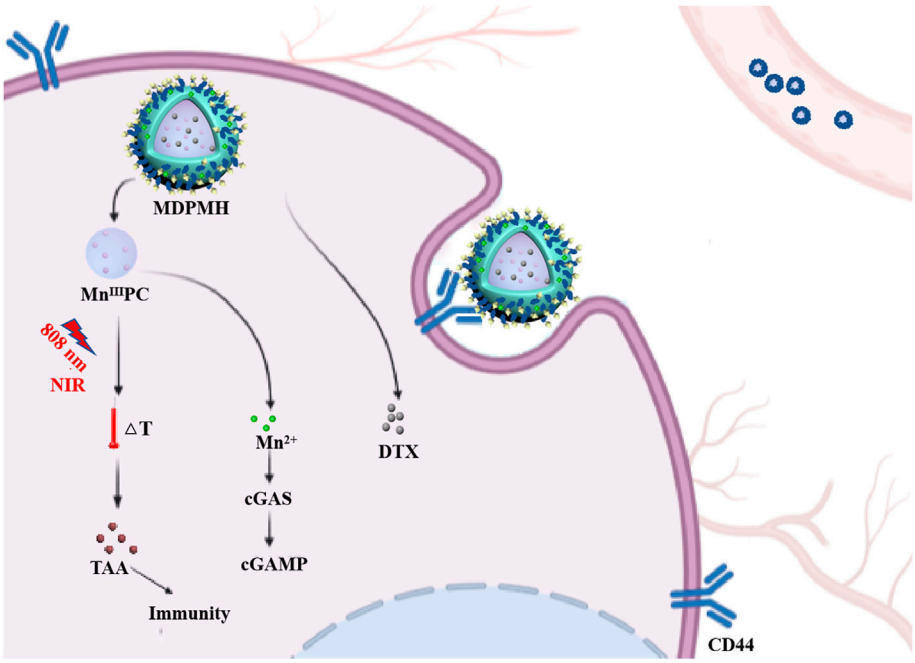


FIGURE 1 | Schematic illustration of combinational therapy of PTT, chemotherapy, and immunotherapy (MDPMH) *via* a combined all-in-one and all-in-control strategy.

region absorption, high stability coefficient, and low phototoxicity. For example, Song et al. (2018) designed a smart theranostic nanoplatform based on a hyaluronic acid-doped polypyrrole-coated bismuth selenide loading with a zinc phthalocyanine nanodish for multimodal imaging-guided combined phototherapy, showing an excellent combined therapeutic effect. Moreover,the combination of PTT and immunotherapy could improve the scavenging capacity of tumor was testified (Li et al., 2017). For example, a photothermal agent IR820 and a programmed death-ligand 1 antibody were loaded into a lipid gel depot, which increased the recruitment of tumor-infiltrating lymphocytes and booted T-cell activity against tumors (Chen et al., 20198).

Further, it was reported that Mn^{2+} could be endocytosed by macrophages, dendritic cells, and lymphocytes and activates the innate immune response, which indicated that Mn^{2+} is a potential immunotherapy strategy (Huang et al., 2019). Hyaluronic acid (HA), composed of repeated units of β-4 linked D-glucuronic acid and β-3 linked N-acetyl-D-glucosamine, has been widely served in antitumor therapies because of its glorious biocompatibility and biodegradable character (Lv et al., 2020). Moreover, HA is the ligand for CD44 receptors, which are overexpressed in multiple tumors (Mattheolabakis et al., 2015; Salwowska et al., 2016).

Based on the current scientific studies, docetaxel (DTX) is one of the well-known and practically effective chemical anticancer agents for the inhibition of NSCLC both as a single agent and in combination treatments (Gao et al., 2019). Several effective drug delivery systems were designed to deliver DTX into tumor cells with high selectivity and efficacy while minimizing negative effects (Jing et al., 2018; Deng et al., 2020). Nanotechnology is a significant method which can be utilized to achieve cancer targeting and efficient treatment while avoiding unnecessary side effects (Rafiei and Haddadi, 2017).

In this study, an intelligent nanoplatform combining PTT, chemotherapy, and immunotherapy was designed (**Figure 1**). Firstly, a novel sonosensitizer, an Mn-modified phthalocyanine derivative ($Mn^{III}PC$), and an HA amphiphilic molecule (HA-HDA) were synthesized, respectively. Secondly, the DTX-loaded nanoparticles ($Mn^{III}PC@DTX@PLGA@Mn^{2+}@HA$, MDPMH) were prepared by mixing DTX, $Mn^{III}PC$, HA-HDA, Mn^{2+}, and PLGA under ultrasound. The physical and chemical properties and cytotoxicity to NSCLC cells of MDPMH were investigated subsequently. MDPMH nanoparticles could handily be internalized by cancer cells due to overexpressed CD44-mediated endocytosis. $Mn^{III}PC$ induced much heat in tumor cells under the irradiation of an 808-nm near-infrared laser; Mn^{2+} deposited on the surface of nanocarriers could activate tumor immunity through cGAS-STING. What is more, DTX released from the carrier could inhibit the proliferation of tumor cells with the biodegradation of HA and nanocarriers. This strategy may shed some light on treating NSCLC in multiple methods.

EXPERIMENTAL SECTION

Materials

1,4,8,11,15,18,22,25-Octabutoxy-29H,31H-phthalocyanine [$(BuO)_8PCH_2$], 1,3-diphenylisobenzofuran (DPBF), and polylactic-co-glycolic acid (PLGA, 50:50) were purchased from

Sigma-Aldrich (Shanghai, China). N-Hydroxysuccinimide (NHS), N-(3-dimethylaminopropyl)-N′-ethyl carbodiimide hydrochloride (EDC·HCl), and DTX were obtained from Sangon Biotech (Shanghai) Co., Ltd. HA (10 kDa) was bought from Rhawn Science and Technology (Shanghai, China) Co., Ltd. Manganese chloride ($MnCl_2$), 1-hexadecanamine (HDA), and hyaluronidase (HAase) were bought from Shanghai Yuanye Bio-Technology Co., Ltd. Dimethyl sulfoxide (DMSO), dimethylformamide (DMF), dichloromethane (DCM), ethanol, and chloroform were derived from Solarbio (Beijing, China). All reagents were of analytical grade and had no additional purification.

Cell Lines

A549 cells were cultured in RPMI 1640 media supplemented with 10% fetal bovine serum and 1% penicillin–streptomycin solution under a 5% CO_2 atmosphere at 37°C.

The Synthesis of Mn(III) $(BuO)_8PCH_2$ ($Mn^{III}PC$)

$(BuO)_8PCH_2$ (109.3 mg, 1.0 mmol, 1.0 eq) and $MnCl_2$ (0.5 mg, 4.0 mmol, 4.0 eq) were dropped into 4 ml DMF under nitrogen atmosphere for 10 min. The above mixture was maintained at 180°C for 3 min. When the reaction system was cooled to room temperature spontaneously, it was dropped into 30 ml water with stirring. The mixture was centrifuged at 12,000 rpm for 5 min and washed with water for two times. The crude product was purified by silica gel column chromatography (eluted with chloroform/ethanol 100:3) to yield a pale yellow solid (80%), which was designated as $Mn^{III}PC$. $Mn^{III}PC$ needs to be kept out of light at 4°C. ^1H NMR ($CDCl_3$) δ: 7.61 (s, 1 H), 4.85 (s, 2 H), 2.22 (t, 2 H), 1.66 (q, 2 H), 1.07-1.09 (t, 3 H).

The Synthesis of HA-HDA

This chemical reaction is designed according to previous literature (Kaczmarek et al., 2018; Wang et al., 2020a). HA (300 mg) was dissolved in pure water (20 ml); afterward, 20 ml DMSO was added to it and the solution was stirred for 10 min. EDC·HCl (30.6 mg dissolved in DMSO) and NHS (18.4 mg dissolved in pure water) were added into the above solution of HA and stirred for 1 h at room temperature. Then HDA (19.3 mg dissolved in DMSO with the help of ultrasound) was dropped into the reaction dropwise. The reaction was processed for 24 h at room temperature and dialysis (MW cutoff 3.5 kDa) against water for 2 days. HA-HDA sponge was fabricated by freeze-drying.

Preparation of the Nanoparticles

$Mn^{III}PC$ (1.0 mg), DTX (1.0 mg), and PLGA (30.0 mg) were dissolved in DCM. Then, under ultrasound conditions, the mixture above was added into the HA-HDA solution (2 mg/ml, 2 ml); the mixture was treated under the ultrasonic probe for 3 min (50%, 3 s on/3 s off). Then, the as-synthesized HA-HDA (0.5 mg/ml, 5 ml) was dropwise added into the beaker and stirred for 4 h at room temperature. The product was used to wash several times to remove the organic solvent and collected by centrifugation (12,000 rpm, 5 min). Ultimately, the nanoparticles were freeze-dried and stored in the dark at 4°C. Homogeneously, $Mn^{III}PC$@PLGA@HA and DTX@PLGA@HA were prepared by altering the amount of $Mn^{III}PC$ and DTX (1.5 mg), respectively.

15 mg MDPH and $MnCl_2$ (0.1 mol/l, 8 ml) aqueous solution were stirred at room temperature for 25 h. Then, the sample was collected by washing and centrifuging with distilled water for 3 times to obtain MDPMH. Finally, it was redissolved in 5% lactose solution, freeze-dried, and stored at −20°C.

The Characterization of the Nanoparticles

Transmission electron microscopy (TEM) images were acquired using the Hitachi H-7650 electron microscope. Dynamic light scattering (DLS) was performed on a Malvern Zetasizer Pro (Mastersizer 3000) to determine the hydrodynamic size and zeta potential. The optical properties of nanoparticles were recorded by ultraviolet-visible spectroscopy (UV-Vis, UV-2600) from 200 to 900 nm. The extinction coefficient of MDPMH was investigated with different concentrations (0.05×10^{-4}, 0.1×10^{-4}, 0.2×10^{-4}, 0.4×10^{-4}, and 0.8×10^{-4} mol l^{-1}).

Drug Loading and Release Behaviors

For the determination of drug loading content (DLC) and drug loading efficiency (DLE), $Mn^{III}PC$@PLGA@HA, DTX@PLGA@HA and MDPMH were dissolved in DMSO at a certain concentrations, respectively. $Mn^{III}PC$ was detected by high-performance liquid chromatography (HPLC, Sepiatec SEPBOX 2D-2000), while DTX was examined by UV-Vis. DLC and DLE were calculated according to the following formula:

$$\mathrm{DLC\,(wt.\%)} = \left(\text{weight of loaded drug}/\text{total weight of loaded drug and carrier}\right)\times 100\%$$

$$\mathrm{DLE\,(\%)} = \left(\text{weight of loaded drug}/\text{weight of the drug added}\right)\times 100\%$$

In order to investigate the drug release behavior, 1 mg MDPMH was dissolved in 1 ml phosphate-buffered saline (PBS) and transferred into a dialysis bag (MW cutoff 3.5 kDa). Then, the dialysis bag was subsequently placed in a centrifuge tube containing 30 ml PBS with different conditions, pH = 7.4, pH = 7.4 + HAase (1,000 units/ml) and pH = 5.5 + HAase (1,000 units/ml), and shaken in a water bath thermostat oscillator (SHZ-C, Shanghai) with the speed of 100 rpm at 37°C. At each specified point, 3 ml dialysate was fetched and replenished with an equal volume of fresh medium. Then, the release rates of DTX and Mn^{2+} were measured by HPLC and inductively coupled plasma-optical emission spectrometry (ICP-OES, PerkinElmer Optima 5,300 DV), respectively.

The Photothermal Properties of MDPMH

The photothermal properties of MDPMH were studied in this section. In detail, MDPMH was dispersed in PBS solution for different concentrations (500, 1,000 and 2,000 μg/ml), which was placed in a 3-ml centrifuge tube under an 808-nm laser (2 W/cm^2) for 10 min, respectively. The temperature was recorded by a thermocouple thermometer (TASI-605) at every minute. Similarly, the properties of MDPMH were tested under different

powers of the laser (1 and 2 W/cm^2). In addition, the thermal cycling stability of MDPMH was repeated four times. During the experiment, PBS was set as blank control. The distance between the laser source and the liquid surface was maintained at 25 mm during the irradiation.

Stability Test

To test the stability of the drug-loaded nanoparticles, 10 μM MDPMH was dispersed in the mixture solution of DMSO and H_2O (volume ratio = 1:10, pH = 7.4). The size and absorption properties were measured and recorded by DLS and UV-Vis every day, respectively.

CCK-8 Assay

A549 cells were seeded in a 96-well plate at a density of 5×10^3 cells per well overnight in an incubator (37°C, 5% CO_2). Then, cells were co-incubated with DTX@PLGA@HA, PLGA@HA, MDPMH, Mn^{III}PC@PLGA@HA, Mn^{III}PC@PLGA@HA + Laser, and MDPMH + Laser at different concentrations (500, 1,000 and 2,000 μg/ml), respectively. In addition, the PBS and laser groups were used as control groups. The photothermal group was irradiated by near-infrared laser (808 nm, 2 W/cm^2) for 4 min each well, and each group was cultured for another 4 h. Then, the solution was discarded and washed with PBS. A 100-μl solution containing 10% CCK-8 was added and incubated for 2 h. The microplate reader (Bio-Rad, Hercules, CA, USA) was used to measure and record the absorbance (OD value) at the 450-nm wavelength. The survival rate was acquired by the following formula:

Survival rate (%) = (experimental hole OD value-blank hole OD value)/(control group OD value-blank hole OD value) × 100%

Cell Apoptosis

Annexin V-FITC/PI staining assay was performed to measure the A549 cell apoptosis after different treatments. The A549 cells were seeded in the 24-well plate at the density of 2×10^5 cells per well and incubated for 12 h. The cells were treated with different treatments (PBS, Laser, PLGA@HA, DTX@PLGA@HA, Mn^{III}PC@PLGA@HA, Mn^{III}PC@PLGA@HA + Laser, MDPMH, and MDPMH + Laser) for 24 h. The cells were collected and washed twice by PBS. The apoptosis rate was determined by Annexin V-FITC/PI Kit and flow cytometric assay.

Calcein AM/PI Dual Staining

The cytotoxicity of MDPMH nanoparticles *in vitro* was further investigated by calcein AM/propidium iodide (PI) dual-staining methods. Briefly, A549 cells (5,000 cells per well) were incubated in a 96-well plate for 24 h. Then, each group with the same concentration (2,000 μg/ml) conducted the following steps as CCK-8. Subsequently, the above cells were dyed by Calcine AM (2 μM) and PI (4.5 μM) at 37°C for 15 min. Finally, fluorescence images were taken under a laser scanning confocal microscopy (TCS-SP8, Leica, Germany).

Western Blot Analysis

A549 cells were inoculated 2×10^5 cells per well in a 6-well plate and cultured overnight (37°C, 5% CO_2). Then, PBS (control group), $MnCl_2$ (50 μM), MDPMH, and MDPMH + Laser were added to each group in sequence. Only the MDPMH + Laser group was irradiated by a near-infrared laser (808 nm, 2 W/cm^2) for 4 min, and each group was cultured for 12 h. Then, cells were harvested and treated according to the manufacturer's instructions. The protein concentrations were detected by the BCA kit. Protein samples were separated on SDS-PAGE gels and transferred to polyvinylidene difluoride membranes. The membranes were blocked with 5% BSA and incubated with anti-beta actin (1:1,000, ab8226), anti-cGAS antibody (1:1,000, ab224144), anti-Bax antibody (1:1,000, ab32503), and anti-Bcl-2 antibody (1:1,000, ab32124), respectively. Then the relevant horseradish peroxidase-conjugated secondary antibodies were inculcated. Ultimately, proteins were detected using the chemiluminescent detection reagents. Besides, the expression of cGAS with different concentrations of $MnCl_2$ was also evaluated.

Statistical Analysis

Results were expressed as mean ± SD. Data were analyzed by *t*-test with the scientific statistic software GraphPad Prism 7.00.

RESULTS

The Preparation and Characterization of the Nanoparticles

Generally, the synthesis route of the MDPMH nanoparticles was described as follows (**Figure 2**). Firstly, the novel photothermal agent Mn^{III}PC was synthesized by $(BuO)_8PCH_2$ and $MnCl_2$. HA and HDA were coupled by the catalysis of the EDC·HCl and NHS. Secondly, MDPH was acquired by the mixture of HA-HDA, Mn^{III}PC, DTX, and PLGA. Finally, the "one-for-all" nanoplatform—MDPMH—was obtained by the electrostatic absorption between MDPH and Mn^{2+}. The spectra of ^{1}H NMR and mass spectrometry are shown in **Supplementary Figure S1A,B**, respectively. The ^{1}H NMR spectrum exhibited in **Supplementary Figure S1C** demonstrated the successful synthesis of PLGA@HA modified by HDA.

MDPMH nanoparticles were measured by TEM with a diameter of about 210 nm (**Figure 3A**). The size of the nanoparticles was further evaluated using DLS, which was mainly distributed around 230 nm (**Figure 3B**). The reason for the difference was possibly owing to the physical state of samples. Then, the zeta potential of each nanoparticle (PLGA, DTX@PLGA@HA, Mn^{III}PC@PLGA@HA, and MDPMH) was determined by -6.18, -18.4, -13.0, and 0.143 mV, respectively (**Figure 3C**). According to the previous reports, the negatively charged or slightly positively charged nanoparticles had better blood circulation stability (Poon et al., 2011). Furthermore, slightly positively charged nanoparticles are beneficial to improving the uptake efficiency of tumor cells. The UV-Vis absorbance spectra of the several samples were measured from 200 to 900 nm and are shown in **Figure 3D**. There were no obvious peaks in PLGA@HA. Particularly, the absorbance at 282 and 832 nm was detected, indicating the absorption of the B band

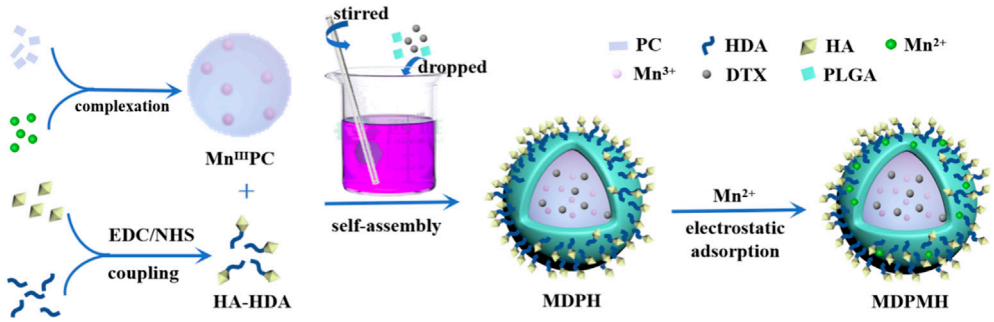


FIGURE 2 | The synthetic route of MDPMH.

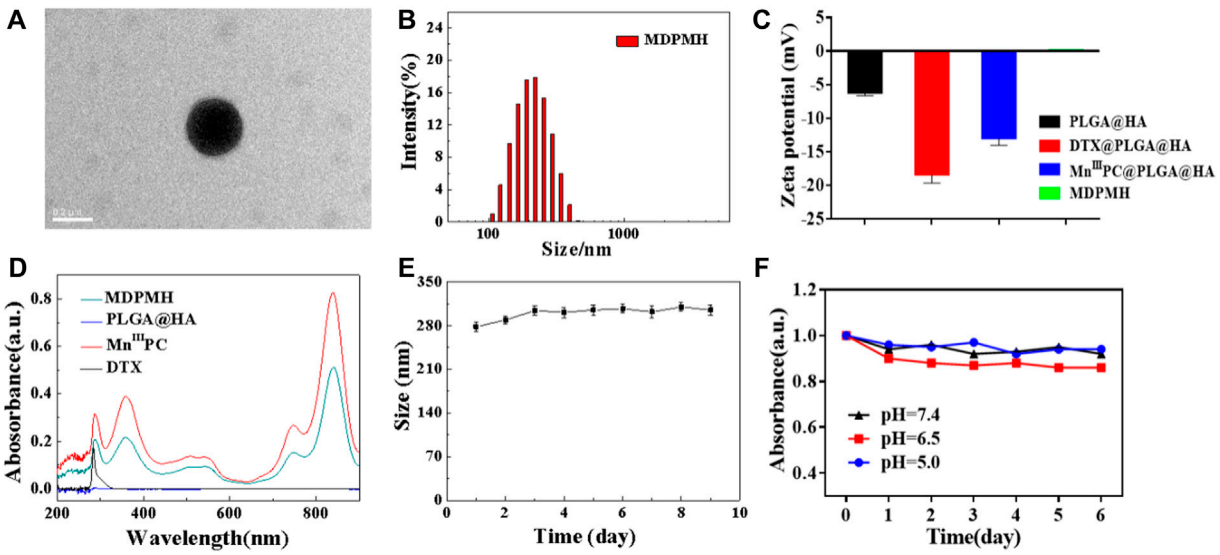


FIGURE 3 | (A) TEM image MDPMH, scale bar = 0.2 μm. **(B)** The size distribution of MDPMH. **(C)** Zeta potential of PLGA@HA, DTX@PLGA@HA, $Mn^{III}PC$@PLGA@HA, and MDPMH. **(D)** The UV-vis spectra of DTX, $Mn^{III}PC$, PLGA@HA, and MDPMH from 200 to 1,000 nm. **(E)** The size change of the MDPMH dispersed in the mixture solution of DMSO and H_2O. **(F)** The absorption spectrum of MDPMH nanoparticle under different pH conditions (5.0, 6.5, 7.4) in 6 days.

TABLE 1 | The drug loading content (DLC) and drug loading efficiency (DLE) in different nanoparticles.

	DLC (wt%)	DLE (%)
$Mn^{III}PC$@PLGA@HA	11.58%	78.00%
DTX@PLGA@HA	28.07%	87.00%
MDPMH	$Mn^{III}PC$: 3.15%:DTX: 37.46%	$Mn^{III}PC$: 54%; DTX: 64%

and Q band from the π electron transition on the benzene ring in the structure of phthalocyanine (Berríos et al., 2007; Göksel, 2016). The UV-vis absorbance spectra demonstrated the successful synthesis of MDPMH. The extinction coefficient of MDPMH was studied by detecting the absorbance at 832 nm with the different concentrations of the sample (**Supplementary Figure S2**), which were $1.025\times10^4\,l\,mol^{-1}\cdot cm^{-1}$. Additionally, the DLS and UV-Vis results demonstrated the good stability of MDPMH (**Figures 3E,F**).

Drug Loading and Release Behaviors

The DLC and drug loading efficiency (DLE) of different nanoparticles were detected and are shown in **Table.1**. The standard curve of DTX is shown in the supporting information. The DLC of $Mn^{III}PC$ in $Mn^{III}PC$@PLGA@HA was 11.58%, while $Mn^{III}PC$ in MDPMH was 3.15%, which might be attributed to the higher total mass of nanoparticles; The DLC of DTX in DTX@PLGA@HA was 28.07%, while the DTX in MDPMH was 37.46%, indicating the stronger absorption effect of DTX. The DLE of $Mn^{III}PC$ in $Mn^{III}PC$@PLGA@HA and DTX in DTX@PLGA@HA was 78.00% and 87.00%, respectively. Additionally, the DLE of $Mn^{III}PC$ and DTX reached 54% and 64%, respectively. The DLC of DTX presented an increasing trend after several drug-loading procedures, which was beneficial to the preparation of the nanoparticles. These results demonstrated that the MDPMH nanocarrier system had a higher loading capacity of $Mn^{III}PC$ and DTX.

To evaluate the release performance of the MDPMH nanoplatform, the *in vitro* release of Mn^{2+} and DTX was

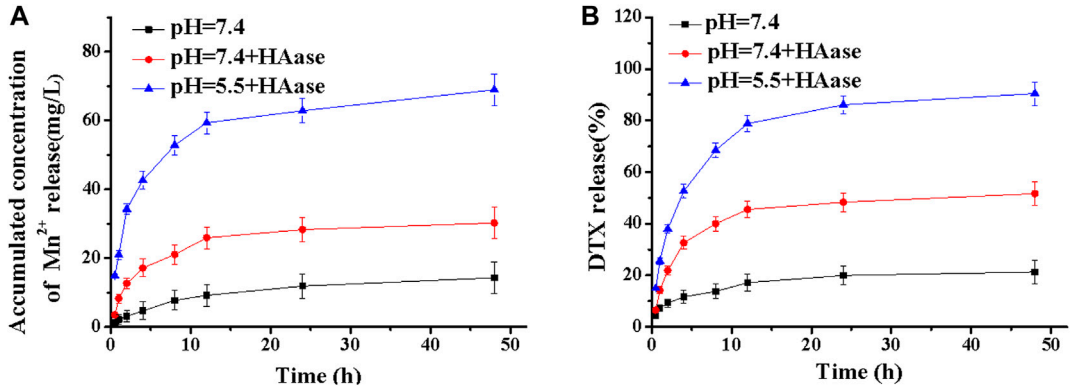


FIGURE 4 | Mass of cumulative Mn^{2+} **(A)** and mass percentage of DTX **(B)** released from MDPMH in buffer solutions (pH = 7.4, pH = 5.5 + HAase and pH = 7.4 + HAase) at 37°C.

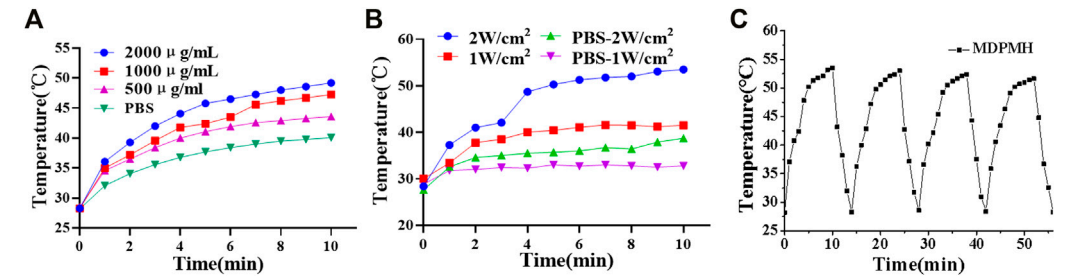


FIGURE 5 | Photothermal curves of the MDPMH at the various conditions with an 808-nm laser, PBS as the control group. **(A)** The photothermal effect of concentrations (500, 1,000 and 2,000 μg/ml) at the power energy of 1 W/cm^2. **(B)** The effect of laser power (1 W/cm^2, 2 W/cm^2). **(C)** The temperature variations of MDPMH at 2,000 μg/ml under 808-nm laser irradiation for 4 cycles.

investigated within 48 h (**Figure 4A**). As shown in **Figures 4A,B**, the concentration of Mn^{2+} and the release rate of DTX were not obvious while the Mn^{2+} concentration of pH = 5.5 + HAase exhibited the highest, which mainly owed to the degradation of HA on the surface of MDPMH under the stimulation of HAase, and the weakly acidic conditions further promoted the release of Mn^{2+} from MDPMH. Similarly, the release rate of DTX in **Figure 4B** also followed the regularity. The above experiments showed that MDPMH had good enzyme response release performance.

The photothermal properties of the MDPMH NPs were evaluated under 808-nm near-infrared laser irradiation (**Figure 5**). Phosphate buffer solution (PBS) containing the various concentrations of MDPMH Nanoparticles (500, 1,000 and 2,000 μg/ml) was irradiated with an 808-nm (2 W/cm^2) laser for 15 min, and the temperature was monitored. As shown in **Figure 5A**, the solution temperature increased with the increasing concentration of MDPMH, indicating a concentration-dependent photothermal effect. Then, the effects of laser **Figure 5B** power were examined (**Figure 5B**). The temperature of MDPMH solution could reach 53.5°C while the laser power was 2 W. Intriguingly, MDPMH nanoparticles could still reach 51.6°C after 808-nm laser irradiation for 4 cycles (**Figure 5C**). The results manifested that MDPMH has good photothermal conversion efficiency and photothermal stability.

Cell Viability and Cytotoxicity Performance *in vitro*

The cell viability of MDPMH *in vitro* was investigated by CCK-8 assay. Different groups [PBS (Control), Laser, PLGA@HA, Mn^{III}PC@PLGA@HA, Mn^{III}PC@PLGA@HA + laser, DTX@PLGA@HA, MDPMH, and MDPMH + laser] and concentrations (500, 1,000, 2,000 μg/ml) were studied on the growth of the A549 cells (**Figure 6A**). Compared with the control group, the cell activity of the Laser group did not change significantly. With the increase in the concentration, the cell activity of the PLGA@HA group did not decrease significantly, indicating that the nanocarrier is not the cause of A549 cytotoxicity. Under an 808-nm laser, MDPMH exhibited the lowest viability (around 5%) when the concentration was up to 2,000 μg/ml. The group of PLGA@HA showed little damage to the A549 cells. Although there was some injury to A549 cells from the groups of Mn^{III}PC@PLGA@HA nanoparticles with laser and DTX@PLGA@HA, the cell survival rate was significantly lower than MDPMH with 808-nm irradiation. These results demonstrated that the obtained nanosystem could effectively inhibit the

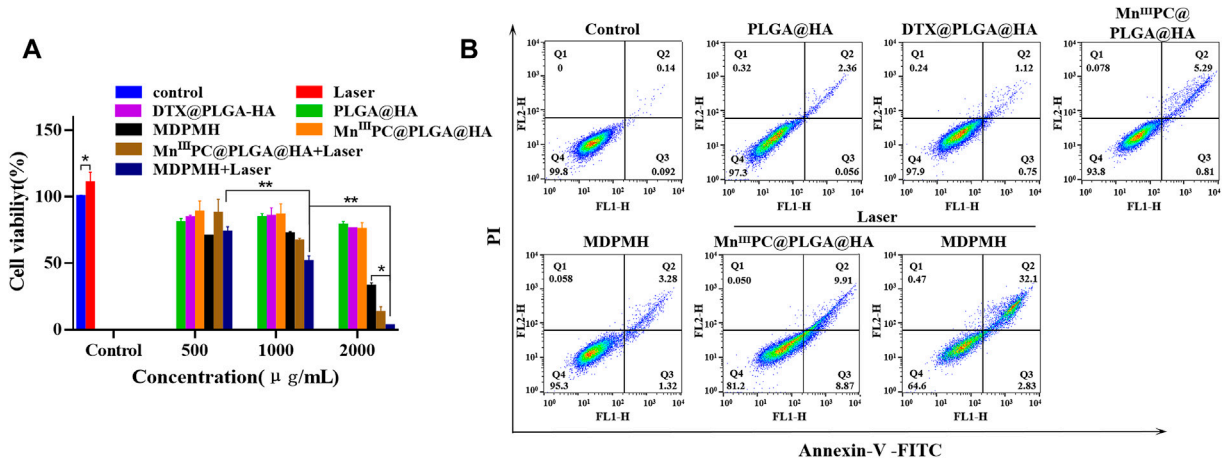


FIGURE 6 | (A) The cytocompatibility assessment of different nanoparticles on A549 by CCK-8 assay. **(B)** Flow cytometric analysis on the apoptosis levels of A549 cell incubation with Control, PLGA@HA, DTX@PLGA@HA, Mn^{III}PC@PLGA@HA, MDPMH, Mn^{III}PC@PLGA@HA + Laser, and MDPMH + Laser, $^{*}p < 0.05$, $^{**}p < 0.01$.

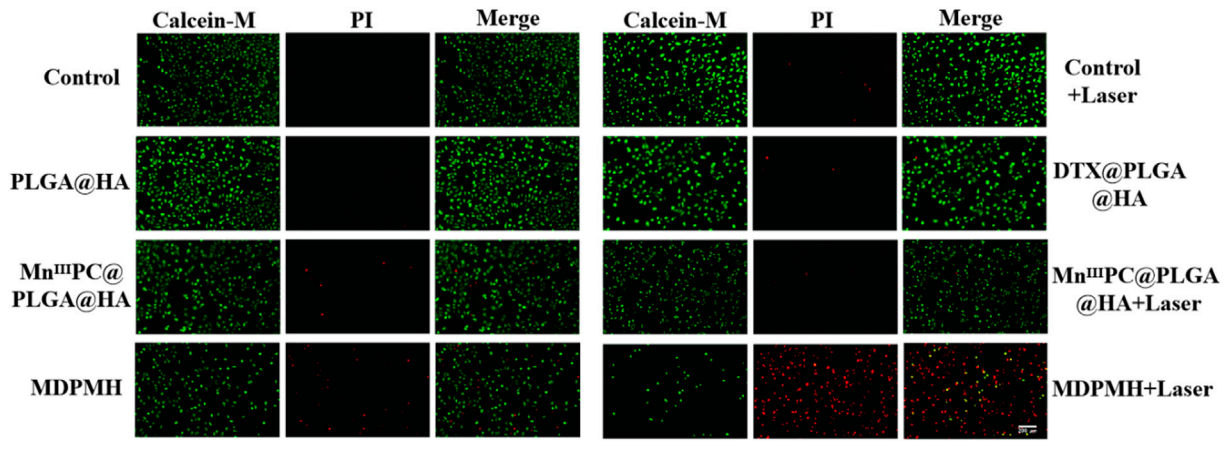


FIGURE 7 | A549 cells stained with calcein-AM under different conditions; live imaging was observed by a fluorescence microscope. Scale bars = 50 μm.

proliferation of tumor cells with the help of irradiation. Moreover, the antitumor effects from the apoptosis assays of various treatment groups were evaluated. As shown in **Figure 6B**, the PBS, PLGA@HA, DTX@PLGA@HA, Mn^{III}PC@PLGA@HA, and MDPMH groups barely affected the apoptosis of A549 cells, while Mn^{III}PC@PLGA@HA with light irradiation (808 nm, 2 W/cm^2) and MDPMH could promote the apoptosis of tumor cells, whose apoptosis ratio was ~20% and ~40%, respectively. As expected, the apoptosis ratio of cells treated by MDPMH under laser irradiation was higher than that of other groups, which could probably be attributed to the effect of PTT. Previous studies had confirmed that PTT could further enhance the permeability of the tumor cell membrane and thus improve the internalization of nanoparticles (Liu et al., 2019; Huang et al., 2021).

To further confirm the cytotoxicity of MDPMH nanoparticle *in vitro*, different nanoparticles were investigated by Calcein-AM/PI staining, respectively (**Figure 7**). Significantly, the strong green fluorescence appeared in the Control, Laser, and PLGA@HA groups, which showed good biocompatibility of nanocarriers and lasers. Compared with the DTX@PLGA@HA and Mn^{III}PC@PLGA@HA groups, the green fluorescence intensity weakened in the MDPMH group. Intriguingly, the MDPMH + Laser group has the strongest red fluorescence and the weakest green fluorescence, indicating the lowest cell viability with the irradiation of laser. Those results demonstrated that MDPMH might have synergistic antitumor effects of photothermal, chemotherapy, and immunotherapy.

Western Blot

To verify whether the release of Mn^{2+} could activate tumor immunity, the protein expression changes of cGAS, Bax, and Bcl-2 were detected with β-actin as internal reference protein. The corresponding results are shown in **Figure 8**. From **Figure 8A**, the expression of Bcl-2 was reduced after medication, while the expression of Bax was higher, which represents the increased apoptosis corresponding with the references (Hassan et al., 2014; Zhang et al., 2019). The corresponding gray values are shown in

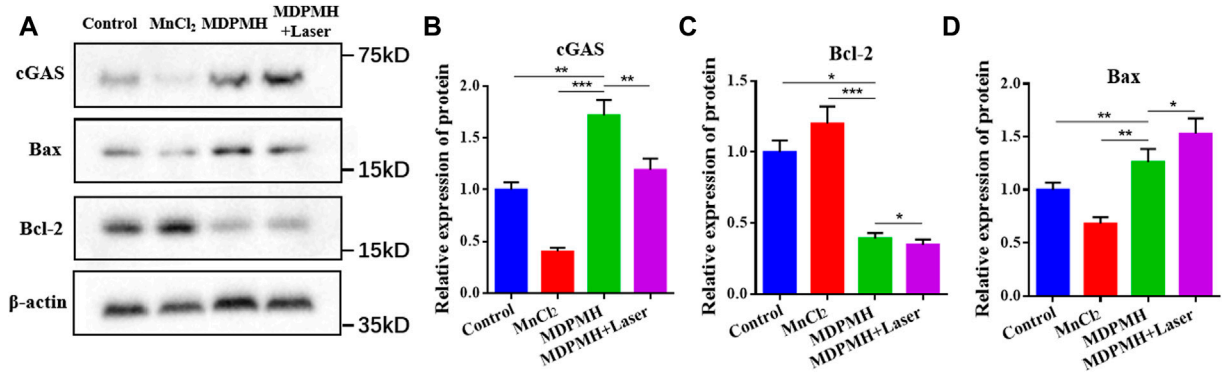


FIGURE 8 | (A) Western blot analysis on the expression of cGAS, Bax, and Bcl-2 in A549 cells after incubation with Control, $MnCl_2$, MDPMH, and MDPMH + Laser; β-actin was selected as internal reference protein. The relative expression of different proteins, cGAS **(B)**, Bax **(C)**, and Bcl-2 **(D)**. $^{*}p < 0.05$, $^{**}p < 0.01$, $^{***}p < 0.001$.

Figures 8B–D, which demonstrated the quantitative changes in relative protein expression. Additionally, the cGAS band in the $MnCl_2$ and control groups was shallow. It might be that the short retention time and low concentration of Mn^{2+} and the cGAS-STING pathway cannot be effectively activated. **Supplementary Figure S4** further clarified the relationship between the concentration of Mn^{2+} and the expression of cGAS. The group of MDPMH and MDPMH + Laser exhibited more deeply, which could probably be attributed to the Mn^{2+} released from MDPMH which could trigger the tumor immune response in the tumor by activating the cGAS-STING pathway (Hopfner and Hornung, 2020; Hou et al., 2020; Wang et al., 2020b). The proteins Bax and Bcl-2 are associated with cell apoptosis. Preclinical studies have shown that tumor PTT is associated with host-specific antitumor immune response (Zhang et al., 2020). After tumor hyperthermia, the immune function of the host body changes, and the antitumor immune response of the body is activated (Xu and Liang, 2020).

DISCUSSION

In this paper, a nanoplatform composed of HA, $Mn^{III}PC$, DTX, etc., was prepared for the NSCLC through PTT, chemotherapy, and immune therapy combination. The UV-visible spectra demonstrated the successful preparation of the nanoparticles (Rajawat and Malik, 2020). The MDPMH nanoparticles were obtained by easy methods such as self-assembly and coagulation, with uniform size distribution, spherical shape, and good stability. Under the 808-nm laser irradiation, MDPMH showed the optimal ability to clear the tumor cells by increasing the expression of apoptosis-related proteins and reducing the expression of proteins that inhibit apoptosis because of the loading of DTX and $Mn^{III}PC$. Besides, once Mn^{2+} could be released from MDPMH, it would activate the immune function of host body changes and the systemic antitumor immune response of the host, which could help remove tumor cells. However, the nanodelivery platform still needs to be improved. An example is the DLC. All in a word, the above mechanisms promise a localized drug-delivery platform for enhancing the therapeutic efficacy of PTT, chemotherapy, and immune therapy combination.

CONCLUSION

In summary, a smart nanodelivery platform was designed which combined multimodal therapy. The synthesized MDPMH with slightly positive electrical properties and surface-modified HA was beneficial to the uptake of NSCLC cells. Under 808-nm laser irradiation, the nanoplatform exhibited good PTT effect and photothermal stability. Importantly, MDPMH could effectively inhibit the growth of A549 cells, which was mainly ascribed to the coordinated effects of DTX, $Mn^{III}PC$, and Mn^{2+} in the nanocarrier system. The combined strategy may exploit great therapeutic effects and development potential.

DATA AVAILABILITY STATEMENT

The original contributions presented in the study are included in the article/**Supplementary Material**, further inquiries can be directed to the corresponding author.

AUTHOR CONTRIBUTIONS

Conceptualization, methodology, experimental design XF and SLM; manuscript writing, XF; reagent preparation and cell experiment, XX; material synthesis, XX writing—review and editing XF; supervision, project administration, funding acquisition, XF. All authors have read and agreed to the published version of the manuscript.

FUNDING

This research was funded by the Key Project of Hangzhou Health Science and Technology Plan (No. 0020190319).

SUPPLEMENTARY MATERIAL

The Supplementary Material for this article can be found online at: https://www.frontiersin.org/articles/10.3389/fphar.2022.832725/full#supplementary-material

REFERENCES

Ai, K., Huang, J., Xiao, Z., Yang, Y., Bai, Y., and Peng, J. (2021). Localized Surface Plasmon Resonance Properties and Biomedical Applications of Copper Selenide Nanomaterials. *Mater. Today Chem.* 20 (1), 100402. doi:10.1016/j.mtchem.2020.100402

Berríos, C., Cardenas-Jirón, G. I., Marco, J. F., Gutiérrez, C., and Ureta-Zañartu, M. S. (2007). Theoretical and Spectroscopic Study of Nickel(II) Porphyrin Derivatives. *J. Phys. Chem. A.* 111 (14), 2706–2714. doi:10.1021/jp0653961

Camidge, D. R., Doebele, R. C., and Kerr, K. M. (2019). Comparing and Contrasting Predictive Biomarkers for Immunotherapy and Targeted Therapy of NSCLC. *Nat. Rev. Clin. Oncol.* 16 (6), 341–355. doi:10.1038/s41571-019-0173-9

Chen, L., Zhou, L., Wang, C., Han, Y., Lu, Y., Liu, J., et al. (2019). Tumor-Targeted Drug and CpG Delivery System for Phototherapy and Docetaxel-Enhanced Immunotherapy with Polarization toward M1-Type Macrophages on Triple Negative Breast Cancers. *Adv. Mater.* 31 (52), e1904997. doi:10.1002/adma.201904997

Deng, L., Zhu, X., Yu, Z., Li, Y., Qin, L., Liu, Z., et al. (2020). Novel T7-Modified pH-Responsive Targeted Nanosystem for Co-Delivery of Docetaxel and Curcumin in the Treatment of Esophageal Cancer. *Int. J. Nanomedicine.* 15, 7745–7762. doi:10.2147/IJN.S257312

Dhas, N., Kudarha, R., Garkal, A., Ghate, V., Sharma, S., Panzade, P., et al. (2021). Molybdenum-Based Hetero-Nanocomposites for Cancer Therapy, Diagnosis and Biosensing Application: Current Advancement and Future Breakthroughs. *J. Control. Release.* 330, 257–283. doi:10.1016/j.jconrel.2020.12.015

Duma, N., Santana-Davila, R., and Molina, J. R. (2019). Non-Small Cell Lung Cancer: Epidemiology, Screening, Diagnosis, and Treatment. *Mayo Clin. Proc.* 94 (8), 1623–1640. doi:10.1016/j.mayocp.2019.01.013

Gao, Q., Wang, S., Chen, X., Cheng, S., Zhang, Z., Li, F., et al. (2019). Cancer-Cell-Secreted CXCL11 Promoted CD8+ T Cells Infiltration through Docetaxel-Induced-Release of HMGB1 in NSCLC. *J. Immunother. Cancer* 7 (1), 42. doi:10.1186/s40425-019-0511-6

Göksel, M. (2016). Synthesis of Asymmetric Zinc(II) Phthalocyanines with Two Different Functional Groups & Spectroscopic Properties and Photodynamic Activity for Photodynamic Therapy. *Bioorg. Med. Chem.* 24 (18), 4152–4164. doi:10.1016/j.bmc.2016.07.003

Hassan, M., Watari, H., AbuAlmaaty, A., Ohba, Y., and Sakuragi, N. (2014). Apoptosis and Molecular Targeting Therapy in Cancer. *Biomed. Res. Int.* 2014, 150845. doi:10.1155/2014/150845

Hopfner, K. P., and Hornung, V. (2020). Molecular Mechanisms and Cellular Functions of cGAS-STING Signalling. *Nat. Rev. Mol. Cel Biol.* 21 (9), 501–521. doi:10.1038/s41580-020-0244-x

Hou, L., Tian, C., Yan, Y., Zhang, L., Zhang, H., and Zhang, Z. (2020). Manganese-Based Nanoactivator Optimizes Cancer Immunotherapy via Enhancing Innate Immunity. *ACS Nano* 14 (4), 3927–3940. doi:10.1021/acsnano.9b06111

Huang, L., Li, Y., Du, Y., Zhang, Y., Wang, X., Ding, Y., et al. (2019). Mild Photothermal Therapy Potentiates Anti-PD-L1 Treatment for Immunologically Cold Tumors via an All-In-One and All-In-Control Strategy. *Nat. Commun.* 10 (1), 4871. doi:10.1038/s41467-019-12771-9

Huang, X., Lu, Y., Guo, M., Du, S., and Han, N. (2021). Recent Strategies for Nano-Based PTT Combined with Immunotherapy: From a Biomaterial Point of View. *Theranostics* 11 (15), 7546–7569. doi:10.7150/thno.56482

Jana, D., Jia, S., Bindra, A. K., Xing, P., Ding, D., and Zhao, Y. (2020). Clearable Black Phosphorus Nanoconjugate for Targeted Cancer Phototheranostics. *ACS Appl. Mater. Inter.* 12 (16), 18342–18351. doi:10.1021/acsami.0c02718

Jin, H. G., Zhong, W., Yin, S., Zhang, X., Zhao, Y. H., Wang, Y., et al. (2019). Lesson from Nature: Biomimetic Self-Assembling Phthalocyanines for High-Efficient Photothermal Therapy within the Biological Transparent Window. *ACS Appl. Mater. Inter.* 11 (4), 3800–3808. doi:10.1021/acsami.8b21299

Jing, F., Guo, Q., Xu, W., Qu, H., and Sui, Z. (2018). Docetaxel Prodrug Self-Assembled Nanosystem: Synthesis, Formulation and Cytotoxicity. *Bioorg. Med. Chem. Lett.* 28 (4), 826–830. doi:10.1016/j.bmcl.2017.07.041

Jonna, S., and Subramaniam, D. S. (2019). Molecular Diagnostics and Targeted Therapies in Non-Small Cell Lung Cancer (NSCLC): An Update. *Discov. Med.* 27 (148), 167–170.

Kaczmarek, B., Sionkowska, A., Kozlowska, J., and Osyczka, A. M. (2018). New Composite Materials Prepared by Calcium Phosphate Precipitation in Chitosan/Collagen/Hyaluronic Acid Sponge Cross-Linked by EDC/NHS. *Int. J. Biol. Macromol.* 107 (Pt A), 247–253. doi:10.1016/j.ijbiomac.2017.08.173

Lee, S. S., and Cheah, Y. K. (2019). The Interplay between MicroRNAs and Cellular Components of Tumour Microenvironment (TME) on Non-Small-Cell Lung Cancer (NSCLC) Progression. *J. Immunol. Res.* 2019, 3046379. doi:10.1155/2019/3046379

Li, X., Kim, C. Y., Lee, S., Lee, D., Chung, H. M., Kim, G., et al. (2017). Nanostructured Phthalocyanine Assemblies with Protein-Driven Switchable Photoactivities for Biophotonic Imaging and Therapy. *J. Am. Chem. Soc.* 139 (31), 10880–10886. doi:10.1021/jacs.7b05916

Li, L., Yang, Q., Shi, L., Zheng, N., Li, Z., Li, K., et al. (2019). Novel Phthalocyanine-Based Polymeric Micelles with High Near-Infrared Photothermal Conversion Efficiency under 808 Nm Laser Irradiation for *In Vivo* Cancer Therapy. *J. Mater. Chem. B.* 7 (14), 2247–2251. doi:10.1039/c9tb00011a

Lim, R. B. (2016). End-of-life Care in Patients with Advanced Lung Cancer. *Ther. Adv. Respir. Dis.* 10 (5), 455–467. doi:10.1177/1753465816660925

Liu, Y., Bhattarai, P., Dai, Z., and Chen, X. (2019). Photothermal Therapy and Photoacoustic Imaging via Nanotheranostics in Fighting Cancer. *Chem. Soc. Rev.* 48 (7), 2053–2108. doi:10.1039/c8cs00618k

Liu, Y., Li, J., Chen, M., Chen, X., and Zheng, N. (2020). Palladium-Based Nanomaterials for Cancer Imaging and Therapy. *Theranostics* 10 (22), 10057–10074. doi:10.7150/thno.45990

Lv, M., Chen, M., Zhang, R., Zhang, W., Wang, C., Zhang, Y., et al. (2020). Manganese Is Critical for Antitumor Immune Responses via cGAS-STING and Improves the Efficacy of Clinical Immunotherapy. *Cell Res* 30 (11), 966–979. doi:10.1038/s41422-020-00395-4

Mattheolabakis, G., Milane, L., Singh, A., and Amiji, M. M. (2015). Hyaluronic Acid Targeting of CD44 for Cancer Therapy: from Receptor Biology to Nanomedicine. *J. Drug Target.* 23 (7-8), 605–618. doi:10.3109/1061186X.2015.1052072

Poon, Z., Lee, J. B., Morton, S. W., and Hammond, P. T. (2011). Controlling *In Vivo* Stability and Biodistribution in Electrostatically Assembled Nanoparticles for Systemic Delivery. *Nano Lett.* 11 (5), 2096–2103. doi:10.1021/nl200636r

Rafiei, P., and Haddadi, A. (2017). Docetaxel-loaded PLGA and PLGA-PEG Nanoparticles for Intravenous Application: Pharmacokinetics and Biodistribution Profile. *Int. J. Nanomedicine.* 12, 935–947. doi:10.2147/IJN.S121881

Rajawat, S., and Malik, M. M. (2020). Targeted Delivery of Colloidal Silver for MCF-7 Breast Cancer Treatment. *Curr. Drug Deliv.* 17 (7), 613–621. doi:10.2174/1567201817666200508095241

Salwowska, N. M., Bebenek, K. A., Żądło, D. A., and Wcisło-Dziadecka, D. L. (2016). Physiochemical Properties and Application of Hyaluronic Acid: A Systematic Review. *J. Cosmet. Dermatol.* 15 (4), 520–526. doi:10.1111/jocd.12237

Song, Y., Wang, J., Liu, L., Sun, Q., You, Q., Cheng, Y., et al. (2018). One-Pot Synthesis of a Bismuth Selenide Hexagon Nanodish Complex for Multimodal Imaging-Guided Combined Antitumor Phototherapy. *Mol. Pharm.* 15 (5), 1941–1953. doi:10.1021/acs.molpharmaceut.8b00106

Taratula, O., Patel, M., Schumann, C., Naleway, M. A., Pang, A. J., He, H., et al. (2015). Phthalocyanine-Loaded Graphene Nanoplatform for Imaging-Guided Combinatorial Phototherapy. *Int. J. Nanomedicine.* 10, 2347–2362. doi:10.2147/IJN.S81097

Wang, L., Dong, S., Liu, Y., Ma, Y., Zhang, J., Yang, Z., et al. (2020). Fabrication of Injectable, Porous Hyaluronic Acid Hydrogel Based on an *In-Situ* Bubble-Forming Hydrogel Entrapment Process. *Polymers (Basel)* 12 (5), 1138. doi:10.3390/polym12051138

Wang, C., Zhang, R., Wei, X., Lv, M., and Jiang, Z. (2020). Metalloimmunology: The Metal Ion-Controlled Immunity. *Adv. Immunol.* 145, 187–241. doi:10.1016/bs.ai.2019.11.007

Xu, P., and Liang, F. (2020). Nanomaterial-Based Tumor Photothermal Immunotherapy. *Int. J. Nanomedicine.* 15, 9159–9180. doi:10.2147/IJN.S249252

Zhang, Y., Yang, X., Ge, X., and Zhang, F. (2019). Puerarin Attenuates Neurological Deficits via Bcl-2/Bax/Cleaved Caspase-3 and Sirt3/SOD2 Apoptotic Pathways in Subarachnoid Hemorrhage Mice. *Biomed. Pharmacother.* 109, 726–733. doi:10.1016/j.biopha.2018.10.161

Zhang, Y., Guo, C., Liu, L., Xu, J., Jiang, H., Li, D., et al. (2020). ZnO-Based Multifunctional Nanocomposites to Inhibit Progression and Metastasis of Melanoma by Eliciting Antitumor Immunity via Immunogenic Cell Death. *Theranostics* 10 (24), 11197–11214. doi:10.7150/thno.44920

Zheng, D., Zhang, K., Chen, B., Zhao, N., and Xu, F. J. (2020). Flexible Photothermal Assemblies with Tunable Gold Patterns for Improved Imaging-Guided Synergistic Therapy. *Small* 16 (34), e2002790. doi:10.1002/smll.202002790

Conflict of Interest: The authors declare that the research was conducted in the absence of any commercial or financial relationships that could be construed as a potential conflict of interest.

Publisher's Note: All claims expressed in this article are solely those of the authors and do not necessarily represent those of their affiliated organizations, or those of the publisher, the editors, and the reviewers. Any product that may be evaluated in this article, or claim that may be made by its manufacturer, is not guaranteed or endorsed by the publisher.

Copyright © 2022 Feng, Xiong and Ma. This is an open-access article distributed under the terms of the Creative Commons Attribution License (CC BY). The use, distribution or reproduction in other forums is permitted, provided the original author(s) and the copyright owner(s) are credited and that the original publication in this journal is cited, in accordance with accepted academic practice. No use, distribution or reproduction is permitted which does not comply with these terms.

frontiers | Frontiers in Pharmacology

TYPE Correction
PUBLISHED 07 September 2022
DOI 10.3389/fphar.2022.964540

Check for updates

OPEN ACCESS

APPROVED BY
Frontiers Editorial Office,
Frontiers Media SA, Switzerland

*CORRESPONDENCE
Shenglin Ma,
mashenglin0607@163.com

SPECIALTY SECTION
This article was submitted to Pharmacology of Anti-Cancer Drugs, a section of the journal Frontiers in Pharmacology

RECEIVED 08 June 2022
ACCEPTED 09 August 2022
PUBLISHED 07 September 2022

CITATION
Feng X, Xiong X and Ma S (2022), Corrigendum: Docetaxel-loaded novel nano-platform for synergistic therapy of non-small cell lung cancer. *Front. Pharmacol.* 13:964540. doi: 10.3389/fphar.2022.964540

COPYRIGHT
© 2022 Feng, Xiong and Ma. This is an open-access article distributed under the terms of the Creative Commons Attribution License (CC BY). The use, distribution or reproduction in other forums is permitted, provided the original author(s) and the copyright owner(s) are credited and that the original publication in this journal is cited, in accordance with accepted academic practice. No use, distribution or reproduction is permitted which does not comply with these terms.

Corrigendum: Docetaxel-loaded novel nano-platform for synergistic therapy of non-small cell lung cancer

Xing Feng[1,2], Xiaoling Xiong[3] and Shenglin Ma[4]*

[1]Department of Thoracic Surgery, The Affiliated Hangzhou Hospital of Nanjing Medical University, Hangzhou, China, [2]Department of Thoracic Surgery, Affiliated Hangzhou First People's Hospital, Zhejiang University School of Medicine, Hangzhou, China, [3]Department of Nephrology, Sir Run Run Shaw Hospital, Zhejiang University School of Medicine, Hangzhou, China, [4]Department of Oncology, The Affiliated Hangzhou Hospital of Nanjing Medical University, Hangzhou, China

KEYWORDS

non-small cell lung cancer, targeted therapy, immunotherapy, photothermal therapy, cGAS-STING

A Corrigendum on
Docetaxel-loaded novel nano-platform for synergistic therapy of non-small cell lung cancer

by Feng X, Xiong X and Ma S (2022). Front. Pharmacol. 13:832725. doi: 10.3389/fphar.2022.832725

In the published article, there was an error in the author list. Author Xing Feng was erroneously listed as corresponding author. The corrected author list appears below:

"Xing Feng[1,2], Xiaoling Xiong[3] and Shenglin Ma[4]*

*Correspondence: Shenglin Ma, mashenglin0607@163.com"

The authors apologize for this error and state that this does not change the scientific conclusions of the article in any way. The original article has been updated.

Publisher's note

All claims expressed in this article are solely those of the authors and do not necessarily represent those of their affiliated organizations, or those of the publisher, the editors and the reviewers. Any product that may be evaluated in this article, or claim that may be made by its manufacturer, is not guaranteed or endorsed by the publisher.

frontiers in Pharmacology

ORIGINAL RESEARCH
published: 08 March 2022
doi: 10.3389/fphar.2022.865065

Study on the Mechanism of Astragalus Polysaccharide in Treating Pulmonary Fibrosis Based on "Drug-Target-Pathway" Network

Pingping Bing, Wenhu Zhou and Songwen Tan**

Academician Workstation, Changsha Medical University, Changsha, China

Pulmonary fibrosis is a chronic, progressive and irreversible heterogeneous disease of pulmonary interstitial tissue. Its incidence is increasing year by year in the world, and it will be further increased due to the pandemic of COVID-19. However, at present, there is no safe and effective treatment for this disease, so it is very meaningful to find drugs with high efficiency and less adverse reactions. The natural astragalus polysaccharide has the pharmacological effect of anti-pulmonary fibrosis with little toxic and side effects. At present, the mechanism of anti-pulmonary fibrosis of astragalus polysaccharide is not clear. Based on the network pharmacology and molecular docking method, this study analyzes the mechanism of Astragalus polysaccharides in treating pulmonary fibrosis, which provides a theoretical basis for its further clinical application. The active components of Astragalus polysaccharides were screened out by Swisstarget database, and the related targets of pulmonary fibrosis were screened out by GeneCards database. Protein-protein interaction network analysis and molecular docking were carried out to verify the docking affinity of active ingredients. At present, through screening, we have obtained 92 potential targets of Astragalus polysaccharides for treating pulmonary fibrosis, including 11 core targets. Astragalus polysaccharides has the characteristics of multi-targets and multi-pathways, and its mechanism of action may be through regulating the expression of VCAM1, RELA, CDK2, JUN, CDK1, HSP90AA1, NOS2, SOD1, CASP3, AHSA1, PTGER3 and other genes during the development of pulmonary fibrosis.

Keywords: Astragalus polysaccharides, pulmonary fibrosis, network pharmacology, molecular docking, mechanism

OPEN ACCESS

Edited by:
Zeming Liu,
Huazhong University of Science and Technology, China

Reviewed by:
Yan Zhang,
Hunan Normal University, China
Yunrun Liu,
Hong Kong Baptist University, Hong Kong SAR, China

****Correspondence:***
Wenhu Zhou
zhouwenhuyaoji@163.com
Songwen Tan
tansongwening@gmail.com

Specialty section:
This article was submitted to Pharmacology of Anti-Cancer Drugs, a section of the journal Frontiers in Pharmacology

Received: *03 February 2022*
Accepted: *16 February 2022*
Published: *08 March 2022*

Citation:
Bing P, Zhou W and Tan S (2022) Study on the Mechanism of Astragalus Polysaccharide in Treating Pulmonary Fibrosis Based on "Drug-Target-Pathway" Network. Front. Pharmacol. 13:865065. doi: 10.3389/fphar.2022.865065

INTRODUCTION

Pulmonary fibrosis is caused by many causes, and it is a chronic, progressive and irreversible heterogeneous disease of pulmonary interstitial tissue (Raghu et al., 2011). Including pulmonary fibrosis caused by secondary factors and idiopathic pulmonary fibrosis. The pathological features of pulmonary fibrosis are mainly the proliferation of lung fibroblasts and excessive deposition of extracellular matrix, which leads to the destruction of lung tissue structure and eventually leads to chronic respiratory failure (Datta et al., 2011; King et al., 2011). There are many factors leading to pulmonary fibrosis, mainly including smoking and environmental exposure, genetic factors, virus infection and complications (Renzoni et al., 2014; Zaman and Lee, 2018). The data show that the incidence of pulmonary fibrosis is increasing year by year in the world and is similar to that of liver

cancer, gastric cancer and cervical cancer (Hutchinson et al., 2015). At present, with the global spread of Coronavirus Disease 2019 (COVID-19), there may be more patients with pulmonary fibrosis. COVID-19 can cause severe lung injury and may lead to pulmonary fibrosis. Previous data of coronavirus infection (SARS-CoV or MERS-CoV) and new data of COVID-19 pandemic indicate that severe fibrosis may occur after SARS-CoV-2 infection (George et al., 2020). Early diagnosis of pulmonary fibrosis is difficult and incurable, and the prognosis is very poor. The median survival time after diagnosis is 2–3 years, The 5-year survival rate is less than 30% (Vancheri and du Bois, 2013; Wuyts et al., 2020). At present, the main treatments for pulmonary fibrosis are drug therapy and lung transplantation. Lung transplantation is the most effective treatment at present, but it is limited by the supply of donor organs, economic situation and patients' situation (Kistler et al., 2014). As for drug therapy, so far only Pirfenidone and Nidanib have been approved by FDA for the treatment of pulmonary fibrosis worldwide (Mora et al., 2017; Lederer and Martinez, 2018). These two anti-fibrosis drugs can improve patients' lung function, but they still can't cure pulmonary fibrosis and have obvious side effects, such as diarrhea and drug-induced liver injury, anorexia, vomiting and photosensitive rash, etc. (Richeldi et al., 2014; King et al., 2014). At present, the pathogenesis of pulmonary fibrosis is not clear, but the incidence of pulmonary fibrosis is on the rise, especially with the pandemic of COVID-19, the incidence of pulmonary fibrosis secondary to COVID-19 will further increase, and seriously affect the health of patients. Although many treatments have been used to treat pulmonary fibrosis, there is still no safe and effective treatment. Therefore, it is of great significance to find drugs with high efficiency and less adverse reactions to improve the quality of life and survival rate of patients with pulmonary fibrosis. A large number of clinical and experimental studies show that traditional Chinese medicine can obviously improve many pathological links of pulmonary fibrosis, and the toxicity of traditional Chinese medicine is relatively small, which can improve the quality of life of patients and reduce the mortality rate, and has a good application prospect (Zhao et al., 2017). Among them, Astragalus membranaceus plays an important role in treating fibrosis (Ma et al., 2020). Astragalus membranaceus has been used in Chinese medicine for nearly 2000 years and is one of the most popular Chinese medicines in the world (Shahrajabian et al., 2019). As one of the traditional Chinese medicines commonly used in clinic, Astragalus membranaceus can improve and treat various diseases, and has many pharmacological effects, such as antioxidation (Shahzad et al., 2016), immunomodulation (Block and Mead, 2003), antifibrosis (Zhou et al., 2016), antitumor (Zhou et al., 2018) and analgesia (Di Cesare Mannelli et al., 2017). The main bioactive components in Astragalus membranaceus include polysaccharides, saponins, flavonoids and alkaloids (Shahrajabian et al., 2019). Among them, Astragalus polysaccharide is the most abundant component in Astragalus membranaceus, which has a variety of pharmacological activities (Zheng et al., 2020). The main components of Astragalus polysaccharides include dextran, heteropolysaccharide, acidic polysaccharide, and neutral polysaccharide. The monosaccharide components of Astragalus polysaccharide include glucose, glucuronic acid, arabinose, rhamnose, fructose, mannose, galactose, galacturonic acid, fucose, etc (Wang et al., 2019). Studies have shown that Astragalus polysaccharide has anti-fibrosis pharmacological activity, and the main active ingredient of Astragalus membranaceus in anti-pulmonary fibrosis may be Astragalus polysaccharide. However, due to the complex components of Astragalus polysaccharide, the research on the anti-pulmonary fibrosis mechanism of Astragalus polysaccharide is relatively lacking at present, and the anti-pulmonary fibrosis mechanism of Astragalus polysaccharide is still unclear (Li et al., 2011).

Network pharmacology is a new discipline of multi-target drug molecular design by network construction and selecting specific signal Nodes. Emphasis is placed on the multi-channel regulation of signal pathway, improving the therapeutic effect of drugs and reducing the toxic and side effects, thus opening up new ways for drug development and utilization and saving the research and development cost of drugs (Zhang et al., 2019). Molecular docking is a computer simulation of the recognition process between two or more molecules, which involves spatial matching and energy matching between molecules. Molecular docking methods are widely used in drug design, screening and other fields (Morris and Lim-Wilby, 2008). Based on network pharmacology and molecular docking technology, this study preliminarily explored the mechanism of Astragalus polysaccharides in anti-pulmonary fibrosis, provided possible therapeutic drugs for the treatment of pulmonary fibrosis, and laid a theoretical foundation for the clinical application of Astragalus polysaccharides in anti-pulmonary fibrosis.

METHODS

Screening of Key Active Components and Targets in Astragalus Polysaccharides

HERB (http://herb.ac.cn/) is a platform for pharmacology of Chinese herbal medicines. The database mainly includes the chemical substances, targets and drug target networks of Chinese herbal medicines (Ru et al., 2014). We searched the HERB database for related chemical components with "Astragalus membranaceus" as the key word, and finally screened the components of Astragalus membranaceus polysaccharides from the above-mentioned searched compounds by combining with references. Pubchem database (https://pubchem.ncbi.nlm.nih.gov/) is a biological activity database of small organic molecules supported by the National Institutes of Health and maintained by the National Biotechnology Information Center (Li et al., 2010). We get the SMILES numbers of the compound components through Pubchem database. SwissTargetPrediction database (www.swisstargetprediction.ch/) is a database for target prediction of more than 3,000 kinds of protein and more than 370,000 kinds of known active substances of different species (Zoete et al., 2016). We import the SMILES of the obtained compounds into Swiss Target Prediction database to predict the target of Astragalus polysaccharide.

Screening of Disease Targets

Enter the keyword "Pulmonary fibrosis" in the human gene database GeneCards (//www.genecards.org), and collect the disease targets related to pulmonary fibrosis (Safran et al., 2002). Then, with the help of jvenn (http://www.bioinformatics.com.cn/static/others/jvenn/example.html), the active ingredient targets of Astragalus polysaccharides screened out are intersected with the targets related to pulmonary fibrosis, and finally, the potential targets of Astragalus polysaccharides for treating pulmonary fibrosis are determined.

Network Construction

Through the software Cytoscape (v3.7.1), the screened active ingredients and the potential targets are visualized by constructing the network between the active ingredients and the potential targets (Lopes et al., 2010). And further construct the target topology network by using BisoGenet. STRING database is a database for searching protein-protein interactions, which contains a large number of PPI data verified by experiments and predicted by bioinformatics methods. In order to analyze the interaction between the potential target genes and proteins of Astragalus polysaccharide in anti-pulmonary fibrosis, a PPI(protein-protein interaction) network was built by STRING database (https://cn.string-db.org/), which was set as *Homo sapiens* and high confidence of 0.700, and the key targets were screened by visualization and network topology heterogeneity analysis in Cytoscape software.

KEGG and GO Enrichment Analysis

In order to describe and annotate the functions of target genes and explore the signal pathways of their functions, we input the selected core targets into the DAVID database (//www.genecards.org) (Huang et al., 2009). The species is limited to human, and the enrichment analysis of GO and KEGG is carried out with $p < 0.05$ as the screening condition. The enrichment analysis of GO includes the enrichment analysis of biological process, BP), cellular component, CC) and molecular function (MF). Through enrichment analysis, the biological processes and potential signal pathways involved in the treatment of pulmonary fibrosis by Astragalus polysaccharides were screened out. In addition, the pathway enrichment analysis of core targets is carried out by ClueGO.

Molecular Docking

Generally, we judge the binding degree of ligand and receptor by the level of energy. When the conformation of compound molecule and receptor is stable, the lower the energy, the greater the possibility of action. We use molecular docking technology to study the binding ability of the selected target protein to active compounds. We obtained the 3D structure of the target protein obtained by the above screening through PDB database. With the active ingredient of Astragalus polysaccharide as the ligand, the processed ligand was molecularly docked with the target protein in Autodock Vina 1.1.2 software (Trott and Olson, 2010). Finally, the docking results are visualized by PyMOL 2.3.4 software.

RESULT

Screening of Key Active Components and Targets in Astragalus Polysaccharides

We searched the HERB database for the keyword "huang qi" to obtain the active ingredient chemistry of Astragalus membranaceus. Finally, we determined the ingredients of Astragalus membranaceus polysaccharide from these ingredients screened from Astragalus membranaceus. We obtained 10 kinds of polysaccharide ingredients, namely D-Galacturonic acid, Alpha-L-Rhamnose, D-ascorbicacid, Vitamin C, L-Rhamnose, DL-Glucuronic acid, L-(-)-Fucose, DL-Xylose, glucose, arabinose. Search the HERB database for related targets of Astragalus polysaccharides, and predict the targets of some polysaccharide components through Swiss Target Prediction database, and finally get 142 targets of Astragalus polysaccharides (**Figure 1**).

Screening of Disease Targets

With "pulmonary fibrosis" as the key word, 5,783 genes were preliminarily screened out from Genecards database, and the potential targets of Astragalus polysaccharides for treating pulmonary fibrosis were obtained by intersecting the selected targets with disease targets by using jvenn (http://www.bioinformatics.com.cn/static/others/jvenn/example.html). As shown in **Figure 1A**, 142 related targets of Astragalus polysaccharides were screened, among which there were 92 potential targets for treating pulmonary fibrosis. We introduced ten compounds and corresponding targets in Astragalus polysaccharide into Cytoscape to construct a polysaccharide component-target network. As shown in **Figure 1B**, it can be seen from the network diagram that compounds act on multiple targets, and some targets also correspond to multiple compounds. Among them, the sub-network degree value of Vitamin C and related targets is high, and most targets are potential targets for treating pulmonary fibrosis, suggesting that Vitamin C may play an important role in the treatment of pulmonary fibrosis by Astragalus polysaccharides.

KEGG and GO Enrichment Analysis

DAVID database was used for GO and KEGG enrichment analysis of Astragalus polysaccharide in treating pulmonary fibrosis. The results of KEGG pathway enrichment analysis are shown in **Figure 2A**, mainly including Pathways in cancer, Malaria, TNF signaling pathway, NF-kappa B signaling pathway, Rheumatoid arthritis, Non-alcoholic fatty liver disease (NAFLD), Leishmaniasis, Pertussis, Inflammatory bowel disease (IBD), PPAR signaling pathway, Tuberculosis, Chagas disease (American trypanosomiasis), Amoebiasis, Herpes simplex infection, Hepatitis B, Amyotrophic lateral sclerosis (ALS), Small cell lung cancer, NOD-like receptor signaling pathway, MAPK signaling pathway etc.

GO enrichment analysis results show that it mainly involves response to hypoxia, response to drug, response to ethanol, aging, positive regulation of cell division, response to antibiotic, inflammatory response, negative regulation of apoptotic

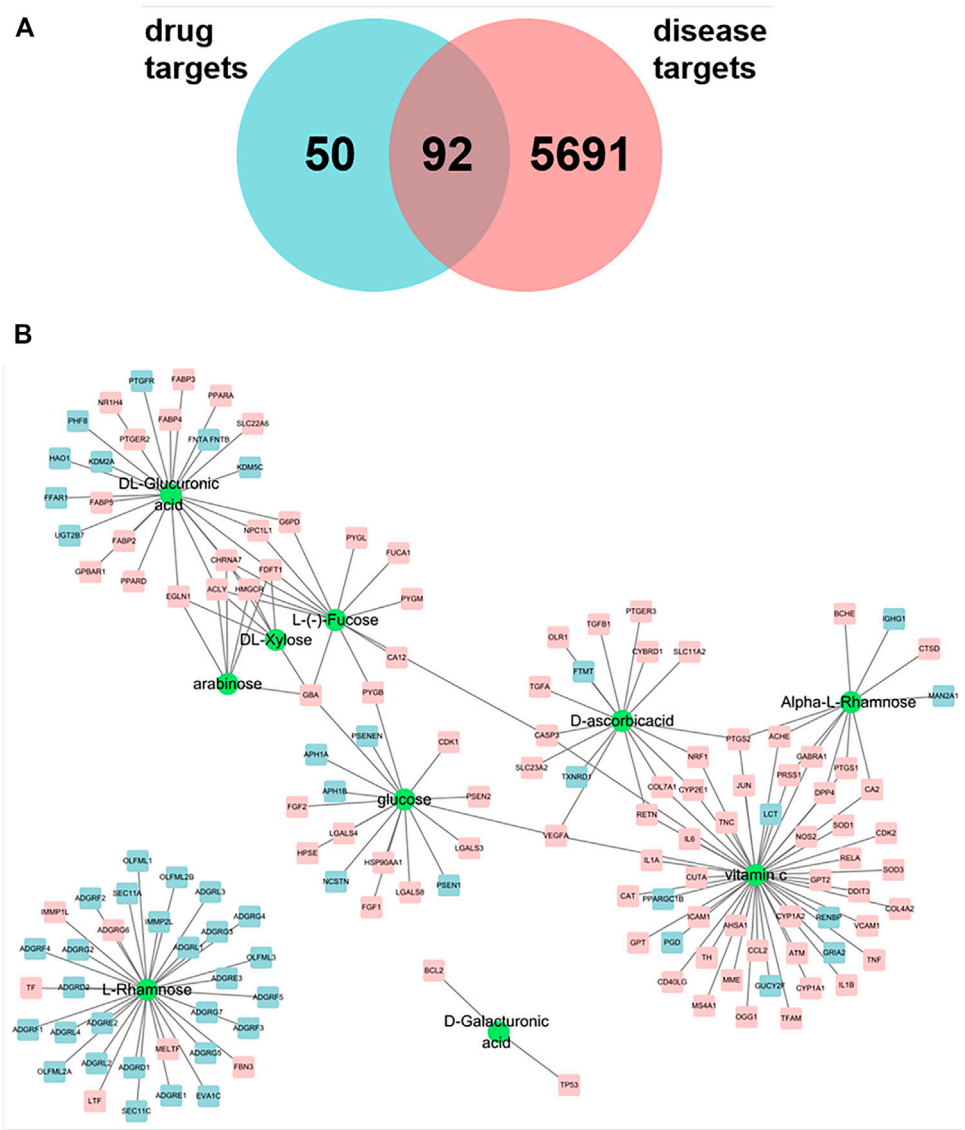


FIGURE 1 | (A) Venn maps of components and disease targets have 92 common targets. **(B)** Components-Target network of astragalus polysaccharide. The green circle indicated the component, and the square was the action target of polysaccharide component, and the pink square was the potential treatment target of pulmonary fibrosis.

process, positive regulation of ERK1 and ERK2 cascade, positive regulation of NF-kappaB transcription factor activity, extracellular space, extracellular exosome, cell surface, extracellular matrix, extracellular region, protein homodimerization activity, enzyme binding, cytokine activity, glycogen phosphorylase activity, heme binding etc. (**Figure 2B**).

Network Construction and Screening of Core Targets

The protein interaction network of potential targets of Astragalus polysaccharide in treating pulmonary fibrosis was obtained by using the BisoGenet plug-in in Cytoscape. As shown in **Figure 3**, there are 4,411 node in network a and 159,341 target interaction relationships. In order to screen out the core targets of the network more accurately, network b was extracted with the median values of the three evaluation indexes of Betweenness, Degree and Closeness as the boundaries, and there were 1770 nodes and 80,027 kinds of target interactions in network b. We continued to extract the targets of the top 500 indexes in network b to build interactive network c, which had 226 nodes and 6,281 kinds of target interactions. In the core network c, we found 11 direct targets, VCAM1, RELA, CDK2, JUN, CDK1, HSP90AA1, NOS2, SOD1, CASP3, AHSA1, PTGER3, which had the greatest

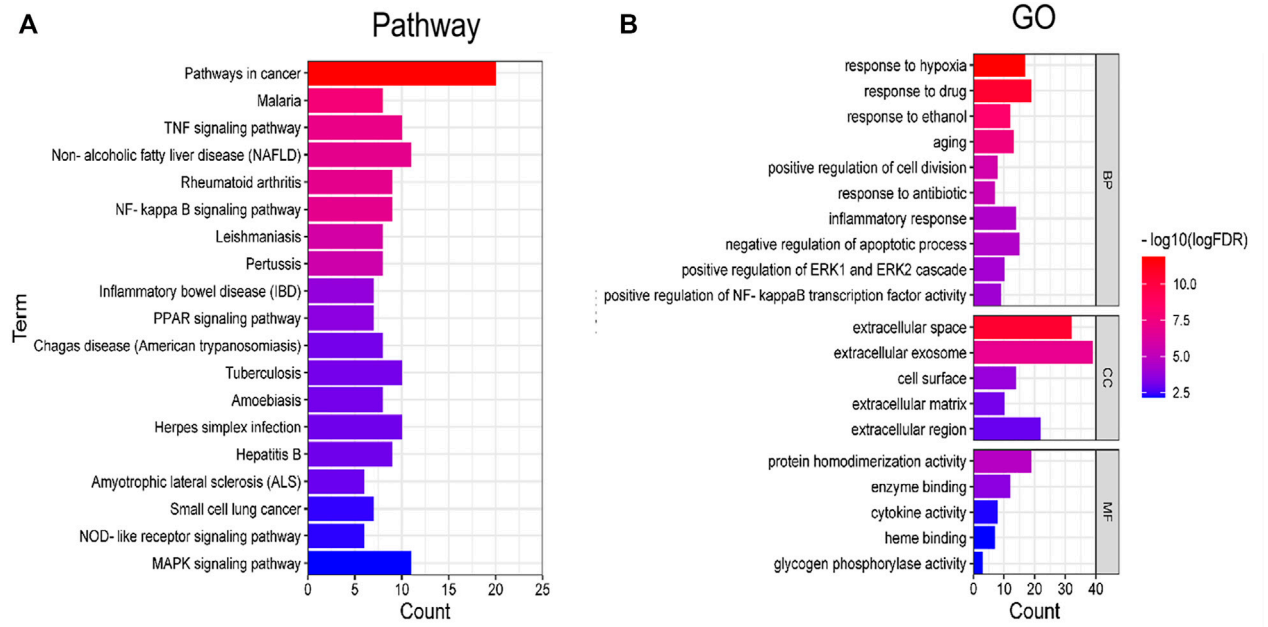


FIGURE 2 | Enrichment analysis of KEGG and GO. **(A)** Pathway enrichment analysis. **(B)** GO enrichment analysis.

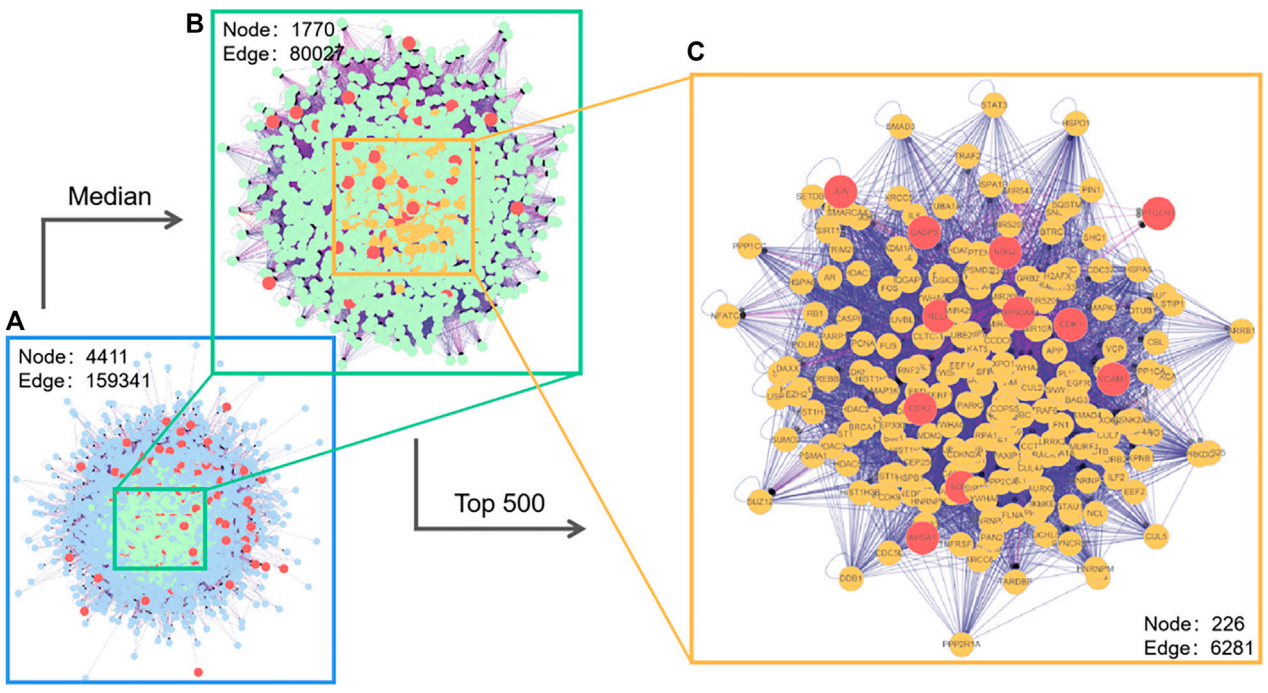


FIGURE 3 | Interaction network of Astragalus polysaccharide targets (with magnified median figure and the top 500 points).

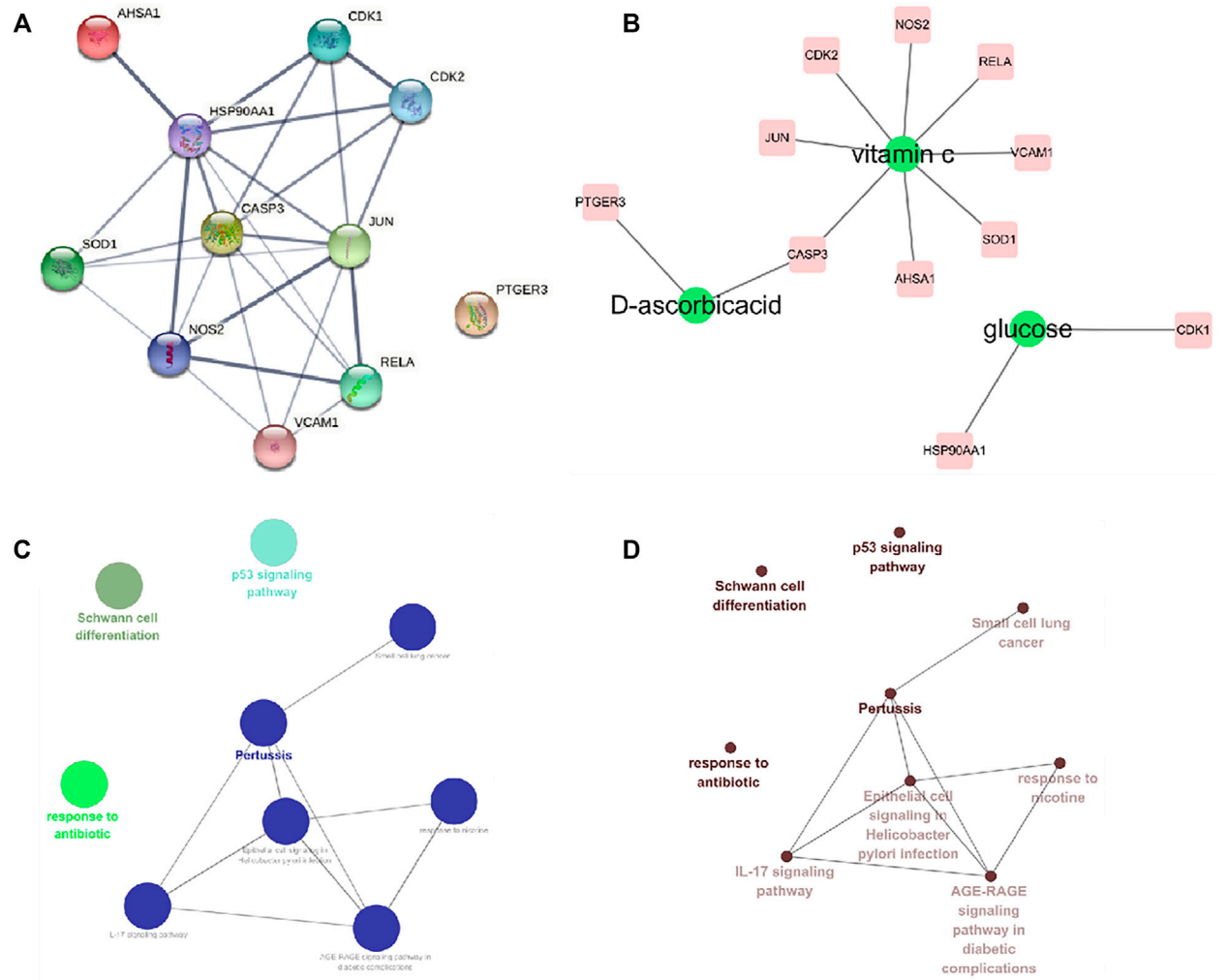


FIGURE 4 | Interaction network of core targets and pathway enrichment analysis. **(A)** Interaction network of core targets. **(B)** Core target component network **(C,D)** Core targets pathway enrichment network.

correlation with Astragalus polysaccharides in treating pulmonary fibrosis. Therefore, we regard these 11 targets as the potential core targets of Astragalus polysaccharides in treating pulmonary fibrosis.

Construction and Enrichment Analysis of Core Target Network

We have further constructed PPI network for these 11 core targets, and found that JUN, CASP3 and HSP90AA1 have higher degrees in the network, suggesting that they may play a key role in the treatment (**Figure 4A**). In addition, we also screened out three components of Astragalus polysaccharides that act on the 11 core targets (D-ascorbicacid, Vitamin C, Glucose) (**Figure 4B**). And ClueGO was used to construct pathways enrichment network for the core targets, and the pathways enrichment includes Schwann cell differentiation, p53 signaling pathway, response to antibiotic, Pertussis, Small cell lung cancer, IL-17 signaling pathway, Epithelial cell signaling in *Helicobacter pylori* infection, response to nicotine, AGE-RAGE signaling pathway in diabetic complications. Among them, four types were obtained by clustering (**Figures 4C,D**).

Molecular Docking

Up to now, only pirfenidone and Nidanib have been approved by FDA to treat pulmonary fibrosis in the world, and these two drugs have a good clinical effect on pulmonary fibrosis. According to previous reports, pirfenidone can inhibit targets such as IL6 and TNFα, and through the previous component target network construction, we found the polysaccharide component (Vitamin C) that acts on these two targets, so we follow up with the docking scores of pirfenidone with IL6 and TNFα as reference values. The results show that the affinity scores of Vitamin C, an active compound in Astragalus polysaccharides, with these two targets are similar to

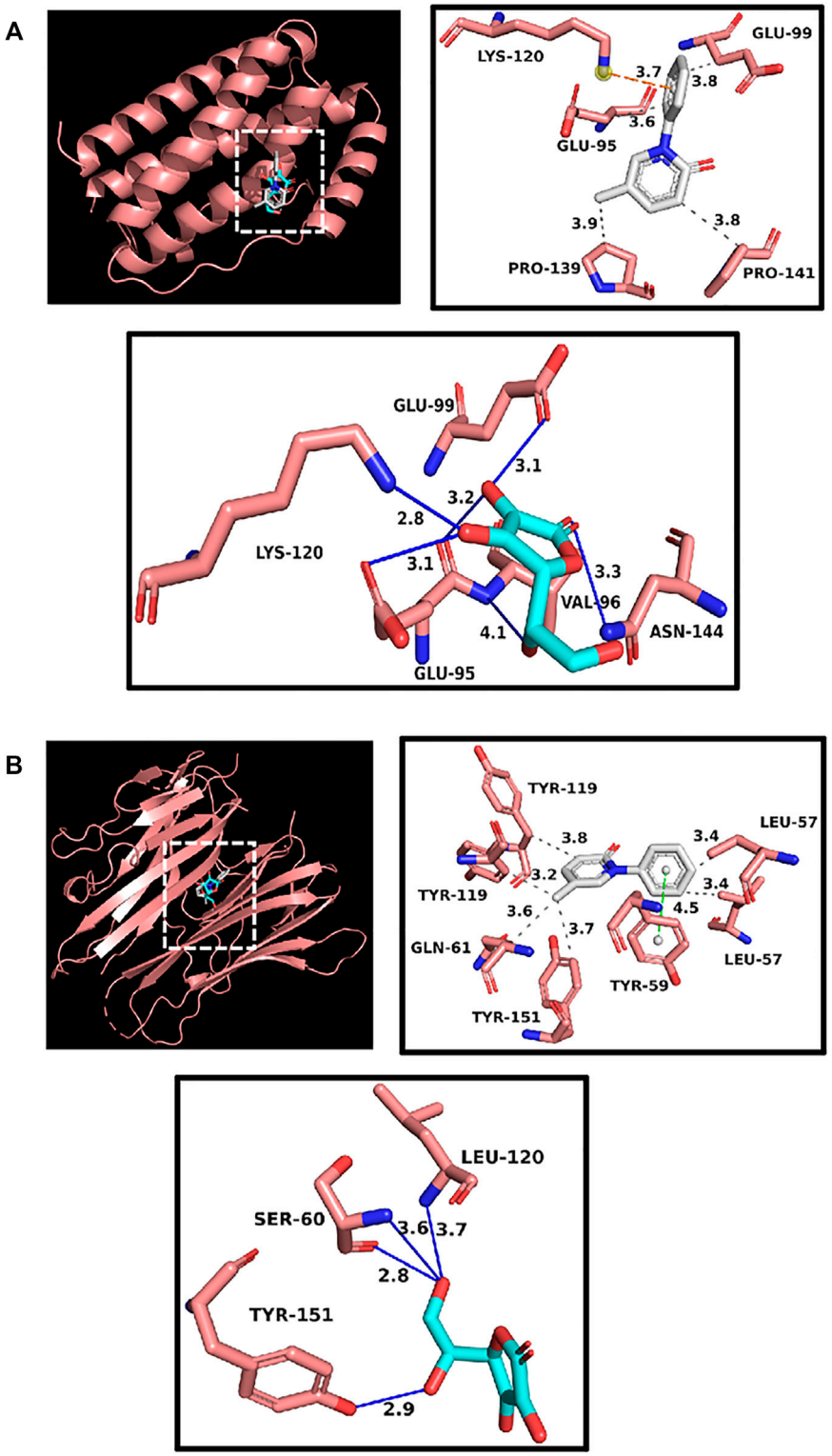


FIGURE 5 | (A) Docking display of pirfenidone and Vitamin C with IL6 respectively. Gray compound represents pirfenidone, and blue compounds represent Vitamin C. **(B)** Docking display of pirfenidone and Vitamin C with TNFα respectively. Gray compound represents pirfenidone, and blue compounds represent Vitamin C.

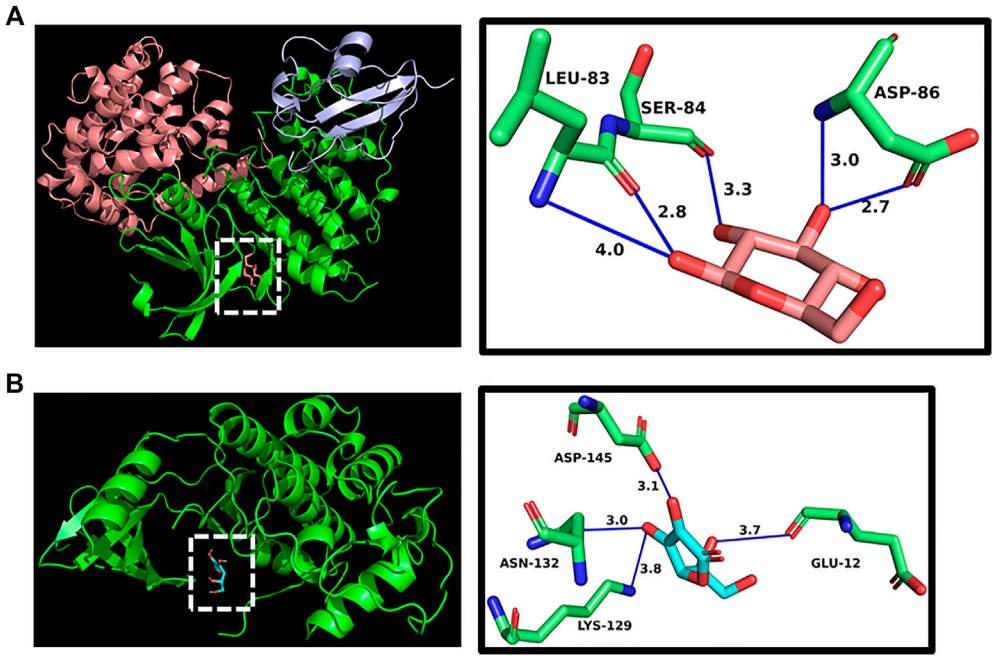


FIGURE 6 | (A) Docking display of CDK1 and glucose. **(B)** Docking display of CDK2 and Vitamin C.

those of pirfenidone, indicating that the key active substances in Astragalus polysaccharides may play an anti-pulmonary fibrosis role, and the molecular docking is shown in **Figure 5**. In addition, we have docked two core targets, CDK1 and CDK2, and docked the Glucose and Vitamin C acting on these two targets into the active pockets of small molecule inhibitors of CDK1 and CDK2, respectively. CDK1 and CDK2 belong to cyclin-dependent protein kinases, which are important factors in cell cycle regulation. It has been reported that lung fibrosis can be controlled to some extent by inhibiting CDKs. It was found that the affinity was similar to the docking scores of IL6 and TNFα, indicating that these key active components may play a key role in the treatment of pulmonary fibrosis (**Figure 6**).

DISCUSSION

For a long time, the treatment of pulmonary fibrosis has been a difficult problem in the world. Except for lung transplantation, there is still a lack of very effective treatment drugs and methods (Kistler et al., 2014). At present, the western medicines used clinically to treat pulmonary fibrosis, such as pirfenidone and Nidanib, can only slow down the decline rate of pulmonary function in patients with mild to moderate pulmonary fibrosis, but the adverse reactions are obvious and expensive. The clinical mortality rate of pulmonary fibrosis is not lower than that of tumor, and the incidence rate is increasing year by year. Due to the pandemic of COVID-19, the incidence rate will further increase (Hutchinson et al., 2015; George et al., 2020). However, there is no ideal therapeutic drug at present, and the pathogenesis is not completely clear and complicated. Therefore, it is very meaningful to find more effective therapeutic targets and drug research and development. In recent years, with the deepening of research on pulmonary fibrosis, the exploration of treating pulmonary fibrosis with traditional Chinese medicine has gradually increased, and great progress has been made in treating pulmonary fibrosis with traditional Chinese medicine, which has attracted much attention because of its multi-channels, multi-targets, few side effects and remarkable curative effect (Ji et al., 2020; Yu et al., 2020). Astragalus polysaccharide is an important active substance in Astragalus membranaceus. Studies have shown that Astragalus polysaccharide has anti-fibrosis pharmacological activities (Li et al., 2011). However, the components of Astragalus polysaccharides are complex, and at present, there is a lack of research on the mechanism of Astragalus polysaccharides against pulmonary fibrosis, and the mechanism of Astragalus polysaccharides against pulmonary fibrosis is still unclear. In this study, the core pharmacodynamic substances and targets were preliminarily determined by network pharmacology, and the core targets were enriched by GO and KEGG pathways. Finally, the molecular docking study of these core active components and core targets was carried out by AutoDock Vina to verify the analysis results of network pharmacology. Ten kinds of active ingredients in Astragalus polysaccharides were screened out, among which Ascorbicacid, Glucose and D-Ascorbicacid are the core targets in the network, suggesting that these active ingredients play an important role in the treatment of pulmonary fibrosis by Astragalus polysaccharides. By analyzing the target interaction network VCAM1,RELA,CDK2,JUN,CDK1,HSP90AA1,NOS2,

SOD1,CASP3,AHSA1, PTGER3 are at the core of the network, which can be regarded as the key targets of Astragalus polysaccharides in treating pulmonary fibrosis.

Marcia Rodrigues et al.' s research shows that Asorbicacid can treat pulmonary fibrosis caused by paraquat poisoning, and the results of animal experiments show that Asorbic acid mainly treats pulmonary fibrosis by reducing the number of macrophages, neutrophils and lymphocytes in fibrotic mice, reducing the levels of IL-6, TGF-β and IL-17 and increasing the activity of antioxidant enzymes in lung homogenate (Rodrigues da Silva et al., 2018). It was suggested that glucose metabolism may be beneficial to prevent myofibroblast differentiation in idiopathic pulmonary fibrosis (Azuelos, 2020). VCAM1 is upregulated in idiopathic pulmonary fibrosis, which can induce TGF-β1, and its main mechanism is to inhibit the proliferation of fibroblasts by reducing G2/M and S phases of cell cycle (Agassandian et al., 2015). Previous studies have shown that the phosphorylation of RELA on Ser536 will affect hepatic myofibroblasts. For pulmonary fibrosis, current studies have shown that the phosphorylation of RELA on Ser536 may be the core regulator of pulmonary fibroblasts (Moles et al., 2013). JNK is a member of mitogen-related protein kinase family. Studies have shown that JNK plays an important role in pulmonary fibrosis, in which JNK1 promotes collagen deposition and leads to further development of pulmonary fibrosis (Alcorn et al., 2009).

Through GO enrichment analysis of the key targets of effective components of Astragalus membranaceus, it is confirmed that Astragalus membranaceus has certain influence on many biological processes, such as response to hypoxia, aging, positive regulation of cell division, response to antibiotic, inflammatory response, negative regulation of apoptotic process, etc. Pathways related to pulmonary fibrosis in KEGG pathway mainly include Pathways in cancer, Malaria, TNF signaling pathway, Non-alcoholic fatty liver disease (NAFLD), Rheumatoid arthritis, NF- kappa B signaling pathway, Pertussis, Tuberculosis, Herpes simplex infection, Hepatitis B, Small cell lung cancer etc.

The results of molecular docking show that the binding properties of the main active components of Astragalus polysaccharides to the key targets selected from the research results are similar to those of the control drug pirfenidone, which indicates that the key active components of Astragalus polysaccharides can stably bind to receptors and play an anti-pulmonary fibrosis role. The molecular docking prediction results provide further evidence for the active components of Astragalus polysaccharide to act on specific targets to treat pulmonary fibrosis.

In this study, a "compound-target" network was established by the method of network pharmacology, and the relationship between pulmonary fibrosis, active components of Astragalus polysaccharides and their targets was studied as a whole. The key compounds and core targets of Astragalus polysaccharides for treating lung cancer and their action pathways were screened, and the multi-component, multi-target and multi-pathway action mechanism of anti-lung cancer was preliminarily discussed, which provided important theoretical clues and basis for further in-depth study on the medicinal material basis and action mechanism of Astragalus polysaccharides for treating pulmonary fibrosis. In this paper, the mechanism of action of Astragalus polysaccharide is discussed based on its chemical components and targets, but it cannot fully reflect the influence of metabolites of Astragalus polysaccharide on the mechanism of action. Therefore, the results of this study still have some limitations, and it is necessary to further verify the results of pharmacological prediction analysis based on network.

DATA AVAILABILITY STATEMENT

The original contributions presented in the study are included in the article/Supplementary Material, further inquiries can be directed to the corresponding authors.

AUTHOR CONTRIBUTIONS

PB contributed to conception and design of the study. WZ organized the database. ST wrote the first draft of the manuscript. All authors contributed to manuscript revision, read, and approved the submitted version.

REFERENCES

Agassandian, M., Tedrow, J. R., Sembrat, J., Kass, D. J., Zhang, Y., Goncharova, E. A., et al. (2015). VCAM-1 Is a TGF-B1 Inducible Gene Upregulated in Idiopathic Pulmonary Fibrosis. *Cell Signal* 27 (12), 2467–2473. doi:10.1016/j.cellsig.2015.09.003

Alcorn, J. F., van der Velden, J., Brown, A. L., McElhinney, B., Irvin, C. G., and Janssen-Heininger, Y. M. (2009). c-Jun N-Terminal Kinase 1 Is Required for the Development of Pulmonary Fibrosis. *Am. J. Respir. Cel Mol Biol* 40 (4), 422–432. doi:10.1165/rcmb.2008-0174OC

Azuelos, I. (2020). Glucose Metabolism in Idiopathic Pulmonary Fibrosis. London: University College London. Thesis.

Block, K. I., and Mead, M. N. (2003). Immune System Effects of Echinacea, Ginseng, and astragalus: a Review. *Integr. Cancer Ther.* 2 (3), 247–267. doi:10.1177/1534735403256419

Datta, A., Scotton, C. J., and Chambers, R. C. (2011). Novel Therapeutic Approaches for Pulmonary Fibrosis. *Br. J. Pharmacol.* 163 (1), 141–172. doi:10.1111/j.1476-5381.2011.01247.x

Di Cesare Mannelli, L., Pacini, A., Micheli, L., Femia, A. P., Maresca, M., Zanardelli, M., et al. (2017). Astragali Radix: Could it Be an Adjuvant for Oxaliplatin-Induced Neuropathy? *Sci. Rep.* 7, 42021–42113. doi:10.1038/srep42021

George, P. M., Wells, A. U., and Jenkins, R. G. (2020). Pulmonary Fibrosis and COVID-19: the Potential Role for Antifibrotic Therapy. *Lancet Respir. Med.* 8 (8), 807–815. doi:10.1016/S2213-2600(20)30225-3

Huang, da. W., Sherman, B. T., and Lempicki, R. A. (2009). Systematic and Integrative Analysis of Large Gene Lists Using DAVID Bioinformatics Resources. *Nat. Protoc.* 4 (1), 44–57. doi:10.1038/nprot.2008.211

Hutchinson, J., Fogarty, A., Hubbard, R., and McKeever, T. (2015). Global Incidence and Mortality of Idiopathic Pulmonary Fibrosis: a Systematic Review. *Eur. Respir. J.* 46 (3), 795–806. doi:10.1183/09031936.00185114

Ji, K., Ma, J., Wang, L., Li, N., Dong, S., Shi, L., et al. (2020). Efficacy and Safety of Traditional Chinese Medicine in Idiopathic Pulmonary Fibrosis: a Meta-Analysis. *Evidence-Based Complement. Altern. Med.* 2020, 1752387. doi:10.1155/2020/1752387

King, T. E., Jr, Bradford, W. Z., Castro-Bernardini, S., Fagan, E. A., Glaspole, I., Glassberg, M. K., et al. (2014). A Phase 3 Trial of Pirfenidone in Patients with Idiopathic Pulmonary Fibrosis. *N. Engl. J. Med.* 370 (22), 2083–2092. doi:10.1056/NEJMoa1402582

King, T. E., Jr, Pardo, A., and Selman, M. (2011). Idiopathic Pulmonary Fibrosis. *Lancet* 378 (9807), 1949–1961. doi:10.1016/S0140-6736(11)60052-4

Kistler, K. D., Nalysnyk, L., Rotella, P., and Esser, D. (2014). Lung Transplantation in Idiopathic Pulmonary Fibrosis: a Systematic Review of the Literature. *BMC Pulm. Med.* 14, 139–212. doi:10.1186/1471-2466-14-139

Lederer, D. J., and Martinez, F. J. (2018). Idiopathic Pulmonary Fibrosis. *N. Engl. J. Med.* 378 (19), 1811–1823. doi:10.1056/nejmra1705751

Li, J., Li, j. Y., Chen, J. J., and Lu, L. C. (2011). Effects of Astragalus Polysaccharides on Level of Cytokines and Pathological Structure of Lung Tissue in Rat Model of Pulmoanry Fibrosis. *Lishizhen Med. Materia Med. Res.* 22 (7), 1684–1685. doi:10.1016/j.carbpol.2020.116740

Li, Q., Cheng, T., Wang, Y., and Bryant, S. H. (2010). PubChem as a Public Resource for Drug Discovery. *Drug Discov. Today* 15 (23-24), 1052–1057. doi:10.1016/j.drudis.2010.10.003

Lopes, C. T., Franz, M., Kazi, F., Donaldson, S. L., Morris, Q., and Bader, G. D. (2010). Cytoscape Web: an Interactive Web-Based Network Browser. *Bioinformatics* 26 (18), 2347–2348. doi:10.1093/bioinformatics/btq430

Ma, L., Wang, R., and Miao, M. (2020). Medication Rule of Chinese Materia Medica in Treatment of Pulmonary Fibrosis Based on Data Mining [Chinese]. *Chin. Traditional Herbal Drugs* 51, 1406–1411. doi:10.7501/j.issn.0253-2670.2020.06.005

Moles, A., Sanchez, A. M., Banks, P. S., Murphy, L. B., Luli, S., Borthwick, L., et al. (2013). Inhibition of RelA-Ser536 Phosphorylation by a Competing Peptide Reduces Mouse Liver Fibrosis without Blocking the Innate Immune Response. *Hepatology* 57 (2), 817–828. doi:10.1002/hep.26068

Mora, A. L., Rojas, M., Pardo, A., and Selman, M. (2017). Emerging Therapies for Idiopathic Pulmonary Fibrosis, a Progressive Age-Related Disease. *Nat. Rev. Drug Discov.* 16 (11), 755–772. doi:10.1038/nrd.2017.170

Morris, G. M., and Lim-Wilby, M. (2008). Molecular Docking, in Molecular Modeling of Proteins. *Methods Mol. Biol.*, 443 365–382. doi:10.1007/978-1-59745-177-2_19

Raghu, G., Collard, H. R., Egan, J. J., Martinez, F. J., Behr, J., Brown, K. K., et al. (2011). An Official ATS/ERS/JRS/ALAT Statement: Idiopathic Pulmonary Fibrosis: Evidence-Based Guidelines for Diagnosis and Management. *Am. J. Respir. Crit. Care Med.* 183 (6), 788–824. doi:10.1164/rccm.2009-040GL

Renzoni, E., Srihari, V., and Sestini, P. (2014). Pathogenesis of Idiopathic Pulmonary Fibrosis: Review of Recent Findings. *F1000prime Rep.* 6, 69. doi:10.12703/P6-69

Richeldi, L., du Bois, R. M., Raghu, G., Azuma, A., Brown, K. K., Costabel, U., et al. (2014). Efficacy and Safety of Nintedanib in Idiopathic Pulmonary Fibrosis. *N. Engl. J. Med.* 370 (22), 2071–2082. doi:10.1056/NEJMoa1402584

Rodrigues da Silva, M., Schapochnik, A., Peres Leal, M., Esteves, J., Bichels Hebeda, C., Sandri, S., et al. (2018). Beneficial Effects of Ascorbic Acid to Treat Lung Fibrosis Induced by Paraquat. *PLoS One* 13, e0205535. doi:10.1371/journal.pone.0205535

Ru, J., Li, P., Wang, J., Zhou, W., Li, B., Huang, C., et al. (2014). TCMSP: a Database of Systems Pharmacology for Drug Discovery from Herbal Medicines. *J. Cheminform* 6 (1), 13–16. doi:10.1186/1758-2946-6-13

Safran, M., Solomon, I., Shmueli, O., Lapidot, M., Shen-Orr, S., Adato, A., et al. (2002). GeneCards 2002: towards a Complete, Object-Oriented, Human Gene Compendium. *Bioinformatics* 18 (11), 1542–1543. doi:10.1093/bioinformatics/18.11.1542

Shahrajabian, M., Sun, W., and Cheng, Q. (2019). *A Review of astragalus Species as Foodstuffs, Dietary Supplements, a Traditional Chinese Medicine and a Part of Modern Pharmaceutical Science. Appl. Ecol. Environ. Res.* 17, 13371–13382.doi:10.15666/aeer/1706_1337113382

Shahzad, M., Shabbir, A., Wojcikowski, K., Wohlmuth, H., and Gobe, G. C. (2016). The Antioxidant Effects of Radix Astragali (Astragalus Membranaceus and Related Species) in Protecting Tissues from Injury and Disease. *Curr. Drug Targets* 17 (12), 1331–1340. doi:10.2174/1389450116666150907104742

Trott, O., and Olson, A. J. (2010). AutoDock Vina: Improving the Speed and Accuracy of Docking with a New Scoring Function, Efficient Optimization, and Multithreading. *J. Comput. Chem.* 31 (2), 455–461. doi:10.1002/jcc.21334

Vancheri, C., and du Bois, R. M. (2013). A Progression-free End-point for Idiopathic Pulmonary Fibrosis Trials: Lessons from Cancer. *Eur. Respir. J.* 41 (2), 262–269. doi:10.1183/09031936.00115112

Wang, J., Jia, J., Song, L., Gong, X., Xu, J., Yang, M., et al. (2019). *Extraction, Structure, and Pharmacological Activities of Astragalus Polysaccharides. Appl. Sci.* 9 (1), 122. doi:10.3390/app9010122

Wuyts, W. A., Wijsenbeek, M., Bondue, B., Bouros, D., Bresser, P., Robalo Cordeiro, C., et al. (2020). Idiopathic Pulmonary Fibrosis: Best Practice in Monitoring and Managing a Relentless Fibrotic Disease. *Respiration* 99 (1), 73–82. doi:10.1159/000504763

Yu, X. Q., Yang, S. G., Xie, Y., and Li, J. S. (2020). Traditional Chinese Medicine in the Treatment of Idiopathic Pulmonary Fibrosis Based on Syndrome Differentiation: Study Protocol of an Exploratory Trial. *J. Integr. Med.* 18 (2), 163–168. doi:10.1016/j.joim.2019.12.005

Zaman, T., and Lee, J. S. (2018). Risk Factors for the Development of Idiopathic Pulmonary Fibrosis: a Review. *Curr. Pulmonol Rep.* 7 (4), 118–125. doi:10.1007/s13665-018-0210-7

Zhang, R., Zhu, X., Bai, H., and Ning, K. (2019). Network Pharmacology Databases for Traditional Chinese Medicine: Review and Assessment. *Front. Pharmacol.* 10, 123. doi:10.3389/fphar.2019.00123

Zhao, G. Z., Guo, Y. H., Li, B., Hu, J., Chen, T. F., Di, H. R., et al. (2017). Research Progress of Traditional Chinese Medicine in Prevention and Treatment of Sepsis. *Zhongguo Zhong Yao Za Zhi* 42 (8), 1423–1429. doi:10.19540/j.cnki.cjcmm.2017.0038

Zheng, Y., Ren, W., Zhang, L., Zhang, Y., Liu, D., and Liu, Y. (2020). A Review of the Pharmacological Action of Astragalus Polysaccharide. *Front. Pharmacol.* 11, 349. doi:10.3389/fphar.2020.00349

Zhou, R., Chen, H., Chen, J., Chen, X., Wen, Y., and Xu, L. (2018). Extract from Astragalus Membranaceus Inhibit Breast Cancer Cells Proliferation via PI3K/AKT/mTOR Signaling Pathway. *BMC Complement. Altern. Med.* 18 (1), 83–88. doi:10.1186/s12906-018-2148-2

Zhou, Y., Tong, X., Ren, S., Wang, X., Chen, J., Mu, Y., et al. (2016). Synergistic Anti-liver Fibrosis Actions of Total astragalus Saponins and Glycyrrhizic Acid via TGF-β1/Smads Signaling Pathway Modulation. *J. Ethnopharmacol* 190, 83–90. doi:10.1016/j.jep.2016.06.011

Zoete, V., Daina, A., Bovigny, C., and Michielin, O. (2016). SwissSimilarity: a Web Tool for Low to Ultra High Throughput Ligand-Based Virtual Screening. *ACS Publications* 56, 1399–1404. doi:10.1021/acs.jcim.6b00174

Conflict of Interest: The authors declare that the research was conducted in the absence of any commercial or financial relationships that could be construed as a potential conflict of interest.

Publisher's Note: All claims expressed in this article are solely those of the authors and do not necessarily represent those of their affiliated organizations, or those of the publisher, the editors and the reviewers. Any product that may be evaluated in this article, or claim that may be made by its manufacturer, is not guaranteed or endorsed by the publisher.

Copyright © 2022 Bing, Zhou and Tan. This is an open-access article distributed under the terms of the Creative Commons Attribution License (CC BY). The use, distribution or reproduction in other forums is permitted, provided the original author(s) and the copyright owner(s) are credited and that the original publication in this journal is cited, in accordance with accepted academic practice. No use, distribution or reproduction is permitted which does not comply with these terms.

frontiers in Oncology

REVIEW
published: 09 March 2022
doi: 10.3389/fonc.2022.858185

Melanoma and Nanotechnology-Based Treatment

Hong Zeng†, *Jia Li*†, *Kai Hou*†, *Yiping Wu*, *Hongbo Chen** *and Zeng Ning**

Department of Plastic and Cosmetic Surgery, Tongji Hospital, Tongji Medical College, Huazhong University of Science and Technology, Wuhan, China

Melanoma is a malignant tumor arising in melanocytes from the basal layer of the epidermis and is the fifth most commonly diagnosed cancer in the United States. Melanoma is aggressive and easily metastasizes, and the survival rate is low. Nanotechnology-based diagnosis and treatment of melanoma have attracted increasing attention. Importantly, nano drug delivery systems have the advantages of increasing drug solubility, enhancing drug stability, prolonging half-life, optimizing bioavailability, targeting tumors, and minimizing side effects; thus, these systems can facilitate tumor cytotoxicity to achieve effective treatment of melanoma. In this review, we discuss current nanosystems used in the diagnosis and treatment of melanoma, including lipid systems, inorganic nanoparticles, polymeric systems, and natural nanosystems. The excellent characteristics of novel and effective drug delivery systems provide a basis for the broad applications of these systems in the diagnosis and treatment of melanoma, particularly metastatic melanoma.

Keywords: melanoma, nanotechnology, drug delivery, cytotoxicity, metastasis

OPEN ACCESS

Edited by:
Kelong Ai,
Central South University, China

Reviewed by:
Jia Huang,
Central South University, China
Honghe Liu,
Johns Hopkins University, United States
Chengzhi Huang,
South China University of Technology, China

****Correspondence:***
Zeng Ning
zengningwhtj@163.com
Hongbo Chen
chenhongbo_xh@sina.com

†These authors have contributed equally to this work

Specialty section:
This article was submitted to Pharmacology of Anti-Cancer Drugs, a section of the journal Frontiers in Oncology

Received: *19 January 2022*
Accepted: *16 February 2022*
Published: *09 March 2022*

Citation:
Zeng H, Li J, Hou K, Wu Y, Chen H and Ning Z (2022) Melanoma and Nanotechnology-Based Treatment. Front. Oncol. 12:858185. doi: 10.3389/fonc.2022.858185

INTRODUCTION

Epidemiology of Melanoma

Melanoma is a type of malignant tumor derived from melanocytes in the basal layer of the epidermis. In the past few decades, the incidence of melanoma has increased rapidly in the developed countries, including the United States, Australia, and Spain, with higher incidence rates in fair-skinned individuals and older men (1). According to the latest SEER data, there were an estimated 106,000 new cases of melanoma in the United States in 2021, accounting for 5.6% of all cancer diagnoses, excluding non-melanoma skin cancer, which has become the fifth most commonly diagnosed cancer in the United States (2). The incidence of melanoma in Australia peaked around 2005, and continued decreases are expected owing to improvements in public health campaigns and the use of sunscreen (3).

In terms of prognosis, melanoma accounts for more than 80% of skin cancer-related deaths, despite representing a low percentage of total skin cancer cases (2). In the United States, with improvements in prevention, screening, diagnosis, and treatment (particularly targeted therapies and immunotherapies) in recent years, the 5-year overall survival rate of patients with melanoma

Abbreviations: DDSs, drug delivery systems; HuIFNb, human interferon B; –Si–O–, silanol; $dSiO_2$, dense silica; MSN, mesoporous silica; BMSN, biodegradable mesoporous silica; PD-1, programmed cell death-1.

has increased to more than 93%. Although the 5-year survival rate of patients with stage I–II disease is 99.4%, those of patients with stage III and IV disease are 68.0% and 29.8%, respectively (2).

Subtypes of Melanoma

Melanoma can be divided into many clinical subtypes according to pathological type and molecular marker expression. Based on pathological type, melanoma can be divided into four common subtypes, as follows: superficial diffusion type, nodular type, malignant melanoma freckles melanoma, and acral freckle-like melanoma. Rarely, melanoma may also present as epithelioid type, which shows characteristics of fiber proliferation, as well as malignant pigmented nevus, balloon sample cells, spindle cells, and giant pigmented nevus malignant melanoma. The superficial diffuse type is most common in Caucasians, and acral freckle-like melanoma is most common in individuals of Asian and African descent (2).

Many studies have evaluated the relationships between molecular biological characteristics, clinical histological characteristics, and gene variations in melanoma in recent years, and the results have shown that specific types of melanoma are related to specific gene variations; therefore, scholars have proposed a new classification method based on molecular biological characteristics, which is more conducive to the application of clinical diagnosis and treatment (4–6). The new classification method can be divided into four basic types: extremum, mucous, chronic sun damage (CSD), and non-CSD (including unknown primary lesions). Notably, 28% of patients with sun damage-related melanoma harbor *KIT* gene mutations, whereas 10% harbor *BRAF* mutations and 5% harbor *NRAS* mutations. *KIT* gene mutations are more common in patients with acral and mucosal types, followed by *BRAF* mutations. The majority of non-CSD types, including trunk melanoma, exhibit *BRAF* gene V600E mutations (60%) or *NRAS* mutations (20%).

Diagnosis of Melanoma

Similar to other diseases, typical clinical manifestations, physical examinations, imaging, and laboratory examinations (e.g., lactate dehydrogenase measurement) are commonly used for the diagnosis of melanoma (7, 8). The gold standard for melanoma diagnosis is pathological examination including immunohistochemical detection, which is of great value for evaluating melanoma stage, treatment, and prognosis (6). Immunohistochemistry is mainly used to assist in the identification of melanoma in pathological examination; for example, S-100, HMB-45, and vimentin are sensitive indicators for the specific diagnosis of melanoma (9, 10).

Treatment of Melanoma

Current treatment methods for melanoma mainly include surgical treatment, adjuvant therapy, radiotherapy, photodynamic therapy, systemic therapy, and transfer to mucosal melanoma treatment (6, 11) (**Figure 1**). Common surgical treatments are biopsy, enlarged resection, sentinel lymph node biopsy, lymph node dissection, and in-transit metastasis (for patients with stage III disease) (6). Adjuvant therapy for melanoma is mainly based on the clinical stage and risk grade of patients (12). At present, although there is a broad consensus on appropriate adjuvant therapy for low-, medium-, and high-risk patients, there is still controversy regarding adjuvant therapy for very high-risk patients. Specific types of melanoma should be treated differently and individually. For example, adjuvant therapy with interferon treatment is important for high-risk patients. Radiotherapy for melanoma can be divided into adjuvant radiotherapy and palliative radiotherapy. Moreover, in patients with advanced melanoma, which is associated with a poor prognosis and a lack of effective treatments, systemic treatment based on internal medicine is typically applied. In recent years, breakthroughs in individualized targeted therapies and immunotherapies have led to improved outcomes in patients with advanced melanoma (13–16).



FIGURE 1 | Therapeutic strategies for melanoma.

Because most targeted drugs are not widely used in the clinical setting in some countries, chemotherapy drugs, such as dacarbazine, temozolomide, paclitaxel, and carboplatin, are essential (17–22). Combined treatments have also been developed for mucosal melanomas originating from the mucous membranes of the head and neck, digestive tract, and genitourinary tract.

NANOTECHNOLOGY

Great progress has been made in the field of nanotechnology in recent decades, particularly with regard to the application of nanotechnology in medicine (23, 24). Nano-agents provide novel strategies for the treatment of many diseases owing to their unique characteristics of improving drug delivery. In the treatment of cancer, for example, conventional chemotherapy drugs do not specifically target the tumor and can also affect the body's normal cells, resulting in various complications and seriously affecting patient's quality of life. By contrast, nanotechnology can be used

to achieve targeted drug delivery, improve pharmacokinetics and bioavailability, and overcome these barriers (25–28). Several different types of nano-agents have been used in clinical studies, including drug delivery, vaccine development, immunotherapy, and imaging diagnosis. However, the full potential of nanotechnology in clinical disease applications is far from being realized (29–31).

The most important approach involving nanomaterials is nanocarrier drug delivery systems (DDSs), which can transport active molecules, such as drugs, to the corresponding target in the body using nanoparticles as carriers. Compared with free drugs, DDSs are more specific and can greatly improve the therapeutic effect of drugs, while reducing potential side effects (32). The application of nano-DDSs in cancer treatment mainly involves using nanotechnology and materials to deliver drugs to tumor cells by passive or active targeting, thereby improving the therapeutic effects of drugs. Passive targeting typically involves the enhanced permeability and retention effect, whereas active targeting applies specific recognition and targeting of tumor-associated antigens by coupling monoclonal antibodies and peptides on the outer surface of DDSs (33–35).

Nanotechnology and Melanoma

Melanoma is aggressive and easily metastatic; therefore, survival rates are low. The clinical treatment of melanoma includes a variety of treatment methods, such as drugs, surgery, radiotherapy. To improve the efficacy of drugs, various new multitarget drugs are often used in combination in the clinical setting. Nanotechnology-based DDSs, such as nanoliposomes, can play key roles in the clinical treatment of advanced melanoma because nanomaterials can target drug delivery at the cellular level by overcoming biological barriers in the body (32, 36, 37).

Nanomaterials have been used as DDSs for several types of cancer, and nanotechnology-based diagnosis and treatment of melanoma have also been proposed and investigated. First, as described above, because of the size and surface characteristics of nanomaterials, targeted drugs wrapped or loaded with nanomaterials easily cross the biological barrier and can be delivered specifically to melanoma cells, where they can exert their cytotoxic effects. Second, nanomaterials can reduce the side effects of off-target tissue toxicity and improve the efficacy of drugs. In addition, nanosystems may prevent the biodegradation of loaded drugs by the body, reduce drug removal, and prolong the half-life of the drug, allowing for dose reductions (38).

Various nanosystems, including lipid systems, inorganic nanoparticles, polymeric systems, and natural nanosystems, have been used for the diagnosis and treatment of melanoma (37, 39). For example, liposomes, solid lipid nanoparticles, and nanoemulsions have been developed as lipid nanosystems, whereas silica nanoparticles, gold nanoparticles, copper nanoparticles, and nanotubes have been used as common inorganic nanoparticle systems. Polymerization systems include polymeric micelles, nanospheres, polymeric nanoparticles, hydrogels, and dendritic macromolecules, and exosomes are a type of natural nanosystem (36).

Liposome Systems

Among various nanoparticle platforms, lipid systems deliver excellent performance in terms of physical stability, controlled release, and biocompatibility. Moreover, such lipid systems are usually biodegradable, show low side effects, and have relatively high physical stability. Therefore, lipid systems, including liposomes, solid lipid nanoparticles, and nanoemulsions, have been extensively studied and applied to clinical diseases.

Liposomes have been used as a type of double nano DDS in cancer treatment owing to their good pharmacokinetic characteristics. Furthermore, liposomes can significantly increase the circulation half-life of drugs and have been shown to enhance the efficacy of drugs in melanoma, particularly for drugs targeting the cell cycle, such as paclitaxel (40, 41). Bedikian et al. reported that the sheath package corpuscle (composed of sphingomyelin/cholesterol) of vincristine liposomes increased circulating half-life, accumulated at the tumor site, and increased therapeutic efficacy, enabling improved outcomes without altering drug dosage (40). Additionally, Matsumoto et al. also showed that cationic liposomes containing the human interferon B (HuIFNb) gene (*IAB-1*) showed higher antitumor activity than the treatment of melanoma with HuIFNb protein (42).

In addition, liposomes may have applications in the development of vaccines to treat and prevent melanoma. Gargett et al. studied a multicomponent dendritic cell-targeted vaccine, Lipovaxin-MM, which is administered intravenously for the treatment of metastatic melanoma (43). During the 12-week study period, Lipovaxin-MM was confirmed to be well tolerated without obvious immunogenicity and clinical toxicity, and the preliminary results suggested that Lipovaxin-MM may have applications as an immunotherapy in melanoma. Cancer vaccines, which have been studied extensively in basic and clinical trials, are characterized by the use of subunit antigens, which have relatively simple chemical compositions, manufacturing processes, and storage requirements; however, the tumor microenvironment is complex, particularly in advanced tumor models, and additional strategies may be required to achieve curative responses (44–46).

Inorganic Nanoparticles

Inorganic nanoparticles, including silica nanoparticles, gold nanoparticles, copper nanoparticles, and nanotubes, have good biocompatibility and enable simultaneous imaging and drug delivery (47, 48). However, these nanoparticles may not permit specific targeting to the affected region and generally need to be coupled with other targeting ligands. As an example, titanium dioxide is a weak dark compatible nanocrystal material with photocatalytic activity. The photoactivity of neat TiO_2 is limited to the ultraviolet region, which limits its application in photodynamic therapy. Kozinska et al. applied functionalized fullerenes and surface-modified TiO_2 as a photosensitizer for melanoma treatment and demonstrated that novel inorganic nanoparticles can achieve photodynamic killing of melanoma cells; this novel inorganic TiO_2 nanoparticle complex was shown to have a longer retention time *in vivo* and to be nontoxic and stable under conditions without light irradiation (47). Ferreira et al. also evaluated a mouse melanoma model in which europium (III)-yttrium vanadate nanoparticles were functionalized with 3-chloropropyl-trimethoxysilane with folic acid; compared with cisplatin alone, cisplatin nanoparticles

modified with or without folic acid exhibited strong antitumor effects (49). Sapino et al. also constructed an inorganic nanoparticle system composed of aminopropyl-functionalized mesoporous silica nanoparticles (NH2-MSNs) as a topical carrier system for quercetin delivery and studied the effects of the topical carrier system on the proliferation of JR8 human melanoma cells; these NH2-MSNs were found to have strong antiproliferative effects in melanoma cells (50).

In addition, through advances in coordination chemistry, the abundant silanol groups (–Si–O–) on the surface of silica or in mesoporous channels have been directly used for radiolabeling of nonchelating compounds and easily modified with appropriate chelating compounds for chelate-based labeling. SiO_2-based nano-inorganic material systems, including dense silica ($dSiO_2$), mesoporous silica (MSN), biodegradable MSN (bMSN), and hollow MSN nanoparticles, have also been used in positron emission tomography imaging systems for patients with metastatic melanoma, providing a highly sensitive, noninvasive, and quantitative readout of organ/tissue distribution, pharmacokinetics, and tumor targeting efficiency. Thus, SiO_2-based inorganic nanomaterials may have promising applications in the diagnosis of melanoma (51).

Polymeric Systems

Polymeric systems include polymeric micelles and nanospheres, polymeric nanoparticles, hydrogels, and dendrimers. Zou et al. provided a unique and secure platform for theranostic aggregates to construct a co-self-assembly of poly(ethylene glycol)-b-poly (dithiolane trimethylene carbonate-co-iodinated trimethylene carbonate) (PEG-P[DTC-IC]) and cRGD-PEG-P(DTC-IC) block copolymers as intelligent polymer antioxidants. Compared with that of iodinated nanosystems, the synthesis process of these polymeric nanosystems is simpler and overcomes the limitations of high viscosity and few applications. Similar to liposome systems, polymeric nanosystems can not only significantly enhance the computed tomography imaging of tumors but also mediate effective targeted chemotherapy for melanoma (52). Wang et al. constructed a cRGD-targeted polymeric oncolytic peptide LTX-315 and CpG adjuvant to combine with an anti-programmed cell death-1 (PD-1) antibody system; this approach provided strong, long-term immunotherapy for mouse malignant B16F10 melanoma and established a novel class of durable immunotherapy for hard-to-target and metastatic tumors, including melanoma (53). Although polymeric systems are diverse and have excellent nanodrug delivery properties, like other nanoplatforms, some polymeric nanoparticle systems exhibit poor physical stability and high toxicity, which limits their translation to the clinical setting.

Natural Nanosystems

Exosomes are nanovesicles containing various biomolecules. Exosomes are produced by cells through exocytosis and are taken up by target cells. They are involved in physiological and pathological processes and can transmit biological signals between local and distant cells. Therefore, exosomes can be modified as drug carriers for therapeutic intervention in diseases.

Exosomes can be used as natural nano DDSs owing to their unique characteristics (54–57). Exosomes are cellular vesicles composed of double membranes and have diameters ranging from 30 to 150 nm. Additionally, these vesicles can carry various biomolecules, including proteins, lipids, and nucleic acids, can pass through cell membranes and the blood–brain barrier, and can target specific cells (58–60). Circulating exosomes can be detected in blood samples, providing a promising diagnostic strategy for melanoma. In addition, exosomes have been evaluated as vehicles for delivery of therapeutic vaccines in melanoma (61). Monitoring exosomal programmed death ligand-1 (PD-L1) levels may enable prediction of the response to immunotherapy (60, 61). Upregulation of PD-L1 enhances interactions with the PD-1 receptor on T cells and triggers an immune checkpoint reaction, thereby allowing escape of immune monitoring (62, 63). However, in metastatic melanoma, melanoma cells typically express PD-L1, and the addition of interferon-γ stimulation increases exosomal PD-L1 levels; this results in the inhibition of CD8 T-cell function and promotes tumor growth, which explains the resistance to PD-1 and treatment failure observed in many patients. Accordingly, tumor PD-L1 has been used as a predictive biomarker of clinical response (64).

CONCLUSIONS

Current therapy for melanoma has reached a limit of clinical responses. Nanotechnology has enabled the development of smaller, safer, and more accurate DDSs, and an increasing number of melanoma drugs are being packaged into nanocapsules as novel treatment systems. Some conventional melanoma drugs have low solubility in water buffer systems, poor bioavailability, rapid metabolism, and low stability, limiting their clinical potential and therapeutic use. Compared with traditional treatment methods, nano-encapsulation of drugs into the body can result in increased solubility, enhanced drug stability, improved epithelial permeability and bioavailability, longer half-life, increased tumor targeting, and minimal side effects. Thus, nano DDSs are expected to improve the therapeutic efficacy of the delivered drugs in patients with melanoma.

Future development challenges mainly focus on further understanding of the mechanisms that make nanosystems more effective than traditional drug formulations for melanoma. Overall, nano DDSs show good histocompatibility, enhanced drug targeting, low toxicity, and many other excellent characteristics, conferring broad applications in the diagnosis and treatment of melanoma, particularly metastatic melanoma.

AUTHOR CONTRIBUTIONS

All authors contributed to the design of the study and writing of the manuscript. KH, HZ, and JL undertook the research. YW, HZ, and NZ wrote the main manuscript text and prepared figures. NZ and HC revised the article critically for important intellectual content and final approval of the version to be submitted. All authors reviewed the manuscript.

REFERENCES

1. Sung H, Ferlay J, Siegel RL, Laversanne M, Soerjomataram I, Jemal A, et al. Global Cancer Statistics 2020: GLOBOCAN Estimates of Incidence and Mortality Worldwide for 36 Cancers in 185 Countries. *CA Cancer J Clin* (2021) 71(3):209–49. doi: 10.3322/caac.21660
2. Saginala K, Barsouk A, Aluru JS, Rawla P, Barsouk A. Epidemiology of Melanoma. *Med Sci (Basel)* (2021) 9(4):63. doi: 10.3390/medsci9040063
3. Whiteman DC, Green AC, Olsen CM. The Growing Burden of Invasive Melanoma: Projections of Incidence Rates and Numbers of New Cases in Six Susceptible Populations Through 2031. *J Invest Dermatol* (2016) 136(6):1161–71. doi: 10.1016/j.jid.2016.01.035
4. Rabbie R, Ferguson P, Molina-Aguilar C, Adams DJ, Robles-Espinoza CD. Melanoma Subtypes: Genomic Profiles, Prognostic Molecular Markers and Therapeutic Possibilities. *J Pathol* (2019) 247(5):539–51. doi: 10.1002/path.5213
5. Swetter SM, Tsao H, Bichakjian CK, Curiel-Lewandrowski C, Elder DE, Gershenwald JE, et al. Guidelines of Care for the Management of Primary Cutaneous Melanoma. *J Am Acad Dermatol* (2019) 80(1):208–50. doi: 10.1016/j.jaad.2018.08.055
6. Seth R, Messersmith H, Kaur V, Kirkwood JM, Kudchadkar R, McQuade JL, et al. Systemic Therapy for Melanoma: ASCO Guideline. *J Clin Oncol* (2020) 38(33):3947–70. doi: 10.1200/JCO.20.00198
7. Garbe C, Peris K, Hauschild A, Saiag P, Middleton M, Bastholt L, et al. Diagnosis and Treatment of Melanoma. European Consensus-Based Interdisciplinary Guideline - Update 2016. *Eur J Cancer* (2016) 63:201–17. doi: 10.1016/j.ejca.2016.05.005
8. Nenclares P, Ap Dafydd D, Bagwan I, Begg D, Kerawala C, King E, et al. Head and Neck Mucosal Melanoma: The United Kingdom National Guidelines. *Eur J Cancer* (2020) 138:11–8. doi: 10.1016/j.ejca.2020.07.017
9. Botella-Estrada R, Boada-Garcia A, Carrera-Alvarez C, Fernandez-Figueras M, Gonzalez-Cao M, Moreno-Ramirez D, et al. Clinical Practice Guideline on Melanoma From the Spanish Academy of Dermatology and Venereology (AEDV). *Actas Dermosifiliogr (Engl Ed)* (2021) 112(2):142–52. doi: 10.1016/j.ad.2020.07.003
10. Katz I, O'Brien B, Clark S, Thompson CT, Schapiro B, Azzi A, et al. Assessment of a Diagnostic Classification System for Management of Lesions to Exclude Melanoma. *JAMA Netw Open* (2021) 4(12):e2134614. doi: 10.1001/jamanetworkopen.2021.34614
11. Aziz HA, Gastman BR, Singh AD. Management of Conjunctival Melanoma: Critical Assessment of Sentinel Lymph Node Biopsy. *Ocul Oncol Pathol* (2015) 1(4):266–73. doi: 10.1159/000381719
12. Wada-Ohno M, Ito T, Furue M. Adjuvant Therapy for Melanoma. *Curr Treat Options Oncol* (2019) 20(8):63. doi: 10.1007/s11864-019-0666-x
13. Albittar AA, Alhalabi O, Glitza Oliva IC. Immunotherapy for Melanoma. *Adv Exp Med Biol* (2020) 1244:51–68. doi: 10.1007/978-3-030-41008-7_3
14. Onitilo AA, Wittig JA. Principles of Immunotherapy in Melanoma. *Surg Clin North Am* (2020) 100(1):161–73. doi: 10.1016/j.suc.2019.09.009
15. Klebaner D, Saddawi-Konefka R, Finegersh A, Yan CH, Califano JA3rd, London NR, et al. Immunotherapy in Sinonasal Melanoma: Treatment Patterns and Outcomes Compared to Cutaneous Melanoma. *Int Forum Allergy Rhinol* (2020) 10(9):1087–95. doi: 10.1002/alr.22628
16. Robert C, Long GV, Brady B, Dutriaux C, Maio M, Mortier L, et al. Nivolumab in Previously Untreated Melanoma Without BRAF Mutation. *N Engl J Med* (2015) 372(4):320–30. doi: 10.1056/NEJMoa1412082
17. Chapman PB, Hauschild A, Robert C, Haanen JB, Ascierto P, Larkin J, et al. Improved Survival With Vemurafenib in Melanoma With BRAF V600E Mutation. *N Engl J Med* (2011) 364(26):2507–16. doi: 10.1056/NEJMoa1103782
18. Ott PA, Chang J, Madden K, Kannan R, Muren C, Escano C, et al. Oblimersen in Combination With Temozolomide and Albumin-Bound Paclitaxel in Patients With Advanced Melanoma: A Phase I Trial. *Cancer Chemother Pharmacol* (2013) 71(1):183–91. doi: 10.1007/s00280-012-1995-7
19. Middleton MR, Grob JJ, Aaronson N, Fierlbeck G, Tilgen W, Seiter S, et al. Randomized Phase III Study of Temozolomide Versus Dacarbazine in the Treatment of Patients With Advanced Metastatic Malignant Melanoma. *J Clin Oncol* (2000) 18(1):158–66. doi: 10.1200/JCO.2000.18.1.158
20. Larkin J, Minor D, D'Angelo S, Neyns B, Smylie M, Miller WHJr., et al. Overall Survival in Patients With Advanced Melanoma Who Received Nivolumab Versus Investigator's Choice Chemotherapy in CheckMate 037: A Randomized, Controlled, Open-Label Phase III Trial. *J Clin Oncol* (2018) 36(4):383–90. doi: 10.1200/JCO.2016.71.8023
21. Kato K, Cho BC, Takahashi M, Okada M, Lin CY, Chin K, et al. Nivolumab Versus Chemotherapy in Patients With Advanced Oesophageal Squamous Cell Carcinoma Refractory or Intolerant to Previous Chemotherapy (ATTRACTION-3): A Multicentre, Randomised, Open-Label, Phase 3 Trial. *Lancet Oncol* (2019) 20(11):1506–17. doi: 10.1016/S1470-2045(19)30626-6
22. Takahashi M, Kato K, Okada M, Chin K, Kadowaki S, Hamamoto Y, et al. Nivolumab Versus Chemotherapy in Japanese Patients With Advanced Esophageal Squamous Cell Carcinoma: A Subgroup Analysis of a Multicenter, Randomized, Open-Label, Phase 3 Trial (ATTRACTION-3). *Esophagus* (2021) 18(1):90–9. doi: 10.1007/s10388-020-00794-x
23. Gharpure KM, Wu SY, Li C, Lopez-Berestein G, Sood AK. Nanotechnology: Future of Oncotherapy. *Clin Cancer Res* (2015) 21(14):3121–30. doi: 10.1158/1078-0432.CCR-14-1189
24. Gao D, Guo X, Zhang X, Chen S, Wang Y, Chen T, et al. Multifunctional Phototheranostic Nanomedicine for Cancer Imaging and Treatment. *Mater Today Bio* (2020) 5:100035. doi: 10.1016/j.mtbio.2019.100035
25. Goldberg MS. Improving Cancer Immunotherapy Through Nanotechnology. *Nat Rev Cancer* (2019) 19(10):587–602. doi: 10.1038/s41568-019-0186-9
26. Xu C, Hong H, Lee Y, Park KS, Sun M, Wang T, et al. Efficient Lymph Node-Targeted Delivery of Personalized Cancer Vaccines With Reactive Oxygen Species-Inducing Reduced Graphene Oxide Nanosheets. *ACS Nano* (2020) 14(10):13268–78. doi: 10.1021/acsnano.0c05062
27. Yadav N, Dahiya T, Chhillar AK, Rana JS, Mohan H. Promising Applications of Nanotechnology in Cancer Diagnostics and Therapeutics. *Curr Pharm Biotechnol* (2021). doi: 10.2174/1389201023666211222165508
28. Zhu D, Li Y, Zhang Z, Xue Z, Hua Z, Luo X, et al. Recent Advances of Nanotechnology-Based Tumor Vessel-Targeting Strategies. *J Nanobiotechnol* (2021) 19(1):435. doi: 10.1186/s12951-021-01190-y
29. Zhou J, Krishnan N, Jiang Y, Fang RH, Zhang L. Nanotechnology for Virus Treatment. *Nano Today* (2021) 36:101031. doi: 10.1016/j.nantod.2020.101031
30. Sahle FF, Kim S, Niloy KK, Tahia F, Fili CV, Cooper E, et al. Nanotechnology in Regenerative Ophthalmology. *Adv Drug Delivery Rev* (2019) 148:290–307. doi: 10.1016/j.addr.2019.10.006
31. Kirtane AR, Verma M, Karandikar P, Furin J, Langer R, Traverso G. Nanotechnology Approaches for Global Infectious Diseases. *Nat Nanotechnol* (2021) 16(4):369–84. doi: 10.1038/s41565-021-00866-8
32. Bensa V, Calarco E, Giusto E, Perri P, Corrias MV, Ponzoni M, et al. Retinoids Delivery Systems in Cancer: Liposomal Fenretinide for Neuroectodermal-Derived Tumors. *Pharm (Basel)* (2021) 14(9):854. doi: 10.3390/ph14090854
33. Torchilin V. Tumor Delivery of Macromolecular Drugs Based on the EPR Effect. *Adv Drug Delivery Rev* (2011) 63(3):131–5. doi: 10.1016/j.addr.2010.03.011
34. Pastorino F, Brignole C, Di Paolo D, Perri P, Curnis F, Corti A, et al. Overcoming Biological Barriers in Neuroblastoma Therapy: The Vascular Targeting Approach With Liposomal Drug Nanocarriers. *Small* (2019) 15(10):e1804591. doi: 10.1002/smll.201804591
35. Attia MF, Anton N, Wallyn J, Omran Z, Vandamme TF. An Overview of Active and Passive Targeting Strategies to Improve the Nanocarriers Efficiency to Tumour Sites. *J Pharm Pharmacol* (2019) 71(8):1185–98. doi: 10.1111/jphp.13098
36. Battaglia L, Scomparin A, Dianzani C, Milla P, Muntoni E, Arpicco S, et al. Nanotechnology Addressing Cutaneous Melanoma: The Italian Landscape. *Pharmaceutics* (2021) 13(10):1617. doi: 10.3390/pharmaceutics13101617
37. Mishra H, Mishra PK, Ekielski A, Jaggi M, Iqbal Z, Talegaonkar S. Melanoma Treatment: From Conventional to Nanotechnology. *J Cancer Res Clin Oncol* (2018) 144(12):2283–302. doi: 10.1007/s00432-018-2726-1
38. Gmeiner WH, Ghosh S. Nanotechnology for Cancer Treatment. *Nanotechnol Rev* (2015) 3(2):111–22. doi: 10.1515/ntrev-2013-0013
39. Kurakula M, Chen L, Tiwari AK, Srinivas NR, Dash RP, Panizzi PR, et al. Recent Advances in Lipid-Based Nanovesicular Delivery Systems for Melanoma Therapy. *Crit Rev Ther Drug Carrier Syst* (2021) 38(4):1–38. doi: 10.1615/CritRevTherDrugCarrierSyst.2021034903
40. Bedikian AY, Vardeleon A, Smith T, Campbell S, Namdari R. Pharmacokinetics and Urinary Excretion of Vincristine Sulfate Liposomes

Injection in Metastatic Melanoma Patients. *J Clin Pharmacol* (2006) 46 (7):727–37. doi: 10.1177/0091270006288953
41. Saengkrit N, Saesoo S, Srinuanchai W, Phunpee S, Ruktanonchai UR. Influence of Curcumin-Loaded Cationic Liposome on Anticancer Activity for Cervical Cancer Therapy. *Colloids Surf B Biointerf* (2014) 114:349–56. doi: 10.1016/j.colsurfb.2013.10.005
42. Matsumoto K, Kubo H, Murata H, Uhara H, Takata M, Shibata S, et al. A Pilot Study of Human Interferon Beta Gene Therapy for Patients With Advanced Melanoma by *In Vivo* Transduction Using Cationic Liposomes. *Jpn J Clin Oncol* (2008) 38(12):849–56. doi: 10.1093/jjco/hyn114
43. Gargett T, Abbas MN, Rolan P, Price JD, Gosling KM, Ferrante A, et al. Phase I Trial of Lipovaxin-MM, a Novel Dendritic Cell-Targeted Liposomal Vaccine for Malignant Melanoma. *Cancer Immunol Immunother* (2018) 67(9):1461–72. doi: 10.1007/s00262-018-2207-z
44. Lu L, Yan H, Shyam-Sundar V, Janowitz T. Cross-Sectional and Longitudinal Analysis of Cancer Vaccination Trials Registered on the US Clinical Trials Database Demonstrates Paucity of Immunological Trial Endpoints and Decline in Registration Since 2008. *Drug Des Devel Ther* (2014) 8:1539–53. doi: 10.2147/DDDT.S65963
45. Faries MB, Morton DL. Therapeutic Vaccines for Melanoma: Current Status. *BioDrugs* (2005) 19(4):247–60. doi: 10.2165/00063030-200519040-00004
46. Liu Q, Das M, Liu Y, Huang L. Targeted Drug Delivery to Melanoma. *Adv Drug Delivery Rev* (2018) 127:208–21. doi: 10.1016/j.addr.2017.09.016
47. Kozinska A, Zadlo A, Labuz P, Broniec A, Pabisz P, Sarna T. The Ability of Functionalized Fullerenes and Surface-Modified TiO2 Nanoparticles to Photosensitize Peroxidation of Lipids in Selected Model Systems. *Photochem Photobiol* (2019) 95(1):227–36. doi: 10.1111/php.13053
48. Wang J, Sui L, Huang J, Miao L, Nie Y, Wang K, et al. MoS2-Based Nanocomposites for Cancer Diagnosis and Therapy. *Bioact Mater* (2021) 6 (11):4209–42. doi: 10.1016/j.bioactmat.2021.04.021
49. Ferreira NH, Furtado RA, Ribeiro AB, de Oliveira PF, Ozelin SD, de Souza LDR, et al. Europium(III)-Doped Yttrium Vanadate Nanoparticles Reduce the Toxicity of Cisplatin. *J Inorg Biochem* (2018) 182:9–17. doi: 10.1016/j.jinorgbio.2018.01.014
50. Sapino S, Ugazio E, Gastaldi L, Miletto I, Berlier G, Zonari D, et al. Mesoporous Silica as Topical Nanocarriers for Quercetin: Characterization and *In Vitro* Studies. *Eur J Pharm Biopharm* (2015) 89:116–25. doi: 10.1016/j.ejpb.2014.11.022
51. Ni D, Jiang D, Ehlerding EB, Huang P, Cai W. Radiolabeling Silica-Based Nanoparticles *via* Coordination Chemistry: Basic Principles, Strategies, and Applications. *Acc Chem Res* (2018) 51(3):778–88. doi: 10.1021/acs.accounts.7b00635
52. Zou Y, Wei Y, Sun Y, Bao J, Yao F, Li Z, et al. Cyclic RGD-Functionalized and Disulfide-Crosslinked Iodine-Rich Polymersomes as a Robust and Smart Theranostic Agent for Targeted CT Imaging and Chemotherapy of Tumor. *Theranostics* (2019) 9(26):8061–72. doi: 10.7150/thno.37184
53. Wang M, Geilich BM, Keidar M, Webster TJ. Killing Malignant Melanoma Cells With Protoporphyrin IX-Loaded Polymersome-Mediated Photodynamic Therapy and Cold Atmospheric Plasma. *Int J Nanomed* (2017) 12:4117–27. doi: 10.2147/IJN.S129266
54. Kalluri R, LeBleu VS. The Biology, Function, and Biomedical Applications of Exosomes. *Science* (2020) 367(6478):eaau6977. doi: 10.1126/science.aau6977
55. Sun Z, Shi K, Yang S, Liu J, Zhou Q, Wang G, et al. Effect of Exosomal miRNA on Cancer Biology and Clinical Applications. *Mol Cancer* (2018) 17(1):147. doi: 10.1186/s12943-018-0897-7
56. Raposo G, Stoorvogel W. Extracellular Vesicles: Exosomes, Microvesicles, and Friends. *J Cell Biol* (2013) 200(4):373–83. doi: 10.1083/jcb.201211138
57. Buratta S, Tancini B, Sagini K, Delo F, Chiaradia E, Urbanelli L, et al. Lysosomal Exocytosis, Exosome Release and Secretory Autophagy: The Autophagic- and Endo-Lysosomal Systems Go Extracellular. *Int J Mol Sci* (2020) 21(7):2576. doi: 10.3390/ijms21072576
58. Yang F, Ning Z, Ma L, Liu W, Shao C, Shu Y, et al. Exosomal miRNAs and miRNA Dysregulation in Cancer-Associated Fibroblasts. *Mol Cancer* (2017) 16(1):148. doi: 10.1186/s12943-017-0718-4
59. Han Y, Jia L, Zheng Y, Li W. Salivary Exosomes: Emerging Roles in Systemic Disease. *Int J Biol Sci* (2018) 14(6):633–43. doi: 10.7150/ijbs.25018
60. Chen G, Huang AC, Zhang W, Zhang G, Wu M, Xu W, et al. Exosomal PD-L1 Contributes to Immunosuppression and is Associated With Anti-PD-1 Response. *Nature* (2018) 560(7718):382–6. doi: 10.1038/s41586-018-0392-8
61. He C, Zheng S, Luo Y, Wang B. Exosome Theranostics: Biology and Translational Medicine. *Theranostics* (2018) 8(1):237–55. doi: 10.7150/thno.21945
62. Chen L, Han X. Anti-PD-1/PD-L1 Therapy of Human Cancer: Past, Present, and Future. *J Clin Invest* (2015) 125(9):3384–91. doi: 10.1172/JCI80011
63. Topalian SL, Taube JM, Anders RA, Pardoll DM. Mechanism-Driven Biomarkers to Guide Immune Checkpoint Blockade in Cancer Therapy. *Nat Rev Cancer* (2016) 16(5):275–87. doi: 10.1038/nrc.2016.36
64. Ribas A, Hamid O, Daud A, Hodi FS, Wolchok JD, Kefford R, et al. Association of Pembrolizumab With Tumor Response and Survival Among Patients With Advanced Melanoma. *JAMA* (2016) 315(15):1600–9. doi: 10.1001/jama.2016.4059

Conflict of Interest: The authors declare that the research was conducted in the absence of any commercial or financial relationships that could be construed as a potential conflict of interest.

Publisher's Note: All claims expressed in this article are solely those of the authors and do not necessarily represent those of their affiliated organizations, or those of the publisher, the editors and the reviewers. Any product that may be evaluated in this article, or claim that may be made by its manufacturer, is not guaranteed or endorsed by the publisher.

Copyright © 2022 Zeng, Li, Hou, Wu, Chen and Ning. This is an open-access article distributed under the terms of the Creative Commons Attribution License (CC BY). The use, distribution or reproduction in other forums is permitted, provided the original author(s) and the copyright owner(s) are credited and that the original publication in this journal is cited, in accordance with accepted academic practice. No use, distribution or reproduction is permitted which does not comply with these terms.

frontiers in Oncology

REVIEW
published: 22 March 2022
doi: 10.3389/fonc.2022.855019

pH-Responsive Polymer Nanomaterials for Tumor Therapy

Shunli Chu[1], *Xiaolu Shi*[1†], *Ye Tian*[1†] *and Fengxiang Gao*[2*]

[1] Department of Implantology, Hospital of Stomatology, Jilin University, Changchun, China, [2] Changchun Institute of Applied Chemistry, Chinese Academy of Sciences, Changchun, China

The complexity of the tumor microenvironment presents significant challenges to cancer therapy, while providing opportunities for targeted drug delivery. Using characteristic signals of the tumor microenvironment, various stimuli-responsive drug delivery systems can be constructed for targeted drug delivery to tumor sites. Among these, the pH is frequently utilized, owing to the pH of the tumor microenvironment being lower than that of blood and healthy tissues. pH-responsive polymer carriers can improve the efficiency of drug delivery *in vivo*, allow targeted drug delivery, and reduce adverse drug reactions, enabling multifunctional and personalized treatment. pH-responsive polymers have gained increasing interest due to their advantageous properties and potential for applicability in tumor therapy. In this review, recent advances in, and common applications of, pH-responsive polymer nanomaterials for drug delivery in cancer therapy are summarized, with a focus on the different types of pH-responsive polymers. Moreover, the challenges and future applications in this field are prospected.

Keywords: tumor, pH-responsive polymer, nanomaterials, tumor microenvironment, drug delivery

OPEN ACCESS

Edited by:
Kelong Ai,
Central South University, China

Reviewed by:
Jia Huang,
Central South University, China
Chao Liu,
Nanjing Stomatological Hospital (NSH), China
Zheng Yang Li,
Tianjin Stomatological Hospital, China

***Correspondence:**
Fengxiang Gao
gfx26@ciac.ac.cn

†These authors contributed to the work equally and should be regarded as co-second authors

Specialty section:
This article was submitted to Pharmacology of Anti-Cancer Drugs, a section of the journal Frontiers in Oncology

Received: *14 January 2022*
Accepted: *24 February 2022*
Published: *22 March 2022*

Citation:
Chu S, Shi X, Tian Y and Gao F (2022) pH-Responsive Polymer Nanomaterials for Tumor Therapy. Front. Oncol. 12:855019. doi: 10.3389/fonc.2022.855019

1 INTRODUCTION

Cancer is a major cause of morbidity and mortality, greatly impacts quality of life, and is a serious threat to human health; the number of diagnosed patients has increased gradually in recent years (1–4). For example, recently, there were 18 million new cancer cases and 9.5 million cancer deaths worldwide in 2018 (1). Many scientists worldwide are committed to researching the diagnosis and treatment of cancerous tumors (5–10). Although this research has achieved some results, to some extent, the complex tumor microenvironment remains a barrier to novel tumor therapy programs. Chemotherapeutic therapy, referred to as chemotherapy, is still one of the main methods of tumor treatment (11–13). Some chemical drugs, such as oxaliplatin, doxorubicin (DOX), and paclitaxel (PTX), are applied to kill tumor cells and shrink or destroy the tumor (14–18). Because drug delivery is generally given systemically, the body itself will also be affected and damaged to some extent, causing side effects, complications, and even death in some serious cases (19–22). Therefore, the development of target-specific or stimuli-sensitive drugs that can identify tumor cells, to achieve the purpose of tumor treatment with no or very little impact on normal tissue cells, is the current focus of research.

During tumor growth, cell proliferation and angiogenesis are uncontrolled and dysfunctional, resulting in a complex tumor microenvironment, comprising severe hypoxia, a slightly acidic pH, and excessive ROS (22–24). Owning to the severely hypoxic microenvironment, a large number of

acid metabolites are produced through glycolysis in tumor cells, leading to a weakly acidic microenvironment (pH < 6.5) around tumor tissues, which is lower than the pH value of blood and healthy tissues (pH 7.4) (25–27). In addition, after endocytosis, the rapid acidification due to proton influx decreases the pH values of intracellular and suborganelle structures (pH 5.0–6.0) and lysosomes (pH 4.0–5.0) (28, 29).

This complex tumor microenvironment can be exploited by researchers to obtain specific responses; for example, pH-responsive stimuli were found to respond to the difference in pH between normal and tumor tissues (30, 31). pH-responsive stimulation is a powerful tool that can be used to regulate the properties of materials (32). Researchers have designed pH-responsive polymer nanomaterials (10–100 nm) (33) that can be engineered to suit the need of the therapy and target area. These materials are relatively stable in the blood and normal tissue but are unstable in the tumor area (acidic pH), leading to rapid changes in the degree of ionization in pH-responsive groups, causing material changes that release the anti-tumor drugs, achieving the goal of targeted tumor therapy (34, 35). Researchers have performed sustainable research on these pH-responsive polymer nanomaterials (36, 37). This review will focus on pH-responsive polymer nanomaterials in tumor therapy and comprises a brief introduction to anti-tumor drug loading methods, a clarification of the mechanism and application of pH-responsive polymer nanomaterials in tumor therapy, an outlook addressing the great recent challenges faced, and suggestions for applications and future research directions.

2 ANTI-TUMOR DRUG LOADING METHODS FOR PH-RESPONSIVE POLYMER NANOMATERIALS

Theoretically, pH-responsive polymer nanomaterials can carry anti-tumor drugs, which are transported into the tumor tissue and are then released to produce therapeutic effects on tumors. pH-responsive nanomaterials are classified into organic nanomaterials (liposomes, polymer micelles, polymer capsules, nano-gels, dendrimers, etc.), inorganic nanomaterials [carbon nanoparticles (NPs), silica NPs, gold NPs, etc.], and composite nanomaterials [metal–organic frameworks (MOFs) and metal-phenolic networks, etc.] (**Table 1**). They exhibit many different

TABLE 1 | Classification of nanomaterials.

Nanomaterials				
Classify			**Morphology or structure**	**Characteristics or deficiency**
Organic Nanomaterials	Liposomes		A hydrophobic phospholipid bilayer, and a central hydrophilic cavity	Low toxicity, good biocompatibility, easy degradation; poor stability *in vitro*, and *in vivo*, and unstable drug release kinetics
	Polymer capsules		A hydrophobic wall, and a hydrophilic cavity	
	Polymer micelles		"Core-shell" structure, hydrophobic cores, and hydrophilic shell	
	Nanogels		Colloidal particles, with an internal cross-linked structure	
	Dendrimers		Spherical structures of multi-branched polymers, central cores, branches of repetitive units, and an outer layer of multivalent functional groups	
	etc.			
Inorganic Nanomaterials	Carbon nanoparticles	Graphene Carbon nanotubes Fullerenes Carbon quantum dots etc.	Network structure from zero-dimensional to three-dimensional, and at least one dimension of the dispersion size is less than 100 nm	Good biocompatibility, electrical conductivity, optical properties, and photothermal properties; carrier surface modification is very important
	Silica nanoparticles		Mesoporous silica nanoparticles, a large number of pore structures, the aperture is in the range of 2-50 nm	The ordered arrangement of pores, tunable pore size, pore volume, and surface chemistry, high chemical stability, and biocompatibility; rely on surface modification to achieve the controlled release of drug molecules
	Metallic nanoparticles	Gold nanoparticles Silver nanoparticles Iron nanoparticles etc.	Core (metal), and shell (functional material)	Gold nanoparticles have a wide range of applications, controllable particle size, easy surface modification, good biocompatibility, excellent photothermal properties, and enzyme activity
	etc.			
Composite Nanomaterials	Metal-Organic Frameworks		An infinitely extended network-like structure, organic bridging ligands linked to metal ions (clusters) by self-assembly or coordination bonds	Large surface area, adjustable performance, a large amount of drug encapsulation, and sustained release effect
	Metal-Phenolic Networks		A network structure formed by the coordination of phenolic hydroxyl groups with various metal ions in polyphenols	Good biocompatibility; poor biological antifouling performance
	etc.			

structures: linear (homopolymer, biblock copolymers, multiblock copolymers, and organic/inorganic hybrid polymers), non-linear branched (branched or hyperbranched polymers), and grid. Linear homopolymers and amphiphilic and amphiphilic block copolymers the most common types, and mainly form micelles, vesicles, dendritic macromolecules, and nanogels. Owing to the different properties of different drug molecules, it is necessary to select the appropriate nanomaterial according to the properties of the particular drug; drugs and nanomaterials can be combined in different ways. The anti-tumor drug loading methods for pH-responsive polymer nanomaterials can be classified into three categories: physical encapsulation, intermolecular force, and chemical bonding, *via* the connection between the pH-responsive polymer nanomaterial and anti-tumor drug (**Figure 1**).

2.1 Physical Encapsulation

Physical encapsulation is the earliest and most effective drug loading method for nanomaterials. It can be used in organic, inorganic, and composite nanomaterials; the most common nanomaterials discussed for its use in the literature are liposomes, polymer micelles, polymer capsules, mesoporous silica NPs, MOFs, and metal–polyphenol nano-networks.

Liposomes were the earliest kinds of nano-drug. They mainly consisted of a bilayer of phospholipid molecules, which could be used to encapsulate the anti-tumor drugs in a hydrophobic phospholipid bilayer or a central hydrophilic cavity; their drug piggybacking was achieved through the physical encapsulation route. Hong et al. (38) designed lipid–polymer hybrid NPs with poly(lactic-co-glycolic acid) as the hydrophobic core to encapsulate afatinib and/or miR-139 encapsulated in an amphiphilic shell of polyethylene glycol (PEG) liposomes, and further modified the shell layer with ligand arginine and pH-sensitive cell-penetrating peptide histidine to enhance the targeting and penetration of these multifunctional NPs in the acidic microenvironment of colorectal cancer cells. Similar to iposomes, physical encapsulation is the main method of drug loading polymer capsules; the polymeric capsules encapsulate hydrophobic drug molecules within the capsule wall and hydrophilic drug molecules in the cavity (39). Zhong et al. (40) synthesized a pH-responsive block polymer, which

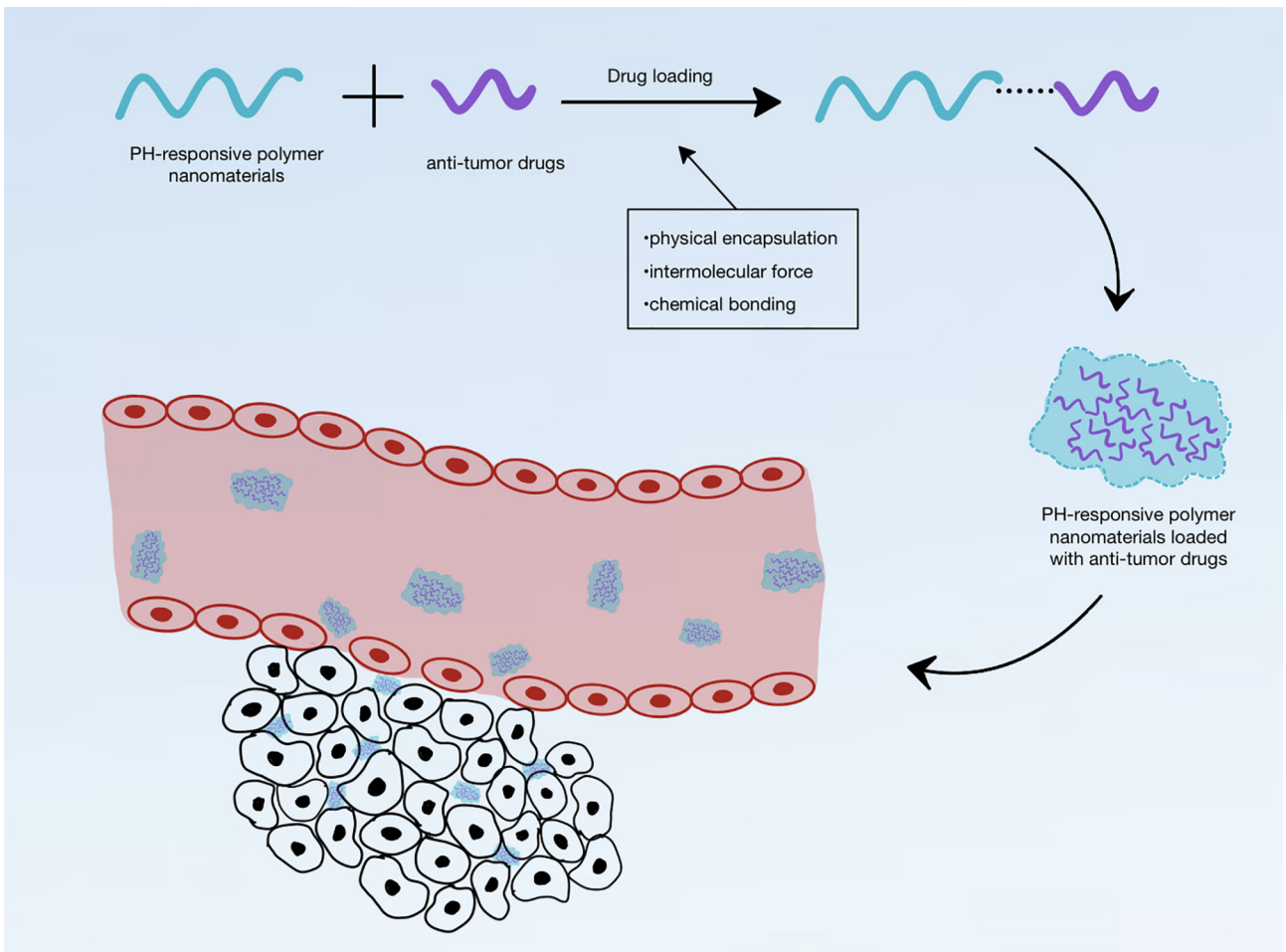


FIGURE 1 | Schematic diagram of pH-responsive polymer nanomaterials loaded with anti-tumor drugs and entering the tumor environment.

comprised methoxy PEG (mPEG) and poly(asparagyl diisopropylethylenediamine-co-phenylalanine), self-assembled into nano-microcapsules as a drug carrier, and encapsulated the hydrophilic hypoxia-activated prodrug tirapamine and hydrophobic photosensitizer dihydroporphyrin [chlorin e6 (Ce6)] to treat breast cancer effectively. Polymeric micelles are the most common carriers of high-molecular-weight polymers. They are thermodynamically stable colloidal solutions formed by the self-assembly of amphiphilic block copolymers in water, and their "core-shell" structure can encapsulate hydrophobic drugs in hydrophobic cores. Xu et al. (41) encapsulated the reactive oxygen species (ROS) generator vitamin K3 with pH/ROS dual-sensitive polymer prodrug PEG-b-P[(LL-g-TK-PTX)-(LL-g-DMA)] micellar NPs to prepare polymeric prodrug-based drug delivery systems (DDSs) with pH-induced surface charge inversion and ROS amplification for ROS-triggered self-accelerated drug release. Mesoporous silica NPs (MSNs) contain a large number of pore structures, which can significantly increase the drug loading capacity and can be blocked by blocking agents, such as surface films or pH-sensitive ZnO quantum dots (QDs), to prevent the drug from leaking at non-targeted positions during transportation *in vivo*. The inorganic material on the walls of MSNs can prevent mechanical, thermal, and biological degradation of the encapsulated drugs to provide safe and effective drug delivery (42). Yan et al. (43) developed a biodegradable pH-responsive hollow MSN for the co-delivery of pheophorbide a and DOX. The NP possessed controllable particle size and a large inner hollow core, giving it excellent encapsulation capacities. MOFs are crystalline materials consisting of organic bridging ligands linked to metal ions (clusters) employing coordination bonds to form an infinitely extended network-like structure, which can physically embed drugs. He et al. (44) loaded cisplatin precursor drugs into UiO nanoscale MOFs with hexagonal-plate morphologies by encapsulation and loaded multiple drug resistance gene-silencing siRNAs by the surface ligand to enhance the therapeutic efficacy against drug-resistant ovarian cancer cells. Liposomes and nanocapsules can carry drugs only by physical encapsulation, unlike other carriers, which can carry drugs through physical encapsulation, using intermolecular forces, or *via* chemical bonding.

2.2 Intermolecular Forces

The use of intermolecular forces is also a common non-chemical bonding method of attaching drugs to carriers. Such forces include electrostatic attraction, hydrogen bonding, π–π interaction, van der Waals forces, and hydrophobic interactions. For water-soluble polymers, drugs can be loaded onto nanomaterials by intermolecular interaction to increase their circulation time and limit their toxicity to normal tissues (45–48). Polymer micelles, nanogels, carbon NPs, and dendritic macromolecules can be combined with drugs *via* one or more intermolecular forces. Polymeric micelles are capable of carrying drug molecules in their cores using hydrophobic forces and hydrogen bonding forces. Wu et al. (49) wrapped hydrophobic DOX in the core of core/shell PEGylated poly(glycerol sebacate) (PEGS)/hydroxyapatite hybrid nanomicelles using hydrogen bonding and fabricated spherical NPs with a high drug loading capacity and pH-sensitive response release by optimizing the coordination of PEG nanomicelles with the hydroxyapatite mineralization-responsive release of spherical NPs. In addition, multi-intermolecular forces can stabilize the bond between carriers and drugs. Zhao et al. fabricated co-loaded NPs using supramolecular assembly, which consisted of a block copolymer of mPEG and polycarbonates, DOX, and Ce6. DOX and Ce6 were mainly dispersed in the hydrophobic core. The hydrophobic polycarbonate chain segments and cationic polycarbonate chain segments generated strong intermolecular interactions between the polymer and cargo, including hydrophobic interactions, hydrogen bonding interactions, and electrostatic interactions. The strong interactions between Ce6 and DOX, including electrostatic interactions, π–π stacking interactions, and hydrophobic interactions, favored the formation of NPs (50). Nanogels with an internal cross-linked structure often adsorb drug molecules through hydrophobic interactions and can use their swelling and anti-swelling characteristics to achieve the stimulus-responsive release of drug molecules. Howaili et al. (51) synthesized a plasmonic nanogel loaded with curcumin (AuNP@Ng/Cur) as a stimuli-responsive nanocarrier, using an incubation method at temperatures above the lower critical solution temperature to promote hydrophobic interactions between the Cur and nanogel to achieve loading. Dendrimers are well-defined spherical structures of multi-branched polymers, characterized by central cores, branches of repetitive units, and an outer layer of multivalent functional groups. Their hydrophobic core can encapsulate uncharged non-polar small molecular drugs, and their functional groups can electrostatically interact with charged polar molecules or chemically bind with immunotherapeutic agents such as therapeutic antibodies. Shi et al. (52) developed a unique polymeric hybrid NP nanoplatform for multi-stage siRNA delivery, which was formed by electrostatic interactions between the copolymer mPEG–poly(l-histidine)-poly (sulfadimethoxine), the dendrimer poly-l-lysine, and PLK1siRNA to efficiently deliver siRNA.

2.3 Chemical Bonding

Researchers often combine drugs with carriers through chemical bonds, such as coordination bonds and acid-unstable bonds, and common nanomaterials, including composite nanomaterials (MOFs), organic nanomaterials (dendrimers), and inorganic nanomaterials (quantum dot nanomaterials).

MOFs are composite nanomaterials with intramolecular pores formed by the self-assembly of organic ligands and metal ions or clusters through coordination bonds (53). Shen et al. (54) prepared a core-shell nanocomposite composed of zeolite imidazole skeleton-90 (ZIF-90) coated with spermine-modified acetal dextran (SAD), in which hydrophilic DOX was covalently bonded to the ZIF-90 skeleton and the hydrophobic photosensitizer IR780 was loaded into the SAD shell, thus allowing combined photodynamic therapy and chemotherapy. Duan et al. (55) fabricated a novel pH-responsive MOF antigen-delivery system to solve the problems in the delivery strategy for tumor-associated antigens (TAAs). Through the one-pot synthesis process, TAAs were loaded into MOFs, which were released into the tumor site and disintegrated due to hydrolysis

caused by the slightly acidic tumor environment, thus enhancing the anti-tumor effect. In dendrimer polymers, such as PAMAM, functional groups can be chemically linked with immunotherapeutic agents. Xia et al. (56) linked DOX to the terminal amino group of PAMAM through a pH-sensitive hydrazone bond [PEG-PAMAM-DOX (PPD) conjugate] and designed a PAMAM-based NP (LMWH/PPD/CpG) loaded with DOX and immunoadjuvant cytosine–phosphate–guanine oligonucleotides (CpGODNs) for the combined chemotherapy and immunotherapy of metastatic melanoma. QDs in inorganic nanocarriers can also combine drugs with carriers through special coordination. Cai et al. (57) synthesized the first acid-decomposable, luminescent aminated ZnO QDs as nanocarriers with ultra-small size, modified with dicarboxyl-terminated PEG and hyaluronic acid (HA), and finally, constructed a ZnO QD-based pH-responsive drug delivery platform, in which DOX molecules were successfully loaded to PEG-functionalized ZnO QDs *via* the formation of a metal–DOX complex and covalent interactions. After the ZnO QDs are taken up by cancer cells, the metal–drug complexes dissociate in the acidic environment of the endosomes or lysosomes, releasing Zn2+ and DOX, achieving synergistic therapy.

In terms of drug loading rate and accurate controlled drug release, the performance of physical encapsulation is poorer than that of the other two drug-loading methods, which can not only reduce the non-specific release of drugs during circulation, but can also increase drug loading by adjusting the ratio of reactants and have obvious advantages in clinical production and application. These benefits may be related to the molecular weight, surface and internal structures of the material, whether the surface is charged, and whether the surface is hydrophobic. Owing to the advantages and disadvantages of these three different loading methods and the complexity of the tumor microenvironment, researchers have constructed nanomaterials with a diverse combination of different drug-loading methods and achieved satisfactory results in drug delivery and tumor treatment. Two pH-sensitive conjugates, pluronic P123-mono–hydrazone bond-P123-single-hydrazone–docetaxel and pluronic P123-double–hydrazone bond–docetaxel, prepared by Su et al. (58) were used as carrier materials to encapsulate docetaxel physically. These polymer micelles, which were prepared using chemical combination and physical encapsulation, can increase the drug loading capacity and drug release control compared to those created by chemical combination or physical encapsulation.

3 MECHANISM OF PH-RESPONSIVE POLYMER NANOMATERIALS IN TUMOR THERAPY

pH-responsive polymer nanomaterials carrying anti-tumor drugs can change their structures or properties with the pH reduction in the tumor microenvironment, thus providing accurate targeted tumor therapy. The common pH-sensitive structures mainly include chemical bonds, which are relatively stable in a neutral or alkaline environment but unstable in an acidic environment and are hydrolyzed or broken; polymers that can change their charge properties according to the change in pH (59); and other special pH-responsive polymers. Since these special pH-responsive structures will change their structures or properties according to changes in pH in the environment, the structure of nano-drug carriers containing these structures will also change (rearrangement, expansion, or degradation) (60). The aim of this is to release the loaded therapeutic drugs, remove the protective layer, cause disintegration close to targeted molecules in areas of pH change, and overall, achieve improved drug delivery efficiency and therapeutic effects (61; 62).

3.1 pH-Sensitive Chemical Bonds

Previously, we have discussed the drug loading methods for nanomaterials. Although the special spatial structure of some nanomaterials allows for the physical loading of drug molecules, combining the drugs and polymer carrier through chemical bonds can better control the distribution and release of drugs, can make the nano-drug system more stable *in vivo*, and only specifically degrade and release drugs in the tumor tissue environment (63–66). At present, we already know that many chemical bonds are unstable and easy to break in a strongly acidic or strongly alkaline environment. We can utilize these unstable chemical bonds in an acidic environment and introduce them into nano-drug carriers to construct a pH-responsive polymer DDS that can specifically release drugs in the slightly acidic tumor microenvironment. The common pH-sensitive bonds mainly include hydrazone/acyl hydrazone, imine, acetal/ketal, oxime, amide, ester/orthoester, β-thiopropionatent, and borate ester (59, 60, 67–69). The general structures of these bonds and the corresponding hydrolyzed products are summarized in **Figure 2**.

3.1.1 Hydrazone/Acyl Hydrazone Bonds

Hydrazone/acyl hydrazone bonds are formed by the condensation reaction of hydrazine groups (-NH-NH2) or hydrazide groups (-CONH-NH2) with ketones or aldehydes. This reaction is relatively stable at pH 7.4, and thus, the hydrolysis rate is very slow but will be accelerated at lower pH levels (70). Based on this, hydrazone/acyl hydrazone bonds are widely used in drug delivery (71).

In the early 1990s, Greenfield et al. (72) and Kaneko et al. (73) had studied various hydrazone bonds formed by the condensation of the ketone groups of DOX with hydrazide groups. The sensitivity of the hydrazone bond to the acidic environment has since been deeply and extensively studied, and it has been applied to various structures, including linear (73), star-shaped (74), and cross-linked (75) molecules. Recently, Long et al. (76) reported a novel strategy to endow cellulose nanocrystals (CNCs) with pH responsiveness and drug loading through the formation of hydrazone bonds between PEG-modified CNCs and the aldehyde group of DOX. DOX was loaded on PEG-modified CNCs and could be specifically released from pH-responsive drug polymer carriers at the tumor site. The results of anti-tumor experiments both *in vivo* and *in vitro* showed that the drug carrier had obvious cytotoxicity and a good anticancer effect.

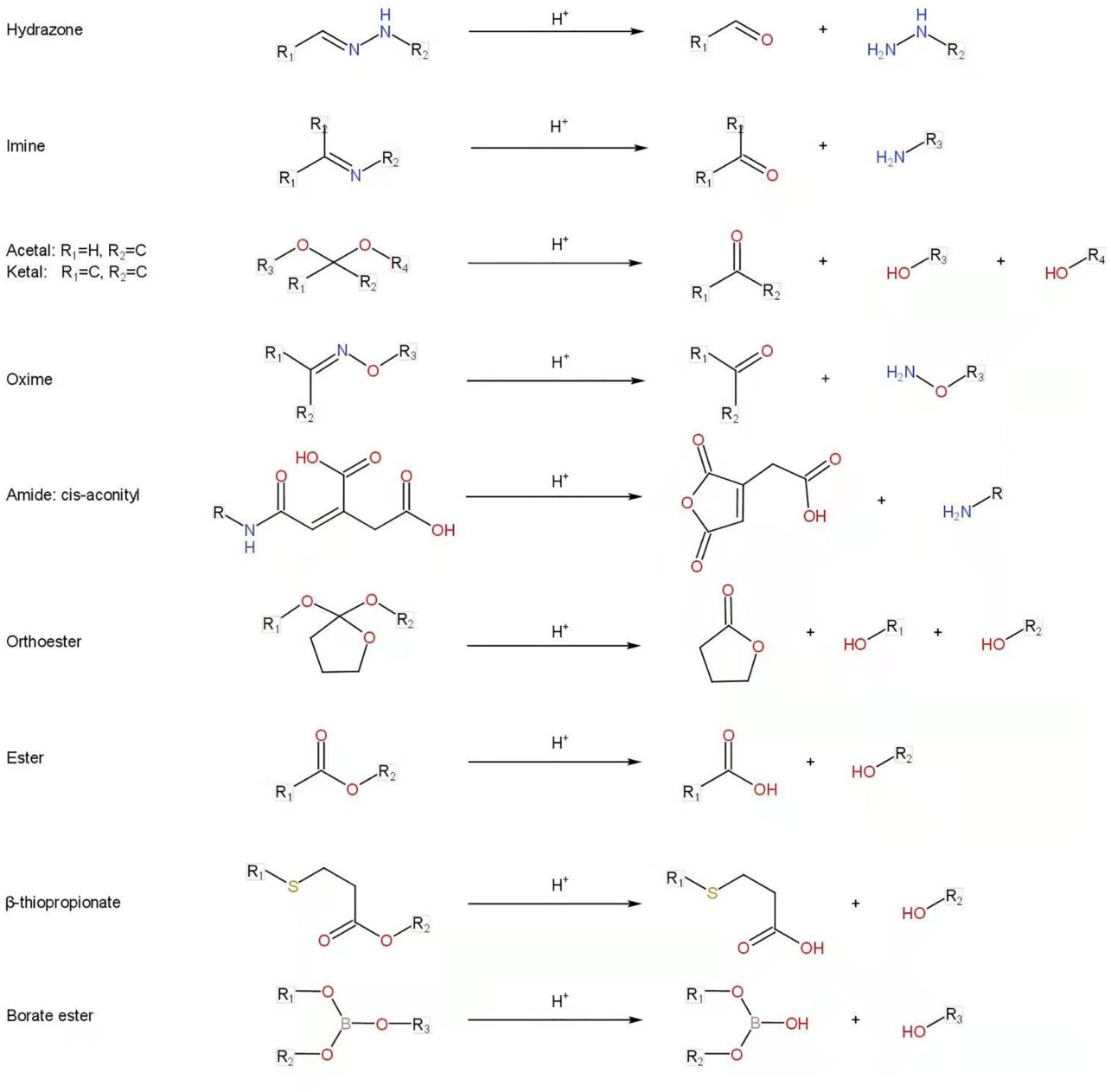


FIGURE 2 | PH-responsive linkages and the corresponding hydrolyzed products.

The most common method of introducing hydrazone bonds into nano-drug carriers is the condensation of hydrazide groups in various polymers with ketones or aldehyde group drugs. Therefore, the existence of ketone or aldehyde functional groups in drug molecules is the main challenge hindering the application of hydrazone bonds (77). Although many researchers have synthesized drug derivatives to obtain ketones or aldehyde groups, such as PTX synthesized by Alani et al. (78), cisplatin synthesized by Aryal et al. (79), and Cur derivatives synthesized by Li et al. (80) and Wang et al. (81) in clinical application, the product development and regulatory approval of these drug derivatives are difficult in practice (77). At the same time, the cationic polymer residues that may be formed after the hydrazone bond breaks in an acidic environment will produce cytotoxicity to a certain extent (82). These limitations in the application of nano-polymers containing hydrazone bonds to tumor therapy require improvement through further research.

3.1.2 Imine Bonds

The structural formula of imine bonds is -C=N-, which is widely known as a pH-sensitive dynamic covalent bond. Its carbon–nitrogen double bond structure is obtained by the condensation reaction of aldehydes or ketones with primary amines, i.e., the "Schiff base reaction". Therefore, the Schiff base structure mainly refers to a class of compounds containing C=N groups. Although it has been proven that the structure can exist stably in an alkaline or neutral environment and accelerate the hydrolysis/breaking rate in an acidic environment (83, 84), some researchers agree that imide bonds are not stable enough under physiological conditions (i.e., pH 7.4 and 37°C) (85, 86). Thus, it has been suggested that increasing the stability by conjugating with the π–π bond to form benzoic–imide bonds could be a solution to this (87).

The synthesis of benzoic–imide bonds involves amines and benzaldehydes, which exist naturally in many raw materials and are easy to obtain and synthesize. They are very suitable for constructing pH-responsive polymer nanomaterials and have been widely used in anti-tumor DDSs. For example, Liao et al. (88) prepared pH-responsive benzoic-imide polymer nanogels as carriers of indocyanine green (ICG) by crosslinking poly (ethylenimine)-g-mPEG (PEI-g-mPEG) copolymers with hydrophobic terephthalaldehyde molecules in an aqueous solution with pH 7.4. The nanogel loaded with ICG not only significantly improved the photostability of ICG in phosphate buffer, but also clearly slowed down the leakage of ICG at pH 7.8, and when the pH was decreased from 7.8 to 6.4, the benzoic–imide bonds in the nanogel broke and released ICG, showing targeted release.

3.1.3 Acetal/Ketal Bonds

The structural formula of acetals/ketals allows for two alkoxy groups to connect on the same carbon; the difference between them is that ketals have one more central carbon substituent than acetals. Under acidic conditions, one of the oxygen atoms is protonated, thus activating the adjacent carbon atoms and leading to the hydrolytic fracture of bonds. Previous studies have shown that polymers containing acetals/ketals can be degraded into soluble monomers in the acidic pH of a tumor microenvironment (89, 90).

Acetal/ketal bonds are also widely used in pH-responsive polymer nano-DDSs (NDDSs). Zhao et al. (91) polymerized cinnamaldehyde (CA) directly with glucose through acid-unstable acetal bonds and encapsulated 10-hydroxy camptothecin (HCPT), and then, synthesized a novel type of pH-responsive DDS comprising HCPT–CA-loaded NPs (PCH). In an acidic environment, both HCPT and CA could be rapidly released by PCH. The results of anti-tumor experiments both *in vivo* and *in vitro* showed that PCH could not only effectively prolong the drug circulation, increasing the drug accumulation in the tumor site and promoting the intake of drugs, but also induced the death of cancer cells by producing intracellular ROS, showing excellent therapeutic performance and improved biosafety.

3.1.4 Oxime Bonds

The structural formula of oxime bonds is -C=N-O-. These bonds are reversible dynamic covalent chemical bonds, similar to imine bonds. The common method for preparing oxime bonds is a condensation of aldehydes or ketones with hydroxylamine groups, which can be hydrolyzed into aldehydes, ketones, and hydroxylamines under acidic conditions (92, 93). Studies have shown that oxime bonds are reversible, have dynamic pH sensitivity, and can form a new type of pH-responsive polymer (94). Jin et al. (94) successfully synthesized a pH-responsive triblock copolymer (PEG-OPCL-PEG) by ligating aminooxy terminals of OPCL with aldehyde-terminated PEG (PEG-CHO), which consisted of hydrophilic PEG and hydrophobic oxime-tethered polycaprolactone (OPCL). DOX was selected as an anti-tumor model drug, which was encapsulated in PEG-OPCL-PEG and self-assembled into micelles in an aqueous solution. The drug release studies showed that the release rate of DOX in micelles at pH 5.0 was significantly faster than that at pH 7.4, which indicated that the oxime bond DDS had the characteristic of pH response. The results of anti-tumor experiments both *in vitro* and *in vivo* also showed that DOX-loaded PEG-OPCL-PEG micelles had a high anti-cancer effect.

3.1.5 Amide Bonds

Amides are an important part of pharmaceutical chemistry, and more than 25% of drugs in the database of pharmaceutical chemistry contain amide bonds (95). The structural formula of amide bonds is (-C=O-N-). The synthesis method involves initial preparation using active carboxylic acid derivatives, such as acyl chloride, anhydride, ester, and azide, followed by development into an acylated preparation using substrates such as alcohols, aldehydes, and alkynes, catalyzed by new catalysts and amines (96, 97). Because some amide bonds with special side chains are hydrolyzed and broken under weakly acidic conditions (98, 99), such as maleic acid (MA) (60), cis-aconitine acid (100), and dimethyl maleic anhydride (DMMA) (101), amide bonds are also widely used in pH-responsive polymer NDDSs. Luo et al. (102) linked stearic acid (SA) to the main chain of carboxymethyl chitosan (CMC) through amide bonds, which then self-assembled into an amphiphilic stearic acid-O-carboxymethyl chitosan conjugate (SA-CMC), and then loaded the anti-tumor drug PTX onto the conjugate to form PTX-SA-CMC NPs. In the acidic environment of the tumor, the NPs disintegrated rapidly and released drugs specifically, owing to the pH sensitivity or acid instability of amide bonds. Both *in vivo* and *in vitro* experimental results showed that compared to those in the free PTX group, the drug uptake rate of tumor cells and killing effect in the PTX-SA-CMC NP group were significantly enhanced, which not only reduced the systemic toxicity but also achieved a noticeable anti-tumor effect.

3.1.6 Ester Bonds

The structure of the ester bonds or orthoester bonds is similar, in which one carbon atom is connected with two or three oxygen atoms. They are also pH-sensitive and degrade faster than acetals, ketals, or hydrazone bonds in an acidic environment (103, 104). At present, ester bonds or orthoester bonds have been widely studied and applied in pH-responsive polymers. Thambi et al. (105) prepared pH-sensitive amphiphilic block copolymers with orthoester bonds using hydrophilic PEG and hydrophobic

poly(γ-benzyl-L-glutamate) (PBLG) as carriers and loaded DOX into them. *In vitro* release studies showed that DOX was released slowly from the carrier in the physiological buffer with pH 7.4, whereas the release rate of DOX increased significantly at pH 5.0. *In vitro* cytotoxicity tests showed that the toxicity of these DOX-loaded nanocarriers to SCC7 cancer cells was higher than that of DOX carriers without orthoester bonds. These results indicated that this pH-responsive copolymer NDDS with orthoester bonds has great potential in tumor therapy.

3.1.7 β-Thiopropionate Bonds

Owing to the inductive effect of the S atom in the β-thiopropionate bond, the hydrolysis of the bond is driven by the positive charge on the carbonyl carbon of the ester. Compared with other pH-resbeponsive chemical bonds, such as hydrazone, imide, and acetal/ketal bonds, which are very sensitive to pH changes, and thus, have a high hydrolysis rate in an acidic environment, β-thiopropionate bonds can be hydrolyzed at a relatively slow rate in a moderately acidic environment (for example, pH 5.5) (106–108).

β-thiopropionate bonds can be synthesized by simple Michael addition reaction of mercaptan methacrylate (106, 107). Samanta et al. (69) copolymerized 2-hydroxyethyl methacrylate and a coumarin-based methacrylate monomer containing a β-thiopropionate moiety *via* reversible addition–fragmentation chain transfer (RAFT) polymerization. The copolymer self-assembled to form vesicular nanoaggregates at physiological pH conditions, and then, photochemical crosslinking was performed *via* coumarin ($2\pi + 2\pi$) cycloaddition reaction to further stabilize the vesicles. In the acidic environment of tumor cells, the slow hydrolysis of β-thiopropionic acid led to the disintegration of the polymers, resulting in the sustainable release of the loaded drugs. The results of the *in vivo* and *in vitro* anti-tumor experiments showed that compared with free DOX, the 50% inhibiting concentration (IC50) of DOX-loaded nanomaterials toward the MG63 cancer cell line decreased significantly, showing excellent anti-tumor effect and good biosafety.

3.1.8 Borate Ester Bonds

Borate ester bonds, formed by the condensation of phenylboronic acid and its derivatives with cis-diol or compounds containing catechol groups, are also reversible dynamic covalent bonds. At acidic pH levels, borate ester bonds can be reversibly hydrolyzed and broken, which gives them broad application prospects in tumor DDSs (109–111). Fang et al. (112) prepared a mitochondrial-targeted polymer, 3,4-dihydroxyphenyl propionic acid-chitosan oligosaccharide-dithiodipropionic acid-berberine (DHPA-CDB), which was used to load Cur and self-assemble into cationic nano-micelles (DHPA-CDB/CUR). Negatively charged oligomeric hyaluronic acid-3-carboxyphenylboric acid (OHA-PBA) was added to the prepared DHPA-CDB/CUR as the ligand of sialic acid and CD44, to shield the positive charge and prolong the circulation time *in vivo*. The OHA-PBA@DHPA-CDB/CUR covalent polymer was formed by OHA-PBA and DHPA-CDB/CUR through pH-sensitive borate ester bonds between PBA and DHPA. The low pH in tumor tissue promoted the degradation of borate ester bonds and the exposure of cationic micelles, which led to the reversal of the polymer surface charge, thus promoting internalization and mitochondrial localization. All experimental results showed that OHA-PBA@DHPA-CDB/CUR had mitochondrial targeting and tumor environmental charge-reversal capabilities, as well as great potential in targeted drug delivery.

3.2 pH-Responsive Charge Conversion

It is well known that nano-drug carriers reach the target position mainly through blood circulation in the human body. If there is a positive charge on the surface of the drug carrier when it encounters the many negatively charged proteins in human plasma, they will attract each other strongly; this makes it very easy for the carriers to be swallowed and cleared by phagocytes in the human body (113, 114), resulting in reduced drug delivery efficiency. The drug uptake efficiency will be reduced due to electrostatic repulsion when a drug carrier with a neutral or electronegative surface encounters the electronegative cell membrane (115, 116), whereas electropositive nano-drug carriers can better target endothelial cells, have higher vascular permeability (117), and are more likely to be swallowed by tumor cells (118–120). However, the liver can act as a charge-selective filtration barrier, which can cause the accumulation of electronegative nano-drug carriers in the liver with consequential potential side-effects. Thus, the long-cycle ability of neutral polymers or amphoteric ionic polymers is a better option (121).

In addition to attaching pH-sensitive acid-unstable bonds to the polymer backbone or side chains, there is another way to make the nano-drug carriers pH-responsive: introduce a chemical group into the nanomaterial that can lead to a change in surface charge properties (protonation or deprotonation) with the change in environmental pH. Such groups include amino, phosphoric acid, and carboxyl groups. These groups have different chemical structures and pKa values, can accept or provide protons, and undergo changes in physical or chemical properties related to pH, such as swelling or solubility, resulting in drug release (59, 60, 122). A nano-drug carrier has been designed, which has neutral or amphoteric ionic when it circulates in the human body, as this allows an improved circulation time for the nano-drug carrier in the body. When the nano-drug carrier reaches the tumor site, the surface charge of the nano-drug carrier is converted to positive, owing to the decreased pH in the tumor microenvironment, which promotes the uptake of tumor cells, thus greatly improving drug delivery efficiency (116, 123). For example, Fang et al. (124) coupled berberine (Ber) and vitamin B6 with oligomeric hyaluronic acid (OHA), creating self-assembled spherical NPs in an aqueous solution to prepare pH-responsive mitochondria-targeting NPs (B6-OHASS-Ber). In the acidic microenvironment of the tumor tissue, the pyridine group of B6 was protonated, and the surface of the carrier changed from negatively to positively charged, which promoted the internalization of NPs. After lysosome escape, it actively targeted mitochondria and released the drugs. The *in vivo* anticancer activity experiment results

showed that B6-OHA-SS-Ber/Cur had an obvious inhibitory effect on tumor growth. As shown in **Figure 3**, the micelles were modified by B6 to give the NPs the ability to convert charges, Ber was induced to focus on mitochondria preferentially by drugs and carriers, and OHA was used to target CD44 receptors (125, 126).

In addition, there also exists a pH-responsive polymer that changes the hydrophilicity or solubility of nano-drug carriers after protonation with a decrease in pH, resulting in the change in carrier structure and drug release (127). For example, some polymers synthesized from acidic monomers, such as poly (methacrylic acid) (128, 129), poly(aspartic acid) (PAsp) (130), and sulfonamide-based polymers (131), change from hydrophilic to hydrophobic when the pH is decreased. Kang and Bae (132) studied oligomeric sulfonamides (OSASs), which could effectively release polymers or transport nucleic acids. Owing to the different pKa values of different sulfonamide groups, OSASs change from hydrophilic to hydrophobic with a decrease in the surrounding pH and show different proton buffering capacities. Kang and Bae (132) combined an OSAS with DNA and then complexed it with poly(L-lysine) (PLL) to form an OSA polymer. The experimental results showed that there was no significant difference in DNA uptake between the OSA polymer and PLL/DNA control group; however, the OSA polymer induced a more extensive distribution of DNA in cells and significantly enhanced the transfection rate of DNA.

3.3 Synergistic Action of pH Stimulus and Other Stimuli

We have previously discussed the two main mechanisms of action of pH-responsive polymers, namely, unstable chemical bonds with pH sensitivity and groups or polymers with charge transfer or water solubility changes. However, these pH-responsive polymers should remain stable when the

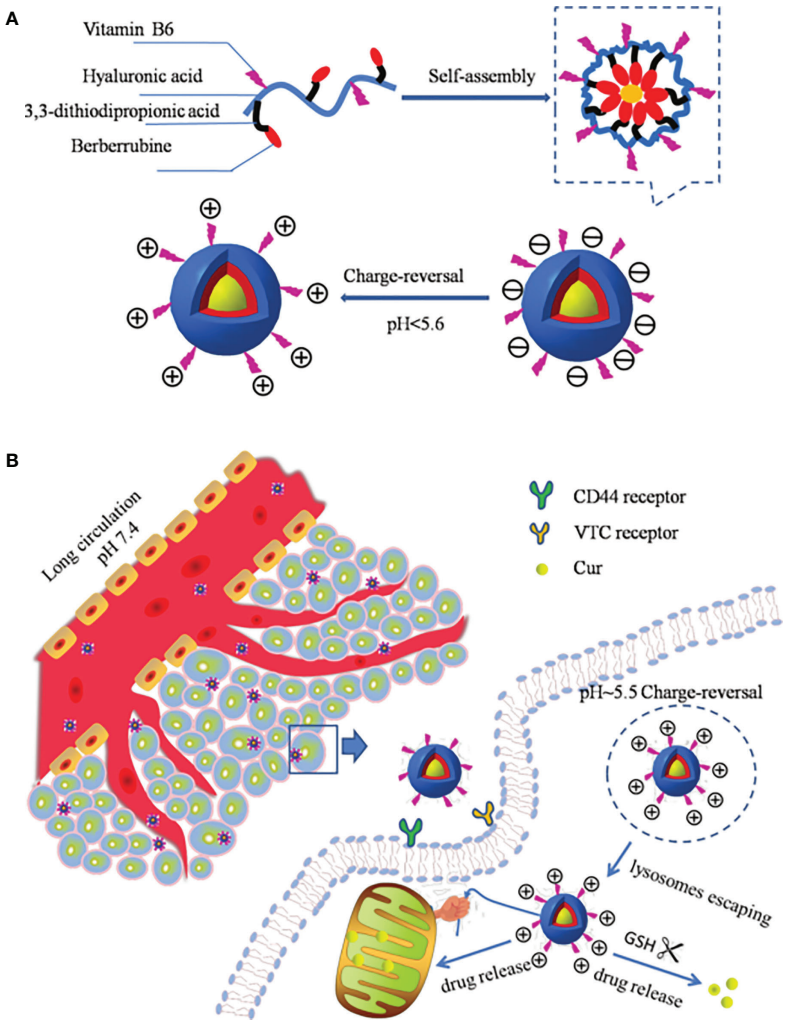


FIGURE 3 | **(A)** Schematic structure of B6-OHA-SS-Ber self-assembly into micelles; **(B)** the micelles entered into tumor cells and concentrated on mitochondria by active targeting and released the drug to tumor cells (124).

physiological pH is 7.4, and it is challenging to ensure sufficient drug release rate or cell uptake rate with a decrease of 1 pH unit (60). At present, many preclinical studies are being conducted at two pH values (7.4 and 5.0). Nevertheless, if there is only a small difference between the targeted position of the nano-drug carriers and the physiological pH, the drug release time of polymers that solely depend on the pH-responsive mechanism, especially the nano-drug carriers that rely on covalent bond cleavage, will be very slow (60). Hence, compared to single stimulus-responsive nano-polymers, dual or multiple stimuli-responsive polymer NDDSs have higher physiological or biological system correlations, can better adapt to the interaction in the real biological system (133), and greatly improve the stability of drug delivery and the sensitivity of controlled release, giving excellent anti-tumor effects and broader application prospects (134).

Compared with normal tissues, tumor tissues show significantly different physiological characteristics, such as differences in pH, redox enzyme levels, ROS levels, owing to their uncontrolled growth and abnormal gene expression. We can select or combine the corresponding stimulus-response factors for tumor-targeted therapy according to specific changes in the tumor microenvironment. In addition, some polymers will change their morphological structure, physical, or chemical properties when exposed to external stimuli (temperature, light, magnetic field, and ultrasound), which can be combined with pH stimulation response for tumor treatment to improve the therapeutic effect (135–139).

To reduce the problem of non-specific drug release in oral DDSs, Song et al. (140) studied the effect of pH response combined with enzyme response (double stimuli) on precisely targeted drug delivery. They anchored polyacrylic acid (PAA) and chitosan (CS) onto Gd3+-doped mesoporous hydroxyapatite NPs (Gd-MHAPNPs) to realize programmed drug release and magnetic resonance imaging at tumor sites. Among them, the grafted PAA acted as a pH-responsive switch to control the release of drugs into the colon. In addition, CS was functionally modified into enzyme-sensitive parts and could be degraded by β-glucosidase in the colon. Chemotherapeutic drugs (5-fluorouracil) and targeted therapy drugs (gefitinib) were encapsulated in Gd-MHAP NPs for synergistic therapy (**Figure 4**). The experimental results showed that CS and PAA protected drug-loaded NPs from various physiological conditions in the gastrointestinal tract, in order for the drug to reach the colon tumor site, prevent premature drug release, and control drug release *via* the dual stimulus-response mechanism (pH and enzyme), which increased the drug load at the colon tumor site and improved the therapeutic effect.

Owing to the high reducibility in the tumor environment, such as the increased glutathione (GSH) content, Kim et al. (141) designed pH- and GSH-responsive fluorescent polymer dots (L-PDs) containing PTX. The core part of the L-PD nano-hybrid system used disulfide bonds as the redox response site, which could not only maintain the stability of the internal structure but could also avoid the leakage of PTX during the cycle. The nano-hybrid system showed fluorescence quenching behavior, with less than 2% of the PTX being released under physiological pH conditions. However, in the tumor microenvironment, fluorescence was restored under the acidic pH, and the PTX release was about 100%, which significantly improved the effectiveness of killing tumor cells. In addition, the experimental results showed that there were differences in the release of PTX under different GSH concentrations, and the explosive release of PTX was detected under a high GSH concentration.

In addition, because of the high levels of reactive oxygen species (ROS) and low pH levels in the tumor microenvironment, Jäger et al. (142) designed functionalized "AND gate" multi-responsive (MR) block amphiphilic copolymers with dual stimulus-response to ROS and pH for cancer drug delivery therapy. The hydrophobic part of the polymer contained masked pH reaction side chains, which were exclusively exposed in response to the high ROS in the tumor microenvironment. These researchers synthesized two kinds of pH-responsive polymers from MR-ethyl and MR-isopropyl and then prepared DOX-loaded nano-drug carriers (multi-responsive nanoparticles, MRPs) and control-free DOX carriers using microfluidic self-assembly technology. The experimental results showed that compared to the control-free DOX carriers, the drug release rate of the MRP group was significantly faster under the influence of the dual ROS and pH response.

In addition to taking the different biochemical indexes of tumor tissue as stimulus-response factors, some polymer components undergo volume phase transition when the external environment, such as temperature, changes, thereby triggering the selective release of drugs. For example, Wang et al. (143) synthesized the temperature and pH double stimuli-responsive NPs consisting of deoxycholic acid and hydroxybutyl-decorated chitosan (DAHBCNPs) and designed a series of DAHBCs with different lower critical solution temperatures (LCSTs, all below 37°C) to load Cur for the oral treatment of colorectal cancer. Owing to the mutual offset of the size change between the polymer expansion after pH response and the polymer contraction after temperature response, the DAHBC NPs were relatively stable under simulated gastric conditions (pH 1.2, 37°C). However, in simulated intestines (pH 7.0–7.4, 37°C), DAHBC NPs promoted the continuous release of Cur into the intestinal tract on account of the single effect of polymer contraction after temperature response. Compared with free Cur, DAHBC NPs at 27°C (DAHBC27) were better absorbed by Caco-2 cells through transcellular and paracellular transport pathways, and the intestinal absorption efficiency of Cur was greatly improved by paracellular transport pathways. In addition, Chen et al. (144) Feng et al. (145), and Lin et al. (146) reported on multifunctional nano-drug carriers with dual pH and temperature-stimuli responses (photothermal therapy). For example, Chen et al. (144) prepared a multifunctional NDDS with pH and temperature response based on an ordered mesoporous silica-sandwiched black phosphorus nanosheet (BP@MS) with vertical pore coating. The special structure of the drug carrier not only

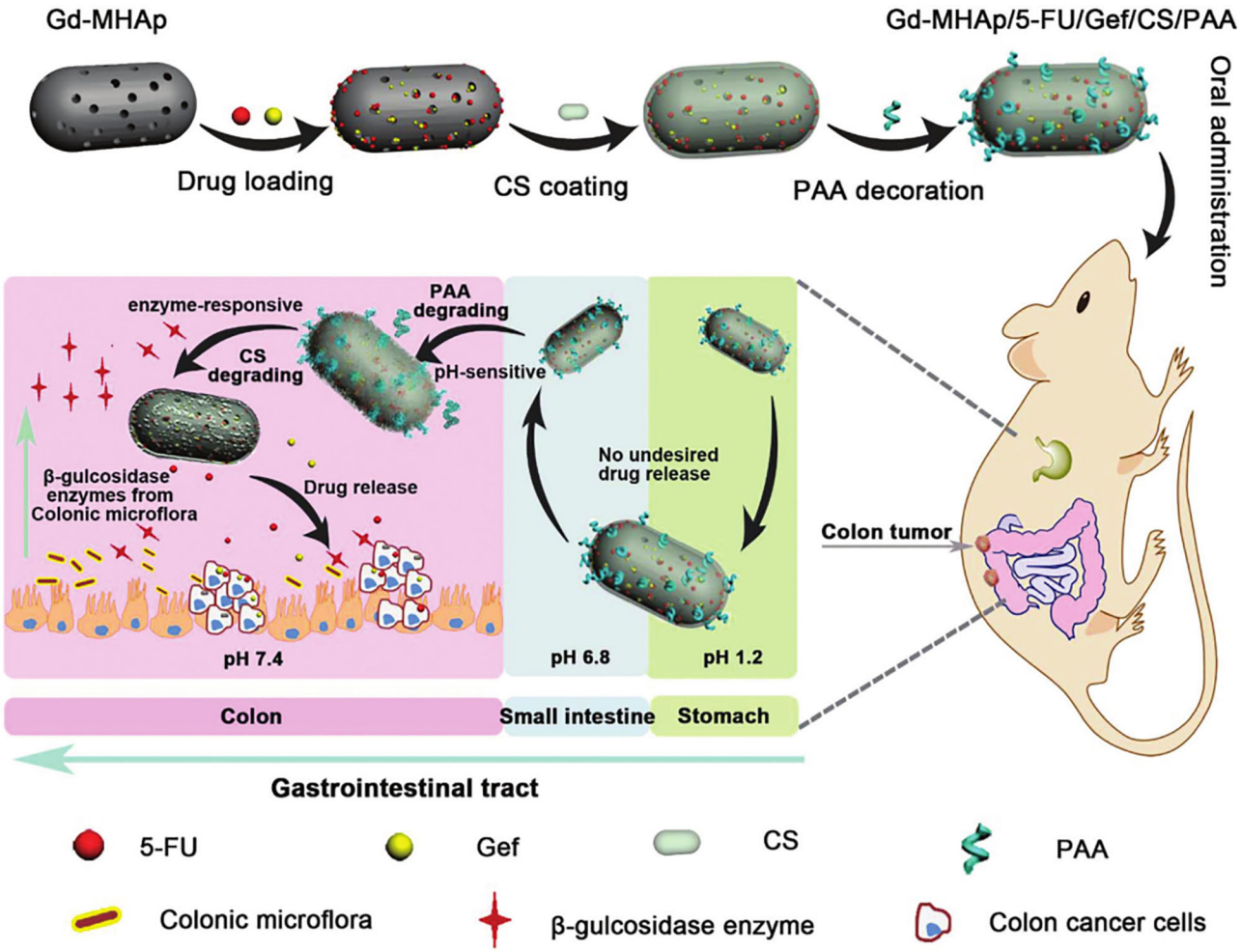


FIGURE 4 | Schematic illustration of the preparation of Gd-MHAPNPs and the mechanism of drug release in different physiological environments in the GIT (140).

enhanced the dispersity of the BP nanosheet and improved the drug loading efficiency (DOX), but also facilitated post-modification, such as the PEGlyation and conjugation of the ligand targeting TKD peptide. The results of *in vivo* and *in vitro* anti-tumor experiments showed that the DOX-loaded BP@MS system (BSPTD) manifested heat-stimulative, pH-responsive, and sustained release behaviors. Moreover, the BSPTD could also significantly inhibit the lung metastasis of tumors, owing to the secondary administration promoted by photothermal degradation.

In addition to dual stimuli, the combined application of multiple stimuli in tumor therapy has been widely studied. Don et al. (147) synthesized a poly(AA-b-NIPAAm) copolymer (PAA-b-PNIPAAm) *via* reversible addition–fragmentation chain transfer polymerization, consisting of PAA and poly(N-isopropylacrylamide) (PNIPAAm), which self-assembled to form nanogels with cationic protein (protamine). Chemical characterization showed that the nanogel exhibited a change in protamine conformation, PAA-b-PNIPAAm disaggregation, and protein enzymatic hydrolysis when stimulated by temperature, pH, and enzyme activity level changes. Changing the pH from 7.4 to 5.0-6.5 increased the mean particle size and converted the surface charge from negative to positive. After cold shock treatment, DOX was rapidly released in the cells. Furthermore, the nanogel could also carry a rose bengal photosensitizer and cause significant damage to cancer cells under irradiation.

3.4 Other Mechanisms

In addition to the two basic principles introduced above, another pH response mechanism has been gradually discovered and studied, the principle of which is that bicarbonate reacts with an acid to produce CO2 and H2O. Therefore, polymer nanomaterials containing bicarbonate structures may also release drugs specifically in an acidic environment, in what is known as a gas-generating pH-sensitive nano-system (59). Kim et al. (148) encapsulated poly(lactide-co-glycolide) (PLGA) NPs with sodium bicarbonate, which could be decomposed to

produce CO2 under acidic conditions, and imidazoquinoline-based synthetic toll-like receptor 7/8 agonist (TLR7/8, also known as "522"). The addition of sodium bicarbonate not only significantly increased the loading dose of 522, but also decomposed and released CO2 through pH response after the NPs were internalized by tumor cells and phagocytized by lysosomes, resulting in the release of 522 into tumor cells. Finally, the experimental results also showed that the new pH-sensitive NPs had a better anti-tumor effect than traditional PLGA NPs.

4 APPLICATION OF PH-RESPONSIVE POLYMER NANOMATERIALS IN TUMOR THERAPY

At present, there are many effective treatment approaches for tumors, from surgical resection, chemotherapy, and radiotherapy to landmark molecular targeted therapy, immunotherapy, gene therapy, photodynamic therapy, photothermal therapy, and chemodynamic therapy, all of which have made great progress and development throughout the years. As is well known, the traditional administration of chemotherapy leads to the poor targeting of drugs to tumors, low drug utilization, and many other challenges. Therefore, scholars have proposed DDSs in which chemotherapeutic drugs are loaded and transported on carriers (149). To improve the efficiency of DDSs, it became a hot spot (150, 151) in tumor therapy research to design nano-drug carriers that can respond to the abnormal biochemical indicators in the tumor microenvironment (152) to release drugs directly into the tumor site. With the development of nanomaterials, nano-systems can enhance the permeability and retention of drugs in solid tumors (59) by introducing different stimulus-responsive structures into DDSs (153), among which pH-responsive polymers have been widely used in stimulus-responsive NDDSs (59, 100). The common applications of pH-responsive polymer nanomaterials in tumor therapy are summarized in **Figure 5**.

4.1 Application of pH-Responsive Polymer Nanomaterials in Tumor Monotherapy

4.1.1 Application of pH-Responsive Polymer Nanomaterials in Combination with Chemotherapy

Single drug therapy will produce serious drug resistance in tumor treatment, but combinations of different drugs have been proven to be very effective in overcoming multidrug resistance (154, 155). Moreover, the combination of two or more drugs can generally reduce the drug dose and toxicity (156). Thus, constructing a multifunctional pH-responsive NDDS provides an effective strategy for chemotherapy. Wang et al. (157) synthesized multifunctional NPs (FTDCAG NPs), using a pH-responsive prodrug (PEG2K-NH-N-DOX), a GSH-responsive prodrug (PEG2K-S-S-CPT), folate-receptor targeting polymers (FA-PEG2K-L8, FA-PEG2K-TOS), and T1-enhanced magnetic resonance imaging contrast agents (Gd-DTPA-N16-16) used to encapsulate combrestatin A4 (CA4). These FTDCAG NPs contained three drugs, namely, CA4, DOX, and CPT. At pH

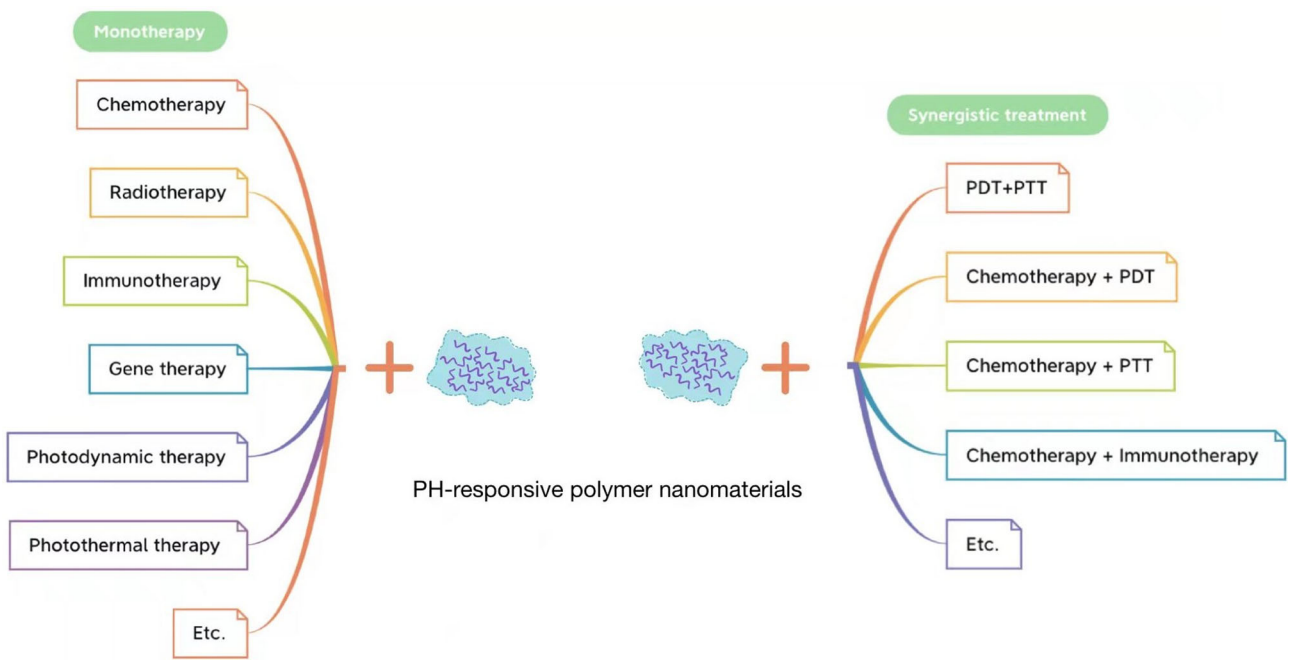


FIGURE 5 | Application of pH-responsive polymer nanomaterials in tumor monotherapy (left) and application of pH-responsive polymer nanomaterials in tumor synergistic treatment (right).

6.5, the drug release rate of CA4 increased by 63.4%. After release, CA4 destroyed angiogenesis in the tumor microenvironment and promoted the uptake of the remaining FTDCG NPs by tumor cells. After entering tumor cells, the FTDCG NPs disintegrated, owing to the increase in intracellular GSH concentration and the decrease in pH levels in the endosomes or lysosomes, releasing CPT and DOX. The results showed that FTDCAG NPs had a significant anti-tumor effect, and controlled drug release in time and space, which could maximize the effect and accuracy of cancer chemotherapy.

4.1.2 Application of pH-Responsive Polymer Nanomaterials in Combination with Radiotherapy

Radiotherapy is the most effective method to treat malignant brain tumors, but it is a challenge to ensure minimum damage to the surrounding normal tissue, while providing the best therapeutic dose to the tumor tissue (158). Therefore, one of the basic treatments for glioblastoma is radiotherapy combined with radiosensitizers. Shirvalilou et al. (159) used 5-iodo-2-deoxyuridine (IUdR) as a radiosensitizer for glioblastoma and magnetic graphene oxide NPs coated with PLGA polymer as drug carriers for IUdR (MNPs). The results of *in vivo* and *in vitro* experiments showed that MNPs not only prolonged the circulation time *in vivo* but also targeted glioma through an external magnetic field after intravenous injection. Moreover, the experiment results illustrated a higher IUdR release rate at pH 5.6 than at pH 7.4, where 82% and 56% of the IUdR was released within 24<n,bsp/>h respectively. The drug release rate was significantly increased when the NPs reached the tumor site due to the degradation of PLGA polymers as a result of charge transfer under acidic pH conditions, revealing the controlled drug release abilities of the MNPs in the acidic environment of the tumor. Under high voltage X-ray irradiation, compared with the control group, IUdR/MNPs showed a stronger radiation sensitization effect and increased apoptosis induced by radiation, which improved the therapeutic effect.

4.1.3 Application of pH-Responsive Polymer Nanomaterials in Combination with Immunotherapy

Compared with chemotherapy, immunotherapy has more advantages in terms of avoiding toxicity and side effects, inhibiting tumor metastasis, and preventing tumor recurrence; it is recognized as the next generation of tumor therapy (160, 161). The complement system plays an important role in promoting antigen-specific immune responses (162). Polymers carrying nucleophilic groups, such as hydroxyl or amino groups, can activate the complement system, resulting in the maturation of dendritic cells and induction of enhanced immune responses (163–165). Li et al. (166) prepared a multifunctional pH-responsive micelle vaccine platform (COOH-NPs) based on a carboxyl-modified deblock copolymer of poly(2-ethyl-2-oxazoline)–poly(D, L-lactide) (COOH-PEOz-PLA). After injection, the vaccine showed good targeting, and the tertiary amine groups in the PEOz backbone became protonated under acidic conditions, imparting the micelle payloads with endosomal escape *via* the "proton sponge" effect (167, 168). Compared with the control group, the nano-vaccine exhibited good laminin targeting, antigen presentation ability of cytotoxic T lymphocyte immune response, and complement activation to promote dendritic cell maturation, which significantly inhibited tumor growth and prolonged survival time.

4.1.4 Application of pH-Responsive Polymer Nanomaterials in Combination with Gene Therapy

Traditional gene therapy generally adopts the method of enhancing host anticancer immunity, antagonizing antioncogenes, expressing suicide genes, or gene modification combined with high-dose chemotherapy. While achieving certain curative effects, it also has some disadvantages, such as low gene vector introduction efficiency and poor accuracy and controllability of foreign gene expression *in vivo*. With the development of genomics and genetic engineering research, recent new technologies, such as targeted gene-viro-therapy (169), RNAi technology (170), and microRNA (171), provide new bases or evidence for the accurate treatment of cancer. In gene therapy, hyperbranched PEI-25k and its derivatives have been widely developed and applied, owing to its high density of positive charges, which can bind closely to DNA and promote its escape from endosomes (172, 173). Chen et al. (174) synthesized a novel pH-responsive polymer shielding system (PAMT) *via* click reaction between poly(γ-allyl-L-glutamate) and thioglycolic acid or 2-(Boc-amino) ethanethiol. PAMT was electrostatically attached to the surface of the positively charged PEI/pDNA complex to form a ternary complex. When the pH in the external environment decreased from 7.4 to 6.8, the PAMT released gene therapy drugs through rapid charge conversion. The *in vivo* anti-tumor experiment showed that the transfection efficiency of the PAMT/PEI/shVEGF group was higher and the inhibitory effect on tumor growth was more obvious, compared to the control group.

4.1.5 Application of pH-Responsive Polymer Nanomaterials in Combination with Photodynamic Therapy

In recent years, photodynamic therapy (PDT) has been widely used in tumor therapy. Earlier, Kelly et al. (175) successfully used hematoporphyrin derivatives as photosensitizers in the treatment of bladder cancer, creating a precedent for the application of PDT on tumors. The traditional DDSs relying on photosensitizers have limited application for the PDT of tumors, owing to their poor pharmacokinetics (176, 177) and long-term biological safety issues (176–178). For example, MoS2 DDSs, the biotoxicity of which is caused by quantum size effects and surface effects, may have adverse effects on the human reproductive system (178). Previous studies have shown that nanomaterial drug carriers have a higher uptake rate of tumor cells and fewer side effects (177), and the specific response of drugs to the tumor can be further enhanced by designing stimulus-responsive nano-drug carriers.

To overcome the shortcomings of the non-specific tumor therapy associated with PDT, Li et al. (179) and He et al. (180) applied nanomaterials with stimulus-response to PDT, which

made the therapeutic drugs release specifically at the tumor site, reducing the non-specific phototoxicity of PDT and improving the anti-tumor effect. Ma et al. (181) combined chidamide as a histone deacetylase inhibitor (HADCi) with pH-responsive block polymer folate PEG-b-poly(aspartic acid) (PEG-b-PAsp)-grafted folate (FA-PEG-b-PAsp) to obtain block polymer folate PEG-b-poly(asparaginyl-chidamide) [FA-PEG-b-PAsp-chidamide (FPPC)]. Then the model photosensitizer pyropheophorbide a (Pha) was coated with FPPC and polymer micelles (Pha@FPPC) were formed in PBS. After the uptake of Pha@FPPC by tumor cells through FA-receptor-mediated endocytosis, PAsp changed from hydrophilic to hydrophobic in the lysosome due to the decrease in pH, which led to the directional release of Pha molecules. The results showed that Pha@FPPC had low dark cytotoxicity *in vitro* and a good therapeutic index, owing to its high dark cytotoxicity:photocytotoxicity ratio. Furthermore, compared with free Pha, Pha@FPPC not only significantly inhibited the growth of the implanted tumor and prolonged the survival time of melanoma-bearing mice, but also remarkably prevented the pulmonary metastasis of mice melanoma through folate-mediated and selective accumulation.

4.1.6 Application of pH-responsive Polymer Nanomaterials in Combination with Photothermal Therapy

Similar to PDT, photothermal therapy (PTT) has become an effective method to treat cancer with high specificity, good anti-tumor effects, controlled drug release, and few side effects (154, 182, 183). As an NIR-absorbing organic photosensitizer, ICG is an amphiphilic tricarbocyanine dye that has been approved by the United States Food and Drug Administration for medical diagnosis and imaging. Although ICG has great potential in PTT applications, it also has many defects (184, 185). To overcome these shortcomings, pH-responsive polymer micelles or NPs have been used to design tumor-targeting ICG delivery methods. Ting et al. (186) co-assembled hybrid polymer NPs (PbCTPNs) comprising hydrophobic PLGA segments, ICG molecules, amphiphilic tocopherol PEG succinate (TPGS), and pH-responsive mPEG-benzoic imine-1-octadecylamine (mPEG-b-C18) segments. PbCTPNs maintained sufficient stability under physiological pH conditions, effectively inhibiting the self-aggregation and leakage of ICG. However, when the pH decreased to 5.5, the unstable imine bond in mPEG-b-C18 was hydrolyzed, which accelerated the release of ICG molecules in combination with near-infrared radiation, significantly killing MCF-7 cells and improving the anticancer efficacy of ICG-mediated PTT.

4.2 Application of pH-Responsive Polymer Nanomaterials in Tumor Synergistic Treatment

Previously, we discussed the application of pH-responsive polymers in tumor monotherapy, such as PDT, PPT, immunotherapy, and gene therapy; although they are still in the early clinical stages, they have shown good efficacy and clinical results. However, studies and clinical experiences have shown that it is difficult for monotherapy to eliminate tumors and control their metastasis; some cell subsets in unevenly distributed tumor tissues are resistant to monotherapy (187, 188). For example, in chemotherapy, long-term use of the same anticancer drug will induce tumor multidrug resistance, resulting in a decline in efficacy (189). Thanks to the rapid development of nanotechnology, we can combine two or more therapies and design multifunctional nano-drug carriers for the targeted delivery of multiple drugs, which can not only improve the curative effects, but can also reduce the side effects caused by high doses of a single therapy and make up for the defects and deficiencies of various other treatments (190, 191).

Photothermal therapeutic agents are also excellent photosensitizers, and the combination of PDT and PTT may have a synergistic effect on phototherapy. Bejjanki et al. (192) studied the efficacy of PTT combined with PDT in treating tumors. They combined ICG, Fe3O4, and palmitoyl ascorbic acid (PA) with pH-responsive PEG-b-PAEMA-PDMA polymers to form nano-drug carriers. The carriers remained stable under physiological pH and the cycle time was prolonged, while drug loading was released *via* charge conversion and tumor cell uptake was promoted in the acidic tumor environment. The results of *in vivo* and *in vitro* tumor cell experiments showed that the nano-drug carrier showed a synergistic PDT/PTT effect, had a high apoptosis rate, and significantly inhibited tumor growth.

Compared with photodynamic therapy, chemodynamic therapy is a new treatment strategy (193). It can kill tumor cells by converting overexpressed hydrogen peroxide into highly toxic hydroxyl free radicals through Fenton and Fenton-like reactions. It has a high tumor selectivity (194, 195). Wang et al. (196) reported a pH and ROS dual-response nano-drug (PtkDOX-NM), which accumulates in the tumor site through the enhanced permeability and retention effect. In the acidic endosomal environment, the poly(2-[diisopropylamino] ethylmethacrylate) segment of the drug changes from hydrophobic to hydrophilic, resulting in β-lapachone (Lap) dissociation and rapid release. The Lap promoted the production of hydrogen peroxide, and a Fenton reaction occurred in the presence of iron ions, which significantly increased the ROS content in the tumor environment, thus promoting the effective cascade release of antineoplastic drugs in response to ROS and enhancing the curative effect through the combination of chemodynamic therapy and chemotherapy.

To verify the synergistic effect between chemotherapy and PDT therapy, Li et al. (197) combined anti-tumor drug GNA002-mediated chemotherapy with PDT therapy through an NDDS, which improved the efficacy of anticancer therapy. They used 5-(4-carboxyphenyl)-10,15,20-triphenylporphyrin as the photosensitizer and GNA002 as the hydrophobic core and cyclic RGD peptide (cRGD)-modified PEG (cRGD-PEG) connected to cell-penetrating peptide hexa-arginine (R6) through an unstable hydrazone bond as a hydrophilic shell to synthesize a nucleus-targeted pH cascade-responsive micelle nano-platform (**Figure 6**). The NPs were accumulated at the tumor site, and then actively internalized into tumor cells through the cRGD ligands. In cells, when the NPs were swallowed by lysosomes, the hydrazone bond was hydrolyzed

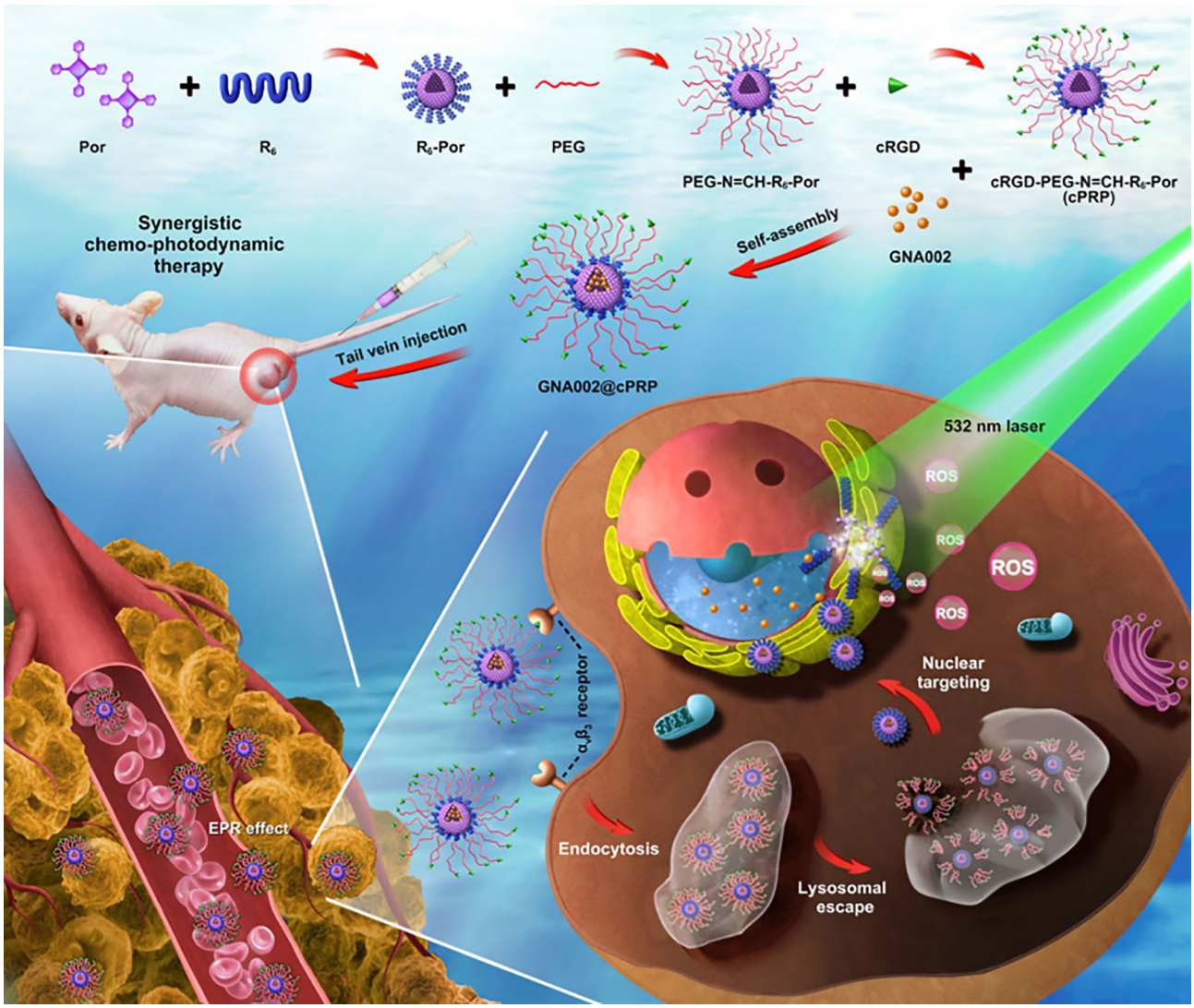


FIGURE 6 | Schematic illustration of a pH cascade-responsive nucleus-targeted nanoplatform for synergistic chemo-photodynamic therapy (197).

and the shell fell off due to the change in pH. Then nucleus-targeted drug delivery mediated by R6 was treated with chemotherapy and PDT under laser irradiation.

In addition, Tang et al. (198) studied whether there was a synergistic effect between chemotherapy and PTT. They designed a biosensor with a MOF coated with multifunctional polydopamine (PDA) for the detection of miRNA-122 with Zn2 +-triggered aggregation-induced enhancement (AIE) and synergistic chemotherapy/PTT. They used ZIF-8 NPs as DOX carriers and modified them with polydopamine to improve the pH response and biocompatibility of the nano-drug carriers. When the nano-drug carrier reached the tumor site, the acidic environment led to a change in the carrier structure and accelerated the release of Zn2+ and DOX. The experimental results not only showed that the nano-drug carrier accurately detected miRNA-122, but also verified the synergistic effect of chemotherapy and PTT on tumor therapy.

To solve the multidrug resistance of chemotherapeutic drugs, the combination of chemotherapy and other therapeutic methods for treating tumors has been widely studied and explored. For instance, Wang et al. (199) studied whether there was a synergy between chemotherapy and tumor immunotherapy. They employed a unique cationic switchable lipid as a pH-responsive drug carrier, which encapsulated the anti-tumor drug sorafenib and was loaded with anti-miRNA27a-loaded anti-GPC3 antibody to form targeted lipid NPs (G-S27LN), enabling targeted release the sorafenib and antibodies in the acidic environment of the tumor. Compared to the control group, the survival rate of tumor cells decreased significantly, and the proportion of apoptotic cells was

remarkably higher than that in the control group, showing a synergistic therapeutic effect.

5 CONCLUSION AND OUTLOOK

pH-responsive polymer nanomaterials can stably carry anti-tumor drugs through the body and release them into tumors through acid-unstable bond fracture or charge conversion for certain targeted therapeutic effects. Compared with conventional tumor chemotherapy, treatment with pH-responsive polymer nanomaterials exhibits improved therapeutic efficiency with minimal invasiveness to the host organism, which highlights its great potential in clinical trials or preclinical studies. Despite the notable progress made in the field of pH-responsive polymer nanomaterials, there are many critical issues that remain to be solved for better clinical application. Therefore, the potential focuses and challenges of pH-responsive polymer nanomaterials have been discussed below.

(1) Few pH-responsive polymer nanomaterials are currently available for clinical use, owing to the enhanced permeability and retention effect, as well as other delivery difficulties (200–204). These polymer nanomaterials are delivered through five stages in tumor therapy: being injected intravenously into the bloodstream, accumulating specifically around the tumor tissue, entering into the solid tumor, cellular internalization, and "CAPIR", i.e., "circulation, accumulation, penetration, internalization, drug release." In the current research stage, it is impossible to consider these five stages, and it is still impossible to achieve the complete treatment of tumors (205–207). This must be the main focus of future research.

(2) Further research is needed to achieve the precise targeting of pH-responsive polymer nanomaterials, to realize an accurate combination of pH-response stimuli and other response stimuli, to optimize pH-responsive stimulation as a tumor therapy, as well as to realize the multifunctional platform function of pH-response stimulation for tumor treatment.

(3) There are some crucial issues associated with pH-responsive polymer nanomaterials, especially those containing synthetic drugs or their derivatives, including manufacturing technique problems, safe application problems, tumor treatment evaluation criteria accuracy problems, and institutional problems, which should be resolved as soon as possible to favor the successful clinical application of treatments after fundamental research is completed. More attention should be paid to establishing the entire standard treatment process, systematic evaluation, and long-term observation.

(4) Finally, the acute short-term toxicity and chronic long-term toxicity of pH-responsive polymer nanomaterials must be considered for the biological safety of clinical application in the future. These nanomaterials should be deeply studied to meet safety standards. At present, some suggested polymer nanomaterials are poisonous to the cells, causing side effects and other disease complications. For example, as mentioned earlier, the polymer nanomaterials containing hydrazone bonds may produce cationic polymer residues after hydrolysis *in vivo*, which are toxic to normal human tissues to some extent. Accordingly, new pH-responsive polymer nanomaterials, which are biodegradable and harmless to the body, should be developed to avoid such side effects. Sustainable materials, such as CO2 copolymers, should be further studied, with focus on ensuring that these materials undergo degradation through the Krebs cycle, metabolize into CO2 and water, and be excreted in a harmless manner *via* exhalation and through the action of kidneys.

In conclusion, pH-responsive polymer nanomaterials possess great potential for tumor therapy, and we believe that their beneficial effects will be recognized on a greater scale with the development of new technology and ongoing research.

AUTHOR CONTRIBUTIONS

FG contributed to the research retrieval and outline drafting. SC, XS and YT contributed to the research retrieval and drafting and critically revised the manuscript. SC critically revised the manuscript. Every author gave final approval and agreed to be accountable for all aspects of the work. All authors have read and agreed to the published version of the manuscript.

FUNDING

Financial support from the Projects directly under Jilin Provincial Department of Finance, China (JCSZ2019378-23), and the Scientific Research Project of Jilin Provincial Department of Education, China (JJKH20211215KJ)

ACKNOWLEDGMENTS

Authors are thankful to their respective departments/institutes/universities for providing space and other necessary facilities, which helped to draft this manuscript.

REFERENCES

1. Bray F, Ferlay J, Soerjomataram I, Siegel RL, Torre LA, Jemal A. Global Cancer Statistics 2018: GLOBOCAN Estimates of Incidence and Mortality Worldwide for 36 Cancers in 185 Countries. *CA Cancer J Clin* (2018) 68 (6):394–424. doi: 10.3322/caac.21492
2. Ryder-Burbidge C, Diaz RL, Barr RD, Gupta S, Nathan PC, McKillop SJ, et al. The Burden of Late Effects and Related Risk Factors in Adolescent and Young Adult Cancer Survivors: A Scoping Review. *Cancers (Basel)* (2021) 13 (19):4870. doi: 10.3390/cancers13194870
3. Seebacher NA, Stacy AE, Porter GM, Merlot AM. Clinical Development of Targeted and Immune Based Anti-Cancer Therapies. *J Exp Clin Cancer Res* (2019) 38(1):156. doi: 10.1186/s13046-019-1094-2
4. Sung H, Ferlay J, Siegel RL, Laversanne M, Soerjomataram I, Jemal A, et al. Global Cancer Statistics 2020: GLOBOCAN Estimates of Incidence and

Mortality Worldwide for 36 Cancers in 185 Countries. *CA Cancer J Clin* (2021) 71(3):209–49. doi: 10.3322/caac.21660
5. Naito Y, Aburatani H, Amano T, Baba E, Furukawa T, Hayashida T, et al. Clinical Practice Guidance for Next-Generation Sequencing in Cancer Diagnosis and Treatment (Edition 2.1). *Int J Clin Oncol* (2021) 26(2):233–83. doi: 10.1007/s10147-020-01831-6
6. Xiong H, Veedu RN, Diermeier SD. Recent Advances in Oligonucleotide Therapeutics in Oncology. *Int J Mol Sci* (2021) 22(7):3295. doi: 10.3390/ijms22073295
7. Atout S, Shurrab S, Loveridge C. Evaluation of the Suitability of RNAscope as a Technique to Measure Gene Expression in Clinical Diagnostics: A Systematic Review. *Mol Diagn Ther* (2021) 26:1–19. doi: 10.1007/s40291-021-00570-2
8. Jayabal P, Ma X, Shiio Y. EZH2 Suppresses Endogenous Retroviruses and an Interferon Response in Cancers. *Genes Cancer* (2021) 12:96–105. doi: 10.18632/genesandcancer.218
9. Bethge WA, Eyrich M, Mielke S, Meisel R, Niederwieser D, Schlegel PG, et al. Results of a Multicenter Phase I/II Trial of Tcrαβ and CD19-Depleted Haploidentical Hematopoietic Stem Cell Transplantation for Adult and Pediatric Patients. *Bone Marrow Transplant* (2021) 24:1–8. doi: 10.1038/s41409-021-01551-z
10. Bandini M, Ahmed M, Basile G, Watkin N, Master V, Zhu Y, et al. A Global Approach to Improving Penile Cancer Care. *Nat Rev Urol* (2021) 22:1–9. doi: 10.1038/s41585-021-00557-y
11. Wang CI, Chu PM, Chen YL, Lin YH, Chen CY. Chemotherapeutic Drug-Regulated Cytokines Might Influence Therapeutic Efficacy in HCC. *Int J Mo l Sci* (2021) 22(24):13627. doi: 10.3390/ijms222413627
12. Zhou H, Alhaskawi A, Sun Q, Dong Y, Kota VG, Hasan Abdulla MHA, et al. Desmoplastic Small Round Cell Tumor in a Pregnant Woman: A Case Report and Literature Review. *Yale J Biol Med* (2021) 94(4):613–22.
13. Volkov I, Radchenko G, Tchernykh A. Digital Twins, Internet of Things and Mobile Medicine: A Review of Current Platforms to Support Smart Healthcare. *Program Comput Soft* (2021) 47(8):578–90. doi: 10.1134/S0361768821080284
14. Abd-Alla HI, Souguir D, Radwan MO. Genus Sophora: A Comprehensive Review on Secondary Chemical Metabolites and Their Biological Aspects From Past Achievements to Future Perspectives. *Arch Pharm Res* (2021) 44 (11):903–86. doi: 10.1007/s12272-021-01354-2
15. Rodríguez M, Alonso-Alonso R, Tomás-Roca L, Rodríguez-Pinilla SM, Manso-Alonso R, Cereceda L, et al. Peripheral T-Cell Lymphoma: Molecular Profiling Recognizes Subclasses and Identifies Prognostic Markers. *Blood Adv* (2021) 5(24):5588–98. doi: 10.1182/bloodadvances.2021005171
16. Mohammed Saleh MF, Kotb A, Abdallah GEM, Muhsen IN, El Fakih R, Aljurf M. Recent Advances in Diagnosis and Therapy of Angioimmunoblastic T Cell Lymphoma. *Curr Oncol* (2021) 28(6):5480–98. doi: 10.3390/curroncol28060456
17. Gopal V, Dubashi B, Kayal S, Penumadu P, Rajaram M, Karunanithi G, et al. Challenges in the Management of Lung Cancer: Real-World Experience From a Tertiary Center in South India. *South Asian J Cancer* (2021) n10 (3):175–82. doi: 10.1055/s-0041-1733312
18. Ding Y, Lv B, Zheng J, Lu C, Liu J, Lei Y, et al. RBC-Hitchhiking Chitosan Nanoparticles Loading Methylprednisolone for Lung-Targeting Delivery. *J Control Release* (2021) 341:702–15. doi: 10.1016/j.jconrel.2021.12.018
19. Masini C, Gallegati D, Gentili N, Massa I, Ciucci R, Altini M. The Challenge of Sustainability of High-Cost Oncological Drugs: A Budgeting Model in an Italian Cancer Center. *Int J Environ Res Public Health* (2021) 18(24):13413. doi: 10.3390/ijerph182413413
20. Nkune NW, Abrahamse H. Nanoparticle-Based Drug Delivery Systems for Photodynamic Therapy of Metastatic Melanoma: A Review. *Int J Mol Sci* (2021) 22(22):12549. doi: 10.3390/ijms222212549
21. Ftouh M, Kalboussi N, Abid N, Sfar S, Mignet N, Bahloul B. Contribution of Nanotechnologies to Vaccine Development and Drug Delivery Against Respiratory Viruses. *PPAR Res* (2021) 2021:6741290. doi: 10.1155/2021/6741290
22. Brasseur K, Gévry N, Asselin E. Chemoresistance and Targeted Therapies in Ovarian and Endometrial Cancers. *Oncotarget* (2017) 8(3):4008–42. doi: 10.18632/oncotarget.14021
23. Patel A, Sant S. Hypoxic Tumor Microenvironment: Opportunities to Develop Targeted Therapies. *Biotechnol Adv* (2016) 34(5):803–12. doi: 10.1016/j.biotechadv.2016.04.005
24. Liu JJ, Chen Q, Feng L, Liu Z. Nanomedicine for Tumor Microenvironment Modulation and Cancer Treatment Enhancement. *Nano Today* (2018) 21:55–73. doi: 10.1016/j.nantod.2018.06.008
25. Estrella V, Chen T, Lloyd M, Wojtkowiak J, Cornnell HH, Ibrahim-Hashim A, et al. Acidity Generated by the Tumor Microenvironment Drives Local Invasion. *Cancer Res* (2013) 73(5):1524–35. doi: 10.1158/0008-5472.CAN-12-2796
26. Li X, Li H, Zhang ZY. Research Progress of Stimuli-Responsive Polymers in Tumor Immunotherapy. *Prog Pharm Sci* (2021) 45(5):325–36.
27. Manchun S, Dass CR, Sriamornsak P. Targeted Therapy for Cancer Using pH-Responsive Nanocarrier Systems. *Life Sci* (2012) 90(11-12):381–7. doi: 10.1016/j.lfs.2012.01.008
28. McMahon HT, Boucrot E. Molecular Mechanism and Physiological Functions of Clathrin-Mediated Endocytosis. *Nat Rev Mol Cell Biol* (2011) 12(8):517–33. doi: 10.1038/nrm3151
29. Qiu L, Qiao M, Chen Q, Tian C, Long M, Wang M, et al. Enhanced Effect of pH-Sensitive Mixed Copolymer Micelles for Overcoming Multidrug Resistance of Doxorubicin. *Biomaterials* (2014) 35(37):9877–87. doi: 10.1016/j.biomaterials.2014.08.008
30. Liu FH, Cong Y, Qi GB, Ji L, Qiao ZY, Wang H. Near-Infrared Laser-Driven *In Situ* Self-Assembly as a General Strategy for Deep Tumor Therapy. *Nano Lett* (2018) 18(10):6577–84. doi: 10.1021/acs.nanolett.8b03174
31. Alsehli M. Polymeric Nanocarriers as Stimuli-Responsive Systems for Targeted Tumor (Cancer) Therapy: Recent Advances in Drug Delivery. *Saudi Pharm J* (2020) 28(3):255–65. doi: 10.1016/j.jsps.2020.01.004
32. Ramírez-García PD, Retamal JS, Shenoy P, Imlach W, Sykes M, Truong N, et al. A pH-Responsive Nanoparticle Targets the Neurokinin 1 Receptor in Endosomes to Prevent Chronic Pain. *Nat Nanotechnol* (2019) 14(12):1150–9. doi: 10.1038/s41565-019-0568-x
33. Wang J, Byrne JD, Napier ME, DeSimone JM. More Effective Nanomedicines Through Particle Design. *Small* (2011) 7(14):1919–31. doi: 10.1002/smll.201100442
34. Asad MI, Khan D, Rehman AU, Elaissari A, Ahmed N. Development and *In Vitro*/*In Vivo* Evaluation of pH-Sensitive Polymeric Nanoparticles Loaded Hydrogel for the Management of Psoriasis. *Nanomater (Basel)* (2021) 11 (12):3433. doi: 10.3390/nano11123433
35. Real DA, Bolaños K, Priotti J, Yutronic N, Kogan MJ, Sierpe R, et al. Cyclodextrin-Modified Nanomaterials for Drug Delivery: Classification and Advances in Controlled Release and Bioavailability. *Pharmaceutics* (2021) 13 (12):2131. doi: 10.3390/pharmaceutics13122131
36. Kanamala M, Wilson WR, Yang M, Palmer BD, Wu Z. Mechanisms and Biomaterials in pH-Responsive Tumor-Targeted Drug Delivery: A Review. *Biomaterials* (2016) 85:152–67. doi: 10.1016/j.biomaterials.2016.01.061
37. Zhang W, Wang F, Wang Y, Wang J, Yu Y, Guo S, et al. pH and Near-Infrared Light Dual-Stimuli Responsive Drug Delivery Using DNA-Conjugated Gold Nanorods for Effective Treatment of Multidrug Resistant Cancer Cells. *J Control Release* (2016) 232:9–19. doi: 10.1016/j.jconrel.2016.04.001
38. Hong ST, Lin H, Wang CS, Chang CH, Lin AM, Yang JC, et al. Improving the Anticancer Effect of Afatinib and microRNA by Using Lipid Polymeric Nanoparticles Conjugated With Dual pH-Responsive and Targeting Peptides. *J Nanobiotech* (2019) 17(1):89. doi: 10.1186/s12951-019-0519-6
39. Ke W, Li J, Mohammed F, Wang Y, Tou K, Liu X, et al. Therapeutic Polymersome Nanoreactors With Tumor-Specific Activable Cascade Reactions for Cooperative Cancer Therapy. *ACS Nano* (2019) 13(2):2357–69. doi: 10.1021/acsnano.8b09082
40. Zhong Y, Huang S, Zheng C, Huang J, Li B, Han S, et al. A Light and Hypoxia-Activated Nanodrug for Cascade Photodynamic-Chemo Cancer Therapy. *Biomater Sci* (2021) 9(15):5218–26. doi: 10.1039/d1bm00660f
41. Xu C, Song R, Lu P, Chen J, Zhou Y, Shen G, et al. A pH-Responsive Charge-Reversal Drug Delivery System With Tumor-Specific Drug Release and ROS Generation for Cancer Therapy. *Int J Nanomed* (2020) 15:65–80. doi: 10.2147/IJN.S230237
42. Mendiratta S, Hussein M, Nasser HA, Ali AAA. Multidisciplinary Role of Mesoporous Silica Nanoparticles in Brain Regeneration and Cancers: From

Crossing the Blood–Brain Barrier to Treatment. *Part Part Syst Charact* (2019) 36:1900195. doi: 10.1002/ppsc.201900195
43. Yan T, He J, Liu R, Liu Z, Cheng J. Chitosan Capped pH-Responsive Hollow Mesoporous Silica Nanoparticles for Targeted Chemo-Photo Combination Therapy. *Carbohydr Polym* (2020) 231:115706. doi: 10.1016/j.carbpol.2019.115706
44. He C, Lu K, Liu D, Lin W. Nanoscale Metal-Organic Frameworks for the Co-Delivery of Cisplatin and Pooled siRNAs to Enhance Therapeutic Efficacy in Drug-Resistant Ovarian Cancer Cells. *J Am Chem Soc* (2014) 136(14):5181–4. doi: 10.1021/ja4098862
45. Hu CM, Zhang L. Nanoparticle-Based Combination Therapy Toward Overcoming Drug Resistance in Cancer. *Biochem Pharmacol* (2012) 83 (8):1104–11. doi: 10.1016/j.bcp.2012.01.008
46. Mattheolabakis G, Rigas B, Constantinides PP. Nanodelivery Strategies in Cancer Chemotherapy: Biological Rationale and Pharmaceutical Perspectives. *Nanomedicine (Lond)* (2012) 7(10):1577–90. doi: 10.2217/nnm.12.128
47. Cho K, Wang X, Nie S, Chen ZG, Shin DM. Therapeutic Nanoparticles for Drug Delivery in Cancer. *Clin Cancer Res* (2008) 14(5):1310–6. doi: 10.1158/1078-0432
48. Minko T. Soluble Polymer Conjugates for Drug Delivery. *Drug Discov Today Technol* (2005) 2(1):15–20. doi: 10.1016/j.ddtec.2005.05.005
49. Wu Z, Ma X, Ma Y, Yang Z, Yuan Y, Liu C. Core/Shell PEGS/HA Hybrid Nanoparticle *Via* Micelle-Coordinated Mineralization for Tumor-Specific Therapy. *ACS Appl Mater Interf* (2020) 12(10):12109–19. doi: 10.1021/acsami.0c00068
50. Zhao M, Wan S, Peng X, Zhang B, Pan Q, Li S, et al. Leveraging a Polycationic Polymer to Direct Tunable Loading of an Anticancer Agent and Photosensitizer With Opposite Charges for Chemo-Photodynamic Therapy. *J Mater Chem B* (2020) 8(6):1235–44. doi: 10.1039/c9tb02400j
51. Howaili F, Özliseli E, Küçüktürkmen B, Razavi SM, Sadeghizadeh M, Rosenholm JM. Stimuli-Responsive, Plasmonic Nanogel for Dual Delivery of Curcumin and Photothermal Therapy for Cancer Treatment. *Front Chem* (2021) 8:602941:602941. doi: 10.3389/fchem.2020.602941
52. Shi M, Zhang J, Huang Z, Chen Y, Pan S, Hu H, et al. Stimuli-Responsive Release and Efficient siRNA Delivery in Non-Small Cell Lung Cancer by a Poly(L-Histidine)-Based Multifunctional Nanoplatform. *J Mater Chem B* (2020) 8(8):1616–28. doi: 10.1039/c9tb02764e
53. Batten SR, Champness NR, Chen XM, Garcia-Martinez J, Kitagawa S, Ohrstrom L, et al. Terminology of Metal-Organic Frameworks and Coordination Polymers (IUPAC Recommendations 2013). *Pure Appl Chermistry* (2013) 85(8):1715–24. doi: 10.1351/PAC-REC-12-11-20
54. Shen J, Ma M, Zhang H, Yu H, Xue F, Hao N, et al. Microfluidics-Assisted Surface Trifunctionalization of a Zeolitic Imidazolate Framework Nanocarrier for Targeted and Controllable Multitherapies of Tumors. *ACS. Appl Mater Interfaces* (2020) 12(41):45838–49. doi: 10.1021/acsami.0c14021
55. Duan F, Feng X, Yang X, Sun W, Jin Y, Liu H, et al. A Simple and Powerful Co-Delivery System Based on pH-Responsive Metal-Organic Frameworks for Enhanced Cancer Immunotherapy. *Biomaterials* (2017) 122:23–33. doi: 10.1016/j.biomaterials.2017.01.017
56. Xia C, Yin S, Xu S, Ran G, Deng M, Mei L, et al. Low Molecular Weight Heparin-Coated and Dendrimer-Based Core-Shell Nanoplatform With Enhanced Immune Activation and Multiple Anti-Metastatic Effects for Melanoma Treatment. *Theranostics* (2019) 9(2):337–54. doi: 10.7150/thno.29026
57. Cai X, Luo Y, Zhang W, Du D, Lin Y. pH-Sensitive ZnO Quantum Dots-Doxorubicin Nanoparticles for Lung Cancer Targeted Drug Delivery. *ACS. Appl Mater Interfaces* (2016) 8(34):22442–50. doi: 10.1021/acsami.6b04933
58. Su Z, Liang Y, Yao Y, Wang T, Zhang N. Polymeric Complex Micelles Based on the Double-Hydrazone Linkage and Dual Drug-Loading Strategy for pH-Sensitive Docetaxel Delivery. *J Mater Chem B* (2016) 4(6):1122–33. doi: 10.1039/c5tb02188j
59. Liu J, Huang Y, Kumar A, Tan A, Jin S, Mozhi A, et al. PH-Sensitive Nano-Systems for Drug Delivery in Cancer Therapy. *Biotechnol Adv* (2014) 32 (4):693–710. doi: 10.1016/j.biotechadv.2013.11.009
60. Deirram N, Zhang C, Kermaniyan SS, Johnston APR, Such GK. PH-Responsive Polymer Nanoparticles for Drug Delivery. *Macromol Rapid Commun* (2019) 40(10):e1800917. doi: 10.1002/marc.201800917
61. Koren E, Apte A, Jani A, Torchilin VP. Multifunctional PEGylated 2C5-Immunoliposomes Containing pH-Sensitive Bonds and TAT Peptide for Enhanced Tumor Cell Internalization and Cytotoxicity. *J Control Release* (2012) 160(2):264–73. doi: 10.1016/j.jconrel.2011.12.002
62. Yu Y, Zhang X, Qiu. The Anti-Tumor Efficacy of Curcumin When Delivered by Size/Charge-Changing Multistage Polymeric Micelles Based on Amphiphilic Poly (β-Amino Ester) Derivates. *Biomaterials* (2014) 35 (10):3467–79. doi: 10.1016/j.biomaterials.2013.12.096
63. Yhaya F, Binauld S, Kim Y, Stenzel MH. Shell Cross-Linking of Cyclodextrin-Based Micelles *via* Supramolecular Chemistry for the Delivery of Drugs. *Macromol Rapid Commun* (2012) 33(21):1868–74. doi: 10.1002/marc.201200473
64. Pang X, Jiang Y, Xiao Q, Leung AW, Hua H, Xu C. PH-Responsive Polymer-Drug Conjugates: Design and Progress. *J Control Release* (2016) 28 (222):116–29. doi: 10.1016/j.jconrel.2015.12.024
65. Kakizawa Y, Kataoka K. Block Copolymer Micelles for Delivery of Gene and Related Compounds. *Adv Drug Deliv Rev* (2002) 54(2):203–22. doi: 10.1016/s0169-409x(02)00017-0
66. Wu D, Pusuluri A, Vogus D, Krishnan V, Shields CW, Kim J, et al. Design Principles of Drug Combinations for Chemotherapy. *J Control Release* (2020) 10(323):36–46. doi: 10.1016/j.jconrel.2020.04.018
67. Zheng T, Wang W, Wu F, Zhang M, Shen J, Sun Y. Zwitterionic Polymer-Gated Au@TiO2 Core-Shell Nanoparticles for Imaging-Guided Combined Cancer Therapy. *Theranostics* (2019) 9(17):5035–48. doi: 10.7150/thno.35418
68. Wu WX, Wang N, Liu BY, Deng QF, Yu XQ. Lipase-Catalyzed Synthesis of Azido-Functionalized Aliphatic Polyesters Towards Acid-Degradable Amphiphilic Graft Copolymers. *Soft Matter* (2014) 10(8):1199–213. doi: 10.1039/c3sm52496e
69. Samanta P, Kapat K, Maiti S, Biswas G, Dhara S, Dhara D. pH-Labile and Photochemically Cross-Linkable Polymer Vesicles From Coumarin Based Random Copolymer for Cancer Therapy. *J Colloid Interface Sci* (2019) 555:132–44. doi: 10.1016/j.jcis.2019.07.069
70. Algar WR, Prasuhn DE, Stewart MH, Jennings TL, Blanco-Canosa JB, Dawson PE, et al. The Controlled Display of Biomolecules on Nanoparticles: A Challenge Suited to Bioorthogonal Chemistry. *Bioconjug Chem* (2011) 22(5):825–58. doi: 10.1021/bc200065z
71. Yoshida T, Lai TC, Kwon GS, Sako K. pH- and Ion-Sensitive Polymers for Drug Delivery. *Expert Opin Drug Deliv* (2013) 10(11):1497–513. doi: 10.1517/17425247.2013.821978
72. Greenfield RS, Kaneko T, Daues A, Edson MA, Fitzgerald KA, Olech LJ, et al. Evaluation *In Vitro* of Adriamycin Immunoconjugates Synthesized Using an Acid-Sensitive Hydrazone Linker. *Cancer Res* (1990) 50(20):6600–7.
73. Kaneko T, Willner D, Monkovíc I, Knipe JO, Braslawsky GR, Greenfield RS, et al. New Hydrazone Derivatives of Adriamycin and Their Immunoconjugates-a Correlation Between Acid Stability and Cytotoxicity. *Bioconjug Chem* (1991) 2(3):133–41. doi: 10.1021/bc00009a001
74. Etrych T, Kovář L, Strohalm J, Chytil P, Říhová B, Ulbrich K. Biodegradable Star HPMA Polymer-Drug Conjugates: Biodegradability, Distribution and Anti-Tumor Efficacy. *J Control Release* (2011) 154(3):241–8. doi: 10.1016/j.jconrel.2011.06.015
75. Říhová B, Etrych T, Sírová M, Kovár L, Hovorka O, Kovár M, et al. Synergistic Action of Doxorubicin Bound to the Polymeric Carrier Based on N-(2-Hydroxypropyl) Methacrylamide Copolymers Through an Amide or Hydrazone Bond. *Mol Pharm* (2010) 7(4):1027–40. doi: 10.1021/mp100121g
76. Long W, Ouyang H, Zhou C, Wan W, Yu S, Qian K, et al. Simultaneous Surface Functionalization and Drug Loading: A Novel Method for Fabrication of Cellulose Nanocrystals-Based pH-Responsive Drug Delivery System. *Int J Biol Macromol* (2021) 1(182):2066–75. doi: 10.1016/j.ijbiomac.2021.05.193
77. Sonawane SJ, Kalhapure RS, Govender T. Hydrazone Linkages in pH-Responsive Drug Delivery Systems. *Eur J Pharm Sci* (2017) 1(99):45–65. doi: 10.1016/j.ejps.2016.12.011

78. Alani AW, Bae Y, Rao DA, Kwon GS. Polymeric Micelles for the pH-Dependent Controlled, Continuous Low Dose Release of Paclitaxel. *Biomaterials* (2010) 31(7):1765–72. doi: 10.1016/j.biomaterials.2009.11.038
79. Aryal S, Hu CM, Zhang L. Polymer-Cisplatin Conjugate Nanoparticles for Acid-Responsive Drug Delivery. *ACS Nano* (2010) 4(1):251–8. doi: 10.1021/nn9014032
80. Li H, Li M, Chen C, Fan A, Kong D, Wang Z, et al. On-Demand Combinational Delivery of Curcumin and Doxorubicin *via* a pH-Labile Micellar Nanocarrier. *Int J Pharm* (2015) 495(1):572–8. doi: 10.1016/j.ijpharm.2015.09.022
81. Wang Z, Chen C, Zhang Q, Gao M, Zhang J, Kong D, et al. Tuning the Architecture of Polymeric Conjugate to Mediate Intracellular Delivery of Pleiotropic Curcumin. *Eur J Pharm Biopharm* (2015) 90:53–62. doi: 10.1016/j.ejpb.2014.11.002
82. Zhang P, Kong J. Doxorubicin-Tethered Fluorescent Silica Nanoparticles for pH-Responsive Anticancer Drug Delivery. *Talanta* (2015) 134:501–7. doi: 10.1016/j.talanta.2014.09.041
83. Tauk L, Schröder AP, Decher G, Giuseppone N. Hierarchical Functional Gradients of pH-Responsive Self-Assembled Monolayers Using Dynamic Covalent Chemistry on Surfaces. *Nat Chem* (2009) 1(8):649–56. doi: 10.1038/nchem.400
84. Rowan SJ, Cantrill SJ, Cousins GR, Sanders JK, Stoddart JF. Dynamic Covalent Chemistry. *Angew Chem Int Ed Engl* (2002) 41(6):898–952. doi: 10.1002/1521-3773(20020315)41:6<898::aid-anie898>3.0.co;2-e
85. Kurita K. Controlled Functionalization of the Polysaccharide Chitin. *Prog In Polymer Sci* (2001) 26(9):1921–71. doi: 10.1016/S0079-6700(01)00007-7
86. Masson C, Garinot M, Mignet N, Wetzer B, Mailhe P, Scherman D, et al. pH-Sensitive PEG Lipids Containing Orthoester Linkers: New Potential Tools for Nonviral Gene Delivery. *J Control Release* (2004) 99(3):423–34. doi: 10.1016/j.jconrel.2004.07.016
87. Engel AK, Yoden T, Sanui K, Ogata N. Synthesis of Aromatic Schiff Base Oligomers at the Air/Water Interface. *J Am Chem Society* (1985) 107 (26):8308–10. doi: 10.1021/ja00312a108
88. Liao SC, Ting CW, Chiang WH. Functionalized Polymeric Nanogels With pH-Sensitive Benzoic-Imine Cross-Linkages Designed as Vehicles for Indocyanine Green Delivery. *J Colloid Interface Sci* (2020) 561:11–22. doi: 10.1016/j.jcis.2019.11.109
89. Binauld S, Stenzel MH. Acid-Degradable Polymers for Drug Delivery: A Decade of Innovation. *Chem Commun (Camb)* (2013) 49(21):2082–102. doi: 10.1039/c2cc36589h
90. Nuhn L, Van Herck S, Best A, Deswarte K, Kokkinopoulou M, Lieberwirth I, et al. FRET Monitoring of Intracellular Ketal Hydrolysis in Synthetic Nanoparticles. *Angew Chem Int Ed Engl* (2018) 57(33):10760–4. doi: 10.1002/anie.201803847
91. Zhao C, Cao W, Zheng H, Xiao Z, Hu J, Yang L, et al. Acid-Responsive Nanoparticles as a Novel Oxidative Stress-Inducing Anticancer Therapeutic Agent for Colon Cancer. *Int J Nanomed* (2019) 14:1597–618. doi: 10.2147/IJN.S189923
92. Szabó I, Manea M, Orbán E, Csámpai A, Bosze S, Szabó R, et al. Development of an Oxime Bond Containing Daunorubicin-Gonadotropin-Releasing Hormone-III Conjugate as a Potential Anticancer Drug. *Bioconjug Chem* (2009) 20(4):656–65. doi: 10.1021/bc800542u
93. Kölmel DK, Kool ET. Oximes and Hydrazones in Bioconjugation: Mechanism and Catalysis. *Chem Rev* (2017) 117(15):10358–76. doi: 10.1021/acs.chemrev.7b00090
94. Jin Y, Song L, Su Y, Zhu L, Pang Y, Qiu F, et al. Oxime Linkage: A Robust Tool for the Design of pH-Sensitive Polymeric Drug Carriers. *Biomacromolecules* (2011) 12(10):3460–8. doi: 10.1021/bm200956u
95. Singh GS. Recent Progress in the Synthesis and Chemistry of Azetidinones. *Tetrahedron* (2003) 59(39):7631–49. doi: 10.1016/S0040-4020(03)01099-8
96. Curtius TH. Synthetische Versuche Mit Hippurazid. *Berichte der deutschen chemischen Gesellschaft* (1902) 35(3):3226–8. doi: 10.1002/cber.190203503125
97. Chan WK, Ho CM, Wong MK, Che CM. Oxidative Amide Synthesis and N-Terminal Alpha-Amino Group Ligation of Peptides in Aqueous Medium. *J Am Chem Soc* (2006) 128(46):14796–7. doi: 10.1021/ja064479s
98. Shao WY, Liu CR, Ma HJ, Hong Z, Xie QL, Lu YH. Fabrication of pH-Sensitive Thin-Film Nanocomposite Nanofiltration Membranes With Enhanced Performance by Incorporating Amine-Functionalized Graphene Oxide. *Appl Surface Sci* (2019) 487:1209–21. doi: 10.1016/j.apsusc.2019.05.157
99. Cai S, Thati S, Bagby TR, Diab HM, Davies NM, Cohen MS, et al. Localized Doxorubicin Chemotherapy With a Biopolymeric Nanocarrier Improves Survival and Reduces Toxicity in Xenografts of Human Breast Cancer. *J Control Release* (2010) 146(2):212–8. doi: 10.1016/j.jconrel.2010.04.006
100. Ofridam F, Tarhini M, Lebaz N, Gagniere E, Mangin D, Elaissari A. pH-Sensitive Polymers: Classification and Some Fine Potential Applications. *Polymers Advanced Technologies* (2021) 32(4):1455–84. doi: 10.1002/pat.5230
101. Huang X, Cao J, Zhang Y, Liu T, Yan H. Polyethylenimine Modified With 2,3-Dimethylmaleic Anhydride Potentiates the Antitumor Efficacy of Conventional Chemotherapy. *Mater Sci Eng C Mater Biol Appl* (2019) 102:558–68. doi: 10.1016/j.msec.2019.04.081
102. Luo F, Fan Z, Yin W, Yang L, Li T, Zhong L, et al. pH-Responsive Stearic Acid-O-Carboxymethyl Chitosan Assemblies as Carriers Delivering Small Molecular Drug for Chemotherapy. *Mater Sci Eng C Mater Biol Appl* (2019) 105:110107. doi: 10.1016/j.msec.2019.110107
103. Heller J, Barr J, Ng SY, Abdellauoi KS, Gurny R. Poly (Orthoesters), Synthesis, Characterization, Properties, and Uses. *Adv Drug Deliv Rev* (2002) 54(7):1015–39. doi: 10.1016/s0169-409x(02)00055-8
104. Tang R, Ji W, Wang C. Amphiphilic Block Copolymers Bearing Ortho Ester Side-Chains: pH-Dependent Hydrolysis and Self-Assembly in Water. *Macromol Biosci* (2010) 10(2):192–201. doi: 10.1002/mabi.200900229
105. Thambi T, Deepagan VG, Yoo CK, Park JH. Synthesis and Physicochemical Characterization of Amphiphilic Block Copolymers Bearing Acid-Sensitive Orthoester Linkage as the Drug Carrier. *POLYMER* (2011) 52(21):4753–9. doi: 10.1016/j.polymer.2011.08.024
106. Dan K, Pan R, Ghosh S. Aggregation and pH-Responsive Disassembly of a New Acid-Labile Surfactant Synthesized by Thiol-Acrylate Michael Addition Reaction. *Langmuir* (2011) 27(2):612–7. doi: 10.1021/la104445h
107. Dan K, Ghosh S. One-Pot Synthesis of an Acid-Labile Amphiphilic Triblock Copolymer and its pH-Responsive Vesicular Assembly. *Angew Chem Int Ed Engl* (2013) 52(28):7300–5. doi: 10.1002/anie.201302722
108. Molla MR, Marcinko T, Prasad P, Deming D, Garman SC, Thayumanavan S. Unlocking a Caged Lysosomal Protein From a Polymeric Nanogel With a pH Trigger. *Biomacromolecules* (2014) 15(11):4046–53. doi: 10.1021/bm501091p
109. Nishiyabu R, Kubo Y, James TD, Fossey JS. Boronic Acid Building Blocks: Tools for Self-Assembly. *Chem Commun (Camb)* (2011) 47(4):1124–50. doi: 10.1039/c0cc02921a
110. He L, Fullenkamp DE, Rivera JG, Messersmith PB. pH-Responsive Self-Healing Hydrogels Formed by Boronate-Catechol Complexation. *Chem Commun (Camb)* (2011) 47(26):7497–9. doi: 10.1039/c1cc11928a
111. Liang E, Zhou H, Ding X, Zheng Z, Peng Y. Fabrication of a Rhythmic Assembly System Based on Reversible Formation of Dynamic Covalent Bonds in a Chemical Oscillator. *Chem Commun (Camb)* (2013) 49 (47):5384–6. doi: 10.1039/c3cc42533a
112. Fang L, Zhang W, Wang Z, Fan X, Cheng Z, Hou X, et al. Novel Mitochondrial Targeting Charge-Reversal Polysaccharide Hybrid Shell/Core Nanoparticles for Prolonged Systemic Circulation and Antitumor Drug Delivery. *Drug Deliv* (2019) 26(1):1125–39. doi: 10.1080/10717544.2019.1687614
113. Page DB, Postow MA, Callahan MK, Allison JP, Wolchok JD. Immune Modulation in Cancer With Antibodies. *Annu Rev Med* (2013) 2014 (65):185–202. doi: 10.1146/annurev-med-092012-112807
114. Oupicky D, Ogris M, Howard KA, Dash PR, Ulbrich K, Seymour LW. Importance of Lateral and Steric Stabilization of Polyelectrolyte Gene Delivery Vectors for Extended Systemic Circulation. *Mol Ther* (2002) 5 (4):463–72. doi: 10.1006/mthe.2002.0568
115. He C, Hu Y, Yin L, Tang C, Yin C. Effects of Particle Size and Surface Charge on Cellular Uptake and Biodistribution of Polymeric Nanoparticles. *Biomaterials* (2010) 31(13):3657–66. doi: 10.1016/j.biomaterials.2010.01.065
116. Shen Y, Zhou Z, Sui M, Tang J, Xu P, Van Kirk EA, et al. Charge-Reversal Polyamidoamine Dendrimer for Cascade Nuclear Drug Delivery. *Nanomedicine (Lond)* (2010) 5(8):1205–17. doi: 10.2217/nnm.10.86

117. Ji T, Zhao Y, Ding Y, Nie G. Using Functional Nanomaterials to Target and Regulate the Tumor Microenvironment: Diagnostic and Therapeutic Applications. *Adv Mater* (2013) 25(26):3508–25. doi: 10.1002/adma.201300299
118. Zarrin A, Foroozesh M, Hamidi M. Carrier Erythrocytes: Recent Advances, Present Status, Current Trends, and Future Horizons. *Expert Opin Drug Deliv* (2014) 11(3):433–47. doi: 10.1517/17425247.2014.880422
119. Arvizo RR, Miranda OR, Thompson MA, Pabelick CM, Bhattacharya R, Robertson JD, et al. Effect of Nanoparticle Surface Charge at the Plasma Membrane and Beyond. *Nano Lett* (2010) 10(7):2543–8. doi: 10.1021/nl101140t
120. Cho EC, Xie J, Wurm PA, Xia Y. Understanding the Role of Surface Charges in Cellular Adsorption Versus Internalization by Selectively Removing Gold Nanoparticles on the Cell Surface With a I2/KI Etchant. *Nano Lett* (2009) 9 (3):1080–4. doi: 10.1021/nl803487r
121. Guo S, Lin CM, Xu Z, Miao L, Wang Y, Huang L. Co-Delivery of Cisplatin and Rapamycin for Enhanced Anticancer Therapy Through Synergistic Effects and Microenvironment Modulation. *ACS. Nano* (2014) 8(5):4996–5009. doi: 10.1021/nn5010815
122. Wong AS, Mann SK, Czuba E, Sahut A, Liu H, Suekama TC, et al. Self-Assembling Dual Component Nanoparticles With Endosomal Escape Capability. *Soft Matter* (2015) 11(15):2993–3002. doi: 10.1039/c5sm00082c
123. Huang Y, Tang Z, Zhang X, Yu H, Sun H, Pang X, et al. pH-Triggered Charge-Reversal Polypeptide Nanoparticles for Cisplatin Delivery: Preparation and *In Vitro* Evaluation. *Biomacromolecules* (2013) 14 (6):2023–32. doi: 10.1021/bm400358z
124. Fang L, Fan H, Guo C, Cui L, Zhang P, Mu H, et al. Novel Mitochondrial Targeting Multifunctional Surface Charge-Reversal Polymeric Nanoparticles for Cancer Treatment. *J BioMed Nanotechnol* (2019) 15(11):2151–63. doi: 10.1166/jbn.2019.2854
125. Chen DQ, Song XY, Wang KL, Guo CJ, Yu YM, Fan HY, et al. Design and Evaluation of Dual CD44 Receptor and Folate Receptor-Targeting Double-Smart pH-Response Multifunctional Nanocarrier. *J Nanoparticle Res* (2017) 19(12):400. doi: 10.1007/s11051-017-4076-3
126. Liang G, Zhu Y, Jing A, Wang J, Hu F, Feng W, et al. Cationic microRNA-Delivering Nanocarriers for Efficient Treatment of Colon Carcinoma in Xenograft Model. *Gene Ther* (2016) 23(12):829–38. doi: 10.1038/gt.2016.60
127. Han K, Zhang J, Zhang W, Wang S, Xu L, Zhang C, et al. Tumor-Triggered Geometrical Shape Switch of Chimeric Peptide for Enhanced *In Vivo* Tumor Internalization and Photodynamic Therapy. *ACS. Nano* (2017) 11(3):3178–88. doi: 10.1021/acsnano.7b00216
128. Luo YL, Yu W, Xu F. pH-Responsive PMAA-B-PEG-B-PMAA Triblock Copolymer Micelles for Prednisone Drug Release and Release Kinetics. *Polymer Bulletin* (2012) 69(5):597–620. doi: 10.1007/s00289-012-0774-2
129. Abbasian M, Roudi MM, Mahmoodzadeh F, Eskandani M, Jaymand M. Chitosan-Grafted-Poly (Methacrylic Acid)/Graphene Oxide Nanocomposite as a pH-Responsive *De Novo* Cancer Chemotherapy Nanosystem. *Int J Biol Macromol* (2018) 118:1871–9. doi: 10.1016/j.ijbiomac.2018.07.036
130. Zhao Y, Su HJ, Fang L, Tan TW. Superabsorbent Hydrogels From Poly (Aspartic Acid) With Salt-, Temperature- and pH-Responsiveness Properties. *Polymer* (2005) 46(14):5368–76. doi: 10.1016/j.polymer.2005.04.015
131. Abel BA, Sims MB, McCormick CL. Tunable pH- and CO2-Responsive Sulfonamide-Containing Polymers by RAFT Polymerization. *Macromolecules* (2015) 48(16):5487–95. doi: 10.1021/acs.macromol.5b01453
132. Kang HC, Bae YH. pH-Tunable Endosomolytic Oligomers for Enhanced Nucleic Acid Delivery. *Advanced Funct Materials* (2007) 17(8):1263–72. doi: 10.1002/adfm.200601188
133. Fu X, Hosta-Rigau L, Chandrawati R, Cui JW. Multi-Stimuli-Responsive Polymer Particles, Films, and Hydrogels for Drug Delivery. *Chem* (2018) 4 (9):2084–107. doi: 10.1016/j.chempr.2018.07.00
134. Cao ZQ, Wang GJ. Multi-Stimuli-Responsive Polymer Materials: Particles, Films, and Bulk Gels. *Chem Rec* (2016) 16(3):1398–435. doi: 10.1002/tcr.201500281
135. Cheng R, Meng FH, Deng C, Zhong ZY. Bioresponsive Polymeric Nanotherapeutics for Targeted Cancer Chemotherapy. *Nano Today* (2015) 10(5):656–70. doi: 10.1016/j.nantod.2015.09.005
136. Gribble FM, Loussouarn G, Tucker SJ, Zhao C, Nichols CG, Ashcroft FM. A Novel Method for Measurement of Submembrane ATP Concentration. *J Biol Chem* (2000) 275(39):30046–9. doi: 10.1074/jbc.M001010200
137. Gorman MW, Feigl EO, Buffington CW. Human Plasma ATP Concentration. *Clin Chem* (2007) 53(2):318–25. doi: 10.1373/clinchem.2006.076364
138. Deng B, Ma P, Xie Y. Reduction-Sensitive Polymeric Nanocarriers in Cancer Therapy: A Comprehensive Review. *Nanoscale* (2015) 7(30):12773–95. doi: 10.1039/c5nr02878g
139. Ganta S, Devalapally H, Shahiwala A, Amiji MA. Review of Stimuli-Responsive Nanocarriers for Drug and Gene Delivery. *J Control Release* (2008) 126(3):187–204. doi: 10.1016/j.jconrel.2007.12.017
140. Song Q, Jia J, Niu X, Zheng C, Zhao H, Sun L, et al. An Oral Drug Delivery System With Programmed Drug Release and Imaging Properties for Orthotopic Colon Cancer Therapy. *Nanoscale* (2019) 11(34):15958–70. doi: 10.1039/c9nr03802g
141. Kim SG, Ryplida B, Phuong PTM, Won HJ, Lee G, Bhang SH, et al. Reduction-Triggered Paclitaxel Release Nano-Hybrid System Based on Core-Crosslinked Polymer Dots With a pH-Responsive Shell-Cleavable Colorimetric Biosensor. *Int J Mol Sci* (2019) 20(21):5368. doi: 10.3390/ijms20215368
142. Jäger E, Humajová J, Dölen Y, Kučka J, Jäger A, Konefał R, et al. Enhanced Antitumor Efficacy Through an "AND Gate" Reactive Oxygen-Species-Dependent pH-Responsive Nanomedicine Approach. *Adv Healthc Mater* (2021) 10(13):e2100304. doi: 10.1002/adhm.202100304
143. Wang T, Wang F, Sun M, Tian M, Mu Y, Chen X, et al. Gastric Environment-Stable Oral Nanocarriers for *In Situ* Colorectal Cancer Therapy. *Int J Biol Macromol* (2019) 139:1035–45. doi: 10.1016/j.ijbiomac.2019.08.088
144. Chen L, Qian M, Jiang H, Zhou Y, Du Y, Yang Y, et al. Multifunctional Mesoporous Black Phosphorus-Based Nanosheet for Enhanced Tumor-Targeted Combined Therapy With Biodegradation-Mediated Metastasis Inhibition. *Biomaterials* (2020) 236:119770. doi: 10.1016/j.biomaterials.2020.119770
145. Feng Y, Cheng Y, Chang Y, Jian H, Zheng R, Wu X, et al. Time-Staggered Delivery of Erlotinib and Doxorubicin by Gold Nanocages With Two Smart Polymers for Reprogrammable Release and Synergistic With Photothermal Therapy. *Biomaterials* (2019) 217:119327. doi: 10.1016/j.biomaterials.2019.119327
146. Lin W, Zhang W, Liu S, Li Z, Hu X, Xie Z, et al. Engineering pH-Responsive BODIPY Nanoparticles for Tumor Selective Multimodal Imaging and Phototherapy. *ACS. Appl Mater Interfaces* (2019) 11(47):43928–35. doi: 10.1021/acsami.9b16403
147. Don TM, Lu KY, Lin LJ, Hsu CH, Wu JY, Mi FL. Temperature/pH/Enzyme Triple-Responsive Cationic Protein/PAA-B-PNIPAAm Nanogels for Controlled Anticancer Drug and Photosensitizer Delivery Against Multidrug Resistant Breast Cancer Cells. *Mol Pharm* (2017) 14(12):4648–60. doi: 10.1021/acs.molpharmaceut.7b00737
148. Kim H, Sehgal D, Kucaba TA, Ferguson DM, Griffith TS, Panyam J. Acidic pH-Responsive Polymer Nanoparticles as a TLR7/8 Agonist Delivery Platform for Cancer Immunotherapy. *Nanoscale* (2018) 10(44):20851–62. doi: 10.1039/c8nr07201a
149. Sun Q, Ma X, Zhang B, Zhou Z, Jin E, Shen Y, et al. Fabrication of Dendrimer-Releasing Lipidic Nanoassembly for Cancer Drug Delivery. *Biomater Sci* (2016) 4(6):958–69. doi: 10.1039/c6bm00189k
150. Langer R, Folkman J. Polymers for the Sustained Release of Proteins and Other Macromolecules. *Nature* (1976) 263(5580):797–800. doi: 10.1038/263797a0
151. Fischel-Ghodsian F, Brown L, Mathiowitz E, Brandenburg D, Langer R. Enzymatically Controlled Drug Delivery. *Proc Natl Acad Sci USA* (1988) 85 (7):2403–6. doi: 10.1073/pnas.85.7.2403
152. Mo R, Gu Z. Tumor Microenvironment and Intracellular Signal-Activated Nanomaterials for Anticancer Drug Delivery. *Materials Today* (2016) 19 (5):274–83. doi: 10.1016/j.mattod.2015.11.025
153. Traitel T, Goldbart R, Kost J. Smart Polymers for Responsive Drug-Delivery Systems. *J Biomater Sci Polym Ed* (2008) 19(6):755–67. doi: 10.1163/156856208784522065
154. Li Z, Yin Q, Chen B, Wang Z, Yan Y, Qi T, et al. Ultra-pH-Sensitive Indocyanine Green-Conjugated Nanoprobes for Fluorescence Imaging-

Guided Photothermal Cancer Therapy. *Nanomedicine* (2019) 17:287–96. doi: 10.1016/j.nano.2019.02.001
155. Li S, Saw PE, Lin C, Nie Y, Tao W, Farokhzad OC, et al. Redox-Responsive Polyprodrug Nanoparticles for Targeted siRNA Delivery and Synergistic Liver Cancer Therapy. *Biomaterials* (2020) 234:119760. doi: 10.1016/j.biomaterials.2020.119760
156. Camacho KM, Kumar S, Menegatti S, Vogus DR, Anselmo AC, Mitragotri S. Synergistic Antitumor Activity of Camptothecin-Doxorubicin Combinations and Their Conjugates With Hyaluronic Acid. *J Control Release* (2015) 210:198–207. doi: 10.1016/j.jconrel.2015.04.031
157. Wang N, Liu C, Yao W, Zhou H, Yu S, Chen H, et al. A Traceable, GSH/pH Dual-Responsive Nanoparticles With Spatiotemporally Controlled Multiple Drugs Release Ability to Enhance Antitumor Efficacy. *Colloids Surf. B Biointerfaces* (2021) 205:111866. doi: 10.1016/j.colsurfb.2021.111866
158. Saucier-Sawyer JK, Seo YE, Gaudin A, Quijano E, Song E, Sawyer AJ, et al. Distribution of Polymer Nanoparticles by Convection-Enhanced Delivery to Brain Tumors. *J Control Release* (2016) 232:103–12. doi: 10.1016/j.jconrel.2016.04.006
159. Shirvalilou S, Khoei S, Khoee S, Mahdavi SR, Raoufi NJ, Motevalian M, et al. Enhancement Radiation-Induced Apoptosis in C6 Glioma Tumor-Bearing Rats *via* pH-Responsive Magnetic Graphene Oxide Nanocarrier. *J Photochem Photobiol B* (2020) 205:111827. doi: 10.1016/j.jphotobiol.2020.111827
160. Song W, Musetti SN, Huang L. Nanomaterials for Cancer Immunotherapy. *Biomaterials* (2017) 148:16–30. doi: 10.1016/j.biomaterials.2017.09.017
161. Liang R, Xie J, Li J, Wang K, Liu L, Gao Y, et al. Liposomes-Coated Gold Nanocages With Antigens and Adjuvants Targeted Delivery to Dendritic Cells for Enhancing Antitumor Immune Response. *Biomaterials* (2017) 149:41–50. doi: 10.1016/j.biomaterials.2017.09.029
162. Liu XY, Wang XY, Li RY, Jia SC, Sun P, Zhao M, et al. Recent Progress in the Understanding of Complement Activation and Its Role in Tumor Growth and Anti-Tumor Therapy. *BioMed Pharmacother* (2017) 91:446–56. doi: 10.1016/j.biopha.2017.04.101
163. Silva AL, Peres C, Conniot J, Matos AI, Moura L, Carreira B, et al. Nanoparticle Impact on Innate Immune Cell Pattern-Recognition Receptors and Inflammasomes Activation. *Semin Immunol* (2017) 34:3–24. doi: 10.1016/j.smim.2017.09.003
164. Moghimi SM, Simberg D. Complement Activation Turnover on Surfaces of Nanoparticles. *Nano Today* (2017) 15:8–10. doi: 10.1016/j.nantod.2017.03.001
165. Wells LA, Guo H, Emili A, Sefton MV. The Profile of Adsorbed Plasma and Serum Proteins on Methacrylic Acid Copolymer Beads: Effect on Complement Activation. *Biomaterials* (2017) 118:74–83. doi: 10.1016/j.biomaterials.2016.11.036
166. Li C, Lu Y, Chen Q, Hu H, Zhao X, Qiao M, et al. Tailored Polymers With Complement Activation Ability to Improve Antitumor Immunity. *Mol Pharm* (2019) 16(6):2648–60. doi: 10.1021/acs.molpharmaceut.9b00195
167. Zhao Y, Zhou Y, Wang D, Gao Y, Li J, Ma S, et al. pH-Responsive Polymeric Micelles Based on Poly(2-Ethyl-2-Oxazoline)-Poly(D,L-Lactide) for Tumor-Targeting and Controlled Delivery of Doxorubicin and P-Glycoprotein Inhibitor. *Acta Biomater* (2015) 17:182–92. doi: 10.1016/j.actbio.2015.01.010
168. Gao Y, Zhou Y, Zhao L, Zhang C, Li Y, Li J, et al. Enhanced Antitumor Efficacy by Cyclic RGDyK-Conjugated and Paclitaxel-Loaded pH-Responsive Polymeric Micelles. *Acta Biomater* (2015) 23:127–35. doi: 10.1016/j.actbio.2015.05.021
169. Zhang ZL, Zou WG, Luo CX, Li BH, Wang JH, Sun LY, et al. An Armed Oncolytic Adenovirus System, ZD55-Gene, Demonstrating Potent Antitumoral Efficacy. *Cell Res* (2003) 13(6):481–9. doi: 10.1038/sj.cr.7290191
170. Masiero M, Nardo G, Indraccolo S, Favaro E. RNA Interference: Implications for Cancer Treatment. *Mol Aspects Med* (2007) 28(1):143–66. doi: 10.1016/j.mam.2006.12.004
171. Zhang L, Huang J, Yang N, Greshock J, Megraw MS, Giannakakis A, et al. microRNAs Exhibit High Frequency Genomic Alterations in Human Cancer. *Proc Natl Acad Sci USA* (2006) 103(24):9136–41. doi: 10.1073/pnas.0508889103
172. Tian H, Lin L, Jiao Z, Guo Z, Chen J, Gao S, et al. Polylysine-Modified Polyethylenimine Inducing Tumor Apoptosis as an Efficient Gene Carrier. *J Control Release* (2013) 172(2):410–8. doi: 10.1016/j.jconrel.2013.06.026
173. Liang L, Chen Y, Chen XM, Zhang Y, Liu Y. Cyclodextrin/polyethylenimine-Based Supramolecular Nanoparticles for Loading and Sustained Release of ATP. *Chem Letters* (2018) 29(6):989–91. doi: 10.1016/j.cclet.2017.12.022
174. Chen J, Guo Z, Jiao Z, Lin L, Xu C, Tian H, et al. Poly (L-Glutamic Acid)-Based Zwitterionic Polymer in a Charge Conversional Shielding System for Gene Therapy of Malignant Tumors. *ACS. Appl Mater Interfaces* (2020) 12 (17):19295–306. doi: 10.1021/acsami.0c02769
175. Kelly JF, Snell ME, Berenbaum MC. Photodynamic Destruction of Human Bladder Carcinoma. *Br J Cancer* (1975) 31(2):237–44. doi: 10.1038/bjc.1975.30
176. Li C, Luo Z, Yang L, Chen J, Cheng K, Xue Y, et al. Self-Assembled Porphyrin Polymer Nanoparticles With NIR-II Emission and Highly Efficient Photothermal Performance in Cancer Therapy. *Mater Today Bio* (2021) 13:100198. doi: 10.1016/j.mtbio.2021.100198
177. Li X, Yuan HJ, Tian XM, Tang J, Liu LF, Liu FY. Biocompatible Copper Sulfide-Based Nanocomposites for Artery Interventional Chemo-Photothermal Therapy of Orthotropic Hepatocellular Carcinoma. *Mater Today Bio* (2021) 12:100128. doi: 10.1016/j.mtbio.2021.100128
178. Wang JL, Sui LH, Huang J, Miao L, Nie Y, Wang KS, et al. MoS_2-Based Nanocomposites for Cancer Diagnosis and Therapy. *Bioactive Materials* (2021) 6(11):4209–42. doi: 10.1016/j.bioactmat.2021.04.021
179. Li Z, Liu Y, Chen L, Hu X, Xie Z. A Glutathione-Activatable Photodynamic and Fluorescent Imaging Monochromatic Photosensitizer. *J Mater Chem B* (2017) 5(22):4239–45. doi: 10.1039/c7tb00724h
180. He DG, Hai L, He X, Yang X, Li HW. Glutathione-Activatable and O-2/Mn2+-Evolving Nanocomposite for Highly Efficient and Selective Photodynamic and Gene-Silencing Dual Therapy. *Funct Materials* (2017) 27(46):1704089. doi: 10.1002/adfm.201704089
181. Ma Z, Hu P, Guo C, Wang D, Zhang X, Chen M, et al. Folate-Mediated and pH-Responsive Chidamide-Bound Micelles Encapsulating Photosensitizers for Tumor-Targeting Photodynamic Therapy. *Int J Nanomed* (2019) 14:5527–40. doi: 10.2147/IJN.S208649
182. Chen Q, Xu L, Liang C, Wang C, Peng R, Liu Z. Photothermal Therapy With Immune-Adjuvant Nanoparticles Together With Checkpoint Blockade for Effective Cancer Immunotherapy. *Nat Commun* (2016) 7:13193. doi: 10.1038/ncomms13193
183. Zhu L, Li P, Gao D, Liu J, Liu Y, Sun C, et al. pH-Sensitive Loaded Retinal/Indocyanine Green Micelles as an "All-in-One" Theranostic Agent for Multi-Modal Imaging *In Vivo* Guided Cellular Senescence-Photothermal Synergistic Therapy. *Chem Commun (Camb)* (2019) 55(44):6209–12. doi: 10.1039/c9cc02567g
184. Yoon HJ, Lee HS, Lim JY, Park JH. Liposomal Indocyanine Green for Enhanced Photothermal Therapy. *ACS. Appl Mater Interfaces* (2017) 9 (7):5683–91. doi: 10.1021/acsami.6b16801
185. Liu R, Tang J, Xu Y, Zhou Y, Dai Z. Nano-Sized Indocyanine Green J-Aggregate as a One-Component Theranostic Agent. *Nanotheranostics* (2017) 1(4):430–9. doi: 10.7150/ntno.19935
186. Ting CW, Chou YH, Huang SY, Chiang WH. Indocyanine Green-Carrying Polymeric Nanoparticles With Acid-Triggered Detachable PEG Coating and Drug Release for Boosting Cancer Photothermal Therapy. *Colloids Surf B Biointerfaces* (2021) 208:112048. doi: 10.1016/j.colsurfb.2021.112048
187. Du JZ, Du XJ, Mao CQ, Wang J. Tailor-Made Dual pH-Sensitive Polymer-Doxorubicin Nanoparticles for Efficient Anticancer Drug Delivery. *J Am Chem Soc* (2011) 133(44):17560–3. doi: 10.1021/ja207150n
188. Danquah MK, Zhang XA, Mahato RI. Extravasation of Polymeric Nanomedicines Across Tumor Vasculature. *Adv Drug Deliv Rev* (2011) 63 (8):623–39. doi: 10.1016/j.addr.2010.11.005
189. Karve S, Werner ME, Sukumar R, Cummings ND, Copp JA, Wang EC, et al. Revival of the Abandoned Therapeutic Wortmannin by Nanoparticle Drug Delivery. *Proc Natl Acad Sci USA* (2012) 109(21):8230–5. doi: 10.1073/pnas.1120508109
190. Yoon HY, Koo H, Choi KY, Lee SJ, Kim K, Kwon IC, et al. Tumor-Targeting Hyaluronic Acid Nanoparticles for Photodynamic Imaging and Therapy. *Biomaterials* (2012) 33(15):3980–9. doi: 10.1016/j.biomaterials.2012.02.016
191. Mauceri HJ, Hanna NN, Beckett MA, Gorski DH, Staba MJ, Stellato KA, et al. Combined Effects of Angiostatin and Ionizing Radiation in Antitumour Therapy. *Nature* (1998) 394(6690):287–91. doi: 10.1038/28412
192. Bejjanki NK, Zhong Y, Liu J, Li Q, Xu H, Shen H, et al. Surface Charge Transition Nano-Theranostics Based on Ultra-Small Fe3O4 Nanoparticles for Enhanced Photodynamic and Photothermal Therapy Against

Nasopharyngeal Carcinoma. *Biochem Biophys Res Commun* (2021) 557:240–6. doi: 10.1016/j.bbrc.2021.03.168
193. Gong NQ, Ma XW, Ye XX, Zhou QF, Chen XA, Tan XL, et al. Carbon-Dot-Supported Atomically Dispersed Gold as a Mitochondrial Oxidative Stress Amplifier for Cancer Treatment. *Nat Nanotechnol* (2019) 14(4):379–87. doi: 10.1038/s41565-019-0373-6
194. Ding YL, Liu FT, Jiang QH, Du B, Sun HD. 12-Hydrothermal Synthesis and Characterization of Fe3O4 Nanorods. *J Inorg Organ P* (2013) 23(2):379–84. doi: 10.1007/s10904-012-9789-2
195. Lacroix LM, Huls NF, Ho D, Sun X, Cheng K, Sun S. Stable Single-Crystalline Body Centered Cubic Fe Nanoparticles. *Nano Lett* (2011) 11(4):1641–5. doi: 10.1021/nl200110t
196. Wang S, Yu G, Wang Z, Jacobson O, Lin LS, Yang W, et al. Enhanced Antitumor Efficacy by a Cascade of Reactive Oxygen Species Generation and Drug Release. *Angew Chem Int Ed Engl* (2019) 58(41):14758–63. doi: 10.1002/anie.201908997
197. Li F, Liang Y, Wang M, Xu X, Zhao F, Wang X, et al. Multifunctional Nanoplatforms as Cascade-Responsive Drug-Delivery Carriers for Effective Synergistic Chemo-Photodynamic Cancer Treatment. *J Nanobiotech* (2021) 19(1):140. doi: 10.1186/s12951-021-00876-7
198. Tang K, Wang W, Song Z, Luo X. Multifunctional Nano-Biosensor Based on Metal-Organic Framework for Enhanced Fluorescence Imaging of Intracellular miRNA-122 and Synergistic Chemo-Photothermal Therapy of Tumor Cells. *Anal Chim Acta* (2021) 1176:338779. doi: 10.1016/j.aca.2021.338779
199. Wang Z, Zhao K, Zhang Y, Duan X, Zhao Y. Anti-GPC3 Antibody Tagged Cationic Switchable Lipid-Based Nanoparticles for the Co-Delivery of Anti-Mirna27a And Sorafenib in Liver Cancers. *Pharm Res* (2019) 36(10):145. doi: 10.1007/s11095-019-2669-5
200. Wang S, Liu Q, Li L, Urban MW. Recent Advances in Stimuli-Responsive Commodity Polymers. *Macromol Rapid Commun* (2021) 42(18):e2100054. doi: 10.1002/marc.202100054
201. Guan GJ, Wu MD, Han MY. Stimuli-Responsive Hybridized Nanostructures. *Adv Funct* (2020) 30:1903439–1903465. doi: 10.1002/adfm.201903439
202. Liao J, Jia Y, Wu Y, Shi K, Yang D, Li P, et al. Physical-, Chemical-, and Biological-Responsive Nanomedicine for Cancer Therapy. *Wiley Interdiscip Rev Nanomed Nanobiotechnol* (2020) 12(1):e1581. doi: 10.1002/wnan.1581
203. Ji T, Zhao Y, Wang J, Zheng X, Tian Y, Zhao Y, et al. Tumor Fibroblast Specific Activation of a Hybrid Ferritin Nanocage-Based Optical Probe for Tumor Microenvironment Imaging. *Small* (2013) 9(14):2427–31. doi: 10.1002/smll.201300600
204. Qin X, Li Y. Strategies To Design and Synthesize Polymer-Based Stimuli-Responsive Drug-Delivery Nanosystems. *Chembiochem* (2020) 21(9):1236–53. doi: 10.1002/cbic.201900550
205. Li HJ, Du JZ, Du XJ, Xu CF, Sun CY, Wang HX, et al. Stimuli-Responsive Clustered Nanoparticles for Improved Tumor Penetration and Therapeutic Efficacy. *Proc Natl Acad Sci USA* (2016) 113(15):4164–9. doi: 10.1073/pnas.1522080113
206. Li HJ, Du JZ, Liu J, Du XJ, Shen S, Zhu YH, et al. Smart Superstructures With Ultrahigh pH-Sensitivity for Targeting Acidic Tumor Microenvironment: Instantaneous Size Switching and Improved Tumor Penetration. *ACS Nano* (2016) 10(7):6753–61. doi: 10.1021/acsnano.6b02326
207. Pi Y, Zhou J, Wang J, Zhong J, Zhang L, Wang Y, et al. Strategies of Overcoming the Physiological Barriers for Tumor-Targeted Nano-Sized Drug Delivery Systems. *Curr Pharm Des* (2015) 21(42):6236–45. doi: 10.2174/1381612821666151027153611

Conflict of Interest: The authors declare that the research was conducted in the absence of any commercial or financial relationships that could be construed as a potential conflict of interest.

Publisher's Note: All claims expressed in this article are solely those of the authors and do not necessarily represent those of their affiliated organizations, or those of the publisher, the editors and the reviewers. Any product that may be evaluated in this article, or claim that may be made by its manufacturer, is not guaranteed or endorsed by the publisher.

Copyright © 2022 Chu, Shi, Tian and Gao. This is an open-access article distributed under the terms of the Creative Commons Attribution License (CC BY). The use, distribution or reproduction in other forums is permitted, provided the original author(s) and the copyright owner(s) are credited and that the original publication in this journal is cited, in accordance with accepted academic practice. No use, distribution or reproduction is permitted which does not comply with these terms.

frontiers in Pharmacology

ORIGINAL RESEARCH
published: 24 March 2022
doi: 10.3389/fphar.2022.850534

Biomimetic ZIF8 Nanosystem With Tumor Hypoxia Relief Ability to Enhance Chemo-Photothermal Synergistic Therapy

Ziming Zhao[1,2], Zhaorong Liu[1], Yabing Hua[1,2], Yuanjie Pan[1], Ge Yi[1], Shengyue Wu[1], Cong He[1], Yanzhuo Zhang[1,2] and Yihua Yang[1,2]**

[1]Jiangsu Key Laboratory of New Drug Research and Clinical Pharmacy, Xuzhou Medical University, Xuzhou, China, [2]Department of Pharmaceutics, School of Pharmacy, Xuzhou Medical University, Xuzhou, China

Tumor hypoxic microenvironment can reduce the therapeutic effects of chemotherapy, radiotherapy, photodynamic therapy, immunotherapy, etc. It is also a potential source of tumor recurrence and metastasis. A biomimetic nanosystem based on zeolitic imidazolate framework 8 (ZIF8), which had multifunctions of hypoxia relief, chemotherapy, and photothermal therapy, was established to improve tumor hypoxic microenvironment and overcome the corresponding therapeutic resistance. ZIF8 enveloped with DOX and CuS nanoparticles (DC@ZIF8) was synthesized by a sedimentation method. Red blood cell membrane and catalase (CAT) were coated onto DC@ZIF8 and biomimetic nanosystem (DC@ZIF8-MEM_C) was formed. The designed DC@ZIF8-MEM_C had a shape of polyhedron with an average particle size around 254 nm. The loading content of DOX, CAT, and CuS was 4.9%, 6.2%, and 2.5%, separately. The release of DOX from DC@ZIF8-MEM_C was pH dependent and significantly faster at pH 5 due to the degradation of ZIF8. DC@ZIF8-MEM_C exhibited outstanding photothermal conversion properties and excellent antitumor effect *in vitro* and *in vivo.* Moreover, the hypoxia relief by CAT was proved to have good sensitization effect on chemo-photothermal combined therapy. DC@ZIF8-MEM_C is a prospective nanosystem, which can realize great chemo-photothermal synergistic antitumor effect under the sensitization of CAT. The biomimetic multifunctional nanoplatform provides a potential strategy of chemo-photothermal synergistic antitumor effect under the sensitization of CAT.

Keywords: biomimetic, ZIF8, photothermal therapy, chemotherapy, hypoxia relief

OPEN ACCESS

Edited by:
Zeming Liu,
Huazhong University of Science and Technology, China

Reviewed by:
Xiongwei Deng,
National Center for Nanoscience and Technology (CAS), China
Haibo Zhou,
Jinan University, China
Yelin Wu,
Tongji University School of Medicine, China

****Correspondence:***
Yanzhuo Zhang
yanzhuozhang@126.com
Yihua Yang
nancyyyh@126.com

Specialty section:
This article was submitted to Pharmacology of Anti-Cancer Drugs, a section of the journal Frontiers in Pharmacology

Received: *07 January 2022*
Accepted: *31 January 2022*
Published: *24 March 2022*

Citation:
Zhao Z, Liu Z, Hua Y, Pan Y, Yi G, Wu S, He C, Zhang Y and Yang Y (2022) Biomimetic ZIF8 Nanosystem With Tumor Hypoxia Relief Ability to Enhance Chemo-Photothermal Synergistic Therapy. Front. Pharmacol. 13:850534. doi: 10.3389/fphar.2022.850534

INTRODUCTION

Cancer has become one of the major diseases threatening human health and life (Li D. et al., 2021). The conventional clinical methods, such as chemotherapy (CT), surgery, radiation therapy, have made remarkable achievement in the treatment of cancer. However, therapeutic outcomes are unsatisfactory, and patient compliance is poor, resulting from far-reaching side effects (Li et al., 2019). Researchers have devoted to develop new approaches, such as photothermal therapy (PTT), photodynamic therapy (PDT), chemodynamic therapy (CDT), immunotherapy, gene therapy, and molecular targeted therapy.

As one of the rising "green" cancer treatment methods, PTT based on photothermal agents converts energy from near infrared (NIR) light into heat, leading to overheating of the surrounding

environment and inducing cancer cell death (Chen et al., 2019; Jiang et al., 2019). Photothermal agents, such as gold nanorods (He et al., 2021), carbon nanorods (Zhao et al., 2021), palladium nanorods (Tang et al., 2014), semiconducting polymer nanoparticles (Zhen et al., 2018), NIR dyes (Yue et al., 2013; Zhao et al., 2014), polydopamine (PDA) (Ding et al., 2016), and copper sulfide (CuS) (Jang et al., 2018; Shi et al., 2018; Li J. et al., 2021) have been reported as having good photothermal effect. However, PTT may lead to uneven heat distribution and subsequent sublethal thermal dose in the treatment area (Jiang et al., 2019; Zhang L. et al., 2019). Moreover, utilizing PTT alone to treat tumor is suboptimal and unreliable. Generally, co-delivery of chemotherapeutic drug and photothermal agent simultaneously exerts two benefits to improve antitumor efficacy. As is well known, a combination therapy of CT and PTT based on nanomaterials exhibits significant advantages over monotherapy for anticancer treatment and usually generates synergistic therapeutic efficacies with minimal side effects (Liu et al., 2011; Li et al., 2018; Li et al., 2019).

CT based on nanocarrier to deliver a chemical drug is effective. As a new kind of porous material, ZIF8 is built from zinc ions and 2-methylimidazolate, which are components of physiological systems (Zhuang et al., 2014). It possesses unique merits including significantly high microporosity, excellent structural regularity, adjustable surface functionality, and intrinsic pH-induced biodegradability (Sun et al., 2012; Liu H et al., 2021). In addition, it is prone to decompose under acidic conditions (pH 5.0–6.0), which is helpful to the pH-controlled delivery and release of the loaded payloads (Park et al., 2006; Lian et al., 2017; Gao et al., 2019). A theranostic nanoplatform based on ZIF8 encapsulated Pd nanosheets and DOX (DOX/Pd@ZIF8@PDA) showed photoacoustic (PA) imaging-guided synergetic photo-chemo cancer therapy (Zhu et al., 2019). A drug delivery nanoplatform based on ZIFs (PDA-PCM@ZIF8/DOX) exhibited drug release as high as 78% under the dual stimulus of NIR and acid environment (Wu et al., 2018).

Moreover, hypoxia is a unique feature of tumor microenvironment due to rapid cell proliferation and abnormal vascular structure (Vaupel and Mayer, 2016; Graham and Unger, 2018). Numerous studies have demonstrated that tumoral hypoxia can activate the overexpression of P-glycoproteins (P-gp), which markedly reduced the effect of CT (Samanta et al., 2014.). Hypoxia also induces tumor gene mutations and subsequent proteomic changes, ultimately impeding the clinical therapeutic effect of cancer therapy (Jing et al., 2019). Additionally, cancerous cells produced excessive amounts of hydrogen peroxide (H_2O_2) in tumor regions, resulting in oxide stress (Szatrowski and Nathan, 1991; Song et al., 2016). Using H_2O_2-responsive enzyme is an intriguing strategy to overcome tumor hypoxia (Szatrowski and Nathan, 1991; Chen et al., 2014; Zhang et al., 2017; Zou et al., 2018; Yin et al., 2020). CAT, an enzyme, is capable of catalyzing H_2O_2 to oxygen (O_2) efficiently, leading to tumor hypoxia relief (Liu et al., 2019; Yin et al., 2020).

Herein, we developed ZIF8 NPs to load CuS NPs and DOX·HCl, then camouflaged with bionic surface material, red cell membrane (MEM) combined with CAT, to construct a biomimetic nanosystem with multifunctions of chemotherapy, hyperthermia treatment, and hypoxia relief (**Figure 1**).

MATERIALS

Reagents

Copper (II) chloride dihydrate ($CuCl_2{\cdot}2H_2O$, analytical grade), sodium citrate dihydrate ($Na_3C_6H_5O_7{\cdot}2H_2O$, analytical grade), sodium sulfide nonahydrate ($Na_2S{\cdot}9H_2O$, analytical grade), and polyvinylpyrrolidone K30 (PVP K30, analytical grade) were obtained from Sinopharm Chemical Reagent Co., Ltd. (Shanghai, China). Zinc acetate dihydrate [Zn (CH_3CO_2) · $2H_2O$, 98%], 2-methylimidazole (98%), catalase (CAT) were purchased from Aladdin Chemistry Co., Ltd. (Shanghai, China). Tris (4,7-diphenyl-1,10-phenanthroline)-ruthenium (II) dichloride [Ru $(dpp)_3Cl_2$, 98%] was obtained from Rhawn Reagent Co., Ltd. (Shanghai, China). Doxorubicin hydrochloride (DOX·HCl, 98%) was supplied from Aladdin Chemistry Co., Ltd. (Shanghai, China). BCA Protein Assay Kit, 3-[4,5-dimethylthiazol-2-yl]-2,5-diphenyltetrazoliumbromide (MTT, 98%) and hoechst 33258 were obtained from Beyotime Biotechnology Co., Ltd. (Shanghai, China). Cell Viability/Cytotoxicity Detec (Calcein AM/PI) was obtained from Yuanye Bio-Technology Co., Ltd (Shanghai, China).

Cells

Mouse breast cancer cells (4T1) and leukemia cells in mouse macrophage (RAW264.7) were obtained from the Chinese Academy of Sciences (Shanghai, China). The 4T1 cells were incubated with DMEM/f12 medium containing 10% FBS, 1% streptomycin (50 U·mL^{-1}), and penicillin (50 U·mL^{-1}) in a 5% CO_2 atmosphere at 37°C. The RAW264.7 cells were cultured in DMEM medium supplemented with 10% FBS, 1% streptomycin (50 U·mL^{-1}), and penicillin (50 U·mL^{-1}) in a 5% CO_2 atmosphere at 37°C.

Animals

BALB/c female mice (20 ± 2 g) were purchased from the Laboratory Animal Center of Xuzhou Medical University (Xuzhou, China), and maintained in a sterile environment, and allowed free access to food and water, and all experiment procedures were approved by the Experimental Animal Ethics Committee of Xuzhou Medical University and carried out by the guidelines of the National Act on the Use of Experimental Animals (People's Republic of China).

METHODS

Preparation of DC@ZIF8-MEM$_C$

Preparation of CuS NPs

$CuCl_2{\cdot}2H_2O$ (0.4 mM) and $Na_3C_6H_5O_7{\cdot}2H_2O$ (0.27 mM) were dissolved in 180 ml of deionized water, and then 20 ml of $Na_2S{\cdot}9H_2O$ (0.4 mM) aqueous solution was added to the mixed solution. After stirring for 5 min at room temperature, the mixed solution was stirred for 15 min at 90°C, until dark

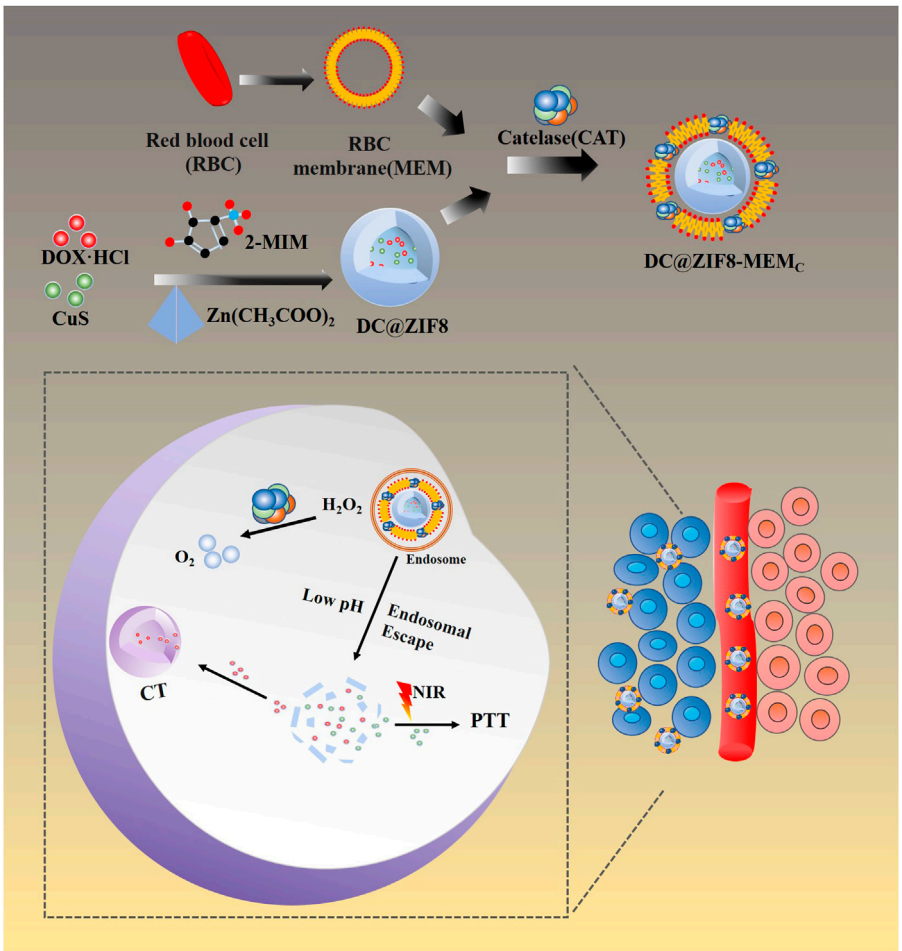


FIGURE 1 | Schematic illustration for the formation of DC@ZIF8-MEM_C nanoplatform.

green was obtained. The synthesized product was centrifuged and then washed with deionized water three times yielding CuS NPs.

Preparation of DC@ZIF8

2-Methylimidazole (460 mg) and PVP K30 (25 mg) were dissolved in 10 ml of CuS aqueous solution (2 mM), 1 ml of zinc acetate methanol solution (0.56 mM) was added and stirred for 10 min, centrifuged, dried under vacuum to obtain CuS NPs-loaded ZIF8 NPs (C@ZIF8). DOX·HCl (1 mg) was mixed with 12 mg C@ZIF8, dissolved in distilled water, and stirred for 10 min, centrifuged, and washed to collect DC@ZIF8.

Extraction of Red Blood Cell Membrane

Red blood cell (RBC) membranes were obtained according to a reported method with modification (Piao et al., 2014). Fresh whole blood from male ICR mice (20–22 g) was collected with heparinized tubes, followed by centrifugation for 10 min with 4,000 rpm at 4°C to remove the plasma and the leukocytes. The collected red blood cells (RBCs) were washed with 1× PBS, suspended with 0.25× PBS for 30 min at 4°C, and then centrifuged at 10,000 rpm for 10 min. The resulting light-pink pellet was purified with 1× PBS, which yielded RBC membrane (Piao et al., 2014).

Preparation of DC@ZIF8-MEM_C

The above prepared DC@ZIF8 and CAT were dispersed in 10 ml of RBC membrane solution and then ultrasonicated with ice bath for 6 min. The precipitation of DC@ZIF8-MEM_C was collected by washing and centrifugation, and placed at 4°C for later use. DC@ZIF8-MEM was prepared by the same method above except for the absence of CAT.

Characterization

Morphology, Size, and Zeta Potential

The particle size and zeta potential were determined by dynamic light scattering (DLS) method using a NicompTM 380 ZLS zeta potential/size analyzer (Particle Sizing Systems, Santa Banta, CA, USA) at 25°C. The morphologies of the NPs

were observed using transmission electron microscopy (TEM) (FEI Tecnai G2 Spirit Twin, Holland).

Load Efficiency

The loading content (LC) was calculated using the following formula: LC = weight of loaded drug/weight of NPs*100%. DOX·HCl was quantitatively analyzed using fluorescence spectrum (excitation wavelength = 488 nm, emission wavelength = 560 nm). The quantification of CAT was determined by ultraviolet spectrophotometer based on ammonium molybdate colorimetric method. The NPs were digested by nitric acid, and Cu^{2+} content was detected by an inductively coupled plasma spectrometer (PQ9000, German), and then the LC of CuS was analyzed.

Spectra Analysis

Infrared spectra and ultraviolet (UV)-visible (UV-vis) spectra were obtained by using a Fourier transform infrared spectrometer (FTIR, BRUKER) and an Evolution 220 UV-Visible Spectrophotometer (Mapada Instruments, Shanghai), respectively.

Drug release *in vitro*

The release study was assessed by the dialysis method. The release media was PBS solutions with different pH values (5.0, 6.5, and 7.4). Briefly, 5 ml of DOX·HCl-loaded NPs was placed in a dialysis bag (MWCO 8,000–14,000) and dialyzed against 45 ml of buffer medium under mechanical shaking (100 rpm) at 37°C. At predesigned time, 5 ml of release medium was withdrawn and replenished with an equal volume of fresh medium. The released DOX·HCl was detected by Fluorescence spectrum.

pH Sensitivity

DC@ZIF8-MEM_C was incubated with 10 mM PBS (pH 7.4 or pH 5.0) at 37°C for 8 h, and the morphology or size was detected.

Stability

DC@ZIF8-MEM_C was suspended in PBS (pH 7.4, 10 mM) or 10% fetal bovine serum (FBS), and measurements were performed in triplicate at different intervals.

Photothermal Activity *in vitro*

The photothermal conversion capability of DC@ZIF8-MEM_C was investigated. Various concentrations of DC@ZIF8-MEM_C (0, 60, 125, 250 $\mu g \cdot mL^{-1}$) were dispersed in 1 ml of deionized water and irradiated by 808 nm NIR laser at 2 $W \cdot cm^{-2}$ for 5 min. The temperature of each sample was monitored by a FLIR imaging instrument.

DC@ZIF8-MEM_C (250 $\mu g \cdot mL^{-1)}$ was dispersed in 1 ml of deionized water and irradiated by 808 nm NIR laser at different power densities (0.5, 1.0, 1.5, 2 $W \cdot cm^{-2}$) for 5 min. The temperature of each sample was monitored by a FLIR imaging instrument.

To evaluate the photothermal stability of NPs, 1 ml of DC@ZIF8-MEM_C was irradiated by 808 nm laser (2 $W \cdot cm^{-2}$) for four laser ON/OFF cycles. The photothermal conversion efficiency (η) of DC@ZIF8-MEM_C was calculated as follows according to a previously reported method (Zhang X. et al., 2019):

$$\eta = \frac{hS(T_{max} - T_{surr}) - Q_{dis}}{I(1 - 10^{-A808})} \times 100\%$$

where h represents heat-transfer coefficient, S represents the irradiated area, T_{max} represents the equilibrium temperature, T_{surr} is ambient temperature of the surrounding, Q_{dis} is the heat associated with the light absorbance of the solvent, I is the power density of the laser (2 $W \cdot cm^{-2}$), and A_{808} is the absorption value of the material at 808 nm (Zhang X. et al., 2019). Photothermal conversion of DC@ZIF8 was performed the same above.

O_2 Generation *in vitro*

The fluorescence of O_2-sensitive fluorescent probe Tris (4,7-diphenyl-1,10-phenanthroline) ruthenium (II) dichloride [Ru $(DPP)_3Cl_2$] will be quenched to a certain extent when O_2 concentration is sufficient. H_2O_2 solution (10 mM), Ru $(DPP)_3Cl_2$ solution (1 mM), and DC@ZIF8-MEM_C (125 $\mu g \cdot mL^{-1}$) were mixed and sealed. The emission spectra were scanned at a predetermined time (0, 10, 20, 30, 45, 60 min).

Additionally, the portable dissolved oxygen meter was used to measure the *in situ* O_2 generation. Free CAT, DC@ZIF8-MEM_C, DC@ZIF8-MEM, and PBS were mixed with H_2O_2 solution (10 mM), and the O_2 production was dynamically detected by the portable dissolved oxygen meter (JPBJ-609L, INESA Scientific Instrument Co., Ltd., China) every 30 s for 600 s.

Catalase activity

Catalase activity was evaluated by the Goth method (Goth, 1991). Free CAT, DC@ZIF8-MEM_C [(CAT) = 2.5 $\mu g \cdot mL^{-1}$] and DC@ZIF8-MEM were incubated with H_2O_2 solution (50 mM) at 37°C, then ammonium molybdate was added to terminate the reaction, and the absorbance was determined at 400 nm according to a standard curve of H_2O_2. CAT was reliable to degrade by the protease K under complicated physiological conditions (Phua et al., 2019). Free CAT and DC@ZIF8-MEM_C was incubated with protease K (100 $\mu g \cdot mL^{-1}$) at 37°C, and then the absorbance was determined according to the method above.

Cell Experiments

Cellular Uptake

4T1 cells were seeded at a density of 2×10^4 cells/well in 48-well plates and treated with samples (DOX·HCl, DC@ZIF8, DC@ZIF8-MEM_C) at an equivalent DOX·HCl concentration of 1 $\mu g \cdot mL^{-1}$, respectively. After incubation for 4 h, the cells were washed by PBS, and then the cell nuclei were stained with Hoechst 33258 for 10 min. Afterward, the cells were observed under an inverted fluorescence microscopy.

The cellular uptake was quantified using a microplate reader following the procedure (Win and Feng, 2005). 4T1 cells were seeded in 96-well plates at a density of 1×10^4 cells/well. After cell

attachment, fresh media containing different formulations [(DOX·HCl) = 1 μg·mL^{-1}] were added and incubated for 4 h. After washing with PBS, the cells were treated with 0.5% of TritonX-100 solution for 30 min. Fluorescence intensity of cell lysates (E_x = 480 nm, E_m = 595 nm) was determined by a fluorescence microplate. Uptake efficiency (%) = W_{sample}/W_{total} *100%

Cytotoxicity *in vitro*

The *in vitro* cytotoxicity was evaluated by using MTT assay. 4T1 cells pre-seeded at a density of 1×10^4 cells/well in 96-well plates were incubated with different samples at gradient concentrations for 24 h. For NIR irradiation treatment, cells were irradiated by 808 nm for 3 min (2 W·cm^{-2}) after 6 h of incubation and then incubated for further 18 h. Then 20 μl of MTT was added and incubated for another 4 h. Subsequently, all of the solutions were replaced with 150 μl dimethyl sulfoxide (DMSO). The absorbance was determined by using a microplate reader at 490 nm. The untreated cells in medium were regarded as control. The cell viabilities (%) were calculated according to the reported literature (Zou et al., 2018).

4T1 cells seeded at a density of 1×10^4 cells/well in 96-well plates and incubated at different samples with hypoxic incubator (1% O_2) for 24 h. Then 10 μM H_2O_2 was added, and the cell viabilities were calculated the same as above.

Calcein AM/PI double staining kit was performed to evaluate live/dead cells (Liu et al., 2019). The 4T1 cells were seeded at a density of 1×10^4 cells/well in 96-well plates and cultured overnight. The media were replaced with DOX·HCl, DC@ZIF8-MEM_C [(DOX·HCl)] = 3.5 μg·mL^{-1}], and incubated for 24 h. For the laser group, the cells were irradiated by 808 nm NIR (2 W·cm^{-2}) for 3 min after 8 h of incubation, and then continued for 16 h of incubation. Calcein-AM (2 μM) and PI (4.5 μM) were added and incubated for 30 min. The cells were washed with PBS and observed under an inverted fluorescence microscope.

Intracellular Location

4T1 cells were inoculated and incubated overnight at a density of 1×10^5 cells/dish in laser confocal Petri dishes. Fresh medium containing DC@ZIF8-MEM_C [(DOX·HCl) = 1 μg·mL^{-1}] was added and incubated for 0.5, 2, 6 h, respectively. The samples were washed with PBS and then stained with Lysotracker for 20 min and Heochst-33258 for 10 min. Intracellular location was observed by confocal laser microscopy (CLMS) and analyzed by ImageJ software (Zhu et al., 2018).

Immune Evasion

RAW 264.7 cells were selected as a macrophage model to demonstrate that the composite vector coated by blood cells can reduce the probability of being phagocytosed by macrophages. RAW 264.7 cells were seeded at density of 1×10^4 cells/well in 96-well plates and incubated overnight. Different samples (DOX·HCl, DC@ZIF8, and DC@ZIF8-MEM_C, with DOX·HCl concentration 1 μg·mL^{-1}) were added, and incubated for 4 h. The medium was discarded, and Heochst-33258 was used as a stain for 10 min. Cell uptake was observed by inverted fluorescence microscopy. The quantitative uptake was investigated similarly as described above.

Intracellular Oxygen Determination

4T1 cells were seeded at a density of 4×10^4 cells/well into 24-well plates, and 10 μM H_2O_2 was added for 2 h with a hypoxic incubator. Different samples were added and incubated for 4 h. Ru $(DPP)_3Cl_2$ (0.5 μM) was added for 1 h and observed by an inverted fluorescence microscopy.

Tumor Inhibition Effect *in vivo*

The animal model was built by subcutaneous injection with 100 μl of 4T1 cells (1×10^6 cells) in the right hind limb of female BALB/c mice. The tumor-bearing mice were randomly divided into seven groups (each group had five mice with similar tumor volume about 200 ± 20 mm^3): 1) PBS group, 2) DOX·HCl group, 3) C@ZIF8-MEM group; 4) D@ZIF8-MEM group; 5) DC@ZIF8-MEM + NIR group; 6) DC@ZIF8-MEM_C group; 7) DC@ZIF8-MEM_C + NIR group. The mice were treated with PBS (group 1), NPs (groups 2 to 7, with a dosage of DOX·HCl 5 mg·kg^{-1}) *via* tail vein injection at day 0, 3, 6, and 9 for an overall of four times. For the NIR groups, the mice were treated with NIR 808 nm irradiation (2 W·cm^{-2}) at the tumor site for 5 min after 8 h post-injection. Tumor volume was calculated by the formula $(a \times b^2)/2$, where a and b are the long and short diameters of the tumor, respectively, which were measured every other day by a vernier caliper (Wu et al., 2018).

On day 14, the mice were sacrificed, and major organs, including the heart, liver, spleen, lungs, kidneys, and tumor were collected for pathological evaluation.

Photothermal Effect *in vivo*

The tumor-bearing mice were tail vein injected with PBS, DC@ZIF8, DC@ZIF8-MEM, and DC@ZIF8-MEM_C. After an 8 h-injection, the mice were anesthetized with 40 μl of 10% chloral hydrate by intraperitoneal injection. The tumor site of the mice was irradiated by 808 nm of NIR (2 W·cm^{-2}) for 5 min. Simultaneously, the photothermal imaging of the tumor site was recorded by the near-infrared imager. The temperature change in the tumor site with time was observed, and the temperature curve was plotted.

Hemolysis Assay

The hemocompatibility was evaluated by hemolysis assay (Yang et al., 2019). First, fresh blood extracted from rabbit heart was centrifuged at 3,000 rpm for 15 min and purified with normal saline (NS) to obtain erythrocytes. DC@ZIF8-MEM_C with various concentrations were mixed with the 2% erythrocytes (v/v) and incubated for 3 h. Afterward, the mixtures were centrifuged at 3,500 rpm for 15 min, and the absorbance (A) of the sample supernatant at 540 nm was measured by UV-vis spectrophotometer. PBS (0.01 M, pH 7.4) and deionized water were regarded as the negative and positive controls, respectively. The hemolysis ratio (HR) was calculated as follows: HR (%) = $(A_{sample} - A_{negative\ control})/(A_{positive\ control} - A_{negative\ control})$ * 100%.

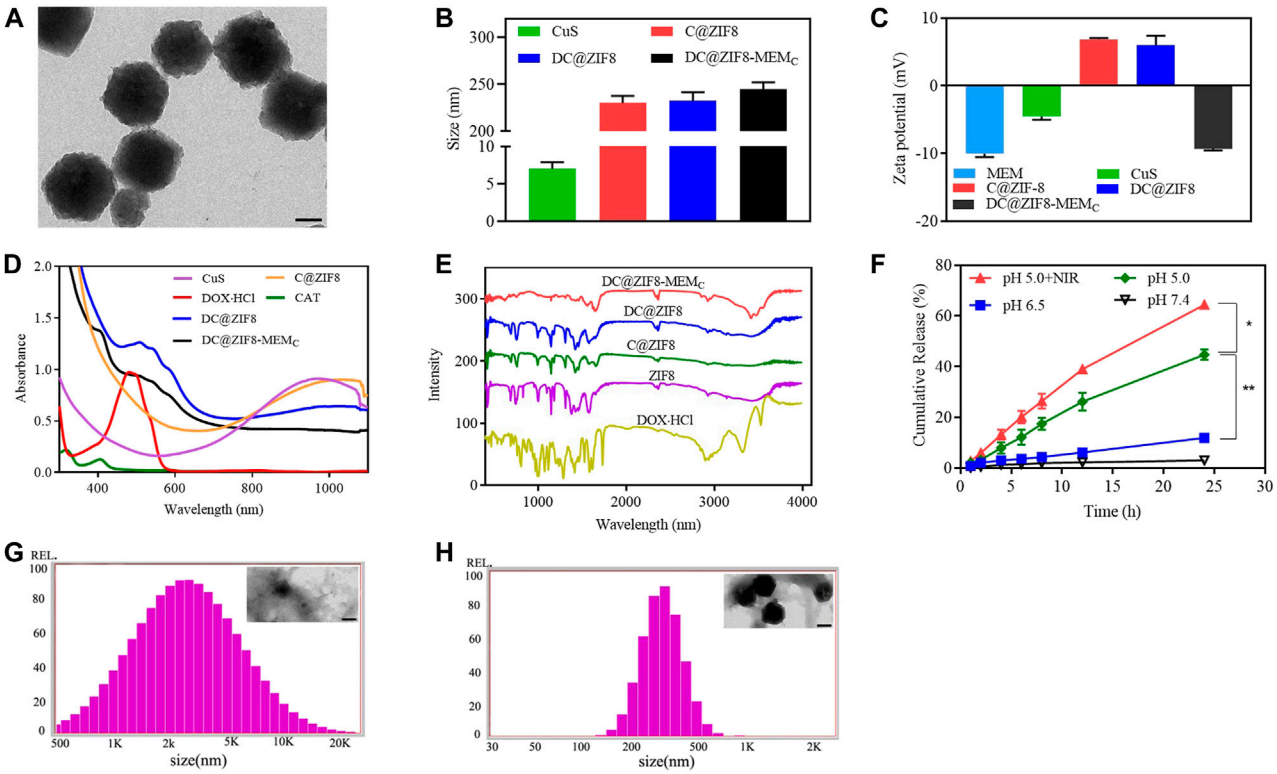


FIGURE 2 | Representative transmission electron microscopy (TEM) image of DC@ZIF8-MEM_C (scale bar = 100 nm) **(A)**. Size of preparations **(B)**. Zeta potential of preparations **(C)**. Ultraviolet (UV)-visible (UV-Vis) analysis **(D)**. Fourier transform infrared (FTIR) analysis **(E)**. DOX·HCl release profiles from DC@ZIF8-MEM_C under PBS at pH values of 5.0, 6.5, and 7.4 **(F)**. Size and TEM image (inserted) of DC@ZIF8-MEM_C with PBS (pH 5.0) for 8 h; scale bar = 100 nm **(G)**. Size and TEM image (inserted) of DC@ZIF8-MEM_C with PBS (pH 7.4) for 8 h; scale bar = 100 nm **(H)**.

Statistical Analysis

The data were expressed as the mean ± standard deviation (SD). Statistical analysis was performed using a two-tailed Student's t-test and analysis of variance (ANOVA) with the software SPSS 23.0. All analyses were shown compared with the control, and the significance of the difference was indicated as $^{*}p < 0.05$, $^{**}p < 0.01$, or $^{***}p < 0.001$.

RESULTS AND DISCUSSION

Synthesis and Characterization

CuS NPs appeared dark green (**Supplementary Figure S1**). Both DC@ZIF8 and DC@ZIF8-MEM_C showed purplish red due to the loaded DOX·HCl (**Supplementary Figure S1**). CuS NPs were spherical, while DC@ZIF8 was polyhedral due to the frame of ZIF8 by TEM (**Supplementary Figure S2**). After coating with MEM-embedded CAT, DC@ZIF8-MEM_C maintained a polyhedral structure by TEM (**Figure 2A**). The size of CuS NPs was only 7 nm, and C@ZIF8 increased to 230 nm due to the framework of ZIF8 (**Figure 2B**). After drug loading, the size of DC@ZIF8 was 232 nm, and the size of DC@ZIF8-MEM_C increased to 254 nm for the coating of cell membrane (**Figure 2B**). Both C@ZIF8 and DC@ZIF8 were positive zeta potential (**Figure 2C**). However, the zeta potential of DC@ZIF8-MEM_C reversed to be negative (−9.3 mV), demonstrating a successful membrane coating (**Figure 2C**). DOX·HCl was quantitatively analyzed by fluorescence spectrum (**Supplementary Figure S3**). The CAT was quantitatively analyzed by ultraviolet spectrophotometer (**Supplementary Figure S4**). The LC of DOX, CAT, and CuS was 4.9%, 6.2%, and 2.5%, separately. Moreover, DC@ZIF8-MEM_C exhibit good colloidal stability in both PBS and 10% FBS, as indicated by the negligible increase in hydrodynamic diameter (**Supplementary Figure S5**).

UV-Vis analysis showed that DC@ZIF8-MEM_C, DC@ZIF8, and CuS NPs all had a very wide absorption band in the near infrared region from 800 to 1,100 nm. Therefore, a near-infrared laser of 808 nm can be used as a heat source for photothermal effect. DC@ZIF8-MEM_C had characteristic absorbance peaks from DOX (480 nm) and CAT (400 nm), confirming the successful loading of these two materials (**Figure 2D**).

By recording Fourier transform infrared (FTIR) spectra, the prepared DC@ZIF8-MEM_C was further characterized. As depicted in **Figure 2E**, DC@ZIF8-MEM_C exhibited a characteristic peak of 1,700 cm^{-1}, which was the C=O stretching vibration of sodium citrate in CuS NP_S, and a –CH stretching vibration peak at 2,800 cm^{-1}, which was consistent with the characteristic peak of DOX·HCl. DC@ZIF8-MEM_C had a characteristic peak of 3,500–3,700 cm^{-1}, which was abundant

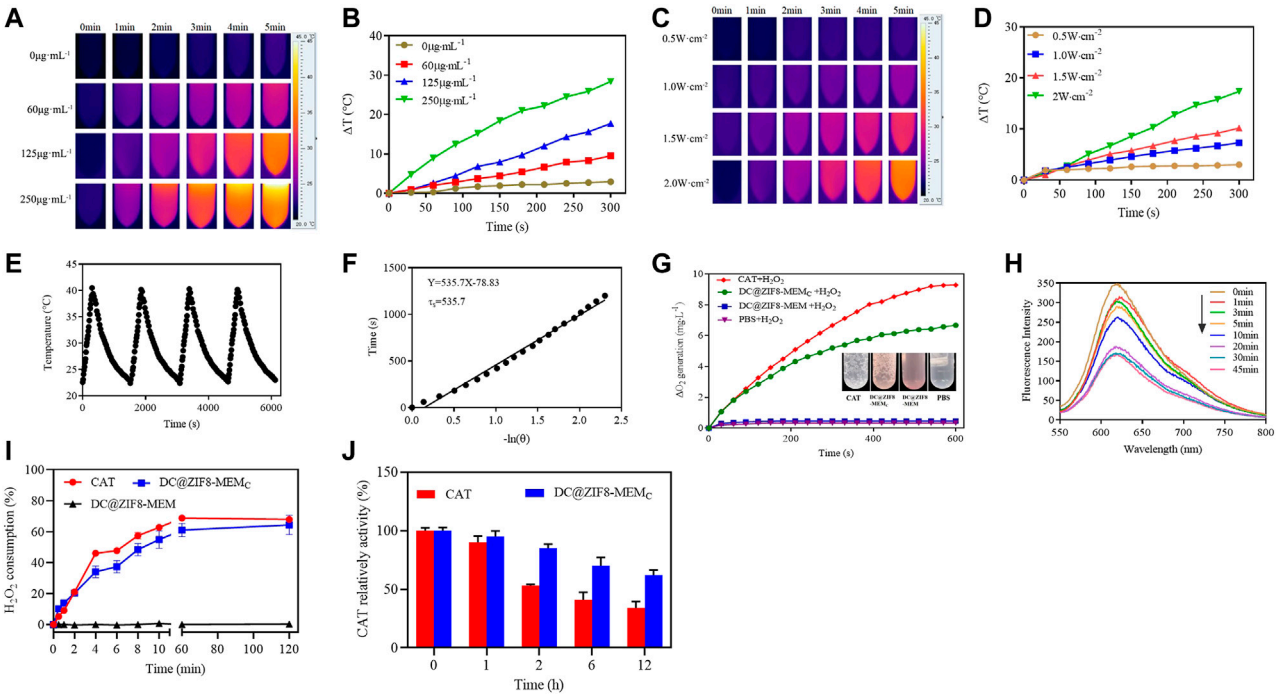


FIGURE 3 | Photothermal images of DC@ZIF8-MEM$_C$ with various concentrations by FLIR **(A)**. Temperature curves by changing concentration of DC@ZIF8-MEM$_C$ with 808 nm near infrared (NIR) at 2 W·cm^{-2} for 5 min **(B)**. Photothermal images of DC@ZIF8-MEM$_C$ with various laser power densities by FLIR **(C)**. Temperature curves of DC@ZIF8-MEM$_C$ by changing the laser power density **(D)**. Temperature variations of DC@ZIF8-MEM$_C$ by repeating on/off (2 W cm^{-2}) **(E)**. Temperature fitting curve of DC@ZIF8-MEM$_C$ **(F)**. The O_2-generating behavior of DC@ZIF8-MEM$_C$, DC@ZIF8-MEM, PBS, and free CAT solution in the presence of H_2O_2. Inset is the corresponding image of these four solutions **(G)**. Fluorescence absorption curves of ruthenium (II) dichloride [Ru (DPP)$_3$Cl$_2$] incubation with DC@ZIF8-MEM$_C$ **(H)**. The H_2O_2 consumption kinetics of free catalase (CAT), DC@ZIF8-MEM$_C$, and DC@ZIF8-MEM at 37°C **(I)**. The relative enzymatic activity of free CAT and DC@ZIF8-MEM$_C$ after treating with protease K for different incubation times **(J)**.

–OH peaks on the surface of CAT and heterozygous membrane. The results of FTIR spectrum analysis and UV analysis were consistent, which showed that DC@ZIF8-MEM$_C$ was successfully constructed.

Drug release *in vitro* showed pH-dependent manners (**Figure 2F**). The cumulative release of DOX·HCl in pH 7.4, pH 6.5, and pH 5.0 media at 24 h was 3.1% 11.9%, and 44.7%, respectively. There was little drug release in pH 7.4, indicating that the developed NPs were stable under physiological conditions. Compared with pH 5.0 group, release from pH 5.0 + NIR group was higher, indicating that NIR accelerated the drug release. Interestingly, pH sensitivity of DC@ZIF8-MEM$_C$ was evident from **Figures 2G, H**. When DC@ZIF8-MEM$_C$ was in a neutral condition (pH 7.4 PBS), the morphology and size changed little for 8 h (**Figure 2H**). It degraded under acidic conditions (pH 5.0), and the size increased to 2,000 nm, 10-fold bigger than that of PBS (pH 7.4) (**Figure 2G**). Under acidic conditions, the release amount of the drug was significantly increased, which may be related to the degradation of the material at lower pH value (Wu et al., 2018). The imidazole groups from ZIF8 were protonated in an acidic environment, and the unstable coordination bonds between zinc ions and imidazole groups became unstable, leading to the disintegration of the skeleton and acceleration of the drug release.

Photothermal Properties

As shown in **Figures 3A, B**, the temperature rise followed a concentration-dependent manner. The temperature of the water increased by only 2.1°C. At concentrations of 60, 125, 250 μg·mL^{-1}, DC@ZIF8-MEM$_C$ increased by 9.5°C, 17.7°C, and 28.4°C, respectively (**Figures 3A, B**). Furthermore, the temperature increased with power. The temperature increased by 17.4°C when the concentration was 125 μg·mL^{-1}, and the power density of the 808 nm laser was 2.0 W·cm^{-2} (**Figures 3C, D**).

Moreover, by measuring the rising/falling temperature, it was found that the photothermal conversion was stable. The photothermal conversion efficiency was calculated to be 51.5%, consistent with a report (Shi et al., 2018), indicating the excellent photothermal performance of DC@ZIF8-MEM$_C$ (**Figures 3E, F**). Intriguingly, the photothermal conversion efficiency of DC@ZIF8 was 54%, similar to that of DC@ZIF8-MEM$_C$, which indicated that there was no influence of membrane coating on photothermal property (**Supplementary Figure S6**).

O_2 Generation *in vitro*

The *in situ* O_2 production was measured by using a portable dissolved oxygen meter. As seen from **Figure 3G**, the DC@ZIF8-

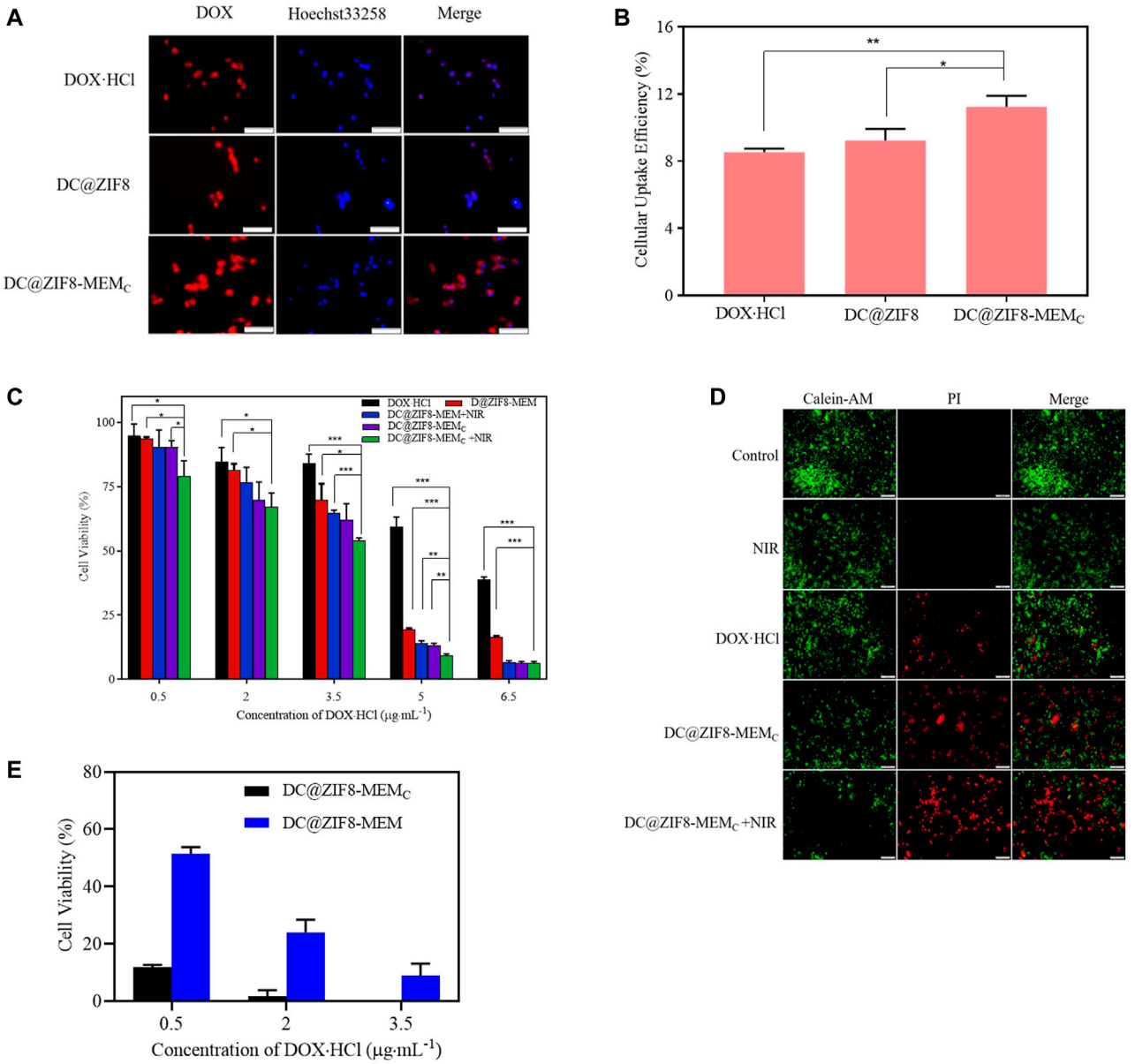


FIGURE 4 | Fluorescence images of mouse breast cancer cells (4T1) incubated with different samples for 4 h, scale bar = 100 μm **(A)**. Cellular uptake efficiency of different samples to 4T1 cells by microplate reader **(B)**. Cytotoxicity of 4T1 cells incubated with different samples at various concentrations for 24 h **(C)**. Labeling of live and dead cells by calcein AM/propidium iodide (PI) for different samples; scale bar = 200 μm **(D)**. Cytotoxicity of 4T1 cells incubated with different samples at various concentrations in hypoxia incubator for 24 h **(E)**. $^{*}p < 0.05$, $^{**}p < 0.01$, $^{***}p < 0.001$.

MEM and PBS groups did not generate any O_2, while the DC@ZIF8-MEM_C and CAT groups generated time-dependent O_2 production due to the activity of CAT. Bubbles were visible in the EP tubes of free CAT and DC@ZIF8-MEM_C, while no bubbles were found with DC@ZIF8-MEM and PBS (**Figure 3G**). As an oxygen-sensitive dye, the fluorescence of Ru $(DPP)_3Cl_2$ was quenched when O_2 was present in the solution. With the prolonging of reaction time, the fluorescence intensity of Ru $(DPP)_3Cl_2$ decreased gradually (**Figure 3H**). When the reaction time was 30 min, the fluorescence intensity of Ru $(DPP)_3Cl_2$ decreased to the lowest.

Catalytic Activity

CAT is an enzyme that catalyzes the decomposition of H_2O_2 to generate O_2. At 2 h, 68% of H_2O_2 was consumed with 2.5 $\mu g \cdot mL^{-1}$ of free CAT, 64% for DC@ZIF8-MEM_C with the same CAT concentration, indicating the same catalytic efficiency as that of free CAT (**Figure 3I**, **Supplementary Figure S7**). Comparatively, DC@ZIF8-MEM consumed barely H_2O_2. Thus, the catalytic activity of DC@ZIF8-MEM_C indeed was derived from CAT. CAT is unstable under physiological conditions, due to enzymic digestion by protein K. At 12 h, the catalytic activity decreased to 34% for free CAT, while 62% was maintained for

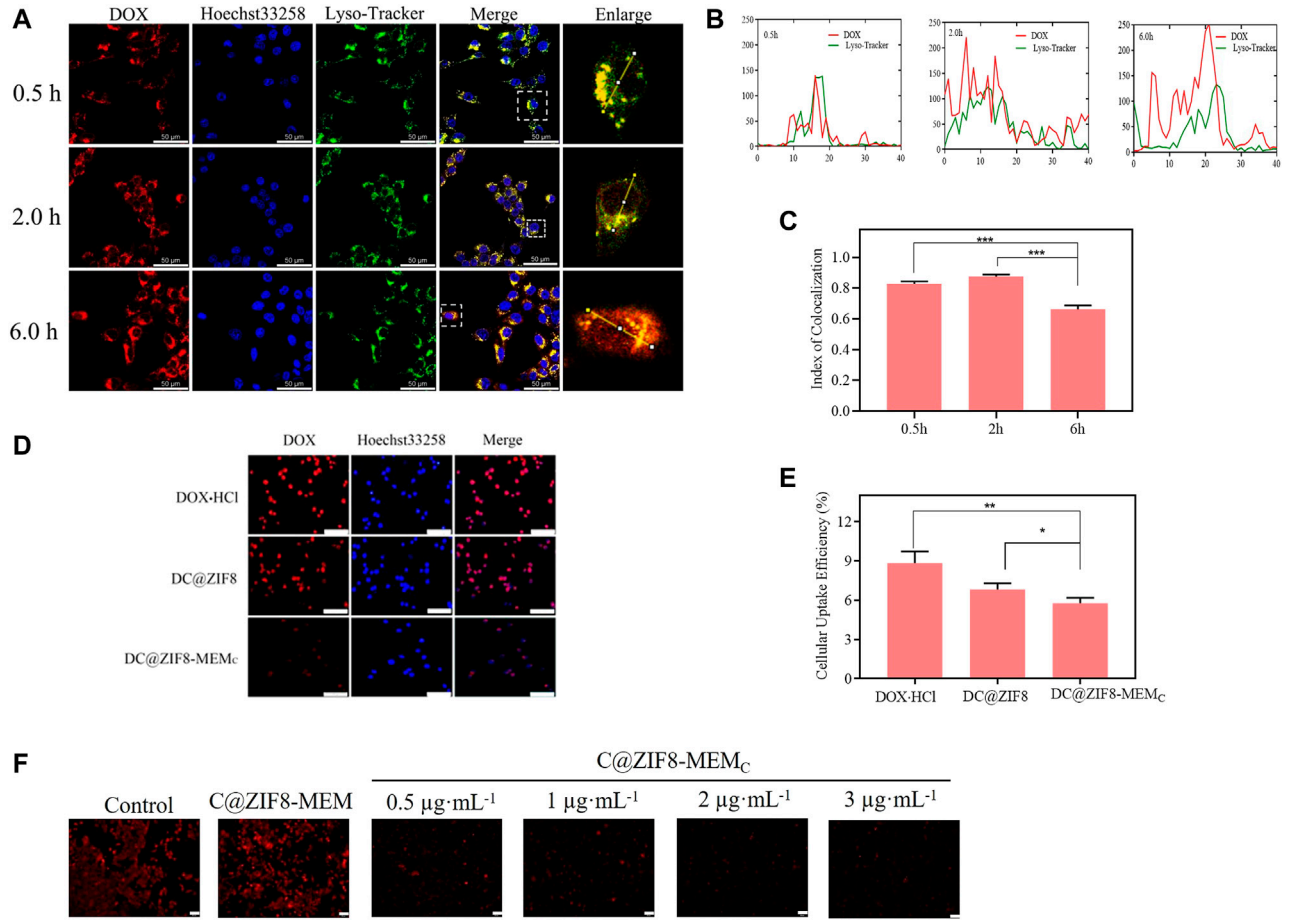


FIGURE 5 | Intracellular distribution fluorescence imaging of DC@ZIF8-MEM_C at different times by confocal laser microscopy (CLMS); scale bar = 50 μm **(A)**. Line-scan profiles of DC@ZIF8-MEM_C and Lysotracker after 0.5, 2, and 6 h incubation by ImageJ software. The level of the overlapped green line and red line is negatively correlated to endosomal escape of DC@ZIF8-MEM_C **(B)**. The index of colocalization of endocytosed DC@ZIF8-MEM_C (red) and endosome (green) was calculated by ImageJ software **(C)**. Cellular uptake of different samples incubated with RAW 264.7 cells for 24 h by fluorescent microscope; scale bar = 100 μm **(D)**. Cellular uptake efficiency of different samples to RAW 264.7cells by microplate reader **(E)**. Fluorescence images of 4T1 cells incubated with different samples and then stained with Ru $(DPP)_3Cl_2$; scale bar = 50 μm **(F)**. $^*p < 0.05$, $^{**}p < 0.01$, $^{***}p < 0.001$.

DC@ZIF8-MEM_C (**Figure 3J**). DC@ZIF8-MEM_C is capable of protecting CAT from degradation, which is useful for CAT delivery to maintain catalytic activity *in vivo*.

Cellular Uptake

To localize the cells, the cell nuclei were stained blue by Heochst-33258. The traffic of DOX·HCl inside the cells could be visualized by its intrinsic red fluorescence (**Figure 4A**). The fluorescence intensity of DC@ZIF8-MEM_C was stronger than that of other treatment groups, presenting the improved cellular uptake through endocytosis (**Figure 4A**). The relative fluorescence intensities were quantified, which suggested a higher uptake efficiency of DC@ZIF8-MEM_C, consistent with the result of qualitative analysis (**Figure 4B**, **Supplementary Figure S8**). It was attributed from MEM coating, which was helpful for accumulation at the tumor sites by passive targeting (Jiang et al., 2017; Ye et al., 2019).

Antitumor Activity *in vitro*

The *in vitro* tumor ablation was measured by MTT assays. The cell killing efficiency was dose dependent (**Figure 4C**). When concentration was at 5 $\mu g \cdot mL^{-1}$, the cell viability was 59%, 19% for free DOX·HCl, DC@ZIF8-MEM_C, respectively. Under laser irradiation, the cell viability of groups treated with DC@ZIF8-MEM_C decreased to 11%. DC@ZIF8-MEM_C indicated that a combination of CT and PTT as well as CAT was better than monotherapy alone.

As seen in **Figure 4E**, both DC@ZIF8-MEM_C and DC@ZIF8-MEM exhibited dose-dependent cytotoxicity. Under hypoxia condition (1% O_2), compared with DC@ZIF8-MEM, the cell viability of DC@ZIF8-MEM_C decreased significantly, demonstrating that the O_2 produced by CAT could alleviate hypoxia-induced resistance to DOX (12 versus 51% at 0.5 $\mu g \cdot mL^{-1}$). These results could explain, to some extent, why the treatment effect of DC@ZIF8-MEM_C was much better than DC@ZIF8-MEM *in vivo* experiment.

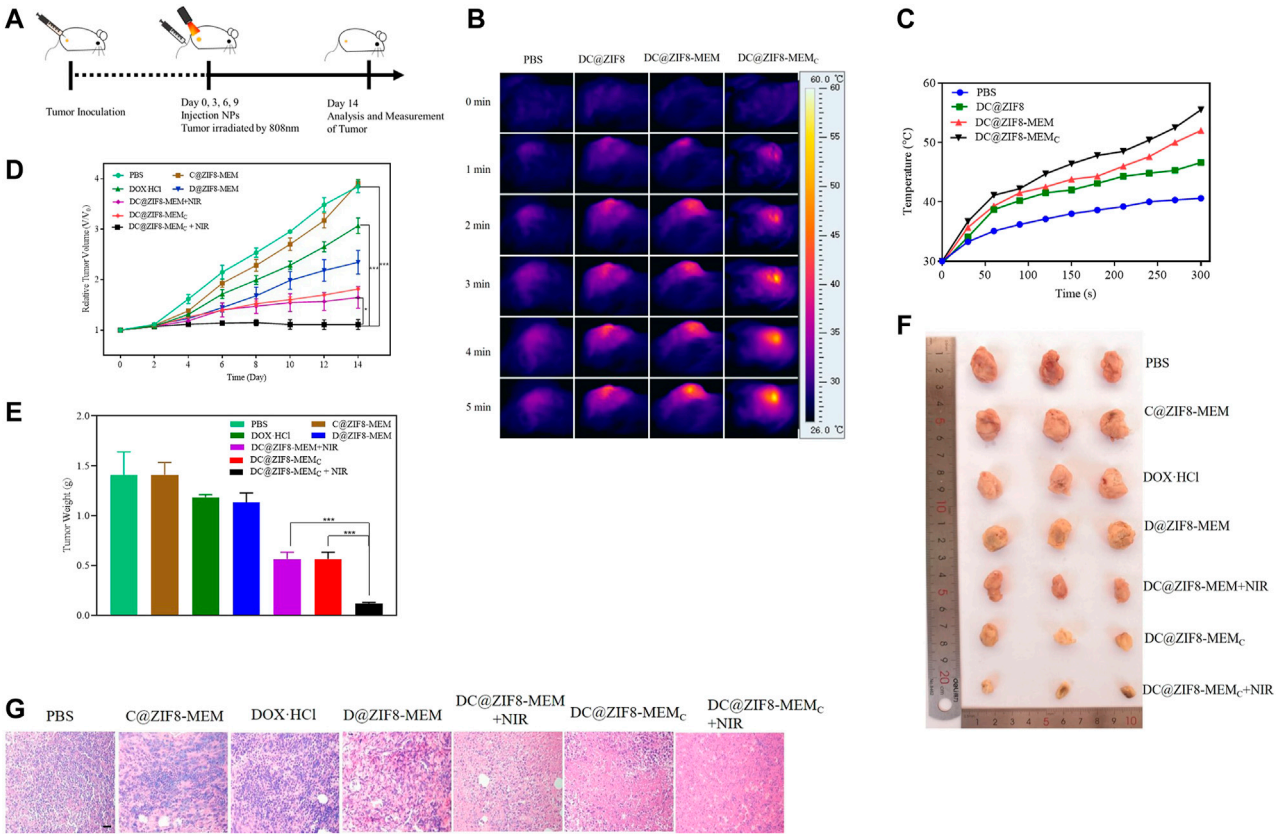


FIGURE 6 | Experimentation for the therapeutic model **(A)**. Photothermal images *in vivo* **(B)**. Temperature curves with 808 nm NIR at 2 W·cm^{-2} for 5 min **(C)**. Relative tumor volumes of mice with different treatments **(D)**. Tumor weights of mice after different treatments **(E)**. Representative digital photographs of excised tumor tissues of mice with different treatments **(F)**. H&E-stained images of tumor tissues from mice after different treatments on the 14th day; scale bar = 20 μm **(G)**. All the above data on mice in each group were averagely calculated (n = 5). *$p < 0.05$, **$p < 0.01$, ***$p < 0.001$.

In addition, when the concentration of NPs was 120 μg·mL^{-1}, the cell survival rate of C@ZIF8-MEM was 80.0%, and the cell survival rate decreased to 35.0% after NIR (**Figure 7A**). The results showed photo-responsive cytotoxicity of NPs.

To further evaluate the therapeutic outcome of the NPs, the treated cells were co-stained by calcein-AM and propidium iodide (PI) for live (green) and dead/late apoptotic cells (red), respectively (Liu et al., 2019). Both the control group and NIR group displayed strong green fluorescence (**Figure 4D**). However, compared with DOX·HCl and DC@ZIF8-MEM$_C$ groups, the red fluorescence was predominant for the DC@ZIF8-MEM$_C$ + NIR group, displaying a significant number of dead cells, which was in line with the results of cytotoxicity *in vitro* (**Figure 4D**).

Intracellular Location

As shown in **Figure 5A**, there were orange spots that emerged from the red and green channels, an evidence that red fluorescence of the majority of DC@ZIF8-MEM$_C$ was in colocalization with green fluorescence (endosomes/lysosomes) at 0.5 h. Over time, the amount of orange spots was weakened, and red color was evenly distributed throughout the cytoplasm, which showed minimal colocalization with the green fluorescence of the endo/lysosomes. The decreased colocalization signal of green and red fluorescence was visualized after 2 h due to the ongoing intracellular transport and rapid endosomal escape. Meaningfully, most of the overlapped signals disappeared after 6 h. The results presented that DC@ZIF8-MEM$_C$ entered the lysosome and then escaped into the cytoplasm after uptake into the cell. To semiquantitatively evaluate the capacity of endosomal escape for DC@ZIF8-MEM$_C$, the index of colocalization and line scanning profiles of fluorescent intensity of the selected 4T1 cells were calculated by ImageJ software, as given in **Figures 5B, C**.

These results jointly corroborated the efficient endosomal/lysosomal escape behaviors of DC@ZIF8-MEM$_C$, which was attributed to the ZIF8 frame. Under the lysosome pH (pH 4.5–5.5), the ZIF8 moiety could release the 2-methylimidazole ligand, which initiated the "proton-sponge" effect due to the protonation of imidazole rings and resulted in the rupture of lysosome membrane. (Liu Z et al., 2021). The rapid lysosomal escape capability of DC@ZIF8-MEM$_C$ was beneficial to maintain the enzymatic activity of CAT and the therapeutic activity of DOX from lysosome to cytoplasm (Varkouhi et al., 2011).

Immune Evasion

Red fluorescence was strong for DOX·HCl group, while weak it was for DC@ZIF8-MEM$_C$ group (**Figure 5D**). As shown in

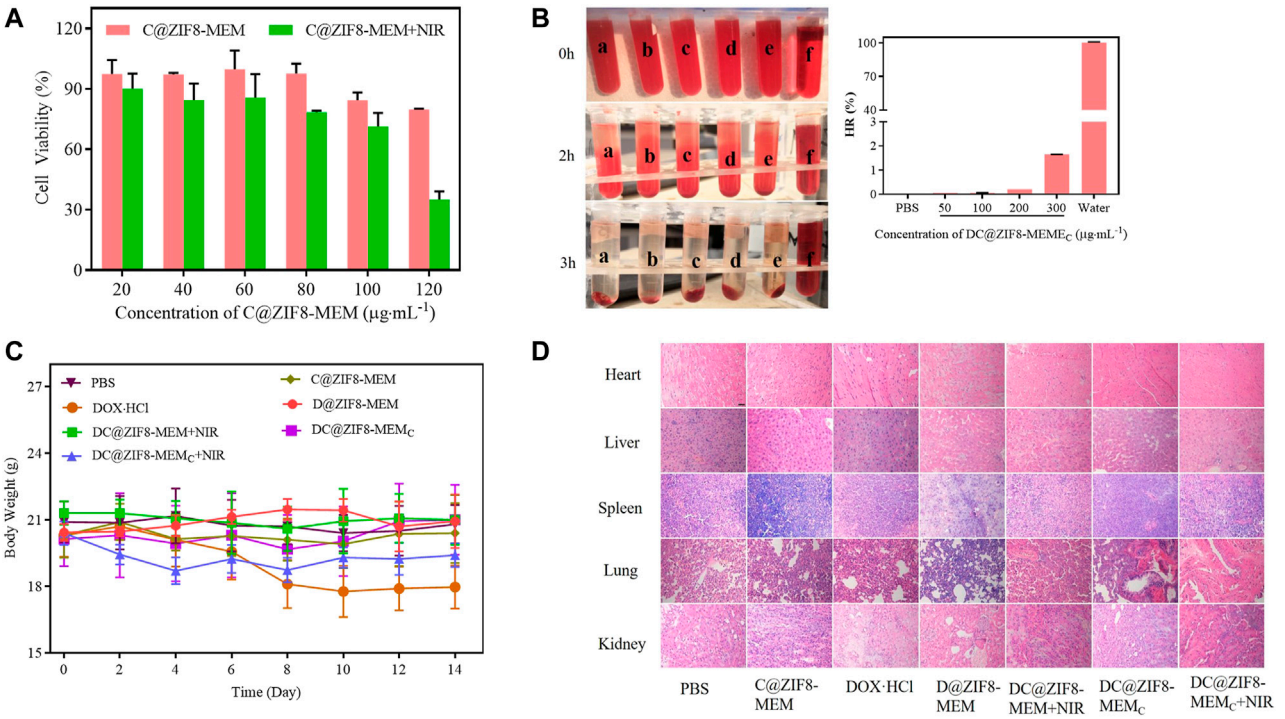


FIGURE 7 | Cell viability of C@ZIF8-MEM to 4T1 cells with and without NIR **(A)**. The hemolytic image (left) and hemolysis ratio of samples (right), PBS (a), 50 μg·mL^{-1} DC@ZIF8-MEM$_C$ (b), 100 μg·mL^{-1} DC@ZIF8-MEM$_C$ (c), 200 μg·mL^{-1} DC@ZIF8-MEM$_C$ (d), 300 μg·mL^{-1} DC@ZIF8-MEM$_C$ (e), deionized water (f) **(B)**. Body weights of mice with different treatments **(C)**. H&E analysis of major organs from mice after treatments; scale bar = 20 μm **(D)**.

Figure 5E, the uptake rate of DC@ZIF8-MEM$_C$ by RAW 264.7 cells were significantly lower than those of the other two groups, displaying that NPs camouflaged by blood cell membranes could avoid the phagocytosis of immune cells. As natural stealth coating, the cell membrane could alleviate immunogenicity and enhance biocompatibility (Graham and Unger, 2018).

Intracellular Oxygen Determination

Oxygen probe Ru(DPP)$_3$Cl$_2$ was applied for intracellular determination. The fluorescence of Ru(DPP)$_3$Cl$_2$ would be weakened in the presence of abundant O_2. As from **Figure 5F**, compared with the control group, the red fluorescence of C@ZIF8-MEM was strong and predominant, while that of the C@ZIF8-MEM$_C$ group was weak and marginal. For C@ZIF8-MEM without embedded CAT, the fluorescence of Ru (DPP)$_3$Cl$_2$ barely changed. However, the fluorescence change was weak due to the O_2 generation for the C@ZIF8-MEM$_C$ group. Moreover, the fluorescence tended to be weaker with the increase in CAT concentration of C@ZIF8-MEM$_C$. The results verified that the intracellular O_2 generation of C@ZIF8-MEM$_C$ originated from embedding the CAT.

Antitumor Effect *in vivo*

The experimentation for the therapeutic model is shown in **Figure 6A**. The antitumor effect was monitored by measuring the tumor size using a caliper every other day. With PBS or C@ZIF8-MEM treatment, the tumor grew rapidly over time (**Figure 6D**). Without irradiation, the DC@ZIF8-MEM$_C$ showed moderate tumor inhibition due to the CT of DOX·HCl and hypoxic improvement of CAT. Combined with irradiation, the tumor inhibition effect was significantly elevated (**Figure 6D**). The tumor weight was only 0.12 g for the DC@ZIF8-MEM$_C$ + NIR group, while the tumor weights were 1.19, 1.13, 0.57, and 0.57 g for DOX·HCl, DC@ZIF8-MEM, DC@ZIF8-MEM + NIR, and DC@ZIF8-MEM$_C$, respectively (**Figure 6E**). It could be clearly seen from the photographs of the extracted tumor tissues after treatment that the tumors treated with DC@ZIF8-MEM$_C$ plus irradiation were ablated significantly (**Figure 6F**). Interestingly, compared with the DC@ZIF8-MEM + NIR, the DC@ZIF8-MEM$_C$ + NIR group exhibited higher tumor inhibition effect, which may be attributed to amelioration of CAT for tumor hypoxia (**Figures 6D–F**). The results were consistent with cytotoxicity *in vitro*. Upon irradiation, DC@ZIF8-MEM$_C$ displayed the most effectivity in tumor inhibition, superior to other groups, indicating the advantages of combined cancer therapy. Tumor slices had a large area of necrosis for the DC@ZIF8-MEM$_C$ + NIR group, consistent with the therapeutic effect (**Figure 6G**).

Photothermal Effect *in vivo*

After continuous irradiation of the tumor site with the 808 nm near-infrared laser (2 W·cm^{-2}) for 5 min, the near-infrared imaging image of the tumor site is shown in **Figure 6B**. The

infrared light intensity of the tumor site for the DC@ZIF8-MEM_C group was significantly stronger than that of the other groups. **Figure 6C** shows the temperature rise curves of each group. The temperature of the DC@ZIF8-MEM group and the DC@ZIF8-MEM_C group changed rapidly within 1 min. After 5 min, the temperature of the tumor site increased to 40.1°C, 46.6°C, 52°C, and 55.5°C for PBS, DC@ZIF8, DC@ZIF8-MEM, and DC@ZIF8-MEM_C, respectively (**Figure 6C**). It presented that DC@ZIF8-MEM_C played an effective photothermal effect.

Biocompatibility and Safety

The biocompatibility of the NPs was evaluated. The cell viability of C@ZIF8-MEM displayed more than 80%, exhibiting good biocompatibility (**Figure 7A**, **Supplementary Figure S9**). The positive control (deionized water) showed obvious hemolysis, with HR as high as 100%. There was no hemolysis found for DC@ZIF8-MEM_C and PBS. HR of DC@ZIF8-MEM_C was less than 2% at a concentration as high as 300 $\mu g \cdot mL^{-1}$ (**Figure 7B**). Therefore, DC@ZIF8-MEM_C was highly biocompatible and could be directly administered by intravenous injection. There was no obvious decrease in body weight for all treatment groups except the DOX·HCl group (**Figure 7C**). Additionally, no significant histopathology changes were noticed for the main organs such as the heart, liver, spleen, lungs, and kidneys, suggesting invisible short-term toxicity during treatments (**Figure 7D**). These results demonstrated DC@ZIF8-MEM_C as promising for biomedicine application with high bio-safety.

CONCLUSION

In summary, biomimic DC@ZIF8-MEM_C was established and investigated. High DOX·HCl loading and self-generation of O_2 which enhanced CT and PTT, were realized. Furthermore, the superior controlled drug release, photothermal efficiency, and excellent biocompatibility of DC@ZIF8-MEM_C were retained for remarkable antitumor effect of chemo-thermo synergistic therapy. Our study sheds light on the great chemo-photothermal synergistic antitumor effect under the sensitization of CAT.

DATA AVAILABILITY STATEMENT

The original contributions presented in the study are included in the article/**Supplementary Material**, further inquiries can be directed to the corresponding authors.

ETHICS STATEMENT

The animal study was reviewed and approved by the Experimental Animal Ethics Committee of Xuzhou Medical University.

AUTHOR CONTRIBUTIONS

ZZ contributed to the design of the experiments, conceptualization, data analysis, and revised the draft. ZL performed the experiments and analyzed the data. YH performed the characterization and data interpretation. YP and GY participated in the cell experiments. SW and CH participated in the data collection and methodology. YZ contributed to the methodology, conceptualization, formal analysis, and revised the draft. YY designed the work and wrote the draft. All authors approved the final version of the manuscript to be submitted.

FUNDING

This work was supported by the National Nature Science Foundation of China (No. 81773643).

SUPPLEMENTARY MATERIAL

The Supplementary Material for this article can be found online at: https://www.frontiersin.org/articles/10.3389/fphar.2022.850534/full#supplementary-material

REFERENCES

Chen, H., He, W., and Guo, Z. (2014). An H_2O_2-Responsive Nanocarrier for Dual-Release of Platinum Anticancer Drugs and O_2: Controlled Release and Enhanced Cytotoxicity against Cisplatin Resistant Cancer Cells. *Chem. Commun.* 50, 9714–9717. doi:10.1039/c4cc03385j

Chen, L., Zhou, L., Wang, C., Han, Y., Lu, Y., Liu, J., et al. (2019). Tumor-Targeted Drug and CpG Delivery System for Phototherapy and Docetaxel-Enhanced Immunotherapy with Polarization toward M1-type Macrophages on Triple Negative Breast Cancers. *Adv. Mater.* 31, e1904997. doi:10.1002/adma.201904997

Ding, X., Liu, J., Li, J., Wang, F., Wang, Y., Song, S., et al. (2016). Polydopamine Coated Manganese Oxide Nanoparticles with Ultrahigh Relaxivity as Nanotheranostic Agents for Magnetic Resonance Imaging Guided Synergetic Chemo-/photothermal Therapy. *Chem. Sci.* 7, 6695–6700. doi:10.1039/c6sc01320a

Gao, L., Chen, Q., Gong, T., Liu, J., and Li, C. (2019). Recent Advancement of Imidazolate Framework (ZIF-8) Based Nanoformulations for Synergistic Tumor Therapy. *Nanoscale* 11, 21030–21045. doi:10.1039/c9nr06558j

Góth, L. (1991). A Simple Method for Determination of Serum Catalase Activity and Revision of Reference Range. *Clin. Chim. Acta* 196, 143–151. doi:10.1016/0009-8981(91)90067-m

Graham, K., and Unger, E. (2018). Overcoming Tumor Hypoxia as a Barrier to Radiotherapy, Chemotherapy and Immunotherapy in Cancer Treatment. *Int. J. Nanomedicine* 13, 6049–6058. doi:10.2147/IJN.S140462

He, T., Jiang, C., He, J., Zhang, Y., He, G., Wu, J., et al. (2021). Manganese-Dioxide-Coating-Instructed Plasmonic Modulation of Gold Nanorods for Activatable Duplex-Imaging-Guided NIR-II Photothermal-Chemodynamic Therapy. *Adv. Mater.* 33, 2008540. doi:10.1002/adma.202008540

Jang, B., Moorthy, M. S., Manivasagan, P., Xu, L., Song, K., Lee, K. D., et al. (2018). Fucoidan-coated CuS Nanoparticles for Chemo-And Photothermal Therapy against Cancer. *Oncotarget* 9, 12649–12661. doi:10.18632/oncotarget.23898

Jiang, Q., Luo, Z., Men, Y., Yang, P., Peng, H., Guo, R., et al. (2017). Red Blood Cell Membrane-Camouflaged Melanin Nanoparticles for Enhanced Photothermal Therapy. *Biomaterials* 143, 29–45. doi:10.1016/j.biomaterials.2017.07.027

Jiang, X., Sun, Y., Shang, L., Yang, C., Kong, L., and Zhang, Z. (2019). Green tea Extract-Assembled Nanoclusters for Combinational Photothermal and Chemotherapy. *J. Mater. Chem. B* 7, 5972–5982. doi:10.1039/c9tb01546a

Jing, X., Yang, F., Shao, C., Wei, K., Xie, M., Shen, H., et al. (2019). Role of Hypoxia in Cancer Therapy by Regulating the Tumor Microenvironment. *Mol. Cancer* 18, 157. doi:10.1186/s12943-019-1089-9

Li, D., Chen, H., Fan, K., Labunov, V., Lazarouk, S., Yue, X., et al. (2021). A Supersensitive Silicon Nanowire Array Biosensor for Quantitating Tumor Marker ctDNA. *Biosens. Bioelectron.* 181, 113147. doi:10.1016/j.bios.2021.113147

Li, J., Cheng, Q., Yue, L., Gao, C., Wei, J., Ding, Y., et al. (2021). Macrophage-hitchhiking Supramolecular Aggregates of CuS Nanoparticles for Enhanced Tumor Deposition and Photothermal Therapy. *Nanoscale Horiz* 6, 907–912. doi:10.1039/d1nh00291k

Li, Q. L., Sun, Y., Ren, L., Wang, X., Wang, C., Li, L., et al. (2018). Supramolecular Nanosystem Based on Pillararene-Capped CuS Nanoparticles for Targeted Chemo-Photothermal Therapy. *ACS Appl. Mater. Inter.* 10, 29314–29324. doi:10.1021/acsami.8b09330

Li, Z., Chen, Y., Yang, Y., Yu, Y., Zhang, Y., Zhu, D., et al. (2019). Recent Advances in Nanomaterials-Based Chemo-Photothermal Combination Therapy for Improving Cancer Treatment. *Front. Bioeng. Biotechnol.* 7, 293. doi:10.3389/fbioe.2019.00293

Lian, X., Fang, Y., Joseph, E., Wang, Q., Li, J., Banerjee, S., et al. (2017). Enzyme-MOF (Metal-organic Framework) Composites. *Chem. Soc. Rev.* 46, 3386–3401. doi:10.1039/c7cs00058h

Liu, H., Chen, D., Li, L., Liu, T., Tan, L., Wu, X., et al. (2011). Multifunctional Gold Nanoshells on Silica Nanorattles: a Platform for the Combination of Photothermal Therapy and Chemotherapy with Low Systemic Toxicity. *Angew. Chem. Int. Ed. Engl.* 50, 891–895. doi:10.1002/anie.201002820

Liu, H., Guo, Z., Zhang, Q., Jin, B., and Peng, R. (2021). Zeolite Imidazolate Frameworks-67 Precursor to Fabricate a Highly Active Cobalt-Embedded N-Doped Porous Graphitized Carbon Catalyst for the Thermal Decomposition of Ammonium Perchlorate. *ACS Omega* 6, 25440–25446. doi:10.1021/acsomega.1c03427

Liu, P., Xie, X., Shi, X., Peng, Y., Ding, J., and Zhou, W. (2019). Oxygen-Self-Supplying and HIF-1α-Inhibiting Core-Shell Nanosystem for Hypoxia-Resistant Photodynamic Therapy. *ACS Appl. Mater. Inter.* 11, 48261–48270. doi:10.1021/acsami.9b18112

Liu, Z., Zhang, L., Cui, T., Ma, M., Ren, J., and Qu, X. (2021). A Nature-Inspired Metal-Organic Framework Discriminator for Differential Diagnosis of Cancer Cell Subtypes. *Angew. Chem. Int. Ed.* 60, 15436–15444. doi:10.1002/anie.202102286

Park, K. S., Ni, Z., Côté, A. P., Choi, J. Y., Huang, R., Uribe-Romo, F. J., et al. (2006). Exceptional Chemical and thermal Stability of Zeolitic Imidazolate Frameworks. *Proc. Natl. Acad. Sci. U S A.* 103, 10186–10191. doi:10.1073/pnas.0602439103

Phua, S. Z. F., Yang, G., Lim, W. Q., Verma, A., Chen, H., Thanabalu, T., et al. (2019). Catalase-Integrated Hyaluronic Acid as Nanocarriers for Enhanced Photodynamic Therapy in Solid Tumor. *Acs Nano* 13, 4742–4751. doi:10.1021/acsnano.9b01087

Piao, J. G., Wang, L., Gao, F., You, Y. Z., Xiong, Y., and Yang, L. (2014). Erythrocyte Membrane Is an Alternative Coating to Polyethylene Glycol for Prolonging the Circulation Lifetime of Gold Nanocages for Photothermal Therapy. *Acs Nano* 8, 10414–10425. doi:10.1021/nn503779d

Samanta, D., Gilkes, D. M., Chaturvedi, P., Xiang, L., and Semenza, G. L. (2014). Hypoxia-inducible Factors Are Required for Chemotherapy Resistance of Breast Cancer Stem Cells. *Proc. Natl. Acad. Sci. U S A.* 111, E5429–E5438. doi:10.1073/pnas.1421438111

Shi, H., Yan, R., Wu, L., Sun, Y., Liu, S., Zhou, Z., et al. (2018). Tumor-targeting CuS Nanoparticles for Multimodal Imaging and Guided Photothermal Therapy of Lymph Node Metastasis. *Acta Biomater.* 72, 256–265. doi:10.1016/j.actbio.2018.03.035

Song, G., Chen, Y., Liang, C., Yi, X., Liu, J., Sun, X., et al. (2016). Catalase-Loaded TaOx Nanoshells as Bio-Nanoreactors Combining High-Z Element and Enzyme Delivery for Enhancing Radiotherapy. *Adv. Mater.* 28, 7143–7148. doi:10.1002/adma.201602111

Sun, C. Y., Qin, C., Wang, X. L., Yang, G. S., Shao, K. Z., Lan, Y. Q., et al. (2012). Zeolitic Imidazolate Framework-8 as Efficient pH-Sensitive Drug Delivery Vehicle. *Dalton Trans.* 41, 6906–6909. doi:10.1039/c2dt30357d

Szatrowski, T. P., and Nathan, C. F. (1991). Production of Large Amounts of Hydrogen Peroxide by Human Tumor Cells. *Cancer Res.* 51, 794–798.

Tang, S., Chen, M., and Zheng, N. (2014). Sub-10-nm Pd Nanosheets with Renal Clearance for Efficient Near-Infrared Photothermal Cancer Therapy. *Small* 10, 3139–3144. doi:10.1002/smll.201303631

Varkouhi, A. K., Scholte, M., Storm, G., and Haisma, H. J. (2011). Endosomal Escape Pathways for Delivery of Biologicals. *J. Control Release* 151, 220–228. doi:10.1016/j.jconrel.2010.11.004

Vaupel, P., and Mayer, A. (2016). Tumor Hypoxia: Causative Mechanisms, Microregional Heterogeneities, and the Role of Tissue-Based Hypoxia Markers. *Adv. Exp. Med. Biol.* 923, 77–86. doi:10.1007/978-3-319-38810-6_11

Win, K. Y., and Feng, S. S. (2005). Effects of Particle Size and Surface Coating on Cellular Uptake of Polymeric Nanoparticles for Oral Delivery of Anticancer Drugs. *Biomaterials* 26, 2713–2722. doi:10.1016/j.biomaterials.2004.07.050

Wu, Q., Niu, M., Chen, X., Tan, L., Fu, C., Ren, X., et al. (2018). Biocompatible and Biodegradable Zeolitic Imidazolate Framework/polydopamine Nanocarriers for Dual Stimulus Triggered Tumor Thermo-Chemotherapy. *Biomaterials* 162, 132–143. doi:10.1016/j.biomaterials.2018.02.022

Yang, Y., Wang, Z., Peng, Y., Ding, J., and Zhou, W. (2019). A Smart pH-Sensitive Delivery System for Enhanced Anticancer Efficacy via Paclitaxel Endosomal Escape. *Front. Pharmacol.* 10, 10. doi:10.3389/fphar.2019.00010

Ye, S., Wang, F., Fan, Z., Zhu, Q., Tian, H., Zhang, Y., et al. (2019). Light/pH-Triggered Biomimetic Red Blood Cell Membranes Camouflaged Small Molecular Drug Assemblies for Imaging-Guided Combinational Chemo-Photothermal Therapy. *ACS Appl. Mater. Inter.* 11, 15262–15275. doi:10.1021/acsami.9b00897

Yin, J., Cao, H., Wang, H., Sun, K., Li, Y., and Zhang, Z. (2020). Phospholipid Membrane-Decorated Deep-Penetrated Nanocatalase Relieve Tumor Hypoxia to Enhance Chemo-Photodynamic Therapy. *Acta Pharm. Sin. B* 10, 2246–2257. doi:10.1016/j.apsb.2020.06.004

Yue, C., Liu, P., Zheng, M., Zhao, P., Wang, Y., Ma, Y., et al. (2013). IR-780 Dye Loaded Tumor Targeting Theranostic Nanoparticles for NIR Imaging and Photothermal Therapy. *Biomaterials* 34, 6853–6861. doi:10.1016/j.biomaterials.2013.05.071

Zhang, L., Zhang, Y., Xue, Y., Wu, Y., Wang, Q., Xue, L., et al. (2019). Transforming Weakness into Strength: Photothermal-Therapy-Induced Inflammation Enhanced Cytopharmaceutical Chemotherapy as a Combination Anticancer Treatment. *Adv. Mater.* 31, e1805936. doi:10.1002/adma.201805936

Zhang, R., Song, X., Liang, C., Yi, X., Song, G., Chao, Y., et al. (2017). Catalase-loaded Cisplatin-Prodrug-Constructed Liposomes to Overcome Tumor Hypoxia for Enhanced Chemo-Radiotherapy of Cancer. *Biomaterials* 138, 13–21. doi:10.1016/j.biomaterials.2017.05.025

Zhang X, X., Xi, Z., Machuki, J. O., Luo, J., Yang, D., Li, J., et al. (2019). Gold Cube-In-Cube Based Oxygen Nanogenerator: A Theranostic Nanoplatform for Modulating Tumor Microenvironment for Precise Chemo-Phototherapy and Multimodal Imaging. *ACS Nano* 13, 5306–5325. doi:10.1021/acsnano.8b09786

Zhao, P., Zheng, M., Yue, C., Luo, Z., Gong, P., Gao, G., et al. (2014). Improving Drug Accumulation and Photothermal Efficacy in Tumor Depending on Size of ICG Loaded Lipid-Polymer Nanoparticles. *Biomaterials* 35, 6037–6046. doi:10.1016/j.biomaterials.2014.04.019

Zhao, Y., Zhao, T., Cao, Y., Sun, J., Zhou, Q., Chen, H., et al. (2021). Temperature-Sensitive Lipid-Coated Carbon Nanotubes for Synergistic Photothermal Therapy and Gene Therapy. *ACS Nano* 15, 6517–6529. doi:10.1021/acsnano.0c08790

Zhen, X., Xie, C., and Pu, K. (2018). Temperature-Correlated Afterglow of a Semiconducting Polymer Nanococktail for Imaging-Guided Photothermal Therapy. *Angew. Chem. Int. Ed. Engl.* 57, 3938–3942. doi:10.1002/anie.201712550

Zhu, W., Chen, M., Liu, Y., Tian, Y., Song, Z., Song, G., et al. (2019). A Dual Factor Activated Metal-Organic Framework Hybrid Nanoplatform for Photoacoustic Imaging and Synergetic Photo-Chemotherapy. *Nanoscale* 11, 20630–20637. doi:10.1039/c9nr06349h

Zhu, Y., Meng, T., Tan, Y., Yang, X., Liu, Y., Liu, X., et al. (2018). Negative Surface Shielded Polymeric Micelles with Colloidal Stability for Intracellular Endosomal/Lysosomal Escape. *Mol. Pharm.* 15, 5374–5386. doi:10.1021/acs.molpharmaceut.8b00842

Zhuang, J., Kuo, C. H., Chou, L. Y., Liu, D. Y., Weerapana, E., and Tsung, C. K. (2014). Optimized Metal-Organic-Framework Nanospheres for Drug Delivery: Evaluation of Small-Molecule Encapsulation. *ACS Nano* 8, 2812–2819. doi:10.1021/nn406590q

Zou, M. Z., Liu, W. L., Li, C. X., Zheng, D. W., Zeng, J. Y., Gao, F., et al. (2018). A Multifunctional Biomimetic Nanoplatform for Relieving Hypoxia to Enhance Chemotherapy and Inhibit the PD-1/pd-L1 Axis. *Small* 14, e1801120. doi:10.1002/smll.201801120

Conflict of Interest: The authors declare that the research was conducted in the absence of any commercial or financial relationships that could be construed as a potential conflict of interest.

Publisher's Note: All claims expressed in this article are solely those of the authors and do not necessarily represent those of their affiliated organizations, or those of the publisher, the editors, and the reviewers. Any product that may be evaluated in this article, or claim that may be made by its manufacturer, is not guaranteed nor endorsed by the publisher.

Copyright © 2022 Zhao, Liu, Hua, Pan, Yi, Wu, He, Zhang and Yang. This is an open-access article distributed under the terms of the Creative Commons Attribution License (CC BY). The use, distribution or reproduction in other forums is permitted, provided the original author(s) and the copyright owner(s) are credited and that the original publication in this journal is cited, in accordance with accepted academic practice. No use, distribution or reproduction is permitted which does not comply with these terms.

frontiers | Frontiers in Oncology

REVIEW
published: 28 April 2022
doi: 10.3389/fonc.2022.898605

Exosome-Based Nanoplatforms: The Emerging Tools for Breast Cancer Therapy

Quan Liu[1†], *Xian Zhang*[2†] *and Jun Zhang*[3*]

[1] Department of Thyroid and Breast Surgery, Xiantao First People's Hospital Affiliated to Yangtze University, Xiantao, China, [2] Ningxia Key Laboratory of Cerebrocranial Diseases, Incubation Base of the National Key Laboratory, Ningxia Medical University, Yinchuan, China, [3] Department of Thyroid and Breast Surgery, Shenzhen Qianhai Shekou Free Trade Zone Hospital, Shenzhen, China

OPEN ACCESS

Edited by:
Zeming Liu,
Huazhong University of Science and Technology, China

Reviewed by:
Yawen Guo
Zhejiang University, China
Yuanbiao Tu,
Jiangxi University of Traditional Chinese Medicine, China
Ji Zhang,
University of Toronto, Canada

***Correspondence:**
Jun Zhang
zhangjunshekou@163.com

[†]*These authors have contributed equally to this work and share first authorship*

Specialty section:
This article was submitted to Pharmacology of Anti-Cancer Drugs, a section of the journal Frontiers in Oncology

Received: *17 March 2022*
Accepted: *04 April 2022*
Published: *28 April 2022*

Citation:
Liu Q, Zhang X and Zhang J (2022) Exosome-Based Nanoplatforms: The Emerging Tools for Breast Cancer Therapy. Front. Oncol. 12:898605. doi: 10.3389/fonc.2022.898605

Breast cancer (BC) remains the leading malignant tumor type among females worldwide. The patients with BC are still faced with undesirable metastasis, relapse rate, and drug resistance. Exosomes are defined as naturally occurring extracellular vesicles (EVs) with typical biomarkers that reflect the characteristics of the parent cells. Exosomes are crucial mediators involved in intercellular communication. By transferring multiple cargoes, represented by proteins, nucleic acids, lipids, metabolites, exosomes contribute to reshaping the recipient cell function and fate. Growing evidence has documented that exosomes originating from BC cells are important participants involved in BC progression and treatments. Nanoparticle-based technology is the cutting-edge field for renewing pharmaceuticals and has endowed deep improvements in precise BC treatment. Additionally, due to their perfect features of the low immune prototype, limited adverse effects, prolongated circulation, and easy modification, exosomes have received much attention as candidates in nano-medicine of BC. The nanoplatforms constructed by exosomes have safety, intelligence, biomimetic, and controlled released advantages for combating BC. Here, we emphasize the multiple exosomes from a variety of cell sources in constructing nanoplatforms for BC therapy, mainly including exosomes and their cargoes, genetically engineered exosomes, and exosome-based carriers. This field would shed light on the promising exosome-based delivery system in BC therapy.

Keywords: breast cancer, exosome, nanoparticle, therapy, drug-resistance

Abbreviations: ADSCs, adipose-derived stem cells; BC, breast cancer; CSCs, cancer stem cells; CARs, chimeric antigen receptors; circRNAs, circular RNA; CTCs, circulating tumor cells; CBSA, conjugating cationic bovine serum albumin; COX-2, cyclooxygenase-2; DPSCs, dental pulp mesenchymal stem cells; DOX, doxorubicin; EPR, enhanced permeability and retention; EGFR, epidermal growth factor receptor; EMT, epithelial to mesenchymal transition; NK-EM, exosome mimetics from NK cells; ENVs, exosome-like nanovesicles; eNVs-FAP, exosome-like nanovesicles; EVs, extracellular vesicles; FAP, fibroblast activation protein-α; FA, folic acid; GNV, grapefruit-derived nanovector; HER2,human epidermal growth factor receptor 2; HUCMSCs human umbilical cord mesenchymal stem cells; HA, hyaluronic acid; HE, hybrid exosomes; lncRNAs, long noncoding RNAs; MSCs, mesenchymal stem cells; MSLN, mesothelin; MIT, mitoxantrone; MVBs, multivesicular bodies (MVBs); MDSCs, myeloid-derived suppressor cells;NK, natural killer; PTX, paclitaxel;ROS, reactive oxygen species;Tregs, regulatory T cells; sEVs, small EVs; TNBC, Triple-negative breast cancer; TME, tumor microenvironment; US, ultrasound.

INTRODUCTION

Breast cancer (BC) remains the leading cause of cancer-caused death in females and its incidence is still rising worldwide (1). Despite the advancement of early diagnosis procedures and mature therapeutic strategies, such as mastectomy, chemotherapy, immunotherapy, and combined therapy, BC patients are still faced with vicious metastasis, relapse rate, and drug resistance (2). BC is a highly heterogeneous and complex entity. The BC tumor microenvironment (TME) consists of tumor cells and stromal cells, soluble cytokines, immune cells, which directly or indirectly impact tumor behaviors and thus establish tumor-favoring niches for supporting tumorous growth and colonization (3). It is still a difficult problem to figure out the detailed mechanism of tumor occurrence and development and improve the efficiency of tumor treatment strategies.

Exosomes are defined as naturally occurring extracellular vesicles (EVs) with approximately 30-150 nm in diameter (4). Exosomes are originated from endocytic multivesicular bodies (MVBs) followed by exosome formation and secretion into extracellular space. In respect of the typical biomarkers, exosomes are particularly rich in a series of conserved proteins that reflect the characteristics of the parent cells, including the tetraspanin transmembrane-4 family (CD9, CD63, and CD81), Hsp90, caveolins, clathrin, and transferrin receptors (5). Generally speaking, exosomes serve as a warehouse that stores a large amount of biologically active molecules, such as lipids, enzymes, mRNAs, metabolites, and various non-coding RNAs, represented by miRNAs, long noncoding RNAs (lncRNAs), and circular RNA (circRNAs) (6). By transferring these cargoes, exosomes play roles in dynamic intercellular communication between tumor cells and adjacent stromal compartments in cancer progression (7). It is well-documented that tumor-derived exosomal RNAs affect the function of recipient cells in the neighborhood and distant sites, leading to tumor growth, metastasis, detection, and drug resistance in BC (8). For example, Ohno et al. used exosomes to deliver let-7a miRNA, which was transferred and internalized to epidermal growth factor receptor (EGFR)-expressing in tumor tissues, exhibiting extraordinary tumor therapeutic effects (9). Santos et al. reported that miR-155 in exosomes isolated from cancer stem cells (CSCs) and resistant cells could be transferred to recipient cells (10). This implies that exosomes may modulate resistance and migration ability to recipient BC cells partially through exosomal transfer to sensitive tumor cells.

Nanoparticle-based technology has endowed deep improvements in precise BC treatment. In consideration of the excellent biosafety, low immunogenicity, carrier properties, and nanoscale penetration effect, exosomes have attracted considerable attention in drug delivery systems for cancer therapy (11). The reported applications of exosomes mainly vary from enhanced efficiency in cancer drug delivery, drug-carrying system, to immunogenicity of cancer vaccines (12). The nanoplatforms constructed by exosomes possess enhanced functionalities with safety, intelligence, biomimetic, and controlled released advantages for combating BC (13). Therefore, this review aims to decipher the exosome potential serving as therapeutic carriers, hoping for offering an in-depth understanding of exosome-based based nanoplatforms for BC therapy.

To summarize the landscape of the potential applications, we have searched exosomes, breast cancer, and therapy on Pubmed over the last 10 years as keywords. These pieces of topically-relevant literature, involving molecular, cellular, and animal studies as well as clinical samples, are all included in this review.

EXOSOMES AND THEIR CARGOES

Exosomes in BC Therapy

Mesenchymal stem cells (MSCs) have gained increasing interest in the field of regeneration and disease treatment due to their multilineage differentiation potential and powerful immunomodulatory and regenerative functions (14). MSC-derived exosomes are a new cell-free alternative to MSCs that has long been a major concern (15). MSC-derived exosomes offer unparalleled advantages in terms of safety, bioactivity, storage, and transport compared to previous MSC transplantation (16). Yu et al. posed that miR-342-3p was down-expressed in advanced BC patients and was of potential to suppress BC metastasis, cell survivability, and drug resistance (17). This result was partially caused by MSC-derived exosome miR-342-3p through binding ID4. The clinical samples with primary BC showed poor expression of miR-148b-3p. In both *in vitro* and *in vitro* validation, human umbilical cord mesenchymal stem cells (HUCMSCs) -derived exosomes carrying miR-148b-3p showed efficient inhibition of MDA-MB-231 cells (18). This suggested that miR-148b-3p-containing exosomes might represent an efficient and facile carrier for BC treatment. In addition, HUCMSC exosomes harboring miR-3182 could inhibit triple-negative breast cancer (TNBC) in invasion *in vitro*, demonstrating that miR-3182-containing exosomes may be a dependable therapeutic option in treating TNBC (19).

Natural killer (NK) cells are intrinsic lymphocytes that play a key role in tumor immune surveillance and are being actively investigated for adoptive cell therapies in cancer immunotherapy (20). NK cell-derived exosomes have a natural and excellent killing effect on tumor cells. The canine NK-exosomes were capable of significantly suppressing tumor size and reducing CD133 expression, representing a promising vehicle for the treatment in an experimental murine BC model (21). Zhu et al. separated the exosome mimetics (NK-EM) from NK cells by extruding NK cells into filters with gradually smaller pore sizes (22). NK-EM exhibited strong tumor-killing activity against tumors in mice such as glioblastoma and BC, compared to low or high doses of NK-Exo.

Exosome Pre-Condition in BC Therapy

Several studies have shown that the use of exosome derivatives or exosome pre-injection can reduce the accumulation of other exosomal carriers or nanodrug carriers in the liver and thus more effectively promote drug enrichment at the target site. Based on exosomes derived from metastatic 4T1 cells, exosome-like nanovesicles (ENVs) were developed (23). Pre-treatment with 4T1 ENVs reduced the evasion of Kupffer cell-mediated

phagocytosis by DOTAP/DOPE liposomes, thereby promoting greater recruitments of DOTAP/DOPE carriers to tumor metastasis, reducing the IC50 of chemotherapeutic drug doxorubicin (DOX), and avoiding adverse side effects. Besides, the accumulation of subsequently injected grapefruit-derived nanovector (GNV) decreased in the lungs, but not the liver, was increased by prior intravenous injection of peripheral blood-derived exosomes in mice (24). Meanwhile, the efficiency of GNV-carrying DOX or paclitaxel (PTX) for the treatment of lung metastases was improved. Exosome-mediated inhibitory effects of GNV into hepatic macrophages were dependent on CD36 and IGFR1 receptor-mediated pathways. Thus, autologous exosome pre-treatment not only accumulated GNV signals in the primary tumor, but also improved the therapeutic efficacy against pulmonary metastases. Melzer et al. treated MSC with sublethal concentrations of PTX and found that the treated MSC exosomes had more potent tumor-specific and targeting properties compared with PTX of equivalent effect (25). In addition, the distribution of MSC PTX exosomes in major organs was reduced by approximately 50% and effectively reduced subcutaneous graft tumor volume by 60%.

GENETICALLY ENGINEERED EXOSOMES

Several features of MSCs may also be transmitted to exosomes, including weak immunogenicity with lack of MHC-II and co-stimulatory ligands, multi-organ homing ability mediated by the expression of specific surface molecules, and high biosafety characteristics (26). The available reports are controversial as to whether MSC-derived exosomes are tumor-promoting or tumor-suppressing in different tumor types. However, MSC-derived exosomes modified by gene editing can certainly overexpress a specific therapeutic RNA or protein to exert tumor-suppressive effects.

MSC exosomes expressing suicide or tumor-killing genes represent an emerging class of tumor-targeting drugs and vector models that act within tumor cells for the treatment of breast tumors (27). Exosomes from generationally modified MSCs can perform as an effective targeting delivery system to specifically target HER2+ cell lines, resulting in corresponding changes in tumor death (28). O'Brien et al. harnessed the tumor homing ability of MSCs to construct miR-379-enriched MSC-EVs, which could significantly inhibit BC tumor growth and promote necrosis, depending on the regulation of cyclooxygenase-2 (COX-2) expression (29). Vakhshiteh et al. established an ex-novo exosome nanocarrier, which was derived from miR-34a-overexpressed dental pulp mesenchymal stem cells (DPSCs), weakened the capability of migration and invasion in MDA-MB-231 cells (30). MSCs-Exo effectively transported LNA-antimiR-142-3p to breast CSC-like cells, thereby reducing miR-142-3p and miR-150 expression (31). Furthermore, inhibiting oncomiRs by transmitting LNA-antimiR-142-3p induced a dramatic lowering of clone formation and tumor initiation capability.

Genetically engineered T cells expressing chimeric antigen receptors (CARs) have become a force to be reckoned with in tumor immunotherapy (32). Exosomes derived from CAR-T cells could facilitate BC immunotherapy by providing higher efficacy and safety (33). Yang et al. successfully isolated exosomes from mesothelin (MSLN)-targeted CAR-T cells, which maintained most of the traits of their parental T cells, including surface expression of CARs and CD3 (34). In addition, CAR-carrying exosomes significantly suppressed the growth of MSLN-positive TNBC cells by secreting perforin and granzyme B, as well as efficiently inhibited the xenograft tumors without noticeable side effects. Conversion of M2 macrophages to the M1 phenotype employing miRNA-containing exosomes is a possible route to inhibit BC tumor invasion and metastasis (35). By using tumor-derived exosomes as carriers, miR-130 was transported to M2 macrophages, which in turn impaired the ability of tumor cells to proliferate, migrate and invade (36). Yue et al. reported that PGRN-/- TAMs restrained BC cell invasion and epithelial to mesenchymal transition (EMT) through releasing their exosomes (37). MiR-5100 upregulation of PGRN-/- TAMs-derived exosomes might modify CXCL12 expression, thereby dampening the CXCL12/CXCR4 axis and consequently resulting in BC malignant alteration. Shi et al. reported the genetically engineered cell-derived platform for developing targeted BC immunotherapy (38). They constructed a dual-targeting exosome platform for T-cell CD3 and BC-specific human epidermal growth factor receptor 2 (HER2) receptors, which was capable of targeted activation of CD8+ T cells and potent killing of HER2 tumor cells, demonstrating promising immunotherapeutic effects.

Adipose-derived stem cells (ADSCs) are considered to be an important tool for cell therapy and regeneration because of their abundant source, easy extraction, and ability to multidirectional differentiation (39). Exosomes are an important bearer form of the secretory profile of ADSCs. Exosomes are capable of delivering to recipient cells some nucleic acids, small molecules, and protein substances that are embedded in MSCs (40). Shojaei et al. successfully isolated ADSC-exosomes and found that miR-381 mimics were efficiently conveyed to MDA-MB-231 cells by ADSC-exosomes (41). Remarkably, ADSC-exosomes loaded with miR-381 inhibited the growth and metastasis ability of MDA-MB-231 cells and promoted apoptosis *in vitro*, showing the excellent RNA therapy potential of ADSC-exosomes. Sheykhhasan et al. constructed miR-145-overexpressing exosomes from ADSCs *via* lentivirus vector (42). These exosomes significantly inhibited tumor cell growth and metastasis by delivering miR-145.

In addition, the study of Li et al. generated the exosomes containing siMTA1 by using the electroporation method, which increased the gemcitabine-mediated inhibition of tumor growth *in vivo* by reversing the EMT effect and inhibiting the autophagic process (43). Limoni et al. transduced HEK293T cells with a lentiviral vector bearing LAMP2B-DARPin G3 chimeric gene for targeting HER2-specific tumors (44). Then, the exosomes generated from these cells were isolated and then loaded with TPD52-silencing siRNAs, which were subsequently delivered to

SKBR3 cells for reducing tumor. Hu et al. constructed exosome-like nanovesicles (eNVs-FAP) from fibroblast activation protein-α (FAP) gene-engineered tumor cells (45). These nanovesicles facilitated dendritic cell (DC) mature, T cell, and FAP+CAFs infiltration, and depressed the ratio of immunosuppressive M2, myeloid-derived suppressor cells (MDSCs), and regulatory T cells (Tregs). Therefore, it implied that eNVs-FAP was a promising oncologic vaccine for targeting both the parenchyma and the stroma of BC tumors.

EXOSOME-BASED CARRIER CONSTRUCTION

Exosomes Serve as Targeted Coating Substances

The use of exosomes to carry conventional clinical chemotherapy drugs can effectively reduce the toxicity of the drugs and improve the enrichment effect of targeted sites (46). Exploiting the targeting capability of BC cell exosomes can empower the homing ability of the nanoplatforms to target homologous tumor cells. Therefore, exosomes of tumor cells or other functional cells can serve as targeted coating substances in nanoplatforms. For example, Chen et al. prepared the smart bionanodrug EXO-GO-CO-γ-PGA-MIT for delivering mitoxantrone (MIT) by exploiting the targeting properties of BC cell-originated exosomes (47). This nanodrug possesses slow-release, tumor aggregation, and enhanced pro-tumor apoptotic ability of MIT. Ghavami et al. established a radiolabeled exosome-based tracer [111In]In-oxine-T-exos, which was markedly internalized by HER2-positive cells for imaging HER2-expressing tumor (48).

Interestingly, a bioactivated exosome-based nanoplatform (EMPCs), was formulated by reactive oxygen species (ROS)-reactive thioether-linked paclitaxel-linoleic acid conjugates (PTX-S-LA), and cucurbitacin B (CuB) was co-loaded in polymeric micelles, with exosome-decorated membranes (49). EMPCs not only displayed enlarged prodrug function, increased blood circulation, the targeted capability of homozygous tumor cells, and improved tumor penetration, but also inhibited BC metastasis through circulating tumor cells (CTCs) elimination and FAK/MMP pathway modulation. Li et al. developed an engineered macrophage exosome to encapsulate poly(lactic-co-glycolic acid) nanoparticles and modified with c-Met-targeting peptide on the exosome surface for tumor targeting (50). This exosome nanocomplex (MEP-D), exhibited significant tumor targeting and tumor killing functions. Zhao et al. designed the CBSA/siS100A4@Exosome by conjugating cationic bovine serum albumin (CBSA) and siS100A4 followed with exosome membrane encapsulation (51). CBSA/siS100A4@Exosome possessed a higher binding affinity to the lung and superiorly exhibited metastasis-associated protein S100A4 expression, showing great inhibition potential in malignant BC growth and lung metastasis. ID@E-MSNs was a tumor cell-derived exosome-mimetic porous silica nanoparticles as an integrated drug delivery platform for carrying both indocyanine green (ICG) and DOX (52). In 4T1 tumor-bearing mice, the nanoparticles were able to enrich at the tumor site and promote ICG thermal effect-induced drug release and tumor ablation under 808 nm NIR irradiation, thus enabling combined chemotherapeutic BC treatment.

Exosomes Serve as Drug Delivery Carriers

The carrier properties of exosomes can be directly used to load chemotherapeutic drugs, photosensitizers or antitumor drugs. Exosomes are natural nanocarriers that can target the cancer-sensitizing agent indocyanine green (ICG) in a biosafe manner. FA-ExoICG was an engineered exosome that possessed tumor-targeting ligand folic acid (FA) and internally loaded ICG (53). Significant inhibition of MCF-7 tumor growth in mice was observed by a single intravenous injection of FA-ExoICG with followed ultrasound (US) irradiation, with a favorable biosafety profile. Tran et al. innovatively used a one-step strategy of loading amorphous nanomatrix formation into exosomes, such as encapsulation of aspirin into exosomes, which could effectively improve the efficiency of drug dissolution and homing targeting effect (54). This compound displayed toxic and killing effects on BC cells and colon cancer cells. Yu et al. developed a nano-carrier Erastin@FA-exo containing erastin-loaded exosomes labeled with FA (55). The results showed that Erastin@FA-exo targeted and inhibited the proliferation and migration of MDA-MB-231 cells and promoted the depletion of intracellular glutathione and activation of ROS to induce ferroptosis. Kalimuthu et al. synthesized personalized exosome mimics (EMs) loaded with PTX, termed PTX-MSC-Ems (56). The exosome carrier significantly inhibited the growth and tumor progression of MDA-MB-231 cells, and was regarded as a powerful drug delivery carrier for BC. Li et al. incorporated Dox in milk exosomes (mExo) and modified with specifically CD44-targeting hyaluronic acid (HA), named HA-mExo-Dox (57). This vector effectively targeted CD44-expressed BC cells and induced cell death *in vitro*. Gong et al. generated a biomimetic delivery system using A15-Exo to package cholesterol-modified miR-159 and chemotherapeutic agent DOX (58). *In vivo*, this delivery system effectively reduced the TCF-7 gene and exhibited potent anti-cancer effects without side effects. Thus, this study demonstrated the synergistic effect of exosomal transport carriers for the co-delivery of gene drugs and chemotherapeutic agents in TNBC treatment.

Immune cell-derived exosomes have parental cell properties and can be used to mimic immune cell targeting of cancer (59). By hybridizing sEV from mouse macrophages with synthetic liposomes, vesicles smaller than 200 nm in size can be designed to mimic the size of exosomes, denoting as hybrid exosomes (HE). The established HE maintained the good property of small EVs (sEVs) with higher colloidal stability, drug carrier feature, and durable release of DOX in response to pH, for killing 4T1 cells. Tian et al. established a well-characterized tool of exosome carrier by an αv integrin-specific iRGD peptide to mouse immature dendritic cells (imDCs) (60). These iRGD-expressing imDCs actively targeted BC tissues with high expression of integrin receptors, leading to significant tumor growth inhibition with limited systemic toxicity.

DISCUSSION

Due to the heterogeneity and biological barriers of tumors, conventional drugs for combating tumors are often difficult to achieve the balance between optimal drug effectiveness and minimum side effect. The majority of anti-cancer agents in clinical practice are toxic to cause adverse damage to normal cells with poor bioavailability, and insufficient *in vivo* stability. Nanoparticle-based technologies provide exciting approaches to BC diagnosis and therapeutics. Novel dosage forms represented by nanoplatforms are a cutting-edge way to improve the delivery efficiency of therapeutic agents. In addition to uploading drugs, the active targeting capability of nanoplatforms is also a factor that cannot be ignored. In terms of diagnosis, it is also worth mentioning that the exosome-related detection still has certain advantages, with non-invasive, high sensitivity and disease specificity, long circulation and stability. Specifically, exosome isolation methods mainly include ultracentrifugation techniques, polymer precipitation, size-based isolation, immunoaffinity chromatography, other isolation techniques. Each method has its own advantages and disadvantages. A more suitable separation method should be selected for different targets. In terms of identification, transmission electron microscopy (TEM) observation and nanoparticle tracking analysis (NTA) are commonly used to identify single exosomes with a diameter of 30-150 nm. Western blot detection can verify specific markers (such as CD63/CD81/CD9/TSG101/Alix), which can also be detected indirectly by immunofluorescence and flow cytometry (FCM). In addition, exosomes are a promising cell-free therapy, and the currently applied protection technologies mainly include freezing, freeze-drying, and spray-drying. In general, the isolation, extraction, identification and preservation technologies of exosomes are relatively mature, but the transformation and efficiency of exosomes are still relatively insufficient.

Currently, tumor targeting of nanoplatforms is mainly achieved *via* enhanced permeability and retention (EPR) effect in tumor internals or receptor-ligand interplay *via* adhering to overexpressed antigens on the tumor cell surface. In developing precisely targeting approaches, exosomes have emerged as ideal drug carriers due to their unique carrier properties and biosafety. In this review, exosome-related nanoplatforms are used for BC treatment, mainly including three aspects, exosomes and their cargoes, genetically engineered exosomes, and exosome-based carrier construction. Specifically, some cell-derived exosomes, or key components of exosomes themselves inhibit tumor proliferation. The genetically editing methods enable researchers to accurately manipulate the overexpression or knockdown of specific genes, thus facilitating the production of anti-tumor exosomes (**Table 1**). Notably, MSCs might secret a considerable amount of functionalized exosomes and are common gene-editing cell tools for yielding expressive-specific exosomes. In nanocarrier construction, surface modification of exosomes can increase specific target recognition and enhance recruitment and abundance at tumor sites. Encapsulation of nanomaterials by exosomes can prolong metabolic cycling, reduce clearance levels, and avoid drug degradation or inactivation. Exosomes can also be used as delivery platforms for carrying chemotherapeutics or other therapeutic agents such as phototherapy and photothermal therapy. Therefore, exosomes are also efficient multimodal synergistic vehicles for BC therapy. In addition, not only for treating BC, exosome carriers are also novel transport means investigated other tumors, including glioma, liver cancer, gastric cancer, and so on.

Most studies suggest that tumor-associated exosomal components are a cancer-promoting factor. Reducing the release of tumor-associated or stromal cell exosomes also enhances the treatment efficacy. However, tumor-associated exosomal components can also act as important antigenic components to activate immune effects (61). At the same time, exosomes are capable to minimize the expression of drug resistance genes by delivering anti-miRNAs. Exosome-originated from MCF-7/ADR cells could promote active drug sequestration and induce drug resistance phenotypes by delivering resistance-related genes MDR-1 and P-glycoprotein (62). By reducing the resistant exosome formation and secretion, psoralen could reverse the development of drug resistance in BC cells. Also, there are some emerging novel exosome nanoplatform that have been developed for BC therapy. For instance, some novel T-cell-based vaccines are expected to perform the excellent tumor-killing function, by equipping polyclonal CD4+ T cells with antigen-specific exosomes (62). Exosomes derived from other cells, especially immune cells with tumor-killing effects, are also expected to be used as formulations for tumor therapy. *In vitro* studies have shown that tumor cells become more capable of activating T cells after DC-Exo uptake, thus potentially producing a more effective anti-tumor immune response, suggesting that DC-derived exosomes are also an effective exosome-related therapeutic tool (63). Or, combine with other treatment modes, exosomes as multifunctional carriers can be fully utilized. For example, heat stress increased the number of doxorubicin-containing exosomes in tumor cells and enhanced the antitumor effect of exosomes from doxorubicin-treated tumor cells (64). This suggests the potential for synergistic kill-expanding effects of combining chemotherapy and heat therapy for BC.

At present, although exosomes provide a variety of comprehensive and desirable properties for drug delivery, there are still many obstacles to be faced in this field. Firstly, there are many sources of cells currently used for exosome delivery, and it is hard to ensure the consistency and stability of the results of different research groups. The isolation and preparation of large amounts of engineered exosomes, including exosome purification, synthesis, stabilization, identification, and drug loading, remains a significant and complex step for BC tumor therapy. Secondly, when exosomes are coupled to nanoparticles or encapsulated with drugs, the metabolic kinetics of exosomes *in vivo* are worthy of further study. When circulating in the body, there may be a large number of liver retention or drug off-target phenomena, which will affect the efficiency of drug delivery. Finally, the current researches are preliminarily at the preclinical level, mostly at the level of cell and animal research. Due to the strict control of clinical trials and the complex nature of exosome components, exosome-based breast tumor therapy still has a

TABLE 1 | The genetically engineered exosomes for combating BC.

Source of exosome	Carrier construction methods	Functions	Ref.
MSCs	an effective targeted delivery system by transduced MSCs	selectively targeted HER2+ cell lines	(28)
MSCs	engineered to secrete EVs enriched with miR-379	innovative therapy for metastatic breast cancer	(29)
DPSCs	miR-34a-overexpressing DPSCs were prepared using XMIRXpress-34a lentivectors	as a therapeutic carrier in BC cells *in vitro*	(30)
MSCs	a feasible nanovesicles to deliver RNA-based therapeutics	inhibited clone-formation and tumor-initiating abilities of the MCF7-derived cancer stem-like cells	(31)
CAR-T cells	MSLN-targeted CAR-T cells with MSLN-CAR construction	inhibited the growth of both endogenous and exogenous MSLN+ TNBC cells by perforin and granzyme B	(34)
4T1 cells	using miRNA-containing exosomes for therapeutic strategy	repolarization of M2 macrophages to M1 phenotype against tumor invasion and metastasis in breast cancer.	(36)
PGRN-/- TAMs	siPGRN-TAMs exosomes and PGRN-/- tumor tissue	inhibited invasion, migration, and EMT of breast cancer cells through their exosomes	(37)
Expi293 cells	developed an exosome platform termed synthetic multivalent antibodies retargeted exosome (SMART-Exo)	dually targeted T cell CD3 and HER2 receptors and exhibited highly potent and specific anti-tumor activity both *in vitro* and *in vivo*	(38)
ADSCs	Introduced miRNA-381-3p mimics to ADSC-exosomes by electroporation	inhibited proliferation, migration, and invasion capacity of MDA-MB-231 and promoted their apoptosis *in vitro*	(41)
MSCs	transfected with lentiviral vectors of miR-145-pLenti-III-enhanced green fluorescent protein (eGFP)	caused an improved anticancer property of miR-145 to inhibit BC	(42)
293T cells	Loading into exosomes of siMTA1 with electroporation.	increased the gemcitabine-mediated tumor growth inhibition effect *in vivo*	(43)
HEK293T cells	HEK293T cells were transduced by a lentiviral vector and seperated the exosomes to loaded with siRNA	bound specifically to HER2/Neu and were capable of delivering siRNA molecules against TPD52 gene into SKBR3 cells	(44)
Tumor cells	FAP gene-engineered tumor cell-derived exosome-like nanovesicles (eNVs-FAP) as a tumor vaccine	suppressed tumor growth by reprogramming TME and promoting tumor ferroptosis	(45)

long way to go. In order to finally achieve clinical application, it is necessary to carry out in-depth explorations on the preparation of exosome carriers, the real efficacy in the human body, and the control of side effects to determine the unification of the safety and effectiveness of exosome delivery.

CONCLUSION

The naturally occurring exosomes, exosomes released by engineered or modified cells, exosomes that upload other substances, or exosomes that act as targeted coating substances, are several common forms of exosome-associated nanoplatforms for effective therapeutic carriers. Therefore, the comprehensive understanding of exosome biogenesis and the progress of efficient exosome engineering techniques will promote the clinical application of exosome-related drug nanoplatforms for combating BC.

AUTHOR CONTRIBUTIONS

All authors contributed to the design of the study and the writing of the manuscript. JZ designed the project and revised the manuscript. QL and XZ performed the literature search and wrote the manuscript. All authors reviewed the manuscript and approved the final version.

REFERENCES

1. Sung H, Ferlay J, Siegel RL, Laversanne M, Soerjomataram I, Jemal A, et al. Global Cancer Statistics 2020: GLOBOCAN Estimates of Incidence and Mortality Worldwide for 36 Cancers in 185 Countries. *CA Cancer J Clin* (2021) 71:209–49. doi: 10.3322/caac.21660
2. Hanker AB, Sudhan DR, Arteaga CL. Overcoming Endocrine Resistance in Breast Cancer. *Cancer Cell* (2020) 37:496–513. doi: 10.1016/j.ccell.2020.03.009
3. Yuan X, Wang J, Huang Y, Shangguan D, Zhang P. Single-Cell Profiling to Explore Immunological Heterogeneity of Tumor Microenvironment in Breast Cancer. *Front Immunol* (2021) 12:643692. doi: 10.3389/fimmu.2021.643692
4. Xiong M, Zhang Q, Hu W, Zhao C, Lv W, Yi Y, et al. The Novel Mechanisms and Applications of Exosomes in Dermatology and Cutaneous Medical Aesthetics. *Pharmacol Res* (2021) 166:105490. doi: 10.1016/j.phrs.2021.105490
5. Dai J, Su Y, Zhong S, Cong L, Liu B, Yang J, et al. Exosomes: Key Players in Cancer and Potential Therapeutic Strategy. *Signal Transduct Target Ther* (2020) 5:145. doi: 10.1038/s41392-020-00261-0
6. Yu W, Hurley J, Roberts D, Chakrabortty SK, Enderle D, Noerholm M, et al. Exosome-Based Liquid Biopsies in Cancer: Opportunities and Challenges. *Ann Oncol* (2021) 32:466–77. doi: 10.1016/j.annonc.2021.01.074
7. Guo Y, Ji X, Liu J, Fan D, Zhou Q, Chen C, et al. Effects of Exosomes on Pre-Metastatic Niche Formation in Tumors. *Mol Cancer* (2019) 18:39. doi: 10.1186/s12943-019-0995-1
8. Dong X, Bai X, Ni J, Zhang H, Duan W, Graham P, et al. Exosomes and Breast Cancer Drug Resistance. *Cell Death Dis* (2020) 11:987. doi: 10.1038/s41419-020-03189-z
9. Ohno S, Takanashi M, Sudo K, Ueda S, Ishikawa A, Matsuyama N, et al. Systemically Injected Exosomes Targeted to EGFR Deliver Antitumor MicroRNA to Breast Cancer Cells. *Mol Ther* (2013) 21:185–91. doi: 10.1038/mt.2012.180
10. Santos JC, Lima N da S, Sarian LO, Matheu A, Ribeiro ML, Derchain SFM. Exosome-Mediated Breast Cancer Chemoresistance *via* miR-155 Transfer. *Sci Rep* (2018) 8:829. doi: 10.1038/s41598-018-19339-5
11. Liang Y, Duan L, Lu J, Xia J. Engineering Exosomes for Targeted Drug Delivery. *Theranostics* (2021) 11:3183–95. doi: 10.7150/thno.52570

12. Li Y-J, Wu J-Y, Liu J, Xu W, Qiu X, Huang S, et al. Artificial Exosomes for Translational Nanomedicine. *J Nanobiotech* (2021) 19:242. doi: 10.1186/s12951-021-00986-2
13. Kim H, Kim EH, Kwak G, Chi S-G, Kim SH, Yang Y. Exosomes: Cell-Derived Nanoplatforms for the Delivery of Cancer Therapeutics. *Int J Mol Sci* (2020) 22:14. doi: 10.3390/ijms22010014
14. Lee J, Henderson K, Massidda MW, Armenta-Ochoa M, Im BG, Veith A, et al. Mechanobiological Conditioning of Mesenchymal Stem Cells for Enhanced Vascular Regeneration. *Nat BioMed Eng* (2021) 5:89–102. doi: 10.1038/s41551-020-00674-w
15. Weiss ARR, Dahlke MH. Immunomodulation by Mesenchymal Stem Cells (MSCs): Mechanisms of Action of Living, Apoptotic, and Dead MSCs. *Front Immunol* (2019) 10:1191. doi: 10.3389/fimmu.2019.01191
16. Wang X, Tang Y, Liu Z, Yin Y, Li Q, Liu G, et al. The Application Potential and Advance of Mesenchymal Stem Cell-Derived Exosomes in Myocardial Infarction. *Stem Cells Int* (2021) 2021:5579904. doi: 10.1155/2021/5579904
17. Yu S, Zhou Y, Niu L, Qiao Y, Yan Y. Mesenchymal Stem Cell-Derived Exosome Mir-342-3p Inhibits Metastasis and Chemo-Resistance of Breast Cancer Through Regulating ID4. *Genes Genomics* (2022). doi: 10.1007/s13258-021-01200-1
18. Yuan L, Liu Y, Qu Y, Liu L, Li H. Exosomes Derived From MicroRNA-148b-3p-Overexpressing Human Umbilical Cord Mesenchymal Stem Cells Restrain Breast Cancer Progression. *Front Oncol* (2019) 9:1076. doi: 10.3389/fonc.2019.01076
19. Khazaei-Poul Y, Shojaei S, Koochaki A, Ghanbarian H, Mohammadi-Yeganeh S. Evaluating the Influence of Human Umbilical Cord Mesenchymal Stem Cells-Derived Exosomes Loaded With miR-3182 on Metastatic Performance of Triple Negative Breast Cancer Cells. *Life Sci* (2021) 286:120015. doi: 10.1016/j.lfs.2021.120015
20. O'Sullivan TE, Sun JC, Lanier LL. Natural Killer Cell Memory. *Immunity* (2015) 43:634–45. doi: 10.1016/j.immuni.2015.09.013
21. Lee J, Lee S-A, Gu N-Y, Jeong SY, Byeon JS, Jeong D-U, et al. Canine Natural Killer Cell-Derived Exosomes Exhibit Antitumor Activity in a Mouse Model of Canine Mammary Tumor. *BioMed Res Int* (2021) 2021:6690704. doi: 10.1155/2021/6690704
22. Zhu L, Gangadaran P, Kalimuthu S, Oh JM, Baek SH, Jeong SY, et al. Novel Alternatives to Extracellular Vesicle-Based Immunotherapy – Exosome Mimetics Derived From Natural Killer Cells. *Artif Cells Nanomed Biotechnol* (2018) 46:S166–79. doi: 10.1080/21691401.2018.1489824
23. Qiu X, Li Z, Han X, Zhen L, Luo C, Liu M, et al. Tumor-Derived Nanovesicles Promote Lung Distribution of the Therapeutic Nanovector Through Repression of Kupffer Cell-Mediated Phagocytosis. *Theranostics* (2019) 9:2618–36. doi: 10.7150/thno.32363
24. Wang Q, Zhuang X, Sriwastva MK, Mu J, Teng Y, Deng Z, et al. Blood Exosomes Regulate the Tissue Distribution of Grapefruit-Derived Nanovector *via* CD36 and IGFR1 Pathways. *Theranostics* (2018) 8:4912–24. doi: 10.7150/thno.27608
25. Melzer C, Rehn V, Yang Y, Bähre H, von der Ohe J, Hass R. Taxol-Loaded MSC-Derived Exosomes Provide a Therapeutic Vehicle to Target Metastatic Breast Cancer and Other Carcinoma Cells. *Cancers (Basel)* (2019) 11:798. doi: 10.3390/cancers11060798
26. Li H, Jin Y, Zhao Y, Li W, He Z, Zhang Q, et al. Targeted Cell Therapy for Partial-Thickness Cartilage Defects Using Membrane Modified Mesenchymal Stem Cells by Transglutaminase 2. *Biomaterials* (2021) 275:120994. doi: 10.1016/j.biomaterials.2021.120994
27. Ursula A, Jana J, Katarina B, Petra P, Martin P, Pavel P, et al. Prodrug Suicide Gene Therapy for Cancer Targeted Intracellular by Mesenchymal Stem Cell Exosomes. *Int J Cancer* (2019) 144:897–908. doi: 10.1002/ijc.31792
28. Gomari H, Forouzandeh Moghadam M, Soleimani M. Targeted Cancer Therapy Using Engineered Exosome as a Natural Drug Delivery Vehicle. *Onco Targets Ther* (2018) 11:5753–62. doi: 10.2147/OTT.S173110
29. O'Brien KP, Khan S, Gilligan KE, Zafar H, Lalor P, Glynn C, et al. Employing Mesenchymal Stem Cells to Support Tumor-Targeted Delivery of Extracellular Vesicle (EV)-Encapsulated microRNA-379. *Oncogene* (2018) 37:2137–49. doi: 10.1038/s41388-017-0116-9
30. Vakhshiteh F, Rahmani S, Ostad SN, Madjd Z, Dinarvand R, Atyabi F. Exosomes Derived From miR-34a-Overexpressing Mesenchymal Stem Cells Inhibit *In Vitro* Tumor Growth: A New Approach for Drug Delivery. *Life Sci* (2021) 266:118871. doi: 10.1016/j.lfs.2020.118871
31. Naseri Z, Oskuee RK, Forouzandeh-moghadam M, Jaafari MR. Delivery of LNA-antimiR-142-3p by Mesenchymal Stem Cells-Derived Exosomes to Breast Cancer Stem Cells Reduces Tumorigenicity. *Stem Cell Rev Rep* (2020) 16:541–56. doi: 10.1007/s12015-019-09944-w
32. Hong M, Clubb JD, Chen YY. Engineering CAR-T Cells for Next-Generation Cancer Therapy. *Cancer Cell* (2020) 38:473–88. doi: 10.1016/j.ccell.2020.07.005
33. Cao Y, Rodgers DT, Du J, Ahmad I, Hampton EN, Ma JSY, et al. Design of Switchable Chimeric Antigen Receptor T Cells Targeting Breast Cancer. *Angew Chemie - Int Ed* (2016) 55:7520–4. doi: 10.1002/anie.201601902
34. Yang P, Cao X, Cai H, Feng P, Chen X, Zhu Y, et al. The Exosomes Derived From CAR-T Cell Efficiently Target Mesothelin and Reduce Triple-Negative Breast Cancer Growth. *Cell Immunol* (2021) 360:104262. doi: 10.1016/j.cellimm.2020.104262
35. Moradi-Chaleshtori M, Bandehpour M, Soudi S, Mohammadi-Yeganeh S, Hashemi SM. *In Vitro* and *In Vivo* Evaluation of Anti-Tumoral Effect of M1 Phenotype Induction in Macrophages by miR-130 and miR-33 Containing Exosomes. *Cancer Immunol Immunother* (2021) 70:1323–39. doi: 10.1007/s00262-020-02762-x
36. Moradi-Chaleshtori M, Shojaei S, Mohammadi-Yeganeh S, Hashemi SM. Transfer of miRNA in Tumor-Derived Exosomes Suppresses Breast Tumor Cell Invasion and Migration by Inducing M1 Polarization in Macrophages. *Life Sci* (2021) 282:119800. doi: 10.1016/j.lfs.2021.119800
37. Yue S, Ye X, Zhou T, Gan D, Qian H, Fang W, et al. PGRN–/– TAMs-Derived Exosomes Inhibit Breast Cancer Cell Invasion and Migration and its Mechanism Exploration. *Life Sci* (2021) 264:118687. doi: 10.1016/j.lfs.2020.118687
38. Shi X, Cheng Q, Hou T, Han M, Smbatyan G, Lang JE, et al. Genetically Engineered Cell-Derived Nanoparticles for Targeted Breast Cancer Immunotherapy. *Mol Ther* (2020) 28:536–47. doi: 10.1016/j.ymthe.2019.11.020
39. Charles-de-Sá L, Gontijo-de-Amorim N, Sbarbati A, Benati D, Bernardi P, Borojevic R, et al. Photoaging Skin Therapy With PRP and ADSC: A Comparative Study. *Stem Cells Int* (2020) 2020:2032359. doi: 10.1155/2020/2032359
40. Liu H, Zhang M, Shi M, Zhang T, Lu W, Yang S, et al. Adipose-Derived Mesenchymal Stromal Cell-Derived Exosomes Promote Tendon Healing by Activating Both SMAD1/5/9 and SMAD2/3. *Stem Cell Res Ther* (2021) 12:338. doi: 10.1186/s13287-021-02410-w
41. Shojaei S, Hashemi SM, Ghanbarian H, Sharifi K, Salehi M, Mohammadi-Yeganeh S. Delivery of miR-381-3p Mimic by Mesenchymal Stem Cell-Derived Exosomes Inhibits Triple Negative Breast Cancer Aggressiveness; an *In Vitro* Study. *Stem Cell Rev Rep* (2021) 17:1027–38. doi: 10.1007/s12015-020-10089-4
42. Sheykhhasan M, Kalhor N, Sheikholeslami A, Dolati M, Amini E, Fazaeli H. Exosomes of Mesenchymal Stem Cells as a Proper Vehicle for Transfecting miR-145 Into the Breast Cancer Cell Line and Its Effect on Metastasis. *BioMed Res Int* (2021) 2021:5516078. doi: 10.1155/2021/5516078
43. Li P, Cao G, Huang Y, Wu W, Chen B, Wang Z, et al. Simta1-Loaded Exosomes Enhanced Chemotherapeutic Effect of Gemcitabine in Luminal-B Type Breast Cancer by Inhibition of EMT/HIF-α and Autophagy Pathways. *Front Oncol* (2020) 10:541262. doi: 10.3389/fonc.2020.541262
44. Limoni SK, Moghadam MF, Moazzeni SM, Gomari H, Salimi F. Engineered Exosomes for Targeted Transfer of siRNA to HER2 Positive Breast Cancer Cells. *Appl Biochem Biotechnol* (2019) 187:352–64. doi: 10.1007/s12010-018-2813-4
45. Hu S, Ma J, Su C, Chen Y, Shu Y, Qi Z, et al. Engineered Exosome-Like Nanovesicles Suppress Tumor Growth by Reprogramming Tumor Microenvironment and Promoting Tumor Ferroptosis. *Acta Biomater* (2021) 135:567–81. doi: 10.1016/j.actbio.2021.09.003
46. Hadla M, Palazzolo S, Corona G, Caligiuri I, Canzonieri V, Toffoli G, et al. Exosomes Increase the Therapeutic Index of Doxorubicin in Breast and Ovarian Cancer Mouse Models. *Nanomedicine* (2016) 11:2431–41. doi: 10.2217/nnm-2016-0154
47. Chen Q, Che C, Liu J, Gong Z, Si M, Yang S, et al. Construction of an Exosome-Functionalized Graphene Oxide Based Composite Bionic Smart Drug Delivery System and Its Anticancer Activity. *Nanotechnology* (2022) 33:175101. doi: 10.1088/1361-6528/ac49bf

48. Ghavami M, Vraka C, Hubert V, Schachner H, Bamminger K, Hacker M, et al. Radiolabeled HER2-Directed Exosomes Exhibit Improved Cell Targeting and Specificity. *Nanomedicine* (2021) 16:553–67. doi: 10.2217/nnm-2020-0408
49. Wang K, Ye H, Zhang X, Wang X, Yang B, Luo C, et al. An Exosome-Like Programmable-Bioactivating Paclitaxel Prodrug Nanoplatform for Enhanced Breast Cancer Metastasis Inhibition. *Biomaterials* (2020) 257:120224. doi: 10.1016/j.biomaterials.2020.120224
50. Li S, Wu Y, Ding F, Yang J, Li J, Gao X, et al. Engineering Macrophage-Derived Exosomes for Targeted Chemotherapy of Triple-Negative Breast Cancer. *Nanoscale* (2020) 12:10854–62. doi: 10.1039/d0nr00523a
51. Zhao L, Gu C, Gan Y, Shao L, Chen H, Zhu H. Exosome-Mediated siRNA Delivery to Suppress Postoperative Breast Cancer Metastasis. *J Control Release* (2020) 318:1–15. doi: 10.1016/j.jconrel.2019.12.005
52. Tian R, Wang Z, Niu R, Wang H, Guan W, Chang J. Tumor Exosome Mimicking Nanoparticles for Tumor Combinatorial Chemo-Photothermal Therapy. *Front Bioeng Biotechnol* (2020) 8:1010. doi: 10.3389/fbioe.2020.01010
53. Nguyen Cao TG, Kang JH, You JY, Kang HC, Rhee WJ, Ko YT, et al. Safe and Targeted Sonodynamic Cancer Therapy Using Biocompatible Exosome-Based Nanosonosensitizers. *ACS Appl Mater Interfaces* (2021) 13:25575–88. doi: 10.1021/acsami.0c22883
54. Tran PHL, Wang T, Yin W, Tran TTD, Barua HT, Zhang Y, et al. Development of a Nanoamorphous Exosomal Delivery System as an Effective Biological Platform for Improved Encapsulation of Hydrophobic Drugs. *Int J Pharm* (2019) 566:697–707. doi: 10.1016/j.ijpharm.2019.06.028
55. Yu M, Gai C, Li Z, Ding D, Zheng J, Zhang W, et al. Targeted Exosome-Encapsulated Erastin Induced Ferroptosis in Triple Negative Breast Cancer Cells. *Cancer Sci* (2019) 110:3173–82. doi: 10.1111/cas.14181
56. Kalimuthu S, Gangadaran P, Rajendran RL, Zhu L, Oh JM, Lee HW, et al. A New Approach for Loading Anticancer Drugs Into Mesenchymal Stem Cell-Derived Exosome Mimetics for Cancer Therapy. *Front Pharmacol* (2018) 9:1116. doi: 10.3389/fphar.2018.01116
57. Li D, Yao S, Zhou Z, Shi J, Huang Z, Wu Z. Hyaluronan Decoration of Milk Exosomes Directs Tumor-Specific Delivery of Doxorubicin. *Carbohydr Res* (2020) 493:108032. doi: 10.1016/j.carres.2020.108032
58. Gong C, Tian J, Wang Z, Gao Y, Wu X, Ding X, et al. Functional Exosome-Mediated Co-Delivery of Doxorubicin and Hydrophobically Modified microRNA 159 for Triple-Negative Breast Cancer Therapy. *J Nanobiotech* (2019) 17:93. doi: 10.1186/s12951-019-0526-7
59. Rayamajhi S, Nguyen TDT, Marasini R, Aryal S. Macrophage-Derived Exosome-Mimetic Hybrid Vesicles for Tumor Targeted Drug Delivery. *Acta Biomater* (2019) 94:482–94. doi: 10.1016/j.actbio.2019.05.054
60. Tian Y, Li S, Song J, Ji T, Zhu M, Anderson GJ, et al. A Doxorubicin Delivery Platform Using Engineered Natural Membrane Vesicle Exosomes for Targeted Tumor Therapy. *Biomaterials* (2014) 35:2383–90. doi: 10.1016/j.biomaterials.2013.11.083
61. Kitai Y, Kawasaki T, Sueyoshi T, Kobiyama K, Ishii KJ, Zou J, et al. DNA-Containing Exosomes Derived From Cancer Cells Treated With Topotecan Activate a STING-Dependent Pathway and Reinforce Antitumor Immunity. *J Immunol* (2017) 198:1649–59. doi: 10.4049/jimmunol.1601694
62. Xu A, Freywald A, Xiang J. Novel T-Cell-Based Vaccines *via* Arming Polyclonal CD4 + T Cells With Antigen-Specific Exosomes. *Immunotherapy* (2016) 8:1265–9. doi: 10.2217/imt-2016-0094
63. Romagnoli GG, Zelante BB, Toniolo PA, Migliori IK, Barbuto JAM. Dendritic Cell-Derived Exosomes May Be a Tool for Cancer Immunotherapy by Converting Tumor Cells Into Immunogenic Targets. *Front Immunol* (2015) 5:692. doi: 10.3389/fimmu.2014.00692
64. Yang Y, Chen Y, Zhang F, Zhao Q, Zhong H. Increased Anti-Tumour Activity by Exosomes Derived From Doxorubicin-Treated Tumour Cells *via* Heat Stress. *Int J Hyperth* (2015) 31:498–506. doi: 10.3109/02656736.2015.1036384

Conflict of Interest: The authors declare that the research was conducted in the absence of any commercial or financial relationships that could be construed as a potential conflict of interest.

Publisher's Note: All claims expressed in this article are solely those of the authors and do not necessarily represent those of their affiliated organizations, or those of the publisher, the editors and the reviewers. Any product that may be evaluated in this article, or claim that may be made by its manufacturer, is not guaranteed or endorsed by the publisher.

Copyright © 2022 Liu, Zhang and Zhang. This is an open-access article distributed under the terms of the Creative Commons Attribution License (CC BY). The use, distribution or reproduction in other forums is permitted, provided the original author(s) and the copyright owner(s) are credited and that the original publication in this journal is cited, in accordance with accepted academic practice. No use, distribution or reproduction is permitted which does not comply with these terms.

frontiers | Frontiers in Pharmacology

MINI REVIEW
published: 03 May 2022
doi: 10.3389/fphar.2022.907943

Principles and Protocols For Post-Cryopreservation Quality Evaluation of Stem Cells in Novel Biomedicine

Jingxian Xie[1,2], *Marlene Davis Ekpo*[2], *Jian Xiao*[1,3]*, *Hongbin Zhao*[4,5], *Xiaoyong Bai*[4,5], *Yijie Liang*[4,5], *Guang Zhao*[6], *Dong Liu*[6] *and Songwen Tan*[2]*

[1]Department of Pharmacy, Xiangya Hospital, Central South University, Changsha, China, [2]Xiangya School of Pharmaceutical Sciences, Central South University, Changsha, China, [3]National Clinical Research Center for Geriatric Disorders, Xiangya Hospital, Central South University, Changsha, China, [4]Hunan Carnation Biotechnology Co. LTD, Changsha, China, [5]Hainan Nova Doctor Group Co. Ltd, Haikou, China, [6]Hunan Sheng Bao Biological Technology Co., Ltd (in Yinfeng Biological Group., Ltd), Changsha, China

Stem cell therapy is a thriving topic of interest among researchers and clinicians due to evidence of its effectiveness and promising therapeutic advantage in numerous disease conditions as presented by novel biomedical research. However, extensive clinical application of stem cells is limited by its storage and transportation. The emergence of cryopreservation technology has made it possible for living organs, tissues, cells and even living organisms to survive for a long time at deep low temperatures. During the cryopreservation process, stem cell preparations are subject to three major damages: osmotic damage, mechanical damage, and peroxidative damage. Therefore, Assessing the effectiveness and safety of stem cells following cryopreservation is fundamental to the quality control of stem cell preparations. This article presents the important biosafety and quality control parameters to be assessed during the manufacturing of clinical grade stem cell products, highlights the significance of preventing cryodamage. and provides a reference for protocols in the quality control of stem cell preparations.

Keywords: stem cells, quality control, safety evaluation, cryopreservation, cell-based therapy

OPEN ACCESS

Edited by:
Zeming Liu,
Huazhong University of Science and Technology, China

Reviewed by:
Yunrun Liu,
Hong Kong Baptist University, Hong Kong, SAR China
Yan Zhang,
Hunan Normal University, China

***Correspondence:**
Jian Xiao
admanoas@163.com
Songwen Tan
stan0309@uni.sydney.edu.au

Specialty section:
This article was submitted to Pharmacology of Anti-Cancer Drugs, a section of the journal Frontiers in Pharmacology

Received: *30 March 2022*
Accepted: *13 April 2022*
Published: *03 May 2022*

Citation:
Xie J, Ekpo MD, Xiao J, Zhao H, Bai X, Liang Y, Zhao G, Liu D and Tan S (2022) Principles and Protocols For Post-Cryopreservation Quality Evaluation of Stem Cells in Novel Biomedicine. Front. Pharmacol. 13:907943. doi: 10.3389/fphar.2022.907943

1 INTRODUCTION

Stem cells are widely studied in the field of biology, and their potential in regenerative medicine and therapy is receiving increasing attention (Krishnan et al., 2021). According to the National Institutes of Health Research Administration's Clinical Research Registry (https://www.clinicaltrials.gov/), as of March 2021, a total of 1,216 mesenchymal stem cells (MSC) clinical research projects were registered worldwide, with 251 in China, accounting for 20.7% of the global total. Stem cells have been broadly classified as adult stem cells (ASCs) and Embryonic stem cells (ESCs) depending on their origin (Pilbauerová and Suchánek, 2018). Stem cell preparations are various types of products obtained by isolating and culturing stem cells from human tissues or healthy donor tissues. Stem cells can be obtained from a variety of tissues such as bone marrow (Tajima et al., 2015), adipose (Yang et al., 2010), umbilical cord (Katheria et al., 2020), umbilical blood (Gil-Kulik et al., 2020), skeletal muscle (Schüler et al., 2021), dental pulp, placenta, amniotic fluid and amniotic membrane (Zare et al., 2021). Stem cell therapy has evolved from basic laboratory research to progressive application in difficult clinical conditions (Chu et al., 2020). Stem cell therapy is the process of implanting human

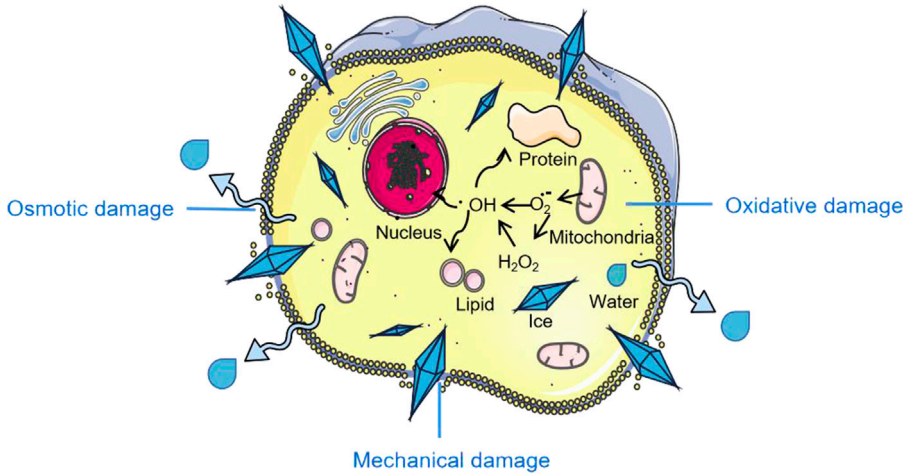


FIGURE 1 | Cryopreservation induced stem cell damage. Parts of the figure are adapted from SMART–Servier Medical Art, Servier: https://smart.servier.com.

stem cells of autologous or allogeneic origin into the human body after *in vitro* manipulation for disease treatment. Such *in vitro* manipulation includes processes such as isolation, purification, expansion, modification of stem cells, establishment of stem cells (lines), induction of differentiation, freezing (cryopreservation) and recovery after freezing (Hao et al., 2020a). The cell preparation techniques and treatment protocols are diverse, complex and specific to each cell type. However, being a novel biotherapeutic product, all stem cell preparations are subject to similar developmental processes ranging from preparation, *in vitro* testing, *in vivo* animal testing, to clinical trials and clinical application via implantation into humans. At each stage of development, relevant studies and quality control used must be performed to ascertain cell quality, safety and biological effects.

Cryopreservation which is basically the storage of biological materials at very low temperatures so as to conserve their viability has become an integral technique in most experimental and clinical protocols including stem cell transplantation (Hao et al., 2020a). Reports obtained from assessing the benefits of cryopreservation in stem cell therapy reveals that the process preserves the quality of the cells from the point of collection, transportation to final implantation without the loss of vital anatomical and physiological properties. In the same vein, it allows ample time for the screening of donors and recipients for markers like human leukocyte antigen (HLA) which may interfere with optimal therapeutic outcome.

Also, multiple passages during culturing and aging of stem cells can lead to reduced cell differentiation potential and genetic alterations (Martin-Piedra et al., 2014), of which cryopreservation becomes the reliable technique to apply in preventing these deleterious effects. None the less, cells are susceptible to damage during freezing, and there are three main types of freezing damage: mechanical damage, osmotic damage, and oxidative damage (Pegg, 2015). Mechanical damage is the irreversible damage to cell membranes and organelles caused by the formation of ice crystals from extracellular and intracellular solutes in cells at low temperatures (Yang et al., 2017). When the extracellular fluid freezes, there is an increase in solute concentration, resulting in cell damage by osmotic dehydration. This event is termed osmotic damage (Finger and Bischof, 2018). On the other hand, oxidative damages are caused by reactive oxygen species (ROS) generated during cryopreservation (Evangelista-Vargas and Santiani, 2017). Ideally, avoiding these undesirable effects is the aim of majority of research studies on cryopreservation as these damages often lead to irreversible harm ranging from the loss of vital functions to even cell death (Calmels et al., 2003) (**Figure 1**). It is therefore extremely important to explore the cryopreservation of stem cells and its preparations for the establishment of medical cell or tissue banks and the development of clinical regenerative medicine. It is also urgent to develop new approaches for stem cell cryopreservation by analyzing the mechanism underlying cell cryoinjury and optimizing the existing deep cryogenic techniques and methods.

Notwithstanding the enormous efforts and advancements in cancer research, Cancer is persistently among the high mortality diseases where the therapeutic efficacy of conventional chemotherapeutics is limited by factors including toxic side effects and the reoccurrence of tumor. To this end, researchers are on deck seeking to discover better approaches in cancer treatment. One of such is stem-cell based therapy which capitalizes on the desirable features of various stem cells with possible modifications to enhance their anti-tumor potential (Han et al., 2018). In addition to being the active therapeutic agents, stem cells can serve as drug carriers in targeted delivery (Wang et al., 2018), be applied in immuno-modulation following radio (chemo) therapy (Abraham et al., 2022), replace damaged organs through tissue regeneration (Grayson et al., 2015), and provide suitable models for research to aid better understanding and development of novel cancer therapies (Jo H et al., 2021).

This paper summarizes the major cryodamages encountered during the cryopreservation of stem cells and approaches used to tackle them, discusses the factors responsible for cytotoxicity of stem cell preparations in clinical applications, their biosafety concerns and recent techniques used in quality evaluation.

This article also provides reference for the quality testing protocols used in the quality control of stem cell preparations, and suggests directions to consider for future quality control and cryopreservation research.

2 CRYOPRESERVATION OF STEM CELLS

Cryoinjury is the irreversible damage that cells may suffer during freezing or thawing process (Ross-Rodriguez et al., 2010), and is mainly classified as osmotic damage, mechanical damage, and oxidative damage. In osmotic damage, the extracellular ice formed during slow freezing causes an osmotically driven removal of water from the intracellular space. The resulting hypertonicity is capable of causing cell death (Yousefian et al., 2018). Mechanical and structural cell damage occurs when the cells are cooled rapidly giving insufficient time for intracellular fluid to exit the cells. As a result, the cell experiences detrimental ice nucleation and recrystallization (Bakhach, 2009). Lastly, Oxidative damage is the injury inflicted by ROS produced during cryopreservation, often amounting to the oxidation of lipids, proteins and nucleic acids (Chen and Li, 2020; Liu et al., 2021a) (**Figure 1**).

Conventionally, the steps in stem cell cryopreservation are as follows: the stem cells of interest are harvested, carefully washed and resuspended in suitable media, then cryopreservation solution containing one or more cryoprotectants (CPAs) is then added (Wang et al., 2022). Till date, Dimethyl sulfoxide (DMSO) is the CPA of choice in stem cell cryopreservation commonly applied at a final concentration of 5–10% (v/v) (Yamatoya et al., 2022). The vial containing the cells and survival promoting additives is later frozen to −80°C using controlled rate freezers usually operated at optimal cooling rates of −1 to −3°C per minute. Finally, the frozen sample is placed in a liquid nitrogen tank mostly at −196°C for long-term preservation (Calmels et al., 2003). On demand, the stem cells are unfrozen by rapid thawing in a in a 37°C water bath and the CPA is removed before administration to patients. Adverse drug reaction monitoring following stem cell implantation procedures has documented some unwanted reactions including symptoms like abdominal cramps, diarrhea, nausea, flushing, and life-threatening events such as acute renal failure, respiratory depression and cardiac arrhythmias (Shu et al., 2014). Some of the observed adverse effects has been linked to toxicity caused by traces of DMSO retained in the infusion (Ataseven et al., 2017; Maral et al., 2018). Although the mechanisms underlying the adverse effects from infusing cryopreserved stem cell products are not completely unraveled, other contributing factors besides the toxicity of DMSO include cell aggregation and presence of apoptotic debris (Schlegel et al., 2009), volume of infused suspension and presence of unnucleated cells (Rohner et al., 2019), hypothermic condition of the cell suspension, and electrolyte imbalance (Calmels et al., 2003).

Predictably, decreasing the quantity of DMSO added during cryopreservation would diminish unwanted side effects. CPAs can be classified as permeable and non-permeable based on their ability or inability to cross the cellular membrane. Generally, permeable CPAs like DMSO are more toxic compared to non-permeable CPAs at equivalent concentrations (Raju et al., 2021). Several studies have shown that the inclusion of trehalose (Zhang et al., 2003), sucrose (Pan et al., 2017), polyampholytes (Matsumura et al., 2010) and antifreeze proteins (AFPs) (Shaliutina-Kolešová et al., 2019) during cryopreservation can greatly reduce the working concentration of DMSO, thereby reducing the cytotoxicity caused by DMSO. Another potent strategy is to develop alternatives to DMSO which should ideally prevent cryodamage and promote survival of the cryopreserved material and concomitantly be biocompatible. CPAs like trehalose and sucrose are suitable candidates as they were found to promote cryopreservation outcome in hematopoietic stem cells by maintaining the CD45+/34+ cell population and retaining cell clonogenicity and viability (Rodrigues et al., 2008).

3 KEY ASPECTS OF QUALITY CONTROL OF STEM CELL PREPARATION

Stem cell products should be generated in compliance with Good Manufacturing Practices (GMP). There are no uniform global guidelines for the production and clinical application of stem cell products. The United States Food and Drug Administration (USFDA), the European Medicines Agency (EMA), the Japanese Pharmaceuticals and Medical Devices Agency (PMDA), and other regulatory agencies currently provide GMPs to promote the safe use of therapies for patients. In addition, China has successively proposed general requirements for stem cells, which is applicable to stem cell research and production (Hao et al., 2020a; Hao et al., 2020b; Zhang et al., 2022). The following are the key aspects of quality control of stem cell preparation summarized in **Table 1**.

3.1 Analysis of Cell Characteristics

Some important methods used to characterize and identify stem cell types include short tandem repeat (STR) typing, morphological examinations, identification of markers, analysis of *in vitro* differentiation and teratoma formation (Zhang et al., 2022). As made known by science, there is yet a great number of undiscovered truths in stem cell research. For instance, new stem cell markers are being identified which could be beneficial in understanding and classifying stem cells. Also, the variations observed in expression of stem cell markers has been attributed to cell isolation and culturing techniques, cell age, culture medium composition, and stage of cell differentiation. Tapia et al. reports varied cell differentiation and expression of stemness markers in human induced pluripotent stem cells (hiPSCs) cells generated with different reprogramming methods (Tapia and Schöler, 2016). Also, the presence of certain growth factors and removal of oxygen from the growth media has induced alterations in stem cell markers (Hagmann et al., 2013).

3.2 Analysis of Biological Safety

3.2.1 Tumorigenicity

The tumorigenicity of stem cells is one of the main factors hindering their clinical use (Yasuda and Sato, 2015). Tumors can be generated through a number of pathways one of which is

TABLE 1 | Routine quality evaluation techniques in stem cell quality control.

Quality Assessed	Aim	Parameter Assessed	Method	Requirements	REF
Identity/Purity	Comprehensive cellular identification of different donors and different types of stem cells	Cell morphology	Electron microscope	Cells grown in 2D conditions shall exhibit growth as colonies with clear boundaries, high nuclear-cytoplasmic ratios and uniform morphology. Within each colony, cell-cell contact should be tight. Zhang et al. (2022)	Gherghiceanu and Popescu (2010)
		Genetics	RT-qPCR, Flow cytometry Single-Cell RNA Sequencing	ND	Jo HY et al. (2021)
		Surface markers	Flow cytometry	Cell surface markers: ≥70.0% of the cell population express any two of the following genes: SSEA3, SSEA4, TRA-1-60, TRA-1-81, for example, TRA1-81–positive rate ≥70.0% and SSEA4–positive rate ≥70.0%; intracellular markers: OCT4-positive rate ≥70.0% and NANOG-positive rate ≥70.0%	Jo HY et al., (2021), Zhang et al. (2022)
		Specific gene expression products	WB RT-qPCR	ND	Zhang et al. (2022)
Viability	Testing for cell activity and growth status	Survival rate	Trypan blue staining MTT	Cell viability shall be ≥ 90% before cryopreservation, and ≥60% post-thaw.	Kamalifar et al. (2020), Zhang et al. (2022)
		Telomerase activity	PCR, High-resolution optical tweezers	ND	Patrick et al. (2020)
		Cell proliferation rate	MTT	ND	Kamalifar et al. (2020)
		Cell cycle	Flow cytometer, Fluorescence Detection	ND	Fendrik et al. (2019)
		Clone forming efficiency	Trypan blue staining Flow cytometer	ND	Dutta et al. (2011)
		Organelle activity	Catalase activity Membrane potential Naþ/Kþ-ATPase, Ca2þ/Mg2þ-ATPase	ND	Liu et al. (2021b)
		Integrity of mitochondrial DNA	ND	ND	Yahata et al. (2017)
		Exosomes	TEM and immunoblotting	ND	Ain et al. (2018)
Sterility	Testing for the presence of mycoplasma, bacterium and fungi	Mycoplasma; bacterium; fungi	Turbidity testing, Chemosensitivity testing, MALDI-TOF MS	Negative	Golay et al. (2018), Hao et al. (2020b), Hartnett et al. (2021)
Adventitious viruses	The viruses to detect should be evaluated case by case by risk analysis	HBV、HCV、HCMV、HIV、HSV、TP, etc	PCR, Cytopathic effect	Negative	Hao et al. (2020b), Fernandez-Muñoz et al. (2021)
Endotoxins	Elimination of the effects of endotoxins	Endotoxins	Limulus amebocyte lysate	<2 EU/ml	Guo et al. (2011) Nomura et al. (2018)
Tumorigenicity	Avoiding Tumors from Stem Cell Therapy	Animal experiments	*In vivo* tumor formation assay in athymic mice	ND	Gowing et al. (2014)
		Tumorigenic transformed cells	ND	ND	Sato et al. (2019)
		Karyotype	Resuscitating and culturing samples for 48–72 h prior to cell harvesting and karyotyping.	46, XY, or 46, XX.	Andrews et al. (2017); Hao et al. (2020b),
		CGH array	CGH	ND	Andrews et al. (2017)
		Colony-forming assays in soft agar	ND	ND	Fernandez-Muñoz et al. (2021)
		migration rate	Scratch test	ND	Matluobi et al. (2018)

(Continued on following page)

TABLE 1 | (*Continued*) Routine quality evaluation techniques in stem cell quality control.

Quality Assessed	Aim	Parameter Assessed	Method	Requirements	REF
Potency	Determining the biological effectiveness of stem cell preparations in relation to therapy	Tri-lineage differentiation potential	ND	ND	Fernandez-Muñoz et al. (2021)
		Cytokines	MB-FIA	ND	Sane et al. (2018)
		Differentiation potential	ELISA, RT-PCR	ND	Matluobi et al. (2018)
		Specific genes and proteins	WB, ELISA	ND	Kang et al. (2019)
DNA Fingerprint	To distinguish the origin of stem cells after transplantation	DNA Fingerprint	STR, VNTR	ND	Blau et al. (1999)
Stem cell-related genes	To assist in assessing the activity and effectiveness of stem cells	Anti-oncogene	PCR	ND	Huang et al. (2013)
		Proto-oncogene	PCR	ND	Daekee et al. (2019)
		Stem cell-related genes (Oct3/4, Nanog, Sox2)	PCR, NGS	ND	Mendes Oliveira et al. (2018) Daekee et al. (2019)
Culture medium	Removal of residual ingredients	Bovine serum protein, antibiotics, cytokines	ELISA	ND	Zhang et al. (2011)

ND: Not determined, VNTR: variable number of tandem repeats, ELISA: enzyme linked immunosorbent assay, PCR: Polymerase chain reaction, WB: Western blot, CGH: Comparative Genomic Hybridization, RT-PCR: reverse transcription PCR, MB-FIA: Magnetic-bead fluorescent immunoassays, MS: mass spectroscopy, MALDI-TOF: Matrix-assisted laser desorption/ionization-time of flight MS, NGS: next generation sequencing, TEM: transmission electron microscopy, HBV: Hepatitis B Virus, HCV: Hepatitis C Virus, HCMV: Human Cytomegalo virus, HIV: Human immunodeficiency virus, HSV: Herpes simplex virus, TP: treponema pallidum.

the malignancy of stem cells induced during proliferation and differentiation (Miyawaki et al., 2017). Additionally, teratomas can originate from undifferentiated stem cells, especially for human induced pluripotent stem cells (hiPSCs) (Yuan, 2015).

3.2.2 Sterility

The microbial contamination of stem cell products (Hartnett et al., 2021) including bacterial, fungal, mycoplasma and bacterial endotoxin contaminations is responsible for a significant number of adverse reaction cases (Golay et al., 2018). Therefore, microbiological testing prior to clinical application is pertinent for preventing unwanted effects. The recently developed and frequently applied BacT/Alert 3D automated culture system is one of the innovations to aid fast and efficient sterility testing; it requires short incubation period and does not differ significantly from pharmacopeial methods in terms of detection capacity (England et al., 2019). Rapid mycoplasma detection methods include nucleic acid amplification technology and mycoplasma metabolic enzyme activity detection (Zhang et al., 2022).

3.2.3 Pathogenic Factors

A combination of *in vivo* and *in vitro* methods should be used to test for human- and animal-derived specific pathogenic factors based on the characteristics of each stem cell preparation. If bovine serum has been used, testing for bovine-derived specific viruses shall be performed; if pig-derived materials such as trypsin are used, testing for at least pig-derived microviruses shall be performed (Zhang et al., 2022).

3.3 Analysis of Biological Activity

The biological effectiveness of various types of stem cells can be basically categorized based on their ability to induce differentiation, immunomodulatory ability and tissue regeneration (Li et al., 2021). Biological potency assay include: secretion of relevant bioactive substances (Matluobi et al., 2018) (e.g., recombinant proteins, glycoproteins or lipoproteins, growth factors, enzymes and cytokines), extracellular matrix/structures, cellular interactions (e.g., immune activation or inhibition), migration differentiation or self-renewal potential of cells (Hao et al., 2020a). To evaluate the immune activity of stem cells, (a combination of) methods like quantitative ribonucleic acid (RNA) analysis, marker assays, secreted protein analysis and immune cell response analysis have been suggested. Furthermore, instrumentations such as immunofluorescence staining, morphological observation, flow cytometry analysis and electrophysiological analysis are applicable in this respect (Rohner et al., 2019).

For MSCs, regardless of their origin, the differentiation ability of multiple cell types (e.g., adipocytes, chondrocytes, osteoblasts, etc.) should be tested *in vitro* to determine their multipotency of cell differentiation (Lee et al., 2015). For undifferentiated ESCs and iPSCs, the pluripotency of cell differentiation must be measured by their ability to form embryoid bodies *in vitro* or teratomas in severe combined immunodeficiency disease (SCID) mice model (Li et al., 2013). In addition to this, biological effects tests relevant to confirming the intended therapeutic activity of stem cells should be performed as specific biological activity assays.

4 FUTURE RESEARCH AND DIRECTIONS FOR QUALITY CONTROL

4.1 Efficient Cryopreservation Solutions

The use of efficient and low toxicity cryopreservation protocols to reduce cryogenic damage would guarantee the effectiveness of

stem cell preparation applications post-thaw. Since different cryoprotectants have different protection mechanisms, a mixture of cryoprotectants is usually used to maximize cell survival (Tao et al., 2020). The combination of cryoprotectants can reduce the concentration of a single CPA used, thus reducing cytotoxicity (Elliott et al., 2017). The addition of trehalose (Yamatoya et al., 2022), sucrose (Shu et al., 2014), polyampholytes (Maral et al., 2018) and antifreeze proteins (Shaliutina-Kolešová et al., 2019) during cryopreservation can greatly minimize the required amount of DMSO, thereby reducing cytotoxicity.

4.2 Elimination of Residual Undifferentiated Stem Cells

Residual undifferentiated hiPSCs pose tumorigenic risk, and methods to eliminate these undifferentiated hiPSCs are crucial to ensuring safety (Blum and Benvenisty, 2008). The introduction of suicide genes (Yagyu et al., 2015), addition of plasma-activated medium (Matsumoto et al., 2016), cell sorting using antibodies against hiPSC surface antigens11 and, the use chemical inhibitors (Ben-David et al., 2013) are useful techniques for separating undifferentiated stem cells. Nevertheless, none of these methods have attained application in clinical grade stem cell production due to high cost, low specificity and retainment of residue in the final product (Mao et al., 2017). Consequently, researchers are beset with the task of discovering new effective ways to eliminate undifferentiated hiPSCs. In this light, Takunori et al. presented in 2018 evidence supporting the ability of high L-alanine concentrations to selectively eliminate undifferentiated hiPSCs through a novel pathway (Nagashima et al., 2018).

This method may contribute to the development of a low-cost, safe, and practical method to eliminate residual undifferentiated hiPSCs.

4.3 The Integrity of Mitochondrial DNA in Pluripotent Stem Cells

Mitochondrial DNA mutations occur at a high rate, causing several debilitating and life-threatening diseases like Kearns–Sayre syndrome and Pearson syndrome (Greaves and Taylor, 2006). According to Prigione et al., pluripotency caused mitochondrial DNA mutations originally absent from the parent PSCs (Prigione et al., 2011). Furthermore, fluctuations in the number of mitochondrial copies have been detected during prolonged culturing of iPSCs isolated from donors presenting with different maladies like lactic acidosis, mitochondrial myopathy, encephalopathy and stroke-like episodes (Gherghiceanu and Popescu, 2010). These reports confirm the need to conduct more research geared at identifying other implacable factors, understanding the mechanism (s) behind these DNA alterations and also to assess the integrity of mitochondrial DNA and genomic DNA before the use of stem cells in humans.

4.4 New Cytogenetic Techniques

Presently, an array of sensitive cytogenetic tools such as fluorescent *in situ* hybridization, comparative genomic hybridization, Giemsa (GTG) karyotyping and whole genome sequencing have been developed to assess the genomic integrity of stem cells (Rohani et al., 2018). Single-cell genome sequencing can rapidly and efficiently detect genetic heterogeneity in large cell samples (Bardy et al., 2016). Single-cell RNA-seq has been used in combination with electrophysiology to evaluate the activity of human iPSCs derived neurons (Bardy et al., 2016). Similarly, single cell sequencing has been applied in the long-term monitoring of trends in cancer development, progression and diversity among populations (Navin, 2015). A collaborative paper published by the International Stem Cell Banking Initiative point out the importance of stem cell genetic integrity, and also mention that other cytogenetic techniques like FISH, SKY, CGH arrays, and whole-genome sequencing would be useful to identify information that GTG karyotyping cannot acquire (Andrews et al., 2015). It is unclear how essential it is to perform more thorough epigenetic screening of pluripotent stem cells prior to clinical application. Report of variable loss of genomic imprinting across lines in iPSCs suggest that standardized epigenetic quality control tests would be beneficial (Pasque et al., 2018).

5 CONCLUSION

Quality control of stem cells and stem cell-based medicines have received widespread attention, and the development of cryopreservation technology has provided a technical guarantee for the application of stem cell preparations. The main risks faced by patients with stem cell preparations are the occurrence of allergic or immune reactions, the formation of tumors, and the occurrence of microbial contamination. These risk-posing factors should be eliminated or reduced to tolerable limits in the preclinical stages by extensive *in vivo/in vitro* evaluation to improve the efficacy and safety of stem cells. To ensure the safety and efficacy of stem cell products, each batch of stem cell preparation shall meet the existing stem cell quality requirements covering cell identification, viability and growth activity, purity and homogeneity, sterility testing and mycoplasma testing, detection of endogenous pathogenic factors, endotoxin testing, abnormal immunological response, tumorigenicity, biological potency testing, residual amount of culture medium and other added components. These strict standards of quality control must be adhered to before stem cells can be used for clinical applications, and such standards must be harmonized and monitored globally to ensure uniformity in the grade of clinically applicable stem cell products. Advanced techniques like single-cell genome sequencing of large samples may provide better understanding of genomic integrity in stem cell lines. Also, these evaluations should be conducted post-cryopreservation during the formulation and testing phases to ensure there is no cryodamage. Furthermore, cryopreservation protocols should be reviewed and tailored to each stem cell, putting into key consideration its efficacy and safety. In any case, more clinical resources and research studies should be targeted at further optimizing the quality control of stem cells before venturing further into application of stem cell therapies.

DATA AVAILABILITY STATEMENT

All data used to support the findings of this review are included within the article.

AUTHOR CONTRIBUTIONS

Writing—original draft preparation, JX and ME. Writing—review and editing, HZ, XB, YL, GZ, and DL. Supervision and approval, JX and ST.

FUNDING

The work is supported by the following projects: Changsha Natural Science Foundation of 2020 (kq2007039); National Clinical Research Center for Geriatric Disorders, Xiangya Hospital (XYYYJSTG-15); Parallel and Distributed Processing for the Stable Support Project of the National Defense Science and Technology Key Laboratory (WDZC20205500121); Key Research Project of Ningxia Hui Autonomous Region in 2021 (Major Project) (2021BEG01001); Natural Science Foundation of Hunan Province (No. 2021JJ31043); Postgraduate Innovative Project of Central South University (No. 207211045).

SUPPLEMENTARY MATERIAL

The Supplementary Material for this article can be found online at: https://www.frontiersin.org/articles/10.3389/fphar.2022.907943/full#supplementary-material

REFERENCES

Abraham, I., Goyal, A., Deniz, B., Moran, D., Chioda, M., MacDonald, K. M., et al. (2022). Budget Impact Analysis of Trilaciclib for Decreasing the Incidence of Chemotherapy-Induced Myelosuppression in Patients with Extensive-Stage Small Cell Lung Cancer in the United States. *J. Manag. Care Spec. Pharm.* 28 (4), 435–448. doi:10.18553/jmcp.2022.21379

Ain, Q. U., Woo, Y. S., Chung, J. Y., and Kim, Y.-H. (2018). Regeneration of Anti-hypoxic Myocardial Cells by Transduction of Mesenchymal Stem Cell-Derived Exosomes Containing Tat-Metallothionein Fusion Proteins. *Macromol. Res.* 26 (8), 709–716. doi:10.1007/s13233-018-6101-5

Andrews, P. W., Baker, D., Benvinisty, N., Miranda, B., Bruce, K., Brüstle, O., et al. (2015). Points to Consider in the Development of Seed Stocks of Pluripotent Stem Cells for Clinical Applications: International Stem Cell Banking Initiative (ISCBI). *Regen. Med.* 10 (2 Suppl. l), 1–44. doi:10.2217/rme.14.93

Andrews, P. W., Ben-David, U., Benvenisty, N., Coffey, P., Eggan, K., Knowles, B. B., et al. (2017). Assessing the Safety of Human Pluripotent Stem Cells and Their Derivatives for Clinical Applications. *Stem Cel Rep.* 9 (1), 1–4. doi:10.1016/j.stemcr.2017.05.029

Ataseven, E., Tüfekçi, Ö., Yilmaz, Ş., Güleryüz, H., and Ören, H. (2017). Neurotoxicity Associated with Dimethyl Sulfoxide Used in Allogeneic Stem Cell Transplantation. *J. Pediatr. Hematol. Oncol.* 39 (5), e297–e9. doi:10.1097/MPH.0000000000000784

Bakhach, J. (2009). The Cryopreservation of Composite Tissues: Principles and Recent Advancement on Cryopreservation of Different Type of Tissues. *Organogenesis* 5 (3), 119–126. doi:10.4161/org.5.3.9583

Bardy, C., van den Hurk, M., Kakaradov, B., Erwin, J. A., Jaeger, B. N., Hernandez, R. V., et al. (2016). Predicting the Functional States of Human iPSC-Derived Neurons with Single-Cell RNA-Seq and Electrophysiology. *Mol. Psychiatry* 21 (11), 1573–1588. doi:10.1038/mp.2016.158

Ben-David, U., Gan, Q. F., Golan-Lev, T., Arora, P., Yanuka, O., Oren, Y. S., et al. (2013). Selective Elimination of Human Pluripotent Stem Cells by an Oleate Synthesis Inhibitor Discovered in a High-Throughput Screen. *Cell Stem Cell* 12 (2), 167–179. doi:10.1016/j.stem.2012.11.015

Blau, I. W., Basara, N., Serr, A., Seidl, C., Seifried, E., Fuchs, M., et al. (1999). A Second Unrelated Bone Marrow Transplant: Successful Quantitative Monitoring of Mixed Chimerism Using a Highly Discriminative PCR-STR System. *Clin. Lab. Haematol.* 21 (2), 133–138. doi:10.1046/j.1365-2257.1999.00188.x

Blum, B., and Benvenisty, N. (2008). The Tumorigenicity of Human Embryonic Stem Cells. *Adv. Cancer Res.* 100, 133–158. doi:10.1016/S0065-230X(08)00005-5

Calmels, B., Houzé, P., Hengesse, J. C., Ducrot, T., Malenfant, C., and Chabannon, C. (2003). Preclinical Evaluation of an Automated Closed Fluid Management Device: Cytomate, for Washing Out DMSO from Hematopoietic Stem Cell Grafts after Thawing. *Bone Marrow Transpl.* 31 (9), 823–828. doi:10.1038/sj.bmt.1703905

Chen, W., and Li, D. (2020). Reactive Oxygen Species (ROS)-Responsive Nanomedicine for Solving Ischemia-Reperfusion Injury. *Front. Chem.* 8, 732. doi:10.3389/fchem.2020.00732

Chu, D. T., Phuong, T. N. T., Tien, N. L. B., Tran, D. K., Thanh, V. V., Quang, T. L., et al. (2020). An Update on the Progress of Isolation, Culture, Storage, and Clinical Application of Human Bone Marrow Mesenchymal Stem/Stromal Cells. *Int. J. Mol. Sci.* 21 (3), 708. doi:10.3390/ijms21030708

Daekee, K., Mi-Jung, H., Minjun, J., Hee-Jin, A., Kwang-Won, S., and Kyung-Sun, K. (2019). Generation of Genetically Stable Human Direct-Conversion-Derived Neural Stem Cells Using Quantity Control of Proto-Oncogene Expression. *Mol. Ther. Nucleic Acids* 14, 388–397. doi:10.1016/j.omtn.2018.12.009

Dutta, R., Malakar, D., Khate, K., Sahu, S., Akshey, Y., and Mukesh, M. (2011). A Comparative Study on Efficiency of Adult Fibroblast, Putative Embryonic Stem Cell and Lymphocyte as Donor Cells for Production of Handmade Cloned Embryos in Goat and Characterization of Putative ntES Cells Obtained from These Embryos. *Theriogenology* 76 (5), 851–863. doi:10.1016/j.theriogenology.2011.03.025

Elliott, G. D., Wang, S., and Fuller, B. J. (2017). Cryoprotectants: A Review of the Actions and Applications of Cryoprotective Solutes that Modulate Cell Recovery from Ultra-low Temperatures. *Cryobiology* 76, 74–91. doi:10.1016/j.cryobiol.2017.04.004

England, M. R., Stock, F., Gebo, J. E. T., Frank, K. M., and Lau, A. F. (2019). Comprehensive Evaluation of Compendial USP, BacT/Alert Dual-T, and Bactec FX for Detection of Product Sterility Testing Contaminants. *J. Clin. Microbiol.* 57 (2), e01548. doi:10.1128/JCM.01548-18

Evangelista-Vargas, S., and Santiani, A. (2017). Detection of Intracellular Reactive Oxygen Species (Superoxide Anion and Hydrogen Peroxide) and Lipid Peroxidation during Cryopreservation of Alpaca Spermatozoa. *Reprod. Domest. Anim.* 52 (5), 819–824. doi:10.1111/rda.12984

Fendrik, A. J., Romanelli, L., and Rotondo, E. (2019). Stochastic Cell Renewal Process and Lengthening of Cell Cycle. *Phys. Biol.* 17 (1), 016004. doi:10.1088/1478-3975/ab576c

Fernandez-Muñoz, B., Garcia-Delgado, A. B., Arribas-Arribas, B., and Sanchez-Pernaute, R. (2021). Human Neural Stem Cells for Cell-Based Medicinal Products. *Cells* 10 (9), 2377. doi:10.3390/cells10092377

Finger, E. B., and Bischof, J. C. (2018). Cryopreservation by Vitrification: a Promising Approach for Transplant Organ Banking. *Curr. Opin. Organ. Transpl.* 23 (3), 353–360. doi:10.1097/MOT.0000000000000534

Gherghiceanu, M., and Popescu, L. M. (2010). Cardiomyocyte Precursors and Telocytes in Epicardial Stem Cell Niche: Electron Microscope Images. *J. Cel Mol. Med.* 14 (4), 871–877. doi:10.1111/j.1582-4934.2010.01060.x

Gil-Kulik, P., Świstowska, M., Kondracka, A., Chomik, P., Krzyżanowski, A., Kwaśniewska, A., et al. (2020). Increased Expression of BIRC2, BIRC3, and BIRC5 from the IAP Family in Mesenchymal Stem Cells of the Umbilical Cord Wharton's Jelly (WJSC) in Younger Women Giving Birth Naturally. *Oxid. Med. Cel Longev.* 2020, 9084730. doi:10.1155/2020/9084730

Golay, J., Pedrini, O., Capelli, C., Gotti, E., Borleri, G., Magri, M., et al. (2018). Utility of Routine Evaluation of Sterility of Cellular Therapy Products with or

without Extensive Manipulation: Best Practices and Clinical Significance. *Cytotherapy* 20 (2), 262–270. doi:10.1016/j.jcyt.2017.11.009

Gowing, G., Shelley, B., Staggenborg, K., Hurley, A., Avalos, P., Victoroff, J., et al. (2014). Glial Cell Line-Derived Neurotrophic Factor-Secreting Human Neural Progenitors Show Long-Term Survival, Maturation into Astrocytes, and No Tumor Formation Following Transplantation into the Spinal Cord of Immunocompromised Rats. *Neuroreport* 25 (6), 367–372. doi:10.1097/WNR.0000000000000092

Grayson, W. L., Bunnell, B. A., Martin, E., Frazier, T., Hung, B. P., and Gimble, J. M. (2015). Stromal Cells and Stem Cells in Clinical Bone Regeneration. *Nat. Rev. Endocrinol.* 11 (3), 140–150. doi:10.1038/nrendo.2014.234

Greaves, L. C., and Taylor, R. W. (2006). Mitochondrial DNA Mutations in Human Disease. *IUBMB Life* 58 (3), 143–151. doi:10.1080/15216540600686888

Guo, C. J., Gao, Y., Hou, D., Shi, D. Y., Tong, X. M., Shen, D., et al. (2011). Preclinical Transplantation and Safety of HS/PCs Expanded from Human Umbilical Cord Blood. *World J. Stem Cell* 3 (5), 43–52. doi:10.4252/wjsc.v3.i5.43

Hagmann, S., Moradi, B., Frank, S., Dreher, T., Kämmerer, P. W., Richter, W., et al. (2013). FGF-2 Addition during Expansion of Human Bone Marrow-Derived Stromal Cells Alters MSC Surface Marker Distribution and Chondrogenic Differentiation Potential. *Cell Prolif.* 46 (4), 396–407. doi:10.1111/cpr.12046

Han, S. W., Kim, Y. Y., Kang, W. J., Kim, H. C., Ku, S. Y., Kang, B. C., et al. (2018). The Use of Normal Stem Cells and Cancer Stem Cells for Potential Anti-cancer Therapeutic Strategy. *Tissue Eng. Regen. Med.* 15 (4), 365–380. doi:10.1007/s13770-018-0128-8

Hao, J., Ma, A., Wang, L., Cao, J., Chen, S., Wang, L., et al. (2020). General Requirements for Stem Cells. *Cel Prolif.* 53 (12), e12926. doi:10.1111/cpr.12926

Hao, J., Cao, J., Wang, L., Ma, A., Chen, S., Ding, J., et al. (2020). Requirements for Human Embryonic Stem Cells. *Cel Prolif.* 53 (12), e12925. doi:10.1111/cpr.12925

Hartnett, K. P., Powell, K. M., Rankin, D., Gable, P., Kim, J. J., Spoto, S., et al. (2021). Investigation of Bacterial Infections Among Patients Treated with Umbilical Cord Blood-Derived Products Marketed as Stem Cell Therapies. *JAMA Netw. Open* 4 (10), e2128615. doi:10.1001/jamanetworkopen.2021.28615

Huang, W., Bei, L., and Eklund, E. A. (2013). Fas-associated Phosphatase 1 Mediates Fas Resistance in Myeloid Progenitor Cells Expressing the Bcr-Abl Oncogene. *Leuk. Lymphoma* 54 (3), 619–630. doi:10.3109/10428194.2012.720979

Jo H, H., Brito, S., Kwak, B. M., Park, S., Lee, M. G., and Bin, B. H. (2021). Applications of Mesenchymal Stem Cells in Skin Regeneration and Rejuvenation. *Int. J. Mol. Sci.* 22 (5), 2410. doi:10.3390/ijms22052410

Jo HY, H. Y., Seo, H. H., Gil, D., Park, Y., Han, H. J., Han, H. W., et al. (2021). Single-Cell RNA Sequencing of Human Pluripotent Stem Cell-Derived Macrophages for Quality Control of the Cell Therapy Product. *Front. Genet.* 12, 658862. doi:10.3389/fgene.2021.658862

Kamalifar, S., Azarpira, N., Sadeghi, L., Ghorbani-Dalini, S., Nekoei, S. M., Aghdaie, M. H., et al. (2020). ROCK Y-27632 Inhibitor, Ascorbic Acid, and Trehalose Increase Survival of Human Wharton Jelly Mesenchymal Stem Cells after Cryopreservation. *Exp. Clin. Transpl.* 18 (4), 505–511. doi:10.6002/ect.2017.0101

Kang, P. J., Zheng, J., Lee, G., Son, D., Kim, I. Y., Song, G., et al. (2019). Glycine Decarboxylase Regulates the Maintenance and Induction of Pluripotency via Metabolic Control. *Metab. Eng.* 53, 35–47. doi:10.1016/j.ymben.2019.02.003

Katheria, A. C., Amino, R., Konop, J. M., Orona, A. J., Kim, E., Liu, Y., et al. (2020). Stem Cell Composition of Umbilical Cord Blood Following Milking Compared with Delayed Clamping of the Cord Appears Better Suited for Promoting Hematopoiesis. *J. Pediatr.* 216, 222–226. doi:10.1016/j.jpeds.2019.07.043

Krishnan, M., Kumar, S., Kangale, L. J., Ghigo, E., and Abnave, P. (2021). The Act of Controlling Adult Stem Cell Dynamics: Insights from Animal Models. *Biomolecules* 11 (5), 667. doi:10.3390/biom11050667

Lee, J., Abdeen, A. A., Kim, A. S., and Kilian, K. A. (2015). Influence of Biophysical Parameters on Maintaining the Mesenchymal Stem Cell Phenotype. *ACS Biomater. Sci. Eng.* 1 (4), 218–226. doi:10.1021/ab500003s

Li, G., Chunxu, Y., and Guisheng, L. (2013). Efficient P53 Gene Targeting by Homologous Recombination in Rat-Induced Pluripotent Stem Cells. *Cel Prolif.* 46 (1), 1–9. doi:10.1111/cpr.12000

Li, H., Wang, W., and Chang, J. (2021). Calcium Silicate Enhances Immunosuppressive Function of MSCs to Indirectly Modulate the Polarization of Macrophages. *Regen. Biomater.* 8 (6), rbab056. doi:10.1093/rb/rbab056

Liu, X., Xu, Y., Liu, F., Pan, Y., Miao, L., Zhu, Q., et al. (2021). The Feasibility of Antioxidants Avoiding Oxidative Damages from Reactive Oxygen Species in Cryopreservation. *Front. Chem.* 9, 648684. doi:10.3389/fchem.2021.648684

Liu, X., Hu, Y., Pan, Y., Fang, M., Tong, Z., Sun, Y., et al. (2021). Exploring the Application and Mechanism of Sodium Hyaluronate in Cryopreservation of Red Blood Cells. *Mater. Today Bio* 12, 100156. doi:10.1016/j.mtbio.2021.100156

Mao, D., Ando, S., Sato, S. I., Qin, Y., Hirata, N., Katsuda, Y., et al. (2017). A Synthetic Hybrid Molecule for the Selective Removal of Human Pluripotent Stem Cells from Cell Mixtures. *Angew. Chem. Int. Ed. Engl.* 56 (7), 1765–1770. doi:10.1002/anie.201610284

Maral, S., Albayrak, M., Pala, C., Yildiz, A., Sahin, O., and Ozturk, H. B. (2018). Dimethyl Sulfoxide-Induced Tonic-Clonic Seizure and Cardiac Arrest during Infusion of Autologous Peripheral Blood Stem Cells. *Cell Tissue Bank* 19 (4), 831–832. doi:10.1007/s10561-018-9718-x

Martin-Piedra, M. A., Garzon, I., Oliveira, A. C., Alfonso-Rodriguez, C. A., Carriel, V., Scionti, G., et al. (2014). Cell Viability and Proliferation Capability of Long-Term Human Dental Pulp Stem Cell Cultures. *Cytotherapy* 16 (2), 266–277. doi:10.1016/j.jcyt.2013.10.016

Matluobi, D., Araghi, A., Maragheh, B. F. A., Rezabakhsh, A., Soltani, S., Khaksar, M., et al. (2018). Carvacrol Promotes Angiogenic Paracrine Potential and Endothelial Differentiation of Human Mesenchymal Stem Cells at Low Concentrations. *Microvasc. Res.* 115, 20–27. doi:10.1016/j.mvr.2017.08.003

Matsumoto, R., Shimizu, K., Nagashima, T., Tanaka, H., Mizuno, M., Kikkawa, F., et al. (2016). Plasma-activated Medium Selectively Eliminates Undifferentiated Human Induced Pluripotent Stem Cells. *Regen. Ther.* 5, 55–63. doi:10.1016/j.reth.2016.07.001

Matsumura, K., Bae, J. Y., and Hyon, S. H. (2010). Polyampholytes as Cryoprotective Agents for Mammalian Cell Cryopreservation. *Cel Transpl.* 19 (6), 691–699. doi:10.3727/096368910X508780

Mendes Oliveira, D., Grillone, K., Mignogna, C., De Falco, V., Laudanna, C., Biamonte, F., et al. (2018). Next-generation Sequencing Analysis of Receptor-type Tyrosine Kinase Genes in Surgically Resected colon Cancer: Identification of Gain-Of-Function Mutations in the RET Proto-Oncogene. *J. Exp. Clin. Cancer Res.* 37 (1), 84. doi:10.1186/s13046-018-0746-y

Miyawaki, S., Okada, Y., Okano, H., and Miura, K. (2017). Teratoma Formation Assay for Assessing Pluripotency and Tumorigenicity of Pluripotent Stem Cells. *Bio Protoc.* 7 (16), e2518. doi:10.21769/BioProtoc.2518

Nagashima, T., Shimizu, K., Matsumoto, R., and Honda, H. (2018). Selective Elimination of Human Induced Pluripotent Stem Cells Using Medium with High Concentration of L-Alanine. *Sci. Rep.* 8 (1), 12427. doi:10.1038/s41598-018-30936-2

Navin, N. E. (2015). The First Five Years of Single-Cell Cancer Genomics and beyond. *Genome Res.* 25 (10), 1499–1507. doi:10.1101/gr.191098.115

Nomura, Y., Fukui, C., Morishita, Y., and Haishima, Y. (2018). A Biological Study Establishing the Endotoxin Limit for Osteoblast and Adipocyte Differentiation of Human Mesenchymal Stem Cells. *Regen. Ther.* 8, 46–57. doi:10.1016/j.reth.2018.01.002

Pan, C.-y., Yu, S., Zhang, P.-f., Wang, B., Zhu, Z.-d., Liu, Y.-y., et al. (2017). Effect of Sucrose on Cryopreservation of Pig Spermatogonial Stem Cells. *J. Integr. Agric.* 16 (5), 1120–1129. doi:10.1016/s2095-3119(16)61489-2

Pasque, V., Karnik, R., Chronis, C., Petrella, P., Langerman, J., Bonora, G., et al. (2018). X Chromosome Dosage Influences DNA Methylation Dynamics during Reprogramming to Mouse iPSCs. *Stem Cel Rep.* 10 (5), 1537–1550. doi:10.1016/j.stemcr.2018.03.019

Patrick, E. M., Slivka, J. D., Payne, B., Comstock, M. J., and Schmidt, J. C. (2020). Observation of Processive Telomerase Catalysis Using High-Resolution Optical Tweezers. *Nat. Chem. Biol.* 16 (7), 801–809. doi:10.1038/s41589-020-0478-0

Pegg, D. E. (2015). Principles of Cryopreservation. *Methods Mol. Biol.* 1257, 3–19. doi:10.1007/978-1-4939-2193-5_1

Pilbauerová, N., and Suchánek, J. (2018). Cryopreservation of Dental Stem Cells. *Acta Med. (Hradec Kralove)* 61, 1–7. doi:10.14712/18059694.2018.16

Prigione, A., Lichtner, B., Kuhl, H., Struys, E. A., Wamelink, M., Lehrach, H., et al. (2011). Human Induced Pluripotent Stem Cells Harbor Homoplasmic and Heteroplasmic Mitochondrial DNA Mutations while Maintaining Human Embryonic Stem Cell-like Metabolic Reprogramming. *Stem Cells* 29 (9), 1338–1348. doi:10.1002/stem.683

Raju, R., Bryant, S. J., Wilkinson, B. L., and Bryant, G. (2021). The Need for Novel Cryoprotectants and Cryopreservation Protocols: Insights into the Importance

of Biophysical Investigation and Cell Permeability. *Biochim. Biophys. Acta Gen. Subj.* 1865 (1), 129749. doi:10.1016/j.bbagen.2020.129749

Rodrigues, J. P., Paraguassú-Braga, F. H., Carvalho, L., Abdelhay, E., Bouzas, L. F., and Porto, L. C. (2008). Evaluation of Trehalose and Sucrose as Cryoprotectants for Hematopoietic Stem Cells of Umbilical Cord Blood. *Cryobiology* 56 (2), 144–151. doi:10.1016/j.cryobiol.2008.01.003

Rohani, L., Johnson, A. A., Naghsh, P., Rancourt, D. E., Ulrich, H., and Holland, H. (2018). Concise Review: Molecular Cytogenetics and Quality Control: Clinical Guardians for Pluripotent Stem Cells. *Stem Cell Transl. Med* 7 (12), 867–875. doi:10.1002/sctm.18-0087

Rohner, N., Passweg, J. R., Tsakiris, D. A., Halter, J. P., Heim, D., Buser, A. S., et al. (2019). The Value of the post-thaw CD34+ Count with and without DMSO Removal in the Setting of Autologous Stem Cell Transplantation. *Transfusion* 59 (3), 1052–1060. doi:10.1111/trf.15107

Ross-Rodriguez, L. U., Elliott, J. A., and McGann, L. E. (2010). Investigating Cryoinjury Using Simulations and Experiments: 2. TF-1 Cells during Graded Freezing (Interrupted Slow Cooling without Hold Time). *Cryobiology* 61 (1), 46–51. doi:10.1016/j.cryobiol.2010.04.005

Sane, M. S., Misra, N., Mousa, O. M., Czop, S., Tang, H., Khoo, L. T., et al. (2018). Cytokines in Umbilical Cord Blood-Derived Cellular Product: a Mechanistic Insight into Bone Repair. *Regen. Med.* 13 (8), 881–898. doi:10.2217/rme-2018-0102

Sato, Y., Bando, H., Di Piazza, M., Gowing, G., Herberts, C., Jackman, S., et al. (2019). Tumorigenicity Assessment of Cell Therapy Products: The Need for Global Consensus and Points to Consider. *Cytotherapy* 21 (11), 1095–1111. doi:10.1016/j.jcyt.2019.10.001

Schlegel, P. G., Wölfl, M., Schick, J., Winkler, B., and Eyrich, M. (2009). Transient Loss of Consciousness in Pediatric Recipients of Dimethylsulfoxide (DMSO)-cryopreserved Peripheral Blood Stem Cells Independent of Morphine Co-medication. *Haematologica* 94 (10), 1473–1475. doi:10.3324/haematol.2009.009860

Schüler, S. C., Dumontier, S., Rigaux, J., and Bentzinger, C. F. (2021). Visualization of the Skeletal Muscle Stem Cell Niche in Fiber Bundles. *Curr. Protoc.* 1 (10), e263. doi:10.1002/cpz1.263

Shaliutina-Kolešová, A., Dietrich, M., Xian, M., and Nian, R. (2019). Seminal Plasma Transferrin Effects on Cryopreserved Common Carp *Cyprinus carpio* Sperm and Comparison with Bovine Serum Albumin and Antifreeze Proteins. *Anim. Reprod. Sci.* 204, 125–130. doi:10.1016/j.anireprosci.2019.03.013

Shu, Z., Heimfeld, S., and Gao, D. (2014). Hematopoietic SCT with Cryopreserved Grafts: Adverse Reactions after Transplantation and Cryoprotectant Removal before Infusion. *Bone Marrow Transpl.* 49 (4), 469–476. doi:10.1038/bmt.2013.152

Tajima, S., Tobita, M., Orbay, H., Hyakusoku, H., and Mizuno, H. (2015). Direct and Indirect Effects of a Combination of Adipose-Derived Stem Cells and Platelet-Rich Plasma on Bone Regeneration. *Tissue Eng. Part. A.* 21 (5-6), 895–905. doi:10.1089/ten.TEA.2014.0336

Tao, Y., Sanger, E., Saewu, A., and Leveille, M. C. (2020). Human Sperm Vitrification: the State of the Art. *Reprod. Biol. Endocrinol.* 18 (1), 17. doi:10.1186/s12958-020-00580-5

Tapia, N., and Schöler, H. R. (2016). Molecular Obstacles to Clinical Translation of iPSCs. *Cell Stem Cell* 19 (3), 298–309. doi:10.1016/j.stem.2016.06.017

Wang, X., Gao, J., Ouyang, X., Wang, J., Sun, X., and Lv, Y. (2018). Mesenchymal Stem Cells Loaded with Paclitaxel-Poly(lactic-Co-Glycolic Acid) Nanoparticles for Glioma-Targeting Therapy. *Int. J. Nanomedicine* 13, 5231–5248. doi:10.2147/IJN.S167142

Wang, J., Shi, X., Xiong, M., Tan, W. S., and Cai, H. (2022). Trehalose Glycopolymers for Cryopreservation of Tissue-Engineered Constructs. *Cryobiology* 104, 47–55. doi:10.1016/j.cryobiol.2021.11.004

Yagyu, S., Hoyos, V., Del Bufalo, F., and Brenner, M. K. (2015). An Inducible Caspase-9 Suicide Gene to Improve the Safety of Therapy Using Human Induced Pluripotent Stem Cells. *Mol. Ther.* 23 (9), 1475–1485. doi:10.1038/mt.2015.100

Yahata, N., Matsumoto, Y., Omi, M., Yamamoto, N., and Hata, R. (2017). TALEN-mediated Shift of Mitochondrial DNA Heteroplasmy in MELAS-iPSCs with m.13513G>A Mutation. *Sci. Rep.* 7 (1), 15557. doi:10.1038/s41598-017-15871-y

Yamatoya, K., Nagai, Y., Teramoto, N., Kang, W., Miyado, K., Nakata, K., et al. (2022). Cryopreservation of Undifferentiated and Differentiated Human Neuronal Cells. *Regen. Ther.* 19, 58–68. doi:10.1016/j.reth.2021.12.007

Yang, Y., Rossi, F. M., and Putnins, E. E. (2010). Periodontal Regeneration Using Engineered Bone Marrow Mesenchymal Stromal Cells. *Biomaterials* 31 (33), 8574–8582. doi:10.1016/j.biomaterials.2010.06.026

Yang, J., Pan, C., Zhang, J., Sui, X., Zhu, Y., Wen, C., et al. (2017). Exploring the Potential of Biocompatible Osmoprotectants as Highly Efficient Cryoprotectants. *ACS Appl. Mater. Inter.* 9 (49), 42516–42524. doi:10.1021/acsami.7b12189

Yasuda, S., and Sato, Y. (2015). Tumorigenicity Assessment of Human Cell-Processed Therapeutic Products. *Biologicals* 43 (5), 416–421. doi:10.1016/j.biologicals.2015.05.008

Yousefian, I., Emamverdi, M., Karamzadeh-Dehaghani, A., Sabzian-Melei, R., Zhandi, M., and Zare-Shahneh, A. (2018). Attenuation of Cryopreservation-Induced Oxidative Stress by Antioxidant: Impact of Coenzyme Q10 on the Quality of post-thawed Buck Spermatozoa. *Cryobiology* 81, 88–93. doi:10.1016/j.cryobiol.2018.02.005

Yuan, B. Z. (2015). Establishing a Quality Control System for Stem Cell-Based Medicinal Products in China. *Tissue Eng. Part. A.* 21 (23-24), 2783–2790. doi:10.1089/ten.TEA.2014.0498

Zare, S., Ahmadi, R., Mohammadnia, A., Nilforoushzadeh, M. A., and Mahmoodi, M. (2021). Biological Characteristics and Optical Reflectance Spectroscopy of Human Placenta Derived Mesenchymal Stem Cells for Application in Regenerative Medicine. *J. Lasers Med. Sci.* 12, e18. doi:10.34172/jlms.2021.18

Zhang, X. B., Li, K., Yau, K. H., Tsang, K. S., Fok, T. F., Li, C. K., et al. (2003). Trehalose Ameliorates the Cryopreservation of Cord Blood in a Preclinical System and Increases the Recovery of CFUs, Long-Term Culture-Initiating Cells, and Nonobese Diabetic-SCID Repopulating Cells. *Transfusion* 43 (2), 265–272. doi:10.1046/j.1537-2995.2003.00301.x

Zhang, Y., Peng, L., Xie, C., Lin, B. L., Huang, Y. S., Xie, J. Q., et al. (2011). Safety Evaluation and Quality Control of MSCs from Hepatitis B Patient *In Vitro*. *Zhonghua Gan Zang Bing Za Zhi* 19 (6), 445–449. doi:10.3760/cma.j.issn.1007-3418.2011.06.013

Zhang, Y., Wei, J., Cao, J., Zhang, K., Peng, Y., Deng, H., et al. (2022). Requirements for Human-Induced Pluripotent Stem Cells. *Cel Prolif.* e13182. doi:10.1111/cpr.13182

Conflict of Interest: HZ, XB and YL are employed by Hunan Carnation Biotechnology Co. LTD, Changsha and Hainan Nova Doctor Group Co., Ltd., Haikou. GZ and DL are employed by Hunan Sheng Bao Biological Technology Co., Ltd (in Yinfeng Biological Group., Ltd), Changsha.

The remaining authors declare that the research was conducted in the absence of any commercial or financial relationships that could be construed as a potential conflict of interest.

Publisher's Note: All claims expressed in this article are solely those of the authors and do not necessarily represent those of their affiliated organizations, or those of the publisher, the editors and the reviewers. Any product that may be evaluated in this article, or claim that may be made by its manufacturer, is not guaranteed or endorsed by the publisher.

Copyright © 2022 Xie, Ekpo, Xiao, Zhao, Bai, Liang, Zhao, Liu and Tan. This is an open-access article distributed under the terms of the Creative Commons Attribution License (CC BY). The use, distribution or reproduction in other forums is permitted, provided the original author(s) and the copyright owner(s) are credited and that the original publication in this journal is cited, in accordance with accepted academic practice. No use, distribution or reproduction is permitted which does not comply with these terms.

frontiers | Frontiers in Oncology

ORIGINAL RESEARCH
published: 10 May 2022
doi: 10.3389/fonc.2022.872502

Synergistic Radiosensitization Mediated by Chemodynamic Therapy *via* a Novel Biodegradable Peroxidases Mimicking Nanohybrid

Jun Zhang[1†], Dazhen Jiang[1†], Meng Lyu[2], Shiqi Ren[3], Yunfeng Zhou[1] and Zhen Cao[1]*

[1] Department of Radiation and Medical Oncology, Hubei Key Laboratory of Tumor Biological Behaviors, Hubei Cancer Clinical Study Center, Zhongnan Hospital of Wuhan University, Wuhan, China, [2] Key Laboratory of Artificial Micro- and Nano-Structures of Ministry of Education, School of Physics and Technology, Wuhan University, Wuhan, China, [3] BGI College & Henan Institute of Medical and Pharmaceutical Sciences, Zhengzhou University, Zhengzhou, China

Purpose: Reactive oxygen species (ROS) are practically essential in radiotherapy to damage cancer cells; however, they are always inadequate for some malignant entities. Here, we designed a biodegradable mesoporous silica decorated with hemin and glucose oxidase (GOD@Hemin-MSN) to generate a chemodynamic therapy in order to enhance the killing capacity of radiotherapy.

Methods: Mesoporous silica, as an outstanding drug carrier, can deliver hemin and glucose oxidase to the tumor site. With high level of metabolism activity, cancer cells are abundant in glucose, which can be oxidized into H_2O_2 by glucose oxidase (GOD) on site. The generated H_2O_2 is subsequently converted into intracellular ROS, especially hydroxyl radical within the tumor microenvironment, by hemin, which has mimetic peroxidase properties. By this means, the ROS can be supplemented or enriched to facilitate the killing of tumor cells.

Results: The chemodynamic therapy induced by GOD@Hemin-MSN produced quantities of ROS, which compensated for their inadequacy as a result of radiotherapy, and exhibited remarkable antitumor efficacy, with a tumor inhibition rate of 91.5% in A549 tumor-bearing mice.

Conclusion: This work has validated GOD@Hemin-MSN as a radiosensitizer in chemodynamic therapy, which showed biocompatibility and potential for translational application.

Keywords: mesoporous silica, peroxidase mimetic, reactive oxygen species, radiotherapy, chemodynamic therapy

OPEN ACCESS

Edited by:
Zeming Liu,
Huazhong University of Science and Technology, China

Reviewed by:
Xing Zhang,
University Hospital RWTH Aachen, Germany
Yang Zhu,
Fuzhou University, China

***Correspondence:**
Zhen Cao
zhencao@whu.edu.cn

[†]These authors have contributed equally to this work

Specialty section:
This article was submitted to Pharmacology of Anti-Cancer Drugs, a section of the journal Frontiers in Oncology

Received: *09 February 2022*
Accepted: *23 March 2022*
Published: *10 May 2022*

Citation:
Zhang J, Jiang D, Lyu M, Ren S, Zhou Y and Cao Z (2022) Synergistic Radiosensitization Mediated by Chemodynamic Therapy via a Novel Biodegradable Peroxidases Mimicking Nanohybrid. Front. Oncol. 12:872502. doi: 10.3389/fonc.2022.872502

INTRODUCTION

Compared with conventional enzymes, nanozymes with some enzyme-mimicking properties have exhibited multiple applications in clinical diagnosis (1–4), bioanalysis (4, 5), biosensors (6, 7), and disease treatment (8, 9), with advantages of facile synthesis, tunable catalytic activities, and high stability. Radicals including O_2^-, O_2^{2-}, OH·, and OOH·, known as reactive oxygen species (ROS),

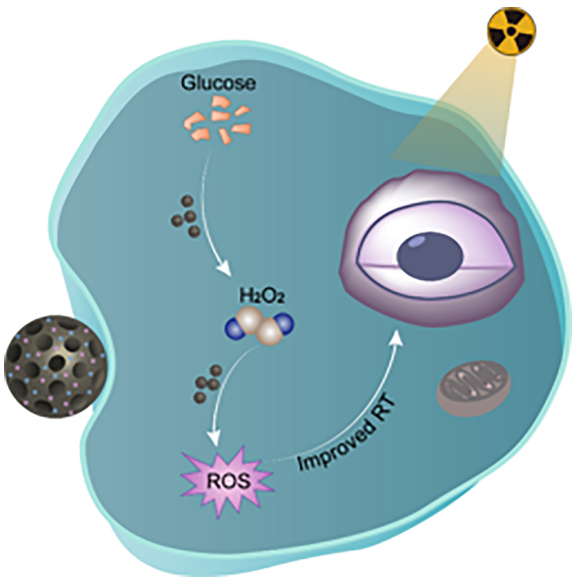
are essentially involved in many processes of cellular metabolism, and some nanozymes are capable of regulating the level of intracellular ROS, which provides possibilities for mediating ROS generation to achieve desired therapeutic outcomes in clinical practice (10, 11). The tumor microenvironment (TME) has unique characteristics including mild acidity (6, 12, 13) and an overexpressed H_2O_2 (14–16), and a highly complex TME might impair the catalytic effects of nanozymes, resulting in failure of obtaining the desired therapeutic outcomes (17, 18). On the other hand, such features could be utilized by some H_2O_2-responsive nanozymes to realize specific antitumor therapies. These nanozymes should be able to decompose H_2O_2 into ROS due to their peroxidase (POD)-mimicking properties under specific TME conditions, i.e., mildly acidic (19–21). However, the amount of intracellular H_2O_2 in tumor cells is still insufficient to generate enough ROS for achieving the desired therapeutic outcomes (22). Hence, a good way to treat tumors is to increase the level of intracellular H_2O_2 and convert it into sufficient ROS in tumor cells.

As one of the most widely used and effective treatments for local control of malignant tumors, radiotherapy (RT) still needs to be improved in many ways, especially for radiation-insensitive tumors (23, 24). Radiotherapy causes tumor cells to undergo apoptosis *via* the induction of direct and indirect damage on the DNA, with the indirect damage primarily caused by the ROS produced during the process of RT (25). Limited by the tolerable dose of adjacent normal tissues, the delivery of radiation with sufficient high dose to specific tumor sites is not always achievable, which seriously impairs the treatment efficacy of RT, especially for radiation-insensitive tumors (26–28). Improving the treatment efficacy of malignant tumors using RT still remains a prominent problem in clinical practice (29), and increasing the energy deposit of ionizing radiation in the tumor region should be a good solution (30). To this end, nano-radiosensitizers with remarkable physical and chemical properties to enhance the killing effect of radiation on tumor cells have caught the attention of radiation oncologists in recent years (22, 24), providing significant opportunities for tumor RT sensitization. Moreover, radiosensitizers with specific targeting abilities can aggregate inside tumor cells with minimal adverse effects on normal tissue cells. Some nano-radiosensitizers enhance the energy deposition on tumor tissues by taking advantage of high-*Z* elements, which improves the photoelectric effect of radiation rays (31–34). Hypoxia, as an obvious characteristic of the TME, hinders the treatment efficacy of RT, resulting in radioresistance, a category of radiosensitizers designed to focus on producing stable radicals in the TME to damage DNA (35). For example, the overexpression of H_2O_2 in the TME could be catalyzed to oxygen by nanozyme radiosensitizers such as MnO_2 (33, 36) and Pt-based nanomaterials (Yan 31, 37), among others. Besides, RT is usually combined with other therapeutic methods such as photothermal therapy (38, 39), photodynamic therapy (40, 41), and chemotherapy (42, 43) to obtain synergistic therapeutic outcomes. These radiosensitizers contribute directly or indirectly to ROS generation to induce accumulated tumor cell apoptosis, enhancing RT performance but maintaining a lower toxicity.

ROS can induce indirect tumor cell apoptosis; however, they can also be eliminated by tumor cells themselves, thereby resulting in a tumor's radioresistance (44, 45). Therefore, incremental amounts of ROS are required to overcome the radiation tolerance induced by the self-protective mechanisms of tumor cells. Here, we designed a biodegradable nanohybrid for radiosensitization by immobilizing glucose oxidize (GOD) and hemin on the surface of mesoporous silica nanospheres (MSN) to induce more production of ROS, as shown in **Scheme 1**. Initially, the nanohybrid was selectively delivered to the tumor site *via* an enhanced permeability and retention effect in the TME. Then, the GOD on the nanohybrid catalyzes intracellular glucose into sufficient H_2O_2, which is decomposed to generate incremental amounts of ROS due to the intrinsic POD enzyme-mimicking activity of hemin in order to achieve chemodynamic therapy. The carrier MSN is biodegradable *in vivo* and can be metabolized in the human body to ensure biological safety. By this means, incremental production of intracellular ROS facilitates the killing effect of ionizing radiation, with minimal damage to adjacent normal tissues.

RESULTS AND DISCUSSION

The design of the present nanohybrid includes decorating GOD and hemin on the MSN. **Figure 1A** demonstrates spherical MSN, Hemin-MSN, and GOD@Hemin-MSN. Moreover, GOD@Hemin-MSN is uniform, with an average size of approximately 190 nm according to particle size statistics (**Supplementary Figure S1**), which is consistent with the *Z*-average diameter



SCHEME 1 | Illustration of biodegradable peroxidases mimicking nanohybrid GOD@Hemin-MSN for chemodynamic therapy to realize radiosensitization.

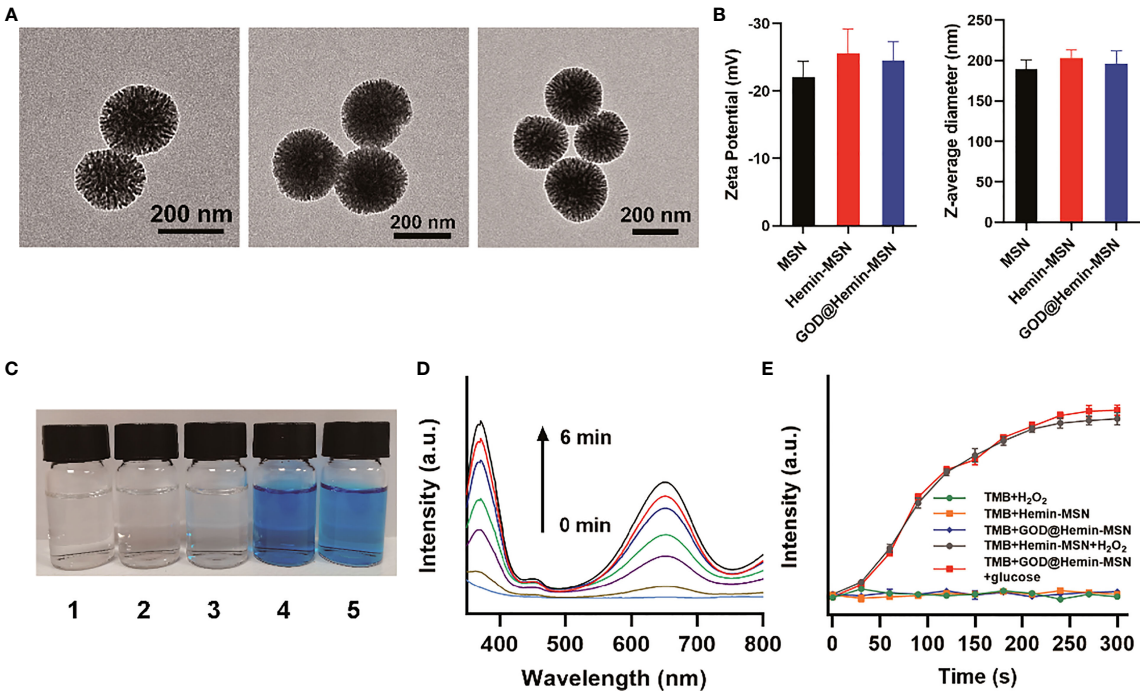


FIGURE 1 | Characterization. **(A)** TEM images of mesoporous silica nanospheres (MSN), hemin-MSN, and MSN decorated with hemin and glucose oxidase (GOD@Hemin-MSN) (*from left to right*). **(B)** Zeta potential and *Z*-average diameter measurements of MSN, hemin-MSN, and GOD@Hemin-MSN. **(C)** Images of the reaction of 3,3′,5,5′-tetramethylbenzidine (TMB) solution (0.1 mM) to (*1*) H_2O_2, (*2*) hemin-MSN, (*3*) GOD@Hemin-MSN, (*4*) hemin-MSN+H_2O_2, and (*5*) GOD@Hemin-MSN+glucose. **(D)** UV–vis spectra of the reaction of TMB solution to GOD@Hemin-MSN+glucose with time variation. **(E)** Time-dependent changes of the absorbance of TMB solution at 652 nm with various solutions.

(**Figure 1B**). In addition, no obvious changes in the zeta potential or *Z*-average diameter were observed after hemin or GOD, and hemin was immobilized on the MSN. The X-ray photoelectron spectroscopy (XPS) measurements of the Si2p orbit of GOD@Hemin-MSN in **Supplementary Figure S2** demonstrate a binding energy of 103.6 eV, confirming the existence of Si^{4+}.

Subsequently, the POD-like property of GOD@Hemin-MSN was then evaluated using 3,3′,5,5′-tetramethylbenzidine (TMB) substrate. TMB is transparent and colorless, but turns blue in the presence of both H_2O_2 and peroxidase. Comparative analyses were performed in TMB solutions with various combinations, including H_2O_2, hemin-MSN, GOD@Hemin-MSN, hemin-MSN+H_2O_2, and GOD@Hemin-MSN+glucose, as shown in **Figure 1C**. No obvious change in color was observed in TMB in the presence of H_2O_2, hemin-MSN, or GOD@Hemin-MSN, proving that they could not oxidize TMB alone. However, the TMB solution turned blue when both hemin-MSN and H_2O_2 were added, suggesting that TMB was oxidized. Similar changes could be found in the presence of GOD@Hemin-MSN and glucose. It should be noted that H_2O_2 was not added in group 5, where the oxidization of TMB occurred induced by catalyzing glucose to H_2O_2 using GOD@Hemin-MSN. Moreover, time-dependent changes in the absorbance spectra of the TMB solution in the presence of GOD@Hemin-MSN and glucose were demonstrated, shown in **Figure 1D**. The characteristic peaks of the absorbance spectra at 370 and 652 nm increased over time. Comparison experiments of TMB with various solutions are demonstrated in **Figure 1E**. Consistent with the results shown in **Figure 1C**, negligible changes were observed regarding the absorbance intensity at 652 nm in the H_2O_2, hemin-MSN, or the GOD@Hemin-MSN group. However, both hemin-MSN+H_2O_2 and GOD@Hemin-MSN+glucose exhibited remarkable catalytic activity with time variance. Moreover, we also studied the effects of temperature and pH on the POD activity of GOD@Hemin-MSN+glucose. The results are shown in **Supplementary Figure S3**. It can be inferred that 37°C was a suitable temperature for POD activity; however, the group in 50°C exhibited more obvious effects. Meanwhile, the POD activity was higher in the mildly acidic solution. These results confirmed the significant enzyme-like properties of GOD@Hemin-MSN in the conversion of glucose into ROS.

Cytotoxicity analysis was performed on a normal human lung fibroblast (NHLF) cell line using the CCK-8 assay. To assess the cytotoxicity of GOD@Hemin-MSN, we incubated NHLF cells with GOD@Hemin-MSN at various therapeutic concentrations (12.5, 25, 50, 100, 200, and 500 μg/ml); the group without any treatment was set as the control group. As shown in **Figure 2A**, the cell survival rate decreased slightly with the increase of GOD@Hemin-MSN concentration. It is notable that the cell

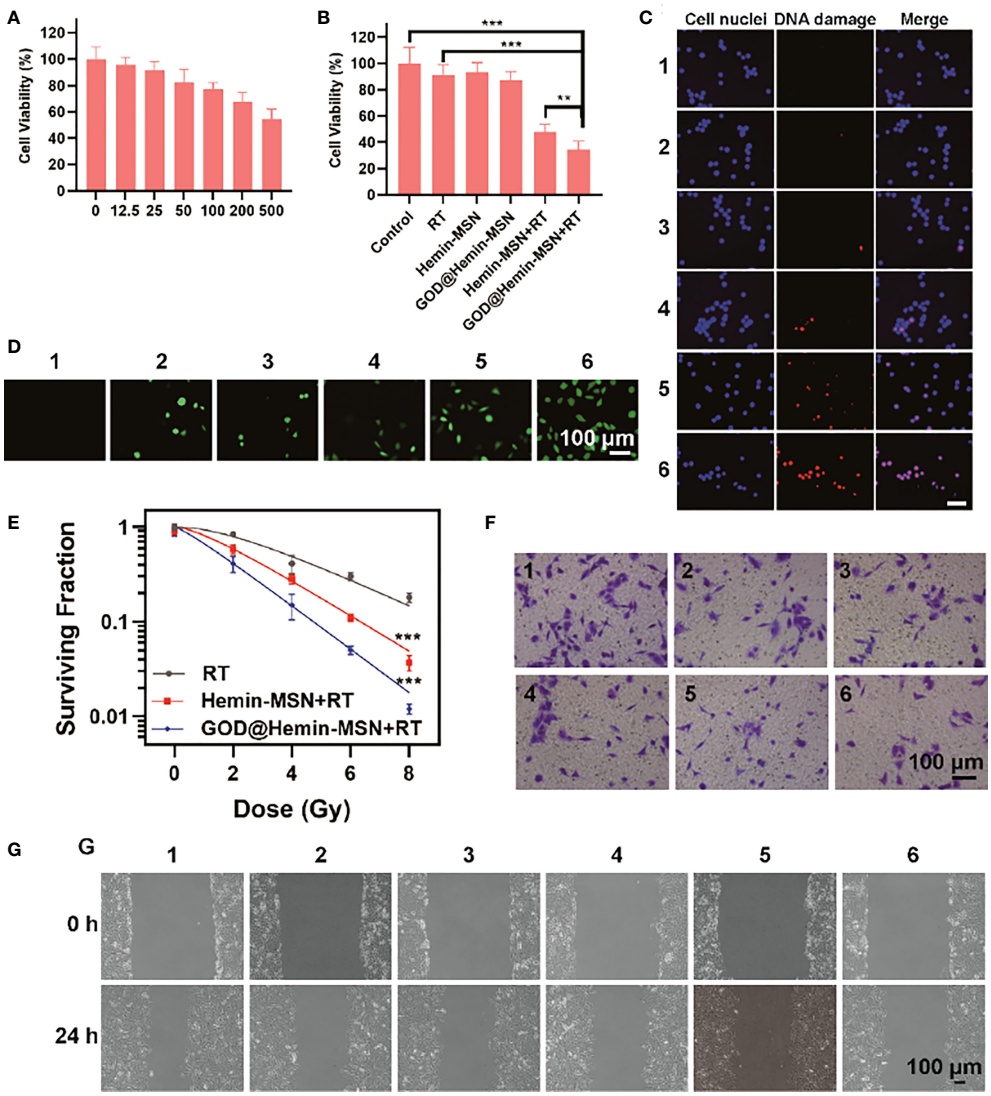


FIGURE 2 | Cell experiments. **(A)** Cell viability of normal human lung fibroblast (NHLF) cells after incubation with mesoporous silica decorated with hemin and glucose oxidase (GOD@Hemin-MSN) at various concentrations. **(B)** Cell viability of A549 cells after various treatments. **(C)** Confocal laser scanning microscopy (CLSM) images of γ-H_2AX staining. **(D)** CLSM images of reactive oxygen species (ROS) staining. **(E)** Colony formation. **(F)** Transwell experiments after various treatments. **(G)** Wounding assay. *1*, control; *2*, radiotherapy (RT); *3*, hemin-MSN; *4*, GOD@Hemin-MSN; *5*, hemin-MSN+RT; and *6*, GOD@Hemin-MSN+RT. Data are presented as the mean ± SD using one-way ANOVA with Tukey's multiple comparison tests. ***$p < 0.001$; **$p < 0.01$.

survival rate still reached more than 60% even at the highest concentration (500 μg/ml), indicating that GOD@Hemin-MSN exhibits no obvious cytotoxicity and good biocompatibility. Subsequently, to verify its killing effect on tumor cells (**Figure 2B**), A549 cells, human lung adenocarcinoma cells, were treated with 6 different treatment combinations: 1) control, 2) RT, 3) hemin-MSN, 4) GOD@Hemin-MSN, 5) hemin-MSN+RT, and 6) GOD@Hemin-MSN+RT. The RT dose was 6 Gy, and the equivalent concentration of hemin-MSN was 50 μg/ml. No obvious cytotoxicity was observed in the control, RT, and hemin-MSN treatment groups. In the hemin-MSN+RT and GOD@Hemin-MSN+RT treatment groups, however, apparent cell death was observed, while the GOD@Hemin-MSN+RT treatment group exhibited much more obvious cytotoxicity than did the hemin-MSN+RT treatment group. The confocal laser scanning microscopy (CLSM) images of the live/dead staining assay further confirmed these results (**Supplementary Figure S4**). These results indicate that GOD is capable of oxidizing glucose to produce abundant amounts of H_2O_2, which, when combined with endogenous H_2O_2, was catalyzed by hemin to produce incremental amounts of ROS, realizing chemodynamic therapy for a greater killing effect on tumor cells in addition to standard RT. We also noticed, after 6 Gy radiotherapy, that the cell killing rate of the GOD@Hemin-

MSN+RT group was significantly higher than that of RT alone, indicating that GOD@Hemin-MSN plays a synergistic role with RT and improves the therapeutic effects. DNA double-strand break (DSB) is the major form of lesion caused by RT that induces the apoptosis of tumor cells. Gamma-H_2AX (γ-H_2AX), a well-known sensitive DNA damage molecular marker, was used for fluorescence staining to indicate DSBs. As shown in **Figure 2C**, γ-H_2AX foci (red fluorescence) were observed in the cell nuclei, and remarkable amounts of DNA damage were found in the GOD@Hemin-MSN+RT group. Corresponding quantitative analysis was conducted using ImageJ software. It is worth noting that hemin-MSN with RT caused 34.4% of the γ-H_2AX foci; however, GOD@Hemin-MSN combined with RT caused 78.2% of the γ-H_2AX foci, indicating the impressive radiosensitization ability of the nanohybrid (**Supplementary Figure S5**). In order to confirm and clarify whether ROS were really produced incrementally, the cells were incubated with dichlorodihydrofluorescein diacetate (DCFH-DA) to examine the ROS production in the different groups (**Figure 2D**). The GOD@Hemin-MSN group showed green fluorescence, confirming that GOD@Hemin-MSN can consume glucose to produce H_2O_2 and, further, to generate ROS. The GOD@Hemin-MSN+RT group showed stronger fluorescence, indicating a higher ROS production. In other words, the GOD@Hemin-

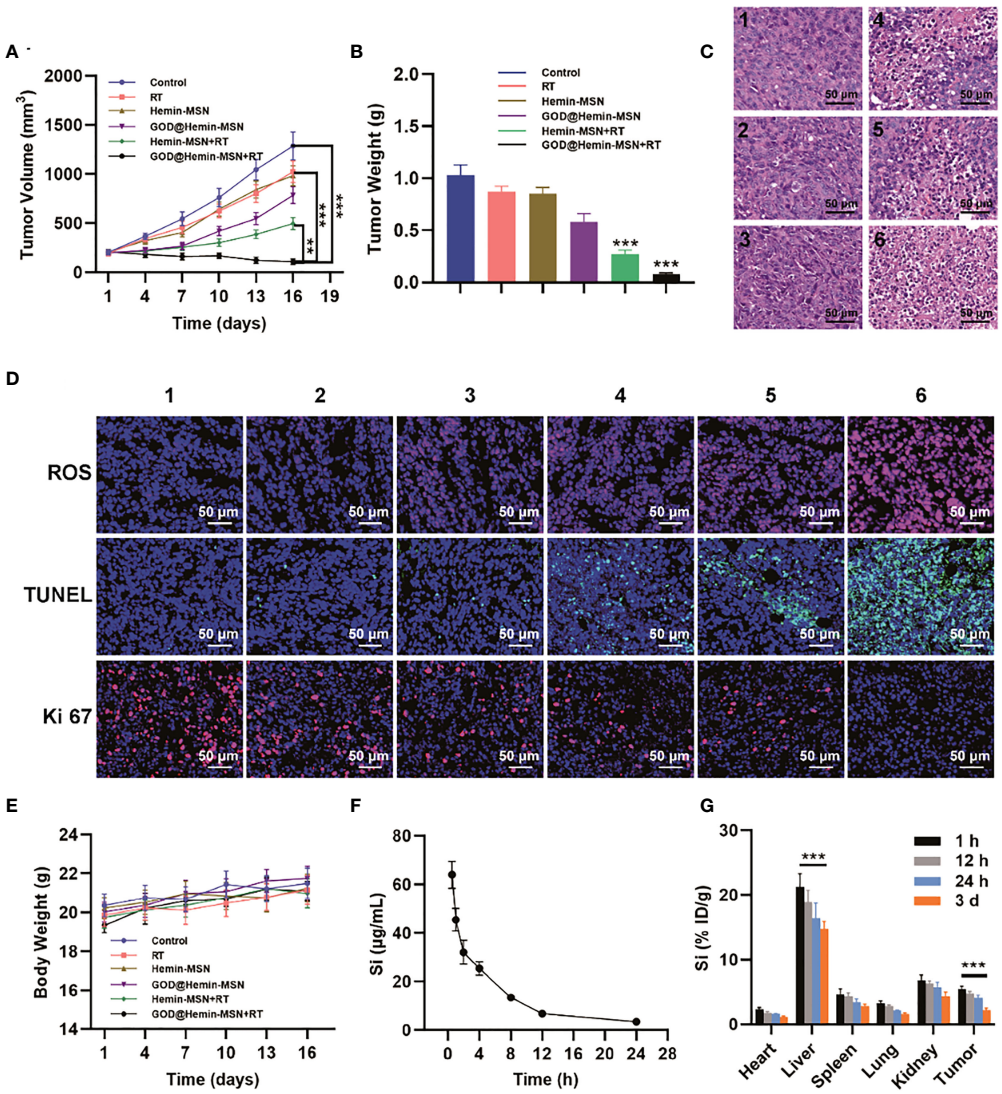


FIGURE 3 | Radiosensitization *in vivo* in tumor xenograft mice. **(A)** Tumor volume changes. **(B)** Tumor weights. **(C)** Hematoxylin–eosin (H&E) staining of the tumor slices [group *1*, control; group *2*, radiotherapy (RT); group *3*, hemin-MSN; group *4*, GOD@Hemin-MSN; group *5*, hemin-MSN+RT; and group *6*, GOD@Hemin-MSN+RT]. **(D)** Immunofluorescence staining. **(E)** Body weights in each group. **(F)** Pharmacokinetic curves. **(G)** Biodistribution at 1, 12, and 24 h and at 3 days post-injection of GOD@Hemin-MSN [the same groups as in **(C)**]. Data are presented as the mean ± SD using one-way ANOVA with Tukey's multiple comparison tests. ***$p < 0.001$; **$p < 0.01$.

MSN nanohybrid can be combined with RT to improve the therapeutic effects by producing incremental amounts of ROS. The results of colony formation are shown in **Figure 2E**. A marked inhibition of the proliferation of tumor cells was observed in the GOD@Hemin-MSN+RT group. The sensitization enhancement ratio of GOD@Hemin-MSN was calculated as 1.60, which was notably higher than that of hemin-MSN (1.32). All these results provided proof that chemodynamic therapy mediated by GOD@Hemin-MSN can substantially improve the killing efficiency of RT through more ROS production. Cell invasion occurs in the process of metastasis of malignant cells. Therefore, studying the mechanisms involved has important implications on a variety of physiological/pathological processes. The invasion and scratch experiments (**Figures 2F, G**) also showed similar results, in which the GOD@Hemin-MSN+RT group had the widest gap among all groups, indicating the strongest suppression on the invasion and the lowest cell fusion rate of A549 cells. With these data, it was deduced that GOD@Hemin-MSN can inhibit A549 cell metastasis by affecting its adhesion, invasion, and migration.

On account of the promising *in vitro* data, the *in vivo* antitumor efficacy of GOD@Hemin-MSN combined with RT was assessed on A549 tumor xenograft mice. When the tumor volume reached approximately 200 mm^3, the mice were divided equally into 6 groups and subjected to various treatments, as follows: 1) control [200 μl phosphates-buffered saline (PBS)]; 2) RT (6 Gy); 3) hemin-MSN (50 μg/ml); 4) GOD@Hemin-MSN (50 μg/ml); 5) hemin-MSN (50 μg/ml) + RT (6 Gy); and 6) GOD@Hemin-MSN (50 μg/ml) + RT (6 Gy). The day the mice were first treated was recorded as day 1. Then, every third day, the body weights and tumor volumes of the mice were monitored and recorded. All mice in the 6 groups were euthanized on day 16. As demonstrated in **Figures 3A, B** and **Supplementary Figure S6**, the tumor volume in the control group increased significantly, reaching an average of 6.3 times on day 16 compared with that on day 1. Most of the mice in the GOD@Hemin-MSN+RT group survived. The tumor volumes in the RT, hemin-MSN, and GOD@Hemin-MSN groups were moderately suppressed. Notably, mice treated with hemin-MSN+RT exhibited remarkably reduced tumor volumes, which was consistent with the results of the *in vivo* experiment, indicating that hemin-MSN imposed a synergistic killing effect when combined with RT on the tumor region; that is, it sensitized RT by producing incremental amounts of ROS. However, this synergistic effect was still restrained by the limited H_2O_2 in tumor tissues. Therefore, GOD@Hemin-MSN compensated for the shortage of H_2O_2 in the TME and exhibited a much higher synergistic damage to the tumor in mice administered with GOD@Hemin-MSN followed by RT, achieving tumor inhibition rates as high as 91.5%. Hematoxylin–eosin (H&E) staining (**Figure 3C**) of the tumor tissue sections of each group also further confirmed our conclusion, as it could be seen that there were significant and abundant areas of necrosis and nuclear pyknosis in the tumor tissues of the GOD@Hemin-MSN+RT

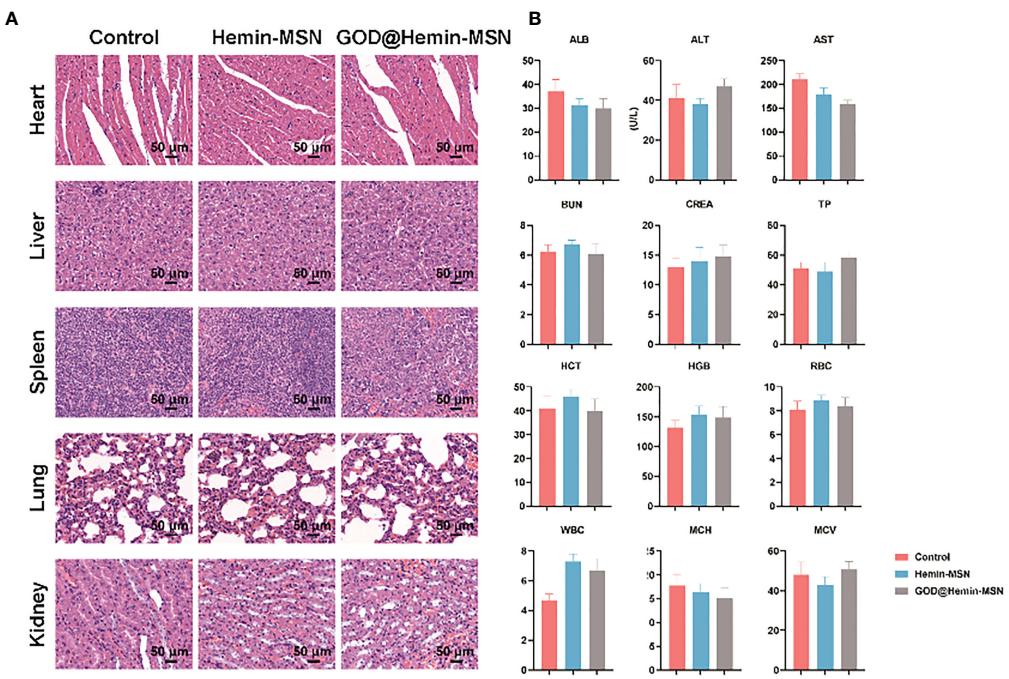


FIGURE 4 | **(A)** Light views of the main organs (heart, liver, spleen, lung, and kidney) with hematoxylin–eosin (H&E) staining. **(B)** Detection of the blood biochemical indicators. ALB, Albumin; ALT, Alanine aminotransferase; AST, Aspartate aminotransferase; BUN, Blood urea nitrogen; CREA, Creatinine; TP, Total protein; HCT, Hematocrit; HGB, Hemoglobin; RBC, Red blood cell; WBC, White blood cell; MCH, Mean corpuscular hemoglobin; MCV, Mean corpuscular volume.

group. As shown in **Figure 3D**, the strongest green fluorescence was observed in tumor specimens of the GOD@Hemin-MSN +RT group. The underlying mechanism can be explained as follows: GOD on the GOD@Hemin-MSN nanohybrid catalyzed the intracellular glucose to produce abundant H_2O_2, which was subsequently catalyzed by hemin to produce incremental amounts of ROS. On the other hand, with the presence of GOD@Hemin-MSN, the ROS produced by ionizing radiation can also be further enhanced, leading to a spike in the ROS levels in the tumor region. Ki-67 and terminal deoxynucleotidyl transferase dUTP nick-end labeling (TUNEL) assays of the tumor tissue specimens of the GOD@Hemin-MSN+RT group further confirmed the enhanced killing efficiency, as indicated by the remarkable proliferation inhibition and tumor cell apoptosis *in vivo*. All treatment methods exhibited no obvious influence on the body weight of mice in all groups within 16 days, as shown in **Figure 3E**. The pharmacokinetic curves in **Figure 3F** demonstrated a blood circulation half-life of GOD@Hemin-MSN of approximately 2.1 h. However, the concentration of Si dropped to 3.5 μg/ml at 24 h post-injection, indicating that GOD@Hemin-MSN was metabolized quickly. The major accumulation of GOD@Hemin-MSN was observed in the kidney and liver at 24 h post-injection, revealing the renal and liver clearance pathway of GOD@Hemin-MSN **(Figure 3G)**. With this method, GOD@Hemin-MSN could be a promising radiosensitizer administered with standard precise intensity-modulated radiotherapy (IMRT) to improve treatment effects or overcome radioresistant tumors for better therapeutic clinical outcomes, such as for the treatment of cancers impossible to be cured by standard RT, although this still needs to be validated in clinical trials.

The biocompatibility of the GOD@Hemin-MSN nanohybrid *in vivo* will be the major concern before it becomes clinically practicable. The main organs including the heart, liver, spleen, lung, and kidney of mice administered PBS, hemin-MSN, and GOD@Hemin-MSN were collected for observation with H&E staining (**Figure 4A**). There was no significant variance in the morphology of all the main organs in the three groups observed, indicating the satisfactory histocompatibility of hemin-MSN and GOD@Hemin-MSN. Peripheral blood was also collected from each group for routine blood biochemical test. As shown in **Figure 4B**, no significant difference was found for all blood indicators among the three groups. The results indicate that the GOD@Hemin-MSN nanohybrid and its synergistic RT sensitization strategy are highly biocompatible.

CONCLUSION

The radioresistance of tumors can sometimes account for the self-clearance of ROS by the tumor cells themselves, which hinders the therapeutic efficacy of RT clinically. POD-like enzymes can catalyze overexpressed H_2O_2 in the TME, which, however, is always insufficient to produce enough ROS to damage the target DNA. We successfully synthesized a novel nanohybrid, GOD@Hemin-MSN, with proven biosafety and biodegradability. GOD@Hemin-MSN can be delivered inside tumor cells and catalyze oxidized glucose to produce abundant H_2O_2. The H_2O_2 is then converted into sufficient ROS to induce chemodynamic therapy, which synergistically works with the direct and indirect DNA damage of RT to perform the killing of tumor cells more efficiently. Our data from both *in vitro* and *in vivo* experiments suggest that GOD@Hemin-MSN overcomes the shortcomings of a standard RT and could be a promising radiosensitization strategy in clinical practice to reverse radioresistance or provide a more efficient therapy for cancer, but with minimal damage to adjacent normal tissues.

DATA AVAILABILITY STATEMENT

The original contributions presented in the study are included in the article/**Supplementary Material**. Further inquiries can be directed to the corresponding author.

ETHICS STATEMENT

All experiments complied with the ethical standards in the Declaration of Helsinki and approved by the Ethics Committee of Zhongnan Hospital of Wuhan University. The animal experiment was permitted by the Institutional Animal Care and Use Committee of Wuhan University. The animal study was reviewed and approved by the Ethics Committee of Zhongnan Hospital of Wuhan University.

AUTHOR CONTRIBUTIONS

JZ and DJ made substantial contributions to the study concept and design, data analysis and interpretation, and the first draft of manuscript. ZC participated in study design and data analysis, drafting and revising the manuscript, had full access to all of the data in the study and take responsibility for the integrity and the accuracy of the data. ML made substantial contributions to the preparation of experimental materials and discussion of experimental puzzles. SR made substantial contributions to assembling of nanohybrid. YZ made substantial revisions to the manuscript. All authors contributed to the article and approved the submitted version.

SUPPLEMENTARY MATERIAL

The Supplementary Material for this article can be found online at: https://www.frontiersin.org/articles/10.3389/fonc.2022.872502/full#supplementary-material

REFERENCES

1. Yu Z, Lou R, Pan W, Li N, Tang B. Nanoenzymes in Disease Diagnosis and Therapy. *Chem Commun* (2020) 56(99):15513–24. doi: 10.1039/D0CC05427E
2. Cong C, He Y, Zhao S, Zhang X, Li L, Wang D, et al. Diagnostic and Therapeutic Nanoenzymes for Enhanced Chemotherapy and Photodynamic Therapy. *J Mater Chem B* (2021) 9(18):3925–34. doi: 10.1039/D0TB02791J
3. Sun P, Hai J, Sun S, Lu S, Liu S, Liu H, et al. Aqueous Stable Pd Nanoparticles/Covalent Organic Framework Nanocomposite: An Efficient Nanoenzyme for Colorimetric Detection and Multicolor Imaging of Cancer Cells. *Nanoscale* (2020) 12(2):825–31. doi: 10.1039/C9NR08486J
4. Li Y, Zhou J, Wang L, Xie Z. Endogenous Hydrogen Sulfide-Triggered MOF-Based Nanoenzyme for Synergic Cancer Therapy. *ACS Appl Mater Interfaces* (2020) 12(27):30213–20. doi: 10.1021/acsami.0c08659
5. Wang X, Qin L, Zhou M, Lou Z, Wei H. Nanozyme Sensor Arrays for Detecting Versatile Analytes From Small Molecules to Proteins and Cells. *Anal Chem* (2018) 90(19):11696–702. doi: 10.1021/acs.analchem.8b03374
6. Hu J, Tang F, Wang L, Tang M, Jiang Y-Z, Liu C. Nanozyme Sensor Based-on Platinum-Decorated Polymer Nanosphere for Rapid and Sensitive Detection of Salmonella Typhimurium With the Naked Eye. *Sensors Actuators B: Chem* (2021) 346:130560. doi: 10.1016/j.snb.2021.130560
7. Karim M, Anderson SR, Singh S, Ramanathan R, Bansal V. Nanostructured Silver Fabric as a Free-Standing NanoZyme for Colorimetric Detection of Glucose in Urine. *Biosens Bioelectron* (2018) 110:8–15. doi: 10.1016/j.bios.2018.03.025
8. Wang D, Wu H, Phua SZF, Yang G, Lim WQ, Gu L, et al. Self-Assembled Single-Atom Nanozyme for Enhanced Photodynamic Therapy Treatment of Tumor. *Nat Commun* (2020) 11(1):357. doi: 10.1038/s41467-019-14199-7
9. Fan K, Xi J, Fan L, Wang P, Zhu C, Tang Y, et al. *In Vivo* Guiding Nitrogen-Doped Carbon Nanozyme for Tumor Catalytic Therapy. *Nat Commun* (2018) 9(1):1440. doi: 10.1038/s41467-018-03903-8
10. Weinberg F, Ramnath N, Nagrath D. Reactive Oxygen Species in the Tumor Microenvironment: An Overview. *Cancers* (2019) 11(8):1191. doi: 10.3390/cancers11081191
11. Lennicke C, Cochemé HM. Redox Metabolism: ROS as Specific Molecular Regulators of Cell Signaling and Function. *Mol Cell* (2021) 81(18):3691–707. doi: 10.1016/j.molcel.2021.08.018
12. Zhu Y, Shi H, Li T, Yu J, Guo Z, Cheng J, et al. A Dual Functional Nanoreactor for Synergistic Starvation and Photodynamic Therapy. *ACS Appl Mater Interfaces* (2020) 12(16):18309–18. doi: 10.1021/acsami.0c01039
13. Zhang X, Machuki JO, Pan W, Cai W, Xi Z, Shen F, et al. Carbon Nitride Hollow Theranostic Nanoregulators Executing Laser-Activatable Water Splitting for Enhanced Ultrasound/Fluorescence Imaging and Cooperative Phototherapy. *ACS Nano* (2020) 14(4):4045–60. doi: 10.1021/acsnano.9b08737
14. Zhu Y, Wang W, Cheng J, Qu Y, Dai Y, Liu M, et al. Stimuli-Responsive Manganese Single-Atom Nanozyme for Tumor Therapy via Integrated Cascade Reactions. *Angew Chem Int Ed* (2021) 60(17):9480–8. doi: 10.1002/anie.202017152
15. Lyu M, Chen M, Liu L, Zhu D, Wu X, Li Y, et al. A Platelet-Mimicking Theranostic Platform for Cancer Interstitial Brachytherapy. *Theranostics* (2021) 11(15):7589–99. doi: 10.7150/thno.61259
16. Chen H, Zheng D, Pan W, Li X, Lv B, Gu W, et al. Biomimetic Nanotheranostics Camouflaged With Cancer Cell Membranes Integrating Persistent Oxygen Supply and Homotypic Targeting for Hypoxic Tumor Elimination. *ACS Appl Mater Interfaces* (2021) 13(17):19710–25. doi: 10.1021/acsami.1c03010
17. Whiteside TL. The Tumor Microenvironment and its Role in Promoting Tumor Growth. *Oncogene* (2008) 27(45):5904–12. doi: 10.1038/onc.2008.271
18. Panieri E, Santoro MM. ROS Homeostasis and Metabolism: A Dangerous Liason in Cancer Cells. *Cell Death Dis* (2016) 7(6):e2253–3. doi: 10.1038/cddis.2016.105
19. Jiang B, Duan D, Gao L, Zhou M, Fan K, Tang Y, et al. Standardized Assays for Determining the Catalytic Activity and Kinetics of Peroxidase-Like Nanozymes. *Nat Protoc* (2018) 13(7):1506–20. doi: 10.1038/s41596-018-0001-1
20. Liu X, Liu Z, Dong K, Wu S, Sang Y, Cui T, et al. Tumor-Activatable Ultrasmall Nanozyme Generator for Enhanced Penetration and Deep Catalytic Therapy. *Biomaterials* (2020) 258:120263. doi: 10.1016/j.biomaterials.2020.120263
21. Wu X, Chen T, Wang J, Yang G. Few-Layered MoSe2 Nanosheets as an Efficient Peroxidase Nanozyme for Highly Sensitive Colorimetric Detection of H2O2 and Xanthine. *J Mater Chem B* (2018) 6(1):105–11. doi: 10.1039/C7TB02434G
22. Jarosz-Biej M, Smolarczyk R, Cichoń T, Kułach N. Tumor Microenvironment as A "Game Changer" in Cancer Radiotherapy. *Int J Mol Sci* (2019) 20(13):3212. doi: 10.3390/ijms20133212
23. Chen Q, Chen J, Yang Z, Xu J, Xu L, Liang C, et al. Nanoparticle-Enhanced Radiotherapy to Trigger Robust Cancer Immunotherapy. *Adv Mater* (2019) 31(10):1802228. doi: 10.1002/adma.201802228
24. Laprise-Pelletier M, Simão T, Fortin M. Gold Nanoparticles in Radiotherapy and Recent Progress in Nanobrachytherapy. *Adv Healthcare Mater* (2018) 7(16):1701460. doi: 10.1002/adhm.201701460
25. Lomax ME, Folkes LK, O'Neill P. Biological Consequences of Radiation-Induced DNA Damage: Relevance to Radiotherapy. *Clin Oncol* (2013) 25(10):578–85. doi: 10.1016/j.clon.2013.06.007
26. Eisbruch A, Harris J, Garden AS, Chao CKS, Straube W, Harari PM, et al. Multi-Institutional Trial of Accelerated Hypofractionated Intensity-Modulated Radiation Therapy for Early-Stage Oropharyngeal Cancer (RTOG 00-22). *Int J Radiat Oncol Biol Physics* (2010) 76(5):1333–8. doi: 10.1016/j.ijrobp.2009.04.011
27. Martens C, Reynaert N, De Wagter C, Nilsson P, Coghe M, Palmans H, et al. Underdosage of the Upper-Airway Mucosa for Small Fields as Used in Intensity-Modulated Radiation Therapy: A Comparison Between Radiochromic Film Measurements, Monte Carlo Simulations, and Collapsed Cone Convolution Calculations. *Med Phys* (2002) 29(7):1528–35. doi: 10.1118/1.1487421
28. Guckenberger M, Richter A, Wilbert J, Flentje M, Partridge M. Adaptive Radiotherapy for Locally Advanced Non–Small-Cell Lung Cancer Does Not Underdose the Microscopic Disease and has the Potential to Increase Tumor Control. *Int J Radiat Oncol Biol Physics* (2011) 81(4):e275–e2825. doi: 10.1016/j.ijrobp.2011.01.067
29. Castelli J, Simon A, Lafond C, Perichon N, Rigaud B, Chajon E, et al. Adaptive Radiotherapy for Head and Neck Cancer. *Acta Oncol* (2018) 57(10):1284–92. doi: 10.1080/0284186X.2018.1505053
30. Sasieni PD, Sawyer EJ. Reply to 'Intraoperative Radiotherapy for Breast Cancer: Powerful Evidence to Change Practice'. *Nat Rev Clin Oncol* (2021) 18(3):188–9. doi: 10.1038/s41571-021-00472-6
31. Li Y, Yun K-H, Lee H, Goh S-H, Suh Y-G, Choi Y. Porous Platinum Nanoparticles as a High-Z and Oxygen Generating Nanozyme for Enhanced Radiotherapy *In Vivo*. *Biomaterials* (2019) 197:12–9. doi: 10.1016/j.biomaterials.2019.01.004
32. Ding Y, Sun Z, Tong Z, Zhang S, Min J, Xu Q, et al. Tumor Microenvironment-Responsive Multifunctional Peptide Coated Ultrasmall Gold Nanoparticles and Their Application in Cancer Radiotherapy. *Theranostics* (2020) 10(12):5195–208. doi: 10.7150/thno.45017
33. Yi X, Chen L, Zhong X, Gao R, Qian Y, Wu F, et al. Core–Shell Au@MnO2 Nanoparticles for Enhanced Radiotherapy *via* Improving Tumor Oxygenation. *Nano Res* (2016) 9(11):3267–78. doi: 10.1007/s12274-016-1205-8
34. Cheng X, Yong Y, Dai Y, Song X, Yang G, Pan Y, et al. Enhanced Radiotherapy Using Bismuth Sulfide Nanoagents Combined With Photo-Thermal Treatment. *Theranostics* (2017) 7(17):4087–98. doi: 10.7150/thno.20548
35. Fan W, Bu W, Zhang Z, Shen B, Zhang H, He Q, et al. X-Ray Radiation-Controlled NO-Release for On-Demand Depth-Independent Hypoxic Radiosensitization. *Angew Chem Int Ed* (2015) 54(47):14026–140305. doi: 10.1002/anie.201504536
36. Sujai PT, Shamjith S, Joseph MM, Maiti KK. Elucidating Gold–MnO2 Core–Shell Nanoenvelope for Real Time SERS-Guided Photothermal Therapy on Pancreatic Cancer Cells. *ACS Appl Bio Mater* (2021) 4(6):4962–72. doi: 10.1021/acsabm.1c00241
37. Li S, Sun W, Luo Y, Gao Y, Jiang X, Yuan C, et al. Hollow PtCo Alloy Nanospheres as a High-Z and Oxygen Generating Nanozyme for Radiotherapy Enhancement in Non-Small Cell Lung Cancer. *J Mater Chem B* (2021) 9(23):4643–53. doi: 10.1039/D1TB00486G
38. Kuang Y, Zhang Y, Zhao Y, Cao Y, Zhang Y, Chong Y, et al. Dual-Stimuli-Responsive Multifunctional Gd2Hf2O7 Nanoparticles for MRI-Guided

Combined Chemo-/Photothermal-/Radiotherapy of Resistant Tumors. *ACS Appl Mater Interfaces* (2020) 12(32):35928–39. doi: 10.1021/acsami.0c09422
39. Yong Y, Cheng X, Bao T, Zu M, Yan L, Yin W, et al. Tungsten Sulfide Quantum Dots as Multifunctional Nanotheranostics for In Vivo Dual-Modal Image-Guided Photothermal/Radiotherapy Synergistic Therap. *ACS Nano* (2015) 9(12):12451–63. doi: 10.1021/acsnano.5b05825
40. Wang GD, Nguyen H, Chen H, Cox PB, Wang L, Nagata K, et al. X-Ray Induced Photodynamic Therapy: A Combination of Radiotherapy and Photodynamic Therapy. *Theranostics* (2016) 6(13):2295–305. doi: 10.7150/thno.16141
41. Zhang M, Cui Z, Song R, Lv B, Tang Z, Meng X, et al. SnWO4-Based Nanohybrids With Full Energy Transfer for Largely Enhanced Photodynamic Therapy and Radiotherapy. *Biomaterials* (2018) 155:135–44. doi: 10.1016/j.biomaterials.2017.11.013
42. Zhang L, Su H, Wang H, Li Q, Li X, Zhou C, et al. Tumor Chemo-Radiotherapy With Rod-Shaped and Spherical Gold Nano Probes: Shape and Active Targeting Both Matter. *Theranostics* (2019) 9(7):1893–908. doi: 10.7150/thno.30523
43. Gao S, Li T, Guo Y, Sun C, Xianyu B, Xu H. Selenium-Containing Nanoparticles Combine the NK Cells Mediated Immunotherapy With Radiotherapy and Chemotherapy. *Adv Mater* (2020) 32(12):1907568. doi: 10.1002/adma.201907568
44. Meng L, Cheng Y, Tong X, Gan S, Ding Y, Zhang Y, et al. Tumor Oxygenation and Hypoxia Inducible Factor-1 Functional Inhibition via React Oxygen Species Responsive Nanoplatform Enhancing Radiat Ther Abscopal Effects. *ACS Nano* (2018) 12(8):8308–22. doi: 10.1021/acsnano.8b03590
45. Bian P, Zhang J, Wang J, Yang J, Wang J, Liu H, et al. Enhanced Catalysis of Ultrasmall Au-MoS2 Clusters Against Reactive Oxygen Species for Radiation Protection. *Sci Bull* (2018) 63(14):925–4. doi: 10.1016/j.scib.2018.05.008

Conflict of Interest: The authors declare that the research was conducted in the absence of any commercial or financial relationships that could be construed as a potential conflict of interest.

Publisher's Note: All claims expressed in this article are solely those of the authors and do not necessarily represent those of their affiliated organizations, or those of the publisher, the editors and the reviewers. Any product that may be evaluated in this article, or claim that may be made by its manufacturer, is not guaranteed or endorsed by the publisher.

Copyright © 2022 Zhang, Jiang, Lyu, Ren, Zhou and Cao. This is an open-access article distributed under the terms of the Creative Commons Attribution License (CC BY). The use, distribution or reproduction in other forums is permitted, provided the original author(s) and the copyright owner(s) are credited and that the original publication in this journal is cited, in accordance with accepted academic practice. No use, distribution or reproduction is permitted which does not comply with these terms.

frontiers | Frontiers in Pharmacology

MINI REVIEW
published: 11 May 2022
doi: 10.3389/fphar.2022.905375

Nucleus-Targeting Phototherapy Nanodrugs for High-Effective Anti-Cancer Treatment

Xingyu Long[1†], Xiaojie Zhang[1†], Qiaohui Chen[1], Min Liu[2,3], Yuting Xiang[1], Yuqi Yang[2,3], Zuoxiu Xiao[1,4], Jia Huang[1,4], Xiaoyuan Wang[1,4], Chong Liu[5,6], Yayun Nan[7] and Qiong Huang[2,3]**

[1]Xiangya School of Pharmaceutical Sciences, Central South University, Changsha, China, [2]Department of Pharmacy, Xiangya Hospital, Central South University, Changsha, China, [3]National Clinical Research Center for Geriatric Disorders, Xiangya Hospital, Central South University, Changsha, China, [4]Hunan Provincial Key Laboratory of Cardiovascular Research, Xiangya School of Pharmaceutical Sciences, Central South University, Changsha, China, [5]Departments of Clinical Pharmacology and Pharmacy, Hunan Key Laboratory of Pharmacogenetics, and National Clinical Research Center for Geriatric Disorders, Xiangya Hospital, Central South University, Changsha, China, [6]Engineering Research Center of Applied Technology of Pharmacogenomics, Institute of Clinical Pharmacology, Ministry of Education, Central South University, Changsha, China, [7]Geriatric Medical Center, People's Hospital of Ningxia Hui Autonomous Region, Yinchuan, China

OPEN ACCESS

Edited by:
Zeming Liu,
Huazhong University of Science and Technology, China

Reviewed by:
Huaxun Wu,
Anhui Medical University, China
Wenbing Dai,
Peking University, China

***Correspondence:**
Qiong Huang
qionghuang@csu.edu.cn
Chong Liu
lclchong@hotmail.com

[†]These authors have contributed equally to this work

Specialty section:
This article was submitted to Pharmacology of Anti-Cancer Drugs, a section of the journal Frontiers in Pharmacology

Received: *27 March 2022*
Accepted: *19 April 2022*
Published: *11 May 2022*

Citation:
Long X, Zhang X, Chen Q, Liu M, Xiang Y, Yang Y, Xiao Z, Huang J, Wang X, Liu C, Nan Y and Huang Q (2022) Nucleus-Targeting Phototherapy Nanodrugs for High-Effective Anti-Cancer Treatment. Front. Pharmacol. 13:905375. doi: 10.3389/fphar.2022.905375

DNA is always one of the most important targets for cancer therapy due to its leading role in the proliferation of cancer cells. Phototherapy kills cancer cells by generating reactive oxygen species (ROS) and local hyperthermia under light. It has attracted extensive interest in the clinical treatment of tumors because of many advantages such as non-invasiveness, high patient compliance, and low toxicity and side effects. However, the short ROS diffusion distance and limited thermal diffusion rate make it difficult for phototherapy to damage DNA deep in the nucleus. Therefore, nucleus-targeting phototherapy that can destroy DNAs *via in-situ* generation of ROS and high temperature can be a very effective strategy to address this bottleneck. Recently, some emerging nucleus-targeting phototherapy nanodrugs have demonstrated extremely effective anticancer effects. However, reviews in the field are still rarely reported. Here, we comprehensively summarized recent advances in nucleus-targeting phototherapy in recent years. We classified nucleus-targeting phototherapy into three categories based on the characteristics of these nucleus-targeting strategies. The first category is the passive targeting strategy, which mainly targets the nucleus by adjusting the physicochemical characteristics of phototherapy nanomedicines. The second category is to mediate the phototherapy nanodrugs into the nucleus by modifying functional groups that actively target the nucleus. The third category is to assist nanodrugs enter into the nucleus in a light-controlled way. Finally, we provided our insights and prospects for nucleus-targeting phototherapy nanodrugs. This minireview provides unique insights and valuable clues in the design of phototherapy nanodrugs and other nucleus-targeting drugs.

Keywords: nucleus-targeting, photodynamic therapy, photothermal therapy, nanomaterials, subcellular organelle

INTRODUCTION

Currently, cancer has surpassed cardiovascular disease as the leading cause of death in many countries (Bray et al., 2018). In the United States, 1,918,030 new cancer cases and 609,360 cancer deaths are projected to occur in 2022 (Siegel et al., 2022). The uncontrolled proliferation of cancer cells is the most striking difference between cancer cells and normal cells (Hanahan, 2022). Destroying the DNA of cancer cells can very effectively inhibit the proliferation of cancer cells (Srinivas et al., 2019). Currently, a variety of anticancer drugs for DNA have been developed and occupied a prominent position in the treatment of cancer, many of which have become the first-line drugs, such as doxorubicin (DOX), cisplatin, and cyclophosphamide (Costoya et al., 2022; Jelinek and Zuchnicka, 2020; Li et al., 2021). Nonetheless, these drugs still have significant limitations in the treatment of cancer. DNA is deeply hidden in the nucleus of the cancer cell, and many drugs targeting DNA must pass through a series of barriers, such as the cytoplasmic membrane, lysosome, and nuclear membrane before entering the nucleus, making a large problem for drug delivery. In fact, only about 1–4% of cisplatin entered the nucleus after cellular internalization and even less (0.4%) of DOX entered the nucleus (Yu Cao et al., 2019; Lasorsa et al., 2019), which inevitably cause some serious side effects and poor prognosis.

DNA is easily destroyed by reactive oxygen species (ROS) with strong nucleophilic activity because the bases of DNA are electrophilic (Srinivas et al., 2019). In addition, DNA is composed of a pair of single strands through Watson-Crick base pairing, and the unique structure is prone to high temperature (Chen et al., 2019; Pan et al., 2018). Phototherapy, mainly divided into photothermal therapy (PTT) and photodynamic therapy (PDT) (Gao et al., 2020), can efficiently damage DNA through ROS and local high temperature generated by photosensitizer (PS) under light irradiation (Chen et al., 2021; Wang et al., 2021). Phototherapy offers higher levels of patient compliance and medical safety thanks to its high selectivity and minimal invasiveness (Hailong Yang et al., 2021). Nevertheless, the "short-life" ROS and limited heat transfer rate greatly compromise the therapeutic effects of phototherapy (Deng et al., 2021; Chen et al., 2022; Zhao et al., 2022). Therefore, DNA-rich nucleus, as the central governor and an organelle that is most susceptible to ROS and high temperature is the ideal target for phototherapy (Jiang et al., 2020). Due to the central regulation of nucleus, nucleus-targeting phototherapy has better anticancer potential than other subcellular organelle-targeting phototherapy. However, the delivery of PS to the nucleus faces significant obstacles (Zhu et al., 2018; Rennick et al., 2021). The nucleus is wholly enclosed by a double nuclear membrane which hinders the connection between the nucleus and cytoplasm. But the nucleus is not completely isolated from the cytoplasm for the nuclear pore complexes (NPCs) embedded in the nuclear membrane mediate material exchange and information transfer. NPC is a hydrophilic channel with a nuclear pore of ~39 nm (Zhen et al., 2021), through which hydrophilic small molecules can be diffused into the nucleus (Zimmerli et al., 2021). However, most biomacromolecules are difficult to enter the nucleus *via* passive diffusion due to their large size. Instead, they need to be recognized by nucleoporins and then enter or exit the nucleus (Shiyi Qin et al., 2021). From this perspective, PSs need to have both small size and hydrophilicity or be modified by the nuclear-driven molecule in order to enter the nucleus. As a matter of fact, most PS agents, such as porphyrin, chlorin e6 (Ce6), phthalocyanines, are hydrophobic and cannot penetrate the nuclear membrane to reach the interior of cancer cell nuclei (Chinna Ayya Swamy et al., 2020; Lo et al., 2020; Zhang et al., 2021). Fortunately, nanotechnology offers a huge opportunity to address the nucleus-targeting bottleneck of PSs (Xie et al., 2020). Recently, some emerging nucleus-targeting phototherapeutic nanodrugs have demonstrated far higher anti-tumor effects than traditional DNA-targeting drugs. Phototherapeutic nanodrugs can be passively targeted to the nucleus by changing surface properties and size because of the highly physicochemical flexibility of nanomaterials (Jiang et al., 2020; Xu et al., 2020). More importantly, active targeting of the nucleus can also be achieved by modifying nucleus-targeting groups such as cell-penetrating peptides [e.g., transactivator of transcription (TAT)] (Su et al., 2020; Tietz et al., 2022), the specific nuclear localization signal/sequence (NLS) peptide (Zelmer et al., 2020; Drescher et al., 2021), and DNA aptamers (Dong et al., 2018; Yang et al., 2018; Zeng et al., 2020) on phototherapeutic nanodrugs. Apart from this, ROS generated by phototherapeutic nanodrugs can also damage the membrane structure to increase permeability (Chen et al., 2021; Su et al., 2021; Chen et al., 2022). Subsequently, the phototherapeutic nanodrugs can remove barriers from lysosomal trapping and nuclear pore restriction, and finally enter the nucleus (Yuanyuan Qin et al., 2021). Currently, nucleus-targeting phototherapeutic nanodrugs have sparked extensive interest in the field of oncotherapy, but sadly, there were few relevant reviews. Herein, we reviewed the latest progress of nucleus-targeting phototherapeutic nanodrugs for cancer treatment based on improving PDT and PTT efficiency. We detailed the design strategies of nuclear passively and actively targeted nanodrugs and discussed future directions and application prospects of nucleus-targeting nanodrugs in tumor therapy (**Figure 1**; **Table 1**). This mini-review provides novel insights for tumor treatment and promotes the clinical application of PDT and PTT.

PASSIVE NUCLEUS-TARGETING NANODRUGS

In order to facilitate the transport of macromolecules such as proteins and RNAs between the cytoplasm and the nucleus, the nuclear membrane maintains some pores that allow the passage of hydrophilic molecules smaller than 39 nm (Panagaki et al., 2021). Theoretically, nanodrugs with dimensions smaller than 39 nm and hydrophilicity have the potential for passive nuclear targeting (Fu et al., 2020). Carbon

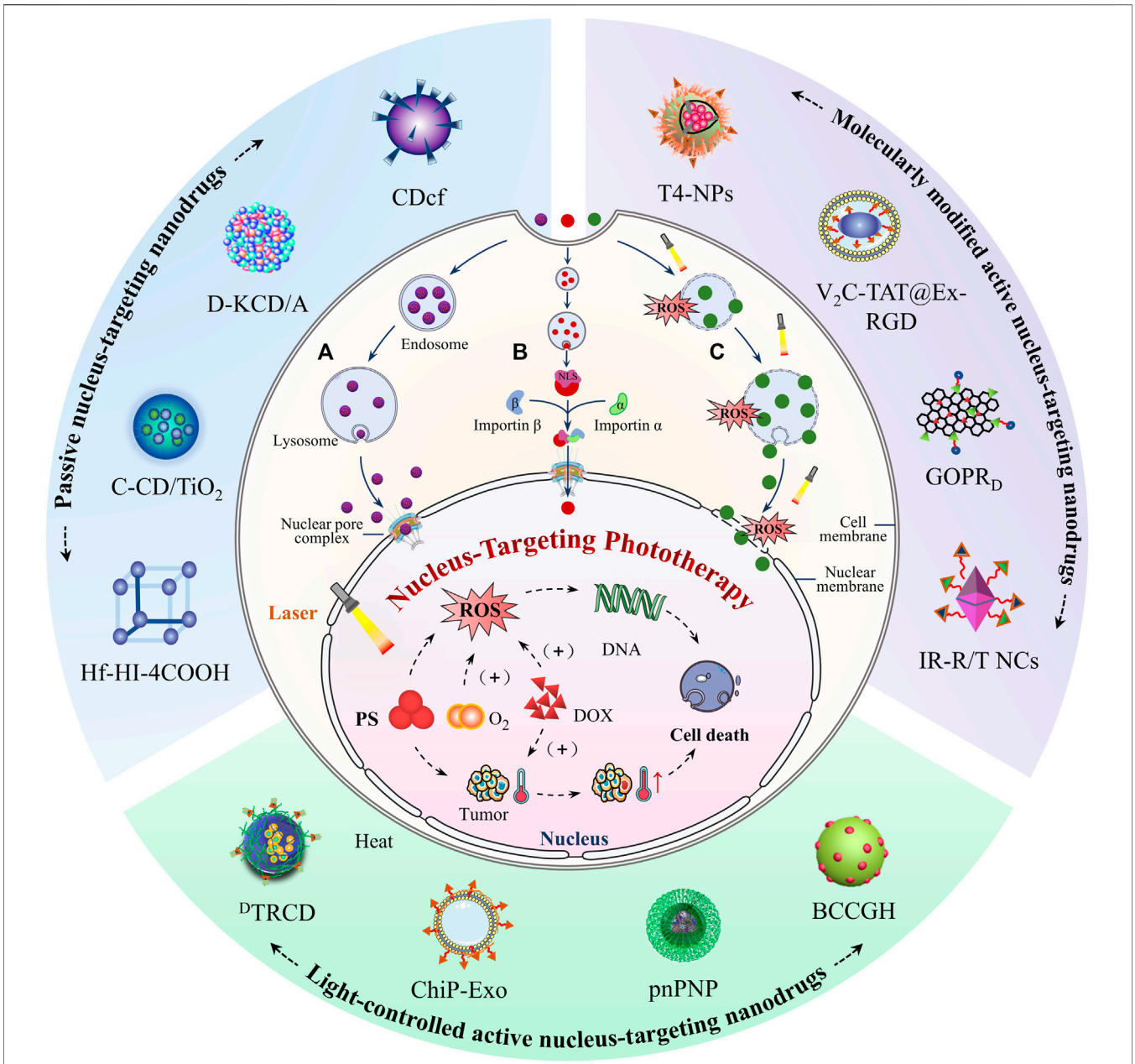


FIGURE 1 | Schematic illustration of nucleus-targeting nanodrugs for enhancing PDT and PTT. According to the way nanodrugs targeting the nucleus, they are divided into two parts: passive nucleus-targeting nanodrugs **(A)** and active nucleus-targeting nanodrugs, which are further divided into molecularly modified active nucleus-targeting nanodrugs **(B)** and light-controlled active nucleus-targeting nanodrugs **(C)**. In **(A)**, nanodrugs that undergo size/hydrophilicity adjustment can passively penetrate the nucleus through NPCs after escaping from the endo/lysosome. In **(B)**, after being modified with the nucleus-targeting groups, nanodrugs can be recognized and then transferred into the nucleus by importin α/β through NPCs. As for **(C)**, ROS generated by nanodrugs under light irradiation will destroy a series of bio-membranes and facilitate the entry of nanodrugs into the nucleus. Nanodrugs accumulated in the nucleus generated a large amount of toxic ROS and local high temperature under light irradiation to destroy DNA and proteins in the nucleus and finally induce tumor cell death.

nanodots have been widely used in PDT, PTT, and fluorescence imaging in recent years due to their excellent optical properties. In addition, many carbon nanodots, which have small size and good hydrophilicity, are particularly suitable for passive targeting to the nucleus (Wareing et al., 2021). Recently, Nasrin et al. (2020) synthesized ultra-small conjugated carbon dots (CDcf) as two-photon active PSs for nucleus-targeting PDT. CDcf were obtained by solvothermal reaction of curcumin and folic acid at high temperature. Interestingly, CDcf retained part of the folic acid group, which enabled them to target folate receptor-positive oral cancer cells. CDcf entered the lysosome through folate

receptor mediated endocytosis and formed a hybrid with the folate receptor. The hybrid released CDcf *via* lysosomal cleavage and then CDcf entered the nucleus due to its abundant hydrophilic amino groups and small size of 8 nm. Subsequently, the multi-conjugate system of CDcf mediated efficient photo-electron transfer to produce ROS and directly attacked DNA in the nucleus under irradiation with 780 nm laser. Benefiting from the effective nucleus-targeting ability, CDcf had much higher anticancer efficacy than CDc without nucleus-targeting ability. Similarly, Xu et al. found that N-doped carbon dots (Xu et al., 2021) and N/Se-doped carbon dots (Xu et al., 2020) with small size not only targeted the nucleus but also specifically bonded to RNA to further improve the treatment precision of carbon dots-mediated PDT. Nanoparticles with intrinsic nucleus-targeting ability can also serve as a drug-loading platform to deliver traditional PSs to the nucleus for high efficiency. For example, Lan Yang et al. (2021) reported an amino acid-based self-assembled nanocarrier with passive nucleus-targeting ability loaded with Ce6 and DOX (D-KCD/A) for the synergistic treatment of chemotherapy and PDT. D-KCD/A was prepared by azide crosslinkers and self-assemblies composed of dibenzocyclooctyne (DIBO)-functionalized lysine (D-K) and Ce6 by copper free click chemistry, followed by DOX loading. Because there were abundant hydrophobic regions, D-KCD/A had a high loading rate (17%) of Ce6, contributing to a higher tumor-killing efficiency. D-KCD/A was endocytosed and then entered the nucleus *via* a non-importin pathway thanks to the amphiphilic amino acid D-K. D-KCD/A exhibited a stronger antitumor effect than free Ce6 and D-KCD because of the synergistic effect of nuclear targeting and enhanced PDT.

In addition to PDT, passively nucleus-targeting PTT has also been developed. Recently, Jiang et al. (2020) developed a Hf-heptamethine indocyanine dye-based nanoscale coordination polymer (Hf-HI-4COOH) for nucleus-targeting PTT with low power density and temperature. Hf-HI-4COOH had a smaller size (36.7 nm) than NPCs and hydrophilicity derived from abundant uncoordinated carboxyl groups, which endowed it with good nuclear targeting ability. Up to 90% of Hf-HI-4COOH were delivered to the nucleus of 4T1 cells when incubated with Hf-HI-4COOH for 4 h. Hf-HI-4COOH significantly improved its photothermal conversion efficiency (39.51%) by the coordination between Hf and the heptamethine indocyanine dye, as demonstrated by a rapid temperature increase of ~15°C within 5 min at the tumor site of tumor-bearing mice. Hf-HI-4COOH achieved effective tumor-killing effects while avoiding damage to the skin and normal organs under low power density (0.3 W/cm^2) laser irradiation due to their high photothermal conversion efficiency and the intrinsic nucleus-targeting property. The tumor extracellular space is slightly acidic (pH = 6.5–6.8) because the tumor microenvironment is rich in lactate (Zhen et al., 2021; Huang et al., 2022; Zhu et al., 2022). To further improve the targeting of cancer therapy, Phuong et al. (2020) developed a slightly acidic environment-responsive carbon dot/TiO_2 nanocomposites for nucleus-targeting PTT. Zwitterionic functionalized-carbon dots (Z-CDs) were attached to the surface of TiO_2 nanocomposites *via* borolipid bonds. Under tumor slightly acidic conditions and visible light irradiation, the cleavage of the borolipid bonds resulted in the release of Z-CD from TiO_2 nanoparticles, and Z-CD was internalized into tumor cells. The sulfobetaine moieties in Z-CD was protonized to lead to excellent hydrophilicity and small size in tumor microenvironment (23.5 nm in pH6.8). Benefiting from this, Z-CD efficiently entered the nucleus from the cytoplasm. The CD/TiO_2 nanocomposites significantly upregulated the pro-apoptotic markers such as P53 and BAX in tumor cells and efficiently ablated tumors after being injected into the tumor and irradiated with Near Infrared (NIR).

ACTIVE NUCLEUS-TARGETING NANODRUGS

The nuclear passive targeting strategy has strict requirements on the size range and surface properties of nanodrugs, which limits the adaptability of this strategy. In addition, most strategies for passively targeting the nucleus rely on the passive diffusion of nanodrugs into the nucleus. Therefore, the delivery efficiency is relatively low and is negatively correlated with the particle size of nanodrugs. To achieve more effective nuclear targeting, many efficient active targeting strategies are currently developed for nanodrug-based phototherapy. These strategies can be divided into two categories. First, modifying the surface of nanodrugs with nucleus-targeting groups endows the nanodrugs with nucleus-targeting ability. Second, targeting the nucleus by light-controlled destruction of the nuclear membrane *via* the PDT or promotion of nanodrugs' diffusion *via* PTT effects.

Modification of Nucleus-Targeting Groups

Nucleus-targeting groups mainly include cell-penetrating peptides (TAT peptides, cyclic R10 peptides), NLS, and DNA aptamers. TAT, as the first discovered cell-penetrating peptide, is a highly cationic peptide with the sequence YGRKKRRQRRR derived from human immunodeficiency virus-1 (HIV-1). TATs have been demonstrated to transfer nanodrugs into the perinuclear region by binding to the import receptors importin α and then translocating through the nuclear pore *via* importin β (karyopherin) (Gao et al., 2019; Wan et al., 2020; Ziyang Cao et al., 2019). Cyclic R10 peptide (cR10), a kind of cyclic cell-penetrating peptide, has higher nucleus-targeting capabilities than both linear TAT and cyclic TAT peptides (Tu et al., 2020). NLS is an amino acid sequence that consists of one or more short sequences of positively charged lysine or arginine (Florio et al., 2022). The mechanism of NLS entry into the nucleus is the same as TAT but NLS does not mediate non-specific membrane penetration and has fewer side effects (Smith et al., 2018; Yue Tan et al., 2021). Histone, as a functional protein that constitutes chromatin, contains nuclear localization sequences that mediate nuclear targeting (Guo et al., 2022). Except for aptamers (Yang et al., 2018), these nucleus-targeting polypeptides and proteins have strong positive charges.

TABLE 1 | Nucleus-targeting nanodrugs for enhancing PDT and PTT.

Category	Nucleus-targeting strategies	Nanomaterials	Nucleus-targeting groups	Size (nm)	Therapy
Passive Nucleus-targeting nanodrugs	Size/hydrophilicity adjustment	CDcf Nasrin et al. (2020)	—	8	PDT
		I-CDs @FA Xu et al. (2021)		4.8(I-CDs)	PDT
		Se/N-CDs Xu et al. (2020)		3.6 ± 0.6	PDT
		D-KCD/A Hailong Yang et al. (2021)		~10	PDT
		Hf-HI-4COOH Jiang et al. (2020)		30	PTT
		C-CD/TiO_2 Phuong et al. (2020)		~25 (Z-CD)	PTT
Active Nucleus-targeting nanodrugs	Modification of nucleus-targeting groups	TPE-TTMN-TPA NPs (T4-NPs) Zhang et al. (2021)	TAT	50–70	PDT
		Pd-TAT Gao et al. (2019)	TAT	19.7 ± 1.9	PTT
		TID NPs Wan et al. (2020)	TAT	108	PTT/ Chemotherapy (CT)
		Ir-R/T NCs Wang et al. (2019)	TAT	<5	PDT/Radio-therapy (RT)
		CuS@MSN-TAT-RGD Li et al. (2018)	TAT	~40	PTT
		V_2C-TAT@Ex-RGD Yu Cao et al. (2019)	TAT	71	PTT
		$GOPR_D$ Tu et al. (2020)	CPPs	~20	PTT/CT
		DIR825@histone Guo et al. (2022)	Histone	~37.5	PDT/CT
		CACH-PEG Yang et al. (2018)	AS1411	~65 (pH6.5) ~70 (pH7.4)	PDT/CT
	Light-controlled nuclear delivery	^{D}TRCD Ziyang Cao et al. (2019)	TAT	63.6 ± 9.6	PDT/CT
		BCCGH Hua et al. (2018)	—	~7.9	PDT/PTT
		pnPNP Cheng et al. (2019a)	NLS	157.6 ± 2.5	PDT
		ChiP-Exo Cheng et al. (2019b)	NLS	132.6	PDT
		PPR NPs Zhu et al. (2018)	—	~75	PDT
		Ce6-C_{18}-PEG/^{125}I-Cur Shiyi Qin et al. (2021)	—	10–30	PDT

Directly modifying these polypeptides and proteins on the surface leads to not only high toxicity but also instability in the blood circulation system because of the highly positive charge of nanodrugs. A general strategy is to modify the surface of these nucleus-targeting polypeptides and proteins based nanodrugs with long-chain polyethylene glycol (PEG) (Li et al., 2018; Wang et al., 2019), or coat a layer of exosomes to increase their biocompatibility (Ziyang Cao et al., 2019). More importantly, the abundant amino groups, hydroxyl groups and sulfhydryl groups in these peptides or proteins make them amenable to modification to mask their positive charge or be functionalized for tumor environmentally responsive activation. For instance, Zhang et al. (2021) developed nucleus-targeting nanodrugs (T4-NPs) cleaved in the lysosome for PDT. T4-NPs were prepared by co-assembly of SA-TAT (succinic anhydride-modified TAT)-PEG (poly (ethylene glycol))-PLA [poly (lactic acid)] and PEG-PLA followed by loading of TPE-TTMN-TPA (a new kind of photosensitizer). Benefiting from the charge masking of TAT by SA modifying, the surface potential of T4-NPs was negative, which made T4-NPs stable in the blood circulation system *in vivo*. When T4-NPs were endocytosed into the lysosomes of cancer cells, the acidic environment of the lysosome (pH = 5) prompted the cleavage of SA from the TAT of T4-NPs to lead a charge reversal (from −15.5 mV to +6.72 mV) and triggered TAT exposure to mediate T4-NPs' entry into the nucleus. T4 NPs had highly efficient nuclear targeting and long nuclear retention (~6 h), and the TPE-TTMN-TPA aggregated in the nuclei of tumor cells and generated a large amount of ROS under light irradiation, which significantly inhibited the proliferation of tumor cells and angiogenesis (anti-tumor rate of 78%).

Very recently, Tu et al. (2020) developed a graphene oxide (GO)-cR10 nuclear translocation nanoplatform loaded with DOX ($GOPR_D$) for the synergistic antitumor effects of chemotherapy and PTT. GO contained abundant carboxyl groups with favorable photothermal property and were easily modified with hyperbranched polyglycerol (hPG) and cR10. In this case, the hPG was modified to improve the biocompatibility of $GOPR_D$. The cR10 effectively promoted the internalization (ten-fold increase in absorption efficiency) and accumulation of $GOPR_D$ in the nucleus. Under NIR light irradiation, $GOPR_D$ exerted a high photothermal effect and effectively killed multi-drug-resistant HeLa cells. As expected, $GOPR_D$ treatment demonstrated stronger anti-tumor activity than the free DOX group and non-nucleus-targeting group.

Light-Controlled Nuclear Delivery

Many phototherapeutic nanodrugs are usually trapped in endo/lysosomes and are difficult to escape from them (Cheng et al., 2019a; Cheng et al., 2019b). Some specially designed nanodrugs

can escape from endo/lysosomes through the proton sponge effect or charge reversal effect to better transport to nuclear. However, they are still likely to be blocked outside the nuclear membrane due to their large size. A strategy for efficient nuclear transport is to destroy endo/lysosomal and nuclear membranes by phototherapy-generated ROS or high temperature (Zhu et al., 2018; Yuanyuan Qin et al., 2021). For instance, Ziyang Cao et al. (2019) reported a PDT-driven nucleus-targeting PDT-nanodrugs (^{D}TRCD) for cancer therapy. ^{D}TRCD was prepared by self-assembly of TAT-modified ROS-responsive polymers followed by loading of Ce6 and DOX. Despite the presence of the nucleus-targeting group TAT peptide, ^{D}TRCD cannot enter the nucleus and can only stay around the nucleus because of the large size of ^{D}TRCD (40–200 nm). The toxic ROS generated by Ce6 directly destroyed the nuclear membrane integrity and the ROS-sensitive thiokel bonds in ^{D}TRCD under light irradiation, which further promoted the intranuclear accumulation of Ce6 and DOX. As a result, ^{D}TRCD treatment plus irradiation achieved the most effective tumor volume reduction compared to the free drug group and single sensitive nanomaterials group. In addition to PDT, PTT also mediates the diffusion of nanodrugs into the nucleus when they are near the nucleus. Recently, Hua et al. (2018) synthesized novel multifunctional nanodots (BCCGH) by mixing bovine serum albumin (BSA), carbon dots, metal ions (Cu^{2+} and Gd^{3+}), and 2-(1-hexyloxyethyl)-2-devinyl pyropheophorbide-α (HPPH, a photosensitizer). BCCGH largely escaped the lysosomal entrapment due to the BSA surface and appropriate size/charge of the nanodots and were distributed mainly around the nucleus-endoplasmic reticulum. BCCGH had a very high photothermal conversion efficiency (68.4%). And high temperature promoted the further diffusion of BCCGH into the nucleus under mild NIR laser irradiation. The BCCGH targeted to the nucleus efficiently killed about 90% of cancer cells *via* ROS under laser light.

CONCLUSION AND PROSPECT

Nucleus-targeting phototherapy drugs can effectively solve the problem caused by the long distance between phototherapy drugs and their target DNA. Therefore, these emerging nucleus-targeting phototherapy nanodrugs have attracted a very wide range of research interests in the field of cancer therapy over the past several years. Herein, we systematically summarize recent advances in nucleus-targeting phototherapy nanodrugs for enhanced antitumor efficacy. To achieve satisfactory nucleus-targeting phototherapy, nanodrugs need to break through multiple hurdles (Zhu et al., 2018; Yu Cao et al., 2019): 1) effective tumor tissue-specific accumulation; 2) high efficiency of cellular internalization; 3) excellent endo/lysosomal escape ability; 4) fully perinuclear or intranuclear translocation, 5) efficient photo-thermal/photochemical energy conversion. Most of these well-designed active/passive nucleus-targeting nanodrugs can overcome these barriers to demonstrate excellent cancer therapeutic efficacy through irreversible and catastrophic thermal or oxidative damage to the nucleus. Despite the substantial advances gained, there are still various obstacles to overcome in furthering the clinical application of nucleus-targeting phototherapy nanodrugs. First, nanodrugs generally require a smaller size to achieve better nuclear targeting, especially for passively nucleus-targeting nanodrugs. However, the too small particle size of nanodrugs leads to the easy excretion of nanodrugs in the blood circulatory system through the kidneys or leakage into other normal tissues (Wei Tan et al., 2021). Second, many actively targeted phototherapeutic nanodrugs require additional modifications to maintain stability in the blood circulation system, which requires very sophisticated designs of nanodrugs to ensure exposure of active nucleus-targeting functional groups at appropriate sites group. Many sophisticated active-targeted nanodrugs are complicated to prepare and have many components, which will lead to a big bottleneck for the subsequent translation from laboratory to clinical. Third, the hypoxic environment at the tumor site can compromise the efficacy of nucleus-targeting nanodrugs PDT-based therapy (Zeng et al., 2020). Oxygen-independent PDT may solve the problems effectively. Fourth, phototherapy generally uses the near-infrared laser as the excitation light source. Although its tissue penetration has been greatly improved compared with visible light, it is still not suitable for many deep tissue tumors (Hailong Yang et al., 2021). To summarize, more efforts are still needed to improve the PDT and PTT effects provided by nucleus-targeting nanodrugs. Nevertheless, nucleus-targeting phototherapy nanodrugs remain intriguing research frontiers in the field of cancer treatment. It is foreseeable that the innovative design of nanodrugs will strongly promote the clinical translation of nucleus-targeting PDT and PTT.

AUTHOR CONTRIBUTIONS

All authors listed have made a substantial, direct, and intellectual contribution to the work and approved it for publication.

FUNDING

This work was supported by the National Natural Science Foundation of China (No. 81974508, 21974134), the Hunan Science Fund for Distinguished Young Scholar of China (No. 2021JJ10067), Innovation-Driven Project of Central South University (No. 202045005), Hunan Provincial Natural Science Foundation of China (No. 2021JJ31066), Changsha Science and Technology Project (No. kq2001048), Key Research Project of Ningxia Hui Autonomous Region in 2021 of China (Major Project) (No. 2021BEG01001).

REFERENCES

Bray, F., Ferlay, J., Soerjomataram, I., Siegel, R. L., Torre, L. A., and Jemal, A. (2018). Global Cancer Statistics 2018: GLOBOCAN Estimates of Incidence and Mortality Worldwide for 36 Cancers in 185 Countries. *CA Cancer J. Clin.* 68 (6), 394–424. doi:10.3322/caac.21492

Chen, W. H., Luo, G. F., and Zhang, X. Z. (2019). Recent Advances in Subcellular Targeted Cancer Therapy Based on Functional Materials. *Adv. Mater.* 31 (18027253), e1802725. doi:10.1002/adma.201802725

Chen, L., Huang, Q., Zhao, T., Sui, L., Wang, S., Xiao, Z., et al. (2021). Nanotherapies for Sepsis by Regulating Inflammatory Signals and Reactive Oxygen and Nitrogen Species: New Insight for Treating COVID-19. *REDOX BIOLOGY* 45, 102046. doi:10.1016/j.redox.2021.102046

Chen, Q., Li, N., Wang, X., Yang, Y., Xiang, Y., Long, X., et al. (2022). Mitochondria-Targeting Chemodynamic Therapy Nanodrugs for Cancer Treatment. *Front. Pharmacol.* 13, 847048. doi:10.3389/fphar.2022.847048

Cheng, H., Fan, J. H., Zhao, L. P., Fan, G. L., Zheng, R. R., Qiu, X. Z., et al. (2019a). Chimeric Peptide Engineered Exosomes for Dual-Stage Light Guided Plasma Membrane and Nucleus Targeted Photodynamic Therapy. *Biomaterials* 211, 14–24. doi:10.1016/j.biomaterials.2019.05.004

Cheng, H., Yuan, P., Fan, G., Zhao, L., Zheng, R., Yang, B., et al. (2019b). Chimeric Peptide Nanorods for Plasma Membrane and Nuclear Targeted Photosensitizer Delivery and Enhanced Photodynamic Therapy. *APPLIED MATERIALS TODAY* 16, 120–131. doi:10.1016/j.apmt.2019.04.017

Chinna Ayya Swamy, P., Sivaraman, G., Priyanka, R. N., Raja, S. O., Ponnuvel, K., Shanmugpriya, J., et al. (2020). Near Infrared (NIR) Absorbing Dyes as Promising Photosensitizer for Photo Dynamic Therapy. *Coord. Chem. Rev.* 411, 213233. doi:10.1016/j.ccr.2020.213233

Costoya, J., Surnar, B., Kalathil, A. A., Kolishetti, N., and Dhar, S. (2022). Controlled Release Nanoplatforms for Three Commonly Used Chemotherapeutics. *Mol. Aspects Med.* 83, 101043. doi:10.1016/j.mam.2021.101043

Deng, X., Shao, Z., and Zhao, Y. (2021). Solutions to the Drawbacks of Photothermal and Photodynamic Cancer Therapy. *Adv. Sci.* 8, 2002504. doi:10.1002/advs.202002504

Dong, K., Wang, Z., Zhang, Y., Ren, J., and Qu, X. (2018). Metal-Organic Framework-Based Nanoplatform for Intracellular Environment-Responsive Endo/Lysosomal Escape and Enhanced Cancer Therapy. *ACS Appl. Mater. Inter.* 10 (38), 31998–32005. doi:10.1021/acsami.8b11972

Drescher, D., Büchner, T., Schrade, P., Traub, H., Werner, S., Guttmann, P., et al. (2021). Influence of Nuclear Localization Sequences on the Intracellular Fate of Gold Nanoparticles. *ACS Nano* 15 (9), 14838–14849. doi:10.1021/acsnano.1c04925

Florio, T. J., Lokareddy, R. K., Yeggoni, D. P., Sankhala, R. S., Ott, C. A., Gillilan, R. E., et al. (2022). Differential Recognition of Canonical NF-Kb Dimers by Importin α3. *Nat. Commun.* 13 (1), 1207. doi:10.1038/s41467-022-28846-z

Fu, X., Shi, Y., Qi, T., Qiu, S., Huang, Y., Zhao, X., et al. (2020). Precise Design Strategies of Nanomedicine for Improving Cancer Therapeutic Efficacy Using Subcellular Targeting. *Signal. Transduct Target. Ther.* 5 (2621), 262. doi:10.1038/s41392-020-00342-0

Gao, G., Jiang, Y. W., Jia, H. R., Sun, W., Guo, Y., Yu, X. W., et al. (2019). From Perinuclear to Intranuclear Localization: A Cell-Penetrating Peptide Modification Strategy to Modulate Cancer Cell Migration under Mild Laser Irradiation and Improve Photothermal Therapeutic Performance. *Biomaterials* 223, 119443. doi:10.1016/j.biomaterials.2019.119443

Gao, D., Guo, X., Zhang, X., Chen, S., Wang, Y., Chen, T., et al. (2020). Multifunctional Phototheranostic Nanomedicine for Cancer Imaging and Treatment. *Mater. Today Bio* 5, 100035. doi:10.1016/j.mtbio.2019.100035

Guo, J., Tan, D., Lou, C., Guo, S., Jin, X., Qu, H., et al. (2022). A Tumor-Penetrable Drug Nanococktail Made from Human Histones for Interventional Nucleus-Targeted Chemophotothermal Therapy of Drug-Resistant Tumors. *Bioact Mater.* 9, 554–565. doi:10.1016/j.bioactmat.2021.07.018

Hailong Yang, H., Xu, B., Li, S., Wu, Q., Lu, M., Han, A., et al. (2021). A Photoresponsive Nanozyme for Synergistic Catalytic Therapy and Dual Phototherapy. *Small* 17 (200709010), 2007090. doi:10.1002/smll.202007090

Hanahan, D. (2022). Hallmarks of Cancer: New Dimensions. *Cancer Discov.* 12 (1), 31–46. doi:10.1158/2159-8290.CD-21-1059

Hua, X. W., Bao, Y. W., Zeng, J., and Wu, F. G. (2018). Ultrasmall All-In-One Nanodots Formed *via* Carbon Dot-Mediated and Albumin-Based Synthesis: Multimodal Imaging-Guided and Mild Laser-Enhanced Cancer Therapy. *ACS Appl. Mater. Inter.* 10 (49), 42077–42087. doi:10.1021/acsami.8b16065

Huang, J., Huang, Q., Liu, M., Chen, Q., and Ai, K. (2022). Emerging Bismuth Chalcogenides Based Nanodrugs for Cancer Radiotherapy. *Front. Pharmacol.* 13, 844037. doi:10.3389/fphar.2022.844037

Jelinek, T., and Zuchnicka, J. (2020). Peripheral T-Cell Lymphoma, NOS, with Rapidly Progressing Leukocytosis Mimicking Acute Lymphoblastic Leukemia. *Blood* 135 (20), 1816. doi:10.1182/blood.2020005020

Jiang, Z., Yuan, B., Wang, Y., Wei, Z., Sun, S., Akakuru, O. U., et al. (2020). Near-infrared Heptamethine Cyanine Dye-Based Nanoscale Coordination Polymers with Intrinsic Nucleus-Targeting for Low Temperature Photothermal Therapy. *Nano Today* 34, 100910. doi:10.1016/j.nantod.2020.100910

Lan Yang, L., He, X., Zeng, Z., Tang, J., Qi, D., Ma, H., et al. (2021). Clickable Amino Acid Tuned Self-Assembly of a Nucleus-Selective Multi-Component Nanoplatform for Synergistic Cancer Therapy. *Chem. Sci.* 12 (24), 8394–8400. doi:10.1039/d1sc01073e

Lasorsa, A., Nardella, M. I., Rosato, A., Mirabelli, V., Caliandro, R., Caliandro, R., et al. (2019). Mechanistic and Structural Basis for Inhibition of Copper Trafficking by Platinum Anticancer Drugs. *J. Am. Chem. Soc.* 141 (30), 12109–12120. doi:10.1021/jacs.9b05550

Li, N., Sun, Q., Yu, Z., Gao, X., Pan, W., Wan, X., et al. (2018). Nuclear-Targeted Photothermal Therapy Prevents Cancer Recurrence with Near-Infrared Triggered Copper Sulfide Nanoparticles. *ACS Nano* 12 (6), 5197–5206. doi:10.1021/acsnano.7b06870

Li, X., Yuan, H. J., Tian, X. M., Tang, J., Liu, L. F., and Liu, F. Y. (2021). Biocompatible Copper Sulfide-Based Nanocomposites for Artery Interventional Chemo-Photothermal Therapy of Orthotropic Hepatocellular Carcinoma. *Mater. Today Bio* 12, 100128. doi:10.1016/j.mtbio.2021.100128

Lo, P. C., Rodríguez-Morgade, M. S., Pandey, R. K., Ng, D. K. P., Torres, T., and Dumoulin, F. (2020). The Unique Features and Promises of Phthalocyanines as Advanced Photosensitisers for Photodynamic Therapy of Cancer. *Chem. Soc. Rev.* 49 (4), 1041–1056. doi:10.1039/c9cs00129h

Nasrin, A., Hassan, M., and Gomes, V. G. (2020). Two-photon Active Nucleus-Targeting Carbon Dots: Enhanced ROS Generation and Photodynamic Therapy for Oral Cancer. *Nanoscale* 12 (40), 20598–20603. doi:10.1039/d0nr05210h

Pan, L., Liu, J., and Shi, J. (2018). Cancer Cell Nucleus-Targeting Nanocomposites for Advanced Tumor Therapeutics. *Chem. Soc. Rev.* 47 (18), 6930–6946. doi:10.1039/c8cs00081f

Panagaki, D., Croft, J. T., Keuenhof, K., Larsson Berglund, L., Andersson, S., Kohler, V., et al. (2021). Nuclear Envelope Budding Is a Response to Cellular Stress. *Proc. Natl. Acad. Sci. U.S.A.* 118, e202099711830. doi:10.1073/pnas.2020997118

Phuong, P. T. M., Won, H. J., Robby, A. I., Kim, S. G., Im, G. B., Bhang, S. H., et al. (2020). NIR-vis-Induced pH-Sensitive TiO2 Immobilized Carbon Dot for Controllable Membrane-Nuclei Targeting and Photothermal Therapy of Cancer Cells. *ACS Appl. Mater. Inter.* 12 (34), 37929–37942. doi:10.1021/acsami.0c11979

Rennick, J. J., Johnston, A. P. R., and Parton, R. G. (2021). Key Principles and Methods for Studying the Endocytosis of Biological and Nanoparticle Therapeutics. *Nat. Nanotechnol.* 16 (3), 266–276. doi:10.1038/s41565-021-00858-8

Shiyi Qin, S., Huang, K., and Szleifer, I. (2021). Design of Multifunctional Nanopore Using Polyampholyte Brush with Composition Gradient. *ACS Nano* 15 (11), 17678–17688. doi:10.1021/acsnano.1c05543

Siegel, R. L., Miller, K. D., Fuchs, H. E., and Jemal, A. (2022). Cancer Statistics, 2022. *CA A. Cancer J. Clinicians* 72 (1), 7–33. doi:10.3322/caac.21708

Smith, K. M., Tsimbalyuk, S., Edwards, M. R., Cross, E. M., Batra, J., Soares da Costa, T. P., et al. (2018). Structural Basis for Importin Alpha 3 Specificity of W Proteins in Hendra and Nipah Viruses. *Nat. Commun.* 9, 3703. doi:10.1038/s41467-018-05928-5

Srinivas, U. S., Tan, B. W. Q., Vellayappan, B. A., and Jeyasekharan, A. D. (2019). ROS and the DNA Damage Response in Cancer. *Redox Biol.* 25, 101084. doi:10.1016/j.redox.2018.101084

Su, W., Chen, C., Wang, T., Li, X., Liu, Y., Wang, H., et al. (2020). Radionuclide-labeled Gold Nanoparticles for Nuclei-Targeting Internal

Radio-Immunity Therapy. *Mater. Horiz.* 7 (4), 1115–1125. doi:10.1039/c9mh01725a

Su, X., Cao, Y., Liu, Y., Ouyang, B., Ning, B., Wang, Y., et al. (2021). Localized Disruption of Redox Homeostasis Boosting Ferroptosis of Tumor by Hydrogel Delivery System. *Mater. Today Bio* 12, 100154. doi:10.1016/j.mtbio.2021.100154

Tietz, O., Cortezon-Tamarit, F., Chalk, R., Able, S., and Vallis, K. A. (2022). Tricyclic Cell-Penetrating Peptides for Efficient Delivery of Functional Antibodies into Cancer Cells. *Nat. Chem.* 14 (3), 284–293. doi:10.1038/s41557-021-00866-0

Tu, Z., Donskyi, I. S., Qiao, H., Zhu, Z., Unger, W. E. S., Hackenberger, C. P. R., et al. (2020). Graphene Oxide-Cyclic R10 Peptide Nuclear Translocation Nanoplatforms for the Surmounting of Multiple-Drug Resistance. *Adv. Funct. Mater.* 30, 2000933. doi:10.1002/adfm.202000933

Wan, G., Cheng, Y., Song, J., Chen, Q., Chen, B., Liu, Y., et al. (2020). Nucleus-targeting Near-Infrared Nanoparticles Based on TAT Peptide-Conjugated IR780 for Photo-Chemotherapy of Breast Cancer. *Chem. Eng. J.* 380, 122458. doi:10.1016/j.cej.2019.122458

Wang, L., Zhang, T., Huo, M., Guo, J., Chen, Y., and Xu, H. (2019). Construction of Nucleus-Targeting Iridium Nanocrystals for Photonic Hyperthermia-Synergized Cancer Radiotherapy. *Small* 15 (190325447), e1903254. doi:10.1002/smll.201903254

Wang, J., Sui, L., Huang, J., Miao, L., Nie, Y., Wang, K., et al. (2021). MoS2-based Nanocomposites for Cancer Diagnosis and Therapy. *Bioact Mater.* 6 (11), 4209–4242. doi:10.1016/j.bioactmat.2021.04.021

Wareing, T. C., Gentile, P., and Phan, A. N. (2021). Biomass-Based Carbon Dots: Current Development and Future Perspectives. *ACS Nano* 15 (10), 15471–15501. doi:10.1021/acsnano.1c03886

Wei Tan, W., Jiang, P., Zhang, W., Hu, Z., Lin, S., Chen, L., et al. (2021). Posttranscriptional Regulation of De Novo Lipogenesis by Glucose-Induced O-GlcNAcylation. *Mol. Cel.* 81 (9), 1890. doi:10.1016/j.molcel.2021.02.009

Xie, Z., Fan, T., An, J., Choi, W., Duo, Y., Ge, Y., et al. (2020). Emerging Combination Strategies with Phototherapy in Cancer Nanomedicine. *Chem. Soc. Rev.* 49 (22), 8065–8087. doi:10.1039/d0cs00215a

Xu, N., Du, J., Yao, Q., Ge, H., Li, H., Xu, F., et al. (2020). Precise Photodynamic Therapy: Penetrating the Nuclear Envelope with Photosensitive Carbon Dots. *Carbon* 159, 74–82. doi:10.1016/j.carbon.2019.12.002

Xu, N., Du, J., Yao, Q., Ge, H., Shi, C., Xu, F., et al. (2021). Carbon Dots Inspired by Structure-Inherent Targeting for Nucleic Acid Imaging and Localized Photodynamic Therapy. *Sensors Actuators B: Chem.* 344 (130322), 130322. doi:10.1016/j.snb.2021.130322

Yang, Y., Zhu, W., Feng, L., Chao, Y., Yi, X., Dong, Z., et al. (2018). G-Quadruplex-Based Nanoscale Coordination Polymers to Modulate Tumor Hypoxia and Achieve Nuclear-Targeted Drug Delivery for Enhanced Photodynamic Therapy. *Nano Lett.* 18 (11), 6867–6875. doi:10.1021/acs.nanolett.8b02732

Yu Cao, Y., Wu, T., Zhang, K., Meng, X., Dai, W., Wang, D., et al. (2019). Engineered Exosome-Mediated Near-Infrared-II Region V2C Quantum Dot Delivery for Nucleus-Target Low-Temperature Photothermal Therapy. *ACS Nano* 13 (2), 1499–1510. doi:10.1021/acsnano.8b07224

Yuanyuan Qin, Y., Shen, M., Liu, X., Gu, J., Zhu, M., and Yi, X. (2021). Photo-Driven Delivery of 125I-Labeled Nanomicelles for Nucleus-Targeted Internal Conversion Electron-Based Cancer Therapy. *ACS Appl. Mater. Inter.* 13 (42), 49671–49681. doi:10.1021/acsami.1c13249

Yue Tan, Y., Chen, M., Chen, H., Wu, J., and Liu, J. (2021). Enhanced Ultrasound Contrast of Renal-Clearable Luminescent Gold Nanoparticles. *Angew. Chem. Int. Ed.* 60 (21), 11713–11717. doi:10.1002/anie.202017273

Zelmer, C., Zweifel, L. P., Kapinos, L. E., Craciun, I., Güven, Z. P., Palivan, C. G., et al. (2020). Organelle-specific Targeting of Polymersomes into the Cell Nucleus. *Proc. Natl. Acad. Sci. U S A.* 117 (6), 2770–2778. doi:10.1073/pnas.1916395117

Zeng, X., Yan, S., Chen, P., Du, W., and Liu, B.-F. (2020). Modulation of Tumor Microenvironment by Metal-Organic-Framework-Derived Nanoenzyme for Enhancing Nucleus-Targeted Photodynamic Therapy. *Nano Res.* 13 (6), 1527–1535. doi:10.1007/s12274-020-2746-4

Zhang, Z., Xu, W., Xiao, P., Kang, M., Yan, D., Wen, H., et al. (2021). Molecular Engineering of High-Performance Aggregation-Induced Emission Photosensitizers to Boost Cancer Theranostics Mediated by Acid-Triggered Nucleus-Targeted Nanovectors. *ACS Nano* 15 (6), 10689–10699. doi:10.1021/acsnano.1c03700

Zhao, T., Wu, W., Sui, L., Huang, Q., Nan, Y., Liu, J., et al. (2022). Reactive Oxygen Species-Based Nanomaterials for the Treatment of Myocardial Ischemia Reperfusion Injuries. *Bioact Mater.* 7, 47–72. doi:10.1016/j.bioactmat.2021.06.006

Zhen, W., An, S., Wang, S., Hu, W., Li, Y., Jiang, X., et al. (2021). Precise Subcellular Organelle Targeting for Boosting Endogenous-Stimuli-Mediated Tumor Therapy. *Adv. Mater.* 33 (51), e2101572. doi:10.1002/adma.202101572

Zhu, Y. X., Jia, H. R., Pan, G. Y., Ulrich, N. W., Chen, Z., and Wu, F. G. (2018). Development of a Light-Controlled Nanoplatform for Direct Nuclear Delivery of Molecular and Nanoscale Materials. *J. Am. Chem. Soc.* 140 (11), 4062–4070. doi:10.1021/jacs.7b13672

Zhu, Y., Zhao, T., Liu, M., Wang, S., Liu, S., Yang, Y., et al. (2022). Rheumatoid Arthritis Microenvironment Insights into Treatment Effect of Nanomaterials. *Nano Today* 42, 101358. doi:10.1016/j.nantod.2021.101358

Zimmerli, C. E., Allegretti, M., Rantos, V., Goetz, S. K., Obarska-Kosinska, A., Zagoriy, I., et al. (2021). Nuclear Pores Dilate and Constrict in Cellulo. *Science* 374 (6573), eabd9776. doi:10.1126/science.abd9776

Ziyang Cao, Z., Li, D., Wang, J., Xiong, M., and Yang, X. (2019). Direct Nucleus-Targeted Drug Delivery Using Cascade pHe/Photo Dual-Sensitive Polymeric Nanocarrier for Cancer Therapy. *Small* 15 (190202236), e1902022. doi:10.1002/smll.201902022

Conflict of Interest: The authors declare that the research was conducted in the absence of any commercial or financial relationships that could be construed as a potential conflict of interest.

Publisher's Note: All claims expressed in this article are solely those of the authors and do not necessarily represent those of their affiliated organizations, or those of the publisher, the editors and the reviewers. Any product that may be evaluated in this article, or claim that may be made by its manufacturer, is not guaranteed or endorsed by the publisher.

Copyright © 2022 Long, Zhang, Chen, Liu, Xiang, Yang, Xiao, Huang, Wang, Liu, Nan and Huang. This is an open-access article distributed under the terms of the Creative Commons Attribution License (CC BY). The use, distribution or reproduction in other forums is permitted, provided the original author(s) and the copyright owner(s) are credited and that the original publication in this journal is cited, in accordance with accepted academic practice. No use, distribution or reproduction is permitted which does not comply with these terms.

frontiers | Frontiers in Pharmacology

MINI REVIEW
published: 17 May 2022
doi: 10.3389/fphar.2022.909504

Nanodrugs Detonate Lysosome Bombs

Yuting Xiang[1†], Niansheng Li[1†], Min Liu[2,3], Qiaohui Chen[1], Xingyu Long[1], Yuqi Yang[2,3], Zuoxiu Xiao[1], Jia Huang[1,4], Xiaoyuan Wang[1,4], Yunrong Yang[2,3], Jinping Zhang[2,3], Chong Liu[5,6] and Qiong Huang[2,3]**

[1]Xiangya School of Pharmaceutical Sciences, Central South University, Changsha, China, [2]Department of Pharmacy, Xiangya Hospital, Central South University, Changsha, China, [3]National Clinical Research Center for Geriatric Disorders, Xiangya Hospital, Central South University, Changsha, China, [4]Hunan Provincial Key Laboratory of Cardiovascular Research, Xiangya School of Pharmaceutical Sciences, Central South University, Changsha, China, [5]Departments of Clinical Pharmacology and Pharmacy, Hunan Key Laboratory of Pharmacogenetics, National Clinical Research Center for Geriatric Disorders, Xiangya Hospital, Central South University, Changsha, China, [6]Institute of Clinical Pharmacology, Engineering Research Center of Applied Technology of Pharmacogenomics, Ministry of Education, Central South University, Changsha, China

Cancer cell lysosomes contain various hydrolases and non-degraded substrates that are corrosive enough to destroy cancer cells. However, many traditional small molecule drugs targeting lysosomes have strong side effects because they cannot effectively differentiate between normal and cancer cells. Most lysosome-based research has focused on inducing mild lysosomal membrane permeabilization (LMP) to release anticancer drugs from lysosomal traps into the cancer cell cytoplasm. In fact, lysosomes are particularly powerful "bombs". Achieving cancer cell-selective LMP induction may yield high-efficiency anticancer effects and extremely low side effects. Nanodrugs have diverse and combinable properties and can be specifically designed to selectively induce LMP in cancer cells by taking advantage of the differences between cancer cells and normal cells. Although nanodrugs-induced LMP has made great progress recently, related reviews remain rare. Herein, we first comprehensively summarize the advances in nanodrugs-induced LMP. Next, we describe the different nanodrugs-induced LMP strategies, namely nanoparticles aggregation-induced LMP, chemodynamic therapy (CDT)-induced LMP, and magnetic field-induced LMP. Finally, we analyze the prospect of nanodrugs-induced LMP and the challenges to overcome. We believe this review provides a unique perspective and inspiration for designing lysosome-targeting drugs.

Keywords: lysosomal membrane permeabilization, nanomaterials, nanodrugs, cancer treatment, chemodynamic therapy, magnetic nanoparticles, subcellular organelle-targeting

OPEN ACCESS

Edited by:
Zeming Liu,
Huazhong University of Science and Technology, China

Reviewed by:
Xiaoli Wang,
Weifang Medical University, China
Marja Jäättelä,
Danish Cancer Society, Denmark

****Correspondence:***
Qiong Huang
qionghuang@csu.edu.cn
Chong Liu
lclchong@hotmail.com

[†]These authors have contributed equally to this work

Specialty section:
This article was submitted to Pharmacology of Anti-Cancer Drugs, a section of the journal Frontiers in Pharmacology

Received: *31 March 2022*
Accepted: *28 April 2022*
Published: *17 May 2022*

Citation:
Xiang Y, Li N, Liu M, Chen Q, Long X, Yang Y, Xiao Z, Huang J, Wang X, Yang Y, Zhang J, Liu C and Huang Q (2022) Nanodrugs Detonate Lysosome Bombs. Front. Pharmacol. 13:909504. doi: 10.3389/fphar.2022.909504

INTRODUCTION

Cancer burdens global public health; it accounts for nearly 10 million deaths annually worldwide, and this number keeps increasing (Sung et al., 2021). The battle against tumors has been ongoing for decades, and a multitude of anticancer drugs have been developed. Many antitumor therapeutic strategies rely on the activation of the apoptosis pathway in tumor cells (Kolenko et al., 2000; Huang et al., 2022), a signaling cascade involving caspases leading to apoptosis (also known as caspase-dependent cell death). However, tumor cells are resistant to apoptosis-inducing and caspase-activating drugs by mutating pro-apoptotic proteins and overexpressing anti-apoptotic proteins (Giampazolias et al., 2017). Interestingly, some cellular components may achieve self-killing by acting as "bombs" (Zhang et al., 2021).

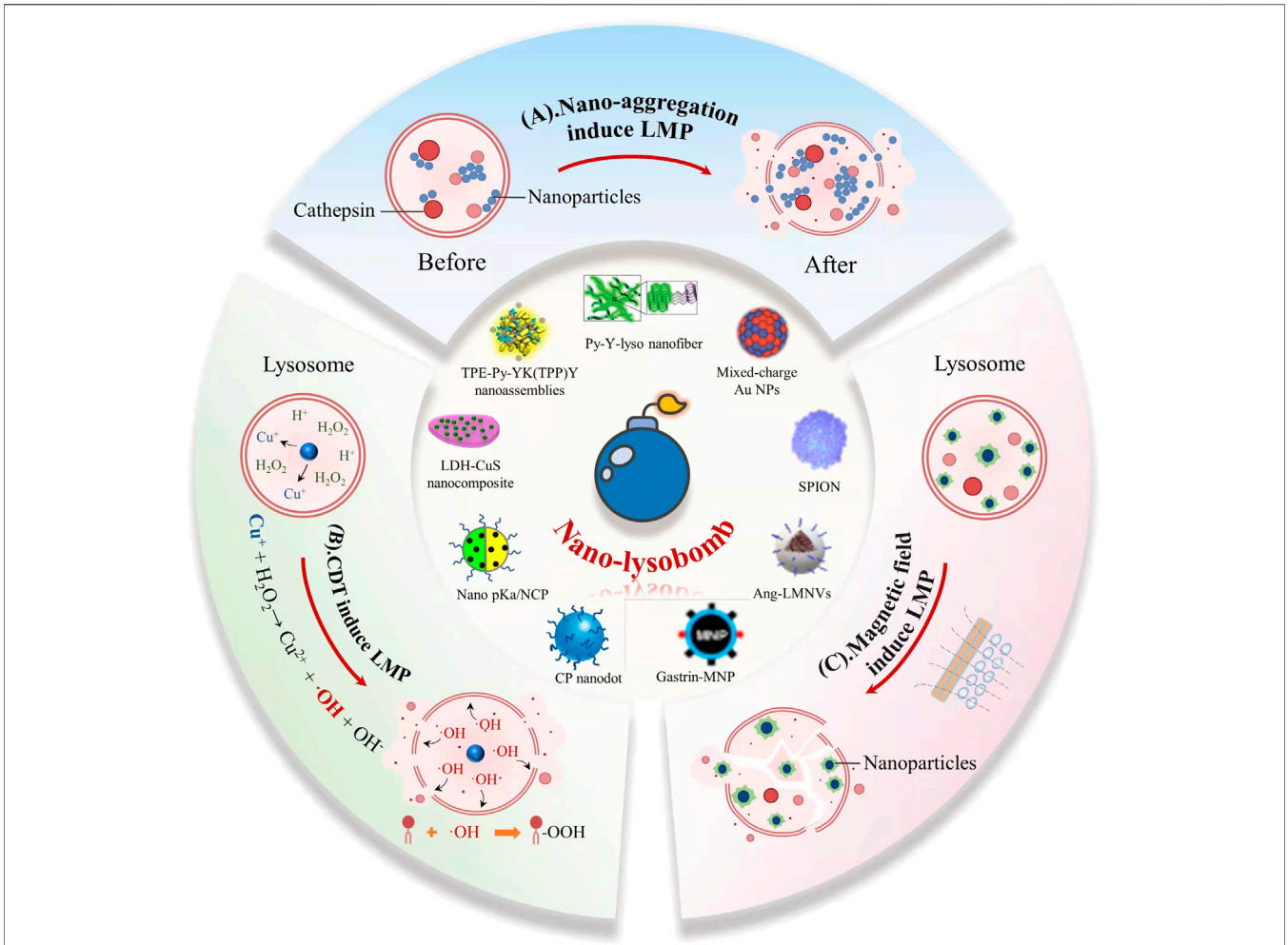


FIGURE 1 | Schematic illustration of nano-lysobombs inducing LMP and lysosome cell death. Nano-lysobombs are classified into three groups according to their action mechanism: nano-aggregation, CDT process, and magnetic field induction **(A)** The first class of nanodrugs triggers osmotic flow and lysosome swelling by self-assembling on the cell membrane or aggregating in lysosomes **(B)** The second class of nanodrugs triggers the Fenton reaction in the lysosomes, using generated OH to induce lipid peroxidation (LPO) of the lysosomal membrane and then trigger LMP **(C)** The third class uses the thermal effects or mechanical stress generated by magnetic field-stimulated magnetic nanoparticles to destroy the lysosomal membranes, eventually killing the cells.

Lysosomes, discovered in 1955, have long been regarded as mere "digesting" machines (De Duve and Wattiaux, 1966). These organelles are essential for endocytosis and autophagy (Piao and Amaravadi, 2016) and contain numerous hydrolases (De Duve and Wattiaux, 1966) responsible for degrading and recycling macromolecules such as exogenous substances and intracellular metabolic waste. In addition, lysosomes play a key role in many cellular biochemical processes, such as cell death and signal transduction (Platt, 2018). Severely damaged lysosomal membranes release the highly active hydrolases from the lysosome into the cytoplasm, where they affect various cellular components and activate death pathways. This process is known as lysosomal membrane permeabilization (LMP)-mediated lysosomal cell death (Kirkegaard and Jäättelä, 2009). The role of LMP in the cell death process is complex and involves various cell death pathways such as apoptosis, necrosis, and pyroptosis (Repnik et al., 2014). In short, leaky and ruptured lysosomes can become bombs threatening cell survival by releasing self-killing enzymes and impairing cellular functions.

These lysosomal bombs have also been called "suicide bags" (De Duve and Wattiaux, 1966). Besides their immense potential power, lysosomes are crucial for the rapid division of tumors; therefore, they have received extensive attention from tumor treatment researchers. Transformation and cancer progression involve dramatic changes in lysosomal volume, composition, and cellular distribution (Serrano-Puebla and Boya, 2018). In tumor cells, lysosomes are hypertrophic and more abundant (Galluzzi et al., 2018) and, therefore, more fragile and prone to rupture than in normal cells (Ma et al., 2020). Moreover, tumor cells have higher lysosomal enzymes levels (Serrano-Puebla and Boya, 2018). For example, increased expression of cathepsin B has been proposed as a marker for colorectal cancer (Abdulla et al., 2017), and various tumors express high cathepsin D levels (Fukuda et al., 2005). The morphological and

TABLE 1 | Nanodrugs detonate lysobombs.

Classification	Nanomaterials	Size	Targeting Strategy	Sources
Nano-aggregation-induced LMP	[+/–] NPs	5.3 ± 0.7 nm of Au NPs ≈200 nm aggregates	Mixed-charge modification for lysosomal targeting	Borkowska et al. (2020)
	Py-Yp-lyso	74.6 ± 11.6 nm aggregates	Alkaline phosphatase guides for tumor targeting; 4-(2-aminoethyl) morpholine for lysosomal targeting	Wu et al. (2021)
	TPE-Py-pYK(TPP)pY	310 nm of aggregates	Alkaline phosphatase guides for tumor targeting; Proper surface charge and nanosize for lysosomal endocytosis	Ji et al. (2021)
CDT-induced LMP	LDH-CuS NCs	≈120 nm (TEM)	LDH plate-like morphology for lysosomal endocytosis	Liu et al. (2020)
	CP nanodot	≈5.0 nm (TEM) ≈ 16.3 nm (hydrodynamic diameter)	—	Lin et al. (2019)
	nano pKa/NCP	≈90 nm (TEM) ≈ 100 nm (hydrodynamic diameter)	—	Deng et al. (2022)
Magnetic field-induced LMP	SPIONs	≈60 nm (hydrodynamic diameter)	—	Lunov et al. (2019)
	Ang—LMNVs	≈179 ± 3 nm (hydrodynamic diameter)	Angiopep-2 guides for tumor targeting	Pucci et al. (2020)
	Gastrin-MNP	≈37–50 nm	Gastrin guides for tumor targeting	Clerc et al. (2018)

physiological changes of lysosomes in tumor cells favor LMP induction. Some "detonators"—such as detergents or lipophilic drugs (Zhitomirsky and Assaraf, 2016)—can accumulate in lysosomes and induce LMP. For example, cationic amphoteric drugs induced LMP-mediated cell death by detaching acid sphingomyelinase from lysosomal membranes (Serrano-Puebla and Boya, 2018). However, these drugs may not be designed for LMP induction and lysosomal cell death pathways activation, and most of them have limitations such as low tumor selectivity and low lysosomal specificity.

The tremendous progress in nanodrugs has enabled the discovery of novel effective "detonators" to ignite lysosome bombs in tumor cells. First, most cellular uptake pathways of nanomedicines mediate endocytosis into lysosomes, including phagocytosis, clathrin-mediated endocytosis, and macropinocytosis (Stern et al., 2012), making this organelle the most common intracellular site of nanoparticle sequestration and degradation. Taking advantage of this, most LMP-inducing nanodrugs can reach their target (lysosomes) with little off-target effects. Second, the enhanced permeability and retention effect (EPR effect) (Kanamala et al., 2016) in tumors allows nanodrugs to achieve high tumor selectivity. In addition, modifying the nanodrugs with functional groups that specifically recognize cancer cells or respond to the tumor microenvironment increases their selectivity (Wang et al., 2021; Yang et al., 2022). Finally, nanodrugs have flexible physicochemical properties, and those with reasonable components and specific functional design can cleave lysosomes more efficiently than small molecule drugs, yielding more potent anticancer effects (Ai et al., 2021). There are growing interests and attempts to design "detonators" of lysosome bombs combining the advantages of nanodrugs (nano-lysobombs). Recently, some anticancer nano-lysobombs have been developed and have demonstrated potent antitumor effects and few side effects. However, to our knowledge, no review summarizes the newly developed anticancer nano-lysobombs. Thus, this minireview discusses the promising nano-lysobombs initiating LMP and lysosomal cell death in tumors. These nano-lysobombs are categorized into three groups based on their initiation process: nano-aggregation, chemodynamic therapy (CDT) and magnetic field induction (**Figure 1**, **Table 1**). Moreover, we detail the advantages and disadvantages of nano-lysobombs to highlight their potential.

NANO-AGGREGATION-INDUCED LYSOSOMAL MEMBRANE PERMEABILIZATION

Cancer cells present an altered lysosomal membrane structure making them more susceptible to osmotic swelling (Ma et al., 2020). Therefore, the idea of constructing nanomedicines inducing lysosome osmotic pressure difference or causing lysosome morphological changes has emerged, and nano-aggregation strategies have been developed. After reaching the plasma membrane of cancer cells, the nanoparticles would first enter early endosomes and then be transported to late endosomes—also called multivesicular bodies (MVB) (Hessvik and Llorente, 2018; Beatriz et al., 2021)—which then fuse with lysosomes. If these specially designed nanoparticles aggregate or self-assemble to a large scale at any stage of internalization, LMP will be induced through ion-induced osmotic pressure and lysosomal swelling, subsequent cancer cell death (Baehr et al., 2021; Wang et al., 2022).

The nano-aggregation strategies aim to selectively target cancer cells to achieve an excellent anticancer effect with few side effects. Currently, two nano-aggregation-induced LMP strategies exist. The first strategy (Borkowska et al., 2020) is based on the difference in lysosomal pH between cancer cells and normal cells. Cancer cell lysosomes and MVBs have lower pH (pH lysosome ≈4.2 in MDA-MB-231 cells) (Borkowska et al., 2020) than normal cell lysosomes (pH ≈ 4.8) and multilamellar bodies (pH < 6.1) (Lajoie et al., 2005). Recently, Borkowska et al. (Borkowska et al., 2020) developed a series of Au nanoparticles [(+/−) NPs] modified with the positively charged *N*,*N*,*N*-trimethyl (11-mercaptoundecyl) ammonium chloride (TMA) and the negatively charged 11-mercaptoundecanoic acid (MUA) at different ratios to specifically induce LMP in cancer cells. A decrease in pH protonates the carboxyl group of

the MUA and decreases the negative charge, rendering MUA hydrophobic. Interestingly (+/−) NPs with a TMA/MUA ratio of 80:20 only aggregated and triggered LMP in the lysosomes of cancer cells, but not in multilamellar bodies of normal cells. These (+/−) NPs (χTMA:χMUA = 80:20) had a particle size of only 5.3 nm and formed very large aggregates with a diameter >2 μm in cancer lysosomes, ultimately resulting in a powerful and broad-spectrum LMP-induced anticancer effect. Furthermore, in normal cells, the 80:20 (+/−) NPs were only present in multilamellar bodies, and most of them were excreted by exocytosis, indicating the potentially low adverse effects.

The second strategy (Ji et al., 2021; Wu et al., 2021) employs an enzyme-instructed self-assembly (EISA) approach. Alkaline phosphatases are highly expressed on the plasma membrane of many types of cancer cells and have been adopted as ELSA-promoting enzymes to induce LMP by mediating nano-aggregation (Wang et al., 2016; Gao et al., 2020a). For example, Wu et al. (Wu et al., 2021) constructed Py-Phe-Phe-Glu-Tyr (H_2PO_3)-Gly-Lyso (Py-Yp-Lyso) to treat cervical cancer through nano-aggregation-inducing LMP. Py-Yp-Lyso consisted of four parts: Glu-Tyr (H_2PO_3) was dephosphorylated by alkaline phosphatases to form Py-Y-Lyso and further self-assembled into nanofibers. The pyrene molecule (Py) served as a monitor due to its concentration-dependent luminescence. Phe-Phe conferred better biostability as a self-assembling structure. Finally, the 4-(2-aminoethyl) morpholine served as a lysosome targeting molecule (Lyso). It is prone to protonation, becomes more hydrophilic into the acidic lysosome, and remains there instead of diffusing to the cytoplasm. Py-Yp-Lyso had a negative charge and was stable in the blood circulation system because it contained a phosphate group. When Py-Yp-Lyso reached the cancer cells, alkaline phosphatases on the surface of the cancer cell plasma membrane dephosphorylated it, reversing its charge. The positively charged surface of the dephosphorylated Py-Y-Lyso promoted endocytosis and protonated the 4-(2-aminoethyl) morpholine moiety, preventing Py-Y-Lyso from diffusing out of the lysosome. In acidic lysosomes, Py-Yp-Lyso aggregation formed large nanofibers which triggered LMP. Py-Yp-Lyso had significantly higher cytotoxicity in Hela cells than in normal cells and inhibited tumor growth to 55.4% of that of control tumors at day 15 following the injection. Similarly, Ji et al. (Ji et al., 2021) constructed an LMP trigger called TPE-Py-pYK(TPP)pY, which was composed of three segments: tetraphenylethylene-pyride (TPE-Py) mainly for imaging, pYKpY (pY = phosphotyrosine) for self-assembly, and triphenylphosphine (TPP) for charge regulation and internalization. Treating Hela cells with TPE-Py-pYK(TPP)pY caused lysosomal destruction and high cytotoxicity. Intriguingly, LMP also effectively induced immunogenic cell death and ameliorated the immunosuppressive microenvironment.

CDT-INDUCED LYSOSOMAL MEMBRANE PERMEABILIZATION

Reactive oxygen species (ROS) are highly reactive and, at high concentrations, they can react with unsaturated lipids in lysosomal membranes to trigger LMP (Huang et al., 2017). CDT kills cancer cells by converting the high concentrations of endogenous H_2O_2 in cancer cells into the highly oxidative OH through the Fenton reaction (Chen et al., 2022). CDT has very excellent selectivity and causes few side effects because tumors have much higher H_2O_2 concentrations than normal tissue (Tang et al., 2019). The CDT reaction requires a low pH (pH ≈ 2–4). However, many Fenton reagents exhibit low efficiency in the weakly acidic tumor microenvironment (pH ≈ 6) (Shi et al., 2021) or cytoplasm (pH > 7.2) (Persi et al., 2018), prompting researchers (Dong et al., 2020; Shi et al., 2021) to search for a more favorable acidic environment for CDT and develop Fenton reagents with broader reaction conditions. The lysosome provides a favorable acidic environment (pH ≈ 4–5) for efficient CDT, and the Fenton reaction exhibits a higher reaction rate in such an acidic environment (Zhao et al., 2019). Moreover, lysosomes rarely contain antioxidant enzymes that inhibit the efficacy of CDT (such as catalase, glutathione peroxidase) (Kurz et al., 2008) but do enclose some small biomolecules that benefit CDT (cysteine, ascorbic acid, and glutathione for reducing oxidated Fenton reagents) (Kurz et al., 2008). Combining the high H_2O_2 levels in tumors and favorable conditions for the Fenton reaction in lysosomes, CDT-induced LMP is highly efficient and has a potent anticancer effect.

Copper-based nanoparticles can be used in a wide range of acidic environments (Jia et al., 2022) and exhibit a more efficient catalytic rate (Zhao et al., 2020) as a Fenton reaction catalyst than traditional ferrous materials. Therefore, copper-based nanomaterials are wildly used in CDT-induced LMP. Recently, Liu et al.(Liu et al., 2020) layered double hydroxide-copper sulfide nanocomposites (LDH-CuS NCs) to effectively treat cancer by CDT-induced LMP. They prepared LDH-CuS NCs by *in situ* growth of CuS on LDH nanosheets. The group chose CuS nanodots for their photothermal activity and better biosafety and performed near-infrared (NIR) excitation to release thermal effects-inducing copper ions to initiate Fenton-like reactions. This process is called NIR-induced CDT. Moreover, the sheet-like structure of LDH allowed CuS to stay in or adhere to lysosomes for longer periods, as 1D and 2D materials remain longer in endocytosis than spherical nanoparticles do. Therefore, LDH-CuS exhibited strong lysosomal localization ability, while free CuS nanodots are prone to diffuse into the cytoplasm. Finally, NIR-excited LDH-CuS efficiently generated OH in lysosomes, inducing LMP and achieving complete tumor suppression, while free CuS nanodots had poor tumor-suppressive effects, demonstrating the importance of lysosomes in CDT.

A continuous H_2O_2 supply is essential to maintain CDT and the subsequent LMP process. The exhaustion of endogenous H_2O_2 in lysosomes of tumor cells hampers CDT efficacy (Jia et al., 2022). To overcome this limitation, Lin et al.(Lin et al., 2019) prepared copper peroxide nanodots (CP nanodots) by combining Cu^{2+} and H_2O_2 in the presence of poly (vinylpyrrolidone) (PVP) as a stabilizer. These nanodots simultaneously release Cu^{2+} and H_2O_2 in the acidic environment, especially in the lysosomes of tumor cells. CP nanodots significantly inhibited the tumor growth of U87MG

tumor-bearing mice *via* CDT-inducing LMP. To further explore the retention behavior of copper-based nanomaterials in lysosomes, Deng et al. (Deng et al., 2022) prepared a series of copper peroxide nanodrugs with different pKa (Nano pKa/NCP). NCPs with low pKa (5.2–6.2) remained in lysosomes for longer and in higher quantities than those with high pKa and increased the ROS levels and LMP in lysosomes. Nano-pKa5.2/NCP treatment displayed the most apparent tumor growth suppression *in vivo*.

MAGNETIC FIELD-INDUCED LYSOSOMAL MEMBRANE PERMEABILIZATION

Cancer treatments based on alternating magnetic fields have numerous advantages over other methods. For example, magnetic fields do not have adverse effects on the human body and have unlimited tissue penetration depth. Many antitumor magnetic nanoparticles (MNPs) have been developed, especially those made from iron oxides, since they have favorable biocompatibility, abundant raw materials, and outstanding biological effects (Soetaert et al., 2020). The MNPs vibrate violently under the alternating magnetic field, which not only induces strong mechanical stress (Lopez et al., 2022) but also increases the temperature near the MNPs (Gobbo et al., 2015). Besides, lysosomal membranes can be disrupted by mechanical stress and thermal expansion, making alternating magnetic field-induced LMP a promising approach for cancer therapy. For example, Lunov et al.(Lunov et al., 2019) experimented with magnetic stimulation-induced LMP through superparamagnetic iron oxide nanoparticles (SPIONs) against liver cancer. Carboxydextran-coated SPIONs passively accumulated in the liver and were efficiently endocytosed into lysosomes by liver cancer cells. SPIONs strongly damaged lysosomes through magneto-mechanical stress with a force ≥700 pN, induced cathepsin B leakage, and eventually killed cells exposed to high-intensity (up to 8 T), short-pulse-width (≈15 μs) pulsed magnetic field.

Pucci et al. (Pucci et al., 2020) also constructed Angiopep-2 functionalized lipid-based magnetic nanovectors (Ang-LMNVs) for magnetic field-induced LMP against glioblastoma multiforme. They added angiopep-2 on LMNVs to target the low-density lipoprotein receptor-related protein 1 (LRP1, overexpressed on the glioma cell surface) and promote blood-brain barrier penetration. Submitting the Ang-LMNVs to an alternating magnetic field induced LMP and glioma cell death through magnetic intra-lysosomal hyperthermia (MILH). Compared with magnetic hyperthermia therapy (which elevates the overall temperature of the tumor), MILH showed better biosafety by only heating the nanoparticles inside the lysosomes and was more energy-efficient (Pucci et al., 2020). In addition, Ang-LMNVs showed prior delivery efficacy and synergistic effects as nanovectors for the nongenotoxic drug nutlin-3a. Notably, Ang-LMNVs submitted to an alternating magnetic field could raise the local temperature to 43°C without affecting heat shock protein 70 (HSP70), bypassing the protection mechanism of HSP70 against magnetocaloric LMP-induced cell death.

Very recently, Clerc et al. (Clerc et al., 2018) constructed gastrin-modified iron oxide magnetic nanoparticles (Gastrin-MNPs) and confirmed their selective cytotoxicity towards various tumors. Gastrin-MNPs targeted tumor cells by recognizing overexpressed gastrin receptors (CCK2R) and inducing LMP through MILH. The MILH-induced local heating increased the ROS level by 7-fold by enhancing the Fenton reaction within lysosomes, in which iron from MNPs was partially involved.

CONCLUSION AND PROSPECTS

In this review, we summarized the three main emerging nanodrug-induced LMP strategies. These nanodrugs demonstrated potent antitumor effects and had ultra-low side effects. Nevertheless, nanodrug-based lysosomal bombs still pose some problems that need to be addressed. For example, HSP70 is overexpressed in malignant tumors and is associated with poor therapeutic outcomes (Kroemer and Jäättelä, 2005; Pucci et al., 2020). HSP70 is localized in the lysosomal membrane and can protect the lysosomal membrane from different stimuli (Kirkegaard and Jäättelä, 2009), including ROS-induced LMP. This suggests that nanodrug-induced LMP researchers should pay particular attention to the factors protecting tumor cells from lysosomal cell death. In addition, the selectivity of nanodrug-induced LMP requires further improvement. For example, EISA-based strategies remain uncommon because alkaline phosphatases are not significantly expressed in some cancer cells (Li et al., 2017). Furthermore, CDT-induced LMP strategies do not differentiate between cancerous and inflamed tissues because many inflammation sites also have elevated H_2O_2 concentrations (Chen et al., 2021; Liu et al., 2022; Zhao et al., 2022; Zhu et al., 2022). Finally, while magnetic field-induced LMP has good spatial selectivity–because the direction of the magnetic field determines the treatment site—it leaves undetected cancer sites untreated.

LMP is a critical process affecting lysosomal function and is an intermediate link in many therapeutic strategies. Multidrug resistance is closely related to lysosomes, as lysosome chelation traps many drugs, rendering them ineffective. Therefore, numerous studies have explored mild LMP induction as a method to mediate lysosomal escape of drugs and thereby increase antitumor efficacy. In fact, due to the highly toxic compounds in lysosomes and their essential role in cellular physiology, strong LMP can directly kill tumors. However, the key to LMP-based therapy is to effectively distinguish cancer cells from normal cells, which dramatically limits the application of this otherwise extremely promising therapy. Fortunately, the many unique and flexible physicochemical properties of nanodrugs allow for specially designed nanodrugs to selectively induce strong LMP in cancer cells, which this minireview highlights. Many

commonly used antitumor strategies have excellent efficiency combined with lysosomal targeting. For example, lysosomal targeting combined with photodynamic therapy (PDT) to overcome the dark toxicity of many photosensitizers (Gao et al., 2020b). To the best of our knowledge, these advantages have not yet been used for LMP-induced cell death in tumor treatment, which may be related to the need for local lighting accuracy. Nevertheless, it provides a research direction for more efficient therapies.

In general, therapeutic strategies that utilize the characteristics of lysosomes in tumor cells are efficient. In addition, the lysosomal cell death mechanism is different from that of most antitumor drugs and provides more opportunities for coping with drug resistance. In addition, processes such as development and aging may be related to the instability of lysosomal membranes. Therefore, LMP-inducing strategies can not only be applied to tumors but may also be worth studying in other aspects leading to treatments for other diseases.

AUTHOR CONTRIBUTIONS

All authors listed have made a substantial, direct, and intellectual contribution to the work and approved it for publication.

FUNDING

This work was supported by the National Natural Science Foundation of China, China (No. 81974508, 21974134), Hunan Science Fund for Distinguished Young Scholar (No. 2021JJ10067), Innovation-Driven Project of Central South University (No. 202045005), Hunan Provincial Natural Science Foundation of China (No. 2021JJ31066), Changsha Science and Technology Project (No. kq2001048), and Key Research Project of Ningxia Hui Autonomous Region in 2021 (Major Project) (No. 2021BEG01001).

REFERENCES

Abdulla, M.-H., Valli-Mohammed, M.-A., Al-Khayal, K., Shkieh, A. A., Zubaidi, A., Ahmad, R., et al. (2017). Cathepsin B Expression in Colorectal Cancer in a Middle East Population: Potential Value as a Tumor Biomarker for Late Disease Stages. *Oncol. Rep.* 37, 3175–3180. doi:10.3892/or.2017.5576

Ai, K., Huang, J., Xiao, Z., Yang, Y., Bai, Y., and Peng, J. (2021). Localized Surface Plasmon Resonance Properties and Biomedical Applications of Copper Selenide Nanomaterials. *Mater Today Chem.* 20, 100402. doi:10.1016/j.mtchem.2020.100402

Baehr, C. M., Zhang, L., Wu, Y., Domokos, A., Xiao, W., Wang, L., et al. (2021). Transformable Amyloid-Beta Mimetic Peptide Amphiphiles for Lysosomal Disruption in Non-small Cell Lung Cancer. *Biomaterials* 277, 121078. doi:10.1016/j.biomaterials.2021.121078

Beatriz, M., Vilaca, R., and Lopes, C. (2021). Exosomes: Innocent Bystanders or Critical Culprits in Neurodegenerative Diseases. *Front. Cell. Dev. Biol.* 9, 635104. doi:10.3389/fcell.2021.635104

Borkowska, M., Siek, M., Kolygina, D. V., Sobolev, Y. I., Lach, S., Kumar, S., et al. (2020). Targeted Crystallization of Mixed-Charge Nanoparticles in Lysosomes Induces Selective Death of Cancer Cells. *Nat. Nanotechnol.* 15, 331–341. doi:10.1038/s41565-020-0643-3

Chen, L., Huang, Q., Zhao, T. J., Sui, L. H., Wang, S. Y., Xiao, Z. X., et al. (2021). Nanotherapies for Sepsis by Regulating Inflammatory Signals and Reactive Oxygen and Nitrogen Species: New Insight for Treating COVID-19. *Redox Biol.* 45, 102046. doi:10.1016/j.redox.2021.102046

Chen, Q. H., Li, N. S., Wang, X. Y., Yang, Y. Q., Xiang, Y. T., Long, X. Y., et al. (2022). *Front. Pharmacol.* 13. doi:10.3389/fphar.2022.847048

Clerc, P., Jeanjean, P., Hallali, N., Gougeon, M., Pipy, B., Carrey, J., et al. (2018). Targeted Magnetic Intra-lysosomal Hyperthermia Produces Lysosomal Reactive Oxygen Species and Causes Caspase-1 Dependent Cell Death. *J. Control. Release* 270, 120–134. doi:10.1016/j.jconrel.2017.11.050

De Duve, C., and Wattiaux, R. (1966). Functions of Lysosomes. *Annu. Rev. Physiol.* 28, 435–492. doi:10.1146/annurev.ph.28.030166.002251

Deng, H., Yang, Z., Pang, X., Zhao, C., Tian, J., Wang, Z., et al. (2022). Self-sufficient Copper Peroxide Loaded pKa-Tunable Nanoparticles for Lysosome-Mediated Chemodynamic Therapy. *Nano Today* 42, 101337. doi:10.1016/j.nantod.2021.101337

Dong, S., Dong, Y., Jia, T., Zhang, F., Wang, Z., Feng, L., et al. (2020). Sequential Catalytic, Magnetic Targeting Nanoplatform for Synergistic Photothermal and NIR-Enhanced Chemodynamic Therapy. *Chem. Mat.* 32, 9868–9881. doi:10.1021/acs.chemmater.9b05170

Fukuda, M. E., Iwadate, Y., Machida, T., Hiwasa, T., Nimura, Y., Nagai, Y., et al. (2005). Cathepsin D Is a Potential Serum Marker for Poor Prognosis in Glioma Patients. *Cancer Res.* 65, 5190–5194. doi:10.1158/0008-5472.can-04-4134

Galluzzi, L., Vitale, I., Aaronson, S. A., Abrams, J. M., Adam, D., Agostinis, P., et al. (2018). Molecular Mechanisms of Cell Death: Recommendations of the Nomenclature Committee on Cell Death 2018. *Cell. Death Differ.* 25, 486–541. doi:10.1038/s41418-017-0012-4

Gao, D., Guo, X., Zhang, X., Chen, S., Wang, Y., Chen, T., et al. (2020). Multifunctional Phototheranostic Nanomedicine for Cancer Imaging and Treatment. *Mater Today Bio* 5, 100035. doi:10.1016/j.mtbio.2019.100035

Gao, Y., Gao, J., Mu, G., Zhang, Y., Huang, F., Zhang, W., et al. (2020). Selectively Enhancing Radiosensitivity of Cancer Cells via *In Situ* Enzyme-Instructed Peptide Self-Assembly. *Acta Pharm. Sin. B* 10, 2374–2383. doi:10.1016/j.apsb.2020.07.022

Giampazolias, E., Zunino, B., Dhayade, S., Bock, F., Cloix, C., Cao, K., et al. (2017). Mitochondrial Permeabilization Engages NF-κb-dependent Anti-tumour Activity under Caspase Deficiency. *Nat. Cell. Biol.* 19, 1116–1129. doi:10.1038/ncb3596

Gobbo, O. L., Sjaastad, K., Radomski, M. W., Volkov, Y., and Prina-Mello, A. (2015). Magnetic Nanoparticles in Cancer Theranostics. *Theranostics* 5, 1249–1263. doi:10.7150/thno.11544

Hessvik, N. P., and Llorente, A. (2018). Current Knowledge on Exosome Biogenesis and Release. *Cell. Mol. Life Sci.* 75, 193–208. doi:10.1007/s00018-017-2595-9

Huang, J., Huang, Q., Liu, M., Chen, Q. H., and Ai, K. L. (2022). Emerging Bismuth Chalcogenides Based Nanodrugs for Cancer Radiotherapy. *Front. Pharmacol.* 13, 844037. doi:10.3389/fphar.2022.844037

Huang, L., Luo, Y., Sun, X., Ju, H., Tian, J., and Yu, B.-Y. (2017). An Artemisinin-Mediated ROS Evolving and Dual Protease Light-Up Nanocapsule for Real-Time Imaging of Lysosomal Tumor Cell Death. *Biosens. Bioelectron.* 92, 724–732. doi:10.1016/j.bios.2016.10.004

Ji, S., Li, J., Duan, X., Zhang, J., Zhang, Y., Song, M., et al. (2021). Targeted Enrichment of Enzyme-Instructed Assemblies in Cancer Cell Lysosomes Turns Immunologically Cold Tumors Hot. *Angew. Chem. Int. Ed.* 60, 26994–27004. doi:10.1002/anie.202110512

Jia, C., Guo, Y., and Wu, F. G. (2022). Chemodynamic Therapy via Fenton and Fenton-Like Nanomaterials: Strategies and Recent Advances. *Small* 18, e2103868. doi:10.1002/smll.202103868

Kanamala, M., Wilson, W. R., Yang, M., Palmer, B. D., and Wu, Z. (2016). Mechanisms and Biomaterials in pH-Responsive Tumour Targeted Drug Delivery: A Review. *Biomaterials* 85, 152–167. doi:10.1016/j.biomaterials.2016.01.061

Kirkegaard, T., and Jäättelä, M. (2009). Lysosomal Involvement in Cell Death and Cancer. *Biochimica Biophysica Acta (BBA) - Mol. Cell. Res.* 1793, 746–754. doi:10.1016/j.bbamcr.2008.09.008

Kolenko, V. M., Uzzo, R. G., Bukowski, R., and Finke, J. H. (2000). Caspase-dependent and -independent Death Pathways in Cancer Therapy. *Apoptosis* 5, 17–20. doi:10.1023/a:1009677307458

Kroemer, G., and Jäättelä, M. (2005). Lysosomes and Autophagy in Cell Death Control. *Nat. Rev. Cancer* 5, 886–897. doi:10.1038/nrc1738

Kurz, T., Terman, A., Gustafsson, B., and Brunk, U. T. (2008). Lysosomes in Iron Metabolism, Ageing and Apoptosis. *Histochem Cell. Biol.* 129, 389–406. doi:10.1007/s00418-008-0394-y

Lajoie, P., Guay, G., Dennis, J. W., and Nabi, I. R. (2005). The Lipid Composition of Autophagic Vacuoles Regulates Expression of Multilamellar Bodies. *J. Cell. Sci.* 118, 1991–2003. doi:10.1242/jcs.02324

Li, Q.-Q., Chen, P.-G., Hu, Z.-W., Cao, Y., Chen, L.-X., Chen, Y.-X., et al. (2017). Selective Inhibition of Cancer Cells by Enzyme-Induced Gain of Function of Phosphorylated Melittin Analogues. *Chem. Sci.* 8, 7675–7681. doi:10.1039/c7sc03217j

Lin, L.-S., Huang, T., Song, J., Ou, X.-Y., Wang, Z., Deng, H., et al. (2019). Synthesis of Copper Peroxide Nanodots for H2O2 Self-Supplying Chemodynamic Therapy. *J. Am. Chem. Soc.* 141, 9937–9945. doi:10.1021/jacs.9b03457

Liu, C.-G., Tang, H.-X., Zheng, X., Yang, D.-Y., Zhang, Y., Zhang, J.-T., et al. (2020). Near-Infrared-Activated Lysosome Pathway Death Induced by ROS Generated from Layered Double Hydroxide-Copper Sulfide Nanocomposites. *ACS Appl. Mat. Interfaces* 12, 40673–40683. doi:10.1021/acsami.0c11739

Liu, M., Huang, Q., Zhu, Y., Chen, L., Li, Y. M., Gong, Z. C., et al. (2022). Harnessing Reactive Oxygen/nitrogen Species and Inflammation: Nanodrugs for Liver Injury. *Mater Today Bio* 13, 100215. doi:10.1016/j.mtbio.2022.100215

Lopez, S., Hallali, N., Lalatonne, Y., Hillion, A., Antunes, J. C., Serhan, N., et al. (2022). Magneto-mechanical Destruction of Cancer-Associated Fibroblasts Using Ultra-small Iron Oxide Nanoparticles and Low Frequency Rotating Magnetic Fields. *Nanoscale Adv.* 4, 421–436. doi:10.1039/d1na00474c

Lunov, O., Uzhytchak, M., Smolkova, B., Lunova, M., Jirsa, M., Dempsey, N. M., et al. (2019). Remote Actuation of Apoptosis in Liver Cancer Cells via Magneto-Mechanical Modulation of Iron Oxide Nanoparticles. *Cancers* 11, 1873. doi:10.3390/cancers11121873

Ma, Z., Li, J., Lin, K., Ramachandran, M., Zhang, D. L., Showalter, M., et al. (2020). Pharmacophore Hybridisation and Nanoscale Assembly to Discover Self-Delivering Lysosomotropic New-Chemical Entities for Cancer Therapy. *Nat. Commun.* 11, 2013. doi:10.1038/s41467-020-18399-4

Persi, E., Duran-Frigola, M., Damaghi, M., Roush, W. R., Aloy, P., Cleveland, J. L., et al. (2018). *Nat. Commun.* 9. doi:10.1038/s41467-018-05261-x

Piao, S., and Amaravadi, R. K. (2016). Targeting the Lysosome in Cancer. *Ann. N.Y. Acad. Sci.* 1371, 45–54. doi:10.1111/nyas.12953

Platt, F. M. (2018). Emptying the Stores: Lysosomal Diseases and Therapeutic Strategies. *Nat. Rev. Drug Discov.* 17, 133–150. doi:10.1038/nrd.2017.214

Pucci, C., De Pasquale, D., Marino, A., Martinelli, C., Lauciello, S., and Ciofani, G. (2020). Hybrid Magnetic Nanovectors Promote Selective Glioblastoma Cell Death through a Combined Effect of Lysosomal Membrane Permeabilization and Chemotherapy. *ACS Appl. Mat. Interfaces* 12, 29037–29055. doi:10.1021/acsami.0c05556

Repnik, U., Hafner Česen, M., and Turk, B. (2014). Lysosomal Membrane Permeabilization in Cell Death: Concepts and Challenges. *Mitochondrion* 19, 49–57. doi:10.1016/j.mito.2014.06.006

Serrano-Puebla, A., and Boya, P. (2018). Lysosomal Membrane Permeabilization as a Cell Death Mechanism in Cancer Cells. *Biochem. Soc. T* 46, 207–215. doi:10.1042/bst20170130

Shi, L., Wang, Y., Zhang, C., Zhao, Y., Lu, C., Yin, B., et al. (2021). An Acidity-Unlocked Magnetic Nanoplatform Enables Self-Boosting ROS Generation through Upregulation of Lactate for Imaging-Guided Highly Specific Chemodynamic Therapy. *Angew. Chem. Int. Ed.* 60, 9562–9572. doi:10.1002/anie.202014415

Soetaert, F., Korangath, P., Serantes, D., Fiering, S., and Ivkov, R. (2020). Cancer Therapy with Iron Oxide Nanoparticles: Agents of Thermal and Immune Therapies. *Adv. Drug Deliv. Rev.* 163-164, 65–83. doi:10.1016/j.addr.2020.06.025

Stern, S. T., Adiseshaiah, P. P., and Crist, R. M. (2012). Autophagy and Lysosomal Dysfunction as Emerging Mechanisms of Nanomaterial Toxicity. *Part. Fibre Toxicol.* 9, 20. doi:10.1186/1743-8977-9-20

Sung, H., Ferlay, J., Siegel, R. L., Laversanne, M., Soerjomataram, I., Jemal, A., et al. (2021). Global Cancer Statistics 2020: GLOBOCAN Estimates of Incidence and Mortality Worldwide for 36 Cancers in 185 Countries. *CA A Cancer J. Clin.* 71, 209–249. doi:10.3322/caac.21660

Tang, Z., Liu, Y., He, M., and Bu, W. (2019). Chemodynamic Therapy: Tumour Microenvironment-Mediated Fenton and Fenton-like Reactions. *Angew. Chem. Int. Ed.* 58, 946–956. doi:10.1002/anie.201805664

Wang, H., Feng, Z., Wang, Y., Zhou, R., Yang, Z., and Xu, B. (2016). Integrating Enzymatic Self-Assembly and Mitochondria Targeting for Selectively Killing Cancer Cells without Acquired Drug Resistance. *J. Am. Chem. Soc.* 138, 16046–16055. doi:10.1021/jacs.6b09783

Wang, J., Hu, L., Zhang, H., Fang, Y., Wang, T., and Wang, H. (2022). Intracellular Condensates of Oligopeptide for Targeting Lysosome and Addressing Multiple Drug Resistance of Cancer. *Adv. Mater* 34, 2270005. doi:10.1002/adma.202270005

Wang, J., Sui, L., Huang, J., Miao, L., Nie, Y., Wang, K., et al. (2021). MoS2-based Nanocomposites for Cancer Diagnosis and Therapy. *Bioact. Mater.* 6, 4209–4242. doi:10.1016/j.bioactmat.2021.04.021

Wu, C., Wang, C., Zhang, T., Gao, G., Wei, M., Chen, Y., et al. (2021). *Advanced Healthcare Materials*.

Yang, Y. Q., Huang, Q., Xiao, Z. X., Liu, M., Zhu, Y., Chen, Q. H., et al. (2022). Nanomaterial-based Biosensor Developing as a Route toward *In Vitro* Diagnosis of Early Ovarian Cancer. *Mater Today Bio* 13, 100218. doi:10.1016/j.mtbio.2022.100218

Zhang, F. L., Hou, Y., Zhu, M. H., Deng, B., Zhao, M., Zhu, X. D., et al. (2021). Death Pathways of Cancer Cells Modulated by Surface Molecule Density on Gold Nanorods. *Adv. Sci.* 8, e2102666. doi:10.1002/advs.202102666

Zhao, B., Zhao, P. H., Jin, Z. K., Fan, M. J., Meng, J., and He, Q. J. (2019). Programmed ROS/CO-releasing Nanomedicine for Synergetic Chemodynamic-Gas Therapy of Cancer. *J. Nanobiotechnol* 17, 75. doi:10.1186/s12951-019-0507-x

Zhao, T., Wu, W., Sui, L., Huang, Q., Nan, Y., Liu, J., et al. (2022). Reactive Oxygen Species-Based Nanomaterials for the Treatment of Myocardial Ischemia Reperfusion Injuries. *Bioact. Mater.* 7, 47–72. doi:10.1016/j.bioactmat.2021.06.006

Zhao, Y., Chen, B.-Q., Kankala, R. K., Wang, S.-B., and Chen, A.-Z. (2020). Recent Advances in Combination of Copper Chalcogenide-Based Photothermal and Reactive Oxygen Species-Related Therapies. *ACS Biomater. Sci. Eng.* 6, 4799–4815. doi:10.1021/acsbiomaterials.0c00830

Zhitomirsky, B., and Assaraf, Y. G. (2016). Lysosomes as Mediators of Drug Resistance in Cancer. *Drug Resist. Updat.* 24, 23–33. doi:10.1016/j.drup.2015.11.004

Zhu, Y., Zhao, T., Liu, M., Wang, S., Liu, S., Yang, Y., et al. (2022). Rheumatoid Arthritis Microenvironment Insights into Treatment Effect of Nanomaterials. *Nano Today* 42, 101358. doi:10.1016/j.nantod.2021.101358

Conflict of Interest: The authors declare that the research was conducted in the absence of any commercial or financial relationships that could be construed as a potential conflict of interest.

Publisher's Note: All claims expressed in this article are solely those of the authors and do not necessarily represent those of their affiliated organizations, or those of the publisher, the editors and the reviewers. Any product that may be evaluated in this article, or claim that may be made by its manufacturer, is not guaranteed or endorsed by the publisher.

Copyright © 2022 Xiang, Li, Liu, Chen, Long, Yang, Xiao, Huang, Wang, Yang, Zhang, Liu and Huang. This is an open-access article distributed under the terms of the Creative Commons Attribution License (CC BY). The use, distribution or reproduction in other forums is permitted, provided the original author(s) and the copyright owner(s) are credited and that the original publication in this journal is cited, in accordance with accepted academic practice. No use, distribution or reproduction is permitted which does not comply with these terms.

frontiers | Frontiers in Oncology

REVIEW
published: 26 May 2022
doi: 10.3389/fonc.2022.907684

Smart Nanoparticles for Breast Cancer Treatment Based on the Tumor Microenvironment

Xiao Luo†, *Qi Zhang*†, *Hongbo Chen*†, *Kai Hou*, *Ning Zeng** *and Yiping Wu**

Department of Plastic and Cosmetic Surgery, Tongji Hospital, Tongji Medical College, Huazhong University of Science and Technology, Wuhan, China

Breast cancer (BC) is the most common malignant tumor in women. There are different risk characteristics and treatment strategies for different subtypes of BC. The tumor microenvironment (TME) is of great significance for understanding the occurrence, development, and metastasis of tumors. The TME plays an important role in all stages of BC metastasis, immune monitoring, immune response avoidance, and drug resistance, and also plays an important role in the diagnosis, prevention, and prognosis of BC. Smart nanosystems have broad development prospect in the regulation of the BC drug delivery based on the response of the TME. In particular, TME-responsive nanoparticles cleverly utilize the abnormal features of BC tissues and cells to achieve targeted transport, stable release, and improved efficacy. We here present a review of the mechanisms underlying the response of the TME to BC to provide potential nanostrategies for future BC treatment.

Keywords: nanomaterial, nanotechnology, nanobiosensors, drug delivery, tumor microenvironment, smart nanoparticles

OPEN ACCESS

Edited by:
Kelong Ai,
Central South University, China

Reviewed by:
Qiong Huang,
Central South University, China
Chengzhi Huang,
South China University of Technology, China

****Correspondence:***
Yiping Wu
wuyipingtj@163.com
Ning Zeng
zengningwhtj@163.com

†*These authors have contributed equally to this work*

Specialty section:
This article was submitted to Pharmacology of Anti-Cancer Drugs, a section of the journal Frontiers in Oncology

Received: *30 March 2022*
Accepted: *28 April 2022*
Published: *26 May 2022*

Citation:
Luo X, Zhang Q, Chen H, Hou K, Zeng N and Wu Y (2022) Smart Nanoparticles for Breast Cancer Treatment Based on the Tumor Microenvironment. Front. Oncol. 12:907684. doi: 10.3389/fonc.2022.907684

INTRODUCTION

Breast cancer (BC) is a common cancer that affects women's health worldwide, and is also the most common malignant tumor among women (1, 2). According to the Report of the American Cancer Society, BC is second only to lung cancer in the number of cancer-related deaths among women. In recent years, the incidence of BC has been increasing at an annual rate of approximately 0.3%, with 2.3 million new cases worldwide in 2020 and a significant increase in mortality from 1990 to 2015 (3, 4). According to Surveillance, Epidemiology and End Results (SEER) data, the 5-year survival rate of patients with stage IIIA and stage IIIB BC was 52% and 48%, respectively, and the median survival of patients with stage III BC was 4.9 years (2, 5–8).

The histological types of BC are (1) non-invasive carcinoma, including ductal carcinoma *in situ* and lobular carcinoma *in situ*; and (2) invasive cancer, including no special type of invasive cancer, invasive lobular carcinoma, tubular carcinoma, and mucinous carcinoma (9–12). Based on molecular evidence, BC can be categorized into three groups: hormone receptor [estrogen

Abbreviations: BC, breast cancer; TME, tumor microenvironment; HER2, human epidermal growth factor receptor 2; ER, estrogen receptors; PR, progesterone receptors; TNBC, triple negative breast cancer; CAFs, cancer-associated fibroblasts; ECM, extracellular matrix; NPs, nanoparticles; ROS, reactive oxygen species; DOX, doxorubicin.

receptor (ER) or progesterone receptor (PR)]-positive, human epidermal receptor 2 (HER2) or ERBB2 receptor-positive, and triple-negative BC (TNBC; ER–, PR–, HER2–). Among them, the luminal subtype can be further divided into luminal A and luminal B tumors, and TNBC can be further divided into six subtypes: basal-like1/basal-like2, mesenchymal, mesenchymal stem-like, immunomodulatory, luminal androgen receptor, and an unspecified group (11, 13–17). The luminal A subtype has the best clinical prognosis, accounting for 40% of all subtypes, and is characterized by high levels of ER expression; therefore, patients with luminal A BC are more likely to benefit from hormone therapy alone. Another less common subtype, luminal B BC (accounting for approximately 20% of all subtypes), is characterized by low levels of ER expression but high expression levels of proliferation-related genes and may require chemotherapy. HER2-enriched tumors (accounting for 15–20% of subtypes) are also characterized by overexpression of proliferation-related genes. The basal-like subtype is characterized by up-regulated expression of genes expressed in basal/myoepithelial cells. The specific molecular pathophysiological mechanism of TNBC tumors is still unclear, accounting for about 15% of all subtypes, and 71% of TNBC tumors are in the basal-like group (18–20).

The three main tumor subtypes of BC, characterized by ER or PR expression and amplification of the *ERBB2* gene, have different risk characteristics and treatment strategies, with the optimal treatment for each patient depending on the tumor subtype, anatomic tumor stage, and patient preference (11, 21–25). In addition, the role of genomic analyses such as detection of *BRCA1* or *BRCA2* germline mutations in treatment decisions has been shown to play an important role in clinical outcomes in BC (26–29).

For patients without metastatic disease, treatment aims to eradicate the tumor from the breast and regional lymph nodes and to prevent recurrence. According to the clinical setting, systemic therapy for non-metastatic BC is mainly based on the molecular characteristics (30–33): patients with hormone receptor-positive tumors receive endocrine therapy and a few patients also receive chemotherapy. Patients with ERBB2-positive tumors are typically treated with ERBB2-targeted antibodies or small-molecule inhibitors (trastuzumab-based) in combination with chemotherapy. Patients with TNBC tumors receive only chemotherapy (6, 14, 18). In addition, local treatment in patients with non-metastatic BC includes surgical excision (including axillary lymph node sampling or excision), and postoperative radiotherapy should be considered if lumpectomy is performed. However, the local treatment of patients with non-metastatic BC is increasingly being performed with some systemic therapy prior to surgery, such as neoadjuvant chemotherapy, followed by postoperative treatment tailored to the preoperative response (18, 34). In contrast, treatment for metastatic BC is also based on molecular subtypes, with the goal of prolonging life and reducing symptoms, which is more complex and personalized (7, 17). Metastatic BC also has a poor prognosis, with a median overall survival of approximately 1 year for metastatic TNBC, compared with approximately 5 years for the other two subtypes (8).

THE TME OF BC

The proliferation of cancer cells and their spread to other parts of the body depend on the microenvironment of the organ, which is also known as the "seed and soil" hypothesis. In brief, cancer-associated fibroblasts (CAFs) in the tumor microenvironment (TME) promote metastasis and secrete large amounts of pro-inflammatory cytokines and chemokines, growth factors, and extracellular matrix (ECM) components. In addition to binding to adjacent tumor cells, CAFs interact with other stromal components in the microenvironment through complex crosstalk. These cells are involved in various activities such as angiogenesis and ECM remodeling, which contribute to tumor growth and metastasis. Thus, the TME is, to some extent, the protagonist of cancer progression, and is more genetically stable than the cancer itself. Therefore, increasing studies aiming toward anticancer drug development are currently focused on strategies targeting the TME (35–37). For example, owing to the genetic and phenotypic heterogeneity of BC cells, the cells or pathways vary among patients or at different periods in the disease course in the same patient, which poses a challenge in conducting targeted research for treatment (38). TME-targeted therapies that use tumor cells, key TME components, or secreted bioactive molecules alone or in combination as therapeutic targets are gaining increasing attention.

Here, we focus on research progress in the development of innovative nanomaterials delivery systems as the key to providing intelligent delivery systems based on active targeting and internalization in the TME and cancer cells (39, 40). In particular, the size and versatility of nano-loaded particles allow for chemical or genetic modification of their surfaces with various targeting groups or active ligands that trigger the specific orientation and recognition of biological targets, enabling them to deliver a steady amount of drugs at the tumor site and control their ability to deliver the drugs effectively (41–43). This review therefore provides an overview of the mechanisms of the TME response to BC, along with examples of the diversity of nanoparticle (NP)-based drug delivery systems developed to date or with potential to target the TME, which can offer an effective dual targeting strategy for BC cells and the TME as the potential key to realizing the successful treatment of BC (44, 45).

The TME is the internal environment in which tumor cells generate and live, which includes not only the tumor cells themselves but also fibroblasts, immune and inflammatory cells, glial cells, and other cells closely related to and interacting with tumor cells. The TME also includes interstitial cells, microvessels, and biomolecules such as secretory factors, proteins, and RNA in the surrounding area (46–49). The TME has long been a key focus of research and the core direction toward gaining a comprehensive understanding of the occurrence and development of tumors. In particular, the TME

plays an important role in the transfer process, immune escape, and drug resistance in tumor metastasis, requiring immune monitoring of the TME at various stages (50) for the diagnosis, prevention, and prognosis of tumors (51–54).

Moreover, the TME plays a key role in several malignant phenotypes associated with tumor progression, including the acquisition of aggressive phenotypes, cell migration ability, chemotherapy resistance, protection from anti-tumor immune responses, and neovasculogenesis (46, 47, 55). The TME can also recombine with the ECM to enhance the permeability of chemotherapeutic drugs, as well as with NPs that enable the intelligent coupling of chemotherapy and immunotherapy by increasing immunogenicity and stimulating anti-tumor immunity (35).

SMART NP-BASED SYSTEMS FOR BC TREATMENT BASED ON THE TME

Nanotechnology has developed rapidly in recent years, providing a good means to overcome the bottleneck problem of non-specific and non-selective damage to body tissues caused by traditional therapies (e.g., chemotherapy, radiotherapy and immunotherapy), and exhibiting unique advantages in improving the effects of drugs and radiation therapy while reducing adverse reactions (44, 56–58). On the one hand, multifunctional nanocarriers can selectively transport therapeutic drugs by utilizing the difference between the tumor tissue and normal tissue to enhance drug permeability and retention. On the other hand, a series of unique physical and chemical properties produced by the TME, such as weak acidity, a reducing environment, abnormal temperature gradient, overexpressed proteins and enzymes, and hypoxia, can be used to regulate the release of loaded drugs by nanocarriers (44, 59).

Reactive Oxygen Species (ROS)-Responsive NPs

Dr. Otto Heinrich Warburg's work on sea urchin embryology led to pioneering research on the physiological effects of ROS. His discoveries in the field of oxidative respiration earned him a Nobel Prize in 1931, and in 1926, Warburg also pioneered a model of tumor maintenance of oxidation and energy, hoping to exert a profound influence on cell physiology and metabolism by deeply exploring the basic properties of ROS (33).

ROS represent the products of single electron reduction of oxygen in the body, as a form of electron leakage before passing to the terminal oxidase respiratory chain, consuming approximately 2% of the oxygen generated, including the single-electron reduction product of oxygen superoxide anion ($O2\cdot^-$), two-electron reduction product hydrogen peroxide (H_2O_2), three-electron product hydroxyl free radical ($\cdot OH$), and nitric oxide, among other highly reactive agents (60). Intracellular ROS are by-products of mitochondrial processes, metabolism, and enzyme activity. Under normal physiological conditions, a large number of electrons are released and reduced by oxygen molecules in the high-oxygen environment and the highly reduced respiratory chain of mitochondria during the transition from state III to state IV (31).

Under normal physiological conditions, ROS can be effectively neutralized by the enzymes superoxide dismutase, catalase, glutathione, and thioredoxin to control the equilibrium oxidation-reduction (redox) state. However, when redox homeostasis is destroyed or relieved, changes in ROS levels will lead to physiological and pathological changes (61, 62). In addition, ROS play a positive role in regulating intracellular signal transduction pathways, with numerous biological conduits being constrained by a variety of ROS species, which are the key to maintaining cellular homeostasis. Any skew in this delicate balance is accompanied by a wave of events that can have either negative or positive impacts for the cell.

From the perspective of cancer, the conventional view that ROS cause widespread damage and chaos within cells has long been debated in the scientific community (63–65). Recently, great progress has been made in the understanding of ROS biology, and there is increasing evidence that the effects of ROS are gradient-dependent, with a threshold of habituation, which affects their signal transduction and toxicity induction function, thus resulting in either "good" or "bad" ROS (33). For example, ROS play a key role in the activation of tumor-promoting signaling pathways (64, 66, 67). Moreover, abnormal production of ROS and ineffective neutralization of excessive ROS levels can lead to tumor growth and progression through different signaling pathways, including phosphatidylinositol 3-kinase/protein kinase inhibitor/mammalian target of rapamycin (PI3/Akt/mTOR), vascular endothelial growth factor (VEGF)/VEGF receptor, phosphatase and tensin congeners (PTEN), and matrix metalloproteinase (MMP) pathways (68). Therefore, an intelligent collaborative treatment system can be developed to ensure the release of chemotherapeutic drugs on demand and reduce ROS production.

pH-Responsive NPs

The acidic microenvironment caused by massive anaerobic glycolysis is one of the important characteristics of malignant tumors, and is also an important factor inducing the occurrence, metastasis, and drug resistance of BC. In recent years, with increasing understanding of the acidic TME, it has been considered a new target for tumor diagnosis and treatment, which is of great significance for the design of pH-responsive nanomedicine and nano-diagnosis (69).

Gong et al. (70) developed a pH-responsive co-delivery platform for metformin and small interfering RNA (siRNA) targeting the immune checkpoint inhibitor FGL1 (siFGL1) based on hybrid biomimetic membrane-camouflaged poly (lactic-co-glycolic acid) NPs. This pH-triggered CO_2 gas generation nanoplatform was developed using the metformin guanidine group, which can react reversibly with CO_2 to produce a metformin-CO_2 complex. Moreover, the capture/release of CO_2 depends on the pH value, thus improving the *in vivo* lysotic escape of the siRNA to achieve the cytoplasmic transfer of siRNA. Metformin promotes programmed death ligand 1

(PD-L1) by activating adenosine monophosphate-induced protein kinase degradation, and then blocks the inhibitory signal of PD-L1, while siFGL1 can silence the *FGL1* gene, promote the T cell-mediated immune response, and enhance anti-tumor immunity. The combination of these two drugs exhibited a high synergistic therapeutic effect on BC *in vivo* and *in vitro* (70).

In addition, Shen et al. (71) developed a robust nanoplatform fabricated from a TME pH-responsive polymer (MEO-PEG-B-PPMEMa) and a cationic lipid compound (G0-C14) for the *in vivo* delivery of cytotoxic saponins in BC treatment. The nanoplatform responds to the TME-specific pH with the rapid release of the saporin/G0-C14 complex, which significantly enhanced the cytoplasmic uptake of saporin and subsequent intracellular escape by tumor cells, thereby effectively inhibiting tumor growth (71).

Enzyme-Responsive NPs

Enzymes play an important role in metabolism. Thus, abnormal metabolism in the TME will result in the overexpression of certain enzymes. Typical examples are MMPs, which are calcium- and zinc-dependent endopeptidases secreted by cancer cells, tumor blood vessels, and CAFs, and play a key role in cancer cell ECM remodeling (72). Other overexpressed enzymes in the TME include hyaluronidase and lysyl oxidase, along with other enzymes that are overexpressed in specific tumors (73).

Kashyap et al. (74) synthesized a hydrophobic acrylate monomer from the natural resource 3-pentachylphenol by enzyme and thermal reactions, which was co-polymerized with the hydrophilic monomer polyethylene glycol acrylate. This copolymer core-shell NP system was then used for the extracellular and intracellular delivery of doxorubicin (DOX)-responsive polymer nanoscaffolds to improve cancer treatment. In the presence of esterase (pH = 7.4, 37°C), the amphiphilic copolymer broke down in a slow and controlled manner within 12 h, releasing >95% of the drugs and achieving controlled release of the drugs in cells (74). For breast cancer, MNPs were successfully conjugated with MTX by Nosrati et al. and this drug delivery system is dependent on the release of the MTX within the lysosomal compartment for BC cells treatment (75).

Hypoxia-Activated NPs

The partial pressure of oxygen (PO_2) in various tumors is generally below 60 mmHg and gradually decreases with tumor progression. This reduction mainly occurs because the structure and function of tumor microvessels are abnormal, and the diffusion distance between blood vessels and the tumor cells increases, thereby preventing the effective transport of O_2 to specific sites. Moreover, the reduced blood oxygenation capacity due to tumor growth or therapeutic anemia also contributes to the local PO_2 reduction (72). The resulting hypoxic environment not only promotes tumor growth, progression, metastasis and damage normal tissues but also reduces the efficacy of radiotherapy and chemotherapy (76).

Mpekris et al. (77) found that the blood vessels of lung metastases of BC were compressed, leading to hypoxia. Based on this principle, mechanical tranilast therapy was used to decompress the blood vessels of lung metastasis in mice so as to restore perfusion and relieve hypoxia. This strategy enabled the immune checkpoint blocker atezolizumab and the nanodrug doxil to more effectively exert cytotoxic effects on metastases and stimulate an antitumor immune response (77).

Thermo-Responsive NPs

Compared with normal tissue, the tumor tissue has a higher temperature, which makes it possible to control and release drugs by external heating at the tumor site, and this property has been exploited in the development of smart drug delivery systems (SDDSs) targeting tumors (74, 78–82). Ding et al. (79) designed a multifunctional SDDS with a double-layer structure: a thermo-sensitive copolymer as the building block of the core-shell structure, two chemotherapeutic drugs [paclitaxel (PTX) and DOX; NP-PD) were encapsulated to form copolymers, and the siRNA (NP-PD-S) affecting survival was absorbed on the surface to form nanostructures, which were finally wrapped by self-polymerizing dopamine (PDA) membranes (NP-PD-S-PDA). This PDA film not only exhibited a photothermal therapeutic effect but also had a protective effect against the uncontrolled release of the drugs. *In vitro* experiments with the MDA-MB-231 BC cell line showed that the survival rate of NP-PD-S-PDA was significantly decreased after 5 min of laser irradiation, indicating that this is an effective combination therapy. *In vivo* experiments with female BALB/C nude mice also showed that in tumors irradiated by NP-PD-S-PDA plus near infrared light, PDA generated sufficient heat, and thermal ablation led to collapse of the NPs, thereby triggering the release of PTX and DOX within the tumor to ultimately achieve antitumor effects (79).

In addition, Hu et al. (80) developed a system for delivery of the hydrophobic chemotherapy drug PTX and the biological macromolecule interleukin (IL)-12 through the low-temperature expansion effect of the acid-sensitive material MPEG-Dlinkm-PDLla and pluronic F127 co-delivered NPs. PTX and IL-12 jointly activated T lymphocytes and natural killer cells to release interferon-gamma, selectively inhibited regulatory T cells, induced the M1-type differentiation of tumor-associated macrophages, improved the tumor immunosuppressive microenvironment, significantly inhibited the growth and metastasis of 4T1 BC cells, and prolonged the overall survival of tumor-bearing mice (80).

CAF-Regulating NPs

The tumor microenvironment is the ecosystem that surrounds a tumor inside the body. It includes immune cells, the extracellular matrix, blood vessels and other cells, like fibroblasts. CAFs are the most abundant cells in the TME matrix, secreting a large number of growth factors (e.g., transforming growth factor-β, VEGF, platelet-derived growth factor), cytokines, interleukins, chemokines, and ECM proteins (e.g., MMPs), which all have an impact on tumor development. CAFs actively reconstruct the

cellular and stromal components of the TME. M2-polarized macrophages promote metastasis and contribute to the development of an immunosuppressive environment. Endothelial cells and pericytes contribute to tumor angiogenesis and handle the oxygen supply. The interstitial ECM supports the tumor structure and regulates drug penetration. The external matrix basement membrane acts as a barrier around the tumor. Both the external matrix and blood vessels contribute to increased interstitial fluid pressure and tumor hypoxia, which is a major barrier to tumor treatment. MMP also supports tumor growth, creates physical barriers to drugs and immune invasion, and promotes cancer invasion (83, 84). In short, normal fibroblasts inhibit tumor formation, whereas CAFs promote BC cell proliferation, angiogenesis, and the inflammatory response, and remodeling the ECM promotes the malignant phenotype of BC cells, resulting in a poor prognosis (85, 86).

Some biological markers of CAFs can be used to identify and target CAFs in the BC TME, which creates opportunities for nanodelivery systems to specifically target the BC metastatic TME. These proteins include fibroblast activating protein (FAP), alpha-smooth muscle actin, fibroblast-specific protein, vimentin, and proline 4-hydroxylase (87, 88). As the most common tumor-targeting CAF antigen, FAP is overexpressed on the surface of CAFs, and nanoparticles can specifically target FAP to promote the infiltration and accumulation of nano-loaded drugs in tumor tissues, thus playing an anti-tumor role. Zhen et al. (89) developed a photoimmunotherapy nanostrategy using ferritin as a photosensitizer carrier and a single-chain variable fragment of anti-FAP antibody conjugated with ferritin.

CONCLUSIONS AND PERSPECTIVES

There has been great progress in the development of intelligent NPs for the effective loading of anti-BC drugs, specific enrichment of tumor cells and tissues, and the controlled release and efficient delivery of drugs. In particular, regulation based on the response of the TME including multifunctional nanoparticles has a broad development prospect for improving BC drug delivery. TME-responsive NPs cleverly utilize the abnormal features of BC tissues to achieve targeted transport, stable release, and improved drug efficacy.

However, there is still room for improvement in TME-responsive nanotechnology. First, there are limitations of the nanomaterials themselves, including limited understanding of the mechanism underlying the interaction between materials and other systems in the body, which makes clinical translation difficult. In addition, the interaction and influence of different components in the nanosystem represent important questions that have not yet been elucidated. Therefore, the design of improved NPs including multifunctional NPs is a promising direction in the future.

AUTHOR CONTRIBUTIONS

All authors contributed to the design of the study and writing of the manuscript. XL, KH, and HC undertook the research, YW and ZN wrote the main manuscript text and prepared figures. QZ and YW revised the article critically for important intellectual content and final approval of the version to be submitted. All authors reviewed the manuscript.

REFERENCES

1. Ferlay J, Colombet M, Soerjomataram I, Parkin DM, Pineros M, Znaor A, et al. Cancer Statistics for the Year 2020: An Overview. *Int J Cancer* (2021). doi: 10.1002/ijc.33588
2. Siegel RL, Miller KD, Fuchs HE, Jemal A. Cancer Statistics, 2021. *CA Cancer J Clin* (2021) 71(1):7–33. doi: 10.3322/caac.21654
3. Shao H, Varamini P. Breast Cancer Bone Metastasis: A Narrative Review of Emerging Targeted Drug Delivery Systems. *Cells* (2022) 11(3):388. doi: 10.3390/cells11030388
4. Azamjah N, Soltan-Zadeh Y, Zayeri F. Global Trend of Breast Cancer Mortality Rate: A 25-Year Study. *Asian Pac J Cancer Prev* (2019) 20 (7):2015–20. doi: 10.31557/APJCP.2019.20.7.2015
5. Gradishar WJ, Anderson BO, Abraham J, Aft R, Agnese D, Allison KH, et al. Breast Cancer, Version 3.2020, NCCN Clinical Practice Guidelines in Oncology. *J Natl Compr Canc Netw* (2020) 18(4):452–78. doi: 10.6004/jnccn.2020.0016
6. Cardoso F, Kyriakides S, Ohno S, Penault-Llorca F, Poortmans P, Rubio IT, et al. Early Breast Cancer: ESMO Clinical Practice Guidelines for Diagnosis, Treatment and Follow-Up. *Ann Oncol* (2019) 30(10):1674. doi: 10.1093/annonc/mdz189
7. Tryfonidis K, Senkus E, Cardoso MJ, Cardoso F. Management of Locally Advanced Breast Cancer-Perspectives and Future Directions. *Nat Rev Clin Oncol* (2015) 12(3):147–62. doi: 10.1038/nrclinonc.2015.13
8. Newman LA. Epidemiology of Locally Advanced Breast Cancer. *Semin Radiat Oncol* (2009) 19(4):195–203. doi: 10.1016/j.semradonc.2009.05.003
9. Fodor A, Brombin C, Mangili P, Borroni F, Pasetti M, Tummineri R, et al. Impact of Molecular Subtype on 1325 Early-Stage Breast Cancer Patients Homogeneously Treated With Hypofractionated Radiotherapy Without Boost: Should the Indications for Radiotherapy be More Personalized? *Breast* (2021) 55:45–54. doi: 10.1016/j.breast.2020.12.004
10. van der Meer DJ, Kramer I, van Maaren MC, van Diest PJ, Linn SC, Maduro JH, et al. Comprehensive Trends in Incidence, Treatment, Survival and Mortality of First Primary Invasive Breast Cancer Stratified by Age, Stage and Receptor Subtype in the Netherlands Between 1989 and 2017. *Int J Cancer* (2021) 148(9):2289–303. doi: 10.1002/ijc.33417
11. Tadros AB, Sevilimedu V, Giri DD, Zabor EC, Morrow M, Plitas G. Survival Outcomes for Metaplastic Breast Cancer Differ by Histologic Subtype. *Ann Surg Oncol* (2021) 28(8):4245–53. doi: 10.1245/s10434-020-09430-5
12. Yalcin B. Overview on Locally Advanced Breast Cancer: Defining, Epidemiology, and Overview on Neoadjuvant Therapy. *Exp Oncol* (2013) 35(4):250–2.
13. Russnes HG, Lingjaerde OC, Borresen-Dale AL, Caldas C. Breast Cancer Molecular Stratification: From Intrinsic Subtypes to Integrative Clusters. *Am J Pathol* (2017) 187(10):2152–62. doi: 10.1016/j.ajpath.2017.04.022
14. Bayani J, Yao CQ, Quintayo MA, Yan F, Haider S, D'Costa A, et al. Molecular Stratification of Early Breast Cancer Identifies Drug Targets to Drive Stratified Medicine. *NPJ Breast Cancer* (2017) 3:3. doi: 10.1038/s41523-016-0003-5
15. Yao K, Goldschmidt R, Turk M, Wesseling J, Stork-Sloots L, de Snoo F, et al. Molecular Subtyping Improves Diagnostic Stratification of Patients With Primary Breast Cancer Into Prognostically Defined Risk Groups. *Breast Cancer Res Treat* (2015) 154(1):81–8. doi: 10.1007/s10549-015-3587-9
16. Wang DY, Jiang Z, Ben-David Y, Woodgett JR, Zacksenhaus E. Molecular Stratification Within Triple-Negative Breast Cancer Subtypes. *Sci Rep* (2019) 9 (1):19107. doi: 10.1038/s41598-019-55710-w
17. Ruswendro D, Syamsu SA, Thabry R, Seweng A, Usman AN. Association Between Molecular Subtype of Local Advanced Breast Cancer With Ca 15-3 Level. *Breast Dis* (2021) 40(S1):S119–22. doi: 10.3233/BD-219018

18. Waks AG, Winer EP. Breast Cancer Treatment: A Review. *JAMA* (2019) 321 (3):288–300. doi: 10.1001/jama.2018.19323
19. Tyagi NK, Dhesy-Thind S. Clinical Practice Guidelines in Breast Cancer. *Curr Oncol* (2018) 25(Suppl 1):S151–60. doi: 10.3747/co.25.3729
20. Xie P, An R, Yu S, He J, Zhang H. A Novel Immune Subtype Classification of ER-Positive, PR-Negative and HER2-Negative Breast Cancer Based on the Genomic and Transcriptomic Landscape. *J Transl Med* (2021) 19(1):398. doi: 10.1186/s12967-021-03076-x
21. Reid S, Haddad D, Tezak A, Weidner A, Wang X, Mautz B, et al. Impact of Molecular Subtype and Race on HR+, HER2- Breast Cancer Survival. *Breast Cancer Res Treat* (2021) 189(3):845–52. doi: 10.1007/s10549-021-06342-0
22. Mills MN, Thawani C, Figura NB, Oliver DE, Soyano AE, Etame A, et al. Breast Cancer Subtype Predicts Clinical Outcomes After Stereotactic Radiation for Brain Metastases. *J Neurooncol* (2021) 152(3):591–601. doi: 10.1007/s11060-021-03735-5
23. Li Y, Wang S, Yang W, Liu H. Prognostic Significance of Molecular Subtype, Metastatic Site and Primary Tumor Surgery for Survival in Primary Metastatic Breast Cancer: A SEER-Based Study. *Med (Baltimore)* (2021) 100(27):e26619. doi: 10.1097/MD.0000000000026619
24. Hong J, Tong Y, He J, Chen X, Shen K. Association Between Tumor Molecular Subtype, Clinical Stage and Axillary Pathological Response in Breast Cancer Patients Undergoing Complete Pathological Remission After Neoadjuvant Chemotherapy: Potential Implications for De-Escalation of Axillary Surgery. *Ther Adv Med Oncol* (2021) 13:1758835921996673. doi: 10.1177/1758835921996673
25. Ding S, Sun X, Lu S, Wang Z, Chen X, Shen K. Association of Molecular Subtype Concordance and Survival Outcome in Synchronous and Metachronous Bilateral Breast Cancer. *Breast* (2021) 57:71–9. doi: 10.1016/j.breast.2021.03.005
26. Im SA, Xu B, Li W, Robson M, Ouyang Q, Yeh DC, et al. Olaparib Monotherapy for Asian Patients With a Germline BRCA Mutation and HER2-Negative Metastatic Breast Cancer: OlympiAD Randomized Trial Subgroup Analysis. *Sci Rep* (2020) 10(1):8753. doi: 10.1038/s41598-020-63033-4
27. Metzger-Filho O, Collier K, Asad S, Ansell PJ, Watson M, Bae J, et al. Matched Cohort Study of Germline BRCA Mutation Carriers With Triple Negative Breast Cancer in Brightness. *NPJ Breast Cancer* (2021) 7(1):142. doi: 10.1038/s41523-021-00349-y
28. Su Y, Yao Q, Xu Y, Yu C, Zhang J, Wang Q, et al. Characteristics of Germline Non-BRCA Mutation Status of High-Risk Breast Cancer Patients in China and Correlation With High-Risk Factors and Multigene Testing Suggestions. *Front Genet* (2021) 12:674094. doi: 10.3389/fgene.2021.674094
29. Atci MM, Geredeli C, Ay S, Sakin A, Erturk B, Secmeler S, et al. Clinical and Pathological Characteristics of Patients With High-Risk Breast Cancer Based on BRCA Mutation Profiles: A Retrospective Study. *Eur J Breast Health* (2021) 17(2):123–7. doi: 10.4274/ejbh.galenos.2020.6346
30. Spring LM, Wander SA, Andre F, Moy B, Turner NC, Bardia A. Cyclin-Dependent Kinase 4 and 6 Inhibitors for Hormone Receptor-Positive Breast Cancer: Past, Present, and Future. *Lancet* (2020) 395(10226):817–27. doi: 10.1016/S0140-6736(20)30165-3
31. Shashni B, Nagasaki Y. Nitroxide Radical-Containing Nanoparticles Attenuate Tumorigenic Potential of Triple Negative Breast Cancer. *Biomaterials* (2018) 178:48–62. doi: 10.1016/j.biomaterials.2018.05.042
32. Reinert T, Barrios CH. Optimal Management of Hormone Receptor Positive Metastatic Breast Cancer in 2016. *Ther Adv Med Oncol* (2015) 7(6):304–20. doi: 10.1177/1758834015608993
33. Raman D, Foo CH, Clement MV, Pervaiz S. Breast Cancer: A Molecular and Redox Snapshot. *Antioxid Redox Signal* (2016) 25(6):337–70. doi: 10.1089/ars.2015.6546
34. Wen N, Qiu J, Xu L, Wang Y, Zhang J, Xie Y, et al. Adjuvant Chemotherapy Guidance for Pt1-3N0-1 Breast Cancer Patients With HR(+), HER2(-) Subtype: A Cohort Study Based on the SEER Database. *Ann Transl Med* (2021) 9(24):1779. doi: 10.21037/atm-21-5937
35. Truffi M, Mazzucchelli S, Bonizzi A, Sorrentino L, Allevi R, Vanna R, et al. Nano-Strategies to Target Breast Cancer-Associated Fibroblasts: Rearranging the Tumor Microenvironment to Achieve Antitumor Efficacy. *Int J Mol Sci* (2019) 20(6):1263. doi: 10.3390/ijms20061263
36. Chen X, Song E. Turning Foes to Friends: Targeting Cancer-Associated Fibroblasts. *Nat Rev Drug Discov* (2019) 18(2):99–115. doi: 10.1038/s41573-018-0004-1
37. Tchou J, Conejo-Garcia J. Targeting the Tumor Stroma as a Novel Treatment Strategy for Breast Cancer: Shifting From the Neoplastic Cell-Centric to a Stroma-Centric Paradigm. *Adv Pharmacol* (2012) 65:45–61. doi: 10.1016/B978-0-12-397927-8.00003-8
38. Stingl J, Caldas C. Molecular Heterogeneity of Breast Carcinomas and the Cancer Stem Cell Hypothesis. *Nat Rev Cancer* (2007) 7(10):791–9. doi: 10.1038/nrc2212
39. Lu P, Wang G, Qian T, Cai X, Zhang P, Li M, et al. The Balanced Microenvironment Regulated by the Degradants of Appropriate PLGA Scaffolds and Chitosan Conduit Promotes Peripheral Nerve Regeneration. *Mater Today Bio* (2021) 12:100158. doi: 10.1016/j.mtbio.2021.100158
40. Han Z, Gong C, Li J, Guo H, Chen X, Jin Y, et al. Immunologically Modified Enzyme-Responsive Micelles Regulate the Tumor Microenvironment for Cancer Immunotherapy. *Mater Today Bio* (2022) 13:100170. doi: 10.1016/j.mtbio.2021.100170
41. Batra H, Pawar S, Bahl D. Curcumin in Combination With Anti-Cancer Drugs: A Nanomedicine Review. *Pharmacol Res* (2019) 139:91–105. doi: 10.1016/j.phrs.2018.11.005
42. Truffi M, Fiandra L, Sorrentino L, Monieri M, Corsi F, Mazzucchelli S. Ferritin Nanocages: A Biological Platform for Drug Delivery, Imaging and Theranostics in Cancer. *Pharmacol Res* (2016) 107:57–65. doi: 10.1016/j.phrs.2016.03.002
43. Colombo M, Rizzuto MA, Pacini C, Pandolfi L, Bonizzi A, Truffi M, et al. Half-Chain Cetuximab Nanoconjugates Allow Multitarget Therapy of Triple Negative Breast Cancer. *Bioconjug Chem* (2018) 29(11):3817–32. doi: 10.1021/acs.bioconjchem.8b00667
44. Tong R, Langer R. Nanomedicines Targeting the Tumor Microenvironment. *Cancer J* (2015) 21(4):314–21. doi: 10.1097/PPO.0000000000000123
45. Omidi Y, Barar J. Targeting Tumor Microenvironment: Crossing Tumor Interstitial Fluid by Multifunctional Nanomedicines. *Bioimpacts* (2014) 4 (2):55–67. doi: 10.5681/bi.2014.021
46. Bezdenezhnykh N, Semesiuk N, Lykhova O, Zhylchuk V, Kudryavets Y. Impact of Stromal Cell Components of Tumor Microenvironment on Epithelial-Mesenchymal Transition in Breast Cancer Cells. *Exp Oncol* (2014) 36(2):72–8.
47. Mao Y, Keller ET, Garfield DH, Shen K, Wang J. Stromal Cells in Tumor Microenvironment and Breast Cancer. *Cancer Metastasis Rev* (2013) 32(1-2):303–15. doi: 10.1007/s10555-012-9415-3
48. Dong M, Shen W, Yang G, Yang Z, Li X. Analysis of M6a Methylation Modification Patterns and Tumor Immune Microenvironment in Breast Cancer. *Front Cell Dev Biol* (2022) 10:785058. doi: 10.3389/fcell.2022.785058
49. Munkacsy G, Santarpia L, Gyorffy B. Gene Expression Profiling in Early Breast Cancer-Patient Stratification Based on Molecular and Tumor Microenvironment Features. *Biomedicines* (2022) 10(2):248. doi: 10.3390/biomedicines10020248
50. Gu X, Gao Y, Wang P, Wang L, Peng H, He Y, et al. Nano-Delivery Systems Focused on Tumor Microenvironment Regulation and Biomimetic Strategies for Treatment of Breast Cancer Metastasis. *J Control Release* (2021) 333:374–90. doi: 10.1016/j.jconrel.2021.03.039
51. Xu Q, Yan X, Han Z, Jin X, Jin Y, Sun H, et al. Immune Cell Infiltration and Relevant Gene Signatures in the Tumor Microenvironment That Significantly Associates With the Prognosis of Patients With Breast Cancer. *Front Mol Biosci* (2022) 9:823911. doi: 10.3389/fmolb.2022.823911
52. Zhu J, Shen Y, Wang L, Qiao J, Zhao Y, Wang Q. A Novel 12-Gene Prognostic Signature in Breast Cancer Based on the Tumor Microenvironment. *Ann Transl Med* (2022) 10(3):143. doi: 10.21037/atm-21-6748
53. Wang X, Xie T, Luo J, Zhou Z, Yu X, Guo X. Radiomics Predicts the Prognosis of Patients With Locally Advanced Breast Cancer by Reflecting the Heterogeneity of Tumor Cells and the Tumor Microenvironment. *Breast Cancer Res* (2022) 24(1):20. doi: 10.1186/s13058-022-01516-0
54. Xu L, Hu Y, Liu W. Pyroptosis-Mediated Molecular Subtypes Are Characterized by Distinct Tumor Microenvironment Infiltration Characteristics in Breast Cancer. *J Inflammation Res* (2022) 15:345–62. doi: 10.2147/JIR.S349186

55. Du Y, Cao M, Liu Y, He Y, Yang C, Zhang G, et al. Tumor Microenvironment Remodeling Modulates Macrophage Phenotype in Breast Cancer Lymphangiogenesis. *FASEB J* (2022) 36(4):e22248. doi: 10.1096/fj.202101230R
56. Zeng N, Chen X, Liu Z. Natural Products and Nanotechnology Against Coronavirus Disease 2019. *Front Chem* (2022) 10:819969. doi: 10.3389/fchem.2022.819969
57. Li Y, Liu Z, Zeng W, Wang Z, Liu C, Zeng N, et al. A Novel H2O2 Generator for Tumor Chemotherapy-Enhanced CO Gas Therapy. *Front Oncol* (2021) 11:738567. doi: 10.3389/fonc.2021.738567
58. Huang C, Liu Z, Chen M, Du L, Liu C, Wang S, et al. Tumor-Derived Biomimetic Nanozyme With Immune Evasion Ability for Synergistically Enhanced Low Dose Radiotherapy. *J Nanobiotechnology* (2021) 19(1):457. doi: 10.1186/s12951-021-01182-y
59. Hou K, Ning Z, Chen H, Wu Y. Nanomaterial Technology and Triple Negative Breast Cancer. *Front Oncol* (2021) 11:828810. doi: 10.3389/fonc.2021.828810
60. Zhao T, Wu W, Sui L, Huang Q, Nan Y, Liu J, et al. Reactive Oxygen Species-Based Nanomaterials for the Treatment of Myocardial Ischemia Reperfusion Injuries. *Bioact Mater* (2022) 7:47–72. doi: 10.1016/j.bioactmat.2021.06.006
61. Choi HW, Lim JH, Kim CW, Lee E, Kim JM, Chang K, et al. Near-Infrared Light-Triggered Generation of Reactive Oxygen Species and Induction of Local Hyperthermia From Indocyanine Green Encapsulated Mesoporous Silica-Coated Graphene Oxide for Colorectal Cancer Therapy. *Antioxid (Basel)* (2022) 11(1):174. doi: 10.3390/antiox11010174
62. Liu L, Liu F, Liu D, Yuan W, Zhang M, Wei P, et al. A Smart Theranostic Prodrug System Activated by Reactive Oxygen Species for Regional Chemotherapy of Metastatic Cancer. *Angew Chem Int Ed Engl* (2022) 61(12):e202116807. doi: 10.1002/anie.202116807
63. Casella D, Palumbo P, Sandroni S, Caponi C, Littori F, Capuano F, et al. Positive ROS (Reactive Oxygen Species) Modulator Engineered Device Support Skin Treatment in Locally Advanced Breast Cancer (LABC) Enhancing Patient Quality of Life. *J Clin Med* (2021) 11(1):126. doi: 10.3390/jcm11010126
64. Wang G, Duan P, Wei Z, Liu F. Curcumin Sensitizes Carboplatin Treatment in Triple Negative Breast Cancer Through Reactive Oxygen Species Induced DNA Repair Pathway. *Mol Biol Rep* (2022) 49(4):3259–70. doi: 10.1007/s11033-022-07162-1
65. Wang C, Guo J, Wu Z. Combinative Treatment of Curdione and Docetaxel Triggers Reactive Oxygen Species (ROS)-Mediated Intrinsic Apoptosis of Triple-Negative Breast Cancer Cells. *Bioengineered* (2021) 12(2):10037–48. doi: 10.1080/21655979.2021.1994737
66. Mishra R, Yuan L, Patel H, Karve AS, Zhu H, White A, et al. Phosphoinositide 3-Kinase (PI3K) Reactive Oxygen Species (ROS)-Activated Prodrug in Combination With Anthracycline Impairs PI3K Signaling, Increases DNA Damage Response and Reduces Breast Cancer Cell Growth. *Int J Mol Sci* (2021) 22(4):2088. doi: 10.3390/ijms22042088
67. Ullah I, Khalil AT, Ali M, Iqbal J, Ali W, Alarifi S, et al. Green-Synthesized Silver Nanoparticles Induced Apoptotic Cell Death in MCF-7 Breast Cancer Cells by Generating Reactive Oxygen Species and Activating Caspase 3 and 9 Enzyme Activities. *Oxid Med Cell Longev* (2020) 2020:1215395. doi: 10.1155/2020/1215395
68. Aggarwal V, Tuli HS, Varol A, Thakral F, Yerer MB, Sak K, et al. Role of Reactive Oxygen Species in Cancer Progression: Molecular Mechanisms and Recent Advancements. *Biomolecules* (2019) 9(11):735. doi: 10.3390/biom9110735
69. Li J, Wang Y, Xu C, Yu Q, Wang X, Xie H, et al. Rapid pH-Responsive Self-Disintegrating Nanoassemblies Balance Tumor Accumulation and Penetration for Enhanced Anti-Breast Cancer Therapy. *Acta Biomater* (2021) 134:546–58. doi: 10.1016/j.actbio.2021.04.022
70. Gong C, Yu X, Zhang W, Han L, Wang R, Wang Y, et al. Regulating the Immunosuppressive Tumor Microenvironment to Enhance Breast Cancer Immunotherapy Using pH-Responsive Hybrid Membrane-Coated Nanoparticles. *J Nanobiotechnol* (2021) 19(1):58. doi: 10.1186/s12951-021-00805-8
71. Shen Q, Xu L, Li R, Wu G, Li S, Saw PE, et al. A Tumor Microenvironment (TME)-Responsive Nanoplatform for Systemic Saporin Delivery and Effective Breast Cancer Therapy. *Chem Commun (Camb)* (2021) 57(20):2563–6. doi: 10.1039/d0cc07808e
72. Qiao Y, Wan J, Zhou L, Ma W, Yang Y, Luo W, et al. Stimuli-Responsive Nanotherapeutics for Precision Drug Delivery and Cancer Therapy. *Wiley Interdiscip Rev Nanomed Nanobiotechnol* (2019) 11(1):e1527. doi: 10.1002/wnan.1527
73. Dong X, Yin W, Zhang X, Zhu S, He X, Yu J, et al. Intelligent MoS2 Nanotheranostic for Targeted and Enzyme-/pH-/NIR-Responsive Drug Delivery To Overcome Cancer Chemotherapy Resistance Guided by PET Imaging. *ACS Appl Mater Interfaces* (2018) 10(4):4271–84. doi: 10.1021/acsami.7b17506
74. Kashyap S, Singh N, Surnar B, Jayakannan M. Enzyme and Thermal Dual Responsive Amphiphilic Polymer Core-Shell Nanoparticle for Doxorubicin Delivery to Cancer Cells. *Biomacromolecules* (2016) 17(1):384–98. doi: 10.1021/acs.biomac.5b01545
75. Nosrati H, Mojtahedi A, Danafar H, Kheiri Manjili H. Enzymatic Stimuli-Responsive Methotrexate-Conjugated Magnetic Nanoparticles for Target Delivery to Breast Cancer Cells and Release Study in Lysosomal Condition. *J BioMed Mater Res A* (2018) 106(6):1646–54. doi: 10.1002/jbm.a.36364
76. Wojtkowiak JW, Verduzco D, Schramm KJ, Gillies RJ. Drug Resistance and Cellular Adaptation to Tumor Acidic pH Microenvironment. *Mol Pharm* (2011) 8(6):2032–8. doi: 10.1021/mp200292c
77. Mpekris F, Panagi M, Voutouri C, Martin JD, Samuel R, Takahashi S, et al. Normalizing the Microenvironment Overcomes Vessel Compression and Resistance to Nano-Immunotherapy in Breast Cancer Lung Metastasis. *Adv Sci (Weinh)* (2021) 8(3):2001917. doi: 10.1002/advs.202001917
78. Rao NV, Ko H, Lee J, Park JH. Recent Progress and Advances in Stimuli-Responsive Polymers for Cancer Therapy. *Front Bioeng Biotechnol* (2018) 6:110. doi: 10.3389/fbioe.2018.00110
79. Ding Y, Su S, Zhang R, Shao L, Zhang Y, Wang B, et al. Precision Combination Therapy for Triple Negative Breast Cancer *via* Biomimetic Polydopamine Polymer Core-Shell Nanostructures. *Biomaterials* (2017) 113:243–52. doi: 10.1016/j.biomaterials.2016.10.053
80. Hu Q, Shang L, Wang M, Tu K, Hu M, Yu Y, et al. Co-Delivery of Paclitaxel and Interleukin-12 Regulating Tumor Microenvironment for Cancer Immunochemotherapy. *Adv Healthc Mater* (2020) 9(10):e1901858. doi: 10.1002/adhm.201901858
81. Niu S, Williams GR, Wu J, Wu J, Zhang X, Chen X, et al. A Chitosan-Based Cascade-Responsive Drug Delivery System for Triple-Negative Breast Cancer Therapy. *J Nanobiotechnol* (2019) 17(1):95. doi: 10.1186/s12951-019-0529-4
82. Huang J, Huang Q, Liu M, Chen Q, Ai K. Emerging Bismuth Chalcogenides Based Nanodrugs for Cancer Radiotherapy. *Front Pharmacol* (2022) 13:844037. doi: 10.3389/fphar.2022.844037
83. Qiao A, Gu F, Guo X, Zhang X, Fu L. Breast Cancer-Associated Fibroblasts: Their Roles in Tumor Initiation, Progression and Clinical Applications. *Front Med* (2016) 10(1):33–40. doi: 10.1007/s11684-016-0431-5
84. Alkasalias T, Moyano-Galceran L, Arsenian-Henriksson M, Lehti K. Fibroblasts in the Tumor Microenvironment: Shield or Spear? *Int J Mol Sci* (2018) 19(5):1532. doi: 10.3390/ijms19051532
85. Costa A, Kieffer Y, Scholer-Dahirel A, Pelon F, Bourachot B, Cardon M, et al. Fibroblast Heterogeneity and Immunosuppressive Environment in Human Breast Cancer. *Cancer Cell* (2018) 33(3):463–79.e10. doi: 10.1016/j.ccell.2018.01.011
86. Bochet L, Lehuede C, Dauvillier S, Wang YY, Dirat B, Laurent V, et al. Adipocyte-Derived Fibroblasts Promote Tumor Progression and Contribute to the Desmoplastic Reaction in Breast Cancer. *Cancer Res* (2013) 73(18):5657–68. doi: 10.1158/0008-5472.CAN-13-0530
87. Ao Z, Shah SH, Machlin LM, Parajuli R, Miller PC, Rawal S, et al. Identification of Cancer-Associated Fibroblasts in Circulating Blood From Patients With Metastatic Breast Cancer. *Cancer Res* (2015) 75(22):4681–7. doi: 10.1158/0008-5472.CAN-15-1633

88. LeBleu VS, Kalluri R. A Peek Into Cancer-Associated Fibroblasts: Origins, Functions and Translational Impact. *Dis Model Mech* (2018) 11(4): dmm029447. doi: 10.1242/dmm.029447
89. Zhen Z, Tang W, Wang M, Zhou S, Wang H, Wu Z, et al. Protein Nanocage Mediated Fibroblast-Activation Protein Targeted Photoimmunotherapy To Enhance Cytotoxic T Cell Infiltration and Tumor Control. *Nano Lett* (2017) 17(2):862–9. doi: 10.1021/acs.nanolett.6b04150

Conflict of Interest: The authors declare that the research was conducted in the absence of any commercial or financial relationships that could be construed as a potential conflict of interest.

Publisher's Note: All claims expressed in this article are solely those of the authors and do not necessarily represent those of their affiliated organizations, or those of the publisher, the editors and the reviewers. Any product that may be evaluated in this article, or claim that may be made by its manufacturer, is not guaranteed or endorsed by the publisher.

Copyright © 2022 Luo, Zhang, Chen, Hou, Zeng and Wu. This is an open-access article distributed under the terms of the Creative Commons Attribution License (CC BY). The use, distribution or reproduction in other forums is permitted, provided the original author(s) and the copyright owner(s) are credited and that the original publication in this journal is cited, in accordance with accepted academic practice. No use, distribution or reproduction is permitted which does not comply with these terms.

frontiers | Frontiers in Oncology

REVIEW
published: 21 June 2022
doi: 10.3389/fonc.2022.919279

Research Progress in Exosome-Based Nanoscale Drug Carriers in Tumor Therapies

Wei Fu[1], *Tingting Li*[1], *Hongbo Chen*[2*], *Shu Zhu*[3*] and *Changkai Zhou*[4*]

[1] Department of Pharmacy, Tongji Hospital, Tongji Medical College, Huazhong University of Science and Technology, Wuhan, China, [2] Department of Plastic and Cosmetic Surgery, Tongji Hospital, Tongji Medical College, Huazhong University of Science and Technology, Wuhan, China, [3] Department of Medical Ultrasound, Tongji Hospital, Tongji Medical College, Huazhong University of Science and Technology, Wuhan, China, [4] Department of Burn and Plastic Surgery, Affiliated Hospital 2 of Nantong University, Nantong First People's Hospital, Nantong, China

OPEN ACCESS

Edited by:
Kelong Ai,
Central South University, China

Reviewed by:
Qiong Huang,
Central South University, China
Wei Fang,
Hubei Academy of Agricultural Sciences, China
Bo An,
GlaxoSmithKline, United States

***Correspondence:**
Changkai Zhou
ntyyzck@outlook.com
Shu Zhu
zhushu0602@126.com
Hongbo Chen
chenhongbo_xh@sina.com

Specialty section:
This article was submitted to Pharmacology of Anti-Cancer Drugs, a section of the journal Frontiers in Oncology

Received: 13 April 2022
Accepted: 12 May 2022
Published: 21 June 2022

Citation:
Fu W, Li T, Chen H, Zhu S and Zhou C (2022) Research Progress in Exosome-Based Nanoscale Drug Carriers in Tumor Therapies. Front. Oncol. 12:919279. doi: 10.3389/fonc.2022.919279

Current antitumor treatment methods have several reported limitations, including multidrug resistance and serious adverse reactions. Targeted drug delivery systems are effective alternatives that can help healthcare providers overcome these limitations. Exosomes can serve as a natural nanoscale drug delivery system, with the advantages of high biocompatibility, low immunogenicity, and efficient tumor targetability. In this paper, we discuss the biological characteristics of exosomes, summarize the drug-carrying mechanisms of exosome-based drug delivery systems, and examine the potential role and applicability of exosomes in clinical tumor treatment approaches. This review can be used as a guideline for the future development of exosome-based delivery systems in clinical precision tumor treatment.

Keywords: exosomes, nanoscale drug carriers, drug-loading strategy, tumor therapy, miRNA

INTRODUCTION

Cancer refers to a range of diseases that are characterized by the unregulated growth of malignant cells that can proliferate beyond the original malignant site. Current cancer treatment options include surgical interventions, immunotherapy, chemotherapy, and radiation therapy or a combination of these options. Existing treatment methods are generally nonselective and can damage healthy normal tissues at the target site, which is associated with unintended severe side effects (1). In fact, adverse effects induced by chemotherapeutic drugs on healthy tissues and organs are partially responsible for the high mortality rate of cancer patients (2). Therefore, it is desirable to develop novel therapeutic strategies for the precise elimination of cancer cells, thereby reducing the potential for adverse side effects while achieving high therapeutic effectiveness.

Exosomes are nanosized vesicle structures that are secreted from cells and are abundant in all fluids and tissues of the human body (3–5). Bioactive substances are transported from donor cells to recipient cells through exosomes, such as nutrients required for cell growth, and exosomal transport plays an important role in the communication between cells (6). Owing to this targeted transport characteristic, exosome-mediated drug delivery can circumvent the P-glycoprotein drug efflux system, which can mitigate the natural drug resistance response in the body (7). Furthermore, exosomes can specifically bind to receptors on the surface of target cells, allowing exosome-

mediated drug transport to be specific to a cell or tissue. In addition, the high biocompatibility and low toxicity of naturally derived exosomes make exosome-based delivery systems superior to synthetic drug carriers in clinical applications (8).

This review is intended to provide a reference for the development and application of exosomes as effective nanoscale drug carriers in tumor therapy by detailing the advantages and challenges that have been reported in recent research.

CHARACTERISTICS AND BIOLOGICAL FUNCTIONS OF EXOSOMES

Basic Characteristics of Exosomes

Exosomes are intracellular vesicular bodies (40–100 nm in diameter) that are secreted from the cell after the fusion of intracellular multivesicular bodies (MVBs) to the cytoplasmic membrane (**Figure 1**). Exosomes were first discovered in 1983 (9) as small vesicles isolated from sheep erythrocyte supernatant by ultracentrifugation. Exosomes have been subject to increasing scholarly and public attention over the past four decades (10, 11). Exosomes are characterized by lipid bilayers with a rounded or cupped shape. They are widely found in biological fluids such as blood, urine, saliva, and cerebrospinal fluid (12).

Initially, exosomes were considered to function as a "cellular trash bag" that removed unnecessary components from cells. However, later studies reported that exosomes can mediate intercellular communication in many biological processes, and ongoing research has gradually elucidated the important and varied biological functions of exosomes (13, 14). Exosomes are formed by the following processes: the cytoplasmic membrane indents into the cell to form intracellular vesicles, and multiple vesicles fuse with each other to form early endosomes; the early endosomes invaginate again to enclose the intracellular fluid or material and form lumen internal vesicles (i.e., MVBs). Finally, MVBs fuse with the cytoplasmic membrane and release small vesicles into the extracellular space, forming exosomes (15). Exosomes are mainly composed of proteins and lipids, such as fusion proteins, transport proteins, heat shock proteins, CD proteins (i.e., CD9, CD63, and CD81), phospholipases, cholesterol, sphingomyelin, and phosphoglyceride (16). In addition, exosomes contain abundant messenger RNA (mRNA), microRNA (miRNA), small interfering RNA (siRNA), and other genetic materials (17).

Because mRNA can be expressed in target cells, exosome-mediated intercellular communication may be involved in the transfer and expression of genetic information. Exosome-transferred miRNAs have been shown to induce functional changes in target cells. Mittelbrunn et al. (18) found that miRNAs from T-cell exosomes caused the repression of target genes in dendritic cells, and miRNAs in exosomes secreted from Epstein–Barr virus–transfected B cells affected the repression of target genes in dendritic cells.

Biological Functions of Exosomes

With the rapid development of analytical technologies such as proteomics and gene sequencing, the complex characteristics of exosomes have been subject to continuous investigation and identification. A series of studies has revealed that exosomes are not simply cell debris but subcellular structures secreted by cells that act as specific carriers for the transfer of genetic material and information between cells (19, 20). Exosomes can specifically bind

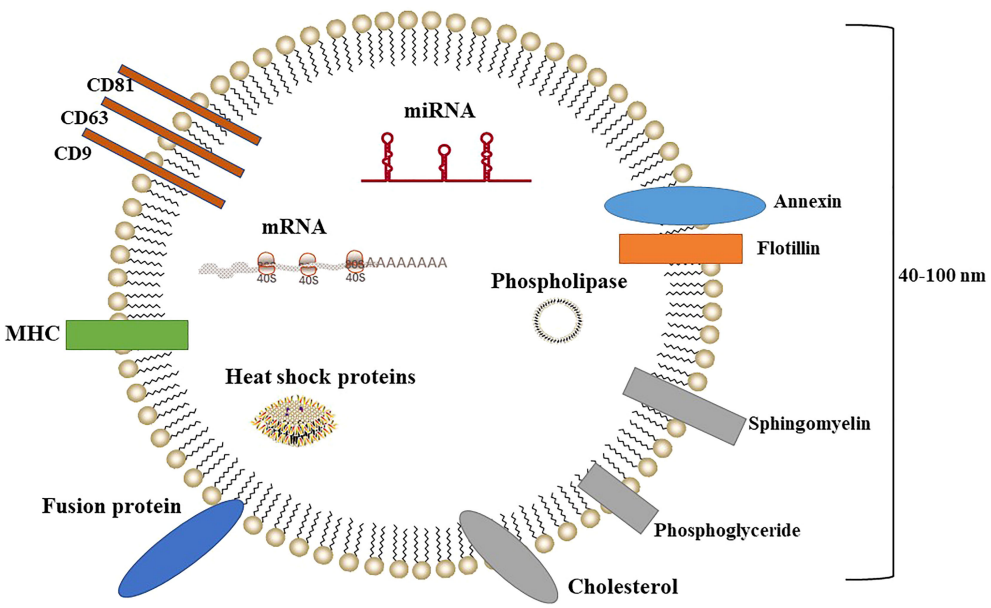


FIGURE 1 | Exosome structure.

to target cells in a variety of ways. Ligands on the surface of exosomes can bind to target cell receptors, and their membrane or internal proteins can bind to target cell receptors following enzymatic hydrolysis or to target cell receptors *via* fusion with target cells or endocytosis. The material within the exosome can then be transferred to exert biologically active effects. Iaccino et al. (21) studied exosomes obtained from multiple myeloma samples and found that these exosomes expressed immunoglobulin receptors on their surfaces that could bind to a unique binding peptide.

Exosomes are now considered promising drug delivery vehicles due to their small size, high biocompatibility, and reduced toxicity in comparison with synthetic nanoformulations. Additionally, anticancer drugs contained in exosomes have been shown to exhibit improved pharmacokinetic and pharmacodynamic properties and enhanced anticancer activity *in vivo* compared to free-drug administration. Similarly, the loading of therapeutic nucleic acids such as siRNA into exosomes protects the RNA from nucleases and increases cellular uptake, thus improving the therapeutic effect compared to free RNAs that are rapidly degraded by nucleases. Notably, exosomes can cross the blood–brain barrier and penetrate deep tissues with improved efficacy compared to synthetic nanocarriers. Thus, exosomes are an effective and necessary tool for delivering anticancer therapeutics.

CHARACTERISTICS OF EXOSOMES AS NANOCARRIERS

Methods for Loading Exosomes

Mounting evidence has demonstrated that exosomes are an excellent candidate platform for cargo delivery in clinical applications. To date, various strategies have been developed for loading materials into exosomes, such as incubation, sonication, electroporation, and chemical conjugation (22–24).

Incubation

The simplest cargo-loading method is incubation, by which the desired cargo is allowed to diffuse into an exosome or exosome-secreting cell *via* a concentration gradient (25). Cargo diffuses across cell and exosomal membranes to then be packaged within exosomes. Two primary incubation methods have been developed: direct incubation and exosome donor cell-mediated incubation followed by isolation of drug-carrying exosomes. The former is suitable for drugs that can interact with the lipid layer of exosomal membranes, while the latter is suitable for small-molecule chemical drugs with low cytotoxicity. Didiot et al. (26) coincubated U-87 glioblastoma with hydrophobically treated small kinetic RNA. The hydrophobic end of siRNA binds to cholesterol on the membrane of U87 glioblastoma-derived exosomes, mediating its entry into exosomes. This coincubation method can yield 10%–50% of siRNA-loaded exosomes. Incubation of exosome donor cells with drugs is another way. Donor cells are treated with the drug, leading to the secretion of loaded exosomes. A combination of paclitaxel and doxorubicin was loaded into exosomes from ovarian cancer cells and breast-to-lung metastatic cells, enabling the inhibitory effects on tumor growth (27).

Incubation loading methods have emerged to load various cargos into exosomes. The main advantages of this strategy are that it is simple and causes only minor damage to exosome integrity. Some disadvantages are that the loading efficiency is limited and the loading quantitation is difficult to control due to physicochemical properties of potential cargo and created exosomes.

Electroporation

Electroporation is a strategy for loading cargo into exosomes with assistance from electrical fields that produce micropores on the exosomal membrane to enhance permeability. Although drugs can diffuse into exosomes *via* incubation, drug loading efficiency can be significantly enhanced using electroporation.

Because high-voltage pulses can penetrate the exosomal membrane, subjecting the mixture of drug and exosomes to a certain voltage can induce drug loading. For example, doxycycline-loaded exosomes generated by electroporation have been reported to target tumor tissues and inhibit tumor growth significantly without exerting observable toxicity to other tissues (28). Kim et al. (29) introduced antisense miRNA oligonucleotides targeting miR-21 into exosomes by electroporation to treat glioblastoma. Electroporation has also been utilized to directly load nucleic acids and nanomaterials into exosomes. Izco et al. (30) loaded short hairpin RNA (shRNA) into murine dendritic cell-derived exosomes, which decreased α-synuclein aggregation and alleviated dopaminergic neuron loss in Parkinson's disease (PD) models.

Transfection

Transfection is the most common strategy for stably loading nucleic acids, proteins, and peptides into exosomes. In this approach, transfection reagents are used to load drugs into exosomes. Cell transfection can be achieved by using the calcium phosphate method or by a commercially available lipid transfection reagent such as Lipofectamine. Choi et al. (31) found that exosomes from osteogenic precursor cells were enriched in let-7 miRNAs under physiological conditions. The introduction of miRNA inhibitors into exosomes by transfection can modulate bone differentiation and improve motor nerve-related diseases and tumor treatment outcomes. Furthermore, Kojima et al. (32) transduced human embryonic kidney cell line 293 (HEK293) cells with designed plasmids to generate catalase mRNA-loaded exosomes that targeted central nervous system (CNS) cells to treat Parkinson's disease. In addition, exosomes can also be directly transfected with nucleic acids by chemical treatment. Pi et al. (33) isolated exosomes from HEK293 cells and transfected exosomes with siRNA using a heat shock protocol.

The ectopic expression of desired materials or molecules that facilitate specific cargo sorting *via* transfection has emerged as a common strategy. However, the loading efficiency achieved using this method remains relatively low as the cargo-sorting mechanisms are difficult to manipulate intracellularly and direct chemical transfection always induces impurities.

Ultrasound

Ultrasound is a physical strategy by which an extra mechanical shear force is applied to weaken the exosomal membrane, which promotes loading of cargo such as drugs, proteins, and nanomaterials. The mechanical shear force generated during sonication disrupts the integrity of the exosomal membrane. The drug enters the exosome during membrane deformation, and the subsequent incubation process restores the integrity of the cell membrane.

Li et al. (34) found that after mixing the drug and exosomes, the drug could be effectively loaded into the exosomes following ultrasound, and the structure and composition of the exosomal membrane did not change significantly after ultrasound. Similarly, Salarpour et al. (35) used sonication and incubation to load paclitaxel (PTX) into U-87 cell-derived exosomes to treat glioblastoma multiforme. Experimental data demonstrate that PTX-loaded exosomes (exoPTX) were more toxic to glioblastoma multiforme cells than free PTX solution.

Recent reports have shown that ultrasound is an effective method for loading drugs into exosomes. However, sonication-induced membrane damage remains a primary roadblock for scaling up this method.

Extrusion

Extrusion is a physical process by which an exosome and cargo mixture are subjected to pressure in an extruder mechanism to induce membrane recombination. The exosome and drug mixture are loaded into a liposome extruder with multiple pore sizes. The pore size of the extruder pore membrane is 100–400 nm, which allows the drug to enter the exosomes *via* extrusion. Kalimuthu et al. (36) mixed PTX with bone marrow mesenchymal stem cells and achieved drug loading using the extrusion method. The drug-loaded exosomes obtained by this method not only efficiently target cancer cells but also exhibit reduced cardiotoxicity and neurotoxicity associated with chemotherapeutic drugs compared to free-drug administration (36). Extrusion has high loading capacities, but a rearrangement of exosome surface structure possibly changes their integrity.

To date, a growing number of approaches have been developed and applied to induce exosomal cargo loading. It remains difficult to efficiently load desired materials into exosomes while minimizing exosomal surface damage. **Table 1** compares the advantages and disadvantages of commonly used drug-loading methods. Although various studies have reported successful drug loading using various methods, the appropriate selection of a candidate method depends on the properties of the target drug and the source and properties of the exosomes (37).

STRATEGIES FOR SURFACE ENGINEERING OF EXOSOMES

Despite being naturally derived, exosomes can be modified by various genetic engineering methods. Genetic engineering approaches fuse genes for signaling proteins or polypeptides with those for selected exosomal membrane proteins, thereby conferring cell-targeted specificity that improves the suitability of the produced exosomes for transport, increasing the concentration and duration of effect of the loaded drugs at the tumor site to achieve desirable treatment outcomes.

Several strategies for modification of the exosome have been tested. For example, exosomes obtained from HEK293 were genetically engineered to express GE11 short peptide and miRNA Let-7a (38). The GE11 peptide binds to the epidermal growth factor receptor, which is highly expressed in many epithelial tumors. The engineered exosomes were labeled with 1,1′-dioctadecyltetramethylindole tricarbocyanine iodine and injected intravenously into tumor-bearing mice. The monitoring results of *in vitro* and *in vivo* imaging showed that three times as many GE11 exosomes reached the tumor site than did those of the control group, and the loaded miRNA Let-7a effectively inhibited tumor growth. Similarly, incorporating ligand modifications on the surface of exosomes is another common strategy widely endorsed. For instance, exosomes obtained from HEK293T cells were anchored with lipophilic hyaluronic acid (lipHA-hEVs) as a ligand to target CD44-overexpressing breast cancer cells to deliver doxorubicin. These lipHA-hEVs were shown to enrich doxorubicin specifically in breast cancer cells, thereby reducing the tumor mass by 89% and increasing the animal survival by 50% (39). In addition, receptor protein engineering is another strategy for preparing exosomes for targeted delivery. Recently, a method was described in HEK293 cells that enabled partitioning of reporter proteins into the inner or outer surface of exosome by utilizing specific locations on the tetraspanin proteins for fusion protein engineering. Such methods immensely allow engineering of exosomes to achieve significantly improved targeting capacity.

In summary, all of these methods significantly improve the tumor-targeted drug delivery of the native exosomes and help reduce the toxicity. Therefore, the latest studies focusing on the development of combined targeting strategies with enhanced exosome homing capacity and drug delivery efficiency have reported promising results that provide a foundation for the clinical application of exosome-based drug delivery systems.

APPLICATION OF EXOSOMES AS NANODRUG CARRIERS IN TUMOR THERAPY

Protein Drugs

Recently, the development of exosome-based vaccines has become a topic of significant interest in clinical research (40, 41). Rivoltini et al. (42) reported that exosomes loaded with tumor necrosis factor α (TNFα)-related apoptosis-inducing ligands promoted cancer cell apoptosis and mitigated tumor development. Similarly, interleukin (IL)-18-rich exosomes promoted proinflammatory cytokine release and monocyte proliferation, inducing specific antitumor immune responses (43). Moreover, Yang et al. (44) found that IL-2-rich exosomes could induce antigen-specific T helper cells I (Th1) polarized and killer T

TABLE 1 | Primary strategies for loading cargos into exosomes.

Types of strategies	Types of cargos	Advantages	Disadvantages
Incubation	Drugs, nucleic acids, proteins, peptides, nanomaterial	Easy operation; Does not require special equipment; Minimal destruction to carrier exosome	Low loading efficiency; Difficult to control;The amount of drug that diffuses into the cells and loads into the exosome is unpredictable
Electroporation	Drugs, nucleic acids, proteins, peptides, nanomaterials	High loading efficiency; Loading large biomolecules	Influence exosome integrity; Cargo aggregation
Transfection	Nucleic acids, proteins, peptides	High loading efficiency for nucleic acids, proteins, and peptides; Stability	Time- and financial consuming; Hard to quantitate
Ultrasound	Drugs, proteins, peptides, nanomaterials	High loading efficiency; Effective method of loading different types of cargo	Disruption of exosome integrity; Attachment of drugs to the surface of exosome
Extrusion	Drugs, nucleic acids, proteins, peptides, nanomaterial	High loading efficiency	Disruption of exosome integrity

lymphocyte-mediated immune responses, leading to significantly inhibited tumor growth in mice.

Exosomes can also be loaded with protein antagonists. For instance, signal regulatory protein α (SIRPα) inhibits macrophage phagocytosis of tumor cells by interacting with CD47. In tumor-bearing mice, exosomes containing SIRPα antagonists were observed to significantly promote tumor phagocytosis (45).

Chemotherapy Drugs

The indiscriminate nature of antitumor chemotherapeutic drugs, leading to cell death in both tumor and normal cells, is associated with severe adverse reactions in the body. Therefore, it is necessary to develop alternative effective drug carriers that specifically target tumor cells.

Tang et al. (46) reported that tumor cell-derived microparticles could be used as carriers for chemotherapeutic drugs, and the chemotherapeutic drugs encapsulated in the microparticles exerted strong antitumor effects *in vitro* and *in vivo*. Kim et al. (47) developed an exosome-based formulation of PTX, which is a commonly used chemotherapy drug. They incorporated PTX into exosomes using three methods: incubation at room temperature, electroporation, and mild sonication. The mild sonication method produced the highest loading efficiency and sustained drug release. The cytotoxicity of exoPTX against drug-resistant MDCKMDR1 (Pgp+) cells was increased by more than 50-fold. In addition, exoPTX was found to effectively target cancer cells following injection into mice with lung cancer, demonstrating a strong antitumor effect. Similarly, Saari et al. (48) found that the use of exosomes from cancer cells as drug carriers enhanced the cytotoxicity of transported PTX to cognate prostate cancer cells. Furthermore, modifying exosome surface proteins is a common method for improving the targeting of chemotherapeutic drugs to cancer cells. Tian et al. (49) obtained mature dendritic cells (IMDCs) expressing Lamp2b iRGD peptide (specific for av integrin) using a genetic engineering method, isolated exosomes from IMDCs, and transported doxorubicin to target cells *via* exosome loading. Their results showed that iRGD-containing exosomes effectively targeted av integrin-expressing breast cancer cells and inhibited tumor growth.

Nucleic Acid Drugs

miRNA

miRNAs are noncoding RNAs of approximately 20 nucleotides in length. Posttranscriptional gene silencing is mediated by binding to the target site in the 3′ untranslated region or open reading frame of the target mRNA (50). Since exosomes naturally carry miRNAs, it can serve as a therapeutic application for tumors. For instance, miR-1290 and miR-375 in exosomes were positively associated with overall survival in castration-resistant prostate cancer patients (51). Katakowski et al. (52) and Zhang et al. (53) reported that anti-glioma miRNA (miRNA-146b)-enriched exosomes inhibited glioma growth *in vitro*, while miR-101-enriched exosomes demonstrated the ability to inhibit the invasion and migration of osteosarcoma cells.

The abovementioned studies provide an illustration as to how the combined effects of miRNAs and exosome-based therapies may be valuable, especially for the future treatment of cancer. The instability and degradability of miRNAs hinder their application in tumor therapy. Exosomes are stable vesicles that can carry functional biologically active molecules with high targeting specificity. Therefore, the miRNA-loaded exosome system is expected to play a key role in emerging tumor therapies.

siRNA

siRNA is a double-stranded RNA with a length of 21–23 nucleotide pairs. In the cytoplasm, RNA-induced silencing complexes interact with complementary mRNAs, leading to their degradation and gene silencing (54). siRNA is the first choice for treating diseases caused by gene overexpression. However, the negative charge of siRNA limits their ability to cross cell membranes, and siRNAs are readily degradable with short half-lives. Therefore, identifying an efficient and reliable method for delivering siRNAs to target cells will significantly improve the efficacy of siRNA-mediated therapies (55).

Alvarez-Erviti et al. (56) exploited the RNA transport ability of exosomes to successfully conduct gene therapy studies in which exogenous siRNA was delivered in a targeted manner for the first time. They transfected IMDCs with a plasmid encoding the exosomal protein Lamp2b and fused it to the brain-specific peptide rabies virus glycoprotein (RVG). RVG-targeted

exosomes were purified from dendritic cell cultures, and Glyceraldehyde-3-phosphate dehydrogenase siRNA was loaded into exosomes by electroporation. Mice were then injected with RVG and Glyceraldehyde-3-phosphate dehydrogenase siRNA-loaded exosomes *via* the tail vein. The results show that this mode of administration can specifically reduce Glyceraldehyde-3-phosphate dehydrogenase expression in the cerebral cortex, striatum, and midbrain of mice. RVG BACE1-siRNA-loaded exosomes reduced *BACE1* gene expression in the cerebral cortex of treated mice by 60% when RVG-loaded exosomes were used to deliver BACE1-siRNA targeting β-secretase. Production of the toxic amyloid $A\beta_{1\text{-}42}$ was also significantly reduced. Notably, these exosomes were used as efficient and specific delivery vehicles for siRNA without associated toxicity or immunogenicity observed even with repeated administration, which is an important feature of siRNA clinical applications (57).

Other Drug Applications

In addition to the abovementioned biologically active molecules, exosomes can silence the expression of related pathogenic genes by transporting specific gene-editing complexes. Lin et al. (58) constructed exosome–liposome composite nanoparticles to effectively transport the gene-editing complex Cas9/Cas9 to the mesenchymal region and subsequently deliver the Cas9-Cas9 complex by being phagocytosed by mesenchymal stem cells. Emerging findings have demonstrated that composite nanoparticles constructed by genetic engineering have a broad application value in novel tumor therapies.

THE CHALLENGES OF USING EXOSOMES IN THERAPEUTIC DRUG DELIVERY SYSTEMS

Several clinical trials have been attempted over the past decade using exosome-based drug delivery for cancer therapy. However, several questions on the optimization of exosomes for clinical usage remain unsettled (**Table 2**).

Sources

The primary consideration in developing therapeutic exosomes is the cell source. Mesenchymal stem cell-derived exosomes are considered promising for cancer therapy, as they are known to be safe and versatile. To optimize their clinical use, critical technological considerations should be addressed and possible side effects identified.

Some research groups have begun isolating exosomes from several types of fruit or vegetables, including ginger, grapes, and lemons, to address problems related to a mammalian cell-derived exosome (59, 60). These exosomes can load small molecules and mediate therapeutic effects on animal models (61). A phase I clinical trial using curcumin-loaded plant-based exosomes for the treatment of colon cancer was conducted.

Loading

The natural biogenesis of exosomes can be used to load them with therapeutics endogenously by direct loading in the producer cell, such as incubation, electroporation, transfection, ultrasound, and extrusion. However, a large load may affect exosome stability or lead to exosome aggregation, and the loading efficiency seems to be quite variable. For instance, electroporation may affect the integrity of exosomes or drugs, especially when loading genetic drugs, thus raising the concern of safety risks (62).

Alternatively, cellular nanoporation for delivering the phosphatase and tensin homolog (PTEN) mRNA in a mouse brain tumor model showed improvement in electroporation-mediated loading. Yang et al. (63) transfected cells with several nucleic acids by using focal and transient electrical stimuli to generate nanopores in targeted cells, which efficiently produced exosomes containing the targeted nucleic acids. The systemically administered PTEN-deficient glioma mouse models with PTEN-loaded exosomes showed a promising effect *in vivo* (63).

Production

The yield of exosomes collected by existing separation technologies cannot meet the standards for clinical use, and the cost of large-scale production is difficult to estimate (64). Serial centrifugation with ultracentrifugation is currently the standard method for exosome production. This method is limited by the risk of macromolecule contaminants, exosome aggregation, time-consuming, and disruption of integrity. To purify exosomes further by ultracentrifugation, a density gradient separation using iodixanol and a sucrose cushion ultracentrifugation step can be applied, leading to higher purity with a minimal risk of sample loss. Furthermore, size-based methods such as tangential flow filtration and size exclusion chromatography are being widely used for exosome isolation and show better yields, integrity, purity, and functionality of exosomes than by ultracentrifugation-based isolation methods.

Finally, methods for transporting and storing drug-encapsulated exosomes are also urgent concerns that require further research. Studies have found that the optimal temperature for storing

TABLE 2 | Advantages and challenges of using exosomes in therapeutic drug delivery systems.

Advantages	Challenges
Nanoscopic size	A large-scale purification method for clinical use is still missing
Low immunogenicity	Efficient cargo loading methods without damaging EV integrity are lacking
High biocompatibility	The exact mechanism of interaction between exosomes and targeted cells needs elucidation
Encapsulation of various cargos	*In vivo* data yet less studied
The ability to overcome biological barriers	Clinical translation for therapeutic delivery is lacking

exosome samples is -80°C, whereas another approach is storing lyophilized powder at room temperature (65, 66).

CONCLUSION

Exosomes have great potential for application in targeted tumor therapy due to their unique biological properties. As nanoscale vesicles secreted by cells, exosomes exhibit unique advantages that make them suitable drug carriers. First, exosomes commonly show high stability, high biocompatibility, and low immunogenicity than other drug delivery platforms (67, 68). Second, nanosized exosomes that bear specific surface proteins can penetrate efficiently the target tumor tissue. These features suggest that exosomes can serve as efficient nanocarriers for the delivery of proteins drugs, chemotherapy drugs, and nucleic acid drugs.

However, the exosome-based drug delivery systems have several limitations in sources, loading, and production. For exosomes to be clinically applicable, the production of functionalized exosomes requires cell culture on a large scale with quality control. Furthermore, given the complexity and heterogeneity of tumors, exosome-based tumor therapy approaches are expected to be the most effective when combined with other nanotherapies (69, 70). There is an urgent need to conduct a large number of clinical trials of exosome-based tumor therapies to determine their efficacy and safety. As these technologies progress and we continue to develop a more comprehensive understanding of exosomal characteristics under various conditions, clinical research on and the applicability of exosomes as a nanoscale drug delivery system in tumor therapies will continue to improve.

AUTHOR CONTRIBUTIONS

All authors contributed to the design of the study and writing of the article. WF, TL, and HC wrote the main article text and prepared figures. CZ and SZ revised the article critically for important intellectual content and final approval of the version to be submitted. All authors reviewed the article.

FUNDING

This work was supported by the Natural Science Foundation of Hubei Province of China (2021CFB348).

REFERENCES

1. Zhou MG, Wang HD, Zeng XY, Yin P, Zhu J, Chen WQ, et al. Mortality, Morbidity, and Risk Factors in China and Its Provinces, 1990-2017: A Systematic Analysis for the Global Burden of Disease Study 2017. *Lancet* (2019) 394:1145–58. doi: 10.1016/S0140-6736(19)30427-1
2. Essa H, Wright DJ, Dobson R, Lip GYH. Chemotherapy-Induced Arrhythmia- Underrecognized and Undertreated. *Am J Med* (2021) 134:1224. doi: 10.1016/j.amjmed.2021.05.026
3. Doyle LM, Wang MZ. Overview of Extracellular Vesicles, Their Origin, Composition, Purpose, and Methods for Exosome Isolation and Analysis. *Cells-Basel* (2019) 8:727. doi: 10.3390/cells8070727
4. Hessvik NP, Llorente A. Current Knowledge on Exosome Biogenesis and Release. *Cell Mol Life Sci* (2018) 75:193–208. doi: 10.1007/s00018-017-2595-9
5. Farooqi AA, Desai NN, Qureshi MZ, Librelotto DRN, Gasparri ML, Bishayee A, et al. Exosome Biogenesis, Bioactivities and Functions as New Delivery Systems of Natural Compounds. *Biotechnol Adv* (2018) 36:328–34. doi: 10.1016/j.biotechadv.2017.12.010
6. Record M, Subra C, Silvente-Poirot S, Poirot M. Exosomes as Intercellular Signalosomes and Pharmacological Effectors. *Biochem Pharmacol* (2011) 81:1171–82. doi: 10.1016/j.bcp.2011.02.011
7. Rountree RB, Mandl SJ, Nachtwey JM, Dalpozzo K, Do L, Lombardo JR, et al. Exosome Targeting of Tumor Antigens Expressed by Cancer Vaccines Can Improve Antigen Immunogenicity and Therapeutic Efficacy. *Cancer Res* (2011) 71:5235–44. doi: 10.1158/0008-5472.Can-10-4076
8. Dad HA, Gu TW, Zhu AQ, Huang LQ, Peng LH. Plant Exosome-Like Nanovesicles: Emerging Therapeutics and Drug Delivery Nanoplatforms. *Mol Ther* (2021) 29:13–31. doi: 10.1016/j.ymthe.2020.11.030
9. Colombo M, Raposo G, Thery C. Biogenesis, Secretion, and Intercellular Interactions of Exosomes and Other Extracellular Vesicles. *Annu Rev Cell Dev Bi* (2014) 30:255–89. doi: 10.1146/annurev-cellbio-101512-122326
10. Thery C, Zitvogel L, Amigorena S. Exosomes: Composition, Biogenesis and Function. *Nat Rev Immunol* (2002) 2:569–79. doi: 10.1038/nri855
11. Valadi H, Ekstrom K, Bossios A, Sjostrand M, Lee JJ, Lotvall JO. Exosome-Mediated Transfer of mRNAs and microRNAs Is a Novel Mechanism of Genetic Exchange Between Cells. *Nat Cell Biol* (2007) 9:654–U72. doi: 10.1038/ncb1596
12. Greening DW, Gopal SK, Xu R, Simpson RJ, Chen WS. Exosomes and Their Roles in Immune Regulation and Cancer. *Semin Cell Dev Biol* (2015) 40:72–81. doi: 10.1016/j.semcdb.2015.02.009
13. Simons M, Raposo G. Exosomes - Vesicular Carriers for Intercellular Communication. *Curr Opin Cell Biol* (2009) 21:575–81. doi: 10.1016/j.ceb.2009.03.007
14. Ventimiglia LN, Alonso MA. Biogenesis and Function of T Cell-Derived Exosomes. *Front Cell Dev Biol* (2016) 4:84. doi: 10.3389/fcell.2016.00084
15. Ibrahim A, Marban E. Exosomes: Fundamental Biology and Roles in Cardiovascular Physiology. *Annu Rev Physiol* (2016) 78:67–83. doi: 10.1146/annurev-physiol-021115-104929
16. Saunderson SC, Dunn AC, Crocker PR, McLellan AD. CD169 Mediates the Capture of Exosomes in Spleen and Lymph Node. *Blood* (2014) 123:208–16. doi: 10.1182/blood-2013-03-489732
17. Sugimachi K, Matsumura T, Hirata H, Uchi R, Ueda M, Ueo H, et al. Identification of a Bona Fide microRNA Biomarker in Serum Exosomes That Predicts Hepatocellular Carcinoma Recurrence After Liver Transplantation. *Brit J Cancer* (2015) 112:532–38. doi: 10.1038/bjc.2014.621
18. Mittelbrunn M, Gutierrez-Vazquez C, Villarroya-Beltri C, Gonzalez S, Sanchez-Cabo F, Gonzalez MA, et al. Unidirectional Transfer of microRNA-Loaded Exosomes From T Cells to Antigen-Presenting Cells. *Nat Commun* (2011) 2:282. doi: 10.1038/ncomms1285
19. Urbanelli L, Magini A, Buratta S, Brozzi A, Sagini K, Polchi A, et al. Signaling Pathways in Exosomes Biogenesis, Secretion and Fate. *Genes-Basel* (2013) 4:152–70. doi: 10.3390/genes4020152
20. Zeng W, Wen Z, Chen H, Duan Y. Exosomes as Carriers for Drug Delivery in Cancer Therapy. *Pharm Res* (2022). doi: 10.1007/s11095-022-03224-y
21. Iaccino E, Mimmi S, Dattilo V, Marino F, Candeloro P, Di Loria A, et al. Monitoring Multiple Myeloma by Idiotype-Specific Peptide Binders of Tumor-Derived Exosomes. *Mol Cancer* (2017) 16:159. doi: 10.1186/s12943-017-0730-8
22. Chen HZ, Wang LY, Zeng XL, Schwarz H, Nanda HS, Peng XS, et al. Exosomes, A New Star for Targeted Delivery. *Front Cell Dev Biol* (2021) 9:751079. doi: 10.3389/fcell.2021.751079

23. Fu SY, Wang Y, Xia XH, Zheng JLC. Exosome Engineering: Current Progress in Cargo Loading and Targeted Delivery. *Nanoimpact* (2020) 20:100261. doi: 10.1016/j.impact.2020.100261
24. Liu CY, Su CQ. Design Strategies and Application Progress of Therapeutic Exosomes. *Theranostics* (2019) 9:1015–28. doi: 10.7150/thno.30853
25. Seo N, Nakamura J, Kaneda T, Tateno H, Shimoda A, Ichiki T, et al. Distinguishing Functional Exosomes and Other Extracellular Vesicles as a Nucleic Acid Cargo by the Anion-Exchange Method. *J Extracell Vesicles* (2022) 11:e12205. doi: 10.1002/jev2.12205
26. Didiot MC, Hall LM, Coles AH, Haraszti RA, Godinho BM, Chase K, et al. Exosome-Mediated Delivery of Hydrophobically Modified siRNA for Huntingtin mRNA Silencing. *Mol Ther* (2016) 24:1836–47. doi: 10.1038/mt.2016.126
27. Wang J, Yeung BZ, Cui MJ, Peer CJ, Lu Z, Figg WD, et al. Exosome is a Mechanism of Intercellular Drug Transfer: Application of Quantitative Pharmacology. *J Control Release* (2017) 268:147–58. doi: 10.1016/j.jconrel.2017.10.020
28. Gehl J. Electroporation: Theory and Methods, Perspectives for Drug Delivery, Gene Therapy and Research. *Acta Physiol Scand* (2003) 177:437–47. doi: 10.1046/j.1365201X.2003.01093.x
29. Kim G, Kim M, Lee Y, Byun JW, Hwang DW, Lee M. Systemic Delivery of microRNA-21 Antisense Oligonucleotides to the Brain Using T7-Peptide Decorated Exosomes. *J Control Release* (2020) 317:273–81. doi: 10.1016/j.jconrel.2019.11.009
30. Izco M, Blesa J, Schleef M, Schmeer M, Porcari R, Al-Shawi R, et al. Systemic Exosomal Delivery of short hairpin RNA Minicircles Prevents Parkinsonian Pathology. *Mol Ther* (2019) 27:2111–22. doi: 10.1016/j.ymthe.2019.08.010
31. Choi SY, Han EC, Hong SH, Kwon TG, Lee Y, Lee HJ. Regulating Osteogenic Differentiation by Suppression of Exosomal MicroRNAs. *Tissue Eng Pt A* (2019) 25:1146–54. doi: 10.1089/ten.tea.2018.0257
32. Kojima R, Bojar D, Rizzi G, Hamri GCE, El-Baba MD, Saxena P, et al. Designer Exosomes Produced by Implanted Cells Intracerebrally Deliver Therapeutic Cargo for Parkinson's Disease Treatment. *Nat Commun* (2018) 9:1305. doi: 10.1038/s41467-018-03733-8
33. Pi FM, Binzel DW, Lee TJ, Li ZF, Sun MY, Rychahou P, et al. Nanoparticle Orientation to Control RNA Loading and Ligand Display on Extracellular Vesicles for Cancer Regression. *Nat Nanotechnol* (2018) 13:82–9. doi: 10.1038/s41565-017-0012-z
34. Li X, Li X, Lin J, Sun X, Ding Q. Exosomes Derived From Low-Intensity Pulsed Ultrasound-Treated Dendritic Cells Suppress Tumor Necrosis Factor-Induced Endothelial Inflammation. *J Ultrasound Med* (2019) 38:2081–91. doi: 10.1002/jum.14898
35. Salarpour S, Forootanfar H, Pournamdari M, Ahmadi-Zeidabadi M, Esmaeeli M, Pardakhty A. Paclitaxel Incorporated Exosomes Derived From Glioblastoma Cells: Comparative Study of Two Loading Techniques. *Daru* (2019) 27:533–39. doi: 10.1007/s40199-019-00280-5
36. Kalimuthu S, Gangadaran P, Rajendran RL, Zhu L, Oh JM, Lee HW, et al. A New Approach for Loading Anticancer Drugs Into Mesenchymal Stem Cell-Derived Exosome Mimetics for Cancer Therapy. *Front Pharmacol* (2018) 9:1116. doi: 10.3389/fphar.2018.01116
37. Syn NL, Wang LZ, Chow EKH, Lim CT, Goh BC. Exosomes in Cancer Nanomedicine and Immunotherapy: Prospects and Challenges. *Trends Biotechnol* (2017) 35:665–76. doi: 10.1016/j.tibtech.2017.03.004
38. Ohno S, Takanashi M, Sudo K, Ueda S, Ishikawa A, Matsuyama N, et al. Systemically Injected Exosomes Targeted to EGFR Deliver Antitumor MicroRNA to Breast Cancer Cells. *Mol Ther* (2013) 21:185–91. doi: 10.1038/mt.2012.180
39. Liu J, Ye Z, Xiang M, Chang B, Cui J, Ji T, et al. Functional Extracellular Vesicles Engineered With Lipid-Grafted Hyaluronic Acid Effectively Reverse Cancer Drug Resistance. *Biomaterials* (2019) 223:119475. doi: 10.1016/j.biomaterials.2019.119475
40. Santos P, Almeida F. Exosome-Based Vaccines: History, Current State, and Clinical Trials. *Front Immunol* (2021) 12:711565. doi: 10.3389/fimmu.2021.711565
41. Tian Y, Cheng C, Wei Y, Yang F, Li G. The Role of Exosomes in Inflammatory Diseases and Tumor-Related Inflammation. *Cells* (2022) 11:1005. doi: 10.3390/cells11061005
42. Rivoltini L, Chiodoni C, Squarcina P, Tortoreto M, Villa A, Vergani B, et al. TNF-Related Apoptosis-Inducing Ligand (TRAIL)-Armed Exosomes Deliver Proapoptotic Signals to Tumor Site. *Clin Cancer Res* (2016) 22:3499–512. doi: 10.1158/1078-0432.Ccr-15-2170
43. Dai SM, Zhou XY, Wang BM, Wang QQ, Fu YX, Chen TY, et al. Enhanced Induction of Dendritic Cell Maturation and HLA-A*0201-Restricted CEA-Specific CD8(+) CTL Response by Exosomes Derived From IL-18 Gene-Modified CEA-Positive Tumor Cells. *J Mol Med* (2006) 84:1067–76. doi: 10.1007/s00109-006-0102-0
44. Yang YS, Xiu FM, Cai ZJ, Wang JL, Wang QQ, Fu YX, et al. Increased Induction of Antitumor Response by Exosomes Derived From Interleukin-2 Gene-Modified Tumor Cells. *J Cancer Res Clin* (2007) 133:389–99. doi: 10.1007/s00432-006-0184-7
45. Koh E, Lee EJ, Nam GH, Hong Y, Cho E, Yang Y, et al. Exosome-SIRP Alpha, a CD47 Blockade Increases Cancer Cell Phagocytosis. *Biomaterials* (2017) 121:121–29. doi: 10.1016/j.biomaterials.2017.01.004
46. Tang K, Zhang Y, Zhang HF, Xu PW, Liu J, Ma JW, et al. Delivery of Chemotherapeutic Drugs in Tumour Cell-Derived Microparticles. *Nat Commun* (2012) 3:1282. doi: 10.1038/ncomms2282
47. Kim MS, Haney MJ, Zhao Y, Mahajan V, Deygen I, Klyachko NL, et al. Development of Exosome-Encapsulated Paclitaxel to Overcome MDR in Cancer Cells. *Nanomed-Nanotechnol* (2016) 12:655–64. doi: 10.1016/j.nano.2015.10.012
48. Saari H, Lazaro-Ibanez E, Viitala T, Vuorimaa-Laukkanen E, Siljander P, Yliperttula M. Microvesicle- and Exosome-Mediated Drug Delivery Enhances the Cytotoxicity of Paclitaxel in Autologous Prostate Cancer Cells. *J Control Release* (2015) 220:727–37. doi: 10.1016/j.jconrel.2015.09.031
49. Tian YH, Li SP, Song J, Ji TJ, Zhu MT, Anderson GJ, et al. A Doxorubicin Delivery Platform Using Engineered Natural Membrane Vesicle Exosomes for Targeted Tumor Therapy. *Biomaterials* (2014) 35:2383–90. doi: 10.1016/j.biomaterials.2013.11.083
50. Treiber T, Treiber N, Meister G. Regulation of microRNA Biogenesis and its Crosstalk With Other Cellular Pathways. *Nat Rev Mol Cell Bio* (2019) 20:321–21:pg 5. doi: 10.1038/s41580-019-0106-6
51. Huang XY, Yuan TZ, Liang MH, Du MJ, Xia S, Dittmar R, et al. Exosomal miR-1290 and miR-375 as Prognostic Markers in Castration-Resistant Prostate Cancer. *Eur Urol* (2015) 67:33–41. doi: 10.1016/j.eururo.2014.07.035
52. Katakowski M, Buller B, Zheng XG, Lu Y, Rogers T, Osobamiro O, et al. Exosomes From Marrow Stromal Cells Expressing miR-146b Inhibit Glioma Growth. *Cancer Lett* (2013) 335:201–04. doi: 10.1016/j.canlet.2013.02.019
53. Zhang KL, Dong C, Chen M, Yang TT, Wang X, Gao YH, et al. Extracellular Vesicle-Mediated Delivery of miR-101 Inhibits Lung Metastasis in Osteosarcoma. *Theranostics* (2020) 10:411–25. doi: 10.7150/thno.33482
54. Schroeder A, Levins CG, Cortez C, Langer R, Anderson DG. Lipid-Based Nanotherapeutics for siRNA Delivery. *J Intern Med* (2010) 267:9–21. doi: 10.1111/j.1365-2796.2009.02189.x
55. Conti DS, Brewer D, Grashik J, Avasarala S, da Rocha SRP. Poly(amidoamine) Dendrimer Nanocarriers and Their Aerosol Formulations for siRNA Delivery to the Lung Epithelium. *Mol Pharmaceut* (2014) 11:1808–22. doi: 10.1021/mp4006358
56. Alvarez-Erviti L, Seow YQ, Yin HF, Betts C, Lakhal S, Wood MJA. Delivery of siRNA to the Mouse Brain by Systemic Injection of Targeted Exosomes. *Nat Biotechnol* (2011) 29:341–U179. doi: 10.1038/nbt.1807
57. Yu Y, Li W, Mao L, Peng W, Long D, Li D, et al. Genetically Engineered Exosomes Display RVG Peptide and Selectively Enrich a Neprilysin Variant: A Potential Formulation for the Treatment of Alzheimer's Disease. *J Drug Target* (2021) 29:1128–38. doi: 10.1080/1061186X.2021.1929257
58. Lin Y, Wu JH, Gu WH, Huang YL, Tong ZC, Huang LJ, et al. Exosome-Liposome Hybrid Nanoparticles Deliver Cas9/Cas9 System in MSCs. *Adv Sci* (2018) 5:1700611. doi: 10.1002/advs.201700611
59. Mu JY, Zhuang XY, Wang QL, Jiang H, Deng ZB, Wang BM, et al. Interspecies Communication Between Plant and Mouse Gut Host Cells Through Edible Plant Derived Exosome-Like Nanoparticles. *Mol Nutr Food Res* (2014) 58:1561–73. doi: 10.1002/mnfr.201300729
60. Raimondo S, Naselli F, Fontana S, Monteleone F, Lo Dico A, Saieva L, et al. Citrus Limon-Derived Nanovesicles Inhibit Cancer Cell Proliferation and Suppress CML Xenograft Growth by Inducing TRAIL-Mediated Cell Death. *Oncotarget* (2015) 6:19514–27. doi: 10.18632/oncotarget.4004
61. Narayanan E. Exosomes as Drug Delivery Vehicles for Cancer Treatment. *Curr Nanosci* (2020) 16:15–26. doi: 10.2174/1573413715666190219112422

62. Li MY, Li SS, Du CY, Zhang YN, Li Y, Chu LQ, et al. Exosomes From Different Cells: Characteristics, Modifications, and Therapeutic Applications. *Eur J Med Chem* (2020) 207:112784. doi: 10.1016/j.ejmech.2020.112784
63. Yang Z, Shi J, Xie J, Wang Y, Sun J, Liu T, et al. Large-Scale Generation of Functional mRNA-Encapsulating Exosomes *via* Cellular Nanoporation. *Nat BioMed Eng* (2020) 4:69–83. doi: 10.1038/s41551-019-0485-1
64. Faruqu FN, Xu LZ, Al-Jamal KT. Preparation of Exosomes for siRNA Delivery to Cancer Cells. *Jove-J Vis Exp* (2018) 142:e58814. doi: 10.3791/58814
65. Charoenviriyakul C, Takahashi Y, Nishikawa M, Takakura Y. Preservation of Exosomes at Room Temperature Using Lyophilization. *Int J Pharmaceut* (2018) 553:1–7. doi: 10.1016/j.ijpharm.2018.10.032
66. Nam GH, Choi Y, Kim GB, Kim S, Kim SA, Kim IS. Emerging Prospects of Exosomes for Cancer Treatment: From Conventional Therapy to Immunotherapy. *Adv Mater* (2020) 32:2002440. doi: 10.1002/adma.202002440
67. Wang JL, Sui LH, Huang J, Miao L, Nie YB, Wang KS, et al. MoS2-Based Nanocomposites for Cancer Diagnosis and Therapy. *Bioact Mater* (2021) 6:4209–42. doi: 10.1016/j.bioactmat.2021.04.021
68. Zhao TJ, Wu W, Sui LH, Huang Q, Nan YY, Liu JH, et al. Reactive Oxygen Species-Based Nanomaterials for the Treatment of Myocardial Ischemia Reperfusion Injuries. *Bioact Mater* (2022) 7:47–72. doi: 10.1016/j.bioactmat.2021.06.006
69. Zhu Y, Zhao TJ, Liu M, Wang SY, Liu SL, Yang YR, et al. Rheumatoid Arthritis Microenvironment Insights Into Treatment Effect of Nanomaterials. *Nano Today* (2022) 42:101358. doi: 10.1016/j.nantod.2021.101358
70. Chen L, Huang Q, Zhao TJ, Sui LH, Wang SY, Xiao ZX, et al. Nanotherapies for Sepsis by Regulating Inflammatory Signals and Reactive Oxygen and Nitrogen Species: New Insight for Treating COVID-19. *Redox Biol* (2021) 45:102046. doi: 10.1016/j.redox.2021.102046

Conflict of Interest: The authors declare that the research was conducted in the absence of any commercial or financial relationships that could be construed as a potential conflict of interest.

Publisher's Note: All claims expressed in this article are solely those of the authors and do not necessarily represent those of their affiliated organizations, or those of the publisher, the editors and the reviewers. Any product that may be evaluated in this article, or claim that may be made by its manufacturer, is not guaranteed or endorsed by the publisher.

Copyright © 2022 Fu, Li, Chen, Zhu and Zhou. This is an open-access article distributed under the terms of the Creative Commons Attribution License (CC BY). The use, distribution or reproduction in other forums is permitted, provided the original author(s) and the copyright owner(s) are credited and that the original publication in this journal is cited, in accordance with accepted academic practice. No use, distribution or reproduction is permitted which does not comply with these terms.

frontiers | Frontiers in Oncology

REVIEW
published: 22 June 2022
doi: 10.3389/fonc.2022.921983

Nanomaterial Technology and Soft Tissue Sarcomas

Changkai Zhou[1†], *Xue Chen*[2†], *Ying Huang*[3], *Qi Zhang*[2*], *Shu Zhu*[4*] *and Wei Fu*[5*]

[1] Department of Burn and Plastic Surgery, Affiliated Hospital 2 of Nantong University, Nantong First People's Hospital, Nantong, China, [2] Department of Plastic and Cosmetic Surgery, Tongji Hospital, Tongji Medical College, Huazhong University of Science and Technology, Wuhan, China, [3] Department of Operation Room, Affiliated Hospital 2 of Nantong University, Nantong First People's Hospital, Nantong, China, [4] Department of Medical Ultrasound, Tongji Hospital, Tongji Medical College, Huazhong University of Science and Technology, Wuhan, China, [5] Department of Pharmacy, Tongji Hospital, Tongji Medical College, Huazhong University of Science and Technology, Wuhan, China

OPEN ACCESS

Edited by:
Kelong Ai,
Central South University, China

Reviewed by:
Ziwei Liu,
Wuhan Institute of Technology, China
Qiong Huang,
Central South University, China
Xue Wang,
AbbVie, United States

***Correspondence:**
Wei Fu
luis9@126.com
Shu Zhu
zhushu0602@126.com
Qi Zhang
zhangqi06172@163.com

[†]These authors have contributed equally to this work

Specialty section:
This article was submitted to Pharmacology of Anti-Cancer Drugs, a section of the journal Frontiers in Oncology

Received: 17 April 2022
Accepted: 24 May 2022
Published: 22 June 2022

Citation:
Zhou C, Chen X, Huang Y, Zhang Q, Zhu S and Fu W (2022) Nanomaterial Technology and Soft Tissue Sarcomas. Front. Oncol. 12:921983. doi: 10.3389/fonc.2022.921983

Soft tissue sarcomas (STSs) are relatively rare heterogeneous solid tumors of the mesenchymal origin. They account for approximately 1% of all malignant tumors in adults and have more than 70 histological subtypes. Consequently, the rarity and heterogeneity of STSs make their diagnosis and treatment very challenging. Nanotechnology has attracted increasing attention from researchers due to the unique physicochemical and biological properties of nanomaterials with potential medical applications as nanoprobes, drug delivery systems, photosensitizers, radioenhancers, antitumor agents, and their combinations for cancer diagnosis and treatment. This review discusses the progress made in the use of nanotechnology for the diagnosis and treatment of STSs and highlights future prospects of the STS multimodality therapy.

Keywords: soft tissue sarcoma, nanotechnology, cancer diagnosis, drug delivery, photodynamic therapy, radiotherapy

INTRODUCTION

Soft tissue sarcomas (STSs) are rare and heterogeneous tumors representing only 1% of all adult malignancies and encompassing more than 70 histological subtypes with variable clinical behavior (1). It is estimated that in 2022, 13,190 new STS cases will be diagnosed in the USA, causing approximately 5,130 deaths (2). These malignant mesenchymal tumors are important and often overlooked causes of death in young patients. According to the American Cancer Society, the average overall five-year STS survival rate is approximately 65% (2). Prognostic prediction accuracy strongly depends on the tumor subtype, size, grade, stage, and response to treatment as well as demographic factors. However, the lack of known risk factors and appropriate preoperative preparation may delay STS diagnosis (3). Thus, referrals often originate from the results of the so-called "whoops" procedures (4). Currently, histologic grade is recognized to be the most important prognostic factor predictive of distant metastasis and disease-specific survival rate (5).

Abbreviation: STS(s), soft tissue sarcoma(s); MRI, magnetic resonance imaging; UPS, undifferentiated pleomorphic sarcoma; TKIs, tyrosine kinase inhibitors; GISTs, gastrointestinal stromal tumors; TAPs, tumor-associated proteins; DDSs, drug delivery systems; GLUTs, glucose transporters; LPR, lipid protamine-siRNA; ARMS, alveolar rhabdomyosarcoma; EPR, enhanced permeability and retention; PTX, paclitaxel; PDT, photodynamic therapy; ROS, reactive oxygen speciesp; PS, photosensitizer; IR, ionizing radiation.

The traditional treatment of patients diagnosed with STS includes surgical resection, radiotherapy, chemotherapy, photodynamic therapy, and their combinations, which are slowly evolving (6). Therefore, it is necessary to investigate effective methods of improving the efficiency of STS diagnosis and treatment.

Nanomaterial technology has attracted significant attention from researchers over the years and tremendous progress has been made in this field. The unique physical and functional properties of nanomaterials make them potentially suitable for the management of many diseases, including cancer (7). Therefore, nanomaterials are widely used for cancer diagnosis, monitoring, imaging, and treatment. For example, various nanovehicles for the efficient delivery of drugs, such as liposomes, micelles, dendrimers, quantum dots, and carbon nanotubes, have been developed (8, 9). Additionally, nanoparticles with certain sizes can convert light into heat, which causes cellular damage during photothermal therapy. Nanoparticles with high electron density and well-defined size and shape are highly efficient at absorbing radiation and, therefore, can be used as radioenhancers in radiotherapy (10). Moreover, a direct antitumor effect was observed for certain nanoparticles (11). Considerable progress has been made in the application of nanotechnology for STS diagnosis and treatment. This review describes the latest developments in the use of nanomaterials for STS diagnosis and treatment, highlighting the future prospects of STS multimodality therapy.

DIAGNOSIS AND SUBTYPES OF STSs

STSs tends to form as a large, painless, and unexplained mass with a consistently increasing volume, which is the best individual indicator of a high malignancy risk (12). Therefore, patients suspected of having STS (especially those having superficial lesions with sizes greater than 5 cm) should initially undergo an ultrasound examination, which is cost-effective and has a high negative predictive value for soft tissue lumps (13). Magnetic resonance imaging (MRI) has a very high negative predictive value in distinguishing lipomatous tumors (14) and is helpful during surgical and radiotherapy planning. Contrast-enhanced computed tomography is an alternative imaging modality for patients with contraindications to MRI, which plays an important role in the evaluation of lungs for metastatic sarcomas. Moreover, core needle biopsy provides a basis for definitive tissue diagnosis, which is critical for cases, in which neoadjuvant therapy is administered (15). Molecular genetic testing plays an increasingly important role in the classification of STSs (16, 17). Therefore, proper sarcoma diagnostics requires a multidisciplinary approach with the participation of an expert team of pathologists, radiologists, medical oncologists, molecular biologists, and surgical oncologists (18).

Most STSs are classified according to their tissue origin and differentiation characteristics. Some of them are named based on their histological patterns (e.g., soft pulmonary alveolar sarcoma and epithelioid sarcoma). Unfortunately, STSs have over 70 histological subtypes (1, 19). Among those, the three most common histologic subtypes of STSs in adults include undifferentiated pleomorphic sarcoma (UPS), liposarcoma, and leiomyosarcoma. Histological diagnosis should be based on the 2020 World Health Organization classification of soft tissues and bone tumors (1). The grading system proposed by the French Federation of Cancer Centers Sarcoma Group is most widely used due to its high reproducibility and precise definitions (20, 21). Unlike other cancers, STSs have a high prognostic value according to the American Joint Committee on Cancer TNM staging system owing to the inclusion of histological grading. In summary, the rarity and heterogeneity of STSs make its diagnostic a very complex and difficult process.

MANAGEMENT OF STSs

Owing to the rarity and heterogeneity of STSs, patients with STSs should be referred to specialized sarcoma centers for curing or palliative care depending on the STS grade (18, 22). First, radical surgical resection is the cornerstone of the treatment of primary STSs. Notably, an adequate preoperative workup, including advanced imaging studies and diagnostic biopsy, should be performed to eliminate the risk of incomplete STS excision (3). In other words, the key principles of surgery include oncological radicality and function sparing. For extremity and truncal STSs, at least 1–2 cm of the healthy tissue around the tumor must be removed. Moreover, for the highly invasive histological subtypes such as locally invasive myxofibrosarcoma, the resection margin should be at least 3 cm (23). However, amputation is a better choice when the tumor involves the major vessels and nerves in the limbs. Fortunately, due to the progress in neoadjuvant treatment, the rate of limb salvage is constantly increasing (24). Resections were classified into R0 (with microscopically negative margins), R1 (with microscopically positive margins), and R2 (with macroscopically positive margins) according to the results of postoperative pathological examination (25). However, R0 resections are sometimes difficult to perform due to anatomic constraints (i.e., retroperitoneal sarcomas, which represent approximately 15% of all STSs). Thus, (neo)adjuvant therapies should be considered to improve prognosis.

Most low-grade and well-edged STSs do not require adjuvant radiotherapy, whereas for the moderate-to-high grade STSs, adjuvant radiotherapy may improve the local control and prognosis (26). Additionally, radiotherapy plays a significant role in the palliative or definitive treatment of patients who cannot undergo R0 resection. Although the effect of radiotherapy on limb STSs is clear, the optimal radio-surgical strategy remains controversial (27–30). However, with the recent advances in radiation techniques, including the use of nanosized radioenhancers (such as hafnium oxide nanoparticles, NBTXR3), the cost/benefit ratio of radiotherapy has considerably decreased (31, 32). Chemotherapy is the first option for metastatic and locally advanced STSs, and the most commonly used drugs include anthracyclines, gemcitabine, and taxanes (33). Nevertheless, the

heterogeneity of various STS subtypes often results in different responses to chemotherapeutic agents. Many studies were performed to explore the role of adjuvant chemotherapy in STS treatment, but their results were contradictory, and the benefits of chemotherapy remained uncertain (34–37). Fortunately, advances in nanosized drug delivery systems may overcome the main drawbacks of traditional chemotherapy, including low efficacy and toxicity. Over the years, significant progress has been made in the field of targeted therapy for STSs (38, 39). Tyrosine kinase inhibitors (TKIs), such as imatinib, sunitinib, and regorafenib, were approved for the treatment of gastrointestinal stromal tumors (GISTs) (40–43). Pazopanib, another TKI, was approved for the treatment for non-GIST STSs (44). Olaratumab, a monoclonal antibody, was approved for the treatment of STSs (45). However, even the best formulation of neo-adjuvant therapies cannot replace R0 resection (46).

NANOTECHNOLOGY AND STSs

Owing to the rarity and multiplicity of clinical behavior, STS diagnosis is sometimes delayed, and the treatment of STSs becomes a complex process; as a result, the prognosis is usually dismal. Therefore, more efforts should be spent on exploring new options for the diagnosis and treatment of STSs. Nanotechnology has attracted scientific interest owing to its various advantages, including desirable bioavailability, specialized structures, and promising drug encapsulation efficiency. Moreover, significant progress has been made in the field of nanomaterials, which exhibit unique physical and chemical properties and are widely used in the health and medical fields (47). The application of nanomaterials offers potential advantages in the diagnosis and treatment of many diseases, including cancer (7, 48, 49). For example, nanomaterials can be used to detect tumor markers for the purpose of diagnosis and evaluating prognosis (50). Drug-loaded nanomaterials may cross many biological barriers and be transported to a target region (51). Additionally, nanomaterials play an important role in photodynamic therapy and radiotherapy.

Nanoprobe and STSs

Early detection is associated with timely treatment and, hence, better prognosis. This is particularly true for STSs, which are often overlooked by the general public and healthcare providers. Traditional diagnostic strategies have various limitations, such as the low sensitivity of imaging techniques and unnecessary contamination of healthy tissues due to a poorly performed biopsy. Researchers are currently exploring potential breakthrough points for tumor diagnostic technologies. Thus, the role of nanoparticles in cancer diagnosis and surveillance has attracted increasing attention over the past few decades due to their intrinsic magnetic, optical, and electrical properties (48). Additionally, nanoprobes coupled with specific ligands can accumulate at the tumor site or generate high responses to very small targets *via* ligand-receptor interactions to produce signals for ultrasensitive detection (50).

Tumor formation is caused by the uncontrolled cell division due to mutations in specific genes that alter the synthesis of specific biomolecules. The overexpression of tumor-associated proteins (TAPs) occurs during tumor formation, and TAPs can regulate proteolysis, making them an important factor in cancer progression. For example, MMP-2 is a TAP overexpressed in most solid tumors including STSs (52), which can be used for the detection of such tumors. Wang et al. (53) developed a nanoprobe containing an MMP-2 substrate sequence for detecting MMP-2-overexpressed tumors, which is highly activated in human fibrosarcoma HT1080 cells *in vitro* and highly expressed in human fibrosarcoma HT1080 cell xenografts compared with MCF-7 cells. Their study demonstrates the sensitivity and specificity of this prodrug-type nanoprobe for tumor detection and imaging. Nevertheless, the heterogeneity of specific biomarkers in each STS subtype makes the development of a foolproof strategy for STS detection a challenging task.

Drug Delivery Nanosystems and STSs

Despite the large number of drugs available for cancer treatment, conventional chemotherapeutic agents have various side effects, such as non-specific distribution, low bioavailability, toxic effects on healthy cells, and resistance development. Therefore, advanced drug delivery systems should be created overcome these drawbacks. Recent developments in nanotechnology-based drug delivery systems (DDSs) are expected to improve the drug delivery process and control drug release using passive or active targeting strategies, thereby reducing the side effects of chemotherapy during tumor treatment. In addition, they can deliver multiple drugs simultaneously to perform a combination therapy (54). Over the years, a large number of nanomedicines have been used to assess their potential for the treatment of STSs, including the balance between efficacy and toxicity (**Table 1**).

Active targeting relies on ligand–receptor binding to deliver drugs to cells and decrease nonspecific interactions in peripheral tissues (**Figure 1**). These high-affinity ligands may include aptamers, proteins, transferrin, antibodies, and other macromolecules that are specifically overexpressed on the surface of tumor cells. For example, the overexpression of glucose transporters (GLUTs) in pediatric sarcomas was used for active targeting. A nano-drug delivery system based on glycosylated polymer nanocapsules targeting dasatinib was reported for the first time by Bukchin et al. (55) In their study, the use of a glycosylated amphiphilic nanocarrier promoted the delivery of dasatinib in tumor parenchyma and reduced its accumulation in the off-target tissues and organs of immunodeficient mice bearing glucose-avid Rh30 xenograft. Additionally, small molecules, such as folic acid, carbohydrates, and nucleic acids, were identified. In another approach utilizing the active targeted delivery of nano-drugs, integrin receptor-targeted lipid protamine-siRNA (LPR) nanoparticles were developed and used to load siRNA targeting the PAX3-FOXO1 (P3F) breakpoint, which was a specific fusion transcript of alveolar rhabdomyosarcoma (ARMS) (56). The results of both *in vitro* and *in vivo* studies verified the specificity and efficacy of

TABLE 1 | Nanomaterials used in the preclinical research of STS treatment.

Nanomaterial	Effect	Target	Cargo	Tumor Cell line/ animal model	Observation	Reference
Glucosylated polymeric nanomicelles	Active targeting	GLUT-1	dasatinib	RMS cell line Rh30. Patient-derivedglucose-avid Rh30 xenograft	In vitro: a 9-fold decrease of the half maximal inhibitory concentration of dasatinib in a RMS cell line, Rh30. In vivo: selective accumulation of dasatnib in a patient-derived RMS model	(55)
LPR nanoparticles	Active targeting	PAX3-FOXO1 (P3F)	siRNA	Human RMS cell lines. Rh30 cells xenograft	Significant tumor growth delay and inhibition of tumor initiation	(56)
4-arm-PEG_{5K}-TPGS nanoparticles	Passive targeting	/	Paclitaxel	S180 sarcoma-bearing mice	Significantly improved tumor growth inhibitory effect	(57)
CP nanoparticles	Passive targeting	/	Doxorubicin	MPNST and UPS sarcoma mouse models	CP-Dox formulation was superior to free doxorubicin in MPNST models, but not in UPS models.	(58)
Cerium oxide nanoparticles	Anticancer effect	/	/	Murine fibrosarcoma cells (WEHI164)	Significant toxicity on WEHI164 cells comparing with L929 cells. ROS generation in the cancer cells but scavenges it in the normal L929 cells.	(59)
	Anticancer effect	/	/	Mice bearing WEHI164 cells (mouse fibrosarcoma cells)	Dominantly accumulation in tumor cells. Significantly decrease tumor growth and volume.	(11)
Gold nanoparticles	Antimigration effect	/	/	Human fibrosarcoma cancer cell line HT-1080	No toxic effects on HT-1080 cells proliferation; Inhibition of cell migration	(60)
	Passive targeting	/	N-aminobacteriopurpurinimide (photoenhancer)	Rats bearing sarcoma M 1	Extended circulation time in the blood and enhanced tumor uptake	(61)
AuNRs/$mSiO_2$	Multy modal phototherapy	/	ICG-Der-02	HT-1080 human fibrosarcoma cells	More damaging to HT-1080 cells and enhanced the effectiveness of photodestruction	(62)

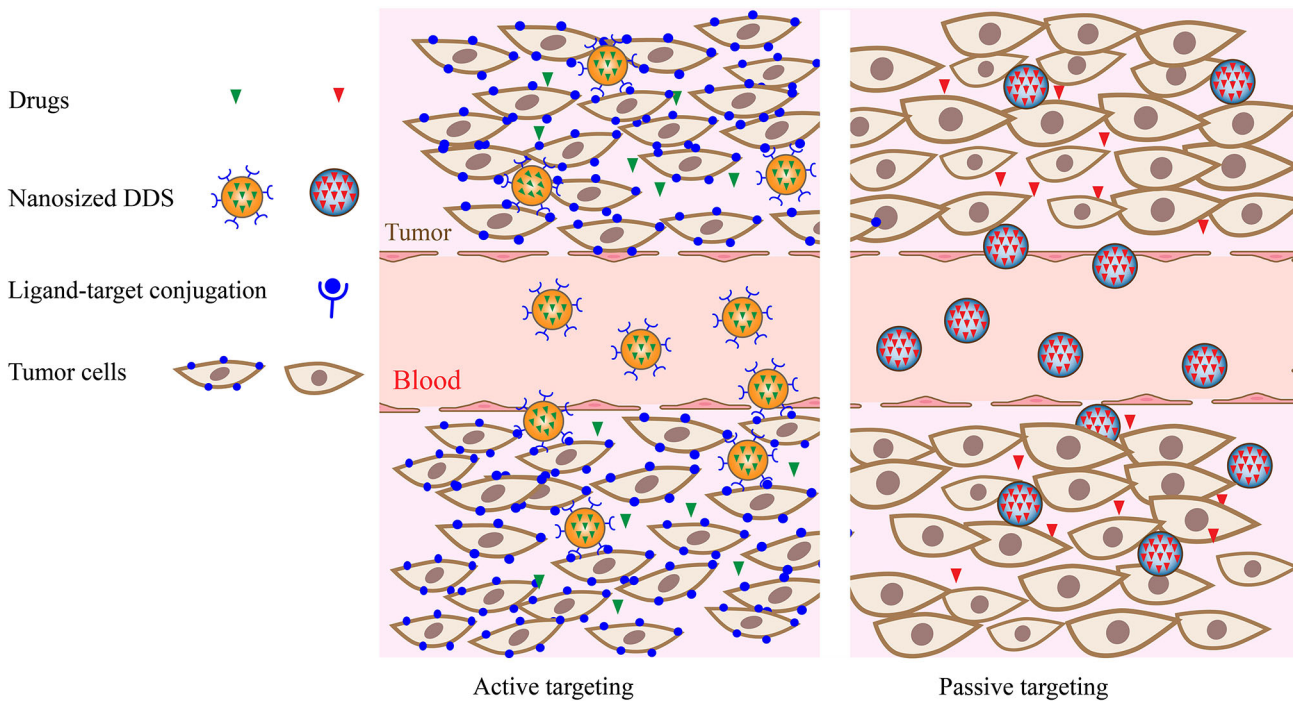


FIGURE 1 | Active and passive targeting strategy of drug delivery nanosystems.

this novel therapeutic strategy. However, the lack of universal STS-specific targets may produce barriers for nanomedicine development due to the heterogeneity of STSs.

Passive targeting involves the diffusion-mediated transport of drugs(**Figure 1**). The enhanced permeability and retention (EPR) effect promotes the passive accumulation of nanodrugs in tumor cells. Thus, the efficiency of the passive targeting strategy is dramatically affected by the inherent properties of drug–carrier complexes, such as molecular size, weight, and surface hydrophilicity. For instance, paclitaxel (PTX) exhibits low aqueous solubility, which limits its delivery to tumors. To overcome this problem, Wu's research group synthesized a novel nanocarrier, 4-arm-PEG_{5K}-TPGS NP, to load PTX for further studies. The S180 sarcoma-bearing mice treated with Taxol® and PTX-loaded 4-arm-PEG_{5K}-TPGS NP *in vivo* exhibited a significantly improved growth inhibitory effect as compared with that observed for the PTX-free group (57). Additionally, the EPR effect differs between different tumor types due to the protean pore dimensions in the vasculature (63). Thus, the heterogeneity of STSs and their stroma can severely impact the efficacy of passively targeted delivery. For example, doxorubicin-based chemotherapy remains the gold standard treatment for recurrent and metastatic STSs (64). Dodd et al. (58) compared the efficacy of nano-encapsulated doxorubicin and free doxorubicin in the treatment of MPNST and UPS mouse sarcoma models and observed different responses of various STS subtypes to the nanoparticle-encapsulated doxorubicin formulation (CP-Dox) treatment.

Furthermore, nanomaterials may be used not only as drug carriers but also as antitumor agents. Recently, the anticancer effect of cerium oxide nanoparticles was observed for mouse sarcoma tumor cells (59). Afterwards, *in vivo* experiments were performed by the same research team to confirm that cerium oxide nanoparticles were mainly concentrated in the mouse fibrosarcoma tissues and exhibited no apparent toxicity to the mouse liver and kidney, suggesting their potential applications in the treatment of fibrosarcoma (11). The proposed mechanism of the antitumor effect of these nanoparticles included antioxidant activity (65, 66) and passive targeting on the tumor side (67). Karuppaiya et al. reported for the first time a detailed procedure for the production of gold nanoparticles using an aqueous extract of *Dysosma pleiantha rhizome (*60). Interestingly, the biosynthesized nanoparticles were able to inhibit the migration of the human fibrosarcoma cell line HT-1080 by interfering with the actin polymerization pathway; however, no toxic effects were observed *in vitro*. Thus, their biocompatibility and anti-migration effect may be utilized to enhance the antitumor effect of the chemotherapeutics currently used in multimodality formulations, especially in metastatic STSs. In summary, the optimal design of nanoparticles for STSs treatment is a daunting task due to the high heterogeneity and constantly evolving nature of STSs.

Use of Nanomaterials in STS Photodynamic Therapy

Photodynamic therapy (PDT) is a tumor-ablative and disease site-specific treatment modality. It involves the generation of cytotoxic reactive oxygen species (ROS) by illuminating a photosensitizer (PS) within tumor cells with the light having a specific wavelength (68). ROS play significant roles in the physiological activities of cells at moderate concentrations. However, the overproduction of ROS may contribute to the development of many diseases, including rheumatoid arthritis (69), cardiovascular disease (70), and even COVID-19 (71). In PDT, ROS cause irreversible damage to the cells and microvasculature of solid tumors followed by a plethora of inflammatory and immune responses. Thus, the ideal PS should be capable of preferentially accumulating in tumor cells and generating a sufficient amount of ROS. Nanomaterials have recently emerged in the field of PDT to overcome most limitations of classic PSs. They may be potentially utilized in PDT as delivery vehicles for PS, PS alone, or PS energy transducers. For example, gold nanoparticles have been used to load a novel PS, N-aminobacteriopurpurinimide, for improving drug delivery through a passive targeting strategy (61). Rats bearing sarcoma M-1 demonstrated an extended circulation time in the blood and enhanced tumor uptake *in vivo*.

Moreover, a combination of different therapeutic methods with PDT may increase the antitumor efficacy (62, 72, 73). For this purpose, Luo et al. (62) introduced hydrophilic indocyanine green derivative (ICG-Der-02) into mesoporous silica-coated gold nanorods (AuNRs/$mSiO_2$). They found that the nanoconjugated AuNRs/$mSiO_2$–ICG-Der-02/RGD-4C system preferentially bound to HT-180 human fibrosarcoma cells and exhibited bimodal photothermal and photochemical effects under the 808-nm irradiation, thus improving the effectiveness of photodynamic therapy. In addition, a nanozyme that can increase the content of H_2O_2 in the tumor microenviroment may further enhance the antitumor effect of phototherapy (72). These novel multimodal treatment approaches may enhance tumor control in localized STSs.

Use of Nanomaterials in STS Radiotherapy

Radiotherapy is one of the most promising tumor control strategies. During radiotherapy, cellular components, especially DNA, are directly or indirectly damaged by delivering ionizing radiation (IR) to tumor tissues. Increasing the radiotherapy efficacy while maintaining the normal tissue toxicity at a tolerable level remains a challenging task. Metal nanoparticles have attracted significant interest in recent years due to their promising role in enhancing the radiosensitizer effect (74). In particular, gold nanoparticles have been most extensively investigated owing to their biocompatibility and multifunctional properties (75–78). For instance, these nanoparticles were used as radiosensitizers and CT contrast agents to develop Au-loaded polymeric micelles (GPMs) in a study conducted by the Tsourkas research group (79). They found that GPMs exhibited a longer circulation half-life and six-fold accumulation in tumors. An *in vivo* study confirmed that the median survival time of the GPM-radiosensitized mice bearing human fibrosarcoma cells (HT1080) in combination with RT was 1.7 times longer than that of the mice treated with radiation alone (79).

Moreover, hafnium oxide nanoparticles NBTXR3 possess the ability to interact with different types of IR and accumulate in cancer cells, thus producing high-dose energy deposition (80). A

preclinical study confirmed the promising uptake rate and encouraging radioenhancing effect of NBTXR3 in fibrosarcoma cell lines (Hs913T, HT-1080) (81). The initial phase I clinical trial of NBTXR3 activated by radiotherapy in patients with locally advanced STSs was performed by Bonvalot et al. (82) In their study, 22 patients with limb or trunk STSs were enrolled into the treatment program, and all of them received a single injection of NBTXR3 followed by external beam radiotherapy and surgical resection. The obtained results revealed that the median decrease in the maximal tumor diameter at the recommended dose was 29% with a median change in volume of −40%. This initial success led to a phase II–III trial (83) aimed to further evaluate the efficiency and safety of NBTXR3 as a radioenhancer in the preoperative treatment of patients with locally advanced STSs. A total of 176 eligible patients out of 180 enrolled ones were evaluated for the primary endpoint (pathological complete response in the intention-to-treat full analysis set). The proportion of patients with a pathological complete response exhibited a significant difference of 16% for the NBTXR3 group versus 8% for the radiotherapy alone group ($p = 0.044$). As a result, NBTXR3 has been approved for the treatment of STSs and became a first-in-class radioenhancer. The described tumor reduction strategy may facilitate surgical resection and provide a reference for the radiation-enhanced therapy of other solid tumors (84).

CONCLUSION

STSs can occur anywhere in the body and originate from mesenchymal tissues. Overall, the patients diagnosed with STSs have poor prognosis, while STS heterogeneity represents a considerable challenge for both detection and treatment. Nanomaterials are playing increasingly important roles in STS detection and treatment. Continuing advances in research studies utilizing nanomaterials as drug delivery systems, therapeutic approaches, and their combinations can help develop an efficient and safe method for the diagnosis and treatment of STSs. However, further optimization of nanomaterials is necessary to achieve rapid diagnosis and effective treatment of STSs.

AUTHOR CONTRIBUTIONS

All authors contributed to the design of the study and writing of the manuscript. CZ, XC and YH undertook the research. QZ, SZ and WF wrote the main manuscript text and prepared figures. WF and SZ revised the article critically for important intellectual content and final approval of the version to be submitted. All authors reviewed the manuscript. All authors contributed to the article and approved the submitted version.

REFERENCES

1. WHO Classification of Tumours Editorial Board. WHO Classification of Tumours of Soft Tissue and Bone. In: *WHO Classification of Tumours of Soft Tissue and Bone, 5th ed*. Lyon, France: International Agency for Research on Cancer. (2020).
2. American Cancer Society. . Available at: https://www.cancer.org/cancer/soft-tissue-sarcoma/about/key-statistics.html (Accessed March 23, 2022).
3. Mesko NW, Wilson RJ, Lawrenz JM, Mathieu JL, Ghiam MK, Mathis SL, et al. Pre-Operative Evaluation Prior to Soft Tissue Sarcoma Excision - Why Can't We Get it Right? *Eur J Surg Oncol J Eur Soc Surg Oncol Br Assoc Surg Oncol* (2018) 44:243–50. doi: 10.1016/j.ejso.2017.11.001
4. Koulaxouzidis G, Schwarzkopf E, Bannasch H, Stark GB. Is Revisional Surgery Mandatory When an Unexpected Sarcoma Diagnosis is Made Following Primary Surgery? *World J Surg Oncol* (2015) 13:306. doi: 10.1186/s12957-015-0719-y
5. Brennan MF, Antonescu CR, Moraco N, Singer S. Lessons Learned From the Study of 10,000 Patients With Soft Tissue Sarcoma. *Ann Surg* (2014) 260:416–21. doi: 10.1097/SLA.0000000000000869
6. Dei Tos AP, Bonvalot S, Haas R. Evolution in the Management of Soft Tissue Sarcoma: Classification, Surgery and Use of Radiotherapy. *Expert Rev Anticancer Ther* (2020) 20:3–13. doi: 10.1080/14737140.2020.1753509
7. Lalotra AS, Singh V, Khurana B, Agrawal S, Shrestha S, Arora D. A Comprehensive Review on Nanotechnology-Based Innovations in Topical Drug Delivery for the Treatment of Skin Cancer. *Curr Pharm Des* (2020) 26:5720–31. doi: 10.2174/1381612826666200819202821
8. Yue X, Dai Z. Liposomal Nanotechnology for Cancer Theranostics. *Curr Med Chem* (2018) 25:1397–408. doi: 10.2174/0929867324666170306105350
9. Bianco A, Kostarelos K, Prato M. Applications of Carbon Nanotubes in Drug Delivery. *Curr Opin Chem Biol* (2005) 9:674–9. doi: 10.1016/j.cbpa.2005.10.005
10. Rancoule C, Magné N, Vallard A, Guy J-B, Rodriguez-Lafrasse C, Deutsch E, et al. Nanoparticles in Radiation Oncology: From Bench-Side to Bedside. *Cancer Lett* (2016) 375:256–62. doi: 10.1016/j.canlet.2016.03.011
11. Nourmohammadi E, Khoshdel-Sarkarizi H, Nedaeinia R, Darroudi M, Kazemi Oskuee R. Cerium Oxide Nanoparticles: A Promising Tool for the Treatment of Fibrosarcoma in-Vivo. *Mater Sci Eng C Mater Biol Appl* (2020) 109:110533. doi: 10.1016/j.msec.2019.110533
12. Dangoor A, Seddon B, Gerrand C, Grimer R, Whelan J, Judson I. UK Guidelines for the Management of Soft Tissue Sarcomas. *Clin Sarcoma Res* (2016) 6:20. doi: 10.1186/s13569-016-0060-4
13. Church DJ, Krumme J, Kotwal S. Evaluating Soft-Tissue Lumps and Bumps. *Mo Med* (2017) 114:289–94.
14. Coran A, Ortolan P, Attar S, Alberioli E, Perissinotto E, Tosi AL, et al. Magnetic Resonance Imaging Assessment of Lipomatous Soft-Tissue Tumors. *Vivo Athens Greece* (2017) 31:387–95. doi: 10.21873/invivo.11071
15. Katz D, Palmerini E, Pollack SM. More Than 50 Subtypes of Soft Tissue Sarcoma: Paving the Path for Histology-Driven Treatments. *Am Soc Clin Oncol Educ Book Am Soc Clin Oncol Annu Meet* (2018) 38:925–38. doi: 10.1200/EDBK_205423
16. Italiano A, Di Mauro I, Rapp J, Pierron G, Auger N, Alberti L, et al. Clinical Effect of Molecular Methods in Sarcoma Diagnosis (GENSARC): A Prospective, Multicentre, Observational Study. *Lancet Oncol* (2016) 17:532–8. doi: 10.1016/S1470-2045(15)00583-5
17. Yao X, Ghert M, Dickson BC, Popovic S, Purgina BM, Verma S, et al. An Evidence-Based Guideline on the Application of Molecular Testing in the Diagnosis, Prediction of Prognosis, and Selection of Therapy in non-GIST Soft Tissue Sarcomas. *Cancer Treat Rev* (2020) 85:101987. doi: 10.1016/j.ctrv.2020.101987
18. Gamboa AC, Gronchi A, Cardona K. Soft-Tissue Sarcoma in Adults: An Update on the Current State of Histiotype-Specific Management in an Era of Personalized Medicine. *CA Cancer J Clin* (2020) 70:200–29. doi: 10.3322/caac.21605
19. Hui JYC. Epidemiology and Etiology of Sarcomas. *Surg Clin North Am* (2016) 96:901–14. doi: 10.1016/j.suc.2016.05.005
20. Guillou L, Coindre JM, Bonichon F, Nguyen BB, Terrier P, Collin F, et al. Comparative Study of the National Cancer Institute and French Federation of Cancer Centers Sarcoma Group Grading Systems in a Population of 410 Adult

Patients With Soft Tissue Sarcoma. *J Clin Oncol Off J Am Soc Clin Oncol* (1997) 15:350–62. doi: 10.1200/JCO.1997.15.1.350
21. Deyrup AT, Weiss SW. Grading of Soft Tissue Sarcomas: The Challenge of Providing Precise Information in an Imprecise World. *Histopathology* (2006) 48:42–50. doi: 10.1111/j.1365-2559.2005.02288.x
22. Blay J-Y, Honoré C, Stoeckle E, Meeus P, Jafari M, Gouin F, et al. Surgery in Reference Centers Improves Survival of Sarcoma Patients: A Nationwide Study. *Ann Oncol Off J Eur Soc Med Oncol* (2019) 30:1143–53. doi: 10.1093/annonc/mdz124
23. Endo M, Lin PP. Surgical Margins in the Management of Extremity Soft Tissue Sarcoma. *Chin Clin Oncol* (2018) 7:37. doi: 10.21037/cco.2018.08.10
24. Eward WC, Lazarides AL, Griffin AM, O'Donnell PW, Sternheim A, O'Neill A, et al. Superficial Soft-Tissue Sarcomas Rarely Require Advanced Soft-Tissue Reconstruction Following Resection. *Plast Reconstr Surg Glob Open* (2017) 5:e1553. doi: 10.1097/GOX.0000000000001553
25. Amin M, Edge S, Greene F, Byrd D, Brookland R, Washington M. AJCC Cancer Staging Manual. In: *Springer International Publishing, 8 Ed*. Chicago: American Joint Commission on Cancer (2017).
26. Dagan R, Indelicato DJ, McGee L, Morris CG, Kirwan JM, Knapik J, et al. The Significance of a Marginal Excision After Preoperative Radiation Therapy for Soft Tissue Sarcoma of the Extremity. *Cancer* (2012) 118:3199–207. doi: 10.1002/cncr.26489
27. O'Sullivan B, Davis AM, Turcotte R, Bell R, Catton C, Chabot P, et al. Preoperative Versus Postoperative Radiotherapy in Soft-Tissue Sarcoma of the Limbs: A Randomised Trial. *Lancet Lond Engl* (2002) 359:2235–41. doi: 10.1016/S0140-6736(02)09292-9
28. Alektiar KM, Velasco J, Zelefsky MJ, Woodruff JM, Lewis JJ, Brennan MF. Adjuvant Radiotherapy for Margin-Positive High-Grade Soft Tissue Sarcoma of the Extremity. *Int J Radiat Oncol Biol Phys* (2000) 48:1051–8. doi: 10.1016/s0360-3016(00)00753-7
29. Jebsen NL, Trovik CS, Bauer HCF, Rydholm A, Monge OR, Hall KS, et al. Radiotherapy to Improve Local Control Regardless of Surgical Margin and Malignancy Grade in Extremity and Trunk Wall Soft Tissue Sarcoma: A Scandinavian Sarcoma Group Study. *Int J Radiat Oncol Biol Phys* (2008) 71:1196–203. doi: 10.1016/j.ijrobp.2007.11.023
30. Gingrich AA, Bateni SB, Monjazeb AM, Darrow MA, Thorpe SW, Kirane AR, et al. Neoadjuvant Radiotherapy is Associated With R0 Resection and Improved Survival for Patients With Extremity Soft Tissue Sarcoma Undergoing Surgery: A National Cancer Database Analysis. *Ann Surg Oncol* (2017) 24:3252–63. doi: 10.1245/s10434-017-6019-8
31. O'Sullivan B, Griffin AM, Dickie CI, Sharpe MB, Chung PWM, Catton CN, et al. Phase 2 Study of Preoperative Image-Guided Intensity-Modulated Radiation Therapy to Reduce Wound and Combined Modality Morbidities in Lower Extremity Soft Tissue Sarcoma. *Cancer* (2013) 119:1878–84. doi: 10.1002/cncr.27951
32. Call JA, Stafford SL, Petersen IA, Haddock MG. Use of Intraoperative Radiotherapy for Upper-Extremity Soft-Tissue Sarcomas: Analysis of Disease Outcomes and Toxicity. *Am J Clin Oncol* (2014) 37:81–5. doi: 10.1097/COC.0b013e31826b9b3d
33. Judson I, Verweij J, Gelderblom H, Hartmann JT, Schöffski P, Blay J-Y, et al. Doxorubicin Alone Versus Intensified Doxorubicin Plus Ifosfamide for First-Line Treatment of Advanced or Metastatic Soft-Tissue Sarcoma: A Randomised Controlled Phase 3 Trial. *Lancet Oncol* (2014) 15:415–23. doi: 10.1016/S1470-2045(14)70063-4
34. Pervaiz N, Colterjohn N, Farrokhyar F, Tozer R, Figueredo A, Ghert M. A Systematic Meta-Analysis of Randomized Controlled Trials of Adjuvant Chemotherapy for Localized Resectable Soft-Tissue Sarcoma. *Cancer* (2008) 113:573–81. doi: 10.1002/cncr.23592
35. Le Cesne A, Ouali M, Leahy MG, Santoro A, Hoekstra HJ, Hohenberger P, et al. Doxorubicin-Based Adjuvant Chemotherapy in Soft Tissue Sarcoma: Pooled Analysis of Two STBSG-EORTC Phase III Clinical Trials. *Ann Oncol Off J Eur Soc Med Oncol* (2014) 25:2425–32. doi: 10.1093/annonc/mdu460
36. Pasquali S, Pizzamiglio S, Touati N, Litiere S, Marreaud S, Kasper B, et al. The Impact of Chemotherapy on Survival of Patients With Extremity and Trunk Wall Soft Tissue Sarcoma: Revisiting the Results of the EORTC-STBSG 62931 Randomised Trial. *Eur J Cancer Oxf Engl 1990* (2019) 109:51–60. doi: 10.1016/j.ejca.2018.12.009
37. Gronchi A, Palmerini E, Quagliuolo V, Martin Broto J, Lopez Pousa A, Grignani G, et al. Neoadjuvant Chemotherapy in High-Risk Soft Tissue Sarcomas: Final Results of a Randomized Trial From Italian (ISG), Spanish (GEIS), French (FSG), and Polish (PSG) Sarcoma Groups. *J Clin Oncol Off J Am Soc Clin Oncol* (2020) 38:2178–86. doi: 10.1200/JCO.19.03289
38. Nakano K, Takahashi S. Current Molecular Targeted Therapies for Bone and Soft Tissue Sarcomas. *Int J Mol Sci* (2018) 19:E739. doi: 10.3390/ijms19030739
39. Nakano K, Takahashi S. Precision Medicine in Soft Tissue Sarcoma Treatment. *Cancers* (2020) 12:E221. doi: 10.3390/cancers12010221
40. van Oosterom AT, Judson I, Verweij J, Stroobants S, Donato di Paola E, Dimitrijevic S, et al. Safety and Efficacy of Imatinib (STI571) in Metastatic Gastrointestinal Stromal Tumours: A Phase I Study. *Lancet Lond Engl* (2001) 358:1421–3. doi: 10.1016/s0140-6736(01)06535-7
41. Blanke CD, Rankin C, Demetri GD, Ryan CW, von Mehren M, Benjamin RS, et al. Phase III Randomized, Intergroup Trial Assessing Imatinib Mesylate at Two Dose Levels in Patients With Unresectable or Metastatic Gastrointestinal Stromal Tumors Expressing the Kit Receptor Tyrosine Kinase: S0033. *J Clin Oncol Off J Am Soc Clin Oncol* (2008) 26:626–32. doi: 10.1200/JCO.2007.13.4452
42. Demetri GD, van Oosterom AT, Garrett CR, Blackstein ME, Shah MH, Verweij J, et al. Efficacy and Safety of Sunitinib in Patients With Advanced Gastrointestinal Stromal Tumour After Failure of Imatinib: A Randomised Controlled Trial. *Lancet Lond Engl* (2006) 368:1329–38. doi: 10.1016/S0140-6736(06)69446-4
43. Demetri GD, Reichardt P, Kang Y-K, Blay J-Y, Rutkowski P, Gelderblom H, et al. Efficacy and Safety of Regorafenib for Advanced Gastrointestinal Stromal Tumours After Failure of Imatinib and Sunitinib (GRID): An International, Multicentre, Randomised, Placebo-Controlled, Phase 3 Trial. *Lancet Lond Engl* (2013) 381:295–302. doi: 10.1016/S0140-6736(12)61857-1
44. van der Graaf WTA, Blay J-Y, Chawla SP, Kim D-W, Bui-Nguyen B, Casali PG, et al. Pazopanib for Metastatic Soft-Tissue Sarcoma (PALETTE): A Randomised, Double-Blind, Placebo-Controlled Phase 3 Trial. *Lancet Lond Engl* (2012) 379:1879–86. doi: 10.1016/S0140-6736(12)60651-5
45. Wagner AJ, Kindler H, Gelderblom H, Schöffski P, Bauer S, Hohenberger P, et al. A Phase II Study of a Human Anti-Pdgfrα Monoclonal Antibody (Olaratumab, IMC-3G3) in Previously Treated Patients With Metastatic Gastrointestinal Stromal Tumors. *Ann Oncol Off J Eur Soc Med Oncol* (2017) 28:541–6. doi: 10.1093/annonc/mdw659
46. O'Donnell PW, Griffin AM, Eward WC, Sternheim A, Catton CN, Chung PW, et al. The Effect of the Setting of a Positive Surgical Margin in Soft Tissue Sarcoma. *Cancer* (2014) 120:2866–75. doi: 10.1002/cncr.28793
47. Nasir A, Khan A, Li J, Naeem M, Khalil AAK, Khan K, et al. Nanotechnology, A Tool for Diagnostics and Treatment of Cancer. *Curr Top Med Chem* (2021) 21:1360–76. doi: 10.2174/1568026621666210701144124
48. Chaturvedi VK, Singh A, Singh VK, Singh MP. Cancer Nanotechnology: A New Revolution for Cancer Diagnosis and Therapy. *Curr Drug Metab* (2019) 20:416–29. doi: 10.2174/1389200219666180918111528
49. Wang J, Sui L, Huang J, Miao L, Nie Y, Wang K, et al. MoS2-Based Nanocomposites for Cancer Diagnosis and Therapy. *Bioact Mater* (2021) 6:4209–42. doi: 10.1016/j.bioactmat.2021.04.021
50. Chi X, Huang D, Zhao Z, Zhou Z, Yin Z, Gao J. Nanoprobes for In Vitro Diagnostics of Cancer and Infectious Diseases. *Biomaterials* (2012) 33:189–206. doi: 10.1016/j.biomaterials.2011.09.032
51. Etheridge ML, Campbell SA, Erdman AG, Haynes CL, Wolf SM, McCullough J. The Big Picture on Nanomedicine: The State of Investigational and Approved Nanomedicine Products. *Nanomedicine Nanotechnol Biol Med* (2013) 9:1–14. doi: 10.1016/j.nano.2012.05.013
52. Temma T, Hanaoka H, Yonezawa A, Kondo N, Sano K, Sakamoto T, et al. Investigation of a MMP-2 Activity-Dependent Anchoring Probe for Nuclear Imaging of Cancer. *PloS One* (2014) 9:e102180. doi: 10.1371/journal.pone.0102180
53. Wang Y, Lin T, Zhang W, Jiang Y, Jin H, He H, et al. Prodrug-Type, MMP-2-Targeting Nanoprobe for Tumor Detection and Imaging. *Theranostics* (2015) 5:787–95. doi: 10.7150/thno.11139
54. Jain RK, Stylianopoulos T. Delivering Nanomedicine to Solid Tumors. *Nat Rev Clin Oncol* (2010) 7:653–64. doi: 10.1038/nrclinonc.2010.139
55. Bukchin A, Pascual-Pasto G, Cuadrado-Vilanova M, Castillo-Ecija H, Monterrubio C, Olaciregui NG, et al. Glucosylated Nanomicelles Target

Glucose-Avid Pediatric Patient-Derived Sarcomas. *J Control Release Off J Control Release Soc* (2018) 276:59–71. doi: 10.1016/j.jconrel.2018.02.034
56. Rengaswamy V, Zimmer D, Süss R, Rössler J. RGD liposome-protamine-siRNA (LPR) Nanoparticles Targeting PAX3-FOXO1 for Alveolar Rhabdomyosarcoma Therapy. *J Control Release Off J Control Release Soc* (2016) 235:319–27. doi: 10.1016/j.jconrel.2016.05.063
57. Wu Y, Chu Q, Tan S, Zhuang X, Bao Y, Wu T, et al. D-α-Tocopherol Polyethylene Glycol Succinate-Based Derivative Nanoparticles as a Novel Carrier for Paclitaxel Delivery. *Int J Nanomed* (2015) 10:5219–35. doi: 10.2147/IJN.S82847
58. Dodd RD, Scherer A, Huang W, McGivney GR, Gutierrez WR, Laverty EA, et al. Tumor Subtype Determines Therapeutic Response to Chimeric Polypeptide Nanoparticle-Based Chemotherapy in Pten-Deleted Mouse Models of Sarcoma. *Clin Cancer Res Off J Am Assoc Cancer Res* (2020) 26:5036–47. doi: 10.1158/1078-0432.CCR-19-2597
59. Nourmohammadi E, Khoshdel-sarkarizi H, Nedaeinia R, Sadeghnia HR, Hasanzadeh L, Darroudi M, et al. Evaluation of Anticancer Effects of Cerium Oxide Nanoparticles on Mouse Fibrosarcoma Cell Line. *J Cell Physiol* (2019) 234:4987–96. doi: 10.1002/jcp.27303
60. Karuppaiya P, Satheeshkumar E, Chao W-T, Kao L-Y, Chen EC-F, Tsay H-S. Anti-Metastatic Activity of Biologically Synthesized Gold Nanoparticles on Human Fibrosarcoma Cell Line HT-1080. *Colloids Surf B Biointerf* (2013) 110:163–70. doi: 10.1016/j.colsurfb.2013.04.037
61. Pantiushenko IV, Rudakovskaya PG, Starovoytova AV, Mikhaylovskaya AA, Abakumov MA, Kaplan MA, et al. Development of Bacteriochlorophyll a-Based Near-Infrared Photosensitizers Conjugated to Gold Nanoparticles for Photodynamic Therapy of Cancer. *Biochem Biokhimiia* (2015) 80:752–62. doi: 10.1134/S0006297915060103
62. Luo T, Qian X, Lu Z, Shi Y, Yao Z, Chai X, et al. Indocyanine Green Derivative Covalently Conjugated With Gold Nanorods for Multimodal Phototherapy of Fibrosarcoma Cells. *J BioMed Nanotechnol* (2015) 11:600–12. doi: 10.1166/jbn.2015.1926
63. Maeda H, Sawa T, Konno T. Mechanism of Tumor-Targeted Delivery of Macromolecular Drugs, Including the EPR Effect in Solid Tumor and Clinical Overview of the Prototype Polymeric Drug SMANCS. *J Control Release Off J Control Release Soc* (2001) 74:47–61. doi: 10.1016/s0168-3659(01)00309-1
64. Linch M, Miah AB, Thway K, Judson IR, Benson C. Systemic Treatment of Soft-Tissue Sarcoma-Gold Standard and Novel Therapies. *Nat Rev Clin Oncol* (2014) 11:187–202. doi: 10.1038/nrclinonc.2014.26
65. Korsvik C, Patil S, Seal S, Self WT. Superoxide Dismutase Mimetic Properties Exhibited by Vacancy Engineered Ceria Nanoparticles. *Chem Commun Camb Engl* (2007), 1056–8. doi: 10.1039/b615134e
66. Heckert EG, Karakoti AS, Seal S, Self WT. The Role of Cerium Redox State in the SOD Mimetic Activity of Nanoceria. *Biomaterials* (2008) 29:2705–9. doi: 10.1016/j.biomaterials.2008.03.014
67. Huo S, Ma H, Huang K, Liu J, Wei T, Jin S, et al. Superior Penetration and Retention Behavior of 50 Nm Gold Nanoparticles in Tumors. *Cancer Res* (2013) 73:319–30. doi: 10.1158/0008-5472.CAN-12-2071
68. Sharman WM, Allen CM, van Lier JE. Role of Activated Oxygen Species in Photodynamic Therapy. *Methods Enzymol* (2000) 319:376–400. doi: 10.1016/s0076-6879(00)19037-8
69. Zhu Y, Zhao T, Liu M, Wang S, Liu S, Yang Y, et al. Rheumatoid Arthritis Microenvironment Insights Into Treatment Effect of Nanomaterials. *Nano Today* (2022) 42:101358. doi: 10.1016/j.nantod.2021.101358
70. Zhao T, Wu W, Sui L, Huang Q, Nan Y, Liu J, et al. Reactive Oxygen Species-Based Nanomaterials for the Treatment of Myocardial Ischemia Reperfusion Injuries. *Bioact Mater* (2022) 7:47–72. doi: 10.1016/j.bioactmat.2021.06.006
71. Chen L, Huang Q, Zhao T, Sui L, Wang S, Xiao Z, et al. Nanotherapies for Sepsis by Regulating Inflammatory Signals and Reactive Oxygen and Nitrogen Species: New Insight for Treating COVID-19. *Redox Biol* (2021) 45:102046. doi: 10.1016/j.redox.2021.102046
72. Zhu D, Chen H, Huang C, Li G, Wang X, Jiang W, et al. H_2O_2 Self-Producing Single-Atom Nanozyme Hydrogels as Light-Controlled Oxidative Stress Amplifier for Enhanced Synergistic Therapy by Transforming "Cold" Tumors. *Adv Funct Mater* (2022) 32:2110268. doi: 10.1002/adfm.202110268
73. Zhu D, Zhang T, Li Y, Huang C, Suo M, Xia L, et al. Tumor-Derived Exosomes Co-Delivering Aggregation-Induced Emission Luminogens and Proton Pump Inhibitors for Tumor Glutamine Starvation Therapy and Enhanced Type-I Photodynamic Therapy. *Biomaterials* (2022) 283:121462. doi: 10.1016/j.biomaterials.2022.121462
74. Pottier A, Borghi E, Levy L. New use of metals as nanosized radioenhancers. *Anticancer Res* (2014) 34:443–53.
75. Hainfeld JF, Slatkin DN, Smilowitz HM. The Use of Gold Nanoparticles to Enhance Radiotherapy in Mice. *Phys Med Biol* (2004) 49:N309–315. doi: 10.1088/0031-9155/49/18/n03
76. Chang M-Y, Shiau A-L, Chen Y-H, Chang C-J, Chen HH-W, Wu C-L. Increased Apoptotic Potential and Dose-Enhancing Effect of Gold Nanoparticles in Combination With Single-Dose Clinical Electron Beams on Tumor-Bearing Mice. *Cancer Sci* (2008) 99:1479–84. doi: 10.1111/j.1349-7006.2008.00827.x
77. Chithrani DB, Jelveh S, Jalali F, van Prooijen M, Allen C, Bristow RG, et al. Gold Nanoparticles as Radiation Sensitizers in Cancer Therapy. *Radiat Res* (2010) 173:719–28. doi: 10.1667/RR1984.1
78. Chattopadhyay N, Cai Z, Kwon YL, Lechtman E, Pignol J-P, Reilly RM. Molecularly Targeted Gold Nanoparticles Enhance the Radiation Response of Breast Cancer Cells and Tumor Xenografts to X-Radiation. *Breast Cancer Res Treat* (2013) 137:81–91. doi: 10.1007/s10549-012-2338-4
79. Al Zaki A, Joh D, Cheng Z, De Barros ALB, Kao G, Dorsey J, et al. Gold-Loaded Polymeric Micelles for Computed Tomography-Guided Radiation Therapy Treatment and Radiosensitization. *ACS Nano* (2014) 8:104–12. doi: 10.1021/nn405701q
80. Maggiorella L, Barouch G, Devaux C, Pottier A, Deutsch E, Bourhis J, et al. Nanoscale Radiotherapy With Hafnium Oxide Nanoparticles. *Future Oncol* (2012) 8:1167–81. doi: 10.2217/fon.12.96
81. Marill J, Anesary NM, Zhang P, Vivet S, Borghi E, Levy L, et al. Hafnium Oxide Nanoparticles: Toward an *In Vitro*predictive Biological Effect? *Radiat Oncol* (2014) 9:150. doi: 10.1186/1748-717X-9-150
82. Bonvalot S, Le Pechoux C, De Baere T, Kantor G, Buy X, Stoeckle E, et al. First-In-Human Study Testing a New Radioenhancer Using Nanoparticles (NBTXR3) Activated by Radiation Therapy in Patients With Locally Advanced Soft Tissue Sarcomas. *Clin Cancer Res* (2017) 23:908–17. doi: 10.1158/1078-0432.CCR-16-1297
83. Bonvalot S, Rutkowski PL, Thariat J, Carrère S, Ducassou A, Sunyach M-P, et al. NBTXR3, a First-in-Class Radioenhancer Hafnium Oxide Nanoparticle, Plus Radiotherapy Versus Radiotherapy Alone in Patients With Locally Advanced Soft-Tissue Sarcoma (Act.In.Sarc): A Multicentre, Phase 2-3, Randomised, Controlled Trial. *Lancet Oncol* (2019) 20:1148–59. doi: 10.1016/S1470-2045(19)30326-2
84. Bagley AF, Ludmir EB, Maitra A, Minsky BD, Li Smith G, Das P, et al. NBTXR3, a First-in-Class Radioenhancer for Pancreatic Ductal Adenocarcinoma: Report of First Patient Experience. *Clin Transl Radiat Oncol* (2022) 33:66–9. doi: 10.1016/j.ctro.2021.12.012

Conflict of Interest: The authors declare that the research was conducted in the absence of any commercial or financial relationships that could be construed as a potential conflict of interest.

Publisher's Note: All claims expressed in this article are solely those of the authors and do not necessarily represent those of their affiliated organizations, or those of the publisher, the editors and the reviewers. Any product that may be evaluated in this article, or claim that may be made by its manufacturer, is not guaranteed or endorsed by the publisher.

Copyright © 2022 Zhou, Chen, Huang, Zhang, Zhu and Fu. This is an open-access article distributed under the terms of the Creative Commons Attribution License (CC BY). The use, distribution or reproduction in other forums is permitted, provided the original author(s) and the copyright owner(s) are credited and that the original publication in this journal is cited, in accordance with accepted academic practice. No use, distribution or reproduction is permitted which does not comply with these terms.

frontiers | Frontiers in Pharmacology

MINI REVIEW
published: 22 June 2022
doi: 10.3389/fphar.2022.924131

Recent Advances in Nanotheranostic Agents for Tumor Microenvironment–Responsive Magnetic Resonance Imaging

Longhai Jin[1], *Chenyi Yang*[2], *Jianqiu Wang*[1], *Jiannan Li*[3]* *and Nannan Xu*[1]*

[1]Department of Radiology, The Second Hospital of Jilin University, Changchun, China, [2]Department of Blood Transfusion, Central Hospital of Changchun, Changchun, China, [3]Department of General Surgery, The Second Hospital of Jilin University, Changchun, China

Nanomaterials integrating a variety of excellent properties (such as controllable/suitable size, surface modifier, and multifunctionality) have attracted increasing attention in the biomedical field and have been considered a new generation of magnetic resonance imaging (MRI) contrast agents (CAs). In recent years, stimuli-responsive nanomaterials with specifically responsive ability have been synthesized as MRI CAs, which can significantly improve the diagnostic sensitivity and accuracy depending on their outstanding performance. Furthermore, the inherent tumor microenvironment (TME) of malignant tumor is considered to possess several unique features, such as low extracellular pH, redox condition, hypoxia, and high interstitial pressure, that are significantly different from healthy tissues. Hence, constructing nanomaterials for TME-responsive MRI as an emerging strategy is expected to overcome the current obstacles to precise diagnosis. This review focuses on recent advances of nanomaterials in their application of TME-responsive MRI that trigger the diagnostic function in response to various endogenous stimulations, including pH, redox, enzyme, and hypoxia. Moreover, the future challenges and trends in the development of nanomaterials serving as TME-responsive MRI CAs are discussed.

Keywords: nanomaterials, tumor microenvironment, stimuli-responsive, MRI, diagnosis of cancer

OPEN ACCESS

Edited by:
Kelong Ai,
Central South University, China

Reviewed by:
Qiong Huang,
Central South University, China
Zhen Liu,
Beijing University of Chemical Technology, China

***Correspondence:**
Jiannan Li
jnli@ciac.ac.cn
Nannan Xu
nnxu@jlu.edu.cn

Specialty section:
This article was submitted to Pharmacology of Anti-Cancer Drugs, a section of the journal Frontiers in Pharmacology

Received: *20 April 2022*
Accepted: *13 May 2022*
Published: *22 June 2022*

Citation:
Jin L, Yang C, Wang J, Li J and Xu N (2022) Recent Advances in Nanotheranostic Agents for Tumor Microenvironment–Responsive Magnetic Resonance Imaging. Front. Pharmacol. 13:924131. doi: 10.3389/fphar.2022.924131

INTRODUCTION

Cancer has become a primary cause of death and a most serious threat to human health worldwide (Sung et al., 2021). Early and accurate diagnosis is crucial to conquering cancer, which can guide clinicians to design the most timely, suitable, and reasonable therapeutic strategies for cancer patients. Magnetic resonance imaging (MRI) as one of the most powerful non-invasive imaging instruments with advantages of non-radiation and excellent spatial resolution. It is widely used in the clinical diagnosis of cancer (Na et al., 2009). It can provide anatomical and functional information of organs and soft tissues, for instance, T1 MRI can display normal anatomy with excellent resolution and T2 MRI is adept at detecting tumors and inflammation lesions with outstanding soft tissue imaging. The introduction of contrast agents (CAs) further improves the sensitivity and capability of MRI to detect lesions, which offers unprecedented and comprehensive diagnostic information for clinicians (Lohrke et al., 2016). Gadolinium (Gd^{3+}) chelate–based MRI CAs are most commonly used in clinics at present. However, these Gd-based CAs have their own limitations, such as very short

internal circulation time, poor specificity, and relatively low relaxation efficiency. In order to overcome the above defects, it is necessary to use large doses of Gd-based CAs to increase the CA concentration in the target area (Raymond and Pierre, 2005). Afterward, high-dose injection of Gd^{3+} chelates may cause severe nephrogenic systemic fibrosis syndrome, as has been warned by the US Food and Drug Administration (FDA) (Penfield and Reilly, 2007; Perez-Rodriguez et al., 2009; Chen et al., 2012). Therefore, the comprehensive performance of currently available CAs in clinic is far from ideal. Research and development of innovative and efficient MRI CAs as a substitute for traditional Gd-based CAs is highly desirable and has become a very promising field.

Over the past decades, nanomaterials integrating a variety of excellent properties have been proposed as a new generation of CAs with great potential in MRI. As imaging CAs, nanomaterials have a series of attractive characteristics: 1) controllable and suitable size, which ensures sufficient circulation time in blood and clearance ability by kidneys or reticuloendothelial system (RES) (Longmire et al., 2011). 2) Surface modifiers, which allow them to be coated with biocompatible materials to improve their biocompatibility or conjugated with ligands to provide additional properties such as target-specific binding ability, barrier-penetrating ability, and long circulation time (Lim et al., 2015). 3) Multifunctionality, integrating multiple imaging modes into one platform, making them capable of providing comprehensive information for detecting lesions. The most frequently developed nanomaterials as T1 MRI CAs are Gd-based complexes (e.g., Gd_2O_3-, $NaGdF_4$-, GdF_3-, and Gd^{3+}-doped nanoparticles [NPs]) (Liu et al., 2011; Kimura et al., 2012; Park et al., 2012; Passuello et al., 2012; Xing et al., 2014; Du et al., 2017) and paramagnetic manganese (Mn)-based composites (e.g., MnO NPs, MnO_2 nanosheets, and Mn_3O_4 NPs) (Kim et al., 2011; Chen et al., 2014; Li et al., 2017), which can shorten their longitudinal relaxation time (T1) due to their excellent ability to interact with hydrogen protons in the surrounding water. Superparamagnetic iron oxide (SPIO) NPs are the other kind of popular CAs which can shorten transverse relaxation time (T2) because of their intrinsic magnetic properties, serving as T2 MRI CAs (Laurent et al., 2008; Tong et al., 2010). Despite the variety of nanomaterials with remarkable performance having been synthesized as MRI CAs which undeniably improved the sensitivity of detecting subtle lesions to a certain extent, there are still some shortages that cannot be neglected. For instance, 1) the majority of current MRI CAs possess the function of enhancing MR contrast signals "always on" regardless of their specific accumulation in target tumors or tissues, leading to poor target-to-background signal ratios. Therefore, it is difficult to distinguish the region of interest from surrounding normal tissues due to non-specific signal enhancement, which may lead to a false-positive diagnosis or missed diagnosis (Yoo and Pagel, 2008; Fu et al., 2021). 2) Dissatisfactory relaxivity causes insufficient sensitivity to detect early-stage tumors or tiny lesions, which may miss the optimal opportunity for treatment (Yu et al., 2014; Lee et al., 2015). 3) Inadequate internal circulation time results in narrow observation window of MRI, reduces diagnostic efficiency, and impedes their applications (Kielar et al., 2010; Ai, 2011; Shen et al., 2017).

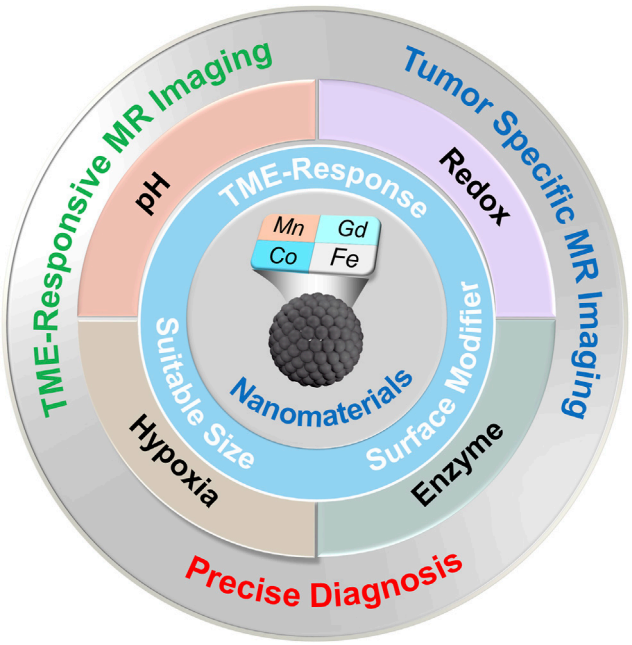


FIGURE 1 | General strategies to synthesize nanotheranostic agents for TME-responsive MRI.

Consequentially, designing stimuli-responsive CAs with specifically responsive ability is expected to overcome the above obstacles. Compared with traditional CAs, these stimuli-responsive CAs have exhibited conspicuously enhanced contrasts between target lesions (especially the small lesions or early-stage tumors) and normal tissues. Many endogenous or exogenous stimuli have been exploited to serve as triggers for stimuli-responsive CAs previously, including endo-stimuli (internal) such as pH, redox, and enzymes, and exo-stimuli (external) such as light, temperature, ultrasound, and electric or magnetic fields (Kang et al., 2017; García-Hevia et al., 2019). In addition, the tumor microenvironment (TME) of various types of malignant tumors, affected by malignant proliferation and metabolism, is considered to possess several unique features such as low extracellular pH, redox conditions, hypoxia, and high interstitial pressure (Danhier et al., 2010; Joyce and Fearon, 2015; Zhu et al., 2022). Nanomaterial-based TME-responsive CAs have attracted widespread attention for personalized cancer diagnosis owing to their outstanding performances in tumor-specific imaging, which could provide more accurate information for precise diagnosis of cancer and optimize treatment strategies (Yang et al., 2018; Wang J. et al., 2021).

This review aims to summarize the recent advances and future prospects of nanomaterial-based CAs in their TME-responsive MRI applications rather than attempting to thoroughly contain the whole field (**Figure 1**). The inherent TME properties of tumors are significantly different from healthy normal tissues, which have been utilized in developing stimuli-responsive nano-MRI CAs for tumor-specific imaging. In this review, TME-responsive MRI CAs are classified according to types of

endogenous stimulation, including pH, redox, enzyme, and hypoxia.

PH-RESPONSIVE MRI CONTRAST AGENTS

According to the Warburg effect, abnormal and rapid proliferation of tumor cells consumes a lot of oxygen and nutrients, leading to acidosis and a reduced pH in the neighboring microenvironment (Vaupel et al., 1989; Webb et al., 2011). Thus, the extracellular pH values in TME are typically acidic in many tumors, differing significantly from those of normal tissues and blood (Lee et al., 2007). The pH-responsive MRI CAs provide noninvasive contrast enhancement depending on pH, which could be applied to tumor-specific imaging. General designs of pH-responsive MRI CAs can be classified by imaging components.

Gd-Based pH-Responsive MRI CAs

Gd chelate is the most commonly used commercial MRI CA, so Gd-based pH-responsive MRI CAs have been widely studied. Zhu et al. attached pH-responsive block polymers on the surface of Gd-based NPs to achieve a surface modified Gd-metal organic frame (MOF) structure as a pH-responsive CA for MRI, which exhibited good performance in a series of characterization tests as well as imaging tests (Zhu et al., 2016). Its longitudinal relaxivity (r_1) changed with the variation of environmental pH. The r_1 value ranged from 6.6 mM^{-1} s^{-1} at pH 7.3 to 11.7 mM^{-1} s^{-1} at pH 6.6. To improve the biocompatibility and biodegradability of CAs, silkworm sericin (SS) was used to cross-link with Gd-based NPs by Huang et al. (Huang et al., 2021). A pH-responsive Gd-based NPs SS@GAH-$GdCl_3$ with r_1 values as 16.4 mM^{-1} s^{-1} at pH 5.8 and 9.2 mM^{-1} s^{-1} at pH 7.4 was obtained that showed a certain degree of increase with the decrease of pH value.

Mn-Based pH-Responsive MRI CAs

As an essential element, manganese participates in many cellular processes *in vivo*, which are of great importance to growth, development, and cellular homeostasis of the normal body (Aschner and Aschner, 2005; Erikson et al., 2005). Apart from Mn ions playing a key role in physiological processes owing to their redox and catalytic nature, Mn also possesses significant magnetic properties. Thus, Mn-based NPs and CAs have entered the field of MR imaging diagnosis and received extensive attention. In spite of some Mn-based CAs serving as regular T1 CAs and having achieved similar effects as clinical Gd-based CAs, a novel class of Mn-based nanomaterials has been designed with improved imaging sensitivity and is potentially expected to be substitutes for traditional CAs. These nanomaterials were constructed to respond to biological microenvironments, mainly to pH and redox potential variations. Chen et al. introduced pH-sensitive degradable manganese oxide (MnO) NPs into mesopores of hollow silica nanocapsules (HMCNs) through in-site redox reaction, then gained MnO-HMCNs as a pH-responsive CA for T_1 MRI (Chen et al., 2012). Under weak acidic conditions, MnO dissolves into Mn ions, causing a great increase in r_1 value (8.81 $mM^{-1}s^{-1}$), which is 11 times higher than that in neutral conditions and 2 times higher than commercial Gd-based CAs. To improve the diagnostic specificity and sensitivity, stimuli-responsive multiple-mode MRI CAs are extremely advisable for obtaining overall and detailed diagnostic information to complement the deficiencies of each other. Our group synthetized cobalt phosphides (Co-P) as core, coating with manganese dioxide (MnO_2) nanosheets to obtain Co-P@$mSiO_2$–MnO_2 for pH-responsive T1/T2 dual-mode MRI-guided synergistic anticancer therapy (Jin et al., 2017). For imaging, Co-P core was applied to T2 MRI owing to its intrinsic magnetic properties, and biodegradable MnO_2 was employed as pH-responsive T1 MRI CA. Under acidic conditions, the r_1 value of Co-P@$mSiO_2$–MnO_2 was determined to be 9.05 $mM^{-1}s^{-1}$, the r_2 value was 253.44 $mM^{-1}s^{-1}$ which increased approximately 1.5 times than under neutral conditions.

Fe-Based pH-Responsive MRI CAs

Fe is another essential element in the human body, mainly existing as ferritin in blood circulation. Paramagnetic Fe^{3+} is regarded as a promising candidate as T1 MR CAs owing to its large number of unpaired electrons (Wu et al., 2014; Zhang et al., 2017). Qu et al. recently fabricated an Fe-based biomimetic melanin-like multifunctional nanoagent (amino-Fe-PDANPs) as a positive pH-responsive MRI CA (Qu et al., 2021). Polydopamine was employed as a pH-responsive sensitizer for imaging. The r_1 value was 10.0 $mM^{-1}s^{-1}$ at pH 7.5, then increasing to 15.4 $mM^{-1}s^{-1}$ at pH 6.5. It has been proven that the approachability of water molecules to the paramagnetic centers is the critical factor for T1 signal enhancement (Taylor et al., 2008). Interestingly, Fe-based NPs are also extensively applied as T2 MR Cas. Their magnetic property reduces rapidly with decreasing size owing to the reduction of magnetic anisotropy and spin disordering on the surface of NPs (Jun et al., 2008). Liu et al. synthesized PEGylated ultrasmall superparamagnetic iron oxide nanoparticles (USPIONs) by incorporating the methods of microemulsion and biomineralization, and coating with $CaCO_3$ to obtain PEG-USPIONs@$CaCO_3$ as a pH-responsive T2-T1–switchable MRI CA (Liu et al., 2021). The USPIONs agglomerated compactly inside the nanostructure, resulting in the enhancement of the T2 signal. While exposed to the acidic conditions in the tumor microenvironment, the $CaCO_3$-layer releases free USPIONs by degradation, then switching to T1 MRI signal enhancement. With the gradual decrease of pH value, the r_2/r_1 ratio reduces substantially. In brief, PEG-USPIONs@$CaCO_3$ will change from T2 CA in the neutral pH condition to T1 CA in the acidic environment of tumors. Not coincidentally, He et al. reported an extremely small iron oxide nanoparticle (ESIONP)–based pH-responsive T1-T2–switchable MRI CA which exhibited good performance (He et al., 2020).

REDOX-RESPONSIVE MRI CONTRAST AGENTS

In addition to weakly acidic pH, redox state as another characteristic biomarker of TME has drawn remarkable attention. Glutathione (GSH), among a variety of redox couples, is usually considered the most important thiol-disulfide redox buffer in charge of maintaining the balance of intracellular redox reactions (Do et al., 2014; Zhao et al., 2022). The concentration of GSH in tumor cells is much higher than that in normal tissues or blood (Cheng et al., 2011). Therefore, reduction-sensitive disulfide bonds and hydrogen peroxide (H_2O_2)–responsive boronated moieties were extensively used as redox-responsive MRI CAs, While Gd itself cannot be redoxed, many other metal ions have been developed, such as Mn, Fe, Co, Eu, and Cu.

Mn-Based Redox-Responsive MRI CAs

Recently, Wang et al. developed an intelligent redox-responsive nanoplatform (MUM NPs) via the coprecipitation process involving upconversion NPs (UCNPs) and aggregation-induced emission-active photosensitizers, as well as an *in situ* generation process of MnO_2 as the outer shell (Wang Y. et al., 2021). MUM NPs exhibited high specificity to TME, rapidly exhausting intracellular GSH and efficiently generating Mn^{2+}, which were instrumental in ROS preservation and T1 MRI enhancement, respectively. This nanoplatform performed well in redox-responsive MR imaging. In addition to single-mode stimuli-responsive MRI, Kim et al. designed a redox-responsive T1/T2 dual-mode MRI CA, integrating a superparamagnetic core (Fe_3O_4) and a paramagnetic shell (Mn_3O_4) into a core-shell structure through a seed-mediated growth process (Kim et al., 2016). Under the stimulation of tumors' intracellular reducing environments by glutathione, the Mn_3O_4 shell will be decomposed into Mn^{2+} for T1 signal enhancement and allow Fe_3O_4 to interact with water protons for T2 signal enhancement. Under GSH-free conditions, the r_1 was 2.4 $mM^{-1}s^{-1}$ and the r_2 was 92.2 $mM^{-1}s^{-1}$. After activation in GSH solution, the r_1 and r_2 values increased to 16.1 and 258.6 $mM^{-1}s^{-1}$, illustrating that this nanoplatform can be qualified as redox-responsive T1/T2 dual-MRI CA.

Fe-Based Redox-Responsive MRI CAs

The yolk-shell type of GSH-responsive nanovesicles (NVs) were synthesized to encapsulate USPIO NPs and chemotherapy drugs by Liu et al.; the obtained USD NVs can respond to GSH-releasing drugs and activate T1 signal enhancement (Liu et al., 2020). The r_1 value increased obviously to 3.1 $mM^{-1}s^{-1}$ in the presence of GSH. For switchable MRI, Cao et al. encapsulated citric acid–modified ESIONPs-CA in disulfide cross-linked poly (CBMA) nanogels, further introducing tumor-targeted c (RGD) ligand to obtain ICNs-RGD (Cao et al., 2020). With the stimulation of GSH, ICNs-RGD are rapidly degraded, and the agglomerated ESIONPs are dispersed evenly, which achieves switching from a T2 CA to a T1 one. ICNs-RGD exhibits a T2 contrast effect (dark) during its transport in the vessel, then switches to a T1 contrast effect (bright) after reaching the tumor region with a redox microenvironment. After stimulation by GSH, the r_1 value was increased mildly from 5.56 to 7.40 $mM^{-1}s^{-1}$ and the r_2 value drastically decreased from 103.01 to 14.36 $mM^{-1}s^{-1}$, which demonstrated that ICNs-RGD had the potential to be an efficient MRI CA in clinics.

ENZYME-RESPONSIVE MRI CONTRAST AGENTS

Because of their unique substrate specificity and high selectivity as well as efficient catalysis in biochemical reactions, enzymes play an indispensable role in most biological and metabolic processes, which can be associated with a series of pathological changes, such as tumors, inflammation, and so on (Zhang et al., 2014; Wang et al., 2019). In particular, cathepsin B and matrix metalloproteinases (MMPs) with elevated expression in the tumor environment participate in numerous biological processes associated with cancer, such as progression, metastasis, and angiogenesis. These tumor-associated enzymes can be regarded as stimulators for enzyme-responsive imaging or treatment of cancer (Hu et al., 2012). By means of one step reaction, Sun et al. synthesized hyperbranched poly (oligo-(ethylene glycol) methacrylate)-Gd complexes (HB-POEGMA-Gd and HB-POEGMA-cRGD-Gd), which employed lysosomal cathepsin B as a stimuli-response component to realize enzyme-responsive T1 CA (Sun et al., 2016). Their r_1 values were 12.25 and 14.65 $mM^{-1}s^{-1}$, respectively. Recently, Yan et al. reported a Gd-based enzyme-responsive MRI and NIR fluorescence imaging CA (P-CyFF-Gd) with alkaline phosphatase (ALP) as a model enzyme (Yan et al., 2019). Upon ALP activation, r_1 increased from 8.9 to 20.1 $mM^{-1}s^{-1}$, which demonstrated that P-CyFF-Gd can be qualified as a new generation of enzyme-responsive T1 CA. Another Gd-based enzyme-responsive T1 CA was designed through a self-assembly approach with caspase-3/7 as an activator by Ye et al. (Ye et al., 2014). The r_1 value significantly increased from 10.2 $mM^{-1}s^{-1}$ before activation to 19.0 $mM^{-1}s^{-1}$ after activation. For enzyme-responsive T2 imaging, Gallo et al. constructed Fe-based MMP, enzyme-activatable, and tumor-specific targeting NPs, which were tethered with CXCR4-targeted peptide ligands for targeting tumors (Gallo et al., 2014). Upon MMP activation, the structure of NPs changes to that of a self-assembled superparamagnetic cluster network through a cycloaddition reaction, resulting in T2 signal enhancement.

HYPOXIA-RESPONSIVE MRI CONTRAST AGENTS

The malignant proliferation of tumors depletes a large amount of oxygen, resulting in the hypoxia of the tumor environment. As an inevitable feature of tumors, hypoxia is considered to be the obvious causative factor of therapeutic resistance and metastasis (Gatenby and Gillies, 2008). Therefore, exploiting novel nanotheranostics to achieve accurate diagnosis of hypoxia and timely treatment simultaneously has drawn great attention in biomedical research as well as clinical studies. The Gd complex of 1,4,7,10-tetraazacyclododecane-1,4,7,10-tetraacetic acid with a 2-nitroimidazole attached to one carboxyl group by an amide linkage was synthesized by Rojas-Quijano et al.; the r_1 value was determined to be 6.38 $mM^{-1}s^{-1}$. The MR imaging results demonstrated that the nitroimidazole-derivant modified nanoprobe could be qualified as a hypoxia-responsive T1 CA

TABLE 1 | Summary of recent work on nanomaterials for TME-responsive MRI.

Nanomaterial	Responsive	Imaging component	Imaging mode	Relaxivity		References
				Before activation	After activation	
GdNPs	pH	Gd	T1	r_1 = 8.3	r_1 = 11.7	Zhu et al. (2016)
Gd-PCNPs	pH	Gd	T1	r_1 = 6.62	r_1 = 10.01	Jiang et al. (2017)
SS@GAH-$GdCl_3$	pH	Gd	T1	r_1 = 9.2	r_1 = 16.4	Huang et al. (2021)
HMCNs	pH	Mn	T1	r_1 = 0.79	r_1 = 8.81	Chen et al. (2012)
Mn-LDH	pH	Mn	T1	r_1 = 1.16	r_1 = 9.48	Li et al. (2017)
Co-P@mSiO_2@DOX-MnO_2	pH	Mn, Co	T1, T2	-	r_1 = 9.05	Jin et al. (2017)
				r_2 = 169.93	r_2 = 253.44	
Amino-Fe-PDANPs	pH	Fe	T1	r_1 = 10.0	r_1 = 15.4	Qu et al. (2021)
ESIONP system	pH	Fe	T1 to T2	r_1 = 5.71	r_1 = 3.88	He et al. (2020)
				r_2 = 9.11	r_2 = 42.2	
PEG-USPIONs@$CaCO_3$	pH	Fe	T2 to T1	-	-	Liu et al. (2021)
MUM NPs	Redox	Mn	T1	r_1 = 0.12	r_1 = 6.89	Wang et al. (2021b)
RANS	Redox	Mn	T1, T2	r_1 = 2.4	r_1 = 16.1	Kim et al. (2016)
				r_2 = 92.2	r_2 = 258.6	
USD NVs	Redox	Fe	T1	-	r_1 = 3.1	Liu et al. (2020)
HIONPs	Redox	Fe	T1, T2	-	r_1 = 41.3	Xu et al. (2021)
					r_2 = 118.7	
ICNs-RGD	Redox	Fe	T2 to T1	r_1 = 5.56	r_1 = 7.4	Cao et al. (2020)
				r_2 = 103.01	r_2 = 14.36	
P-CyFF-Gd	Enzyme	Gd	T1	r_1 = 8.9	r_1 = 20.1	Yan et al. (2019)
HB-POEGMA-cRGD-Gd	Enzyme	Gd	T1	-	r_1 = 14.65	Sun et al. (2016)
C-SNAM	Enzyme	Gd	T1	r_1 = 10.2	r_1 = 19.0	Ye et al. (2014)
IONPs	Enzyme	Fe	T2	-	-	Gallo et al. (2014)
Gd-complexes	Hypoxia	Gd	T1	-	r_1 = 6.38	Rojas-Quijano et al. (2012)
DOX-UCHSM-PEG-DOTA	Hypoxia	Mn	T1	r_1 = 0.112	r_1 = 1.137	Song et al. (2018)
CoTPAx complexes	Hypoxia	Co	T2	-	-	O'Neill et al. (2017)

to distinguish hypoxic from normoxic tissues. For Mn-based CAs, Song et al. constructed a rattle-structured NP consisting of a UCNP core, a hollow mesoporous silica shell, and hypoxia-sensitive MnO_2 nanosheet modification (Song et al., 2018). MnO_2 could be disintegrated into Mn^{2+} to achieve hypoxia-responsive T1 signal enhancement, and the r_1 value is 1.137 $mM^{-1}s^{-1}$ after activation. O'Neill et al. studied the possibility of Co-based bioreductive prodrugs working as a hypoxia-responsive MRI CA. Once in the hypoxic environment of tumors, the diamagnetic Co(III) ions of the CA will be reduced to ions of paramagnetic Co(II), ones which could significantly shorten the T2 relaxation to realize a T2 signal enhancement.

DISCUSSION

TME-responsive MRI CAs have been widely developed for accurate diagnosis of cancer because of their outstanding properties. The recent work on nanomaterials for TME-responsive MRI is summarized in **Table 1**. Although great efforts have been devoted to exploring a variety of TME-responsive MRI CAs in the biomedical field, there are still some problems that need to be solved for accelerating their clinical transformation. For instance, 1) up to date, most studies of stimuli-responsive CAs based on nanomaterials stay in the stage of concept verification as well as the research of laboratory application; systematic and in-depth researches are needed to promote their clinical application. 2) The safety concerns of these CAs need to be investigated more thoroughly, including their long-term biocompatibility, pharmacokinetics, biodistribution, biodegradability, and excretion, which are vitally important for their clinical transformation. 3) Despite numerous stimuli-responsive CAs exhibiting good performance, nanomaterials with better properties (such as high relaxivity, adequate circulation time, and appropriate stimuli-response function) should be explored to further improve the imaging effect and diagnostic efficiency. We believe that ingenious design and construction of TME-responsive MRI CAs will greatly promote the development of early and accurate cancer diagnosis in the future.

AUTHOR CONTRIBUTIONS

JL and NX conceived the topic and structure of the article. LJ conducted the literature research and drafted the manuscript. CY and JW prepared the figures, tables, and manuscript amendments. JL and NX reviewed and refined the manuscript.

FUNDING

This work was supported by the National Natural Science Foundation of China (Grant No. 32000953), the Natural Science Foundation of Jilin Province (Grant No. 20210101287JC), the Financial Department of Jilin Province (Grant No. 2019SCZT045), the Fundamental Research Funds for the Central Universities (Grant No. 415010200060), and the Education Project of Jilin University (#419070600046 and 45121031D024).

REFERENCES

Ai, H. (2011). Layer-by-layer Capsules for Magnetic Resonance Imaging and Drug Delivery. *Adv. Drug Deliv. Rev.* 63 (9), 772–788. doi:10.1016/j.addr.2011.03.013

Aschner, J. L., and Aschner, M. (2005). Nutritional Aspects of Manganese Homeostasis. *Mol. Asp. Med.* 26 (4-5), 353–362. doi:10.1016/j.mam.2005.07.003

Cao, Y., Mao, Z., He, Y., Kuang, Y., Liu, M., Zhou, Y., et al. (2020). Extremely Small Iron Oxide Nanoparticle-Encapsulated Nanogels as a Glutathione-Responsive T1 Contrast Agent for Tumor-Targeted Magnetic Resonance Imaging. *ACS Appl. Mater Interfaces* 12 (24), 26973–26981. doi:10.1021/acsami.0c07288

Chen, Y., Ye, D., Wu, M., Chen, H., Zhang, L., Shi, J., et al. (2014). Break-up of Two-Dimensional MnO2 Nanosheets Promotes Ultrasensitive pH-Triggered Theranostics of Cancer. *Adv. Mater* 26 (41), 7019–7026. doi:10.1002/adma.201402572

Chen, Y., Yin, Q., Ji, X., Zhang, S., Chen, H., Zheng, Y., et al. (2012). Manganese Oxide-Based Multifunctionalized Mesoporous Silica Nanoparticles for pH-Responsive MRI, Ultrasonography and Circumvention of MDR in Cancer Cells. *Biomaterials* 33 (29), 7126–7137. doi:10.1016/j.biomaterials.2012.06.059

Cheng, R., Feng, F., Meng, F., Deng, C., Feijen, J., and Zhong, Z. (2011). Glutathione-responsive Nano-Vehicles as a Promising Platform for Targeted Intracellular Drug and Gene Delivery. *J. Control Release* 152 (1), 2–12. doi:10.1016/j.jconrel.2011.01.030

Danhier, F., Feron, O., and Préat, V. (2010). To Exploit the Tumor Microenvironment: Passive and Active Tumor Targeting of Nanocarriers for Anti-cancer Drug Delivery. *J. Control Release* 148 (2), 135–146. doi:10.1016/j.jconrel.2010.08.027

Do, Q. N., Ratnakar, J. S., Kovács, Z., and Sherry, A. D. (2014). Redox- and Hypoxia-Responsive MRI Contrast Agents. *ChemMedChem.* 9 (6), 1116–1129. doi:10.1002/cmdc.201402034

Du, F., Zhang, L., Zhang, L., Zhang, M., Gong, A., Tan, Y., et al. (2017). Engineered Gadolinium-Doped Carbon Dots for Magnetic Resonance Imaging-Guided Radiotherapy of Tumors. *Biomaterials* 121, 109–120. doi:10.1016/j.biomaterials.2016.07.008

Erikson, K. M., Syversen, T., Aschner, J. L., and Aschner, M. (2005). Interactions between Excessive Manganese Exposures and Dietary Iron-Deficiency in Neurodegeneration. *Environ. Toxicol. Pharmacol.* 19 (3), 415–421. doi:10.1016/j.etap.2004.12.053

Fu, S., Cai, Z., and Ai, H. (2021). Stimulus-Responsive Nanoparticle Magnetic Resonance Imaging Contrast Agents: Design Considerations and Applications. *Adv. Healthc. Mat.* 10 (5), 2001091. doi:10.1002/adhm.202001091

Gallo, J., Kamaly, N., Lavdas, I., Stevens, E., Nguyen, Q. D., Wylezinska-Arridge, M., et al. (2014). CXCR4-targeted and MMP-Responsive Iron Oxide Nanoparticles for Enhanced Magnetic Resonance Imaging. *Angew. Chem. Int. Ed. Engl.* 53 (36), 9550–9554. doi:10.1002/anie.201405442

García-Hevia, L., Bañobre-López, M., and Gallo, J. (2019). Recent Progress on Manganese-Based Nanostructures as Responsive MRI Contrast Agents. *Chem. Eur. J.* 25 (2), 431–441. doi:10.1002/chem.201802851

Gatenby, R. A., and Gillies, R. J. (2008). A Microenvironmental Model of Carcinogenesis. *Nat. Rev. Cancer* 8 (1), 56–61. doi:10.1038/nrc2255

He, Y., Mao, Z., Zhang, Y., Lv, H., Yan, J., Cao, Y., et al. (2020). Tumor Acid Microenvironment-Triggered Self-Assembly of ESIONPs for T1/T2 Switchable Magnetic Resonance Imaging. *ACS Appl. Bio Mat.* 3 (11), 7752–7761. doi:10.1021/acsabm.0c00958

Hu, J., Zhang, G., and Liu, S. (2012). Enzyme-responsive Polymeric Assemblies, Nanoparticles and Hydrogels. *Chem. Soc. Rev.* 41 (18), 5933–5949. doi:10.1039/C2CS35103J

Huang, Z., Wang, Y., Wu, M., Li, W., Zuo, H., Xiao, B., et al. (2021). Sericin-based Gadolinium Nanoparticles as Synergistically Enhancing Contrast Agents for pH-Responsive and Tumor Targeting Magnetic Resonance Imaging. *Mater. Des.* 203, 109600. doi:10.1016/j.matdes.2021.109600

Jiang, D., Zhang, X., Yu, D., Xiao, Y., Wang, T., Su, Z., et al. (2017). Tumor-Microenvironment Relaxivity-Changeable Gd-Loaded Poly(L-lysine)/Carboxymethyl Chitosan Nanoparticles as Cancer-Recognizable Magnetic Resonance Imaging Contrast Agents. *J. Biomed. Nanotechnol.* 13 (3), 243–254. doi:10.1166/jbn.2017.2346

Jin, L., Liu, J., Tang, Y., Cao, L., Zhang, T., Yuan, Q., et al. (2017). MnO2-Functionalized Co-P Nanocomposite: A New Theranostic Agent for pH-Triggered T1/T2 Dual-Modality Magnetic Resonance Imaging-Guided Chemo-Photothermal Synergistic Therapy. *ACS Appl. Mater Interfaces* 9 (48), 41648–41658. doi:10.1021/acsami.7b10608

Joyce, J. A., and Fearon, D. T. (2015). T Cell Exclusion, Immune Privilege, and the Tumor Microenvironment. *Science* 348 (6230), 74–80. doi:10.1126/science.aaa6204

Jun, Y. W., Lee, J. H., and Cheon, J. (2008). Chemical Design of Nanoparticle Probes for High-Performance Magnetic Resonance Imaging. *Angew. Chem. Int. Ed. Engl.* 47 (28), 5122–5135. doi:10.1002/anie.200701674

Kang, T., Li, F., Baik, S., Shao, W., Ling, D., and Hyeon, T. (2017). Surface Design of Magnetic Nanoparticles for Stimuli-Responsive Cancer Imaging and Therapy. *Biomaterials* 136, 98–114. doi:10.1016/j.biomaterials.2017.05.013

Kielar, F., Tei, L., Terreno, E., and Botta, M. (2010). Large Relaxivity Enhancement of Paramagnetic Lipid Nanoparticles by Restricting the Local Motions of the Gd(III) Chelates. *J. Am. Chem. Soc.* 132 (23), 7836–7837. doi:10.1021/ja101518v

Kim, M. H., Son, H. Y., Kim, G. Y., Park, K., Huh, Y. M., and Haam, S. (2016). Redoxable Heteronanocrystals Functioning Magnetic Relaxation Switch for Activatable T1 and T2 Dual-Mode Magnetic Resonance Imaging. *Biomaterials* 101, 121–130. doi:10.1016/j.biomaterials.2016.05.054

Kim, T., Cho, E. J., Chae, Y., Kim, M., Oh, A., Jin, J., et al. (2011). Urchin-shaped Manganese Oxide Nanoparticles as pH-Responsive Activatable T1 Contrast Agents for Magnetic Resonance Imaging. *Angew. Chem. Int. Ed. Engl.* 50 (45), 10589–10593. doi:10.1002/anie.201103108

Kimura, Y., Kamisugi, R., Narazaki, M., Matsuda, T., Tabata, Y., Toshimitsu, A., et al. (2012). Size-controlled and Biocompatible Gd2 O3 Nanoparticles for Dual Photoacoustic and MR Imaging. *Adv. Healthc. Mater* 1 (5), 657–660. doi:10.1002/adhm.201200103

Laurent, S., Forge, D., Port, M., Roch, A., Robic, C., Vander Elst, L., et al. (2008). Magnetic Iron Oxide Nanoparticles: Synthesis, Stabilization, Vectorization, Physicochemical Characterizations, and Biological Applications. *Chem. Rev.* 108 (6), 2064–2110. doi:10.1021/cr068445e

Lee, E. S., Oh, K. T., Kim, D., Youn, Y. S., and Bae, Y. H. (2007). Tumor pH-Responsive Flower-like Micelles of poly(L-Lactic Acid)-B-Poly(ethylene Glycol)-B-poly(L-Histidine). *J. Control Release* 123 (1), 19–26. doi:10.1016/j.jconrel.2007.08.006

Lee, Y. J., Lee, J. M., Lee, J. S., Lee, H. Y., Park, B. H., Kim, Y. H., et al. (2015). Hepatocellular Carcinoma: Diagnostic Performance of Multidetector CT and MR Imaging-A Systematic Review and Meta-Analysis. *Radiology* 275 (1), 97–109. doi:10.1148/radiol.14140690

Li, B., Gu, Z., Kurniawan, N., Chen, W., and Xu, Z. P. (2017). Manganese-Based Layered Double Hydroxide Nanoparticles as a T1 -MRI Contrast Agent with Ultrasensitive pH Response and High Relaxivity. *Adv. Mater* 29 (29), 1. doi:10.1002/adma.201700373

Lim, E. K., Kim, T., Paik, S., Haam, S., Huh, Y. M., and Lee, K. (2015). Nanomaterials for Theranostics: Recent Advances and Future Challenges. *Chem. Rev.* 115 (1), 327–394. doi:10.1021/cr300213b

Liu, D., Zhou, Z., Wang, X., Deng, H., Sun, L., Lin, H., et al. (2020). Yolk-shell Nanovesicles Endow Glutathione-Responsive Concurrent Drug Release and T1 MRI Activation for Cancer Theranostics. *Biomaterials* 244, 119979. doi:10.1016/j.biomaterials.2020.119979

Liu, W., Yin, S., Hu, Y., Deng, T., and Li, J. (2021). Microemulsion-Confined Biomineralization of PEGylated Ultrasmall Fe3O4 Nanocrystals for T2-T1 Switchable MRI of Tumors. *Anal. Chem.* 93 (42), 14223–14230. doi:10.1021/acs.analchem.1c03128

Liu, Y., Ai, K., Yuan, Q., and Lu, L. (2011). Fluorescence-enhanced Gadolinium-Doped Zinc Oxide Quantum Dots for Magnetic Resonance and Fluorescence Imaging. *Biomaterials* 32 (4), 1185–1192. doi:10.1016/j.biomaterials.2010.10.022

Lohrke, J., Frenzel, T., Endrikat, J., Alves, F. C., Grist, T. M., Law, M., et al. (2016). 25 Years of Contrast-Enhanced MRI: Developments, Current Challenges and Future Perspectives. *Adv. Ther.* 33 (1), 1–28. doi:10.1007/s12325-015-0275-4

Longmire, M. R., Ogawa, M., Choyke, P. L., and Kobayashi, H. (2011). Biologically Optimized Nanosized Molecules and Particles: More Than Just Size. *Bioconjug Chem.* 22 (6), 993–1000. doi:10.1021/bc200111p

Na, H. B., Song, I. C., and Hyeon, T. (2009). Inorganic Nanoparticles for MRI Contrast Agents. *Adv. Mat.* 21 (21), 2133–2148. doi:10.1002/adma.200802366

O'Neill, E. S., Kaur, A., Bishop, D. P., Shishmarev, D., Kuchel, P. W., Grieve, S. M., et al. (2017). Hypoxia-Responsive Cobalt Complexes in Tumor Spheroids: Laser Ablation

Inductively Coupled Plasma Mass Spectrometry and Magnetic Resonance Imaging Studies. *Inorg. Chem.* 56 (16), 9860–9868. doi:10.1021/acs.inorgchem.7b01368

Park, Y. I., Kim, H. M., Kim, J. H., Moon, K. C., Yoo, B., Lee, K. T., et al. (2012). Theranostic Probe Based on Lanthanide-Doped Nanoparticles for Simultaneous *In Vivo* Dual-Modal Imaging and Photodynamic Therapy. *Adv. Mater* 24 (42), 5755–5761. doi:10.1002/adma.201202433

Passuello, T., Pedroni, M., Piccinelli, F., Polizzi, S., Marzola, P., Tambalo, S., et al. (2012). PEG-capped, Lanthanide Doped GdF3 Nanoparticles: Luminescent and T2 Contrast Agents for Optical and MRI Multimodal Imaging. *Nanoscale* 4 (24), 7682–7689. doi:10.1039/c2nr31796f

Penfield, J. G., and Reilly, R. F., Jr. (2007). What Nephrologists Need to Know about Gadolinium. *Nat. Clin. Pract. Nephrol.* 3 (12), 654–668. doi:10.1038/ncpneph0660

Perez-Rodriguez, J., Lai, S., Ehst, B. D., Fine, D. M., and Bluemke, D. A. (2009). Nephrogenic Systemic Fibrosis: Incidence, Associations, and Effect of Risk Factor Assessment-Rreport of 33 Cases. *Radiology* 250 (2), 371–377. doi:10.1148/radiol.2502080498

Qu, J., Guillory, D., Cheah, P., Tian, B., Zheng, J., Liu, Y., et al. (2021). Synthesis of Biomimetic Melanin-like Multifunctional Nanoparticles for pH Responsive Magnetic Resonance Imaging and Photothermal Therapy. *Nanomater. (Basel)* 11 (8). doi:10.3390/nano11082107

Raymond, K. N., and Pierre, V. C. (2005). Next Generation, High Relaxivity Gadolinium MRI Agents. *Bioconjug Chem.* 16 (1), 3–8. doi:10.1021/bc049817y

Rojas-Quijano, F. A., Tircsó, G., Tircsóné Benyó, E., Baranyai, Z., Tran Hoang, H., Kálmán, F. K., et al. (2012). Synthesis and Characterization of a Hypoxia-Sensitive MRI Probe. *Chemistry* 18 (31), 9669–9676. doi:10.1002/chem.201200266

Shen, Z., Chen, T., Ma, X., Ren, W., Zhou, Z., Zhu, G., et al. (2017). Multifunctional Theranostic Nanoparticles Based on Exceedingly Small Magnetic Iron Oxide Nanoparticles for T1-Weighted Magnetic Resonance Imaging and Chemotherapy. *ACS Nano* 11 (11), 10992–11004. doi:10.1021/acsnano.7b04924

Song, R., Zhang, M., Liu, Y., Cui, Z., Zhang, H., Tang, Z., et al. (2018). A Multifunctional Nanotheranostic for the Intelligent MRI Diagnosis and Synergistic Treatment of Hypoxic Tumor. *Biomaterials* 175, 123–133. doi:10.1016/j.biomaterials.2018.05.018

Sun, L., Li, X., Wei, X., Luo, Q., Guan, P., Wu, M., et al. (2016). Stimuli-Responsive Biodegradable Hyperbranched Polymer-Gadolinium Conjugates as Efficient and Biocompatible Nanoscale Magnetic Resonance Imaging Contrast Agents. *ACS Appl. Mater Interfaces* 8 (16), 10499–10512. doi:10.1021/acsami.6b00980

Sung, H., Ferlay, J., Siegel, R. L., Laversanne, M., Soerjomataram, I., Jemal, A., et al. (2021). Global Cancer Statistics 2020: GLOBOCAN Estimates of Incidence and Mortality Worldwide for 36 Cancers in 185 Countries. *CA Cancer J. Clin.* 71 (3), 209–249. doi:10.3322/caac.21660

Taylor, K. M., Kim, J. S., Rieter, W. J., An, H., Lin, W., and Lin, W. (2008). Mesoporous Silica Nanospheres as Highly Efficient MRI Contrast Agents. *J. Am. Chem. Soc.* 130 (7), 2154–2155. doi:10.1021/ja710193c

Tong, S., Hou, S., Zheng, Z., Zhou, J., and Bao, G. (2010). Coating Optimization of Superparamagnetic Iron Oxide Nanoparticles for High T2 Relaxivity. *Nano Lett.* 10 (11), 4607–4613. doi:10.1021/nl102623x

Vaupel, P., Kallinowski, F., and Okunieff, P. (1989). Blood Flow, Oxygen and Nutrient Supply, and Metabolic Microenvironment of Human Tumors: a Review. *Cancer Res.* 49 (23), 6449–6465.

Wang, J., Sui, L., Huang, J., Miao, L., Nie, Y., Wang, K., et al. (2021a). MoS2-based Nanocomposites for Cancer Diagnosis and Therapy. *Bioact. Mater* 6 (11), 4209–4242. doi:10.1016/j.bioactmat.2021.04.021

Wang, X., Wang, X., Jin, S., Muhammad, N., and Guo, Z. (2019). Stimuli-Responsive Therapeutic Metallodrugs. *Chem. Rev.* 119 (2), 1138–1192. doi:10.1021/acs.chemrev.8b00209

Wang, Y., Li, Y., Zhang, Z., Wang, L., Wang, D., and Tang, B. Z. (2021b). Triple-Jump Photodynamic Theranostics: MnO 2 Combined Upconversion Nanoplatforms Involving a Type-I Photosensitizer with Aggregation-Induced Emission Characteristics for Potent Cancer Treatment. *Adv. Mater.* 33 (41), 2103748. doi:10.1002/adma.202103748

Webb, B. A., Chimenti, M., Jacobson, M. P., and Barber, D. L. (2011). Dysregulated pH: a Perfect Storm for Cancer Progression. *Nat. Rev. Cancer* 11 (9), 671–677. doi:10.1038/nrc3110

Wu, M., Meng, Q., Chen, Y., Xu, P., Zhang, S., Li, Y., et al. (2014). Ultrasmall Confined Iron Oxide Nanoparticle MSNs as a pH-Responsive Theranostic Platform. *Adv. Funct. Mat.* 24 (27), 4273–4283. doi:10.1002/adfm.201400256

Xing, H., Zhang, S., Bu, W., Zheng, X., Wang, L., Xiao, Q., et al. (2014). Ultrasmall NaGdF4 Nanodots for Efficient MR Angiography and Atherosclerotic Plaque Imaging. *Adv. Mater* 26 (23), 3867–3872. doi:10.1002/adma.201305222

Xu, X., Zhou, X., Xiao, B., Xu, H., Hu, D., Qian, Y., et al. (2021). Glutathione-Responsive Magnetic Nanoparticles for Highly Sensitive Diagnosis of Liver Metastases. *Nano Lett.* 21 (5), 2199–2206. doi:10.1021/acs.nanolett.0c04967

Yan, R., Hu, Y., Liu, F., Wei, S., Fang, D., Shuhendler, A. J., et al. (2019). Activatable NIR Fluorescence/MRI Bimodal Probes for *In Vivo* Imaging by Enzyme-Mediated Fluorogenic Reaction and Self-Assembly. *J. Am. Chem. Soc.* 141 (26), 10331–10341. doi:10.1021/jacs.9b03649

Yang, G., Zhang, R., Liang, C., Zhao, H., Yi, X., Shen, S., et al. (2018). Manganese Dioxide Coated WS2 @Fe3 O4/sSiO2 Nanocomposites for pH-Responsive MR Imaging and Oxygen-Elevated Synergetic Therapy. *Small* 14 (2), 1. doi:10.1002/smll.201702664

Ye, D., Shuhendler, A. J., Pandit, P., Brewer, K. D., Tee, S. S., Cui, L., et al. (2014). Caspase-responsive Smart Gadolinium-Based Contrast Agent for Magnetic Resonance Imaging of Drug-Induced Apoptosis. *Chem. Sci.* 4 (10), 3845–3852. doi:10.1039/C4SC01392A

Yoo, B., and Pagel, M. D. (2008). An Overview of Responsive MRI Contrast Agents for Molecular Imaging. *Front. Biosci.* 13, 1733–1752. doi:10.2741/2796

Yu, M. H., Kim, J. H., Yoon, J. H., Kim, H. C., Chung, J. W., Han, J. K., et al. (2014). Small (≤1-cm) Hepatocellular Carcinoma: Diagnostic Performance and Imaging Features at Gadoxetic Acid-Enhanced MR Imaging. *Radiology* 271 (3), 748–760. doi:10.1148/radiol.14131996

Zhang, H., Li, L., Liu, X. L., Jiao, J., Ng, C. T., Yi, J. B., et al. (2017). Ultrasmall Ferrite Nanoparticles Synthesized via Dynamic Simultaneous Thermal Decomposition for High-Performance and Multifunctional T1 Magnetic Resonance Imaging Contrast Agent. *ACS Nano* 11 (4), 3614–3631. doi:10.1021/acsnano.6b07684

Zhang, H. W., Wang, L. Q., Xiang, Q. F., Zhong, Q., Chen, L. M., Xu, C. X., et al. (2014). Specific Lipase-Responsive Polymer-Coated Gadolinium Nanoparticles for MR Imaging of Early Acute Pancreatitis. *Biomaterials* 35 (1), 356–367. doi:10.1016/j.biomaterials.2013.09.046

Zhao, T., Wu, W., Sui, L., Huang, Q., Nan, Y., Liu, J., et al. (2022). Reactive Oxygen Species-Based Nanomaterials for the Treatment of Myocardial Ischemia Reperfusion Injuries. *Bioact. Mater* 7, 47–72. doi:10.1016/j.bioactmat.2021.06.006

Zhu, L., Yang, Y., Farquhar, K., Wang, J., Tian, C., Ranville, J., et al. (2016). Surface Modification of Gd Nanoparticles with pH-Responsive Block Copolymers for Use as Smart MRI Contrast Agents. *ACS Appl. Mater Interfaces* 8 (7), 5040–5050. doi:10.1021/acsami.5b12463

Zhu, Y., Zhao, T., Liu, M., Wang, S., Liu, S., Yang, Y., et al. (2022). Rheumatoid Arthritis Microenvironment Insights into Treatment Effect of Nanomaterials. *Nano Today* 42, 101358. doi:10.1016/j.nantod.2021.101358

Conflict of Interest: The authors declare that the research was conducted in the absence of any commercial or financial relationships that could be construed as a potential conflict of interest.

Publisher's Note: All claims expressed in this article are solely those of the authors and do not necessarily represent those of their affiliated organizations, or those of the publisher, the editors, and the reviewers. Any product that may be evaluated in this article, or claim that may be made by its manufacturer, is not guaranteed or endorsed by the publisher.

Copyright © 2022 Jin, Yang, Wang, Li and Xu. This is an open-access article distributed under the terms of the Creative Commons Attribution License (CC BY). The use, distribution or reproduction in other forums is permitted, provided the original author(s) and the copyright owner(s) are credited and that the original publication in this journal is cited, in accordance with accepted academic practice. No use, distribution or reproduction is permitted which does not comply with these terms.

frontiers | Frontiers in Oncology

REVIEW
published: 28 June 2022
doi: 10.3389/fonc.2022.928797

Nanoparticle-Based Combination Therapy for Melanoma

Hongbo Chen[1†], *Kai Hou*[1†], *Jing Yu*[1†], *Le Wang*[2*] *and Xue Chen*[1*]

[1] *Department of Plastic and Cosmetic Surgery, Tongji Hospital, Tongji Medical College, Huazhong University of Science and Technology, Wuhan, China,* [2] *Department of Nephrology, Tongji Hospital, Tongji Medical College, Huazhong University of Science and Technology, Wuhan, China*

Melanoma is a cutaneous carcinoma, and its incidence is rapidly increasing with every year. The treatment options for melanoma have been comprehensively studied. Conventional treatment methods (e.g., radiotherapy, chemotherapy and photodynamic therapy) with surgical removal inevitably cause serious complications; moreover, resistance is common. Nanoparticles (NPs) combined with conventional methods are new and promising options to treat melanoma, and many combinations have been achieving good success. Due to their physical and biological features, NPs can help target intended melanoma cells more efficiently with less damage. This creates new hope for a better treatment strategy for melanoma with minimum damage and maximum efficacy.

Keywords: nanoparticles, combined therapy, melanoma, chemotherapy, immunotherapy, photodynamic therapy

OPEN ACCESS

Edited by:
Kelong Ai,
Central South University, China

Reviewed by:
Huan He,
Jilin University, China
Qiong Huang,
Central South University, China

***Correspondence:**
Xue Chen
chenxue_tongji@outlook.com
Le Wang
lwang1@foxmail.com

[†]These authors have contributed equally to this work

Specialty section:
This article was submitted to Pharmacology of Anti-Cancer Drugs, a section of the journal Frontiers in Oncology

Received: *26 April 2022*
Accepted: *31 May 2022*
Published: *28 June 2022*

Citation:
Chen H, Hou K, Yu J, Wang L and Chen X (2022) Nanoparticle-Based Combination Therapy for Melanoma. Front. Oncol. 12:928797. doi: 10.3389/fonc.2022.928797

INTRODUCTION

Overview of Melanoma

Melanoma is a malignant tumour originating from cells called melanocytes. The melanocytes can synthesise melanin, which imparts colour to the skin (1). They are located in the deepest layer of the epidermis and usually protect us from sunburn. Excessive exposure to ultraviolet (UV) radiation increases the occurrence of melanoma (2–5).

Melanoma can form from a congenital or *de novo* nevus. It can appear anywhere on the body, mainly on the parts that are more exposed to the sun, such as the face, leg, arm, and body (6). Low exposed parts have less possibilities to develop the disease, such as the feet.

Although the clinical appearance of a pigmented or unpigmented (amelanotic) lesion with sudden change can be clues for diagnosis, histological staining and classification can predict the prognosis (7). The prognosis is very poor when there is distant metastasis (8, 9).

Epidemiology of Melanoma

Although melanoma accounts for only 1% of all skin cancers, it causes the highest number of deaths among all skin cancers (10). In the world, 324,635 new cases of melanoma were diagnosed in 2020

Abbreviations: AM, Acral melanoma; BRAF, v-raf murine sarcoma viral oncogene homolog B1; CTLs, Cytotoxic T-lymphocytes; CM, Cutaneous melanoma; DGBA-OVA-CpG, Guanidinobenzoic acid-ovalbumin-cytosine-guanine dinucleotides; EPR, Permeation and retention effect; UV, Ultraviolet; PDT, Photodynamic therapy; NPs, Nanoparticles; PSs, Photosensitisers; TWT, Triple wild type; MM, Mucosal melanoma; MAPK, The mitogen-activated protein kinase; MEK, Mitogen-activated protein kinase kinase; VEGF, Vascular endothelial growth factor; PBS, Phosphate-buffered saline; ROS, Reactive oxygen species; UVB, Ultraviolet B-rays; RAS, Rat sarcoma virus; NF1, Neurofibromatosis 1; UM, Uveal melanoma; DTIC, Dacarbazine.

and US constituted 106,000 new cases, which is nearly one third. Among all these new cases, 57,043 were dead around the world (11). It was the fifth most common cancer (excluding non-melanoma skin cancer). The incidence is slightly higher in men and usually occurs in people aged 55–84 years (10). It has increased rapidly during the last 50 years in the US, and the incidence varies with age, sex, and geographical location (12–15). There are some factors influencing the incidence of melanoma, and these are important for preventing the disease.

First one is Ethnicity: It is reported that fair-skinned Caucasian populations are more likely to be affected by melanoma (15, 16). This is because the absorption of UVB (Ultraviolet B-rays) radiation is 50% higher in dark-skinned people and results in lower cell death and malignant transformation (17). Geography also plays an important role: "Latitude gradient" is a phenomenon described by Lancaster; it shows a higher incidence of melanoma with increasing proximity to the equator (18–20). The third factor is Age: Elderly people are more susceptible to melanoma, and the highest incidence is among those aged 70–80 years (21). The last factor is sex: Men are more likely to develop melanoma in part because it is androgen driven (22).

The mortality rate due to melanoma is higher in men than in women worldwide (23), with the proportion of annual deaths in the US being 4.0:100,000 in men compared to 1.7:100,000 in women (24). The peak mortality rate is in the age group of 75–84 years and declines thereafter (24).

Subtypes of Melanoma

There are four subtypes of melanoma based on the tissue from which the primary tumour arises. The major subtype is cutaneous melanoma (CM), which usually accompanies the *BRAF*(v-raf murine sarcoma viral oncogene homolog B1), *RAS* (Rat sarcoma virus), *NF1*(Neurofibromatosis 1), and *TWT*(triple wild-type) mutations (25, 26). Acral melanoma (AM), a distinct form that originates in the palms, soles, and nail beds, is associated more with the *TWT* mutation (27).

Mucosal melanoma (MM), the rarest subtype, has a progressive onset in clinics. Compared to other mutations, loss of *PTEN* mutation or activation of *KIT* and *CCND1* or *CDK4* are more common in MM (28). The last subtype is uveal melanoma (UM), which develops from melanocytes in the uveal tract of the eye with predominantly *GNAQ* and *GNA11* mutations (29). In recent times, the cutaneous melanoma subtype has shown a better prognosis.

Melanoma divided according to the driving mutations also has four subtypes: *BRAF*-mutant, *NRAS*-mutant, *NF1*-loss, and *TWT*. The *BRAF*, *NRAS*, and *NF1* mutations activate the mitogen-activated protein kinase (MAPK) pathway and usually occur during the early stage of tumour (30).

Prognosis biomarkers and related treatments are under investigation, and most data comes from European countries. More sequencing data is needed from non-European countries in order to have a blueprint of the whole mutated genes from different races.

Molecular Pathology of Melanoma

Melanocytic neoplasms include benign lesions named melanocytic naevi, to malignant types termed melanomas, or even progressive stage, termed metastatic melanoma. Melanocytes, from which all melanocytic neoplasms originate, can grow out of control with excessive UV damage. There are almost 3 billion melanocytes in the skin of an average human being (31). Normally, melanocytes divide less than twice a year (32), and when the adjacent keratinocytes are damaged by UV radiation, melanocytes secrete melanin to protect the keratinocyte nucleus from DNA damage (33).

Melanocytic naevi are benign proliferation of melanocytes and are normally unlikely to progress to melanoma. A common naevus is usually derived from the $BRAF^{V600E}$ mutation (34). Dysplastic naevi are an intermediate stage between naevi and melanoma (35, 36). The mutations that activate MAPK signalling and *TERT* promoter mutations or hemizygous alterations of *CDKN2A* are drivers of dysplastic naevi (34). Multiple dysplastic naevi are considered high risk factors for melanoma (35, 37)and they are obtaining *NRAS* mutation except $BRAF^{V600E}$ (34). *BRAF*, *NRAS*, and *TERT* mutations have been reported as the most likely mutations in melanoma *in situ* (38, 39). As MARK signalling plays an important role in melanoma, *TERT* mutations can lead to progression to invasive melanoma. *ARID2* and *ARID1A* are two genes that also influence the progression (34). For melanoma to metastasise to distant organs, the key is activation of genes in the WNT signalling pathway (40–42).

Treatment Strategies for Melanoma

Each tumour has its own feature, such as location, stage, and genetic profile; thus, the treatment strategy can be quite varied. The treatment options include surgical resection, chemotherapy, radiotherapy, photodynamic therapy (PDT), immunotherapy, or targeted therapy. For stage I–IIIB melanoma, surgical resection is the first choice (43–45) followed by targeted therapy and combined immunotherapy (44, 46). In case of distant metastasis, chemotherapy is necessary (45, 46). Chemotherapy is a good choice for advanced melanoma, and dacarbazine (DTIC) is the key agent (47); however, temozolomide can also be a good choice (47). BRAF inhibitors and MEK inhibitors were a breakthrough in the treatment of melanoma and around 15–20% of tumors finally show primary resistance to this treatment, and moreover, some patients even develop acquired resistance to therapy. The causes of drug resistance can be reactivation of MAPK pathway due to changes in the BRAF protein or interactions of BRAF inhibitors with wild type BRAF proteins (48). Electrochemotherapy is used as a tunnel to deliver drugs to the cells through an electric pulse (49, 50). No adverse effects have been reported, and 85% of patients responded to the treatment (49). However, there are few reports about this treatment, and more research is necessary. Some researchers combined PDT and DTIC, and it successfully reduced the resistance in metastatic melanoma (51).

Since the 19th century, researchers have found that the immune system plays an essential role in tumour metastasis (52). T cells can recognise the tumour cell antigens and destroy them. Interferon α-2b was reported to reduce the recurrence of melanoma and thus increase the patient survival (53); however, few patients responded to the treatment (54). Following this,

many more agents to treat melanoma were approved by the United States Food and Drug Administration, including Interleukin-2 in 1998 (55), Ontak (Treg inhibition) in 1999 (56), Peginterferon α-2b (Peg-IFN) and Ipilimumab (Cytotoxic T lymphocyte-associated antigen 4 (CTLA-4) blockade) in 2011 (53, 57),, Nivolumab (Programmed cell death protein 1 (PD-1)/ PD-1 ligand (PD-L1) blockade) in 2014 (58), and Talimogene laherparepvec as the first oncolytic virus therapy in 2015 (59). Other immune therapies are under investigation, such as Adoptive T-cell therapy (NCT03060356 and NCT02830724).

Bio-chemotherapy is the combination of chemotherapy and immunotherapy, and it did not show an overall improvement in survival (60). As mentioned earlier, melanoma is triggered by a bunch of gene mutations involved in different signalling pathways. *BRAF* inhibitors, including vemurafenib in 2011 (61), dabrafenib in 2013 (62), and encorafenib, which is currently undergoing clinical trials, are some choices to increase the overall survival; however, these agents have severe adverse effects. *MEK* (Mitogen-activated protein kinase kinase) inhibitors, tametinib in 2013 (63), cobimetinib in 2015 (64) are always administered in combination with *BRAF* inhibitors to treat melanoma. *VEGF* (Vascular endothelial growth factor) inhibitors (65), PI3K-AKT-mTOR pathway inhibitors (66), cyclin-dependent kinase inhibitors (67), and ErbB4 inhibitors (68) also target different signalling pathways to inhibit the growth of melanoma cells.

OVERVIEW OF NANOTECHNOLOGY IN CANCER

Nanotechnology is used to deliver medications to the cancer cells *via* nanoparticles (NPs) with minimum adverse effects (69). It is also used in cancer diagnosis, gene therapy, biomarker making, targeted therapy, and imaging. NPs, due to their biological features, can target the cancer cells precisely with little damage to the healthy organs (70). Nanocarriers including liposomes, carbon nanotubes, polymeric micelles, dendrimers, and quantum dots are increasingly widely used in cancer treatment. Liposomes are nanocarriers composed of lipid bilayers encapsulating an aqueous core. The structure of carbon nanotubes is a hollow sphere, ellipsoid and/or tube. Polymeric micelles are nanoscopic core structures derived from amphiphilic block copolymers. Dendrimers are formed by a small atom or group of atoms surrounded by dendrons, which can be classified as nanosized, symmetrical molecules. Quantum dots are nanoscale crystals which are made by human to transport electrons. All of them are applied in different fields and help to delivery drugs.

Some NPs are used to diagnose cancer, like MoS2 nanomaterials used as a platform material in bladder cancer diagnosis (71);NPs as biomarker in the diagnosis of early ovarian cancer (72).And some NPs are used to treat diseases, like NPs based on ROS even can be used in the treatment of myocardial ischemia reperfusion injury (73):NPs based on rheumatoid arthritis microenvironment can be a new direction for rheumatoid arthritis treatment (74). Different NPs based on different physical properties can be used in different ways.

NPs for Drug Delivery

Drug delivery is the process by which the medication from outside the body reaches the organs or cells (**Figure 1**). The reticuloendothelial system of the liver and kidney can filter most of the intravenously administered NPs (75). Most of the NPs are degraded, and few that are not degraded are retained. The Kupffer cells, which are phagocytic immune cells lining the liver sinusoids, are the key cells for the elimination of NPs (76). Actually, if the target system is reticuloendothelial system, the NPs can perfectly satisfy the demands since they can always reach the renal system effectively (77). While the NPs pass through the other organs, they are eliminated depending on their physical and biological features.

Once the NPs reach the target organs, they need to exit the vasculature and enter the targeted cells. They exit from the vasculature depends on the physiology of the vessel. In the liver, the NPs should be <100 nm (78), while in the kidney, it should be <6 nm (79). Transferring the NPs to the brain is even more difficult because of the blood–brain barrier (80). Extracellular matrix and connective tissue cells are tissue stroma, and these become barriers for NPs to enter the target cells. The cells absorb the particles in different ways, such as membrane fusion (81), caveolin-mediated endocytosis (82), clathrin-mediated endocytosis (83), micropinocytosis (84), or phagocytosis (85). The last step is when the NPs reach to the actual subcellular location for action. In this process, the challenge is how to escape the endosome.

There are two methods to increase the delivery efficiency: 1. Reduce the number of barriers by changing the route of administration. More barriers, more degradation. How to reach the destinated organs or cells with less elimination is of great concern. 2. Change the targeted position to make the delivery easier. For example, if the melanoma cells are hard to target, maybe we can aim to target the microenvironment easier. How to design the best NPs and the routes of administration are the two current areas of research advances in NPs and Melanoma.

With conventional treatments, such as surgical resection, chemotherapy, radiotherapy, PDT, immunotherapy, or targeted therapy, chemotherapy drugs lack specificity for tumor sites, and melanoma cells often develop drug resistance to these drugs. Sometimes the drugs achieve minimal therapeutic effect but lots of side effects. Also, tumor-driven immunosuppression makes the immunotherapy hard to work and metastasis rate is still high (86). More and more researchers are trying to find new therapeutic approaches to treat melanoma. The aim is to target the melanoma cells more specifically with minimal adverse effects, using the small size and components of NPs (87). Liposomes and niosomes, polymeric NPs, inorganic particles, carbon nanotubes, and others are good vesicular carriers. The factors concerned in the melanoma NPs carriers included the core, targeting ligands, and the stimulation triggers of releasing the cargo (88). We discuss in the following sections,

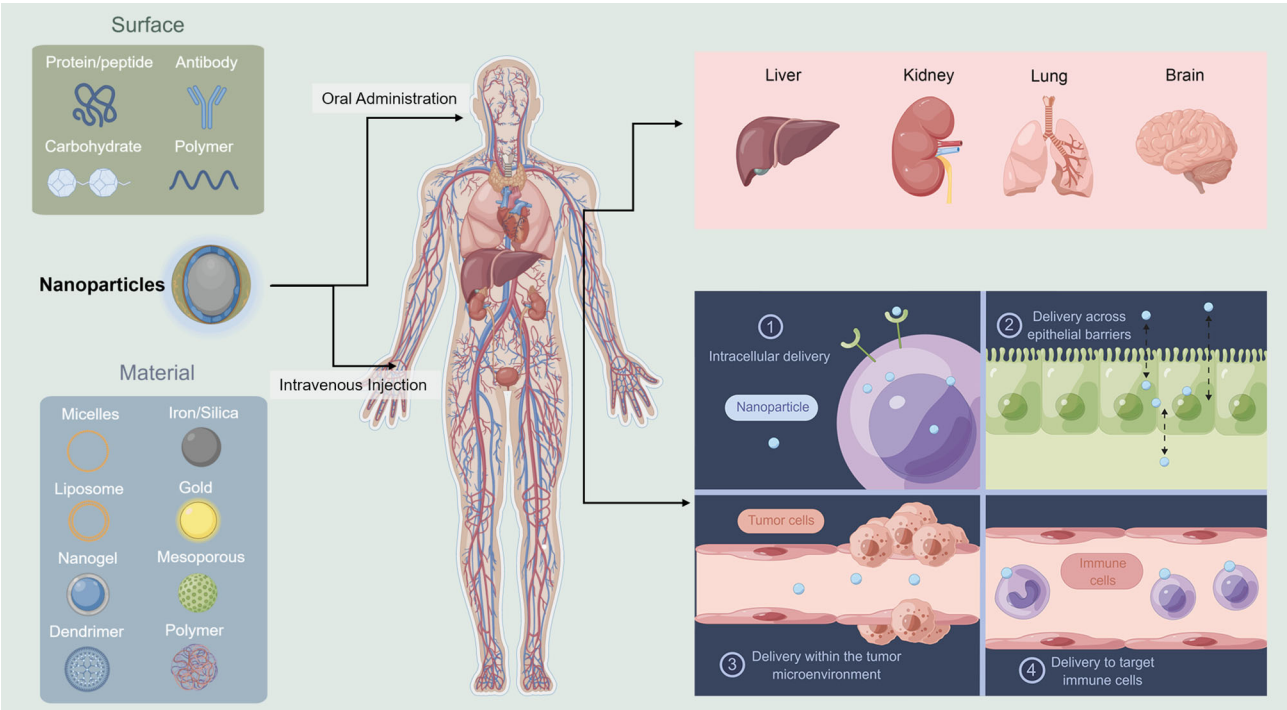


FIGURE 1 | Schematic illustration of nanoparticles delivery system. Liver and kidney can filter most of the NPs. Different NPs are used in different administration ways (This figure was drawn by Figdraw).

NPs in combination with chemotherapy, immunotherapy, or radiotherapy for the treatment of melanoma (**Figure 2**) (89).

NPs and Chemotherapy Combined Treatment

Chemotherapy with DTIC is the standard treatment approved by the United States Food and Drug Administration. In a British study, the response rate to DTIC was 16%, with a 6-year survival rate of 31% (47). Monotherapy can achieve little in the treatment of melanoma, and even polytherapy cannot prolong the overall survival (89). Chemotherapy has a low response rate (12%) and combination with immune checkpoint inhibitor also cannot cure advanced melanoma (90). Adverse effects, less sensitivity, high toxicity, and drug resistance are the most common challenges associated with chemotherapy.

NPs are used as carriers to deliver drugs to the intended cells in the organs. NPs reduce systemic toxicity and degradation through the delivery process (87, 91). Meanwhile, NPs have the preferential accumulation in the melanoma, owing to the enhanced EPR (permeation and retention effect), which could promote their cellular uptake. They can regulate the pH, temperature, and responsiveness of enzymes due to their physical characteristics. They can pass easily through the vessels because of their small size and reach the targeted cells. NPs can also increase the concentration of the chemotherapy drugs in the intended organs. There are two mechanisms by which NPs deliver the drugs to the targeted cells: passive and active targeting. In passive targeting, NPs can increase the permeability and retention of drugs in the designated organs. In active targeting, NPs increase the accuracy of targeting and uptake of the drug by increasing the ability of ligands to recognise the tumour cell receptors.

There are many successful investigations with the combination of NPs and chemotherapy. The drug doxorubicin encoded by carbon nanotubes increased cell death (90%) by inducing a moderate G2-M phase arrest (17.7 ± 1.1%) and reduced tumour size in mice bearing B16–F10 melanoma (92). Another group of researchers tried to encode doxorubicin with chitosan/alginate NPs and showed a lower rate of release of doxorubicin, better transport, and higher intracellular concentration (93) due to the sustained release of the drug which provided better accumulation and longer cytotoxic effect of encapsulated doxorubicin in melanoma cell lines. More and more NPs were developed to encode chemotherapeutic agents. NPs/10-Hydroxycamptothecin encapsulated by NPs was designed to enhance the tumour penetration capability for chemotherapy. The proliferation of melanoma cell lines (B16F10 and B16F1) decreased, and apoptosis increased with this treatment (94). The tumour growth was also inhibited compared to that seen in PBS (Phosphate-buffered saline) injected tumour-bearing mice. This effect was considers derived from the positive surface of NPs/HCPT enhanced cells internalization through endocytosis. A new nanoformulation of paclitaxel-loaded cholic acid-functionalised star-shaped poly

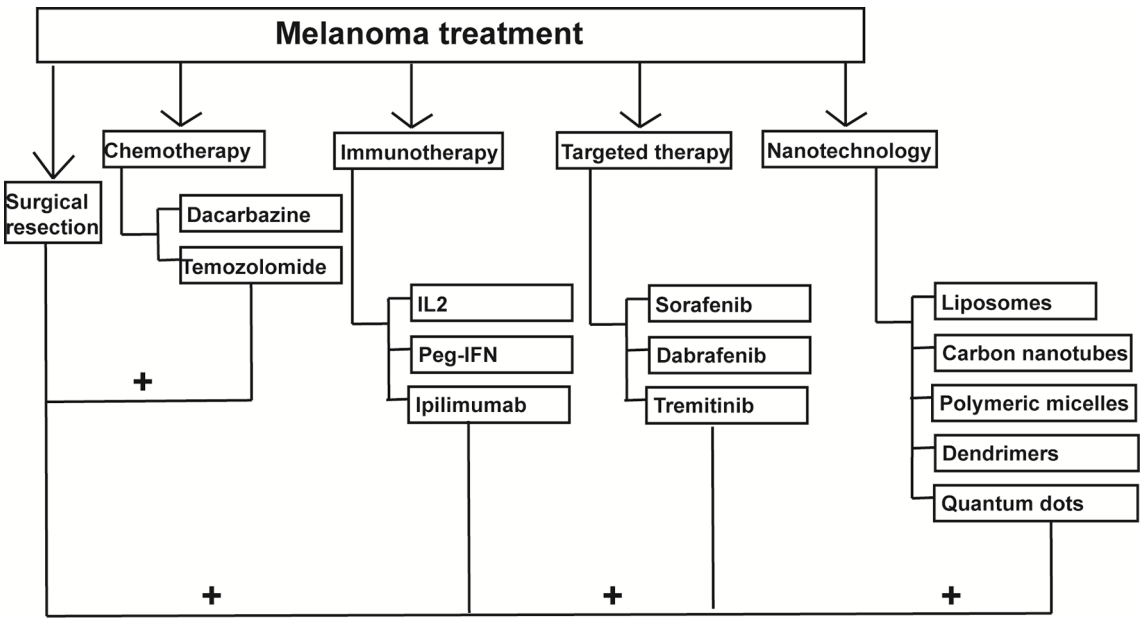


FIGURE 2 | Nanoparticles-mediated combination therapies for melanoma treatment. Nanoparticles can be combined with chemotherapy, immunotherapy and photodynamic therapy to treat melanoma.

(lactide-co-glycolide) (PLGA)-d-α-tocopheryl polyethylene glycol 1000 succinate (TPGS) NPs (PTX-loaded CAPLGA-TPGS NPs) was produced by Yongsheng et al. to treat malignant melanoma, and it showed a higher rate of release rate (78.69%), higher cellular uptake efficiency, and reduced growth of tumours in mice compared to those treated with saline (95). This year, DTIC (Dacarbazine)-NPs(Cholic acid -poly (lactide-co-glycolide)-b-polyethylene glycol)-Apt(nucleic acid aptamer AS1411) was developed to treat melanoma cell lines and showed good toxicity to MM but few side effects (96). The combination of NPs and chemotherapy have increased the EPR of the chemotherapy drug although different mechanisms.

Combined Treatment Using NPs and Immunotherapy

Immunotherapy aims to enhance or inhibit the immune system and can be classified as active and passive immunotherapy (97), depending on the method of boosting the immune response i.e., using an antigen or the intrinsic immune response itself. However, immunotherapy can cause many adverse effects, like attacking healthy organs, changing the immune system, or resistance (98). The rate of primary and secondary resistance to immunotherapy drugs like checkpoint inhibitors is increasing every year.

NPs help in enhancing the effect of immunotherapy in melanoma through different mechanisms (86, 99): 1. As the tumour cells inhibit the immune response, the accumulation of NPs at the site of the primary tumour can relieve the immunosuppressive effect and help the immune system recognise the tumour cells and kill them. Cancer immunoediting is a process that targets the microenvironment and enables the melanoma cells to escape the killing effect of the immune system. NPs try to target the macrophages and NK cells to boost the immune system, inhibit tumour growth, and prevent recurrence. NPs can also induce tumour immunogenic cell death or generate more tumour-associated antigens. 2. NPs can target the peripheral immune cells to inhibit tumour growth or mimic the artificial immune cells or improve the efficacy of adoptive T cells. 3. NPs prevent the formation of the pre-metastatic niche by reducing inflammation and myeloid-derived suppressor cells. 4. Prevent recurrence by directly applying the NPs on the surgical wounds.

Many NPs are under investigation for clinical use. Nanovaccine is one option. DGBA-OVA-CpG (Guanidinobenzoic acid-ovalbumin-cytosine-guanine dinucleotides) nanovaccine increased the antigen-presenting cells such as dendritic cells *in vitro* and *in vivo*. It also increased the generation of circulating interferon-γ+ CTLs (Cytotoxic T-lymphocytes) 4 times compared to that in the control group. The combination of DGBA-OVA-CpG nanovaccine with anti-PD-1 blockade significantly reduced the growth of melanoma in mice compared to that in the control group (by more than 50%), and the survival rate increased by nearly 37.5% (100). It raised great interest for researchers to develop vaccines constructed by dendrimers capable of cytosol delivery of proteins to treat melanoma. A hydrogel system was used to deliver celecoxib and PD-1 blockade to treat B16-F10 melanoma in mice to increase the antitumour effect of PD-1 blockade. This method decreased the tumour size to nearly 10% compared to that in the control group and increased the survival in mice (101). Synergistically delivery both celecoxib and PD-1 from this hydrogel system enhanced the presence of $CD4^+$ T cells and $CD8^+$ T cells in the immune system and finally formed an impaired pro-tumor angiogenic and inflammatory microenvironment.

NPs and Photodynamic Therapy (PDT) Combined Treatment

PDT promotes the accumulation of photosensitisers (PSs) activated by irradiation in the targeted organs or cells and kills the disease cells through ROS generated by photosensitizers. Permeability and retention are the most important challenges in conventional photodynamic therapy. Although PS is not recommended by the guidelines, it is still a useful adjuvant therapy, and many researchers have attempted to increase the efficacy of PS. NPs, which have a smaller size, can increase the permeability, target the cells more precisely and reduce the degradation of PDT. NPs can increase the solubility of PSs in water and thus increase their absorption rate. Furthermore, NPs reduce the elimination of PSs and increase the retention time. NPs, due to their small size and physical characteristics, make the penetration of PSs to the targeted cells easier. As diseased cells can adapt their own oxidative system and develop resistance to the treatment, NPs help overcome this challenge through high ROS (Reactive oxygen species) production.

5-aminolaevulinic acid-mediated photodynamic therapy was used to treat the A375 melanoma cell lines and showed decreased survival and increased apoptosis (102). 5-ALA caused the accumulation of endogenous photosensitizer protoporphyrin IX (PpIX) in the mitochondria of cells, thus increasing the apoptosis of melanoma cells and the mechanism of this can contribute to improve the therapeutic efficacy. Zhao et al. tried to encapsulate phthalocyanine 4 using silica NPs to treat different melanoma cell lines and showed higher permeability and lower cell survival than controls (103). Modifying the surface of silicon nanoparticles to encapsulate the photosensitizers and the antibodies specific to melanoma cells can be a new method in melanoma treatment. Yttrium oxide NPs were also used in combination with X-rays to treat melanoma cells. Porosnicu found that it increased the production of ROS,thus influenced the integrity of the mitochondria and increased the DNA damage (104). Magnetic NPs and albumin-stabilised paclitaxel NPs are also under investigation for combination therapy.

There are some clinical trials about the combination of NPs and PDT. Verteporfin with laser irradiation was the most used combination, and it reduced tumour growth with less regression; however, more data of the clinical trials is necessary.

CONCLUSIONS AND PERSPECTIVES

The incidence of melanoma is increasing rapidly, and several patients develop distant metastasis. The main cause of melanoma is excess UV light exposure. Although surgical removal is the core strategy to treat melanoma, adjuvant therapies, including chemotherapy, immunotherapy, PDT therapy are also combined with surgery. Due to the low permeability, short retention, and high resistance to the existing therapeutic agents, new methods to treat melanoma are urgently needed.

NPs due to their unique physical features, are under investigation. Combinations of liposomes, carbon nanotubes, polymeric micelles, dendrimers and quantum dots, and other technologies with conventional adjuvant therapies are being attempted to deliver the drug more efficiently, reduce the degradation and toxicity, and target the intended cells more accurately. Although considerable progress has been achieved in the previous years, agents with further increased specificity, smaller size, and lower toxicity are needed and the technologies to combine them with conventional medications are still necessary. Moreover, clinical trials should be initiated to test the NPs to increase their use in clinics.

AUTHOR CONTRIBUTIONS

All authors contributed to the design of the study and writing of the manuscript. HC, KH, and JY undertook the research. KH, HC, and XC wrote the main manuscript text and prepared figures. LW and XC revised the article critically for important intellectual content and final approval of the version to be submitted. JY responded to the reviewers' questions and revision manuscript preparation. All authors reviewed the manuscript.

FUNDING

This study was financially support by the foundation from the National Natural Science Foundation of China (No.81873630).

REFERENCES

1. Goldsmith HS. Melanoma: An Overview. *CA Cancer J Clin* (1979) 29:194–215. doi: 10.3322/canjclin.29.4.194
2. Kelly JW, Rivers JK, MacLennan R, Harrison S, Lewis AE, Tate BJ. Sunlight: A Major Factor Associated With the Development of Melanocytic Nevi in Australian Schoolchildren. *J Am Acad Dermatol* (1994) 30:40–8. doi: 10.1016/S0190-9622(94)70005-2
3. Pavlotsky F, Azizi E, Gurvich R, Lusky A, Barell V, Weiner M, et al. Prevalence of Melanocytic Nevi and Freckles in Young Israeli Males: Correlation With Melanoma Incidence in Jewish Migrants: Demographic and Host Factors. *Am J Epidemiol* (1997) 146:78–86. doi: 10.1093/oxfordjournals.aje.a009193
4. Breitbart M, Garbe C, Büttner P, Weiss J, Soyer HP, Stocker U, et al. Ultraviolet Light Exposure, Pigmentary Traits and the Development of Melanocytic Naevi and Cutaneous Melanoma. A Case-Control Study of the German Central Malignant Melanoma Registry. . *Acta Derm Venereol* (1997) 77:374–8. doi: 10.2340/0001555577374378
5. Luther H, Altmeyer P, Garbe C, Ellwanger U, Jahn S, Hoffmann K, et al. Increase of Melanocytic Nevus Counts in Children During 5 Years of Follow-Up and Analysis of Associated Factors. *Arch Dermatol* (1996) 132:1473–8. doi: 10.1001/archderm.132.12.1473
6. Mort RL, Jackson IJ, Patton EE. The Melanocyte Lineage in Development and Disease. *Development* (2015) 142:620–32. doi: 10.1242/dev.106567
7. Breslow A. Thickness, Cross-Sectional Areas and Depth of Invasion in the Prognosis of Cutaneous Melanoma. *Ann Surg* (1970) 172:902–8. doi: 10.1097/00000658-197011000-00017
8. Bombelli FB, Webster CA, Moncrieff M, Sherwood V. The Scope of Nanoparticle Therapies for Future Metastatic Melanoma Treatment. *Lancet Oncol* (2014) 15:e22–32. doi: 10.1016/S1470-2045(13)70333-4
9. Jiang B-P, Zhang L, Guo X-L, Shen X-C, Wang Y, Zhu Y, et al. Poly (N -Phenylglycine)-Based Nanoparticles as Highly Effective and Targeted Near-Infrared Photothermal Therapy/Photodynamic Therapeutic Agents

for Malignant Melanoma. *Small* (2017) 13:1602496. doi: 10.1002/smll.201602496
10. *National Cancer Institute Melanoma of the Skin-Cancer Stat Facts*. Available at: https://seercancergov/statfacts/html/.melan.html (Accessed 10 May 2021).
11. Saginala K, Barsouk A, Aluru JS, Rawla P, Barsouk A. Epidemiology of Melanoma. *Med Sci* (2021) 9:63. doi: 10.3390/medsci9040063
12. Erdei E, Torres SM. A New Understanding in the Epidemiology of Melanoma. *Expert Rev Anticancer Ther* (2010) 10:1811–23. doi: 10.1586/era.10.170
13. Whiteman DC, Green AC, Olsen CM. The Growing Burden of Invasive Melanoma: Projections of Incidence Rates and Numbers of New Cases in Six Susceptible Populations Through 2031. *J Invest Dermatol* (2016) 136:1161–71. doi: 10.1016/j.jid.2016.01.035
14. Olsen CM, Neale RE, Green AC, Webb PMthe QSkin Study, the Epigene Study, , Whiteman DC. Independent Validation of Six Melanoma Risk Prediction Models. *J Invest Dermatol* (2015) 135:1377–84. doi: 10.1038/jid.2014.533
15. Padovese V, Franco G, Valenzano M, Pecoraro L, Cammilli M, Petrelli A. Skin Cancer Risk Assessment in Dark Skinned Immigrants: The Role of Social Determinants and Ethnicity. *Ethn Health* (2018) 23:649–58. doi: 10.1080/13557858.2017.1294657
16. Chao LX, Patterson SSL, Rademaker AW, Liu D, Kundu RV. Melanoma Perception in People of Color: A Targeted Educational Intervention. *Am J Clin Dermatol* (2017) 18:419–27. doi: 10.1007/s40257-016-0244-y
17. Brenner M, Hearing VJ. The Protective Role of Melanin Against UV Damage in Human Skin. *Photochem Photobiol* (2008) 84:539–49. doi: 10.1111/j.1751-1097.2007.00226.x
18. Lancaster HO. Some Geographical Aspects of the Mortality From Melanoma in Europeans. *Med J Aust* (1956) 43:1082–7. doi: 10.5694/j.1326-5377.1956.tb36084.x
19. Lancaster HO, Nelson J. Sunlight as a Cause of Melanoma; a Clinical Survey. *Med JAust.* (1957) 44:452–6. doi: 10.5694/j.1326-5377.1957.tb59648.x
20. Elwood JM, Lee JAH, Walter SD, Mo T, Green AES. Relationship of Eelanoma and Other Skin Cancer Mortality to Latitude and Ultraviolet Radiation in the United States and Canada. *Int J Epidemiol* (1974) 3:325–32. doi: 10.1093/ije/3.4.325
21. GLOBOCAN 2012 V1.0. Cancer Incidence and Mortality Worldwide. In: *IARC CancerBase No 11*. IARC CancerBase: GLOBOCAN
22. Li W-Q, Qureshi AA, Ma J, Goldstein AM, Giovannucci EL, Stampfer MJ, et al. Personal History of Prostate Cancer and Increased Risk of Incident Melanoma in the United States. *J Clin Oncol* (2013) 31:4394–9. doi: 10.1200/JCO.2013.51.1915
23. Shen W, Sakamoto N, Yang L. Melanoma-Specific Mortality and Competing Mortality in Patients With non-Metastatic Malignant Melanoma: A Population-Based Analysis. *BMC Cancer* (2016) 16:413. doi: 10.1186/s12885-016-2438-3
24. Surveillance, Epidemiology and End Results (SEER) Program Cancer Statistics Review. 1975–2013. In: *Natl Cancer Inst [Internet] Novemb 2015 SEER Data Submiss [Cited Posted to SEER Web Site, 2016 Apr]* (2015). Natl Cancer Inst: SEER database
25. Vidak S, Foisner R. Molecular Insights Into the Premature Aging Disease Progeria. *Histochem Cell Biol* (2016) 145:401–17. doi: 10.1007/s00418-016-1411-1
26. Akbani R, Akdemir KC, Aksoy BA, Albert M, Ally A, Amin SB, et al. Genomic Classification of Cutaneous Melanoma. *Cell* (2015) 161:1681–96. doi: 10.1016/j.cell.2015.05.044
27. Liang WS, Hendricks W, Kiefer J, Schmidt J, Sekar S, Carpten J, et al. Integrated Genomic Analyses Reveal Frequent TERT Aberrations in Acral Melanoma. *Genome Res* (2017) 27:524–32. doi: 10.1101/gr.213348.116
28. Furney SJ, Turajlic S, Stamp G, Nohadani M, Carlisle A, Thomas JM, et al. Genome Sequencing of Mucosal Melanomas Reveals That They Are Driven by Distinct Mechanisms From Cutaneous Melanoma. *J Pathol* (2013) 230:261–9. doi: 10.1002/path.4204
29. Moore AR, Ceraudo E, Sher JJ, Guan Y, Shoushtari AN, Chang MT, et al. Recurrent Activating Mutations of G-Protein-Coupled Receptor CYSLTR2 in Uveal Melanoma. *Nat Genet* (2016) 48:675–80. doi: 10.1038/ng.3549
30. Shain AH, Joseph NM, Yu R, Benhamida J, Liu S, Prow T, et al. Genomic and Transcriptomic Analysis Reveals Incremental Disruption of Key Aignaling Pathways During Melanoma Evolution. *Cancer Cell* (2018) 34:45–55.e4. doi: 10.1016/j.ccell.2018.06.005
31. Kanitakis J. Anatomy, Histology and Immunohistochemistry of Normal Human Skin. *Eur J Dermatol* (2002) 12:390–9.
32. Jimbow K, Roth SI, Fitzpatrick TB, Szabo G. Mitotic Activity in non-Neoplastic Melanocytes *In Vivo* as Determined by Histochemical, Autoradiographic, and Electron Microscope Studies. *J Cell Biol* (1975) 66:663–70. doi: 10.1083/jcb.66.3.663
33. Kaidbey KH, Agin PP, Sayre RM, Kligman AM. Photoprotection by Melanin—A Comparison of Black and Caucasian Skin. *J Am Acad Dermatol* (1979) 1:249–60. doi: 10.1016/S0190-9622(79)70018-1
34. Shain AH, Yeh I, Kovalyshyn I, Sriharan A, Talevich E, Gagnon A, et al. The Genetic Evolution of Melanoma From Precursor Lesions. *N Engl J Med* (2015) 373:1926–36. doi: 10.1056/NEJMoa1502583
35. Duffy K, Grossman D. The Dysplastic Nevus: From Historical Perspective to Management in the Modern Era. *J Am Acad Dermatol* (2012) 67:1. doi: 10.1016/j.jaad.2012.02.047
36. Kanzler MH, Mraz-Gernhard S. Primary Cutaneous Malignant Melanoma and Its Precursor Lesions: Diagnostic and Therapeutic Overview. *J Am Acad Dermatol* (2001) 45:260–76. doi: 10.1067/mjd.2001.116239
37. Rigel DS, Rivers JK, Kopf AW, Friedman RJ, Vinokur AF, Heilman ER, et al. Dysplastic Nevi.Markers for Increased Risk for Melanoma. *Cancer* (1989) 63:386–9. doi: 10.1002/1097-0142(19890115)63:2<386::AID-CNCR2820630231>3.0.CO;2-6
38. Dong J, Phelps RG, Qiao R, Yao S, Benard O, Ronai Z, et al. BRAF Oncogenic Mutations Correlate With Progression Rather Than Initiation of Human Melanoma. *Cancer Res* (2003) 63:3883–5.
39. Yazdi AS, Palmedo G, Flaig MJ, Puchta U, Reckwerth A, Rütten A, et al. Mutations of the BRAF Gene in Benign and Malignant Melanocytic Lesions. *J Invest Dermatol* (2003) 121:1160–2. doi: 10.1046/j.1523-1747.2003.12559.x
40. Turajlic S, Furney SJ, Lambros MB, Mitsopoulos C, Kozarewa I, Geyer FC, et al. Whole Genome Sequencing of Matched Primary and Metastatic Acral Melanomas. *Genome Res* (2012) 22:196–207. doi: 10.1101/gr.125591.111
41. Gartner JJ, Davis S, Wei X, Lin JC, Trivedi NS, Teer JK, et al. Comparative Exome Sequencing of Metastatic Lesions Provides Insights Into the Mutational Progression of Melanoma. *BMC Genomics* (2012) 13:505. doi: 10.1186/1471-2164-13-505
42. Ding L, Kim M, Kanchi KL, Dees ND, Lu C, Griffith M, et al. Clonal Architectures and Driver Mutations in Metastatic Melanomas. *PloS One* (2014) 9:e111153. doi: 10.1371/journal.pone.0111153
43. Miller KD, Siegel RL, Lin CC, Mariotto AB, Kramer JL, Rowland JH, et al. Cancer Treatment and Survivorship Statistics, 2016. *CA Cancer J Clin* (2016) 66:271–89. doi: 10.3322/caac.21349
44. van Zeijl MCT, van den Eertwegh AJ, Haanen JB, Wouters MWJM. (Neo) adjuvant Systemic Therapy for Melanoma. *Eur J Surg Oncol* (2017) 43:534–43. doi: 10.1016/j.ejso.2016.07.001
45. Batus M, Waheed S, Ruby C, Petersen L, Bines SD, Kaufman HL. Optimal Management of Metastatic Melanoma: Current Strategies and Future Directions. *Am J Clin Dermatol* (2013) 14:179–94. doi: 10.1007/s40257-013-0025-9
46. Austin E, Mamalis A, Ho D, Jagdeo J. Laser and Light-Based Therapy for Cutaneous and Soft-Tissue Metastases of Malignant Melanoma: A Systematic Review. *Arch Dermatol Res* (2017) 309:229–42. doi: 10.1007/s00403-017-1720-9
47. Kim C, Lee CW, Kovacic L, Shah A, Klasa R, Savage KJ. Long-Term Survival in Patients With Metastatic Melanoma Treated With DTIC or Temozolomide. *Oncologist* (2010) 15:765–71. doi: 10.1634/theoncologist.2009-0237
48. Czarnecka AM, Bartnik E, Fiedorowicz M, Rutkowski P. Targeted Therapy in Melanoma and Mechanisms of Resistance. *Int J Mol Sci* (2020) 21:4576. doi: 10.3390/ijms21134576
49. Miklavčič D, Serša G, Brecelj E, Gehl J, Soden D, Bianchi G, et al. Electrochemotherapy: Technological Advancements for Efficient Electroporation-Based Treatment of Internal Tumors. *Med Biol Eng Comput* (2012) 50:1213–25. doi: 10.1007/s11517-012-0991-8

50. Testori A, Ribero S, Bataille V. Diagnosis and Treatment of in-Transit Melanoma Metastases. *Eur J Surg Oncol* (2017) 43:544–60. doi: 10.1016/j.ejso.2016.10.005
51. Biteghe FN, Davids L. A Combination of Photodynamic Therapy and Chemotherapy Displays a Differential Cytotoxic Effect on Human Metastatic Melanoma Cells. *J Photochem Photobiol B Biol* (2017) 166:18–27. doi: 10.1016/j.jphotobiol.2016.11.004
52. Balkwill F, Mantovani A. Inflammation and Cancer: Back to Virchow? *Lancet* (2001) 357:539–45. doi: 10.1016/S0140-6736(00)04046-0
53. Ives NJ, Suciu S, Eggermont AMM, Kirkwood J, Lorigan P, Markovic SN, et al. Adjuvant Interferon-α for the Treatment of High-Risk Melanoma: An Individual Patient Data Meta-Analysis. *Eur J Cancer* (2017) 82:171–83. doi: 10.1016/j.ejca.2017.06.006
54. Eggermont AMM, Suciu S, Rutkowski P, Kruit WH, Punt CJ, Dummer R, et al. Long Term Follow Up of the EORTC 18952 Trial of Adjuvant Therapy in Resected Stage IIB–III Cutaneous Melanoma Patients Comparing Intermediate Doses of Interferon-Alpha-2b (IFN) With Observation: Ulceration of Primary is Key Determinant for IFN-Sensitivity. *Eur J Cancer* (2016) 55:111–21. doi: 10.1016/j.ejca.2015.11.014
55. Krieg C, Létourneau S, Pantaleo G, Boyman O. Improved IL-2 Immunotherapy by Selective Stimulation of IL-2 Receptors on Lymphocytes and Endothelial Cells. *Proc Natl Acad Sci* (2010) 107:11906–11. doi: 10.1073/pnas.1002569107
56. Bobo D, Robinson KJ, Islam J, Thurecht KJ, Corrie SR. Nanoparticle-Based Medicines: A Review of FDA-Approved Materials and Clinical Trials to Date. *Pharm Res* (2016) 33:2373–87. doi: 10.1007/s11095-016-1958-5
57. Waterhouse P, Penninger JM, Timms E, Wakeham A, Shahinian A, Lee KP, et al. Lymphoproliferative Disorders With Early Lethality in Mice Deficient in Ctla-4. *Science (80-)* (1995) 270:985–8. doi: 10.1126/science.270.5238.985
58. Raedler LA. Opdivo (Nivolumab): Second PD-1 Inhibitor Receives FDA Approval for Unresectable or Metastatic Melanoma. *Am Heal Drug benefits* (2015) 8:180–3.
59. Pol J, Kroemer G, Galluzzi L. First Oncolytic Virus Approved for Melanoma Immunotherapy. *Oncoimmunology* (2016) 5:e1115641. doi: 10.1080/2162402X.2015.1115641
60. Samlowski WE, Moon J, Witter M, Atkins MB, Kirkwood JM, Othus M, et al. High Frequency of Brain Metastases After Adjuvant Therapy for High-Risk Melanoma. *Cancer Med* (2017) 6:2576–85. doi: 10.1002/cam4.1223
61. Chapman PB, Hauschild A, Robert C, Haanen JB, Ascierto P, Larkin J, et al. Improved Survival With Vemurafenib in Melanoma With BRAF V600E Mutation. *N Engl J Med* (2011) 364:2507–16. doi: 10.1056/NEJMoa1103782
62. Ballantyne AD, Garnock-Jones KP. Dabrafenib: First Global Approval. *Drugs* (2013) 73:1367–76. doi: 10.1007/s40265-013-0095-2
63. Livingstone E, Zimmer L, Vaubel J, Schadendorf D. BRAF. MEK and KIT Inhibitors for Melanoma: Adverse Events and Their Management. *Chin Clin Oncol* (2014) 3:29. doi: 10.3978/j.issn.2304-3865.2014.03.03
64. Niezgoda A, Niezgoda P, Czajkowski R. Novel Approaches to Treatment of Advanced Melanoma: A Review on Targeted Therapy and Immunotherapy. *BioMed Res Int* (2015) 2015:1–16. doi: 10.1155/2015/851387
65. Kim KJ, Li B, Winer J, Armanini M, Gillett N, Phillips HS, et al. Inhibition of Vascular Endothelial Growth Factor-Induced Angiogenesis Suppresses Tumour Growth *in vivo*. *Nature* (1993) 362:841–4. doi: 10.1038/362841a0
66. Li X, Wu D, Shen J, Zhou M, Lu Y. Rapamycin Induces Autophagy in the Melanoma Cell Line M14 *via* Regulation of the Expression Levels of Bcl-2 and Bax. *Oncol Lett* (2013) 5:167–72. doi: 10.3892/ol.2012.986
67. O'Leary B, Finn RS, Turner NC. Treating Cancer With Selective CDK4/6 Inhibitors. *Nat Rev Clin Oncol* (2016) 13:417–30. doi: 10.1038/nrclinonc.2016.26
68. Prickett TD, Agrawal NS, Wei X, Yates KE, Lin JC, Wunderlich JR, et al. Analysis of the Tyrosine Kinome in Melanoma Reveals Recurrent Mutations in ERBB4. *Nat Genet* (2009) 41:1127–32. doi: 10.1038/ng.438
69. Huang L, Hu J, Huang S, Wang B, Siaw-Debrah F, Nyanzu M, et al. Nanomaterial Applications for Neurological Diseases and Central Nervous System Injury. *Prog Neurobiol* (2017) 157:29–48. doi: 10.1016/j.pneurobio.2017.07.003
70. Chaturvedi VK, Singh A, Singh VK, Singh MP. Cancer Nanotechnology: A New Revolution for Cancer Diagnosis and Therapy. *Curr Drug Metab* (2019) 20:416–29. doi: 10.2174/1389200219666180918111528
71. Wang J, Sui L, Huang J, Miao L, Nie Y, Wang K, et al. MoS2-Based Nanocomposites for Cancer Diagnosis and Therapy. *Bioact Mater* (2021) 6:4209–42. doi: 10.1016/j.bioactmat.2021.04.021
72. Yang Y, Huang Q, Xiao Z, Liu M, Zhu Y, Chen Q, et al. Nanomaterial-Based Biosensor Developing as a Route Toward *In Vitro* Diagnosis of Early Ovarian Cancer. *Mater Today Bio* (2022) 13:100218. doi: 10.1016/j.mtbio.2022.100218
73. Zhao T, Wu W, Sui L, Huang Q, Nan Y, Liu J, et al. Reactive Oxygen Species-Based Nanomaterials for the Treatment of Myocardial Ischemia Reperfusion Injuries. *Bioact Mater* (2022) 7:47–72. doi: 10.1016/j.bioactmat.2021.06.006
74. Zhu Y, Zhao T, Liu M, Wang S, Liu S, Yang Y, et al. Rheumatoid Arthritis Microenvironment Insights Into Treatment Effect of Nanomaterials. *Nano Today* (2022) 42:101358. doi: 10.1016/j.nantod.2021.101358
75. Sadauskas E, Danscher G, Stoltenberg M, Vogel U, Larsen A, Wallin H. Protracted Elimination of Gold Nanoparticles From Mouse Liver. *Nanomedicine Nanotechnology Biol Med* (2009) 5:162–9. doi: 10.1016/j.nano.2008.11.002
76. Tsoi KM, MacParland SA, Ma X-Z, Spetzler VN, Echeverri J, Ouyang B, et al. Mechanism of Hard-Nanomaterial Clearance by the Liver. *Nat Mater* (2016) 15:1212–21. doi: 10.1038/nmat4718
77. Liliemark E, Sjöström B, Liliemark J, Peterson C, Kållberg N, Larsson BS. Targeting of Teniposide to the Mononuclear Phagocytic System (MPS) by Incorporation in Liposomes and Submicron Lipid Particles; an Autoradiographic Study in Mice. *Leuk Lymphoma* (1995) 18:113–8. doi: 10.3109/10428199509064930
78. Poon W, Zhang Y-N, Ouyang B, Kingston BR, Wu JLY, Wilhelm S, et al. Elimination Pathways of Nanoparticles. *ACS Nano* (2019) 13:5785–98. doi: 10.1021/acsnano.9b01383
79. Soo Choi H, Liu W, Misra P, Tanaka E, Zimmer JP, Itty Ipe B, et al. Renal Clearance of Quantum Dots. *Nat Biotechnol* (2007) 25:1165–70. doi: 10.1038/nbt1340
80. Saraiva C, Praça C, Ferreira R, Santos T, Ferreira L, Bernardino L. Nanoparticle-Mediated Brain Drug Delivery: Overcoming Blood–Brain Barrier to Treat Neurodegenerative Diseases. *J Control Release* (2016) 235:34–47. doi: 10.1016/j.jconrel.2016.05.044
81. Düzgüneş N, Nir S. Mechanisms and Kinetics of Liposome–Cell Interactions. *Adv Drug Delivery Rev* (1999) 40:3–18. doi: 10.1016/S0169-409X(99)00037-X
82. Sahay G, Kim JO, Kabanov AV, Bronich TK. The Exploitation of Differential Endocytic Pathways in Normal and Tumor Cells in the Selective Targeting of Nanoparticulate Chemotherapeutic Agents. *Biomaterials* (2010) 31:923–33. doi: 10.1016/j.biomaterials.2009.09.101
83. Harush-Frenkel O, Debotton N, Benita S, Altschuler Y. Targeting of Nanoparticles to the Clathrin-Mediated Endocytic Pathway. *Biochem Biophys Res Commun* (2007) 353:26–32. doi: 10.1016/j.bbrc.2006.11.135
84. Meng H, Yang S, Li Z, Xia T, Chen J, Ji Z, et al. Aspect Ratio Determines the Quantity of Mesoporous Silica Nanoparticle Uptake by a Small GTPase-Dependent Macropinocytosis Mechanism. *ACS Nano* (2011) 5:4434–47. doi: 10.1021/nn103344k
85. Lunov O, Syrovets T, Loos C, Beil J, Delacher M, Tron K, et al. Differential Uptake of Functionalized Polystyrene Nanoparticles by Human Macrophages and a Monocytic Cell Line. *ACS Nano* (2011) 5:1657–69. doi: 10.1021/nn2000756
86. Bei D, Meng J, Youan B-BC. Engineering Nanomedicines for Improved Melanoma Therapy: Progress and Promises. *Nanomedicine* (2010) 5:1385–99. doi: 10.2217/nnm.10.117
87. Gmeiner WH, Ghosh S. Nanotechnology for Cancer Treatment. *Nanotechnol Rev* (2014) 3:111–22. doi: 10.1515/ntrev-2013-0013
88. Song M, Liu C, Chen S, Zhang W. Nanocarrier-Based Drug Delivery for Melanoma Therapeutics. *Int J Mol Sci* (2021) 22:1873. doi: 10.3390/ijms22041873
89. Eigentler TK, Caroli UM, Radny P, Garbe C. Palliative Therapy of Disseminated Malignant Melanoma: A Systematic Review of 41 Randomised Clinical Trials. *Lancet Oncol* (2003) 4:748–59. doi: 10.1016/S1470-2045(03)01280-4
90. Goldinger SM, Buder-Bakhaya K, Lo SN, Forschner A, McKean M, Zimmer L, et al. Chemotherapy After Immune Checkpoint Inhibitor Failure in Metastatic Melanoma: A Retrospective Multicentre Analysis. *Eur J Cancer* (2022) 162:22–33. doi: 10.1016/j.ejca.2021.11.022

91. Su S, Kang PM. Systemic Review of Biodegradable Nanomaterials in Nanomedicine. *Nanomaterials* (2020) 10:656. doi: 10.3390/nano10040656
92. Chaudhuri P, Soni S, Sengupta S. Single-Walled Carbon Nanotube-Conjugated Chemotherapy Exhibits Increased Therapeutic Index in Melanoma. *Nanotechnology* (2010) 21:25102. doi: 10.1088/0957-4484/21/2/025102
93. Yoncheva K, Merino M, Shenol A, Daskalov NT, Petkov PS, Vayssilov GN, et al. Optimization and *in-Vitro/in-Vivo* Evaluation of Doxorubicin-Loaded Chitosan-Alginate Nanoparticles Using a Melanoma Mouse Model. *Int J Pharm* (2019) 556:1–8. doi: 10.1016/j.ijpharm.2018.11.070
94. Guo H, Li F, Qiu H, Liu J, Qin S, Hou Y, et al. Preparation and Characterization of Chitosan Nanoparticles for Chemotherapy of Melanoma Through Enhancing Tumor Penetration. *Front Pharmacol* (2020) 11:317. doi: 10.3389/fphar.2020.00317
95. Su Y, Hu J, Huang Z, Huang Y, Peng B, Xie N, et al. Paclitaxel-Loaded Star-Shaped Copolymer Nanoparticles for Enhanced Malignant Melanoma Chemotherapy Against Multidrug Resistance. *Drug Des Devel Ther* (2017) 11:659–68. doi: 10.2147/DDDT.S127328
96. Xiong W, Guo Z, Zeng B, Wang T, Zeng X, Cao W, et al. Dacarbazine-Loaded Targeted Polymeric Nanoparticles for Enhancing Malignant Melanoma Therapy. *Front Bioeng Biotechnol* (2022) 10:847901. doi: 10.3389/fbioe.2022.847901
97. Lesterhuis WJ, Haanen JBAG, Punt CJA. Cancer Immunotherapy – Revisited. *Nat Rev Drug Discov* (2011) 10:591–600. doi: 10.1038/nrd3500
98. Rothermel LD, Sarnaik AA, Khushalani NI, Sondak VK. Current Immunotherapy Practices in Melanoma. *Surg Oncol Clin N Am* (2019) 28:403–18. doi: 10.1016/j.soc.2019.02.001
99. Zhang P, Meng J, Li Y, Yang C, Hou Y, Tang W, et al. Nanotechnology-Enhanced Immunotherapy for Metastatic Cancer. *Innov* (2021) 2:100174. doi: 10.1016/j.xinn.2021.100174
100. Xu J, Wang H, Xu L, Chao Y, Wang C, Han X, et al. Nanovaccine Based on a Protein-Delivering Dendrimer for Effective Antigen Cross-Presentation and Cancer Immunotherapy. *Biomaterials* (2019) 207:1–9. doi: 10.1016/j.biomaterials.2019.03.037
101. Li Y, Fang M, Zhang J, Wang J, Song Y, Shi J, et al. Hydrogel Dual Delivered Celecoxib and Anti-PD-1 Synergistically Improve Antitumor Immunity. *Oncoimmunology* (2016) 5:1–12. doi: 10.1080/2162402X.2015.1074374
102. Cai J, Zheng Q, Huang H, Li B. 5-Aminolevulinic Acid Mediated Photodynamic Therapy Inhibits Survival Activity and Promotes Apoptosis of A375 and A431 Cells. *Photodiagnosis Photodyn Ther* (2018) 21:257–62. doi: 10.1016/j.pdpdt.2018.01.004
103. Pauff SM, Miller SC. Enhanced Photodynamic Efficacy Towards Melanoma Cells by Encapsulation of Pc4 *in Silica* Nanoparticles. *Bone* (2012) 78:711–6. doi: 10.1016/j.taap.2009.08.010.Enhanced
104. Porosnicu I, Butnaru CM, Tiseanu I, Stancu E, Munteanu CVA, Bita BI, et al. Y2O3 Nanoparticles and X-Ray Radiation-Induced Effects in Melanoma Cells. *Molecules* (2021) 26:3403. doi: 10.3390/molecules26113403

Conflict of Interest: The authors declare that the research was conducted in the absence of any commercial or financial relationships that could be construed as a potential conflict of interest.

Publisher's Note: All claims expressed in this article are solely those of the authors and do not necessarily represent those of their affiliated organizations, or those of the publisher, the editors and the reviewers. Any product that may be evaluated in this article, or claim that may be made by its manufacturer, is not guaranteed or endorsed by the publisher.

Copyright © 2022 Chen, Hou, Yu, Wang and Chen. This is an open-access article distributed under the terms of the Creative Commons Attribution License (CC BY). The use, distribution or reproduction in other forums is permitted, provided the original author(s) and the copyright owner(s) are credited and that the original publication in this journal is cited, in accordance with accepted academic practice. No use, distribution or reproduction is permitted which does not comply with these terms.

frontiers | Frontiers in Oncology

ORIGINAL RESEARCH
published: 30 June 2022
doi: 10.3389/fonc.2022.918416

Cu-Hemin Nanosheets and Indocyanine Green Co-Loaded Hydrogel for Photothermal Therapy and Amplified Photodynamic Therapy

Shu Zhu[1,2†], *Shuntao Wang*[3†], *Chunping Liu*[3†], *Meng Lyu*[4] *and Qinqin Huang*[1*]

[1] Department of Molecular Pathology, The Second Affiliated Hospital of Zhengzhou University, Zhengzhou, China, [2] Department of Medical Ultrasound, Tongji Hospital, Tongji Medical College, Huazhong University of Science and Technology, Wuhan, China, [3] Department of Breast and Thyroid Surgery, Union Hospital, Tongji Medical College, Huazhong University of Science and Technology, Wuhan, China, [4] Department of Radiation and Medical Oncology, Hubei Key Laboratory of Tumor Biological Behaviors, Hubei Cancer Clinical Study Center, Zhongnan Hospital of Wuhan University, Wuhan, China

OPEN ACCESS

Edited by:
Kelong Ai,
Central South University, China

Reviewed by:
Qiong Huang,
Central South University, China
Yawen Guo,
Zhejiang University, China
Xue-Xin Cheng,
Nanchang University, China

***Correspondence:**
Qinqin Huang
qqhuang@zzu.edu.cn

[†]These authors have contributed equally to this work

Specialty section:
This article was submitted to Pharmacology of Anti-Cancer Drugs, a section of the journal Frontiers in Oncology

Received: 12 April 2022
Accepted: 10 May 2022
Published: 30 June 2022

Citation:
Zhu S, Wang S, Liu C, Lyu M and Huang Q (2022) Cu-Hemin Nanosheets and Indocyanine Green Co-Loaded Hydrogel for Photothermal Therapy and Amplified Photodynamic Therapy. Front. Oncol. 12:918416. doi: 10.3389/fonc.2022.918416

Near-infrared (NIR) organic small molecule indocyanine green (ICG) could respond well to 808 nm laser to promote local high temperature and ROS generation for realizing photothermal therapy (PTT)/photodynamic therapy (PDT). However, the high content of GSH in the tumor microenvironment (TME) limited the further therapeutic performance of ICG. Herein, injectable agarose *in situ* forming NIR-responsive hydrogels (CIH) incorporating Cu-Hemin and ICG were prepared for the first time. When CIH system was located to the tumor tissue through local injection, the ICG in the hydrogel could efficiently convert the light energy emitted by the 808 nm laser into thermal energy, resulting in the heating and softening of the hydrogel matrix, which releases the Cu-Hemin. Then, the over-expressed GSH in the TME could also down-regulated by Cu-Hemin, which amplified ICG-mediated PDT. *In vivo* experiments validated that ICG-based PDT/PTT and Cu-Hemin-mediated glutathione depletion could eliminate cancer tissues with admirable safety. This hydrogel-based GSH-depletion strategy is instructive to improve the objective response rate of PDT.

Keywords: indocyanine green, glutathione, photothermal therapy, photodynamic therapy, hydrogel

INTRODUCTION

At present, the clinical treatment based on cancer has fallen into a great predicament, which has become a treatment difficulty and research hotspot in the current medical field. Tumor microenvironment (TME) is different from healthy tissue environment. For example, TME is usually weakly acidic with high content of GSH and high heat sensitivity, which has encouraged researchers to develop new treatments to treat tumors (1). In recent years, the emergence and rapid development of photothermal therapy (PTT) has provided new ideas for the treatment of solid tumors (2–4). PTT is a new photophysical technology that converts the light energy into heat energy through photothermal conversion reagent, and then generates a local high temperature at a specific lesion, thereby using the heat energy to directly kill tumor cells (5, 6). PTT is less invasive and more

precise than traditional chemotherapy, surgery and radiotherapy (7–9). Many copper-based compounds have good photothermal efficiency and are used as PTAs, and molybdenum-based compounds are also widely used in PTT (10, 11). Among them, the photothermal reagent indocyanine green (ICG) has attracted the attention of researchers due to its excellent biocompatibility and photothermal properties as it has strong near-infrared (NIR) light absorption at 808 nm (12). Not only that, ICG can act as a photosensitizer and transfer the energy to the surrounding oxygen molecules to generate chemically active reactive oxygen species (ROS) (13, 14). ROS could interact with biofilms, destroy cell structure and function, and inactivate cellular proteins, thereby killing cancer cells (15–17). ROS (such as superoxide anion, hydroxyl radical, hydrogen peroxide) could induce apoptosis and even leads to cell necrosis through oxidative stress (18, 19). However, the high content of the reducing substance glutathione (GSH) in the tumor microenvironment (TME) neutralizes the toxicity of ROS and largely inhibits the efficiency of ICG-based PDT (17, 20, 21).

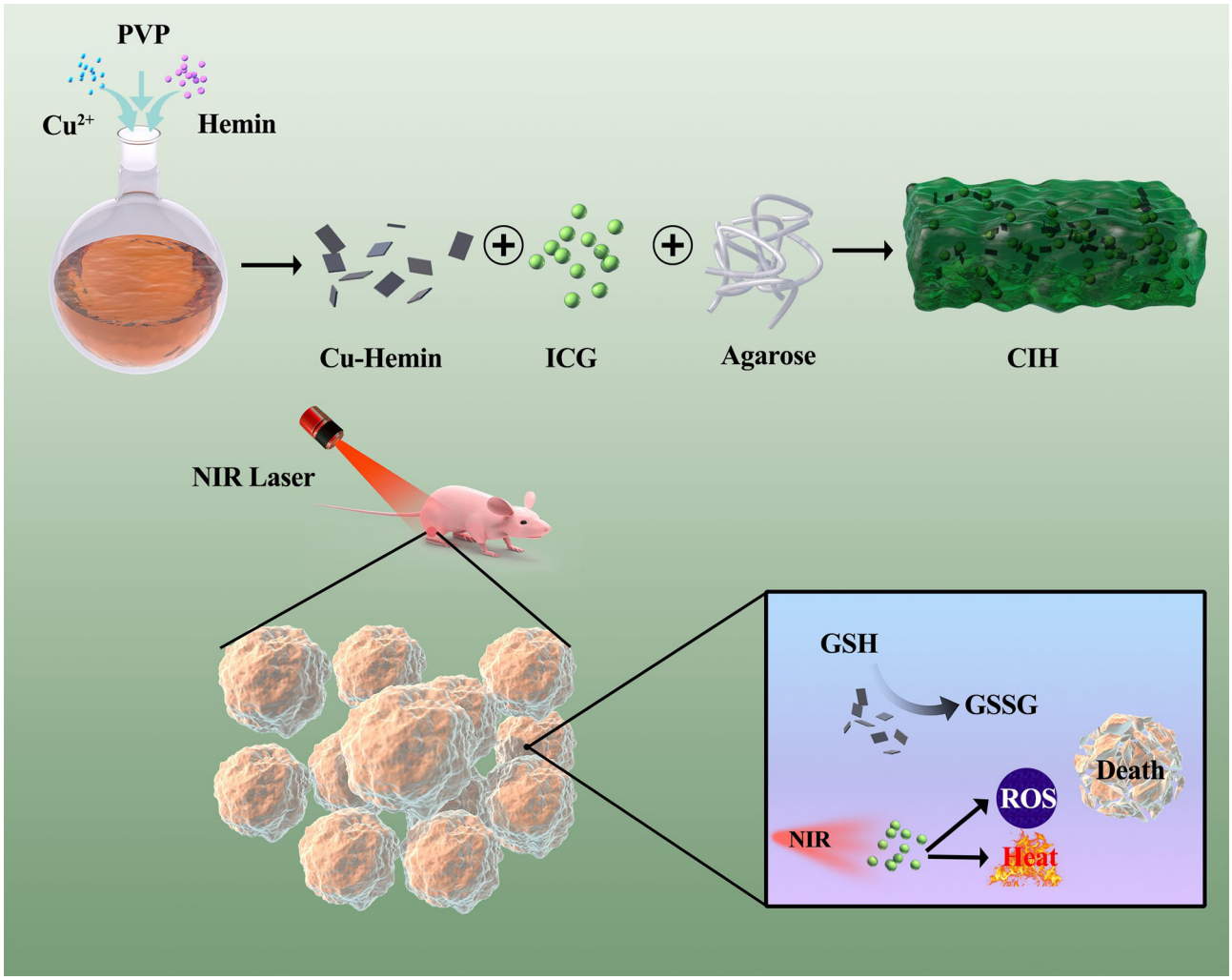
As a typical tumor marker, GSH is widely present in TME, it is the most abundant biological thiol in cells, and plays a crucial role in pathological processes and biochemical pathways (22, 23). It exists in both reduced and oxidized states, and more than 90% of cellular GSH exists in reduced form (24, 25). Therefore, the regulation of reduced glutathione (GSH) is the focus in tumor therapy. The intracellular concentration of GSH (≈10 mM in TME) in cancer cells is much higher than that in normal cells, therefore the effect of ROS-based therapeutics is easily regulated by GSH (24, 26). Nanomaterials can treat various diseases due to their particularity (18, 19, 27), to this end, researchers have developed various GSH-consumable nanomaterials to address this challenge. For example, Fan et al. designed a FeS_2-based nanozyme with high glutathione oxidase (GSH-OXD) activity and enhanced its tumor permeability through folic acid (FA) modification, thereby disrupting the redox homeostasis of the tumor site (28). Thus, FeS_2 effectively depletes intracellular GSH, and at the same time produces a large amount of ·OH to kill tumors. Cai et al. developed novel Cu-Hemin-PEG-LA nanosheets to achieve synchronized GSH depletion and ferroptosis (29). As a new type of nanomaterial, Cu-Hemin has a good tumor killing effect, and the synthesis method is simple and convenient. It can kill tumor tissue well at low doses. Cu-Hemin depletes intracellular GSH and enhances oxidative stress levels. Therefore, Cu-Hemin could well cooperate with ICG to optimize the therapeutic window of individualized medicine, achieving powerful tumor ablation effect. However, it is difficult to co-deliver ICG and Cu-Hemin to tumor sites simultaneously.

Although the traditional intravenous injection of nanomaterials to the tumor site improves the therapeutic efficiency to a certain extent, the uncontrollable release of nanomaterials and the complex physiological environment of the body make the accumulation of nanocarriers in tumor tissue still less than 10% (30–32). Macroscopic drug delivery systems such as light-responsive hydrogels (LRH) are promising smart controlled release systems (33–35). The hydrogel-carrying nanomaterials can aggregate at the tumor site and achieve almost 100% drug penetration (31). And LRH could achieve controlled release carriers for precise on-demand treatment. For example, Zhu et al. simultaneously encapsulated the photothermal agent Pd-C SAzyme and the chemotherapeutic drug camptothecin (CPT) into agarose hydrogels to form a light-controlled oxidative stress amplifier, achieving better photothermal/immunotherapy (15). Notably, this stimuli-responsive hydrogel can tune the rate and extent of carrier release by changing external parameters such as laser power, irradiation time, gel size. Therefore, the simultaneous delivery of ICG and Cu-Hemin into tumor sites using hydrogels is an ideal macroscopic transport mode.

In this study, we performed a simple treatment of the tumor microenvironment regulator Cu-Hemin nanosheets and the photothermal agent ICG with agarose to form a composite hydrogel Cu-Hemin-ICG-hydrogel (CIH) (**Scheme 1**). CIH can stay at the tumor site for a long time after injection, and respond intelligently to 808nm laser. The ICG converts light energy into heat under NIR laser irradiation, and softens the hydrogel to release the Cu-Hemin while generating local high temperature in the mean time. ICG can also absorb 808 nm laser energy to stimulate surrounding oxygen molecules to generate ROS, and Cu-Hemin can amplify ROS generation by depleting intracellular GSH. This combination of modulating redox homeostasis and phototherapy achieved good tumor-suppressive effects in both *in vitro* and *in vivo* experiments. Importantly, agarose is regardas a safe drug approved by American Food and Drug Administration (FDA) (31). The experimental group of CIH combined with 808 nm laser did not have any adverse reactions during the treatment. This indicates that our designed therapeutic system achieves the unification of treatment and system safety. This way of ICG-based enhancing photothermal/photodynamic therapy by depleting GSH is instructive for the subsequent development of novel nano-therapeutic systems.

RESULTS AND DISCUSSION

Cupric nitrate, PVP and hemin were mixed and stirred overnight, and the Cu-Hemin nanosheets were obtained by centrifugation (29). The transmission electron microscopy (TEM) images of Cu-Hemin are shown in **Figure 1A**, Cu-Hemin exhibits a random sheet-like structure with small nanoscale dimensions. The Cu-Hemin was characterized by XRD and XPS (**Figures 1B–D**), and the results showed that the Cu-Hemin was successfully prepared, which was similar to the Cu-Hemin Metal-organic frame (MOF) prepared by the predecessors (29). The results of zeta potential values (**Figure S1**) for Cu-Hemin nanosheets showed that our parpared Cu-MOF is stable. GSH, as an important intracellular regulatory metabolite, is overexpressed in tumor cells (36, 37). We configured different concentrations of Cu-Hemin to explore its ability to destroy GSH. As shown in the **Figure 1E**, GSH was depleted to different degrees after co-incubating with Cu-Hemin



SCHEME 1 | Schematic illustration of Cu-Hemin nanosheets and indocyanine green co-loaded hydrogel for photothermal therapy and amplified photodynamic therapy.

for several hours, and showed a concentration-dependent relationship. This result is encouraging that Cu-Hemin can respond to high intracellular levels of GSH and disrupt redox homeostasis after reaching the tumor site.

Then we prepared pure hydrogel and CIH by a simple method. As shown in the **Figure 2A**, the hydrogel will solidify at room temperature and will not flow down the tube wall, while the solidification performance of CIH with ICG and Cu-Hemin showed no difference. Scanning electron microscopy (SEM) results showed that the hydrogels displayed a typical porous structure with uniform distribution and neat arrangement of pore structures, which are essential in drug delivery and facilitate drug diffusion (**Figure S2**). Simultaneously, the storage modulus of this thermosensitive hydrogel varies with temperature. **Figure 2B** showed that the storage modulus of CIH decreases significantly at hyperthermia, which reflected that CIH softens with increasing temperature. We continued to study the time-temperature profiles of ICG solutions exposed to low-power NIR laser irradiation. Firstly, the absorption spectrum of ICG confirms that it has good absorption ability at 808 nm (**Figure 2D**). We configured different concentrations of ICG solutions (0, 20 and 100 μg/mL) and continuously exposed them to laser irradiation. Infrared thermal imaging (**Figure 2C**) shows that ICG can exert strong photothermal conversion performance under the irradiation of low-power laser. The temperature of the ICG solution (200 ug/mL) increased about 19°C (**Figure 2E**) after irradiation, thus confirming that ICG is an efficient photothermal conversion agent.

The good photothermal properties of ICG prompted us to move forward. We placed CIH in a glass dish, and after standing for a while, laser irradiation was performed, and infrared thermal images were recorded. As shown in the **Figures 3A, B**, the hydrogel temperature increased significantly after irradiation and gradually softened. Relevant 3D temperature diagram

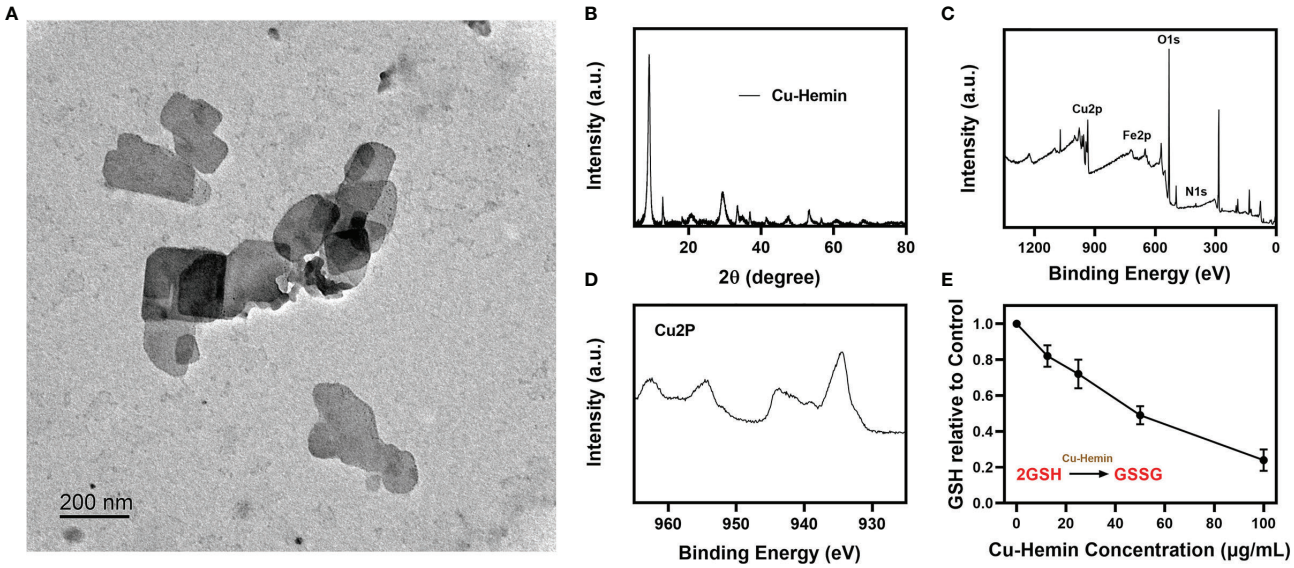


FIGURE 1 | Characterization analysis of Cu-Hemin. **(A)** TEM image of Cu-Hemin nanosheets. **(B)** XRD pattern of Cu-Hemin. **(C)** The XPS spectrum of Cu-Hemin. **(D)** The Cu 2p XPS spectra of Cu-Hemin nanosheets. **(E)** The relative GSH content of the supernatant after the reaction of various concentrations Cu-hemin and 10 mm GSH in mixed solution for 24 h.

(**Figure 3C**) also verified similar results. This indicates that the encapsulated ICG has satisfactory photothermal performance and can be used for subsequent investigations.

The good antitumor effect of PDT mainly comes from the direct cytotoxic effect on tumor cells and the indirect destruction of TME to regulate cell death (38–41). A large amount of ROS is generated during the PDT process (42). Based on this, we used DCFH-DA to verify the content of ROS in cells treated with different groups. In the presence of ROS, DCFH is oxidized to form a fluorescent substance DCF, and the green fluorescence intensity is proprtional to the intracellular reactive oxygen species level (43). The control group and the NIR-treated group exhibited weak green fluorescence, which is the interference signal of endogenous H_2O_2 in the TME (**Figure 4A**). Although Cu-Hemin could induce a fast decline of cellular GSH contents, encapsulation of hydrogels hampered its efficiency of diffusion to tumor cells. As a result, the CIH group exhibited a completely different difference in fluorescence intensity with or without NIR treatment. The IH + NIR group produced moderately intense green fluorescence, which was benefited from the effect of the photosensitizer ICG. The convergence of CIH with NIR achieved the strongest fluorescence effect, as ICG could generate a large amount of ROS in response to laser irradiation, furthermore, Cu-Hemin could reduce intracellular GSH to protect ROS from being consumed. Corresponding quantitative analysis of ROS generation are consistent with fluorescence images (**Figure 4B**). ROS combined with high temperature could eradicate cancer cells. We used the MTT assay kit to explore the cell viability after different treatments, and the results are shown in **Figure 4C**. The efficacy of ICG-based PTT/PDT was limited by TME, while the introduction of Cu-Hemin greatly enhanced the efficacy of PDT. Cell viability between CIH + NIR and IH + NIR groups had significant difference. We fixed the concentration of Cu-Hemin to tackle with TME, and changed the concentration of ICG to perform gradient control experiments, the relative results were shown in **Figure 4D**. It is difficult to evoke cell death in the presence of low concentration of ICG + power laser, and the killing effect increases with the increase of ICG concentration.

Many photothermal agents are used to achieve PTT, although many gold nanomaterials have localized surface plasmon resonance (LSPR) properties, they could strongly absorb near-infrared light and efficiently convert the light into localized heat, thereby generating heat (44, 45). However, the photothermal conversion efficiency of gold nanoparticles at 808 nm is less than 20%, which obviously cannot meet the clinical needs (13). Carbon-based materials are widely used in photothermal therapy, including graphene oxide and graphene quantum dots (46, 47). ICG has good biocompatibility and NIR light-absorbing abilities, which makes it have good clinical potential in photothermal/photodynamic therapy. We continued to explore the light-heat responsive effect of CIH *in vivo*. Compared with the control group, the tumor temperature of the mice treated by CIH + NIR group increased by about 17°C after 10 minutes, which is conducive to killing tumor cells (**Figures S3, S4**). In view of the above results, we continued to explore CIH-based *in vivo* anti-tumor effect. In this study, 4T1 cells were injected subcutaneously into the mice to establish a 4T1 breast cancer subcutaneous tumor model. As tumors reached approximately 200 mm^3 in size, tumor-bearing BALB/c mice were randomly assigned into five groups: (1) PBS; (2) NIR; (3) CIH; (4) IH + NIR and (5) CIH + NIR. Each group was given corresponding treatment. As shown in the **Figure 5A**, the NIR

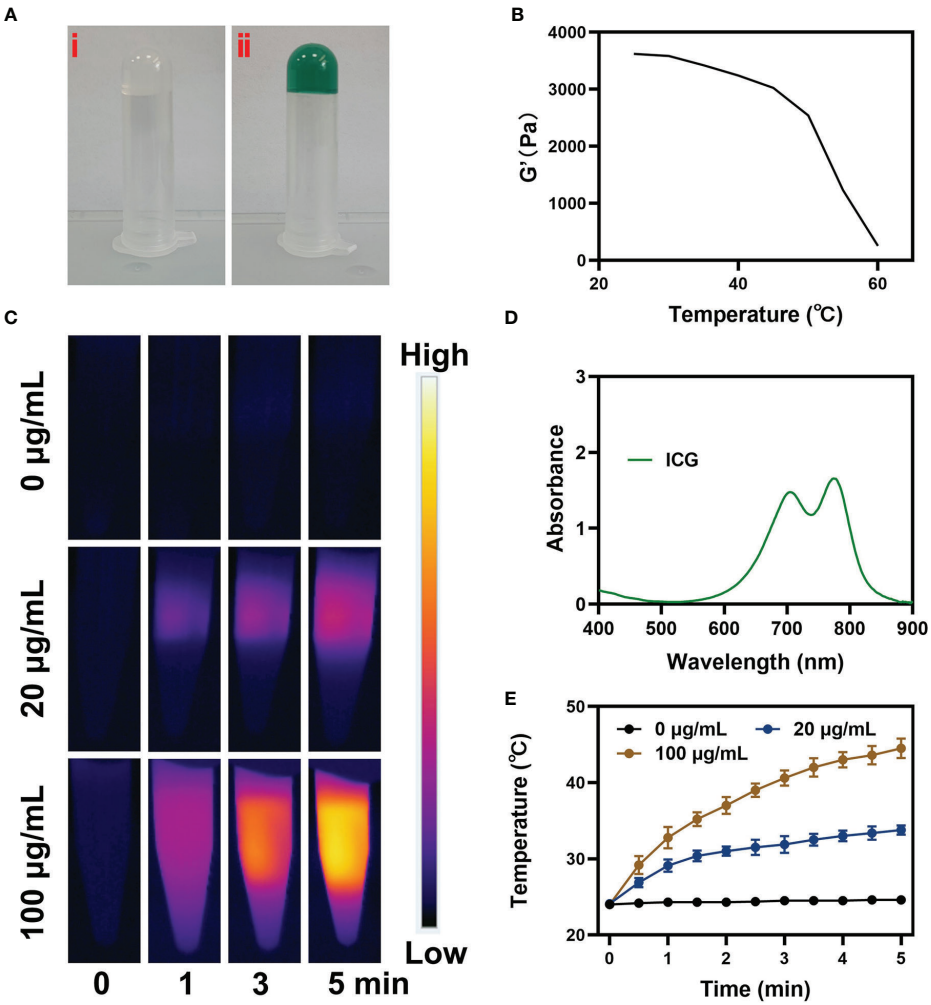


FIGURE 2 | Characterization analysis of ICG. **(A)** The prepared image of pure hydrogel (i) and CIH (ii). **(B)** Rheological and temperature curves for the prepared CIH. **(C)** The corresponding thermal images and **(E)** photothermal heating curves of CIH at different concentrations (ICG: 0, 20 and 100 μg/mL) under an 808 nm (NIR-I) laser irradiation at a power density of 0.5 W/cm. **(D)** Absorption spectrum of ICG solution.

group and the PBS group alone hardly had any tumor suppressive effect, and IH-based PTT/PDT produced a moderate tumor suppression rate. As CIH partly exchanges with external media, a small amount of Cu-Hemin penetrates into the tumor site to achieve slightly antitumor effect. Notably, CIH combined with NIR group could eliminate tumor tissues, as Cu-Hemin could impart oxidative damage toward the tumor, then, ICG fully utilized abnormal TME modulated by Cu-Hemin to intensify PDT. And our treatment was safe, as the mice body weight did not change drastically during the treatment period (**Figure 5B**), but increased slowly. After the treatment, we took vital organs (heart, liver, spleen, lungs, and kidney) of the mice for pathological analysis, and the results also showed that the mice did not have any inflammation and adverse conditions (**Figure S5**). This result is clinically significant, as many cargos permitted good therapeutic effects, but are also associated with high long-term risks. **Figure 5C** showed that the mice tumor weight and volume change curve is consistent. Furthermore, after the treatment of CIH combined with laser irradiation group, tumor proliferation signal Ki-67 was significantly inhibited (**Figure 5D).** Terminal deoxynucleotidyl transferase-mediated dUTP-biotin nick end labeling (TUNEL) also demonstrated CIH + NIR group induced profound cell apoptosis. Our designed GSH-consuming strategy amplified the ICG-mediated PDT efficiency, PTT also assisted certain therapeutic effects without any side effects.

CONCLUSION

In conclusion, our designed CIH-based PTT/PDT can induce a large amount of ROS, which can damage cellular and protein structures, thereby inducing tumor cell apoptosis. The over-

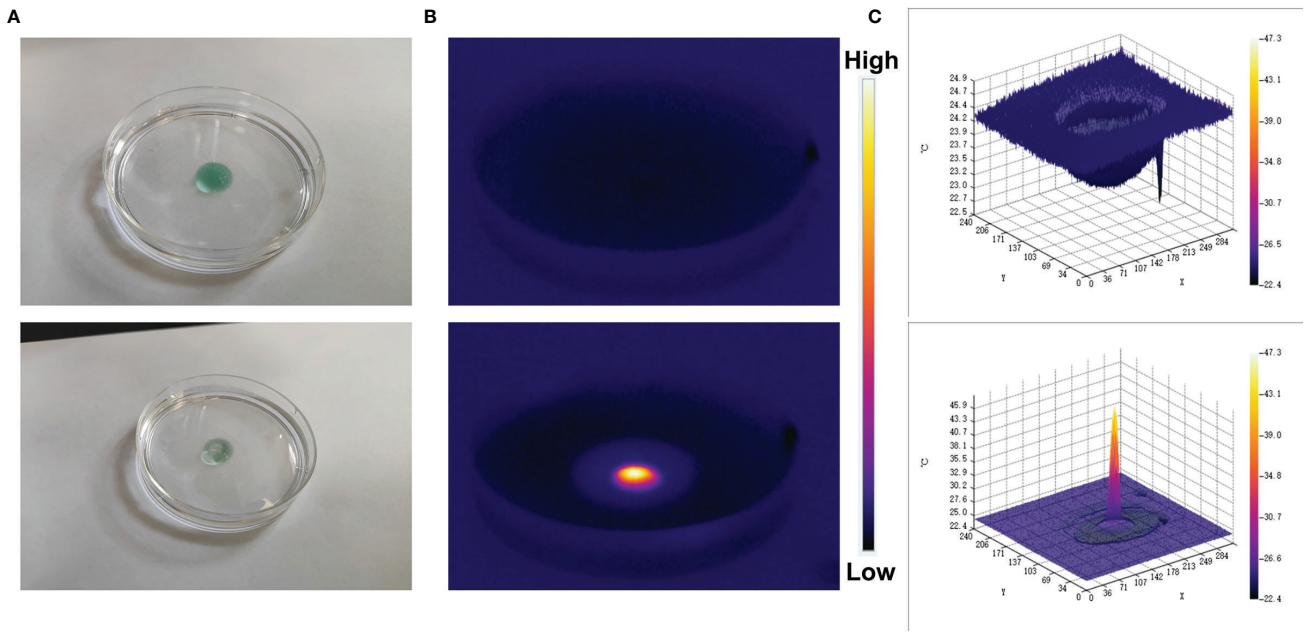


FIGURE 3 | Digital image analysis of softening effect of CIH. **(A)** The morphology of the prepared CIH before and after 0.5 W/cm^2 808 nm laser irradiation for 5 min. **(B)** The infrared thermal images of the prepared CIH before and following irradiation. **(C)** Relevant 3D temperature diagram in 2B.

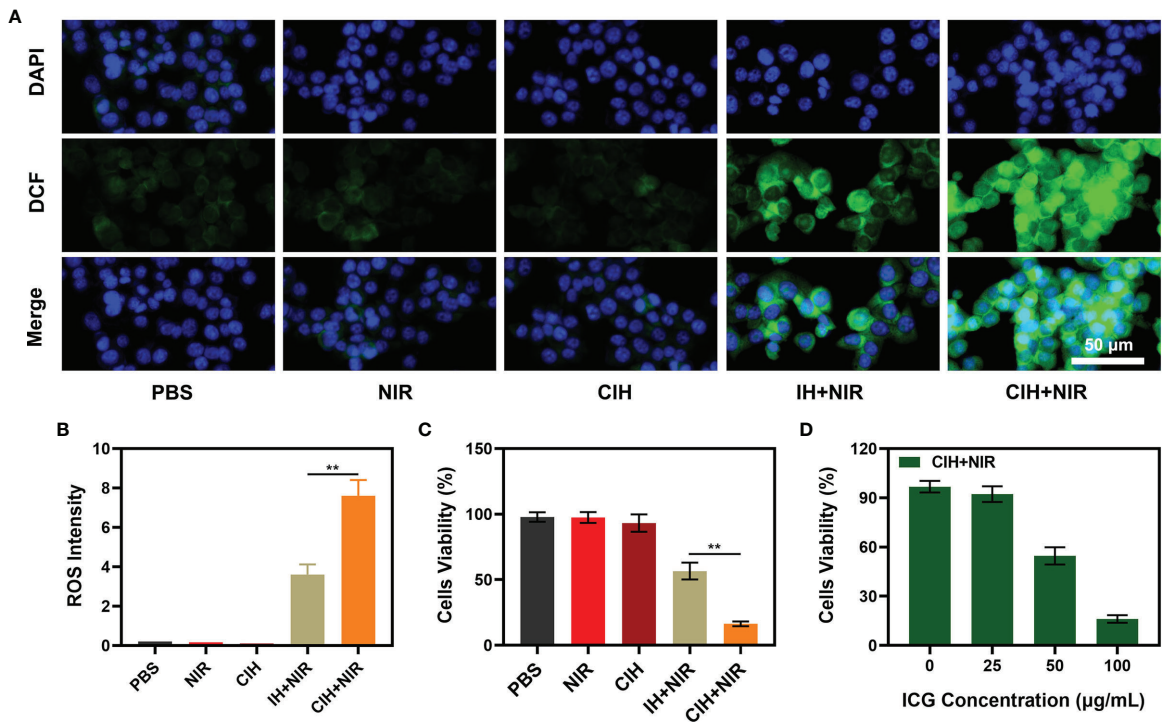


FIGURE 4 | *In vitro* experiments. **(A)** Fluorescence images of 4T1 cells stained by DCFH-DA to indicate nanoparticle-induced ROS generation. Scar bar: 50 μm. **(B)** Corresponding quantitative analysis of ROS generation in 4A. **(C)** Viability of 4T1 cells cultured in the presence of various formulations. **(D)** Cell viability of 4T1 cells following the CIH treatments under different ICG concentration. $^{**}P < 0.01$; Student's t-test.

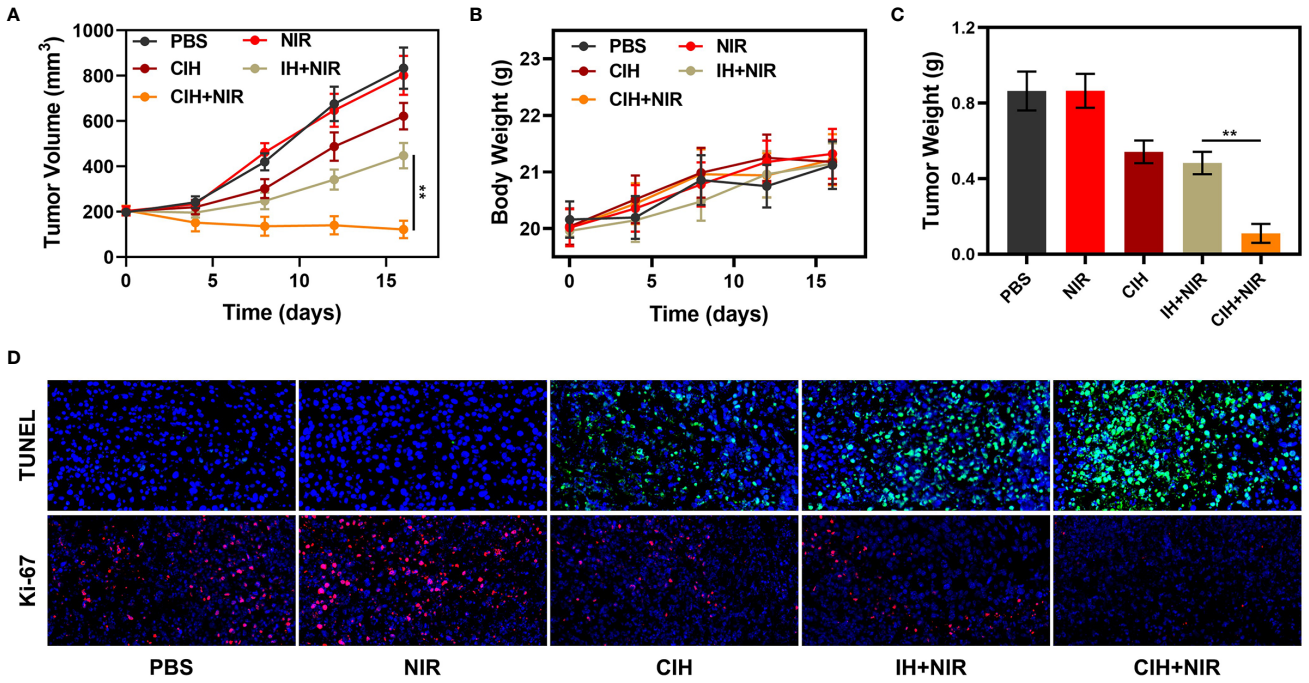


FIGURE 5 | *In vivo* experiments. **(A)** Relative changes of tumor volume in mice bearing 4T1 tumors after indicated treatments. **(B)** Body weight changes of treated mice. **(C)** Tumor weight measured following the indicated treatments. **(D)** Representative digital photos of tumors collected from various groups. **(D)** TUNEL and Ki-67 tumor sections from the indicated treatment groups. $^{**}P < 0.01$; Student's t-test.

expressed GSH in the tumor microenvironment was also down-regulated by Cu-Hemin, thereby alleviating the degree of ROS neutralization and further enhancing the therapeutic effect of PDT. Both animal and cell models demonstrate the potent therapeutic effects of our combined system. Hydrogels with safe properties will benefit further clinical applications in the future, and we will continue to develop novel nano-systems for biological applications.

DATA AVAILABILITY STATEMENT

The original contributions presented in the study are included in the article/**Supplementary Material**. Further inquiries can be directed to the corresponding author.

ETHICS STATEMENT

The animal experiments were carried out according to the protocol approved by the Ministry of Health in People's Republic of PR China and were approved by Wuhan University.

AUTHOR CONTRIBUTIONS

SZ and SW: Methodology, Validation, Formal analysis, Roles, Writing – original draft. CL: Conceptualization, Writing – review and editing. ML: Conceptualization, Writing – review and editing. QH: Project administration, Funding acquisition, Formal analysis, Data curation. All authors contributed to the article and approved the submitted version.

FUNDING

This work was supported by National Natural Science Foundation of China (31800085).

SUPPLEMENTARY MATERIAL

The Supplementary Material for this article can be found online at: https://www.frontiersin.org/articles/10.3389/fonc.2022.918416/full#supplementary-material

REFERENCES

1. Su X, Cao Y, Liu Y, Ouyang B, Ning B, Wang Y, et al. Localized Disruption of Redox Homeostasis Boosting Ferroptosis of Tumor by Hydrogel Delivery System. *Mater Today Bio* (2021) 12:100154. doi: 10.1016/j.mtbio.2021.100154
2. Ding K, Zheng C, Sun L, Liu X, Yin Y, Wang L. NIR Light-Induced Tumor Phototherapy Using ICG Delivery System Based on Platelet-Membrane-

Camouflaged Hollow Bismuth Selenide Nanoparticles. *Chin Chem Lett* (2020) 31(5):1168–72. doi: 10.1016/j.cclet.2019.10.040
3. Lin H, Gao S, Dai C, Chen Y, Shi J. A Two-Dimensional Biodegradable Niobium Carbide (MXene) for Photothermal Tumor Eradication in NIR-I and NIR-II Biowindows. *J Am Chem Soc* (2017) 139(45):16235–47. doi: 10.1021/jacs.7b07818
4. Jiang Y, Upputuri PK, Xie C, Lyu Y, Zhang L, Xiong Q, et al. Broadband Absorbing Semiconducting Polymer Nanoparticles for Photoacoustic Imaging in Second Near-Infrared Window. *Nano Lett* (2017) 17(8):4964–9. doi: 10.1021/acs.nanolett.7b02106
5. Lyu M, Zhu D, Duo Y, Li Y, Quan H. Bimetallic Nanodots for Tri-Modal CT/MRI/PA Imaging and Hypoxia-Resistant Thermoradiotherapy in the NIR-II Biological Windows. *BioMater* (2019) 233:119656. doi: 10.1016/j.bioMater.2019.119656
6. Zhu D, Lyu M, Huang Q, Suo M, Liu Y, Jiang W, et al. Stellate Plasmonic Exosomes for Penetrative Targeting Tumor NIR-II Thermo-Radiotherapy. *ACS Appl Mater Interfaces* (2020) 12(33):36928–37. doi: 10.1021/acsami.0c09969
7. Chen N, Fu W, Zhou J, Mei L, Yang J, Tian Y, et al. Mn2+-Doped ZrO2 PDA Nanocomposite for Multimodal Imaging-Guided Chemo-Photothermal Combination Therapy. *Chin Chem Lett* (2021) 32(8):2405–10. doi: 10.1016/j.cclet.2021.02.030
8. Yu X, Ma H, Xu G, Liu Z. Radiotherapy Assisted With BioMater to Trigger Antitumor Immunity. *Chin Chem Lett.* (2022) 3(3):1331–6. doi: 10.1016/j.cclet.2021.07.073
9. Huang C, Chen T, Zhu D, Huang Q. Enhanced Tumor Targeting and Radiotherapy by Quercetin Loaded Biomimetic Nanoparticles. *Front Chem* (2020) 8:225. doi: 10.3389/fchem.2020.00225
10. Ai K, Huang J, Xiao Z, Yang Y, Bai Y, Peng J. Localized Surface Plasmon Resonance Properties and Biomedical Applications of Copper Selenide NanoMater. *Mater Today Chem* (2021) 20:100402. doi: 10.1016/j.mtchem.2020.100402
11. Wang J, Sui L, Huang J, Miao L, Nie Y, Wang K, et al. MoS2-Based Nanocomposites for Cancer Diagnosis and Therapy. *Bioact Mater* (2021) 6 (11):4209–42. doi: 10.1016/j.bioactmat.2021.04.021
12. Chen Q, Xu L, Liang C, Wang C, Peng R, Liu Z. Photothermal Therapy With Immune-Adjuvant Nanoparticles Together With Checkpoint Blockade for Effective Cancer Immunotherapy. *Nat Commun* (2016) 7:13193. doi: 10.1038/ncomms13193
13. Liu Y, Bhattarai P, Dai Z, Chen X. Photothermal Therapy and Photoacoustic Imaging *via* Nanotheranostics in Fighting Cancer, Chemical Society Reviews. *Chem So. Rev* (2019) 48:2053–2108. doi: 10.1039/C8CS00618K
14. Jiang N, Zhou Z, Xiong W, Chen J, Shen J, Li R, et al. Tumor Microenvironment Triggered Local Oxygen Generation and Photosensitizer Release From Manganese Dioxide Mineralized Albumin-ICG Nanocomplex to Amplify Photodynamic Immunotherapy Efficacy. *Chin Chem Lett* (2021) 32(12):3948–53. doi: 10.1016/j.cclet.2021.06.053
15. Zhu D, Chen H, Huang C, Li G, Wang X, Jiang W, et al. H_2O_2 Self-Producing Single-Atom Nanozyme Hydrogels as Light-Controlled Oxidative Stress Amplifier for Enhanced Synergistic Therapy by Transforming "Cold" Tumors. *Adv Funct Mater* (2022):32(16):2110268. doi: 10.1002/adfm.202110268
16. Zhu D, Zhang J, Luo G, Duo Y, Tang BZ. Bright Bacterium for Hypoxia-Tolerant Photodynamic Therapy Against Orthotopic Colon Tumors by an Interventional Method. *Adv Sci* (2021):8(15):2004769. doi: 10.1002/advs.202004769
17. Zhu D, Zhang T, Li Y, Huang C, Suo M, Xia L, et al. Tumor-Derived Exosomes Co-Delivering Aggregation-Induced Emission Luminogens and Proton Pump Inhibitors for Tumor Glutamine Starvation Therapy and Enhanced Type-I Photodynamic Therapy. *BioMater* (2022) 283:121462. doi: 10.1016/j.bioMater.2022.121462
18. Zhao T, Wu W, Sui L, Huang Q, Nan Y, Liu J, et al. Reactive Oxygen Species-Based NanoMater for the Treatment of Myocardial Ischemia Reperfusion Injuries. *Bioact Mater* (2022) 7:47–72. doi: 10.1016/j.bioactmat.2021.06.006
19. Chen L, Huang Q, Zhao T, Sui L, Wang S, Xiao Z, et al. Nanotherapies for Sepsis by Regulating Inflammatory Signals and Reactive Oxygen and Nitrogen Species: New Insight for Treating COVID-19. *Redox Biol* (2021) 45:102046. doi: 10.1016/j.redox.2021.102046
20. Cao R, Sun W, Zhang Z, Li X, Du J, Fan J, et al. Protein Nanoparticles Containing Cu(II) and DOX for Efficient Chemodynamic Therapy *via* Self-Generation of H2O2. *Chin Chem Lett* (2020) 31(12):3127–30. doi: 10.1016/j.cclet.2020.06.031
21. Dai Y, Ding Y, Li L. Nanozymes for Regulation of Reactive Oxygen Species and Disease Therapy. *Chin Chem Lett* (2021) 32(9):2715–28. doi: 10.1016/j.cclet.2021.03.036
22. Zhou Z, Liang H, Yang R, Yang Y, Dong J, Di Y, et al. GSH Depletion-Induced Activation of Dimersomes for Potentiating the Ferroptosis and Immunotherapy of "Cold" Tumor. *Angewandte Chemie* (2022) 61(22): e202204830. doi: 10.1002/ange.202202843
23. Wang Q, Sun M, Li D, Li C, Luo C, Wang Z, et al. Cytochrome P450 Enzyme-Mediated Auto-Enhanced Photodynamic Cancer Therapy of Co-Nanoassembly Between Clopidogrel and Photosensitizer. *Theranostics* (2020) 10(12):5550–64. doi: 10.7150/thno.42633
24. Mishchenko TA, Balalaeva IV, Vedunova MV, Krysko DV. Ferroptosis and Photodynamic Therapy Synergism: Enhancing Anticancer Treatment. *Trends Cancer* (2021) 7(6):484–7. doi: 10.1016/j.trecan.2021.01.013
25. Xiong Y, Xiao C, Li Z, Yang X. Engineering Nanomedicine for Glutathione Depletion-Augmented Cancer Therapy. *Chem Soc Rev* (2021) 50(10):6013–41. doi: 10.1039/D0CS00718H
26. Niu B, Liao K, Zhou Y, Wen T, Quan G, Pan X, et al. Application of Glutathione Depletion in Cancer Therapy: Enhanced ROS-Based Therapy, Ferroptosis, and Chemotherapy. *BioMater* (2021) 277:121110. doi: 10.1016/j.bioMater.2021.121110
27. Zhu Y, Zhao T, Liu M, Wang S, Liu S, Yang Y, et al. Rheumatoid Arthritis Microenvironment Insights Into Treatment Effect of NanoMater. *Nano Today* (2022) 42:101358. doi: 10.1016/j.nantod.2021.101358
28. Meng X, Li D, Chen L, He H, Wang Q, Hong C, et al. High-Performance Self-Cascade Pyrite Nanozymes for Apoptosis-Ferroptosis Synergistic Tumor Therapy. *ACS Nano* (2021) 15:5735–51. doi: 10.1021/acsnano.1c01248
29. Li K, Xu K, He Y, Lu L, Mao Y, Gao P, et al. Functionalized Tumor-Targeting Nanosheets Exhibiting Fe(II) Overloading and GSH Consumption for Ferroptosis Activation in Liver Tumor. *Small* (2021) 17(40):e2102046. doi: 10.1002/smll.202102046
30. Yang D. Recent Advances in Hydrogels. *Chem Mater* (2022) 34(5):1987–9. doi: 10.1021/acs.chemmater.2c00188
31. Qiu M, Wang D, Liang W, Liu L, Zhang Y, Chen X, et al. Novel Concept of the Smart NIR-Light-Controlled Drug Release of Black Phosphorus Nanostructure for Cancer Therapy. *Proc Natl Acad Sci USA* (2018) 115 (3):501–6. doi: 10.1073/pnas.1714421115
32. Zhu D, Zheng Z, Luo G, Suo M, Li X, Duo Y, et al. Single Injection and Multiple Treatments: An Injectable Nanozyme Hydrogel as AIEgen Reservoir and Release Controller for Efficient Tumor Therapy. *Nano Today* (2021) 37:101091. doi: 10.1016/j.nantod.2021.101091
33. Xing R, Liu K, Jiao T, Zhang N, Ma K, Zhang R, et al. An Injectable Self-Assembling Collagen-Gold Hybrid Hydrogel for Combinatorial Antitumor Photothermal/Photodynamic Therapy. *Adv Mater* (2016) 28(19):3669–76. doi: 10.1002/adma.201600284
34. Zhao S, Zhang L, Deng L, Ouyang J, Xu Q, Gao X, et al. NIR-II Responsive Hydrogel as an Angiogenesis Inhibition Agent for Tumor Microenvironment Reprogramming. *Small* (2021) 17(47):e2103003. doi: 10.1002/smll.202103003
35. Huang C, Chen B, Chen M, Jiang W, Liu W. Injectable Hydrogel for Cu(2+) Controlled Release and Potent Tumor Therapy. *Life (Basel)* (2021) 11(5):391 doi: 10.3390/life11050391
36. Meng X, Deng J, Liu F, Guo T, Liu M, Dai P, et al. Triggered All-Active Metal Organic Framework: Ferroptosis Machinery Contributes to the Apoptotic Photodynamic Antitumor Therapy. *Nano Lett* (2019) 19(11):7866–76. doi: 10.1021/acs.nanolett.9b02904
37. Shen L, Zhou T, Fan Y, Chang X, Wang Y, Sun J, et al. Recent Progress in Tumor Photodynamic Immunotherapy. *Chin Chem Lett* (2020) 31(7):1709–16. doi: 10.1016/j.cclet.2020.02.007
38. Yu CY, Xu H, Ji S, Kwok RT, Lam JW, Li X, et al. Mitochondrion-Anchoring Photosensitizer With Aggregation-Induced Emission Characteristics Synergistically Boosts the Radiosensitivity of Cancer Cells to Ionizing Radiation. *Adv Mater* (2017) 29(15):1606167. doi: 10.1002/adma.201606167
39. Zhang T, Zhang J, Wang FB, Cao H, Zhu D, Chen X, et al. Mitochondria-Targeting Phototheranostics by Aggregation-Induced NIR-II Emission

Luminogens: Modulating Intramolecular Motion by Electron Acceptor Engineering for Multi-Modal Synergistic Therapy. *Adv Funct Mater* (2022) 32(16):12110526. doi: 10.1002/adfm.202110526
40. Duo Y, Zhu D, Sun X, Suo M, Zheng Z, Jiang W, et al. Patient-Derived Microvesicles/AIE Luminogen Hybrid System for Personalized Sonodynamic Cancer Therapy in Patient-Derived Xenograft Models. *BioMater* (2021) 272:120755. doi: 10.1016/j.bioMater.2021.120755
41. Gao D, Guo X, Zhang X, Chen S, Wang Y, Chen T, et al. Multifunctional Phototheranostic Nanomedicine for Cancer Imaging and Treatment. *Mater Today Bio* (2020) 5:100035. doi: 10.1016/j.mtbio.2019.100035
42. Li J, Zhuang Z, Zhao Z, Tang BZ. Type I AIE Photosensitizers: Mechanism and Application. *View* (2021) 3(2):20200121. doi: 10.1002/VIW.20200121
43. Huang C, Liu Z, Chen M, Du L, Liu C, Wang S, et al. Tumor-Derived Biomimetic Nanozyme With Immune Evasion Ability for Synergistically Enhanced Low Dose Radiotherapy. *J Nanobiotech* (2021) 19(1):457. doi: 10.1186/s12951-021-01182-y
44. Ding X, Liow CH, Zhang M, Huang R, Li C, Shen H, et al. Surface Plasmon Resonance Enhanced Light Absorption and Photothermal Therapy in the Second Near-Infrared Window. *J Am Chem Soc* (2014) 136(44):15684–93. doi: 10.1021/ja508641z
45. Zhou J, Jiang Y, Hou S, Upputuri PK, Wu D, Li J, et al. Compact Plasmonic Blackbody for Cancer Theranosis in the Near-Infrared II Window. *ACS Nano* (2018) 12(3):2643–51. doi: 10.1021/acsnano.7b08725
46. Tchounwou C, Sinha SS, Viraka Nellore BP, Pramanik A, Kanchanapally R, Jones S, et al. Hybrid Theranostic Platform for Second Near-IR Window Light Triggered Selective Two-Photon Imaging and Photothermal Killing of Targeted Melanoma Cells. *ACS Appl Mater Interfaces* (2015) 7(37):20649–56. doi: 10.1021/acsami.5b05225
47. Guo W, Chen Z, Feng X, Shen G, Huang H, Liang Y, et al. Graphene Oxide (GO)-Based Nanosheets With Combined Chemo/Photothermal/Photodynamic Therapy to Overcome Gastric Cancer (GC) Paclitaxel Resistance by Reducing Mitochondria-Derived Adenosine-Triphosphate (ATP). *J Nanobiotech* (2021) 19(1):146. doi: 10.1186/s12951-021-00874-9

Conflict of Interest: The authors declare that the research was conducted in the absence of any commercial or financial relationships that could be construed as a potential conflict of interest.

Publisher's Note: All claims expressed in this article are solely those of the authors and do not necessarily represent those of their affiliated organizations, or those of the publisher, the editors and the reviewers. Any product that may be evaluated in this article, or claim that may be made by its manufacturer, is not guaranteed or endorsed by the publisher.

Copyright © 2022 Zhu, Wang, Liu, Lyu and Huang. This is an open-access article distributed under the terms of the Creative Commons Attribution License (CC BY). The use, distribution or reproduction in other forums is permitted, provided the original author(s) and the copyright owner(s) are credited and that the original publication in this journal is cited, in accordance with accepted academic practice. No use, distribution or reproduction is permitted which does not comply with these terms.

frontiers | Frontiers in Oncology

ORIGINAL RESEARCH
published: 30 June 2022
doi: 10.3389/fonc.2022.904960

Injectable Hydrogel System for Camptothecin Initiated Nanocatalytic Tumor Therapy With High Performance

Shuntao Wang[1,2†], Qi Zhang[3†], Ning Zeng[3†], Pengyuan Qi[4], Chunyu Huang[5] and Qinqin Huang[1]*

[1] Department of Molecular Pathology, The Second Affiliated Hospital of Zhengzhou University, Zhengzhou, China, [2] Department of Breast and Thyroid Surgery, Union Hospital, Tongji Medical College, Huazhong University of Science and Technology, Wuhan, China, [3] Department of Plastic Surgery, Tongji Hospital, Tongji Medical College, Huazhong University of Science and Technology, Wuhan, China, [4] The Institute for Advanced Studies, Wuhan University, Wuhan, China, [5] Department of Radiation and Medical Oncology, Hubei Key Laboratory of Tumor Biological Behaviors, Hubei Cancer Clinical Study Center, Zhongnan Hospital of Wuhan University, Wuhan, China

OPEN ACCESS

Edited by:
Kelong Ai,
Central South University, China

Reviewed by:
Qiong Huang,
Central South University, China
Wei Wei,
Memorial Sloan Kettering Cancer Center, United States

***Correspondence:**
Qinqin Huang
qqhuang@zzu.edu.cn

[†]These authors have contributed equally to this work

Specialty section:
This article was submitted to Pharmacology of Anti-Cancer Drugs, a section of the journal Frontiers in Oncology

Received: 26 March 2022
Accepted: 04 May 2022
Published: 30 June 2022

Citation:
Wang S, Zhang Q, Zeng N, Qi P, Huang C and Huang Q (2022) Injectable Hydrogel System for Camptothecin Initiated Nanocatalytic Tumor Therapy With High Performance. Front. Oncol. 12:904960. doi: 10.3389/fonc.2022.904960

Single photothermal therapy (PTT) has many limitations in tumor treatments. Multifunctional nanomaterials can cooperate with PTT to achieve profound tumor killing performance. Herein, we encapsulated chemotherapeutic drug camptothecin (CPT) and pyrite (FeS_2) with dual enzyme activity (glutathione oxidase (GSH-OXD) and peroxidase (POD) activities) into an injectable hydrogel to form a CFH system, which can improve the level of intratumoral oxidative stress, and simultaneously realize FeS_2-mediated PTT and nanozymes catalytic treatment. After laser irradiation, the hydrogel gradually heats up and softens under the photothermal agent FeS_2. The CPT then released from CFH to tumor microenvironment (TME), thereby enhancing the H_2O_2 level. As a result, FeS_2 can catalyze H_2O_2 to produce •OH, and cooperate with high temperature to achieve high-efficiency tumor therapy. It is worth noting that FeS_2 can also deplete excess glutathione (GSH) in the cellular level, further amplifying oxidative stress. Both *in vivo* and *in vitro* experiments show that our CFH exhibits good tumor-specific cytotoxicity. The CFH we developed provides new insights for tumor treatment.

Keywords: hydrogel, pyrite nanozyme, camptothecin, photothermal therapy, catalytic treatment

INTRODUCTION

As the main cancer treatment methods in the world, surgical resection, chemotherapy and radiotherapy have achieved certain results, but the side effects and other limitations after treatment limit their effects (1–4). In recent years, photothermal therapy has been proposed for non-invasive treatment of tumors (5, 6). Photothermal therapy uses nanomaterials with high near-infrared absorption characteristics to generate heat under laser irradiation and subsequently induce tumor ablation (7). Since near-infrared light penetrates biological bodies more easily than ultraviolet light and visible light, near-infrared light is widely used in PTT (8). In order to enhance the effect of penetration therapy, researchers have designed a variety of new nanomaterials, including metal

nanoparticles, organic polymer nanoparticles, carbon-based nanoparticles, etc. to improve the light-to-heat conversion ability (9, 10). Photothermal nanomaterials must have high photothermal conversion efficiency, high surface modification activity, high bio-histocompatibility, and low toxicity (11, 12). PTT is safer than radiotherapy and many molecular drugs (11–13). Although certain effects have been achieved, due to the complexity of the tumor microenvironment, a single PTT is difficult to completely eradicate the tumor tissue (14, 15). Therefore, it is necessary to develop multifunctional nanomaterials, which can not only realize PTT, but also achieve better therapeutic effects in response to the tumor microenvironment.

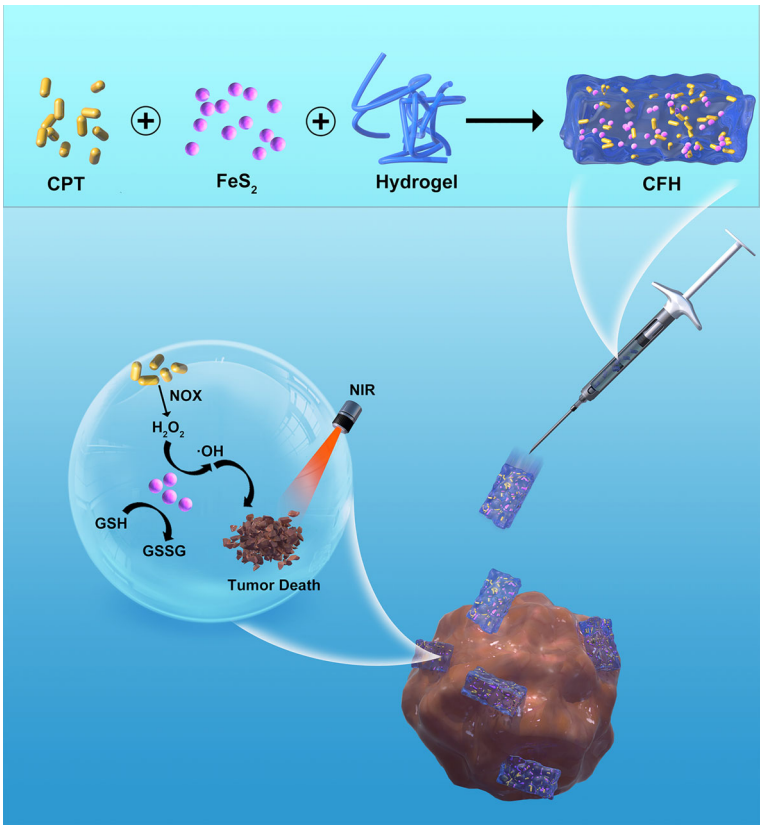
Nanozymes with mimic biological enzyme activity can be combined with photothermal therapy to inhibit the growth of malignant tumors, as nanozymes can affect biological activity at the molecular or cellular level according to the particularity of the tumor microenvironment (16, 17). For example, Fe3O4 nanoparticles can catalyze endogenous tumor hydrogen peroxide (H_2O_2) to produce hydroxyl radical (•OH), which realizes tumor catalysis treatment, simultaneously, Fe3O4 nanoparticles have a good photothermal effect (18). Furthermore, Cui and his team synthesized a novel type of FePPy nanozyme (19). Under laser irradiation, FePPy nanoparticles located in tumor tissue can trigger photothermal transformation and enhance ferroptosis by enhancing fenton reaction (19). Both in vito and in vivo experiments showed that FePPy combined with photothermal treatment has observed significant tumor suppression. However, tumor microenvironment (TME) often contains high levels of glutathione (GSH) (10 mM in TME) (20), and GSH could react with •OH, thereby reducing the corresponding treatment efficiency. As a novel type of photothermal nanomaterial, pyrite (FeS_2) nanozymes can not only respond to near-infrared light and generate a lot of heat to destroy tumor tissues, but also have multiple nanozyme activities (21). FeS_2 nanozyme can oxidize GSH to oxidized glutathione (GSSG), that is, it has similar activity with glutathione oxidase (GSH-OXD) (22). At the same time, as pyrite has a very high affinity for the substrate H_2O_2, it can also effectively catalyze the limited H_2O_2 in the TME and produce more cytotoxic •OH for tumor treatment. However, due to the limited content of endogenous H_2O_2 in tumor, it is difficult to maintain the catalytic effect of nanozyme for a long time (16, 23). Therefore, in order to improve the therapeutic effect of FeS_2-based tumor catalysis and photothermal treatment, a self-produced H_2O_2 system is urgently needed.

In addition, the traditional methods of delivering nanomaterials to tumor sites are through oral or vein injection (13, 24), which will lead to a series of problems such as premature release of the carrier, missing the optimal treatment time of the carrier, and long-term toxic and side effects caused by the carrier's residence time in the body and other problems (25–27). Local therapeutic drug delivery is an attractive alternative to systemic intravenous drug delivery, enabling researchers to achieve sustained and precise release of nanomaterials without any risk of off-target toxicity (28, 29). NIR light-responsive hydrogel is a satisfactory and controllable drug delivery platform (30). The hydrogel is gradually solidified after being injected into the tumor tissue. It can be used as a long-term reservoir. Zhu et al. designed an injectable nano-enzyme hydrogel as the storage and controlled release of AIEgen to achieve effective tumor treatment (31). Given these findings, we hypothesized that the use of hydrogels to deliver FeS_2 to TME would improve photothermal efficacy.

Here, we design an intratumoral administration method of an injectable composite hydrogel (CFH) (**Scheme 1**) containing the chemotherapeutic drug camptothecin (CPT) and FeS_2 nanoparticles for the combined use of photothermal and nanozyme-catalyzed therapy, CFH can be used to regulate the release of FeS_2 and CPT under light irradiation. Once irradiated by NIR irradiation, FeS_2 can realize the conversion of light energy to heat energy, and at the same time realize local tumor ablation and hydrogel dissolution, thereby releasing the CPT in CFH. CPT will spread to the local TME to kill tumor cells, and increase the production of H_2O_2 by activating nicotinamide adenine dinucleotide phosphate (NADPH) oxidase (NOX) (32), so that FeS_2 can produce enough •OH to further enhance the death of tumor cells. Since CFH can stay at the tumor site for a long time after injection, we could change the laser parameters to adjust the release of nanomaterials and CPT to keep it within its treatment window. Both in vivo and in vitro experiments show that our CFH drug delivery platform achieves good anti-tumor efficacy of FeS_2-based photothermal therapy without systemic toxicity. Therefore, the CFH drug delivery platform can not only expand the application field of FeS_2 nanozymes, but it is also the first system that enhances FeS_2-based cancer treatment by rationally designing functional nanocarriers with H_2O_2 self-supply and tumor specificity.

RESULTS AND DISCUSSION

We mixed the low melting point agarose hydrogel with FeS_2 nanozyme and CPT, and kept stirring at 60 degrees to prepare the CFH system. **Figure 1A** shows the transmission electron microscope (TEM) of FeS_2. The particle size of FeS_2 we prepared is about 150 nm. As shown in **Figure 1B**, the scanning electron microscope (SEM) showed that the hydrogel presented a three-dimensional complex network structure. We first verified the stability of FeS_2 and measured the Zeta potential and particle size of FeS_2 for three days. As shown in **Figure 1C**, the particle diameters are about 148.2 ± 5.6 nm, 153 ± 4.7 nm and 152.6 ± 6.2 nm respectively. There is almost no change in the particle size, and the zeta potential also tends to be stable (**Figure S1**). The rheological measurement results of CFH at different temperatures show that as the temperature rises, CFH will gradually soften, and the storage modulus of CFH will continue to decrease (**Figure 1D**). This result is consistent with the rheological properties of the hydrogel (33), as shown in **Figure 1D**. After CFH is prepared, it will be very stable when stored at room temperature. Under continuous laser irradiation, CFH will gradually release FeS_2 in it, and the solution will become turbid (**Figure 1E**). Infrared thermal images verify the



SCHEME 1 | Schematic illustration of injectable hydrogel system for camptothecin initiated nano-catalytic tumor therapy with high performance.

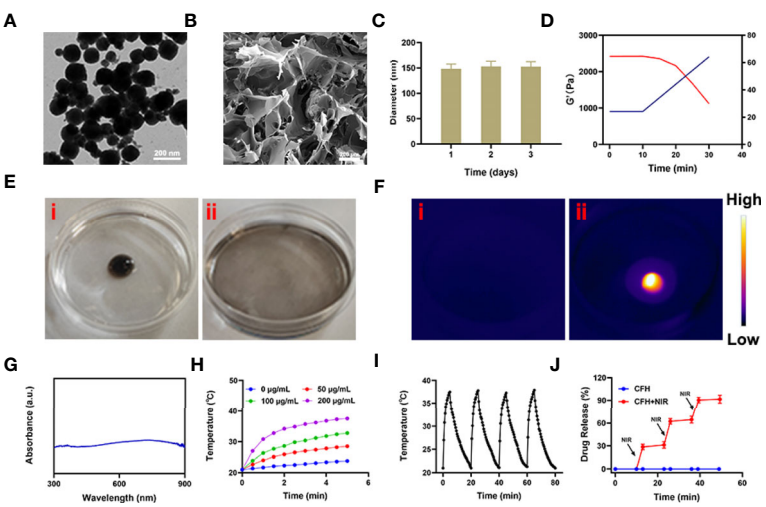


FIGURE 1 | **(A)** TEM image of FeS_2 nanozymes. **(B)** SEM image of hydrogel. **(C)** Statistical graph of measured diameter size of FeS_2. **(D)** Rheological and temperature curves (red and blue, respectively) for the prepared CFH under conditions that simulate an exposure to 0.5 W/cm^2 808 nm laser irradiation. **(E)** The morphology of the prepared CFH before (i) and after (ii) 0.5 W/cm^2 808 nm laser irradiation for 10 min. **(F)** The infrared thermal image of the prepared CFH before (i) and after (ii) irradiation. **(G)** UV–vis spectra of FeS_2. **(H)** Temperature changes of FeS_2 at different concentrations under a 5 min irradiation from an 808 nm laser at 0.5 W/cm^2. **(I)** Temperature variations of a FeS_2 solution over four cycles of heating and natural cooling. **(J)** *In vitro* CFH CPT release profile in the presence and absence of 808 nm laser irradiation.

temperature difference before and after irradiation (**Figure 1F**). FeS_2 can promote the conversion of light energy to heat energy, leading to an increase in temperature. The UV-Vis absorption spectrum verifies FeS_2 has an absorption value at 808nm, showing a wide absorption region in the near infrared region. (**Figure 1G**), which is also the factor that it can respond to 808 nm laser irradiation. A good photothermal agent is conducive to photothermal treatment. We prepared FeS_2 solutions of different concentrations (0, 50, 100, 200 μg/mL) and utilized 0.5 W/cm2 laser for processing (**Figure 1H**). The results showed that the solution heating effect was positively correlated with the material concentration, and the 200 μg/mL FeS_2 solution could rise by about 16.5 degrees under 5 minutes of laser irradiation. One of the most important factors for evaluating photothermal agent (PTA) is the photothermal stability (34). Next, we continue to use the 808 nm near-infrared laser to repeatedly heat the FeS_2 solution, and close the switch after 5 min to allow the FeS_2 to naturally cool to ambient temperature (**Figure S2**). We performed four heating and cooling cycles (**Figure 1I**). The temperature curve shows that the peak temperature of FeS_2 has a small change, and the cooling trend is similar, which also shows photothermal stability of FeS_2 nanoparticles. As shown in **Figure 1J**, once the CFH is exposed to laser radiation, it will achieve a photothermal response drug release. After the temperature rises, the CPT is gradually released. After the irradiation is stopped, the hydrogel continues to restore the colloidal state. This result shows that the CFH prepared by us can achieve good storage and release of the CPT.

The photothermal conversion efficiency (η) of FeS_2 was 33.2% (**Figure 2A)** in our experiments. Only nanomaterials with good biocompatibility can be applied for subsequent biological experiments (35). As shown in **Figure 2B**, FeS_2 is stable in blood, and even 200 μg/mL FeS_2 would not cause hemolysis. We continued to explore the effect of pH on the POD-like activity of FeS_2. The result showed FeS_2 has the strongest POD enzyme activity under acidic conditions with a pH of 4.5, while the enzyme activity is lower under normal neutral conditions (**Figure 2C)**. TME is weakly acidic, which promotes POD activity of FeS_2 enzyme. We applied 5,5′-dithiobis (2-nitrobenzoic acid) (DTNB) as a probe to analyze the GSH-OXD enzyme activity of FeS_2 at different concentrations. The co-incubation of FeS_2 and GSH will lead to a significant decrease in GSH content (**Figure 2D**), and it has a positive correlation curve with time and concentration. These results verified the good dual enzyme activity of FeS_2, and FeS_2 can also be used as an ideal photothermal agent.

Due to the good nanozyme activity of FeS_2, we verified the ability of FeS_2 to generate ROS in vitro. Although the content of H_2O_2 in tumor cells (up to 0.1-1 mM) is higher than that in normal cells, its content is still limited and is not conducive to continuous tumor treatment (36). Our CFH system contains CPT that can increase H_2O_2 and can cooperate with FeS_2 to produce reactive oxygen (ROS) (**Figure S3**). As shown in **Figure 3A**, the dichlorofluorescein diacetate (DCFH-DA) probe was used to detect the ability of CFH to produce ROS. There was almost no green fluorescence of ROS in the control group, and CFH group. We prepared a hydrogel containing only FeS_2 (FH) for exploratory experiments to verify the ability of CPT to produce H_2O_2. As shown in **Figures 3A, C**, the FH combined with NIR group produced moderate fluorescence effect and CFH + NIR motivate the strongest green fluorescence. We then used a live dead cell staining kit (Fluorescein diacetate and propidium iodide are living and dying cell fluorescent tracer probe) to explore the tumor cell killing effect of CFH (**Figure 3B**). Under laser irradiation, the hydrogel containing only FeS_2 can realize the conversion of light energy to heat energy, and induce the death of some tumor cells, with moderate Cell killing effect. The CFH + NIR group achieved the best therapeutic effect. The content of GSH is high in tumors, and GSH is common in various types of cancer tissues. GSH is a highly reducing substance, which generally exists in a simplified form in cells, and can react with oxidative reaction substances

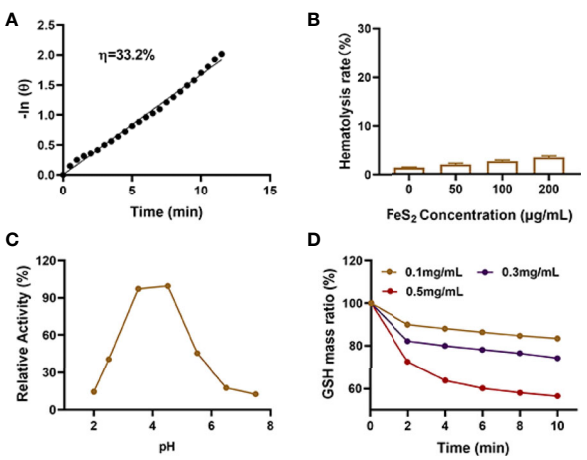


FIGURE 2 | **(A)** Calculation of the time constant for heat transfer using a linear regression of the cooling profile. **(B)** Hemolysis ratio of FeS_2 at different FeS_2 concentrations. **(C)** pH-dependent POD activity of FeS_2. **(D)** Time-dependent reduction of GSH after incubating with the indicated concentrations of FeS_2.

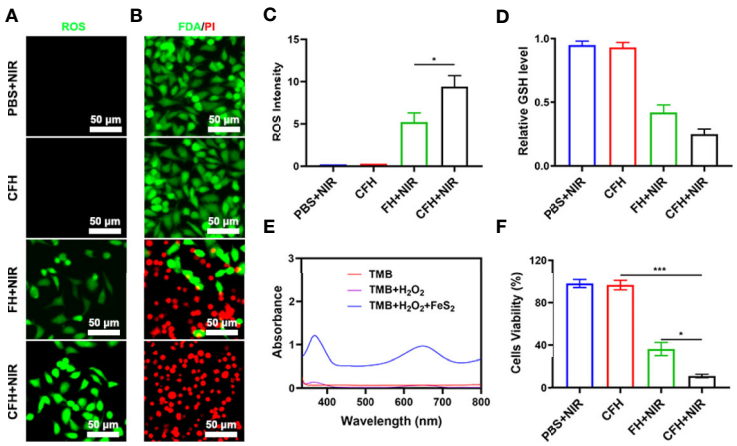


FIGURE 3 | **(A)** DCFH-DA fluorescence image under the indicated treatments. **(B)** Fluorescence images of CT26 cells stained with fluorescein diacetate (FDA) (live cells, green fluorescence) and propidium iodide (PI) (dead cells, red fluorescence) after incubation with different formulations. **(C)** DCFH-DA fluorescence intensity after the indicated treatments. **(D)** The impact of FeS_2 on the intracellular level of GSH was estimated using a GSH assay kit (n = 5). **(E)** UV – vis absorbance spectra and color changes of TMB in different reaction systems. **(F)** MTT assays were conducted using CT26 cells treated with different formulations. *P < 0.05, ***P < 0.005; Student's t-test.

(37). GSH reacts with reactive oxygen species to be oxidized and subsequently forms GSSG, thereby inhibiting the anti-tumor effect based on ROS. Based on the depletion of glutathione, free radicals destroy the redox balance of cells, cause oxidative stress, and ultimately lead to cell apoptosis (38). We have verified the effect of CFH in cooperating with NIR irradiation to consume GSH (**Figure 3D**). The results show that FeS_2 can well reduce intracellular GSH levels, and CPT can also produce a certain amount of H_2O_2 to promote GSH consumption, thereby further improving FeS_2 nanozymes catalytic therapeutic effect. **Figure 3E** also exhibit good POD-like activity of FeS_2. We use the MTT assay to further verify the therapeutic effect of CFH + NIR. The cell viability of the control group and the CFH group was very high, while the cell viability of the FH+NIR group was about 36.5%, while the cell viability of the CFH+NIR group was the lowest, only 10.8% (**Figure 3F**). This also shows that CFH has good anti-tumor ability in vitro.

In view of the fact that FeS_2 exhibits better photothermal performance in vitro, we continue to explore the photothermal effect of CFH in vivo. As shown in **Figure 4A**, the control group achieved a temperature rise of less than 5°C after five minutes under the 808 nm laser irradiation. CFH + NIR, on the other hand, resulted in a temperature rise of about 16.4°C (**Figure 4A**). It shows that CFH is suitable for photothermal therapy, and the low power density we utilized is also conducive to reducing the damage of hyperthermia to surrounding healthy tissues. The heat resistance of tumor tissue is lower than that of normal cells, causing active substances such as proteins in tumor cells to be destroyed at high temperature (42-47°C), and then induce cell apoptosis (39). To explore the synergistic in vivo antitumor ability of CFH and NIR in mice with CT26 tumors, BALB/c mice were injected subcutaneously with 1 × 106 CT26 cells to assess the main effect of CFH. The mice were treated after reaching the primary tumor volume to about 200 mm3. Tumor-bearing mice were randomly arranged into 4 groups (5 mice per group) (1): PBS + NIR (2); CFH (3); FH + NIR and (4) CFH + NIR. The FeS_2 concentration was 20 mg/kg in group 2, 3 and 4. Then, mice in group 1, 3 and 4 were exposed to 808 nm laser radiation (0.5 W/cm2) for 10 min. Mice body weight was monitored every 2 days. During the continuous treatment cycle, the tumor volumes in the control group (PBS + NIR) increased significantly, while the CFH group achieved only a negligible tumor suppression effect. FH + NIR group indicates a better therapeutic effect. Although FH combined with laser has a certain tumor ablation effect, the intracellular H_2O_2 content limits the further catalytic therapeutic effect of FeS_2. The treatment group of CFH combined with NIR showed the best tumor suppression curve (**Figure 4B**). This is because after laser irradiation, the chemotherapy drug CPT can not only promote tumor cell apoptosis, but also increase H_2O_2 levels and further enhance FeS_2-mediated ·OH production, while FeS_2 can also deplete intracellular GSH to achieve oxidative stress damage. The tumor weight in mice after treatment was consistent with the results (**Figure 4C**). The agarose hydrogel was safe and non-toxic, and there were no abnormal changes in the body weight of the mice throughout the treatment cycle, indicating that our treatment regimen was safe (**Figure S4**). Furthermore, staining of Ki-67 was conducted and observed to be obviously decreased after the treatment of CFH combined with laser irradiation group. The hematoxylin and eosin (H&E) staining results demonstrated that the structure of solid tumor tissue was destroyed, and many tumor cells are necrotic after treatments of CFH synergistic with NIR and the cells in the tissue (**Figure 4D**) were contracted with disappeared nuclei. These results suggested that our CFH can cooperate with laser irradiation to realize tumor treatment. The potential in vivo

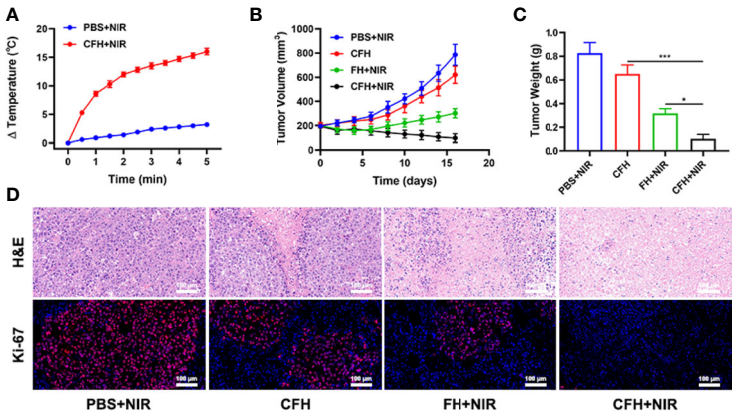


FIGURE 4 | **(A)** Temperature increases in mice implanted with CT26 tumors following 808 nm laser irradiation (0.5 W/cm^2) for 5 min in the indicated treatment groups. **(B)** Tumor volume change over time in groups treated as indicated. **(C)** Average tumor weight values associated with the indicated treatments. **(D)** H&E and Ki-67 stained tumor sections from the indicated treatment groups. *P < 0.05, ***P < 0.005; Student's t-test.

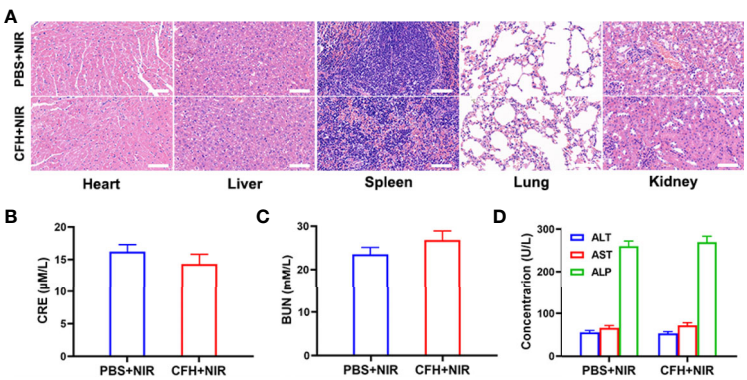


FIGURE 5 | **(A)** Histopathological analysis results (H&E stained images) of the major organs, heart, lung, liver, kidneys, and spleen, of mice that were exposed to different treatments 16 days post-injection. Scale bars: 100 μm. **(B)** Liver function markers: CRE, **(C)** BUN and **(D)** ALT, AST and ALP after various treatments.

toxicity of nanomaterials has limited their clinical biological applications (40, 41). After the treatment, all mice were euthanized, and their blood and major organs were collected for further analysis. We obtain the vital organs (Heart, liver, spleen, lung and kidney) of the mice for histopathological analysis, and the results showed that our treatment system was safe and non-toxic, and the liver and kidney indexes were also normal. In summary, in vivo studies have shown that our CFH can not only achieves the optimal tumor killing effect, but also has a good in vivo safety.

CONCLUSION

In conclusion, we prepared a CFH system for tumor ablation using agarose hydrogel with high safety, combined with chemotherapeutic drug CPT and FeS_2 nanozyme with both GSH-OXD and POD activities. FeS_2 can guide the conversion of light energy to heat energy and promote the release of CPT. The hydrogen peroxide produced can further enhance the therapeutic effect of FeS_2. *In vivo* experiments have shown that CFH combined with NIR can destroy tumor tissue and inhibit tumor growth with good safety. Tumor tissue has a unique pathological environment, including dense extracellular matrix (ECM) and abnormal vascular system. Hydrogels can help FeS_2 reach tumor tissue and achieve the good anti-tumor effect. This platform has great potential for treating solid tumors.

DATA AVAILABILITY STATEMENT

The original contributions presented in the study are included in the article/**Supplementary Material**. Further inquiries can be directed to the corresponding author.

ETHICS STATEMENT

The animal experiments were carried out according to the protocol approved by the Ministry of Health in People's Republic of PR China and were approved by the Administrative Committee on Animal Research of the Wuhan University.

AUTHOR CONTRIBUTIONS

SW: methodology, validation, formal analysis, roles, and data curation. QZ: investigation, formal analysis, formal analysis, and writing – original draft. NZ: conceptualization and project administration. PQ: writing – review and editing. CH: conceptualization and writing – original draft. QH: funding acquisition, writing – original draft, writing – review and editing, and resources. All authors contributed to the article and approved the submitted version.

FUNDING

This work was supported by National Natural Science Foundation of China (31800085).

SUPPLEMENTARY MATERIAL

The Supplementary Material for this article can be found online at: https://www.frontiersin.org/articles/10.3389/fonc.2022.904960/full#supplementary-material

REFERENCES

1. Chen X, Kang R, Kroemer G, Tang DL. Broadening Horizons: The Role of Ferroptosis in Cancer. *Nat Rev Clin Oncol* (2021) 18(5):280–96. doi: 10.1038/s41571-020-00462-0
2. Jin L, Hu P, Wang Y, Wu L, Qin K, Cheng H, et al. Fast-Acting Black-Phosphorus-Assisted Depression Therapy With Low Toxicity. *Adv Mater* (2020) 32(2):e1906050. doi: 10.1002/adma.201906050
3. Wang J, Zhu M, Nie G. Biomembrane-Based Nanostructures for Cancer Targeting and Therapy: From Synthetic Liposomes to Natural Biomembranes and Membrane-Vesicles. *Adv Drug Deliv Rev* (2021) 178:113974. doi: 10.1016/j.addr.2021.113974
4. Zhu D, Zhang J, Luo G, Duo Y, Tang BZ. Bright Bacterium for Hypoxia-Tolerant Photodynamic Therapy Against Orthotopic Colon Tumors by an Interventional Method. *Adv Sci* (2021) 8(15):e2004769. doi: 10.1002/advs.202004769
5. Zhu D, Lyu M, Huang Q, Suo M, Liu Y, Jiang W, et al. Stellate Plasmonic Exosomes for Penetrative Targeting Tumor NIR-II Thermo-Radiotherapy. *ACS Appl Mater Interfaces* (2020) 12(33):36928–37. doi: 10.1021/acsami.0c09969
6. Liu Y, Zhen W, Wang Y, Liu J, Jin L, Zhang T, et al. Double Switch Biodegradable Porous Hollow Trinickel Monophosphide Nanospheres for Multimodal Imaging Guided Photothermal Therapy. *Nano Lett* (2019) 19 (8):5093–101. doi: 10.1021/acs.nanolett.9b01370
7. Cao C, Zou H, Yang N, Li H, Cai Y, Song X, et al. Fe3 O4 /Ag/Bi2 MoO6 Photoactivatable Nanozyme for Self-Replenishing and Sustainable Cascaded Nanocatalytic Cancer Therapy. *Adv Mater* (2021) 33(52):e2106996. doi: 10.1002/adma.202106996
8. Liu C, Xing J, Akakuru OU, Luo L, Sun S, Zou R, et al. Nanozymes-Engineered Metal-Organic Frameworks for Catalytic Cascades-Enhanced Synergistic Cancer Therapy. *Nano Lett* (2019) 19(8):5674–82. doi: 10.1021/acs.nanolett.9b02253
9. Fan L, Xu X, Zhu C, Han J, Gao L, Xi J, et al. Tumor Catalytic–Photothermal Therapy With Yolk–Shell Gold@Carbon Nanozymes. *ACS Appl Mater Interfaces* (2018) 10(5):4502–11. doi: 10.1021/acsami.7b17916
10. Fan K, Xi J, Fan L, Wang P, Zhu C, Tang Y, et al. *In Vivo* Guiding Nitrogen-Doped Carbon Nanozyme for Tumor Catalytic Therapy. *Nat Commun* (2018) 9(2018):1440. doi: 10.1038/s41467-018-03903-8
11. Wang J, Sui L, Huang J, Miao L, Nie Y, Wang K, et al. MoS2-Based Nanocomposites for Cancer Diagnosis and Therapy. *Bioactive Mater* (2021) 6(11):4209–42. doi: 10.1016/j.bioactmat.2021.04.021
12. Huang J, Huang Q, Liu M, Chen Q, Ai K. Emerging Bismuth Chalcogenides Based Nanodrugs for Cancer Radiotherapy. *Front Phar* (2022) 13:844037. doi: 10.3389/fphar.2022.844037
13. Su X, Cao Y, Liu Y, Ouyang B, Ning B, Wang Y, et al. Localized Disruption of Redox Homeostasis Boosting Ferroptosis of Tumor by Hydrogel Delivery System. *Mater Today Bio* (2021) 12:100154. doi: 10.1016/j.mtbio.2021.100154
14. Chen J, Ning C, Zhou Z, Yu P, Zhu Y, Tan G, et al. Nanomaterials as Photothermal Therapeutic Agents. *Prog Mater Sci* (2019) 99:1–26. doi: 10.1016/j.pmatsci.2018.07.005
15. Zhu D, Chen H, Huang C, Li G, Wang X, Jiang W, et al. H_2O_2 Self-Producing Single-Atom Nanozyme Hydrogels as Light-Controlled Oxidative Stress Amplifier for Enhanced Synergistic Therapy by Transforming "Cold" Tumors. *Adv Funct Mater* (2022) 32(16):2110268. doi: 10.1002/adfm.202110268
16. Liu F, Lin L, Zhang Y, Wang YB, Sheng S, Xu CN, et al. A Tumor-Microenvironment-Activated Nanozyme-Mediated Theranostic Nanoreactor for Imaging-Guided Combined Tumor Therapy. *Adv Mater* (2019) 31(40):11. doi: 10.1002/adma.201902885
17. Zhang X, Li G, Wu D, Li X, Hu N, Chen J, et al. Recent Progress in the Design Fabrication of Metal-Organic Frameworks-Based Nanozymes and Their Applications to Sensing and Cancer Therapy. *Biosensors Bioelectron* (2019) 137:178–98. doi: 10.1016/j.bios.2019.04.061
18. Dai Y, Xu C, Sun X, Chen X. Nanoparticle Design Strategies for Enhanced Anticancer Therapy by Exploiting the Tumour Microenvironment. *Chem Soc Rev* (2017) 46(12):3830–52. doi: 10.1039/C6CS00592F
19. Cui X, Lu G, Fang F, Xiong Y, Tian S, Wan Y, et al. Iron Self-Boosting Polymer Nanoenzyme for Low-Temperature Photothermal-Enhanced Ferrotherapy. *ACS Appl Mater Interfaces* (2021) 13(26):30274–83. doi: 10.1021/acsami.1c01658
20. Yin W, Li J, Ke W, Zha Z, Ge Z. Integrated Nanoparticles To Synergistically Elevate Tumor Oxidative Stress and Suppress Antioxidative Capability for Amplified Oxidation Therapy. *ACS Appl Mater Interfaces* (2017) 9 (35):29538–46. doi: 10.1021/acsami.7b08347
21. Meng X, Li D, Chen L, He H, Wang Q, Hong C, et al. High-Performance Self-Cascade Pyrite Nanozymes for Apoptosis–Ferroptosis Synergistic Tumor Therapy. *ACS Nano* (2021) 15(3):5735–51. doi: 10.1021/acsnano.1c01248
22. Huang C, Liu Z, Chen M, Du L, Liu C, Wang S, et al. Tumor-Derived Biomimetic Nanozyme With Immune Evasion Ability for Synergistically Enhanced Low Dose Radiotherapy. *J Nanobiotechnol* (2021) 15(3): 5735–51. doi: 10.1186/s12951-021-01182-y
23. Liu X, Liu Z, Dong K, Wu S, Sang Y, Cui T, et al. Tumor-Activatable Ultrasmall Nanozyme Generator for Enhanced Penetration and Deep Catalytic Therapy. *Biomaterials* (2020) 258:120263. doi: 10.1016/j.biomaterials.2020.120263
24. Li C, Luo Z, Yang L, Chen J, Cheng K, Xue Y, et al. Self-Assembled Porphyrin Polymer Nanoparticles With NIR-II Emission and Highly Efficient Photothermal Performance in Cancer Therapy. *Mater Today Bio* (2022) 13:100198. doi: 10.1016/j.mtbio.2021.100198
25. Zhang L, Wang Z, Zhang Y, Cao F, Dong K, Ren J, et al. Erythrocyte Membrane Cloaked Metal-Organic Framework Nanoparticle as Biomimetic Nanoreactor for Starvation-Activated Colon Cancer Therapy. *ACS Nano* (2018) 12(10):10201–11. doi: 10.1021/acsnano.8b05200

26. Chang M, Wang M, Wang M, Shu M, Ding B, Li C, et al. A Multifunctional Cascade Bioreactor Based on Hollow-Structured Cu2 MoS4 for Synergetic Cancer Chemo-Dynamic Therapy/Starvation Therapy/Phototherapy/Immunotherapy With Remarkably Enhanced Efficacy. *Adv Mater* (2019) 31(51):e1905271. doi: 10.1002/adma.201905271
27. Yang S, Tang Z, Hu C, Zhang D, Shen N, Yu H, et al. Selectively Potentiating Hypoxia Levels by Combretastatin A4 Nanomedicine: Toward Highly Enhanced Hypoxia-Activated Prodrug Tirapazamine Therapy for Metastatic Tumors. *Adv Mater* (2019) 31(11):e1805955. doi: 10.1002/adma.201805955
28. Qiu M, Wang D, Liang W, Liu L, Zhang Y, Chen X, et al. Novel Concept of the Smart NIR-Light-Controlled Drug Release of Black Phosphorus Nanostructure for Cancer Therapy. *Proc Natl Acad Sci USA* (2018) 115(3):501–6. doi: 10.1073/pnas.1714421115
29. Chen M, Wang Z, Suo W, Bao Z, Quan H. Injectable Hydrogel for Synergetic Low Dose Radiotherapy, Chemodynamic Therapy and Photothermal Therapy. *Front Bioeng Biotechnol* (2021) 9. doi: 10.3389/fbioe.2021.757428
30. Huang C, Chen B, Chen M, Jiang W, Liu W. Injectable Hydrogel for Cu(2+) Controlled Release and Potent Tumor Therapy. *Life (Basel)* (2021) 11(5):391. doi: 10.3390/life11050391
31. Zhu D, Zheng Z, Luo G, Suo M, Li X, Duo Y, et al. Single Injection and Multiple Treatments: An Injectable Nanozyme Hydrogel as AIEgen Reservoir and Release Controller for Efficient Tumor Therapy. *Nano Today* (2021) 37:101091. doi: 10.1016/j.nantod.2021.101091
32. Tang Y, Lu X, Yin C, Zhao H, Hu W, Hu X, et al. Chemiluminescence-Initiated and in Situ-Enhanced Photoisomerization for Tissue-Depth-Independent Photo-Controlled Drug Release. *Chem Sci* (2019) 10(5):1401–9. doi: 10.1039/C8SC04012E
33. Hou M, Yang R, Zhang L, Zhang L, Liu G, Xu Z, et al. Injectable and Natural Humic Acid/Agarose Hybrid Hydrogel for Localized Light-Driven Photothermal Ablation and Chemotherapy of Cancer. *ACS Biomater Sci Eng* (2018) 4(12):4266–77. doi: 10.1021/acsbiomaterials.8b01147
34. Song G, Liang C, Gong H, Li M, Zheng X, Cheng L, et al. Core-Shell MnSe@Bi2 Se3 Fabricated *via* a Cation Exchange Method as Novel Nanotheranostics for Multimodal Imaging and Synergistic Thermoradiotherapy. *Adv Mater* (2015) 27(40):6110–7. doi: 10.1002/adma.201503006
35. Zhu DM, Duo YH, Suo M, Zhao YH, Xia LG, Zheng Z, et al. Tumor-Exocytosed Exosome/Aggregation-Induced Emission Luminogen Hybrid Nanovesicles Facilitate Efficient Tumor Penetration and Photodynamic Therapy. *Angew Chem-Int Edit* (2020) 59(33):13836–43. doi: 10.1002/anie.202003672
36. Chen Z, Niu M, Chen G, Wu Q, Tan L, Fu C, et al. Oxygen Production of Modified Core-Shell CuO@ZrO2 Nanocomposites by Microwave Radiation to Alleviate Cancer Hypoxia for Enhanced Chemo-Microwave Thermal Therapy. *ACS Nano* (2018) 12(12):12721–32. doi: 10.1021/acsnano.8b07749
37. Wu Y, Guo T, Qiu Y, Lin Y, Yao Y, Lian W, et al. An Inorganic Prodrug, Tellurium Nanowires With Enhanced ROS Generation and GSH Depletion for Selective Cancer Therapy. *Chem Sci* (2019) 10(29):7068–75. doi: 10.1039/C9SC01070J
38. Huang C, Ding S, Jiang W, Wang F-B. Glutathione-Depleting Nanoplatelets for Enhanced Sonodynamic Cancer Therapy. *Nanoscale* (2021) 13(8):4512–8. doi: 10.1039/D0NR08440A
39. Liu S, Pan X, Liu H. Two-Dimensional Nanomaterials for Photothermal Therapy. *Angewandte Chemie* (2020) 59(15):5890–900. doi: 10.1002/anie.201911477
40. Wu W, Huang L, Wang E, Dong S. Atomic Engineering of Single-Atom Nanozymes for Enzyme-Like Catalysis. *Chem Sci* (2020) 11(36):9741–56. doi: 10.1039/D0SC03522J
41. Gao C, Cheng Q, Wei J, Sun C, Lu S, Kwong CHT, et al. Bioorthogonal Supramolecular Cell-Conjugation for Targeted Hitchhiking Drug Delivery. *Mater Today* (2020) 40:9–17. doi: 10.1016/j.mattod.2020.05.023

Conflict of Interest: The authors declare that the research was conducted in the absence of any commercial or financial relationships that could be construed as a potential conflict of interest.

Publisher's Note: All claims expressed in this article are solely those of the authors and do not necessarily represent those of their affiliated organizations, or those of the publisher, the editors and the reviewers. Any product that may be evaluated in this article, or claim that may be made by its manufacturer, is not guaranteed or endorsed by the publisher.

Copyright © 2022 Wang, Zhang, Zeng, Qi, Huang and Huang. This is an open-access article distributed under the terms of the Creative Commons Attribution License (CC BY). The use, distribution or reproduction in other forums is permitted, provided the original author(s) and the copyright owner(s) are credited and that the original publication in this journal is cited, in accordance with accepted academic practice. No use, distribution or reproduction is permitted which does not comply with these terms.

frontiers | Frontiers in Oncology

ORIGINAL RESEARCH
published: 04 July 2022
doi: 10.3389/fonc.2022.888855

Nanozyme Hydrogels for Self-Augmented Sonodynamic/ Photothermal Combination Therapy

Shuntao Wang[1,2†], *Ning Zeng*[3†], *Qi Zhang*[3†], *Mingzhu Chen*[4] *and Qinqin Huang*[1*]

[1] Department of Molecular Pathology, The Second Affiliated Hospital of Zhengzhou University, Zhengzhou, China, [2] Department of Breast and Thyroid Surgery, Union Hospital, Tongji Medical College, Huazhong University of Science and Technology, Wuhan, China, [3] Department of Plastic Surgery, Tongji Hospital, Tongji Medical College, Huazhong University of Science and Technology, Wuhan, China, [4] Department of Radiation and Medical Oncology, Hubei Key Laboratory of Tumor Biological Behaviors, Hubei Cancer Clinical Study Center, Zhongnan Hospital of Wuhan University, Zhengzhou, China

OPEN ACCESS

Edited by:
Kelong Ai,
Central South University, China

Reviewed by:
Meng Suo,
Wuhan University, China
Pengyuan Qi,
Wuhan University, China
Dongdong Wang,
Nanyang Technological University, Singapore

***Correspondence:**
Qinqin Huang
qqhuang@zzu.edu.cn

[†]These authors have contributed equally to this work

Specialty section:
This article was submitted to Pharmacology of Anti-Cancer Drugs, a section of the journal Frontiers in Oncology

Received: 03 March 2022
Accepted: 26 April 2022
Published: 04 July 2022

Citation:
Wang S, Zeng N, Zhang Q, Chen M and Huang Q (2022) Nanozyme Hydrogels for Self-Augmented Sonodynamic/Photothermal Combination Therapy. Front. Oncol. 12:888855. doi: 10.3389/fonc.2022.888855

Sonosensitizer-mediated sonodynamic therapy (SDT) has emerged as a promising anti-tumor strategy. However, this strategy of continuous oxygen consumption further exacerbates the hypoxic tumor microenvironment, which limits its therapeutic efficacy. In this study, we designed a multifunctional hydrogel (PB+Ce6@Hy) that simultaneously co-delivers nanozyme prussian blue (PB) and sonosensitizer chlorin e6 (Ce6) for the realization of photothermal therapy (PTT) and enhanced SDT. When the hydrogel reaches the tumor tissue through local injection, the 808 nm laser can induce the hydrogel to warm up and soften, thereby triggering the release of PB and Ce6. PB can interact with endogenous H_2O_2 *in situ* and generate sufficient oxygen to promote the Ce6-mediated SDT effect. Besides, due to the good encapsulation ability of the hydrogel, the nanomaterials can be released in a controlled manner by changing laser parameter, irradiation time, etc. The experimental results show that the PB+Ce6@Hy system we developed can generate a large amount of reactive oxygen species (ROS), which can be combined with the photothermal effect to kill tumor cells, as a result, tumor proliferation has been adequately inhibited. This combined PTT/SDT dynamic strategy provides a new perspective for Ce6-induced cancer therapy, showing great potential for clinical application.

Keywords: prussian blue, chlorin e6, oxygen regulation, photothermal therapy, sonodynamic therapy

INTRODUCTION

Due to the limited penetration depth of light, phototherapy is not enough for deep tumors, which limits the development potential of photothermal therapy (PTT) and photodynamic therapy (PDT) (1–4). Based on this, Yumita et al. proposed sonodynamic therapy (SDT) based on PTT (5). SDT is a new treatment method for malignant tumors using a combination of sonosensitizers and low-intensity ultrasound (US) (6, 7). It has the advantages of high accuracy, deep tissue penetration, good patient compliance, and few adverse reactions. Ultrasound can penetrate deep tissue and focus on the tumor area, thereby activating the sonosensitizer, realizing ultrasonic cavitation, reactive

oxygen species-induced cell damage, apoptosis, and autophagy, which provide the possibility for targeted non-invasive radical cure of solid tumors (8, 9). It is generally believed that the one of the main mechanisms of SDT is the generation of reactive oxygen species (ROS) through cavitation or cavitation-activated sonosensitizers (10). ROS can effectively destroy intracellular proteins, damage DNA, promote intracellular lipid peroxidation, further induce tumor cell apoptosis, and achieve the purpose of inhibiting tumor growth (11, 12). However, due to the malignant growth of tumor cells, solid tumor areas are usually partially hypoxic, furthermore, SDT could activate sonosensitizers agent to consume oxygen, thereby exacerbating local tissue hypoxia (13). Therefore, the tumor hypoxic state and sustained oxygen consumption during oxygen-dependent SDT severely affect the therapeutic effect.

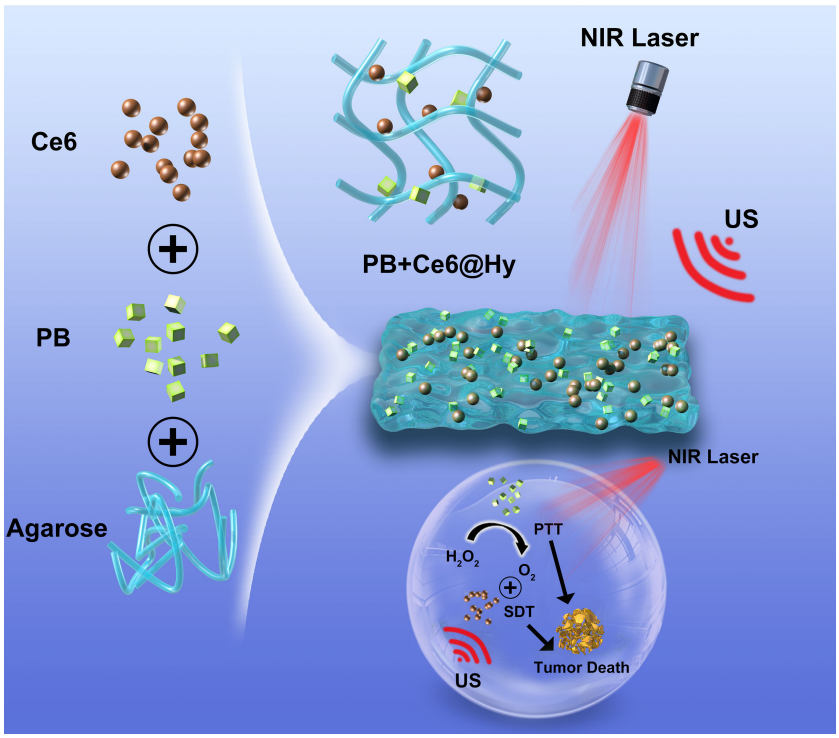
Prussian blue nanoparticles (PB) are a class of inorganic substances assembled from transition metal ions or lanthanides through cyano bridging ligands (14). Because of its unique safety and high photothermal conversion efficiency, it has aroused great interest of researchers. PB have excellent absorption and photothermal conversion properties in the near-infrared first (NIR-I) window region (15). It is worth mentioning that compared with gold nanorods, PB nanoparticles have higher photothermal conversion efficiency, and PB nanoparticles also have better photothermal stability than general organic photothermal conversion agents (16, 17). Recently, PB has also been found to have a catalase (CAT)-like effect (18). PB can catalyze endogenous hydrogen peroxide (H_2O_2) in tumors to generate oxygen, which is expected to alleviate the hypoxic microenvironment of tumors. Hu et al. designed a novel PMPT nanomaterial that not only alleviates hypoxia tolerance and enhances ROS generation during photodynamic processes, but also inhibits the MTH1-regulated DNA damage repair pathway, resulting in aggravated oxidative damage and cell death (19). It has also achieved good results in animal models. Therefore, PB, which can alleviate tumor hypoxia levels, is expected to have a good synergistic effect when used in conjunction with SDT.

Although nanodrugs have greatly improved the toxicity of chemotherapeutic drugs and enhanced the enrichment of drugs in tumor sites (20), the drug accumulation in tumor tissues through nanocarriers is still less than 10% due to the complexity of the body environment (21–23). It is difficult to efficiently deliver PB nanoparticles and sonosensitizers to tumor tissues due to the interference of *in vivo* biological barriers such as liver and kidney clearance effects. Traditional drug delivery systems (i.e. intravenous injection) have a series of problems such as low efficiency of nanomaterials reaching tumor tissue, premature leakage of cargo, and profound toxicity caused by the long-term existence of the carrier in the body (24–26). Numerous studies have shown that hydrogel delivery system can prolong the sustained release time of materials, prolong the effect of materials, and improve the effect of tumor treatment (27). Adding nanomaterials into hydrogel solution by diffusion or grafting to hydrogel materials can directly hit the lesion site by implantation or injection to achieve the effect of local slow-release drugs (28, 29). As one of the popular macroscopic drug delivery carriers, light-responsive hydrogels have very broad application prospects due to their unique properties (30, 31). And the controlled release of the material can be achieved by changing the external parameters (laser power, spot size, etc.) (32). For example, Dong et al. designed a novel MXene hydrogel by combining photothermal agent MXene nanosheets with low-melting-point agarose and loading DOX into it to prepare a smart hydrogel with reversible phase transition, and *in vitro* cells experiments verified its good cell killing ability (33). These results motivate our attempts to realize enhanced SDT treatment using hydrogels.

In this study, we simultaneously encapsulated the sonosensitizer chlorin e6 (Ce6) and nanozyme PB into a lowmelting agarose hydrogel to prepare a multifunctional nanosystem (PB+Ce6@Hy) for enhanced SDT/PTT (**Scheme 1**). PB+Ce6@Hy could reach the tumor site by local injection, and it could be enriched here after solidification. After being irradiated by 808 nm laser, PB absorbed light energy and converts it into heat energy, causing the hydrogel to heat up and soften, then Ce6 and PB were released on demand. PB would sustainably catalyze endogenous H_2O_2 to generate O_2 *in situ* to alleviate the hypoxic microenvironment, which in turn enhances the subsequent Ce6-mediated SDT. Both *in vitro* and *in vivo* experiments showed that the prepared PB+Ce6@Hy achieved the synergistic therapeutic effect of PTT and SDT on tumors. This mutually reinforcing system overcomes the deficiencies of SDT and significantly inhibits subcutaneous tumors with negligible toxic side effects. The convergence of PTT with enhanced SDT strategy provides a novel insight for Ce6-induced tumor therapy.

RESULTS AND DISCUSSION

We prepared PB according to the previous work (30), and characterized the morphology of PB by transmission electron microscopy (TEM), as shown in **Figure 1A**. Subsequently, hybrid hydrogel containing PB and Ce6 (PB+Ce6@Hy) was prepared by simple hydrothermal method. The blue PB+Ce6@Hy loses its fluidity after solidification and does not flow down with the tube wall (**Figure S1**). Scanning electron microscopy (SEM) image showed that the as-prepared hydrogels had complex three-dimensional pore morphologies (**Figure 1B**). Next, its photothermal conversion ability was verified. As shown in **Figure 1C**, the hydrogel will gradually soften and release the material after being irradiated by 808 nm laser, and the thermal energy generation ability of PB is verified by the infrared thermal image. The particle size of PB did not change significantly during the week storage period, confirming its stability (**Figure 1D**). This property is beneficial for long-term sequestration of PB in hydrogels for subsequent effects. As many unstable nanomaterials are unsuitable for long-time storage and biological applications (34). We evaluated the catalase (CAT)-like properties of PB nanozymes in aqueous solutions containing hydrogen peroxide. The results showed that PB could induce substantial oxygen production after incubation with hydrogen peroxide for five minutes (**Figure 1E**). This encourages us to use PB for enhancing SDT. UV–vis spectra of



SCHEME 1 | Nanozyme hydrogels for self-augmented sonodynamic/photothermal combination therapy.

PB (**Figure 1F**) exhibited that it has strong absorbance in the NIR-I region. We prepared PB solutions with different concentration gradients to verify their photothermal properties, the control group had almost no heating effect under 808 nm laser irradiation, while the 50 μg/mL PB solution could achieve a temperature rise of nearly 15 degrees within three minutes of irradiation, and the heating effect of PB is positively correlated with its concentration (**Figure 1H**). We utilized three consecutive ON-OFF cycles of laser irradiation, that is, the PB solution was irradiated with 808 nm laser for 5 minutes and then cooled back to the initial temperature naturally, and the cycle was repeated three times. The results are shown in **Figure S2**, the heating ability of PB does not fluctuate much, confirming the photothermal stability of PB, which is also beneficial for the controllable release of PB *in vivo* for tumor therapy. Simultaneously, rheological curves of agarose hydrogel were detected, as the temperature increases (**Figure 1G**), the hydrogel will slowly transform from a solid colloidal state to a liquid state, and the storage modulus gradually decreases. We continued to study the controlled drug release kinetics of the PB+Ce6@Hy. **Figure 1I** shows the drug release curve with or without laser irradiation. When the laser switch is turned on, the temperature of the system begins to increase, and the carrier encapsulated in it is gradually released slowly. After the irradiation was stopped, the hydrogel slowly solidified and continued to encapsulate the cargo.

Inspired by the well-characterized properties of the prepared PB+Ce6@Hy, we further explored its *in vitro* cell killing effect. SDT has a strong ability to penetrate biological tissues (35), it can concentrate acoustic energy into deeper tissues and activate the sonosensitizers (such as Ce6 in this study) in tumor tissues, ultimately playing an anti-tumor effect (36). However, SDT will continue to consume oxygen, this increased hypoxia, in turn, affects the effectiveness of SDT. So we constructed normoxic and hypoxic cell growth environments to verify the effect of PB+Ce6@Hy in regulating cell death. First, the ability of PB+Ce6@Hy combined with US and NIR to generate ROS was explored, and 2′,7′-dichlorofluorescin diacetate (DCFH-DA) was utilized as a ROS indicator. As shown in **Figures 2A, C**, the control, NIR + US, PB+Ce6@Hy and PB@Hy + NIR groups produced negligible ROS, while Ce6+US could mediate a strong green fluorescence under normoxic conditions. However, hypoxic conditions inhibited the effect of Ce6-mediated SDT to generate ROS. We quantitatively analyzed the ROS intensity under different conditions. **Figure 2B** showed that PB+Ce6@Hy + NIR + US produced bright green ROS fluorescence regardless of normoxic or hypoxic conditions, as the release of PB nanozymes upon 808 nm laser irradiation could convert endogenous H_2O_2 into O_2. Since PB+Ce6@Hy has a good effect on regulating the tumor ecological environment, we continued to use the MTT experiment to test the killing effect of PB+Ce6@Hy combined with US and NIR. As shown in **Figures 2D, E**, the survival state of cells in the control group was almost unaffected. the convergence of sonosensitizers Ce6 with US in normoxic environment could achieve a moderate tumor killing effect, but

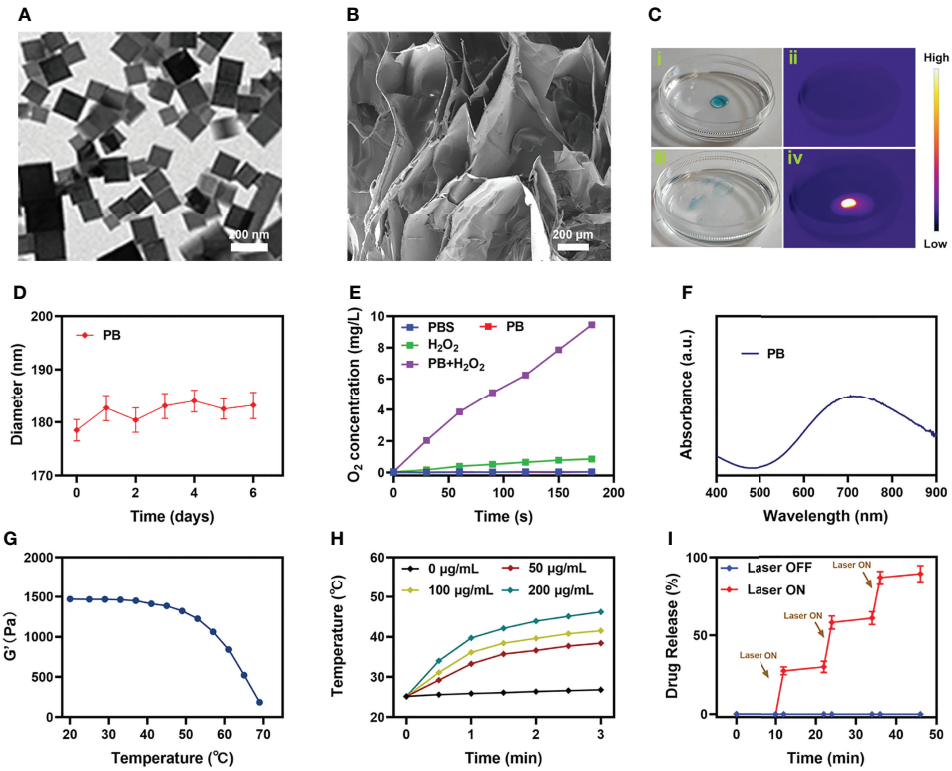


FIGURE 1 | Characterization analysis of PB+Ce6@Hy. **(A)** TEM image of PB. **(B)** SEM image of agarose hydrogel. **(C)** The morphology of the prepared PB+Ce6@Hy before (i) and after (iii) 0.5 W/cm^2 808 nm laser irradiation for 10 min and infrared thermal images (ii, iv) of the prepared PB+Ce6@Hy following irradiation. **(D)** Hydrodynamic diameter of PB at different time points. **(E)** Oxygen generation in different conditions as measured by a dissolved oxygen meter. **(F)** UV–vis–NIR absorbance spectra of PB. **(G)** Rheological curves of agarose hydrogel. **(H)** Temperature elevation curves with the different concentration of PB at 808 nm laser irradiation. **(I)** *In vitro* Ce6 release profile in the presence and absence of 808 nm laser irradiation, with arrows being used to indicate irradiation time points.

the effect was adequately reduced in hypoxia. It is worth noting that PB+Ce6@Hy + NIR + US has achieved a superior therapeutic benefits and is not affected by the oxygen environment. The results of live and dead assay in the hypoxic group also fully demonstrated the killing effect of PB+Ce6@Hy system (**Figure S3**). This is attributed to the fact that PB produces O_2 to promote SDT, and PB also has PTT effect. This dynamic oxygen-producing strategy has achieved good effects.

In situ injection of hydrogels can greatly increase the content of nanomaterials in tumor tissues. Light-responsive hydrogels are ideal biomaterials for various biomedical applications (37). The PB+Ce6@Hy we prepared has a three-dimensional cross-linked structure and good biodegradability. and biocompatibility and sensitive response to light stimuli, showing great potential in cancer therapy. We continue to explore its photothermal conversion effect *in vivo*. As shown in **Figure 3A**, PB+Ce6@Hy can achieve a good local heating effect of tumor tissue under the cooperation of 808 nm laser. PB+Ce6@Hy (10 min irradiation, 0.5W/cm^2) could raise the tumor temperature to nearly 48 degrees. A large number of basic researches and clinical applications have proved that when tumor tissue is continuously heated for a certain period of time, the growth of tumor cells is blocked, disintegrated, and even leads to death (38). The formation of tumor thermotherapy is based on two characteristics of tumor tissue: First, there are abnormal blood vessels in tumor tissue so its heat dissipation is extremely poor (39). Local heating by appropriate methods can easily make the temperature of tumor tissue 5% to 15% higher than that of surrounding normal tissue; second, the temperature resistance of tumor tissue is significantly lower than that of normal tissue, and tumor tissue will occur at a temperature of 42°C irreversible damage (40, 41). Inspired by this result, we aimed to investigate the synergistic antitumor ability of PB+Ce6@Hy and NIR + US in 4T1 tumor mice.100 μL of 4T1 cell suspension (1×10^6 cells per mL) were subcutaneously injected into each mouse to establish the tumor models. Subsequently, tumor growth was monitored every 2 days to assess the primary effect of the treatment system. As shown in **Figure 3B**, the injected PB+Ce6@Hy alone remained in the tumor tissue for a long time, but did not produce any tumor-toxicity, and the tumor volume growth curve was hardly inhibited. In this regard, PB@Hy containing only PB combined with laser irradiation produced a certain photothermal treatment effect. The tumor ablation effect induced by PB+Ce6@Hy plus NIR and US is the best. First, PB achieves precise hyperthermia effect, and then the softening of the hydrogel promotes the release of PB and Ce6 into the tumor site. PB can improve TME *in situ* and generate O_2, which greatly strengthens Ce6-induced ROS production effect, tumor

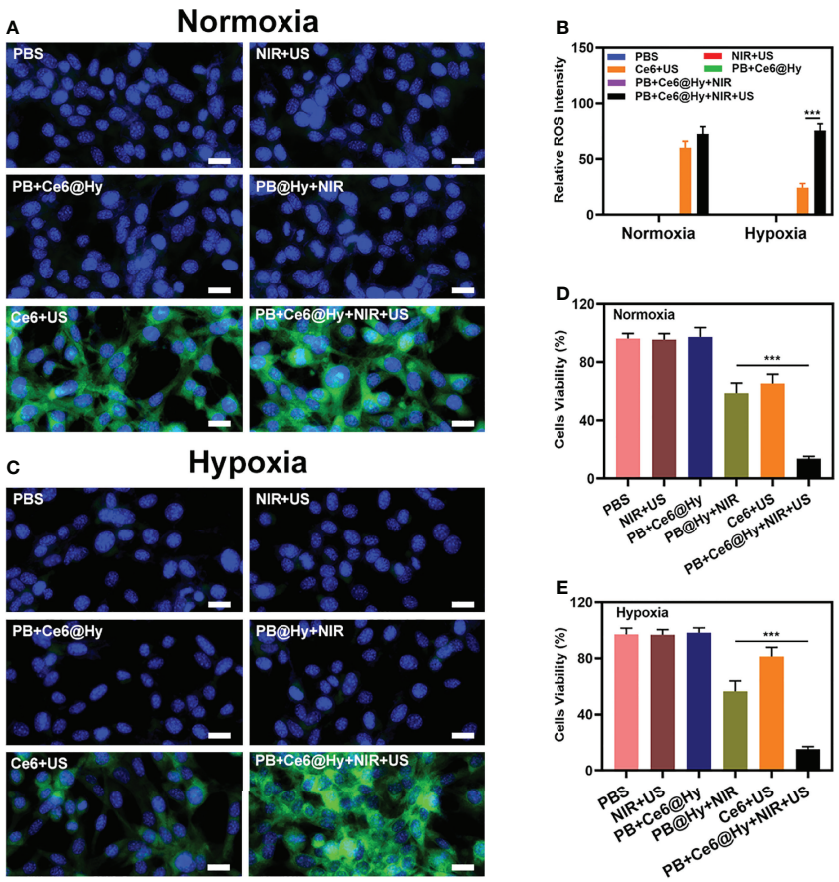


FIGURE 2 | Results of *in vitro* experiments. Fluorescence microscopy images of DCFH-DA to detect intracellular ROS with various treatments under normoxic **(A)** and hypoxia **(C)** condition. Scale bar = 20 μm. **(B)** DCFH-DA fluorescence intensity after the indicated treatments. **(D)** Cell viability of 4T1 cells cultured in the presence of various formulations under normoxic condition. **(E)** Cell viability of 4T1 cells cultured in the presence of various formulations under hypoxia condition. ***P < 0.005; Student's t-test.

growth was greatly inhibited. **Figure S4** also showed that the tumor mass and volume curves are consistent. After treatment, the average tumor weight was only 0.12 g. It is worth noting that the weight of mice in each group did not increase or decrease sharply during the treatment cycle, and showed a normal growth trend, which also indicated that our treatment regimen was safe (**Figure 3C**). Hypoxia-inducible factor 1α (HIF-1α) was highly expressed under hypoxia, tumor cells under hypoxic conditions strongly expressed HIF-1α in the form of green fluorescence. We verified in an *in vivo* model that both PB@Hy and PB+Ce6@Hy systems could alleviate the hypoxic microenvironment (**Figure 3D**). In addition, PB+Ce6@Hy combined with NIR and US can also generate a large amount of ROS (**Figure 3E**) in an *in vivo* tumor model, and simultaneously increase the level of tumor cell apoptosis (**Figure 3F**). After the treatment cycle, mice in all groups were euthanized, followed by collection of major organs for further analysis and blood for biochemical analysis (**Figure 4**). The relevant results of both the experimental group and the conventional control group showed that the mice functioned normally after treatment, and our treatment method did not show short-term toxic and side effects.

CONCLUSION

In conclusion, a biocompatible hydrogel containing both nanozyme PB and Ce6 sonosensitizer was constructed to achieve cooperative PTT/SDT against tumor. PB+Ce6@Hy can controllably deliver the loaded material to the tumor site and simultaneously realize on-demand release. After the hydrogel was irradiated by laser, photothermal heating was triggered, and the released PB catalyzed H_2O_2 to generate oxygen *in situ*, which promoted SDT. *In vitro* and *in vivo* experiments showed that PB+Ce6@Hy induced a large number of apoptosis and inhibited tumor growth without any physiological toxicity. This study provides a new mode of combination therapy and expands the application of PB nanozymes in sonodynamic therapy. Based on the fact that a single treatment method is

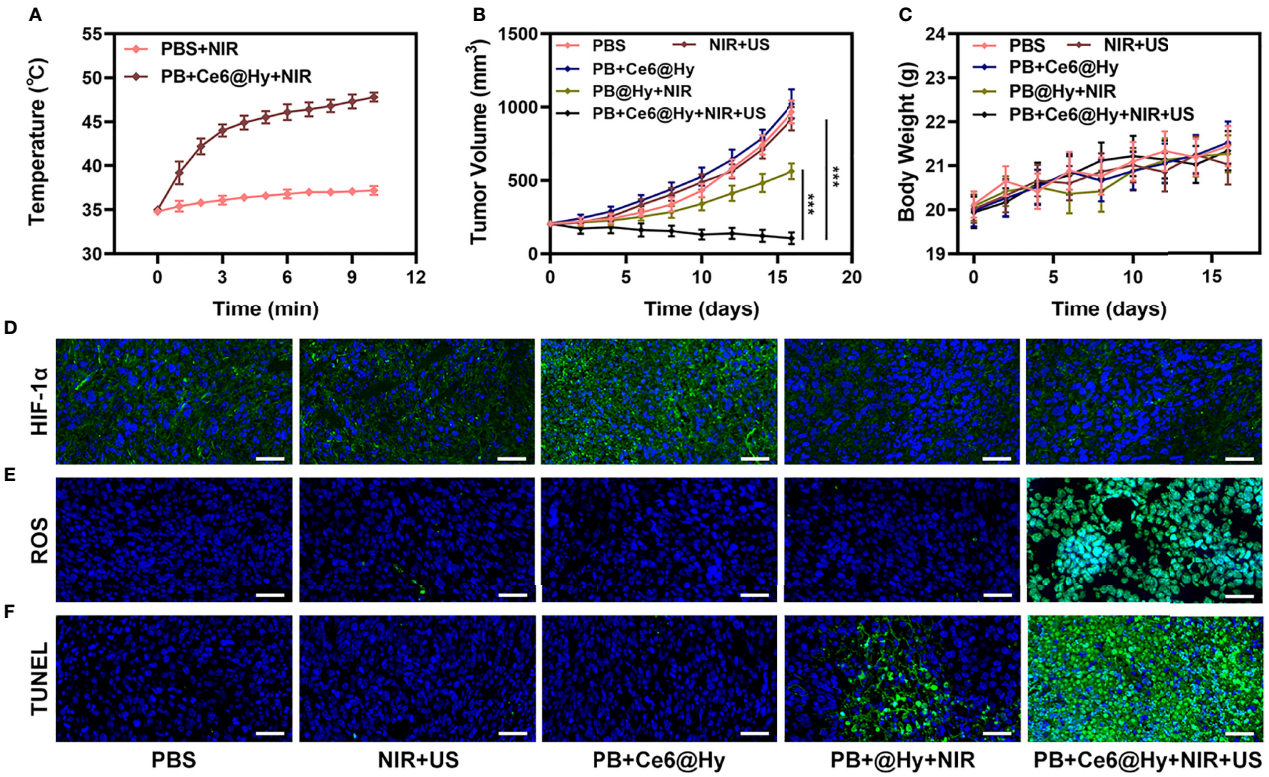


FIGURE 3 | Results of *in vivo* experiments. **(A)** Temperature increases in mice implanted with 4T1 tumors following 808 nm laser irradiation (0.5 W/cm^2) for 10 min in the indicated treatment groups. **(B)** Tumor volume change over time in groups treated as indicated. **(C)** Time-dependent body-weight curves of mice in different groups. **(D)** HIF-1α, **(E)** ROS and **(F)** TUNEL stained tumor sections from the indicated treatment groups Scale bar = 100 μm. ***P < 0.005; Student's t-test.

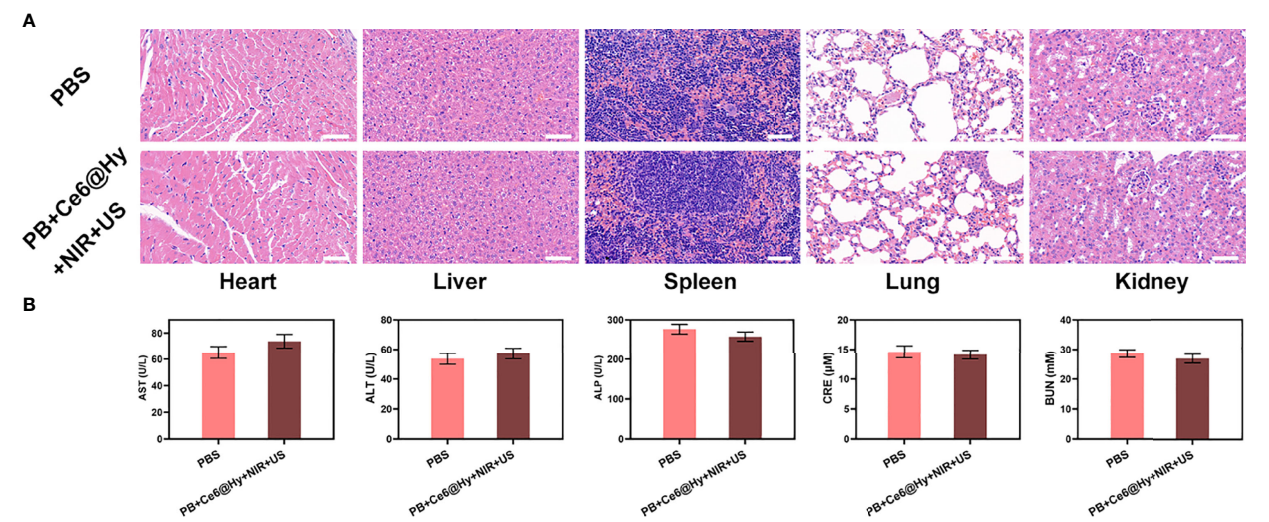


FIGURE 4 | Result of *in vivo* safety experiments. **(A)** Histopathological analysis results (H&E stained images) of the major organs, heart, lung, liver, kidneys, and spleen, of mice that were exposed to different treatments 16 days post-injection. Scale bars: 100 μm. **(B)** Liver, kidney and blood function markers: AST, ALT, ALP, CRE and BUN after various treatments.

difficult to suppress tumor cell proliferation for a long time, we will continue to develop new and safe nanozymes for multimodal treatment in the future.

DATA AVAILABILITY STATEMENT

The original contributions presented in the study are included in the article/**Supplementary Material**. Further inquiries can be directed to the corresponding author.

ETHICS STATEMENT

The animal experiments were carried out according to the protocol approved by the Ministry of Health in People's Republic of PR China and were approved by the Administrative Committee on Animal Research of the Wuhan University.

AUTHOR CONTRIBUTIONS

SW, NZ, and QZ contributed to conception and design of the study. MC and QH wrote the first draft of the manuscript. SW performed the statistical analysis. NZ organized the database. All authors contributed to manuscript revision, read, and approved the submitted version.

FUNDING

This work was supported by National Natural Science Foundation of China (31800085).

SUPPLEMENTARY MATERIAL

The Supplementary Material for this article can be found online at: https://www.frontiersin.org/articles/10.3389/fonc.2022.888855/full#supplementary-material

REFERENCES

1. Zhu D, Lyu M, Huang Q, Suo M, Liu Y, Jiang W, et al. Stellate Plasmonic Exosomes for Penetrative Targeting Tumor NIR-II Thermo-Radiotherapy. *ACS Appl Mater Interfaces* (2020) 12(33):36928–37. doi: 10.1021/acsami.0c09969
2. Wang J, Sui L, Huang J, Miao L, Nie Y, Wang K, et al. MoS2-Based Nanocomposites for Cancer Diagnosis and Therapy. *Bioact Mater* (2021) 6 (11):4209–42. doi: 10.1016/j.bioactmat.2021.04.021
3. Xu K, Wu X, Cheng Y, Yan J, Feng Y, Chen R, et al. A Biomimetic Nanoenzyme for Starvation Therapy Enhanced Photothermal and Chemodynamic Tumor Therapy. *Nanoscale* (2020) 12(45):23159–65. doi: 10.1039/D0NR05097K
4. Ding K, Zheng C, Sun L, Liu X, Yin Y, Wang L. NIR Light-Induced Tumor Phototherapy Using ICG Delivery System Based on Platelet-Membrane-Camouflaged Hollow Bismuth Selenide Nanoparticles. *Chin Chem Lett* (2020) 31(5):1168–72. doi: 10.1016/j.cclet.2019.10.040
5. Son S, Kim JH, Wang X, Zhang C, Yoon SA, Shin J, et al. Multifunctional Sonosensitizers in Sonodynamic Cancer Therapy. *Chem Soc Rev* (2020) 49 (11):3244–61. doi: 10.1039/C9CS00648F
6. Xu T, Zhao S, Lin C, Zheng X, Lan M. Recent Advances in Nanomaterials for Sonodynamic Therapy. *Nano Res* (2020) 13(11):2898–908. doi: 10.1007/s12274-020-2992-5
7. Liang S, Deng X, Chang Y, Sun C, Shao S, Xie Z, et al. Intelligent Hollow Pt-CuS Janus Architecture for Synergistic Catalysis-Enhanced Sonodynamic and Photothermal Cancer Therapy. *Nano Lett* (2019) 19(6):4134–45. doi: 10.1021/acs.nanolett.9b01595
8. Huang P, Qian X, Chen Y, Yu L, Lin H, Wang L, et al. Metalloporphyrin-Encapsulated Biodegradable Nanosystems for Highly Efficient Magnetic Resonance Imaging-Guided Sonodynamic Cancer Therapy. *J Am Chem Soc* (2017) 139(3):1275–84. doi: 10.1021/jacs.6b11846
9. Jiang F, Yang C, Ding B, Liang S, Zhao Y, Cheng Z, et al. Tumor Microenvironment-Responsive MnSiO3-Pt@BSA-Ce6 Nanoplatform for Synergistic Catalysis-Enhanced Sonodynamic and Chemodynamic Cancer Therapy. *Chin Chem Lett* (2022) 19:2. doi: 10.1016/j.cclet.2021.12.096
10. Zhang H, Pan X, Wu Q, Guo J, Wang C, Liu H. Manganese Carbonate Nanoparticles-Mediated Mitochondrial Dysfunction for Enhanced Sonodynamic Therapy. *Exploration* (2021) 1(2). doi: 10.1002/EXP.20210010
11. Xiong Y, Xiao C, Li Z, Yang X. Engineering Nanomedicine for Glutathione Depletion-Augmented Cancer Therapy. *Chem Soc Rev* (2021) 50(10):6013–41. doi: 10.1039/D0CS00718H
12. Huang C, Zhu C, Chen J, Huang K, Li F, Ding S, et al. Nano-Platelets as an Oxygen Regulator for Augmenting Starvation Therapy Against Hypoxic Tumor. *Front Bioeng Biotechnol* (2020) 8. doi: 10.3389/fbioe.2020.571993
13. Tong Z, Gao Y, Yang H, Wang W, Mao Z. Nanomaterials for Cascade Promoted Catalytic Cancer Therapy. *View* (2021) 2(6):20200133. doi: 10.1002/VIW.20200133
14. Zhang K, Wu J, Zhao X, Qin J, Xue Y, Zheng W, et al. Prussian Blue/Calcium Peroxide Nanocomposites-Mediated Tumor Cell Iron Mineralization for Treatment of Experimental Lung Adenocarcinoma. *ACS Nano* (2021) 15 (12):19838–52. doi: 10.1021/acsnano.1c07308
15. Qin Z, Chen B, Mao Y, Shi C, Li Y, Huang X, et al. Achieving Ultrasmall Prussian Blue Nanoparticles as High-Performance Biomedical Agents With Multifunctions. *ACS Appl Mater Interfaces* (2020) 12(51):57382–90. doi: 10.1021/acsami.0c18357
16. Zhao S, Luo Y, Chang Z, Liu C, Li T, Gan L, et al. BSA-Coated Gold Nanorods for NIR-II Photothermal Therapy. *Nanoscale Res Lett* (2021) 16(1):170. doi: 10.1186/s11671-021-03627-7
17. Cao C, Zou H, Yang N, Li H, Cai Y, Song X, et al. Fe3 O4 /Ag/Bi2 MoO6 Photoactivatable Nanozyme for Self-Replenishing and Sustainable Cascaded Nanocatalytic Cancer Therapy. *Adv Mater* (2021):e2106996. doi: 10.1002/adma.202106996
18. Ai Y, Hu ZN, Liang X, H.b. Sun H, Liang Q. Recent Advances in Nanozymes: From Matters to Bioapplications. *Adv Funct Mater* (2021) 32(14):2110432. doi: 10.1002/adfm.202110432
19. Hu JJ, Chen Y, Li ZH, Peng SY, Sun Y, Zhang XZ. Augment of Oxidative Damage With Enhanced Photodynamic Process and MTH1 Inhibition for Tumor Therapy. *Nano Lett* (2019) 19(8):5568–76. doi: 10.1021/acs.nanolett.9b02112
20. Zhang X, He C, Chen Y, Chen C, Yan R, Fan T, et al. Cyclic Reactions-Mediated Self-Supply of H_2O_2 and O_2 for Cooperative Chemodynamic/Starvation Cancer Therapy. *Biomaterials* (2021) 275:120987. doi: 10.1016/j.biomaterials.2021.120987
21. Yang B, Yao H, Tian H, Yu Z, Guo Y, Wang Y, et al. Intratumoral Synthesis of Nano-Metalchelate for Tumor Catalytic Therapy by Ligand Field-Enhanced Coordination. *Nat Commun* (2021) 12(1):3393. doi: 10.1038/s41467-020-20522-4
22. Cui X, Lu G, Fang F, Xiong Y, Tian S, Wan Y, et al. Iron Self-Boosting Polymer Nanoenzyme for Low-Temperature Photothermal-Enhanced Ferrotherapy. *ACS Appl Mater Interfaces* (2021) 13(26):30274–83. doi: 10.1021/acsami.1c01658
23. Koo S, Park OK, Kim J, Han SI, Yoo TY, Lee N, et al. Enhanced Chemodynamic Therapy by Cu-Fe Peroxide Nanoparticles: Tumor

Microenvironment-Mediated Synergistic Fenton Reaction. *ACS Nano* (2022) 16(2):2535–2545. doi: 10.1021/acsnano.1c09171
24. Lin LS, Huang T, Song J, Ou XY, Wang Z, Deng H, et al. Synthesis of Copper Peroxide Nanodots for H_2O_2 Self-Supplying Chemodynamic Therapy. *J Am Chem Soc* (2019) 141(25):9937–45. doi: 10.1021/jacs.9b03457
25. Hao YN, Gao YR, Li Y, Fei T, Shu Y, Wan JH. Ultrasmall Copper–Gallic Acid Nanodots for Chemodynamic Therapy. *Adv Mater Interfaces* (2021) 8 (24):2101173. doi: 10.1002/admi.202101173
26. Lu X, Gao S, Lin H, Yu L, Han Y, Zhu P, et al. Bioinspired Copper Single-Atom Catalysts for Tumor Parallel Catalytic Therapy. *Adv Mater* (2020) 32 (36):e2002246. doi: 10.1002/adma.202002246
27. Zhao S, Zhang L, Deng L, Ouyang J, Xu Q, Gao X, et al. NIR-II Responsive Hydrogel as an Angiogenesis Inhibition Agent for Tumor Microenvironment Reprogramming. *Small* (2021) 17(47):e2103003. doi: 10.1002/smll.202103003
28. Qiu M, Wang D, Liang W, Liu L, Zhang Y, Chen X, et al. Novel Concept of the Smart NIR-Light-Controlled Drug Release of Black Phosphorus Nanostructure for Cancer Therapy. *Proc Natl Acad Sci USA* (2018) 115 (3):501–6. doi: 10.1073/pnas.1714421115
29. Chen M, Tan Y, Dong Z, Lu J, Han X, Jin Q, et al. Injectable Anti-Inflammatory Nanofiber Hydrogel to Achieve Systemic Immunotherapy Post Local Administration. *Nano Lett* (2020) 20:(9):6763–73. doi: 10.1021/acs.nanolett.0c02684
30. Zhu D, Zheng Z, Luo G, Suo M, Li X, Duo Y, et al. Single Injection and Multiple Treatments: An Injectable Nanozyme Hydrogel as AIEgen Reservoir and Release Controller for Efficient Tumor Therapy. *Nano Today* (2021) 37:101091. doi: 10.1016/j.nantod.2021.101091
31. Zhu D, Chen H, Huang C, Li G, Wang X, Jiang W, et al. H2O2 Self-Producing Single-Atom Nanozyme Hydrogels as Light-Controlled Oxidative Stress Amplifier for Enhanced Synergistic Therapy by Transforming "Cold" Tumors. *Adv Funct Mater* (2022) 32(16):2110268. doi: 10.1002/adfm.202110268
32. Chen D, Chen C, Huang C, Chen T, Liu Z. Injectable Hydrogel for NIR-II Photo-Thermal Tumor Therapy and Dihydroartemisinin-Mediated Chemodynamic Therapy. *Front Chem* (2020) 8:251. doi: 10.3389/fchem.2020.00251
33. Dong Y, Li S, Li X, Wang X. Smart MXene/agarose Hydrogel With Photothermal Property for Controlled Drug Release. *Int J Biol Macromol* (2021) 190:693–9. doi: 10.1016/j.ijbiomac.2021.09.037
34. Zhu D, Zhang J, Luo G, Duo Y, Tang BZ. Bright Bacterium for Hypoxia-Tolerant Photodynamic Therapy Against Orthotopic Colon Tumors by an Interventional Method. *Adv Sci* (2021):e2004769. doi: 10.1002/advs.202004769
35. Zhu J, Ouyang A, Shen Z, Pan Z, Banerjee S, Zhang Q, et al. Sonodynamic Cancer Therapy by Novel Iridium-Gold Nanoassemblies. *Chin Chem Lett* (2022) 33(4):1907–12. doi: 10.1016/j.cclet.2021.11.017
36. Huang C, Ding S, Jiang W, Wang F-B. Glutathione-Depleting Nanoplatelets for Enhanced Sonodynamic Cancer Therapy. *Nanoscale* (2021) 13(8):4512–8. doi: 10.1039/D0NR08440A
37. Meng Z, Zhou X, Xu J, Han X, Dong Z, Wang H, et al. Light-Triggered *In Situ* Gelation to Enable Robust Photodynamic-Immunotherapy by Repeated Stimulations. *Adv Mater* (2019) 31(24):e1900927. doi: 10.1002/adma.201900927
38. Chen WH, Luo GF, Lei Q, Hong S, Qiu WX, Liu LH, et al. Overcoming the Heat Endurance of Tumor Cells by Interfering With the Anaerobic Glycolysis Metabolism for Improved Photothermal Therapy. *ACS Nano* (2017) 11 (2):1419–31. doi: 10.1021/acsnano.6b06658
39. She D, Peng S, Liu L, Huang H, Zheng Y, Lu Y, et al. Biomimic FeS2 Nanodrug With Hypothermal Photothermal Effect by Clinical Approved NIR-II Light for Augmented Chemodynamic Therapy. *Chem Eng J* (2020) 400:125933. doi: 10.1016/j.cej.2020.125933
40. Yang X, Wang D, Shi Y, Zou J, Zhao Q, Zhang Q, et al. Black Phosphorus Nanosheets Immobilizing Ce6 for Imaging-Guided Photothermal/Photodynamic Cancer Therapy. *ACS Appl Mater Interfaces* (2018) 10 (15):12431–40. doi: 10.1021/acsami.8b00276
41. Wang H, Yang J, Cao P, Guo N, Li Y, Zhao Y, et al. Functionalization of Bismuth Sulfide Nanomaterials for Their Application in Cancer Theranostics. *Chin Chem Lett* (2020) 31(12):3015–26. doi: 10.1016/j.cclet.2020.05.003

Conflict of Interest: The authors declare that the research was conducted in the absence of any commercial or financial relationships that could be construed as a potential conflict of interest.

The reviewers MS and PQ declared a shared parent affiliation with the author MC at the time of review.

Publisher's Note: All claims expressed in this article are solely those of the authors and do not necessarily represent those of their affiliated organizations, or those of the publisher, the editors and the reviewers. Any product that may be evaluated in this article, or claim that may be made by its manufacturer, is not guaranteed or endorsed by the publisher.

Copyright © 2022 Wang, Zeng, Zhang, Chen and Huang. This is an open-access article distributed under the terms of the Creative Commons Attribution License (CC BY). The use, distribution or reproduction in other forums is permitted, provided the original author(s) and the copyright owner(s) are credited and that the original publication in this journal is cited, in accordance with accepted academic practice. No use, distribution or reproduction is permitted which does not comply with these terms.

frontiers | Frontiers in Oncology

REVIEW
published: 06 July 2022
doi: 10.3389/fonc.2022.939365

Research Progress of Photothermal Nanomaterials in Multimodal Tumor Therapy

Xiaolu Shi[1†], *Ye Tian*[1†], *Yang Liu*[1], *Zhengrong Xiong*[2,3], *Shaobo Zhai*[1], *Shunli Chu*[1*] *and Fengxiang Gao*[2,3*]

[1] Department of Implantology, Hospital of Stomatology, Jilin University, Changchun, China, [2] University of Science and Technology of China, Hefei, China, [3] Changchun Institute of Applied Chemistry, Chinese Academy of Sciences, Changchun, China

OPEN ACCESS

Edited by:
Kelong Ai,
Central South University, China

Reviewed by:
Peng Zhang,
Nanjing Stomatological Hospital Medical School of Nanjing University, China
Zheng Yang Li,
Tianjin Stomatological Hospital, China

***Correspondence:**
Shunli Chu
chusl@jlu.edu.cn
Fengxiang Gao
gfx26@ciac.ac.cn

[†]These authors have contributed equally to this work and share first authorship

Specialty section:
This article was submitted to Pharmacology of Anti-Cancer Drugs, a section of the journal Frontiers in Oncology

Received: 09 May 2022
Accepted: 26 May 2022
Published: 06 July 2022

Citation:
Shi X, Tian Y, Liu Y, Xiong Z, Zhai S, Chu S and Gao F (2022) Research Progress of Photothermal Nanomaterials in Multimodal Tumor Therapy. Front. Oncol. 12:939365. doi: 10.3389/fonc.2022.939365

The aggressive growth of cancer cells brings extreme challenges to cancer therapy while triggering the exploration of the application of multimodal therapy methods. Multimodal tumor therapy based on photothermal nanomaterials is a new technology to realize tumor cell thermal ablation through near-infrared light irradiation with a specific wavelength, which has the advantages of high efficiency, less adverse reactions, and effective inhibition of tumor metastasis compared with traditional treatment methods such as surgical resection, chemotherapy, and radiotherapy. Photothermal nanomaterials have gained increasing interest due to their potential applications, remarkable properties, and advantages for tumor therapy. In this review, recent advances and the common applications of photothermal nanomaterials in multimodal tumor therapy are summarized, with a focus on the different types of photothermal nanomaterials and their application in multimodal tumor therapy. Moreover, the challenges and future applications have also been speculated.

Keywords: photothermal therapy, nanomaterial, tumor, multimodal therapy, photothermal agents, synergistic effect

1 INTRODUCTION

Cancer poses a serious threat to human health worldwide, despite the developments in modern medical technology. Cancer is difficult or impossible to cure because it involves various genetic changes and cell abnormalities. Moreover, its complexity and heterogeneity promote the aggressive growth of cancer cells, resulting in significant incidence and mortality rates (1–3). The three traditional methods of tumor treatment include surgery, radiotherapy, and chemotherapy. However, due to severe surgical trauma, nonspecific and excessive radiation, and the irreplaceable defects of these therapies in targeting, bio-compatibility, multidrug resistance, and drug accumulation, patients may suffer from serious physiological side effects, resulting in poor quality of life and difficulty in achieving the target treatment effect (4–6).

These treatment deficiencies have inspired the development of new, precise, and more effective treatment strategies for tumors. For example, several emerging treatment methods, such as photodynamic therapy (PDT) (7, 8), photothermal therapy (PTT) (9, 10), and photoacoustic therapy (11, 12) have improved or can potentially improve therapeutic outcomes. Among them,

PTT is a new type of minimally invasive tumor light therapy that has developed rapidly in recent years. It mainly uses photothermal conversion nanomaterials with strong absorption in the near-infrared light region (wavelength range 700–1300 nm) (13–15) to convert the absorbed light energy into heat energy effectively under the irradiation of the near-infrared laser, resulting in an increase in the temperature of local tumor tissues up to 40–45°C (hyperthermia) or above 45°C (thermal ablation) (14, 16). This results in degeneration and necrosis of tumor cells to achieve the goal of tumor therapy. The destruction of tumor tissue by PTT mainly occurs through killing tumor cells and destroying tumor blood vessels. The ability of tumor cells to tolerate high temperatures is much lower than that of normal cells. Specifically, the thermal lethal temperature of most tumor cells is between 42 and 43°C, while normal cells can tolerate such temperatures for a prolonged period. Therefore, the local hyperthermia produced by PTT can selectively kill tumor cells and cause irreversible damage, while normal cells are not damaged. Regarding blood vessels, compared with the blood vessels of normal tissue, those of tumor tissue have abnormal morphological growth, imperfect tissue and function, and are prone to rupture when the temperature and pressure increase. This causes tumor tissue to be more prone to damage by hyperthermia. Thus, PTT can effectively destroy tumor blood vessels, killing tumor cells without damaging normal tissues or causing systemic toxic reactions. Because PTT has the advantages of rapid targeted killing, being minimally invasive, and minimal toxic side effects, it is also known as "green therapy," which carries significant potential in the field of alternative surgical resection (14, 17, 18).

It has been reported that PTT requires a temperature above 50°C to achieve tumor thermal ablation. In addition, cancer cells treated at low temperatures (around 43°C) may survive through self-repair of their heat shock proteins (HSPs), which could lead to treatment resistance and reduce treatment efficiency (19, 20). In recent years, the great progress in nanomaterials, medicine, and biology has promoted the application of nanomaterials in tumor therapy (21, 22). Moreover, great progress has been made in the construction of multifunctional photothermal nanomaterials, which can integrate a variety of treatment modes into a single nano platform. Compared with monotherapy, the combination of multiple therapies usually shows superiority in therapeutic effect. This advanced synergistic therapy can not only maintain the advantages of non-invasive, low toxicity, and convenient administration of PTT, but also relieve the problems of non-selectivity and multidrug resistance of traditional chemotherapy, and has achieved good therapeutic results (20).

This review will focus on the research progress of photothermal nanomaterials in multimodal tumor therapy and consists of a brief introduction to the classification of photothermal nanomaterials and their relative merits. Subsequently, multimodal treatments of tumors based on photothermal nanomaterials are clarified in detail. Finally, an outlook is provided to address recent challenges and suggest better treatment applications and research focuses to pursue new opportunities ahead.

2 CLASSIFICATION OF PHOTOTHERMAL NANOMATERIALS

The goal of PTT is to make use of the hyperthermic effect of photothermal agents (PTAs), which can absorb light energy and convert it into heat energy, raising the temperature of the lesion site and ultimately causing the death of tumor cells (23, 24). To reduce the influence of localized high temperatures on normal tissue, near-infrared (NIR) light is usually selected for PTT because it has less tissue absorption and scattering and is able to penetrate deep tissue (15, 25). In addition, the ideal photothermal material should have higher photothermal conversion efficiency (PCE) and be accumulated effectively in tumor tissue (26). With the progress of PTT research and the rapid development of nanomaterials, photothermal nanomaterials have been more widely used than other photothermal materials because of their higher PCE and ability to be used in a multimodal tumor therapy platform (27–29). This review summarizes the common photothermal nanomaterials, which are divided into inorganic, organic, and composite photothermal nanomaterials (**Table 1**).

2.1 Inorganic Photothermal Nanomaterials

2.1.1 Precious Metal Nanomaterials

Precious metal nanomaterials, including gold, silver, palladium, and platinum, are considered to be simple and effective PTAs (23, 67, 68) due to their strong surface plasmon resonance (SPR), synthetic tunability, biological imaging potential, and excellent photothermal properties, such as high PCE in the high-absorption cross-section and NIR region.

Studies have shown that gold is one of the most popular nanomaterials for mediating PTT (69, 70), as it has good biocompatibility and low cytotoxicity (71). The photothermal conversion phenomenon in gold nanoparticles (GNPs) is based on the collective oscillation of free electrons on the surface of GNPs under electromagnetic radiation. The local area around GNPs is heated by electronic excitation and relaxation, which leads to the destruction of tumor tissue (72). At present, several gold nanomaterials with unique size and morphology have been developed, including nanorods, nanospheres, nanostars, nanocages, and nanoshells, among others. Choe et al. (30) loaded high concentration gold nanoparticles into mesoporous silica nanocapsules to form yolk-shell-structured gold nanospheres (aAuYSs) to study their photothermal effect on drug-resistant ovarian cancer cells. Under 808-nm laser irradiation, the cultured cancer cells were eliminated when the concentration of aAuYSs was 300 μg/mL. Moreover, *in vivo* experiments showed that after the combined treatment of aAuYSs and doxorubicin (Dox), the tumor volume and size were significantly reduced, and the number of Ki-67-positive proliferating cancer cells sharply decreased, indicating that aAuYSs can be used as a multifunctional photothermal nanoplatform for PTT and combined therapy.

TABLE 1 | Summary of photothermal nanomaterials in this review.

PTAs	Nanomaterials	Wavelength	PCE	Applications	Reference
Inorganic photothermal nanomaterials	aAuYSs	808nm	-	PTT+CT	(30)
	BSA-Silver NPs	690nm	–	PTT	(31)
	Pd nanosheets	808nm	-	PTT	(32)
	DPCN	808nm	–	PTT+CT	(33)
	USPIO-PEG-sLe^x	808nm	-	PTT	(34)
	FA-BSA-PEG/MoOx@DTX	808nm	43.41%	PTT+CT	(35)
	WO_3 nanosheets	808nm	41.6%	PTT	(36)
	Z@CD/P	808nm	–	PTT+CT	(37)
	mBMNI NPs	808nm	45.9%	PTT+PDT+CDT	(38)
	NB/CuS@PCM NPs	1060nm	–	PTT+CDT	(39)
	MoS_2@DOX/MnO_2-PEG	808nm	33.7%	PTT+CT	(40)
	TiS_2 nanosheets	808nm	46.82% (808nm)	PTT+IT	(41)
		1064nm	45.51% (1064nm)		
	HMC-SS-PDA@CDs	808nm	35.9%	PTT+CT	(42)
	CdTeSe/ZnS@QDs	457nm	11%	PTT+PDT	(43)
	CNTs-PS/siRNA	808nm	59.3% (SCNT-PS)	PTT+GT	(44)
			57.8% (MCNT-PS)		
	HPP	1064nm	45.1%	PTT	(45)
	mGOG	808nm	-	PTT+CT	(46)
	DOX-Fe_3O_4@CGA	808nm	–	PTT+CT	(47)
	Nb_2C@PDA-R837@RBC NPs	1064nm	27.6%	PTT+IT	(48)
	BP NS-PAMAM@DOX-HA	808nm	–	PTT+CT	(49)
	Co-P@$mSio_2$@DOX-MnO_2	808nm	-	PTT+CT	(50)
	UCNPs@$mSiO_2$FePc-MC540	808nm		PTT+PDT	(51)
	PCM+PTX@mPBs/PEG	808nm	16,9%	PTT+CT	(52)
Organic photothermal nanomaterials	Cy5.5&ICG@ZIF-8-Dex	780nm	27.9%	PTT	(53)
	PPor NPs	808nm	70%	PTT+IT	(54)
	T-MPs	808nm	16.8%	PTT+Operation	(55)
	BBDP	690nm	54.2%	PTT+PDT	(56)
	DTPADPP/TPADDPP	635nm	48.1% (DTPADPP)	PTT	(57)
			41.7% (TPADDPP)		
	CMC/CS@PPy+5Fu NPs	808nm	21.6%	PTT+CT	(58)
	PANITG	808nm	55%	PTT+Starvation therapy	(59)
	NIRb14 NPs	808nm	31.2%	PTT	(60)
	MNP@PEDOT : PSS NPs	808nm	–	PTT	(61)
	Cu-PDA-FA NPs	808nm	46.84%	PTT+CDT+IT	(62)
	OMCNs	808nm	37.3%	PTT	(63)
	MNPs	808nm	87.65%	PTT+PDT	(64)
Organic–inorganic hybrid photothermal nanomaterials	Fe_2O_3@PEDOT-siRNA NPs	808nm	54.3%	PTT+GT	(65)
	RCDS@MIL-100	660nm	31.2%	PTT+CDT	(66)

PCE, photothermal conversion efficiency; PTT, photothermal therapy; CT, chemotherapy; CDT, chemodynamic therapy; IT, immunotherapy; GT, gene therapy.

Silver nanoparticles (SNPs), another type of precious metal nanomaterial, have been widely used due to their unique properties, such as controllable size and shape, easy modification, and excellent optoelectronic properties. Similar to GNPs, the SPR of SNPs can be adjusted to the infrared region by changing their size and shape (73). Additionally, Kim et al. (31) prepared SNPs coated with bovine serum albumin (BSA) (BSA-SNPs), which could internalize and kill melanoma cells by inducing ROS through cell analysis. These nanoparticles were also found to play a potential role in inhibiting angiogenesis. In addition, BSA-SNPs showed a significant increase in the temperature of a suspension under the irradiation of a laser at 690 nm and had a strong photothermal conversion capability, which could be used for photothermal cancer therapy.

Palladium-based nanomaterials, such as palladium nanosheets (74), porous/hollow palladium nanoparticles (75), and palladium@M (M=Ag, Au, Pt, SiO_2, ZIF-8) (76–80) nanocomposites, also show strong absorption in the NIR region, as well as ideal PCE, excellent photothermal stability, and good biocompatibility (81). Therefore, palladium-based photothermal nanomaterials have become an option for cancer imaging contrast agents and therapeutic agents. Chen et al. (32) designed palladium nanosheets with a thickness of 1.8 nm and a diameter of 5–80 nm to evaluate the effect of size on the biological behavior of these nanosheets through cell and animal model experiments. The experimental results showed that compared with the large palladium nanowires, the smaller nanowires demonstrated a better photothermal effect under ultra-low laser irradiation. In addition, *in vivo* experiments revealed that 5-nm palladium nanosheets could escape the reticuloendothelial system with a longer blood half-life and be excreted from the kidneys, while the large nanosheets accumulated in the liver and spleen.

As a photothermal nanomaterial, platinum nanoparticles (PtNPs) slowly and continuously increase the temperature with

light irradiation, not exceeding 46°C, which can effectively avoid normal cell damage (82, 83). Apart from good optical and photothermal stability, PtNPs can also be involved in the design of multimodal tumor treatment platforms, which can be used in combination with chemotherapy or radiotherapy (84, 85). Zhou et al. synthesized dendritic platinum-copper alloy nanoparticles (DPCNs) as a multimodal, therapeutic, tumor imaging platform (33). The PTT *in vitro* assay revealed that DPCNs ingested by PC-9 cells could effectively kill cancer cells under NIR irradiation. In addition, compared with the control group treated with DPCNs/NIR or Dox alone, the killing rate of cancer cells treated with DPCNs/Dox and irradiated with NIR laser was higher, indicating that DPCNs have potential for photothermal and chemotherapy.

2.1.2 Transition Metal Dichalcogenide Nanomaterials

Transition metal dichalcogenides (TMDCs) are usually composed of one layer of transition metal atoms and two layers of chalcogenide atoms, and their generalized formula is MX_2. M refers to the transition metals of groups 4–10, such as copper, molybdenum, tungsten, titanium, etc., while X refers to a chalcogen (86). It has been found that monolayer TMDCs exhibit strong NIR absorption, good PCE, and excellent photothermal stability (87, 88), giving TMDCs the potential to be used as PTAs (89).

In recent years, copper nanomaterials have been widely used in cancer therapy (90). Among those used in PTT for cancer, such as copper selenide, copper telluride, and copper oxide, copper sulfide is the most explored (91). It has been found that as a P-type semiconductor, copper chalcogenide nanomaterials have composition-dependent localized SPR and ideal PCE in the NIR region (92, 93). Moreover, Huang et al. (39) combined monoterpenoid sensitizer, borneol, and NIR-II PTA copper sulfide to make thermo-responsive vehicle NB/CuS@PCMNPs. Under the irradiation of a 1060-nm laser, the high temperature produced by copper sulfide nanoparticles can be used in PTT. The results of animal experiments showed that NB/CuS@PCMNPs could aggregate in the tumor site and significantly inhibit tumor growth.

Titanium disulfide is another common material for TMDCs with excellent stability, electrical conductivity, and strong absorption in the NIR window (41). In addition, due to the local SPR effect, the absorption peak of these nanosheets can be shifted from red to the range of 1000–1350 nm by adjusting the thickness and width of the nanowires (94). Fu et al. (41) made a multifunctional NIR-II nano-preparation based on titanium disulfide, which can be used in magnetic targeted NIR-II photoacoustic/magnetic resonance imaging-guided synergistic photothermal-immune combination therapy. The results of *in vivo* experiments showed that the primary tumors in the group that underwent PTT combined with immunotherapy disappeared without recurrence after 16 days of treatment. This significantly inhibited the tumor growth rate, indicating that titanium disulfide has great potential in the field of PTT combined with immunotherapy and imaging.

In addition, the crystal structure of molybdenum disulfide is a honeycomb, similar to graphene, which can be obtained through stripping or synthesis and has a variety of forms, such as nanosheets and quantum dots, among others (95–98). It has been found that molybdenum disulfide nanoparticles have become commonly used PTAs in cancer treatment due to their good biocompatibility, strong SPR, excellent PCE, and low production cost (99). Liu et al. (40) synthesized a mesoporous core-shell structure with molybdenum disulfide as the core and manganese dioxide as the shell. This structure was used to wrap the chemotherapeutic drug, Dox, and then modified with mPEG-NH_2 to prepare MoS_2@Dox/MnO_2-PEG (MDMP) composite antitumor nanocomposites. The *in vivo* and *in vitro* experiments showed that MDMP had excellent antitumor activity (tumor survival rate: 11.8%) and good PCE (33.7%).

2.1.3 Metal Oxide Nanomaterials

In addition to TMDC nanomaterials, nanomaterials containing transition metal oxides have also received extensive attention in the field of PTT (100) due to their excellent PCE good biocompatibility, excellent chemical stability, adjustable band gap, and low cost. Iron oxide, molybdenum oxide, tungsten oxide, zinc oxide, and manganese oxide are used as common metal oxide nanomaterials.

Magnetic nanoparticles, mainly including magnetite (Fe_3O_4), maghemite (γ-Fe_2O_3), or a combination of the two (101) show great potential in cancer therapy in the form of magnetic resonance imaging-guided chemotherapy (102, 103), PDT (104, 105), and PTT (106, 107) due to their unique superparamagnetic iron oxide nanoparticles. In addition, iron oxide nanoparticles show excellent PCE in a biological environment and have good chemical stability and low cytotoxicity (108). Moreover, the US Food and Drug Administration has approved its application in the human body (109). Liu et al. (34) synthesized USPIO-PEG-sLe^x, which consists of nanocomposites of ultrasmall superparamagnetic iron oxide nanoparticles coated with polyethylene glycol (PEG) coupled with Sialyl Lewis X. The USPIO-PEG-sLex nanoparticles have good photothermal conversion properties, and the temperature and concentration of the solution are positively correlated with the power density of NIR on 808-nm wavelengths. The results of PTT *in vitro* showed that as the nanoparticle concentration increased, the survival rate of 5-8F cells significantly decreased, which could effectively inhibit the development of tumors (**Figure 1**).

Molybdenum-based materials can be divided into two categories: transition metal oxides composed of molybdenum dioxide and molybdenum trioxide, and TMDCs composed of molybdenum disulfide. Transition metal molybdenum oxide has a similar, adjustable, local SPR effect to precious metal nanomaterials (110). Molybdenum trioxide nanoparticles have been reported to have excellent light absorption ability in the NIR region and can produce singlet oxygen under the irradiation of NIR light. Thus, molybdenum oxide nanomaterials can be used in PDT or PTT for tumors (111, 112). Qiu et al. (35) combined folic acid and α-lipoic acid-conjugated mPEG-NH_2 (LA-PEG) and modified BSA with molybdenum oxide nanosheets to prepare multi-functional degradable FA-BSA-PEG/MoOx nanosheets (**Figure 2**). The results of *in vivo* and

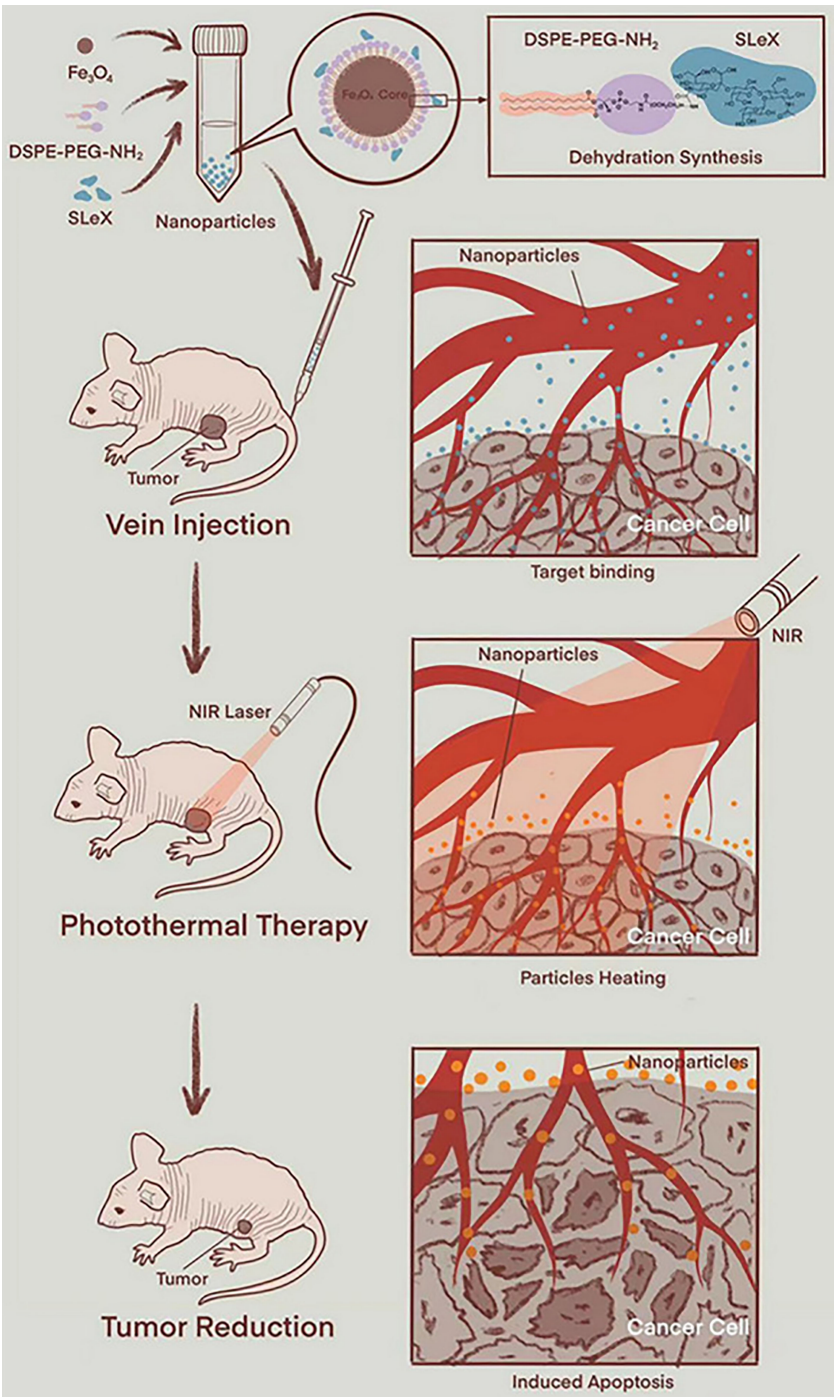


FIGURE 1 | Schematic diagram of PTT (using animal experimental research as a model) (34). Reproduced with permission from Liu et al., 2021.

in vitro anti-tumor experiments showed that FA-BSA-PEG/MoOx nanosheets significantly increased the temperature of the tumor site, inducing immunogenic cell death, which triggered an immune response *in vivo* through the combination of PTT and chemotherapy, inhibiting primary tumor growth (inhibition rate: 51.7%) and lung metastasis (inhibition rate: 93.6%). This novel nanosheet is a promising avenue for combination therapy for breast tumors.

Tungsten nanomaterials, similar to precious metal nanomaterials, exhibit a local SPR effect because of their outer-d valence electrons, which can be used to produce a photothermal effect (113). The size and shape of the

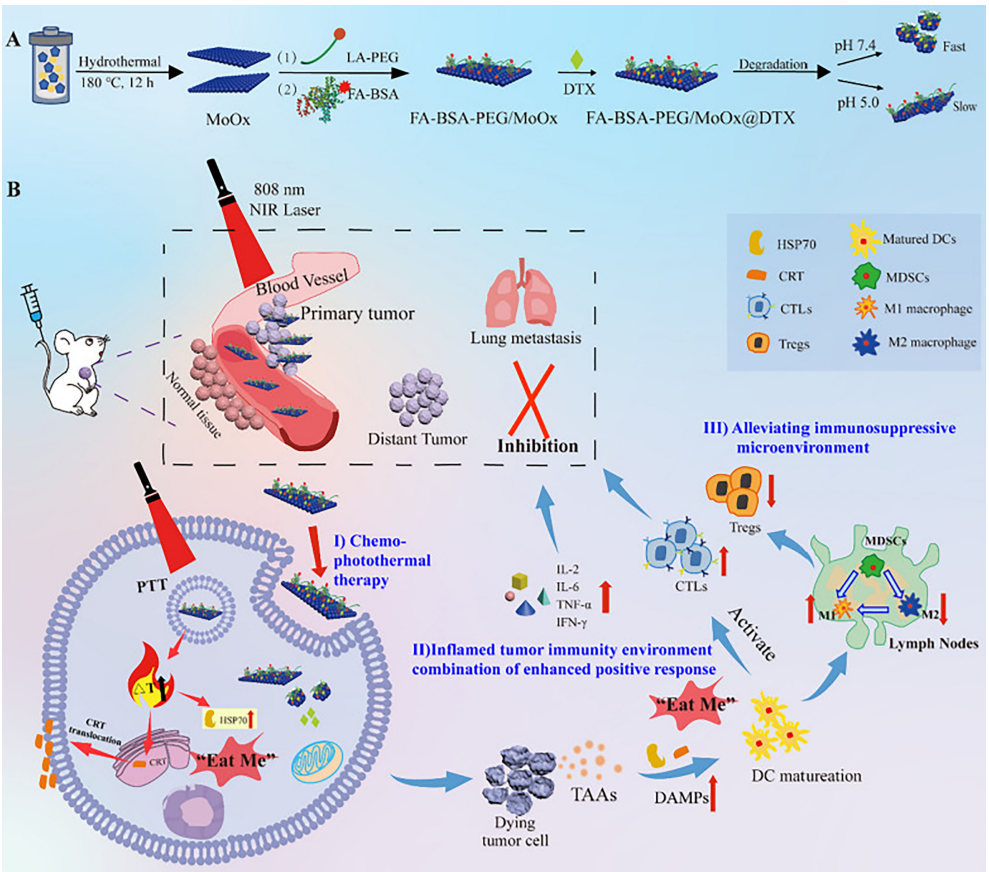


FIGURE 2 | The schematic illustration of the multi-strategy for cancer treatment. **(A)** The preparation route of the FA-BSA-PEG/MoOx@DTX nanosheet and the *in vitro* antitumor and degradation experimental design; **(B)** the elucidation of the mechanism of FA-BSA-PEG/MoOx@DTX + NIR combination therapy for meliorating tumor immunosuppression, inhibiting distant tumor and lung metastasis (35). Reproduced with permission from (35).

nanoparticles also play a role in the SPR effect of tungsten nanomaterials (114, 115). Among tungsten nanomaterials with different stoichiometry, tungsten oxide nanomaterials are among the most widely used materials in the biomedical field (116, 117). In particular, $W_{20}O_{58}$, $W_{18}O_{49}$, and $W_{24}O_{68}$ are more common PTAs because of their excellent optical absorption capacity in the NIR region (118). Liang et al. (36) introduced oxygen vacancy (OV) tuning into oxygen-deficient tungsten trioxide nanosheets to optimize the chemical and electrical properties. The experimental results show that under the irradiation of single-wavelength NIR (808 nm), tungsten trioxide-OVs exhibited good PCE (41.6%) and an effective tumor inhibition rate (96.8%).

Zinc oxide is a multi-functional material with unique physical and chemical properties, such as high chemical stability, high electrochemical coupling coefficient, wide radiation absorption range, and high light stability (119, 120). Zinc oxide nanomaterials can appear in one-dimensional (121), two-dimensional (122), and three-dimensional (123) structures, providing one of the greatest assortments of particle structures among all known materials (124). Thus, zinc oxide is a potential alternative for PTT (72). Deng et al. (37) prepared multifunctional nanoparticles (Z@CD/P) using ZnO@CuS as the carrier, as well as β-cyclodextrin (β-CD) modified by 2,3-dimethyl maleic anhydride (DMA) (β-CD-DMA), and mPEG-NH_2 modified by DMA (PEG-DMA) to increase stability. They were loaded with Dox and pirfenidone (PFD). Zinc oxide and copper sulfide were found to promote tumor cell death by regulating the pathway of ROS production as well as that of GSH-GPX_4, and their photothermal conversion ability further promotes the anti-tumor effect.

Manganese oxide nanomaterials have great potential as PTAs and signal contrast agents for traditional PTT because of their excellent T1-weighted contrast signals, low cytotoxicity, and high PCE (72, 125). Liu et al. (126) proposed for the first time that ultra-thin manganese dioxide nanosheets have pH and redox responses as well as T1-weighted magnetic resonance imaging capabilities. Moreover, photothermal *in vivo* and *in vitro* experiments showed that these nanosheets also had good photothermal conversion ability (η: 21.4%) and a high inhibition rate on tumor growth (**Figure 3**). Xu et al. (38) designed bismuth/manganese oxide nanoparticles (mBMNI NPs) for targeting triple-negative breast cancer, which were encapsulated in the tumor cell membrane and loaded with

indocyanine green. The result of the photothermal experiment showed that mBMNI NPs absorbed NIR laser efficiently and generated a large amount of heat for PTT. Apart from high-efficiency PTT, mBMNI NPs also performed chemodynamic therapy (CDT) and PDT synergistically through the generated singlet oxygen and ICG, offering great potential for targeted triple-negative breast cancer therapy.

2.1.4 Carbon-Based Nanomaterials

In recent years, carbon-based nanomaterials have been widely studied as inorganic materials for PTT for tumors (100). Many carbon-based nanostructures have been developed for biomedical applications, such as carbon dots, quantum dots, graphene, and carbon nanotubes, among others. The graphitic structure of carbon-based materials endows them with strong absorption in the NIR region and good PCE (127, 128). In addition, the ultra-high surface area of carbon-based materials enables them to build multifunctional nanoplatforms, which have optimistic application prospects in tumor therapy (129).

2.1.4.1 Carbon Dots

As a new type of 0 dimensionality material, carbon dots (CDs) not only inherit the advantages of small molecules (such as fluorophores) and traditional semiconductors (such as inorganic quantum dots), but they also have additional properties (130). For example, CDs have excellent photostability, good biocompatibility, permeability, low toxicity, low cost, and are easy to prepare (131). However, most CDs usually absorb light in the short wavelength region due to the π-π^* transition of the C=C bond; therefore, other nanomaterials, such as metal nanoparticles (132) or semiconducting polymers (133) are needed as NIR-assisted PTAs (131). Lu et al. (42) assembled polydopamine (PDA) and carbon points on hollow mesoporous carbon (HMC) to construct a photothermal enhanced multi-functional system (HMC-SS-PDA@CDs). The results of *in vivo* experiments showed that under low-power, 808-nm laser radiation of 0.75 W/cm^2, the antitumor drug-loaded HMC-SS-PDA@CDs inhibited tumor growth by 92.6% and significantly reduced the toxicity of Dox to cells, indicating that Dox/HMC-SS-PDA@CD nanoparticles have good photothermal chemotherapeutic synergism and ideal biocompatibility.

2.1.4.2 Quantum Dots

Compared with traditional fluorescent dyes and proteins, quantum dots (QDs) have significant advantages, such as broad luminescence excitation spectra and narrow symmetrical emission spectra with large Stokes shifts (134, 135). Different types of quantum dots have varying chemical compositions and properties, which can affect their potential applications. The new generation of quantum dots, including non-cadmium and NIR-II window quantum dots, have excellent optical properties and biocompatibility required for *in vivo* applications and good prospects in the field of tumor therapy and imaging (136–138). Wang et al. (43) have developed cadmium tellurium selenium/

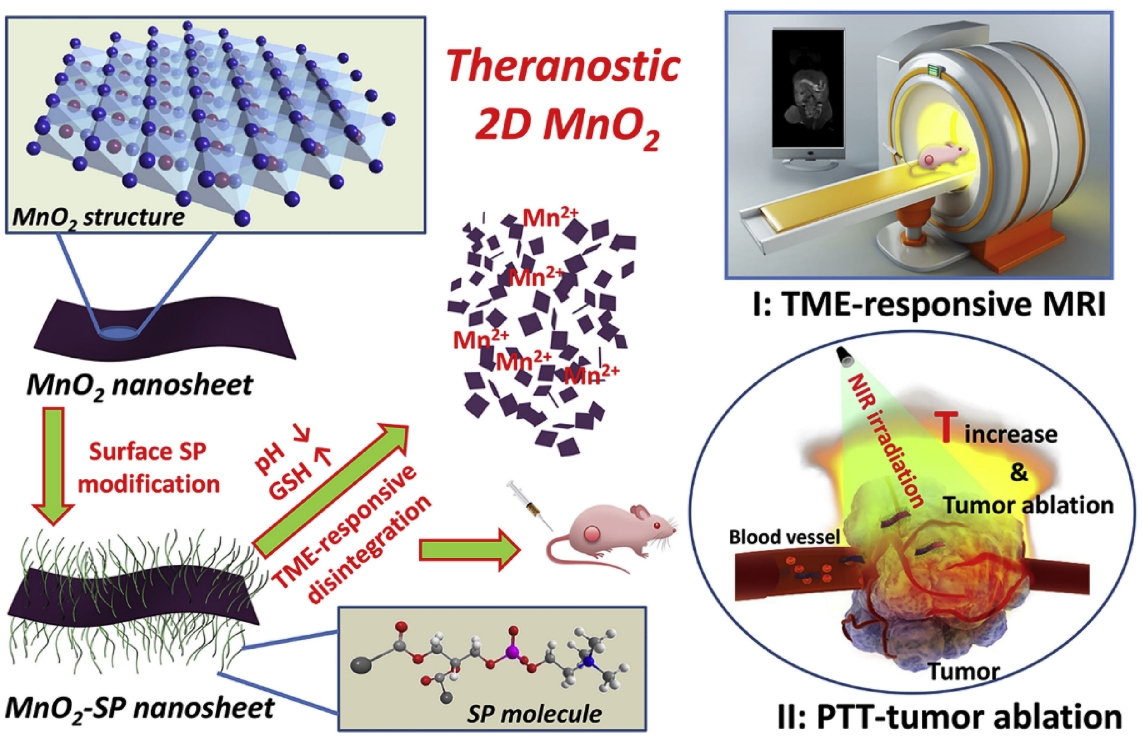


FIGURE 3 | Schematic illustration of synthetic procedure for MnO2-SPs nanosheets and their specific functions for tumor theranostics with TME sensitivity, including the acidic/reducing condition-triggered T1-weighted MR imaging and efficient PTT against tumor (126). Reproduced with permission from (126).

zinc sulfide core-shell quantum dots with excellent biocompatibility for PTT and fluorescence imaging of tumors. After being irradiated with blue light (80 mW/cm^2 blue laser) for 20 min, the quantum dots were heated rapidly. Due to their photothermal and photodynamic effects, the quantum dots induce complete apoptosis of the Huh7 hepatoma cell line, providing a new avenue for tumor therapy.

2.1.4.3 Carbon Nanotubes

Carbon nanotubes (CNTs), originally proposed by Iijima (139), are currently the most widely used carbon-based nanomaterials in the biomedical field (140, 141). CNTs are divided into two types according to the number of layers in their structure: single-walled CNTs (SCNTs), which consist of a single graphene sheet, and multi-walled CNTs (MCNTs), which consist of several sheets forming concentric cylinders (142). CNTs have been reported to have broad NIR absorption and are affected by the size and shape of the nanomaterials (143). CNTs exposed to NIR laser absorbs light energy and converts it into thermal energy, which can be used to ablate cancer cells (144). Zhao et al. (44) coated SCNTs and MCNTs with peptide lipid and sucrose laurate, respectively and loaded anti-survivin siRNA to synthesize a nano-delivery system (denoted SCNT-PS and MCNT-PS, respectively) with good temperature sensitivity and photothermal properties for tumor immunity and combination PTT. The results showed that CNT/siRNA inhibited tumor growth by silencing the expression of survivin and exhibiting a photothermal effect under NIR laser. SCNT-PS/siRNA showed high antitumor activity and had a complete inhibitory effect on some tumors. Neither SCNT-PS nor MCNT-PS nanoparticles had obvious cytotoxicity at a concentration of up to 60 μg/mL.

2.1.4.4 Mesoporous Carbon Nanoparticles

Mesoporous carbon nanoparticles (MCNs) or hollow carbon nanospheres (HCNs) are mesoporous nanomaterials with high pore volume and specific surface area, which have attracted attention in recent years (145, 146). It has been found that MCNs have a unique structure that can load a large number of hydrophobic drugs as well as excellent biocompatibility, which makes them an effective drug carrier (147, 148). In addition, MCNs have high efficiency in converting NIR laser energy into thermal energy and can be used in tumor PTT (72, 149). Xu et al. (45) designed polyethylene glycol-graft-polyethylenimine (HPP)-modified HCNs as NIR-II responsive PTAs. The experimental results showed that HPP-HCNs have a PCE of 45.1% under 1064nm laser irradiation. The *in vivo* and *in vitro* experiments showed that HPP had limited cytotoxicity to mice and good photothermal activity towards killing cancer cells in the xenograft 4T1 tumor-bearing mice model, which significantly inhibited tumor growth.

2.1.4.5 Graphene-Based Nanomaterials

Graphene, as a common carbon-based nanomaterial, has a wide range of applications as a biosensor, drug carrier, and tumor PTA because of its strong NIR absorption (150, 151). However, graphene has poor dispersibility in physiological fluid and is considered to have certain biological toxicity (152). To overcome these limitations, graphene requires surface modification with specific materials (153). Therefore, graphene-based nanomaterials (GBNs) have received increasing attention (154–156). For example, GBNs have been found to have a large surface area and can be used as drug carriers (157). GBNs are also widely used as PTAs in tumor therapy because of their good photothermal conversion ability in the NIR region (158, 159). Generally, GBNs can be divided into several types, including graphene with varied layers, graphene oxide (GO), and reduced graphene oxide (rGO) (160).

GO and rGO have great potential in the field of biomedicine, especially in drug delivery, biosensors, and targeted tumor therapy because of their tunable physicochemical properties, excellent biocompatibility, and outstanding photothermal properties (160–163). Dash et al. (46) modified rGO with citrate-coated magnetic nanoparticles, coupled with gastrin-releasing peptide receptor-binding peptide, and loaded Dox through the π-π bond to synthesize an rGO-based magnetic nanocomposite (mGOG). The results of the *in vitro* experiments showed that after being combined with 808-nm laser irradiation, the 50% inhibiting concentration and apoptosis rate of tumor cells were 0.19 μg/mL and 76.8%, respectively. At the same time, the increased expression of heat shock protein HSP70 confirmed the magnitude of the photothermal effect of mGOG. In addition, the mouse model experiment showed that, after 5 min of NIR laser irradiation, the tumor volumes in the mice in the experimental group were significantly reduced, the survival time was significantly prolonged, and the antitumor effect was significant.

With the continuous study of GBNs, graphene quantum dots (GQDs) first discovered by Ponomarenko and Geim (164), have undergone vigorous development in the biomedical field. GQDs exhibit inherent fluorescence properties, low cytotoxicity, stable photoluminescence, good biocompatibility, and superior resistance to photobleaching (165). After NIR light irradiation, GQDs also show excellent photothermal conversion ability (166, 167). These unique physicochemical properties endow GQDs with excellent potential in tumor therapy. Chen et al. (47) combined aptamer-modified GQDs with magnetic chitosan to form novel photothermal-chemotherapy drug delivery nanosystems (DOX-Fe_3O_4@CGA). The results of an *in vivo* antitumor experiment showed that under NIR laser irradiation, the temperature of the tumor site in mice increased rapidly to 43–45°C, and the tumor volume and weight significantly decreased over time. Thus, DOX-Fe_3O_4@CGA significantly inhibited tumor growth and prolonged survival time in mice, demonstrating excellent synergistic therapeutic ability.

2.1.5 Other Inorganic Photothermal Nanomaterials

MXenes refer to a series of carbides, nitrides, and carbonitrides containing transition metals (mainly from groups 3 and 4), with unique structure and excellent physicochemical properties (168–170) (**Figure 4**). The typical molecular formula is expressed as Mn $+1X_nT_x$ (e.g, $Ti_3C_2T_x$). Notably, MXenes have good optical properties for bioimaging and biosensors, and their excellent PCE and biocompatibility make them ideal candidates as efficient PTAs (172, 173). Lu et al. (48) coated a layer of red blood cell membrane on polydopamine-modified niobium carbide nanosheets coated with immunoadjuvant R837 to synthesize a new type of

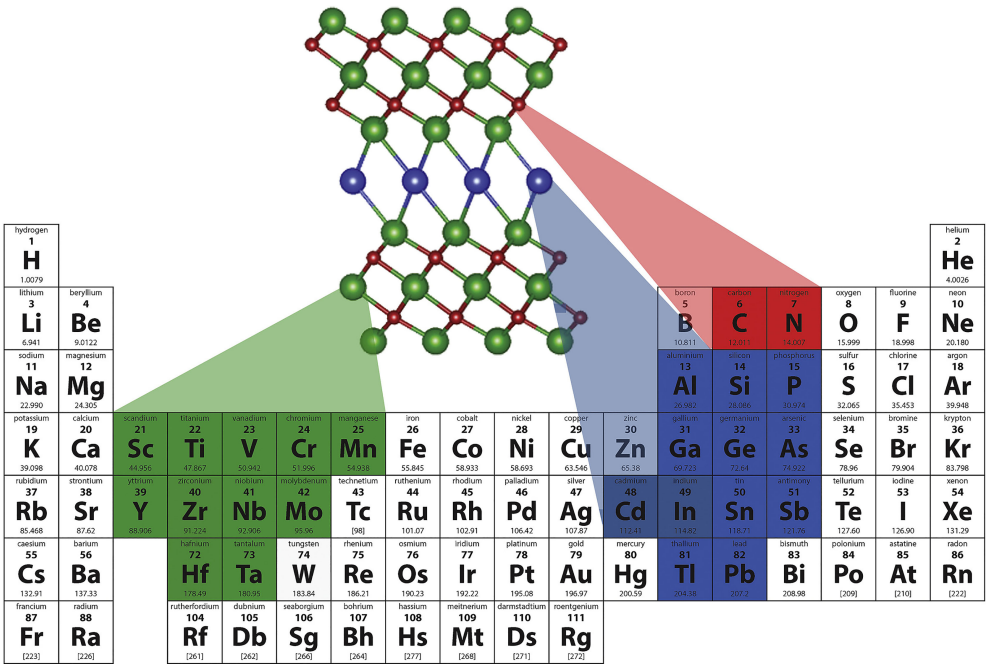


FIGURE 4 | MAX phases Mn+1AXn forming elements (171). Reproduced with permission from (171).

multifunctional niobium carbide nanoparticle (Nb_2C@PDA-R837@RBCNP) for NIR-II PTT combined with immunotherapy. Nb_2C@PDA-R837@RBCNPs exhibited high PCE under 1064-nm laser irradiation. Additionally, the circulation time *in vivo* was significantly prolonged, and the primary tumors were completely cleared in mice. Finally, the secondary tumor growth inhibition rate was as high as 89.8% due to the enhanced immune response.

Compared with other two-dimensional nanomaterials, black phosphorus nanosheets (BPNSs) have a larger extinction coefficient and higher PCE and are often used as PTAs for PTT (174–176). In addition, BPNSs have been widely used in biomedicine because of their large specific surface area, good biocompatibility, and biodegradability (177). Peng et al. (49) prepared BPNS-based multifunctional nanocomposites (BPNS-PAMAM@DOX-HA) by modifying BPNSs with hyaluronic acid and poly-amidoamine dendrimer and loading them with Dox. The results of the *in vivo* and *in vitro* experiments showed that BPNS-PAMAM@DOX-HA exhibited excellent tumor cytotoxicity and cellular uptake efficiency under 808-nm laser irradiation, significantly inhibited the growth of tumors in mice, and showed a more significant antitumor effect than chemotherapy or PTT alone.

Metal phosphorus-based nanomaterials (metal-PNMs) mainly include metal phosphide nanomaterials (e.g., ferrous phosphide) (178), metal phosphate nanomaterials (e.g., calcium phosphate) (179), and metal-black phosphorous nanocomposites (180). Among PNMs, metal-PNMs have been widely studied for tumor diagnosis and treatment due to their unique advantages such as excellent light absorption, inherent magnetism, and biodegradability (181). Jin et al. (50) created a novel anticancer nanoplatform (Co-P@$mSiO_2$@DOX-MnO_2) for the synergistic treatment of tumor chemotherapy and PTT, which used cobalt phosphide nanocomposite as the core and mesoporous silica as the shell, loaded with Dox, and combined with manganese dioxide nanosheets. The results showed that under the irradiation of 808-nm NIR laser, Co-P@$mSio_2$@DOX-MnO_2 rapidly increased the temperature of the tumor, reflecting the excellent photothermal conversion ability. Compared with the control group, the tumor growth inhibition of the Co-P@$mSio_2$@DOX-MnO_2 group was greater and the antitumor effect was significantly improved.

In recent years, upconversion nanoparticles (UCNPs) have attracted attention for their ability to convert NIR light into visible light or ultraviolet light with a shorter wavelength (182). UCNPs have the advantages of minimizing light damage, deep tissue penetration, low light bleaching, and good chemical stability (183–185), which give them great potential for application in tumor therapy (186). Zhang et al. (51) designed a lanthanide-doped UCNP nanotherapy platform (UCNPs@$mSiO_2$FePc-MC540) coated with mesoporous silica for synergistic PDT and PTT, which included $NaYF_4$:Yb, Er@$NaLuF_4$:Nd@$NaLuF_4$ UCNPs, and dual photosensitizing agents (merocyanine 540 and iron phthalocyanine). The results of the antitumor experiment showed that the survival rate of A549 cells in the UCNPs@$mSiO_2$FePc-MC540 group decreased significantly under 808-nm light, while the tumor volume decreased to approximately 10% of the original volume, showing a significant antitumor effect.

Prussian blue (PB) is an iron-centered compound ($Fe_4[Fe(CN)_6]_3$-xH2O, where x is the number of water molecules), which has been widely studied as a coordination compound (187, 188). PBNPs are widely used in immunosensors, biological imaging, drug release, and tumor therapy due to their large inner pore volume, adjustable size, easy synthesis, surface modification, good thermal stability, and biocompatibility (189–193). Liu et al. (52) mixed paclitaxel (PTX) and phase change materials (PCM) and loaded them onto polyethylene glycol-modified mesoporous PBNPs (mPBs) to construct a biocompatible nano-drug delivery system (PCM+PTX@mPBs/PEG). The *in vitro* cell experiment showed that the cellular uptake rate of PCM+PTX@mPBs/PEG increased significantly after 808-nm NIR laser irradiation. The *in vivo* antitumor experiment showed that PCM+PTX@mPBs/PEG could accumulate in the tumor site of mice by passive transport and significantly inhibit tumor growth by delivering chemotherapeutic drugs and a photothermal effect.

2.2 Organic Photothermal Nanomaterials

Inorganic photothermal nanomaterials are easy to prepare and highly modifiable (141), and tend to have higher PCE and better photothermal stability than organic nanomaterials (26, 194). However, the potential cytotoxicity caused by the poor biodegradability of inorganic materials hinders their clinical application (195). In contrast, organic photothermal nanomaterials are more biodegradable and biocompatible (26, 196) and mainly include organic small-molecule nanomaterials and conjugated polymer nanomaterials (14, 197). These two types of PTAs have shown good therapeutic effects and are frequently used for tumor imaging and treatment (198, 199). The most common organic photothermal nanomaterials are introduced below.

2.2.1 Organic Small-Molecule Nanomaterials

Common organic small-molecule photothermal materials include cyanine dyes, porphyrins, phthalocyanines, boron dipyrromethene, and diketopyrrolopyrrole (DPP). Although these small molecules have excellent photothermal conversion ability and biosafety, they also have limitations, such as poor water solubility and limited tumor accumulation. Through functional modification, nanocarriers can be designed to improve the solubilization and pharmacokinetics of small organic molecules and enhance the penetration and retention of therapeutic agents in tumor tissue, enhancing the therapeutic effect (26).

After modification to improve the photophysical properties, cyanine dyes are widely used in tumor PTT, imaging, and sensing because of their excellent biocompatibility and strong NIR absorption (200, 201). Cyanine molecules such as ICG, IR825, IR780, and cypate, are common PTAs that show potential for widespread application in fluorescence imaging and tumor therapy (26, 202). Guo etal. (53) synthesized zeolitic imidazolate framework-8 (ZIF-8) composite nanoparticles (Cy5.5&ICG@ZIF-8-Dex) using dimethyl sulfoxide/water solvent mixtures and loaded ICG and cyanine-5.5 (Cy5.5) for tumor imaging and PTT. The results of PTT showed that the A549 cells in the Cy5.5&ICG@ZIF-8-Dex group died in large numbers, and the tumor growth rate in mice was significantly inhibited, achieving an excellent therapeutic effect.

Porphyrin-based nanomaterials, with good photophysical properties and biocompatibility, have gained extensive attention in clinical tumor therapy and diagnostic imaging (203, 204). Studies have found that assembling porphyrin monomers with supramolecular nanostructures not only improves their physical and chemical properties and strengthens tumor accumulation, but also greatly enhances the range of application of porphyrin in the biomedical field (205, 206). Cao et al. (54) synthesized amphiphilic porphyrin (PPor) through conjugation with two PEG chains, and integrated perylene diimide into the porphyrin skeleton to form a D-A structure. The *in vivo* and *in vitro* antitumor experiments showed that under 808-nm laser irradiation, PPor nanoparticles completely disappeared from the primary tumor in mice and stimulated robust systemic antitumor immunity by releasing a large number of damage-associated molecular patterns and tumor-associated antigens, which significantly inhibited tumor metastasis.

Phthalocyanines (PCs) are regarded as second-generation photosensitizers in PDT because of their high molar absorption and excellent photostability (202, 207). With further research on PCs, it was found that PC nanomaterials also exhibit high PCE after irradiation with NIR light, giving them great potential in the application of PTT (208, 209). Feng et al. (55) designed T-MP nanoplatforms based on HER2 and targeted micellular PC. The results of *in vivo* and *in vitro* antitumor experiments showed that after 808-nm laser irradiation, the killing rate of HT-29 cells in the T-MP group was much higher than that in the control group. Additionally, primary tumor growth was significantly suppressed, and tumor lymph node metastasis was effectively overcome, greatly prolonging the survival time of mice.

Compared with other organic photothermal nanomaterials, boron dipyrromethene (BODIPY) has gained interest because of its strong absorption of long wavelengths, good photostability, excellent water solubility, and biocompatibility (210–214). Through chemical modification with a conjugated system, the nano-photosensitizer based on BODIPY has a higher absorption coefficient in the NIR region, which gives it the potential to be used as a PTA (215–217). Yu et al. (56) fabricated an NIR BODIPY dye with an upper phenyl-fused segment (BBDP). The photothermal experimental results demonstrated the PCE of BBDP nanoparticles to be as high as 54.2%, suggesting excellent photothermal capability. Moreover, *in vitro* antitumor experiments showed that under 690-nm laser irradiation, as the concentration of BBDP-NPs increased, the survival rate of tumor cells gradually decreased, indicating that BBDP-NPs have a good phototherapeutic effect.

DPP and its derivatives are widely used in fluorescence imaging and tumor therapy because of their easy modification, high molar extinction coefficient, and good photothermal stability (218, 219). In recent years, nanomaterials with a D-A-D structure based on DPP derivatives have received increasing attention (220, 221). Zheng et al. (57) synthesized three self-assembled nanoparticles with PEG as the side chain using three

amphiphilic DPP derivatives (TPADPP, DTPADPP, and TPADDPP). The experimental results showed that these three nanoparticles can not only effectively gather in the tumor site, but also have good biological safety and low cytotoxicity in dark environments. Under the irradiation of a 635-nm laser, DTPADPP and TPADDPP nanoparticles showed an efficient photothermal effect, and tumor growth in mice was significantly inhibited, suggesting that they have a tumor ablation effect.

2.2.2 Conjugated Polymer Nanomaterials

Conjugated polymers with a large π-conjugated backbone and high electron delocalized structure have been widely used in tumor therapy because of their high extinction coefficient and good biocompatibility (222, 223). Moreover, because of their π-electrons, which can easily cause delocalization and transition, conjugated polymers can effectively convert absorbed light energy into heat, making it a suitable PTA (224). At present, the conjugated polymer nanomaterials mainly include polypyrrole (PPy), polyaniline (PANI), and donor-acceptor (D-A)-conjugated polymers, as well as poly-(3,4-ethylenedioxythiophene): poly(4-styrene sulfonate) (PEDOT : PSS).

As a potential PTA, PPy has good biocompatibility, excellent photothermal properties, photostability, and accessible synthesis characteristics (225, 226). Wang et al. (58) combined CS and carboxymethyl cellulose (CMC) through electrostatic interactions and loaded PPy and 5-fluorouracil (5-Fu) to prepare a novel composite nanoparticle: CMC/CS@PPy +5FuNP. *In vitro* biological studies showed that CMC/CS@PPy +5FuNPs can be effectively internalized by HepG2 cancer cells. The combination of the photothermal effect of PPy and toxicity of 5-FU can significantly improve the therapeutic efficiency on tumors, indicating that CMC/CS@PPy+5FuNPs have great potential in synergistic chemotherapy and PTT.

PANI has been reported as a type of organic photothermal nanomaterial with good stability, biocompatibility, and strong NIR absorptivity. It has been widely used in photoacoustic imaging (PAI) and PTT for tumors (227–229). Wu et al. (59) synthesized a glucose oxidase (GOx)-conjugated PANI nanoplatform (PANITG) for PTT for tumors. Under the irradiation of NIR laser, PANITG activates PTT in slightly acidic tumor microenvironments. The released GOx reacts with excess glucose in the tumor tissue, resulting in cancer starvation. The *in vitro* and *in vivo* antitumor experiments showed that glutamate produced by GOx-mediated catalytic reactions enhances the photothermal effect. Meanwhile, PTT also plays a role in promoting the catalytic reaction, indicating that the two synergistically exhibit a significant antitumor effect.

D-A-conjugated polymers have been widely used in PTT for tumors because of their extended light absorption ability and good PCE (230, 231). Liu et al. (60) synthesized D-A-conjugated nanoparticles using thiophene and triphenylamine (TPA) as donors and benzo[1,2-c:4,5-c′]bis([1,2,5]thiadiazole) (BBTD) as the acceptor. The molecular rotors and bulky alkyl chains were then introduced into the center Dmura core to reduce intermolecular interaction. NIRb14 nanoparticles (NIRb14NPs) with long alkyl chains exhibit better photothermal properties. Additionally, the *in vivo* and *in vitro* antitumor experiments showed that NIRb14NPs had a longer circulation time *in vivo*, demonstrating significant tumor growth inhibition and biosafety.

Poly(3,4-ethylenedioxythiophene): poly(styrene-sulfonate) (PEDOT : PSS) is a complex of conjugated polymer PEDOT and negatively charged polymer PSS (232–234). PEDOT : PSS is an aqueous-based conductive polymer nanoparticle with strong NIR absorption that has become a popular NIR PTA for its water-dispersibility, high PCE, excellent light stability, and good biocompatibility (235–237). Ko et al. (61) synthesized a kind of magneto-conjugated polymer core-shell nanoparticle (MNP@PEDOT : PSSNP) based on PEDOT : PSS by *in situ* surface polymerization. PTT experiments showed that after laser irradiation, compared with the control group, the tumor volume of tumor-bearing mice did not significantly change, while the tumors in the MNP@PEDOT : PSSNP group were completely cleared. Additionally, these nanoparticles did not affect other organs, showing an effective and safe anti-tumor effect.

PDA has a similar chemical structure to eumelanin and may have similar properties, including NIR-responsiveness, chelation, and drug-binding capability (238). Liu et al. (239) first discovered that PDA has remarkable photothermal conversion ability and applied PDA as PTA to tumors. Xu et al. (62) designed biodegradable folic acid-modified Cu_{2+}-chelated PDA nanoparticles (Cu-PDA-FANPs) as an immunogenic cell death (ICD) inducer and multimodal tumor therapy technique (**Figure 5**). Experimental results showed that under the irradiation of 808-nm NIR light, Cu-PDA-FANPs could effectively convert light into heat and cooperate with Cu_{2+}-mediated chemical dynamic therapy, promoting a systemic antitumor immune response, which can eliminate tumors *in vivo* and significantly inhibit tumor metastasis.

2.2.3 Other Organic Photothermal Nanomaterials

Melanin is a natural polyphenol substance that can be divided into eumelanin and pheomelanin (240), according to the precursor molecular. Apart from their chelating function and drug-binding ability, natural melanin-based nanomaterials have many beneficial physical and chemical properties, including UV-Vis absorption and excellent PCE. Therefore, the application of natural and artificial melanin-based nanomaterials or melanin-like nanoparticles has achieved remarkable results in the field of biomedicine, especially as antitumor PTT (241, 242). For example, Xie et al. (63) prepared melanin and cellulose nanosheets (OMCNs) using black sesame hell as raw material by facile liquid-phase exfoliation. They then tested the photothermal properties and ability to kill cells of the OMCNs. The extinction coefficient of OMCNs at 808 nm was 3.1 L/g/cm, the PCE was approximately 37.3%, and the OMCNS demonstrated good light stability. The results of cell experiments showed that almost all SMCC-7721 and B16 cells were killed after NIR laser irradiation, indicating that OMCNs have a significant photothermal killing effect on cancer cells and great potential in antitumor therapy *in vivo*. In addition, Kang etal. (64) prepared dual laser-responsive multifunctional melanin-like nanoparticles (MNPs) for PDT, PTT, and chemotherapy, based on the KMnO4-oxidative polymerization

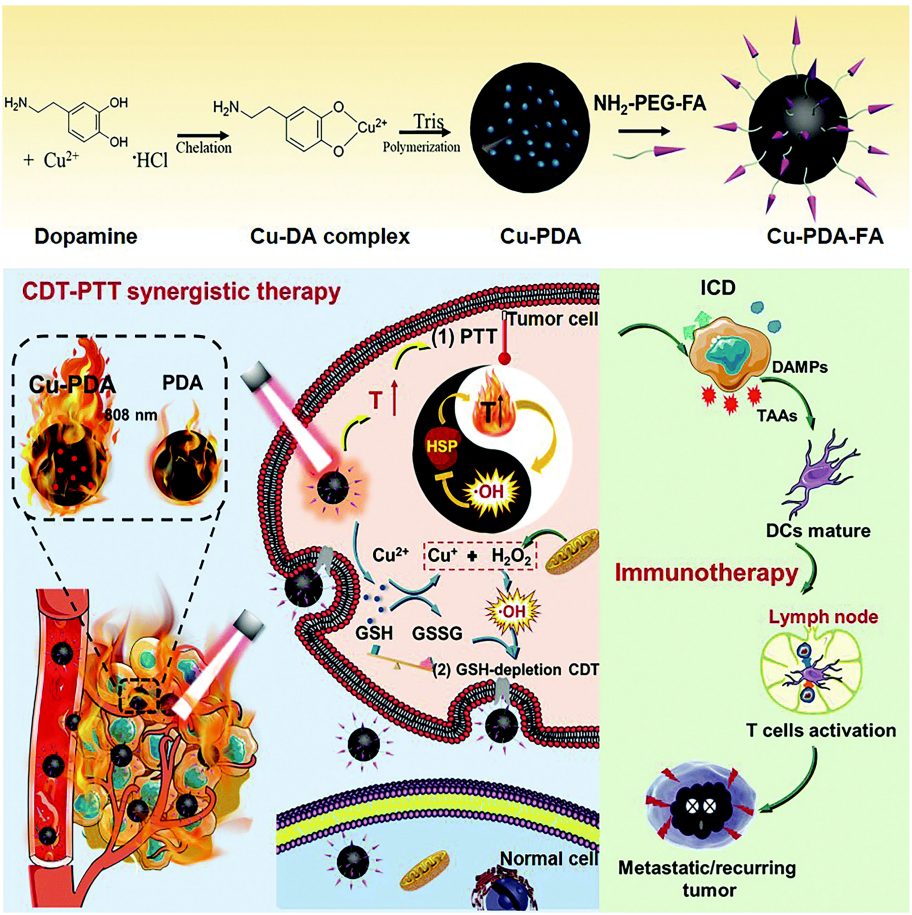


FIGURE 5 | Schematic illustration of Cu–PDA–FA NP synthesis and Cu–PDA–FA NP-mediated PTT/CDT synergistic effect and antitumor immune activation (62). Reproduced with permission from Xu et al., 2022 (62).

of L-3,4-dihydroxyphenylalanine (L-DOPA), pheophorbide a, and Dox, and modified by FA. The results of antitumor experiments showed that after 670-nm and 808-nm laser irradiation, the MNP group showed more extensive damage and apoptosis than the control group, showing great potential for antitumor therapy.

2.3 Organic-Inorganic Hybrid Photothermal Nanomaterials

Inorganic photothermal nanomaterials have unique physicochemical properties, such as high molar extinction coefficients, good photothermal conversion rate, excellent photothermal stability, and easy modification; however, their poor biodegradability and potential cytotoxicity limit their use in clinical treatment (91, 243). In contrast, organic photothermal nanomaterials have ideal biodegradability and biocompatibility; however, the photothermal properties of most organic photothermal nanomaterials often require further modification to be used in the treatment of tumors *in vivo* (244, 245). Due to the unsatisfactory effect of inorganic or organic photothermal nanomaterials alone, the application of organic-inorganic composite nanomaterials in PTT has attracted attention. Organic-inorganic composites not only integrate their respective advantages and improve their physical and chemical properties, but also exhibit synergistm (246–248).

Common organic-inorganic composite nanomaterials include core-shell nanoparticles and metal-organic frameworks (MOFs) (249, 250). Odda etal. (65) synthesized surface-engineered iron oxide nanoparticles (α-Fe_2O_3NPs) and PEDOT into a novel core-shell photothermal nanoparticle (Fe_2O_3@PEDOT-siRNANP), which was loaded with siRNA for synergistic tumor gene therapy and PTT. The experimental results of photothermal conversion performance showed that Fe_2O_3@PEDOT-siRNANPs not only had good biocompatibility and water dispersibility but also demonstrated a high PCE (η = 54.3%) in the NIR region. *In vitro* and *in vivo* experiments showed that Fe_2O_3@PEDOT-siRNANPs induced greater cancer cell apoptosis and more pronounced tumor suppression after laser irradiation compared with GT or PTT alone. Bai etal. (66) were the first to prepare NIR emission carbon dots (RCDs) based on glutathione (GSH). They then synthesized a novel metal-organic framework nano-platform (RCDS@MIL-100) using

RCDs, $FeCl_3$, and trimesic acid solutions. In the tumor microenvironment, RCDS@MIL-100 NPs consumed GSH and released Fe^{2+}, which could react with hydrogen peroxide to produce hydroxyl radicals. Under the irradiation of 660-nm laser, RCDs showed excellent photothermal conversion ability, promoted a Fenton reaction, and enhanced the therapeutic effect of CDT. The results of antitumor experiments indicated that tumors in the mice of the RCDS@MIL-100 group were completely removed, showing a highly effective antitumor effect.

3 MULTIMODAL THERAPY FOR TUMORS BASED ON PHOTOTHERMAL NANOMATERIALS

Currently, chemotherapy (251), radiotherapy (252), and high-intensity focused ultrasound therapy (253) are widely used and successfully inhibit the growth or spread of tumors and prolong the survival time of patients. PDT (254) has also been shown to have significant advantages in the treatment of non-small cell lung cancer and esophageal cancer. Other treatments, such as PTT (194), immunotherapy (255), gene therapy (256), and magnetothermal therapy (257), have undergone significant research, though most are still in the preliminary clinical stage of research. These emerging tumor treatments have been shown to have ideal anticancer effects in many laboratory and preclinical studies and have broad applications for clinical treatment in the future. For example, ICG, a hydrophobic photosensitizer, is the only NIR imaging reagent approved by the USFDA and has been widely used in the biomedical field, especially for tumor therapy (258, 259). However, ICG has not achieved the eradication of all tumors or the prediction and prevention of metastasis, which is the limitation of single-mode immunotherapy. For example, some cancer cell subsets in heterogeneous tumor tissues may achieve mono-drug resistance to antineoplastic drugs (260). Moreover, long-term use of anticancer drugs often induces multidrug resistance in tumor tissues, which leads to reduced efficacy of chemotherapy (261). Additionally, because of the insensitivity of anoxic cancer cells to ionizing radiation, radiotherapy alone is often unable to achieve an ideal therapeutic effect in a hypoxic tumor environment (262).

Similarly, although PTT has unique advantages, its inherent limitations affect its clinical application. Because the temperature of the tumor site rises to 41–47°C during PTT, necrosis may also occur in the surrounding normal tissue. This leads to the infiltration of pro-inflammatory and immune suppressor cells, triggers a chronic inflammatory response, and promotes immunosuppression through the activation of checkpoint pathways that inhibit T cell responses (263–265). In addition, due to the limited depth of NIR light penetration into the tissue, the tumor cells outside the irradiation area are not completely removed, resulting in possible tumor recurrence and metastasis (263). These limitations inhibit the clinical applications of PTT.

To overcome these barriers of single-mode therapy, combination therapy by integrating two or more treatment modalities has been proposed as a solution (266). Combination therapy is based on synergistic and enhanced interactions between two or more treatments, which tends to produce super additive effects, known as "1+1>2" (267). Therefore, multi-functional nanomaterials are constructed by combining different types of therapeutic agents in a single nanostructure through physical adsorption or chemical binding, which can be used to create multimodal, collaborative therapy for tumors (268–270).

3.1 Dual-Modal Therapy Based on PTT

PTT facilitates other tumor treatment methods by its ability to increase the temperature of the tumor site and change the microenvironment. The heat generated during PTT can also promote the intracellular transmission and release of drugs, genes, and immune adjuvants and the disintegration of thermosensitive nanocarriers to enhance the therapeutic effects of chemotherapy, gene therapy, and immunotherapy. It can also accelerate the production of physical/chemical injury factors, such as ROS synthesis, to enhance the efficacy of PDT, sonodynamic therapy (SDT), and CDT based on the principle of oxygen injury. Additionally, due to the increase in temperature from PTT, the vascular permeability of tumor tissue increases, which promotes hemoperfusion, increases oxygen saturation, improves the hypoxic tumor environment, and enhances the efficacy of radiotherapy limited by hypoxia. At the same time, light induces ICD and upregulates tumor immunogenicity, which improves lymphocyte permeability and enhances antitumor immunity (263, 271). In this section, representative studies will be introduced to explain the synergy between PTT and additional therapies (**Figure 6**).

3.1.1 PTT Acts Synergistically by Promoting the Uptake of Therapeutic Agents

Studies have found that the high temperatures produced by PTT can promote the uptake of nanocarriers by tumor cells and accelerate the decomposition of nanocarriers to enhance intracellular drug concentration and cytotoxicity (272). In addition, some anticancer drugs (e.g., cisplatin) exhibit a significantly enhanced ability to kill tumor cells under the high temperature produced by PTT (273). However, due to the thermal expansion of PTT, chemotherapeutic drugs can be more evenly distributed in tumor tissues, enhance heterogeneity, and inhibit tumor drug resistance and metastasis. Wang et al. (274) prepared an intelligent polymer-drug vehicle (MPPD@IR825/DTX) for chemo-photothermal combination therapy, which used poly(ethyleneimine)-poly (ϵ-caprolactone) block polymers as the core and dimethylmaleic anhydride-modified PEG as the shell, encapsulating docetaxel (DTX) and IR825. Compared with the free drug, IR825, MPPD@IR825/DTX nanoparticles exhibited higher temperatures under 808-nm NIR laser irradiation, which increased cytotoxicity and promoted apoptosis of tumor cells more effectively. Furthermore, the results of an *in vivo* antitumor experiment showed that the combination of chemotherapy and PTT has a better effect on tumor

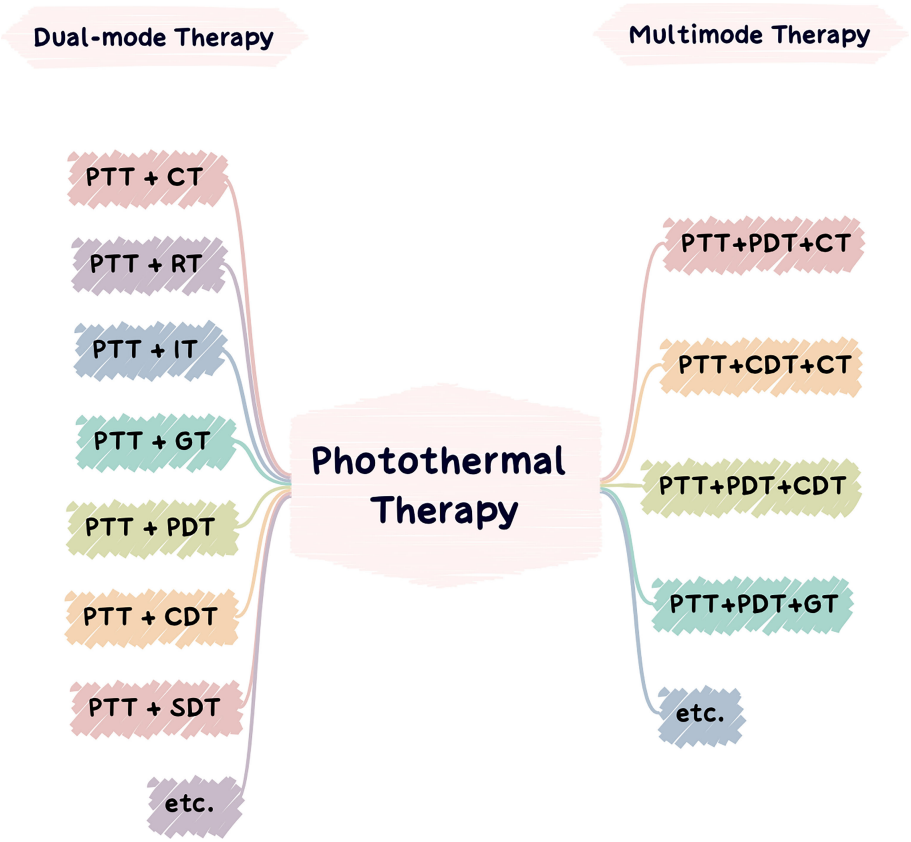


FIGURE 6 | Applications of photothermal nanomaterials in tumor dual-mode therapy (left) and applications of photothermal nanomaterials in tumor multimode therapy (right).

eradication, while chemotherapy or PTT alone cannot eliminate the tumor completely.

Similar to combination chemotherapy, PTT can enhance immunotherapy by promoting the uptake of immune adjuvants and the disintegration of nanocarriers by tumor cells. Some PTAs can also be used as immune adjuvants to promote the maturation of dendritic cells and the production of antitumor cytokines (275). After PTT, tumor tissue responds to high-temperature stress and promotes ICD of tumor cells, thereby enhancing antitumor immune responses (276, 277). Wang et al. (278) loaded immune adjuvants, imiquimod (IMQ) and ICG onto amorphous iron oxide nanoparticles (IONs) to design a tumor microenvironment-responsive nanoplatform (IMQ@IONs/ICG). The results of antitumor experiments *in vivo* and *in vitro* showed that IMQ@IONs/ICG had good photothermal conversion ability under 805-nm laser irradiation, induced *in situ* ICD, and cooperated with released IMQ to enhance the antitumor immune response and significantly inhibit tumor metastasis. Compared with the ICG alone group, the primary tumors in the IMQ@IONs/ICG group were completely eradicated after treatment, mesenteric metastasis was significantly reduced, and the survival time of mice was significantly prolonged.

Similarly, PTT can enhance the efficiency of tumor cell uptake by loosening the cell membrane and promoting the release of genes from nanocarriers to enhance gene therapy effects (279). Gene therapy can improve the efficacy of PTT by inhibiting the expression of specific heat shock proteins and overcoming the resistance of cancer cells to thermal damage (280). Xu et al. (281) synthesized a polypyrrole-poly(ethyleneimine)-siILK nanocomplex (PPRILK) gene PTT nanosystem based on the siRNA of integrin-linked kinase (ILK). The results of *in vivo* and *in vitro* experiments showed that after 808-nm laser irradiation, the tumor growth of the PPRILK treatment group was significantly slower and the damage to normal tissue was minimized compared to the laser and gene therapy groups, indicating that the combination of gene therapy and PTT can effectively ablate tumors and inhibit tumor recurrence.

3.1.2 PTT Acts Synergistically by Promoting the Production of Damaging Factors

As an innovative ROS-based cancer treatment, CDT mainly relies on *in situ* Fenton or Fenton-like reactions to generate hydroxyl radical and trigger oxidative damage (282, 283). A kinetic study found that when the temperature increased from 20°C to 50°C, the rate of Fenton reaction was significantly

accelerated, giving PTT an unparalleled position in promoting CDT (284). A limitation of PTT is that the expression of HSPs inhibits heat-induced apoptosis (285). HSPs include redress misfolded proteins, such as HSP90 and HSP70, which can alleviate tumor ablation mediated by PTT. Interestingly, studies have found that ROS can effectively inhibit the expression of HSP70, suggesting that CDT, which can generate hydroxyl radicals, is suitable for inhibiting HSP activity and enhancing the efficacy of PTT (286). Huang etal. (287) mixed Ag_2S nanodot-conjugated Fe-doped bioactive glass nanoparticles (BGN-Fe-Ag_2S) with PEG double acrylates (PEGDA) and 2,2′-azobis[2-(2-imidazolin-2-yl)propane]-dihydrochloride solution to form a novel light-activated injectable nano-hydrogel (PBFA). The results of *in vitro* experiments showed that under the irradiation of an 808-nm laser, the solution temperature of the PBFA group increased significantly, the concentration of intracellular ROS increased, and the survival rate of tumor cells was much lower than that of the control groups at 33%. Additionally, compared with the control group, the PBFA group could inhibit tumor growth more effectively and showed better biological safety.

The principle of PDT is that photosensitizers are selectively activated and produce cytotoxic ROS through a specific wavelength of light induction, thus inducing tumor cell death (288). It has been reported that PTT produces mildly high-temperatures, can enhance cell membrane permeability to enhance tumor cell uptake of photosensitizer-loaded nanocarriers, and increases intracellular photosensitizer concentration to promote ROS synthesis, enhancing the therapeutic effect of PDT (289, 290). Sun et al. (291) prepared a novel target nanoprobe (Fe/ICG@HA) with porous Fe_3O_4 nanoparticles modified by HA and loaded with ICG. The results of antitumor experiments showed that the temperature of the tumor site in the Fe/ICG@HA group increased rapidly to 42.3°C after 808-nm NIR laser irradiation. After 14 days of treatment, the tumor volume of the Fe_3O_4 and ICG groups increased slightly, while that of the Fe/ICG@HA group decreased significantly. At the same time, histological examination showed that a large amount of singlet oxygen was produced between tumor cells, indicating that Fe/ICG@HA nanoprobe is a promising nanoplatform for combination PDT/PTT.

In recent years, SDT has been widely revered as a non-invasive tumor treatment method, whose action is to promote acoustic cavitation in tumor cells through the impact of ultrasound on sonosensitizers, thus producing an antitumor effect (292). Additionally, the energy generated by ultrasound can be converted into ROS in the presence of ultrasonic sensitizers (293). Because the lipid arrangement in the biofilm is affected by temperature and membrane permeability increases with temperature, PTT can enhance the SDT cavitation effect (263). Moreover, the ROS and oxygen environment on which SDT depends may enhance PTT/SDT synergism (294). Soratijahromi et al. (295) designed gold/manganese dioxide nanocomposite (Au/MnO_2 NC) for combination therapy of SDT/PTT. The experimental results showed that under the irradiation of an 808-nm laser and ultrasound, Au/MnO_2 NC shows excellent photothermal and acoustodynamic conversion ability. Compared with the control group, the production of ROS in the phototherapy/sonotherapy group was significantly increased, which was the most effective in inhibiting melanoma and showed good synergism.

3.1.3 PTT Acts Synergistically by Improving Tumor Hypoxic Environment

PTT can not only promote the generation of ROS to enhance the therapeutic effect of PDT but the mildly high-temperature can also accelerate blood flow to increase the saturated oxygen concentration of blood vessels, which improves the tumor hypoxia environment to promote oxygen production in oxygen-dependent PDT (296, 297). In addition, difficulty in distinguishing normal cells from tumor cells as well as hypoxia-limited ROS production are common pitfalls of radiotherapy (298). Currently, PTT-induced hyperthermia has been observed to accelerate intratumoral blood flow to improve tumor oxygenation (299), thereby reducing hypoxia-induced radioresistance to enhance radiotherapy efficacy (300). In addition, PTT can effectively inhibit the repair of DNA damage caused by X-ray radiation, increase the radiosensitivity of tumor cells, and improve synergism (301, 302). Ni et al. (303) assembled UCNPs coated with manganese dioxide and copper sulfide to create a multifunctional nanoplatform (UCCM) for combined radiotherapy and PTT. The results showed that the manganese dioxide coating produced a large amount of oxygen by interacting with hydrogen peroxide, which can improve the anoxic microenvironment and enhance the efficacy of radiotherapy. Meanwhile, under NIR laser irradiation, the dispersed copper sulfide nanoparticles absorbed light energy and converted it into thermal energy, which significantly inhibited tumor growth. Compared with the radiotherapy or PTT groups, the tumor-bearing mice in the UCCM group had lower cancer cell activity levels and more significant antitumor effects.

3.1.4 PTT Acts Synergistically With Other Methods

In addition to the synergistic effects of PTT with the methods described above, PTT can also promote synergism in other ways. For example, Yang et al. (304) combined superparamagnetic iron oxide nanoparticles and luminescent lead sulfide/cadmium sulfide quantum dots (Pb-based QDs) to create supernanoparticles (SASNs), which verified the feasibility of magnetothermal and photothermal dual-modal hyperthermia. Dual-modal heating with SASN as the heating agent showed an efficient heating output, which was better than magnetothermal and photothermal heating alone. Lu et al. (305) explored the synergism between gas therapy and PTT by designing sulfur dioxide prodrug-doped nanorattles. The experimental results showed that sulfur dioxide had goodPCE, while sulfur dioxide gas had certain cytotoxicity, which could effectively induce tumor cell apoptosis through pH-precise targeting. Compared with the control group without laser irradiation, the expression of pro-inflammatory proteins (Bax, P53, caspase-3) was significantly upregulated in superficial and deep tumors in the combined treatment group after 808-nm laser irradiation, while that of the anti-inflammatory protein, Bcl2, was significantly downregulated, and the apoptosis rate of tumor cells was higher.

3.2 Multimodal Therapy Based on PTT

Since the 1960s, the combination of two or more treatment strategies has shown a strong synergistic effect and reduced side effects. Hence, dual-modal or multimodal treatments have skillfully integrated the advantages of a single treatment into one system (282). In contrast to the limited therapeutic effects and possible side effects of single-modal immunotherapy, multimodal synergistic therapy may have the overall advantages of a variety of single-modal immunotherapies and produce higher anticancer effects at lower doses, avoiding high-dose side effects (306). Although dual-modal therapy shows better therapeutic effects than single-modal therapy, multimodal therapies (three or more based on PTT treatments), can further overcome the shortcomings and improve anticancer effectiveness (282). The potential synergistic effect of different treatments has been largely ignored in previous literature because of the complexity of the synergy among treatments. When multiple treatment modes are superimposed, whether contradictions or adverse effects will occur requires further systematic research and analysis. For example, compared with PTT or PDT alone, although their combination can provide a simpler treatment process and more ideal result, it requires higher laser power and irradiation time to initiate synergism. Whether this results in adverse effects on normal human tissue has not been reported (12). Based on the research experience of several groups (307, 308), a variety of therapeutic agents can be assembled in nanocarriers for combination treatment of multiple therapies with higher efficacy and almost no side effects. Below, we provide examples to introduce the research of several multimodal tumor therapy methods.

3.2.1 PTT Combined With PDT and Chemotherapy

Previous studies have shown that drugs, photosensitizers, and PTAs can be integrated into one nanostructure, thus enabling the combination of chemotherapy, PDT, and PTT (309). Because ROS produced during PDT can promote intracellular drug delivery by avoiding uptake of nuclear endosomes, PDT can effectively enhance chemotherapy. Therefore, the combination of PTT/PDT/chemotherapy may be more effective than their dual-modal combinations. Chen et al. (310) synthesized a new multimodal therapy system based on BP nanotablets using Dox as a model drug, which has pH/light-responsive drug release properties. In other words, drug release is further promoted under 808-nm illumination. The results of antitumor therapy *in vivo* showed that, compared with other control groups, the tumor growth inhibition of mice in the three-mode immunotherapy group was the most significant (inhibition rate as high as 95.5%), and the therapeutic effect was significantly enhanced, indicating that the multi-modal combination of PTT/PDT/chemotherapy is feasible.

3.2.2 PTT Combined With Chemotherapy and CDT

The synergistic effect between CDT and PTT has been widely studied and verified (219, 311, 312), but tumor tissues adapt stronger ROS defensive systems at high ROS levels, resulting in poor therapeutic effects from CDT (219, 311, 312). A study (313) found that when PTT andCDT are combined with chemotherapy, this multimodal method can not only overcome the limitation of PTT penetration depth and avoid drug resistance, but also improve the sensitivity of tumor tissue to ROS, achieving significant synergism. Wang et al. (314) designed a nanoparticle based on redox and light-responsiveness (RLR), which consists of ultrasmall iron oxide nanoparticles embedded in an amorphous hollow carbon framework as the core and stacked manganese dioxide flower-like nanosheet structures as the shell. RLR nanoparticles were synergistically treated by manganese dioxide consumption of GSH, iron ion-induced Fenton reaction, PTT, and chemotherapy (Dox). The *in vivo* and *in vitro* results showed that the RLR nanoparticles successfully achieved 99.4% and 99.0% tumor-killing rates, respectively through the synergistic action of CDT, photochemotherapy, and anticancer drugs on a single platform. These results show the potential of the RLR nanoparticle-based platform in multimodal tumor therapy.

3.2.3 PTT Combined With PDT and CDT

PDT and CDT are mainly ROS-mediated tumor therapy methods. Thus, combining them to construct an antitumor nanoplatform is a promising strategy to improve the antitumor effect (315, 316). Because PTT can improve the hypoxia of PDT, and CDT can inhibit the expression of HSP from PTT, the establishment of a PTT/PDT/CDT multimodal therapeutic platform has attracted attention. For example, Liu et al. (317) prepared biocompatible copper ferrite nanospheres (CFNs) (**Figure 7**). Under 650-nm laser irradiation, the Fenton reaction mediated by copper and iron ions was significant. Meanwhile, CFNs regulated the tumor microenvironment to enhance the therapeutic effect of PDT by promoting the production and consumption of GSH by oxygen. Under the irradiation of 808-nm laser, CFNs exhibited excellent photothermal conversion ability. The experimental results *in vivo* and *in vitro* also showed that when the two wavelengths of laser were irradiated at the same time, almost all tumor cells were killed and the tumors in tumor-bearing mice were eliminated, demonstrating an excellent synergistic antitumor effect.

3.2.4 PTT Combined With PDT and Gene Therapy

Studies have found that some specific types of siRNA (e.g., BAG3-siRNA) used in gene therapy can inhibit the expression of HSPs in cancer cells, which provides the possibility of gene therapy and PTT synergism (318). Among the nanomaterials that have been used to construct multifunctional platforms for tumor therapy and imaging, ultrathin BP nanosheets can not only act as photosensitizers for PDT by effectively promoting the production of large amounts of singlet oxygen (310), but also be widely used in PTT because of their excellent extinction coefficient and PCE (319). Therefore, the construction of a PTT/PDT/gene multimodal therapy nanosystem, based on a BP multifunctional nanoplatform, has aroused interest among researchers (320). Chen et al. (321) used PEG and polyethyleneimine-modified ultrathin BP nanoparticles (PPBP) as a human telomerase reverse transcriptase (hTERT) siRNA delivery system. When irradiated by different wavelengths of laser, PPBP nanoparticles showed excellent PDT and PTT

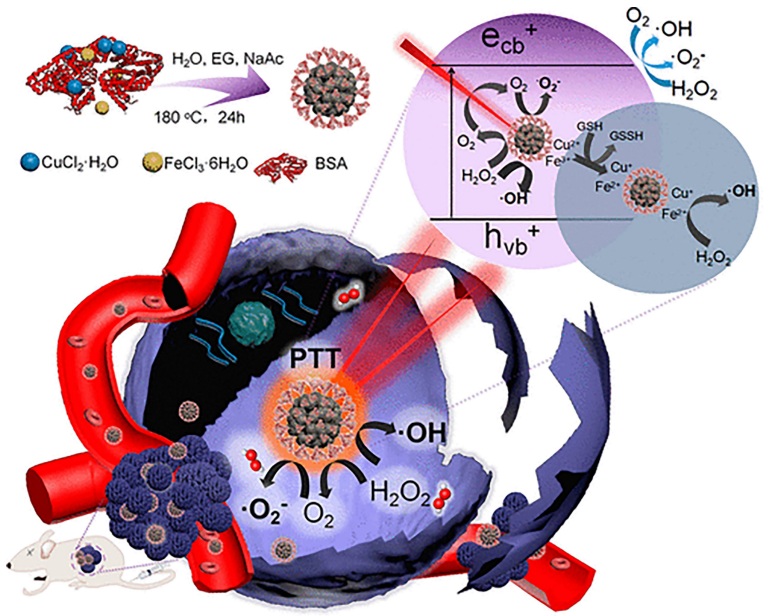


FIGURE 7 | Schematic illustration of synthetic process and therapeutic mechanism of CFNs (317). Reproduced with permission from Liu et al., 2018.

activities, which further promoted the specific release of siRNA for gene silencing antitumor therapy. Experimental *in vivo* and *in vitro* results showed that compared with single-wavelength irradiation, when 660-nm and 808-nm lasers were irradiated together, the expression of hTERT mRNA in mice was significantly reduced and tumor growth was significantly inhibited under the action of PPBP-siRNA nanosheets. After 42 days of treatment, no obvious lung metastases were found. This study demonstrates that the PPBP-siRNA nanoplatform effectively inhibits tumor growth and metastasis through PTT/PDT/gene therapy synergism and verifies the feasibility of this multimodal therapy.

4 CONCLUSION AND OUTLOOK

Relying on the rapid development of nanoscience and polymer material technology, the research of photothermal nanomaterials in tumor treatment has made significant progress (322). Although the common inorganic and organic photothermal nanomaterials have great differences in their structures, they all have high PCE and tumor ablation capabilities. Nano phototherapy can not only directly kill tumor cells and reverse drug resistance, but also enhance immune responses (323). In addition, photothermal nanomaterials are becoming increasingly multifunctional through the modification of nanomaterials. Moreover, tumor treatment is becoming increasingly multimodal through the combination of various treatment methods, such as PTT and chemotherapy or PTT and PDT, which have achieved improved therapeutic effects. However, most of these methods are still in the laboratory stage, and these nanomaterials may have defects that limit their clinical application. Thus, the application of photothermal nanomaterials faces many challenges, such as:

1) Due to the different locations of tumor growth and tumor distances from the body surface, the tissue penetrated by laser irradiation has absorbs light, resulting in light weakening or extinction during PTT. In the future, more efforts should be focused on the research and development of PTAs with greater extinction coefficients. In addition, the application method of penetrating the body should also be developed to avoid laser attenuation, such as the administration of PTT at the same time as surgery.

2) The targeting of photothermal nanomaterials in the treatment of tumors, especially in temperature targeting, and avoidance of HSP should be improved. In the future, more attention should be paid to the modification of photothermal nanomaterials to achieve multifunctional uses. For example, treatment based on temperature sensitivity in combination with the application of pH-responsiveness can increase targeting capablities while realizing the multimodality of tumor treatment.

3)Although nanocarriers can co-assemble various therapeutic agents into a single system to build a multifunctional nanoplatform for tumor diagnosis, imaging, and multimodal therapy, the compatibility and composition of therapeutic agents in this technique require further exploration. For example, while PTT and PDT or CDT exert significant synergism, whether the proportion of PTAs and photosensitizer or chemodynamic drugs will inhibit the curative effect of synergistic therapy, as well as the optimal constituent ratio to achieve the best outcome have yet to be determined.

4)PTT is convenient for other treatment modes by virtue of its unique treatment principle; however, the deeper mechanism of the synergy between multimodal treatments remains to be explored. For example, PTT and PDT have an obvious synergistic effect, but the dominant modality has yet to be determined. In addition to the composition ratio of nanodrugs, whether promoting ROS production or alleviating tumor hypoxia is more significant, and how to design drug carriers to best exploit this synergism require further investigation.

5)Finally, the most important aspect is the biosafety of photothermal nanomaterials that remain in the body, which can administer toxicity to the human body. In addition, most solvents and chemicals in these nanomaterials are also harmful to the human body. Although nanomaterials may show low short-term cytotoxicity to cells, tissues, or organs, their long-term cytotoxicity and related immune reactions should be carefully evaluated. One possible method to reduce toxicity is to design biodegradable and cleanable PTAs. However, improving the biodegradability and clearance of PTAs may sacrifice their stability and retention time in the blood, resulting in reduced tumor uptake. Therefore, a balance must be achieved.

In all, photothermal nanomaterials in multimodal tumor therapy present great potential and will become increasingly beneficial with further research.

AUTHOR CONTRIBUTIONS

FG contributed to the research retrieval and outline drafting. SC, XS and YT contributed to the research retrieval and drafting and critically revised the manuscript. YL, ZX and SZ critically revised the manuscript. Every author gave final approval and agreed to be accountable for all aspects of the work. All authors have read and agreed to the published version of the manuscript. All authors contributed to the article and approved the submitted version.

FUNDING

Financial support from the Projects directly under Jilin Provincial Department of Finance, China (JCSZ2019378-23), and the Scientific Research Project of Jilin Provincial Department of Education, China (JJKH20211215KJ).

ACKNOWLEDGMENTS

Authors are thankful to their respective departments/institutes/universities for providing space and other necessary facilities, which helped to draft this manuscript.

REFERENCES

1. Sun XK. *Construction of Multifunctional Composite Nanomaterials and Multi-Mode Tumor Therapy. [Dissertation Thesis]*. China (JL): Jilin University (2019).
2. Das M, Mohanty C, Sahoo SK. Ligand-Based Targeted Therapy for Cancer Tissue. *Expert Opin Drug Deliv* (2009) 6(3):285–304. doi: 10.1517/17425240902780166
3. Mohanty C, Das M, Kanwar JR, Sahoo SK. Receptor Mediated Tumor Targeting: An Emerging Approach for Cancer Therapy. *Curr Drug Deliv* (2011) 8(1):45–58. doi: 10.2174/156720111793663606
4. Baumann M, Krause M, Hill R. Exploring the Role of Cancer Stem Cells in Radioresistance. *Nat Rev Cancer* (2008) 8(7):545–54. doi: 10.1038/nrc2419
5. Huang P, Wang D, Su Y, Huang W, Zhou Y, Cui D, et al. Combination of Small Molecule Prodrug and Nanodrug Delivery: Amphiphilic Drug-Drug Conjugate for Cancer Therapy. *J Am Chem Soc* (2014) 136(33):11748–56. doi: 10.1021/ja505212y
6. Kalbasi A, Komar C, Tooker GM, Liu M, Lee JW, Gladney WL, et al. Tumor-Derived CCL2 Mediates Resistance to Radiotherapy in Pancreatic Ductal Adenocarcinoma. *Clin Cancer Res* (2017) 23(1):137–48. doi: 10.1158/1078-0432.CCR-16-0870
7. Alzeibak R, Mishchenko TA, Shilyagina NY, Balalaeva IV, Vedunova MV, Krysko DV. Targeting Immunogenic Cancer Cell Death by Photodynamic Therapy: Past, Present and Future. *J Immunother Cancer* (2021) 9(1):e001926. doi: 10.1136/jitc-2020-001926
8. Kirillin M, Kurakina D, Khilov A, Orlova A, Shakhova M, Orlinskaya N, et al. Red and Blue Light in Antitumor Photodynamic Therapy With Chlorin-Based Photosensitizers: A Comparative Animal Study Assisted by Optical Imaging Modalities. *BioMed Opt Express* (2021) 12(2):872–92. doi: 10.1364/BOE.411518
9. Yim W, Borum RM, Zhou J, Mantri Y, Wu Z, Zhou J, et al. Ultrasmall Gold Nanorod-Polydopamine Hybrids for Enhanced Photoacoustic Imaging and Photothermal Therapy in Second Near-Infrared Window. *Nanotheranostics* (2022) 6(1):79–90. doi: 10.7150/ntno.63634
10. Li CL, Fisher CJ, Wilson BC, Weersink RA. Preclinical Evaluation of a Clinical Prototype Transrectal Diffuse Optical Tomography System for Monitoring Photothermal Therapy of Focal Prostate Cancer. *J Biomed Opt* (2022) 27(2):026001. doi:–10.1117/1.JBO.27.2.026001
11. Sun IC, Jo S, Dumani D, Yun WS, Yoon HY, Lim DK, et al. Theragnostic Glycol Chitosan-Conjugated Gold Nanoparticles for Photoacoustic Imaging of Regional Lymph Nodes and Delivering Tumor Antigen to Lymph Nodes. *Nanomater (Basel)* (2021) 11(7):1700. doi: 10.3390/nano11071700
12. Younis MR, Wang C, An R, Wang S, Younis MA, Li ZQ, et al. Low Power Single Laser Activated Synergistic Cancer Phototherapy Using Photosensitizer Functionalized Dual Plasmonic Photothermal Nanoagents. *ACS Nano* (2019) 13(2):2544–57. doi: 10.1021/acsnano.8b09552
13. Jain PK, Huang X, El-Sayed IH, El-Sayed MA. Noble Metals on the Nanoscale: Optical and Photothermal Properties and Some Applications in Imaging, Sensing, Biology, and Medicine. *Acc Chem Res* (2008) 41(12):1578–86. doi: 10.1021/ar7002804
14. Li J, Rao J, Pu K. Recent Progress on Semiconducting Polymer Nanoparticles for Molecular Imaging and Cancer Phototherapy. *Biomaterials* (2018) 155:217–35. doi: 10.1016/j.biomaterials.2017.11.025
15. Weissleder R. A Clearer Vision for *In Vivo* Imaging. *Nat Biotechnol* (2001) 19(4):316–7. doi: 10.1038/86684
16. Huang X, Zhang W, Guan G, Song G, Zou R, Hu J. Design and Functionalization of the NIR-Responsive Photothermal Semiconductor Nanomaterials for Cancer Theranostics. *Acc Chem Res* (2017) 50(10):2529–38. doi: 10.1021/acs.accounts.7b00294
17. Fiedler VU, Schwarzmaier HJ, Eickmeyer F, Müller FP, Schoepp C, Verreet PR. Laser-Induced Interstitial Thermotherapy of Liver Metastases in an Interventional 0.5 Tesla MRI System: Technique and First Clinical Experiences. *J Magn Reson Imaging* (2001) 13(5):729–37. doi: 10.1002/jmri.1101
18. Tian Q, Tang M, Sun Y, Zou R, Chen Z, Zhu M, et al. Hydrophilic Flower-Like CuS Superstructures as an Efficient 980 Nm Laser-Driven Photothermal Agent for Ablation of Cancer Cells. *Adv Mater* (2011) 23(31):3542–7. doi: 10.1002/adma.201101295
19. Li GC, Mivechi NF, Weitzel G. Heat Shock Proteins, Thermotolerance, and Their Relevance to Clinical Hyperthermia. *Int J Hyperthermia* (1995) 11(4):459–88. doi: 10.3109/02656739509022483

20. Luo Z. *Construction of Nanocarriers for Photothermal/Chemotherapy Combined Cancer Treatment and Study on Their Anti-Tumor Mechanism. [Master's Thesis]*. China (TJ): Tianjin Univ Technol (2021)
21. Zhu Y, Zhao TJ, Liu M, Wang SW, Liu SL, Ai KL. Rheumatoid Arthritis Microenvironment Insights Into Treatment Effect of Nanomaterials. *Nano Today* (2022) 42:101358. doi: 10.1016/j.nantod.2021.101358
22. Zhao TJ, Wu W, Sui LH, Huang Q, Nan YY, Ai KL. Reactive Oxygen Species-Based Nanomaterials for the Treatment of Myocardial Ischemia Reperfusion Injuries. *Bioactive Mater* (2022) 7:42–72. doi: 10.1016/j.bioactmat.2021.06.006
23. Huang X, Jain PK, El-Sayed IH, El-Sayed MA. Plasmonic Photothermal Therapy (PPTT) Using Gold Nanoparticles. *Lasers Med Sci* (2008) 23 (3):217–28. doi: 10.1007/s10103-007-0470-x
24. Doughty ACV, Hoover AR, Layton E, Murray CK, Howard EW, Chen WR. Nanomaterial Applications in Photothermal Therapy for Cancer. *Mater (Basel)* (2019) 12(5):779. doi: 10.3390/ma12050779
25. He YL, Cao YY, Wang YP. Progress on Photothermal Conversion in the Second NIR Window Based on Conjugated Polymers. *Asian J Organic Chem* (2018) 7(11):2201–12. doi: 10.1002/ajoc.201800450
26. Liu Y, Bhattarai P, Dai Z, Chen X. Photothermal Therapy and Photoacoustic Imaging *via* Nanotheranostics in Fighting Cancer. *Chem Soc Rev* (2019) 48 (7):2053–108. doi: 10.1039/c8cs00618k
27. Xu Y, Liang X, Bhattarai P, Sun Y, Zhou Y, Wang S, et al. Enhancing Therapeutic Efficacy of Combined Cancer Phototherapy by Ultrasound-Mediated *In Situ* Conversion of Near-Infrared Cyanine/Porphyrin Microbubbles Into Nanoparticles. *Adv Funct Mater* (2017) 27(48):1704096. doi: 10.1002/adfm.201704096
28. Lin LS, Yang X, Zhou Z, Yang Z, Jacobson O, Liu Y, et al. Yolk-Shell Nanostructure: An Ideal Architecture to Achieve Harmonious Integration of Magnetic-Plasmonic Hybrid Theranostic Platform. *Adv Mater* (2017) 29 (21):1606681. doi: 10.1002/adma.201606681
29. Wang Z, Huang P, Jacobson O, Wang Z, Liu Y, Lin L, et al. Biomineralization-Inspired Synthesis of Copper Sulfide-Ferritin Nanocages as Cancer Theranostics. *ACS Nano* (2016) 10(3):3453–60. doi: 10.1021/acsnano.5b07521
30. Choe HS, Shin MJ, Kwon SG, Lee H, Kim DK, Choi KU, et al. Yolk-Shell-Type Gold Nanoaggregates for Chemo- and Photothermal Combination Therapy for Drug-Resistant Cancers. *ACS Appl Mater Interfaces* (2021) 13 (45):53519–29. doi: 10.1021/acsami.1c10036
31. Kim D, Amatya R, Hwang S, Lee S, Min KA, Shin MC. BSA-Silver Nanoparticles: A Potential Multimodal Therapeutics for Conventional and Photothermal Treatment of Skin Cancer. *Pharmaceutics* (2021) 13(4):575. doi: 10.3390/pharmaceutics13040575
32. Chen M, Chen S, He C, Mo S, Wang X, Liu G, et al. Safety Profile of Two-Dimensional Pd Nanosheets for Photothermal Therapy and Photoacoustic Imaging. *Nano Res* (2017) 10(4):1234–48. doi: 10.1007/s12274-016-1349-6
33. Zhou ZJ, Hu KW, Ma R, Yan Y, Ni B, Zhang YJ, et al. Dendritic Platinum-Copper Alloy Nanoparticles as Theranostic Agents for Multimodal Imaging and Combined Chemophotothermal Therapy. *Adv Funct Mater* (2016) 26 (33):5971–8. doi: 10.1002/adfm.201601754
34. Liu Q, Liu L, Mo C, Zhou X, Chen D, He Y, et al. Polyethylene Glycol-Coated Ultrasmall Superparamagnetic Iron Oxide Nanoparticles-Coupled Sialyl Lewis X Nanotheranostic Platform for Nasopharyngeal Carcinoma Imaging and Photothermal Therapy. *J Nanobiotech* (2021) 19(1):171. doi: 10.1186/s12951-021-00918-0
35. Qiu N, Yang X, Zhang Y, Zhang J, Ji J, Zhang Y, et al. A Molybdenum Oxide-Based Degradable Nanosheet for Combined Chemo-Photothermal Therapy to Improve Tumor Immunosuppression and Suppress Distant Tumors and Lung Metastases. *J Nanobiotech* (2021) 19(1):428. doi: 10.1186/s12951-021-01162-2
36. Liang H, Xi H, Liu S, Zhang X, Liu H. Modulation of Oxygen Vacancy in Tungsten Oxide Nanosheets for Vis-NIR Light-Enhanced Electrocatalytic Hydrogen Production and Anticancer Photothermal Therapy. *Nanoscale* (2019) 11(39):18183–90. doi: 10.1039/c9nr06222j
37. Deng H, Yang Y, Zuo T, Fang T, Xu Y, Yang J, et al. Multifunctional ZnO@CuS Nanoparticles Cluster Synergize Chemotherapy and Photothermal Therapy for Tumor Metastasis. *Nanomedicine* (2021) 34:102399. doi: 10.1016/j.nano.2021.102399
38. Xu X, Zhang R, Yang X, Lu Y, Yang Z, Peng M, et al. A Honeycomb-Like Bismuth/Manganese Oxide Nanoparticle With Mutual Reinforcement of Internal and External Response for Triple-Negative Breast Cancer Targeted Therapy. *Adv Healthc Mater* (2021) 10(18):e2100518. doi: 10.1002/adhm.202100518
39. Huang B, Huang Y, Han H, Ge Q, Yang D, Hu Y, et al. An NIR-II Responsive Nanoplatform for Cancer Photothermal and Oxidative Stress Therapy. *Front Bioeng Biotechnol* (2021) 9:751757. doi: 10.3389/fbioe.2021.751757
40. Liu Q, Song P, Zhang W, Wang Z, Yang K, Luo J, et al. Acid-Sensitive Nanoparticles Based on Molybdenum Disulfide for Photothermal-Chemo Therapy. *ACS Biomater Sci Eng* (2022) 8(4):1706–16. doi: 10.1021/acsbiomaterials.1c01390
41. Fu Q, Li Z, Ye J, Li Z, Fu F, Lin SL, et al. Magnetic Targeted Near-Infrared II PA/MR Imaging Guided Photothermal Therapy to Trigger Cancer Immunotherapy. *Theranostics* (2020) 10(11):4997–5010. doi: 10.7150/thno.43604
42. Lu J, Wang K, Lei W, Mao Y, Di D, Zhao Q, et al. Polydopamine-Carbon Dots Functionalized Hollow Carbon Nanoplatform for Fluorescence-Imaging and Photothermal-Enhanced Thermochemotherapy. *Mater Sci Eng C Mater Biol Appl* (2021) 122:111908. doi: 10.1016/j.msec.2021.111908
43. Wang J, Su X, Zhao P, Gao D, Chen R, Wang L. Cancer Photothermal Therapy Based on Near Infrared Fluorescent CdSeTe/ZnS Quantum Dots. *Analytical Methods* (2021) 13(45):5509–15. doi: 10.1039/D1AY01635K
44. Zhao YN, Zhao TY, Cao YN, Sun J, Zhou Q, Chen HY, et al. Temperature-Sensitive Lipid-Coated Carbon Nanotubes for Synergistic Photothermal Therapy and Gene Therapy. *ACS Nano* (2021) 15(4):6517–29. doi: 10.1021/acsnano.0c08790
45. Xu ZR, Zhang YL, Zhou WX, Wang LJ, Xu GX, Ma MZ, et al. NIR-II-Activated Biocompatible Hollow Nanocarbons for Cancer Photothermal Therapy. *J Nanobiotech* (2021) 19(1):137. doi: 10.1186/s12951-021-00884-7
46. Dash BS, Lu Y-J, Chen H-A, Chuang C-C, Chen J-P. Magnetic and GRPR-Targeted Reduced Graphene Oxide/Doxorubicin Nanocomposite for Dual-Targeted Chemo-Photothermal Cancer Therapy. *Mater Sci Eng: C* (2021) 128:112311. doi: 10.1016/j.msec.2021.112311
47. Chen LL, Hong WZ, Duan SL, Li YP, Wang J, Zhu JM. Graphene Quantum Dots Mediated Magnetic Chitosan Drug Delivery Nanosystems for Targeting Synergistic Photothermal-Chemotherapy of Hepatocellular Carcinoma. *Cancer Biol Ther* (2022) 23(1):281–93. doi: 10.1080/15384047.2022.2054249
48. Lu Y, Zhang X, Hou X, Feng M, Cao Z, Liu J. Functionalized 2d Nb2C Nanosheets for Primary and Recurrent Cancer Photothermal/Immune-Therapy in the NIR-II Biowindow. *Nanoscale* (2021) 13(42):17822–36. doi: 10.1039/D1NR05126A
49. Peng FF, Zhao FX, Shan LW, Li RR, Jiang SS, Zhang P. Black Phosphorus Nanosheets-Based Platform for Targeted Chemo-Photothermal Synergistic Cancer Therapy. *Colloids Surfaces B-Biointerfaces* (2021) 198:111467. doi: 10.1016/j.colsurfb.2020.111467
50. Jin L, Liu J, Tang Y, Cao L, Zhang T, Yuan Q, et al. MnO2-Functionalized Co–P Nanocomposite: A New Theranostic Agent for pH-Triggered T1/T2 Dual-Modality Magnetic Resonance Imaging-Guided Chemo-Photothermal Synergistic Therapy. *ACS Appl Mater Interfaces* (2017) 9(48):41648–58. doi: 10.1021/acsami.7b10608
51. Zhang YH, Zhu XH, Zhang J, Wu YH, Liu JL, Zhang Y. Synergistic Upconversion Photodynamic and Photothermal Therapy Under Cold Near-Infrared Excitation. *J Colloid Interface Sci* (2021) 600:513–29. doi: 10.1016/j.jcis.2021.05.017
52. Liu R, Sang LH, Wang TY, Liu YH, Wang ZR, Li J, et al. Phase-Change Mesoporous Prussian Blue Nanoparticles for Loading Paclitaxel and Chemo-Photothermal Therapy of Cancer. *Colloids Surfaces B-Biointerfaces* (2021) 207:112018. doi: 10.1016/j.colsurfb.2021.112018
53. Guo H, Liu L, Hu Q, Dou H. Monodisperse ZIF-8@Dextran Nanoparticles Co-Loaded With Hydrophilic and Hydrophobic Functional Cargos for Combined Near-Infrared Fluorescence Imaging and Photothermal Therapy. *Acta Biomater* (2022) 137:290–304. doi: 10.1016/j.actbio.2021.10.006
54. Cao Y, Wei D, Yang L, Luo Z, Yu P, Li H, et al. Nanoplatform Self-Assembly From Small Molecules of Porphyrin Derivatives for NIR-II Fluorescence Imaging Guided Photothermal-Immunotherapy. *Adv Healthc Mater* (2022), e2102526. doi: 10.1002/adhm.202102526

55. Feng HY, Yuan Y, Zhang Y, Liu HJ, Dong X, Yang SC, et al. Targeted Micellar Phthalocyanine for Lymph Node Metastasis Homing and Photothermal Therapy in an Orthotopic Colorectal Tumor Model. *Nanomicro Lett* (2021) 13(1):145. doi: 10.1007/s40820-021-00666-8
56. Yu T, Zhang D, Wang J, Sun C, Cui T, Xu Z, et al. Near-Infrared Upper Phenyl-Fused BODIPY as a Photosensitizer for Photothermal-Photodynamic Therapy. *J Mater Chem B* (2022) 10(16):3048–54. doi: 10.1039/d2tb00012a
57. Zheng X, Bian S, Liu W, Zhang C, Wu J, Ren H, et al. Amphiphilic Diketopyrrolopyrrole Derivatives for Efficient Near-Infrared Fluorescence Imaging and Photothermal Therapy. *ACS Omega* (2021) 6(40):26575–82. doi: 10.1021/acsomega.1c03947
58. Wang F, Li J, Chen C, Qi H, Huang K, Hu S. Preparation and Synergistic Chemo-Photothermal Therapy of Redox-Responsive Carboxymethyl Cellulose/Chitosan Complex Nanoparticles. *Carbohydr Polym* (2022) 275:118714. doi: 10.1016/j.carbpol.2021.118714
59. Wu J, Zhang Y, Jiang K, Wang X, Blum NT, Zhang J, et al. Enzyme-Engineered Conjugated Polymer Nanoplatform for Activatable Companion Diagnostics and Multistage Augmented Synergistic Therapy. *Adv Mater* (2022) 34(18):e2200062. doi: 10.1002/adma.202200062
60. Liu S, Zhou X, Zhang H, Ou H, Lam JWY, Liu Y, et al. Molecular Motion in Aggregates: Manipulating TICT for Boosting Photothermal Theranostics. *J Am Chem Soc* (2019) 141(13):5359–68. doi: 10.1021/jacs.8b13889
61. Ko Y, Kim J, Jeong HY, Kwon G, Kim D, Ku M, et al. Antibacterial Poly (3,4-Ethylenedioxythiophene):Poly(Styrene-Sulfonate)/Agarose Nanocomposite Hydrogels With Thermo-Processability and Self-Healing. *Carbohydr Polym* (2019) 203:26–34. doi: 10.1016/j.carbpol.2018.09.026
62. Xu N, Hu A, Pu X, Wang J, Liao X, Huang Z, et al. Cu-Chelated Polydopamine Nanoparticles as a Photothermal Medium and "Immunogenic Cell Death" Inducer for Combined Tumor Therapy. *J Mater Chem B* (2022) 10(16):3104–18. doi: 10.1039/d2tb00025c
63. Xie Z, Lu R, Zhu Y, Peng M, Fan T, Ren P, et al. Liquid-Phase Exfoliation of Black Sesame to Create a Nanoplatform for *In Vitro* Photoluminescence and Photothermal Therapy. *Nanomed (Lond)* (2020) 15(21):2041–52. doi: 10.2217/nnm-2020-0151
64. Kang S, Baskaran R, Ozlu B, Davaa E, Kim JJ, Shim BS, et al. T1-Positive Mn2+-Doped Multi-Stimuli Responsive Poly(L-DOPA) Nanoparticles for Photothermal and Photodynamic Combination Cancer Therapy. *Biomedicines* (2020) 8(10):417. doi: 10.3390/biomedicines8100417
65. Odda AH, Cheang TY, Alesary HF, Liu L, Qian X, Ullah N, et al. A Multifunctional α-Fe2O3@PEDOT Core-Shell Nanoplatform for Gene and Photothermal Combination Anticancer Therapy. *J Mater Chem B* (2022) 10 (9):1453–62. doi: 10.1039/d1tb02625a
66. Bai Y, Zhao J, Zhang L, Wang S, Hua J, Zhao S, et al. A Smart Near-Infrared Carbon Dot-Metal Organic Framework Assemblies for Tumor Microenvironment-Activated Cancer Imaging and Chemodynamic-Photothermal Combined Therapy. *Adv Healthc Mater* (2022), e2102759. doi: 10.1002/adhm.202102759
67. Lv Z, He S, Wang Y, Zhu X. Noble Metal Nanomaterials for NIR-Triggered Photothermal Therapy in Cancer. *Adv Healthc Mater* (2021) 10(6): e2001806. doi: 10.1002/adhm.202001806
68. Kim M, Lee JH, Nam JM. Plasmonic Photothermal Nanoparticles for Biomedical Applications. *Adv Sci (Weinh)* (2019) 6(17):1900471. doi: 10.1002/advs.201900471
69. Yao CP, Zhang LW, Wang J, He YL, Xin J, Wang SJ, et al. Gold Nanoparticle Mediated Phototherapy for Cancer. *J Nanomater* (2016) 2016:5497136. doi: 10.1155/2016/5497136
70. Amendoeira A, Garcia LR, Fernandes AR, Baptista PV. Light Irradiation of Gold Nanoparticles Toward Advanced Cancer Therapeutics. *Advanced Ther* (2020) 3(1):1900153. doi: 10.1002/adtp.201900153
71. Hu M, Chen J, Li ZY, Au L, Hartland GV, Li X, et al. Gold Nanostructures: Engineering Their Plasmonic Properties for Biomedical Applications. *Chem Soc Rev* (2006) 35(11):1084–94. doi: 10.1039/b517615h
72. Pivetta TP, Botteon CEA, Ribeiro PA, Marcato PD, Raposo M. Nanoparticle Systems for Cancer Phototherapy: An Overview. *Nanomater (Basel)* (2021) 11(11):3132. doi: 10.3390/nano11113132
73. Thompson EA, Graham E, MacNeill CM, Young M, Donati G, Wailes EM, et al. Differential Response of MCF7, MDA-MB-231, and MCF 10A Cells to Hyperthermia, Silver Nanoparticles and Silver Nanoparticle-Induced Photothermal Therapy. *Int J Hyperthermia* (2014) 30(5):312–23. doi: 10.3109/02656736.2014.936051
74. Huang X, Tang S, Mu X, Dai Y, Chen G, Zhou Z, et al. Freestanding Palladium Nanosheets With Plasmonic and Catalytic Properties. *Nat Nanotechnol* (2011) 6(1):28–32. doi: 10.1038/nnano.2010.235
75. Xiao JW, Fan SX, Wang F, Sun LD, Zheng XY, Yan CH. Porous Pd Nanoparticles With High Photothermal Conversion Efficiency for Efficient Ablation of Cancer Cells. *Nanoscale* (2014) 6(8):4345–51. doi: 10.1039/c3nr06843a
76. Huang X, Tang S, Liu B, Ren B, Zheng N. Enhancing the Photothermal Stability of Plasmonic Metal Nanoplates by a Core-Shell Architecture. *Adv Mater* (2011) 23(30):3420–5. doi: 10.1002/adma.201100905
77. Chen M, Tang S, Guo Z, Wang X, Mo S, Huang X, et al. Core-Shell Pd@Au Nanoplates as Theranostic Agents for in-Vivo Photoacoustic Imaging, CT Imaging, and Photothermal Therapy. *Adv Mater* (2014) 26(48):8210–6. doi: 10.1002/adma.201404013
78. Wei J, Li J, Sun D, Li Q, Ma J, Chen X, et al. A Novel Theranostic Nanoplatform Based on Pd@Pt-PEG-Ce6 for Enhanced Photodynamic Therapy by Modulating Tumor Hypoxia Microenvironment. *Adv Funct Mater* (2018) 28(17):1706310. doi: 10.1002/adfm.201706310
79. Tang S, Huang X, Zheng N. Silica Coating Improves the Efficacy of Pd Nanosheets for Photothermal Therapy of Cancer Cells Using Near Infrared Laser. *Chem Commun* (2011) 47(13):3948–50. doi: 10.1039/c1cc10451a
80. Zhu W, Chen M, Liu Y, Tian Y, Song Z, Song G, et al. A Dual Factor Activated Metal-Organic Framework Hybrid Nanoplatform for Photoacoustic Imaging and Synergetic Photo-Chemotherapy. *Nanoscale* (2019) 11(43):20630–7. doi: 10.1039/c9nr06349h
81. Liu Y, Li J, Chen M, Chen X, Zheng N. Palladium-Based Nanomaterials for Cancer Imaging and Therapy. *Theranostics* (2020) 10(22):10057–74. doi: 10.7150/thno.45990
82. Zhu YY, Li W, Zhao X, Zhou ZJ, Wang YT, Cheng YY, et al. Hyaluronic Acid-Encapsulated Platinum Nanoparticles for Targeted Photothermal Therapy of Breast Cancer. *J BioMed Nanotechnol* (2017) 13(11):1457–67. doi: 10.1166/jbn.2017.2446
83. Chen DH, Gao SP, Ge W, Li QW, Jiang H, Wang XM. One-Step Rapid Synthesis of Fluorescent Platinum Nanoclusters for Cellular Imaging and Photothermal Treatment. *RSC Adv* (2014) 4(76):40141–5. doi: 10.1039/c4ra07121b
84. Deng Y, Li E, Cheng X, Zhu J, Lu S, Ge C, et al. Facile Preparation of Hybrid Core-Shell Nanorods for Photothermal and Radiation Combined Therapy. *Nanoscale* (2016) 8(7):3895–9. doi: 10.1039/c5nr09102k
85. Zhao H, Xu J, Huang W, Zhan G, Zhao Y, Chen H, et al. Spatiotemporally Light-Activatable Platinum Nanocomplexes for Selective and Cooperative Cancer Therapy. *ACS Nano* (2019) 13(6):6647–61. doi: 10.1021/acsnano.9b00972
86. Chhowalla M, Shin HS, Eda G, Li LJ, Loh KP, Zhang H. The Chemistry of Two-Dimensional Layered Transition Metal Dichalcogenide Nanosheets. *Nat Chem* (2013) 5(4):263–75. doi: 10.1038/Nchem.1589
87. Wang C, Bai J, Liu YW, Jia XD, Jiang X. Polydopamine Coated Selenide Molybdenum: A New Photothermal Nanocarrier for Highly Effective Chemo-Photothermal Synergistic Therapy. *ACS Biomater-Sci Eng* (2016) 2 (11):2011–7. doi: 10.1021/acsbiomaterials.6b00416
88. Zhu HJ, Lai ZC, Fang Y, Zhen X, Tan CL, Qi XY, et al. Ternary Chalcogenide Nanosheets With Ultrahigh Photothermal Conversion Efficiency for Photoacoustic Theranostics. *Small* (2017) 13(16):1604139. doi: 10.1002/smll.201604139
89. Li Z, Chen Y, Yang Y, Yu Y, Zhang Y, Zhu D, et al. Recent Advances in Nanomaterials-Based Chemo-Photothermal Combination Therapy for Improving Cancer Treatment. *Front Bioeng Biotechnol* (2019) 7:293. doi: 10.3389/fbioe.2019.00293
90. Gawande MB, Goswami A, Felpin FX, Asefa T, Huang X, Silva R, et al. Cu and Cu-Based Nanoparticles: Synthesis and Applications in Catalysis. *Chem Rev* (2016) 116(6):3722–811. doi: 10.1021/acs.chemrev.5b00482
91. Fernandes N, Rodrigues CF, Moreira AF, Correia IJ. Overview of the Application of Inorganic Nanomaterials in Cancer Photothermal Therapy. *Biomater Sci* (2020) 8(11):2990–3020. doi: 10.1039/d0bm00222d
92. Hessel CM, Pattani VP, Rasch M, Panthani MG, Koo B, Tunnell JW, et al. Copper Selenide Nanocrystals for Photothermal Therapy. *Nano Lett* (2011) 11(6):2560–6. doi: 10.1021/nl201400z

93. Lie SQ, Wang DM, Gao MX, Huang CZ. Controllable Copper Deficiency in Cu2-xSe Nanocrystals With Tunable Localized Surface Plasmon Resonance and Enhanced Chemiluminescence. *Nanoscale* (2014) 6(17):10289–96. doi: 10.1039/c4nr02294g
94. Zhu Z, Zou Y, Hu W, Li Y, Gu Y, Cao B, et al. Near-Infrared Plasmonic 2D Semimetals for Applications in Communication and Biology. *Adv Funct Mater* (2016) 26(11):1793–802. doi: 10.1002/adfm.201504884
95. Yuwen L, Zhou J, Zhang Y, Zhang Q, Shan J, Luo Z, et al. Aqueous Phase Preparation of Ultrasmall MoSe2 Nanodots for Efficient Photothermal Therapy of Cancer Cells. *Nanoscale* (2016) 8(5):2720–6. doi: 10.1039/c5nr08166a
96. Ding D, Guo W, Guo C, Sun J, Zheng N, Wang F, et al. MoO3-X Quantum Dots for Photoacoustic Imaging Guided Photothermal/Photodynamic Cancer Treatment. *Nanoscale* (2017) 9(5):2020–9. doi: 10.1039/c6nr09046j
97. Song G, Hao J, Liang C, Liu T, Gao M, Cheng L, et al. Degradable Molybdenum Oxide Nanosheets With Rapid Clearance and Efficient Tumor Homing Capabilities as a Therapeutic Nanoplatform. *Angew Chem Int Ed Engl* (2016) 55(6):2122–6. doi: 10.1002/anie.201510597
98. Wang JL, Sui LH, Huang J, Miao L, Nie YB, Ai KL. MoS2-Based Nanocomposites for Cancer Diagnosis and Therapy. *Bioactive Mater* (2021) 6(11):4209–42. doi: 10.1016/j.bioactmat.2021.04.021
99. Li S, Tan L, Xu W, Liu C, Wu Q, Fu C, et al. Doxorubicin-Loaded Layered MoS_2 Hollow Spheres and Its Photothermo-Chemotherapy on Hepatocellular Carcinoma. *J BioMed Nanotechnol* (2017) 13(11):1557–64. doi: 10.1166/jbn.2017.2461
100. Jeong H, Park W, Kim DH, Na K. Dynamic Nanoassemblies of Nanomaterials for Cancer Photomedicine. *Adv Drug Delivery Rev* (2021) 177:113954. doi: 10.1016/j.addr.2021.113954
101. Estelrich J, Antònia Busquets M. Iron Oxide Nanoparticles in Photothermal Therapy. *Molecules* (2018) 23(7):1567. doi: 10.3390/molecules23071567
102. Maeng JH, Lee DH, Jung KH, Bae YH, Park IS, Jeong S, et al. Multifunctional Doxorubicin Loaded Superparamagnetic Iron Oxide Nanoparticles for Chemotherapy and Magnetic Resonance Imaging in Liver Cancer. *Biomaterials* (2010) 31(18):4995–5006. doi: 10.1016/j.biomaterials.2010.02.068
103. Hu J, Qian Y, Wang X, Liu T, Liu S. Drug-Loaded and Superparamagnetic Iron Oxide Nanoparticle Surface-Embedded Amphiphilic Block Copolymer Micelles for Integrated Chemotherapeutic Drug Delivery and MR Imaging. *Langmuir* (2012) 28(4):2073–82. doi: 10.1021/la203992q
104. Lai CW, Wang YH, Lai CH, Yang MJ, Chen CY, Chou PT, et al. Iridium-Complex-Functionalized Fe3O4/SiO2 Core/Shell Nanoparticles: A Facile Three-in-One System in Magnetic Resonance Imaging, Luminescence Imaging, and Photodynamic Therapy. *Small* (2008) 4(2):218–24. doi: 10.1002/smll.200700283
105. Ding J, Zhao J, Cheng K, Liu G, Xiu D. *In Vivo* Photodynamic Therapy and Magnetic Resonance Imaging of Cancer by TSPP-Coated Fe3O4 Nanoconjugates. *J BioMed Nanotechnol* (2010) 6(6):683–6. doi: 10.1166/jbn.2010.1165
106. Ma X, Tao H, Yang K, Feng L, Cheng L, Shi X, et al. A Functionalized Graphene Oxide-Iron Oxide Nanocomposite for Magnetically Targeted Drug Delivery, Photothermal Therapy, and Magnetic Resonance Imaging. *Nano Res* (2012) 5(3):199–212. doi: 10.1007/s12274-012-0200-y
107. Dong W, Li Y, Niu D, Ma Z, Gu J, Chen Y, et al. Facile Synthesis of Monodisperse Superparamagnetic Fe3O4 Core@Hybrid@Au Shell Nanocomposite for Bimodal Imaging and Photothermal Therapy. *Adv Mater* (2011) 23(45):5392–7. doi: 10.1002/adma.201103521
108. Zhu L, Zhou Z, Mao H, Yang L. Magnetic Nanoparticles for Precision Oncology: Theranostic Magnetic Iron Oxide Nanoparticles for Image-Guided and Targeted Cancer Therapy. *Nanomed (Lond)* (2017) 12(1):73–87. doi: 10.2217/nnm-2016-0316
109. Soetaert F, Korangath P, Serantes D, Fiering S, Ivkov R. Cancer Therapy With Iron Oxide Nanoparticles: Agents of Thermal and Immune Therapies. *Adv Drug Delivery Rev* (2020) 163-164:65–83. doi: 10.1016/j.addr.2020.06.025
110. Dhas N, Kudarha R, Garkal A, Ghate V, Sharma S, Panzade P, et al. Molybdenum-Based Hetero-Nanocomposites for Cancer Therapy, Diagnosis and Biosensing Application: Current Advancement and Future Breakthroughs. *J Control Release* (2021) 330:257–83. doi: 10.1016/j.jconrel.2020.12.015
111. Odda AH, Xu Y, Lin J, Wang G, Ullah N, Zeb A, et al. Plasmonic MoO3-X Nanoparticles Incorporated in Prussian Blue Frameworks Exhibit Highly Efficient Dual Photothermal/Photodynamic Therapy. *J Mater Chem B* (2019) 7(12):2032–42. doi: 10.1039/c8tb03148g
112. Bazaka K, Levchenko I, Lim JWM, Baranov O, Corbella C, Xu S, et al. MoS2-Based Nanostructures: Synthesis and Applications in Medicine. *J Phys D. Appl Phys* (2019) 52(18):183001. doi: 10.1088/1361-6463/ab03b3
113. Manthiram K, Alivisatos AP. Tunable Localized Surface Plasmon Resonances in Tungsten Oxide Nanocrystals. *J Am Chem Soc* (2012) 134 (9):3995–8. doi: 10.1021/ja211363w
114. Guo W, Guo C, Zheng N, Sun T, Liu S.). Csx WO3 Nanorods Coated With Polyelectrolyte Multilayers as a Multifunctional Nanomaterial for Bimodal Imaging-Guided Photothermal/Photodynamic Cancer Treatment. *Adv Mater* (2017) 29(4):1604157. doi: 10.1002/adma.201604157
115. Ghosh S, Khamarui S, Saha M, De SK. Fabrication of Tungsten Nanocrystals and Silver–Tungsten Nanonets: A Potent Reductive Catalyst. *RSC Advances* (2015) 5(49):38971–6. doi: 10.1039/c4ra16567e
116. Zuo H, Tao J, Shi H, He J, Zhou Z, Zhang C. Platelet-Mimicking Nanoparticles Co-Loaded With W18O49 and Metformin Alleviate Tumor Hypoxia for Enhanced Photodynamic Therapy and Photothermal Therapy. *Acta Biomater* (2018) 80:296–307. doi: 10.1016/j.actbio.2018.09.017
117. Yang ZY, Wang JF, Liu S, Sun F, Miao J, Xu E, et al. Tumor-Targeting W18O49 Nanoparticles for Dual-Modality Imaging and Guided Heat-Shock-Response-Inhibited Photothermal Therapy in Gastric Cancer. *Particle Particle Syst Characterization* (2019) 36(7):1900124. doi: 10.1002/ppsc.201900124
118. Zheng HD, Ou JZ, Strano MS, Kaner RB, Mitchell A, Kalantar-Zadeh K. Nanostructured Tungsten Oxide–Properties, Synthesis, and Applications. *Advanced Funct Mater* (2011) 21(12):2175–96. doi: 10.1002/adfm.201002477
119. Segets D, Gradl J, Taylor RK, Vassilev V, Peukert W. Analysis of Optical Absorbance Spectra for the Determination of ZnO Nanoparticle Size Distribution, Solubility, and Surface Energy. *ACS Nano* (2009) 3(7):1703–10. doi: 10.1021/nn900223b
120. Lou X, Shen H, Shen Y. Development of ZnO Series Ceramic Semiconductor Gas Sensors. *J Sens Trans Technol* (1991) 03:1–5. doi: 10.13873/j.1000-97871991.03.001
121. Nikoobakht B, Wang X, Herzing A, Shi J. Scalable Synthesis and Device Integration of Self-Registered One-Dimensional Zinc Oxide Nanostructures and Related Materials. *Chem Soc Rev* (2013) 42(1):342–65. doi: 10.1039/c2cs35164a
122. Chiua WS, Khiew PS, Clokea M, Isaa D, Tana TK, Radimanb S, et al. Photocatalytic Study of Two-Dimensional ZnO Nanopellets in the Decomposition of Methylene Blue. *Chem Eng J* (2010) 158(2):345–352. doi: 10.1016/j.cej.2010.01.052
123. Bitenc M, Orel ZC. Synthesis and Characterization of Crystalline Hexagonal Bipods of Zinc Oxide. *Mater Res Bull* (2009) 44(2):381–387. doi: 10.1016/j.materresbull.2008.05.005
124. Kołodziejczak-Radzimska A, Jesionowski T. Zinc Oxide-From Synthesis to Application: A Review. *Mater (Basel)* (2014) 7(4):2833–81. doi: 10.3390/ma7042833
125. Cai X, Zhu Q, Zeng Y, Zeng Q, Chen X, Zhan Y. Manganese Oxide Nanoparticles as Mri Contrast Agents in Tumor Multimodal Imaging and Therapy. *Int J Nanomed* (2019) 14:8321–44. doi: 10.2147/IJN.S218085
126. Liu Z, Zhang S, Lin H, Zhao M, Yao H, Zhang L, et al. Theranostic 2D Ultrathin MnO2 Nanosheets With Fast Responsibility to Endogenous Tumor Microenvironment and Exogenous NIR Irradiation. *Biomaterials* (2018) 155:54–63. doi: 10.1016/j.biomaterials.2017.11.015
127. Han B, Zhang YL, Chen QD, Sun HB. Carbon-Based Photothermal Actuators. *Advanced Funct Mater* (2018) 28(40):1802235. doi: 10.1002/adfm.201802235
128. Yu J, Lin YH, Yang L, Huang CC, Chen L, Wang WC, et al. Improved Anticancer Photothermal Therapy Using the Bystander Effect Enhanced by Antiarrhythmic Peptide Conjugated Dopamine-Modified Reduced Graphene Oxide Nanocomposite. *Adv Healthc Mater* (2017) 6(2):1600804. doi: 10.1002/adhm.201600804

129. Lim DJ, Sim M, Oh L, Lim K, Park H. Carbon-Based Drug Delivery Carriers for Cancer Therapy. *Arch Pharm Res* (2014) 37(1):43–52. doi: 10.1007/s12272-013-0277-1
130. Ding CQ, Zhu AW, Tian Y. Functional Surface Engineering of C-Dots for Fluorescent Biosensing and in Vivo Bioimaging. *Acc Chem Res* (2014) 47 (1):20–30. doi: 10.1021/ar400023s
131. Du J, Xu N, Fan J, Sun W, Peng X. Carbon Dots for *In Vivo* Bioimaging and Theranostics. *Small* (2019) 15(32):e1805087. doi: 10.1002/smll.201805087
132. Zhang YJ, Sha R, Zhang L, Zhang WB, Jin PP, Xu WG, et al. Harnessing Copper-Palladium Alloy Tetrapod Nanoparticle-Induced Pro-Survival Autophagy for Optimized Photothermal Therapy of Drug-Resistant Cancer. *Nat Commun* (2018) 9:4236. doi: 10.1038/s41467-018-06529-y
133. Li DD, Zhang GB, Xu WG, Wang JX, Wang YC, Qiu LZ, et al. Investigating the Effect of Chemical Structure of Semiconducting Polymer Nanoparticle on Photothermal Therapy and Photoacoustic Imaging. *Theranostics* (2017) 7 (16):4029–40. doi: 10.7150/thno.19538
134. Bilan R, Nabiev I, Sukhanova A. Quantum Dot-Based Nanotools for Bioimaging, Diagnostics, and Drug Delivery. *Chembiochem* (2016) 17 (22):2103–14. doi: 10.1002/cbic.201600357
135. Yao J, Li L, Li P, Yang M. Quantum Dots: From Fluorescence to Chemiluminescence, Bioluminescence, Electrochemiluminescence, and Electrochemistry. *Nanoscale* (2017) 9(36):13364–83. doi: 10.1039/c7nr05233b
136. Yao J, Li PF, Li L, Yang M. Biochemistry and Biomedicine of Quantum Dots: From Biodetection to Bioimaging, Drug Discovery, Diagnostics, and Therapy. *Acta Biomaterialia* (2018) 74:36–55. doi: 10.1016/j.actbio.2018.05.004
137. Li LP, Zhang RP, Lu CX, Sun JH, Wang LJ, Qu BT, et al. *In Situ* Synthesis of NIR-Light Emitting Carbon Dots Derived From Spinach for Bio-Imaging Applications. *J Mater Chem B* (2017) 5(35):7328–34. doi: 10.1039/c7tb00634a
138. Zhang J, Hao GY, Yao CF, Yu JN, Wang J, Yang WT, et al. Albumin-Mediated Biomineralization of Paramagnetic NIR Ag2S QDs for Tiny Tumor Bimodal Targeted Imaging in Vivo. *ACS Appl Mater Interfaces* (2016) 8(26):16612–21. doi: 10.1021/acsami.6b04738
139. Iijima S. Helical Microtubules of Graphitic Carbon. *Nature* (1991) 354 (6348):56–8. doi: 10.1038/354056a0
140. Augustine S, Singh J, Srivastava M, Sharma M, Das A, Malhotra BD. Recent Advances in Carbon Based Nanosystems for Cancer Theranostics. *Biomater Sci* (2017) 5(5):901–52. doi: 10.1039/c7bm00008a
141. Jaque D, Martínez Maestro L, del Rosal B, Haro-Gonzalez P, Benayas A, Plaza JL, et al. Nanoparticles for Photothermal Therapies. *Nanoscale* (2014) 6 (16):9494–530. doi: 10.1039/C4NR00708E
142. He H, Pham-Huy LA, Dramou P, Xiao DL, Zuo PL, Pham-Huy C. Carbon Nanotubes: Applications in Pharmacy and Medicine. *BioMed Res Int* (2013) 2013:578290. doi: 10.1155/2013/578290
143. Iancu C, Mocan L. Advances in Cancer Therapy Through the Use of Carbon Nanotube-Mediated Targeted Hyperthermia. *Int J Nanomed* (2011) 6:1675–84. doi: 10.2147/ijn.S23588
144. Kam NWS, O'Connell M, Wisdom JA, Dai HJ. Carbon Nanotubes as Multifunctional Biological Transporters and Near-Infrared Agents for Selective Cancer Cell Destruction. *Proc Natl Acad Sci United States America* (2005) 102(33):11600–5. doi: 10.1073/pnas.0502680102
145. Wang LM, Sun Q, Wang X, Wen T, Yin JJ, Wang PY, et al. Using Hollow Carbon Nanospheres as a Light-Induced Free Radical Generator To Overcome Chemotherapy Resistance. *J Am Chem Soc* (2015) 137(5):1947–55. doi: 10.1021/ja511560b
146. Fang Y, Gu D, Zou Y, Wu ZX, Li FY, Che RC, et al. A Low-Concentration Hydrothermal Synthesis of Biocompatible Ordered Mesoporous Carbon Nanospheres With Tunable and Uniform Size. *Angewandte Chemie-International Edition* (2010) 49(43):7987–91. doi: 10.1002/anie.201002849
147. Li X, Liu C, Wang SY, Jiao J, Di DH, Jiang TY, et al. Poly(acrylic Acid) Conjugated Hollow Mesoporous Carbon as a Dual-Stimuli Triggered Drug Delivery System for Chemo-Photothermal Synergistic Therapy. *Mater Sci Eng C-Materials Biol Appl* (2017) 71:594–603. doi: 10.1016/j.msec.2016.10.037
148. Karavasili C, Amanatiadou EP, Sygellou L, Giasafaki DK, Steriotis TA, Charalambopoulou GC, et al. Development of New Drug Delivery System Based on Ordered Mesoporous Carbons: Characterisation and Cytocompatibility Studies. *J Mater Chem B* (2013) 1(25):3167–74. doi: 10.1039/c3tb20304b
149. Wang XD, Li X, Mao YL, Wang D, Zhao QF, Wang SL. Multi-Stimuli Responsive Nanosystem Modified by Tumor-Targeted Carbon Dots for Chemophototherapy Synergistic Therapy. *J Colloid Interface Sci* (2019) 552:639–50. doi: 10.1016/j.jcis.2019.05.085
150. Jin Y, Wang J, Ke H, Wang S, Dai Z. Graphene Oxide Modified PLA Microcapsules Containing Gold Nanoparticles for Ultrasonic/CT Bimodal Imaging Guided Photothermal Tumor Therapy. *Biomaterials* (2013) 34 (20):4794–802. doi: 10.1016/j.biomaterials.2013.03.027
151. Chen YW, Chen PJ, Hu SH, Chen IW, Chen SY. NIR-Triggered Synergic Photo-Chemothermal Therapy Delivered by Reduced Graphene Oxide/Carbon/Mesoporous Silica Nanocookies. *Adv Func Mater* (2014) 24 (4):451–9. doi: 10.1002/adfm.201301763
152. Hussein EA, Zagho MM, Nasrallah GK, Elzatahry AA. Recent Advances in Functional Nanostructures as Cancer Photothermal Therapy. *Int J Nanomedicine* (2018) 17(13):2897–906 doi: 10.2147/IJN.S161031
153. Kostarelos K, Novoselov KS. Exploring the Interface of Graphene and Biology. *Science* (2014) 344(6181):261–3. doi: 10.1126/science.1246736
154. Cheng C, Li S, Thomas A, Kotov NA, Haag R. Functional Graphene Nanomaterials Based Architectures: Biointeractions, Fabrications, and Emerging Biological Applications. *Chem Rev* (2017) 117(3):1826–914. doi: 10.1021/acs.chemrev.6b00520
155. Orecchioni M, Cabizza R, Bianco A, Delogu LG. Graphene as Cancer Theranostic Tool: Progress and Future Challenges. *Theranostics* (2015) 5 (7):710–23. doi: 10.7150/thno.11387
156. de Melo-Diogo D, Costa EC, Alves CG, Lima-Sousa R, Ferreira P, Louro RO, et al. POxylated Graphene Oxide Nanomaterials for Combination Chemophototherapy of Breast Cancer Cells. *Eur J Pharmaceutics Biopharmaceutics* (2018) 131:162–9. doi: 10.1016/j.ejpb.2018.08.008
157. Moore TL, Podilakrishna R, Rao A, Alexis F. Systemic Administration of Polymer-Coated Nano-Graphene to Deliver Drugs to Glioblastoma. *Particle Particle Syst Characterization* (2014) 31(8):886–94. doi: 10.1002/ppsc.201300379
158. de Melo-Diogo D, Lima-Sousa R, Alves CG, Costa EC, Louro RO, Correia IJ. Functionalization of Graphene Family Nanomaterials for Application in Cancer Therapy. *Colloids Surfaces B-Biointerfaces* (2018) 171:260–75. doi: 10.1016/j.colsurfb.2018.07.030
159. de Melo-Diogo D, Pais-Silva C, Dias DR, Moreira AF, Correia IJ. Strategies to Improve Cancer Photothermal Therapy Mediated by Nanomaterials. *Advanced Healthcare Mater* (2017) 6(10):1700073. doi: 10.1002/adhm.201700073
160. Yao J, Sun Y, Yang M, Duan YX. Chemistry, Physics and Biology of Graphene-Based Nanomaterials: New Horizons for Sensing, Imaging and Medicine. *J Mater Chem* (2012) 22(29):14313–29. doi: 10.1039/c2jm31632c
161. Lin J, Chen XY, Huang P. Graphene-Based Nanomaterials for Bioimaging. *Advanced Drug Delivery Rev* (2016) 105:242–54. doi: 10.1016/j.addr.2016.05.013
162. Shim G, Kim MG, Park JY, Oh YK. Graphene-Based Nanosheets for Delivery of Chemotherapeutics and Biological Drugs. *Advanced Drug Delivery Rev* (2016) 105:205–27. doi: 10.1016/j.addr.2016.04.004
163. Jaleel JA, Sruthi S, Pramod K. Reinforcing Nanomedicine Using Graphene Family Nanomaterials. *J Controlled Release* (2017) 255:218–30. doi: 10.1016/j.jconrel.2017.04.041
164. Ponomarenko LA, Schedin F, Katsnelson MI, Yang R, Hill EW, Novoselov KS, et al. Chaotic Dirac Billiard in Graphene Quantum Dots. *Science* (2008) 320(5874):356–8. doi: 10.1126/science.1154663
165. Tade RS, Patil PO. Theranostic Prospects of Graphene Quantum Dots in Breast Cancer. *ACS Biomater Sci Eng* (2020) 6(11):5987–6008. doi: 10.1021/acsbiomaterials.0c01045
166. Fan HY, Yu XH, Wang K, Yin YJ, Tang YJ, Tang YL, et al. Graphene Quantum Dots (GQDs)-Based Nanomaterials for Improving Photodynamic Therapy in Cancer Treatment. *Eur J Medicinal Chem* (2019) 182:111620. doi: 10.1016/j.ejmech.2019.111620

167. Yao XX, Tian ZF, Liu JX, Zhu YF, Hanagata N. Mesoporous Silica Nanoparticles Capped With Graphene Quantum Dots for Potential Chemo-Photothermal Synergistic Cancer Therapy. *Langmuir* (2017) 33 (2):591–9. doi: 10.1021/acs.langmuir.6b04189
168. Szuplewska A, Kulpinska D, Dybko A, Chudy M, Jastrzebska AM, Olszyna A, et al. Future Applications of MXenes in Biotechnology, Nanomedicine, and Sensors. *Trends Biotechnol* (2020) 38(3):264–79. doi: 10.1016/j.tibtech.2019.09.001
169. Wojciechowski T, Rozmysłowska-Wojciechowska A, Matyszczak G, Wrzecionek M, Olszyna A, Peter A, et al. Ti2C MXene Modified With Ceramic Oxide and Noble Metal Nanoparticles: Synthesis, Morphostructural Properties, and High Photocatalytic Activity. *Inorganic Chem* (2019) 58(11):7602–14. doi: 10.1021/acs.inorgchem.9b01015
170. Kalambate PK, Gadhari NS, Li X, Rao ZX, Navale ST, Shen Y, et al. Recent Advances in MXene-Based Electrochemical Sensors and Biosensors. *Trac-Trends Analytical Chem* (2019) 120:115643. doi: 10.1016/j.trac.2019.115643
171. Ronchi RM, Arantes JT, Santos SF. Synthesis, Structure, Properties and Applications of MXenes: Current Status and Perspectives. *Ceramics Int* (2019) 45(15):18167–88. doi: 10.1016/j.ceramint.2019.06.114
172. Iravani S, Varma RS. MXenes for Cancer Therapy and Diagnosis: Recent Advances and Current Challenges. *ACS Biomater Sci Eng* (2021) 7(6):1900–13. doi: 10.1021/acsbiomaterials.0c01763
173. Zhang JB, Fu Y, Mo AC. Multilayered Titanium Carbide MXene Film for Guided Bone Regeneration. *Int J Nanomed* (2019) 14:10091–102. doi: 10.2147/ijn.S227830
174. Shao JD, Xie HH, Huang H, Li ZB, Sun ZB, Xu YH, et al. Biodegradable Black Phosphorus-Based Nanospheres for *In Vivo* Photothermal Cancer Therapy. *Nat Commun* (2016) 7:12967. doi: 10.1038/ncomms12967
175. Chen L, Zhou GM, Liu ZB, Ma XM, Chen J, Zhang ZY, et al. Scalable Clean Exfoliation of High-Quality Few-Layer Black Phosphorus for a Flexible Lithium Ion Battery. *Advanced Mater* (2016) 28(3):510–+. doi: 10.1002/adma.201503678
176. Cheng L, Liu J, Gu X, Gong H, Shi X, Liu T, et al. PEGylated WS2 Nanosheets as a Multifunctional Theranostic Agent for *In Vivo* Dual-Modal CT/Photoacoustic Imaging Guided Photothermal Therapy. *Adv Mater* (2014) 26(12):1886–93. doi: 10.1002/adma.201304497
177. Qin L, Jiang SS, He HY, Ling GX, Zhang P. Functional Black Phosphorus Nanosheets for Cancer Therapy. *J Controlled Release* (2020) 318:50–66. doi: 10.1016/j.jconrel.2019.12.013
178. Liu Y, Zhen WY, Wang YH, Liu JH, Jin LH, Zhang TQ, et al. One-Dimensional Fe2P Acts as a Fenton Agent in Response to NIR II Light and Ultrasound for Deep Tumor Synergetic Theranostics. *Angewandte Chemie-International Edition* (2019) 58(8):2407–12. doi: 10.1002/anie.201813702
179. Huang KW, Hsu FF, Qiu JTT, Chern GJ, Lee YA, Chang CC, et al. Highly Efficient and Tumor-Selective Nanoparticles for Dual-Targeted Immunogene Therapy Against Cancer. *Sci Adv* (2020) 6(3):eaax5032. doi: 10.1126/sciadv.aax5032
180. Yao X, Yang B, Wang S, Dai Z, Zhang D, Zheng X, et al. A Novel Multifunctional FePt/BP Nanoplatform for Synergistic Photothermal/Photodynamic/Chemodynamic Cancer Therapies and Photothermally-Enhanced Immunotherapy. *J Mater Chem B* (2020) 8(35):8010–21. doi: 10.1039/D0TB00411A
181. Liu Y, Wang YH, Song SY, Zhang HJ. Tumor Diagnosis and Therapy Mediated by Metal Phosphorus-Based Nanomaterials. *Advanced Mater* (2021) 33(49):e2103936. doi: 10.1002/adma.202103936
182. Chen GY, Qiu HL, Prasad PN, Chen XY. Upconversion Nanoparticles: Design, Nanochemistry, and Applications in Theranostics. *Chem Rev* (2014) 114(10):5161–214. doi: 10.1021/cr400425h
183. Chatterjee DK, Rufaihah AJ, Zhang Y. Upconversion Fluorescence Imaging of Cells and Small Animals Using Lanthanide Doped Nanocrystals. *Biomaterials* (2008) 29(7):937–43. doi: 10.1016/j.biomaterials.2007.10.051
184. Idris NM, Li ZQ, Ye L, Sim EKW, Mahendran R, Ho PCL, et al. Tracking Transplanted Cells in Live Animal Using Upconversion Fluorescent Nanoparticles. *Biomaterials* (2009) 30(28):5104–13. doi: 10.1016/j.biomaterials.2009.05.062
185. Zhang F, Shi QH, Zhang YC, Shi YF, Ding KL, Zhao DY, et al. Fluorescence Upconversion Microbarcodes for Multiplexed Biological Detection: Nucleic Acid Encoding. *Advanced Mater* (2011) 23(33):3775–+. doi: 10.1002/adma.201101868
186. Liu YQ, Qin LY, Li HJ, Wang YX, Zhang R, Shi JM, et al. Application of Lanthanide-Doped Upconversion Nanoparticles for Cancer Treatment: A Review. *Nanomedicine* (2021) 16(24):2207–42. doi: 10.2217/nnm-2021-0214
187. Griffith WP. Cyanide Complexes of the Transition Metals. *Q Rev Chem Soc* (1962) 16(2):188–207. doi: 10.1039/QR9621600188
188. Adak S, Daemen LL, Hartl M, Williams D, Summerhill J, Nakotte H. Thermal Expansion in 3d-Metal Prussian Blue Analogs-A Survey Study. *J Solid State Chem* (2011) 184(11):2854–61. doi: 10.1016/j.jssc.2011.08.030
189. Long J, Guari Y, Guerin C, Larionova J. Prussian Blue Type Nanoparticles for Biomedical Applications. *Dalton Trans* (2016) 45(44):17581–7. doi: 10.1039/c6dt01299j
190. Wang D, Zhou J, Chen R, Shi R, Zhao G, Xia G, et al. Controllable Synthesis of Dual-MOFs Nanostructures for pH-Responsive Artemisinin Delivery, Magnetic Resonance and Optical Dual-Model Imaging-Guided Chemo/Photothermal Combinational Cancer Therapy. *Biomaterials* (2016) 100:27–40. doi: 10.1016/j.biomaterials.2016.05.027
191. Xiao F, Fan JL, Tond CY, Xiao C, Wang Z, Liu B, et al. An Erythrocyte Membrane Coated Mimetic Nano-Platform for Chemo-Phototherapy and Multimodal Imaging. *Rsc Adv* (2019) 9(48):27911–26. doi: 10.1039/c9ra05867b
192. Gautam M, Poudel K, Yong CS, Kim JO. Prussian Blue Nanoparticles: Synthesis, Surface Modification, and Application in Cancer Treatment. *Int J Pharmaceutics* (2018) 549(1-2):31–49. doi: 10.1016/j.ijpharm.2018.07.055
193. Busquets MA, Novella-Xicoy A, Guzman V, Estelrich J. Facile Synthesis of Novel Prussian Blue-Lipid Nanocomplexes. *Molecules* (2019) 24(22):4137. doi: 10.3390/molecules24224137
194. Cheng L, Wang C, Feng LZ, Yang K, Liu Z. Functional Nanomaterials for Phototherapies of Cancer. *Chem Rev* (2014) 114(21):10869–939. doi: 10.1021/cr400532z
195. Kowada T, Maeda H, Kikuchi K. BODIPY-Based Probes for the Fluorescence Imaging of Biomolecules in Living Cells. *Chem Soc Rev* (2015) 44(14):4953–72. doi: 10.1039/c5cs00030k
196. Guha S, Shaw SK, Spence GT, Roland FM, Smith BD. Clean Photothermal Heating and Controlled Release From Near-Infrared Dye Doped Nanoparticles Without Oxygen Photosensitization. *Langmuir* (2015) 31 (28):7826–34. doi: 10.1021/acs.langmuir.5b01878
197. Song XJ, Chen Q, Liu Z. Recent Advances in the Development of Organic Photothermal Nano-Agents. *Nano Res* (2015) 8(2):340–54. doi: 10.1007/s12274-014-0620-y
198. Rajora MA, Lou JWH, Zheng G. Advancing Porphyrin's Biomedical Utility *via* Supramolecular Chemistry. *Chem Soc Rev* (2017) 46(21):6433–69. doi: 10.1039/c7cs00525c
199. Bhattarai P, Dai Z. Cyanine Based Nanoprobes for Cancer Theranostics. *Adv Healthc Mater* (2017) 6(14):1700262. doi: 10.1002/adhm.201700262
200. Sun W, Guo S, Hu C, Fan J, Peng X. Recent Development of Chemosensors Based on Cyanine Platforms. *Chem Rev* (2016) 116(14):7768–817. doi: 10.1021/acs.chemrev.6b00001
201. Luo S, Zhang E, Su Y, Cheng T, Shi C. A Review of NIR Dyes in Cancer Targeting and Imaging. *Biomaterials* (2011) 32(29):7127–38. doi: 10.1016/j.biomaterials.2011.06.024
202. Lan M, Zhao S, Liu W, Lee CS, Zhang W, Wang P. Photosensitizers for Photodynamic Therapy. *Adv Healthc Mater* (2019) 8(13):e1900132. doi: 10.1002/adhm.201900132
203. Zhou Y, Liang X, Dai Z. Porphyrin-Loaded Nanoparticles for Cancer Theranostics. *Nanoscale* (2016) 8(25):12394–405. doi: 10.1039/c5nr07849k
204. Lu K, He C, Lin W. Nanoscale Metal-Organic Framework for Highly Effective Photodynamic Therapy of Resistant Head and Neck Cancer. *J Am Chem Soc* (2014) 136(48):16712–5. doi: 10.1021/ja508679h
205. Liu K, Xing R, Zou Q, Ma G, Möhwald H, Yan X. Simple Peptide-Tuned Self-Assembly of Photosensitizers Towards Anticancer Photodynamic Therapy. *Angew Chem Int Ed Engl* (2016) 55(9):3036–9. doi: 10.1002/anie.201509810
206. Lu K, He C, Lin W. A Chlorin-Based Nanoscale Metal-Organic Framework for Photodynamic Therapy of Colon Cancers. *J Am Chem Soc* (2015) 137 (24):7600–3. doi: 10.1021/jacs.5b04069

207. Lim CK, Shin J, Lee YD, Kim J, Oh KS, Yuk SH, et al. Phthalocyanine-Aggregated Polymeric Nanoparticles as Tumor-Homing Near-Infrared Absorbers for Photothermal Therapy of Cancer. *Theranostics* (2012) 2 (9):871–9. doi: 10.7150/thno.4133
208. Zhao YY, Zhang L, Chen Z, Zheng BY, Ke M, Li X, et al. Nanostructured Phthalocyanine Assemblies With Efficient Synergistic Effect of Type I Photoreaction and Photothermal Action to Overcome Tumor Hypoxia in Photodynamic Therapy. *J Am Chem Soc* (2021) 143(34):13980–9. doi: 10.1021/jacs.1c07479
209. Mei L, Shi Y, Cao F, Liu X, Li XM, Xu Z, et al. PEGylated Phthalocyanine-Functionalized Graphene Oxide With Ultrahigh-Efficient Photothermal Performance for Triple-Mode Antibacterial Therapy. *ACS Biomater Sci Eng* (2021) 7(6):2638–48. doi: 10.1021/acsbiomaterials.1c00178
210. Turan IS, Yildiz D, Turksoy A, Gunaydin G, Akkaya EU. A Bifunctional Photosensitizer for Enhanced Fractional Photodynamic Therapy: Singlet Oxygen Generation in the Presence and Absence of Light. *Angew Chem Int Ed Engl* (2016) 55(8):2875–8. doi: 10.1002/anie.201511345
211. Kolemen S, Akkaya EU. Reaction-Based BODIPY Probes for Selective Bio-Imaging. *Coordination Chem Rev* (2018) 354:121–34. doi: 10.1016/j.ccr.2017.06.021
212. He L, Huang Y, Chang Y, You Y, Hu H, Leong KW, et al. A Highly Selective Dual-Therapeutic Nanosystem for Simultaneous Anticancer and Antiangiogenesis Therapy. *J Mater Chem B* (2017) 5(41):8228–37. doi: 10.1039/c7tb02163a
213. Chen HM, Zhang WZ, Zhu GZ, Xie J, Chen XY. Rethinking Cancer Nanotheranostics. *Nat Rev Mater* (2017) 2(7):17024. doi: 10.1038/natrevmats.2017.24
214. Shen G, Xing R, Zhang N, Chen C, Ma G, Yan X. Interfacial Cohesion and Assembly of Bioadhesive Molecules for Design of Long-Term Stable Hydrophobic Nanodrugs Toward Effective Anticancer Therapy. *ACS Nano* (2016) 10(6):5720–9. doi: 10.1021/acsnano.5b07276
215. Xu Y, Feng T, Yang T, Wei H, Yang H, Li G, et al. Utilizing Intramolecular Photoinduced Electron Transfer to Enhance Photothermal Tumor Treatment of Aza-BODIPY-Based Near-Infrared Nanoparticles. *ACS Appl Mater Interfaces* (2018) 10(19):16299–307. doi: 10.1021/acsami.8b03568
216. Sun W, Zhao X, Fan J, Du J, Peng X. Boron Dipyrromethene Nano-Photosensitizers for Anticancer Phototherapies. *Small* (2019) 15(32): e1804927. doi: 10.1002/smll.201804927
217. Ma C, Zhang T, Xie Z. Leveraging BODIPY Nanomaterials for Enhanced Tumor Photothermal Therapy. *J Mater Chem B* (2021) 9(36):7318–27. doi: 10.1039/d1tb00855b
218. Yang Z, Xu W, Wang J, Liu L, Chu Y, Wang Y, et al. Diketopyrrolopyrrole-Based Multifunctional Ratiometric Fluorescent Probe Andγ-Glutamyltranspeptidase-Triggered Activatable Photosensitizer for Tumor Therapy. *J Mater Chem C.* (2020) 8(24):8183–90. doi: 10.1039/d0tc01836h
219. Tang A, Zhan C, Yao J, Zhou E. Design of Diketopyrrolopyrrole (DPP)-Based Small Molecules for Organic-Solar-Cell Applications. *Adv Mater* (2017) 29(2):1600013. doi: 10.1002/adma.201600013
220. Cai Y, Liang P, Tang Q, Si W, Chen P, Zhang Q, et al. Diketopyrrolopyrrole-Based Photosensitizers Conjugated With Chemotherapeutic Agents for Multimodal Tumor Therapy. *ACS Appl Mater Interfaces* (2017) 9 (36):30398–405. doi: 10.1021/acsami.7b09025
221. Deng W, Wu Q, Sun P, Yuan P, Lu X, Fan Q, et al. Zwitterionic Diketopyrrolopyrrole for Fluorescence/Photoacoustic Imaging Guided Photodynamic/Photothermal Therapy. *Polym Chem* (2018) 9(20):2805–12. doi: 10.1039/c8py00244d
222. Qian CG, Chen YL, Feng PJ, Xiao XZ, Dong M, Yu JC, et al. Conjugated Polymer Nanomaterials for Theranostics. *Acta Pharmacol Sin* (2017) 38 (6):764–81. doi: 10.1038/aps.2017.42
223. Zhen X, Pu K, Jiang X. Photoacoustic Imaging and Photothermal Therapy of Semiconducting Polymer Nanoparticles: Signal Amplification and Second Near-Infrared Construction. *Small* (2021) 17(6):e2004723. doi: 10.1002/smll.202004723
224. Feng G, Zhang GQ, Ding D. Design of Superior Phototheranostic Agents Guided by Jablonski Diagrams. *Chem Soc Rev* (2020) 49(22):8179–234. doi: 10.1039/d0cs00671h
225. Xiao Z, Peng C, Jiang X, Peng Y, Huang X, Guan G, et al. Polypyrrole-Encapsulated Iron Tungstate Nanocomposites: A Versatile Platform for Multimodal Tumor Imaging and Photothermal Therapy. *Nanoscale* (2016) 8(26):12917–28. doi: 10.1039/c6nr03336a
226. Lu TY, Chiang CY, Fan YJ, Jheng PR, Quiñones ED, Liu KT, et al. Dual-Targeting Glycol Chitosan/Heparin-Decorated Polypyrrole Nanoparticle for Augmented Photothermal Thrombolytic Therapy. *ACS Appl Mater Interfaces* (2021) 13(8):10287–300. doi: 10.1021/acsami.0c20940
227. Zhou Y, Hu Y, Sun W, Zhou B, Zhu J, Peng C, et al. Polyaniline-Loaded γ-Polyglutamic Acid Nanogels as a Platform for Photoacoustic Imaging-Guided Tumor Photothermal Therapy. *Nanoscale* (2017) 9(34):12746–54. doi: 10.1039/c7nr04241h
228. Wang W, Wang L, Li Y, Liu S, Xie Z, Jing X. Nanoscale Polymer Metal-Organic Framework Hybrids for Effective Photothermal Therapy of Colon Cancers. *Adv Mater* (2016) 28(42):9320–5. doi: 10.1002/adma.201602997
229. Zhou J, Lu Z, Zhu X, Wang X, Liao Y, Ma Z, et al. NIR Photothermal Therapy Using Polyaniline Nanoparticles. *Biomaterials* (2013) 34(37):9584–92. doi: 10.1016/j.biomaterials.2013.08.075
230. Men X, Wang F, Chen HB, Liu YB, Men XX, Yuan Y, et al. Ultrasmall Semiconducting Polymer Dots with Rapid Clearance for Second Near-Infrared Photoacoustic Imaging and Photothermal Cancer Therapy. *Advanced Funct Mater* (2020) 30(24):Article 1909673. doi: 10.1002/adfm.201909673
231. Wei Z, Xue F, Xin F, Wu M, Wang B, Zhang X, et al. A Thieno-Isoindigo Derivative-Based Conjugated Polymer Nanoparticle for Photothermal Therapy in the NIR-II Bio-Window. *Nanoscale* (2020) 12(38):19665–72. doi: 10.1039/d0nr03771k
232. Khodagholy D, Doublet T, Gurfinkel MG, Quilichini P, Ismailova E, Leleux P, et al. Highly Conformable Conducting Polymer Electrodes for in Vivo Recordings. *Adv Mater* (2011) 23(36):H268–72. doi: 10.1002/adma.201102378
233. Vosgueritchian M, Lipomi DJ, Bao Z. Highly Conductive and Transparent PEDOT:PSS Films With a Fluorosurfactant for Stretchable and Flexible Transparent Electrodes. *Adv Funct Mater* (2011) 22(2):421–8. doi: 10.1002/adfm.201101775
234. Yun JM, Yeo JS, Kim J, Jeong HG, Kim DY, Noh YJ, et al. Solution-Processable Reduced Graphene Oxide as a Novel Alternative to PEDOT:PSS Hole Transport Layers for Highly Efficient and Stable Polymer Solar Cells. *Adv Mater* (2011) 23(42):4923–8. doi: 10.1002/adma.201102207
235. Jeong CJ, Sharker SM, In I, Park SY. Iron Oxide@PEDOT-Based Recyclable Photothermal Nanoparticles With Poly(Vinylpyrrolidone) Sulfobetaines for Rapid and Effective Antibacterial Activity. *ACS Appl Mater Interfaces* (2015) 7(18):9469–78. doi: 10.1021/acsami.5b02737
236. Khan S, Narula AK. Bio-Hybrid Blended Transparent and Conductive Films PEDOT: PSS:Chitosan Exhibiting Electro-Active and Antibacterial Properties. *Eur Polymer J* (2016) 81:161–72. doi: 10.1016/j.eurpolymj.2016.06.005
237. Ko Y, Kim D, Kim UJ, You J. Vacuum-Assisted Bilayer PEDOT:PSS/cellulose Nanofiber Compositefilm for Self-Standing,Flexible, Conductive Electrodes. *Carbohydr Polymers* (2017) 173:383–91. doi: 10.1016/j.carbpol.2017.05.096
238. Hong ZY, Feng HY, Bu LH. Melanin-Based Nanomaterials: The Promising Nanoplatforms for Cancer Diagnosis and Therapy. *Nanomedicine* (2020) 28:102211. doi: 10.1016/j.nano.2020.102211
239. Liu Y, Ai K, Liu J, Deng M, He Y, Lu L. Dopamine-Melanin Colloidal Nanospheres: An Efficient Near-Infrared Photothermal Therapeutic Agent for *In Vivo* Cancer Therapy. *Adv Mater* (2013) 25(9):1353–9. doi: 10.1002/adma.201204683
240. Liu Y, Ai K, Lu L. Polydopamine and its Derivative Materials: Synthesis and Promising Applications in Energy, Environmental, and Biomedical Fields. *Chem Rev* (2014) 114(9):5057–115. doi: 10.1021/cr400407a
241. Liu H, Yang Y, Liu Y, Pan J, Wang J, Man F, et al. Melanin-Like Nanomaterials for Advanced Biomedical Applications: A Versatile Platform With Extraordinary Promise. *Adv Sci* (2020) 7(7):1903129. doi: 10.1002/advs.201903129
242. Yue Y, Zhao X. Melanin-Like Nanomedicine in Photothermal Therapy Applications. *Int J Mol Sci* (2021) 22(1):399. doi: 10.3390/ijms22010399
243. Xiong J, Bian Q, Lei S, Deng Y, Zhao K, Sun S, et al. Bi19S27I3 Nanorods: A New Candidate for Photothermal Therapy in the First and Second Biological

Near-Infrared Windows. *Nanoscale* (2021) 13(10):5369–82. doi: 10.1039/d0nr09137e
244. Zhou B, Li Y, Niu G, Lan M, Jia Q, Liang Q. Near-Infrared Organic Dye-Based Nanoagent for the Photothermal Therapy of Cancer. *ACS Appl Mater Interfaces* (2016) 8(44):29899–905. doi: 10.1021/acsami.6b07838
245. Yu CC, Xu LJ, Zhang YY, Timashev PS, Huang YY, Liang XJ. Polymer-Based Nanomaterials for Noninvasive Cancer Photothermal Therapy. *ACS Appl Polym Mater* (2020) 2(10):4289–305. doi: 10.1021/acsapm.0c00704
246. Hao MQ, Chen BB, Zhao XY, Zhao NN, Xu FJ. Organic/inorganic Nanocomposites for Cancer Immunotherapy. *Mater Chem Front* (2020) 4 (9):2571–609. doi: 10.1039/d0qm00323a
247. Yu H, Chen M, Rice PM, Wang SX, White RL, Sun S. Dumbbell-Like Bifunctional Au–Fe3O4 Nanoparticles. *Nano Lett* (2005) 5(2):379–82. doi: 10.1021/nl047955q
248. Mezni A, Balti I, Mlayah A, Jouini N, Smiri LS. Hybrid Au-Fe3O4 Nanoparticles: Plasmonic, Surface Enhanced Raman Scattering, and Phase Transition Properties. *J Phys Chem C.* (2013) 117(31):16166–74. doi: 10.1021/jp4040826
249. Seaberg J, Montazerian H, Hossen MN, Bhattacharya R, Khademhosseini A, Mukherjee P. Hybrid Nanosystems for Biomedical Applications. *ACS Nano* (2021) 15(2):2099–142. doi: 10.1021/acsnano.0c09382
250. Park W, Shin H, Choi B, Rhim WK, Na K, Han DK. Advanced Hybrid Nanomaterials for Biomedical Applications. *Prog Mater Sci* (2020) 114:100686. doi: 10.1016/j.pmatsci.2020.100686
251. Ulbrich K, Hola K, Subr V, Bakandritsos A, Tucek J, Zboril R. Targeted Drug Delivery With Polymers and Magnetic Nanoparticles: Covalent and Noncovalent Approaches, Release Control, and Clinical Studies. *Chem Rev* (2016) 116(9):5338–431. doi: 10.1021/acs.chemrev.5b00589
252. Hogle WP. The State of the Art in Radiation Therapy. *Semin Oncol Nurs* (2006) 22(4):212–20. doi: 10.1016/j.soncn.2006.07.004
253. Zhang K, Chen HR, Li FQ, Wang Q, Zheng SG, Xu HX, et al. A Continuous Tri-Phase Transition Effect for HIFU-Mediated Intravenous Drug Delivery. *Biomaterials* (2014) 35(22):5875–85. doi: 10.1016/j.biomaterials.2014.03.043
254. Gao H, Liu R, Gao FP, Wang YL, Jiang XL, Gao XY. Plasmon-Mediated Generation of Reactive Oxygen Species From Near-Infrared Light Excited Gold Nanocages for Photodynamic Therapy in Vitro. *ACS Nano* (2014) 8 (7):7260–71. doi: 10.1021/nn502325j
255. Wang C, Sun WJ, Wright G, Wang AZ, Gu Z. Inflammation-Triggered Cancer Immunotherapy by Programmed Delivery of CpG and Anti-PD1 Antibody. *Advanced Mater* (2016) 28(40):8912–20. doi: 10.1002/adma.201506312
256. Jayakumar MKG, Bansal A, Huang K, Yao R, Li BN, Zhang Y. Near-Infrared-Light-Based Nano-Platform Boosts Endosomal Escape and Controls Gene Knockdown in Vivo. *ACS Nano* (2014) 8(5):4848–58. doi: 10.1021/nn500777n
257. Canfarotta F, Piletsky SA. Engineered Magnetic Nanoparticles for Biomedical Applications. *Adv Healthcare Mater* (2014) 3(2):160–75. doi: 10.1002/adhm.201300141
258. Xue X, Fang T, Yin L, Jiang J, He Y, Dai Y, et al. Multistage Delivery of CDs-DOX/ICG-Loaded Liposome for Highly Penetration and Effective Chemo-Photothermal Combination Therapy. *Drug Deliv* (2018) 25(1):1826–39. doi: 10.1080/10717544.2018.1482975
259. Deng G, Zhu T, Zhou L, Zhang J, Li S, Sun Z, et al. Bovine Serum Albumin-Loaded Nano-Selenium/ICG Nanoparticles for Highly Effective Chemo-Photothermal Combination Therapy. *RSC Adv* (2017) 7(49):30717–24. doi: 10.1039/c7ra02384g
260. Valastyan S, Weinberg RA. Tumor Metastasis: Molecular Insights and Evolving Paradigms. *Cell* (2011) 147(2):275–92. doi: 10.1016/j.cell.2011.09.024
261. Dean M, Fojo T, Bates S. Tumour Stem Cells and Drug Resistance. *Nat Rev Cancer* (2005) 5(4):275–84. doi: 10.1038/nrc1590
262. Brown JM. Exploiting the Hypoxic Cancer Cell: Mechanisms and Therapeutic Strategies. *Mol Med Today* (2000) 6(4):157–62. doi: 10.1016/S1357-4310(00)01677-4
263. Xu C, Pu K. Second Near-Infrared Photothermal Materials for Combinational Nanotheranostics. *Chem Soc Rev* (2021) 50(2):1111–37. doi: 10.1039/d0cs00664e
264. Dong Q, Wang XW, Hu XX, Xiao LQ, Zhang L, Song LJ, et al. Simultaneous Application of Photothermal Therapy and an Anti-Inflammatory Prodrug Using Pyrene-Aspirin-Loaded Gold Nanorod Graphitic Nanocapsules. *Angewandte Chemie-International Edition* (2018) 57(1):177–81. doi: 10.1002/anie.201709648
265. Aggarwal BB, Vijayalekshmi RV, Sung B. Targeting Inflammatory Pathways for Prevention and Therapy of Cancer: Short-Term Friend, Long-Term Foe. *Clin Cancer Res* (2009) 15(2):425–30. doi: 10.1158/1078-0432.Ccr-08-0149
266. Piccolo MT, Menale C, Crispi S. Combined Anticancer Therapies: An Overview of the Latest Applications. *Anti-Cancer Agents Medicinal Chem* (2015) 15(4):408–22. doi: 10.2174/1871520615666150113123039
267. Grau C, Prakash Agarwal J, Jabeen K, Rab Khan A, Abeyakoon S, Hadjieva T, et al. Radiotherapy With or Without Mitomycin C in the Treatment of Locally Advanced Head and Neck Cancer: Results of the IAEA Multicentre Randomised Trial. *Radiother Oncol* (2003) 67(1):17–26. doi: 10.1016/S0167-8140(03)00020-3
268. Smith BR, Gambhir SS. Nanomaterials for *In Vivo* Imaging. *Chem Rev* (2017) 117(3):901–86. doi: 10.1021/acs.chemrev.6b00073
269. Brodin NP, Guha C, Tome WA. Photodynamic Therapy and Its Role in Combined Modality Anticancer Treatment. *Technol Cancer Res Treat* (2015) 14(4):355–68. doi: 10.1177/1533034614556192
270. Tian G, Zhang X, Gu ZJ, Zhao YL. Recent Advances in Upconversion Nanoparticles-Based Multifunctional Nanocomposites for Combined Cancer Therapy. *Advanced Mater* (2015) 27(47):7692–712. doi: 10.1002/adma.201503280
271. Sweeney EE, Cano-Mejia J, Fernandes R. Photothermal Therapy Generates a Thermal Window of Immunogenic Cell Death in Neuroblastoma. *Small* (2018) 14(20):e1800678. doi: 10.1002/smll.201800678
272. Zhang YX, Hou ZY, Ge YK, Deng KR, Liu B, Li XJ, et al. DNA-Hybrid-Gated Photothermal Mesoporous Silica Nanoparticles for MR-Responsive and Aptamer-Targeted Drug Delivery. *ACS Appl Mater Interfaces* (2015) 7 (37):20696–706. doi: 10.1021/acsami.5b05522
273. Huang CC, Liu TM. Controlled Au-Polymer Nanostructures for Multiphoton Imaging, Prodrug Delivery, and Chemo-Photothermal Therapy Platforms. *ACS Appl Mater Interfaces* (2015) 7(45):25259–69. doi: 10.1021/acsami.5b07110
274. Wang XW, Gu YX, Li Q, Xu YP, Shi YF, Wang ZR, et al. Synergistic Chemo-Photothermal Cancer Therapy of pH-Responsive Polymeric Nanoparticles Loaded IR825 and DTX With Charge-Reversal Property. *Colloids Surfaces B-Biointerfaces* (2022) 209(Pt 2):112164. doi: 10.1016/j.colsurfb.2021.112164
275. Zhou FF, Wu S, Song S, Chen WR, Resasco DE, Xing D. Antitumor Immunologically Modified Carbon Nanotubes for Photothermal Therapy. *Biomaterials* (2012) 33(11):3235–42. doi: 10.1016/j.biomaterials.2011.12.029
276. Galluzzi L, Buqué A, Kepp O, Zitvogel L, Kroemer G. Immunogenic Cell Death in Cancer and Infectious Disease. *Nat Rev Immunol* (2017) 17(2):97–111. doi: 10.1038/nri.2016.107
277. Li J, Luo Y, Pu K. Electromagnetic Nanomedicines for Combinational Cancer Immunotherapy. *Angew Chem Int Ed Engl* (2020) 60(23):12682–705. doi: 10.1002/anie.202008386
278. Wang M, Li Y, Wang M, Liu KL, Hoover AR, Li M, et al. Synergistic Interventional Photothermal Therapy and Immunotherapy Using an Iron Oxide Nanoplatform for the Treatment of Pancreatic Cancer. *Acta Biomaterialia* (2022) 138:453–62. doi: 10.1016/j.actbio.2021.10.048
279. Kim J, Kim J, Jeong C, Kim WJ. Synergistic Nanomedicine by Combined Gene and Photothermal Therapy. *Advanced Drug Delivery Rev* (2016) 98:99–112. doi: 10.1016/j.addr.2015.12.018
280. Jung BK, Lee YK, Hong J, Ghandehari H, Yun CO. Mild Hyperthermia Induced by Gold Nanorod-Mediated Plasmonic Photothermal Therapy Enhances Transduction and Replication of Oncolytic Adenoviral Gene Delivery. *ACS Nano* (2016) 10(11):10533–43. doi: 10.1021/acsnano.6b06530
281. Xu M, Zhao D, Chen Y, Chen C, Zhang L, Sun L, et al. Charge Reversal Polypyrrole Nanocomplex-Mediated Gene Delivery and Photothermal Therapy for Effectively Treating Papillary Thyroid Cancer and Inhibiting Lymphatic Metastasis. *ACS Appl Mater Interfaces* (2022) 14(12):14072–86. doi: 10.1021/acsami.1c25179

282. Yao J, Zheng F, Yao C, Xu X, Akakuru OU, Chen T, et al. Rational Design of Nanomedicine for Photothermal-Chemodynamic Bimodal Cancer Therapy. *Wiley Interdiscip Rev Nanomed Nanobiotechnol* (2021) 13(3):e1682. doi: 10.1002/wnan.1682
283. Zhang C, Bu W, Ni D, Zhang S, Li Q, Yao Z, et al. Synthesis of Iron Nanometallic Glasses and Their Application in Cancer Therapy by a Localized Fenton Reaction. *Angew Chem Int Ed Engl* (2016) 55(6):2101–6. doi: 10.1002/anie.201510031
284. Sun SP, Li CJ, Sun JH, Shi SH, Fan MH, Zhou Q. Decolorization of an Azo Dye Orange G in Aqueous Solution by Fenton Oxidation Process: Effect of System Parameters and Kinetic Study. *J Hazard Mater* (2009) 161(2-3):1052–7. doi: 10.1016/j.jhazmat.2008.04.080
285. Yang Y, Zhu W, Dong Z, Chao Y, Xu L, Chen M, et al. 1d Coordination Polymer Nanofibers for Low-Temperature Photothermal Therapy. *Adv Mater* (2017) 29(40):1703588. doi: 10.1002/adma.201703588
286. Wu H, Liu L, Song L, Ma M, Gu N, Zhang Y. Enhanced Tumor Synergistic Therapy by Injectable Magnetic Hydrogel Mediated Generation of Hyperthermia and Highly Toxic Reactive Oxygen Species. *ACS Nano* (2019) 13(12):14013–23. doi: 10.1021/acsnano.9b06134
287. Huang H, Wang X, Wang W, Qu X, Song X, Zhang Y, et al. Injectable Hydrogel for Postoperative Synergistic Photothermal-Chemodynamic Tumor and Anti-Infection Therapy. *Biomaterials* (2022) 280:121289. doi: 10.1016/j.biomaterials.2021.121289
288. Castano AP, Demidova TN, Hamblin MR. Mechanisms in Photodynamic Therapy: Part Three-Photosensitizer Pharmacokinetics, Biodistribution, Tumor Localization and Modes of Tumor Destruction. *Photodiagnosis Photodyn Ther* (2005) 2(2):91–106. doi: 10.1016/S1572-1000(05)00060-8
289. Bhana S, Lin G, Wang L, Starring H, Mishra SR, Liu G, et al. Near-Infrared-Absorbing Gold Nanopopcorns With Iron Oxide Cluster Core for Magnetically Amplified Photothermal and Photodynamic Cancer Therapy. *ACS Appl Mater Interfaces* (2015) 7(21):11637–47. doi: 10.1021/acsami.5b02741
290. Melancon MP, Elliott AM, Shetty A, Huang Q, Stafford RJ, Li C. Near-Infrared Light Modulated Photothermal Effect Increases Vascular Perfusion and Enhances Polymeric Drug Delivery. *J Control Release* (2011) 156(2):265–72. doi: 10.1016/j.jconrel.2011.06.030
291. Sun X, Xu Y, Guo Q, Wang N, Wu B, Zhu C, et al. A Novel Nanoprobe for Targeted Imaging and Photothermal/Photodynamic Therapy of Lung Cancer. *Langmuir* (2022) 38(4):1360–7. doi: 10.1021/acs.langmuir.1c02434
292. Tachibana K, Feril L, Ikeda-Dantsuji Y. Sonodynamic Therapy. *Ultrasonics* (2008) 48(4):253–9. doi: 10.1016/j.ultras.2008.02.003
293. Son S, Kim JH, Wang X, Zhang C, Yoon SA, Shin J, et al. Multifunctional Sonosensitizers in Sonodynamic Cancer Therapy. *Chem Soc Rev* (2020) 49(11):3244–61. doi: 10.1039/c9cs00648f
294. Qian X, Zheng Y, Chen Y. Micro/Nanoparticle-Augmented Sonodynamic Therapy (SDT): Breaking the Depth Shallow of Photoactivation. *Adv Mater* (2016) 28(37):8097–129. doi: 10.1002/adma.201602012
295. Soratijahromi E, Mohammadi S, Dehdari Vais R, Azarpira N, Sattarahmady N. Photothermal/sonodynamic Therapy of Melanoma Tumor by a Gold/Manganese Dioxide Nanocomposite: In Vitro and *In Vivo* Studies. *Photodiagnosis Photodyn Ther* (2020) 31:101846. doi: 10.1016/j.pdpdt.2020.101846
296. Vijayaraghavan P, Liu CH, Vankayala R, Chiang CS, Hwang KC. Designing Multi-Branched Gold Nanoechinus for NIR Light Activated Dual Modal Photodynamic and Photothermal Therapy in the Second Biological Window. *Adv Mater* (2014) 26(39):6689–95. doi: 10.1002/adma.201400703
297. Zhao R, Han X, Li Y, Wang H, Ji T, Zhao Y, et al. Photothermal Effect Enhanced Cascade-Targeting Strategy for Improved Pancreatic Cancer Therapy by Gold Nanoshell@Mesoporous Silica Nanorod. *ACS Nano* (2017) 11(8):8103–13. doi: 10.1021/acsnano.7b02918
298. Baskar R, Lee KA, Yeo R, Yeoh KW. Cancer and Radiation Therapy: Current Advances and Future Directions. *Int J Med Sci* (2012) 9(3):193–9. doi: 10.7150/ijms.3635
299. Cheng L, Yuan C, Shen SD, Yi X, Gong H, Yang K, et al. Bottom-Up Synthesis of Metal-Ion-Doped WS2 Nanoflakes for Cancer Theranostics. *ACS Nano* (2015) 9(11):11090–101. doi: 10.1021/acsnano.5b04606
300. Chao Y, Wang GL, Liang C, Yi X, Zhong XY, Liu JJ, et al. Rhenium-188 Labeled Tungsten Disulfide Nanoflakes for Self-Sensitized, Near-Infrared Enhanced Radioisotope Therapy. *Small* (2016) 12(29):3967–75. doi: 10.1002/smll.201601375
301. Mao FX, Wen L, Sun CX, Zhang SH, Wang GL, Zeng JF, et al. Ultrasmall Biocompatible Bi2Se3 Nanodots for Multimodal Imaging-Guided Synergistic Radiophotothermal Therapy Against Cancer. *ACS Nano* (2016) 10(12):11145–55. doi: 10.1021/acsnano.6b06067
302. Li Q, Hang LF, Jiang W, Dou JX, Xiao L, Tang XF, et al. Pre- and Post-Irradiation Mild Hyperthermia Enabled by NIR-II for Sensitizing Radiotherapy. *Biomaterials* (2020) 257:120235. doi: 10.1016/j.biomaterials.2020.120235
303. Ni J, Xu H, Zhong Y, Zhou Y, Hu S. Activatable UCL/CT/MR-Enhanced *In Vivo* Imaging-Guided Radiotherapy and Photothermal Therapy. *J Mater Chem B* (2022) 10(4):549–61. doi: 10.1039/D1TB02006D
304. Yang F, Skripka A, Tabatabaei MS, Hong SH, Ren F, Benayas A, et al. Multifunctional Self-Assembled Supernanoparticles for Deep-Tissue Bimodal Imaging and Amplified Dual-Mode Heating Treatment. *ACS Nano* (2019) 13(1):408–20. doi: 10.1021/acsnano.8b06563
305. Lu Q, Lu T, Xu M, Yang L, Song Y, Li N. SO(2) Prodrug Doped Nanorattles With Extra-High Drug Payload for "Collusion Inside and Outside" Photothermal/pH Triggered - Gas Therapy. *Biomaterials* (2020) 257:120236. doi: 10.1016/j.biomaterials.2020.120236
306. Fan W, Shen B, Bu W, Chen F, Zhao K, Zhang S, et al. Rattle-Structured Multifunctional Nanotheranostics for Synergetic Chemo-/Radiotherapy and Simultaneous Magnetic/Luminescent Dual-Mode Imaging. *J Am Chem Soc* (2013) 135(17):6494–503. doi: 10.1021/ja312225b
307. Wang X, Chen H, Zhang K, Ma M, Li F, Zeng D, et al. An Intelligent Nanotheranostic Agent for Targeting, Redox-Responsive Ultrasound Imaging, and Imaging-Guided High-Intensity Focused Ultrasound Synergistic Therapy. *Small* (2014) 10(7):1403–11. doi: 10.1002/smll.201302846
308. Xie J, Lee S, Chen X. Nanoparticle-Based Theranostic Agents. *Adv Drug Delivery Rev* (2010) 62(11):1064–79. doi: 10.1016/j.addr.2010.07.009
309. Gong H, Cheng L, Xiang J, Xu H, Feng LZ, Shi XZ, et al. Near-Infrared Absorbing Polymeric Nanoparticles as a Versatile Drug Carrier for Cancer Combination Therapy. *Advanced Funct Mater* (2013) 23(48):6059–67. doi: 10.1002/adfm.201301555
310. Chen W, Ouyang J, Liu H, Chen M, Zeng K, Sheng J, et al. Black Phosphorus Nanosheet-Based Drug Delivery System for Synergistic Photodynamic/Photothermal/Chemotherapy of Cancer. *Adv Mater* (2017) 29(5):1603864. doi: 10.1002/adma.201603864
311. Tang ZM, Zhao PR, Ni DL, Liu YY, Zhang M, Wang H, et al. Pyroelectric Nanoplatform for NIR-II-Triggered Photothermal Therapy With Simultaneous Pyroelectric Dynamic Therapy. *Mater Horizons* (2018) 5(5):946–52. doi: 10.1039/c8mh00627j
312. Hu P, Wu T, Fan W, Chen L, Liu Y, Ni D, et al. Near Infrared-Assisted Fenton Reaction for Tumor-Specific and Mitochondrial DNA-Targeted Photochemotherapy. *Biomaterials* (2017) 141:86–95. doi: 10.1016/j.biomaterials.2017.06.035
313. He C, Liu D, Lin W. Self-Assembled Core-Shell Nanoparticles for Combined Chemotherapy and Photodynamic Therapy of Resistant Head and Neck Cancers. *ACS Nano* (2015) 9(1):991–1003. doi: 10.1038/s41565-019-0373-6
314. Wang S, Yang L, Cho HY, Dean Chueng ST, Zhang H, Zhang Q, et al. Programmed Degradation of a Hierarchical Nanoparticle With Redox and Light Responsivity for Self-Activated Photo-Chemical Enhanced Chemodynamic Therapy. *Biomaterials* (2019) 224:119498. doi: 10.1016/j.biomaterials.2019.119498
315. Zhuang X, Ma X, Xue X, Jiang Q, Song L, Dai L, et al. A Photosensitizer-Loaded DNA Origami Nanosystem for Photodynamic Therapy. *ACS Nano* (2016) 10(3):3486–95. doi: 10.1021/acsnano.5b07671
316. Shen Z, Song J, Yung BC, Zhou Z, Wu A, Chen X. Emerging Strategies of Cancer Therapy Based on Ferroptosis. *Adv Mater* (2018) 30(12):e1704007. doi: 10.1002/adma.201704007
317. Liu Y, Zhen W, Jin L, Zhang S, Sun G, Zhang T, et al. All-In-One Theranostic Nanoagent With Enhanced Reactive Oxygen Species Generation and Modulating Tumor Microenvironment Ability for Effective Tumor Eradication. *ACS Nano* (2018) 12(5):4886–93. doi: 10.1021/acsnano.8b01893
318. Du X, Zhao C, Zhou M, Ma T, Huang H, Jaroniec M, et al. Hollow Carbon Nanospheres With Tunable Hierarchical Pores for Drug, Gene, and

Photothermal Synergistic Treatment. *Small* (2017) 13(6):1602592. doi: 10.1002/smll.201602592
319. Tao W, Zhu X, Yu X, Zeng X, Xiao Q, Zhang X, et al. Black Phosphorus Nanosheets as a Robust Delivery Platform for Cancer Theranostics. *Adv Mater* (2017) 29(1):1603276. doi: 10.1002/adma.201603276
320. Lei W, Liu G, Zhang J, Liu M. Black Phosphorus Nanostructures: Recent Advances in Hybridization, Doping and Functionalization. *Chem Soc Rev* (2017) 46(12):3492–509. doi: 10.1039/c7cs00021a
321. Chen L, Chen C, Chen W, Li K, Chen X, Tang X, et al. Biodegradable Black Phosphorus Nanosheets Mediate Specific Delivery of hTERT siRNA for Synergistic Cancer Therapy. *ACS Appl Mater Interfaces* (2018) 10 (25):21137–48. doi: 10.1021/acsami.8b04807
322. Cheng K, Zhou J, Chen Y, Chen DZ. Progress of Stimulation Re-sponse Strategy Based on Nanomaterials in Tumor Therapy. *Cancer Res Prev Treat* (2019) 46(9):841–46 doi: 10.3971/j.issn.1000-8578.2019.19.0285
323. Hou X, Tao Y, Pang Y, Li X, Jiang G, Liu Y. Nanoparticle-Based Photothermal and Photodynamic Immunotherapy for Tumor Treatment. *Int J Cancer* (2018) 143(12):3050–60. doi: 10.1002/ijc.31717

Conflict of Interest: The authors declare that the research was conducted in the absence of any commercial or financial relationships that could be construed as a potential conflict of interest.

Publisher's Note: All claims expressed in this article are solely those of the authors and do not necessarily represent those of their affiliated organizations, or those of the publisher, the editors and the reviewers. Any product that may be evaluated in this article, or claim that may be made by its manufacturer, is not guaranteed or endorsed by the publisher.

Copyright © 2022 Shi, Tian, Liu, Xiong, Zhai, Chu and Gao. This is an open-access article distributed under the terms of the Creative Commons Attribution License (CC BY). The use, distribution or reproduction in other forums is permitted, provided the original author(s) and the copyright owner(s) are credited and that the original publication in this journal is cited, in accordance with accepted academic practice. No use, distribution or reproduction is permitted which does not comply with these terms.

frontiers | Frontiers in Oncology

REVIEW
published: 07 July 2022
doi: 10.3389/fonc.2022.933125

Nanotech Probes: A Revolution in Cancer Diagnosis

Qi Zhang[†], *Kai Hou*[†], *Hongbo Chen*[†], *Ning Zeng*[*] *and Yiping Wu*[*]

Department of Plastic and Cosmetic Surgery, Tongji Hospital, Tongji Medical College, Huazhong University of Science and Technology, Wuhan, China

Recent advances in nanotechnologies for cancer diagnosis and treatment have received considerable attention worldwide. Nanoparticles are being used to create nanodrugs and probes to diagnose and treat a variety of diseases, including cancer. Nanomedicines have unique advantages, such as increased surface-to-volume ratios, which enable them to interact with, absorb, and deliver small biomolecules to a very specific target, thereby improving the effectiveness of both probes and drugs. Nanoprobe biotechnology also plays an important role in the discovery of novel cancer biomarkers, and nanoprobes have become an important part of early clinical diagnosis of cancer. Various organic and inorganic nanomaterials have been developed as biomolecular carriers for the detection of disease biomarkers. Thus, we designed this review to evaluate the advances in nanoprobe technology in tumor diagnosis.

Keywords: nanomaterial, nanotechnology, cancer, diagnosis, nanotech probes

OPEN ACCESS

Edited by:
Kelong Ai,
Central South University, China

Reviewed by:
Daoming Zhu,
Wuhan University, China
Qiong Huang,
Central South University, China

***Correspondence:**
Yiping Wu
wuyipingtj@163.com
Ning Zeng
zengningwhtj@163.com

[†]*These authors have contributed equally to this work*

Specialty section:
This article was submitted to Pharmacology of Anti-Cancer Drugs, a section of the journal Frontiers in Oncology

Received: *30 April 2022*
Accepted: *14 June 2022*
Published: *07 July 2022*

Citation:
Zhang Q, Hou K, Chen H, Zeng N and Wu Y (2022) Nanotech Probes: A Revolution in Cancer Diagnosis. Front. Oncol. 12:933125. doi: 10.3389/fonc.2022.933125

INTRODUCTION

Cancer is currently one of the leading causes of death worldwide, with the number of cancer patients expected to increase over the next 50 years as demographic changes, such as population aging and growth, strongly influence cancer incidence and trends across different regions. Assuming that the latest incidence trends of major cancer types continue, the combined incidence of all cancers would double by 2070 (1). Cancer is often fatal, with early diagnosis generally acting as the deciding factor in therapeutic response. Thus, novel cancer prevention strategies and diagnostic tools must be developed to effectively reduce the number of future cancer cases and save more cancer patients.

Cancer is characterized by abnormal cell differentiation and proliferation, uncontrolled growth, invasion, and metastasis, and its occurrence is a complex multi-factor and multi-step process (2). Earlier cancer detection improves survival rate; however, about 50% of cancers are already in

Abbreviations: ACQ, Aggregation-caused quenching; NPC, nasopharyngeal carcinoma; PA, Photoacoustic; PET, Positron emission tomography; SPION, Superparamagnetic iron oxide

advanced stages of pathogenesis at their time of diagnosis (3–5). Early detection of cancer or precancerous lesions allows early intervention attempting to slow or prevent cancer progression and mortality. In addition to a better understanding of risk susceptibility for certain cancers, the biology and trajectory of precancerous and early cancer lesions must be assessed in order to identify secondary diseases that may require intervention. These efforts are best accelerated by early detection research translated into sensitive and specific early detection technologies (6). This need is supported by the observations following the COVID-19 pandemic, which has had a significant impact on cancer patients across the globe. Pandemic responses have resulted in delayed diagnosis and disruptions in treatment and follow-up care, increasing overall infection rates and premature deaths (7–9). This has highlighted the need to reduce the delays in cancer diagnosis associated with traditional diagnostic models and to address the inaccuracy and disruptions in diagnosis caused by COVID-19 (10). In this review, we aim to explore the application of tumor nanotechnology in tumor diagnosis.

NANOMATERIALS AND CANCER DIAGNOSIS

Nanomedicine is an emerging science often applied in cancer therapy, as it is characterized by tumor-specific drug delivery, conferring a significant therapeutic advantage over traditional interventions (11–15). The integration of imaging and nanoprobes for cancer diagnosis and treatment may facilitate better responses and reduced side effects in normal tissues (14, 16, 17). This means that nano-biosensors are likely to be critical to the development of novel cancer therapies and diagnostics, as they can be used to detect cancer biomarkers, map cancer cells, and monitor metastasis in response to different substrates and conditions (18, 19). Thus, the cancer diagnosis and treatment landscape has expanded considerably over the last decade, propelled by advances in novel therapies and improved diagnostics (14, 16, 17, 20). This recent success in nanomedicine research has also paved the way for accurate diagnosis through the interaction of nanoprobes with specific biological systems (21, 22).

NANOPROBE TECHNOLOGY

Fluorescent Probes

Optical tumor detection is becoming more and more common in biomedical research, but its limitations, including light penetration depth and signal attenuation in tissues, need to be overcome (23). Therefore, different optical imaging methods using nanoprobe technology have been developed for application in the fields of fluorescence, phosphorescence, and photoacoustic (PA) imaging. These methods are more sensitive than traditional techniques, providing higher resolution images and making it easier to get information pointing to anoxic areas.

Fluorescent probes are most common in optical sensors. Fluorescent probes bound to selected nanocarriers can produce dense hydrophobic aggregates following self-assembly in aqueous solutions. The probes can be activated by stimulus-specific "off-on" activation, improving the signal-to-noise ratio within the region of interest, resulting in extremely high sensitivity and increased resolution. Many of these probes are used to evaluate multiple tissues and subcellular structures (24).

Aggregation-caused quenching (ACQ) refers to the strong coupling reactions between ground state fluorophores that form a stable non-influenza fluorescence complex with a unique absorption spectrum (25), which is a typical activatable design. Yang et al. (26) took advantage of this simplicity to develop a scalable hypoxic-responsive human serum albumin-triggered nanosystem, consisting of human serum albumin, the near-infrared imaging photosensitizer chlore6, an oxaliplatin precursor, and a hypoxic-sensitive linker, azobenzene 4,4 'dicarboxylic acid. When exposed to a hypoxic tumor microenvironment, the nanosystem is cleaved by nitrogen reductase, breaking up the ultra-small human serum albumin aggregates and restoring chlore6 fluorescence, facilitating clear hypoxic imaging (27). Although the ACQ probe is simple to use, the quenching state of the dye largely depends on the assembly state of the nanocarrier. Thus, the status of the ACQs in any given carrier may be influenced by a variety of *in vivo* factors, including protein binding and enzyme degradation, which may lead to decreased selectivity and specificity for tumors.

In addition to general activatable designs, imaging strategies targeting tumor biomarkers *via in situ* luminescence can also be used to effectively image tumors *in vivo*. For example, the HIF-1α-induced transmembrane protein CAIX, which is a biomarker for hypoxic environments, is widely expressed on the surface of hypoxic cells (28). Huang et al. (29) evaluated the application of a CAIX-specific IRDye 800CW probe (CAIX-800) for hypoxia detection in a mouse model of orthotopic nasopharyngeal carcinoma (NPC). Their data revealed that a combination of this dye and fluorescence molecular tomography or computed tomography could be used to accurately locate early-stage NPC tumors, with detection as early as 2 weeks. Lymph node metastases from advanced NPC (6 weeks) were then observed using multispectral PA imaging. Taken together, the results of this study show that molecular conjugation combining appropriate targeting groups and near-infrared dyes can facilitate the selective imaging of specific anoxic analytes *in vivo*.

In addition, anaerobe integration in nanocarriers can also facilitate tumor targeting, as these microbes can only survive in anoxic environments; thus, their inclusion would force aggregation to the hypoxic areas of the tumor. In addition, bacterial migration to hypoxic tumors can also be facilitated by external stimulation. F. Chen et al. (30) attached lipid nanoparticles loaded with indocyanine green to bacterial surfaces to target and ablate hypoxic tumors through photothermal therapy. Fluorescent probes based on nanocarriers are used more and more frequently in tumor diagnosis.

Phosphorescent Probes

Following photoexcitation, an excited electron passes through the excited triplet state between the systems, inducing a spin transition, which returns a singlet to the ground state and emits photons in the form of phosphorescence. Phosphorescence can then be converted to pO_2 by calibrating the probe using the Sterne-Volmer equation. Several research groups have gone on to develop phosphorescence probes for various applications, including direct pO_2 measurement (31, 32). Phosphorescent probes have the advantages of high spatial resolution and direct and reversible pO_2 quantitative analysis. Yoshihara et al. (33) reported that Ru (II) complexes could be coupled with oligodeoxy nucleotides containing pyrene and nitroimidazole ligands, and that the hydrophilicity of the modified metal complex molecules could facilitate the induction of nanoaggregates, which could then be used to support qualitative analysis of tumor burden. In addition, Liu et al. (34) recently combined complementary imaging technology with nanoparticles to achieve high-quality, reliable, and quantitative hypoxia detection in several different cancer models. In this study, the research team encapsulated benzene-substituted Pd (II) porphyrin (PdTPTBP) into dSPE-PEG 2K phospholipid micelles (Pd-) in MX, to produce a phosphorescent nanoprobe, which could then be applied as a time-resolved lifetime imaging system. By combining the wide field of view of luminescent lifetime imaging with O_2-sensitive nanoprobes, this group were able to quantify O_2 localization in tumors and thus identify hotspots for likely tumor formation.

PA Probes

PA tomography may be another potential approach for addressing the limitations of modern imaging associated with maximum tissue penetration depth. This system works by converting excited light energy to heat/sound energy, facilitating a significant increase in penetration depth while maintaining near-microscopic spatial resolution. PA signals are generated by photon absorption, which causes rapid thermoelastic expansion and sound wave propagation. These pressure waves can be detected by transducers, and PA images can then be produced. These images are characterized by improved tissue penetration depth (35). A recent study (36) used endogenous PA imaging to detect tumor hypoxia in a multicancer model, providing anatomical and functional information on hypoxia. Knox et al. (37) developed a hyper-1-based hypoxic response probe for radiographic PA imaging, which utilized the aza-Bodipy platform and a dialkyl aniline substitutive group, facilitating further oxidation of the system to produce the single n-oxide probe RHP-1. Probe evaluations revealed a two-fold increase in PA 820 nm/PA 770 nm emissions when these sensors were placed under hypoxic conditions. Furthermore, *in vivo* PA imaging revealed that the hypoxic regions of the tumor could be mapped for 3D reconstruction when using a RHP-1 probe. Recently, M. Chen et al. (38) applied the bioreducible N-oxide hypoxia-sensitive probe Hyper-650 with enhanced molar absorption to high resolution PA microscopy. This system facilitated the simultaneous and constant monitoring of vascular sO_2 and tissue oxygenation, following its combination with endogenous contrast agents. These images revealed that the identified tumor hypoxia center signals were consistent with those identified using traditional sO_2 imaging, supporting their clinical value.

Tumor Imaging Based on Dendritic Cells

The tumor microenvironment is characterized by gradual changes in both spatial and temporal heterogeneity, which can be used to explore its diagnostic application in tumors. Fluorescent imaging probes responsive to various conditions, including hypoxia, pH, and protease expression, may be used to evaluate and diagnose specific tumor conditions (39–42). In precision medicine, molecular imaging is primarily used to identify cancer-specific targets, design therapeutic methods, and monitor drug administration responses. DCs, for example, are the most adept antigen-presenting cells, transmitting information to the cells in the adaptive immune system (27, 28). Accurate antigen delivery and effective activation of immune pathways are key to the development of DC anticancer vaccines and successful immunotherapy. However, DC viability, function, and their ability to migrate *in vivo* remain unknown. Superparamagnetic iron oxide (SPION) is an excellent MRI contrast agent that can be easily absorbed by DCs and tracked using MRI. Thus, MRI using SPIONs can provide more anatomical information and more detailed visualization than other methods, but at lower sensitivity (43, 44). To overcome this limitation Y.C. Chen et al. (45) pioneered the development of a novel dual-mode nanoprobe, SPIONIR797, for tracking DC migration *in vivo* and detection *via* a non-invasive combined method. Thus, leveraging the advantages of high sensitivity, high spatial resolution, and relatively simple operation, it is becoming increasingly easy to visualize various diseases and use these imaging techniques to draw critical diagnostic conclusions. Many of these systems focus on a variety of disease models, including tumors, inflammation, and atherosclerosis.

Other Imaging Nanoprobe Technologies

In addition to the technologies described above, other research groups continue to work on a variety of alternatives. For example, gold, silver, and bimetallic and magnetic nanoparticles are widely used in the manufacture of sensing tools due to their unique optical properties and biocompatibility (22, 46–51). The functionalization of these nanoparticles with different components provides an excellent opportunity to assemble selective and sensitive sensing materials for the detection of various cancer-related biomolecules. This was exemplified in the Zhang et al. (52) study, where a multifunctional ASnFAp : Gd/Tb system was synthesized using a new bionic strategy. Subsequent *in vitro* and *in vivo* experiments then confirmed improved tumor imaging and recognition ability, compared with conventional methods. The generated nanoparticles could be used as drug carriers for tumor imaging and treatment with good tumor recognition, treatment capacity, and superior biocompatibility. Thus, this study supports the very important potential clinical application of nanomaterials in diagnosis.

PATH TO CLINICAL TRANSLATION

Given the complexity of the tumor microenvironment and the diversity of analytes that contribute to global hypoxia, there is currently no "gold standard" for measuring tumor hypoxia (53). Nevertheless, several novel methods designed to detect and evaluate tumor hypoxia have been developed, with several entering clinical evaluations. These include oxygen electrodes, electron paramagnetic resonance oximetry, positron emission tomography (PET), and more.

One example is the system created by de Georgia (54), which facilitates pO_2 evaluation in invasive tumors *via* electrochemical probes. This system has been successfully employed in critical care settings focused on retaining nerve function. However, when the oxygen is completely consumed, the electrode undergoes electrochemical reduction, resulting in reduced signal sensitivity and increasing inaccurate readings. This system is also invasive and can lead to edema and hemorrhage in some tissues. Daimiel et al. (55) developed an alternative technique for repeatable quantitative pO_2 measurement in tumors using electron paramagnetic resonance oximetry. This non-invasive method requires the use of a paramagnetic probe, which responds to the oxygen in any given environment and evaluates pO_2 levels by measuring relaxation rates.

In addition, recent developments in 2-nitroimidazole-based radiotracers may facilitate an increase in PET application as an alternative non-invasive technique for detecting tumor hypoxia. Relatively short-lived radionuclides, such as 18F, can be easily bound *via* isotope exchange reactions to produce novel probes. Several studies have evaluated 18F LA-Beled FMISO, pentafluorinated etanidazole, hydrophilic fluoridazole, and arabinosfluorroazomycin as PET probes for hypoxia imaging (56).

However, the development of a new probe must always be followed by preclinical evaluation and scaled-up good manufacturing practices to facilitate clinical trials. Obstacles in each specific area must be overcome before probes can be incorporated into routine clinical practice. Despite all the immediate challenges of clinical transformation, nanoprobe imaging offers significant opportunities to provide improved non-invasive diagnostic tools. Combining optical imaging with other biomedical imaging methods may also facilitate multimodal imaging, providing even better tumor detection.

CONCLUSION AND PERSPECTIVES

Nanoprobes have a unique set of physical advantages, including flexible biocompatibility and pharmacokinetics, and most present various unique nanoscale properties, providing more convenient tumor imaging. Nanostructures can also promote the production of organic dye aggregates. Thus, cancer diagnostic specialists have continued to focus on biomedical sensing and imaging. Nanosensors can also provide a protective substrate to prevent unnecessary interactions within the biological environment and improve *in vivo* circulation time and system delivery. With improved understanding of the basic physical phenomena resulting from nanoconstraints, nanosensors can be designed to facilitate both assembly and disassembly in response to specific physicochemical conditions, providing the possibility for the further development of "smart" responsive nanosensors.

In addition, the high degree of heterogeneity between and within tumors can result in complex diagnostic and evaluation issues, including a large discrepancy in imaging results (57). This highlights the importance of further studies on different tumor types. Considering the temporal and spatial variability of tumors, the development of sensors that can accurately track treatment dynamics in real time is a promising concept. Thus, we believe that nanoprobe sensors are likely to play a fundamental role in our understanding of tumors and are almost guaranteed to become increasingly important in the detection and treatment of various cancers due to their physical, pharmacokinetic, and nanoscopic properties.

AUTHOR CONTRIBUTIONS

All authors contributed to the design of the study and writing of the manuscript. QZ, KH, and HC undertook the research. YW and NZ wrote the main manuscript text. QZ and YW revised the article critically for important intellectual content and granted final approval of the submitted version. All authors reviewed the manuscript.

REFERENCES

1. Soerjomataram I, Bray F. Planning for Tomorrow: Global Cancer Incidence and the Role of Prevention 2020-2070. *Nat Rev Clin Oncol* (2021) 18(10):663–72. doi: 10.1038/s41571-021-00514-z
2. Yang Y, Huang Q, Xiao Z, Liu M, Zhu Y, Chen Q, et al. Nanomaterial-Based Biosensor Developing as a Route Toward *In Vitro* Diagnosis of Early Ovarian Cancer. *Mater Today Bio* (2022) 13:100218. doi: 10.1016/j.mtbio.2022.100218
3. Crosby D, Bhatia S, Brindle KM, Coussens LM, Dive C, Emberton M, et al. Early Detection of Cancer. *Science* (2022) 375(6586):eaay9040. doi: 10.1126/science.aay9040
4. Hricak H, Ward ZJ, Atun R, Abdel-Wahab M, Muellner A, Scott AM. Increasing Access to Imaging for Addressing the Global Cancer Epidemic. *Radiology* (2021) 301(3):543–6. doi: 10.1148/radiol.2021211351
5. Liu Y, Ai K, Lu L. Nanoparticulate X-Ray Computed Tomography Contrast Agents: From Design Validation to *In Vivo* Applications. *Acc Chem Res* (2012) 45(10):1817–27. doi: 10.1021/ar300150c
6. Wang J, Sui L, Huang J, Miao L, Nie Y, Wang K, et al. MoS2-Based Nanocomposites for Cancer Diagnosis and Therapy. *Bioact Mater* (2021) 6 (11):4209–42. doi: 10.1016/j.bioactmat.2021.04.021
7. Hesary FB, Salehiniya H. The Impact of the COVID-19 Epidemic on Diagnosis, Treatment, Concerns, Problems, and Mental Health in Patients With Gastric Cancer. *J Gastrointest Cancer* (2021) 1–8. doi: 10.1007/s12029-021-00692-0
8. Tuech JJ, Gangloff A, Di Fiore F, Benyoucef A, Michel P, Schwarz L. The Day After Tomorrow: How Should We Address Health System Organization to Treat Cancer Patients After the Peak of the COVID-19 Epidemic? *Oncology* (2020) 98(12):827–35. doi: 10.1159/000509650

9. Huynh I. When COVID-19 Saves Lives: Accidental Cancer Diagnosis in an Epidemic Context. *Ethics Med Public Health* (2021) 18:100666. doi: 10.1016/j.jemep.2021.100666
10. Parihar A, Singhal A, Kumar N, Khan R, Khan MA, Srivastava AK. Next-Generation Intelligent MXene-Based Electrochemical Aptasensors for Point-Of-Care Cancer Diagnostics. *Nanomicro Lett* (2022) 14(1):100. doi: 10.1007/s40820-022-00845-1
11. Zhu D, Liu Z, Li Y, Huang Q, Xia L, Li K. Delivery of Manganese Carbonyl to the Tumor Microenvironment Using Tumor-Derived Exosomes for Cancer Gas Therapy and Low Dose Radiotherapy. *Biomaterials* (2021) 274:120894. doi: 10.1016/j.biomaterials.2021.120894
12. Zeng H, Li J, Hou K, Wu Y, Chen H, Ning Z. Melanoma and Nanotechnology-Based Treatment. *Front Oncol* (2022) 12:858185. doi: 10.3389/fonc.2022.858185
13. Qi P, Zhang J, Bao Z, Liao Y, Liu Z, Wang J. A Platelet-Mimicking Single-Atom Nanozyme for Mitochondrial Damage-Mediated Mild-Temperature Photothermal Therapy. *ACS Appl Mater Interfaces* (2022) 14(17):19081–90. doi: 10.1021/acsami.1c22346
14. Huang C, Liu Z, Chen M, Du L, Liu C, Wang S, et al. Tumor-Derived Biomimetic Nanozyme With Immune Evasion Ability for Synergistically Enhanced Low Dose Radiotherapy. *J Nanobiotechnol* (2021) 19(1):457. doi: 10.1186/s12951-021-01182-y
15. Zhao T, Wu W, Sui L, Huang Q, Nan Y, Liu J, et al. Reactive Oxygen Species-Based Nanomaterials for the Treatment of Myocardial Ischemia Reperfusion Injuries. *Bioact Mater* (2022) 7:47–72. doi: 10.1016/j.bioactmat.2021.06.006
16. Huang C, Ding S, Jiang W, Wang FB. Glutathione-Depleting Nanoplatelets for Enhanced Sonodynamic Cancer Therapy. *Nanoscale* (2021) 13(8):4512–8. doi: 10.1039/d0nr08440a
17. Huang C, Zhu C, Chen J, Huang K, Li F, Ding S, et al. Nano-Platelets as an Oxygen Regulator for Augmenting Starvation Therapy Against Hypoxic Tumor. *Front Bioeng Biotechnol* (2020) 8:571993. doi: 10.3389/fbioe.2020.571993
18. Shahbazi N, Zare-Dorabei R, Naghib SM. Multifunctional Nanoparticles as Optical Biosensing Probe for Breast Cancer Detection: A Review. *Mater Sci Eng C Mater Biol Appl* (2021) 127:112249. doi: 10.1016/j.msec.2021.112249
19. Mohammadpour Z, Majidzadeh AK. Applications of Two-Dimensional Nanomaterials in Breast Cancer Theranostics. *ACS Biomater Sci Eng* (2020) 6(4):1852–73. doi: 10.1021/acsbiomaterials.9b01894
20. Huang C, Wang FB, Liu L, Jiang W, Liu W, Ma W, et al. Hypoxic Tumor Radiosensitization Using Engineered Probiotics. *Adv Healthc Mater* (2021) 10(10):e2002207. doi: 10.1002/adhm.202002207
21. Kundu P, Singh D, Singh A, Sahoo SK. Cancer Nanotheranostics: A Nanomedicinal Approach for Cancer Therapy and Diagnosis. *Anticancer Agents Med Chem* (2020) 20(11):1288–99. doi: 10.2174/1871520619666190820145930
22. Xiao Z, Huang Q, Yang Y, Liu M, Chen Q, Huang J, et al. Emerging Early Diagnostic Methods for Acute Kidney Injury. *Theranostics* (2022) 12(6):2963–86. doi: 10.7150/thno.71064
23. Ntziachristos V. Going Deeper Than Microscopy: The Optical Imaging Frontier in Biology. *Nat Methods* (2010) 7(8):603–14. doi: 10.1038/nmeth.1483
24. Shashkova S, Leake MC. Single-Molecule Fluorescence Microscopy Review: Shedding New Light on Old Problems. *Biosci Rep* (2017) 37(4):BSR20170031. doi: 10.1042/BSR20170031
25. Luby BM, Walsh CD, Zheng G. Advanced Photosensitizer Activation Strategies for Smarter Photodynamic Therapy Beacons. *Angew Chem Int Ed Engl* (2019) 58(9):2558–69. doi: 10.1002/anie.201805246
26. Yang G, Phua SZF, Lim WQ, Zhang R, Feng L, Liu G, et al. A Hypoxia-Responsive Albumin-Based Nanosystem for Deep Tumor Penetration and Excellent Therapeutic Efficacy. *Adv Mater* (2019) 31(25):e1901513. doi: 10.1002/adma.201901513
27. Cui D, Huang J, Zhen X, Li J, Jiang Y, Pu K. A Semiconducting Polymer Nano-Prodrug for Hypoxia-Activated Photodynamic Cancer Therapy. *Angew Chem Int Ed Engl* (2019) 58(18):5920–4. doi: 10.1002/anie.201814730
28. Tafreshi NK, Lloyd MC, Proemsey JB, Bui MM, Kim J, Gillies RJ, et al. Evaluation of CAIX and CAXII Expression in Breast Cancer at Varied O2 Levels: CAIX is the Superior Surrogate Imaging Biomarker of Tumor Hypoxia. *Mol Imaging Biol* (2016) 18(2):219–31. doi: 10.1007/s11307-015-0885-x
29. Huang W, Wang K, An Y, Meng H, Gao Y, Xiong Z, et al. *In Vivo* Three-Dimensional Evaluation of Tumour Hypoxia in Nasopharyngeal Carcinomas Using FMT-CT and MSOT. *Eur J Nucl Med Mol Imaging* (2020) 47(5):1027–38. doi: 10.1007/s00259-019-04526-x
30. Chen F, Zang Z, Chen Z, Cui L, Chang Z, Ma A, et al. Nanophotosensitizer-Engineered Salmonella Bacteria With Hypoxia Targeting and Photothermal-Assisted Mutual Bioaccumulation for Solid Tumor Therapy. *Biomaterials* (2019) 214:119226. doi: 10.1016/j.biomaterials.2019.119226
31. O'Riordan TC, Fitzgerald K, Ponomarev GV, Mackrill J, Hynes J, Taylor C, et al. Sensing Intracellular Oxygen Using Near-Infrared Phosphorescent Probes and Live-Cell Fluorescence Imaging. *Am J Physiol Regul Integr Comp Physiol* (2007) 292(4):R1613–20. doi: 10.1152/ajpregu.00707.2006
32. Cheng MHY, Mo Y, Zheng G. Nano Versus Molecular: Optical Imaging Approaches to Detect and Monitor Tumor Hypoxia. *Adv Healthc Mater* (2021) 10(2):e2001549. doi: 10.1002/adhm.202001549
33. Yoshihara K, Takagi K, Son A, Kurihara R, Tanabe K. Aggregate Formation of Oligonucleotides That Assist Molecular Imaging for Tracking of the Oxygen Status in Tumor Tissue. *Chembiochem* (2017) 18(16):1650–8. doi: 10.1002/cbic.201700116
34. Liu Y, Gu Y, Yuan W, Zhou X, Qiu X, Kong M, et al. Quantitative Mapping of Liver Hypoxia in Living Mice Using Time-Resolved Wide-Field Phosphorescence Lifetime Imaging. *Adv Sci (Weinh)* (2020) 7(11):1902929. doi: 10.1002/advs.201902929
35. Li M, Tang Y, Yao J. Photoacoustic Tomography of Blood Oxygenation: A Mini Review. *Photoacoustics* (2018) 10:65–73. doi: 10.1016/j.pacs.2018.05.001
36. Ron A, Dean-Ben XL, Gottschalk S, Razansky D. Volumetric Optoacoustic Imaging Unveils High-Resolution Patterns of Acute and Cyclic Hypoxia in a Murine Model of Breast Cancer. *Cancer Res* (2019) 79(18):4767–75. doi: 10.1158/0008-5472.CAN-18-3769
37. Knox HJ, Kim TW, Zhu Z, Chan J. Photophysical Tuning of N-Oxide-Based Probes Enables Ratiometric Photoacoustic Imaging of Tumor Hypoxia. *ACS Chem Biol* (2018) 13(7):1838–43. doi: 10.1021/acschembio.8b00099
38. Chen M, Knox HJ, Tang Y, Liu W, Nie L, Chan J, et al. Simultaneous Photoacoustic Imaging of Intravascular and Tissue Oxygenation. *Opt Lett* (2019) 44(15):3773–6. doi: 10.1364/OL.44.003773
39. Wu Y, Zhang W, Li J, Zhang Y. Optical Imaging of Tumor Microenvironment. *Am J Nucl Med Mol Imaging* (2013) 3(1):1–15.
40. Li Y, Shen B, Zou G, Hu R, Pan Y, Qu J, et al. Super-Multiplex Nonlinear Optical Imaging Unscrambles the Statistical Complexity of Cancer Subtypes and Tumor Microenvironment. *Adv Sci (Weinh)* (2022) 9(5):e2104379. doi: 10.1002/advs.202104379
41. Vakoc BJ, Lanning RM, Tyrrell JA, Padera TP, Bartlett LA, Stylianopoulos T, et al. Three-Dimensional Microscopy of the Tumor Microenvironment *In Vivo* Using Optical Frequency Domain Imaging. *Nat Med* (2009) 15(10):1219–23. doi: 10.1038/nm.1971
42. Penet MF, Krishnamachary B, Chen Z, Jin J, Bhujwalla ZM. Molecular Imaging of the Tumor Microenvironment for Precision Medicine and Theranostics. *Adv Cancer Res* (2014) 124:235–56. doi: 10.1016/B978-0-12-411638-2.00007-0
43. Long CM, van Laarhoven HW, Bulte JW, Levitsky HI. Magnetovaccination as a Novel Method to Assess and Quantify Dendritic Cell Tumor Antigen Capture and Delivery to Lymph Nodes. *Cancer Res* (2009) 69(7):3180–7. doi: 10.1158/0008-5472.CAN-08-3691
44. Kobukai S, Baheza R, Cobb JG, Virostko J, Xie J, Gillman A, et al. Magnetic Nanoparticles for Imaging Dendritic Cells. *Magn Reson Med* (2010) 63(5):1383–90. doi: 10.1002/mrm.22313
45. Chen YC, Wen S, Shang SA, Cui Y, Luo B, Teng GJ. Magnetic Resonance and Near-Infrared Imaging Using a Novel Dual-Modality Nano-Probe for Dendritic Cell Tracking In Vivo. *Cytotherapy* (2014) 16(5):699–710. doi: 10.1016/j.jcyt.2013.09.006
46. Lee SJ, Kim HJ, Huh YM, Kim IW, Jeong JH, Kim JC, et al. Functionalized Magnetic PLGA Nanospheres for Targeting and Bioimaging of Breast Cancer. *J Nanosci Nanotechnol* (2018) 18(3):1542–7. doi: 10.1166/jnn.2018.14220
47. Zong J, Cobb SL, Cameron NR. Peptide-Functionalized Gold Nanoparticles: Versatile Biomaterials for Diagnostic and Therapeutic Applications. *Biomater Sci* (2017) 5(5):872–86. doi: 10.1039/c7bm00006e
48. Azharuddin M, Zhu GH, Das D, Ozgur E, Uzun L, Turner APF, et al. A Repertoire of Biomedical Applications of Noble Metal Nanoparticles. *Chem Commun (Camb)* (2019) 55(49):6964–96. doi: 10.1039/c9cc01741k

49. Li X, Yang T, Lin J. Spectral Analysis of Human Saliva for Detection of Lung Cancer Using Surface-Enhanced Raman Spectroscopy. *J BioMed Opt* (2012) 17(3):37003. doi: 10.1117/1.JBO.17.3.037003
50. Ravalli A, Marrazza G. Gold and Magnetic Nanoparticles-Based Electrochemical Biosensors for Cancer Biomarker Determination. *J Nanosci Nanotechnol* (2015) 15(5):3307–19. doi: 10.1166/jnn.2015.10038
51. Li RD, Yin BC, Ye BC. Ultrasensitive, Colorimetric Detection of microRNAs Based on Isothermal Exponential Amplification Reaction-Assisted Gold Nanoparticle Amplification. *Biosens Bioelectron* (2016) 86:1011–6. doi: 10.1016/j.bios.2016.07.042
52. Zhang W, Zhou R, Yang Y, Peng S, Xiao D, Kong T, et al. Aptamer-Mediated Synthesis of Multifunctional Nano-Hydroxyapatite for Active Tumour Bioimaging and Treatment. *Cell Prolif* (2021) 54(9):e13105. doi: 10.1111/cpr.13105
53. Tatum JL, Kelloff GJ, Gillies RJ, Arbeit JM, Brown JM, Chao KS, et al. Hypoxia: Importance in Tumor Biology, Noninvasive Measurement by Imaging, and Value of its Measurement in the Management of Cancer Therapy. *Int J Radiat Biol* (2006) 82(10):699–757. doi: 10.1080/09553000601002324
54. De Georgia MA. Brain Tissue Oxygen Monitoring in Neurocritical Care. *J Intensive Care Med* (2015) 30(8):473–83. doi: 10.1177/0885066614529254
55. Daimiel I. Insights Into Hypoxia: Non-Invasive Assessment Through Imaging Modalities and Its Application in Breast Cancer. *J Breast Cancer* (2019) 22 (2):155–71. doi: 10.4048/jbc.2019.22.e26
56. Fleming IN, Manavaki R, Blower PJ, West C, Williams KJ, Harris AL, et al. Imaging Tumour Hypoxia With Positron Emission Tomography. *Br J Cancer* (2015) 112(2):238–50. doi: 10.1038/bjc.2014.610
57. Bhandari V, Hoey C, Liu LY, Lalonde E, Ray J, Livingstone J, et al. Molecular Landmarks of Tumor Hypoxia Across Cancer Types. *Nat Genet* (2019) 51 (2):308–18. doi: 10.1038/s41588-018-0318-2

Conflict of Interest: The authors declare that the research was conducted in the absence of any commercial or financial relationships that could be construed as a potential conflict of interest.

Publisher's Note: All claims expressed in this article are solely those of the authors and do not necessarily represent those of their affiliated organizations, or those of the publisher, the editors and the reviewers. Any product that may be evaluated in this article, or claim that may be made by its manufacturer, is not guaranteed or endorsed by the publisher.

Copyright © 2022 Zhang, Hou, Chen, Zeng and Wu. This is an open-access article distributed under the terms of the Creative Commons Attribution License (CC BY). The use, distribution or reproduction in other forums is permitted, provided the original author(s) and the copyright owner(s) are credited and that the original publication in this journal is cited, in accordance with accepted academic practice. No use, distribution or reproduction is permitted which does not comply with these terms.

frontiers | Frontiers in Pharmacology

ORIGINAL RESEARCH
published: 11 July 2022
doi: 10.3389/fphar.2022.915822

Genetic Variants in Double-Strand Break Repair Pathway Genes to Predict Platinum-Based Chemotherapy Prognosis in Patients With Lung Cancer

Jun-Yan Liu[1], Ting Zou[2], Ji-Ye Yin[3,4], Zhan Wang[5], Chong Liu[4], Han-Xue Huang[4], Fei-Xiang Ding[4], Meng-Rong Lei[4], Ying Wang[6], Min Liu[7], Zhao-Qian Liu[2,3], Li-Ming Tan[8] and Juan Chen[9,10]**

[1]Department of Orthopaedics, Xiangya Hospital, Central South University, Changsha, China, [2]National Institution of Drug Clinical Trial, Xiangya Hospital, Central South University, Changsha, China, [3]Departments of Clinical Pharmacology, Xinagya Hospital, Central South University, Changsha, China, [4]Institute of Clinical Pharmacology and Hunan Key Laboratory of Pharmacogenetics, Central South University, Changsha, China, [5]Lung Cancer and Gastrointestinal Unit, Department of Medical Oncology, Hunan Cancer Hospital, Affiliated Cancer Hospital of Xiangya School of Medicine, Changsha, China, [6]Hunan Clinical Research Center in Gynecologic Cancer, Hunan Cancer Hospital, Affiliated Cancer Hospital of Xiangya School of Medicine, Changsha, China, [7]Xiangya School of Pharmaceutical Sciences, Central South University, Changsha, China, [8]Department of Pharmacy, The Second People's Hospital of Huaihua City, Huaihua, China, [9]Department of Pharmacy, Xinagya Hospital, Central South University, Changsha, China, [10]National Clinical Research Center for Geriatric Disorders, Xiangya Hospital, Central South University, Changsha, China

OPEN ACCESS

Edited by:
Zeming Liu,
Huazhong University of Science and Technology, China

Reviewed by:
Jun-Li Luo,
The Scripps Research Institute, United States
Jessy Abraham,
All India Institute of Medical Sciences Raipur, India

***Correspondence:**
Li-Ming Tan
limingtan@126.com
Juan Chen
cj1028@csu.edu.cn

Specialty section:
This article was submitted to Pharmacology of Anti-Cancer Drugs, a section of the journal Frontiers in Pharmacology

Received: 08 April 2022
Accepted: 30 May 2022
Published: 11 July 2022

Citation:
Liu J-Y, Zou T, Yin J-Y, Wang Z, Liu C, Huang H-X, Ding F-X, Lei M-R, Wang Y, Liu M, Liu Z-Q, Tan L-M and Chen J (2022) Genetic Variants in Double-Strand Break Repair Pathway Genes to Predict Platinum-Based Chemotherapy Prognosis in Patients With Lung Cancer. Front. Pharmacol. 13:915822. doi: 10.3389/fphar.2022.915822

Objective: The purpose of this study was to investigate the associations of genetic variants in double-strand break (DSB) repair pathway genes with prognosis in patients with lung cancer treated with platinum-based chemotherapy.

Methods: Three hundred ninety-nine patients with lung cancer who received platinum-based chemotherapy for at least two cycles were included in this study. A total of 35 single nucleotide polymorphisms (SNPs) in DSB repair, base excision repair (BER), and nucleotide excision repair (NER) repair pathway genes were genotyped, and were used to evaluate the overall survival (OS) and the progression-free survival (PFS) of patients who received platinum-based chemotherapy using Cox proportional hazard models.

Results: The PFS of patients who carried the *MAD2L2* rs746218 GG genotype was shorter than that in patients with the AG or AA genotypes (recessive model: $p = 0.039$, OR = 5.31, 95% CI = 1.09–25.93). Patients with the TT or GT genotypes of *TNFRSF1A* rs4149570 had shorter OS times than those with the GG genotype (dominant model: $p = 0.030$, OR = 0.57, 95% CI = 0.34–0.95). We also investigated the influence of age, gender, histology, smoking, stage, and metastasis in association between SNPs and OS or PFS in patients with lung cancer. DNA repair gene SNPs were significantly associated with PFS and OS in the subgroup analyses.

Conclusion: Our study showed that variants in *MAD2L2* rs746218 and *TNFRSF1A* rs4149570 were associated with shorter PFS or OS in patients with lung cancer who

received platinum-based chemotherapy. These variants may be novel biomarkers for the prediction of prognosis of patients with lung cancer who receive platinum-based chemotherapy.

Keywords: lung cancer, platinum-based chemotherapy, prognosis, genetic polymorphisms, MAD2L2, TNFRSF1A

INTRODUCTION

Lung cancer has one of the highest rates of cancer-related mortality (Parkin et al., 1999; Siegel et al., 2021). Approximately 2.2 million new lung cancer cases and 1.8 million deaths resulting from lung cancer were reported in 2020, which was double the number reported 30 years earlier (Parkin et al., 1999; Siegel et al., 2021). The overall 5-year survival rate for lung cancer is less than 18% due to rapid progression and late-stage diagnosis (Alam et al., 2020). Lung cancer mainly consists of non–small cell lung cancer (NSCLC) and small cell lung cancer (SCLC), which occur in 85:15 ratio (Shi and Sun, 2015; Schwartz and Cote, 2016). Surgery, radiotherapy, chemotherapy, immunotherapy, and targeted therapy are the primary approaches for the treatment of lung cancer. Specific management is contingent on staging and pathohistological type (Kalemkerian et al., 2018; Ettinger et al., 2019). Development of targeted therapies and immunotherapy has resulted in substantial clinical benefits. However, the majority of patients do not have activating mutations and do not experience long-term stable remission (Hirsch et al., 2017; Arbour and Riely, 2019). Chemotherapy is the main treatment for lung cancer, with platinum-based chemotherapy the most widely-used approach.

Platinum-based chemotherapy has been widely used as a therapeutic regimen to treat cancer, including patients with lung cancer, since the first platinum agent, cisplatin, was approved over 40 years ago (Rottenberg et al., 2021). Cisplatin, carboplatin, and oxaliplatin are the three main platinum-based antineoplastic drugs (Low et al., 2021). Cisplatin is the standard treatment for NSCLC, and is the first choice to treat patients with advanced cancers without treatable gene mutations (Kryczka et al., 2021). The platinum-doublet chemotherapy, platinum combined with etoposide, is recommended as a first-line treatment for late-stage SCLC (Thai et al., 2021; Zugazagoitia and Paz-Ares, 2022). Although platinum-based chemotherapy can improve survival rate, patients treated with platinum-based drugs often suffered from drug resistance, resulting in poor prognosis and therapeutic failure. There are many prognostic factors such as genetic polymorphisms, age, gender, histology type, smoking, metastasis, and clinical stage that have been reported to be connected to platinum-based chemotherapy sensitivity (Cescon et al., 2015; Chen et al., 2016; Yin et al., 2016). Therapeutic efficacy is unsatisfactory and unpredictable. Therefore, the identification of novel biomarkers may help to identify therapeutic avenues that can improve survival time.

Investigation of mechanisms of drug resistance is of great importance for the improvement of the prognosis of lung cancer in response to platinum-based chemotherapy. Given that platinum-based drugs induce DNA fragmentation through crosslinking with DNA to form DNA adducts, alteration of DNA repair mechanisms can affect tumor sensitivity to platinum drugs (Rottenberg et al., 2021). Base excision repair (BER), nucleotide excision repair (NER), DNA mismatch repair (MMR), homologous recombination (HR), and non-homologous end joining (NHEJ) are the major DNA repair pathways, among which HR and NHEJ are responsible for repairing double-strand breaks (DSBs). Furthermore, NHEJ plays an important role in the DNA damage response system (Gupta et al., 2018; Xu and Xu, 2020; Jiang et al., 2021), which can directly link the ends of DSBs by DNA ligase to promote ligation of DNA ends. This process is characterized by impedance of homologous DNA sequences, while HR uses the intact sister chromatid as a template (Huang and Dynan, 2002; Andres et al., 2015; Xing et al., 2015; Almohaini et al., 2016; Kulkarni et al., 2016; Menon and Povirk, 2017; Reid et al., 2017). Previous studies have shown the importance of double-strand break repair (DSBR) pathways in platinum chemotherapy resistance (Kryczka et al., 2021). A numbers of DNA repair genes have been confirmed to be related to platinum-based chemotherapy resistance in patients with lung cancer, including the *XRCC5* and *HSPB1* genes. However, few studies have focused on polymorphisms in the DSBR pathway genes.

We investigated the associations between SNPs in the *MAD2L2*, *XPC*, *XRCC3*, *BRCA2*, *RAD52*, *NFKB1*, *NFKBIA*, *TNFRSF1A*, or *FASN* genes and prognosis in patients with lung cancer who received platinum-based chemotherapy.

PATIENTS AND METHODS

Patients and Data Collection

The inclusion criteria for 399 patients with lung cancer were as follows: 1) all patients attended at the Xiangya Hospital of Central South University or Affiliated Cancer Hospital of Xiangya School of Medicine (Changsha, Hunan, China) from August 2009 to May 2013; 2) patients with lung cancer received platinum-based chemotherapy for at least two cycles; 3) patients with lung cancer had not undergone surgery, radiotherapy, targeted drug therapy, or other biological therapy before chemotherapy. The research proposal was approved by the Ethics Committee of Xiangya Hospital, Central South University. All patients provided written informed consent prior to participating in the study.

The deadline for patient enrollment was 15 July 2019. Standard follow-up clinical data included age, gender, smoking history, histology classification, TNM stage, and metastasis. The two main data processing approaches were PFS, which was defined as the time period from diagnosis until disease progression. Patients without OS and PFS data were removed from the study at the final follow-up. The overall survival was

TABLE 1 | 35 gene polymorphisms examined in this study.

Gene	SNP	Alleles	Call Rate (%)	MAF
ERCC1	rs2298881	C/A,G,T	96.24	0.402
ERCC2	rs1052555	G/A	100	0.143
	rs238406	T/G	96.24	0.471
ERCC4	rs1799801	T/C	98.50	0.298
ERCC6	rs2228527	T/A,C	100	0.118
	rs3793784	G/C	98.25	0.337
XPC	rs2228000	G/A	96.24	0.340
	rs2228001	G/C,T	98.50	0.411
XRCC1	rs25489	C/A,G,T	99.75	0.172
XRCC3	rs1799794	T/C	97.24	0.470
	rs861539	G/A	99.50	0.098
BRCA1	rs799917	G/A,C,T	97.49	0.423
BRCA2	rs543304	T/C,G	96.74	0.240
BRCA2	rs206118	A/C,G	98.25	0.246
RAD51	rs12593359	T/A,C,G	97.74	0.266
	rs1801320	G/C	96.49	0.226
	rs1801321	G/C,T	97.24	0.124
RAD52	rs1051669	C/T	96.24	0.245
	rs7963551	T/G	99.75	0.273
POLH	rs6941583	A/T	99.75	0.079
MAD2L2	rs2233004	G/A	99.25	0.090
	rs746218	G/A	92.48	0.211
	rs2233006	T/A	94.99	0.447
NFKB1	rs230529	A/G	95.99	0.491
	rs1585215	A/G	95.99	0.420
	rs4648068	A/G	99.75	0.474
NFKBIA	rs2233406	C/T	99.75	0.196
TNF	rs1800629	G/A	95.74	0.102
TNFRSF1A	rs4149570	T/G	95.74	0.487
	rs2234649	A/C	99.50	0.147
TNFRSF1B	rs1061622	T/G	99.50	0.247
FASN	rs1140616	C/T	97.49	0.372
	rs2228309	T/C	96.74	0.246
	rs4246445	A/G	97.99	0.453
	rs4485435	G/C	99.25	0.216

MAF, minor allele frequency.

calculated as the time between lung cancer diagnosis and follow-up or death.

Single Nucleotide Polymorphism Selection, DNA Extraction, and Genotyping

The SNPs genotyped in our study were *ERCC1* SNPs (rs2298881), *ERCC2* SNPs (rs1052555, rs238406), *ERCC4* SNP (rs1799801), *ERCC6* SNPs (rs2228527, rs3793784), *XPC* SNPs (rs2228000, rs2228001), *XRCC1* SNP (rs25489), *XRCC3* SNPs (rs1799794, rs861539), *BRCA1* SNP (rs799917), *BRCA2* SNPs (rs543304,rs206118), *RAD51* SNPs (rs12593359, rs1801320, rs1801321), *RAD52* SNPs (rs1051669, rs7963551), *POLH/POLR1C* SNP (rs6941583), *MAD2L2* SNPs (rs2233004, rs746218, rs2233006), *NFKB1* SNPs (rs230529, rs1585215, rs4648068), *NFKBIA* SNP (rs2233406), *TNF* SNP (rs1800629), *TNFRSF1A* SNPs (rs4149570, rs2234649), *TNFRSF1B* SNP (rs1061622), and *FASN* SNPs (rs1140616, rs2228309, rs4246445, rs4485435). Haploview was used to choose pair-wise tagging SNPs with pair wise r^2 threshold ≥0.8, and all SNPs had a minor allele frequency (MAF) greater than 0.05 (**Table 1**).

All blood samples were collected and stored in EDTA tubes. We used a genomic DNA Purification Kit (Promega) to extract genomic DNA. Genotyping of all SNPs was performed using the Sequenom MassARRAY Genotyping Platform (Sequenom, San Diego, CA, United States).

Statistical Analysis

Logistic regression was used to select covariates using the Cox proportional hazard model. The covariates included age, gender, histologic type, smoking status, clinical stage, and metastasis status. Three analysis models (additive model: compares major allele homozygotes versus heterozygotes versus minor allele homozygotes; dominant model: compares major allele homozygous versus combined heterozygotes and minor allele homozygous groups; recessive model: compares major allele-carrying genotypes with homozygous variant genotype) were used to calculate the associations between SNPs and prognosis. In the association analyses, we divided the patients into two or three groups by their genotypes of the SNPs. In additive model and dominant model, patients with wild type were used as a control group; and in recessive model, patients with wild type and heterozygote were used as a control group. The Cox proportional hazard regression analysis was used to analyze OS and PFS. All data were analyzed using SPSS 18.0 software (SPSS Inc., Chicago, IL, United States), PLINK (version 1.9, http://pngu.mgh.harvard.edu/purcell/plink/), and R 4.1.0. The associations between PFS or OS and SNPs were calculated as odds ratio (OR) and their 95% confidence intervals (95% CI) using unconditional logistic regression.

RESULTS

Demographic Characteristics of Patient Characteristics

Three hundred ninety-nine patients with lung cancer were enrolled in this study. All included patients had received platinum-based chemotherapy as the first-line treatment. The patients were 21–75 years old, with a median age of 56 years old. In this study, 317 (79.4%) patients were male and 82 (20.6%) were female. Furthermore, 152 (38.1%) patients were non-smokers and 247 (61.9%) were smokers. In addition, 311 (77.9%) patients had NSCLC and 88 (22.1%) had SCLC. Finally, 351 (88.0%) patients were at advanced stages (stage III/IV/ED), and the remaining 48 (12.0%) were at early stages (stage I/II/LD) (**Table 2**).

Association Between *MAD2L2* rs746218 and PFS in Patients With Lung Cancer

Multivariate Cox regression adjusted for age, gender, histology type, smoking status, stage, and metastasis showed that the *MAD2L2* rs746218 polymorphism was significantly related to PFS in patients with lung cancer in the recessive model ($p = 0.039$, OR = 5.31, and 95% CI = 1.09–25.93) (**Table 3**). Patients carrying the AG or AA genotype had a significantly longer PFS times than those carrying the GG genotype (**Figure 1A**). Compared with other SNPs, *MAD2L2* rs746218 was significantly associated with

TABLE 2 | Distribution of characteristics in patients with patients with lung cancer and prognosis analysis.

Variable	Patients (N%)	Death (N%)	MST-OS (year)	MST-PFS (year)
Age				
≤55	197 (49.4)	153 (77.6)	3.75	2.94
>55	202 (50.6)	168 (83.2)	4.67	4.37
Gender				
Male	317 (79.4)	256 (80.8)	4.39	3.87
Female	82 (20.6)	65 (79.3)	4.11	3.21
Histology				
NSCLC	311 (77.9)	256 (82.3)	4.34	3.26
SCLC	88 (22.1)	65 (73.9)	4.32	4.48
Smoking status				
Non-smoker	152 (38.1)	120 (78.9)	4.02	3.12
Smoker	247 (61.9)	200 (81.0)	4.45	3.91
Stage				
I/II/LD	48 (12.0)	36 (75.0)	5.00	4.38
III/IV/ED	351 (88.0)	281 (80.1)	4.31	3.34

MST, median survival time; LD, limitation disease; ED, extensive disease.

TABLE 3 | Association of the *MAD2L2* rs746218 polymorphisms and PFS in lung cancer patients.

Gene	Polymorphisms	Genotypes	MPFS (year)	Additive		Dominant		Recessive	
				OR (95%CI)	*p* value	OR (95%CI)	*p* value	OR (95%CI)	*p* value
MAD2L2	rs746218	GG	5.84	1.26 (0.84–1.90)	0.263	1.12 (0.7–1.78)	0.633	5.31 (1.09–25.9)	0.039*
		GA	3.67						
		AA	3.25						

MPFS, median progression-free survival; OR, odds ratio; CI, confidence interval; additive model: comparison between minor allele subjects and major allele subjects. Dominant model: comparison between minor allele carriers and major homozygous subjects. Recessive model: comparison between major allele carriers and minor homozygous subjects.

PFS in the recessive model analysis in patients with lung cancer who received platinum-based chemotherapy.

Association Between *TNFRSF1A* rs4149570 and OS in Patients With Lung Cancer

Univariate Cox regression analysis was used to evaluate OS, and the results were adjusted for age, gender, histology type, smoking status, stage, and metastasis status. As shown in **Table 4**, *TNFRSF1A* rs4149570 was associated with OS in patients with lung cancer in the dominant model (p = 0.030, OR = 0.57, and 95% CI = 0.34–0.95). In the dominant model, the OS of patients who carried the rs4149570 GG genotype was significantly longer than that of patients carrying the TT or GT genotypes (**Figure 1B**). Compared with other SNPs, *TNFRSF1A* rs4149570 was most significantly associated with OS in the dominant model in patients with lung cancer who received platinum-based chemotherapy.

Stratification Analyses

In the stratification analyses, age (≤56, >56), smoking status (no, yes), gender (male, female), histological type (NSCLC, SCLC), metastasis (no, yes), and Stage (I/II/LD, III/IV/ED) were evaluated as covariates for associations between SNPs and PFS. The following SNPs were significantly associated with PFS: *BRCA2* rs206118 in patients ≤56 years old (additive model: p = 0.039, OR = 0.56, and 95% CI = 0.33–0.97; dominant model: p = 0.041, OR = 0.52, and 95% CI = 0.27–0.97); *XRCC3* rs1799794 in patients >56 years old (dominant model p = 0.036, OR = 2.03, and 95% CI = 1.05–3.92); *NFKB1* rs230529 in patients >56 years old (recessive model p = 0.012, OR = 2.40, and 95% CI = 1.21–4.74) and *NFKB1* rs1585215 in patients with SCLC (recessive model: p = 0.045, OR = 14.66, and 95% CI = 1.06–203.60); *RAD52* rs7963551 in male patients (additive model: p = 0.046, OR = 1.49, and 95% CI = 1.01–2.22); *NFKBIA* rs2233406 (additive model: p = 0.029, OR = 6.73, and 95% CI = 1.22–37.16 dominant model: p = 0.029, OR = 6.73, 95% CI = 1.22–37.16); and *TNFRSF1A* rs4149570 in patients with lung cancer with stage III/IV cancer (dominant model: p = 0.050, OR = 0.26, and 95% CI = 0.07–1.00) (**Table 5**; **Figure 2**).

For OS stratification analyses, the results were as follows: *TNFRSF1A* rs4149570 in patients >56 years old (dominant model: p = 0.048, OR = 0.48, and 95% CI = 0.23–0.99); *TNFRSF1A* rs4149570 in patients with advanced stage cancer (additive model: p = 0.049, OR = 0.70, and 95% CI = 0.48–1.00; dominant model: p = 0.049, OR = 0.58, and 95% CI = 0.34–1.00); *XRCC3* rs1799794 in patients with SCLC (dominant model: p = 0.048, OR = 2.27, and 95% CI = 1.01–5.13); *XPC* rs2228000 in non-smokers (dominant model: p = 0.023, OR = 2.53, and 95% CI = 1.13–5.64); and *FASN* rs4246445 in non-smokers (dominant model: p = 0.043, OR = 0.43, 95% CI = 0.19–0.97) (**Table 6**; **Figure 3**).

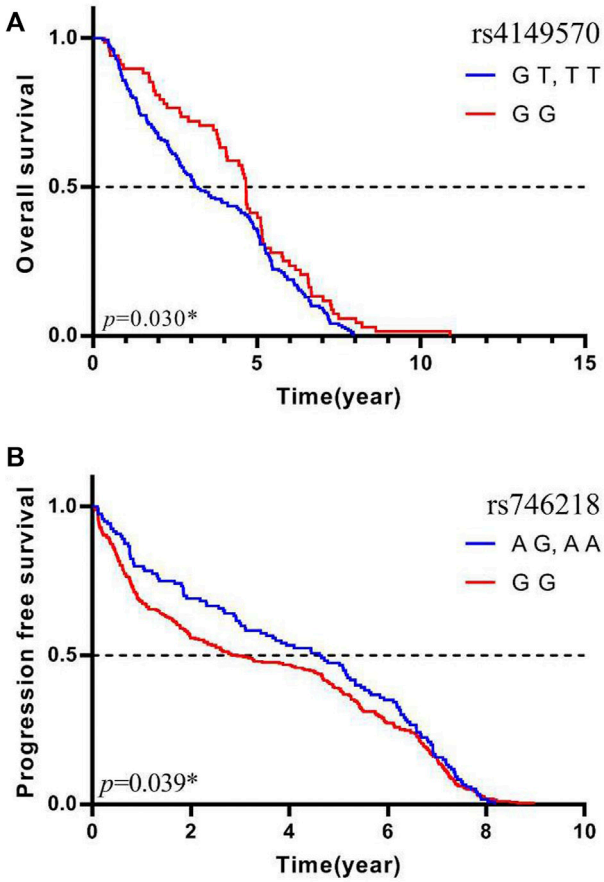


FIGURE 1 | *MAD2L2* rs746218 and *TNFRSF1A* rs4149570 were significantly associated with platinum-based chemotherapy prognosis in patients with lung cancer. **(A)** *TNFRSF1A* rs4149570 was significantly associated with OS. **(B)** *MAD2L2* rs746218 was significantly associated with PFS.

Our results showed that *MAD2L2* rs746218 and *TNFRSF1A* rs4149570 were significantly associated with prognosis in patients with lung cancer who received platinum-based chemotherapy. The PFS time of patients with GG genotype (Median PFS: 3.45 (0.10–9.17) years) of *MAD2L2* rs746218 was longer than that in patients with GA or AA genotypes (Median PFS: 2.56 (0.04–11.85) years). Furthermore, OS was longer in patients with the GG genotype of *TNFRSF1A* rs4149570 than that in patients with the AA or AG genotypes. In the subgroup analysis, *BRCA2* rs206118, *XRCC3* rs1799794, *NFKB1* rs230529, *RAD52* rs7963551, *NFKB1* rs1585215, *NFKBIA* rs2233406, and *TNFRSF1A* rs4149570 were associated with the PFS time. Patients younger than 56 years old with the TT or TC genotype of rs206118 had longer PFS times than those with the CC genotype. For *XRCC3* rs1799794, the AA and AG genotypes were associated with shorter PFS times in patients >56 years old. For *NFKB1* rs230529, the AA and AG genotypes were associated with longer PFS times in patients greater than 56 years old). For *NFKB1* rs1585215, patients with squamous cell carcinoma (SCC) patients carrying the GG genotype had significantly shorter PFS times. The TT and TG genotypes of *RAD52* rs7963551 were associated with significantly shorter PFS times compared with the GG genotype in male patients. For *NFKBIA* rs2233406, the CC and CT genotypes were associated with shorter PFS times than the TT genotype in patients with stage III/IV cancer. For *TNFRSF1A* rs4149570 in patients with stage III/IV cancer, the TT and TG genotypes were associated with longer PFS times than the GG genotype. In the subgroup analyses, *TNFRSF1A* rs4149570, *XRCC3* rs1799794, *XPC* rs2228000, and *FASN* rs4246445 were significantly associated with OS. In patients older than 56 years old, the TT and TG genotypes of *TNFRSF1A* rs4149570 were associated with longer OS than that associated with the GG genotype. For *TNFRSF1A* rs4149570, the TT and TG genotypes were associated with longer OS in patients with stage III/IV cancer. For *XRCC3* rs1799794, the GG genotype was associated with longer OS in patients with SCLC. Non-smokers with the GG or GA genotypes of *XPC* rs2228000 had shorter OS than those with the AA genotype. Non-smokers with the AA or AG genotypes of *FASN* rs4246445 had longer OS than those with the GG genotype.

DISCUSSION

Platinum chemotherapy is one of the most important approaches for treatment of lung cancer. Platinum agents are typically used in combination with other antitumor drugs, but efficacy is limited due to resistance (Garufi et al., 2020; Yu et al., 2020). The DNA repair system contributes to platinum resistance, which influences the curative effects of chemotherapy and negatively impacts the clinical outcomes (Simon et al., 2007; Sullivan et al., 2014; Jiang et al., 2019; Peng et al., 2020). Polymorphism research has shown that gene polymorphisms affect prognosis, the folate metabolism pathway, drug transporters, and metabolic enzymes. The DNA repair system is essential for maintaining genome

TABLE 4 | Association of the *TNFRSF1A* rs4149570 polymorphisms and OS in lung cancer patients.

Gene	Polymorphisms	Genotype	MST (year)	Additive		Dominant		Recessive	
				OR (95%CI)	*p* value	OR (95%CI)	*p* value	OR (95%CI)	*p* value
TNFRSF1A	rs4149570	TT	5.32	0.74 (0.53–1.04)	0.084	0.57 (0.34–0.95)	0.030*	0.86 (0.48–1.52)	0.594
		TG	3.53						
		GG	4.66						

MST, median survival time; OR, odds ratio; CI, confidence interval; Additive model: comparison between minor allele subjects and major allele subjects, Dominant model: comparison between minor allele carriers and major homozygous subjects, Recessive model: comparison between major allele carriers and minor homozygous subjects.

TABLE 5 | Stratification analyses of Association between the seven polymorphisms and PFS in lung cancer patients.

Genes	SNPs	Subgroups	Additive		Dominant		Recessive	
			OR (95%CI)	*p* value	OR (95%CI)	*p* value	OR (95%CI)	*p* value
BRCA2	rs206118	Age (≤56)	0.56 (0.33–0.97)	0.039*	0.52 (0.27–0.97)	0.041*	0.41 (0.08–2.05)	0.279
XRCC3	rs1799794	Age (>56)	1.38 (0.93–2.04)	0.112	2.03 (1.05–3.92)	0.036*	1.17 (0.61–2.25)	0.641
NFKB1	rs230529	Age (>56)	1.36 (0.90–2.06)	0.150	0.94 (0.48–1.82)	0.854	2.40 (1.21–4.74)	0.012*
	rs1585215	SCLC	1.78 (0.72–4.41)	0.216	1.13 (0.35–3.67)	0.840	14.66 (1.06–203.6)	0.045*
RAD52	rs7963551	Male	1.49 (1.01–2.22)	0.046*	1.52 (0.96–2.43)	0.077	2.29 (0.73–7.17)	0.154
NFKBIA	rs2233406	Stage (III/IV/ED)	6.73 (1.22–37.16)	0.029*	6.73 (1.22–37.16)	0.029*		
TNFRSF1A	rs4149570	Stage (III/IV/ED)	0.63 (0.28–1.43)	0.271	0.26 (0.07–1.00)	0.049*	1.19 (0.30–4.68)	0.803

Additive model: comparison between minor allele subjects and major allele subjects. Dominant model: comparison between minor allele carriers and major homozygous subjects. Recessive model: comparison between major allele carriers and minor homozygous subjects. OR, odds ratio; CI, confidence interval; p, p-*value for binary logistic regression analysis; Ref., reference.* *p < *0.05.*

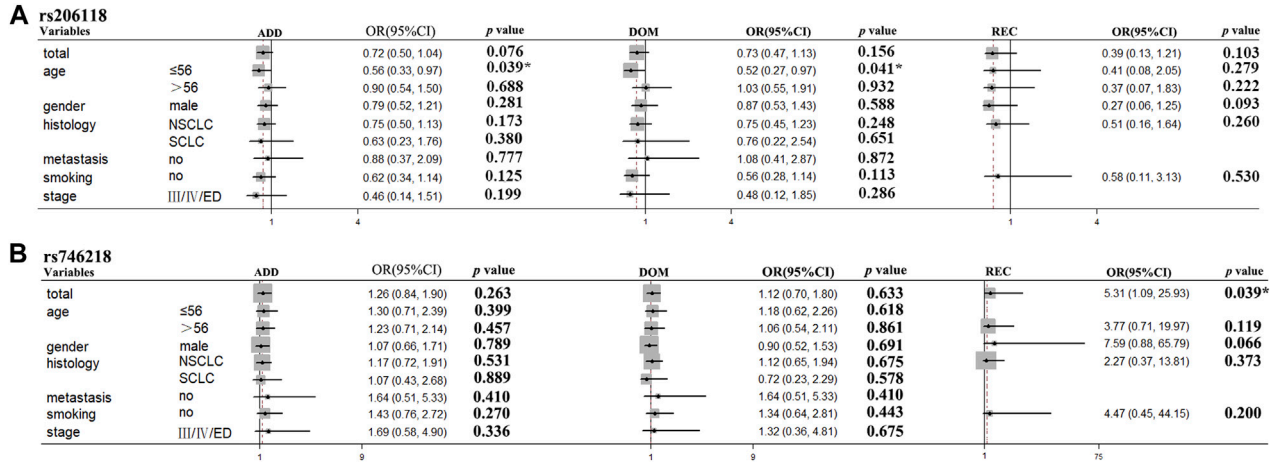


FIGURE 2 | *BRCA2* rs206118 and *MAD2L2* rs746218 polymorphisms were significantly associated with survival time in the subgroups of patients with lung cancer treated with platinum-based chemotherapy. **(A)** *BRCA2* rs206118 polymorphism was significantly associated with PFS time in patients less than 55 years of age. **(B)** *MAD2L2* rs746218 polymorphism was significantly associated with PFS time in patients treated with platinum-based chemotherapy.

TABLE 6 | Stratification analyses of association between the four polymorphisms and OS in lung cancer patients.

Genes	SNPs	Subgroups	Additive		Dominant		Recessive	
			OR (95%CI)	*p* value	OR (95%CI)	*p* value	OR (95%CI)	*p* value
TNFRSF1A	rs4149570	Age (>56)	0.73 (0.46–1.16)	0.180	0.48 (0.23–0.99)	0.048*	0.97 (0.45–2.10)	0.934
		Stage (III/IV/ED)	0.70 (0.48–1.00)	0.049*	0.58 (0.34–1.00)	0.049*	0.69 (0.37–1.29)	0.240
XRCC3	rs1799794	SCLC	2.27 (1.01–5.13)	0.048*	2.28 (0.71–7.30)	0.164	4.47 (0.97–20.71)	0.055
XPC	rs2228000	Non-smoker	1.70 (0.94–3.09)	0.081	2.53 (1.13–5.64)	0.023*	0.99 (0.27–3.63)	0.992
FASN	rs4246445	Non-smoker	0.72 (0.41–1.25)	0.242	0.43 (0.19–0.97)	0.043*	1.18 (0.45–3.08)	0.735

Additive model: comparison between minor allele subjects and major allele subjects. Dominant model: comparison between minor allele carriers and major homozygous subjects. Recessive model: comparison between major allele carriers and minor homozygous subjects. OR, odds ratio; CI, confidence interval; p, p-*value for binary logistic regression analysis; Ref., reference.* *p < *0.05.*

integrity and preventing genome instability-associated diseases, such as lung cancer (Chen et al., 2014; Anoushirvani et al., 2019; Zhao et al., 2020). Polymorphisms in DNA repair genes play a significant role in the ability to repair DNA damage. The relationship between repair gene polymorphisms and platinum chemoresistance has received a great deal of attention with regard to sensitivity of lung cancer to chemotherapy (Longhese et al., 2010; Li et al., 2018; Makovec, 2019; Schmid et al., 2020). In this study, DNA repair gene polymorphisms were studied to identify significant biomarkers for the prediction of platinum-based chemotherapy response.

In this study, we also investigated the correlations between 35 polymorphisms in 9 DNA repair genes (*XRCC3*, *BRCA2/ZAR1L*, *XPC*, *RAD52*, *MAD2L2*, *NFKB1*, *NFKBIA*, *TNFRSF1A*,

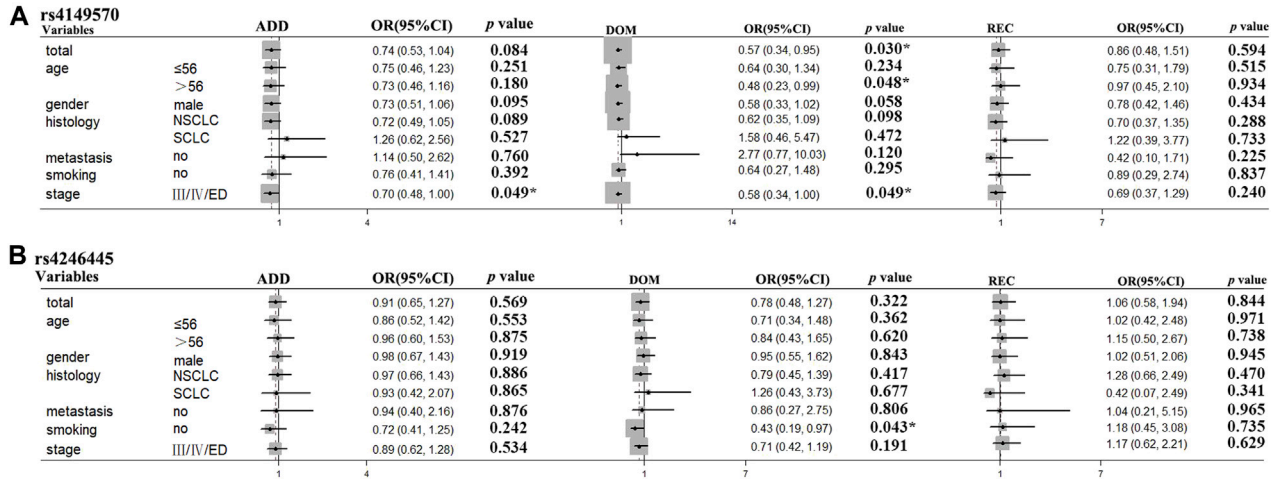


FIGURE 3 | *TNFRSF1A* rs4149570 and *FASN* rs4246445 polymorphisms were significantly associated with survival times in the subgroups of patients with lung cancer treated with platinum-based chemotherapy. **(A)** *TNFRSF1A* rs4149570 polymorphism was significantly associated with OS time in patients less than 55 years of age. **(B)** *FASN* rs4246445 polymorphism was significantly associated with PFS time in patients who received platinum-based chemotherapy.

and *FASN*) with platinum-based chemotherapy prognosis in 399 patients with lung cancer. A previous study showed that *XRCC3*, *BRCA2*, and *RAD52* were involved in the HR-mediated DBS repair. *XRCC3* is a *RAD51* paralog in the HR-mediated DBS repair pathway that assists *RAD51* with HR initiation (Brenneman et al., 2002). *BRCA2* is a tumor suppressor gene critical to multiple cellular processes including DNA repair, the cell cycle, and apoptosis (Cleary et al., 2020). Mutation of *BRCA2* was shown to promote tumor sensitivity towards PARP inhibitors (Farmer et al., 2005). In addition, *RAD52* has been shown to play a major role in facilitating restart of damaged replication forks (Mortensen et al., 2009). *XPC* is the main DNA damage sensor in NER, and *MAD2L2* is a controller of NHEJ-mediated DBS repair (Van Cuijk et al., 2015; Vassel et al., 2020). *NFKB1*, *NFKBIA*, *TNFRSF1A*, and *FASN* were found to be related to DNA repair, which affects tumor sensitivity to DNA-damaging agents (Chui et al., 2010; Bredel et al., 2011; Park et al., 2012; Jones and Infante, 2015). Gene variations in these genes have been reported to correlate to onset and progression of several types of tumors.

Our results showed that *MAD2L2* rs746218 and *TNFRSF1A* rs4149570 may be biomarkers for predicting the prognosis of patients with lung cancer in response to platinum-based chemotherapy. The *MAD2L2* gene, which is essential for DNA repair, localizes to uncapped telomeres and promotes the non-homologous end-joining (NHEJ)-mediated fusion of deprotected chromosome ends and genomic instability. In addition, *MAD2L2* can control DNA breaks by inhibiting 5' end resection (Tomida et al., 2015; Dai et al., 2020). The *TNFRSF1A* gene plays a crucial role in non-small cell lung cancer growth, invasion, and metastasis (Lee et al., 2010; Fujikawa et al., 2014; Hu et al., 2019). The *MAD2L2* containing new shield complex protein plays a critical role in the choice between homologous recombination (HR) and non-homologous end-joining (NHEJ)-mediated repair. Upregulation of *MAD2L2* (also known as *MAD2B* or *REV7*) decreases DNA end resection, which increases NHEJ and chromosomal abnormalities, resulting mitotic catastrophe in PARP inhibitor treated HR-proficient cells. In addition, *MAD2L2* can also inhibit end-resection in irradiation (IR)-induced DNA double-strand breaks (DSBs) (Boersma et al., 2015; Simonetta et al., 2018; De Krijger et al., 2021). *MAD2L2* accelerates end-joining of DNA double-strand breaks in several settings, including immunoglobulin class switch recombination through ATM kinase activity (Xu et al., 2015; Batenburg et al., 2017; Noordermeer et al., 2018). Previous studies showed that *MAD2L2* promoted DNA repair activity through 53BP1 and promotes NHEJ by inhibiting 5′ end resection downstream of RIF1 protein (Ghezraoui et al., 2018; Liang et al., 2020). Both *MAD2L2* Rs746218 and *TNFRSF1A* rs4149570 are upstream transcript variants, and might affect gene expression by interacting with promoters to influence gene transcription. Therefore, *MAD2L2* rs746218 could influence the choice between HR and NHEJ by affecting the expression of *MAD2L2*. In addition, the *TNFRSF1A* gene was shown to play a crucial role in NSCLS growth, invasion, and metastasis (Lee et al., 2010; Fujikawa et al., 2014; Hu et al., 2019). However, the mechanism by which the *TNFRSF1A* gene affects prognosis associated with platinum-based chemotherapy has not been characterized. Future studies should characterize the mechanism by which *MAD2L2* rs746218 participates in the double-strand break repair pathway and the mechanism by which the *TNFRSF1A* gene contributes to platinum chemoresistance. Characterization of these mechanisms may allow for the development of new drug candidates and more effective use of combination therapies including platinum-based drugs and DNA repair regulators.

Our study was subject to the following limitations. Our study was a single-center study, which limits the generalizability of the results. In addition, the small sample size resulted in a broad confidence interval for *MAD2L2*

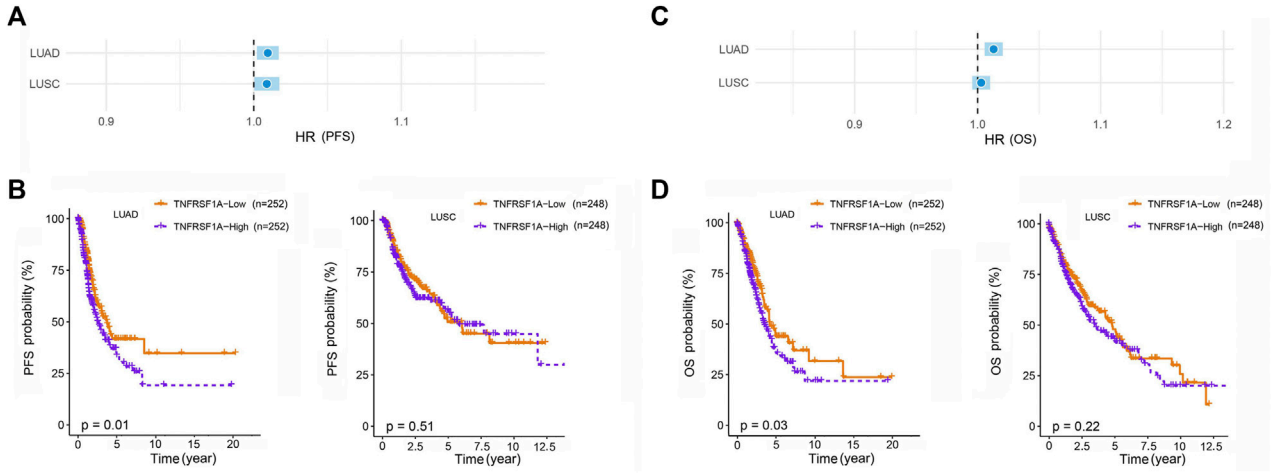


FIGURE 4 | Association of the expression of *TNFRSF1A* with lung cancer prognosis in patients with LUAD (Lung adenocarcinoma) and LUSC (Lung squamous cell carcinoma). Low expression of *TNFRSF1A* in patients with LUAD was associated with significantly longer **(A,B)** progression-free survival (PFS) and overall survival **(C,D)** (OS).

rs746218, and more samples are needed to confirm the results. Potential mechanisms by which *MAD2L2* rs746218 and *TNFRSF1A* rs4149570 impacted prognosis in patients with lung cancer who received platinum-based chemotherapy were determined using TCGA data (https://portal.gdc.cancer.gov/). This analysis showed that low expression of *TNFRSF1A* in LUAD (lung adenocarcinoma) was associated with significantly longer PFS and OS (**Figure 4**). However, the mechanisms of these effects require further investigation.

In summary, our study showed that *MAD2L2* rs746218 was significantly associated with platinum-based chemotherapy, and PFS and *TNFRSF1A* rs4149570 was significantly associated with OS time in patients with lung cancer treated with platinum-based chemotherapy. Polymorphisms of *MAD2L2* rs746218 and *TNFRSF1A* rs4149570 polymorphisms may be biomarkers for predicting prognosis in patients with lung cancer treated with platinum-based chemotherapy.

DATA AVAILABILITY STATEMENT

The original contributions presented in the study are included in the article/Supplementary Materials; further inquiries can be directed to the corresponding authors.

ETHICS STATEMENT

The studies involving human participants were reviewed and approved by the Ethics Committee of Xiangya Hospital, Central South University. The patients/participants provided their written informed consent to participate in this study.

AUTHOR CONTRIBUTIONS

Study design was contributed by JC, J-YL, and L-MT. J-YL, TZ, JC, and ZW took the lead in data collection and data analysis, assisted by CL, H-XH, F-XD, M-RL, ML, and YW. Data interpretation was performed by J-YL, with assistance from the other authors. The manuscript was written primarily by J-YL and TZ, and revised by J-YY, Z-QL, L-MT, and JC. All authors contributed to the article and approved the submitted version.

FUNDING

This work was supported by the National Nature Science Foundation of China (81803640, 81603207) and Hunan Provincial Natural Science Foundation of China (2020JJ5885).

REFERENCES

Alam, H., Tang, M., Maitituoheti, M., Dhar, S. S., Kumar, M., Han, C. Y., et al. (2020). KMT2D Deficiency Impairs Super-enhancers to Confer a Glycolytic Vulnerability in Lung Cancer. *Cancer Cell* 37, 599. doi:10.1016/j.ccell.2020.03.005

Almohaini, M., Chalasani, S. L., Bafail, D., Akopiants, K., Zhou, T., Yannone, S. M., et al. (2016). Nonhomologous End Joining of Complex DNA Double-Strand Breaks with Proximal Thymine Glycol and Interplay with Base Excision Repair. *DNA Repair (Amst)* 41, 16–26. doi:10.1016/j.dnarep.2016.03.003

Andres, S. N., Schellenberg, M. J., Wallace, B. D., Tumbale, P., and Williams, R. S. (2015). Recognition and Repair of Chemically Heterogeneous Structures at DNA Ends. *Environ. Mol. Mutagen* 56, 1–21. doi:10.1002/em.21892

Anoushirvani, A. A., Aghabozorgi, R., Ahmadi, A., Arjomandzadegan, M., Khalili, S., Sahraei, M., et al. (2019). The Relationship between rs3212986C>A Polymorphism and Tumor Stage in Lung Cancer Patients. *Cureus* 11, e4423. doi:10.7759/cureus.4423

Arbour, K. C., and Riely, G. J. (2019). Systemic Therapy for Locally Advanced and Metastatic Non-small Cell Lung Cancer: A Review. *JAMA* 322, 764–774. doi:10.1001/jama.2019.11058

Batenburg, N. L., Walker, J. R., Noordermeer, S. M., Moatti, N., Durocher, D., and Zhu, X. D. (2017). ATM and CDK2 Control Chromatin Remodeler CSB to Inhibit RIF1 in DSB Repair Pathway Choice. *Nat. Commun.* 8, 1921. doi:10.1038/s41467-017-02114-x

Boersma, V., Moatti, N., Segura-Bayona, S., Peuscher, M. H., Van Der Torre, J., Wevers, B. A., et al. (2015). MAD2L2 Controls DNA Repair at Telomeres and DNA Breaks by Inhibiting 5' End Resection. *Nature* 521, 537–540. doi:10.1038/nature14216

Bredel, M., Scholtens, D. M., Yadav, A. K., Alvarez, A. A., Renfrow, J. J., Chandler, J. P., et al. (2011). NFKBIA Deletion in Glioblastomas. *N. Engl. J. Med.* 364, 627–637. doi:10.1056/NEJMoa1006312

Brenneman, M. A., Wagener, B. M., Miller, C. A., Allen, C., and Nickoloff, J. A. (2002). XRCC3 Controls the Fidelity of Homologous Recombination: Roles for XRCC3 in Late Stages of Recombination. *Mol. Cell* 10, 387–395. doi:10.1016/s1097-2765(02)00595-6

Cescon, D. W., She, D., Sakashita, S., Zhu, C. Q., Pintilie, M., Shepherd, F. A., et al. (2015). NRF2 Pathway Activation and Adjuvant Chemotherapy Benefit in Lung Squamous Cell Carcinoma. *Clin. Cancer Res.* 21, 2499–2505. doi:10.1158/1078-0432.CCR-14-2206

Chen, J., Wu, L., Wang, Y., Yin, J., Li, X., Wang, Z., et al. (2016). Effect of Transporter and DNA Repair Gene Polymorphisms to Lung Cancer Chemotherapy Toxicity. *Tumour Biol.* 37, 2275–2284. doi:10.1007/s13277-015-4048-0

Chen, J., Yin, J., Li, X., Wang, Y., Zheng, Y., Qian, C., et al. (2014). WISP1 Polymorphisms Contribute to Platinum-Based Chemotherapy Toxicity in Lung Cancer Patients. *Int. J. Mol. Sci.* 15, 21011–21027. doi:10.3390/ijms151121011

Chui, Y. L., Ching, A. K., Chen, S., Yip, F. P., Rowlands, D. K., James, A. E., et al. (2010). BRE Over-expression Promotes Growth of Hepatocellular Carcinoma. *Biochem. Biophys. Res. Commun.* 391, 1522–1525. doi:10.1016/j.bbrc.2009.12.111

Cleary, J. M., Aguirre, A. J., Shapiro, G. I., and D'andrea, A. D. (2020). Biomarker-Guided Development of DNA Repair Inhibitors. *Mol. Cell* 78, 1070–1085. doi:10.1016/j.molcel.2020.04.035

Dai, Y., Zhang, F., Wang, L., Shan, S., Gong, Z., and Zhou, Z. (2020). Structural Basis for Shieldin Complex Subunit 3-mediated Recruitment of the Checkpoint Protein REV7 during DNA Double-Strand Break Repair. *J. Biol. Chem.* 295, 250–262. doi:10.1074/jbc.RA119.011464

De Krijger, I., Föhr, B., Pérez, S. H., Vincendeau, E., Serrat, J., Thouin, A. M., et al. (2021). MAD2L2 Dimerization and TRIP13 Control Shieldin Activity in DNA Repair. *Nat. Commun.* 12, 5421. doi:10.1038/s41467-021-25724-y

Ettinger, D. S., Wood, D. E., Aggarwal, C., Aisner, D. L., Akerley, W., Bauman, J. R., et al. (2019). NCCN Guidelines Insights: Non-small Cell Lung Cancer, Version 1.2020. *J. Natl. Compr. Canc Netw.* 17, 1464–1472. doi:10.6004/jnccn.2019.0059

Farmer, H., Mccabe, N., Lord, C. J., Tutt, A. N., Johnson, D. A., Richardson, T. B., et al. (2005). Targeting the DNA Repair Defect in BRCA Mutant Cells as a Therapeutic Strategy. *Nature* 434, 917–921. doi:10.1038/nature03445

Fujikawa, K., Migita, K., Shigemitsu, Y., Umeda, M., Nonaka, F., Tamai, M., et al. (2014). MEFV Gene Polymorphisms and TNFRSF1A Mutation in Patients with Inflammatory Myopathy with Abundant Macrophages. *Clin. Exp. Immunol.* 178, 224–228. doi:10.1111/cei.12407

Garufi, G., Palazzo, A., Paris, I., Orlandi, A., Cassano, A., Tortora, G., et al. (2020). Neoadjuvant Therapy for Triple-Negative Breast Cancer: Potential Predictive Biomarkers of Activity and Efficacy of Platinum Chemotherapy, PARP- and Immune-Checkpoint-Inhibitors. *Expert Opin. Pharmacother.* 21, 687–699. doi:10.1080/14656566.2020.1724957

Ghezraoui, H., Oliveira, C., Becker, J. R., Bilham, K., Moralli, D., Anzilotti, C., et al. (2018). 53BP1 Cooperation with the REV7-Shieldin Complex Underpins DNA Structure-specific NHEJ. *Nature* 560, 122–127. doi:10.1038/s41586-018-0362-1

Gupta, R., Somyajit, K., Narita, T., Maskey, E., Stanlie, A., Kremer, M., et al. (2018). DNA Repair Network Analysis Reveals Shieldin as a Key Regulator of NHEJ and PARP Inhibitor Sensitivity. *Cell* 173, 972. doi:10.1016/j.cell.2018.03.050

Hirsch, F. R., Scagliotti, G. V., Mulshine, J. L., Kwon, R., Curran, W. J., Jr., Wu, Y. L., et al. (2017). Lung Cancer: Current Therapies and New Targeted Treatments. *Lancet* 389, 299–311. doi:10.1016/S0140-6736(16)30958-8

Hu, Z., Li, H., Xie, R., Wang, S., Yin, Z., and Liu, Y. (2019). Genomic Variant in Porcine TNFRSF1A Gene and its Effects on TNF Signaling Pathway *In Vitro*. *Gene* 700, 105–109. doi:10.1016/j.gene.2019.03.046

Huang, J., and Dynan, W. S. (2002). Reconstitution of the Mammalian DNA Double-Strand Break End-Joining Reaction Reveals a Requirement for an Mre11/Rad50/NBS1-Containing Fraction. *Nucleic Acids Res.* 30, 667–674. doi:10.1093/nar/30.3.667

Jiang, M., Jia, K., Wang, L., Li, W., Chen, B., Liu, Y., et al. (2021). Alterations of DNA Damage Response Pathway: Biomarker and Therapeutic Strategy for Cancer Immunotherapy. *Acta Pharm. Sin. B* 11, 2983–2994. doi:10.1016/j.apsb.2021.01.003

Jiang, Y., Dai, H., Li, Y., Yin, J., Guo, S., Lin, S. Y., et al. (2019). PARP Inhibitors Synergize with Gemcitabine by Potentiating DNA Damage in Non-small-cell Lung Cancer. *Int. J. Cancer* 144, 1092–1103. doi:10.1002/ijc.31770

Jones, S. F., and Infante, J. R. (2015). Molecular Pathways: Fatty Acid Synthase. *Clin. Cancer Res.* 21, 5434–5438. doi:10.1158/1078-0432.CCR-15-0126

Kalemkerian, G. P., Loo, B. W., Akerley, W., Attia, A., Bassetti, M., Boumber, Y., et al. (2018). NCCN Guidelines Insights: Small Cell Lung Cancer, Version 2.2018. *J. Natl. Compr. Canc Netw.* 16, 1171–1182. doi:10.6004/jnccn.2018.0079

Kryczka, J., Kryczka, J., Czarnecka-Chrebelska, K. H., and Brzeziańska-Lasota, E. (2021). Molecular Mechanisms of Chemoresistance Induced by Cisplatin in NSCLC Cancer Therapy. *Int. J. Mol. Sci.* 22, 8885. doi:10.3390/ijms22168885

Kulkarni, S., Vella, E. T., Coakley, N., Cheng, S., Gregg, R., Ung, Y. C., et al. (2016). The Use of Systemic Treatment in the Maintenance of Patients with Non-small Cell Lung Cancer: A Systematic Review. *J. Thorac. Oncol.* 11, 989–1002. doi:10.1016/j.jtho.2016.03.007

Lee, E. B., Jeon, H. S., Yoo, S. S., Choi, Y. Y., Kang, H. G., Cho, S., et al. (2010). Polymorphisms in Apoptosis-Related Genes and Survival of Patients with Early-Stage Non-small-cell Lung Cancer. *Ann. Surg. Oncol.* 17, 2608–2618. doi:10.1245/s10434-010-1082-4

Li, Y. Q., Chen, J., Yin, J. Y., Liu, Z. Q., and Li, X. P. (2018). Gene Expression and Single Nucleotide Polymorphism of ATP7B Are Associated with Platinum-Based Chemotherapy Response in Non-small Cell Lung Cancer Patients. *J. Cancer* 9, 3532–3539. doi:10.7150/jca.26286

Liang, L., Feng, J., Zuo, P., Yang, J., Lu, Y., and Yin, Y. (2020). Molecular Basis for Assembly of the Shieldin Complex and its Implications for NHEJ. *Nat. Commun.* 11, 1972. doi:10.1038/s41467-020-15879-5

Longhese, M. P., Bonetti, D., Manfrini, N., and Clerici, M. (2010). Mechanisms and Regulation of DNA End Resection. *EMBO J.* 29, 2864–2874. doi:10.1038/emboj.2010.165

Low, H. B., Wong, Z. L., Wu, B., Kong, L. R., Png, C. W., Cho, Y. L., et al. (2021). DUSP16 Promotes Cancer Chemoresistance through Regulation of Mitochondria-Mediated Cell Death. *Nat. Commun.* 12, 2284. doi:10.1038/s41467-021-22638-7

Makovec, T. (2019). Cisplatin and beyond: Molecular Mechanisms of Action and Drug Resistance Development in Cancer Chemotherapy. *Radiol. Oncol.* 53, 148–158. doi:10.2478/raon-2019-0018

Menon, V., and Povirk, L. F. (2017). XLF/Cernunnos: An Important but Puzzling Participant in the Nonhomologous End Joining DNA Repair Pathway. *DNA Repair (Amst)* 58, 29–37. doi:10.1016/j.dnarep.2017.08.003

Mortensen, U. H., Lisby, M., and Rothstein, R. (2009). Rad52. *Curr. Biol.* 19, R676–R677. doi:10.1016/j.cub.2009.06.001

Noordermeer, S. M., Adam, S., Setiaputra, D., Barazas, M., Pettitt, S. J., Ling, A. K., et al. (2018). The Shieldin Complex Mediates 53BP1-dependent DNA Repair. *Nature* 560, 117–121. doi:10.1038/s41586-018-0340-7

Park, Y. Y., Jung, S. Y., Jennings, N. B., Rodriguez-Aguayo, C., Peng, G., Lee, S. R., et al. (2012). FOXM1 Mediates Dox Resistance in Breast Cancer by Enhancing DNA Repair. *Carcinogenesis* 33, 1843–1853. doi:10.1093/carcin/bgs167

Parkin, D. M., Pisani, P., and Ferlay, J. (1999). Global Cancer Statistics. *CA Cancer J. Clin.* 49, 3331. doi:10.3322/canjclin.49.1.33

Peng, S., Sun, Y., Luo, Y., Ma, S., Sun, W., Tang, G., et al. (2020). MFP-FePt-GO Nanocomposites Promote Radiosensitivity of Non-small Cell Lung Cancer via Activating Mitochondrial-Mediated Apoptosis and Impairing DNA Damage Repair. *Int. J. Biol. Sci.* 16, 2145–2158. doi:10.7150/ijbs.46194

Reid, D. A., Conlin, M. P., Yin, Y., Chang, H. H., Watanabe, G., Lieber, M. R., et al. (2017). Bridging of Double-Stranded Breaks by the Nonhomologous End-Joining Ligation Complex Is Modulated by DNA End Chemistry. *Nucleic Acids Res.* 45, 1872–1878. doi:10.1093/nar/gkw1221

Rottenberg, S., Disler, C., and Perego, P. (2021). The Rediscovery of Platinum-Based Cancer Therapy. *Nat. Rev. Cancer* 21, 37–50. doi:10.1038/s41568-020-00308-y

Schmid, S., Omlin, A., Higano, C., Sweeney, C., Martinez Chanza, N., Mehra, N., et al. (2020). Activity of Platinum-Based Chemotherapy in Patients with Advanced Prostate Cancer with and without DNA Repair Gene Aberrations. *JAMA Netw. Open* 3, e2021692. doi:10.1001/jamanetworkopen.2020.21692

Schwartz, A. G., and Cote, M. L. (2016). Epidemiology of Lung Cancer. *Adv. Exp. Med. Biol.* 893, 21–41. doi:10.1007/978-3-319-24223-1_2

Shi, Y., and Sun, Y. (2015). Medical Management of Lung Cancer: Experience in China. *Thorac. Cancer* 6, 10–16. doi:10.1111/1759-7714.12168

Siegel, R. L., Miller, K. D., Fuchs, H. E., and Jemal, A. (2021). Cancer Statistics, 2021. *CA A Cancer J. Clin.* 71, 7–33. doi:10.3322/caac.21654

Simon, G. R., Ismail-Khan, R., and Bepler, G. (2007). Nuclear Excision Repair-Based Personalized Therapy for Non-small Cell Lung Cancer: from Hypothesis to Reality. *Int. J. Biochem. Cell Biol.* 39, 1318–1328. doi:10.1016/j.biocel.2007.05.006

Simonetta, M., De Krijger, I., Serrat, J., Moatti, N., Fortunato, D., Hoekman, L., et al. (2018). H4K20me2 Distinguishes Pre-replicative from Post-replicative Chromatin to Appropriately Direct DNA Repair Pathway Choice by 53BP1-RIF1-Mad2l2. *Cell Cycle* 17, 124–136. doi:10.1080/15384101.2017.1404210

Sullivan, I., Salazar, J., Majem, M., Pallarés, C., Del Río, E., Páez, D., et al. (2014). Pharmacogenetics of the DNA Repair Pathways in Advanced Non-small Cell Lung Cancer Patients Treated with Platinum-Based Chemotherapy. *Cancer Lett.* 353, 160–166. doi:10.1016/j.canlet.2014.07.023

Thai, A. A., Solomon, B. J., Sequist, L. V., Gainor, J. F., and Heist, R. S. (2021). Lung Cancer. *Lancet* 398, 535–554. doi:10.1016/S0140-6736(21)00312-3

Tomida, J., Takata, K., Lange, S. S., Schibler, A. C., Yousefzadeh, M. J., Bhetawal, S., et al. (2015). REV7 Is Essential for DNA Damage Tolerance via Two REV3L Binding Sites in Mammalian DNA Polymerase ζ. *Nucleic Acids Res.* 43, 1000–1011. doi:10.1093/nar/gku1385

Van Cuijk, L., Van Belle, G. J., Turkyilmaz, Y., Poulsen, S. L., Janssens, R. C., Theil, A. F., et al. (2015). SUMO and Ubiquitin-dependent XPC Exchange Drives Nucleotide Excision Repair. *Nat. Commun.* 6, 7499. doi:10.1038/ncomms8499

Vassel, F. M., Bian, K., Walker, G. C., and Hemann, M. T. (2020). Rev7 Loss Alters Cisplatin Response and Increases Drug Efficacy in Chemotherapy-Resistant Lung Cancer. *Proc. Natl. Acad. Sci. U. S. A.* 117, 28922–28924. doi:10.1073/pnas.2016067117

Xing, M., Yang, M., Huo, W., Feng, F., Wei, L., Jiang, W., et al. (2015). Interactome Analysis Identifies a New Paralogue of XRCC4 in Non-homologous End Joining DNA Repair Pathway. *Nat. Commun.* 6, 6233. doi:10.1038/ncomms7233

Xu, G., Chapman, J. R., Brandsma, I., Yuan, J., Mistrik, M., Bouwman, P., et al. (2015). REV7 Counteracts DNA Double-Strand Break Resection and Affects PARP Inhibition. *Nature* 521, 541–544. doi:10.1038/nature14328

Xu, Y., and Xu, D. (2020). Repair Pathway Choice for Double-Strand Breaks. *Essays Biochem.* 64, 765–777. doi:10.1042/EBC20200007

Yin, J. Y., Li, X., Zhou, H. H., and Liu, Z. Q. (2016). Pharmacogenomics of Platinum-Based Chemotherapy Sensitivity in NSCLC: toward Precision Medicine. *Pharmacogenomics* 17, 1365–1378. doi:10.2217/pgs-2016-0074

Yu, C., Wang, Z., Sun, Z., Zhang, L., Zhang, W., Xu, Y., et al. (2020). Platinum-Based Combination Therapy: Molecular Rationale, Current Clinical Uses, and Future Perspectives. *J. Med. Chem.* 63, 13397–13412. doi:10.1021/acs.jmedchem.0c00950

Zhao, L., Bao, C., Shang, Y., He, X., Ma, C., Lei, X., et al. (2020). The Determinant of DNA Repair Pathway Choices in Ionising Radiation-Induced DNA Double-Strand Breaks. *Biomed. Res. Int.* 2020, 4834965. doi:10.1155/2020/4834965

Zugazagoitia, J., and Paz-Ares, L. (2022). Extensive-Stage Small-Cell Lung Cancer: First-Line and Second-Line Treatment Options. *J. Clin. Oncol.* 40, 671–680. doi:10.1200/jco.21.01881

Conflict of Interest: The authors declare that the research was conducted in the absence of any commercial or financial relationships that could be construed as a potential conflict of interest.

Publisher's Note: All claims expressed in this article are solely those of the authors and do not necessarily represent those of their affiliated organizations, or those of the publisher, the editors, and the reviewers. Any product that may be evaluated in this article, or claim that may be made by its manufacturer, is not guaranteed or endorsed by the publisher.

Copyright © 2022 Liu, Zou, Yin, Wang, Liu, Huang, Ding, Lei, Wang, Liu, Liu, Tan and Chen. This is an open-access article distributed under the terms of the Creative Commons Attribution License (CC BY). The use, distribution or reproduction in other forums is permitted, provided the original author(s) and the copyright owner(s) are credited and that the original publication in this journal is cited, in accordance with accepted academic practice. No use, distribution or reproduction is permitted which does not comply with these terms.

frontiers | Frontiers in Pharmacology

MINI REVIEW
published: 12 July 2022
doi: 10.3389/fphar.2022.949001

Nanodrugs Manipulating Endoplasmic Reticulum Stress for Highly Effective Antitumor Therapy

Yuting Xiang[1,2†], Min Liu[3,4†], Yunrong Yang[3,4], Yubo Wang[1,2], Yige Qiu[1,2], Shiqi Tu[1,2], Yitian Jiang[1], Yayun Nan[5], Xiaojie Zhang[1,2] and Qiong Huang[3,4]**

[1]Xiangya School of Pharmaceutical Sciences, Central South University, Changsha, China, [2]Hunan Provincial Key Laboratory of Cardiovascular Research, Xiangya School of Pharmaceutical Sciences, Central South University, Changsha, China, [3]Department of Pharmacy, Xiangya Hospital, Central South University, Changsha, China, [4]National Clinical Research Center for Geriatric Disorders, Xiangya Hospital, Central South University, Changsha, China, [5]Geriatric Medical Center, People's Hospital of Ningxia Hui Autonomous Region, Yinchuan, China

Cancer is one of the leading causes of death worldwide due to high morbidity and mortality. Many attempts and efforts have been devoted to fighting cancer. Owing to the significant role of the endoplasmic reticulum (ER) in cell function, inducing ER stress can be promising for cancer treatment. However, the sustained activation of cytoprotective unfolded protein response (UPR) presents a tremendous obstacle for drugs in inducing unsolved ER stress in tumor cells, especially small-molecule drugs with poor bioavailability. Therefore, many emerging nanodrugs inducing and amplifying ER stress have been developed for efficient cancer treatment. More importantly, the novel discovery of ER stress in immunogenic cell death (ICD) makes it possible to repurpose antitumor drugs for immunotherapy through nanodrug-based strategies amplifying ER stress. Therefore, this mini-review aims to provide a comprehensive summary of the latest developments of the strategies underlying nanodrugs in the treatment of cancer *via* manipulating ER stress. Meanwhile, the prospects of ER stress–inducing nanodrugs for cancer treatment are systematically discussed, which provide a sound platform for novel therapeutic insights and inspiration for the design of nanodrugs in treating cancer.

Keywords: endoplasmic reticulum stress, tumor, immunogenic cell death, nanodrugs, photodynamic therapy

OPEN ACCESS

Edited by:
Zeming Liu,
The Huazhong University of Science and Technology, China

Reviewed by:
Wu-Yi Sun,
Anhui Medical University, China
Jianhua Liu,
The Second Affiliated Hospital of Jilin University, China

****Correspondence:***
Qiong Huang
qionghuang@csu.edu.cn
Xiaojie Zhang
803375@csu.edu.cn

[†]These authors have contributed equally to this work

Specialty section:
This article was submitted to Pharmacology of Anti-Cancer Drugs, a section of the journal Frontiers in Pharmacology

Received: *20 May 2022*
Accepted: *09 June 2022*
Published: *12 July 2022*

Citation:
Xiang Y, Liu M, Yang Y, Wang Y, Qiu Y, Tu S, Jiang Y, Nan Y, Zhang X and Huang Q (2022) Nanodrugs Manipulating Endoplasmic Reticulum Stress for Highly Effective Antitumor Therapy. Front. Pharmacol. 13:949001. doi: 10.3389/fphar.2022.949001

INTRODUCTION

Consistently, cancer treatment is a long-standing conundrum within the field of medicine. Currently, the main treatment modalities for cancer are still based on chemotherapy, radiotherapy, and surgery. However, these traditional treatments elicit significant side effects and even tissue damage. For example, chemotherapy often causes severe hepatotoxicity and nephrotoxicity (Zhao et al., 2018; Zhao et al., 2022a; Liu et al., 2022; Xiao et al., 2022), which are responsible for severe deleterious hepatic and renal dysfunctions in patients. Therapeutic strategies targeting key organelles have attracted considerable attention, on account of the important role of organelles in maintaining the normal physiological function of cells. The endoplasmic reticulum (ER) is a central organelle that carries out many important functions such as synthesizing and folding proteins, modifying secreted and transmembrane proteins, regulating lipid synthesis and metabolism, storing calcium, and mediating signal transduction (King and Wilson, 2020). In addition, ER is closely apposed and dynamically tethered to other organelles through membrane networks, such as the nucleus,

TABLE 1 | Nanodrugs manipulating ER stress for highly effective antitumor therapy.

Category	Nanodrugs	Factors that induce or amplify ER stress	Tumor/ER-targeting strategies	Ref.
ER stress–inducing nanodrugs for cancer treatment				
In situ formation–based ER-targeted nanoparticles	Phosphotetrapeptide (1P)-based assemblies	\	d-phosphotyrosine	Feng et al. (2018)
	branched peptide (1)–based assemblies	\	KYDKKKKDG substance	Kim et al. (2021)
	1-Nap nanofiber	\	RVRR substance	Fu et al. (2020)
Nanocarriers with small-molecule drugs	Cc/Glt NM	Curcumin	\	Cheng et al. (2020)
	PRN@MSN	Propranolol; Mesoporous silica nanoparticle	\	Wu et al. (2020)
	GNS@MSNs-FA/Ly	Gold nanostars; Lycorine	Folate	Hu et al. (2021)
Multifunctional photosensitizer–based nanodrugs	Ru-1@TPP-PEG-biotin SAN	Ruthenium complex 1; Tetraphenylporphyrin	Biotin	Purushothaman et al. (2020)
	RDDG/DC	2-deoxy-glucose; Dithiophene-benzotriazole groups	ROS-sensitive bond	Dong et al. (2019)
Nanodrug-based strategies to amplify ER stress for immunotherapy				
ER-targeting nanodrugs based on ICD inducers	Ds-sP/TCPP-TER NPs	Meso-tetra(4-carboxyphenyl) porphyrin	Reduction-sensitive polymeric;	Deng et al. (2020)
	FAL-ICG-HAuNS	Indocyanine green; Gold nanospheres	*p*-toluene sulfonyl group Pardaxin peptides	Li et al. (2019)
ER stress–inducing nanodrugs combined with ICD inducers	3-NPs	Cisplatin; Adjudin; WKYMVm	pH sensitivity; GSH sensitivity	Liu et al. (2019)
	ETP-PtFeNP	Oxaliplatin; Magnetic nanoparticle	α-enolase targeting peptide	Chen et al. (2019)

mitochondria, and Golgi apparatus (Chen and Cubillos-Ruiz, 2021). Once the ER is injured, the physiology of the entire cell gets adversely affected. Therefore, the tightly regulated process of ER function is crucial for cell fate determination.

Many factors, such as intracellular reactive oxygen species (ROS) and nutrient deprivation, disturb ER functioning in inducing ER stress based on the accumulation of unfolded and misfolded proteins in the ER (Yao et al., 2017). The initial adaptive mechanisms such as unfolded protein response (UPR) in tumor cells provide a possibility to restore and maintain protein homeostasis, but unsolved ER stress still leads to cell death (Chen and Cubillos-Ruiz, 2021). Some clinical chemotherapeutics are found to be associated with ER stress induction, while the upregulation of UPR promotes resistance (Bahar et al., 2019). Therefore, many drugs have been proposed to induce and exacerbate severe ER stress in killing tumor cells as potential therapeutics. For example, molecular chaperone binding immunoglobulin (BiP), an ER stress sensor, is highly expressed in mediating tumor chemotherapy resistance by activating UPR to restore ER homeostasis in cancer cells (Hetz et al., 2020). Currently, many BiP inhibitors have been developed for killing tumors, such as KP1339 (Wernitznig et al., 2019) and HA15 (Cerezo et al., 2016).

However, the clinical application of these ER-targeted small-molecule drugs faces great bottlenecks, such as the lack of tumor targeting and strong side effects. The development of nanodrugs offers a possibility to address the dilemma in traditional drugs (Shi et al., 2021). The enhanced penetration and retention (EPR) effects mediate the accumulation of nanodrugs at tumor sites (Huang et al., 2022) to reduce the risk of toxicity in normal tissues. Moreover, nanodrugs can be modified with specific ligands targeting tumor cells or ER (Li et al., 2020) to further improve the enrichment of nanodrugs in tumor sites (Yang et al., 2022) and anticancer efficacy. Notably, nanodrugs can induce immunogenic cell death (ICD) to effectively improve immunotherapy by amplifying ER stress. Specifically, when the nanodrugs disrupt the ER, ER stress induces imbalances in calcium homeostasis, and calreticulin (CRT) transfers from the ER to the cell membrane to act as an "eat-me" signal, inducing inflammatory cell infiltration and enhancing tumor cell antigens presented.

To our knowledge, no similar reviews have been published in summarizing newly developed nanodrugs based on ER stress for cancer treatment. Herein, this review covers the recent progress in oncology therapeutics about nanodrugs for ER stress induction, recapitulating the design of nanodrugs that induce ER stress, together with the strategies of nanodrugs that amplify ER stress to repurpose antitumor drugs for cancer immunotherapy (**Figure 1**) (**Table 1**). Finally, the obstacles and prospects of ER stress–based nanodrugs for cancer treatment are discussed.

ENDOPLASMIC RETICULUM STRESS–INDUCING NANODRUGS FOR CANCER TREATMENT

ER stress is a cellular condition characterized by the unsolved accumulation of misfolded proteins, which is detrimental to the

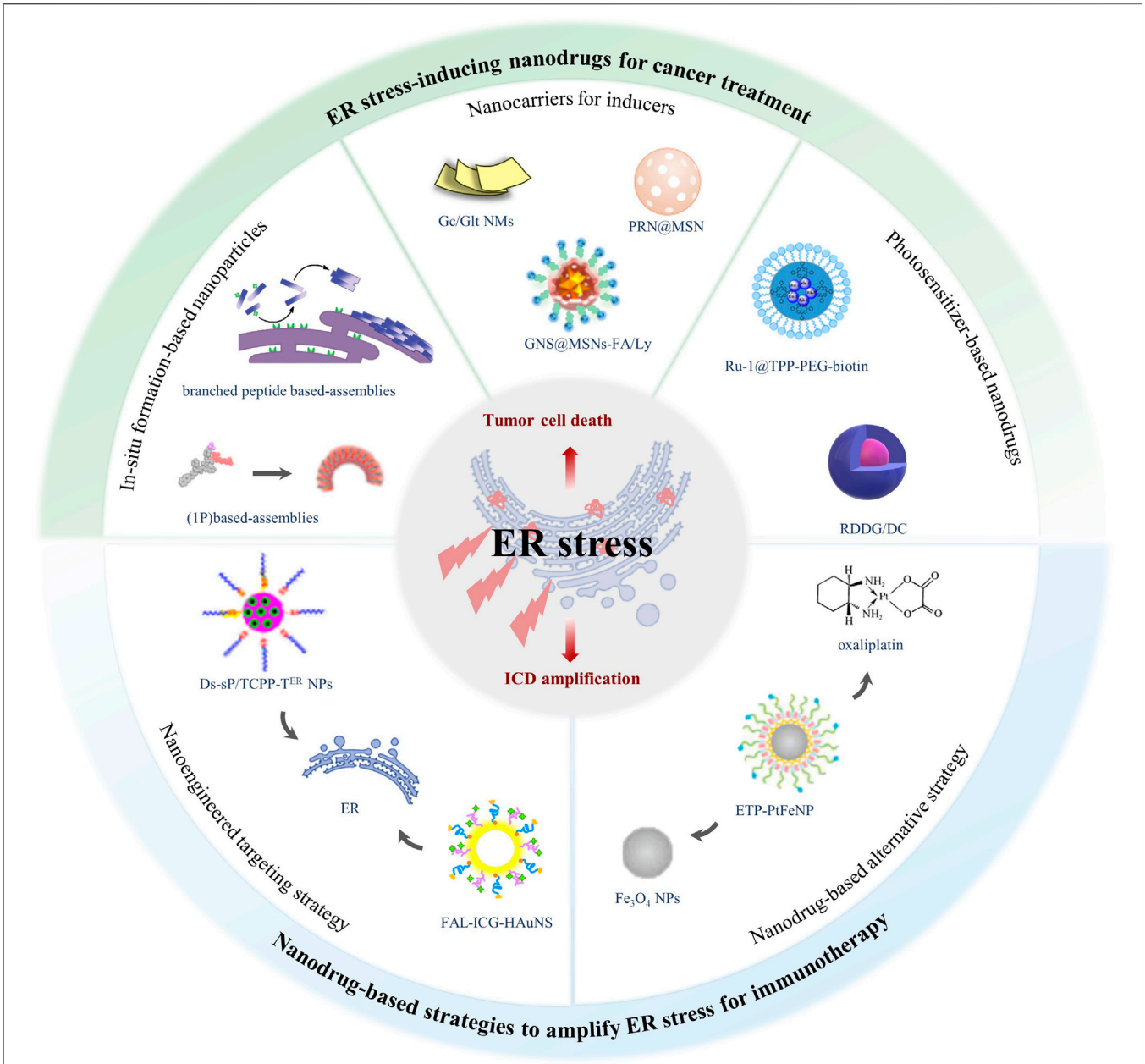


FIGURE 1 | The scope and focus of this article. Accumulation of misfolded protein results in ER stress, which can induce antitumor effects by triggering tumor cell death and amplifying ICD. ER stress–inducing nanodrugs can treat cancer through activating unsolved ER stress. In addition, nanodrugs amplifying ER stress *via* ER-targeting strategy and combination strategy make it possible for traditional ICD inducers to initiate antitumor immunotherapy.

organism. Misfolded proteins have a higher affinity to molecular chaperone BiP and activate sensors of ER stress *via* titrating BiP from sensors [PKR-like ER kinase (PERK), activating transcription factor 6 (ATF6), and inositol-requiring enzyme 1 (IRE1α)], termed UPR. Subsequently, the activation of sensors initiate cytoprotective mechanisms, including inducing transcription of the cell-protective molecule, directing the protein to the ubiquitin-proteasome system (UPS), promoting protective autophagy, and so on. Therefore, there are two strategies to induce ER stress as expected: promoting the production of misfolded proteins and inhibiting UPR-mediated protective effects (Marciniak et al., 2022). Currently, many emerging nanodrugs targeting ER have been developed for efficient cancer treatment. According to the pharmacological mechanism, these nanodrugs are mainly divided into the following three categories: the first category, the *in situ* formation-based ER-targeted nanoparticles to induce ER stress by enzyme-instructed self-assembly (EISA); the second category, nanocarriers for small-molecule drugs substantially induce ER stress by improving the targeting efficiency; the third category,

photodynamic therapy (PDT)–based nanodrugs amplify ER stress by generating uncontrolled ROS.

In Situ Formation–Based Endoplasmic Reticulum–Targeted Nanoparticles

EISA technology is an effective method for *in situ* self-assembly, which is a benefit for organelles targeting and inducing stress (Ji et al., 2021). The overexpressed enzymes in tumor cells can achieve targeted enrichment and improve selectivity for some molecules containing specific amino acid sequence substrates for these enzymes. These specially designed molecules can self-assemble into ER-targeted nanoforms to induce ER stress through membrane lipid action in cancer cells after the substrate fragments are cleaved by these enzymes (Gao et al., 2020; Xiang et al., 2022a). Recently, Feng et al. (2018) adopted alkaline phosphatase (ALP), highly expressed in tumor cells (HeLa cells), to construct an EISA-related phosphotetrapeptide (1P)-based ER inducer for cancer therapy. The 1P precursor contained a d-phosphotyrosine as a specific substrate of ALP, and positively charged l-homoarginine, which targeted the ER. After the 1P precursor was catalyzed by ALP to generate 1P, 1P self-assembled on the surface of the cancer cell membrane to form unique crescent-shaped 1P nanoparticles. Subsequently, the 1P nanoparticles were selectively enriched in the ER to induce ER stress. Similarly, Kim et al. (2021) utilized trypsin-1, which was overexpressed in the ER of a high-grade serous ovarian cancer cell line (OVSAHO), to develop a trypsin-1 (PRSS1)–based branched peptide chain. After proteolysis, the branched peptide chains formed peptide assemblies to accumulate in the ER, upregulated ER stress-related proteins, and killed OVSAHO cells through various death pathways. In addition, furin that is highly expressed in many malignant tumor cells (Fu et al., 2020) has been used to treat cancer. Based on its location in the trans-Golgi network, furin-instruct EISA blocked the transport of ER to the Golgi apparatus to induce ER stress and cancer cell death.

Nanocarriers With Small-Molecule Drugs

Nanocarriers were also developed for ER-targeted small-molecule drugs to improve their efficacy in tumors (Wang et al., 2021). Cheng et al. (2020) encapsulated curcumin in gelatin-blended nanofibrous mat (Cc/Glt NM) to address the inherent insolubility, instability, poor absorption, and rapid systemic elimination of curcumin. Cc/Glt NM effectively entered cancer cells to release curcumin, which activated the BiP/p-PERK/p-elF2a pathway to induce ER stress. As expected, Cc/Glt NM significantly reduced the tumor volume in pancreatic adenocarcinoma (PDAC) tumor–bearing mice with enhanced ER stress levels after topical application. In addition, Wu et al. (2020) adopted mesoporous silica nanoparticle (MSN) to deliver propranolol (PRN), the first-line therapy for hemangiomas. PRN@MSN strongly inhibited the formation of microvessels in murine hemangioma models *via* increased ER stress, where MSN induced ER stress and PRN inhibited autophagy that was resistant to ER stress. Moreover, Hu et al. (2021) integrated gold nanostars (GNS) and the antineoplastic drug lycorine (Ly) into MSNs with modified tumor-targeted folate (FA). GNS@MSNs-FA/Ly exhibited highly specific tumor growth inhibition in osteosarcoma cell tumor–bearing mice without additional side effects, among which Ly promoted mitochondrial dysfunction to interfere with ER *via* endoplasmic reticulum–mitochondrial contact (Giacomello et al., 2020).

Multifunctional Photosensitizer-Based Nanodrugs

PDT is one of the potential therapeutic strategies for cancers that generates cytotoxic ROS by the reaction of photosensitizers with oxygen (O_2) under the light (Zhao et al., 2022b; Long et al., 2022). The ROS generated during PDT attack proteins to form toxic ROS-modified proteins, which can provoke ER stress by inducing the accumulation of toxic protein (Chen et al., 2021; Zhu et al., 2022) in the ER. In addition, excessive intracellular ROS affect ER-resident calcium channels (Görlach et al., 2015) and promote lipid peroxidation (Vladykovskaya et al., 2012), which also disturb the homeostasis of the ER. However, a single photosensitizer has limited utility to induce ER as well. Further amplification of ER stress is also essential for photosensitizers. Multifunctional nanodrugs can combine varying molecules and materials with photosensitizers into one nanoscale entity to bring the most efficient functionality against tumors.

Recently, Purushothaman et al. (2020) developed Ru-1@TPP-PEG-biotin self-assembled nanoparticles (Ru-1@TPP-PEG-biotin SAN) for cancer therapy. Ru-1@TPP-PEG-biotin SAN was loaded with ruthenium complex 1 (Ru-1, an inhibitor of chaperone GRP78 functions) as an ER stress inducer and photosensitizer. Ru-1@TPP-PEG-biotin SAN induced degradation of the lysosome and inhibition of autophagy, which benefited the release of Ru-1 and the induction of ER stress to cause strong cytotoxicity in MCF-7 and HepG2 cells. Combining photosensitizers and various ER stress inducers presented more potent and efficient antitumor effects than separately administering them. Dong et al. (2019) further developed a multifunctional photosensitizer-based nanodrug (RDDG/DC NPs) for treating breast cancer. The photosensitizers (polymers with dithiophene-benzotriazole groups, abbreviated with the letter C) and doxorubicin (a widely used chemotherapy drug, abbreviated with the letter D) were encapsulated in the ROS-sensitive dextran with 2-deoxy-glucose (2-DG, an ER stress inducer that interferes with N-linked glycosylation). The 2-DG and photosensitizers synthetically induced severe ER stress, which significantly increased CHOP mRNA (related to ER stress), and high cytotoxicity was observed in MCF-7 breast cancer cells treated with RDDG/DC NPs and light irradiation. Eventually, the well-fabricated multifunctional nanodrugs targeted the tumor site and exhibited the most potent suppressing effects on tumor growth under light illumination.

NANODRUG-BASED STRATEGIES TO AMPLIFY ENDOPLASMIC RETICULUM STRESS FOR IMMUNOTHERAPY

Antitumor immunotherapy, which boosts the body's own immune system's ability to recognize and attack tumor cells,

represents one of the most promising advances in modern medicine (Wang et al., 2021). However, the immunosuppressive tumor microenvironment and poor tumor immunogenicity discourage tumor cells from immune attack, which confronts immunotherapy with enormous challenges (Dong et al., 2021). ICD is a special form of cell death, activating an immune response to recognize antigens of dead or dying tumor cells (Banstola et al., 2021). The expression and release of death-association molecular patterns (DAMPs), such as CRT and high mobility group box 1 (HMGB1), promote dendritic cell (DC) maturation and antigen presentation during ICD (Kroemer et al., 2022). More immunogen exposure to tumors' signals potentiates an immune effect, which is beneficial for treating malignant tumors. However, most ICD inducers have poor antitumor immunity because ICD-related danger signaling is not their original pharmacology mechanism but a consequence of collateral ER stress effects.

ER stress has been shown to contribute to ICD. When ER stress occurs, abundant CRTs in the ER translocate to the cell surface as a signal for immune system recognition and antigen presentation, often referred to as the "eat me" signaling. Photosensitizers have the potential to be ICD inducers due to their ability to induce ER stress, but only a small amount of them have been applied in ER-associated ICD-induced research on account of their existing but limited influences on ER stress. Some promising strategies of nanodrugs to amplify ER stress benefit antitumor immunotherapy of these limited ICD inducers.

Endoplasmic Reticulum–Targeting Nanodrugs Based on Immunogenic Cell Death Inducers

A few ICD inducers, such as hypericin (an ER-target photosensitizer) (Lin et al., 2017), induce highly efficient ICD by directly and selectively targeting the ER. Therefore, engineering ER-targeting nanodrugs based on ICD inducers is an effective strategy for enhancing the ICD-associated antitumor immunity. Deng et al. (2020) modified meso-tetra(4-carboxyphenyl) porphyrin (TCPP) with N-tosylethylenediamine to form an ER-targeting photosensitizer TCPP-T^{ER}. Notably, the *p*-toluene sulfonyl group of TCPP-T^{ER} recognized the ATP-sensitive K^+ channel (sulfonylurea receptor) on the ER. Then, TCPP-T^{ER} was loaded to reduction-sensitive polymer (Ds-sP) to respond to the tumor microenvironment. The dual-targeting of smart Ds-sP/TCPP-T^{ER} nanoparticles released TCPP-T^{ER} in tumor sites with high GSH levels and ensured the accumulation of TCPP-T^{ER} in the ER. The ROS generated from TCPP-T^{ER} under light exposure activated ER stress directly and increased the translocation of CRTs to the cell membrane in 4T1 cells (human breast cancer cell lines). The Ds-sP/TCPP-T^{ER} nanoparticles successfully inhibited the growth of primary and distant tumors along with evaluating the proportion of $CD8^+$ T cells in tumor tissues.

Additionally, Li et al. (2019) fabricated an ER target nanodrug, pardaxin (FAL) peptides–modified indocyanine green (ICG)–conjugated hollow gold nanospheres (FAL-ICG-HAuNS). The AuNS were an excellent carrier with both photothermal properties and ER stress–inducing function, which exerted a synergistic effect with photosensitizer ICG. FAL-ICG-HAuNS increased CHOP and CRTs on the cell surface under light exposure. The ER stress induced by FAL-ICG-HAuNS was ROS-dependent and was blocked by antioxidant vitamin C. To overcome the limitations of the hypoxia tumor microenvironment on PDT, the oxygen-delivering hemoglobin (Hb) liposome (FAL-Hb lipo) was adopted to provide sufficient O_2. FAL-ICG-HAuNS inhibited tumor growth and prolonged survival time of CT-26 tumor–bearing mice and B16 tumor–bearing mice, which was reversed by depleting either $CD4^+$ or $CD8^+$ T cells, demonstrating the important role of ICD in tumor killing. In summary, the nanoengineered targeting strategy successfully enhanced ICD and related antitumor immunity by amplifying ER stress.

Endoplasmic Reticulum Stress–Inducing Nanodrugs Combined With Immunogenic Cell Death Inducers

Clinically available chemotherapeutic drugs, such as DOX, platinum-based drugs, cyclophosphamide, and so on, belong to the ICD inducers *via* collateral ER stress effects (Tham et al., 2020). The increasing targeting of ER benefits the ICD-inducing ability of these inducers. However, the increasing immunogenicity is accompanied by less cytotoxicity because they initiate cell death *via* non–ER-related targets (Xiang et al., 2022b). Therefore, combining different ER stress inducers and ICD inducers to form an alternative ICD inducer with strong antitumor efficacy is a promising strategy to promote ICD-associated immunogenicity and preserve original cytotoxicity.

Recently, Xu et al. (2019) combined cisplatin and adjudin (ADD) into a multi-responsive peptide-based prodrug platform for cancer therapy. ADD was a derivative of lonidamine with potent antitumor effects, and it significantly increased intracellular ROS levels by attacking the mitochondria. The combination of cisplatin and ADD along with tumor targeting from the nanoplatform amplified CRTs exposure, ATP secretion, and HMGB-1 release. To further improve antitumor immunity, WKYMVm were loaded to nanoparticles to form 3-NPs assembled from 2-(Nap)-FFKPt-2TPA-ADDGGGPLGVRG-WKYMVm-mPEG1000. WKYMVm was an agonist of formyl peptide receptor 1 (FRR-1) which facilitated DCs to touch and contact with dying tumor cells stably. More importantly, 3-NPs demonstrated minimal lung metastases surprising rate of tumor shrinkage, as high as 93.1% in the 4T1 orthotopic tumor model. Therefore, 3-NPs were efficient in treating triple-negative breast cancer (TNBC) and inhibiting tumor metastasis *via* provoking innate and adaptive anti-TNBC immunity. In addition, Chen et al. (2019) constructed a core-shell magnetic nanoparticle (FeNP) to load oxaliplatin (the third-generation star product of platinum-based drugs) with a modified tumor-targeting peptide (α-enolase-targeting peptide, ETP) (ETP-PtFeNP). The ETP-PtFeNP induced intracellular Fenton's reaction and elicited ROS bursting (Chen et al., 2022), which was partially beneficial for ICD. ERS-mediated ICD activation was demonstrated by markedly elevated levels of CRT on the cell surface in the

ETP-PtFeNP–treated group. ETP-PtFeNP eventually activated entire-body immunity and suppressed tumor growth in the 4T1 tumor–bearing balb/c mice.

CONCLUSION AND PROSPECTS

This article reviewed the tumor treatment strategies of ER stress–inducing nanodrugs. Nanodrugs are specifically enriched in tumor sites and achieve efficient treatment of cancer *via* the enhancement of ER stress. Moreover, a combination of various ER stress inducers in a nanoplatform can further amplify ER stress and demonstrate attractive antitumor effects. In addition, nanodrug-based strategies to amplify ER stress repurposed those antitumor drugs for immunotherapy and acquired amazing results, considering the importance of ER stress for ICD.

Although significant progress has been made in this emerging field, there are still some unsolved questions about these nanodrugs. First, ER exists in almost all cells, which represents the wide toxic side effects of ER-targeting nanodrugs. As such, precise tumor cell targeting is imperative. Second, many ROS-based drugs are limited by tumor environment hypoxia in tumor therapy, especially the strategy that requires direct utilization of O_2 like PDT (Long et al., 2022). Although the work conducted by Li et al. (2019) provided a direction for breaking the restriction, there was still a long way to overcome this challenge. Finally, the ER targeting of many nanodrugs is achieved through the modification of targeting peptides, but the modification of macromolecules such as proteins increases the difficulty of synthesis. More superior ER targeting strategies, such as nanoliposome targeting ER, require further deep study (Shi et al., 2021).

Overall, nanodrugs-induced/amplified ER stress is available to increase ICD and antitumor effects. Of whatever function as cytotoxic antitumor drugs or immunotherapeutic drugs, the ER stress-inducing nanodrugs are potential and promising for cancer treatment. At the same time, the ideas of nanodrugs-based strategies based on ER stress are also beneficial for the treatment of other diseases.

AUTHOR CONTRIBUTIONS

All authors listed have made a substantial, direct, and intellectual contribution to the work and approved it for publication.

FUNDING

This work was supported by the National Natural Science Foundation of China, China (Nos. 81974508, 21974134), the Hunan Science Fund for Distinguished Young Scholar (No. 2021JJ10067), Innovation-Driven Project of Central South University (No. 202045005), Hunan Provincial Natural Science Foundation of China (No. 2021JJ31066), Key Research Project of Ningxia Hui Autonomous Region in 2021 (Major Project) (No. 2021BEG01001), and The Key Program of Ningxia Hui Autonomous Region Natural Science Foundation of China (No. 2022JJ21059).

REFERENCES

Bahar, E., Kim, J.-Y., and Yoon, H. (2019). Chemotherapy Resistance Explained through Endoplasmic Reticulum Stress-dependent Signaling. *Cancers* 11, 338. doi:10.3390/cancers11030338

Banstola, A., Poudel, K., Kim, J. O., Jeong, J.-H., and Yook, S. (2021). Recent Progress in Stimuli-Responsive Nanosystems for Inducing Immunogenic Cell Death. *J. Control. Release* 337, 505–520. doi:10.1016/j.jconrel.2021.07.038

Cerezo, M., Lehraiki, A., Millet, A., Rouaud, F., Plaisant, M., Jaune, E., et al. (2016). Compounds Triggering ER Stress Exert Anti-melanoma Effects and Overcome BRAF Inhibitor Resistance. *Cancer Cell.* 29, 805–819. doi:10.1016/j.ccell.2016.04.013

Chen, L., Huang, Q., Zhao, T., Sui, L., Wang, S., Xiao, Z., et al. (2021). Nanotherapies for Sepsis by Regulating Inflammatory Signals and Reactive Oxygen and Nitrogen Species: New Insight for Treating COVID-19. *Redox Biol.* 45, 102046. doi:10.1016/j.redox.2021.102046

Chen, Q., Li, N., Wang, X., Yang, Y., Xiang, Y., Long, X., et al. (2022). Mitochondria-Targeting Chemodynamic Therapy Nanodrugs for Cancer Treatment. *Front. Pharmacol.* 13, 847048. doi:10.3389/fphar.2022.847048

Chen, Q., Liu, L., Lu, Y., Chen, X., Zhang, Y., Zhou, W., et al. (2019). Tumor Microenvironment-Triggered Aggregated Magnetic Nanoparticles for Reinforced Image-Guided Immunogenic Chemotherapy. *Adv. Sci.* 6, 1802134. doi:10.1002/advs.201802134

Chen, X., and Cubillos-Ruiz, J. R. (2021). Endoplasmic Reticulum Stress Signals in the Tumour and its Microenvironment. *Nat. Rev. Cancer* 21, 71–88. doi:10.1038/s41568-020-00312-2

Cheng, T., Zhang, Z., Shen, H., Jian, Z., Li, J., Chen, Y., et al. (2020). Topically Applicated Curcumin/gelatin-Blended Nanofibrous Mat Inhibits Pancreatic Adenocarcinoma by Increasing ROS Production and Endoplasmic Reticulum Stress Mediated Apoptosis. *J. Nanobiotechnol* 18, 126. doi:10.1186/s12951-020-00687-2

Deng, H., Zhou, Z., Yang, W., Lin, L.-s., Wang, S., Niu, G., et al. (2020). Endoplasmic Reticulum Targeting to Amplify Immunogenic Cell Death for Cancer Immunotherapy. *Nano Lett.* 20, 1928–1933. doi:10.1021/acs.nanolett.9b05210

Dong, M., Xiao, X. Z., Su, Z. G., Yu, Z. H., Qian, C. G., Liu, J. H., et al. (2019). *Small* 15, e1900212. doi:10.1002/smll.201900212

Dong, Y., Zhang, S., Gao, X., Yin, D., Wang, T., Li, Z., et al. (2021). HIF1α Epigenetically Repressed Macrophages via CRISPR/Cas9-EZH2 System for Enhanced Cancer Immunotherapy. *Bioact. Mater.* 6, 2870–2880. doi:10.1016/j.bioactmat.2021.02.008

Feng, Z., Wang, H., Wang, S., Zhang, Q., Zhang, X., Rodal, A. A., et al. (2018). Enzymatic Assemblies Disrupt the Membrane and Target Endoplasmic Reticulum for Selective Cancer Cell Death. *J. Am. Chem. Soc.* 140, 9566–9573. doi:10.1021/jacs.8b04641

Fu, C., Zhan, J., Huai, J., Ma, S., Li, M., Chen, G., et al. (2020). Furin-instructed Molecular Self-Assembly Actuates Endoplasmic Reticulum Stress-Mediated Apoptosis for Cancer Therapy. *Nanoscale* 12, 12126–12132. doi:10.1039/d0nr00151a

Gao, J., Zhan, J., and Yang, Z. (2020). Enzyme-Instructed Self-Assembly (EISA) and Hydrogelation of Peptides. *Adv. Mat.* 32, 1805798. doi:10.1002/adma.201805798

Giacomello, M., Pyakurel, A., Glytsou, C., and Scorrano, L. (2020). The Cell Biology of Mitochondrial Membrane Dynamics. *Nat. Rev. Mol. Cell. Biol.* 21, 204–224. doi:10.1038/s41580-020-0210-7

Görlach, A., Bertram, K., Hudecova, S., and Krizanova, O. (2015). Calcium and ROS: A Mutual Interplay. *Redox Biol.* 6, 260–271. doi:10.1016/j.redox.2015.08.010

Hetz, C., Zhang, K., and Kaufman, R. J. (2020). Mechanisms, Regulation and Functions of the Unfolded Protein Response. *Nat. Rev. Mol. Cell. Biol.* 21, 421–438. doi:10.1038/s41580-020-0250-z

Hu, H., Yang, W., Liang, Z., Zhou, Z., Song, Q., Liu, W., et al. (2021). Amplification of Oxidative Stress with Lycorine and Gold-Based Nanocomposites for Synergistic Cascade Cancer Therapy. *J. Nanobiotechnol* 19, 221. doi:10.1186/s12951-021-00933-1

Huang, J., Huang, Q., Liu, M., Chen, Q., and Ai, K. (2022). Emerging Bismuth Chalcogenides Based Nanodrugs for Cancer Radiotherapy. *Front. Pharmacol.* 13, 844037. doi:10.3389/fphar.2022.844037

Ji, S., Li, J., Duan, X., Zhang, J., Zhang, Y., Song, M., et al. (2021). Targeted Enrichment of Enzyme-Instructed Assemblies in Cancer Cell Lysosomes Turns Immunologically Cold Tumors Hot. *Angew. Chem. Int. Ed.* 60, 26994–27004. doi:10.1002/anie.202110512

Kim, B. J., Fang, Y., He, H., and Xu, B. (2021). *Adv. Healthc. Mater* 10, e2000416. doi:10.1002/adhm.202000416

King, A. P., and Wilson, J. J. (2020). Endoplasmic Reticulum Stress: an Arising Target for Metal-Based Anticancer Agents. *Chem. Soc. Rev.* 49, 8113–8136. doi:10.1039/d0cs00259c

Kroemer, G., Galassi, C., Zitvogel, L., and Galluzzi, L. (2022). Immunogenic Cell Stress and Death. *Nat. Immunol.* 23, 487–500. doi:10.1038/s41590-022-01132-2

Li, J., Gao, H., Liu, R., Chen, C., Zeng, S., Liu, Q., et al. (2020). Endoplasmic Reticulum Targeted AIE Bioprobe as a Highly Efficient Inducer of Immunogenic Cell Death. *Sci. China Chem.* 63, 1428–1434. doi:10.1007/s11426-020-9846-4

Li, W., Yang, J., Luo, L., Jiang, M., Qin, B., Yin, H., et al. (2019). Targeting Photodynamic and Photothermal Therapy to the Endoplasmic Reticulum Enhances Immunogenic Cancer Cell Death. *Nat. Commun.* 10, 3349. doi:10.1038/s41467-019-11269-8

Lin, S., Yang, L., Shi, H., Du, W., Qi, Y., Qiu, C., et al. (2017). Endoplasmic Reticulum-Targeting Photosensitizer Hypericin Confers Chemo-Sensitization towards Oxaliplatin through Inducing Pro-death Autophagy. *Int. J. Biochem. Cell. Biol.* 87, 54–68. doi:10.1016/j.biocel.2017.04.001

Liu, M., Huang, Q., Zhu, Y., Chen, L., Li, Y., Gong, Z., et al. (2022). Harnessing Reactive Oxygen/nitrogen Species and Inflammation: Nanodrugs for Liver Injury. *Mater. Today Bio* 13, 100215. doi:10.1016/j.mtbio.2022.100215

Liu, P., Xiang, Y., Liu, X., Zhang, T., Yang, R., Chen, S., et al. (2019). *Molecules* 24. doi:10.3390/molecules24030647

Long, X., Zhang, X., Chen, Q., Liu, M., Xiang, Y., Yang, Y., et al. (2022). Nucleus-Targeting Phototherapy Nanodrugs for High-Effective Anti-cancer Treatment. *Front. Pharmacol.* 13, 905375. doi:10.3389/fphar.2022.905375

Marciniak, S. J., Chambers, J. E., and Ron, D. (2022). Pharmacological Targeting of Endoplasmic Reticulum Stress in Disease. *Nat. Rev. Drug Discov.* 21, 115–140. doi:10.1038/s41573-021-00320-3

Purushothaman, B., Lee, J., Hong, S., and Song, J. M. (2020). Multifunctional TPP-PEG-Biotin Self-Assembled Nanoparticle Drug Delivery-Based Combination Therapeutic Approach for Co-targeting of GRP78 and Lysosome. *J. Nanobiotechnol* 18, 102. doi:10.1186/s12951-020-00661-y

Shi, Y., Wang, S., Wu, J., Jin, X., and You, J. (2021). Pharmaceutical Strategies for Endoplasmic Reticulum-Targeting and Their Prospects of Application. *J. Control. Release* 329, 337–352. doi:10.1016/j.jconrel.2020.11.054

Tham, M. J. R., Babak, M. V., and Ang, W. H. (2020). PlatinER: A Highly Potent Anticancer Platinum(II) Complex that Induces Endoplasmic Reticulum Stress Driven Immunogenic Cell Death. *Angew. Chem. Int. Ed.* 59, 19070–19078. doi:10.1002/anie.202008604

Vladykovskaya, E., Sithu, S. D., Haberzettl, P., Wickramasinghe, N. S., Merchant, M. L., Hill, B. G., et al. (2012). Lipid Peroxidation Product 4-Hydroxy-Trans-2-Nonenal Causes Endothelial Activation by Inducing Endoplasmic Reticulum Stress. *J. Biol. Chem.* 287, 11398–11409. doi:10.1074/jbc.m111.320416

Wang, J., Sui, L., Huang, J., Miao, L., Nie, Y., Wang, K., et al. (2021). MoS2-based Nanocomposites for Cancer Diagnosis and Therapy. *Bioact. Mater.* 6, 4209–4242. doi:10.1016/j.bioactmat.2021.04.021

Wernitznig, D., Kiakos, K., Del Favero, G., Harrer, N., Machat, H., Osswald, A., et al. (2019). First-in-class Ruthenium Anticancer Drug (KP1339/IT-139) Induces an Immunogenic Cell Death Signature in Colorectal Spheroids *In Vitro*. *Metallomics* 11, 1044–1048. doi:10.1039/c9mt00051h

Wu, H., Wang, X., Liang, H., Zheng, J., Huang, S., and Zhang, D. (2020). Enhanced Efficacy of Propranolol Therapy for Infantile Hemangiomas Based on a Mesoporous Silica Nanoplatform through Mediating Autophagy Dysfunction. *Acta Biomater.* 107, 272–285. doi:10.1016/j.actbio.2020.02.033

Xiang, Y., Chen, L., Liu, C., Yi, X., Li, L., and Huang, Y. (2022). *Small* 18, e2104591. doi:10.1002/smll.202104591

Xiang, Y., Li, N., Liu, M., Chen, Q., Long, X., Yang, Y., et al. (2022). Nanodrugs Detonate Lysosome Bombs. *Front. Pharmacol.* 13, 909504. doi:10.3389/fphar.2022.909504

Xiao, Z., Huang, Q., Yang, Y., Liu, M., Chen, Q., Huang, J., et al. (2022). Emerging Early Diagnostic Methods for Acute Kidney Injury. *Theranostics* 12, 2963–2986. doi:10.7150/thno.71064

Xu, C., Yu, Y., Sun, Y., Kong, L., Yang, C., Hu, M., et al. (2019). Transformable Nanoparticle-Enabled Synergistic Elicitation and Promotion of Immunogenic Cell Death for Triple-Negative Breast Cancer Immunotherapy. *Adv. Funct. Mater.* 29, 1905213. doi:10.1002/adfm.201905213

Yang, Y., Huang, Q., Xiao, Z., Liu, M., Zhu, Y., Chen, Q., et al. (2022). Nanomaterial-based Biosensor Developing as a Route toward *In Vitro* Diagnosis of Early Ovarian Cancer. *Mater. Today Bio* 13, 100218. doi:10.1016/j.mtbio.2022.100218

Yao, Y., Lu, Q., Hu, Z., Yu, Y., Chen, Q., and Wang, Q. K. (2017). A Non-canonical Pathway Regulates ER Stress Signaling and Blocks ER Stress-Induced Apoptosis and Heart Failure. *Nat. Commun.* 8, 133. doi:10.1038/s41467-017-00171-w

Zhao, H., Huang, J., Miao, L., Yang, Y., Xiao, Z., Chen, Q., et al. (2022). Toward Urease-free Wearable Artificial Kidney: Widened Interlayer Spacing MoS2 Nanosheets with Highly Effective Adsorption for Uremic Toxins. *Chem. Eng. J.* 438, 135583. doi:10.1016/j.cej.2022.135583

Zhao, R., Liu, X., Yang, X., Jin, B., Shao, C., Kang, W., et al. (2018). Nanomaterial-Based Organelles Protect Normal Cells against Chemotherapy-Induced Cytotoxicity. *Adv. Mat.* 30, 1801304. doi:10.1002/adma.201801304

Zhao, T., Wu, W., Sui, L., Huang, Q., Nan, Y., Liu, J., et al. (2022). Reactive Oxygen Species-Based Nanomaterials for the Treatment of Myocardial Ischemia Reperfusion Injuries. *Bioact. Mater.* 7, 47–72. doi:10.1016/j.bioactmat.2021.06.006

Zhu, Y., Zhao, T., Liu, M., Wang, S., Liu, S., Yang, Y., et al. (2022). Rheumatoid Arthritis Microenvironment Insights into Treatment Effect of Nanomaterials. *Nano Today* 42, 101358. doi:10.1016/j.nantod.2021.101358

Conflict of Interest: The authors declare that the research was conducted in the absence of any commercial or financial relationships that could be construed as a potential conflict of interest.

Publisher's Note: All claims expressed in this article are solely those of the authors and do not necessarily represent those of their affiliated organizations, or those of the publisher, the editors, and the reviewers. Any product that may be evaluated in this article, or claim that may be made by its manufacturer, is not guaranteed or endorsed by the publisher.

Copyright © 2022 Xiang, Liu, Yang, Wang, Qiu, Tu, Jiang, Nan, Zhang and Huang. This is an open-access article distributed under the terms of the Creative Commons Attribution License (CC BY). The use, distribution or reproduction in other forums is permitted, provided the original author(s) and the copyright owner(s) are credited and that the original publication in this journal is cited, in accordance with accepted academic practice. No use, distribution or reproduction is permitted which does not comply with these terms.

frontiers | Frontiers in Oncology

MINI REVIEW
published: 14 July 2022
doi: 10.3389/fonc.2022.930125

Current Progress in Cancer Treatment Using Nanomaterials

Ruirui Zhu[1], *Fangyuan Zhang*[2], *Yudong Peng*[1], *Tian Xie*[1*], *Yi Wang*[3*] *and Yin Lan*[1*]

[1] Department of Cardiology, Union Hospital, Tongji Medical College, Huazhong University of Science and Technology, Wuhan, China, [2] Department of Dermatology, Union Hospital, Tongji Medical College, Huazhong University of Science and Technology, Wuhan, China, [3] Department of Cardiovascular Ultrasound, Zhongnan of Wuhan University, Wuhan University, Wuhan, China

The pathological processes of cancer are complex. Current methods used for chemotherapy have various limitations, such as cytotoxicity, multi-drug resistance, stem-like cells growth, and lack of specificity. Several types of nanomaterials are used for cancer treatment. Nanomaterials 1–100 nm in size have special optical, magnetic, and electrical characteristics. Nanomaterials have been fabricated for cancer treatments to overcome cytotoxicity and low specificity, and improve drug capacity and bioavailability. Despite the increasing number of related studies, few nanodrugs have been approved for clinical use. To improve translation of these materials, studies of targeted drug delivery using nanocarriers are needed. Cytotoxicity, enhanced permeability and retention effects, and the protective role of the protein corona remain to be addressed. This mini-review summarizes new nanomaterials manufactured in studies and in clinical use, analyses current barriers preventing their translation to clinical use, and describes the effective application of nanomaterials in cancer treatment.

Keywords: nanomaterial, cancer treatment, tumor microenvironment, drug delivery, chemotherapy, bioavailability, nanodrug

OPEN ACCESS

Edited by:
Kelong Ai,
Central South University, China

Reviewed by:
Qiong Huang,
Central South University, China
Wen Zeng,
Zhongnan Hospital of Wuhan University, China
Mahmood Barani,
Kerman University of Medical Sciences, Iran

***Correspondence:**
Tian Xie
715494934@qq.com
Yi Wang
kingyi32154768@163.com
Yin Lan
lanyinuh@126.com

Specialty section:
This article was submitted to Pharmacology of Anti-Cancer Drugs, a section of the journal Frontiers in Oncology

Received: *27 April 2022*
Accepted: *16 June 2022*
Published: *14 July 2022*

Citation:
Zhu R, Zhang F, Peng Y, Xie T, Wang Y and Lan Y (2022) Current Progress in Cancer Treatment Using Nanomaterials. Front. Oncol. 12:930125. doi: 10.3389/fonc.2022.930125

INTRODUCTION

Cancer is a common, complex, and heterogeneous disease. As the population ages, cancer is becoming a leading cause of morbidity and mortality worldwide, with approximately 9.5 million cancer-related deaths annually (1). Therefore, studies aimed at developing treatments for cancer are urgently needed. Surgery, chemotherapy, and radiotherapy are the three main treatments for cancer but often lead to unsatisfactory outcomes and side effects (2, 3). With increasing advances in oncology research, more effective therapies have become available to overcome these limitations, such as immunotherapy, gene therapy, photothermal therapy (PTT), photodynamic therapy (PDT), chemodynamic therapies (CDT), sonodynamic therapy (SDT) and nanomaterial-based chemotherapy (4–9). Among them, nanomaterial-based chemotherapy is a promising therapy for cancer because of its low toxicity, high specificity, and excellent bioavailability (10).

Medical nanotechnology is one of the most promising frontiers in cancer. Typical nanomaterials are 1–100 nm in size and exhibit a high surface to volume ratio, unique fluorescence properties, enhanced permeability, and outstanding biocompatibility (11, 12). These properties offer several advantages in cancer treatment. The high surface to volume ratio facilitates the assembly of biomolecules, which can improve the specificity of chemical drugs, thereby increasing the efficacy of targeted therapy and reducing its toxicity (10).

PDT and PTT are promising approaches for improving the effects of cancer treatment; both methods are related to optical interference. The materials used in PDT and PTT have obtained wide interest in recent years. The temperature of the targeted region can be elevated by the photothermal conversion efficiency of PTT to promote cancer cell death. In contrast, in PDT, photosensitizers and certain wavelengths of light are utilized to produce singlet oxygen, leading to the death of cancer cells (13). Because of their excellent fluorescence properties, various nanomaterials are utilized in PDT and PTT (14). In tumor site, toxic ROS was generated by endogenous H2O2 and therefore cancer cells were killed in the absence of external O2 (15). This is one of the unique advantages of CDT. So far, CDT nanodrugs with mitochondria-targeting displayed outstanding spatial specificity and anti-tumor effect (9).

Nanoparticles are a better choice for cancer treatment compared to microparticles because nanoparticles are more biodegradable than microparticles (16). Nanoparticles are not small enough to penetrate into normal blood vessels because they have a dense extracellular matrix. As tumor grows, lymphatic drainage was inhibited by immature vasculatures generated by tumor-induced angiogenesis (17). The suppressed lymphatic drainage makes it possible for nanoparticles to penetrate targeted cells. This phenomenon is known as "enhanced permeability and retention effect" (EPR) and the passive targeting of nanoparticles is largely dependent on EPR effect (18).

The superparamagnetic behavior of nanomaterials facilitates the diagnosis and treatment of cancer. For example, superparamagnetic iron oxide nanoparticles offer unique advantages. They are small, display high targeting specificity, and show a powerful ability to evade the immune system, thereby exhibiting potential for cancer treatment (19).

ADVANCES IN NANOTECHNOLOGY FOR TARGETED DELIVERY

Cancer treatment based on nanomaterials shows advantages over using free drugs, particularly for targeted delivery. Compared to free drugs, targeted delivery exhibits reduced toxicity, decreased degradation, increased half-life, and enhanced capacity (20, 21). Recent advances have been made in nanomaterial-based targeted drug delivery systems, including in active or passive targeting. Active targeting is achieved using antibodies or small molecule-conjugated nanoparticles, whereas passive targeting occurs through enhanced permeability and retention effects. Active targeting displays great potential and acted as an alternative strategy to passive targeting and the ability of tumor localization in active targeting was improved by increased efficiency and retention (22). Compared with traditional chemical therapies, nanomaterial-based drugs display increased specificity, improved bioavailability, lower cytotoxicity, better loading capacity, and a longer half-life. To date, many nanomaterials for cancer treatment have been developed based on remarkable advances in nanoscience, technology, and cancer pathology. However, few nanomaterial-based drugs have been intensively studied and utilized in clinical practice. Nanomaterials can be broadly classified into several categories (**Figure 1**).

NANOMATERIALS IN CANCER THERAPY

Several well-studied nanoparticles are listed in **Supplementary Table 1** (23–28). Chemical drugs can be delivered and sustainably released to target sites by Polymeric nanoparticles (PNPs) (10 to 1000 nm) (29). Nanoparticle components have evolved over the past few decades; they were initially manufactured from non-biodegradable polymers, including polymethyl methacrylate and polyacrylates (30, 31). Because they cause chronic inflammation and toxicity, one challenge to using these types of PNPs is their timely removal. To overcome this difficulty, biodegradable polymers such as polylactic acid, poly (lactic-co-glycolic acid), and poly (amino acids) have been fabricated (32), which exhibit excellent advantages depending on their structures and properties. PNPs protect drugs from degradation, improve loading ability, and increase stability (33). However, metal nanomaterials are not considered for

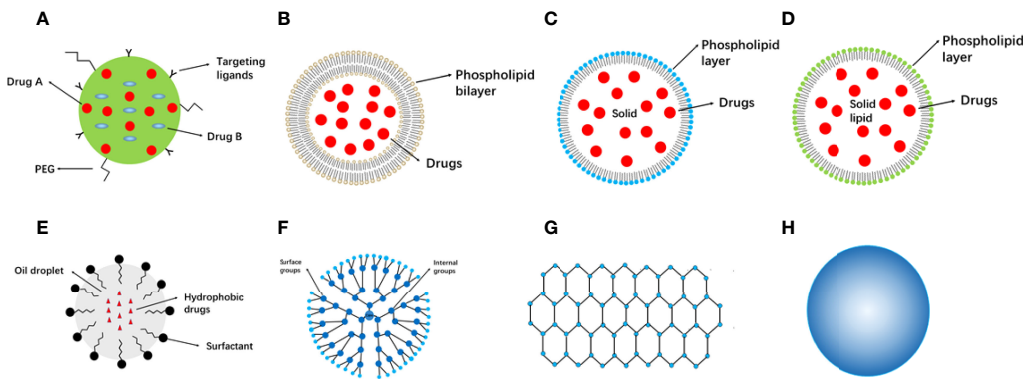


FIGURE 1 | Categories of nanomaterials used in cancer therapy. **(A)** Nanoparticles. **(B)** Liposomes. **(C)** Solid lipid nanoparticles. **(D)** Nanostructured lipid carriers. **(E)** Nanoemulsions. **(F)** Dendrimers. **(G)** Graphene. **(H)** Metallic nanoparticles. PEG, poly (ethylene glycol).

cancer treatment because renal and brain toxicity and denaturation of enzymes may be caused by excessive heavy metal element in-take (34, 35).

Drug delivery plays an important role in cancer therapy, and non-conjugated polymers with intrinsic luminescence show its special advantage in drug delivery (36). Drug delivery are including passive and active targeting (**Figure 2A**). A crucial issue is the size of the drug. It is difficult for drugs to infiltrate the dense extracellular matrix. However, tumor induced angiogenesis promoted generation of numerous immature vasculatures and inhibited lymphatic drainage (37). Because these immature vasculatures are "leaky", nanoparticles are small enough to penetrate the target sites. It is convenient to attach targeting peptides to the surface of PNPs because of excellent surface to volume ratio. Polysorbates surfactant effect can promote solubilization and fluidization. Coating polymers with polysorbates can improve bioavailability, thereby promoting the interaction of PNPs with endothelial cell membranes of the blood-brain barrier and facilitating endocytosis (38, 39). Compared with conventional chemical drugs, PNPS can deliver anticancer drugs to target sites and react to ultrasound. Theragnostics is a novel strategy that includes both diagnosis and therapy, in which fluorescent PNPs play a crucial role. In recent years, fluorescent PNPs with complex structures have been used as theragnostic materials. Fluorescent PNPs are typically composed of biocompatible biopolymers, fluorescent proteins, and organic dyes (40). Moreover, the anticancer effect of nanomedicine is strengthened by hydrophobic interactions or π–π bonds according to fluorescence assays (41). Radionuclides, such as I-125, can be stored in the stable core by electrophilic aromatic substitution of nanoparticles (42, 43). In addition, a self-assembling protein nanoparticle (11 nm) was developed and showed stability and biocompatibility in vivo, revealing its potential for drug delivery in cancer therapy (44). Ultrasound-sensitive PNPs are effective for cancer diagnosis and therapy. Side effects were reduced by using ultrasound in nanoparticle fabrication to overcome "obstacles" (such as endothelial blood vessels, tissue endothelium, and blood-brain barrier) associated with the traversing ability of cancer treatments, thus enhancing drug delivery (45–47). Ultrasound displays a thermal effect and can be utilized to trigger the controlled release of chemical drugs (48). However, some degraded PNPs are toxic; therefore, their fabrication and properties are still to be improved (49).

MONOCLONAL ANTIBODY NANOPARTICLES

Because of their anticancer effect and specific targeting ability, monoclonal antibodies (mAbs) are widely used in targeted treatment. More recently, mAbs have been utilized in

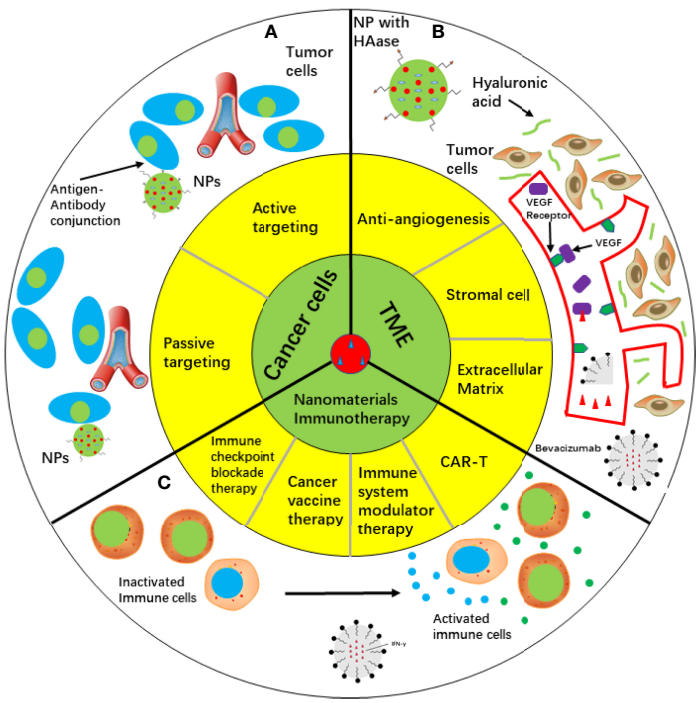


FIGURE 2 | Cancer therapy approaches depending on nanomaterials. **(A)** Targeting cancer cells by passive targeting or active targeting. **(B)** Targeting TME, such as anti-angiogenesis, stromal cell and extracellular matrix. Bevacizumab was loaded in liposome and conjugated with VEGF to suppress angiogenesis. HAase was fabricated onto NP surface and penetration ability of NP was increased. c IFN-γ as an immune regulator delivered by liposomes activated immune cells in cancer immunotherapy. HAase, hyaluronidase; IFN-γ, Interferon gamma; NP, nanoparticle; TME, tumor microenvironment; VEGF, vascular endothelial growth factor.

anticancer nanoplatforms and as frontlines in the fight against cancer. Cytotoxic drugs are conjugated with mAbs to strengthen the therapeutic efficacy of anticancer drugs, known as antibody-drug conjugates. According to the specific antigens expressed in cancer cells, less toxicity and higher specificity can be achieved (50). Different antibody-drug conjugate systems display enhanced therapeutic efficacy in breast cancer (26, 51). Based on these effects of antibody-drug conjugates, trastuzumab nanoparticles are promising and widely studied nanoplatforms for cancer treatment (52–54).

LIPID-BASED NANOMATERIALS

Liposomes, solid lipid nanoparticles (SLNs), and nanostructured lipid carriers are three main categories of lipid-based nanomaterials. Liposomes (20 nm to >1 μm) were the first microcosmic phospholipid bilayer nanosystem (55). Both hydrophilic and hydrophobic drugs can be delivered depending on the liposome structure (56). Drugs are shielded from degradation by the central cavity of liposomes (57). Liposomes may be phagocytized by the mononuclear phagocyte system, known as human guards; therefore, liposome membranes should be modified to prolong their half-life (58). This can be achieved through polyethylene glycol conjugation. For example, PEG-liposomes carrying doxorubicin (DOX) were developed and applied to treat Kaposi sarcoma (59). Liposomes are widely applied in co-delivery and controlled release and have been combined with chemical drugs. How to load drugs and control release must be considered when designing liposome nanocarriers. Drug efficacy is affected by bioavailability in cancer chemotherapy, and DOX liposomes have a lower bioavailability than free DOX, suggesting that bioavailability should be improved during liposome design (60). A new PEGylated liposome carrying cobimetinib and ncl-240 displayed an enhanced cytotoxic effect through synergistic effects, leading to higher efficacy (61). Moreover, liposomes loaded with floxuridine and irinotecan exhibited better effects on advanced solid tumors, whereas a new liposome containing multilayer siRNA molecules and that co-delivered DOX displayed better DOX efficacy, decreasing the tumor mass in breast cancer (62, 63). Notably, specific liposomes can release drugs depending on the pH value, as cancerous regions are more acidic compared to healthy tissues (64). pH-sensitive cationic liposomes were prepared using a pH-sensitive material. The release of sorafenib was increased at pH 6.5 (65). In summary, liposomes exhibit low immunogenicity, low cytotoxicity, and high biodegradability (66). However, the disadvantages of liposomes include their rapid removal by the mononuclear phagocyte system, low stability, and obstacles in membrane transfer. Therefore, the application of liposomes remains limited.

SLNs have been acted as alternative carriers to liposomes. Because of the rigid confinement of the scale, SLNs (1–100 nm) are known as "zero-dimensional" nanomaterials compared with other larger nanomaterials. SLNs contain solid materials, in contrast to liposomes. Examples of these materials include solid lipids, emulsifiers, and water. PEGylated lipids, triglycerides, and fatty acids are utilized in SLNs (20). The outer layer and delivery function of SLNs are similar but show some differences from conventional liposomes. Some SLNs have a micelle-like structure rather than a contiguous bilayer, with drugs packaged in the core (67). Compared with liposomes, SLNs show higher stability and longer release. However, because of their crystalline structure, SLNs exhibit some limitations, such as inherently low incorporation rates and an unpredictable gelation tendency (68). Nanostructured lipid carriers (NLCs) have been fabricated to overcome the drawbacks of SLNs and termed as the second lifetime of lipid nanoparticles. Compared with SLNs, NLCs exhibit a higher loading capacity and show a less inclination of gelation (69). NLCs have received considerable attention in recent years because many drugs used in cancer therapy are lipophilic and can be administered through various routes (oral, parenteral, inhalational, and ocular) (70). NLCs are manufactured as systems that carry both liquid and solid lipids. Over the past two decades, the stability and loading capacity of NLCs have evolved.

NANOEMULSIONS

Nanoemulsions (NEs) are colloidal nanoparticles with an aqueous phase, emulsifying agents, and oil (71). NEs are widely utilized drug nanocarriers. They have a lipophilic surface and solid spheres; three typical NE types are water-in-oil NE systems, oil-in-water NE systems, and bi-continuous NE (71). Compared with most lipid-based nanomaterials, NEs show the advantages of optical clarity, excellent biodegradability, and improved molecule release profiles (72). In contrast to conventional delivery vehicles, nanoemulsions are superior in efficacy and stability, and a serial of routes they can use to administer (73, 74). Intranasal route was used to carry small interfering RNA to the brain by nanoemulsions. In glioblastoma, CD73 small interfering RNA was successfully carried to the brain for gene silencing in a cationic nanoemulsion and show its great potential in drug delivery (75). Co-delivery using NEs can be performed to improve the effects and bioavailability of drugs. A previous study showed that an NE carrier containing paclitaxel (PTX) and Spirulina polysaccharides displayed improved anticancer effects by regulating the TLR4/NF-κB signaling pathways (76). An NE system composed of rapamycin and bevacizumab was developed. Increased inhibition of tumor migration and angiogenesis and improved cytotoxicity against cancer cells were observed in advanced melanoma (77) (**Figure 2B**).

NEs can also be used in immune therapies. A modified NE loaded with interferon-γ inhibited the viability of MCF-7 breast cancer cells and enhanced the activity of phagocytes. These results indicate the potential of these NEs for cancer therapy (78) (**Figure 2C**). A new NE carried baicalein and paclitaxel was produced enhanced oxidative stress and decreased glutathione levels in MCF-7/Tax cells, providing a suitable approach for increasing the sensitivity of cells to paclitaxel (74, 79). Compared

to conventional paclitaxel production, baicalein-paclitaxel NE displayed higher anticancer efficacy in vivo (74, 79). These studies indicate that applying elaborately fabricated NEs is useful for managing multi-drug resistance.

NEs are transitioning to clinical application but require many improvements, despite their potential advantages. A high temperature and pressure are typically needed to fabricate NEs, for which few materials are suitable. It is difficult to commercially manufacture NEs. Moreover, compared to other conventional production methods, homogenizers and microfluidizers are often used to prepare NEs, making the process more energy-efficient. Further studies of NE metabolism are needed to evaluate the safety of NEs in clinical applications (72).

DENDRIMERS

Dendrimers (1–15 nm) exhibit an architecture with highly branched surfaces (80, 81). Dendrimer molecules are composed of three parts: a central core, branches, and an exterior surface. A few dendrimers have been investigated for cancer therapy, including polyamidoamine (PAMAM), polypropylenimine, 5-aminolevulinic acid, and triethanolamine (82).

Depending on their unique structure, dendrimers exert specific functions, such as adjustable branches, outstanding solubility, and excellent bioavailability. Cationic dendrimers can form complexes with nucleic acids because of their positively charged surfaces. Hence, dendrimers can be utilized as efficacious nucleic acid nanocarriers. PAMAM and polypropylenimine have been extensively investigated. A PAMAM dendrimer composed of two parts was developed for simultaneously monitoring cancer cells and managing multi-drug resistance through fluorescence imaging. The first part was a carbon dot/DOX complex and the other part was composed of five PAMAM dendrimers with cyclic arginine-glycine-aspartic acid and d-α-tocopheryl polyethylene glycol 1000 succinate (TPGS). These two parts were combined via electrostatic interactions to obtain a PAMAM dendrimer. The carbon dots produced fluorescence, and arginine-glycine-aspartic acid ligands targeting αvβ3 integrin receptors induced targeting specificity; TPGS showed a remarkable ability to inhibit cancer cells (83).

Dendrimers are also useful for co-delivery. Tumor necrosis factor-related apoptosis-inducing ligand (TRAIL) is an important factor in the apoptotic pathway. In addition, colon cancer is typically treated using DOX. TRAIL and DOX plasmids were carried in a dendrimer nanocarrier, which showed enhanced anticancer effects compared to modified carriers containing the TRAIL or DOX plasmids alone (84). Depending on the dendrimer, a PAMAN nanocarrier was prepared and used to treat liver cancer. PAMAN dendrimers without decoration exhibit inefficient cellular internalization, low transfection efficiency, and unstable encapsulation; however, the competitive characteristics of nanomaterials exhibit many advantages in combination therapy (85, 86).

GRAPHENE

Because of its important mechanical and electronic characteristics, graphene has been widely studied in cancer therapy (87). Based on their composition, structure, and characteristics, single-layer and multi-layer graphene, graphene oxide (GO), and reduced graphene oxide have been defined (88). Graphene shows unique mechanical and electrochemical advantages. Optical transmittance, high density, and hydrophobicity are outstanding properties (89, 90). In addition, high drug-carrying ability and thermal conductivity are important properties in cancer theragnostic (91, 92). However, the poor solubility of graphene causes toxicity and prevents its manufacture (93). Hence, more bioavailable graphene-based nanomaterials are needed. A classical GO molecule is composed of functional oxygen groups, carbonyl groups, and epoxy groups (94). GO and the reduced derivative of GO display improved biological effects compared to graphene. Powerful hydrophilicity contributes to dispersions in aqueous solvents, avoiding aggregation induced by van der Waals and hydrophobic interactions (95). Additionally, nanosheets are a versatile platform on which hydrophilic functional groups can be combined with various materials, offering many advantages in targeted therapy and cancer diagnosis (96).

Direct immunogenicity is exhibited in graphene compared to in other nanomaterials, and the extent of the immunostimulatory capability can be modulated by changing the lateral size (97). Macrophages and dendritic cells can be activated by graphene, revealing their potential for cancer therapy. TNF-α was remarkably increased by 6-armed GO in RAW264.7 macrophages without altering IL-1β and IL-6 levels (98). Graphene can also suppress some cancer cells. Treatment of human osteosarcoma cells and normal osteoblasts with GO displayed significant cytotoxicity against osteosarcoma, and the apoptosis rate of osteosarcoma cells was remarkably higher than that of hFOB1.19 normal osteoblast cells (99). Cancer stem cells (CSCs) are cancer cells with self-renewability and high tumorigenic potency; these cells are associated with multi-drug resistance and interact with the TME (100). Hence, damage to CSCs is vital for preventing malignancy. GO can distinctively target CSCs and suppress several pivotal signaling pathways, such as Notch and STAT signaling. Moreover, GO can induce CSC differentiation (101). This effect was named as differentiation-based nanotherapy. However, the anti-CSC phenomenon are still to be evaluated.

NANOMATERIALS FOR CANCER IMMUNOTHERAPY

Nanomaterials exhibit great potential in promoting the efficacy of cancer immunotherapy. Cancer immunotherapy include two aspects: cancer vaccines and TME modulation. Cancer vaccines are developed to present cancer antigen to DCs and promote robust effector T-cell response, while TME modulation aims to expand the ability of cytotoxic T cells for killing cancer cells (102, 103). Moreover, nanomaterials preloaded with targeting ligands

can be taken up by specific cells (104). Interestingly, a recent research reported that a D-enantiomeric supermolecule nanoparticle was fabricated and its p53-dependent antiproliferative activity was exhibited and therefore antitumor immunity was enhanced (105). Immunotherapy will be benefited from delivery of tumor antigens by nanomaterials and the immune response can be also modulated by nanomaterials because of their specific characteristics (106, 107). Of note, the stimulator of interferon genes pathway was activated by the PC7A nanoparticles and therefore contribute a robust response in anti-tumor immunotherapy (108).

BIOINFORMATICS IN CANCER RESEARCH

Recently, bioinformatics gained lots of interest in the medicine and especially in the field of cancer research. The best cancer therapy depends largely on the right identification of the origin of cancers. With the developments of bioinformatics, machine learning methods have been used to predict the origin of cancer, depending on the mRNA expression, or miRNA expression. An interesting publication showed that tissue specific miRNA and DNA methylation markers have been used to detect the origin of cancer and classifiers based on DNA methylation are more powerful than miRNA-based classifiers (109). Moreover, multimodal deep learning was successfully used in the identification of choroidal neovascularization activity (110). The above classifiers and relevant biomarkers (such as mRNA) will promote the specific therapy of cancer in the future.

DISCUSSION

Nanomaterials display different properties, such as composition, structure, and immunogenicity. Cancer treatment based on these nanomaterials have been widely studied. Diverse modification can be obtained on nanomaterials and anti-tumor drugs can be preloaded into nanocarriers. Both the characteristics of the nanoplatform and agents are of vital importance. The efficacy, targeting ability, and biocompatibility are based on the modification of the nanomaterials. Drugs, peptide and small molecules can be carried by nanomaterials in targeted delivery and non-targeted delivery. In this mini-review, we focused on the properties of common nanomaterials and evolution of their applications in cancer treatment. Of note, we summarized the categories of nanomaterials used in cancer therapy and diverse cancer therapy approaches depending on nanomaterials. Nanoplatforms can also be designed to target the TME environment. With further studies of the pathophysiology of cancer genesis and multi-drug resistance germination, additional nanomaterial-based therapies will be explored. Although extensive research has been conducted, few nanomaterial-based therapies are currently in clinical use, and thus further studies are needed to address this issue. Overall, the development of nanobiotechnology will lead to progress in clinical translation. Nanomaterial-based drugs can lead to beneficial effects in patients with cancer.

AUTHOR CONTRIBUTIONS

RZ, FZ, and YP contributed equally to this work. RZ, FZ, and YP wrote the manuscript. YL, YW and TX edited the manuscript. RZ and FZ finished the figures. All authors contributed to the article and approved the submitted version.

ACKNOWLEDGMENTS

We would like to thank Editage (www.editage.cn) for English language editing.

SUPPLEMENTARY MATERIAL

The Supplementary Material for this article can be found online at: https://www.frontiersin.org/articles/10.3389/fonc.2022.930125/full#supplementary-material

REFERENCES

1. Sung H, Ferlay J, Siegel RL, Laversanne M, Soerjomataram I, Jemal A, et al. Global Cancer Statistics 2020: GLOBOCAN Estimates of Incidence and Mortality Worldwide for 36 Cancers in 185 Countries. *CA Cancer J Clin* (2021) 71:209–49. doi: 10.3322/caac.21660
2. Perez-Herrero E, Fernandez-Medarde A. Advanced Targeted Therapies in Cancer: Drug Nanocarriers, the Future of Chemotherapy. *Eur J Pharm Biopharm* (2015) 93:52–79. doi: 10.1016/j.ejpb.2015.03.018
3. Baumann M, Krause M, Hill R. Exploring the Role of Cancer Stem Cells in Radioresistance. *Nat Rev Cancer* (2008) 8:545–54. doi: 10.1038/nrc2419
4. Zou L, Wang H, He B, Zeng L, Tan T, Cao H, et al. Current Approaches of Photothermal Therapy in Treating Cancer Metastasis With Nanotherapeutics. *Theranostics* (2016) 6:762–72. doi: 10.7150/thno.14988
5. Fan W, Huang P, Chen X. Overcoming the Achilles' Heel of Photodynamic Therapy. *Chem Soc Rev* (2016) 45:6488–519. doi: 10.1039/C6CS00616G
6. Hu Q, Sun W, Wang C, Gu Z. Recent Advances of Cocktail Chemotherapy by Combination Drug Delivery Systems. *Adv Drug Delivery Rev* (2016) 98:19–34. doi: 10.1016/j.addr.2015.10.022
7. Ribas A, Wolchok JD. Cancer Immunotherapy Using Checkpoint Blockade. *Science* (2018) 359:1350–5. doi: 10.1126/science.aar4060
8. Hartshorn CM, Bradbury MS, Lanza GM, Nel AE, Rao J, Wang AZ, et al. Nanotechnology Strategies To Advance Outcomes in Clinical Cancer Care. *ACS Nano* (2018) 12:24–43. doi: 10.1021/acsnano.7b05108
9. Chen Q, Li N, Wang X, Yang Y, Xiang Y, Long X, et al. Mitochondria-Targeting Chemodynamic Therapy Nanodrugs for Cancer Treatment. *Front Pharmacol* (2022) 13:847048. doi: 10.3389/fphar.2022.847048
10. Xu JJ, Zhao WW, Song S, Fan C, Chen HY. Functional Nanoprobes for Ultrasensitive Detection of Biomolecules: An Update. *Chem Soc Rev* (2014) 43:1601–11. doi: 10.1039/C3CS60277J
11. Song Y, Li X, Wang L, Rojanasakul Y, Castranova V, Li H, et al. Nanomaterials in Humans: Identification, Characteristics, and Potential Damage. *Toxicol Pathol* (2011) 39:841–9. doi: 10.1177/0192623311413787

12. Zhao CY, Cheng R, Yang Z, Tian ZM. Nanotechnology for Cancer Therapy Based on Chemotherapy. *Molecules* (2018) 23:1–29. doi: 10.3390/molecules23040826
13. Osaki T, Yokoe I, Sunden Y, Ota U, Ichikawa T, Imazato H, et al. Efficacy of 5-Aminolevulinic Acid in Photodynamic Detection and Photodynamic Therapy in Veterinary Medicine. *Cancers (Basel)* (2019) 11:1–18. doi: 10.3390/cancers11040495
14. Gao W, Wang Z, Lv L, Yin D, Chen D, Han Z, et al. Photodynamic Therapy Induced Enhancement of Tumor Vasculature Permeability Using an Upconversion Nanoconstruct for Improved Intratumoral Nanoparticle Delivery in Deep Tissues. *Theranostics* (2016) 6:1131–44. doi: 10.7150/thno.15262
15. Qin X, Wu C, Niu D, Qin L, Wang X, Wang Q, et al. Peroxisome Inspired Hybrid Enzyme Nanogels for Chemodynamic and Photodynamic Therapy. *Nat Commun* (2021) 12:5243. doi: 10.1038/s41467-021-25561-z
16. Obireddy SR, Lai WF. Preparation and Characterization of 2-Hydroxyethyl Starch Microparticles for Co-Delivery of Multiple Bioactive Agents. *Drug Delivery* (2021) 28:1562–8. doi: 10.1080/10717544.2021.1955043
17. Maeda H, Wu J, Sawa T, Matsumura Y, Hori K. Tumor Vascular Permeability and the EPR Effect in Macromolecular Therapeutics: A Review. *J Control Release* (2000) 65:271–84. doi: 10.1016/S0168-3659(99)00248-5
18. Zhao T, Wu W, Sui L, Huang Q, Nan Y, Liu J, et al. Reactive Oxygen Species-Based Nanomaterials for the Treatment of Myocardial Ischemia Reperfusion Injuries. *Bioact Mater* (2022) 7:47–72. doi: 10.1016/j.bioactmat.2021.06.006
19. Horst MF, Coral DF, Fernandez van Raap MB, Alvarez M, Lassalle V. Hybrid Nanomaterials Based on Gum Arabic and Magnetite for Hyperthermia Treatments. *Mater Sci Eng C Mater Biol Appl* (2017) 74:443–50. doi: 10.1016/j.msec.2016.12.035
20. Ali ES, Sharker SM, Islam MT, Khan IN, Shaw S, Rahman MA, et al. Targeting Cancer Cells With Nanotherapeutics and Nanodiagnostics: Current Status and Future Perspectives. *Semin Cancer Biol* (2021) 69:52–68. doi: 10.1016/j.semcancer.2020.01.011
21. Rosenblum D, Joshi N, Tao W, Karp JM, Peer D. Progress and Challenges Towards Targeted Delivery of Cancer Therapeutics. *Nat Commun* (2018) 9:1410. doi: 10.1038/s41467-018-03705-y
22. Shi J, Xiao Z, Kamaly N, Farokhzad OC. Self-Assembled Targeted Nanoparticles: Evolution of Technologies and Bench to Bedside Translation. *Acc Chem Res* (2011) 44:1123–34. doi: 10.1021/ar200054n
23. Le Broc-Ryckewaert D, Carpentier R, Lipka E, Daher S, Vaccher C, Betbeder D, et al. Development of Innovative Paclitaxel-Loaded Small PLGA Nanoparticles: Study of Their Antiproliferative Activity and Their Molecular Interactions on Prostatic Cancer Cells. *Int J Pharm* (2013) 454:712–9. doi: 10.1016/j.ijpharm.2013.05.018
24. Bellocq NC, Pun SH, Jensen GS, Davis ME. Transferrin-Containing, Cyclodextrin Polymer-Based Particles for Tumor-Targeted Gene Delivery. *Bioconjug Chem* (2003) 14:1122–32. doi: 10.1021/bc034125f
25. Zhang X, Liu J, Li X, Li F, Lee RJ, Sun F, et al. Trastuzumab-Coated Nanoparticles Loaded With Docetaxel for Breast Cancer Therapy. *Dose Response* (2019) 17:1559325819872583. doi: 10.1177/1559325819872583
26. Abedin MR, Powers K, Aiardo R, Barua D, Barua S. Antibody-Drug Nanoparticle Induces Synergistic Treatment Efficacies in HER2 Positive Breast Cancer Cells. *Sci Rep* (2021) 11:7347. doi: 10.1038/s41598-021-86762-6
27. Bao S, Zheng H, Ye J, Huang H, Zhou B, Yao Q, et al. Dual Targeting EGFR and STAT3 With Erlotinib and Alantolactone Co-Loaded PLGA Nanoparticles for Pancreatic Cancer Treatment. *Front Pharmacol* (2021) 12:625084. doi: 10.3389/fphar.2021.625084
28. Hadla M, Palazzolo S, Corona G, Caligiuri I, Canzonieri V, Toffoli G, et al. Exosomes Increase the Therapeutic Index of Doxorubicin in Breast and Ovarian Cancer Mouse Models. *Nanomedicine (Lond)* (2016) 11:2431–41. doi: 10.2217/nnm-2016-0154
29. Masood F. Polymeric Nanoparticles for Targeted Drug Delivery System for Cancer Therapy. *Mater Sci Eng C Mater Biol Appl* (2016) 60:569–78. doi: 10.1016/j.msec.2015.11.067
30. Vijayan V, Reddy KR, Sakthivel S, Swetha C. Optimization and Charaterization of Repaglinide Biodegradable Polymeric Nanoparticle Loaded Transdermal Patchs: *In Vitro* and *In Vivo* Studies. *Colloids Surf B Biointerfaces* (2013) 111:150–5. doi: 10.1016/j.colsurfb.2013.05.020
31. Shastri VP. Non-Degradable Biocompatible Polymers in Medicine: Past, Present and Future. *Curr Pharm Biotechnol* (2003) 4:331–7. doi: 10.2174/1389201033489694
32. Elsabahy M, Wooley KL. Design of Polymeric Nanoparticles for Biomedical Delivery Applications. *Chem Soc Rev* (2012) 41:2545–61. doi: 10.1039/c2cs15327k
33. Martin-Saldana S, Palao-Suay R, Aguilar MR, Ramirez-Camacho R, San Roman J. Polymeric Nanoparticles Loaded With Dexamethasone or Alpha-Tocopheryl Succinate to Prevent Cisplatin-Induced Ototoxicity. *Acta Biomater* (2017) 53:199–210. doi: 10.1016/j.actbio.2017.02.019
34. Wang J, Sui L, Huang J, Miao L, Nie Y, Wang K, et al. MoS2-Based Nanocomposites for Cancer Diagnosis and Therapy. *Bioact Mater* (2021) 6:4209–42. doi: 10.1016/j.bioactmat.2021.04.021
35. Huang J, Huang Q, Liu M, Chen Q, Ai K. Emerging Bismuth Chalcogenides Based Nanodrugs for Cancer Radiotherapy. *Front Pharmacol* (2022) 13:844037. doi: 10.3389/fphar.2022.844037
36. Lai W-F. Non-Conjugated Polymers With Intrinsic Luminescence for Drug Delivery. *J Drug Delivery Sci Technol* (2020) 59:101916. doi: 10.1016/j.jddst.2020.101916
37. Bernier-Latmani J, Petrova TV. Intestinal Lymphatic Vasculature: Structure, Mechanisms and Functions. *Nat Rev Gastroenterol Hepatol* (2017) 14:510–26. doi: 10.1038/nrgastro.2017.79
38. Ajorlou E, Khosroushahi AY. Trends on Polymer- and Lipid-Based Nanostructures for Parenteral Drug Delivery to Tumors. *Cancer Chemother Pharmacol* (2017) 79:251–65. doi: 10.1007/s00280-016-3168-6
39. Teixeira MC, Carbone C, Souto EB. Beyond Liposomes: Recent Advances on Lipid Based Nanostructures for Poorly Soluble/Poorly Permeable Drug Delivery. *Prog Lipid Res* (2017) 68:1–11. doi: 10.1016/j.plipres.2017.07.001
40. Andreiuk B, Reisch A, Lindecker M, Follain G, Peyrieras N, Goetz JG, et al. Fluorescent Polymer Nanoparticles for Cell Barcoding *In Vitro* and In Vivo. *Small* (2017) 13:1–24. doi: 10.1002/smll.201701582
41. Kang EB, Lee JE, Mazrad ZAI, In I, Jeong JH, Park SY. pH-Responsible Fluorescent Carbon Nanoparticles for Tumor Selective Theranostics *via* pH-Turn on/Off Fluorescence and Photothermal Effect *In Vivo* and In Vitro. *Nanoscale* (2018) 10:2512–23. doi: 10.1039/C7NR07900A
42. Tang C, Edelstein J, Mikitsh JL, Xiao E, Hemphill AH2nd, Pagels R, et al. Biodistribution and Fate of Core-Labeled ^{125} I Polymeric Nanocarriers Prepared by Flash NanoPrecipitation (FNP). *J Mater Chem B* (2016) 4:2428–34. doi: 10.1039/C5TB02172C
43. Peltek OO, Muslimov AR, Zyuzin MV, Timin AS. Current Outlook on Radionuclide Delivery Systems: From Design Consideration to Translation Into Clinics. *J Nanobiotechnology* (2019) 17:90. doi: 10.1186/s12951-019-0524-9
44. Dey R, Xia Y, Nieh MP, Burkhard P. Molecular Design of a Minimal Peptide Nanoparticle. *ACS Biomater Sci Eng* (2017) 3:724–32. doi: 10.1021/acsbiomaterials.6b00243
45. Thakkar D, Gupta R, Mohan P, Monson K, Rapoport N. Overcoming Biological Barriers With Ultrasound. *AIP Conf Proc* (2012) 1481:381–7. doi: 10.1063/1.4757365
46. Barua S, Mitragotri S. Challenges Associated With Penetration of Nanoparticles Across Cell and Tissue Barriers: A Review of Current Status and Future Prospects. *Nano Today* (2014) 9:223–43. doi: 10.1016/j.nantod.2014.04.008
47. Zhou Y, Peng Z, Seven ES, Leblanc RM. Crossing the Blood-Brain Barrier With Nanoparticles. *J Control Release* (2018) 270:290–303. doi: 10.1016/j.jconrel.2017.12.015
48. Tharkar P, Varanasi R, Wong WSF, Jin CT, Chrzanowski W. Nano-Enhanced Drug Delivery and Therapeutic Ultrasound for Cancer Treatment and Beyond. *Front Bioeng Biotechnol* (2019) 7:324. doi: 10.3389/fbioe.2019.00324
49. Lockman PR, Mumper RJ, Khan MA, Allen DD. Nanoparticle Technology for Drug Delivery Across the Blood-Brain Barrier. *Drug Dev Ind Pharm* (2002) 28:1–13. doi: 10.1081/DDC-120001481
50. Sievers EL, Senter PD. Antibody-Drug Conjugates in Cancer Therapy. *Annu Rev Med* (2013) 64:15–29. doi: 10.1146/annurev-med-050311-201823

51. Nieto C, Vega MA, Martin Del Valle EM. Trastuzumab: More Than a Guide in HER2-Positive Cancer Nanomedicine. *Nanomaterials (Basel)* (2020) 10:1–21. doi: 10.3390/nano10091674
52. Xu P, Wang R, Yang W, Liu Y, He D, Ye Z, et al. A DM1-Doped Porous Gold Nanoshell System for NIR Accelerated Redox-Responsive Release and Triple Modal Imaging Guided Photothermal Synergistic Chemotherapy. *J Nanobiotechnology* (2021) 19:77. doi: 10.1186/s12951-021-00824-5
53. Fu Q, Wang J, Liu H. Chemo-Immune Synergetic Therapy of Esophageal Carcinoma: Trastuzumab Modified, Cisplatin and Fluorouracil Co-Delivered Lipid-Polymer Hybrid Nanoparticles. *Drug Delivery* (2020) 27:1535–43. doi: 10.1080/10717544.2020.1837294
54. Liang S, Sun M, Lu Y, Shi S, Yang Y, Lin Y, et al. Cytokine-Induced Killer Cells-Assisted Tumor-Targeting Delivery of Her-2 Monoclonal Antibody-Conjugated Gold Nanostars With NIR Photosensitizer for Enhanced Therapy of Cancer. *J Mater Chem B* (2020) 8:8368–82. doi: 10.1039/D0TB01391A
55. Samad A, Sultana Y, Aqil M. Liposomal Drug Delivery Systems: An Update Review. *Curr Drug Delivery* (2007) 4:297–305. doi: 10.2174/156720107782151269
56. Zhang L, Gu FX, Chan JM, Wang AZ, Langer RS, Farokhzad OC. Nanoparticles in Medicine: Therapeutic Applications and Developments. *Clin Pharmacol Ther* (2008) 83:761–9. doi: 10.1038/sj.clpt.6100400
57. Portney NG, Ozkan M. Nano-Oncology: Drug Delivery, Imaging, and Sensing. *Anal Bioanal Chem* (2006) 384:620–30. doi: 10.1007/s00216-005-0247-7
58. Cattel L, Ceruti M, Dosio F. From Conventional to Stealth Liposomes: A New Frontier in Cancer Chemotherapy. *Tumori* (2003) 89:237–49. doi: 10.1177/030089160308900302
59. James ND, Coker RJ, Tomlinson D, Harris JR, Gompels M, Pinching AJ, et al. Liposomal Doxorubicin (Doxil): An Effective New Treatment for Kaposi's Sarcoma in AIDS. *Clin Oncol (R Coll Radiol)* (1994) 6:294–6. doi: 10.1016/S0936-6555(05)80269-9
60. Laginha KM, Verwoert S, Charrois GJ, Allen TM. Determination of Doxorubicin Levels in Whole Tumor and Tumor Nuclei in Murine Breast Cancer Tumors. *Clin Cancer Res* (2005) 11:6944–9. doi: 10.1158/1078-0432.CCR-05-0343
61. Sriraman SK, Geraldo V, Luther E, Degterev A, Torchilin V. Cytotoxicity of PEGylated Liposomes Co-Loaded With Novel Pro-Apoptotic Drug NCL-240 and the MEK Inhibitor Cobimetinib Against Colon Carcinoma In Vitro. *J Control Release* (2015) 220:160–8. doi: 10.1016/j.jconrel.2015.10.037
62. Batist G, Gelmon KA, Chi KN, Miller WHJr., Chia SK, Mayer LD, et al. Safety, Pharmacokinetics, and Efficacy of CPX-1 Liposome Injection in Patients With Advanced Solid Tumors. *Clin Cancer Res* (2009) 15:692–700. doi: 10.1158/1078-0432.CCR-08-0515
63. Deng ZJ, Morton SW, Ben-Akiva E, Dreaden EC, Shopsowitz KE, Hammond PT. Layer-By-Layer Nanoparticles for Systemic Codelivery of an Anticancer Drug and siRNA for Potential Triple-Negative Breast Cancer Treatment. *ACS Nano* (2013) 7:9571–84. doi: 10.1021/nn4047925
64. Zhang H, Li RY, Lu X, Mou ZZ, Lin GM. Docetaxel-Loaded Liposomes: Preparation, pH Sensitivity, Pharmacokinetics, and Tissue Distribution. *J Zhejiang Univ Sci B* (2012) 13:981–9. doi: 10.1631/jzus.B1200098
65. Yao Y, Su Z, Liang Y, Zhang N. pH-Sensitive Carboxymethyl Chitosan-Modified Cationic Liposomes for Sorafenib and siRNA Co-Delivery. *Int J Nanomedicine* (2015) 10:6185–97. doi: 10.2147/IJN.S90524
66. Naseri N, Valizadeh H, Zakeri-Milani P. Solid Lipid Nanoparticles and Nanostructured Lipid Carriers: Structure, Preparation and Application. *Adv Pharm Bull* (2015) 5:305–13. doi: 10.15171/apb.2015.043
67. Kraft JC, Freeling JP, Wang Z, Ho RJ. Emerging Research and Clinical Development Trends of Liposome and Lipid Nanoparticle Drug Delivery Systems. *J Pharm Sci* (2014) 103:29–52. doi: 10.1002/jps.23773
68. Das S, Chaudhury A. Recent Advances in Lipid Nanoparticle Formulations With Solid Matrix for Oral Drug Delivery. *AAPS PharmSciTech* (2011) 12:62–76. doi: 10.1208/s12249-010-9563-0
69. Selvamuthukumar S, Velmurugan R. Nanostructured Lipid Carriers: A Potential Drug Carrier for Cancer Chemotherapy. *Lipids Health Dis* (2012) 11:159. doi: 10.1186/1476-511X-11-159
70. Iqbal MA, Md S, Sahni JK, Baboota S, Dang S, Ali J. Nanostructured Lipid Carriers System: Recent Advances in Drug Delivery. *J Drug Target* (2012) 20:813–30. doi: 10.3109/1061186X.2012.716845
71. Jaiswal M, Dudhe R, Sharma PK. Nanoemulsion: An Advanced Mode of Drug Delivery System. *3 Biotech* (2015) 5:123–7. doi: 10.1007/s13205-014-0214-0
72. Gorain B, Choudhury H, Nair AB, Dubey SK, Kesharwani P. Theranostic Application of Nanoemulsions in Chemotherapy. *Drug Discovery Today* (2020) 25:1174–88. doi: 10.1016/j.drudis.2020.04.013
73. Gadhave DG, Kokare CR. Nanostructured Lipid Carriers Engineered for Intranasal Delivery of Teriflunomide in Multiple Sclerosis: Optimization and *In Vivo* Studies. *Drug Dev Ind Pharm* (2019) 45:839–51. doi: 10.1080/03639045.2019.1576724
74. Sanchez-Lopez E, Guerra M, Dias-Ferreira J, Lopez-Machado A, Ettcheto M, Cano A, et al. Current Applications of Nanoemulsions in Cancer Therapeutics. *Nanomaterials (Basel)* (2019) 9:1–29. doi: 10.3390/nano9060821
75. Azambuja JH, Schuh RS, Michels LR, Gelsleichter NE, Beckenkamp LR, Iser IC, et al. Nasal Administration of Cationic Nanoemulsions as CD73-siRNA Delivery System for Glioblastoma Treatment: A New Therapeutical Approach. *Mol Neurobiol* (2020) 57:635–49. doi: 10.1007/s12035-019-01730-6
76. Du M, Yang Z, Lu W, Wang B, Wang Q, Chen Z, et al. Design and Development of Spirulina Polysaccharide-Loaded Nanoemulsions With Improved the Antitumor Effects of Paclitaxel. *J Microencapsul* (2020) 37:403–12. doi: 10.1080/02652048.2020.1767224
77. Dianzani C, Monge C, Miglio G, Serpe L, Martina K, Cangemi L, et al. Nanoemulsions as Delivery Systems for Poly-Chemotherapy Aiming at Melanoma Treatment. *Cancers (Basel)* (2020) 12:1–18. doi: 10.3390/cancers12051198
78. Ribeiro EB, de Marchi PGF, Honorio-Franca AC, Franca EL, Soler MAG. Interferon-Gamma Carrying Nanoemulsion With Immunomodulatory and Anti-Tumor Activities. *J BioMed Mater Res A* (2020) 108:234–45. doi: 10.1002/jbm.a.36808
79. Meng L, Xia X, Yang Y, Ye J, Dong W, Ma P, et al. Co-Encapsulation of Paclitaxel and Baicalein in Nanoemulsions to Overcome Multidrug Resistance *via* Oxidative Stress Augmentation and P-Glycoprotein Inhibition. *Int J Pharm* (2016) 513:8–16. doi: 10.1016/j.ijpharm.2016.09.001
80. Baker JRJr. Dendrimer-Based Nanoparticles for Cancer Therapy. *Hematol Am Soc Hematol Educ Program* (2009) 2009:708–19. doi: 10.1182/asheducation-2009.1.708
81. Lim J, Kostiainen M, Maly J, da Costa VC, Annunziata O, Pavan GM, et al. Synthesis of Large Dendrimers With the Dimensions of Small Viruses. *J Am Chem Soc* (2013) 135:4660–3. doi: 10.1021/ja400432e
82. Lo ST, Kumar A, Hsieh JT, Sun X. Dendrimer Nanoscaffolds for Potential Theranostics of Prostate Cancer With a Focus on Radiochemistry. *Mol Pharm* (2013) 10:793–812. doi: 10.1021/mp3005325
83. Li D, Fan Y, Shen M, Banyai I, Shi X. Design of Dual Drug-Loaded Dendrimer/Carbon Dot Nanohybrids for Fluorescence Imaging and Enhanced Chemotherapy of Cancer Cells. *J Mater Chem B* (2019) 7:277–85. doi: 10.1039/C8TB02723D
84. Pishavar E, Ramezani M, Hashemi M. Co-Delivery of Doxorubicin and TRAIL Plasmid by Modified PAMAM Dendrimer in Colon Cancer Cells, *In Vitro* and *In Vivo* Evaluation. *Drug Dev Ind Pharm* (2019) 45:1931–9. doi: 10.1080/03639045.2019.1680995
85. Tarach P, Janaszewska A. Recent Advances in Preclinical Research Using PAMAM Dendrimers for Cancer Gene Therapy. *Int J Mol Sci* (2021) 22:1–30. doi: 10.3390/ijms22062912
86. Jedrzak A, Grzeskowiak BF, Coy E, Wojnarowicz J, Szutkowski K, Jurga S, et al. Dendrimer Based Theranostic Nanostructures for Combined Chemo- and Photothermal Therapy of Liver Cancer Cells In Vitro. *Colloids Surf B Biointerfaces* (2019) 173:698–708. doi: 10.1016/j.colsurfb.2018.10.045
87. Novoselov KS, Geim AK, Morozov SV, Jiang D, Zhang Y, Dubonos SV, et al. Electric Field Effect in Atomically Thin Carbon Films. *Science* (2004) 306:666–9. doi: 10.1126/science.1102896
88. Liu J, Dong J, Zhang T, Peng Q. Graphene-Based Nanomaterials and Their Potentials in Advanced Drug Delivery and Cancer Therapy. *J Control Release* (2018) 286:64–73. doi: 10.1016/j.jconrel.2018.07.034

89. Geim AK, Novoselov KS. The Rise of Graphene. *Nat Mater* (2007) 6:183–91. doi: 10.1038/nmat1849
90. Verde V, Longo A, Cucci LM, Sanfilippo V, Magri A, Satriano C, et al. Anti-Angiogenic and Anti-Proliferative Graphene Oxide Nanosheets for Tumor Cell Therapy. *Int J Mol Sci* (2020) 21:1–23. doi: 10.3390/ijms21155571
91. Rebuttini V, Fazio E, Santangelo S, Neri F, Caputo G, Martin C, et al. Chemical Modification of Graphene Oxide Through Diazonium Chemistry and Its Influence on the Structure-Property Relationships of Graphene Oxide-Iron Oxide Nanocomposites. *Chemistry* (2015) 21:12465–74. doi: 10.1002/chem.201500836
92. Balandin AA, Ghosh S, Bao W, Calizo I, Teweldebrhan D, Miao F, et al. Superior Thermal Conductivity of Single-Layer Graphene. *Nano Lett* (2008) 8:902–7. doi: 10.1021/nl0731872
93. Ema M, Gamo M, Honda K. A Review of Toxicity Studies on Graphene-Based Nanomaterials in Laboratory Animals. *Regul Toxicol Pharmacol* (2017) 85:7–24. doi: 10.1016/j.yrtph.2017.01.011
94. Zhang Z, Liu Q, Gao D, Luo D, Niu Y, Yang J, et al. Graphene Oxide as a Multifunctional Platform for Raman and Fluorescence Imaging of Cells. *Small* (2015) 11:3000–5. doi: 10.1002/smll.201403459
95. Geim AK. Graphene: Status and Prospects. *Science* (2009) 324:1530–4. doi: 10.1126/science.1158877
96. Goenka S, Sant V, Sant S. Graphene-Based Nanomaterials for Drug Delivery and Tissue Engineering. *J Control Release* (2014) 173:75–88. doi: 10.1016/j.jconrel.2013.10.017
97. Ma J, Liu R, Wang X, Liu Q, Chen Y, Valle RP, et al. Crucial Role of Lateral Size for Graphene Oxide in Activating Macrophages and Stimulating Pro-Inflammatory Responses in Cells and Animals. *ACS Nano* (2015) 9:10498–515. doi: 10.1021/acsnano.5b04751
98. Feito MJ, Vila M, Matesanz MC, Linares J, Goncalves G, Marques PA, et al. *In Vitro* Evaluation of Graphene Oxide Nanosheets on Immune Function. *J Colloid Interface Sci* (2014) 432:221–8. doi: 10.1016/j.jcis.2014.07.004
99. Burnett M, Abuetabh Y, Wronski A, Shen F, Persad S, Leng R, et al. Graphene Oxide Nanoparticles Induce Apoptosis in Wild-Type and CRISPR/Cas9-IGF/IGFBP3 Knocked-Out Osteosarcoma Cells. *J Cancer* (2020) 11:5007–23. doi: 10.7150/jca.46464
100. Najafi M, Mortezaee K, Majidpoor J. Cancer Stem Cell (CSC) Resistance Drivers. *Life Sci* (2019) 234:116781. doi: 10.1016/j.lfs.2019.116781
101. Fiorillo M, Verre AF, Iliut M, Peiris-Pages M, Ozsvari B, Gandara R, et al. Graphene Oxide Selectively Targets Cancer Stem Cells, Across Multiple Tumor Types: Implications for non-Toxic Cancer Treatment, *via* "Differentiation-Based Nano-Therapy". *Oncotarget* (2015) 6:3553–62. doi: 10.18632/oncotarget.3348
102. Melero I, Gaudernack G, Gerritsen W, Huber C, Parmiani G, Scholl S, et al. Therapeutic Vaccines for Cancer: An Overview of Clinical Trials. *Nat Rev Clin Oncol* (2014) 11:509–24. doi: 10.1038/nrclinonc.2014.111
103. Zou W, Wolchok JD, Chen L. PD-L1 (B7-H1) and PD-1 Pathway Blockade for Cancer Therapy: Mechanisms, Response Biomarkers, and Combinations. *Sci Transl Med* (2016) 8:328rv324. doi: 10.1126/scitranslmed.aad7118
104. Sykes EA, Dai Q, Sarsons CD, Chen J, Rocheleau JV, Hwang DM, et al. Tailoring Nanoparticle Designs to Target Cancer Based on Tumor Pathophysiology. *Proc Natl Acad Sci U.S.A.* (2016) 113:E1142–1151. doi: 10.1073/pnas.1521265113
105. Yan J, Yao Y, Yan S, Gao R, Lu W, He W. Chiral Protein Supraparticles for Tumor Suppression and Synergistic Immunotherapy: An Enabling Strategy for Bioactive Supramolecular Chirality Construction. *Nano Lett* (2020) 20:5844–52. doi: 10.1021/acs.nanolett.0c01757
106. Bolhassani A, Safaiyan S, Rafati S. Improvement of Different Vaccine Delivery Systems for Cancer Therapy. *Mol Cancer* (2011) 10:3. doi: 10.1186/1476-4598-10-3
107. Smith MJ, Brown JM, Zamboni WC, Walker NJ. From Immunotoxicity to Nanotherapy: The Effects of Nanomaterials on the Immune System. *Toxicol Sci* (2014) 138:249–55. doi: 10.1093/toxsci/kfu005
108. Luo M, Wang H, Wang Z, Cai H, Lu Z, Li Y, et al. A STING-Activating Nanovaccine for Cancer Immunotherapy. *Nat Nanotechnol* (2017) 12:648–54. doi: 10.1038/nnano.2017.52
109. Tang W, Wan S, Yang Z, Teschendorff AE, Zou Q. Tumor Origin Detection With Tissue-Specific miRNA and DNA Methylation Markers. *Bioinformatics* (2018) 34:398–406. doi: 10.1093/bioinformatics/btx622
110. Jin K, Yan Y, Chen M, Wang J, Pan X, Liu X, et al. Multimodal deep learning with feature level fusion for identification of choroidal neovascularization activity in agerelated macular degeneration. *Acta Ophthalmol* (2022) 100: e512–20. doi: 10.1111/aos.14928

Conflict of Interest: The authors declare that the research was conducted in the absence of any commercial or financial relationships that could be construed as a potential conflict of interest.

The reviewer WZ declared a shared affiliation with the author YW to the handling editor at the time of review.

Publisher's Note: All claims expressed in this article are solely those of the authors and do not necessarily represent those of their affiliated organizations, or those of the publisher, the editors and the reviewers. Any product that may be evaluated in this article, or claim that may be made by its manufacturer, is not guaranteed or endorsed by the publisher.

Copyright © 2022 Zhu, Zhang, Peng, Xie, Wang and Lan. This is an open-access article distributed under the terms of the Creative Commons Attribution License (CC BY). The use, distribution or reproduction in other forums is permitted, provided the original author(s) and the copyright owner(s) are credited and that the original publication in this journal is cited, in accordance with accepted academic practice. No use, distribution or reproduction is permitted which does not comply with these terms.

frontiers | Frontiers in Pharmacology

REVIEW
published: 22 July 2022
doi: 10.3389/fphar.2022.929854

Recent Advance in Tumor Microenvironment-Based Stimuli-Responsive Nanoscale Drug Delivery and Imaging Platform

Fengzhi Cui, Jianhua Liu, Siwen Pang and Bo Li**

Department of Radiology, The Second Hospital of Jilin University, Changchun, China

The tumor microenvironment (TME) plays an important role in the development, progression, and metastasis of cancer, and the extremely crucial feature is hypoxic and acidic. Cancer-associated fibroblasts (CAFs), extracellular matrix (ECM), mesenchymal cells, blood vessels, and interstitial fluid are widely recognized as fundamentally crucial hallmarks for TME. As nanotechnology briskly boomed, the nanoscale drug delivery and imaging platform (NDDIP) emerged and has attracted intensive attention. Based on main characteristics of TME, NDDIP can be classified into pH-sensitive delivery and imaging platforms, enzyme-sensitive delivery and imaging platforms, thermo-sensitive delivery and imaging platforms, redox-sensitive delivery and imaging platforms, and light-sensitive delivery and imaging platforms. Furthermore, imageology is one of the significant procedures for disease detection, image-guided drug delivery, and efficacy assessment, including magnetic resonance imaging (MRI), computed tomography (CT), ultrasound (US), and fluorescence imaging. Therefore, the stimuli-responsive NDDIP will be a versatile and practicable tumor disease diagnostic procedure and efficacy evaluation tool. In this review article, we mainly introduce the characteristics of TME and summarize the progress of multitudinous NDDIP as well as their applications.

Keywords: stimuli-responsive nanoscale drug delivery, imaging platform, nanomaterials, TME, cancer therapy

OPEN ACCESS

Edited by:
Zeming Liu,
Huazhong University of Science and Technology, China

Reviewed by:
Meng Li,
Hebei Medical University, China
Zhen Yang,
Fujian Normal University, China

****Correspondence:***
Jianhua Liu
jian_hua@jlu.edu.cn
Bo Li
l_b99@jlu.edu.cn

Specialty section:
This article was submitted to Pharmacology of Anti-Cancer Drugs, a section of the journal Frontiers in Pharmacology

Received: *27 April 2022*
Accepted: *30 May 2022*
Published: *22 July 2022*

Citation:
Cui F, Liu J, Pang S and Li B (2022) Recent Advance in Tumor Microenvironment-Based Stimuli-Responsive Nanoscale Drug Delivery and Imaging Platform. Front. Pharmacol. 13:929854. doi: 10.3389/fphar.2022.929854

INTRODUCTION

Cancer is the most common cause of death worldwide threatening human health seriously. According to cancer statistics in 2021, approximately nearly one million new cancer deaths and six hundred thousand cancer deaths were reported. The incidence and mortality rates of cancer have continuously increased for the past few years (Siegel et al., 2021). Despite traditional therapies for cancer, surgery, radiotherapy, chemotherapy, and all kinds of other therapy have made significant and remarkable achievements. These also lead to many systemic side effects such as 1) although cancer resection greatly prolongs patients' survival time, it reduces the survival quality (Nam and Shin, 2021); 2) chemotherapy drug is known to have adverse side effects such as drug resistance, nonspecific toxicity, and short circulating half-life (YAN et al., 2020); 3) in view of the conventional radiotherapy with many restrictions lead to long-term destruction of normal organ functions as well as the immune system (Zhang et al., 2019). In consequence, novel and efficient therapeutic methods

(Naidoo and Chuturgoon, 2021) with fewer side effects, high efficiency, and low toxicity still urgently need to be explored.

With the remarkable and rapid progress of nanotechnology, the nanomaterial is gradually emerging and has become a global research spotlight (Bhutta et al., 2021). Based on their unique advantages, such as extremely small size, high stability performance, and favourable biocompatibility properties, nanomaterials have attracted intensive attention, giving rise to the novel bellwether as nanomedicine, especially in noninvasive diagnosis, precise therapy (Jiang et al., 2021), and prevention of cancer (Xiang et al., 2020; El-Sayed and Kamel, 2020; Wang et al., 2021; HE et al., 2015). Nanomaterials can be produced into a variety of spatial structures, morphology, forms, and surface modification based on their intrinsic thermal, electrical, magnetic, and optical physical properties. Nanomaterial is widely used as a theranostic agent in PTT (photothermal therapy) (Huang et al., 2021), PDT (photodynamic therapy) (Bharathiraja et al., 2018; Wu et al., 2021), CDT (chemodynamic therapy) (Wang et al., 2022; Yang et al., 2022), and NDDS (Bai et al., 2021; Foglietta et al., 2021) to overcome the limitations of standard cancer treatments.

A variety of nanomaterials have attracted a lot of research attention as diagnostic and therapeutic tools to promote the exploration of nanomedical cancer therapy. As a typical paradigm, Liu et al. have synthesized $NaYbF_4$:Tm@$NaGdF_4$: Yb-PVP nanoparticles to serve as the most attractive candidates to achieve UCL/MRI/CT tri-modal imaging and improve the detected rate of early-stage tumor (Wang et al., 2017). In another representative work, Li et al. constructed a magnetic composite nanoplatform using cancer PTT, by coating with the PDA on the surface of Fe_3O_4 nanoparticles. Such a well-designed composite therapeutic nanoparticles exert its cancer therapeutic effect, promoting the application of nanomedical in cancer therapy (Li et al., 2020). In a significant work in 2018, Liu et al. further demonstrated the protective effects of CFNs, integrated PDT, CDT, PTT, and MRI imaging capabilities, achieving synergistic cancer treatment. The "all-in-one" nanoplatform has tremendous potential in cancer theranostics (Liu et al., 2018). In light of this, Deng et al. prepared targeted multifunctional UCHNs-PAMA nanocarriers that offered the enhanced T_1-weighted MRI, CT, and upconverting luminescence (UCL) imaging. Meanwhile, the nanoparticle-loaded Pt(VI) has effective inhibition for combinational therapy of cancer *via* the *in vitro* and *in vivo* experiments confirmed. In consequence, UCHNs-PAMA-Pt(IV) possesses a multifunctional platform for trimodal imaging and therapeutic applications (Deng et al., 2015). Further experimental results manifest that such nanocarriers are capable of exerting significant therapeutic efficacy in cancer. In conclusion, many research studies have certified that nanomaterials represent excellent and remarkable merits in the therapy of cancer.

Herein, we categorize the diversity of NDDIP based on stimulus and emphasize the most recent treatment research for cancerous diseases. Simultaneously, we discuss the latest application and development trends of NDDIP in the future.

CHARACTERISTICS OF THE TUMOR MICROENVIRONMENT

TME is of crucial effect on cancer generation, progression, invasion, metastasis, and drug resistance. It is composed of CAFs, ECM, mesenchymal cells, blood vessels, and interstitial fluid (Barati Bagherabad et al., 2017; Anderson and Simon, 2020). CAFs, as the main components of the tumor stroma, are mainly located in the perivascular or peripheral interstitial fibers, secreting cytokines and related enzyme molecules. ECM deposition can produce a dense fibrous interstitium that encapsulates the tumor, making the tumor tissue more fragile and stiffer than normal tissue, forming a physical barrier to immune cell infiltration and inhibiting the targeting of antitumor drugs. Meanwhile, CAFs secrete proteases that remodel the ECM and release chemokines, growth factors, and proangiogenic factors, promoting the malignant transformation of tumors (Jiang et al., 2020). With rapid tumor growth and vascular anisotropy, the intratumor blood supply is often inadequate, causing the tumor microenvironment in a long-term hypoxic environment (Wang et al., 2018a; Chamundeeswari et al., 2019). Additionally, aerobic glycolysis significantly enhanced, further aggravating the acidification in the tumor microenvironment. Generally, the extracellular pH of normal tissues fluctuates within an appropriate range of 7.2–7.4. But the pH value in the majority of tumor extracellular sites is typically lower than that of normal tissue, within the scope of 6.2–6.9 (Ma et al., 2018). Therefore, novel pH-sensitive NDDIPs as a target are promising in the therapeutic efficacy of cancer therapy.

Glutathione (GSH), as an antioxidant, is one of the most important enzymatic platforms which keep the intracellular redox balance in cancer cells. Cysteine, glutamic acid, and glycine compose of GSH exist in two interconvertible and active forms: reduced form (GSH) and oxidized form (GSSG). Intracellularly, a large proportion of GSH is existed in the cytosol with more than 90%, while mitochondria exist at nearly 10% and the endoplasmic reticulum contains an extremely small amount (Rozanov et al., 2015). Many malignant tumor cells are especially dependent on elevated GSH. Therefore, the GSH system has attracted the intensive attention of pharmacologists as a hope target for medical intervention against cancer progression (Nunes and Serpa, 2018; Marengo et al., 2019).

ROS, as byproducts of incomplete aerobic respiration, refer to a series of the highly reactive substances, existing in two forms of radical and nonradical, which include hydrogen peroxide (H_2O_2), singlet oxygen ($^1O_2$), peroxide (O_2^{2-}), superoxide (O_2^-), and hydroxyl radical (•OH) (Sai et al., 2021; Zhu et al., 2022). ROS functions as a double-edged sword *in vivo* (Zhao et al., 2022; Chen et al., 2021). Some research confirmed that ROS has the capability of stimulating physiological cellular proliferation, and the substances can be utilized by a tumor to promote survival and differentiation. However, high levels of ROS can have

TABLE 1 | Illustrative examples of NDDIP and their biomedical applications.

Nanomaterials platform	Type	Imaging	Application	Characteristic	Ref
Mesoporous silica nanoparticle	pH-sensitive	T_1-weighted MRI	Tumor tissue	The acetal at acidic pH could generate physicochemical property variations to the removal of the S-NPs to release DOX in the cancer sites	Chen et al. (2015)
HER-DMNPs	pH-sensitive	T_2-weighted MRI	Tumor tissue	The π–π interactions between DOX and pyrene groups could be decreased at acidic pH to release DOX	Lim et al. (2011)
Poly[N-(2-hydroxypropyl) methacrylamide] (polyHPMA) copolymer	Enzyme- and pH-sensitive	—	Breast cancer	The conformational changes of HPMA take place in DOX releasing from the conjugate under the high concentration of cathepsin B and lower pH value	Wei et al. (2016)
Gelatin nanoparticle	Enzyme-sensitive	Fluorescence imaging	Tumor tissue	Gelatin NPs could be degraded when exposed to a higher concentration of matrix metalloproteinase-2 enzymes in the TME, achieved PAMAM dendrimers release, and improved intracellular uptake into tumor cells	Fan et al. (2017)
Fe_3O_4@P(MEO_2MA_{60}-$OEGMA_{40}$)NP	Thermo-sensitive	—	Tumor tissue	The drug release is accelerated based on the high temperature which is raised above the CST, inducing polymer chains to shrink to release DOX.	Jamal Al Dine et al. (2017)
M-MNCs	pH- and thermo-sensitive	T_2-weighted MRI	Lung cancer cell	M-MNCs possessed pH- and thermo-sensitive release behavior in which the released amount was highest	Farshbaf et al. (2018)
mPEG-ss-Tripp	Redox-sensitive	AIE imaging	Tumor tissue	Disulfide bonds are sensitive to reductive substance GSH, which quickly cleaved through thiol-disulfide exchange to release DOX	Sun et al. (2021)
DOX@MSN-ss-GHA	Redox-sensitive	T_1-weighted MRI	Tumor tissue	A higher concentration of GSH prompted the disulfide linkage in MSN-ss-GHA to cleave occurring in the cancer cellular environment which achieved drug efflux rapidly	Chen et al. (2016)
FCCP NPs (Fe3O4@CS/CuS NPs)	Redox-sensitive	T_2-weighted MRI	Tumor tissue	The generation of •OH as a therapeutic agent and the concurrent production of O_2 as a conditioning agent for cancer theranostics	Zhang et al. (2018b)
AuNSt-MSNP	Light-sensitive	—	Tumor tissue	Thiolated photolabile molecule is sensitive to the NIR light, leading to the formation of succinic acid which triggered controlled DOX-specific release based on irradiation with NIR-light	Hernández Montoto et al. (2019)
Multifunctional anticancer-drug carrier	Light-sensitive	T_2-weighted MRI	Tumor tissue	The temperature increases from laser irradiation for precise control of the DOX release	Yoon et al. (2019)

deleterious effects, breaking down lipids, proteins, and genetic material DNA. Furthermore, many research studies have confirmed that ROS regarded as an effective tumor inhibitor to achieve potent cancer treatment (Ming et al., 2020; Malla et al., 2021). In conclusion, concentrations of ROS in tumor tissues and intracellular cancerous cells are enormously higher in comparison with normal cells (Weinberg et al., 2019).

NANOSCALE DRUG DELIVERY AND IMAGING PLATFORM

NDDIP is one of the most spectacular and significant prospects in the targeted drug delivery therapeutics and efficacy evaluation agents (Aminu et al., 2020). It has been used to deliver multitudinous chemotherapeutic drugs, inhibitors, vaccines, and proteins. Among them, the most tremendous promise of nanotechnology is NDDIP complexes.

Smart NDDIP combined with stimuli-sensitive properties that can either respond to physical or biological stimuli has recently become the center of attention. According to special characteristics of the diseased microenvironment, NDDIP for drug delivery and imaging platforms can be classified into pH-sensitive delivery and imaging platforms, enzyme-sensitive delivery and imaging platforms, thermo-sensitive delivery and imaging platforms, redox-sensitive delivery and imaging platforms, and light-sensitive delivery and imaging platforms as seen in **Table 1** and **Figure 1**.

pH-Sensitive Delivery and Imaging Platforms

In the midst of the various sensitive nanoscale drug delivery platforms, pH-sensitive delivery and imaging platform is known as the most comprehensive strategy as a result of the acidification in the solid tumor microenvironment obviously. It is known that the pH value of the tumor extracellular microenvironment is approximately 6.5, lower than that of normal tissue. Therefore, pH-sensitive delivery and imaging platforms are capable of generating physicochemical property variations at a mild acidic tumor microenvironment for their structure or conformation characteristics, resulting in anticancer drugs or contrast enhancement at the desired site. Then, multiple imaging methods were used to observe the changes in lesion

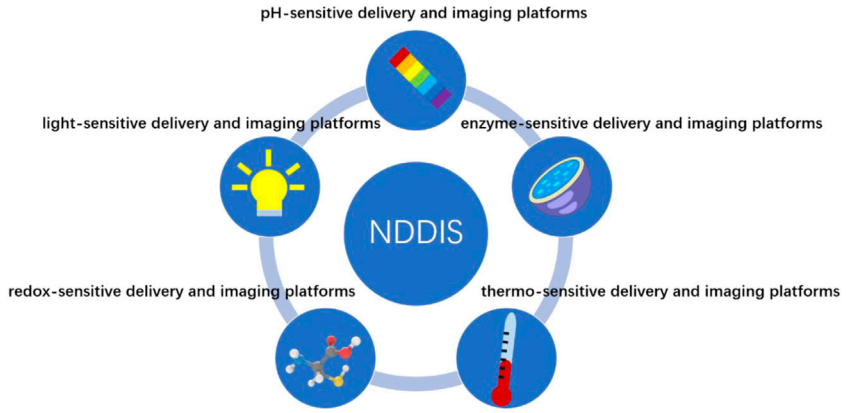


FIGURE 1 | Graphical summarization of five different types of stimuli put into the design of stimuli-sensitive nanocarriers for drug delivery and imaging platforms: pH-sensitive delivery and imaging platforms, enzyme-sensitive delivery and imaging platforms, thermo-sensitive delivery and imaging platforms, redox-sensitive delivery and imaging platforms, and light-sensitive delivery and imaging platforms.

size and evaluate the therapeutic effect of the tumor (Yang et al., 2019).

On account of this sensitive reaction, Chen et al. developed a multifunctional mesoporous silica nanoparticle system for drug delivery and magnetic resonance imaging (MRI) by a classic method (Chen et al., 2015) (see **Table 1**). The pH-responsive MS@S-NPs are the essential component of the mesoporous silica nanoparticle system. DOX hermetically loaded into the holes of MS, and then the holes were sealed with S-NP to prevent premature drug release. As the experiment proves, MS@S-NPs were stable under conditions similar to physiological status (pH = 7.4), and the DOX release generally ignored. On the contrary, the DOX release markedly increased with the reduction of pH. This is principally because the acid–labile acetal bridges the gaps between MS and S-NPs, and the hydrolysis of the acetal at acidic pH as triggers could generate physicochemical property variations to remove the S-NPs achieving the DOX specific-targeting and controlled release. Due to the presence of Gd^{3+}, MS@S-NPs, as an efficient contrast agent, realized T_1-weighted MR images successfully at the tumor site for image-guided drug delivery and efficacy assessment. Hence, MS@S-NPs, as high effective NDDIP, play important roles in tumor therapy and real-time monitoring (Hrubý et al., 2005; Devalapally et al., 2007).

On this point, a new study has claimed that Lim et al. (see **Table 1**) designed HER-DMNPs as pH-triggered NDDIP through employing α-pyrenyl-ω-carboxyl poly(ethylene glycol) (Py-PEG-COOH or pyrenyl-PEG) to encapsulate magnetic resonance (MR)-sensitive $MnFe_2O_4$ nanocrystals (MNCs) and doxorubicin (DOX). In this research, the authors demonstrated that the π–π interactions between DOX and pyrene groups could be decreased at acidic pH to release DOX. Meanwhile, the loaded DOX could be effectively conveyed to tumor tissues reducing toxicity to normal tissues, which realizes targeted cancer therapy. In addition, the authors verified that the $MnFe_2O_4$ nanocrystals possessed T_2-weighted MR imaging capability through experiments that could be monitored by MRI to guide personalized cancer regimens. In summary, HER-DMNPs, as high effective nanoparticles, have a good T_2-weighted MRI imaging effect for tumor therapeutic effect evaluation (Lim et al., 2011).

Enzyme-Sensitive Delivery and Imaging Platforms

Enzymes often play pivotal roles in metabolism and their intimate connection with human health greatly. However, there are several enzymes with specific chemical properties overexpressed in the tumor microenvironment, such as hydrolases, cathepsins, kinases, esterases, and gelatinase (Lou et al., 2021; Dhaval et al., 2022; Wang et al., 2018b; Zhang et al., 2018a). Therefore, overexpression of dysregulated enzyme as a favorable potential biological target is of new innovations. In brief, smart NDDIP stimulated by enzymes has a tremendous and excellent foreground to develop as one of the promising cancer therapies (Chau and Zhong, 2011; Rastegari et al., 2017).

Cathepsin B overexpression has been related to more premalignant lesions playing an important role in adjusting the tumor microenvironment in a wide variety of cancer types. Hence, the cathepsin B-sensitive delivery platform has been conceived, using enzyme as triggers, to deliver the drug to the targeted diseased site where the cathepsin B is overexpressed. Wei and coworkers developed functional polyHPMA copolymer-loaded DOX as enzyme- and pH-sensitive delivery platforms with favorable promising efficiency for breast cancer therapy (Wei et al., 2016) (see **Table 1**). HPMA was prepared by RAFT polymerization, possessing cathepsin B sensitive moiety (GFLGK) loaded to branched copolymers. Then, obtained copolymer covalently bound to the DOX via pH-sensitive hydrazine bond. In this study, an enzyme complex based on cathepsin B could develop rapid and efficient cleavage. Moreover, the DOX release lies on the pH of the tumor environment. Therefore, the conformational changes of HPMA take place in DOX releasing from the conjugate under a higher concentration of cathepsin B and lower pH value. The novel HPMA copolymer

had successfully applied to 4T1 tumor models with enhanced antitumor efficacies. In conclusion, the enzyme-sensitive delivery platforms are regarded as a safe and high effective nanoparticle for breast cancer therapy.

Fan et al. designed gelatin nanoparticles containing PAMAM dendrimer-loaded MTX to improve antitumor efficiency (see **Table 1**). The high concentration of matrix metalloproteinase-2 enzymes in TME effectively promoted gelatin nanoparticle cracking, which achieved PAMAM dendrimers release and improved intracellular uptake into tumor cells. Meanwhile, the results demonstrate that the multistage nanocarrier guaranteed the therapeutic effect of antitumor drugs. Nanocarriers have ascendancy in fluorescence imaging to assess drug distribution in real time (Fan et al., 2017).

Thermo-Sensitive Delivery Platforms

Thermal is one of the most-explored external stimuli-sensitive for NDDIP, which is delicately sensitive to the thermal within an imperceptible transformation, especially in cancer therapy and diagnosis. The normal body temperature is about 37°C, while the temperature rises in the existence of pyrogens or pathogens, diverging from the normal temperature, which can be exploited to motivate the release of active ingredient pharmaceutical compounds for thermo-sensitive drug delivery platforms. Favorable thermo-sensitive delivery platforms stably reserve therapeutic drugs at physiological temperatures, and they merely released them to the targeted diseased site where the temperature is higher than the critical temperature of drugs. In addition, admired NDDIPs possessed favorable biocompatible and well-stable loading capacity (Qian et al., 2013; Limjeerajarus et al., 2020).

Recent research by Enaam et al. demonstrated that Fe_3O_4@P(MEO_2MA_{60}-$OEGMA_{40}$)NP is equipped with reversible aggregation in response to the temperature used to make a targeting drug-carried platform (Jamal Al Dine et al., 2017). (see **Table 1**). Fe_3O_4@P(MEO_2MA_{60}-$OEGMA_{40}$)NP, as targeted drug carriers, was composited by a mild method, and then the nanoparticles encapsulated DOX by noncovalent interactions bounding to thermo-responsive polymers which possessed a critical temperature of around 41°C. The properties of DOX drug release increase from the nanocarriers above 40°C was proved by a series of experimental investigations. It was found that the drug release efficiency of the nanocarriers might be concerned with thermo-responsive polymers. The main cause for the release of DOX is that the polymer chains shrunk when the temperature is higher than the critical temperature. In brief, the favorable thermo-sensitive delivery platforms of Fe_3O_4@P (MEO_2MA_{60}-$OEGMA_{40}$)NP with precisely regulated might provide great significance and potential for drug delivery.

Masoud and coworkers synthesized multifunctional pH- and thermo-sensitive delivery platforms (M-MNCs) through a multistep, and then mesoporous silica successfully connected to polymers as an anticancer drug payload to realize release of loaded medicine in specific circumstances (see **Table 1**). The authors prove by experiment that the M-MNCs showed pH- and thermo-sensitive release behavior which the released amount was highest (92.3%) at pH 5 and 40°C. Therefore, the multifunctional delivery platforms have excellent capability in drug loading and releasing. Besides, the study results showed that M-MNCs retained superparamagnetic characteristics as promising T_2-weighted contrast agents to evaluate the therapeutic effect (Farshbaf et al., 2018).

Redox-Sensitive Delivery and Imaging Platforms

Redox-sensitive delivery platforms have moved into the spotlight based on the high concentrations of redox agents such as ROS and GSH in the solid tumor microenvironment, compared with their concentration in normal sites sharply. It has extensively enormous potential utilized as favorable potential triggers to controlled drug-specific release contenting in response to intracellular conditions for cancer therapeutic strategy without damaging the other normal sites surrounding the tumor mass. Herein, redox-responsive NDDIPs are promising in realizing efficient intracellular stimulus-responsive drug platforms (Zhao et al., 2016).

As is known to all, the GSH concentration in tumor cells is typically higher than the values of healthy cells (Mirhadi et al., 2020). Sun and colleagues took advantage of this characteristic to explore a redox-sensitive delivery platform (mPEG-ss-Tripp) used for controlled drug delivery and simultaneous AIE imaging (Sun et al., 2021) (see **Table 1**). By the self-assembled method, mPEG-ss-Tripp was synthesized and simultaneously loaded doxorubicin via a disulfide bond. Disulfide bonds are sensitive to reductive substance GSH, which is quickly cleaved through thiol-disulfide exchange, especially in the cancer intracellular environment under a higher concentration of GSH. On the contrary, disulfide bonds have fixed construction in normal tissues at a lower level of GSH. *In vitro* cytotoxicity of micelles experiments proved that the toxicity of DOX-loaded micelles to 293 T cells is extremely low. However, DOX-loaded micelles can prevent 4T1 cell growth and show great cell toxicity. Therefore, mPEG-ss-Tripp has good tumor selectivity between cancer cells and normal cells. At the same time, the mPEG-ss-Tripp with AIE property achieved cellular imaging for monitoring the distribution of the drug as seen in **Figure 2**.

Chen et al. explored an effective NDDIP for multipurpose cancer theranostics (see **Table 1**). Obtained MSN-ss-GHA could not only achieve medicine transportation under a strong reducing condition but also dramatically improve 4T1 intracellular uptake. With the assistance of an ultrasonic bath, anticancer drugs were successfully loaded into MSN-SS-GHA to further synthesize DOX@MSN-ss-GHA. A higher concentration of GSH prompted the disulfide linkage in MSN-ss-GHA to cleave occurring in the cancer cellular environment which achieved anticancer drug efflux rapidly. Moreover, the presence of Gd component is the basis of excellent T_1-weighted MRI imaging. In conclusion, the new redox-sensitive delivery platforms with accurately cleaved disulfide linkage revealed enormous meaningful and promising for neoadjuvant chemotherapy. At the same time, redox-sensitive delivery and imaging platforms are regarded as high effective nanoparticle in tumor precision therapy and real-time monitoring by MRI. (Chen et al., 2016).

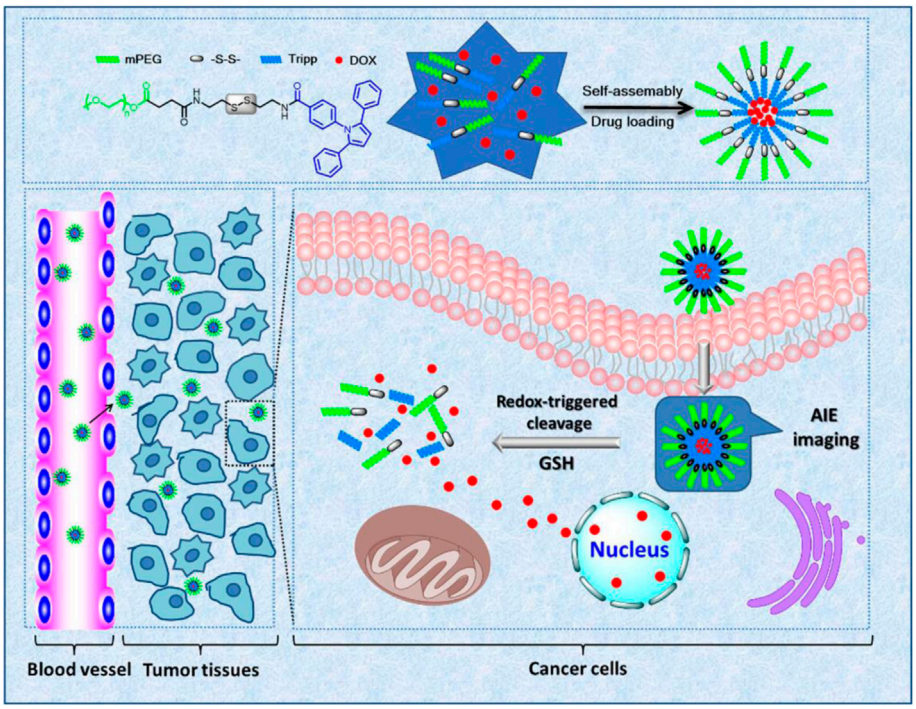


FIGURE 2 | | Malignant tumor cells are characterized by intracellular high concentrations of GSH. Advantage is taken from this in developing the redox-responsive drug delivery platform. Sun and colleagues explore redox-sensitive delivery platform (mPEG-ss-Tripp). Synthesized mPEG-ss-Tripp was loaded with doxorubicin via a disulfide bond, which is sensitive to reductive substance GSH and then quickly cleaved through thiol-disulfide exchange, in order to release the DOX at targeted sites without damaging normal tissues (Sun et al., 2021).

Zhang et al. synthesized FCCP NPs (Fe_3O_4@CS/CuS NPs) nanoclusters to achieve multimodal imaging and synergetic therapy (see **Table 1**). As obtained, Fe_3O_4@CS/CuS NPs performed important functions in improving intrinsic peroxidase to generate •OH and O_2 from endogenous H_2O_2, in which the generation of •OH as a therapeutic agent suppresses the cancerous cells and the concurrent production of O_2 as a conditioning agent modulates the hypoxic microenvironment of tumors with remarkable efficiency. In conclusion, ROS is regarded as an effective tumor inhibitor to achieve potent cancer treatment. Due to the presence of Fe, the nanoparticle is a potential T_2 contrast agent for MRI which is proportionate to the increase of the Fe concentration. *In vivo* and *in vitro* experiments proved that FCCP NPs inhibiting tumor growth were remarkably improved. T_2-weighted MR imaging was achieved to effectively evaluate the targeting of nanoparticles. In summary, FCCP NPs could apply in the precise diagnosis and efficient therapeutic and are expected to contribute to personalized medicine (Zhang et al., 2018b).

Light-Sensitive Delivery and Imaging Platforms

Innocuous electromagnetic radiation contained ultraviolet (UV), visible light (VIS), and near-infrared light (NIR), as light-sensitiveness stimuli have moved into the considerable spotlight due to favorable biocompatibility and tissue penetration. Novel light-sensitive delivery platforms based on electromagnetic radiation with an external light source have been recently exploited to achieve more drug delivery at well-delimited sites of the body, guaranteed selective drug accumulation and reduced drug side effects, and improved pharmacokinetics and pharmacodynamics, to realize secure and efficient cancer therapy. Taking advantage of light-sensitive delivery platforms, external stimuli can be used to develop light-sensitive delivery platforms to improve a range of applications.

At present, multifarious NIR-sensitive delivery platforms using different responsive mechanisms have been generated and investigated for the treatment of cancer (Chamundeeswari et al., 2018).

In a recent study, Andy and colleagues investigated the NIR-light-triggered drug delivery approach (Hernández Montoto et al., 2019) (see **Table 1**). AuNSt with a thiolated photolabile molecule was firstly acquired via a simple and mild method, and then the thiol groups were connected AuNSt and MSNP@DOX together in order to synthesize the satisfying NIR-sensitive drug delivery. The principle of AuNSt-MSNP is that thiolated photolabile molecule is sensitive to the NIR light leading to the formation of succinic acid which is triggered to controlled DOX specific release based on irradiation with NIR-light. *In vitro* cytotoxicity of AuNSt-MSNP experiments proved that DOX-loaded nanoparticles revealed nontoxicity to HeLa cells without NIR light, while under NIR laser, AuNSt-

MSNP severely inhibited HeLa cells viability by effectively releasing DOX. In conclusion, this novel NIR-light-triggered drug delivery platform has provided a promising potential for achieving the synchronism of treatment to strengthen the efficiency of combination therapy (Xiang and Chen, 2020).

In another study, Yoon et al. have developed a multifunctional anticancer-drug carrier containing GNR, IONP, and DOX, with a desirable small size (see **Table 1**). GNR is efficiently able to transform light into heat energy under NIR. IONP serves as an MRI contrast agent monitoring with the MRI T_2 imaging precisely. Experiments have proved that the temperature increase from laser irradiation to achieve drug release precisely, reducing damage to normal surrounding tissue. Meanwhile, the workers proved the property of drug release *via* MTT which utilized HeLa cells as a stable cell model. The result reflects that DOX is released from the multifunctional anticancer-drug carrier by laser stimulation to effectively kill cancer cells. In conclusion, the multifunctional light-sensitive delivery and imaging platforms could not only resoundingly release DOX into the cancer cells under NIR but also achieve MRI T_2 imaging (Yoon et al., 2019).

FUTURE OUTLOOKS

With the therapeutic strategy of carcinoma flourishing, and life-span lengthening, the solicitude for the patients' quality of life appears to be more significantly momentous. The current modalities of traditional cancer therapies comprise surgery, chemotherapy, radiotherapy, and their combinations and is extremely effective to make tumor shrink or disappear, simultaneously inevitably damaging the other normal sites surrounding the tumor mass. Therefore, probing into how to suppress tumor growth and prolong the survival, while simultaneously not injuring the human organism, is a crucial and aggressive cancer treatment protocol. Nanomedicine, especially NDDIP, has recently promoted immense and innovative preclinical and utility progress in health care. NDDIP as efficient and favorable drug delivery and diagnostic tools would witness deep involvement of various diseases, with targeted and stimuli-responsive ability to deliver drugs. Synchronously, it has solved side effects caused by the traditional therapeutic strategies of carcinoma and achieved the development of precision medicine *via* reduced systemic cytotoxicity, improved cancerous tissue permeability, and prolonged circulation time.

As we have evidenced by the studies in this review, the performance of NDDIP is verified via substantial preclinical studies, which possesses promising efficiency to suppress the growing progress of cancer (Wu et al., 2016). In this field, plenty of nanoparticles, possessing the characteristics of responding to pH, enzyme, thermal, redox, and light, have been prepared and developed to achieve precise and targeted therapy. Not long afterward, abundant and varied NDDIPs with specific tumor targeting and on-demand antitumor efficiency will appear soon in the clinical application (Zhao et al., 2018).

In conclusion, scientists continuously look for opportunities to improve favorable and profound ways to treat many kinds of cancer by optimizing and innovating nanoparticles and technologies. Therefore, the appearance of smart NDDIP platforms would enable to perform therapy and diagnostics of oncology patients at a totally new and advanced level, maximizing the therapeutic effects, and improving the patients' quality of life.

AUTHOR CONTRIBUTIONS

JL conceived the presented research. JL and FC designed the structure of the paper. FC drafted the manuscript. BL provided critical revision of this article. JL, BL, and SP supervised the findings of the work and approved the manuscript for submission. All authors agreed with the final version of this manuscript.

FUNDING

This work was supported by the National Natural Science Foundation of China (Nos. 82071981 and 21635007), the Program of Science and Technology Development Plan of Jilin Province of China (No. 2018010119JC), the Health Special Project of Jilin Province Department of Finance (No. 3D518V283429), and the Fundamental Research Funds for the Central Universities (No. 419070600032).

REFERENCES

Aminu, N., Bello, I., Umar, N. M., Tanko, N., Aminu, A., and Audu, M. M. (2020). The Influence of Nanoparticulate Drug Delivery Systems in Drug Therapy. *J. Drug Deliv. Sci. Technol.* 60, 101961. [J]. doi:10.1016/j.jddst.2020.101961

Anderson, N. M., and Simon, M. C. (2020). The Tumor Microenvironment. *Curr. Biol.* 30 (16), R921–R925. doi:10.1016/j.cub.2020.06.081

Bai, M., Yang, M., Gong, J., Xu, H., and Wei, Z. (2021). Progress and Principle of Drug Nanocrystals for Tumor Targeted Delivery. *AAPS PharmSciTech* 23 (1), 41. doi:10.1208/s12249-021-02200-w

Barati Bagherabad, M., Afzaljavan, F., Shahidsales, S., Hassanian, S. M., and Avan, A. (2017). Targeted Therapies in Pancreatic Cancer: Promises and Failures. *J. Cell Biochem.* 120, 2726–2741. [J]. doi:10.1002/jcb.26284

Bharathiraja, S., Manivasagan, P., Santha Moorthy, M., Bui, N. Q., Jang, B., Phan, T. T. V., et al. (2018). Photo-based PDT/PTT Dual Model Killing and Imaging of Cancer Cells Using Phycocyanin-Polypyrrole Nanoparticles. *Eur. J. Pharm. Biopharm.* 123, 20–30. doi:10.1016/j.ejpb.2017.11.007

Bhutta, Z. A., Kanwal, A., Ali, M., Kulyar, M. F., Yao, W., Shoaib, M., et al. (2021). Emerging Nanotechnology Role in the Development of Innovative Solutions against COVID-19 Pandemic. *Nanotechnology* 32. [J]. doi:10.1088/1361-6528/ac189e

Chamundeeswari, M., Jeslin, J., and Verma, M. L. (2018). Nanocarriers for Drug Delivery Applications. *Environ. Chem. Lett.* 17 (2), 849–865. [J]. doi:10.1007/s10311-018-00841-1

Chamundeeswari, M., Jeslin, J., and Verma, M. L. (2019). Nanocarriers for Drug Delivery Applications. *Environ. Chem. Lett.* 17, 849–865. [J]. doi:10.1007/s10311-018-00841-1

Chau, Y., and Zhong, J. (2011). Enzyme-Sensitive Biomaterials for Drug Delivery. *Compr. Biotechnol.* 5, 605–624. doi:10.1016/b978-0-08-088504-9.00158-6

Chen, L., Huang, Q., Zhao, T., Sui, L., Wang, S., Xiao, Z., et al. (2021). Nanotherapies for Sepsis by Regulating Inflammatory Signals and Reactive

Oxygen and Nitrogen Species: New Insight for Treating COVID-19. *Redox Biol.* 45, 102046. doi:10.1016/j.redox.2021.102046

Chen, L., Zhou, X., Nie, W., Zhang, Q., Wang, W., Zhang, Y., et al. (2016). Multifunctional Redox-Responsive Mesoporous Silica Nanoparticles for Efficient Targeting Drug Delivery and Magnetic Resonance Imaging. *ACS Appl. Mater Interfaces* 8 (49), 33829–33841. doi:10.1021/acsami.6b11802

Chen, Y., Ai, K., Liu, J., Sun, G., Yin, Q., and Lu, L. (2015). Multifunctional Envelope-type Mesoporous Silica Nanoparticles for pH-Responsive Drug Delivery and Magnetic Resonance Imaging. *Biomaterials* 60, 111–120. doi:10.1016/j.biomaterials.2015.05.003

Deng, X., Dai, Y., Liu, J., Zhou, Y., Ma, P., Cheng, Z., et al. (2015). Multifunctional Hollow CaF2:Yb(3+)/Er(3+)/Mn(2+)-Poly(2-Aminoethyl Methacrylate) Microspheres for Pt(IV) Pro-drug Delivery and Tri-modal Imaging. *Biomaterials* 50, 154–163. [J]. doi:10.1016/j.biomaterials.2015.01.040

Devalapally, H., Shenoy, D., Little, S., Langer, R., and Amiji, M. (2007). Poly(ethylene Oxide)-Modified Poly(beta-Amino Ester) Nanoparticles as a pH-Sensitive System for Tumor-Targeted Delivery of Hydrophobic Drugs: Part 3. Therapeutic Efficacy and Safety Studies in Ovarian Cancer Xenograft Model. *Cancer Chemother. Pharmacol.* 59 (4), 477–484. doi:10.1007/s00280-006-0287-5

Dhaval, M., Vaghela, P., Patel, K., Sojitra, K., Patel, M., Patel, S., et al. (2022). Lipid-based Emulsion Drug Delivery Systems - a Comprehensive Review. *Drug Deliv. Transl. Res.* 12, 1616–1639. [J]. doi:10.1007/s13346-021-01071-9

El-Sayed, A., and Kamel, M. (2020). Advances in Nanomedical Applications: Diagnostic, Therapeutic, Immunization, and Vaccine Production. *Environ. Sci. Pollut. Res. Int.* 27 (16), 19200–19213. doi:10.1007/s11356-019-06459-2

Fan, Y., Yuan, S., Huo, M., Chaudhuri, A. S., Zhao, M., Wu, Z., et al. (2017). Spatial Controlled Multistage Nanocarriers through Hybridization of Dendrimers and Gelatin Nanoparticles for Deep Penetration and Therapy into Tumor Tissue. *Nanomedicine* 13 (4), 1399–1410. doi:10.1016/j.nano.2017.01.008

Farshbaf, M., Salehi, R., Annabi, N., Khalilov, R., Akbarzadeh, A., and Davaran, S. (2018). pH-And Thermo-Sensitive MTX-Loaded Magnetic Nanocomposites: Synthesis, Characterization, and *In Vitro* Studies on A549 Lung Cancer Cell and MR Imaging. *Drug Dev. Ind. Pharm.* 44 (3), 452–462. doi:10.1080/03639045.2017.1397686

Foglietta, F., Serpe, L., and Canaparo, R. (2021). The Effective Combination between 3D Cancer Models and Stimuli-Responsive Nanoscale Drug Delivery Systems. *Cells* 10 (12), 3295. doi:10.3390/cells10123295

He, W., Ai, K., and Lu, L. (2015). Nanoparticulate X-Ray CT Contrast Agents. *Sci. China Chem.* 58 (5), 753–760. doi:10.1007/s11426-015-5351-8

Hernández Montoto, A., Llopis-Lorente, A., Gorbe, M., M Terrés, J., Cao-Milán, R., Díaz de Greñu, B., et al. (2019). Janus Gold Nanostars-Mesoporous Silica Nanoparticles for NIR-Light-Triggered Drug Delivery. *Chemistry* 25 (36), 8471–8478. doi:10.1002/chem.201900750

Hrubý, M., Konák, C., and Ulbrich, K. (2005). Polymeric Micellar pH-Sensitive Drug Delivery System for Doxorubicin. *J. Control Release* 103 (1), 137–148. [J]. doi:10.1016/j.jconrel.2004.11.017

Huang, X., Lu, Y., Guo, M., Du, S., and Han, N. (2021). Recent Strategies for Nano-Based PTT Combined with Immunotherapy: from a Biomaterial Point of View. *Theranostics* 11 (15), 7546–7569. doi:10.7150/thno.56482

Jamal Al Dine, E., Ferjaoui, Z., Ghanbaja, J., Roques-Carmes, T., Meftah, A., Hamieh, T., et al. (2017). Thermo-responsive Magnetic Fe3O4@ P(MEO2MAX-OEGMA100-X) NPs and Their Applications as Drug Delivery Systems. *Int. J. Pharm.* 532 (2), 738–747. doi:10.1016/j.ijpharm.2017.09.019

Jiang, Q., Liu, L., Li, Q., Cao, Y., Chen, D., Du, Q., et al. (2021). NIR-laser-triggered Gadolinium-Doped Carbon Dots for Magnetic Resonance Imaging, Drug Delivery and Combined Photothermal Chemotherapy for Triple Negative Breast Cancer. *J. Nanobiotechnol* 19 (1), 64. doi:10.1186/s12951-021-00811-w

Jiang, X., Wang, J., Deng, X., Xiong, F., Zhang, S., Gong, Z., et al. (2020). The Role of Microenvironment in Tumor Angiogenesis. *J. Exp. Clin. Cancer Res.* 39 (1), 204. doi:10.1186/s13046-020-01709-5

Li, B., Gong, T., Xu, N., Cui, F., Yuan, B., Yuan, Q., et al. (2020). Improved Stability and Photothermal Performance of Polydopamine-Modified Fe3 O4 Nanocomposites for Highly Efficient Magnetic Resonance Imaging-Guided Photothermal Therapy. *Small* 16 (45), e2003969. doi:10.1002/smll.202003969

Lim, E. K., Huh, Y. M., Yang, J., Lee, K., Suh, J. S., and Haam, S. (2011). pH-triggered Drug-Releasing Magnetic Nanoparticles for Cancer Therapy Guided by Molecular Imaging by MRI. *Adv. Mater* 23 (21), 2436–2442. doi:10.1002/adma.201100351

Limjeerajarus, C. N., Kreua-Ongarjnukool, N., Seang, S., Pavasant, P., and Niyomthai, S. T. (2020). Characterization of a Thermo-Sensitive Injectable Hydrogel as an Iloprost Delivery System for Dental Use. *Key Eng. Mater.* 856, 391–398. [J]. doi:10.4028/www.scientific.net/KEM.856.391

Liu, Y., Zhen, W., Jin, L., Zhang, S., Sun, G., Zhang, T., et al. (2018). All-in-One Theranostic Nanoagent with Enhanced Reactive Oxygen Species Generation and Modulating Tumor Microenvironment Ability for Effective Tumor Eradication. *ACS Nano* 12 (5), 4886–4893. doi:10.1021/acsnano.8b01893

Lou, X. F., Du, Y. Z., and Xu, X. L. (2021). Endogenous Enzyme-Responsive Nanoplatforms for Anti-tumor Therapy. *Curr. Drug Targets* 22 (8), 845–855. doi:10.2174/1389450122666210114095614

Ma, T., Zhang, P., Hou, Y., Ning, H., Wang, Z., Huang, J., et al. (2018). "Smart" Nanoprobes for Visualization of Tumor Microenvironments. *Adv. Healthc. Mater* 7, e1800391. doi:10.1002/adhm.201800391

Malla, R., Surepalli, N., Farran, B., Malhotra, S. V., and Nagaraju, G. P. (2021). Reactive Oxygen Species (ROS): Critical Roles in Breast Tumor Microenvironment. *Crit. Rev. Oncology/Hematology* 160 (11), 103285. doi:10.1016/j.critrevonc.2021.103285

Marengo, B., Pulliero, A., Izzotti, A., and Domenicotti, C. (2019). MiRNA Regulation of Glutathione Homeostasis in Cancer Initiation, Progression and Therapy Resistance. *Microrna* 9, 187–197. [J]. doi:10.21742F2211536609666191218103220 10.2174/2211536609666191218103220

Ming, L., Cheng, K., Chen, Y., Yang, R., and Chen, D. (2020). Enhancement of Tumor Lethality of ROS in Photodynamic Therapy. *Cancer Med.* 10, 257–268. [J]. doi:10.1002/cam4.3592

Mirhadi, E., Mashreghi, M., Faal Maleki, M., Alavizadeh, S. H., Arabi, L., Badiee, A., et al. (2020). Redox-sensitive Nanoscale Drug Delivery Systems for Cancer Treatment. *Int. J. Pharm.* 589, 119882. doi:10.1016/j.ijpharm.2020.119882

Naidoo, D. B., and Chuturgoon, A. A. (2021). Nanobodies Enhancing Cancer Visualization, Diagnosis and Therapeutics. *Int. J. Mol. Sci.* 22 (18). doi:10.3390/ijms22189778

Nam, K., and Shin, J. E. (2021). Risk Factors of Advanced Metachronous Neoplasms in Surveillance after Colon Cancer Resection. *Korean J. Intern Med.* 36 (2), 305–312. doi:10.3904/kjim.2019.053

Nunes, S., and Serpa, J. (2018). Glutathione in Ovarian Cancer: A Double-Edged Sword. *Ijms* 19 (7), 1882. [J]. doi:10.3390/ijms19071882

Qian, Q. W., Kong, M., Yi, A., Liu, Y., Li, J. J., Zhou, X., et al. (2013). Hydroxybutyl Chitosan Thermo-Sensitive Hydrogel: A Potential Drug Delivery System. *J. Mater. Sci.* 48 (16), 5614–5623. [J]. doi:10.1007/s10853-013-7356-z

Rastegari, B., Karbalaei-Heidari, H. R., Zeinali, S., and Sheardown, H. (2017). The Enzyme-Sensitive Release of Prodigiosin Grafted β-cyclodextrin and Chitosan Magnetic Nanoparticles as an Anticancer Drug Delivery System: Synthesis, Characterization and Cytotoxicity Studies. *Colloids Surfaces B Biointerfaces* 158, 589–601. [J]. doi:10.1016/j.colsurfb.2017.07.044

Rozanov, D., Cheltsov, A., Sergienko, E., Vasile, S., Golubkov, V., Aleshin, A. E., et al. (2015). TRAIL-Based High Throughput Screening Reveals a Link between TRAIL-Mediated Apoptosis and Glutathione Reductase, a Key Component of Oxidative Stress Response. *Plos One* 10, e0129566. doi:10.1371/journal.pone.0129566

Sai, D. L., Lee, J., Nguyen, D. L., and Kim, Y. P. (2021). Tailoring Photosensitive ROS for Advanced Photodynamic Therapy. *Exp. Mol. Med.* 53, 495–504. [J]. doi:10.1038/s12276-021-00599-7

Siegel, R. L., Miller, K. D., Fuchs, H. E., and Jemal, A. (2021). Cancer Statistics, 2021. *CA A Cancer J. Clin.* 71 (1), 7–33. doi:10.3322/caac.21654

Sun, C., Lu, J., Wang, J., Hao, P., Li, C., Qi, L., et al. (2021). Redox-sensitive Polymeric Micelles with Aggregation-Induced Emission for Bioimaging and Delivery of Anticancer Drugs. *J. Nanobiotechnol* 19 (1), 14. doi:10.1186/s12951-020-00761-9

Wang, D., Zou, L., Jin, Q., Hou, J., Ge, G., and Yang, L. (2018). Human Carboxylesterases: a Comprehensive Review. *Acta Pharm. Sin. B* 8 (05), 699–712. doi:10.1016/j.apsb.2018.05.005

Wang, J., Sui, L., Huang, J., Miao, L., Nie, Y., Wang, K., et al. (2021). MoS2-based Nanocomposites for Cancer Diagnosis and Therapy. *Bioact. Mater* 6 (11), 4209–4242. doi:10.1016/j.bioactmat.2021.04.021

Wang, N., Cheng, X., Li, N., Wang, H., and Chen, H. (2018). Nanocarriers and Their Loading Strategies. *Adv. Healthc. Mat.* 8, 1801002. [J]. doi:10.1002/adhm.201801002

Wang, S., Yang, Y., Wu, H., Li, J., Xie, P., Xu, F., et al. (2022). Thermosensitive and Tum or Microenvironment Activated Nanotheranostics for the Chemodynamic/photothermal Therapy of Colorectal Tumor. *J. Colloid Interface Sci.* 612, 223–234. doi:10.1016/j.jcis.2021.12.126

Wang, T., Yang, M., Huang, J., Zhao, Y., Wang, H., Leng, S., et al. (2017). NIR-to-NIR UCL/ T 1 -weighted MR/CT Multimodal Imaging by NaYbF 4 :Tm@ NaGdF 4 :Yb-PVP Upconversion Nanoparticles. *Sci. Bull.* 62 (13), 903–912. doi:10.1016/j.scib.2017.05.028

Wei, X., Luo, Q., Sun, L., Li, X., Zhu, H., Guan, P., et al. (2016). Enzyme- and pH-Sensitive Branched Polymer-Doxorubicin Conjugate-Based Nanoscale Drug Delivery System for Cancer Therapy. *ACS Appl. Mater Interfaces* 8 (18), 11765–11778. doi:10.1021/acsami.6b02006

Weinberg, F., Ramnath, N., and Nagrath, D. (2019). Reactive Oxygen Species in the Tumor Microenvironment: An Overview. *Cancers (Basel)* 11 (8). doi:10.3390/cancers11081191

Wu, A., Zeng, L., and Yu, Z. (2016). Near-infrared Light Responsive Upconversion Nanoparticles for Imaging, Drug Delivery and Therapy of Cancers. *Curr. Nanosci.* 12 (1), 18–32. [J]. doi:10.2174/1573413711666150624172433

Wu, F., Zhang, Q., Sun, B., Chu, X., Zhang, M., She, Z., et al. (2021). MoO3-x Nanosheets-Based Platform for Single NIR Laser Induced Efficient PDT/PTT of Cancer. *J. Control. Release* 338, 33846–33855. doi:10.1016/j.jconrel.2021.08.022

Xiang, W., and Chen, L. (2020). In Light-Sensitive Drug Delivery System Nanoparticles Mediate Oxidative Stress. *Am. J. Transl. Res.* 12 (5), 1469–1480.

Xiang, Z., Qi, Y., Lu, Y., Hu, Z., Wang, X., Jia, W., et al. (2020). MOF-derived Novel Porous Fe3O4@C Nanocomposites as Smart Nanomedical Platforms for Combined Cancer Therapy: Magnetic-Triggered Synergistic Hyperthermia and Chemotherapy. *J. Mater Chem. B* 8 (37), 8671–8683. doi:10.1039/d0tb01021a

Yan, L., Shen, J., Wang, J., Yang, X., Dong, S., and Lu, S. (2020). Nanoparticle-Based Drug Delivery System: A Patient-Friendly Chemotherapy for Oncology. *Dose Response* 18 (3), 1559325820936161. doi:10.1177/1559325820936161

Yang, Y., Wang, Z., Peng, Y., Ding, J., and Zhou, W. (2019). A Smart pH-Sensitive Delivery System for Enhanced Anticancer Efficacy via Paclitaxel Endosomal Escape. *Front. Pharmacol.* 10, 10. doi:10.3389/fphar.2019.00010

Yang, Z., Yang, A., Ma, W., Ma, K., Lv, Y.-K., Peng, P., et al. (2022). Atom-precise Fluorescent Copper Cluster for Tumor Microenvironment Targeting and Transient Chemodynamic Cancer Therapy. *J. Nanobiotechnol* 20 (1), 20. doi:10.1186/s12951-021-01207-6

Yoon, S., Chang, J., Kwon, N., Moon, S., Park, Y., Han, K. H., et al. (2019). Multifunctional Nanomaterial-Alginate Drug Delivery and Imaging System for Cancer Therapy. *BioChip J.* 13 (3), 236–242. doi:10.1007/s13206-019-3309-1

Zhang, K., Chen, D., Ma, K., Wu, X., Hao, H., and Jiang, S. (2018a). NAD(P)H: Quinone Oxidoreductase 1 (NQO1) as a Therapeutic and Diagnostic Target in Cancer. *J. Med. Chem.* 61, 6983–7003. doi:10.1021/acs.jmedchem.8b00124

Zhang, K., Yang, Z., Meng, X., Cao, Y., Zhang, Y., Dai, W., et al. (2018b). Peroxidase-like Fe3O4 Nanocomposite for Activatable Reactive Oxygen Species Generation and Cancer Theranostics. *Mat. Chem. Front.* 2 (6), 1184–1194. doi:10.1039/c8qm00098k

Zhang, L. X., Sun, X. M., Xu, Z. P., and Liu, R. T. (2019). Development of Multifunctional Clay-Based Nanomedicine for Elimination of Primary Invasive Breast Cancer and Prevention of Its Lung Metastasis and Distant Inoculation. *ACS Appl. Mater Interfaces* 11 (39), 35566–35576. doi:10.1021/acsami.9b11746

Zhao, D., Zhang, H., Yang, S., He, W., and Luan, Y. (2016). Redox-sensitive mPEG-SS-PTX/TPGS Mixed Micelles: An Efficient Drug Delivery System for Overcoming Multidrug Resistance - ScienceDirect. *Int. J. harmaceutics* 515 (1–2), 281–292. doi:10.1016/j.ijpharm.2016.10.029

Zhao, T., Chen, L., Li, Q., and Li, X. (2018). Near-infrared Light Triggered Drug Release from Mesoporous Silica Nanoparticles. *J. Mater Chem. B* 6, 7112–7121. doi:10.1039/c8tb01548a

Zhao, T., Wu, W., Sui, L., Huang, Q., Nan, Y., Liu, J., et al. (2022). Reactive Oxygen Species-Based Nanomaterials for the Treatment of Myocardial Ischemia Reperfusion Injuries. *Bioact. Mater* 7, 47–72. doi:10.1016/j.bioactmat.2021.06.006

Zhu, Y., Zhao, T., Liu, M., Wang, S., Liu, S., Yang, Y., et al. (2022). Rheumatoid Arthritis Microenvironment Insights into Treatment Effect of Nanomaterials. *Nano Today* 42, 101358. doi:10.1016/j.nantod.2021.101358

Sahoo, B M, Banik, B K, and Borah, P (2021). Reactive Oxygen Species (ROS): Key components in Cancer Therapies. *Anti-Cancer Agents in Medicinal Chemistry*. 22, 215–222. doi:10.2174/1871520621666210608095512

Conflict of Interest: The authors declare that the research was conducted in the absence of any commercial or financial relationships that could be construed as a potential conflict of interest.

Publisher's Note: All claims expressed in this article are solely those of the authors and do not necessarily represent those of their affiliated organizations or those of the publisher, the editors, and the reviewers. Any product that may be evaluated in this article, or claim that may be made by its manufacturer, is not guaranteed or endorsed by the publisher.

Copyright © 2022 Cui, Liu, Pang and Li. This is an open-access article distributed under the terms of the Creative Commons Attribution License (CC BY). The use, distribution or reproduction in other forums is permitted, provided the original author(s) and the copyright owner(s) are credited and that the original publication in this journal is cited, in accordance with accepted academic practice. No use, distribution or reproduction is permitted which does not comply with these terms.

Frontiers in Oncology

Advances knowledge of carcinogenesis and tumor progression for better treatment and management

The third most-cited oncology journal, which highlights research in carcinogenesis and tumor progression, bridging the gap between basic research and applications to imrpove diagnosis, therapeutics and management strategies.

Discover the latest Research Topics

See more →



Frontiers

Avenue du Tribunal-Fédéral 34
1005 Lausanne, Switzerland
frontiersin.org

Contact us

+41 (0)21 510 17 00
frontiersin.org/about/contact